

# **Paleoclimatology and Paleometeorology: Modern and Past Patterns of Global Atmospheric Transport**

# NATO ASI Series

## Advanced Science Institutes Series

*A Series presenting the results of activities sponsored by the NATO Science Committee, which aims at the dissemination of advanced scientific and technological knowledge, with a view to strengthening links between scientific communities.*

The Series is published by an international board of publishers in conjunction with the NATO Scientific Affairs Division

**A Life Sciences**

**B Physics**

**C Mathematical  
and Physical Sciences**

**D Behavioural and Social Sciences**

**E Applied Sciences**

**F Computer and Systems Sciences**

**G Ecological Sciences**

**H Cell Biology**

Plenum Publishing Corporation  
London and New York

Kluwer Academic Publishers  
Dordrecht, Boston and London

Springer-Verlag  
Berlin, Heidelberg, New York, London,  
Paris and Tokyo



# Paleoclimatology and Paleometeorology: Modern and Past Patterns of Global Atmospheric Transport

edited by

**Margaret Leinen**

Graduate School of Oceanography,  
University of Rhode Island,  
Narragansett, RI, U.S.A.

and

**Michael Sarnthein**

Geologisches Paleontologisches Institut,  
Christian Albrechts Universität,  
Kiel, F.R.G.



**Kluwer Academic Publishers**

Dordrecht / Boston / London

Published in cooperation with NATO Scientific Affairs Division

Proceedings of the NATO Advanced Research Workshop on  
Paleoclimatology and Paleometeorology: Modern and Past Patterns of Global  
Atmospheric Transport  
Oracle, AZ, U.S.A.  
November 17–19, 1987

**Library of Congress Cataloging in Publication Data**

NATO Advanced Research Workshop (1987 : Oracle, Ariz.)  
Paleoclimatology and paleometeorology.

(NATO ASI series. Series C, Mathematical and physical  
sciences ; vol. 282)

Includes index.

1. Climatic changes--Congresses. 2. Paleoclimatology  
--Congresses. 3. Atmospheric circulation--Congresses.  
4. Dust--Congresses. 5. Eolian processes--Congresses.  
I. Leinen, Margaret, 1946- . II. Sarnthein, M.  
III. North Atlantic Treaty Organization. IV. Title.  
V. Series: NATO ASI series. Series C, Mathematical and  
physical sciences ; no. 282.

QC981.8.C5N37 1987 551.6 89-11219

ISBN-13:978-94-010-6937-3 e-ISBN-13:978-94-009-0995-3

DOI: 10.1007/978-94-009-0995-3

---

Published by Kluwer Academic Publishers,  
P.O. Box 17, 3300 AA Dordrecht, The Netherlands.

Kluwer Academic Publishers incorporates the publishing programmes of  
D. Reidel, Martinus Nijhoff, Dr W. Junk and MTP Press.

Sold and distributed in the U.S.A. and Canada  
by Kluwer Academic Publishers,  
101 Philip Drive, Norwell, MA 02061, U.S.A.

In all other countries, sold and distributed  
by Kluwer Academic Publishers Group,  
P.O. Box 322, 3300 AH Dordrecht, The Netherlands.

*Printed on acid free paper*

---

All Rights Reserved

© 1989 by Kluwer Academic Publishers

Softcover reprint of the hardcover 1st edition 1989

No part of the material protected by this copyright notice may be reproduced or  
utilized in any form or by any means, electronic or mechanical, including photo-  
copying, recording or by any information storage and retrieval system, without written  
permission from the copyright owner.

This book contains the proceedings of a NATO Advanced Research Workshop held within the programme of activities of the NATO Special Programme on Global Transport Mechanisms in the Geo-Sciences running from 1983 to 1988 as part of the activities of the NATO Science Committee.

Other books previously published as a result of the activities of the Special Programme are:

- BUAT-MENARD, P. (Ed.) – *The Role of Air-Sea Exchange in Geochemical Cycling* (C185) 1986
- CAZENAIVE, A. (Ed.) – *Earth Rotation: Solved and Unsolved Problems* (C187) 1986
- WILLEBRAND, J. and ANDERSON, D.L.T. (Eds.) – *Large-Scale Transport Processes in Oceans and Atmosphere* (C190) 1986
- NICOLIS, C. and NICOLIS, G. (Eds.) – *Irreversible Phenomena and Dynamical Systems Analysis in Geosciences* (C192) 1986
- PARSONS, I. (Ed.) – *Origins of Igneous Layering* (C196) 1987
- LOPER, E. (Ed.) – *Structure and Dynamics of Partially Solidified Systems* (E125) 1987
- VAUGHAN, R. A. (Ed.) – *Remote Sensing Applications in Meteorology and Climatology* (C201) 1987
- BERGER, W. H. and LABEYRIE, L. D. (Eds.) – *Abrupt Climatic Change – Evidence and Implications* (C216) 1987
- VISCONTI, G. and GARCIA, R. (Eds.) – *Transport Processes in the Middle Atmosphere* (C213) 1987
- SIMMERS, I. (Ed.) – *Estimation of Natural Recharge of Groundwater* (C222) 1987
- HELGESON, H. C. (Ed.) – *Chemical Transport in Metasomatic Processes* (C218) 1987
- CUSTODIO, E., GURGUI, A. and LOBO FERREIRA, J. P. (Eds.) – *Groundwater Flow and Quality Modelling* (C224) 1987
- ISAKSEN, I. S. A. (Ed.) – *Tropospheric Ozone* (C227) 1988
- SCHLESINGER, M.E. (Ed.) – *Physically-Based Modelling and Simulation of Climate and Climatic Change 2 vols.* (C243) 1988
- UNSWORTH, M. H. and FOWLER, D. (Eds.) – *Acid Deposition at High Elevation Sites* (C252) 1988
- KISSEL, C. and LAY, C. (Eds.) – *Paleomagnetic Rotations and Continental Deformation* (C254) 1988
- HART, S. R. and GULEN, L. (Eds.) – *Crust/Mantle Recycling at Subduction Zones* (C258) 1989
- GREGERSEN, S. and BASHAM, P. (Eds.) – *Earthquakes at North-Atlantic Passive Margins: Neotectonics and Postglacial Rebound* (C266) 1989
- MOREL-SEYTOUX, H. J. (Ed.) – *Unsaturated Flow in Hydrologic Modeling* (C275) 1989
- BRIDGWATER, D. (Ed.) – *Fluid Movements – Element Transport and the Composition of the Crust* (C281) 1989
- ANDERSON, D.L.T. and WILLEBRAND, J. (Eds.) – *Ocean Circulation Models: Combining Data and Dynamics* (C284) 1989
- BERGER, A., SCHNEIDER, S. and DUPLESSY, J. Cl. (Eds.) – *Climate and Geo-Sciences* (C285) 1989

## TABLE OF CONTENTS

PREFACE	xiii
LIST OF PARTICIPANTS	xvii
SECTION 1. DUST FORMATION, INJECTION, AND CONTINENTAL ARIDITY	1
<i>William Nickling, Chair</i>	
1. PYE, K., "Processes of fine particle formation, dust source regions, and climatic changes"	3
2. BREUNINGER, R.H., D.A. Gillette, and R. Kihl, "Formation of wind-erodible aggregates for salty soils and soils with less than 50% sand composition in natural terrestrial environments"	31
3. BRAZEL, A.J., "Dust and climate in the American Southwest"	65
4. MIDDLETON, N.J., "Climatic controls on the frequency, magnitude and distribution of dust storms: examples from India/Pakistan, Mauritania and Mongolia"	97
5. NICKLING, W.G. and J.A. Gillies, "Emission of fine-grained particulates from desert soils"	133
6. ROGNON, P., G. Coudé-Gaussen, G. Bergametti, and L. Gomes, "Relationships between the characteristics of soils, the wind energy and dust near the ground, in the western sandsea (N.W. Sahara)"	167
7. TETZLAFF, G., M. Peters, W. Janssen, and L.J. Adams, "Aeolian dust transport in West Africa"	185

**SECTION 2. DUST TRANSPORT AND TRANSPORT MODELING** 205

*John Merrill, Chair*

1. MERRILL, J.T., "Modeling long-range transport using trajectory techniques" 207
2. BERGAMETTI, G., L. Gomes, E. Remoudaki, M. Desbois, D. Martin and P. Buat-Ménard, "Present transport and deposition patterns of African dusts to the North-western Mediterranean" 227
3. JOUSSAUME, S., "Desert dust and climate: an investigation using an atmospheric general circulation model" 253

**SECTION 3. DUST COMPOSITION AND FACTORS CONTROLLING IT: EVIDENCE FROM AEROSOLS AND SEDIMENTS** 265

*Gerd Tetzlaff, Chair*

1. TOMADIN, L. and R. Lenaz, "Eolian dust over the Mediterranean and their contribution to the present sedimentation" 267
2. TOMADIN, L., G. Cesari, S. Fuzzi, V. Landuzzi, R. Lenaz, A. Lobietti, P. Mandrioli, M. Mariotti, A. Mazzucotelli, and R. Vannucci, "Eolian dust collected in springtime (1979 and 1984 Years) at the seawater-air interface of the Northern Red Sea" 283
3. D'ALMEIDA, G.A., "Desert aerosol: characteristics and effects on climate" 311
4. COUDÉ-GAUSSSEN, G., "Local, proximal and distal Saharan dusts: characterization and contribution to the sedimentation" 339
5. SCHUETZ, L., "Atmospheric mineral dust — properties and source markers" 359
6. GROUSSET, F.E. and P.E. Biscaye, "Nd and Sr isotopes as tracers of wind transport: Atlantic aerosols and surface sediments" 385
7. SIROCKO, F. and M. Sarnthein, "Wind-borne deposits in the Northwestern Indian Ocean: record of Holocene sediments versus modern satellite data" 401

8.	POYNTER, J.G., P. Farrimond, N. Robinson, and G. Eglinton, "Aeolian-derived higher plant lipids in the marine sedimentary record: links with palaeoclimate"	435
9.	PFIRMAN, S., I. Wollenburg, J. Thiede, and M.A. Lange, "Lithogenic sediment on Arctic pack ice: potential aeolian flux and contribution to deep sea sediment"	463
<b>SECTION 4. MODELING ATMOSPHERIC CIRCULATION IN THE PAST</b>		<b>495</b>
<i>John Kutzbach, Chair</i>		
1.	NEWELL, R.E. and J. Hsiung, "Past and present oceanic energy balance patterns"	497
2.	KUTZBACH, J.E., "Possible effects of orbital variations on past sources and transports of eolian material: estimates from general circulation model experiments"	513
<b>SECTION 5. INFERENCES FROM THE SEDIMENTARY RECORD: LOESS, ICE CORES, AND OTHER LAND EVIDENCE</b>		<b>523</b>
<i>Jean Maley, Chair</i>		
1.	ISSAR, A., H. Tsoar, and D. Levin, "Climatic changes in Israel during historical times and their impact on hydrological, pedological and socio-economic systems"	525
2.	WAGENBACH, D. and K. Geis, "The mineral-dust record in a high- altitude Alpine Glacier (Colle Gnifetti, Swiss Alps)"	543
3.	BUCHER, A., "Fallout of Saharan dust in the Northwestern Mediterranean Region"	565
4.	MALEY, J., "Late Quaternary climatic changes in the African Rain Forest: forest refugia and the major role of sea-surface temperature variations"	585
5.	DAVIS, O.K., "The regionalization of climatic change in Western North America"	617



6. PETIT-MAIRE, N., "Interglacial environments in presently Hyperarid Sahara: palaeoclimatic implications" 637

**SECTION 6. REPORT OF THE GROUP STUDYING: INFERENCES FROM THE MARINE SEDIMENTARY RECORD** 663

*Michael Sarnthein and Margaret Leinen, Co-Chair*

1. HEUSSER, L.E., "Northeast Asian climatic change over the last 140,000 years inferred from pollen in marine cores taken off the Pacific Coast of Japan" 665
2. LEINEN, M., "The Late Quaternary record of atmospheric transport to the Northwest Pacific from Asia" 693
3. HOOGHEIMSTRA, H., "Variations of the NW African trade wind regime during the last 140,000 years: changes in pollen flux evidenced by marine sediment records" 733
4. STABELL, B., "Deflation and humidity during the last 700 ka in NW Africa from the marine record" 771
5. DUPONT, L.M., "Palynology of the last 680,000 years of ODP Site 658 (off NW Africa): fluctuations in paleowind systems" 779
6. POKRAS, E.M., "Pliocene history of South Saharan/Sahelian aridity: record of freshwater diatoms (Genus *Melosira*) and opal phytoliths, ODP Sites 662 and 664" 795
7. SCHRAMM, C.T., "Cenozoic climatic variation recorded by quartz and clay minerals in North Pacific sediments" 805
8. REA, D.K., "Geologic record of atmospheric circulation on tectonic time scales" 841

**SECTION 7. REPORTS AND RECOMMENDATIONS OF WORKING GROUPS** 859

1. DUST FORMATION, INJECTION, AND CONTINENTAL ARIDITY 861

*William Nickling, Chair*

2. DUST TRANSPORT AND TRANSPORT MODELING	865
<i>John Merrill, Chair</i>	
3. DUST COMPOSITION AND FACTORS CONTROLLING IT: EVIDENCE FROM AEROSOLS AND SEDIMENTS	869
<i>Gerd Tetzlaff, Chair</i>	
4. MODELING ATMOSPHERIC CIRCULATION IN THE PAST	873
<i>John Kutzbach, Chair</i>	
5. INFERENCES FROM THE SEDIMENTARY RECORD: LOESS, ICE CORES, AND OTHER LAND EVIDENCE	877
<i>Jean Maley, Chair</i>	
6. REPORT OF THE GROUP STUDYING: INFERENCES FROM THE MARINE SEDIMENTARY RECORD	883
<i>Michael Sarnthein and Margaret Leinen, Co-Chair</i>	
INDEX	889

## PREFACE

The NATO Advanced Research Workshop on "Paleoclimatology and Paleometeorology: Modern and Past Patterns of Global Atmospheric Transport" (held at Oracle, Arizona, USA from November 17-19, 1987) brought together atmospheric chemists, physicists, and meteorologists who study the origin and transport of modern-day mineral and biological aerosols with geologists and paleobotanists who study the sedimentary record of eolian and hydrologic processes along with modelers who study and conceptualize the processes influencing atmospheric transport at present and in the past. Presentations at the workshop provided a guide to our present knowledge of the entire spectrum of processes and phenomena important to the generation, transport, and deposition of eolian terrigenous material that ultimately becomes part of the geologic record and the modeling techniques that used to represent these processes. The presentations on the geologic record of eolian deposition documented our present understanding of the nature and causes of climate change on time scales of the last glacial ages (tens of thousands of years) to time scales over which the arrangement of continents, mountains, and oceans has changed substantially (tens of millions of years).

There has been a growing recognition of the importance of global climatic changes to the future well-being of humanity. In particular, the climatic response to human alterations to the earth's surface and chemical composition has led to concern over the agricultural, ecological, and societal impacts of such potential global changes. Recently, scientists have become very interested in using the geologic record of past climates as a data base for studying global climate change. These studies address fundamental questions about the present climate system — How correct is our understanding of the role of radiatively active gases like CO<sub>2</sub> in controlling climate? — and our ability to understand past and future climate change — What are the mechanisms of climate? How linearly do the equations we use to model climate parameters behave when extrapolated beyond the range of present climatic variation? How does Earth's climate respond to catastrophic perturbation of the atmosphere? In order to answer these questions, earth scientists need to be able to make very sophisticated inferences about climate from the geologic record. It is no longer enough to know that a climatic event or change occurred in the past. We need to know how it occurred, how fast it occurred, and the conditions that were

antecedent and subsequent to it. Within this context the study of atmospheric transport and deposition in the past has gained momentum as a result of its importance for understanding the perturbations to Earth's environment that may result from changes in the composition of atmospheric aerosol and amount of atmospheric transport.

Studies of atmospheric transport in the past also provides data to evaluate the performance of the atmospheric circulation models that are used to predict the results of man's alteration of Earth's climate. In order to predict both climatic changes and the environmental consequences of such changes, it is necessary to construct mathematical models of climate and to drive these models with scenarios of human alteration to land surfaces and atmospheric chemical composition — especially "greenhouse" gases such as CO<sub>2</sub> or methane. But before society can be expected to make changes to activities that modify the environment, it is necessary to validate the predictions of mathematical models of climate. Because the anticipated changes to atmospheric conditions are larger than any modern experience, the only viable examples against which to test the models come from Earth's history.

The ability of climatic models to predict the location of ancient deserts and the patterns of ancient winds can be inferred from studies of the paleoclimatic pattern of deserts and dusts and their comparison with model-predicted simulations of ancient deserts and dust transport patterns. Because the ability of state-of-the-art climatic models to forecast the regional consequences of human alteration of the climate is both more important for impact assessment than hindcasting past conditions and less verifiable, excellent performance by models in predicting paleoclimatic regimes is critical to have confidence in model simulation. Thus, we view studies of atmospheric transport in the past as the meter-stick against which we can calibrate our understanding of how climatic changes evolve and how human activities are altering our climatic future. Without such understanding, public policy making will be based on speculative formulations.

Other recent studies suggest that we do not fully understand the role of natural terrigenous materials in geochemical cycling. For example, terrigenous material transported to the oceans may influence biological productivity in areas remote from surface runoff and regenerated nutrients. Like climate models, these hypotheses are heavily biased by present-day compositions and fluxes of terrigenous material to the ocean. An evaluation of the variability in the type and amount of terrigenous material transported to the oceans in the past can put such hypotheses into perspective.

Eolian dust and other terrigenous materials that are transported by atmospheric processes are potent indicators of climate change in the geologic record, and reconciling the geological record of dust deposition with theories and models of climate is a challenging, but rewarding effort. Climate can be influenced by dust and by radiative processes; such as, redistribution of heating in the atmospheric column and by microphysical processes as nucleation. Modeling these factors is at present difficult, but the small amount that has been done has yielded tantalizing results. Because the resultant climate depends upon so many factors, this work impinges upon climate prediction problems of obvious importance to society.

In order to assess our present understanding of paleoclimate and the tools and models used to study this topic, the NATO Advanced Research Workshop on Paleoclimatology and Paleometeorology brought together 43 participants representing 9 nations. The scientific expertise of the participants ranged from instrumental measurement of aerosol particle size in the free troposphere to modeling of general atmospheric circulation several millions of years ago. The workshop was organized into several sessions which followed aerosol from its formation to its deposition and geologic record:

- Dust Formation, Injection and Continental Aridity;
- Meteorology of Transport, Transport Mechanisms and Trajectories;
- Dust Composition and Controls on Composition: Evidence from Aerosols and Sediments;
- Inferences from the Sedimentary Record: Loess, Ice Cores, and Other Land Evidence;
- Inferences from Deep-Sea Sediments; and
- Modeling Atmospheric Circulation in the Past.

The presentations made at the workshop provided the participants with summaries of the state of our present understanding of each of these topics. This volume includes papers based on these presentations and is also organized to follow aerosol from formation to deposition. The greatest value of the workshop for its participants came from the questions and discussions which followed each presentation and set of presentations. These discussions identified new directions for research in each of the fields to answer important questions. In some cases the discussions identified problems of interest to those in other fields and opportunities which would open cross-disciplinary work. These discussions and recommendations are summarized by topic in a separate section at the end of the volume.

We would like to acknowledge the assistance of several organizations and individuals. Our planning was assisted by a Steering Committee which included John Kutzbach (U.S.), Jean Maley (France), John Merrill (U.S.), William Nickling (Canada), and Gerd Tetzlaff (FRG). These individuals also assisted us in identifying the exciting group of scientists who attended the workshop and qualified reviewers of the many manuscripts. We are grateful to these reviewers for their efforts in improving this volume.

We are indebted to the NATO Scientific Affairs Division and the Special Programme on "Global Transport Mechanisms in the Geo-sciences" for their financial support (Advanced Research Workshops Programme (ARW.934/86) and sponsorship of the workshop. Additional funds for the workshop were provided by the United States National Science Foundation (NSF) through a grant to Margaret Leinen (NSF ATM88-00044) and by the French Centre National de la Recherche Scientifique (CNRS) through travel grants to individuals.

The personnel of the SunSpace Ranch Conference Center made our stay there a fruitful and pleasant one. The logistics of the conference were handled with efficiency and grace by Ms. Tammy King Walsh. Special thanks are due to Ms. Rhonda Kenny, who typed and reformatted the U.S. manuscripts and who also prepared the abstracts volume for the conference. We would also like to thank Mrs. Nel Pols-van der Heijden along with Mrs. Nel de Boer and staff at Kluwer for their patience and guidance in preparing this volume.

**Margaret Leinen**  
Narragansett, RI (U.S.A.)

**Michael Sarnthein**  
Kiel, FRG

**March, 1989**

## LIST OF PARTICIPANTS NATO-ASI

*November 17-19, 1987*  
*Oracle, Arizona - U.S.A.*

### **DIRECTORS**

*M. Leinen*  
Graduate School of Oceanography, University of Rhode Island,  
Narragansett, RI 02882-1197, U.S.A.

*M. Sarnthein*  
Geologisches Paleontologisches Institut, Christian Albrechts Universität,  
Olshausenstrasse, Kiel, FEDERAL REPUBLIC OF GERMANY

### **STEERING COMMITTEE**

*J. Kutzbach*  
Center for Climatic Reserach, Dept. of Meteorology, University of  
Wisconsin, Madison, WI 53706, U.S.A.

*J. Maley*  
ORSTOM, Laboratoire de Palynologie, Université des Sciences et Techniques  
du Languedoc, 34060 Montpellier Cèdex, FRANCE

*W. Nickling*  
Dept. of Geography, University of Guelph, Guelph, Ontario, CANADA  
W1G 2W1

*G. Tetzlaff*  
Institut für Meteorologie, Universität Hannover, Herrenhauserstrasse 2,  
D-3000 Hannover 21, FEDERAL REPUBLIC OF GERMANY

### **PARTICIPANTS**

#### ***England***

*G. Eglinton*  
School of Chemistry, University of Bristol, Bristol B58 1TS

*N.J. Middleton*

University of Oxford, Mansfield Road, Oxford OX1 3TB, Oxford 271919

*K. Pye*

Dept. of Earth Sciences, Cambridge University, Cambridge, CB2 3RS

*Federal Republic of Germany*

*G.A. d'Almeida*

Meteorologisches Institut, Universität München, 8000 München 2, den

*L.M. Dupont*

Institut für Palynologie, Wilhem-Weberstrasse 2, D-3400 Göttingen

*H. Hooghiemstra*

Institute of Palynology and Quaternary Sciences, University of Göttingen, Göttingen

*L. Schütz*

Institut für Meteorologie der Universität Mainz, Anselm-von-Bentzel-Weg 12, D-6500 Mainz

*F. Sirocko*

Geologisches Paleontologisches Institut, Christian Albrechts Universität, Olshausenstrasse, Kiel

*R. Tiedemann*

Geologisches Paleontologisches Institut, Christian Albrechts Universität, Olshausenstrasse, Kiel

*D. Wagenbach*

Institut für Umweltphysik, Neuenhemer Feld 366, D-6900 Heidelberg

*I. Wollenburg*

Geologisches Paleontologisches Institut, Christian Albrechts Universität, Olshausenstrasse, Kiel



**France***G. Bergametti*

Laboratoire de Physico-Chimie de l'Atmosphère, Université Paris VII 2,  
place Jussieu, 75251 Paris, Cedex 05

*A. Bücher*

Ministère de l'éducation Nationale, Université Paul Sabatier, Observatoires  
du Pic-du-Midi et de Toulouse, 65200 Bagnères-de-Bigorre

*G. Coude-Gaussen*

Géologie des ensembles continentaux, Université P.M. Curie, 4 place  
Jussieu, 75230 Paris

*F.E. Grousset*

UA CNRS #197, Université Bordeaux 1, 351 Crs. de la Libération,  
33405 Talence, Cedex

*S. Joussaume*

Laboratoire de Météorologie Dynamique, 24 rue Lhomond, 75231 Paris,  
Cedex 5

*A. Juillet-Leclerc*

Centre des Faibles Radioactivités, Domaine du CNRS, 91 190 Gif-sur-Yvette

*J.R. Petit*

Laboratoire de Géochimie Isotopique, LODYC/CEA/IRDI/DESICP/DPC,  
91191 Gif-sur-Yvette, Cedex

*N. Petit-Maire*

Laboratoire de Géologie du Quaternaire CNRS, Faculté sciences Luminy,  
C. Postale 902, 13288 Marseille, Cedex

*P. Rognon*

Laboratoire de Géodynamique des milieux continentaux, 4 place Jussieu,  
Tour 16, 4ème étage, 75252 Paris, Cedex 05

**Israel***A. Issar*

The Jacob Blaustein Institute for Desert Research, Ben-Gurion University of  
NEGEV, Sede Boqer Campus, 84993

*Italy*

*F. Giorgi*  
National Center for Atmospheric Research, Boulder, CO

*L. Tomadin*  
Istituto di Mineralogia e Petrografia, Università di Urbino

*Norway*

*B. Stabell*  
Dept. of Geology, University of Oslo, P.O. Box 1047, Blindern, N-0316 Oslo 3

*U.S.A.*

*Richard Arimoto*  
Center for Atmospheric Chemistry Studies, Graduate School of  
Oceanography, University of Rhode Island, Narragansett, RI 02882-1997

*Anthony Brazel*  
Laboratory of Climatology, Arizona State University, Tempe, AZ 85287

*O.K. Davis*  
Dept. of Geosciences, The University of Arizona, Tucson, AZ 85721

*D.A. Gillette*  
Geophysical Monitoring for Climatic Change, Air Resource Laboratory,  
NOAA, Boulder, CO 80303

*L. Heusser*  
Lamont-Doherty Geological Observatory, University of Columbia, Palisades,  
NY 10964

*J.T. Merrill*  
Center for Atmospheric Chemistry Studies, Graduate School of  
Oceanography, University of Rhode Island, Narragansett, RI 02882

*R.E. Newell*  
Dept. of Earth, Atmospheric, and Planetary Sciences, 54-1522 Massachusetts  
Institute of Technology, Cambridge, MA 02139

*E.M. Pokras*

Lamont-Doherty Geological Observatory, Columbia University, Palisades,  
NY 10964

*D.K. Rea*

Dept. of Geological Sciences, The University of Michigan, Ann Arbor,  
MI 48109

*S. Schneider*

National Center for Atmospheric Research, Boulder, CO

*C.T. Schramm*

Graduate School of Oceanography, University of Rhode Island,  
Narragansett, RI 02882-1197

*S. Thompson*

National Center for Atmospheric Research, Boulder, CO

*D.L. Westphal*

Pennsylvania State University, Dept. of Meteorology, University Park,  
PA 16802

**SECTION 1.**

**DUST FORMATION, INJECTION, AND CONTINENTAL ARIDITY**

# PROCESSES OF FINE PARTICLE FORMATION, DUST SOURCE REGIONS, AND CLIMATIC CHANGES

K. Pye  
Department of Earth Sciences  
University of Cambridge  
Downing Street  
Cambridge CB2 3EQ  
England

**ABSTRACT.** Atmospheric dust has been supplied by two main types of source region during the Quaternary. At times of maximum continental glaciation much dust was blown from outwash plains and braided river channels adjacent to continental ice sheets and valley glaciers in mid-latitudes. Dust flux from these sources was low in the Holocene and earlier interglacials. Arid regions have been important sources of dust during both glacial and interglacial periods. Based on observed variations in the abundance of dust in oceans cores, several authors have suggested that the flux of desert dust is directly related to the intensity or areal extent of continental aridity. However, this interpretation is based on an oversimplified view of the factors which control dust supply. It is argued in this paper that dust flux is greater from arid areas than hyper-arid areas. Sudden increases in dust flux observed in ocean cores can be caused either by a change from semi-arid to arid or from hyperarid to arid conditions, or by changes in the pattern of meso- and macro-scale atmospheric processes which control dust dispersion.

## 1. INTRODUCTION

Interpretation of climatic history from dust records in ocean cores and loess sections is presently hampered by a limited understanding of the precise nature of dust source regions, the relative importance of processes which form fine particles and the atmospheric processes which control dust dispersion. Sedimentary evidence from the continents indicates a large increase in the scale of atmospheric dust transport around the time of the last glacial maximum (18,000 B.P.). Much of this dust was derived from glacial outwash at the margins of continental ice sheets, but there is also evidence of increased dust flux from at least some deserts. Two factors may have contributed to this: (1) an increase in the magnitude of dust source areas and/or the rate of dust formation, and (2) higher wind energy. Several authors have inferred that there is a positive relationship between the magnitude of non-glacial dust flux and the intensity and extent of continental aridity. However, this inter-

pretation is not based on a close examination of the factors which control dust supply and atmospheric dust dispersion. The aim of this paper is to critically review what is presently known or not known about the processes of fine particle formation, the terrain types which favour high rates of dust deflation, and their relationship to climatic change.

## 2. EVENT SEQUENCES LEADING TO THE FORMATION OF DUST DEPOSITS

The formation of dust deposits requires (a) a source of dust, (b) adequate wind energy to entrain and transport the dust to the deposition site, and (c) conditions which favour preservation of the dust at the deposition site (Isoar and Pye, 1987). Event sequences are involved in the formation of all dust deposits (Smalley, 1980; Smalley and Smalley, 1983). In complex cases up to a dozen stages of particle formation, transport, deposition, remobilization and redeposition may be involved, but there are many simple cases involving only three or four. The three most common types of event sequence are shown in Figure 1. Weathering and glacial abrasion/crushing are believed to be the two most important groups of processes which form fine particles (Smalley, 1966; Nahon and Trompette, 1982) although some fine material is also produced by abrasion and crushing during fluvial, aeolian and marine transport, and some is released from existing fine-grained rocks (Moss et al., 1973; Whalley et al., 1982, 1987).

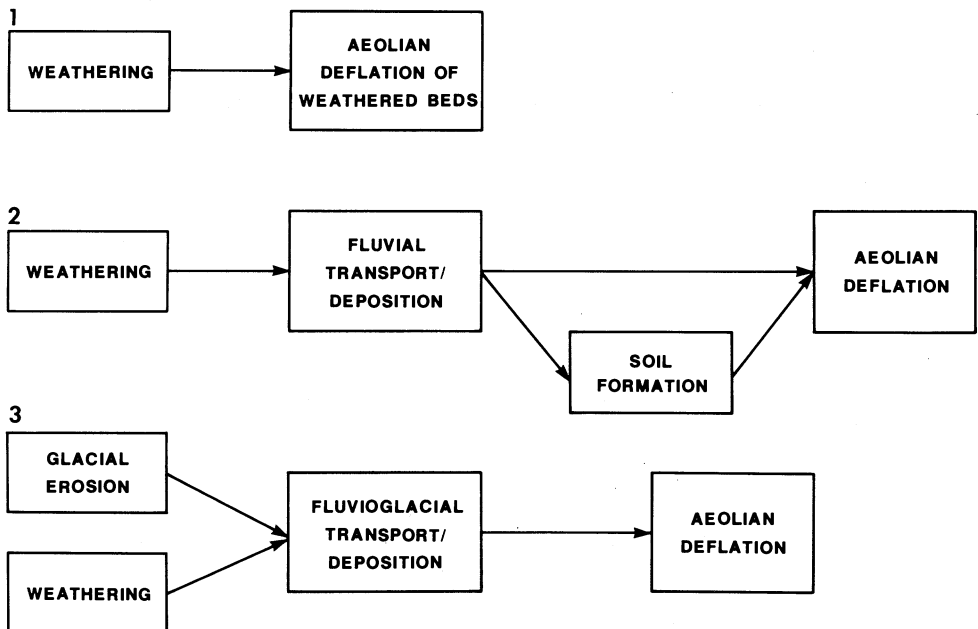


Fig. 1 Three important event sequences leading to the formation of aeolian dust deposits.

Production of fines by fluvial processes is most important in high energy mountain streams. Aeolian abrasion and direct aeolian removal of weathering debris is most important in hyper-arid environments (case 1 of Figure 1). In arid and semi-arid areas much weathered debris experiences a phase of fluvial transport (and sometimes soil formation) before deflation (case 2 of Figure 1). At high latitudes and in high mountain environments, glacial erosion and frost weathering provide debris which is transported by fluvio-glacial meltwater to the sites of deflation (case 3 of Figure 1). Although the sites of fine particle formation and aeolian deflation are frequently geographically separate, the distance of fluvial transport can range from only a few metres to thousands of kilometres. Some fines are unquestionably produced under arid conditions, but in many cases, as in the Lake Chad Basin (McTainsh, 1987), weathered sediment has been supplied to an arid depositional environment by fluvial transport from a humid source region. The relative proportions of autochthonous and allochthonous fine grained material in arid zone basins are difficult to determine, since quantitative data about rates of particle formation under different climatic conditions are sparse, and many such basins have experienced dramatic climatic changes (and hence fluctuations in the rates of operation of different processes) during the Quaternary.

### 3. PRODUCTION OF FINES BY WEATHERING PROCESSES

A full review of the literature dealing with the formation of fine particles is beyond the scope of this paper, but some general comments can appropriately be made.

The nature of weathering products is governed by climate, relief and the physical and chemical properties of the source rocks. The grain size, porosity, permeability, mineral composition, degree of microcracking and residual strain are critical factors which influence the effectiveness of weathering processes.

Weathering processes include cyclic wetting and drying, temperature fluctuations, chemical reactions, frost and salt action. In most natural environments several processes operate together, either simultaneously or at different times of the year.

Although the qualitative operation of these processes is relatively well understood, there is a lack of quantitative field data about natural weathering rates.

#### 3.1 Frost Weathering

Laboratory experiments have demonstrated that frost can cause disintegration of many rocks in a critical degree of water saturation is achieved (at least 80% of the porosity must be filled with water, Thomas, 1938). When water freezes there is a 9% increase in volume which creates stresses which may exceed the rock tensile strength if the expansion cannot be accommodated by internal voids (Litvan, 1976). More important, however, may be stresses created as supercooled moisture moves towards the freezing front (White, 1976; Walder & Hallet, 1986).

Soft rocks with large numbers of small pores but low permeability, including chalks and many mudrocks, are especially prone to frost damage and can produce a large amount of fine grained material in a relatively short time (Lautridou and Ozouf, 1982).

Several authors have questioned the effectiveness of frost action in cold, dry environments because the critical degree of moisture saturation is rarely attained (White, 1976; McGreevy and Whalley, 1985; Hall, 1986). Laboratory experiments have shown that "Antarctic" or "Siberian-type" winter conditions, with low relative humidity and small number of freeze-thaw cycles, tend to cause less damage in unit time than "Icelandic-type" conditions in which humidity is higher and the number of freezing cycles is greater (Tricart, 1956; Wiman, 1963; Martini, 1967; Potts, 1970). In general, the effectiveness of frost action increases with the annual number of freeze-thaw cycles and winter precipitation total. The intensity of freezing is of relatively minor importance (Wiman, 1963; Potts, 1970).

Field observations suggest frost action is an important silt-forming process on Mount Kenya (Zeuner, 1949), in sub-Arctic Canada (St. Arnaud and Whiteside, 1963), and in Siberia (Konischev, 1982). It appears to be less important in cold arid environments (Hall, 1986).

### 3.2 Salt Weathering

Laboratory experiments have also shown that the physical action of salts is very effective in causing rock breakdown under simulated hot desert conditions (Kwaad, 1970; Goudie et al., 1970; Goudie, 1974, 1986a,b), although there is conflicting evidence regarding their effectiveness at low temperatures (Williams and Robinson, 1981; McGreevy and Smith, 1982). Significant quantities of silt-size material have been produced in some of these investigations (Goudie et al., 1979; Goudie, 1986b; Pye and Sperling, 1983). Doubts have been expressed about how well the laboratory experiments simulate salt weathering in nature (McGreevy and Smith, 1982; Smith and McGreevy, 1983), but a large volume of field observational and experimental evidence indicates salt weathering can be rapid, at least locally (Beaumont, 1968; Chapman, 1980; Goudie and Day, 1980; Cooke, 1981; Goudie and Watson, 1984; Smith and McAlister, 1987). Salt action is most intense on the margins of salt lakes or playas where saline groundwater rises by capillary action and salts are precipitated at the surface by evaporation. Seasonal wetting and drying of playa crusts produces significant amounts of fine saline dust which is easily deflated (St. Amand et al., 1986). In hyperarid environments airborne salts accumulate on rock outcrops and surface sediments, where they may contribute to weathering and tafoni development. However, rates of airborne salt accumulation are low (Dan and Yaalon, 1982; Dan and Koyumdjisky, 1987), and the intensity of salt weathering is much less than in lake-marginal settings. Where mean annual rainfall exceeds 100 mm, salts accumulate in a sub-surface horizon. Little of the fine material produced by sub-surface salt weathering can be deflated unless the sediments are disturbed.

Three physical processes are involved in salt weathering (Cooke and Smalley, 1968; Evans, 1970; Cooke and Sperling, 1985): (1) crystallization pressure exerted by salt crystals growing in a saturated or supersaturated



solution; (2) pressure exerted during thermal expansion of salt crystals; (3) pressure caused by an increase in volume when salts undergo hydration. Chemical reactions between highly saline pore fluids and the host rock may also be important in some cases (Young, 1987). Repeated fluctuations in temperature and humidity increase the intensity of salt weathering since the solubility of many salts is temperature dependent, and many salts hydrate or dehydrate in response to temperature and humidity fluctuations. Large diurnal differences in ambient conditions favour intense salt weathering.

Although the local effectiveness of salt action in causing rock disintegration has been convincingly demonstrated, its quantitative importance as a producer of large amounts of fines is not proven. The presence of salts in soils and sediments need not imply it is the dominant weathering mechanism. Similarly, the presence of fine material in saline desert soils is not proof of its in-situ formation by salt-weathering, since much of it may represent deposited dust formed elsewhere (Peterson, 1980; Amit and Gerson, 1986; Gerson et al., 1985).

### 3.3 Chemical Weathering

Chemical weathering occurs under all climatic regimes, although the rates are much higher in humid than in arid climates. The rate of chemical reactions also increases with temperature, being higher in the humid tropics than in humid temperate areas. The principal chemical reactions involved are hydrolysis and solution. In addition to temperature, these processes are strongly dependent on the pH, concentration of organic and inorganic acids, salinity and flow rate of near-surface waters. In humid, vegetated areas, soil waters are commonly charged with carbonic and organic acids which readily dissolve carbonates and form complexes with the products of silicate weathering. By contrast, arid zone soil waters are frequently alkaline and/or saline. Carbonates are less readily dissolved and hydrolysis of silicates is retarded. However, such waters may accomplish significant dissolution of quartz and alumino-silicate minerals (van Lier et al., 1960; Yariv and Cross, 1979; Young, 1987).

In the humid tropics, silicate minerals rapidly decompose to form clay and iron oxyhydroxides, whereas in the sub-humid and arid tropics chemical alteration is limited mainly to grain boundaries and rocks break down mainly by granular disintegration (Pye, 1985). The silt/clay ratio of weathering products in arid and semi-arid areas is normally much higher than in humid tropical or humid temperate areas. For example, in the Kora area of semi-arid Kenya, Pye et al. (1985) found that soils developed on a range of lithologies contained up to 50% silt but less than 10% clay.

### 3.4 Other Weathering Processes

Stresses caused by diurnal temperature fluctuations, thermal gradients, and the differential coefficients of thermal expansion of different minerals have long been suspected to be important in weathering of bare rock surfaces in deserts, but their significance is still uncertain (Roth, 1965; Peel, 1974; Rice, 1976; Winkler, 1977; Smith, 1977). Early labora-

tory experimental work (Blackwelder, 1925; Griggs, 1936) showed that temperature variations alone do not cause disintegration of small rock cubes, but that combined temperature and moisture fluctuations are effective. It has been suggested that sudden reductions in rock surface temperatures due to rain might cause thermal shock cracking. Stresses might also be generated by the formation of an electrical double layer following moisture absorption into fine capillaries (Ravina and Zaslavsky, 1974). Surface temperature and moisture fluctuations are ubiquitous in deserts and their effects warrant further investigation.

Spontaneous breakdown of rocks due to the release of strain energy is a further process of potential importance in both humid and arid environments (Durrance, 1965). "Sheeting" of large rock slabs due to the formation of unloading joints has long been recognised to be important in the formation of inselbergs (Twidale, 1982). Unloading can also weaken the bonds between individual mineral grains, leading to microfracturing and chemical weathering at grain boundaries (Pye, 1986). The tectonic history and residual strain characteristics of rocks must have a profound effect on the weathering behaviour of rocks but remain to be accurately demonstrated.

#### 4. PARTICLE FORMATION BY ABRASION AND CRUSHING PROCESSES

##### 4.1 Fluvial Abrasion and Crushing

Kuenen (1959) found in laboratory tumbling mill experiments that large amounts of fine material are not produced during simulated fluvial abrasion of crushed Brazilian quartz, but more fine debris was produced when steel balls were added to the mill to simulate crushing by cobbles. However, as noted by Moss (1966), much first cycle plutonic quartz contains microfractures which enhance its rate of breakdown during fluvial transport. Moss et al. (1973) and Moss and Green (1975) demonstrated experimentally that silt is produced by abrasion of such material.

The amount of silt produced by fluvial processes will depend on the size distribution, mineral composition and strain history of the source material. High rates of silt production are likely in high energy mountain streams which transport a wide range of particle sizes including cobbles. Fewer fines are likely to be generated in rivers which transport only sand or finer material. The widely observed downstream increase in roundness of cobbles and gravel testifies to the effectiveness of fluvial abrasion processes.

##### 4.2 Aeolian Abrasion

Aeolian abrasion experiments performed on a variety of materials by Kuenen (1960) showed that rates of abrasion increase with particle size, wind velocity, particle angularity and surface roughness. Polished quartz sand grains suffered virtually no abrasion. Only very fine flour ( $<2\mu\text{m}$ ) and a few coarse silt particles ( $>50\mu\text{m}$ ) were produced by abrasion of crushed Brazilian quartz, though medium and coarse silt were produced by erosion of crushed feldspar. However, Whalley et al. (1982) reported

the production of both coarse and fine silt during simulated aeolian abrasion of crushed vein quartz. Whalley et al. (1987) subsequently found that the total amount of silt produced decreases with time while the proportion of fine silt increases as the grains are progressively rounded. These results imply that significant quantities of dust should be produced by abrasion of angular, polymineralic, first-cycle sands, but only a small amount of fine dust will be produced by abrasion of mature, rounded quartz sands.

The occurrence of yardangs and ventifacts in deserts, together with the results of laboratory experiments (Dietrich, 1977; Suzuki and Takahashi, 1981), provides direct evidence that blowing sand can abrade rock surfaces, but there are no published data regarding the size of the particles produced.

#### 4.3 Glacial Grinding

The glacial origin of much loessic silt was recognised in the late 19th century (Tutovskii, 1899, 1900; Geikie, 1898) and subsequently emphasised by Smalley (1966). Analysis of sub-glacial deposits (Vivian, 1975; Boulton, 1978, 1979) confirmed the presence of large quantities of silt and clay, but there is still debate about how much is formed sub-glacially and how much represents reworked weathered material (Whalley, 1979; Haldorsen, 1981, 1983; Nahon and Trompette, 1982; Sharp and Gomez, 1985). Most of the fine material in the loess of North America, Europe, Siberia, Argentina and New Zealand has undoubtedly been glacially transported, if not glacially formed. Some of the Soviet Central Asian and Chinese loess must also have been formed by glacial or cold weathering processes in the adjacent mountains (Smalley and Krinsley, 1978; Smalley, 1980; Smalley and Smalley, 1983), but an unknown proportion is of desert origin (Derbyshire, 1983; Liu et al., 1985). There is no evidence that glacial processes have contributed to the much smaller Quaternary dust accumulations in Australia, Nigeria, Tunisia and Israel.

### 5. MAJOR DUST SOURCE REGIONS

Present day dust storms are most frequent and most extensive in and around the major deserts (Goudie, 1978, 1983; Middleton et al., 1986). Continental ice sheets are much less extensive than during the last glacial maximum, and areas of unvegetated outwash sediment are of restricted extent, principally in high latitudes and some high mountain valleys. Deflation of dust from outwash plains occurs today in parts of Iceland, Alaska and Antarctica (Ashwell, 1986; Péwé, 1951), but on a relatively small scale compared with the Pleistocene. Much larger dust storms occur in the deserts and desert fringe areas of the Sahara, Central Asia, the Middle East, the northwest Indian subcontinent, the American southwest and Australia. Not all these areas are hyperarid. Available observational data suggest that dust storm frequency is in fact almost twice as high in arid areas with a mean annual rainfall of 100-200 mm compared with hyperarid areas (<100 mm) and semi-arid areas (200-400 mm) (Figure 2; Goudie, 1983). To some extent this must reflect

recent human disturbance on desert margins, but three natural may contribute to the lower frequency of dust storms in hyperarid areas compared with arid areas: (1) lower rates of debris production by weathering, (2) less fluvial transport and disturbance of wind-stable surfaces by surface wash, and (3) rarity of strong winds associated with mid-latitude depressions in very arid core areas.

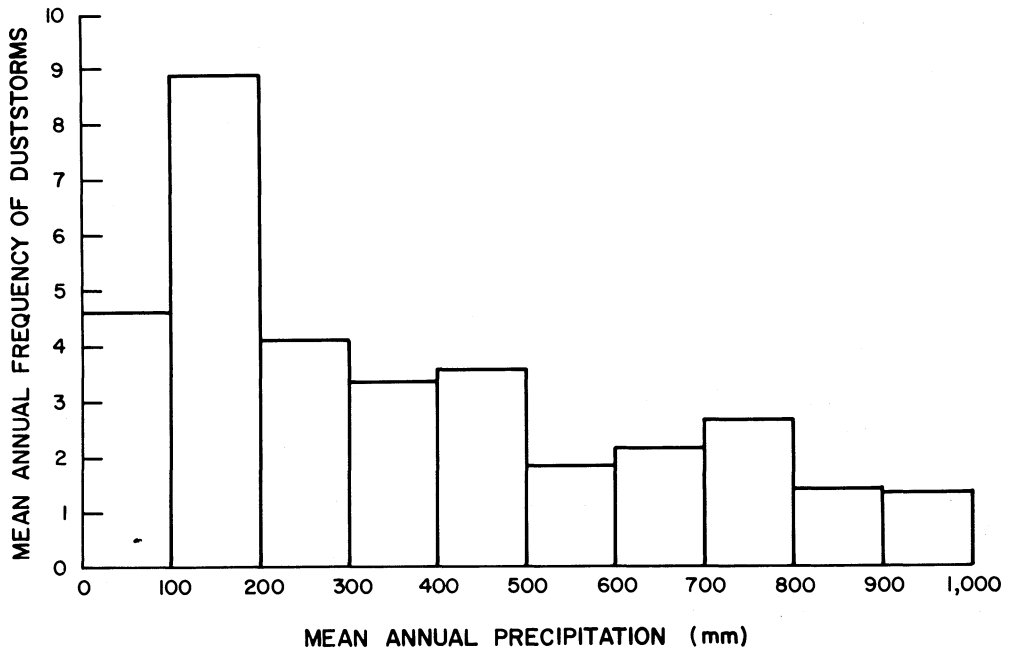


Fig. 2 Frequency of modern dust storms in relation to rainfall (after Goudie, 1983).

## 6. TERRAIN TYPES FAVOURABLE FOR DUST DEFLATION

Dust is raised when the drag velocity of the wind ( $u_*$ ) exceeds the threshold ( $u_{*t}$ ) required to entrain the most erodible surface particles, or when the surface is disturbed (e.g. by saltating sand grains). Different terrain types have widely varying values of  $u_{*t}$ , reflecting the nature of the vegetation cover, surface roughness, grain size, moisture content and cohesion of the surface sediment. Field wind tunnel measurements have shown that threshold velocity cannot be accurately predicted from particle size distribution alone. This is due largely to the effect of soil moisture and surface crusting by salts, clay skins or organic matter (Clements et al., 1963; Gillette et al., 1980, 1982; Nickling and Gillies, 1986). Measured values of  $u_{*t}$  range from  $0.17 \text{ m s}^{-1}$  for uncrusted river channel deposits and dune sands to  $2.5 \text{ m s}^{-1}$  for crusted or

armoured alluvial fan sediments and playa deposits. These values correspond to mean wind velocities (at a height of 10 m) of 5 - 15 m s<sup>-1</sup>, assuming a logarithmic wind profile (Table I).

Table I. Minimum mean wind speed (10m) required to generate blowing dust on various arid surfaces in the American Southwest

Surface Type	$\bar{U}$ (m s <sup>-1</sup> )	Author
Playa, undisturbed	15	Clements et al. (1963)
Alluvial fan, crusted	16	"
Alluvial fan, loose material	9	"
Mature desert pavement	16	"
Partially formed desert pavement	8	"
Dry wash	10	"
Desert flat, partial vegetation	11	"
Sand dunes	6	"
Santa Cruz River, Tucson	5	Nickling & Gillies (1986)
Salt River, Tempe	5	"
Mine tailings	5-7	"
Scrub desert, Yuma	11	"
Inter-dune desert flat, Algodones	18	"
Disturbed desert, Yuma	8	"
Abandoned agricultural land, Casa Grande	8	"

A high silt and clay content does not guarantee that a sediment will be an important source of airborne dust. The total amount of clay and the sand/silt plus clay ratio are important controls. Sediments containing more than 10% clay are not easily eroded unless the surface has a fine aggregate structure or consists of clay curls. Equally, fine-grained sediments which contain few particles larger than 60  $\mu\text{m}$ , such as loess, fluvial silts and lacustrine silts, have high fluid threshold velocities because small particles with large particle Reynolds numbers remain immersed in the viscous sub-layer, and because cohesive forces between adjoining small particles are strong (Bagnold, 1941; Iversen and White, 1982). Entrainment of such material is commonly initiated by saltating sand grains from upwind rather than by fluid drag (Gillette et al., 1974).

Field tunnel tests have shown that sediments which can be classified as "sand", "loamy sand", and "sandy loam" are potentially important sources of dust. Such sediments may have a surface crust, but if this is disturbed the rate of deflation is high. Figure 3 shows that playa deposits, takyrs soils, loess, and humid tropical soils are much less important potential sources of dust than dune sands, sandy alluvium and many semi-arid soils. Field studies (Jones et al., 1986; Khalaf et al., 1985) have demonstrated that fluvial sediments are particularly important sources of dust in arid environments because they have a high silt/clay ratio and are often not cemented or crusted.

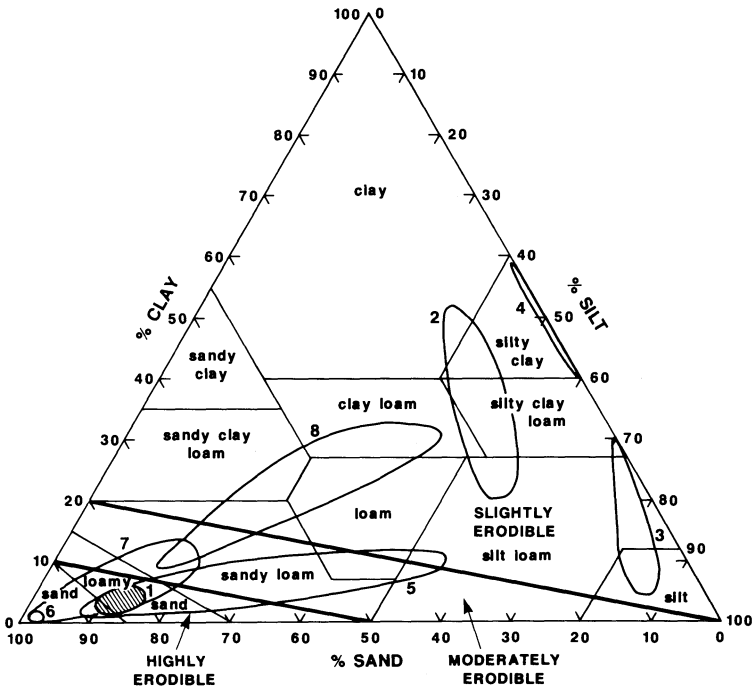


Fig. 3 Soil texture classification diagram showing sediments which provide the most potentially important dust sources (compiled from data in Pye, 1987; Pye et al., 1985; Gerson et al., 1985; and Gillette et al., 1980, 1982). 1: Non-gravel fraction of coarse desert alluvium; 2: playa sediments, takyrs and solonchaks soils; 3: loess; 4: long-range dust deposits; 5: semi-arid soils and regolith; 6: active dune sands; 7: stabilised, weathered dune sands; 8: humid tropical soils and regolith.

Arid weathering produces debris with a high content of coarse particles. Fine particles at the surface are either blown away by the wind or washed down into the subsurface by runoff. Hammadas and reg soils are wind-stable, and such surfaces act as net dust sinks rather than dust sources (Gerson et al., 1985; Amit and Gerson, 1986; Gerson and Amit, 1987). Other net dust sinks in deserts include lakes, playas filled with wet sediment, stabilised dunes and vegetated fluvial deposits (Table II).

Table II. Net dust sources and sinks in arid regions

NET DUST SOURCES	NET DUST SINKS
Active fluvial channels & fans	Relict alluvial channel& fan deposits
Dry lake beds & playas	Hammadass
Active sand dune fields	Stabilised dune fields
Soft, easily abraded rock outcrops	Lakes and wet playas
Bare loamy soils	Reg soils
Dirt roads	
Urban areas & construction sites	
Mine tailings	

All types of stable sediments, including stabilised dune sands, accumulate fine material which includes airborne dust, opal phytoliths, and products of situ weathering (Figure 4A). If these sediments are remobilised they provide an important dust source (Figure 4B). However, the reserve of dust is finite, so that after an initial increase, the rate of dust emission declines again to a constant rate determined by the rate of particle formation (Figure 5).

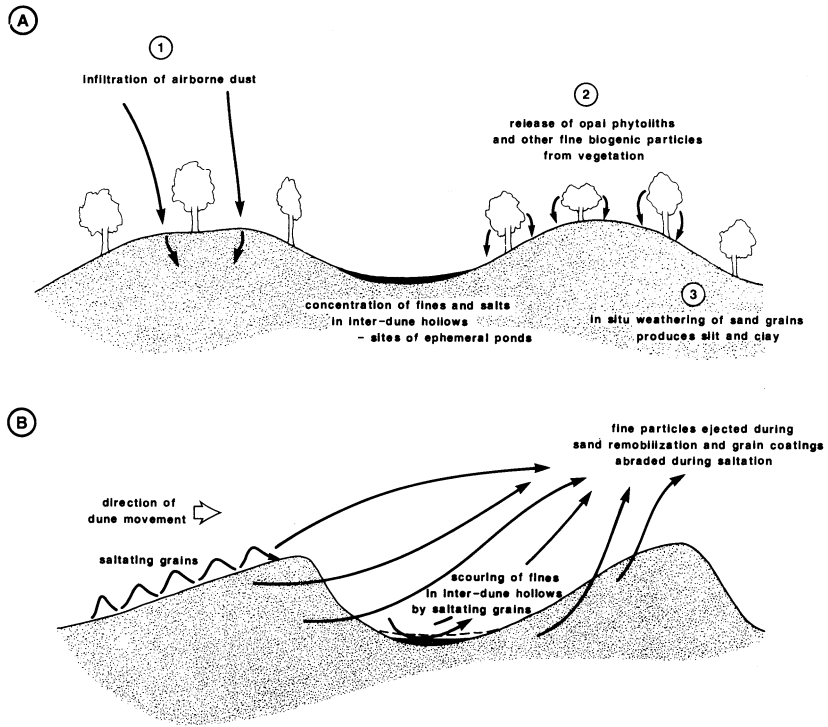


Fig. 4 Build-up of fine-grained material in stabilised dune sands (A) and subsequent release of dust in suspension when dunes are reactivated (B).

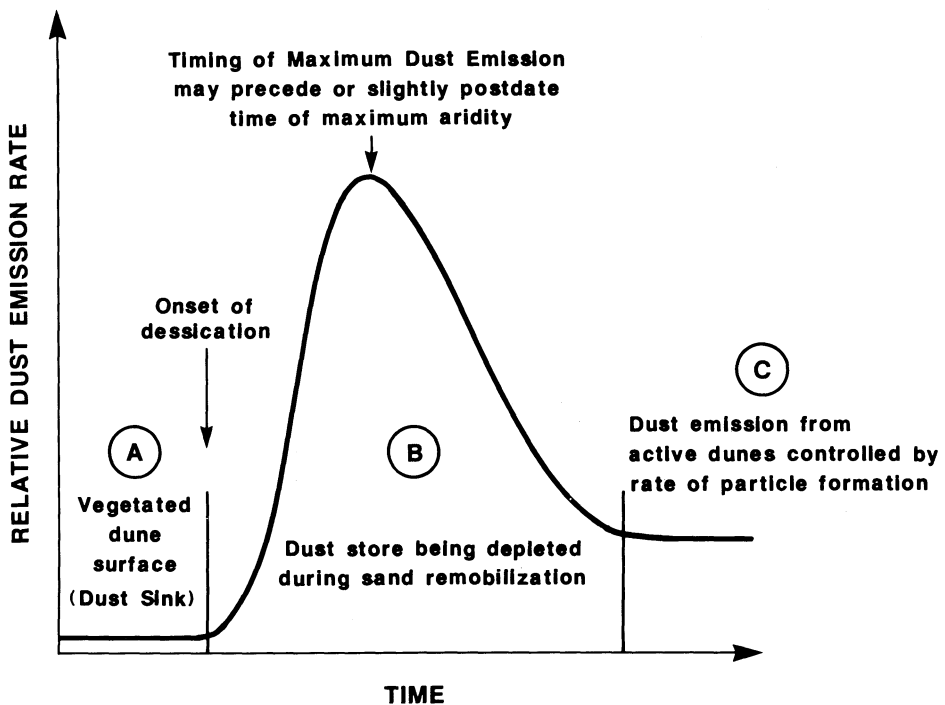


Fig. 5 Schematic diagram showing changes in the relative rate of dust emission with time after the reactivation of a stabilised dune field.

## 7. CHANGES IN PARTICLE FORMATION RATES, EXTENT OF DUST SOURCE AREAS AND DUST FLUX DUE TO CLIMATIC CHANGE

### 7.1 Ice Marginal Outwash Plains

A large body of evidence indicates that the major periods of dust blowing and loess formation in mid latitudes coincided with cold stages of the Quaternary when both ice sheets and glacial outwash sediments were much more extensive than at present. During interstadials and interglacials, the ice sheets retreated, the area of seasonally exposed outwash sediment was reduced and loess deposition slowed or ceased, allowing soils to form (Fink and Kukla, 1977; Maruszczak, 1980). Radiocarbon and thermoluminescence dating of numerous loess sections in North America, Europe and China (e.g. Pye and Johnson, 1988; Lu et al., 1987) has shown general agreement that during the last 100,000 years dust deposition rates were highest in stadial periods (oxygen isotope stages 2 and 4),



intermediate during interstadial conditions (stage 3), and low in the Holocene and the last interglacial (stages 1 and 5). There are currently no reliable dates for the Argentinian loess, but peak dust concentrations recorded in Antarctic ice of last glacial maximum age (Petit et al., 1981; Thompson and Mosley-Thompson, 1981) may correspond to maximum ice extent in Argentina.

A dissimilar pattern is indicated by the loess-soil record of Soviet Central Asia, where the last glacial period appears to be represented by four major paleosols and intervening loess units, and the last interglacial by two loess units and at least one paleosol (Dodonov, 1979; Lazarenko et al., 1981). If the stratigraphic and age interpretations are correct, this suggests that dust transport and loess accumulation in Soviet Central Asia has varied in response both to regional and global factors (Pye, 1987).

At least in Europe and North America, there is strong evidence that large-scale dust transport during cold stages mainly reflected larger dust source areas and seasonal replenishment of the dust supply by glacial meltwaters, though the drier, windy nature of the glacial climate may also have contributed to the increased dust flux. Hobbs (1943a,b) suggested that dust was transported mainly by strong northerly or northeasterly winds blowing from anticyclones over the major continental ice sheets. This is consistent with observed thickness and grain size trends observed in the northwest European loess (Catt, 1977; 1979), but in North America these criteria indicate dust transport predominantly from the northwest (Lugn, 1960; Frye et al., 1962; Snowden and Priddy, 1968; Saucier, 1978), possibly by mid-latitude westerlies. There is no direct evidence that winds were stronger than at present.

## 7.2 Dust Transport from Desert Source Regions

Climatic fluctuations might hypothetically affect dust flux from deserts by causing changes in the following: (1) the rate of fine particle formation, (2) the efficiency of fluvial transport/sorting processes, (3) the area covered by unvegetated, easily deflated sediments, (4) antecedent moisture conditions, and (5) wind energy. These changes need not all act in the same direction at the same time and the cumulative effect could differ depending on the balance of regional environmental conditions.

The likely effects of changes in precipitation and temperature on different fine particle formation processes in dry regions are summarised in Table III. Other things being constant, an increase in precipitation will increase the rate or scale of glacial abrasion, frost weathering, chemical weathering and fluvial abrasion. Only salt weathering and wind abrasion are likely to be less effective. A reduction in precipitation would have the opposite effect. Increased temperature acting in isolation would probably reduce the effectiveness of glaciation, frost weathering and fluvial abrasion due to its effect on evaporation and the moisture budget. Reduced temperature would have a similar, though less marked, effect as increased precipitation, with the exception that the rate of chemical weathering might be lowered. The net effect of a trend from hyperarid conditions to a cooler, more humid climate is likely to be an increase in the rate of fine particle formation. A change from aridity to hyperaridity would have a reverse effect.

Table III. Net effect of environmental changes on fine debris production by different processes in arid regions. Brackets indicate minor change.

Process	Precipitation increase	Precipitation decrease	Temperature increase	Temperature decrease
Glacial crushing & abrasion	+	-	-	+
Frost weathering	+	-	-	+
Salt weathering	-	+	(+)	(-)
Chemical weathering	+	-	(+)	(-)
Wind abrasion	-	+	(+)	(-)
Fluvial abrasion	+	-	(-)	(+)

Many authors have assumed that greater continental aridity, caused either by low rainfall or higher temperatures (evaporation), is the most important cause of increased dust flux from deserts, whereas increases in wind strength are responsible for increases in size of transported dust (Parkin, 1974; Rea et al., 1985). According to this model, reduced soil moisture leads to a reduction in vegetation cover and lowering of  $u_x$ . The area of bare ground increases as desert margins expand and lake levels fall. Conversely, wetter conditions reduce dust flux through higher soil moisture, greater vegetation cover, rising lake levels and dune stabilisation. The occurrence of such a sequence of events during Pleistocene arid phases is supported by observed increases in dust activity during recent droughts (Chepil et al., 1963; Lockertz, 1978; Prospero and Nees, 1986; Middleton, 1985, 1987). Ocean core evidence indicates an increase in dust flux to the eastern Atlantic around the time of the last glacial maximum when there was a large expansion of active dunefields in the western and southern Sahara, rivers dried up and lake levels (Sarnthein, 1978; Sarnthein and Diester-Hass, 1977; Sarnthein and Koopman, 1980; Street and Grove, 1979). During the early to mid Holocene, which was warmer and wetter in the southern Sahara than at present, dust sedimentation in the eastern Atlantic was much reduced, though it remained centred at about 18°N (Sarnthein et al., 1981). The grain size of dust deposited in the eastern Atlantic indicates that at 18,000 yr B.P. the surface trade winds north of Cape Verde were more vigorous, probably due to steeper meridional temperature gradients (Parkin and Padgham, 1975), but zonal wind speeds over the eastern Atlantic were apparently reduced by more than a third (Sarnthein et al., 1981).

An apparent association between late glacial aridity and increased dustiness is indicated by evidence from southeast Australia. Although no true loess is found in Australia, discontinuous sheets of silty clay (parna) were deposited mainly during the later part of the last glacial period (Dare-Edwards, 1984). There was also an increase in dust deposition in the southwest Pacific at this time (Thiede, 1979). The period 25,000-12,000 B.P. saw falling lake levels and dune reactivation in south-

east Australia (Bowler et al., 1976; Bowler, 1978). Some quartz dust was derived from the reactivated dunefields and deposited in lakes and soils downwind, but much of the parna clay was derived in pellet form from dry alluvial deposits. Increased frequency of strong winds associated with mid-latitude depressions which penetrated into the Central Australian desert during the glacial maxima probably contributed to increased sand and dust movement (Bowler, 1978).

The evidence regarding changes in the dust flux from the Chinese deserts during the last 30,000 years is somewhat conflicting. Rea and Leinen (1988) concluded from Northwest Pacific ocean core data that dust flux was at a minimum around 18,000 B.P. and attained a maximum in the mid Holocene. They suggested their results indicate maximum aridity in the Central Asian deserts in the early to mid Holocene, which is in accordance with the model predictions of Kutzbach and Guetter (1986). However, Pye and Zhou (1989) have pointed out that loess accumulation rates in the Chinese Central Loess Plateau were much higher in the late last glacial period than in the mid Holocene. This apparent discrepancy may be explained by the fact that different wind systems are responsible for dust transport to the two areas. Whereas the loess was transported mainly by low level northerly and northwesterly winds generated by outbreaks of cold, dry air from the Mongolian anticyclone, long-range dust transport over the North Pacific requires dust to be lifted to high levels where it can be incorporated into a strong westerly jet. Vertical lifting of dust occurs mainly in spring when the Mongolian anticyclone begins to break down and dry frontal depressions cross the deserts from the west (Pye and Zhou, 1989). Apparent changes in dust flux indicated by the Northwest Pacific cores may reflect variations in the frequency and effectiveness of the dust lifting mechanism (i.e. frequency of frontal depressions) rather than degree of aridity in the desert source areas. Support for this interpretation is provided by the fact that many desert basins in northwest China have experienced progressive dessication during the Holocene, but at the same time there has been a relative decline in the rate of dust deposition in the North Pacific since 6,000 yr B.P. The rate of dust deposition on the Central Loess Plateau has been lower throughout most of the Holocene, compared with the late last glacial period, possibly because of a weakening of the Mongolian anticyclone and weaker outbreaks of cold, northerly air in late winter and spring.

There is also no clear relationship between aridity and scale of dust transport in the northeastern Sahara and Sinai, as indicated by the accumulation history of loess in the northern Negev. It should be noted, however, that all loess - soil sequences record changes in the rate of net dust accumulation, rather than simply rate of deposition. The nature and thickness of loess accumulated in unit time is strongly influenced by the rates of pedogenesis and fluvial reworking, which are partly controlled by vegetation cover and rainfall at the deposition site. It is therefore difficult to identify precisely the magnitude of changes in dust deposition (Pye and Isoar, 1987).

Allowing for these difficulties, radiocarbon and archaeological dating has clearly shown that most of the Negev loess is of late Pleistocene age (Margaritz, 1986; Margaritz and Goodfriend, 1987;

Goodfriend and Margaritz, 1988). Thin deposits of primary Holocene loess are found in some areas (Gerson and Amit, 1987), but fluvial erosion and redeposition of the loess has been dominant throughout much of the Holocene. Present-day rates of dust deposition, which are of the order of 0.02–0.04 mm yr (Ganor and Mamane, 1982), are too low for the formation of loess. This is despite the fact that the dust source areas in Sinai and the Western Desert of Egypt have experienced an arid to hyper-arid climate since the mid Holocene (the present mean annual rainfall is < 50 mm). Issar and Bruins (1983) and Pye and Isoar (1987) concluded that dust accumulation rates in the northern Negev were significantly higher in the late Pleistocene than in the Holocene. During the period 40,000–10,000 yr B.P., there is evidence of three relatively wet periods centred around 37,000, 28,000 and 13,000 B.P., separated by drier phases centred around 33,000 and 18,000 B.P. (Goodfriend and Margaritz, 1988). During the wet periods, which appear to correspond with high latitude interstadials, rainfall in the northern Negev must have exceeded 500 mm p.a. (> 300 mm higher than today), allowing carbonate leaching and pedogenesis to occur. The fact that measured rates of dust deposition are too low at the present day, despite the existence of hyperarid conditions in the source areas of North Africa, Sinai and the southern Negev, strongly suggests that wetter conditions in the source areas must have been associated with increased rates of dust supply and loess accumulation in the late Pleistocene. Three main factors may have been involved: (1) more frequent slopewash and wadi floods during wet phases would have provided a larger potential source of dust; (2) large dust storms are likely to have been more common due to a higher incidence of mid-latitude depressions which took a more southerly track than at present across the southern Mediterranean and North Africa, and (3) thicker vegetation in the northern Negev would have reduced the rate at which deposited dust was re-eroded by fluvial processes. There is clear evidence of a large increase in the scale of wadi sedimentation in northern Sinai between 25,000 and 30,000 B.P. (Sneh, 1982), and these sediments may have provided a source of dust analogous to the glacial outwash sediments of mid and high latitudes.

A similar situation seems to have occurred in southern Tunisia, where loess formed on the Matmata Plateau between 35,000 and 10,000 years ago under conditions more humid than today (Coudé-Gaussen and Rognon, 1988). Loess accumulated during a short humid period in the mid-Holocene (4,000–6,000 B.P.). During the intervening drier periods the loess deposits were eroded and redeposited by colluvial and fluvial processes.

## 8. CONCLUSION

Large scale dust activity requires (1) a large area of bare, uncrusted and unarmoured silty sediment, and (2) incidence of strong winds capable of entraining dust and dispersing it over large distances. At the present day favourable dust source areas are much less extensive than during glacial stages of the Pleistocene, when poorly sorted fluvioglacial outwash was deposited over thousands of square kilometres in mid-latitudes. Some of this sediment was produced directly by glacial and cold weathering processes, but a considerable amount consisted of reworked soil material

formed by chemical weathering under earlier periods of temperate climate. Fluvio-glacial meltwaters played a crucial role in sorting this material and depositing sediments with a high silt/clay ratio which could be easily deflated during times of low flow.

Arid regions have provided a second important source of dust during both glacial and interglacial periods of the Quaternary. Rates of particle formation by weathering in deserts are generally lower than in more humid climates, and fluvial activity is restricted by low rainfall. Nevertheless, fluvial processes (both slopewash and channel flow) play a crucial role in maintaining the dust supply in deserts by disturbing wind-stable gravel layers on hillslopes, by sorting the products of weathering, and forming sediments with a high silt/clay ratio and low value of  $u_{*t}$ . Periodic floods carry fine material onto the surfaces of playas where it can be readily deflated. Periodic floods also moisten the clay and crust salts on playas, leading to formation of wind-erodible clay curls and fluffy salt efflorescences during subsequent drying (Figure 6B).

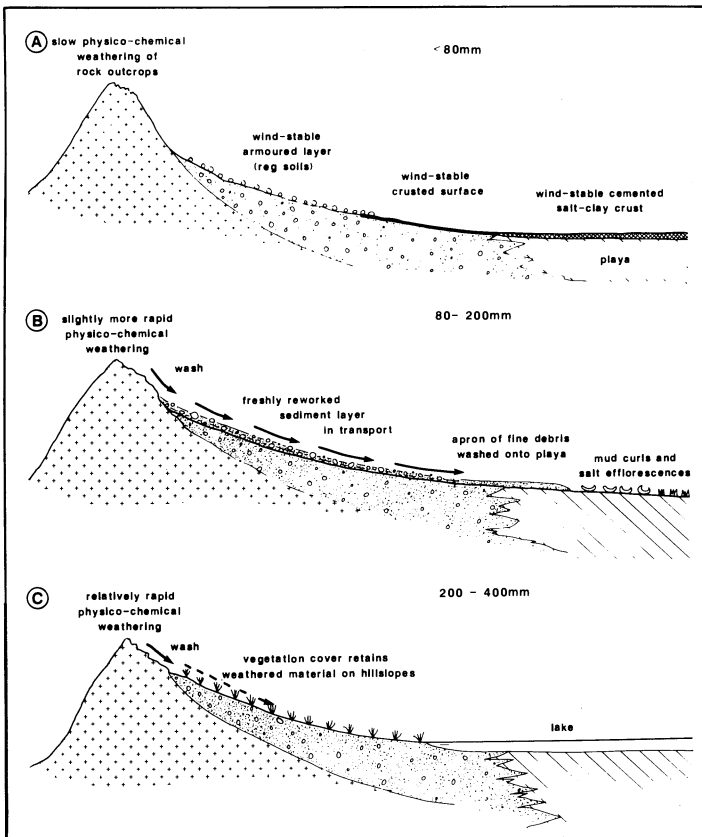


Fig. 6 Weathering and surface sediment transport regimes under hyperarid (A), arid (B) and semi-arid (C) climatic conditions.

Under hyperarid conditions (mean annual rainfall  $< 80$  mm), coarse weathering debris accumulates in upland source areas and much of the landscape becomes covered by wind-stable reg soils which act as dust sinks (Gerson, 1982; Gerson and Amit, 1987). Extreme flash flood events occur, but they are infrequent and of limited geographical extent (Figure 6A). In areas which receive an average rainfall of 200 mm, vegetation is able to colonise large areas of the hillsides. This increases the aerodynamic roughness and allows crusted soils to form, thereby raising  $u_{*t}$ . Furthermore, coarse sediment transport into the river channels is reduced, leading to the formation of fine-grained channel deposits which also have a relatively high  $u_{*t}$  (Figure 6C).

Modern day dust storms are almost twice as frequent in areas with a mean annual rainfall of 100 - 200 mm compared with drier and wetter areas (Goudie, 1983). The incidence of dust-transporting winds in different climatic regions is obviously important, but the extent of erodible terrain types containing fines, and their rate of regeneration by fluvial processes, is also of crucial importance.

With respect to climatic changes during the Quaternary, it is clear from the above discussion that an increase in dust flux could be brought about either by a change from semi-arid to arid conditions or from hyperarid to arid conditions. In the former case, thinning of vegetation cover would result in fluvial and aeolian erosion of soils and sediments formed under semi-arid conditions. Areas of old, weathered dune sands would be reactivated, and dry lake beds exposed to aeolian action. In the case of a transition from hyperarid to arid conditions, accumulated weathering products would be flushed from the uplands by more effective fluvial processes, forming fan and channel deposits of relatively coarse, poorly sorted sediment. The storms responsible for the more frequent runoff might also increase the frequency of dust-transporting winds. The effects of changes from aridity to hyperaridity or aridity to semi-arid conditions would be opposite to those described. Repeated landscape instability resulting from rapid fluctuations from arid to relatively wetter conditions and vice versa would maximise the potential for a long-term high level of dust emission from deserts.

## 9. REFERENCES

- Amit, R. and Gerson, R. (1986) 'The evolution of Holocene reg (gravelly) soils in deserts - an example from the Dead Sea region.' Catena 13, 59-79.
- Ashwell, I.Y. (1986) 'Meteorology and duststorms in Central Iceland,' Arctic Alpine Res. 18, 223-234.
- Bagnold, R.A. (1941) The Physics of Blown Sand and Desert Dunes. Methuen, London, 241 p.
- Beaumont, P. (1968) 'Salt weathering on the margin of the Great Kavir, Iran.' Geol. Soc. Am. Bull. 79, 1683-1684.
- Blackwelder, E. (1925) 'Exfoliation as a phase of rock weathering.' J. Geol. 33, 793-806.
- Blackwelder, E. (1933) 'The insolation hypothesis of rock weathering.' Am. J. Sci. 26, 97-113.
- Boulton, G.S. (1978) 'Boulder shapes and grain size distribution of debris as indicators of transport paths through a glacier and till genesis.' Sedimentology 25, 773-799.
- Boulton, G.S. (1979) 'Processes of glacial erosion on different substrata.' J. Glaciol. 23, 15-38.
- Bowler, J.M. (1978) 'Glacial age events at high and low latitudes. In E.M. Van Zinderen Bakker' (ed.), Antarctic Glacial History and World Palaeoenvironments. Balkema, Rotterdam, 149-172.
- Bowler, J.M., Hope, G.S., Jennings, J.N., Singh, G. and Walker, D. (1976) 'Late Quaternary climates of Australia and New Guinea.' Quat. Res. 6, 359-394.
- Catt, J.A. (1977) Loess and coversands. In F.W. Shotton (ed.) British Quaternary Studies: Recent Advances. Oxford University Press, 221-229.
- Catt, J.A. (1979) 'Distribution of loess in Britain.' Proc. Geol. Ass. 90, 93-95.
- Chapman, R.W. (1980) 'Salt weathering by sodium chloride in the Saudi Arabian desert.' Am. J. Sci. 280, 116-129.
- Chepil, W.S., Siddoway, F.H. and Armbrust, D.V. (1963) 'Climatic Index of wind erosion conditions in the Great Plains.' Proc. Soil Sci. Soc. Am. 27, 449-451.
- Clements, T., Stone, R.O., Mann, J.F. and Eymann, J.L. (1963) 'A study of

- windborne sand and dust in desert areas.' U.S. Army Natick Laboratories, Earth Sci. Div., Tech. Report ES8, 61 p.
- Cooke, R.U. (1981) 'Salt weathering in deserts.' Proc. Geol. Ass. 92, 1-16.
- Cooke, R.U. and Smalley, I.J. (1968) 'Salt weathering in deserts.' Nature 220, 1226-1227.
- Coudé-Gaussens, G. and Rognon, P. (1988) 'The Upper Pleistocene loess of southern Tunisia: a statement.' Earth Surf. Proc. Landf. 13, 137-152.
- Dan, Y. and Yaalon, D.H. (1982) 'Automorphic saline soils in Israel.' Catena Supp. 1, 103-115.
- Dan, J. and Koyumdjisky, H. (1987) 'Distribution of salinity in the soils of Israel.' Israel J. Earth Sci. 36, 213-223.
- Dare-Edwards, A.J. (1984) 'Aeolian clay deposits of southeastern Australia: parna or loessic clay.' Trans. Inst. Brit. Geog. N.S. 9, 337-344.
- Derbyshire, E. (1983) 'On the morphology, sediments and origin of the Loess Plateau of Central China.' In R. Gardner and H. Scoging (eds.), Megageomorphology. Oxford University Press, 172-194.
- Dietrich, R.V. (1977) 'Impact abrasion of harder by softer materials.' J. Geol. 85, 242-246.
- Dodonov, A.E. (1979) 'Stratigraphy of the Upper Pliocene - Quaternary deposits of Tajikistan (Soviet Central Asia).' Acta Geol. Acad. Scient. Hung. 22, 63-73.
- Durrance, E.M. (1965) 'Release of strain energy as a mechanism for the mechanical weathering of granular rock material.' Geol. Mag. 102, 496-497.
- Evans, I. (1970) 'Salt crystallization and rock weathering: a review.' Rev. Geomorph. Dyn. 19, 153-177.
- Fink, J. and Kukla, G.J. (1977) 'Pleistocene climates of central Europe: at least seventeen interglacials after the Olduvai event.' Quat. Res. 7, 111-124.
- Frye, J.C., Glass, H.D. and Willman, H.B. (1962) 'Stratigraphy and mineralogy of the Wisconsin loess of Illinois.' Illinois Geol. Surv. Circ. 334, 1-55.
- Ganor, E. and Mamane, Y. (1982) 'Transport of Saharan dust across the eastern Mediterranean.' Atmos. Env. 16, 581-587.



- Geikie, J. (1898) 'The tundras and steppes of perhistoric Europe.' Scott. Geog. Mag. 14, 281-294, 346-357.
- Gerson, R. (1982) 'The Middle east: landforms of a planetary desert through environmental changes.' Striae 17, 52-78.
- Gerson, R. and Amit, R. (1987) 'Rates and modes of dust accretion and deposition in an arid region - the Negev, Israel.' In L. Frostick and I. Reid (eds.) Desert Sediments Ancient and Modern. Geol. Soc. Spec. Pub. 35, Blackwell, Oxford, 157-169.
- Gerson, R., Amit, R. and Grossman, S. (1985) Dust Availability in Desert Terrains - A study of the Deserts of Israel and Sinai. Report to the U.S. Army Research, Development and Standardization Group, U.K., Contract No. DAJA 45-83-C-0041.
- Gillette, D.A., Blifford, D.A. and Fryrear, D.W. (1974) 'The influence of wind velocity on the size distribution of aerosols generated by the wind erosion of soils.' J. Geophys. Res. 79, 4068-4075.
- Gillette, D.A., Adams, J., Endo, L. and Smith, D. (1980) 'Threshold velocities for input of soil particles into the air by desert soils.' J. Geophys. Res. C85, 5621-5630.
- Gillette, D.A., Adams, J., Muhs, D and Kihl, R. (1982) 'Threshold friction velocities required and rupture moduli for crushed desert soils for input of soil particles into air.' J. Geophys. Res. 87, 9003-9015.
- Goodfriend, G.A. and Magaritz, M. (1988) 'Palaeosols and Late Pleistocene rainfall fluctuations in the Negev Desert.' Nature 332, 144-146.
- Goudie, A.S. (1974) 'Further experimental investigation of rock weathering by salt and other mechanical processes.' Zeit. Geomorph. Supp. Bd. 21, 1-12.
- Goudie, A.S. (1978) 'Dust storms and their geomorphological implications.' J. Arid Env. 1, 291-310.
- Goudie, A.S. (1983) 'Dust storms in space and time.' Prog. Phys. Geog. 7, 502-530.
- Goudie, A.S. (1986a) 'Salt Weathering.' School of Geography, Univ. of Oxford Res. Pap. 33, 31 p.
- Goudie, A.S. (1986b) 'Laboratory simulation of the 'wick effect' in salt weathering of rock.' Earth Surf. Proc. Landf. 11, 275-285.
- Goudie, A.S. and Day, M.J. (1980) 'Disintegration of fan sediments in Death Valley, California, by salt weathering.' Phys. Geog. 1, 126-137.
- Goudie, A.S. and Watson, A. (1984) 'Rock block monitoring of rapid salt

- weathering in southern Tunisia.' Earth Surf. Proc. Landf. 9, 95-99.
- Goudie, A.S., Cooke, R.U. and Evans, I. (1970) 'Experimental investigation of rock weathering by salts.' Area 4, 42-48.
- Goudie, A.S., Cooke, R.U. and Doornkamp, J.C. (1979) 'The formation of silt from quartz dune sand by salt processes in deserts.' J. Arid. Environ. 2, 105-112.
- Griggs, D. (1936) 'The factor of fatigue in rock exfoliation.' J. Geol. 44, 781-796.
- Haldorsen, S. (1981) 'Grain size distribution of subglacial till and its relation to glacial crushing and abrasion.' Boreas 10, 91-105.
- Haldorsen, S. (1983) 'Mineralogy and geochemistry of basal tills and their relationship to till forming processes.' Norsk Geol. Tidsskr. 63, 15-25.
- Hall, K. (1986) 'Rock moisture content in the field and its relationship to mechanical weathering studies.' Earth Surf. Proc. Landf. 11, 131-142.
- Hobbs, W.H. (1943a) 'The glacial anticyclones and the European continental glacier.' Am. J. Sci. 241, 333-336.
- Hobbs, W.H. (1943b) 'The glacial anticyclone and the continental glaciers of North America.' Proc. Am. Phil. Soc. 86, 368-559.
- Issar, A.S. and Bruins, H.J. (1983) 'Special climatological conditions in the deserts of Sinai and the Negev during the latest Pleistocene.' Palaeogeog., Palaeoclimatol., Palaeoecol. 43, 63-72.
- Iversen, J.D. and White, B.R. (1982) 'Saltation threshold on Earth, Mars and Venus.' Sedimentology 29, 111-119
- Jones, D.K.C., Cooke, R.U. and Warren, A. (1986) Geomorphological investigation, for engineering purposes, of blowing sand and dust hazard. Quart. J. Eng. Geol. 19, 251-270.
- Khalaf, F.I., Al-Kadi, A. and Al-Saleh, S. (1985) 'Mineralogical composition and potential sources of dust fallout deposits in Kuwait, northern Arabian Gulf.' Sedim. Geol. 42, 255-278.
- Konischev, V.N. (1982) 'Characteristics of cryogenic weathering in the permafrost zone of the European USSR.' Arctic Alpine Res. 14, 261-265.
- Kuenen, P.H. (1959) 'Experimental abrasion. 3. Fluvial action on sand.' Am. J. Sci. 257, 172-190.
- Kuenen, P.H. (1960) 'Experimental abrasion. 4. Eolian action.' J. Geol.

68, 427-449.

- Kutzbach, J.E. and Guetter, P.J. (1986) 'The influence of changing orbital parameters and surface boundary conditions on climate simulations for the past 18,000 years.' J. Atmos. Sci. 43, 1726-1759.
- Kwaad, F.J.P.M. (1970) 'Experiments on the disintegration of granite by salt action.' Univ. Amsterdam Fys. Geog. Boden. Kundig. Lab. Pub. 16, 67-80.
- Lautridou, J.P. and Ozouf, J.C. (1982) 'Experimental frost shattering: fifteen years of research at the Centre de Geomorphologie du CNRS.' Prog. Phys. Geog. 6, 215-232.
- Lazarenko, A.A., Bolikhovskaya, N.S. and Semenov, V.V. (1981) 'An attempt at a detailed stratigraphic subdivision of the loess association of the Tashkent region.' Int. Geol. Rev. 23, 1335-1346.
- Litvan, G.G. (1976) 'Frost action in the presence of deicers.' Cement Concrete Res. 6, 351-356.
- Lui Tung Sheng et al. (1985) Loess and the environment. China Ocean Press, Beijing, xii + 251 p.
- Lockertz, W. (1978) 'The lessons of the dust bowl'. Am. Scient. 66, 560-569.
- Lu Yanchou, Prescott, J.R., Robertson, G.B. and Hutton, J.T. (1987) 'Thermoluminescence dating of the Malan Loess at Zhaitang, China.' Geology 15, 603-645.
- Lugn, A.L. (1960) 'The origin and sources of loess in the Great Plains of North America.' Proc. 21st Int. Geol. Cong., 223-235.
- McGreevy, J.P. and Smith, B.J. (1982) 'Salt weathering in hot deserts: observations on the design of simulation experiments.' Geog. Ann. 64A, 161-170.
- McGreevy, J.P. and Whalley, W.B. (1985) 'Rock moisture content and frost weathering under natural and experimental conditions: a comparative discussion.' Arctic Alpine Res. 17, 337-346.
- McTainsh, G. (1987) 'Desert loess in northern Nigeria.' Zeit. Geomorph. NF 31, 145-165.
- Magaritz, M. (1986) 'Environmental changes recorded in the upper Pleistocene along the desert boundary, southern Israel.' Palaeogeog., Palaeoclimatol., Palaeoecol. 53, 213-229.
- Magaritz, M. and Goodfriend, G.A. (1987) 'Movement of the desert boundary in the Levant from latest Pleistocene to Early Holocene.' In:

W.H. Berger and L.D. Labeyrie<sup>1</sup> (eds.) Abrupt Climatic Change - Evidence and Implications. Reidel, Dordrecht, 173-183.

- Martini, A. (1967) 'Preliminary experimental studies on frost weathering of certain rock types from the West Sudentes.' Biul. Peryglac. 16, 147-194.
- Maruszczak, H. (1980) 'Stratigraphy and chronology of the Vistulian loess in Poland.' Quat. Stud. Poland 2, 57-76.
- Middleton, N.J. (1985) 'Effect of drought on dust production in the Sahel.' Nature 316, 431-434.
- Middleton, N.J. (1987) 'Desertification and wind erosion in the western Sahel: the example of Mauritania.' School of Geography, University of Oxford, Res. Pap. 40, 26 p.
- Middleton, N.J. Goudie, A.S. and Wells, G.L. (1986) 'The frequency and source areas of dust storms.' In W.G. Nickling (ed.), Aeolian Geomorphology. Allen and Unwin, New York, 237-259.
- Moss, A.J. (1966) 'Origin, shaping and significance of quartz sand grains.' J. Geol. Soc. Aust. 13, 97-136.
- Moss, A.J. and Green, P. (1975) 'Sand and silt grains: predetermination of their formation and properties by microfractures in quartz.' J. Geol. Soc. Aust. 22, 485-495.
- Moss, A.J., Green, P. and Hutka, J. (1973) 'Fragmentation of granitic quartz in water.' Sedimentology 20, 489-511.
- Nahon, D. and Trompette, R. (1982) 'Origin of siltstones: glacial grinding versus weathering.' Sedimentology 29, 25-35.
- Nickling, W.G. and Gillies, J.A. (1986) Evaluation of Aerosol Production Potential of Type Surfaces in Arizona. Unpub. Report by MND Associates for EPA Contract No. 68-02-388, 84 p. + 7 tables + 34 figs.
- Parkin, D.W. (1974) 'Trade winds during the glacial cycles.' Proc. Roy. Soc. Lond. A., 337, 73-100.
- Parkin, D.W. and Pagdham, R.C. (1975) 'Further studies on the trade winds during the glacial cycles.' Proc. Roy. Soc. Lond. A 346, 245-260.
- Peel, R.F. (1974) 'Insolation weathering: some measurements of diurnal temperature changes in exposed rocks in the Tibesti region, central Sahara.' Zeit. Geomorph. Supp. Bd. 21, 19-28.
- Peterson, F.F. (1980) 'Holocene desert soil formation under sodium salt

- influence in a playa-margin environment.' Quat. Res. 13, 172-186.
- Petit, J.R., Briat, M. and Royer, A. (1981) 'Ice-age aerosol content from east Antarctic ice core samples and past wind strength.' Nature 293, 391-394.
- Péwé, T.L. (1951) 'An observation on windblown silt.' J. Geol. 59, 399-401.
- Potts, A.S. (1970) 'Frost action in rocks: some experimental data.' Trans. Inst. Brit. Geog. 49, 109-124.
- Prospero, J.M. and Nees, R.T. (1986) 'Impact of the North African drought and el Nino on mineral dust in the Barbados trade winds.' Nature 320, 735-738.
- Pye, K. (1985) 'Granular disintegration of gneiss and migmatites.' Catena 12, 191-199.
- Pye, K. (1986) 'Mineralogical and textural controls on the weathering of granitoid rocks.' Catena 13, 47-57.
- Pye, K. (1987) Aeolian Dust and Dust Deposits. Academic Press, London, 334 p.
- Pye, K. and Sperling, C.H.B. (1983) 'Experimental investigation of silt formation by static breakage processes; the effect of temperature, moisture and salt on quartz dune sand and granitic regolith.' Sedimentology 30, 49-62.
- Pye, K. and Tsoar, H. (1987) 'The mechanics and implications of dust transport and deposition in deserts, with particular reference to loess formation and dune sand diagenesis in the northern Negev, Israel.' In L. Frostick and I. Reid (eds.) Desert Sediments Ancient and Modern. Geol. Soc. Spec. Pub. 35, Blackwell, Oxford, 139-156.
- Pye, K. and Johnson, R. (1988) 'Stratigraphy, geochemistry and thermoluminescence ages of Lower Mississippi Valley loess.' Earth Surf. Proc. Landf. 13, 103-124.
- Pye, K. and Zhou Li-Ping (1989) 'Late Pleistocene and Holocene aeolian dust deposition in North China and the northwest Pacific Ocean.' Palaeogeog.Palaeoclimatol. Palaeoecol. (in press).
- Pye, K., Goudie, A.S. and Watson, A. (1985) 'An introduction to the physical geography of the Kora area of central Kenya. Geog. J. 151, 168-181.
- Ravina, I. and Zaslavsky, D. (1974) 'The electrical double layer as a possible factor in desert weathering.' Zeit. Geomorph. Supp. Bd. 21, 13-18.

- Rea, D. and Leinen, M. (1988) 'Asian aridity and the zonal westerlies: late Pleistocene and Holocene record of eolian deposition in the northwest Pacific Ocean.' Palaeogeog. Palaeoclimatol. Palaeoecol. 66, 1-8.
- Rea, D., Leinen, M. and Janacek, T.R. (1985) 'Geologic approach to the long-term history of atmospheric circulation.' Science 227, 721-725.
- Rice, A.R. (1976) 'Insolation warmed over.' Geology 4, 61-62.
- Roth, E.S. (1965) 'Temperature and water content as factors in desert weathering.' J. Geol. 73, 454-468.
- Sarnthein, M. (1978) 'Sand deserts during glacial maximum and climatic optimum.' Nature 272, 434-436.
- Sarnthein, M. and Diester-Haas, L. (1977) 'Eolian sand turbidites.' J. Sedim. Petrol. 47, 868-890.
- Sarnthein, M. and Koopman, B. (1980) 'Late Quaternary deep-sea record of northwest African dust supply and wind circulation.' Palaeoecol. Africa Surround. Is. 12, 239-253.
- Sarnthein, M., Tetzlaaf, G., Koopman, B., Wolter, K. and Pflaumann, U. (1981) 'Glacial and interglacial wind regimes over the eastern subtropical Atlantic and northwest Africa.' Nature 293, 193-196.
- Saucier, R.T. (1978) 'Sand dunes and related eolian features of the Lower Mississippi Valley alluvial valley.' Geoscience and Man 19, 23-40.
- Sharp, M. and Gomez, B. (1985) 'Processes of debris comminution in the glacial environment and implications for quartz sand grain micro-morphology.' Sedim. Geol. 46, 33-47.
- Smalley, I.J. (1966) 'The properties of glacial loess and the formation of loess deposits.' J. Sedim. Petrol. 36, 669-676.
- Smalley, I.J. (1980) 'The formation of loess materials and loess deposits: some observations on the Tashkent loess.' Geophys. Geol. Geophys. Ver. K.M.U. Leipzig Bd II, H2, 247-357.
- Smalley, I.J. and Krinsley, D.H. (1978) 'Loess deposits associated with deserts.' Catena 5, 53-66.
- Smalley, I.J. and Smalley, V. (1983) 'Loess material and loess deposits: formation, distribution and consequences.' In M.E. Brookfield and T.S. Ahlbrandt (eds.) Eolian Sediments and Processes. Elsevier, Amsterdam, 51-68.
- Smith, B.J. (1977) 'Rock temperature measurements from the northwest

- Sahara and their implications for rock weathering.' Catena 4, 41-63.
- Smith, B.J. and McGreevy, J.P. (1983) 'A simulation study of salt weathering in hot deserts.' Geog. Ann. 65A, 127-133.
- Smith, B.J. and McAlister, J.J. (1986) 'Observations on the occurrence and origins of salt weathering phenomena near Lake Magadi, southern Kenya.' Zeit. Geomorph. NF 30, 445-460.
- Snowden, J.O. and Priddy, R.R. (1968) 'Geology of Mississippi loess.' Miss. Geol. Surv. Bull. 111, 13-203.
- Sperling, C.H.B. and Cooke, R.U. (1985) 'Laboratory simulation of rock weathering by salt crystallisation and hydration processes in hot deserts.' Earth Surf. Proc. Landf. 10, 541-555.
- St. Amand, P., Mathews, L.A., Gaines, C. and Reinking, R. (1986) 'Dust Storms from Owens and Mono Valleys, California.' U.S. Naval Weapons Center Tech. Pub. 6731, 79 p.
- St. Arnaud, R.J. and Whiteside, E.P. (1963) 'Physical breakdown in relation to soil development.' J. Soil Sci. 14, 267-281.
- Street, F.A. and Grove, A.I. (1979) 'Global maps of lake level fluctuations since 30,000 yr B.P.' Quat. Res. 12, 83-118.
- Suzuki, T. and Takahashi, K. (1981) 'An experimental study of wind abrasion.' J. Geol. 89, 23-36.
- Thiede, J. (1979) 'Wind regimes over the late Quaternary southwest Pacific Ocean.' Geology 7, 259-262.
- Thomas, W.N. (1938) 'Experiments on the freezing of certain building materials.' D.S.I.R. Building Research Station Tech. Pap. 17, 146 p.
- Thompson, L.G. and Mosley-Thompson, E. (1981) 'Microparticle concentration variation linked with climatic change: evidence from polar ice cores.' Science 21, 812-815.
- Tricart, J. (1956) 'Étude expérimentale du problème de la gélivation.' Biul. Peryglac. 4, 285-318.
- Tsoar, H. and Pye, K. (1987) 'Dust transport and the question of desert loess formation.' Sedimentology 34, 139-153.
- Tutovskii, P.A. (1899) 'The question of the method of loess formation.' Zemlevenie 1-2, 213-311 (in Russian).
- Tutovskii, P.A. (1900) 'Paul Tutowski on the origin of loess.' Scott.

- Geog. Mag. 16, 171-174.
- Twidale, C.R. (1982) Granite Landforms. Elsevier, Amsterdam, 372 p.
- van Lier, J.A., de Bruyn, P.L. and Overbeek, J. (1960) 'The solubility of quartz.' J. Phys. Chem. 64, 1675-1682.
- Vivian, R.A. (1975) Les Glaciers des Alpes Occidentales. Imprimerie Allier, Grenoble.
- Walder, J.S. and Hallet, B. (1986) 'The physical basis of frost weathering: toward a more fundamental and unified perspective.' Arctic Alpine Res. 18, 27-32.
- Whalley, W.B., Marshall, J.R. and Smith, B.J. (1982) 'Origin of desert loess from some experimental observations.' Nature 300, 433-435.
- Whalley, W.B., Smith, B.J., McAlister, J.J. and Edwards, A. (1987) 'Aeolian abrasion of quartz particles and the production of silt-size fragments, preliminary results and some possible implications for loess and silcrete formation.' In L. Frosticks and I. Reid (eds.) Desert Sediments Ancient and Modern. Geol. Soc. Spec. Pub. 35, Blackwell, Oxford.
- White, S.E. (1976) 'Is frost action only hydration shattering.' Arctic Alpine Res. 8, 1-6.
- Williams, R.G.B. and Robinson, D.A. (1981) 'Weathering of sandstone by the combined action of frost and salt.' Earth Surf. Proc. Landf. 6, 1-9.
- Wiman, S. (1963) 'A preliminary study of experimental frost shattering.' Geog. Ann. 45, 113-121.
- Winkler, E.M. (1977) 'Insolation of stones: a hot item.' Geology 5, 188-189.
- Yariv, S. and Cross, H. (1979) Geochemistry of Colloid Systems. Springer, Heidelberg, 450 p.
- Young, A.R.M. (1987) 'Salt as an agent in the development of cavernous weathering.' Geology 15, 962-966.
- Zeuner, F.E. (1949) 'Frost soils on Mount Kenya.' J. Soil Sci. 1, 20-30.



# FORMATION OF WIND-ERODIBLE AGGREGATES FOR SALTY SOILS AND SOILS WITH LESS THAN 50% SAND COMPOSITION IN NATURAL TERRESTRIAL ENVIRONMENTS

RAY H. BREUNINGER<sup>1</sup>, DALE A. GILLETTE<sup>2</sup>,  
AND ROLF KIHLE<sup>3</sup>

<sup>1</sup> Carroll College  
Helena, Montana 59601  
U.S.A.

<sup>2</sup> Geophysical Monitoring for Climatic Change,  
Air Resources Laboratories/NOAA  
Boulder, Colorado 80303  
U.S.A.

<sup>3</sup> Institute for Arctic and Alpine Research  
University of Colorado  
Boulder, Colorado 80303  
U.S.A.

**ABSTRACT.** Of nine possible mechanisms for the formation of non-sandy, wind-erodible aggregates from a more homogeneous soil or sediment, five are found to be widespread in arid and semiarid regions. In approximate order of significance, the most important mechanisms are tension and compression fracturing of shrinkable mud or soil during wet/dry cycles; tension fracturing and molding by compression during freeze/thaw cycles; direct abrasion (corrosion); fracturing and aggregation produced by salt efflorescence; and mechanical disturbance of surface materials by animals. A sixth mechanism (in soils) is by surface films, colloidal matting, or cements. Minor mechanisms are: floatation and lofting of foam and fracturing caused by hydration expansion or other chemical weathering of fine-grained bedrock. The flocculation of small particles in a water suspension or wet mud is a possible minor mechanism not yet observed. Surface soils and sediments with more than 28% clay and more than 2% organic material formed wind-erodible aggregates, but organic-poor materials did not. Calcareous loams, silt loams, silty clay loams, and clay

loams formed wind-erodible aggregates, but non-calcareous materials of the same textures did not. Salt efflorescence was locally a major mechanism for production of wind-erodible aggregates. An experiment with expandible (high smectite content) clay shows that wet/dry cycles (such as might result from several summer rain showers on a dry lake bed) can produce wind-erodible aggregates without high temperatures or lengthy droughts and in the absence of salt efflorescence. For example, cold-climate clay dunes (now inactive) fringe ephemeral lakes in deflation basins in Montana at windy semiarid sites with short hot summers and intensely cold winters.

## 1. INTRODUCTION

Dune formation has been a major topic of study in geomorphology. Recent work on mechanisms of wind erosion and dune formation were reported in the Binghamton Symposium in Geomorphology (Nickling, 1986), which supplements the classical work of Bagnold (1941) and the more recent work of Greeley and Iversen (1985). As described in these texts and in much other published work on aeolian geomorphology, dunes are dominantly composed of sandy material. However, dunes have been recognized to arise from a non-sandy parent material. Clay dunes have been widely observed in dry lakes in the form of "lunettes" that form on the downwind side of the dry lake (Bowler, 1973). Sand-sized, clayey pellets may be physically broken into clay or silt-sized grains and lofted away by the wind (Dare-Edwards, 1982). The clayey pellets may also be carried into sand dunes. For instance, clayey pellets are a widespread, minor (typically less than 5%) constituent of longitudinal dunes in the Strzelecki dunefield of Australia (Wasson, 1983).

To form dunes, a necessary condition is to have particles that may be erodible by the wind. Gillette (1978, 1984a, b) and Gillette, *et al.*, (1980, 1982) studied the threshold friction velocities for wind erosion of natural sediments. They found that the strongest predictor of wind erosion other than wind statistics is the size of the surface aggregates. The mode of the size distribution of dry surface aggregates correlates with threshold wind velocity; smaller dry aggregates are erodible for smaller wind speeds. This result is consistent with more idealized studies of wind erosion threshold velocities, for example, those of Arvidson (1972), Chepil (1945), Greeley, *et al.*, (1974), Hess (1973), Ishihara and Iwagaki (1952), Iversen, *et al.*, (1976), Phillips (1980), Ryan (1964), Sagan and Pollack (1969), and Wood (1974).

Studies of non-sandy dunes have been made. In his review of clay dunes, Bowler (1973) gives a number of examples of clay dunes, relying principally on Price's (1963) study of Texas Gulf Coast clay dunes. The studies reviewed by Bowler conclude that seasonal flooding by salty water, followed by drying out, leads to formation of clayey grain aggregates. The aggregates reportedly form by salt crystallization and by disintegration of thin, curled, sun-dried mud flakes and domal blisters. Some are modified by filamentous algae. Bowler notes that there are no records of cold-desert clay dunes. He argues that seasonally high temperatures with consequent high evaporation rates are necessary; otherwise, the water table is not lowered enough to form wide and bare salty mud flats, and clay aggregates will not form early enough in the dry season "to permit the wind to do its work before the onset of the next humid season...."(p.334)

Notwithstanding Bowler's (1973) conclusions, the literature is not clear as to whether extended periods of high temperatures and no atmospheric precipitation are necessary for clay dune formation. For instance, clay-pellet dunes on saline tidal flats in south Texas (Huffman and Price, 1949) grow most rapidly during prolonged droughts and during the drier months of the summer, but movement of clay pellets can start as early as March and continue until November. Movement of pellets ceases only when the flats become continuously wet, frozen, or snowcovered. And, Marrs and Kolm (1982) describe high-elevation, saline playas in Wyoming, with clay and silt dunes and long streaks of deflated salts; winters there are very cold, and summers are brief but hot.

Likewise, in the formation of wind-erodible pellets, we do not know the relative importance of salt efflorescence versus desiccation cracking and mechanical breakage of crust by wind acting on drying sediment flats. There are only a few modern sites of active pellet formation, all of them in small areas (Dare-Edwards, 1984). Price (1963) states that "There seems to be no way in which non-saline clay disintegrates in nature to produce such large percentages of sand-sized aggregates" (p. 772). But Price (1963) and Huffman and Price (1949) both describe how the wind physically rolls and breaks up desiccated, cracked mud curls.

Perhaps specific salts or clay minerals promote the development and strength of grain aggregates, or inhibit their formation. For instance, Bryan (1974) found that the type and amount of clay minerals is important in forming water-stable aggregates. Price (1963) suggested that the disintegration of clay crusts is promoted by the swelling of hygroscopic saline clay on dewey nights, followed by contraction during sunny days, and that this process does not occur in non-saline clay.

Caine, *et al.*, (1977) suggested that the action of ice needles was efficient in mechanically breaking soil aggregates into erodible sizes. Generation of the small aggregates in the extensive erodible clay soils of the Red River Valley of North Dakota is attributed to the freeze/thaw cycle (Norman Prochnow, Soil Conservation Service, personal communication, 1987).

It was our purpose to study natural formation of non-sandy surface aggregates, with emphasis on those aggregates that are subject to wind erosion. In carrying out this research, our strategy was to find naturally formed aggregates in a wide variety of environments including both recently deposited sediments and natural soils. To restrict our quest somewhat, we chose to examine only materials having composition of less than 50% sand. For surface material having observable salt efflorescence, however, we considered all compositions. Examination of the aggregates for size and other characteristics then allowed us to describe a probable cause for the aggregate formation.

## **2. NATURAL MECHANISMS FOR THE FORMATION OF NON-SANDY, WIND-ERODIBLE AGGREGATES**

Observations of conditions of non-sandy surface material led us to hypothesize the following possible causes for formation of wind-erodible aggregates:

- (1) cracking caused by wetting and drying;
- (2) fracturing of brittle sediment or molding of soft sediment caused by ice crystals during freeze-thaw cycles;
- (3) fracturing or molding by salt efflorescence in the capillary fringe;
- (4) direct abrasion by wind-driven clasts (Here we include related processes such as the breaking of thin, brittle mud curls and other large clasts as they are flipped and tumbled by the wind.);
- (5) breakup of fine-grained bedrock as a result of stresses produced by hydration swelling and related chemical weathering (This process may be aided by freeze/thaw action and wet/dry swelling and shrinking related to pore water.);

- (6) flocculation of clay and other fine-grained material in a sediment-water suspension or wet mud;
- (7) in soils, the formation of grain aggregates (peds) by surface films, colloidal material, or cements; and related processes (In natural environments, bare surfaces affected by these processes typically crust over rather than forming into loose grain aggregates.);
- (8) floatation and lofting of foam; and
- (9) mechanical disturbance of surface material by animals (Since it is obvious that this mechanism can produce some wind-erodible surface material, it is not of primary interest to this investigation.).

The above mechanisms may act on soil or sedimentary material that is preconditioned to break into erodible units more easily. Examples of such preconditioning are these:

- (1) vesicular structures in the soil,
- (2) small laminae, and
- (3) spicules of salt efflorescence.

In our investigation, observations and detailed examination of sediment samples were made to determine whether and how much the first eight mechanisms could be attributed to actually produce wind-erodible surface material. On the basis of our observations, we also ranked the mechanisms among all the natural (non-animal and non-anthropogenic) causes of wind erosion.

### 3. EXPERIMENTAL DETAILS

Locations and details, such as descriptions of the land and geological setting for each soil or sediment sample, are given in Table 1. All soil samples were tested for *in situ* conditions. Sampling locations were chosen to be representative for surface materials having less than 50% sand composition. Some of our samples came from mature soils (North Dakota) exposed to wind action by tilling, natural erosion, or drought destruction of ground cover, but most were recently deposited sediments little affected by long-term soil processes. As far as possible, locations were chosen where

Table 1. Identification and Location for Surface Samples

Group	Number	Description	Location	Comment
I	301	cracked crust	mid, Danby L., CA	curled peds
	302	cracked crust	mid, Danby L., CA	curled peds
	305a	2-5 mm pellets	Hale Co., TX	UdicPellustert; fine,montmoril., thermic
	305b	0.3-2 mm pellets	Hale Co., TX	flat, erodible
	306	thin peels	Battle Mtn., NV	center of playa
	308	smooth crust	El Mirage L., CA	center of playa
	310	cracked crust	Harper L., CA	center of playa
	311	cracked crust	Emerson L., CA	center of playa
	312	curled peels	Emerson L., CA	edge of playa
	313	cracked crust	Lucerne L., CA	center of playa
	314	cracked crust	Soggy L., CA	center of playa
	317	crust	Silver L., CA	center of playa
	318	cracked crust	Silver L., CA	edge of playa
	LEW-4-4	cracked crust	Wild Horse L., MT	edge of playa
	LEW-4-6	cracked crust	Wild Horse L., MT	edge of playa
	LEW-2-1	thin cr. crust	Petroleum Co., MT	dry bed of pond
	RND11-2	fluffy salty aggregate	North L., Broadview, MN	edge of playa
	NM 1	cracked crust	Las Cruces, NM	crusted soil
	ND 7	fine aggregates	Fargo, ND	small aggregates
	ND 1	fine aggregates	Mapleton, ND	field
	ND 2	fine aggregates	Fargo, ND	field
	CO 3	fine aggregates	Erie, CO	flat wet soil
	CO 4	fine aggregates	Erie, CO	flat wet soil
CO 5	fine aggregates	Erie, CO	flat wet soil	
CO 6 (GW)	fine aggregates	Longmont, CO	flat wet soil	
NM 2	cracked crust	Las Cruces, NM	crusted soil	
II	304	smooth crust	Danby L., CA	edge of playa
	309	smooth crust	El Mirage L., CA	edge of playa
	315	thin crust	Pueblo, CO	prairie flat
	NM 3	cracked crust	Las Cruces, NM	center of playa
	ND 3	flat,bare soil	Casleton, ND	small aggregates
	ND 4	flat,bare soil	Casleton, ND	small aggregates
	ND 5	Plowed field	Casleton, ND	flat soil
	NE 1	bare soil	Sidney, NE	flat soil
	NE 2	bare soil	Sidney, NE	flat soil
	NE 4	bare soil	Sidney, NE	flat soil
	NE 3	bare soil	Sidney, NE	flat soil
	ND 6	flat, bare soil	Jamestown, ND	flat soil

Table 1. (Continued)

Group	Number	Description	Location	Comment
III	101	salty crust	Danby L., CA	center of playa
	102	sand-salt crust	Searles L., CA	center of playa
	103	salty crust	Searles L., CA	center of playa
	104	salt crust	Searles L., CA	center of playa
	105	salty crust	Searles L., CA	center of playa
	106	salty crust	Searles L., CA	center of playa
	107	fluffy salt	Soda L., CA	center of playa
	108	fluffy salt	Soda L., CA	center of playa
	109	salty crust	Soda L., CA	center of playa
	110	loose salty soil	Soda L., CA	center of playa
	111	salty crust	Soda L., CA	center of playa
	112	loose salt soil	Owens L., CA	center of playa
	113	salt crust	Owens L., CA	center of playa

natural processes were undisturbed. As might be expected for aeolian geomorphology, our sample locations were largely in semiarid and arid settings. Specifically, our principal sampling locations were in the Mojave Desert, central Montana, part of the Great Basin Desert, west Texas, North Dakota, and Colorado.

The mode of the size distribution of the surface aggregates is used by us as a surrogate for wind erodibility. In this study, modes larger than 1 mm are generally not wind erodible for all but unusually high winds; modes smaller than 1 mm are erodible for winds experienced in the western United States. The soil samples were carefully transported to our laboratory to avoid breakage of aggregates. The dry-aggregate size distribution was determined for each sample by dry sieving. Sieving was done slowly by hand with care taken to minimize breakage of aggregates in the sieving process. Dry sieving did not significantly effect sample modes, however, it is possible that the fine fraction of the aggregate size distribution was slightly exaggerated. From the size distribution the modes were obtained for each sample. Mode was determined as described by Gillette, *et al.*, 1982.

Mass percentages and size distributions of the test soils were determined after water-soluble material, calcium carbonate, and organic material were removed. The Pipette method and Sedigraph method were used to determine the size distributions. The resulting compositions of sampled soils listed in Table 1 are shown in Table 2 for those soils having more than 28% clay composition (Group I), in Table III for those soils having less than 28% clay composition (Group II), and in Table 4 for the salty samples (Group III). Results of size distributions are reported using U. S. Department of Agriculture (USDA) definitions for sand, silt, and clay: sand designates particles with size between 50  $\mu\text{m}$  and 2 mm; silt has sizes between 2 and 50  $\mu\text{m}$ , and clay has sizes smaller than 2  $\mu\text{m}$  (Buckman and Brady, 1970).

Other components of the test soils are given in Tables 2, 3, and 4. Soluble material was measured gravimetrically from a soil-water extract of a suspension formed by intermittent stirring of soil in water for 3 hours. The pH values, organic matter, and carbonate material were determined by standard laboratory procedures. Obvious organic detritus was hand-picked out before organic matter was determined. For determination of clay mineralogy, the following procedure was used: The sample was placed in a plastic centrifuge tube, where carbonates and soluble salts were removed with 1N NaOAc (pH=5), by use of Jackson's (1975) centrifuge washing procedure. The carbonate- and salt-free sample was then transferred to a beaker, and organic matter was destroyed by treatment with  $\text{H}_2\text{O}_2$  and



**Table 2. Composition of Samples that had More than 28% by Mass Clay and Less than 50% Sand (Group I)**

Number	Silt,%	Clay,%	Soluble,%	CO <sup>3</sup> ,%	Organic,%	pH	Mode,cm
301	23.2	62.0	0.35	5.6	1.58	8.2	3.500
302	23.1	76.5	0.63	8.0	1.51	8.0	1.500
305a	13.5	86.0	0.09	1.9	2.66	7.5	0.150
305b	32.5	51.5	0.04	0.6	2.96	7.5	0.075
306	29.9	64.2	0.24	18.8	0.33	9.8	9.99
308	34.8	52.0	2.11	2.8	0.39	9.0	9.99
310	29.9	60.2	3.02	6.4	1.08	8.4	1.5
311	32.9	44.1	22.17	2.7	0.58	8.3	3.5
312	50.9	38.3	0.29	4.3	1.31	9.1	0.3
313	29.5	64.0	3.36	14.0	0.3	8.2	3.5
314	29.4	50.1	0.27	13.9	0.44	8.7	3.5
317	23.8	52.0	0.35	5.2	0.3	9.2	1.2
318	9.4	61.6	0.26	5.1	0.3	8.9	1.2
LEW-4-4	2.0	97.71	0.0	1.0	0.65	8.6	1.05
LEW-4-6	14.4	85.44	0.0	1.19	0.84	8.5	0.6
LEW-2-1	17.86	81.84	0.0	1.03	0.97	8.4	0.3
RND11-2	46.93	45.77	0.0	7.49	2.42	8.8	0.03
NM2	22.2	35.8	0.0	14.41	1.35	8.3	5.0
NM 1	33.45	42.05	0.0	19.19	1.33	8.3	5.0
ND 7	36.2	58.8	0.0	0.98	5.73	7.1	0.0605
ND 1	60.25	34.63	0.0	0.67	5.79	7.4	0.061
ND 2	52.17	44.72	0.0	2.58	5.08	7.8	0.043
CO 3	33.7	31.3	0.0	0.00	1.01	6.3	0.043
CO 4	37.7	31.0	0.0	2.0	1.03	7.3	0.061
CO 5	33.6	35.4	0.0	2.0	0.81	7.3	0.043
CO 6	29.6	35.8	0.0	2.0	1.1	7.5	0.043

**Table 3. Composition of Samples that have had Less than 28% Mass Clay and Less than 50% Sand (Group II)**

Number	Silt,%	Clay,%	Soluble,%	CO <sup>3</sup> ,%	Organic,%	pH	Mode,cm
304	36.0	24.9	1.49	8.3	1.87	7.7	1.5
309	61.5	21.5	0.07	1.6	0.87	8.8	1.5
315	32.8	20.4	0.04	9.5	0.67	7.9	3.5
NM 3	46.4	25.6	0.0	15.55	2.42	8.3	5.0
ND 3	57.18	19.21	0.0	1.45	4.32	7.6	9.9
ND 4	59.74	16.19	0.0	2.42	1.51	7.8	9.9
ND 5	65.16	11.8	0.0	6.59	5.94	7.9	0.06
NE 3	51.3	25.2	0.0	0.0	2.0	5.8	9.9
NE 1	46.5	23.5	0.0	0.0	1.7	6.6	9.9
NE 2	34.0	23.1	0.0	0.0	1.06	6.1	9.9
NE 4	32.0	19.1	0.0	2.0	1.55	7.3	9.9
ND 6	28.84	13.64	0.0	15.52	1.29	8.0	9.9

**Table 4. Composition of Salty Samples (Group III)**

Number	Silt,%	Clay,%	Soluble,%	CO <sup>3</sup> ,%	Organic,%	pH	Mode,cm
101	54.8	19.1	26.26	2.1	0.07	8.1	10.0
102	44.1	16.3	38.6	11.8	0.0	9.5	4.8
103	23.5	1.9	34.1	31.1	0.0	9.9	4.8
104	56.2	6.9	30.4	10.2	0.0	9.6	10.0
105	33.8	56.1	86.3	6.0	0.35	9.9	10.0
106	32.3	48.6	22.9	9.3	0.0	9.9	0.0
107	27.3	72.0	72.3	4.6	0.0	9.4	0.3
108	29.7	68.9	46.4	5.0	0.0	9.4	0.02
109	41.6	47.4	11.5	5.2	0.0	8.7	10.0
110	43.6	47.7	24.6	4.3	0.0	8.5	0.02
111	39.5	33.4	0.9	4.9	0.0	8.0	4.8
112	38.8	9.1	13.0	8.9	0.32	9.9	0.0
113	53.8	10.2	23.2	16.7	0.0	9.9	0.0

dispersed with 25 ml of  $\text{Na}_4\text{P}_2\text{O}_7$ . Stirring and ultrasonication followed. Clays were isolated by sedimentation after removal of the sand fraction by wet sieving.

Dominant mineralogy of the clay fraction was determined by x-ray diffraction using the method described by Gillette, *et al.*, 1982. The x-ray diffractograms were examined by one of us (RB), and relative abundances of the clay minerals were assigned. Table 5 lists these minerals. Some information on the mineralogy of the soluble material is given in Table 6.

## 4. RESULTS

We have organized our observations into those related to the first eight mechanisms for producing erodible non-sandy aggregates given in Sec. 2.

### 4.1. *Shrink/Swell Cracking Caused by Drying and Wetting*

When a wet mud dries slowly, it shrinks and cracks under tension. This process is complex, because of inhomogeneities in the material, redistribution of stress as cracks propagate, changes in drying and shrinking rates along growing cracks, and the material's increasing resistance to further shrinkage as it compacts.

On natural, bare, drying surfaces, the cracking progresses only so far: a typical end result is a network of desiccation cracks separating polygonal blocks several centimeters or decimeters in diameter (Corte and Higashi, 1964). We investigated which factors promote further cracking so that centimeter-sized clasts could be reduced to a loose rubble of less-than-2-mm-sized, wind-erodible grain aggregates (also termed pellets or "peds").

We found four major variables, all related to shrink/swell cracking of desiccating soils and sediments, which explain much of the variation in grain size of our grain aggregates:

- (1) texture: the percent of clay relative to silt and sand in disaggregated samples;
- (2) the percentage of organic material and calcium;
- (3) the occurrence and timing of alternating episodes of wetting and drying; and

**Table 5. Clay Mineralogy for Surface Material (in tenths)**

Number	Smectite	Mica	Kaolinite	Chlorite	Vermiculite
301	3	4	2	1	0
302	3	4	2	1	0
305a	1	6	3	0	0
305b	1	5	4	0	0
306	1	7	2	0	0
308	1	2	5	2	0
310	4	4	1	1	0
311	5	3	2	0	0
312	6	3	1	0	0
313	2	5	2	0	1
314	3	4	2	1	0
317	6	3	0	1	0
318	6	2	0	2	0
LEW-4-4	4	5	1	0	0
LEW-4-6	4	5	1	0	0
LEW-2-1	4	5	1	0	0
RND11-2	0	5	3	2	0
NM 2	1	6	2	1	0
NM 1	0	6	2	2	0
ND 1	4	5	1	0	0
ND 2	5	3	2	0	0
304	3	5	2	0	0
309	1	2	5	2	0
315	1	3	5	1	0
NM 3	1	5	2	2	0
ND 3	4	4	2	0	0
ND 4	4	5	1	0	0
ND 5	4	4	2	0	0
ND 6	6	3	1	0	0
101	3	4	2	0	1
102	1	6	1	2	0
103	1	1	1	1	1
104	1	7	0	2	0
105	2	5	0	2	1
106	2	6	0	2	0
107	5	3	0	2	0
108	4	4	0	2	0
109	6	3	0	1	0
110	7	3	0	0	0
111	6	2	0	3	0
112	4	4	2	0	0
113	4	3	1	1	0

**Table 6. Salt Mineralogy for Surface Material (in tenths)**

<b>Number</b>	<b>Calcite</b>	<b>Halite</b>	<b>Borax</b>	<b>Anhydrite</b>	<b>Sylvite</b>	<b>Soda Niter</b>
101	1	9	0	0	0	0
102	1	7	0	1	1	0
103	2	5	0	3	0	0
104	2	8	0	0	0	0
105	0	10	0	0	0	0
106	0	4	1	2	1	2
107	0	10	0	0	0	0
108	0	10	0	0	0	0
109	0	6	1	1	0	2
110	0	8	0	0	0	2
111	0	0	0	0	0	10
112	8	2	0	0	0	0
113	4	3	0	0	3	0

- (4) inhomogeneities, especially bedding and laminations, in the original sediment.

#### 4.1.1 Texture (the percent clay relative to silt and sand in disaggregated pellets)

If the soil has a "skeleton" of hard, relatively incompressible grains such as quartz sand and silt, then shrinkage volumetric changes are strongly limited, and there can be little or no desiccation cracking (Vershinin, 1958). The grain-size distributions of our disaggregated pellet samples bear this out. We plotted the data on pellet size versus the variables that were given in Sec. 4.1. The most visible correlation resulted from a plot of the aggregate size versus organic composition for a division of the data set into samples having more or less than 28% clay composition (Groups I and II). Since we used the USDA textural definitions, this separated our data set into clay, silty clay, clay loam, and silty clay loam textures (Group I) and loam and silt loam textures (Group II). The observed mode of the dry-aggregate size distribution is plotted in Figure 1 versus organic percentage of the soil for Group I. We also searched for relationships between mode value and silt, clay, and pH but did not find any obvious relationships.

#### 4.1.2 Percentage of organic material and calcium carbonate

Studies of soils (for example, Vershinin, 1958; Baver, *et al.*, 1972) show that there is stronger desiccation cracking and formation of aggregates in soils with higher content of organic matter, and also in soils saturated with bivalent cations (especially  $\text{Ca}^{2+}$  or  $\text{Mg}^{2+}$ ), compared with weaker cracking and aggregate formation with monovalent cations (such as  $\text{Na}^+$ ).

Of these chemical parameters, our data suggest that organic content and calcium content are very significant for Group I (more than 28% clay content). The soils from North Dakota, Montana, and Texas that were rich in organic material (more than 2% by mass) had aggregates that were much smaller and were wind erodible. The other surface samples were lower in organic content, larger, and for the most part not wind erodible. These samples were largely from more arid regions.

The organic percentage versus mode of dry-aggregate size distribution for Group II is plotted in Figure 2. We see no significant trend of mode size with organic matter. We suggest that this is because desiccation cracking is inhibited by silt and sand grains that are mostly in contact, forming a rigid framework that resists shrinkage; the effect of high organic content is

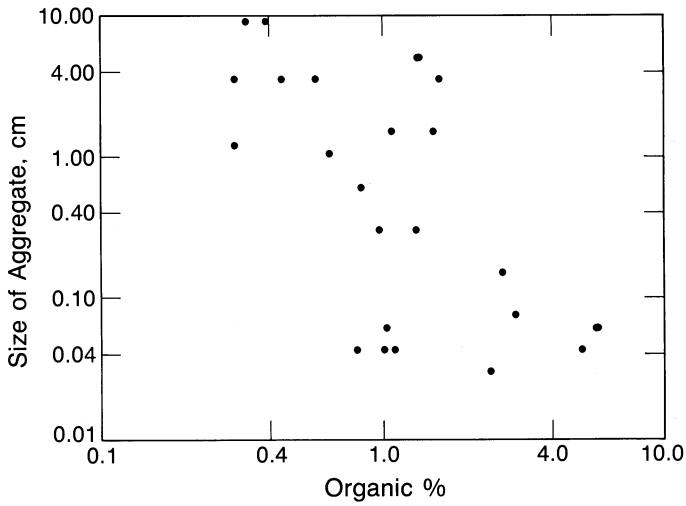


Figure 1: Mode size (cm) of dry surface aggregates having more than 28% clay by mass (Group I) versus organic composition (percent). All surface material had less than 50% sand composition.

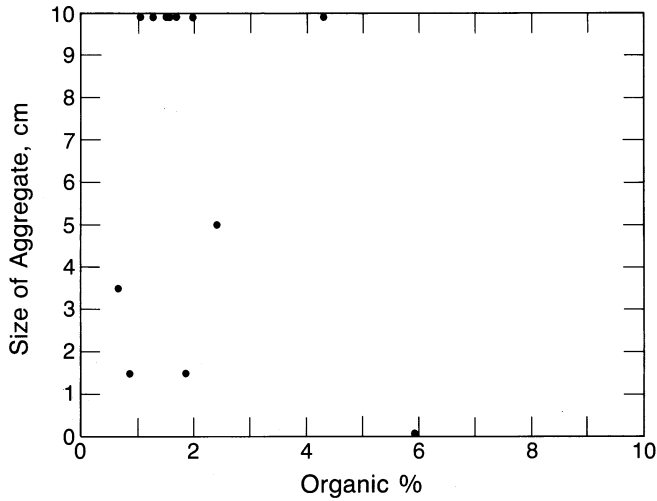


Figure 2: Mode size (cm) of dry surface aggregates having less than 28% clay by mass (Group II) versus organic composition (percent). All surface material had less than 50% sand composition.

masked. The contrast between Figures 1 and 2 shows that the clay percentage and organic percentage are major variables for production of erodible-sized aggregates.

A second important compositional difference was pointed out by the work of Chepil and Woodruff (1963). In establishing the Wind Erodibility Group 4L classification, they recognized the effect of high calcium carbonate percentage in increasing wind erodibility. The expected effect would be to produce smaller, loose surface aggregates. Indeed, for example, soils ND 3 and ND 5 (in Group II) were located within 2 km of each other; both soils were similarly farmed, flat, and had similar (approximately 3cm-thick) crusts. ND 5 was rich in calcium carbonate, with 6.59%, while ND 3 had 1.45% carbonate. Both soils were classified as silt loam soils. Close-up examination of the surfaces of both soils showed that the more calcareous soil had a more disaggregated surface with an approximately 1-mm-thick layer of loose particles having an aggregate mode of 0.06 cm. The less calcareous soil had a smoother surface that did not possess any loose particles.

#### 4.1.3 Alternating episodes of wetting and drying of non-sandy soils

Atmospheric precipitation is important in production of dry aggregates subject to wind erosion. For agricultural soils, it is observed that clods of soil "melt" into a flattened soil structure following intense rainfall or melting of a sufficient quantity of snow. Thus, precipitation can profoundly modify the aggregate structure of a soil or sediment. The following selected observations on the response of surface aggregates to precipitation are organized by our Group I and Group II classifications.

Group I. Two samples of a clay soil, 305 A and 305 B, were obtained prior to and following major precipitation events. 305A and B were typical of clay soils that are rich in organic matter and that break into small erodible aggregates after sufficient drying. Aggregate size mode was measured at smaller than 1 mm prior to a 4-cm rain storm that soaked the soil for 2 days. The erodible clay material was thoroughly wetted and became a thick layer of water-saturated mud. The precipitation event was followed by a long, dry period. Within a month, the clay had cracked into aggregates 1-2 mm in size. The aggregates were eroded by winds at that time, but because of their rather large size did not become suspended and were deposited within a few tens of meters of their origin. During the next several months of severe drought and frequent winds larger than threshold, the clay aggregates were mechanically worn down to a size distribution having a mode of 0.075 cm.



NM 1 and NM 2 were typical of low-organic-composition desert clay and clay loam crusts. During a period of about 1 1/2 years, the crusts of the two samples were never broken into a wind-erodible size.

Soils CO 4 and CO 5 were two clay loam soils located within 1 km of each other. In October 1985, CO 4 had a smooth-loose soil condition and CO 5 had a cloddy soil condition. Following the melting of a snow layer on February 15, 1986 (6 cm cumulative precipitation), high winds caused drying and wind erosion on the top layer of the water-soaked soils. The aggregate size mode for each soil was 0.06 and 0.04 cm respectively. The melting of the snow had destroyed the cloddy structure of soil CO 5 but had not significantly changed the structure of soil CO 4. Had the high winds not immediately followed the melting of the snow covering the soils, both soils might have dried more slowly, forming wind-erosion-resistant crusts.

Experiments in wetting and drying mud chips showed that several light rain showers on a dry mud flat could reduce large chips to loose piles of smaller, deflatable chips. With more intense wetting, the end product could be a weakly cohesive mass of grain aggregates that are susceptible to erosion by wind-driven grains. The experiments also demonstrated that order-of-magnitude reduction in grain size can occur in a short time (several wet-dry cycles of a few hours each), with no salt efflorescence or high temperatures required.

The chips, sample LEW-4-4, were collected from the desiccated, sun-dried and cracked surface of the basin of Wild Horse Lake, 17 km north of Teigen, central Montana. We noted no evidence of active deflation of grain aggregates, but inactive clay dunes (lunettes) fringe the east shore of the lake basin about 100 m east of the sampled site. At 47° 11' North latitude, the basin is the northernmost large deflation basin in Montana and has the northernmost clay dunes known to us anywhere.

The sediment (Tables 1 and 2) has 0.65% organic matter, and a very high clay content (98%, highest of all our samples), with much smectite and no obvious salt efflorescence (although an overflight on June 4, 1987, showed broad, white salt crusts about 0.5 km west of our sample site). The chips were weakly laminated. The chips were from a recently cracked mud surface that showed no evidence of wetting by rain. The original size of the mud chips was approximately 1 x 2 x 3 cm.

Within seconds after adding water to the upper surface of a chip, the water began to soak into a chip, expanding the outer 1-2 mm of the wetted

top and sides of the chip. This put the interior of the chip under tension and the exterior under compression.

Beginning about 5 seconds after addition of the water, the chip fractured in its compressed outer layer and probably also within its interior; this was accompanied by audible snaps and crackles. Compressive stress in the expanded surface layer was partially relieved by outward spalling of flakes and needles. This was most obvious on acute edges of the chip, where elongated needles and rods (triangular in cross section) were formed. A few tiny flakes and needles (typically 1-3 mm long) popped off the sides of the chip, some landing several centimeters away; others remained loosely attached to the sides of the chip. Some needles were oriented parallel to the lamination in the chip. The rate of audible cracking rapidly decreased after 2 or 3 minutes, but continued sporadically for as long as 30 minutes.

The audible cracking is probably in part caused by entrapment and compression of pore air in front of the rapidly advancing wetting front within the chip. Baver (1972) reviewed studies that suggest air entrapment is the dominant mechanism in internally fracturing (and even violently shattering) illite and kaolinite clods, whereas both air entrapment and differential swelling are important in fracturing montmorillonite clods.

The water puddle on the top of the chip was gradually absorbed and the surface eventually, after about 3-5 minutes, no longer glistened with water. Capillarity drew some of the water into the chip interior, reducing the pore-water content of the previously expanded surface layer; some of the water was retained in the surface layer by smectite clay minerals. In consequence, the interior of the chip swelled and was compressed, while the surface layer was placed under tension and cracked. These cracks were crudely parallel to the primary depositional laminae of the sediment and were spaced 0.1-1.0 mm apart. Most tapered inward several millimeters and ended. A few propagated to the center of the chip and joined. Some were curved, and possibly intersected other cracks on the upper and lower surfaces of the chip.

After air-drying then rewetting the samples at room temperature, and (repeating this cycle several times) many of the cracks enlarged and joined or intersected. The original chip was reduced to a mass of many nested, small, flat-to-slightly-cupped tabular flakes and roughly equidimensional polyhedra. These grains were all more or less still in place, but many were loose or adhered only weakly to one another. This mass was surrounded by many completely detached, sand-sized chips of three morphotypes: rods,

many with triangular cross sections and needle-shaped, slightly curved points at one or both ends; roughly equidimensional polyhedra; and tabular flakes.

Overwetting caused our experimental clay chips to disaggregate completely. Larger chips began to crack as described above, then "melt" into a mass of poorly defined silt- and fine-sand-sized aggregates and disaggregated clay grains; upon drying the material formed a porous, slightly cohesive mass, which would probably be easily eroded as silt- and clay-sized dust by saltating sand-sized pellets. Our experimental chips had little cementing or bonding agents such as salts, carbonates, or iron hydroxides, so did not crust upon drying.

Group II. Of our Group II samples, only ND 5 developed erodible-sized aggregates. We observed soils NE 1, NE 2, NE 3, and NE 4 during a several-month period. At no time during that period, however, did the soils develop erodible-sized aggregates. It has been observed, however, that high winds following driving rain and clod destruction of silt loam and loam soils cause intense wind erosion (Tom Nightingale, University of Nebraska, personal communication, 1986). This was also observed for the clay loam soil CO 5 by the authors. The rather ambiguous results that intense precipitation may be followed by intense wind erosion or by crusting and no erosion may be differentiated by the timing of the strong drying wind following wetting — if the wind occurs while the surface layer is still wet, wind erosion is possible; if it occurs after the soil crust has at least partially formed on the surface, wind erosion will probably be prevented.

#### 4.1.4 Bedding and laminations in the original sediment

Thin beds of drying mud have a greater potential for breaking into small, wind-erodible chips than do thick layers. Our field work suggests that this is because thin layers of desiccating soil or sediment have more cracks that are more closely spaced. This is supported by the work of Corte and Higashi (1964), who studied desiccation cracks by drying soil-water slurries in shallow trays. With a thinner layer of drying mud, the total crack length increased, and thus the average cell area (made by intersecting cracks) decreased.

We studied a good example of this phenomenon in central Montana. Sediment LEW-2-1 is sun-dried, very angular chips and shards of a very clayey sediment. The sediment was deposited from suspension as a thin layer, about 0.5 cm thick in a shallow, ephemeral pond in a small deflation basin northeast of Grass Range, Montana. The mode of the chips is about

0.25 cm (Fig. 3). The clay chips would be deflatable by a strong wind. We think that the clay bed cracked so extensively for three reasons: it contains much water-expandible smectite clay, and thus shrinks greatly when desiccated; it has a moderate content of organic material (0.97%), which promotes close-spaced shrinkage cracks; and it started as a very thin layer tightly adhered to an underlying, relatively rigid bed of laminated clayey silt, 1 cm thick, which did not shrink much.

Thin desiccating layers also have a greater potential for separating from an underlying bed as thin mud curls, which although large, can be moved by the wind. This has been observed by us and described by many workers, for instance, Huffman and Price (1949) and Roth (1960).

Lamination boundaries, even if very weakly developed, act as planes of weakness in desiccating muds, concentrating tension stress and leading to smaller pellets with a more tabular shape. Experiments, such as the one described in Sec. 4.1.3 with the clayey mud chips LEW-4-4, graphically show this.

#### 4.2 *The Freeze/Thaw Cycle*

The freeze/thaw cycle is commonly thought to be an important mechanism for formation of wind-erodible aggregates. Evidence for the efficacy of this mechanism is that clay soils are often broken into erodible pellets in the spring after fall plowing had formed the soil into clods of several centimeters in size. This is especially evident in North Dakota and Montana where cold, dry winters are common. In Colorado, the action of ice needles on loosening of the surface soil has been documented by Caine, *et al.*, 1977.

Surface aggregate formation resulting from the freeze/thaw cycle is, however, quite difficult to distinguish from aggregation resulting from shrink/swell fracturing during wet/dry cycles. For example, the clay pellets produced in a West Texas dry lake (samples 305a and b) are similar to those in North Dakota agricultural soils (samples ND 1 and ND 7). And yet, the Texas samples did not experience a severe winter during their formation, whereas the North Dakota samples experienced a severe winter with numerous freeze/thaw episodes.

The North Dakota samples were particularly susceptible to shrink/swell breakdown during wet/dry cycles because they contained much expandable clay (approximately 40% of the clay in ND 1 is smectite). In North Dakota, temporary thawing and desiccation of the ground surface



Figure 3: Sample LEW-2-1, a thin layer of very clayey, loose, sun-dried, angular chips. The chips lie on a relatively rigid layer of very light-grey-colored, sun-cracked, clayey silt.

is common on warm winter and spring days during low-snow years when the ground is bare. This leads us to believe that much of the clay pellet formation that takes place in the winter at many sites may be caused by expansion and contraction during wet/dry cycles, with or without the additional effects of freeze/thaw action.

One clear-cut example of the action of freeze/thaw cycles in producing erodible aggregates was related to one of the authors by S. Vick (P. E., Geotechnical Engineer, personal communication, 1988). The sediment disturbed by freeze/thaw was a dried pond of silt-sized mining waste containing no sand, no organic material, and no smectite. The material was flat and did not display cracking in the summer. Following freezing and thawing during the Irish winter, the material, previously crusted into a smooth nonerodible surface, eroded in the wind until the crusted surface was restored.

#### *4.3 Salt Efflorescence in the Capillary Fringe of the Soil*

The effect of salt efflorescence has been widely attributed to be a leading cause of small pellet formation. Indeed, in a study of several Mojave playas by Gillette, *et al.*, 1982, salt efflorescence was observed in one of them to generate wind-erodible aggregates.

Three dry lakes in the Mojave that were examined by us had large quantities of surficial salt: Searles Lake, Owens Lake, and Soda Lake (all located in southeastern California). The condition of the salt encrustation for all three lakes was such that the surface material was actually cemented into non-erodible crusts in most cases (samples 101, 106, 109, 111, and 113). At Searles Lake and at Owens Lake, the salt formed dry and hard spicules that were subject to abrasion by sandblasting but that did not erode by the force of the wind. At Soda Lake most of the salt-encrusted soil was nonerodible. However, there were several dome-crust, blisterlike structures. Some of these blisters were split open, and fine soil and salt material was in abundance in the inside of these structures (sample 110). It was evident that some of this material had been eroded out of the blisters in several locations. The total area covered by these blisters was less than 1% of the entire dry lake area, so we do not feel that we saw evidence for salt efflorescence as a major mechanism in producing erodible-sized aggregates.

#### *4.4 Direct Abrasion*

Several observers have noted that wind erosion often spreads into agricultural fields from upwind eroding areas such as unpaved roads,

barrow pits, or other agricultural fields. We have noted several examples of erosion taking place in fields having sufficient cloddiness to prevent erosion, or in fields having sufficient vegetative residue to prevent erosion, by the incursion of sandblasting sand from an upwind source having a low threshold friction velocity.

One of us has witnessed a 3-day-long dust storm at Owens Lake in Southern California (Gillette, 1984b). Careful observations of the erosion during that time gave evidence that the primary eroding areas of the lake were loose deposits of relatively salt-free sand. Indeed, the areas of minimum wind speed for active wind erosion were the areas where low-salt-composition dunes were present. Sand was carried from these areas onto large areas of salt efflorescence on the lake. It was evident that the salty material was being sandblasted and that significant salty material was being made airborne as a result of the sandblasting. Sample 112 was collected at Owens Lake far downwind of the primary sand areas and immediately downwind of a sandblasted salt crust area. For winds higher than those initiating the relatively salt-free sand movement, some of the sandy lake bottom having salt efflorescence continuously eroded, showing that the salt had increased, not decreased, the threshold velocity. Thus, our observations were interpreted such that the salt efflorescence increased aggregate size, rather than decreased it. Presence of salty material in aerosols from Owens Lake as was observed by Barone, *et al.* (1981), does not demonstrate that salt efflorescence decreases dry aggregate size.

#### 4.5 *Weathering of Fine-Grained Bedrock by Hydration*

The direct physical and chemical weathering of fine-grained bedrock, such as shale and siltstone, can produce sand- and silt-sized, wind-erodible rock fragments at windy, dry sites with little ground cover. Our observations at two sites in Montana suggest that this is a common but volumetrically insignificant process, in cold-temperate, semiarid areas. Results confirm Pye's (1987) comment that it is difficult to distinguish the effects of ice crystallization and moisture absorption in cold environments. We also expected to find significant hydration swelling and other evidences of chemical weathering, but did not. Previous studies (reviewed by Pye, 1987, pp. 14-15) have not dealt with the disintegration of fine-grained parent rocks, such as shale, mudstone, and clayey siltstone. These "soft" rocks by no means necessarily decompose by weathering to their component clay and silt mineral grains, but rather may be reduced by weathering to sand- and silt-sized grains suitable for deflation.

#### 4.5.1 Wind-erodible shale fragments

We studied coppice dunes consisting mostly of shale flakes deflated from nearby outcrops. The shale is finely fissile, medium-dark-gray colored, and contains subordinate siltstone laminae (Colorado Shale, Upper Cretaceous age). Deflation of the shale fragments, along with siltstone fragments, occurs on the upper sides and crest of wind-swept knobs and escarpments 7-9 km north of Teigen, in central Montana.

The wind-erodible fragments form by weathering of the parent rock on bare hillslopes, micropediments, and in water-eroded gulches less than 1 m deep. At most sites the shale bedrock is poorly exposed and is covered with a weathering mantle of angular shale flakes several centimeters deep. Many of the deflating surfaces show evidence of recent sheetflow erosion and local deposition of miniature alluvial fans and terraces. This suggests that water erosion is the main agent that keeps the shale slopes free of vegetation, thereby enabling episodic, strong winds to also erode the weathered bedrock grains.

Ground juniper traps the deflated sand- and fine-gravel-sized shale and siltstone flakes, forming coppice dunes up to 2 m high. Each dune is typically within 10 m of its sediment source.

Samples collected from both the shale-fragment mantle on bedrock surfaces and from the coppice dunes have a bimodal grain-size distribution, with one mode of silt and fine sand, another of medium sand to fine gravel. The maximum diameter of shale flakes in coppice dunes is about 1 cm. The larger shale flakes are typically very angular, 0.5-1.0 mm thick and 2-10 mm in diameter. Most sand-sized shale fragments are more equidimensional; some are well rounded, but others are very angular. This suggests that many of them formed mechanically by the transverse breaking of larger flakes at the site of weathering. There is no evidence of chemical alteration, such as swelling by hydration, other than a slight yellowish discoloration on some shale and siltstone grains, probably caused by iron oxides.

We interpret the sand- and gravel-sized shale fragments as having formed primarily by frost wedging along parting planes in the thinly laminated parent shale. The abundant silt-sized grains in the coppice dunes are mostly individual quartz grains. They are probably released by *in situ* mechanical weathering (frost action) of the siltstone grains after being deposited in the coppice dunes.



#### 4.5.2 Wind-erodible clayey siltstone fragments

Deflation of sand-sized, roughly equidimensional siltstone fragments is occurring at a windy hillcrest site 4 km east of Augusta, Montana. Gray-colored siltstone of the Upper Cretaceous Two Medicine Formation is exposed in low rock knobs along the ridgecrest, and on adjacent bare slopes facing northwest into the prevailing wind. The bare areas are mantled with sand- and gravel-sized siltstone fragments formed by erosion of the underlying bedrock. Wind abrasion has locally sculpted small siltstone yardangs ringed by deflation moats.

There are several tiny deflation basins about 15 m southeast of the ridge crest. Portions of their beds are vegetated and stabilized with range grasses and forbs. The remaining portions of the deflation basins are bare of vegetation and are mantled by a thin layer of sand- and gravel-sized siltstone fragments. The siltstone fragments increase in size with depth and pass into irregularly jointed siltstone bedrock 3-6 cm down.

We suggest that freeze/thaw action, supplemented by cracks formed by swelling and contraction during wetting/drying episodes, enlarges primary joints and creates new fractures, reducing the parent siltstone into deflatable fragments. Hydration swelling may also contribute to cracking the siltstone, but there is no evidence of significant chemical alteration of the rock fragments.

Production of sand-sized fragments of clayey siltstone by freeze/thaw action can be quite rapid and efficient. We experimentally weathered seven gravel-sized clayey siltstone chips (CHO-9-2), soaking the chips for 1 hour, then freezing and thawing them, and repeating for a total of three cycles. Numerous (24) curved, angular, sand-sized fragments were spalled off the edges and corners of five of the seven chips, and four of the chips also split crossways into two to three roughly equidimensional polyhedra. A similar experiment with seven chips (not frozen, but wetted and dried) resulted in eight sand-sized spalls; two chips split in half.

#### 4.6 *Flocculation of Sediment in a Water Suspension or Soft Mud*

This hypothetical process has not been documented, to our knowledge. Wasson (1983) suggests, in reference to clay pellets in the Strzelecki dunefield of Australia, that "The saline water with montmorillonitic clays may have aided pelletization by means of flocculation."

#### **4.7 Grain Aggregates Formed by Surface Films, Colloidal Material, or Cements**

In the soils of semiarid and arid regions where natural wind erosion typically occurs, the clumping of grains into water-stable aggregates is promoted primarily by organic matter and clay (Baver, *et al.*, 1972). Our work bears this out.

There are many other mechanisms for forming aggregates in soils. Flocculation of clay and binding of the flocs and other microaggregates to one another is aided by divalent and trivalent cations, especially calcium. Films and cements of silica, calcite, gypsum, and iron oxides also bind and link soil grains into water-stable aggregates. Sodium ion content is critical in determining the presence or absence of grain aggregates in salty soils and sediments. Very high concentrations of sodium cause flocculation of colloidal material and clays, but moderate concentrations cause dispersion of colloids, and breakup of grain aggregates (Baver, *et al.*, 1972).

Soil-grain aggregates in natural, uncultivated semiarid regions are typically protected from wind erosion by vegetative ground cover and in more arid regions by surface crusts. We conclude that, in natural environments the wind erodes these soil aggregates mainly when extended drought has destroyed the ground cover or where grazing has broken up surface crusts.

#### **4.8 Flootation and Lofting of Foam**

This mechanism was observed by one of us (DAG). It required standing water on a playa (Soggy Dry Lake, California) and high wind that suspended a mixture of both organic-rich residue and mineral grains in the shallow water, which became a foamy material on the water surface. This foam was made airborne at the downwind side of the playa by the strong wind. It also was blown against the downwind shore of the 2cm-deep lake where it accumulated and was aerosolized by high winds after it dried. Another example of such accumulation of soil foam was a more salty, dried foam found at Soda Lake (sample 108). This mechanism is thought to represent conditions having fairly low probability of occurring.

## 5. DISCUSSION

The large variety of clay mineralogies found in the California dry lakes did not yield any that produced wind-erodible clay aggregates. Rather, it seems that the organic additive is necessary, along with the shrinking/swelling properties of the clay, to produce small aggregates. A possible explanation for this behavior was offered by Robert Grossman (USDA Soil Conservation Service, National Soils Testing Laboratory, Lincoln, Nebraska, personal communication, 1986) that the stresses of shrinking/swelling were resolved in a smaller distance when organic matter was present. Thus low-organic content desert clays could develop long cracks and large aggregates; more organic-rich areas would develop smaller sized aggregates, more subject to wind erosion.

Our results showing that calcium carbonate in the soil results in smaller dry aggregates supports the results of Chepil and Woodruff (1963). Their work uses a group of soil textures including loam, silt loam, clay loam, and silty clay loam that are more erodible when calcium carbonate is significant in their composition. This increased erodibility would be manifested in smaller dry-aggregate size for surface material.

Our work did not add to investigations of increased wind erodibility caused by freeze/thaw disturbance, including the action of ice needles. Nonetheless, we feel that others have shown this to be an important mechanism. We also feel that some disaggregation that has been attributed to freeze/thaw may actually be due to clay lattice expansion/contraction accompanying the changes of moisture in the winter environment.

The effect of salt efflorescence in many of our observations increases aggregate size and inhibits wind erosion. In some cases, however, efflorescence has caused loose-fine material to be available to wind ablation. Direct abrasion by particles already of wind-erodible sizes, especially sand grains, is very important in producing erodible-sized material. We found this mechanism especially important in producing salty material in Owens Valley dust storms. Clayey sediment deposited in thin beds or laminae crack into smaller wind-erodible fragments than does the same sediment deposited in thick beds.

Our experiment in wetting and drying clay chips shows that wet/dry cycles (such as might result from several brief, nonsoaking summer rainshowers on a dry lake bed) can produce wind-erodible clay pellets without high temperatures or lengthy droughts and in the absence of salt

efflorescence. This may have happened in cold-climate clay dunes (now inactive) that fringe ephemeral lakes in deflation basins in Montana at windy, semiarid sites with short, hot summers and intensely cold winters.

The swelling and consequent cracking of fine-grained bedrock, such as shale and clayey siltstone, by means of freeze/thaw and, less important, wetting/drying cycles is an efficient means of producing sand-sized, wind-erodible grains that can superficially look much like clay or clay-silt pellets formed by other processes.

We did not observe hydration cracking or flocculation of fine-grained sediment as agents for production of wind-erodible pellets.

The process of wind lofting of foam was observed for two lakes in California. We feel, however, that this mechanism operates only during high winds following occasional flooding of the lakes. Thus, the probability of this mechanism producing much erodible material is fairly low.

## 6. CONCLUSIONS

We used 28% clay composition as a division for non-sandy surface material with respect to organic-rich and organic-poor soils. Organic-rich (more than 2% by mass) surface material formed wind-erodible aggregates; organic-poor surface material did not. Calcareous loams, silt loams, silty clay loams, and clay loams were distinguished from non-calcareous soils of the same textural classes by forming erodible surface aggregates, whereas non-calcareous soil of the same textures did not. The effect of wetting and drying the soils by precipitation is less for the less-than-28%-clay soils than it is for the greater-than-28%-clay soils. The timing of high, drying winds after thorough soil wetting is critical for loamy soils. If the wind occurs while the soil is still wet, wind erosion is quite likely to occur; if it follows after surface crusting has taken place, wind erosion is avoided.

Salt efflorescence was not seen to be a major mechanism for erodible aggregation production. Some of the erosion that has been formerly attributed to salt efflorescence may actually be due to direct abrasion of sandblasting and by floatation and lofting of foam. Moderate concentrations of soluble sodium salts disperse flocculated material such as organic colloids and clay aggregates. In such cases, and also where salts of various compositions have formed hard surface crusts, wind erosion would be strongly inhibited, rather than promoted.

Our observations lead to the following ranking for mechanisms producing wind-erodible, non-sandy aggregates — not including animal or human disturbance:

- (1) clay lattice expansion/contraction during wet/dry cycles;
- (2) freeze/thaw cycle;
- (3) direct abrasion;
- (4) salt efflorescence;
- (5) surface films, colloidal material, or cements;
- (6) floatation and lofting of foam;
- (7) hydration cycles in fine-grained bedrock; and
- (8) flocculation of clay and other fine-grained material.

## 7. ACKNOWLEDGMENTS

This work has been supported by The National Oceanic and Atmospheric Administration as part of the National Acid Precipitation Assessment Program. The authors gratefully acknowledge the contribution of many other researchers (arranged alphabetically): Charles Fenster of the University of Nebraska was extremely helpful in locating sites in western Nebraska. Robert Gibbens obtained soil crusts for us from three sites for over 1 year at the USDA Jornada Experimental Range. Steven Holzhey kindly agreed to test soil samples at the Soil Conservation Service, National Soil Laboratory, Lincoln, Nebraska. Tom Nightingale provided us with valuable information and sampling sites at the University of Nebraska High Plains Experiment Station. Norman Prochnow and C. Murrell Thompson located sampling sites for us in North Dakota and Texas and provided us with valuable suggestions and discussions.

## REFERENCES

- Arvidson, R.E., 1972: Aeolian processes on Mars: Erosive velocities, settling velocities, and yellow clouds, *Geol. Soc. Amer. Bull.*, 83: 1503-1508.
- Bagnold, R.A., 1941: *The Physics of Blown Dust and Desert Dunes*, Methuen, London, 265 pp.

- Barone, J.B., Ashbaugh, L.L., Kusko, B.H., and Cahill, T.A., 1981: The effect of Owens Dry Lake on air quality in the Owens Valley with implications for the Mono Lake Area, *Am. Chem. Soc. Sympos.*, Ser. 67: 237-345.
- Baver, L.D., Gardner, W.H., and Gardner, W.R., 1972: *Soil Physics*, Fourth Edition, John Wiley and Sons, New York, 498 pp.
- Bowler, J.M., 1973: Clay dunes: Their occurrence, formation and environmental significance, *Earth Sci. Rev.*, 9: 315-338.
- Bryan, R.B., 1974: Water erosion by splash and wash and the erodibility of Albertan soils, *Geograf. Annal.*, 56: 159-181.
- Buckman, H.O., and Brady, N.C., 1970: *The Nature and Properties of Soils*, Macmillan, London, 653 pp.
- Caine, N., Morin, P., and Nicholas, R.M., 1977: Significance of frost action and surface soil characteristics to wind erosion at Rocky Flats, Colorado, Third Progress Report, Oct. 1, 1976-June 1977, ERDA-510500, ERDA-510100, U7805, 65 pp.
- Chepil, W.S., 1945: Dynamics of wind erosion, II: Initiation of soil movement, *Soil Sci.*, 60: 397-411.
- Chepil, W.S., and Woodruff, N.P., 1963: The physics of wind erosion and its control, In: Norman, A.G. (Ed.), *Advances in Agronomy*, v. 15, Academic Press, New York, pp. 1-301.
- Corte, A., and Higashi, A., 1964: Experimental research on desiccation cracks in soil, Research Report 66, U.S. Army Materiel Command, Cold Regions Research and Engineering Laboratory, Hanover, New Hampshire, 72 pp.
- Dare-Edwards, A.J., 1982: Clay pellets of clay dunes: Types, mineralogy, origin and effect of pedogenesis, In: Wassen, R.J. (Ed.), *Quaternary Dust Mantles of China, New Zealand and Australia*, Australian National University, Canberra, pp. 179-189.
- Dare-Edwards, A.J., 1984: Aeolian clay deposits of south-eastern Australia: parna or loessic clay?, *Trans. Inst. Br. Geogr.*, M.S. 9: 337-344.

- DeGraff, J.M., and Aydin, A. , 1987: Surface morphology of columnar joints and its significance to mechanics and direction of joint growth, *Geol. Soc. Amer. Bull.*, 99: 605-617.
- Gillette, D., 1978: Tests with a portable wind tunnel for determining wind erosion threshold velocities, *Atmos. Environ.*, 12: 2309-2313.
- Gillette, D., 1984a: Threshold velocities for wind erosion on natural terrestrial arid surfaces (a summary), *In: Pruppacher, Semonin, and Slinn (Eds.), Precipitation Scavenging, Dry Deposition, and Resuspension*, Elsevier, New York, pp. 1047-1057.
- Gillette, D., 1984b: Threshold friction velocities and moduli of rupture at Owens Lake, California, *In: Results of Test Plot Studies at Owens Dry Lake, Inyo County, California*, Report prepared for State Lands Commission, by WESTEC Services, San Diego, CA.
- Gillette, D., Adams, J., Endo, A., Smith, D., and Kihl, R., 1980: Threshold velocities for input of soil particles into the air by desert soils, *J. Geophys. Res.*, 85: 5621-5630.
- Gillette, D., Adams, J., Muhs, D., and Kihl, R., 1982: Threshold friction velocities and rupture moduli for crusted desert soil for the input of soil particles into the air, *J. Geophys. Res.*, 87: 9003-9015.
- Greeley, R., and Iversen, J.D., 1985: *Wind as a Geological Process on Earth, Mars, Venus and Titan*, Cambridge University Press, Cambridge, 333 pp.
- Greeley, R., Iversen, J.D., Pollack, J.B., and White, B.R., 1974: Wind tunnel studies of Martian aeolian processes, *Proc. Roy. Soc. London A*, 341: 331-336.
- Hess, S.L., 1973: Martian winds and dust clouds, *Planet. Space Sci.*, 21: 1549-1557.
- Huffman, G.G., and Price, W.A., 1949: Clay dune formation near Corpus Christi, Texas, *J. Sed. Pet.*, 19: 118-127.
- Ishihara, T., and Iwagaki, Y., 1952: On the effect of sand storm in controlling the mouth of the Kiku River, Bulletin No. 2, Disaster Prevention Research Institute, Kyoto University, Kyoto, Japan.

- Iversen, J.D., Pollack, J., Greeley, R., and White, B., 1976: Saltation threshold on Mars: The effect of interparticle force, surface roughness, and low atmospheric density, *Icarus*, 29: 381-393.
- Jackson, M.L., 1975: *Soil Chemical Analysis*, Originally published by Prentice-Hall, now published by the author, Department of Soil Science, University of Wisconsin, Madison, WI.
- Marrs, R.W., and Kolm, K.E. (Eds.), 1982: Interpretation of wind flow characteristics from eolian landforms, *Geol. Soc. Amer. Spec. Paper*, 192, 112 pp.
- Nickling, W.G. (Ed.), 1986: *Aeolian Geomorphology*, Allen and Unwin, Boston, 311 pp.
- Phillips, M., 1980: A force balance model for particle entrainment in a fluid stream, *J. Phys. D: Appl. Phys.*, 13: 221-233.
- Price, W.A., 1963: Physicochemical and environmental factors in clay dune genesis, *J. Sed. Pet.*, 33: 766-778.
- Pye, K., 1987: *Aeolian Dust and Dust Deposits*, Academic Press, London, pp. 10-28.
- Roth, E.S., 1960: The silt-clay dunes of Clark Dry Lake, California, *The Compass*, 38: 18-27.
- Ryan, J.A., 1964: Notes on the Martian yellow clouds, *Geophys. Res.*, 69: 3750-3770.
- Sagan, C., and Pollack, J., 1969: Wind blown dust on Mars, *Nature* (London), 223: 791-794.
- Vershinin, P.V., 1958: *The Background of Soil Structure*, (Pochvennaya Struktura i Usloviya ee Formirovaniya). S.I. Dolgov (Ed.), Izdatel'stvo Akademii Nauk SSSR, Moskva-Leningrad. (Translated from Russian, Israel Program for Scientific Translations, Jerusalem, 1971, 128 pp.)
- Wasson, R.J., 1983: Dune sediment types, sand colour, sediment provenance and hydrology in the Strzelecki-Smpson dunefield, Australia, In: Brookfield, M.E. and T.S. Ahlbrandt, (Eds.), *Eolian Sediments and Processes, Developments in Sedimentology*, 38, Elsevier, Amsterdam, 165-195.



Wood, G.P., Weaver, W., and Henry, R., 1974: The minimum free-stream wind for initiating motion of surface material on Mars, NASA TM X-71959, Langley Research Center, Hampton, VA.

# DUST AND CLIMATE IN THE AMERICAN SOUTHWEST

**ANTHONY J. BRAZEL**  
Laboratory of Climatology  
Arizona State University  
Tempe, AZ 85287  
U.S.A.

## 1. INTRODUCTION

The primary purpose of this paper is to present a dust climatology of the American Southwest, emphasizing data tabulation from weather sites in Arizona, discussing related issues of dust generating factors, and hypothesizing on the reasons for the variability of dust frequencies and interrelated forcing factors across the southwestern landscape. Much of this paper is from the analyses of Nickling and Brazel (1984); Brazel and Nickling (1986); Brazel, Nickling, and Lee (1986); Brazel and Nickling (1987); and Lougeay, Brazel, and Miller (1987). The major point of this review paper is to coalesce individual analyses into a synthesis of ideas, and to highlight the variability of dust generation and dust frequencies across differing environments of the American Southwest region of the Sonoran and Mojave Deserts.

## 2. THE STUDY REGION

Figure 1 shows the Southwest study region and stations for which dust frequency information is readily obtainable (Changery, 1983). Records are also available for some sites not shown, but of main concern are the Sonoran and Mojave desert areas of the region. One additional station not shown in Figure 1 in Arizona (Winslow, in the high desert country of the Colorado Plateau northeast of Prescott) will be discussed in sections on synoptic weather types and wind characteristics of dust events in Arizona.

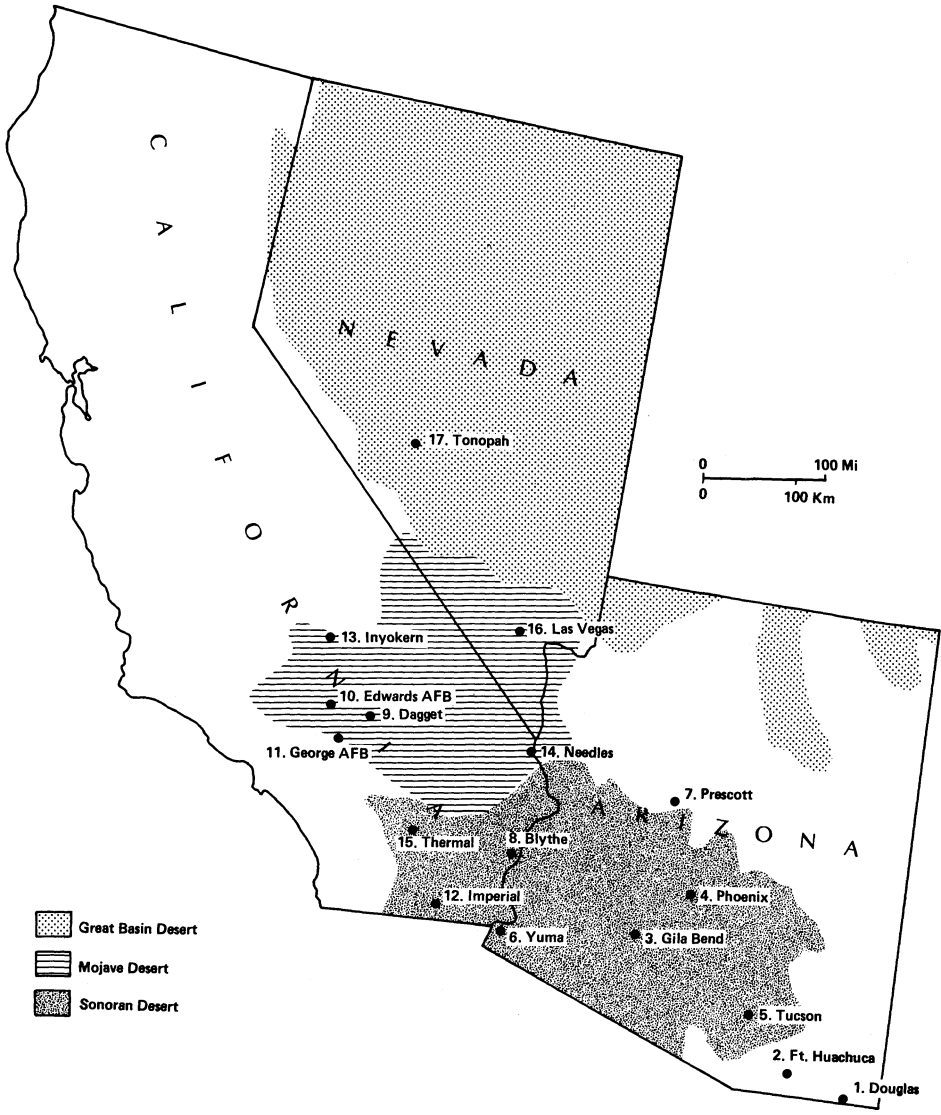


Figure 1: Station locations (coded by number, see Tables 1 and 2) which record blowing dust (after Brazel and Nickling, 1987).

A tabular summary of climate for the region is given in Table 1. Stations range from -34m to over 1500m in elevation and experience annual precipitation from less than 100 mm to over 400 mm. Average minimum temperatures are above freezing and maximums commonly exceed 25-30°C. Potential evaporation far exceeds precipitation (by 500 to 1000%). Thunderstorm probabilities associated with blowing dust range from 1-41% and indicate that the summer monsoon promotes dust processes particularly in the eastern sector of the desert region, whereas in Nevada and California blowing dust is primarily generated by cyclonic activity during winter and spring.

The surface terrain across this region is highly variable and consists of the classical basin and range topography, with over 400 mountain ranges and intervening basins evident (Dohrenwend, 1987). Correspondingly, sediment sources for blowing dust are quite variable, with large playa environments in the western portions and basin silts and clays in colluvial-alluvial deposits generally throughout the area. Ephemeral streams are widespread. Natural vegetation cover in the region is highly variable depending on elevation and precipitation sources. Very little desert vegetation cover exists in the southwestern and southcentral portions of the region.

### **3. DUST DATA USED IN THE STUDY**

Station weather records from 17 locations were accessed to identify blowing dust events in the region for the period 1948-1982. These records were obtained from Changery (1983). Detailed records of dust and weather conditions were catalogued from original surface weather observation forms for the sites in Arizona. Two major sources of dust information are the MF-10A surface weather observation forms of the National Weather Service of NOAA and the Local Climatological Data (LCD) publication of the U.S. Department of Commerce. The former form is not generally available to a researcher without extended efforts of acquisition. The latter publication can be readily obtained from state or federal climate offices.

Dust information from weather records consists of visual observations by an observer of obstructions to vision less than 11.3 km (7 miles). Details of visibility changes during a blowing dust event are logged on the MF-10A form by the observer. A key in this process is the network of visibility markers used to determine close-in degradation of visibility. Also important is the timing of the dust event relative to the routine standard hourly observation that is taken at each weather station. Consulting the

TABLE 1. Southwestern United States Climate Summary for the Sonoran-Mojave Desert Region

STATION	ELEV (m)	Precipitation † (mm)			Temp. (°C) †			EVAP* (mm)	CS (%)	Thunderstorm (%) prob*
		S	W	A	Max.	Min.				
(1) Douglas	1249	204	105	309	25.4	7.4	1143	48	25	
(2) Ft. Huachuca	1422	222	101	323	23.9	9.7	1016	18	13	
(3) Gila Bend	224	56	92	148	31.6	13.4	1143	283	35	
(4) Phoenix	340	66	115	181	29.5	14.1	1143	88	34	
(5) Tucson	788	153	125	278	27.6	12.3	1067	143	41	
(6) Yuma	63	21	46	67	31.0	15.4	1397	485	7	
(7) Prescott	1679	219	260	479	20.4	2.9	940	10	27	
(8) Blythe	120	31	55	86	30.6	15.3	1778	502	12	
(9) Daggett	584	30	67	97	24.0	9.3	1448	975	3	
(10) Edwards AFB	702	5	135	140	24.4	7.8	1397	172	2	
(11) George AFB	879	0	129	129	23.9	8.9	1524	225	4	
(12) Imperial	-20	18	46	64	30.9	14.7	1270	445	3	
(13) Inyokern	699	10	93	103	26.1	10.0	1270	312	1	
(14) Needles	278	39	73	112	29.7	15.4	1651	135	18	
(15) Thermal	-34	18	54	72	31.1	13.7	1397	483	2	
(16) Las Vegas	659	38	68	106	26.2	11.3	1346	573	10	
(17) Tonopah	1654	50	74	124	18.9	2.2	1016	140	4	

† Data from U.S. Department of Commerce, U.S. Air Force Weather Service and Brazel, *et al.* (1981)

S = summer (June - Sept); W = winter (Oct. - May); A = annual

• Data from Farnsworth, *et al.* (1982)

§ Data from Lyles (1983)

\* Thunderstorm probabilities from Changery (1983)

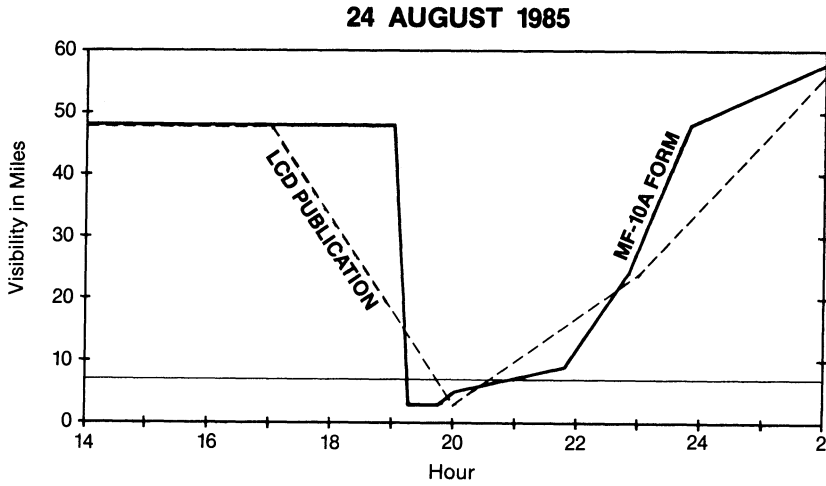


Figure 2a: Sample of Local Climatological Data Publication and MF-10A Form of the National Weather Service recording of August 24, 1985 dust event at Phoenix, AZ by listing and visibility values.

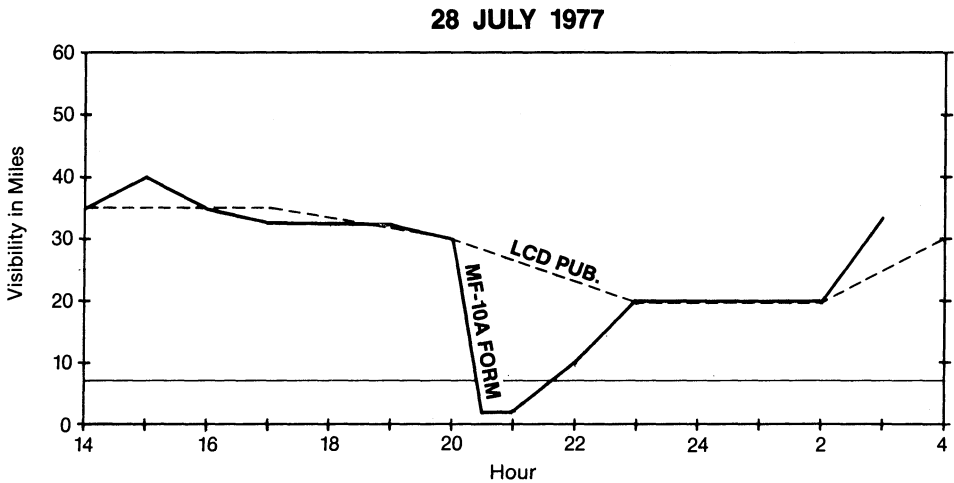


Figure 2b: Sample of MF-10A Form identification of blowing dust event at Phoenix, AZ for July 28, 1977. The LCD publication omitted this event.

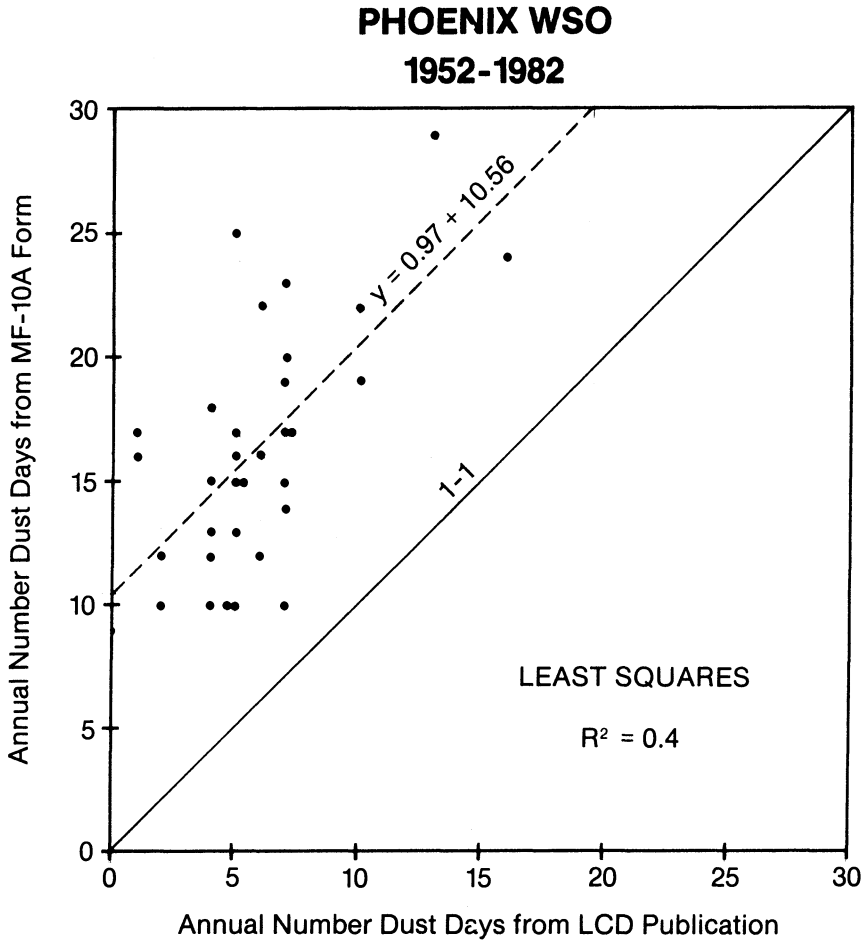


Figure 3: Correlation of dust day identification from the LCD and MF-10A Form summaries, for Phoenix, AZ, 1952-1982.

**TABLE 2. Southwestern United States Dust Event Summary†**

STATION	FREQUENCY PER YEAR		
	11.3 km	1 km	Ratio (1 km/11.3 km)
(1) Douglas	1.8	0.1	0.06
(2) Ft. Huachuca	0.9	0.3	0.33
(3) Gila Bend	10.8	2.1	0.19
(4) Phoenix	18.1	1.6	0.08
(5) Tucson	3.8	0.3	0.08
(6) Yuma	23.9	4.7	0.19
(7) Prescott	0.5	0.03	0.06
(8) Blythe	12.7	3.0	0.23
(9) Daggett	9.1	1.2	0.13
(10) Edwards AFB	20.3	5.0	0.25
(11) George AFB	13.0	3.0	0.23
(12) Imperial	22.8	2.5	0.11
(13) Inyokern	8.0	1.8	0.22
(14) Needles	2.8	0.2	0.07
(15) Thermal	35.6	5.1	0.14
(16) Las Vegas	13.2	3.6	0.27
(17) Tonopah	2.0	0.2	0.10
Mean	12.0	2.1	0.16

† Data from Changery (1983)



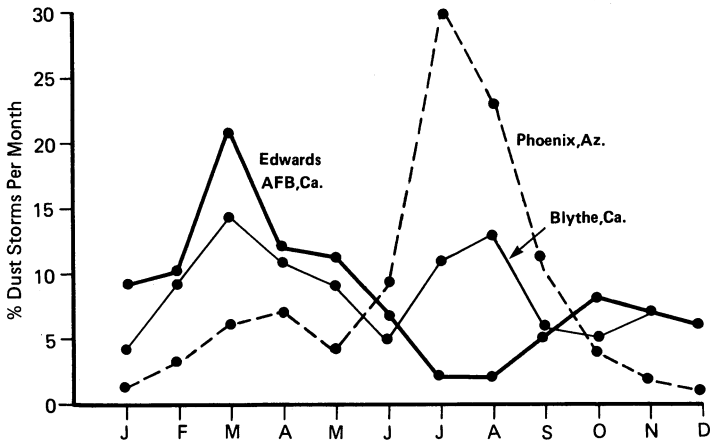


Figure 4: Percentage of dust events (vis. < 11.3 km) by month in a transect across the southwestern U.S.A. (after Brazel and Nickling, 1987).

abbreviated LCD dust data source for the identification of frequencies of blowing dust may skew results. Many events are not shown in this source, although they are captured by referring to the original MF-10A forms. Figures 2a, 2b, and Figure 3 show an illustration of this problem. For August 24, 1985 in Phoenix, a dust event is indicated in both sources and the visibility drops well below 7 miles (visibility is plotted directly from the data in the MF-10A and LCD). However, for July 28, 1977 the MF-10A data indicates a dust event occurred, while the LCD data do not. An analysis of the 1952-1982 period (in reference to both MF-10A and LCD dust event detection for Phoenix) indicates a low correlation between the two sources and a very large absolute difference in frequencies between the two sources (Fig. 3). One must also remember, of course, that both sources of information omit the detection of blowing dust events which may affect visibility but do not drop the values below 7 miles.

The data from Changery (1983) and for Arizona (Nickling and Brazel, 1984) were extracted from the more detailed records of the MF-10A forms. The data, however, only capture the more severe blowing dust conditions around a particular site. Intervening areas and more mild events are not sampled adequately at present with the available network of stations in the region. Historical dust records from these stations, therefore, have limited value in any analysis.

#### 4. REGIONAL VARIABILITY OF DUST

Table 2 displays an annual summary of dust frequencies for the 17-station network shown in Figure 1. Two frequency values are shown for each station: (1) frequency of events that impair visibility to less than 11.3 km, and (2) frequency of events that reduce visibility to less than 1 km (the international definition of the threshold that can be labeled a dust storm, Goudie, 1983). The annual mean frequency for the entire region attains a value of 12.0 and 2.1, respectively. However, note considerable variation among sites, ranging from 0.5 to 35.6 (11.3 km) and 0.03 to 5.1 (1 km). Some of this variation relates to the nature of individual site attributes and some to differences in atmospheric effects. The higher ratios of 1 km/11.3 km blowing dust events might suggest more frequent intense storms when they do occur and/or higher concentrations of dust per event.

In addition to the spatial variation of dust frequencies throughout the region, the timing of frequent blowing dust incidences during the year differs from place to place. Figure 4 illustrates monthly frequencies of blowing dust from west (Edwards Air Force Base, California), to central

(Blythe, California), to east (Phoenix, Arizona) across the study region. These data reflect the dominant synoptic controls. Note the shift from frequent winter/spring blowing dust in the west to the summer monsoon-related peak frequencies experienced in the east. Blythe, California lies in a transitional location where equal frequencies occur in winter and summer.

Raw frequencies per month shadow another important, variable characteristic of dust in the region. Table 3 illustrates two frequencies that are considerably different in some cases: (1) the percent of events occurring in a month, and (2) the percent of the time that blowing dust occurs. This latter characteristic includes the concept of duration time of blowing dust. In general, the more frequent the events are for a month, the longer the total time of blowing dust for that month. This would be particularly true if the same kind of storm consistently led to blowing dust events. However, for Yuma, Arizona (as indicated in Table 3), the month with the most frequent dust events is not the month with the longest duration of time of blowing dust. In August, 27% of all dust events occur. However, the percent of time blowing dust is observed is highest in April due to sustained cyclonic wind activity. During summertime short duration thunderstorm activity causes blowing dust to occur for only minutes in some cases. Note that to a lesser extent, the same can be said for Phoenix dust regimes. Even for Tucson the month with the highest frequency does not match the month with the longer time of blowing dust.

## 5. ROLE OF WEATHER TYPES IN DUST GENERATION

Weather types should play a significant role in dust generation, dust frequencies, and % time of blowing dust during various seasons and on an annual basis. Tables 4 and 5 list characteristics of dust events and weather types associated with dust events for selected stations in Arizona. An analysis by Brazel and Nickling (1986) of dust events for the period 1965 to 1980 included identification of 5 major synoptic types (see footnote of Table 5) associated with dust generation at major weather stations. Type 1 is subdivided into pre-frontal (1B) and post-frontal (1A) blowing dust. The thunderstorm type (2) requires much further subdivision based on an understanding of a mesoscale convective system, which we do not have. In Table 4 the mean time of occurrence, wind direction (in degrees), degradation rate of visibility from 11.3 to 1.6 km during an event (labeled Delta Time [min]), and event duration (min) are listed. These data are organized by the five synoptic conditions. In addition, Table 5 presents the total number of dust events by synoptic type (Dust) and the total number of that synoptic type whether dust was observed or not (Tot).

TABLE 3. Seasonal dust, % per month, and % time observed for Yuma, Phoenix, and Tucson, Arizona

MONTH	YUMA		PHOENIX		TUCSON	
	% per Month	% Time Blowing Dust	% per Month	% Time Blowing Dust	% per Month	% Time Blowing Dust
JAN	3	.12	0	.00	0	.00
FEB	3	.11	1	.02	0	.00
MAR	6	.18	1	.01	0	.00
APR	17	.28	3	.13	0	.00
MAY	6	.17	6	.03	9	.01
JUN	3	.03	8	.05	37	.01
JUL	18	.08	28	.15	27	.02
AUG	27	.17	35	.20	27	.01
SEP	12	.21	15	.15	0	.00
OCT	0	.00	2	.00	0	.00
NOV	2	.03	1	.01	0	.00
DEC	3	.10	0	.00	0	.00

\* Relative to less than 1.6 km visibility obstruction, as defined in Nickling and Brazel (1984)

TABLE 4. Synoptic and Event Characteristics of Blowing Dust for Yuma, Phoenix, Tucson, and Winslow, Arizona 1965-1980 (After Brazel and Nickling, 1986)

TYPE	n	YUMA				PHOENIX				TUCSON				WINSLOW							
		Time (h)	Direction (degrees)	$\Delta$ Time (min)	Duration (min)	n	Time (h)	Direction (degrees)	$\Delta$ Time (min)	Duration (min)	n	Time (h)	Direction (degrees)	$\Delta$ Time (min)	Duration (min)	n	Time (h)	Direction (degrees)	$\Delta$ Time (min)	Duration (min)	
<i>Intense dust storms</i>																					
1A	9	1325*	250 (410)†	140 (117)	208 (172)	2	1389	260	42	78	0	—	—	—	—	1	0858	190	28	140	
1B	13	1622	291 (378)	299 (20)	428 (254)	5	1534 (942)	204 (91)	132 (102)	229 (220)	0	—	—	—	—	10	1159	223	124	240	
2	25	1439	140 (748)	140 (87)	75 (63)	57	1834 (431)	129 (79)	9 (19)	54 (37)	7	1813 (144)	106 (46)	4 (4)	17 (17)	6	1616 (169)	165 (99)	4 (5)	31 (27)	
3	2	1439	110	16	258	2	1847	150	26	75	2	1715	110	14	13	0	—	—	—	—	
4	2	1459	240	125	218	5	1708	238	23	32	2	1530	110	9	12	0	—	—	—	—	
										<u>71</u>						<u>11</u>				<u>17</u>	
<i>Moderate to weak dust storms</i>																					
1A	30	1427	283 (512)	—	138 (102)	1	1646	340	—	54	0	—	—	—	—	2	1315	160	—	373	
1B	51	1228	283 (675)	—	248 (197)	9	1507 (672)	260 (35)	—	135 (82)	4	1118	233	—	261	11	1138 (495)	236 (49)	—	239 (191)	
2	19	1122	167 (927)	—	106 (70)	28	1637 (703)	167 (67)	—	57 (72)	0	—	—	—	—	0	—	—	—	—	
3	1	2140	260	—	95	0	—	—	—	—	0	—	—	—	—	0	—	—	—	—	
4	12	1619	270 (782)	—	214 (84)	3	1631	227	—	103	0	—	—	—	—	0	—	—	—	—	
						<u>41</u>										<u>4</u>				<u>13</u>	

\* Mean

† Standard deviation where appropriate

TABLE 5. Weather Types Associated with Blowing Dust (Dust) and all Weather Events (Tot.) by Station (Dust/Tot. relates ratio of number of dust events to all events, coded by weather typed)

ANNUAL PRECIPITATION (mm)	YUMA 67		PHOENIX 180		TUCSON 278		WINSLOW 194		FOUR STATION MEAN 180	
	Dust	Tot.	Dust	Tot.	Dust	Tot.	Dust	Tot.	Dust	Tot.
Weather	Dust	Tot.	Dust	Tot.	Dust	Tot.	Dust	Tot.	Dust	Tot.
1 A & B	103	404	17	463	4	432	24	584	37	470
2	44	80	85	304	7	544	6	528	36	364
3	14	176	8	176	2	176	0	176	24	704
4	3	16	2	16	2	16	0	16	7	65
All types	164	676	112	959	15	1168	30	1304	80	1027
			Dust/ Tot.	Dust/ Tot.	Dust/ Tot.	Dust/ Tot.	Dust/ Tot.	Dust/ Tot.	Dust/ Tot.	Dust/ Tot.
			0.25	0.04	0.04	0.01	0.04	0.04	0.04	0.08
			0.55	0.28	0.28	0.01	0.01	0.01	0.01	0.10
			0.08	0.05	0.05	0.01	0.01	0.00	0.00	0.00
			0.19	0.13	0.13	0.13	0	0.00	0.00	0.11
			0.24	0.12	0.12	0.01	0.01	0.02	0.02	0.08

1A & B = Frontal type  
 2 = Thunderstorm/convective type  
 3 = Tropical disturbance type  
 4 = Upper level/cutoff low type

If synoptic forcing were the only control on dust generation and dust frequencies, the ratio of Dust/Tot should remain relatively constant among all sites. Of the Arizona sites Yuma has the highest ratios of Dust/Tot followed by Phoenix, Winslow, and Tucson. Ratios are inversely related to the total annual number of synoptic weather events at respective sites. Therefore, dust storms are not generated simply because a localized region experiences a higher number of synoptic events during a year than other locales. Instead, the four sites rank directly in order with the annual precipitation of respective sites; that is, the drier the location, the higher the ratio. Despite similarities in synoptic conditions, the local pressure gradients for a given event may not be sufficient to generate winds of a high enough velocity to initiate sediment transport. Beyond the immediate scope of this paper is the issue of within-type variance of surface wind fields associated with the general synoptic types identified for the region. The western sectors of the study region, areas of more winter generation of dust, have not yet been analyzed in the manner of the Arizona sites. In the eastern areas of the region, summer convective patterns are more influential in dust generation.

A further test of the importance of interannual variability in synoptic conditions related to dust generation over time can be achieved by examining the Circulation Index of Carleton (1987). Carleton developed several indices of circulation for the period 1945 to 1985 by analyzing daily surface and 500 mb weather maps. He performed a synoptic classification exercise yielding summer synoptic types. Some of these types were associated with major "bursts" in the summer monsoon period in Arizona. Others were correlated with "breaks" in the flow of monsoon air. Usually, burst periods are characterized by massive mesoscale convective system development and imbedded thunderstorm activity. Often dust storms accompany these outbreaks. The break periods are lulls in the action. Carleton (1987) found that upon northward expansion of the Bermuda High Pressure Ridge, more burst activities occurred in Arizona. His index relates the ratio of anticyclonic (wet) to anticyclonic (dry) synoptic types as influenced by the latitudinal location of centers of ridging activity in summer (Fig. 5a). This ratio varied from less than 0.2 to over 7.0 during the 1945 to 1985 period. The time series of this index was random according to Carleton, 1987. Dust frequencies by year for Yuma and Phoenix (Figs. 5b and 5c) were correlated with this index as a test of the sole importance of large-scale synoptics on interannual variability of dust generation. For Phoenix, an  $r^2$  value of 0.0341 was obtained; for Yuma, a value of only 0.0995. Also, annual dust frequencies correlated between Phoenix and Yuma attained an  $r^2$  value of only 0.183. None of these  $r^2$  values are significant at the 95% confidence level. From this analysis and that of Nickling and Brazel (1986),

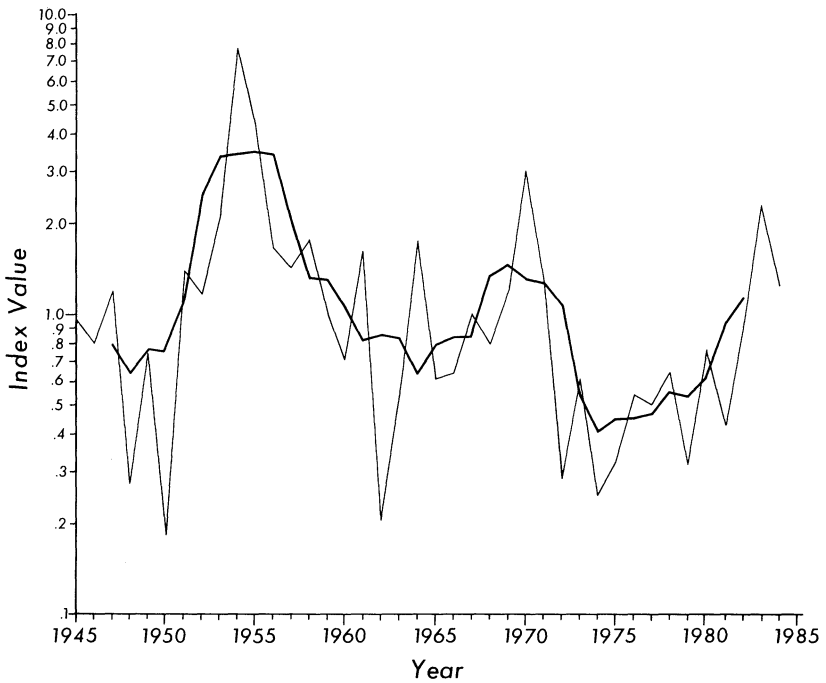


**Figure 5a:** Annual and five-year moving averages of the Carleton circulation index for the 1945-84 summers (see text for explanation; after Carleton, 1987). High values indicate burst activity leading to high winds and thunderstorms.



### Annual Dust Events Yuma, Arizona

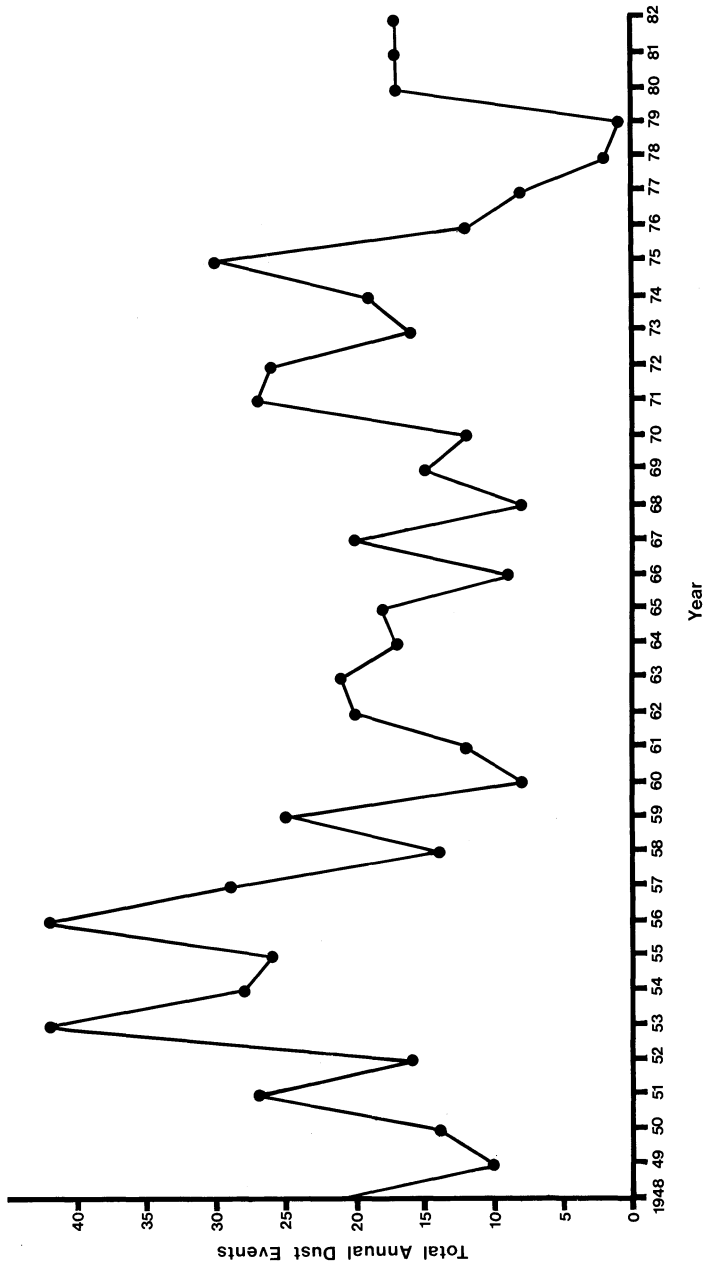


Figure 5b: Time series of Yuma, Arizona annual dust events, 1948-1982.

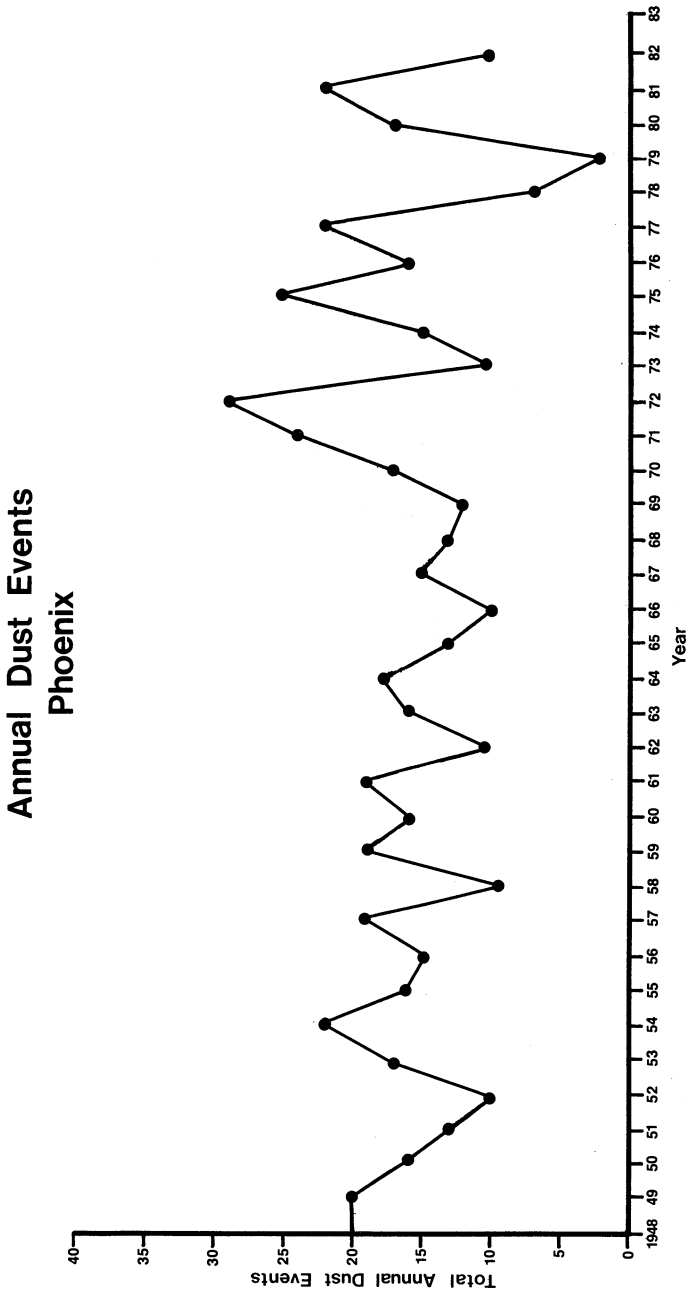


Figure 5c: Time series of Phoenix, Arizona annual dust events, 1948-1982.

dust event frequencies across the study region do not appear to be solely predictable by large-scale parameters of the general circulation, nor even by thunderstorm frequencies, although some general correspondence is indicated.

## 6. ROLE OF ANNUAL AND SEASONAL MOISTURE

Surficial conditions, both annually and seasonally, control dust generation (Chepil, *et al.*, 1962; Gillette, *et al.*, 1982; Kimberlin, *et al.*, 1977; Lyles, 1983; Nickling, 1984; and Pewe, 1981). Goudie (1978 and 1983), Middleton (1984), and others have illustrated a moderate correlation of annual dust frequencies with precipitation. Table 6 lists the results of a regression and correlation analysis of sites within and near Arizona. Interannual variations of precipitation and dust frequencies have a low correlation. A mean spatial correlation of these two parameters is stronger (see Fig. 6). The mean conditions of moisture over the long term at a location do indeed attain a statistically significant correlation with mean frequencies (e.g., Goudie, 1978 and 1983; Middleton, 1984). However, surface conditions, such as crusting effects and variable year-to-year percent cover of vegetation, apparently decreases this mean regional correlation when an interannual timeframe is analyzed.

A search for a link between moisture and dust frequencies over short time periods (less than a year) assists in the understanding of dust generation, restricted in this case to the eastern portions of the study area (i.e., primarily Arizona). Two straightforward analyses were performed: (1) moisture and dust correlations on a seasonal basis, and (2) short-term antecedent relationships (daily) between dust frequencies and precipitation.

Addressing the second point first, a measure of the significance of antecedent conditions on blowing dust is the comparison of antecedent precipitation as recorded at a station prior to dust events with conditions prior to non-dust days chosen at random from the population of summer days as a whole. Seventy days were chosen at random from the Phoenix weather records as well as 70 dust days from the period 1948 to 1980. A calculation of antecedent dryness was performed on these two data sets (how far back in time to precipitation of various magnitudes). Several levels of moisture amounts prior to both dust days and non-dust days were analyzed. A non-parametric Kolmogorov-Smirnov test, using a Chi-Square test statistic at a 0.05 level of significance was used to determine if the two antecedent dryness data sets were significantly different. The data sets were composed of a 1-to-30 day antecedence data set and a 30-to-180 day

TABLE 6. Correlation of Annual Precipitation (calendar year) and Frequency of Dust Events at Selected Sites

SITE	$r^2$ †	Intercept	Slope	Std. Error	Precip. (mm)	N	Events/Year
(1) Douglas	0.02	0.92	0.056	1.58	309	29	1.8
(4) Phoenix	0.09	19.67	-0.589	5.46	181	36	18.1
(5) Tucson	0.04	13.74	-0.839	6.18	278	35	9.2
(6) Yuma	0.14	24.86	-2.406	8.88	67	35	23.9
(7) Prescott	0.00	0.63	-0.008	0.69	479	29	0.5
(8) Blythe	0.06	13.74	-0.839	5.46	86	29	12.7
(14) Needles	0.00	2.99	-0.131	3.44	112	27	2.8

† All  $r^2$  values are insignificant at the 0.05 level of significance.

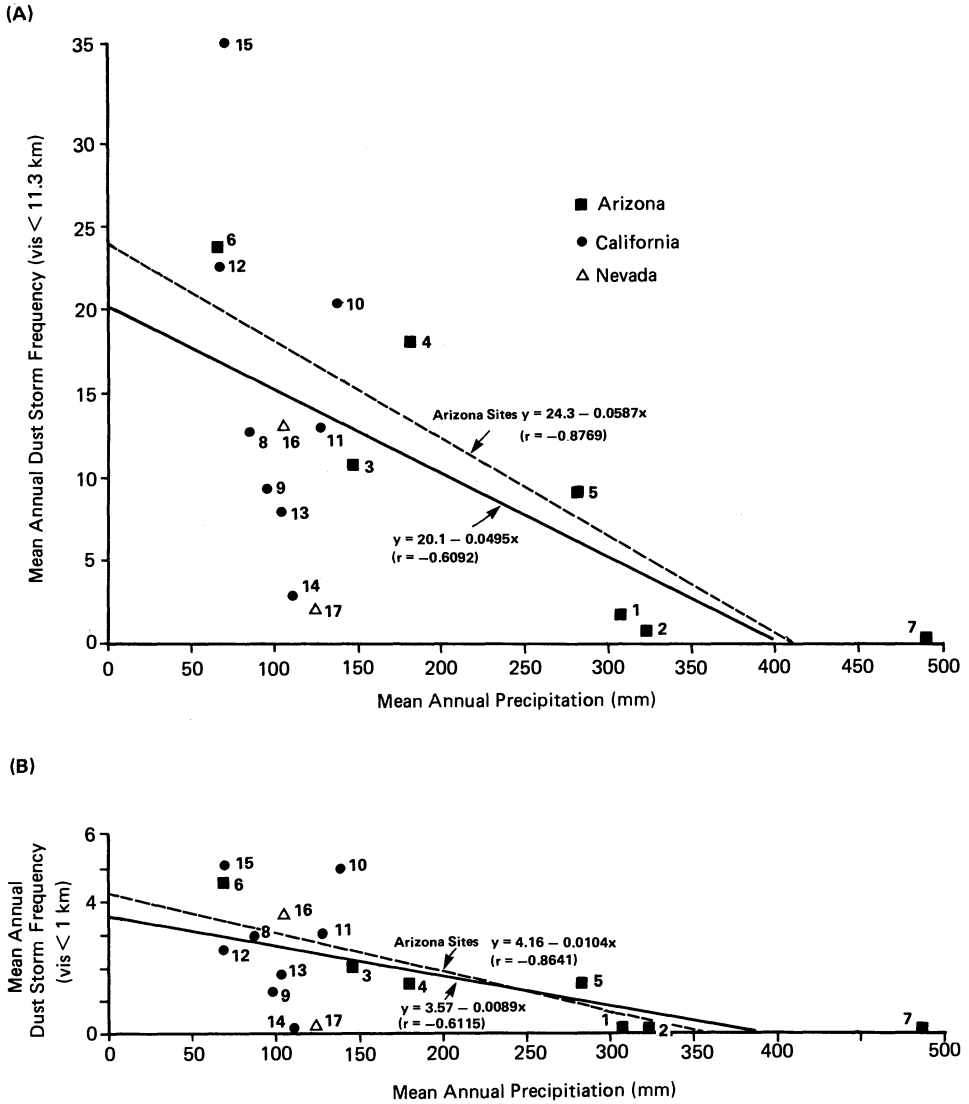


Figure 6: Mean annual precipitation (calendar year) in mm versus dust storm frequency for: (A) visibility less than 11.3 km, and (B) visibility less than 1 km across the study region. Arizona, California, and Nevada (after Brazel and Nickling, 1987).

antecedence data set. Results suggest that there was no significant difference at both these time scales in the timing of antecedent precipitation for non-dust days and dust days.

Part of the problem is the erroneous nature of point rainfall evaluated for a station and used to represent what really should be a "spatial zone, or dust source" antecedent moisture value. At present, the weather network is not adequate to capture such zones or source areas, unless they are immediately around a site. Figure 7 illustrates the drop in correlation between the single Phoenix station antecedent dryness time period and an aggregate antecedent length from a network of stations surrounding Phoenix (approximately 100 km radius). For low daily rainfall totals (e.g., 0.05 inches), Phoenix station dryness prior to dust events correlates well with the larger region. For intense, more significant rainfall correlations are low. Beyond about 25 km, Phoenix antecedent dryness length has no statistically significant correlation with the surrounding region in summer. These findings are typical of the eastern monsoon summer regions of the Sonoran desert.

Longer term antecedence reveals a clearer picture of moisture controls on dust frequencies. Figure 8 shows for Yuma and Phoenix regionally averaged Palmer Drought Severity Index (Palmer, 1965; Karl and Knight, 1985) correlations with dust frequencies. The prior November to April mean PDSI correlates significantly with dust frequencies for the year (January to December). Ten stations in Figure 1 were tested for this relationship, using mean PDSI winter values as the independent variable (PDSI values are for large areas surrounding each site) and annual dust frequencies as the dependent variable. Six of the sites have such low frequency values that they were eliminated from this analysis (Douglas, Ft. Huachuca, Tucson, Prescott, Needles, and Tonopah). The  $r^2$  values developed ranged from over 0.38 to virtually zero across the network of sites. Table 7 lists the ranks of the  $r^2$  values and the corresponding sites. Note that  $r^2$  values are progressively lower from the eastern sectors of the region to the western zones of the Sonoran and Mojave desert. The exact explanation for this systematic progression is unclear. One hypothesis may relate to initiation of a wet winter development of substantial vegetation cover on the surface of the desert that may persist (even in stubble form) into the moist monsoon summer season of the eastern zones of the Sonoran region. This cover provides a mechanism for dust suppression over widespread areas and surfaces prone to blowing dust. Lougeay, Brazel, and Miller (1987) have suggested this process in analysis of Central Arizona MSS Landsat data for very dry and very wet years.

***r* DECAY OF PHOENIX WSO VERSUS SURROUNDING STATIONS FOR ANTECEDENT DRYNESS RELATIVE TO STATED PRECIPITATION VALUE.**

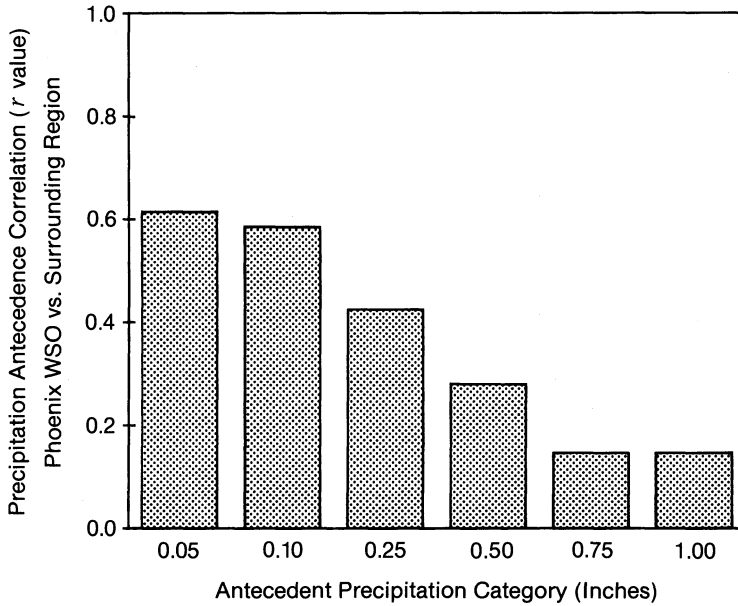
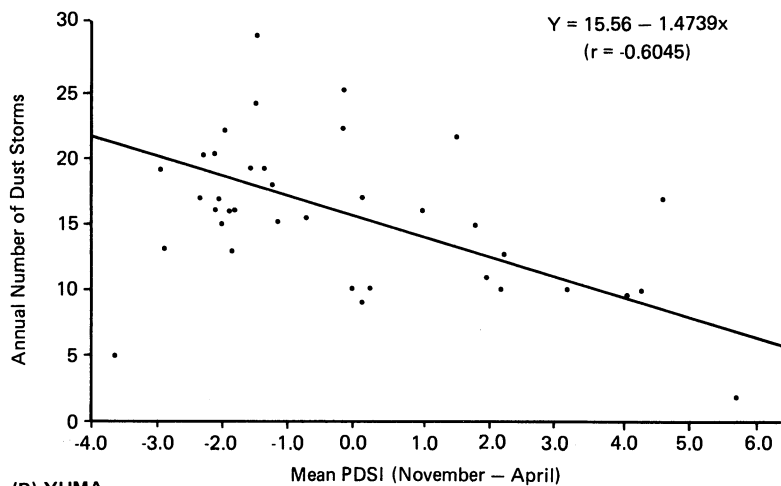


Figure 7: Antecedent dryness by precipitation category for Phoenix, WSO versus surrounding stations within 100 km of Phoenix, AZ.

## (A) PHOENIX



## (B) YUMA

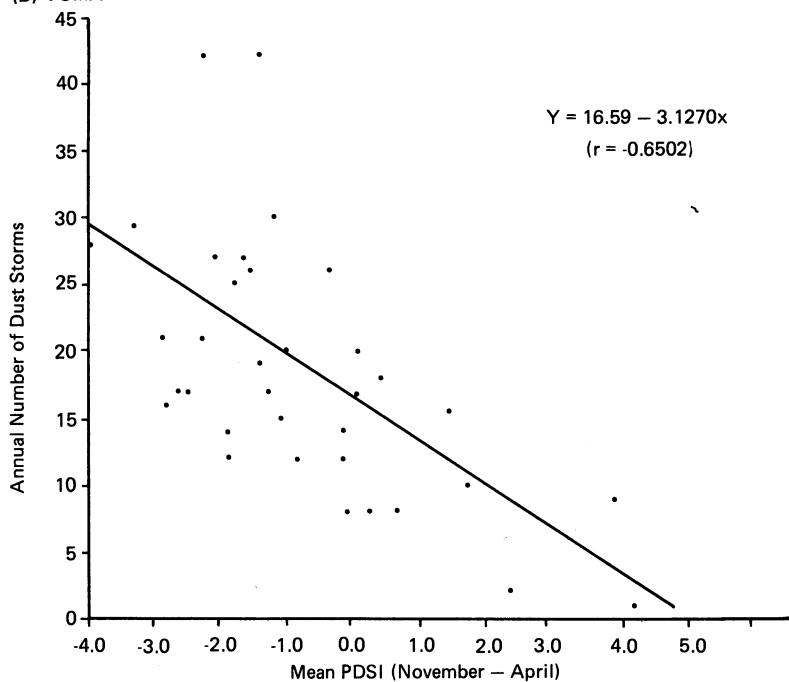


Figure 8: Mean Palmer Drought Severity Index (for the period November-April each year) versus frequency of dust events per year for: (A) Phoenix, and (B) Yuma, AZ (after Brazel and Nickling, 1987).



**Table 7: Correlation of PDSI (November-April) with annual dust frequencies (January-December) for ten selected stations in Figure 1.**

Site	$r^2$ Values
Yuma	0.38
Phoenix	0.36
Blythe	0.26
Las Vegas	0.21
Inyokern	0.14
Edwards	0.08
Daggett	0.08
Imperial	0.06
George	0.04
Thermal	0.00

\* The top four places, all in the central and eastern portions of the region, attain significant  $r^2$  values at the 95% confidence level. All others show no statistical significance at the 95% confidence level.

The clearest signal from analysis of antecedent moisture is a winter season moisture control on subsequent annual dust frequencies. However, this finding is restricted spatially to specific zones of the study region — primarily the summer monsoon dust regions of the central to eastern Sonoran desert. Processes of winter dust generation in the playa environments of the Mojave Desert (for example) also relate to more complex factors of surface crusting, saltation, and surficial disturbances (Cahill, 1984; Gillette, *et al.*, 1978 and 1982).

## 7. WIND CHARACTERISTICS OF DUST STORMS

Wind characteristics and threshold wind velocities for various surface types have been extensively studied (e.g., Gillette, *et al.*, 1972, 1974, 1982; Nickling, 1978; Nickling and Gillies, 1986). An example of threshold values is shown in Table 8 after Clements, *et al.*, (1963) and Nickling and Gillies (1986) for various surface types in the Southwest. An example of the variable wind characteristics associated with Arizona dust events is illustrated in Figure 9. Wind frequency data for the Arizona sites for all hours indicate that speeds in excess of 5-15 m/s occur between 12 to less than 1.0 % of the time (Andersen, *et al.*, 1981). However, dust events occur with high winds only 0.05-1.5 % of the time (see Table 3). Thus, even when thresholds are attained or even exceeded, blowing dust may not occur.

Mean and peak gust wind speeds for dust events were analyzed for Yuma, Phoenix, Tucson, and Winslow. Mean speeds are 9.0, 11.0, 15.0, and 15.5 m/sec, respectively. Mean peak gusts are 16.8, 17.8, 21.2, and 22.3 m/sec, respectively. For reference, mean cumulative frequencies for eight Western Sahara sites recently investigated by Helgren and Prospero (1987) are shown in Figure 9 in addition to the data for Arizona. The mean speeds associated with dust events in Arizona range from 9.0 to 15.5 m/sec, and in general, exceed those for the Western Sahara. However, Yuma values very closely approximate those of the Sahara sites.

The values for Yuma and Phoenix exceed stated threshold wind speeds for alluvial fans (loose), partially formed desert pavement, dry washes, sparsely vegetated desert flats, mine tailings (not near each of these places in this case), abandoned land, and disturbed desert surfaces. Thus, sources of blowing dust are highly variable depending on wind direction and distances to source areas. Most of these surface types exist nearby these two sites.

**Table 8: Wind Threshold Values for Type Surfaces in the Southwest (after Clements, *et al.*, 1963 and Nickling and Gillies, 1986).**

Surface Type	Threshold Speed (m/sec)
Mine Tailings	5.1
River Channel	6.7
Abandoned Land	7.8
Desert Pavement, Partly Formed	8.0
Disturbed Desert	8.1
Alluvial Fan, Loose	9.0
Dry Wash	10.0
Desert Flat, Partly Vegetated	11.0
Scrub Desert	11.3
Playa (dry lake) Undisturbed	15.0
Agriculture	15.6
Alluvial Fan, Crusted	16.0
Desert Pavement, Mature	>16.0

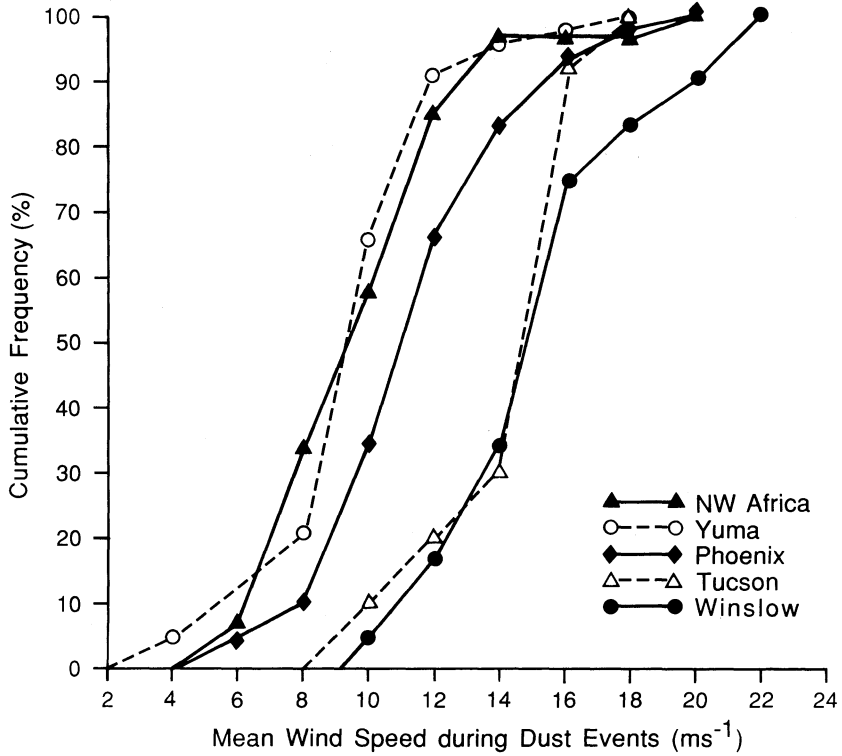


Figure 9: Cumulative frequencies of dust event mean wind speeds for NW Africa (after Helgren and Prospero, 1987), Yuma, Phoenix, Tucson, and Winslow, AZ.

Agriculturally induced dust storms during the mid-summer period are unlikely due to irrigation practices and the high threshold velocities required, as indicated by the data of Nickling and Gillies (1987).

For Tucson and Winslow, mean speeds during dust events are higher. These sites are more typical of scrub desert terrain with substantial vegetation cover. The results presented here for mean speeds and peak gust values follow closely the analysis of Hall (1981). Hall also suggests that mean speeds for these two sites coincide with threshold values for undisturbed surfaces in an analysis of the data from 1940 to 1950. The more recent data suggest lower mean speeds during dust events and closer to threshold values for disturbed surfaces. Thus, Hall implies a long-term increased anthropogenic effect on dust generation may be evidenced in the dust frequency and wind records for these two sites. This long-term, increased anthropogenic effect has not been investigated for the other sites.

Considerable spatial variability of mean speeds associated with dust events is seen from these data. Part of this variability may be attributed to spatial differences in storm dynamics. This point remains as a major research objective. Note, however, that the ranking of the speeds follows the environmental moisture and vegetation cover gradient among sites (see Fig. 9).

## 8. CONCLUSIONS

Data are available on dust event frequency and climatic characteristics of the Sonoran and Mojave desert regions of the Southwest, U.S.A.. Although the dust/weather record indeed has limitations in understanding dust emission rates, dust source areas, and system control factors, insights still can be achieved of the relative importance of various controlling factors on dust generation.

In this study, long-term records reveal the spatial and temporal complexity of dust generation within relatively small regions of the desert environment. Mean annual and seasonal dust frequency patterns across the Southwest correspond to dominant synoptic and moisture controls. However, temporal variability of dust frequencies among sites appears to show some correspondence to the interannually variable vegetative cover, crusting effects, and possible anthropogenic effects over time.

More detailed dynamic and synoptic climatic research, historical land surveys, research on vegetative distributions, and anthropogenic disturbance effect identification are required to fully explain changes in dust storm activity both geographically and through time. All of these processes cannot be adequately modeled at present solely with historical weather records of visibility. The analysis using the meteorological data base yields still a significant degree of unexplained variance in the variability of dust generation from place to place and through time across the desert Southwest.

## ACKNOWLEDGEMENTS

I am indebted to my co-author on much of this research, Dr. William G. Nickling, Department of Geography, University of Guelph, Ontario. This research was made possible through grants from Arizona State University (Provost Research Fund), Arizona Department of Transportation (Contract # N-800-251), National Science and Engineering Research Council of Canada (Dr. Nickling, Grant A7427), and the National Science Foundation (Dr. R. Lougeay, Grant # SES-8407587). The following people helped in field and/or data analysis: H. Bulk, J. Gillies, V. Gobel, S. Kelly, R. Kelly, A. Marcus, T. Miller, K. Nast, and M. Puddister.

## REFERENCES

- Andersen, S.R., Barchet, W.R., Elliott, D.L., Freeman, D.L., George, R.L., and Hadley, D.L., 1981: WIND ENERGY RESOURCE ATLAS, Volume 8 - The Southern Rocky Mountain Region, Prepared by ERT/Western Scientific Services, Inc. for Pacific Northwest Laboratory, Richland, Washington, 166 pp.
- Brazel, A.J., Quinn, J.A., McQueen, J.D., Catalano, J.A., and Chico, T., 1981: Final Report Arizona Climate Inventory, v. 1, Aero Comp., Inc., BLM Contract YA-553-CT1-1021.
- Brazel, A.J., and Nickling, W.G., 1986: The relationship of weather types to dust storm generation in Arizona (1965-1980), *J. Climatology*, 6: 255-275.
- Brazel, A.J., Nickling, W.G., and Lee, J., 1986: Effect of antecedent moisture conditions on dust storm generation in Arizona, *In: Nickling, W.G., Ed., Aeolian Geomorphology*, Allen & Unwin Press, pp. 261-271.

- Brazel, A.J., and Nickling, W.G., 1987: Dust storms and their relation to moisture in the Sonoran-Mojave Desert Region of the southwestern United States, *J. Environ. Mgmt.*, 24: 279-291.
- Cahill, T.A., 1984: Study of particulate episodes at Mono Lake, Final Report to the California Air Resources Board, Contract No. A1-144-32, 16 pp.
- Carleton, A.M., 1987: Summer circulation climate of the American southwest, 1945-1984, *Annals of the Association of American Geographers*, 77, No. 4: 619-634.
- Changery, M. J., 1983: A dust climatology of the western United States, Prepared for the Division of Health, Siting, and Waste Management Office, Nuclear Regulatory Commission, National Climatic Data Center, Asheville, NC, 25 pp.
- Chepil, W.S., Siddoway, F.H., and Armburst, D.V., 1962: Climatic factor for estimating wind erodibility of farm fields, *J. Soil and Water Conservation*, 17: 162-165.
- Clements, T., Mann, J.F., Jr., Stone, R.O., and Erymann, J.L., 1963: A study of windborne sand and dust in desert areas, Tech. Report ES-8, U. S. Army Natick Laboratories, Earth Science Division, 61pp.
- Dohrenwend, J.C., 1987: *Basin and range in geomorphic systems of North America*, (Ed. W. L. Graf), Centennial Special Volume 2, The Geological Society of America, pp. 303-342.
- Farnsworth, R.K., Thompson, E.S., and Peck, E.L., 1982: Evaporation Atlas for the Contiguous 48 States, NOAA Technical Report NWS 33, Office of Hydrology, National Weather Service, Washington, DC.
- Gillette, D.A., Blifford, I.H. , Jr., and Fenster, C.R., 1972: Measurements of aerosol size distributions and vertical fluxes of land subject to wind erosion, *J. App. Met.*, 11: 977-987.
- Gillette, D.A., Blifford, I.H., and Fryrear, D.W., 1974: The influence of wind velocity on the size distribution of aerosols generated by the erosion of soils, *J. Geo. Res.*, 79, 4068-4075.
- Gillette, D.A., Clayton, R.N., Mayeda, T.K., Jackson, M.L. , and Sridhar, K., 1978: Tropospheric aerosols from some major dust storms of the southwestern United States, *J. App. Met.*, 17: 832-845.

- Gillette, D. A., Adams, J., Muhs, D., and Kihl, R., 1982: Threshold friction velocities and rupture moduli for crusted desert soils for the input of soil particles into the air, *J. Geo. Res.*, 87: 9003-9015.
- Goudie, A.S., 1978: Dust storms and their geomorphological implications, *J. Arid Environments*, 1: 291-310.
- Goudie, A.S., 1983: Dust storms in space and time, *Prog. Phys. Geography*, 7: 502-530.
- Hall, F.F., Jr., 1981: Visibility reductions from soil dust in the Western U. S., *Atmo. Environment*, 15: 1929-1933.
- Helgren, D.M., and Prospero, J.M., 1987: Wind velocities associated with dust deflation events in the western Sahara, *J. Climate App. Met.*, 26: 1147-1151.
- Karl, T.R., and Knight, R.W., 1985: Atlas of palmer drought severity indices (1931-1983) for the contiguous United States, National Climatic Data Center, Historical Climatology Series, No. 11, Asheville, NC.
- Kimberlin, L.W., Hidlebaugh, A.L., and Grunewald, A.R., 1977: The potential wind erosion problem in the United States, *Transactions of the American Society of Agricultural Engineers*, 20: 873-879.
- Lougeay, R., Brazel, A.J., and Miller, T.A., 1987: Monitoring changing desert biomass through video digitization of Landsat MSS data: an application to dust storm generation, *Photogrammetric Engineering and Remote Sensing*, 53: 1251-1254.
- Lyles, L., 1983: Erosive wind energy distributions and climatic factors for the West," *J. Soil Water Conservation*, 38: 106-109.
- Middleton, N.J., 1984: Dust storms in australia: frequency, distribution, and seasonality, *Search*, 15: 46-47.
- Nickling, W.G., 1978: Eolian sediment transport during dust storms: Slims River Valley, Yukon Territory, *Canadian J. Earth Sciences*, 15: 1069-1084.
- Nickling, W.G., and Brazel, A.J., 1984: Temporal and spatial characteristics of Arizona dust storms (1965-1980), *J. Clim.*, 4: 645-660.



- Nickling, W.G., 1984: The stabilizing role of bonding agents on the entrainment of sediment by wind, *Sedimentology*, 31: 111-117.
- Nickling, W.G., and Gillies, J.A., 1986: Evaluation of aerosol production potential of type surfaces in Arizona, EPA Contract No. 68-02-388, MND Associates, Guelph, Ontario, 48 pp.
- Palmer, W.C., 1965: Meteorological drought, Research Paper 45, U. S. Weather Bureau, U.S. Department of Commerce.
- Pewe, T.L., 1981: Desert dust: origin, characteristics and effect on man, U. S. Geological Survey Special Paper 186., Boulder, Colorado, 303 pp.

CLIMATIC CONTROLS ON THE FREQUENCY, MAGNITUDE AND  
DISTRIBUTION OF DUST STORMS: EXAMPLES FROM INDIA/PAKISTAN,  
MAURITANIA AND MONGOLIA

Nicholas J. Middleton  
School of Geography  
University of Oxford  
Mansfield Road  
Oxford OX1 3TB  
England

ABSTRACT. Analysis of terrestrially observed meteorological data is used to fill some of the gaps in our knowledge of the dust storm systems in a number of world regions.

In NW India and Pakistan, dust is raised from the alluvial soils of the Ganges and Indus and the Thar desert by localised convective cells ('Andhi'), while synoptic scale dust-raising and transport is caused by the 'Loo' wind, a pressure gradient airflow. Mapping of twice-daily meteorological reports enables tracking of dust events which follow distinct patterns of dust transport. A tentative model of dust raising and transport in the area is proposed.

Below-average rainfall in the Sahelian latitudes of Mauritania, West Africa, which began in the late 1960s, has been partly instrumental in causing increases in dust-raising activity. At Nouakchott, data show the drought to have continued into 1986, with continued high levels of dust storm activity. Correlations of annual dust storm frequency with 3-year antecedent rainfall averages at Nouakchott, show significant relationships.

The frequency and distribution of dust storms in the Mongolian People's Republic are mapped, showing highest activity in the Gobi desert and Great Lakes regions. The seasonality of dust storms (which occur largely in the spring) is controlled by ground surface conditions, the frequency of dust-raising meteorological systems, and in some areas by the actions of human populations. At Ulan Bator, increases in dust storms during the 1980s are related to human activities in and around the city.

## 1. DISTRIBUTION AND FREQUENCY OF DUST STORMS

Dust storms are generally characteristic of the world's arid zones where soils are often dry and unconsolidated and vegetation cover is sparse. A range of techniques has been used to study their occurrence and environmental impact, these include analysis of remotely sensed images, the

collection of aerosols and soil samples, and the study of terrestrially observed meteorological data.

Meteorological data on dust storm occurrence are collected using a 'target' method for dust storm identification, so that when an object at a known distance of 1,000 metres from the observer is obscured by dust being raised then a 'dust storm' is recorded. If visibility is obscured by dust that is not being raised at the time of observation then a 'dust haze' is recorded, the visibility may or may not be below 1,000 metres. The range of codes used by observers is shown in figure 1.

The availability of data for global appraisal of dust storm source location and strength is a problem. The reliability, coherence and length of data period often vary from country to country and region to region. But standardised meteorological data provide the best long-term record of dust storm occurrence over periods of decades, while also providing useful cross reference data for satellite studies and aerosol monitoring, as well as enabling investigation between dust storm occurrence and other meteorological parameters such as rainfall and wind speeds.

The global distribution of major dust storm areas as determined by long-term meteorological data is shown in figure 2. Inclusion of areas as major dust storm regions was made according to the arbitrary limit of 15 dust storm days a year, the annual dust storm frequencies of key stations in each of the 19 dust storm regions are given in table I. This distribution has been compiled from meteorological data supplied by national meteorological departments who use the standardised international coding practices, but as will be seen below in the case of India there are some national practices that use a slightly different definition of dust storms in that a wind speed criterion is introduced. In this light, therefore, the present global distribution should be treated as an approximation of the true picture, but the best approximation given the level of data available.

The main body of this paper illustrates some of the various ways in which meteorologically observed dust storm data can be used in further investigation of some of the areas shown in figure 2.

## 2. NORTHWESTERN INDIA AND PAKISTAN

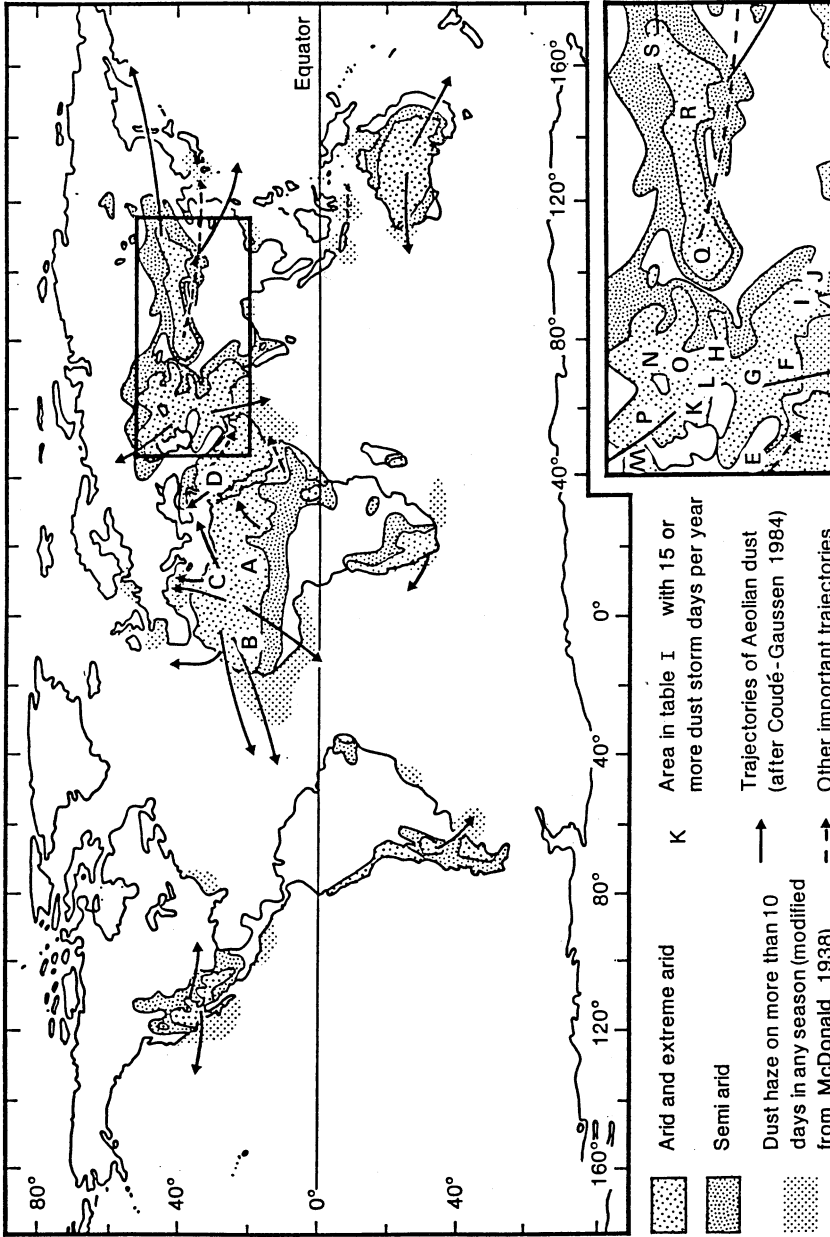
A previous study (Middleton 1986) of dust storm distribution in south-west Asia noted that no significant relationship existed between dust storm distribution in northwestern India and the climatic index C3 developed by Chepil *et al* (1963). The failure of this test inspired the author to further investigate the dust storm system of the area using a method similar to that developed by Bertrand (1977) and Morales (1979).

TABLE I Major global dust source areas with key station dust storm day frequency per year (D) (modified after Middleton *et al* 1986)

Source	Ref to Fig 2	Station	D	Number of years data
AFRICA				
Bodele Depression	A	Maiduguri	22.5	25
S Mauritania/N Mali/ C Algeria	B	Nouakchott	27.4	25
Libya/Egypt	C	Sirte	17.8	22
MIDDLE EAST				
N Saudi/Jordan/ Syria	D	Abou Kamal	14.9	21
Lower Mesopotamia	E	Kuwait	27.0	23
S-W ASIA				
Makran coast	F	Jask	27.3	4
Seistan Basin	G	Zabol	80.7	7
Afghan Turkestan	H	Chardarrah	46.7	7
Upper Indus plain	I	Jhelum	18.9	8
Thar desert	J	Fort Abbas	17.8	8
USSR				
Turkmenistan	K	Repetek	65.5	25
Kara Kum	L	Nebit Dag	60.0	25
Rostov	M	Zavetnoe	23.3	25
Altay	N	Rubtsovsk	25.1	25
Alma Alta	O	Bakanas	47.7	25
Kazakhstan	P	Dzhambeiti	45.9	25
CHINA				
Taklimakan desert	Q	Hotien	32.9	28
Gansu Corridor	R	Minqin	37.3	28
MONGOLIA				
Gobi desert	S	Dzamiin Uud	34.4	31

Code figure ww	Symbol	Description	
05	∞	Haze	
06	S	Widespread dust in suspension in the air, not raised by wind at or near the station at the time of observation	
07	\$	Dust or sand raised by wind at or near the station at the time of observation, but no well-developed dust whirl(s) and no duststorm or sandstorm seen	
08	⊞	Well-developed dust whirl(s) or sand whirl(s) seen at or near the station during the preceding hour or at the time of observation, but no duststorm or sandstorm	
09	(S→)	Duststorm or sandstorm within sight at the time of observation or at the station during the preceding hour	
30	S→	Slight or moderate duststorm or sandstorm	- has decreased during the preceding hour
31			- no appreciable change during the preceding hour
32			- has begun or has increased during the preceding hour
33	⊞→	Severe duststorm or sandstorm	- has decreased during the preceding hour
34			- no appreciable change during the preceding hour
35			- has begun or has increased during the preceding hour
98	⊞→ ⚡	Thunderstorm combined with duststorm or sandstorm at time of observation	

1. SYNOP present weather codes for dust events.



2. Global distribution of major dust storm areas with main seasonal dust trajectories.

## 2.1. Meteorological systems generating dust events in northwestern India and Pakistan

Two distinct synoptic situations are commonly responsible for dust-raising in north-west India and both are related to the easterly movement of 'western disturbances'. A western disturbance is a low pressure zone or trough either at the surface or in the upper westerly wind regime, north of the subtropical high pressure belt, and such systems moving across Iran and Soviet Turkestan affect the Indian subcontinent north of  $30^{\circ}$  N. Weak circulations, called induced lows, may simultaneously develop over central parts of Pakistan and Rajasthan and move ENE wards (Rao 1981). The two situations commonly created by these induced lows are the creation of an area prone to thunderstorm generation, where dust storms are caused by the dry thunderstorm downdraft, and the setting up of a steep pressure gradient where strong winds may cause dust storms in dry areas. For all dust storms the Indian Meteorological Department has adopted three classes according to their intensities: light; moderate and severe, details are given in table II.

2.1.1. Thunderstorm or convective dust storms. Dust is raised and advances as a thick wall of dust at the turbulent gust front that precedes the main cumulonimbus clouds of the thunderstorm. In north-west India these storms are known as 'Andhi' ('blinding', from the Sanskrit word 'andha' meaning blind man). As the name suggests, the arrival of such a storm is characterised by a dramatic fall in visibility, often to below 100 metres, and also by a fall in temperature (by as much as 10 to  $15^{\circ}$  C) and a rise in humidity, while wind speed increases and changes direction (Joseph *et al* 1980). Examination of past charts shows that all spells of convective activity in northwestern India and west Uttar Pradesh and adjoining areas are associated with a western disturbance or its associated induced lows over Pakistan, north-west India and adjacent areas. The western disturbances and induced lows may be seen either as a closed low or only as a trough; in the low levels of the troposphere a trough may extend eastwards or southeastwards from the induced low, and this trough region is a potent field for thunderstorm activity (Srinivasan *et al* 1973). The effect of the western disturbance is to cause incursions of humid air of maritime origin at all levels, making the formation of convective clouds possible in the normally very unstable pre-monsoon air of northwestern India. The exact mechanisms governing whether such convective activity will produce a thunderstorm or a dust storm are not clear, the idea proposed at one time that dust storms are associated with less moisture than thunderstorms has been disproved by Bhalotra (1951, 1955) who shows that humidity values for both systems are similar at all levels.

TABLE II Classification of dust storms in India according to intensity.

Intensity of dust storm	Wind force on Beaufort scale	Visibility
Light	4 to 6	<1000m, upto 500m
Moderate	7 to 8	<500m, upto 200m
Severe	9 or more	<200m



At Delhi, Andhis seem to be more commonly associated with 'severe thunderstorms' (or squall line thunderstorms) as opposed to ordinary cellular thunderstorms (Joseph, pers. comm. 1986). These systems can be identified on radar by the long bank of cloud from which the downdraft dust storm is generated. They are typically 200 km long, with the dust front situated some 30 km in advance of the cumulonimbus clouds. Severe thunderstorms commonly form when wind speed increases rapidly with height, and are generally predominant in India north of about 20° N due to the steep wind gradient up to the westerly jet. These dust storms, therefore, last less than an hour at any one station, although the severe thunderstorm itself may be relatively long-lived (5 to 10 hours) moving with typical speed of 60 kmhr<sup>-1</sup>. Convective dust storms in northwestern India are thus mesoscale phenomena. Joseph *et al* (1980) have classified Andhi into four types from the nature of variation of visibility and wind speeds.

2.1.2. Pressure gradient dust storms. The pressure gradient dust storm, by contrast, is typically a synoptic scale feature, with dust-raising and transport occurring over large areas and often continuing for several days. Dust-raising winds occur when the pressure gradient is strong, and this situation typically occurs when an induced low moves east/northeastwards from west Pakistan to the northern Thar desert producing a strong pressure gradient to the south of the low where the isobars are oriented east-west. Thus, the most common area for pressure gradient dust-raising is in Rajasthan. Such lows usually have a large pressure departure from normal and are associated with strong upper winds in the very low levels (upto 1.5 km).

The Indian Meteorological Department uses the term 'steep pressure gradient' for a pressure gradient of 1 to 1.5 mb per degree of latitude and 'very strong pressure gradient' for more than 1.5 mb per degree of latitude. When the pressure gradient is steep, according to this definition, and/or the lowest level upper winds are of the order of 30 knots or more, strong dust-raising winds may be expected over the area (Srinivasan *et al* 1973). Dust-raising winds may start in the morning and continue throughout the day, but their intensity reaches a maximum in the afternoon/evening, at the time of the maximum temperature epoch, when the superadiabatic lapse rates close to the ground favour the raising of dust. Dust may remain suspended in the atmosphere for upto a few days and generally is transported eastwards or northeastwards by the pressure gradient winds. To the south-east and east of the low pressure system, however, the pressure gradient is generally weaker and thus the winds are slight. Dust transported in this way, arriving at areas to the east and north-east of the dust source in light winds is the cause of conditions known as 'Loo'.

Loo is typically experienced to the east and north-east of Rajasthan, in Delhi and down the Gangetic plain, as far as Bihar to the east (Singh 1971), although it is also felt in Rajasthan itself when dust is raised to the west on the Indus plains. In meteorological terms, therefore, Loo is a dust haze, and indeed it is usually recorded as such by observers due to the low wind speeds involved because a dust event is only recorded as a dust storm in India when dust reduces visibility to below 1,000 m in association with a wind of Beaufort 4 (about  $5.5 \text{ ms}^{-1}$ ) or greater.

## 2.2. Dust event tracking in northwestern India and Pakistan

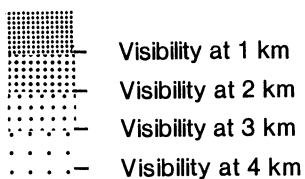
It has been noted above that Andhis are a mesoscale phenomenon, and as such, attempts to adequately track their movement were not successful given the low density of frequent-interval observatories in the region. Pressure gradient dust storms, however, are synoptic scale features, and thus tracking is possible using surface station reports and synoptic maps.

Three pressure gradient dust events are tracked using daily surface station observed data and synoptic maps, both for 0830 Indian Summer Time IST (0300 GMT) and 1730 IST (1200 GMT). Maps of events tracked show the surface pressure distribution, taken from hand drawn forecasting maps, and the station wind speed and direction and present weather code (ww) relating to dust in the atmosphere (see fig I). To complement this information station visibility is indicated by visibility isopleths at intervals of 4.0 km, 3.0 km, 2.0 km and 1.0 km as decoded from present visibility values (VV) (see fig 3). These data were obtained from the Indian Meteorological Department at Pune. Three dust events are mapped, illustrating typical dust-raising conditions with differing durations and transport paths. Figure 4 shows the distribution of stations used in this mapping exercise.

2.2.1. 20-22 May 1965. On the 20 May 0830 IST a shallow low pressure system is located over western Pakistan and dust is being raised by NNWly winds at Nokkundi in Baluchistan where the pressure gradient is steep on the southwestern side of the system (fig 5). The pressure gradient over the rest of Pakistan and northwestern India is very gentle and winds are light and variable. By the late afternoon the low has moved northeastwards and deepened; winds are still light over north-west India and much of Pakistan but dust-raising is now occurring to the south-west of the low over much of Baluchistan from the NNW and at the coastal station of Pasni on the Makran coast.

By 0830 IST on 21 May the low has deepened considerably (24 hour pressure change is -8 mb, and the pressure departure from normal is -8 mb at the centre). In Baluchistan the dust-raising winds have developed into a full dust storm, the wind now from the north with an increased speed of 35 knots, while on the Makran coast the winds have subsided and haze is recorded at Pasni. In the Thar desert and upper Indus plains winds have picked up as the pressure gradient has steepened and dust is being raised at Khanpur and Lahore in east Pakistan and at Jammu in northwestern India. Down the Ganges plain Delhi is experiencing a dust haze and Bareilly dust-raising, while the strongest winds from the south-west are blowing at 20 knots causing a dust storm at Phalodi in Rajasthan.

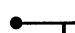
The low continues to deepen during the 21st so that by 1730 IST the 24 hour pressure change is -10 mb and dust-

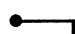


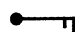
~~988~~ Isobar (mb)

Wind arrow points in direction  
the wind is blowing

 1 - 2 knots

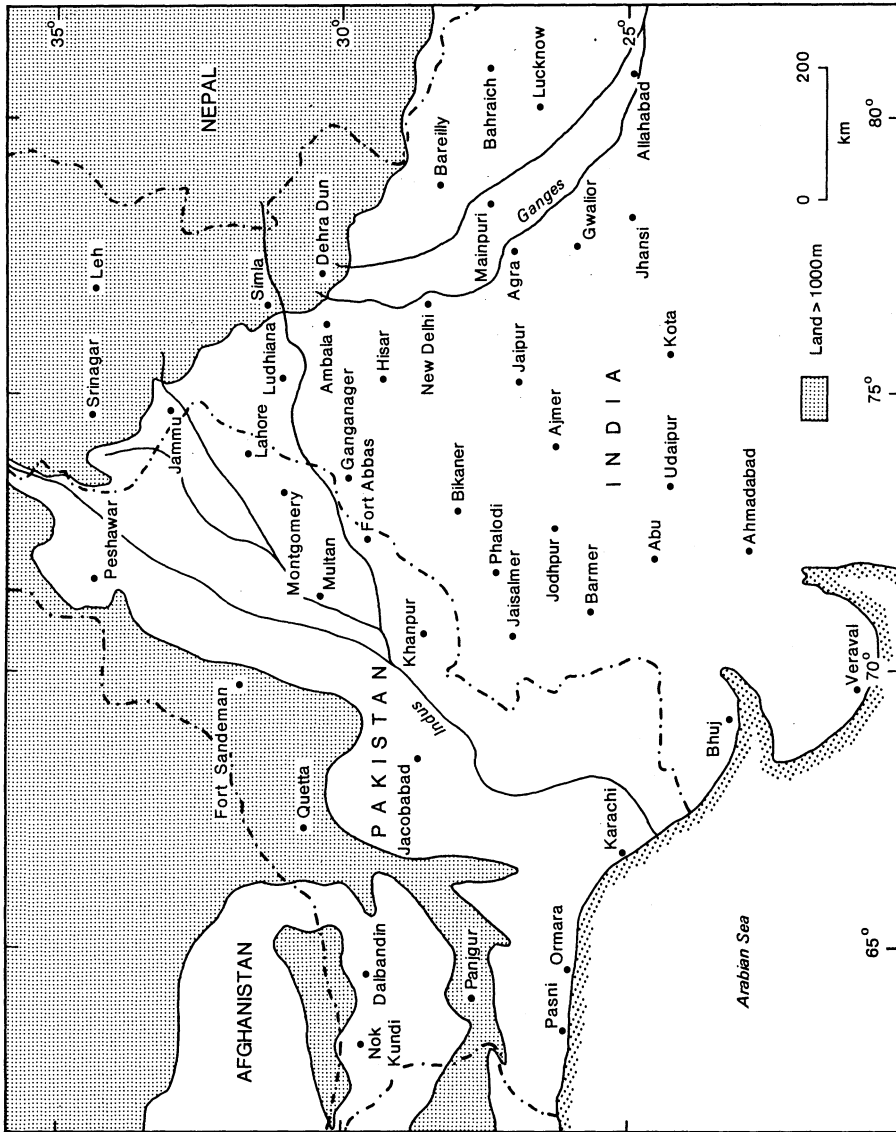
 3-7 knots

 8-12 knots

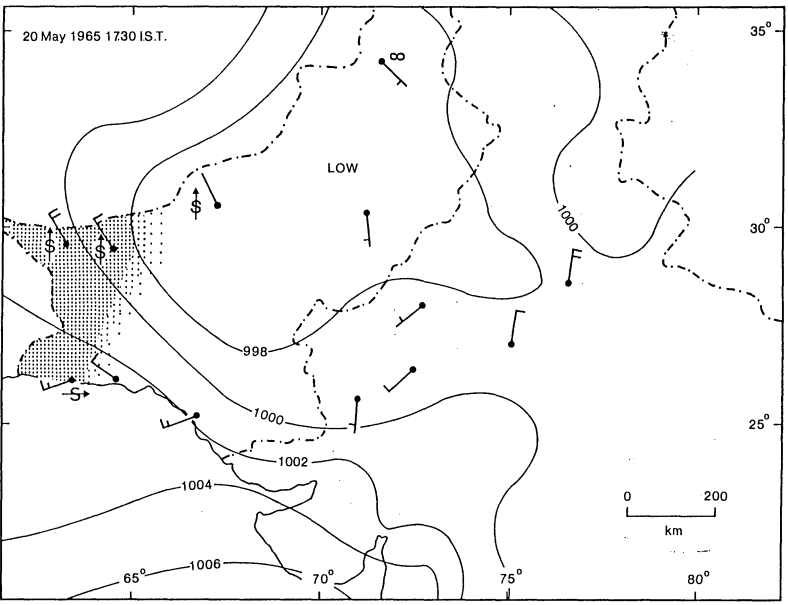
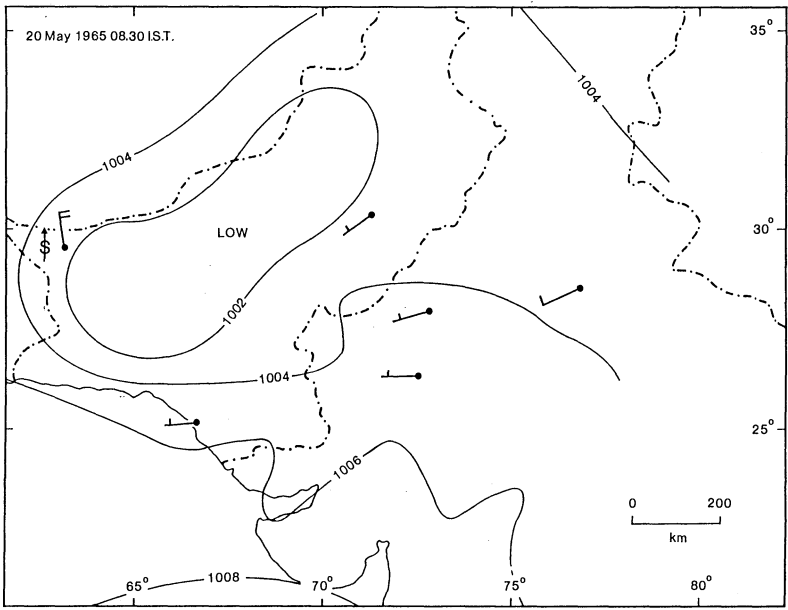
 13-17 knots etc.

(Full fleche 10 knots)

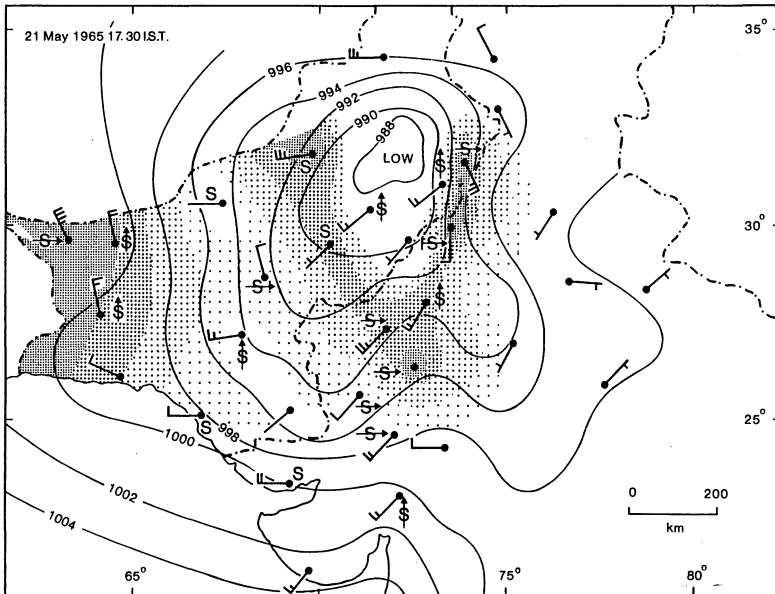
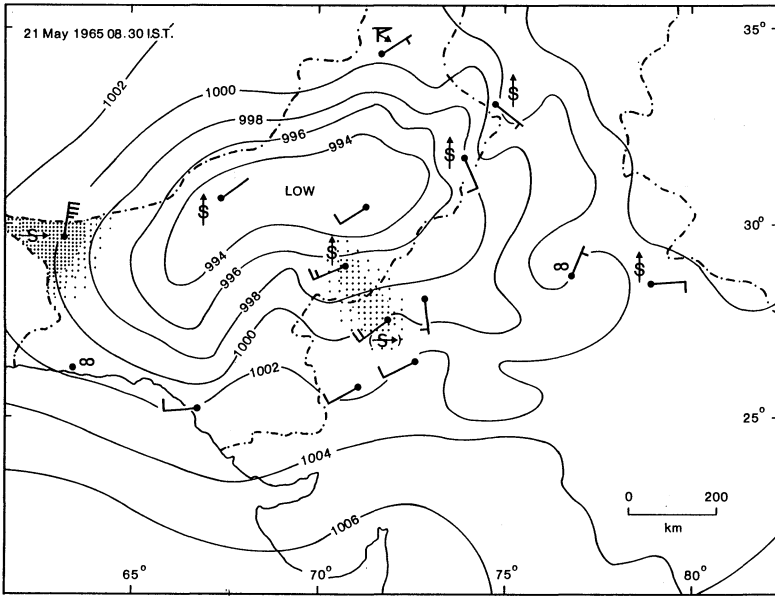
3. Explanation of symbols used in figures 5 to 7 (see also fig 1).

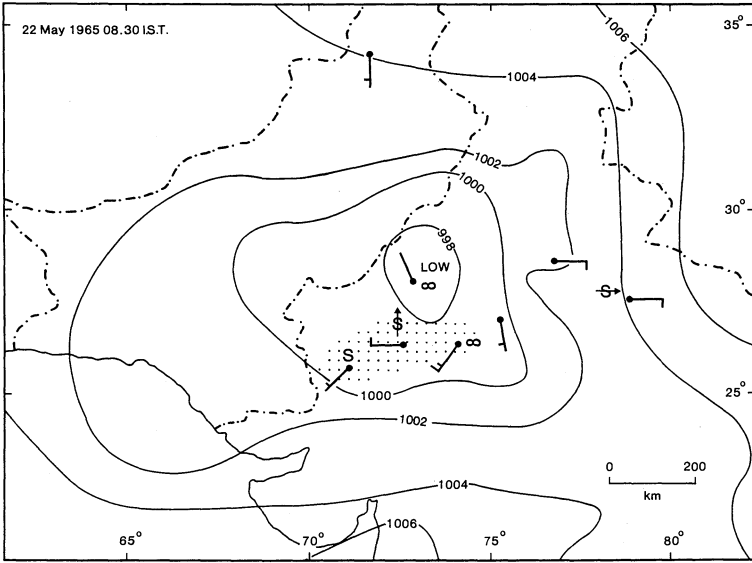


4. Geographical distribution of stations used in figures 5 to 7.



5. Weather charts based on SYNOP observations for 20-22 May 1965.





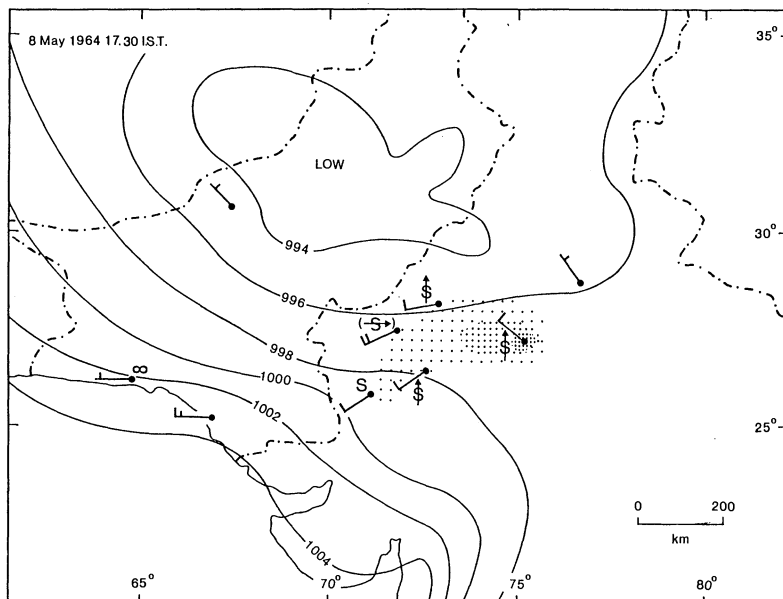
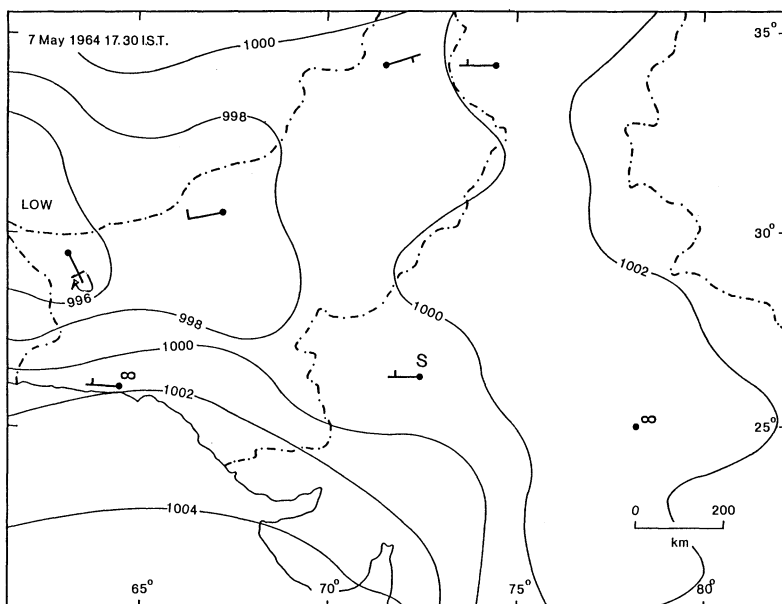


raising is occurring over virtually all of Pakistan south of about  $33^{\circ}$  N and much of northwestern India due to the steepening of the pressure gradient and solar heating during the day. In Baluchistan dust winds are still from the north-west, in the rear of the pressure zone, while over southern Pakistan and Gujarat winds are mainly westerlies of 10 to 15 knots and blowing dust at the stations or bringing it in suspension from further west. In Rajasthan the winds are generally stronger and from the south-west and are causing dust storms, the visibility isopleths show that maximum dust-raising is in an area that describes a horseshoe shape around the low pressure centre. Across the upper Indus plains to Peshawar thick dust haze is being transported from the south and west, while in the northern Thar dust storms are caused by southerly winds at Ganganagar and south-easterlies at Lahore. This last point is particularly interesting in that most texts that refer to the pressure gradient type dust-raising make no mention of a southeasterly component in a predominantly westerly flow.

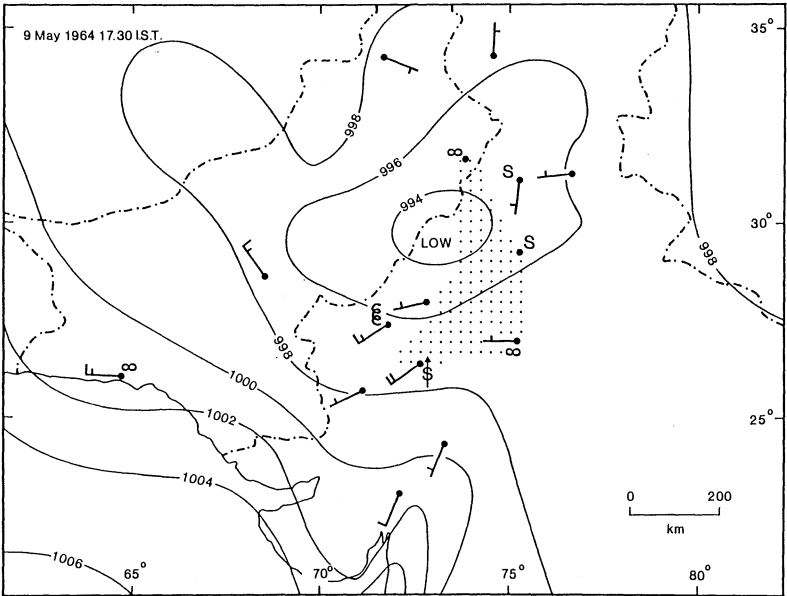
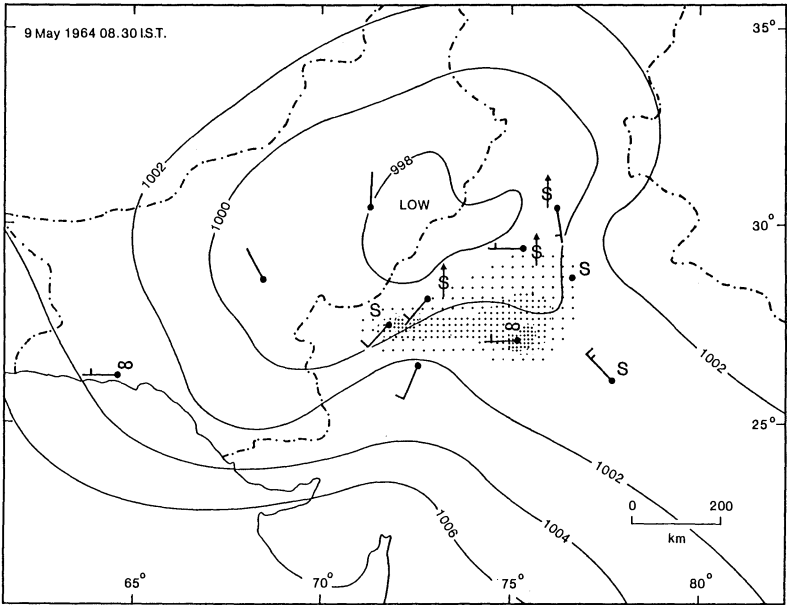
By the morning of the 22nd the low has moved south-east and filled, pressure gradients are much reduced, winds have calmed and much of the suspended dust has settled except over a number of stations in Rajasthan where visibility is <4 km with light winds. At Jodhpur dust is still being raised at this time, but at Barmer and Ajmer the suspended dust represents a Loo event.

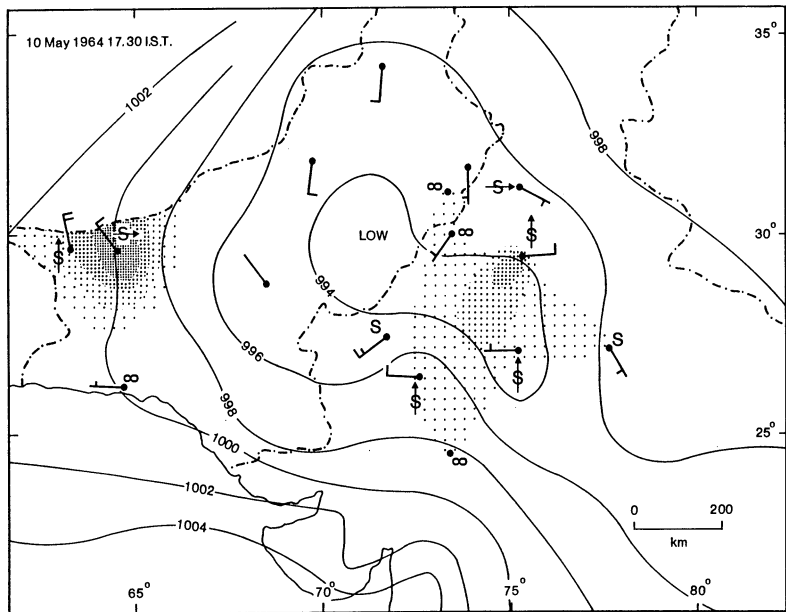
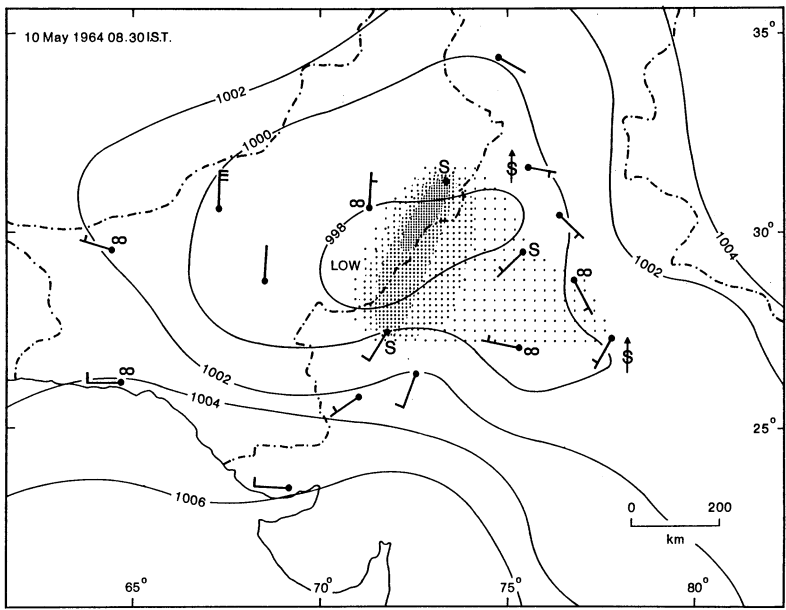
2.2.2. 7-12 May 1964. A low pressure system, centred over the Seistan Basin north-west of Baluchistan at 1730 IST on 7 May, arrives over the upper Indus plain at 1730 IST, 8 May (fig 6). Its arrival causes pressure gradient dust-raising in an area of Rajasthan broadly elongated west-east from Barmer to Jaipur, with 20 knot winds blowing a dust storm at Phalodi. By 0830 IST on the 9th the dust haze has been blown ENEwards as the low pressure system has moved over the northern Thar, the haze has reached Hissar and Delhi as suspended dust with light winds or calms (Loo) and Gwalior where there are light northwesterly winds.

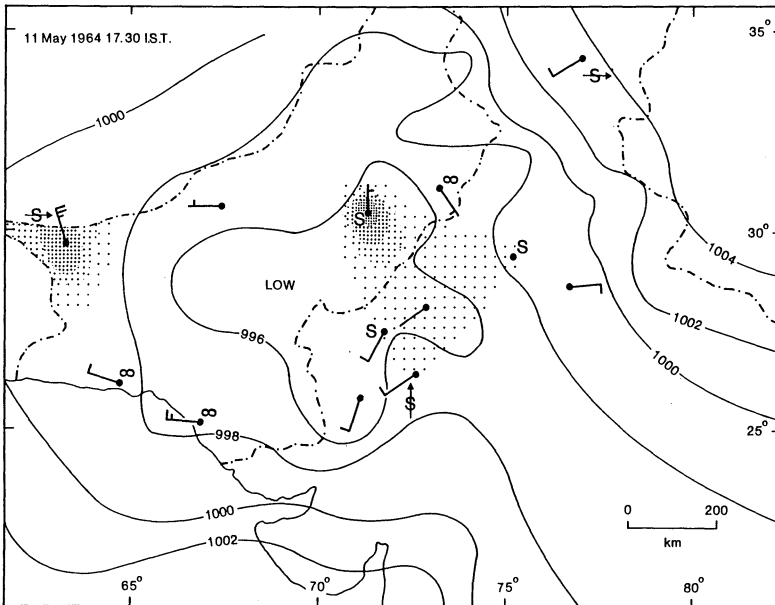
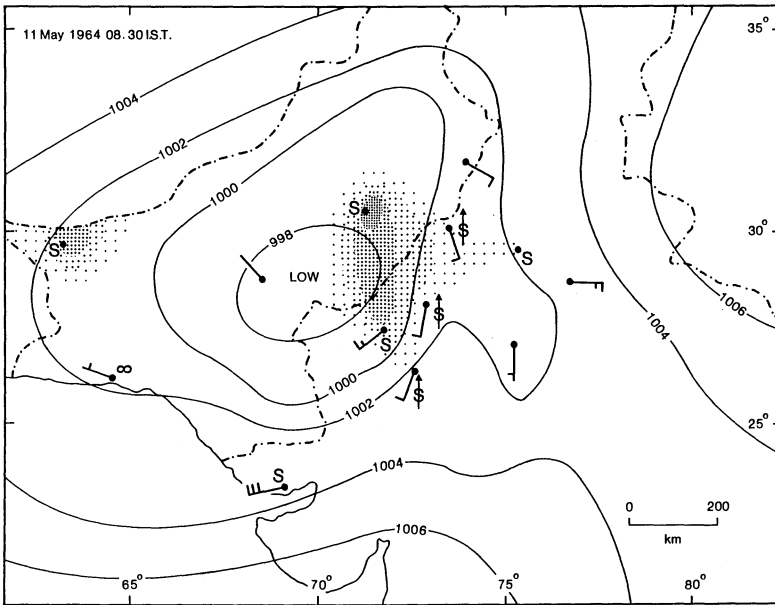
By the afternoon of the 9th the situation has changed; the low has become more localised and the dust haze has drifted northwards affecting Ludhiana and Lahore (pressure departure from normal at the centre of the low is -6 mb at this time). On the 10th May the maximum dust haze is centered over the northern Thar with a tongue being advected down the Ganges plain with light winds. The 4 km isopleth has reached Gwalior. By the afternoon of the 10th this pattern of haze has shifted eastwards and the maximum haze is located over Hissar as the low pressure system becomes elongated to the south-east. In north-west India pressure gradients are not steep enough to produce dust storm strength winds, although at 1730 IST over Baluchistan, Nokkundi and Dalbandin are recording dust-raising winds from the north-west of up to 20 knots. During 11th and 12th May the low fills slightly and retreats toward the south-west, pressure gradients and winds

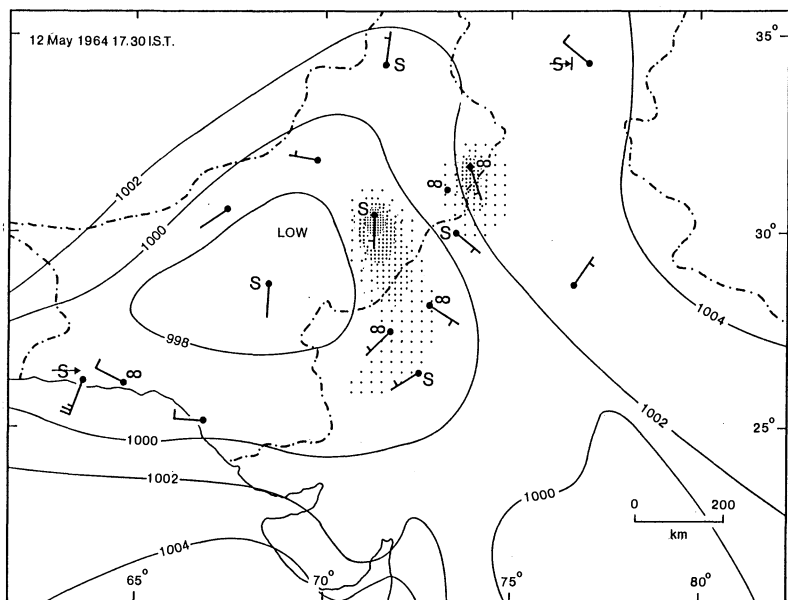
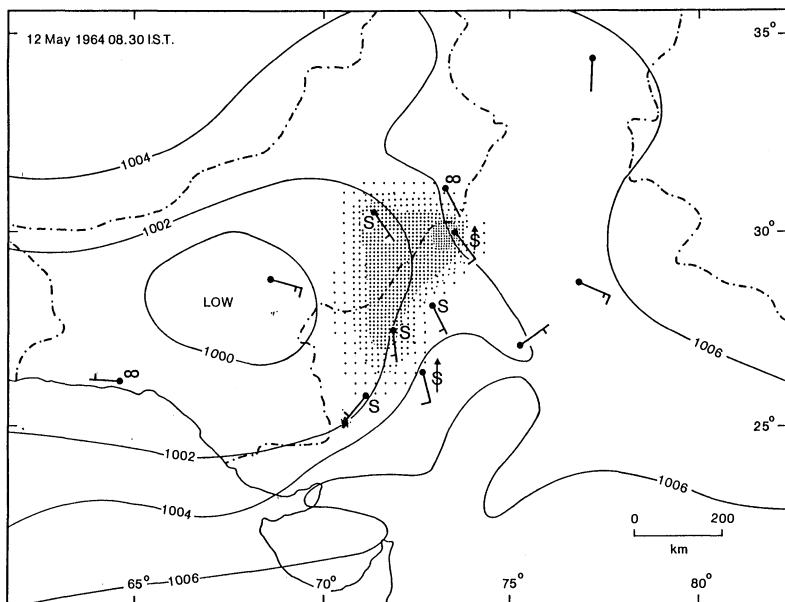


6. Weather charts based on SYNOP observations for 7-12 May 1964.







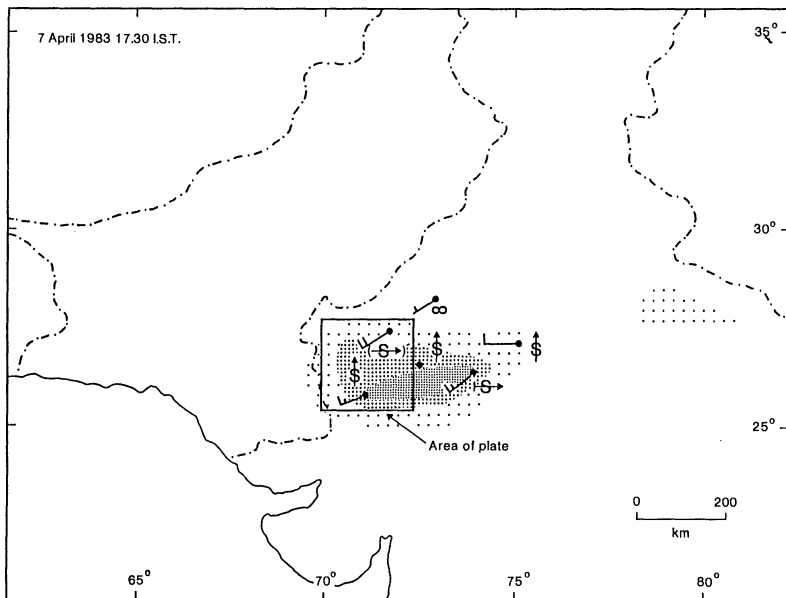
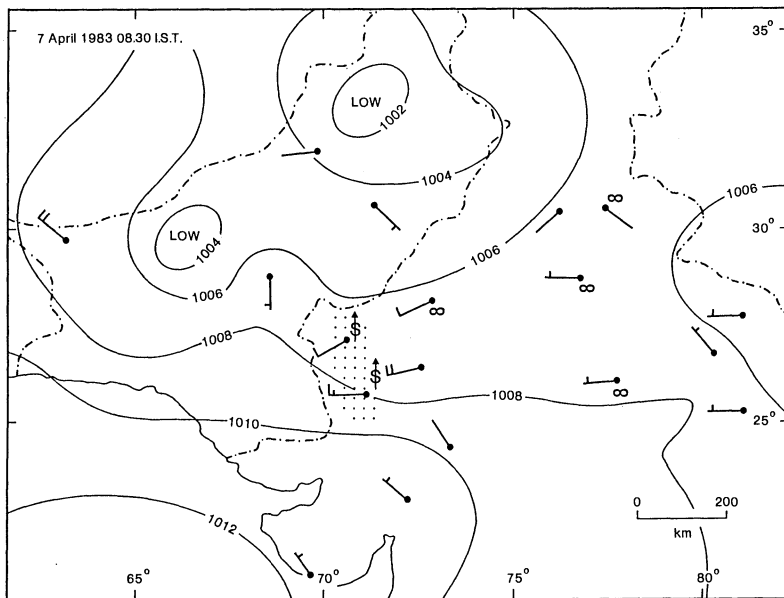


are still low but there remains a considerable amount of suspended dust in the atmosphere over the Thar, while the transport of material down the Ganges plain appears to have been much reduced. As the low retreats, winds in the vicinity of Ganganagar and Bikaner veer from S/SSEly at 0830 IST 11th May to southeasterly on 12th May, blowing suspended material, with dust still being raised at Ganganagar and Jodhpur, towards the north-west to the stations of Lahore, Montgomery and Multan, producing a recurved dust transport path. Also during these two days afternoon winds at Leh are sufficient to produce localised dust storm activity in Kashmir.

2.2.3. 7-10 April 1983. Two western disturbances are located over Pakistan: one over Baluchistan and a second over northern Pakistan, Jammu and Kashmir and Punjab, on 7th April 1983, 0830 IST (fig 7). Pressure gradient winds from the south-east over Rajasthan are 10-12 knots raising dust at Barmer and Jaisalmer, with haze recorded at Bikaner. No meteorological charts were available for 1730 IST on April 7th, but observations at stations in Rajasthan indicate that winds have strengthened to 15-20 knots at Barmer, Phalodi and Ajmer, probably due to a steepened pressure gradient as the low over Baluchistan has moved eastwards, causing dust-raising and dust storms with a large area of reduced visibility. The large scale dust-raising has built up during the day as shown in plate I, a Space Shuttle photograph taken at about 1200 IST on April 7 over western Rajasthan.

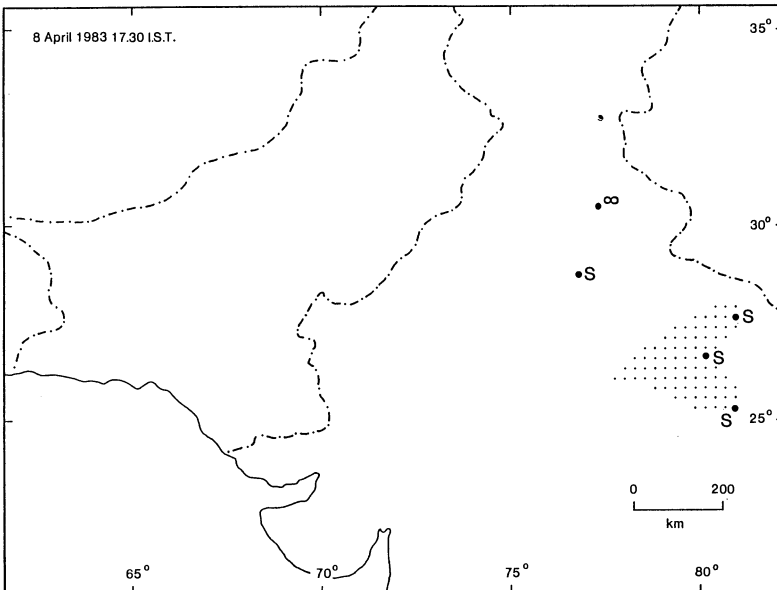
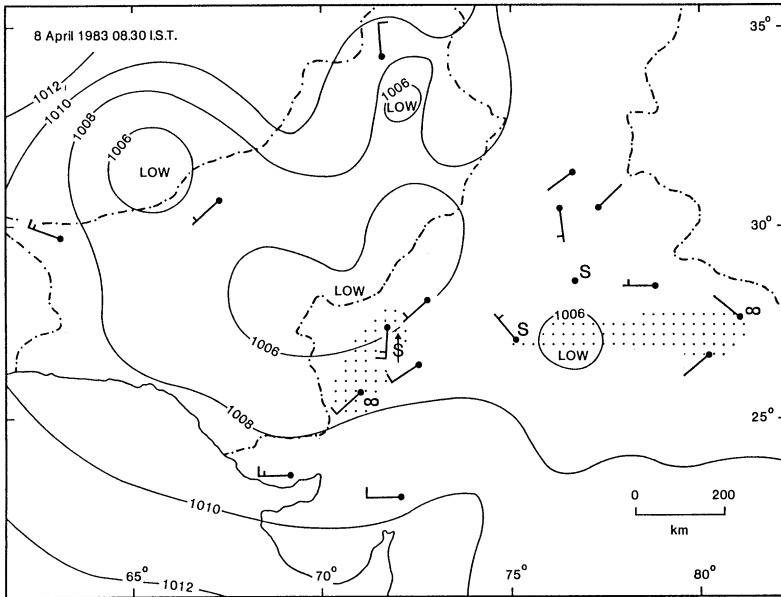
By 0830 IST on the 8th the low over the Thar has filled out and winds have weakened over Rajasthan, though the atmosphere is still heavily dust-laden. Much of the material raised in Rajasthan has been advected eastwards and the widespread haze is reducing visibility to <4km over the upper Ganges plain with light winds ("Loo"). By 1730 IST there is widespread dust haze reported at Bahraich, Lucknow and Allahabad, and this haze continues to travel slowly down the Ganges in very light winds. On 9th April 0830 IST this suspended dust has reached stations not shown on the map : Patna (visibility <4km in haze), Kanpur (visibility <2km by dust in suspension) and Varanasi (visibility <1km in haze).

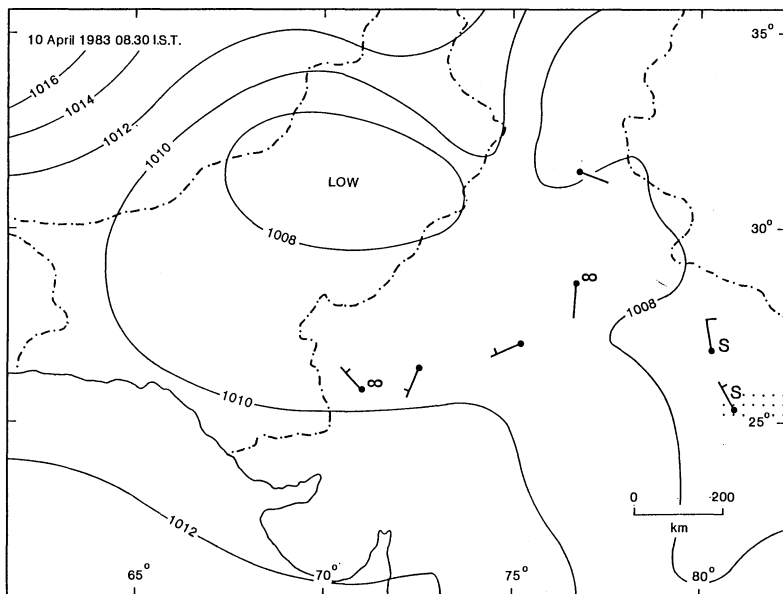
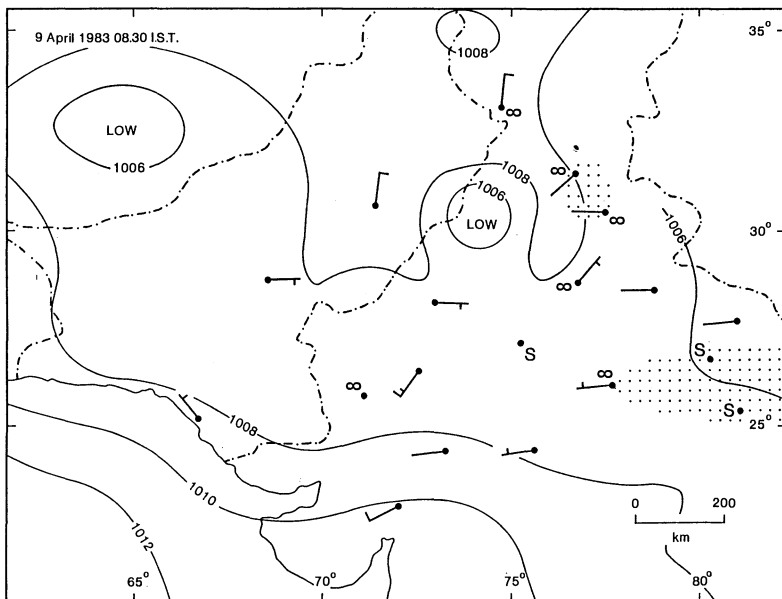
2.2.3. Discussion. The foregoing analyses of dust events have been selected from a systematic study of synoptic charts during such events, and illustrate the typical area of dust-raising during pressure gradient type storms in northwestern India and Pakistan, with typical transport paths of dust once raised. From long experience of forecasting dust events, the Indian Meteorological Department state that 'Rajasthan, in particular, experiences dust-raising winds more frequently than the other sub-divisions.' (Srinivasan et al 1973, p.40). At stations east of Rajasthan, Andhi dust storms are probably more important (Joseph, pers. comm. 1986) as the induced lows associated



7. Weather charts based on SYNOP observations for 7-10 April 1983.







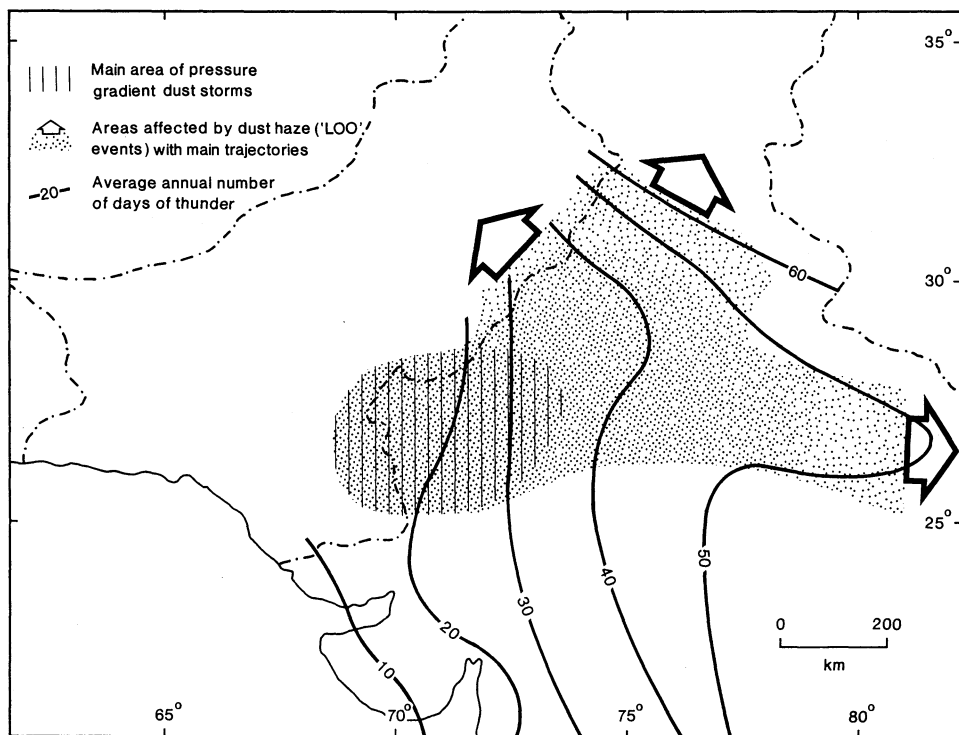
with western disturbances seldom move further east than the Punjab.

From observations at Delhi airport Joseph *et al* (1980) conclude that 'most of the dust storms that occur at Delhi are of the Andhi type' (p.431) and in one of the earliest studies of dust storms at Agra Sreenivasaiah and Sur (1939) also suggest that Andhi is the most important type of dust storm occurring at that station.

It has been noted above that the frequency of thunderstorms is often underestimated over large areas, especially at stations manned by part-time observers, and also because, being localised systems, they may occur in areas where no observer is present to record them. The first of these problems has been overcome for India by Rao *et al* (1971) who base their analysis of thunderstorms on records from stations that cater to aviation and thus have continuous observations, and are particularly alert to adverse weather conditions such as thunderstorms or peals of thunder that are observed and reported for warning purposes.

The map of annual thunderstorm frequency produced by Rao *et al* (1971) is shown in figure 8 in combination with a schematic representation of the findings of the dust tracking exercise : the most common source area of pressure gradient dust storms and the trajectories of transported dust which are more or less synonymous with Loo events. Although the large majority of Andhis occur during the pre-monsoon hot season (April - June) the annual frequency map of thunderstorms is broadly similar to the monthly frequency distribution for these three months, in that minimum activity is shown over Rajasthan and north Gujarat increasing northwards to the Himalayan foothills and southeastwards down the Gangetic plain. Since this frequency distribution includes all thunderstorms, both Andhis and 'wet' systems, it does not, of course, prove conclusively that Andhis become increasingly important as dust-raising systems north and east of Rajasthan. In conjunction with observations in the literature referred to above, however, and the views of the forecasters at the Indian Meteorological Department, the general pattern broadly confirms this suspicion. The relationship is not simple, however, in that with increasing southeasterly distance down the Gangetic plain dust storm frequency declines (Middleton 1986) whereas thunderstorm frequency continues to increase to a maximum over northern Bangladesh and Assam. This lack of correlation is due to higher rainfall totals towards this area.

Although the above conclusion, that pressure gradient dust storms become less important and Andhis become more significant north and east of Rajasthan, seems reasonable, the situation should not be oversimplified. Andhis occur in Rajasthan (Vaidyanathan 1969) and in Gujarat (Upadhaya 1954) and Loo or thick dust haze conditions may be experienced in these states due to pressure gradient dust-raising to the west, on the Indus plains. Indeed, Vaidyanathan (1969)



8. Model of the dust storm system in northwestern India.

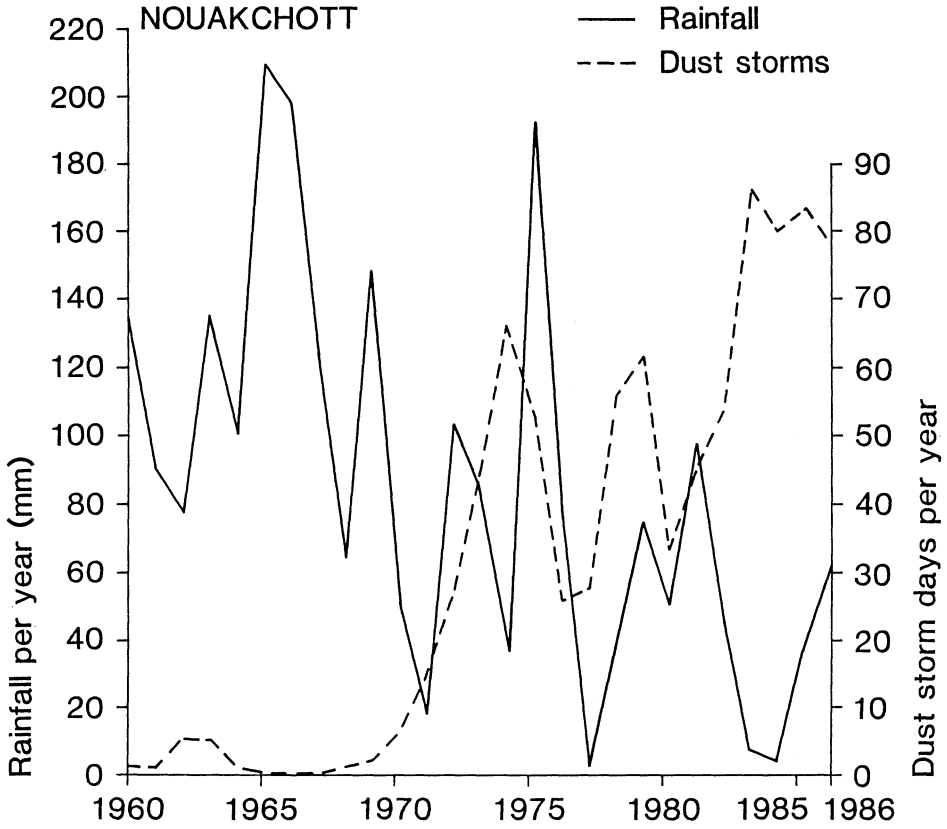
documents a case of severe dust haze (visibility <500m, wind speed <6knots) that was apparently due to an unrecorded Andhi occurring in the Rajasthan Desert.

The complexity of the dust storm system has been illustrated by the apparent lack of correlation between dust storm frequency and rainfall, both for northwestern India (Middleton 1986) and for many other of the world's drylands (Goudie 1983). From this study it seems that a significant proportion of dust events in north-west India and Pakistan are due to dust raised and advected to a station from afar (Loo). In most cases, however, such events are not recorded as dust storms, which does not explain the lack of correlation in this area. In the case of Andhi the characteristic advancing dust wall is a dynamic entity that probably consists of material both raised and brought from afar and material that is continually being raised along its path, so that this convective system combines both the ideas of a dust storm and a thick dust haze. If the land over which such a storm passes has a constant erodibility, and the downdraft maintains constant velocity and turbulence characteristics, therefore, it follows that Andhi would increase in intensity as it continues along its path until the wind's carrying capacity is reached. Case studies using a dense network of continual visibility observations would evaluate such a suggestion.

In Rajasthan, some degree of correlation between annual dust storm frequency and monsoonal rainfall of the preceding year is shown by Krishnan (1977). At Delhi the incidence of dusty weather in May and June was found to be closely related to the frequency of western disturbances affecting the weather of Delhi State by Roy (1954) as would be expected from the above analysis of the synoptic meteorology of dust-raising events. In Roy's study 'dusty weather' refers to both numbers of Andhis occurring and also the number of hours of visibility reduced to <1000m, more representative of Loo events as Andhis typically involve severe visibility reduction of less than one hour. Nevertheless, the incidence of western disturbances and dusty weather were not related by a simple rule of ratio, as antecedent rainfall among other factors, is also an important influence.

### 3. MAURITANIA

Meteorological data have been used to investigate the relationship between dust generation and rainfall deficits in the west African state of Mauritania (Middleton 1985a, 1985b, 1987). The variation in frequency of annual dust storm days and annual rainfall totals at Nouakchott is updated in figure 9 from the initial investigation by Middleton (1985a). This graph illustrates that dust storm frequencies have continued at high levels, relative to pre-



9. Annual rainfall totals and dust storm frequencies at Nouakchott, Mauritania (1960-86).

drought frequencies, into 1986 as rainfall totals have continued to be low.

Further investigation of the dust storm/rainfall relationship at Nouakchott is shown in figures 10 and 11. Figure 10 compares dust storm frequency to the previous year's rainfall (note that the dust storm season at Nouakchott is primarily in the first six months of the year, before the onset of the rainy season). The linear correlation coefficient is  $-0.53$  (28 per cent explanation) which is significant at the 5 per cent level. The relationship between dust storms and antecedent rainfall is stronger, however, when annual dust storm days are compared to the average annual rainfall over the previous three years. The linear correlation coefficient is  $-0.75$  (56 per cent explanation), significant at the 0.1 per cent level. This strong relationship with three-year antecedent rainfall is similar to that found by Bertrand *et al* (1979) for Agadez and Bilma in Niger.

#### 4. MONGOLIA

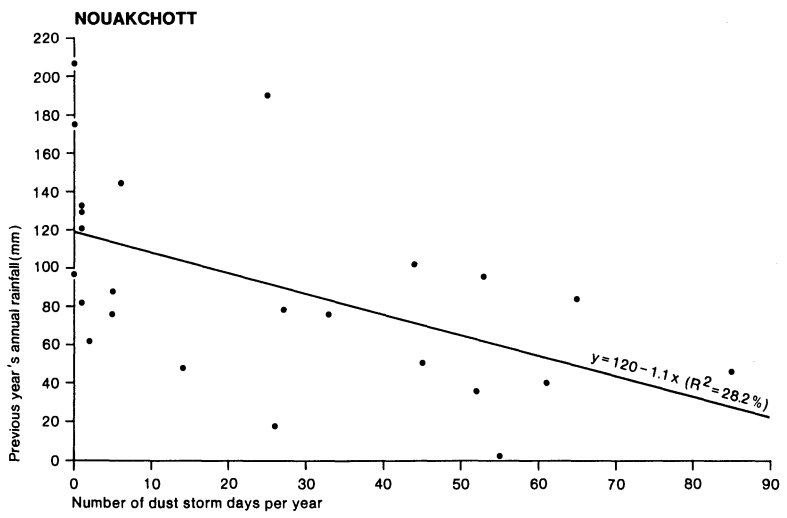
The world dust storm frequency map shown in figure 2 gives a good indication of the geographical distribution of dust storm activity. Some of the source areas shown on this map are much better studied than others. The Sahara, for example, is perhaps the best understood source area, although much still remains to be explained. The People's Republic of Mongolia lies in perhaps the least studied source area. Whereas significant work has been carried out on dust that has its origins in northern China and Mongolia, little work has been done in the source areas themselves.

Figure 12 shows the distribution of annual average numbers of dust storm days recorded in the Mongolian People's Republic. The highest frequencies are recorded in the southern Gobi region and in the northwestern Great Lakes area. Dzamiin Uud, on the Chinese border with Inner Mongolia, records the highest average annual number of dust storm days: 34.4.

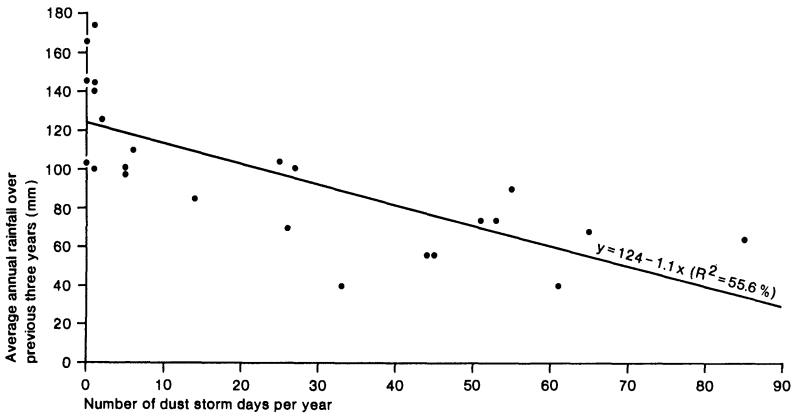
Dust storms are most common in the spring months of March, April and May. During the winter Mongolia is dominated by the position of the Central Asian high which is characteristically positioned over the basins of Tannu Tuva in the USSR or the Great Lakes Basin of western Mongolia. This system creates dry, stable conditions over most of Mongolia from October to April. As spring approaches the influence of this high weakens as a rapid progression of frontal cyclones moves generally from west to east across the country bringing strong winds.

##### 4.1. Ulan Bator

Analysis of the dust storm system of Ulan Bator, the nation's capital, was made using meteorological observations

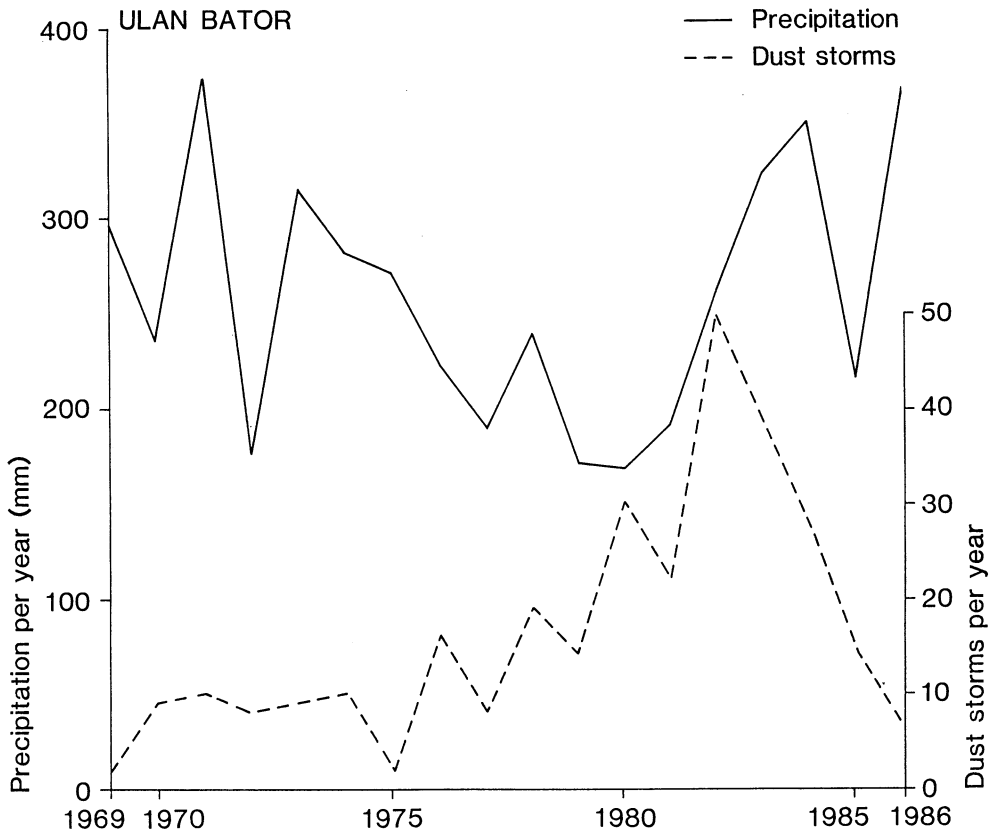


10. Frequency of dust storms in relation to previous year's rainfall at Nouakchott.



11. Frequency of dust storms in relation to mean annual rainfall over the previous three years at Nouakchott.





12. Distribution of dust storms in the Mongolian People's Republic.

of rainfall and dust storm occurrence. The data, shown in figure 13, are for a station moved to a new site in 1968 on the northwestern side of the city.

A trend of increasing dust storms is clear, dating from the mid-1970s, reaching a peak in 1982. At the same time a declining trend in rainfall totals is also discernable from the late 1960s to the early 1980s. Several dust sources can be identified in Ulan Bator:

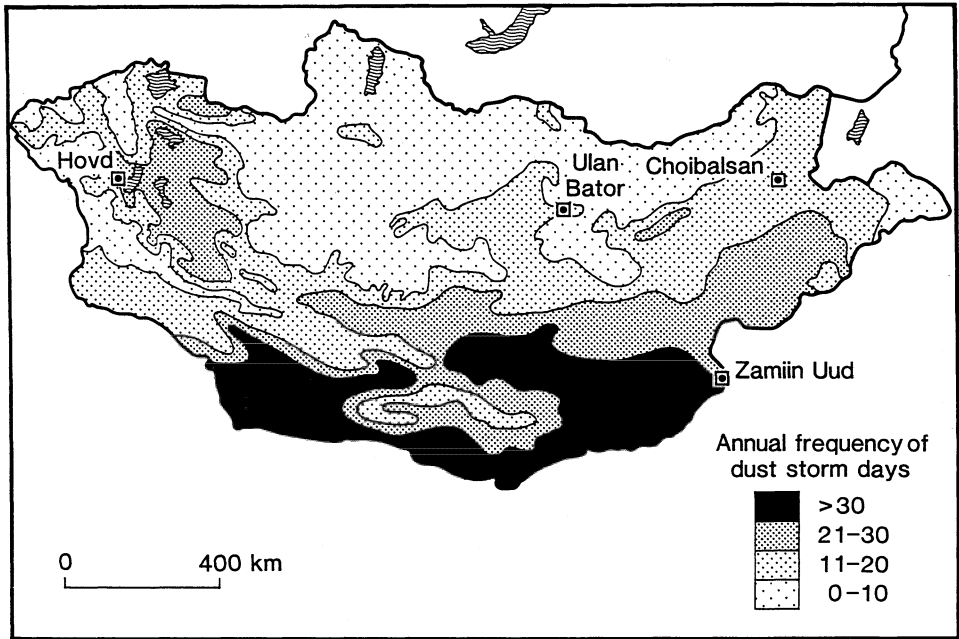
- a. Unvegetated alluvium of the River Tuul that flows down the south side of the valley in which Ulan Bator is situated.
- b. Unpaved roads and tracks both outside the city centre and in and around the compounds of traditional felt tents or 'gers' that surround the modern centre.
- c. Areas cleared for construction work. Construction work and associated activities such as the movement of heavy lorries on dirt tracks are significant dust-raising agents in Ulan Bator. This process probably also has a bearing on the peak of dust activity at the Ulan Bator meteorological station since new building of housing blocks reached within 200 metres of the station in the early 1980s.
- d. On the outskirts of the city off road vehicles on dirt tracks generate much dust. This mechanism has been becoming more effective in recent years according to Ulan Bator meteorologists as more vehicles have driven on the grass beside tracks thus increasing the width of the unvegetated tracks and exposing more sediment to aeolian entrainment.
- e. Pollution from power stations and factories at the western end of the valley.

## 5. CONCLUSION

This paper has attempted to illustrate some of the ways in which meteorologically observed dust storm data can be used to investigate dust processes. Although there are problems associated with such data, they provide a useful insight to the workings of dust entrainment and transport processes and related meteorological variables. In the field of palaeoclimatic and palaeometeorological studies the location and strength of today's major dust source areas is of particular significance when trying to reconstruct past patterns and processes. Present day meteorological data provide a good indication of these locations and strengths and their patterns of dispersal, representing a useful input to palaeo studies as well as to studies of present day problems associated with dust storms.

## 6. REFERENCES

Bertrand, J. (1977) 'Action des poussières sub-sahariennes sur le pouvoir glaciogène de l'air en Afrique de l'ouest', Ph.D. Thesis, Université de Clermont-Ferrand, France.



13. Annual rainfall totals and dust storm frequencies at Ulan Bator, Mongolian People's Republic (1969-86).

- Bertrand, J., Cerf, A. & Domergue, J.L. (1979) 'Repartition in space and time of dust haze south of the Sahara.' WMO, 538: 409-415.
- Bhalotra, Y.P.R. (1951) 'Will it be a dust storm or a thunderstorm?' Indian Journal of Meteorology and Geophysics, 5: 290-291.
- Bhalotra, Y.P.R. (1955) 'On the role of upper level advection of cold air in the development of duststorms and thunderstorms over Delhi.' Indian Journal of Meteorology and Geophysics, 6: 81-82.
- Coude-Gaussen, G. (1984) Le cycle des poussières éoliennes désertiques actuelles et la sédimentation des loess péridésertiques quaternaires. Bulletin Centre Recherche et Exploration-Production Elf-Aquitaine, 8: 167-182.
- Goudie, A.S. (1983) 'Dust storms in space and time.' Progress in Physical Geography, 7: 502-530.
- Joseph, P.V., Raipal, D.K. & Deka, S.N. (1980) ''Andhi', the convective duststorm of northwest India.' Mausam, 31: 431-442.
- Krishnan, A. (1977) 'A climatic analysis of the arid zone of northwestern India.' In Jaiswal, P.L. (ed) Desertification and its Control. New Delhi: Indian Council of Agricultural Research: 42-57.
- McDonald, W.F. (1938) Atlas of Climatic charts of the Oceans. Washington DC, Department of Agriculture: Weather Bureau.
- Middleton, N.J. (1985a) 'Effect of drought on dust production in the Sahel.' Nature, 316: 431-434.
- Middleton, N.J. (1985b) 'Dust production in the Sahel: reply to M. Hulme.' Nature, 318: 488.
- Middleton, N.J. (1986) 'A geography of dust storms in south-west Asia.' Journal of Climatology, 6: 183-196.
- Middleton, N.J. (1987) 'Desertification and wind erosion in the western Sahel: the example of Mauritania.' Oxford: School of Geography Research Paper, 40.
- Middleton, N.J., Goudie, A.S. & Wells, G.L. (1986) 'The frequency and source areas of dust storms.' In Nickling, W.G. (ed) Aeolian Geomorphology. Boston: Unwin Hyman: 237-259.
- Morales, C. (1979) 'The use of meteorological observations for studies of the mobilization, transport and deposition of Saharan dust. In Morales, C. (ed) Saharan Dust. SCOPE Report 14, Chichester: J. Wiley: 119-131.
- Rao, Y.P. (1981) 'The climate of the Indian subcontinent. In Takiatash, K. & Arakawa, H. (eds) Climates of Southern and Western Asia. World Survey of Climatology, 9. Amsterdam: Elsevier: 67-118.
- Rao, K.N., Daniel, C.E.J, & Balasubramaniam, L.V. (1971) 'Thunderstorms over India.' Indian Meteorological Department Scientific Report No. 153.
- Roy, S.C. (1951) 'Is the incidence of unusually dusty weather over Delhi in May and June for two consecutive summers of 1952 and 1953 an indication that the Rajasthan

- Desert is advancing towards Delhi?' Indian Journal of Meteorology and Geophysics, 5: 1-15.
- Singh, R.L. (ed) (1971) India: a regional Geography. Varanasi: National Geographical Society of India.
- Sreenivasaiiah, B.N. & Sur, N.K. (1939) 'A study of the duststorms of Agra.' Memoirs of the Indian Meteorology Department, 27, part 1.
- Srinivasan, V., Ramamurthy, K. & Nene, Y.R. (1973) 'Summer - Nor'westers and Andhis and large-scale convective activity over peninsula and central parts of the country. Indian Meteorological Department, Pune, Forecasting Manual, part 3.2.2.
- Upadhyaya, V.C. (1954) 'Dust and thunderstorms on 23 March 1954 at Ahmedabad. Indian Journal of Meteorology and Geophysics, 5: 295.
- Vaidyanathan, M. (1969) 'Unusual type of dust haze over Jodhpur Airfield and neighbourhood on May 13, 1963.' Indian Journal of Meteorology and Geophysics, 20: 56-57.

## EMISSION OF FINE-GRAINED PARTICULATES FROM DESERT SOILS

W. G. NICKLING & J. A. GILLIES

Department of Geography  
University of Guelph  
Guelph, Ontario  
CANADA, N1G 2W1

### 1. INTRODUCTION

During the past decade, considerable interest has been focused on the emission, transport, deposition and climatological effects of natural and anthropogenic aerosols (e.g. Gillette, *et al.*, 1982; 1978; Deluise, *et al.*, 1977; Péwé, 1981). Several studies have also considered the effects of mass particle concentration on light extinction (Pilat and Ensor, 1971), climate (Idso and Brazel, 1974), human health hazards (Leathers, 1981), visibility (Patterson and Gillette, 1977b) and ambient air quality (Hagen and Woodruff, 1973). In addition, a large volume of literature has been developed on the atmospheric, textural and surface conditions which interact to produce atmospheric aerosols.

Despite this, few studies have attempted to identify and classify (in a quantitative manner) the relative aerosol production potential of natural and anthropogenic surfaces. As part of a long-range program to investigate dust emissions in the Southwestern U.S., an initial detailed field study was carried out in Arizona to determine the relative aerosol production potential of selected surface types. A total of 13 representative sample sites were selected for the evaluation of dust emission factors using a newly designed, portable field wind tunnel. Information of this nature is needed to understand total suspended particulate loadings; especially in areas such as the U.S. Southwest, Africa, and the Middle East, where dust storm frequencies and total suspended particulate (T.S.P.) loadings are relatively high (Nickling and Brazel, 1984; Brazel and Nickling, 1986). High particulate loadings in these areas have frequently resulted in serious environmental and human health hazards. For example, in the U.S.

Southwest, considerable controversy has arisen over the sources of high background dust concentrations (Nickling and Brazel, 1984). Various individuals and groups, including government agencies, have disputed the primary sources of high dust concentrations. Potential sources have included agricultural fields, major construction sites, natural desert surfaces, mine tailings as well as stack and vehicle exhaust emissions. Despite these ongoing controversies, little quantitative data is presently available to substantiate or refute most arguments.

Although a relative wealth of information exists on the horizontal flux of soils, few detailed studies have been carried out on the vertical flux of fine-grained aerosols from natural surfaces. Chepil and Woodruff (1957) provided the first detailed data on the variation of sediment concentration with height during dust storms in Colorado and Kansas. More recent studies on vertical aerosol fluxes have been carried out in the High Plains of Texas by Gillette (1977) and in Texas and Nevada by Shinn, *et al.* (1976). Complementary studies have also been undertaken in Canada by Complin and Piersol (1978) on uranium mill tailings and on undisturbed natural soils by Nickling (1978; 1983). The results of Shinn, *et al.* (1976) are not directly comparable to the present work because their investigation focused on long range transport once sediment was entrained. In contrast, the present study focuses on the emission rate from different surface types.

The relative lack of information on the vertical fluxes of aerosols from natural surfaces in part reflects the logistical problems associated with instrumentation. In almost all the above studies, particulate concentration data were collected during wind erosion events using various types of aerosol collectors and wind instrumentation placed on towers at selected sites. Empirical relationships derived from such long-term field studies have been used with varying degrees of success by other authors to produce emission factors for specific sites.

The recent decision by the U.S. Environmental Protection Agency to modify the current T.S.P. standards to a limitation based on particulates having a mass mean aerodynamic diameter  $<10 \mu\text{m}$  has necessitated a more detailed understanding of the potential sources and land use activities which result in high aerosol fluxes so that appropriate environmental standards can be established.

## 2. FIELD SITES

The thirteen sites selected for the evaluation of aerosol production potential represent a range of surface types suspected by the authors and local environmental officials of being major contributors to background dust concentrations in Southern Arizona. The sites were selected on the basis of their soil textural characteristics, vegetative cover, land use and degree of anthropogenic disturbance. The surface types include: active agricultural lands, abandoned agricultural fields, natural desert surfaces, construction sites and mine tailings. The locations of the sites are shown in Figure 1 and a brief description of each site's surface and textural characteristics is given in Table 1.

## 3. FIELD MEASUREMENT OF AEROSOL FLUXES

A fundamental problem in identifying and evaluating the aerosol production potential of surfaces is the need for the direct monitoring of sediment loss under a wide range of atmospheric and surface conditions. However, direct field observations using specialized monitoring equipment (e.g. Gillette, 1977; Nickling, 1978; 1983), despite their usefulness, do have several serious drawbacks:

- 1) they are extremely costly in terms of the instrumentation and the logistical support necessary to investigate several sites;
- 2) field studies are very much dependent on the vagaries of the weather, and as a result, one often spends considerable time waiting for the right weather or surface conditions that in the end may severely limit the quality and quantity of data obtained; and
- 3) data obtained in such studies are often extremely complex because of the lack of control on the many atmospheric and surface variables involved in the wind erosion process.

### 3.1 *The Portable Field Wind Tunnel*

In order to overcome some of the limitations associated with direct soil loss monitoring under natural wind conditions, a portable field wind tunnel was designed and constructed for *in situ* testing. The wind tunnel is similar in design, although considerably larger than portable wind tunnels reported by Wooding (1968) and Gillette (1978). The tunnel has a 0.75 x 1.0 x 12.0 m open-floored working section constructed of fiberglass with



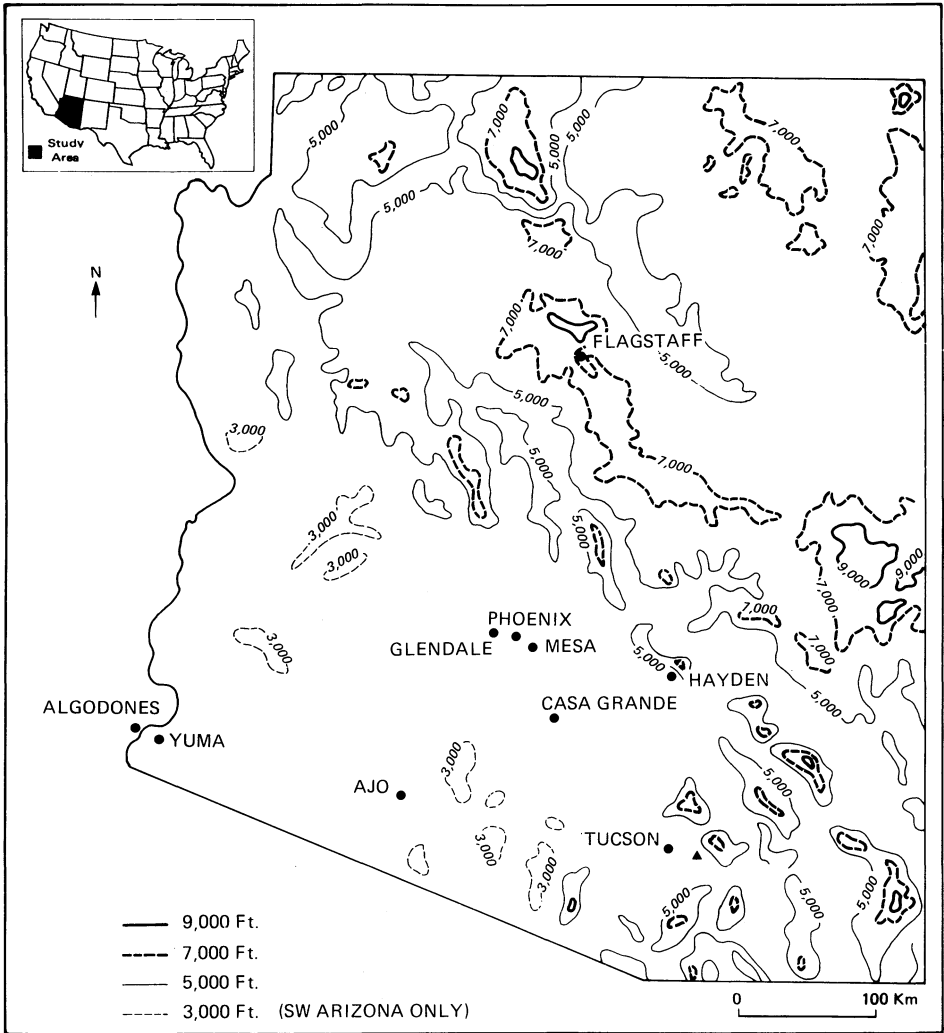


Figure 1: Locations of the study sites.

TABLE 1. Site Surface and Textural Characteristics

SITE	SITE CHARACTERISTICS
Mesa, Arizona (agricultural land)	Flat, laser leveled for irrigation; no vegetation or surface trash; double disked 2 days prior to testing; large clods of varying size covering the surface
Maricopa, Arizona (agricultural land)	Flat, laser leveled for irrigation; no vegetation or surface trash; secondary tillage operations in preparation for cotton planting; large clods of varying size covered the surface
Yuma, Arizona (agricultural land)	Flat, laser leveled for irrigation; no vegetation or surface trash; surface was loose and friable with few large clods
Casa Grande, Arizona (abandoned agricultural land)	Flat, smooth, laser leveled at some previous time; sparse vegetation; primarily annual grasses; weakly crusted surface; easily disturbed
Glendale, Arizona (construction site)	Flat, smooth, machine-leveled surface; no vegetation; surface soil heavily pulverized by earthmoving machinery and regularly watered for dust control; easily disturbed by vehicular traffic
Tucson, Arizona (construction site)	Very flat, machine-leveled surface; no vegetation; surface soil heavily pulverized by earthmoving; fetch lengths over 1 km in all directions; regularly watered for dust control
Ajo, Arizona (mine tailings)	Extremely flat, extensive copper mine tailings; no vegetation; mainly unconsolidated sediment with some sparsely intermixed crusted areas; fetch lengths greater than 1 km
Hayden, Arizona (mine tailings)	Extremely flat copper mine tailings; no vegetation; light crust is easily disturbed; fetch lengths greater than 1 km
Algodones, California (dune flats)	Relatively flat, extensive outwash deposits adjacent to Algodones Dune complex; sparse vegetation cover; surface weakly crusted; lag of fine pebbles; heavily disturbed by offroad vehicles

TABLE 1. (Continued)

SITE	SITE CHARACTERISTICS
Yuma, Arizona (scrub desert)	Relatively flat; sparse vegetation cover; surface is weakly crusted; lag of fine pebbles; heavily disturbed by offroad vehicles
Yuma, Arizona (disturbed scrub desert)	Slightly undulating surface; sparse vegetation cover; primarily annual grasses, sagebrush, and creosote bush; surface soil is very loose with little cohesive structure; heavily disturbed by offroad vehicles
Tucson, Arizona (Santa Cruz river terrace)	Flat terrace deposits adjacent to river; sparse vegetation cover; high silt content with fine gravel lag deposit
Mesa, Arizona (salt river channel)	Slightly undulating river bed; no vegetation; surface is very loose with no evidence of crusting; heavily disturbed by offroad vehicles

plexiglass viewing/access windows (Fig. 2). The tunnel uses a two-dimensional, molded fiberglass inlet bell with a honeycomb flow straightener and a conical fiberglass diffuser. Air flow for the wind tunnel is provided by a 95 cm centrifugal fan powered by a 35 h.p. diesel engine. The fan and engine are transported and operated from the bed of a one-ton pickup truck and connected to the main working section by 1.0 m diameter flexible hosing. The inlet bell, working sections and diffuser are transported on a 8 m flatbed trailer.

### 3.2 Testing Procedures

At each test site the wind tunnel was carefully placed over the undisturbed surface and the wind velocity sensors and sediment collectors installed into the test section. Velocity was measured with four N.P.L. type pitot tubes connected to magnehelic differential pressure gauges. The pitot tubes were positioned above the soil surface at heights of 5, 15, 25 and 35 cm.

Suspended sediment was collected in two streamlined isokinetic samplers mounted downwind and to either side of the pitot tubes, 50 cm above the surface (Fig. 3). The samplers were connected to a high-volume vacuum pump. Sediment was collected during each run by drawing air isokinetically through preweighed 3.7 cm diameter membrane filters (0.1  $\mu\text{m}$  pore diameter) held in commercially available sampling cassettes within the samplers. Isokinetic flow through the 0.64 cm sample orifice was maintained during each test by means of a needle valve and flow meter incorporated into each vacuum line.

Sediment transported in saltation and creep was collected in a Bagnold (1941) type catcher installed along the center line of the wind tunnel 10 cm behind the suspended sediment collectors (Fig. 3).

Following installation of the instrumentation, velocity in the wind tunnel was slowly raised until movement of particles was noted by observers positioned at the plexiglass viewing windows. After the threshold test was completed, a predetermined shear velocity ( $u_*$ ) above threshold was established in the wind tunnel and the suspended sediment nozzle flow rate set to the center line velocity at the instrument height. Shear velocity was determined from the wind velocity profile above the bed using the Prandtl equation:

$$U = \frac{u_*}{k} \ln \frac{z}{z_0} \quad (1)$$

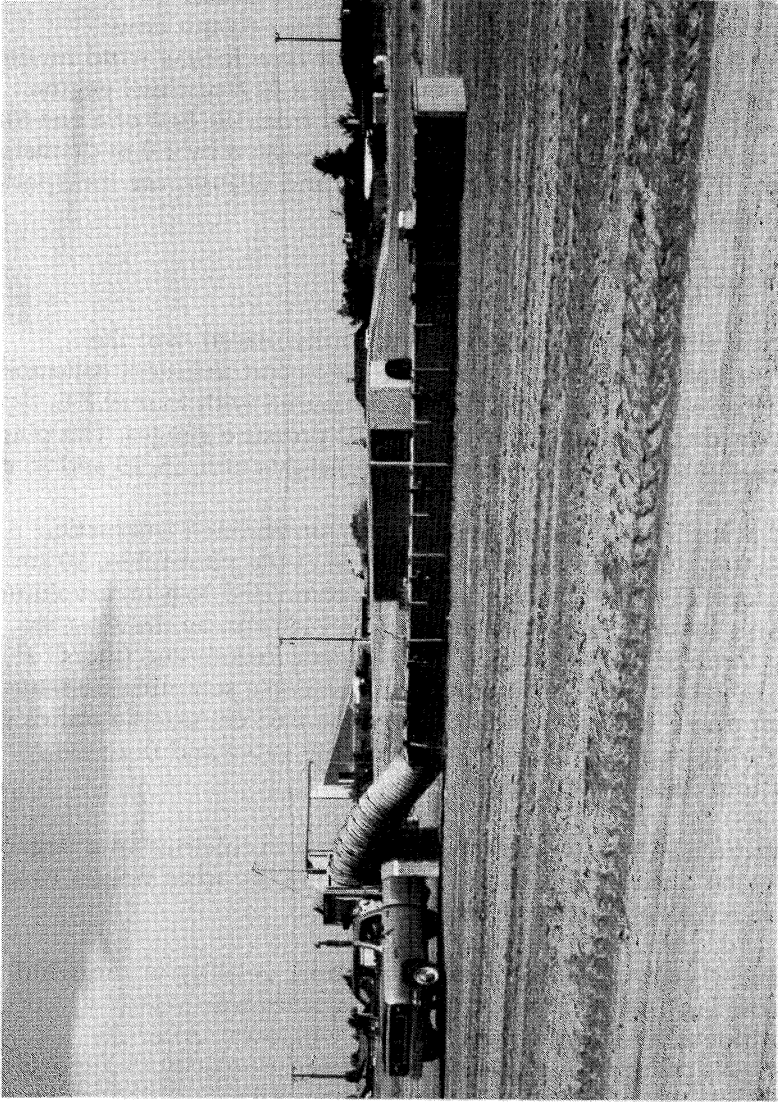


Figure 2: The portable field wind tunnel used in the aerosol emission tests.

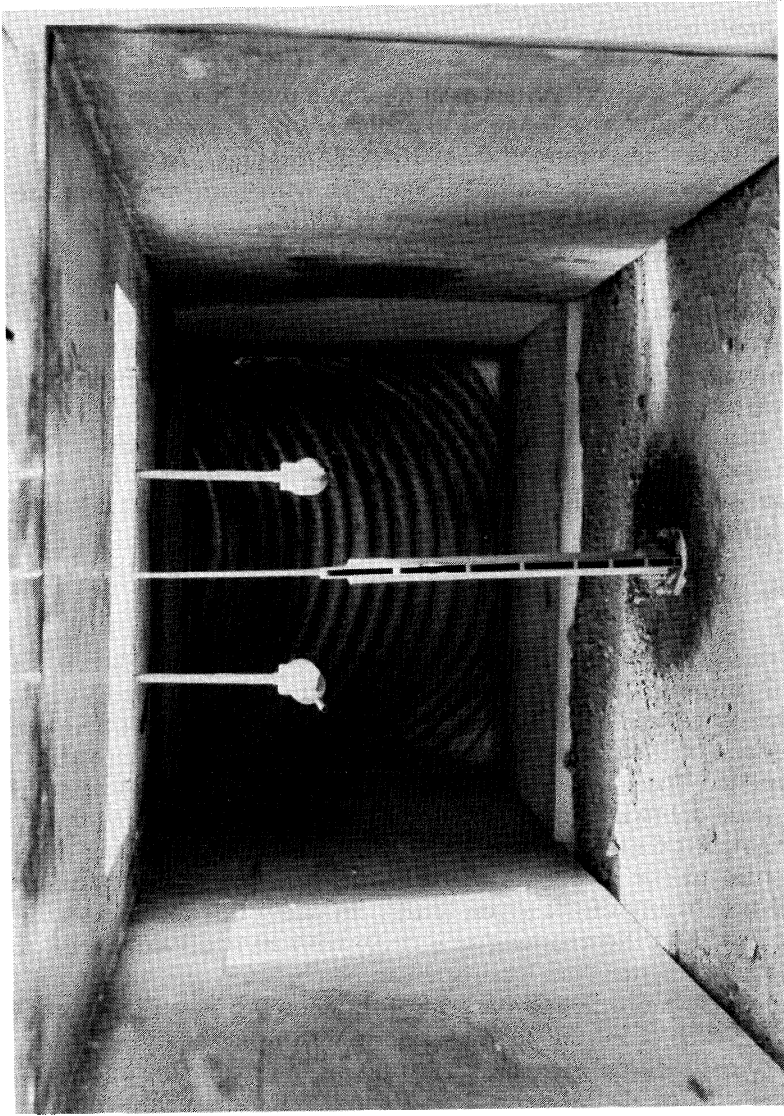


Figure 3: Suspended sediment samplers and Bagnold-type saltation/creep trap installed in the wind tunnel. The saltation/creep trap is 50 cm in height.

where  $u$  is the velocity at length  $z$ ,  $z_0$  is roughness length of the surface and  $k$  is Von Karman's constant (0.4).

The length of an individual test was dependent on the amount of sediment transported and was longer for surfaces with lower flux rates. Duration of individual tests ranged from 10 to 30 minutes. At the completion of the test run, the sediment samples were removed from the samplers and carefully stored for subsequent weighing and grain-size analysis.

Since the soil surface may become depleted of erodible grains during the test, it was necessary to move the tunnel to a new location for each sample run. Subsequent test locations were normally within 10 m of the original site, with the long axis of the tunnel parallel to the initial orientation. Once the wind tunnel was repositioned, the threshold determination and flux measurements were repeated. In general, five or six runs at different shear velocities above threshold were carried out at each of the 13 selected sites.

### 3.3 *Grain-Size Analysis*

Size analysis of the suspended sediment collected during each run was done using a Quantimet 720 image analyzing computer following the method of Perrie and Peach (1973). In this technique, a small portion of an aqueous dispersion of the sample is placed on a gelatin-coated microscope slide with a pipette. The water is quickly absorbed by the gelatin, leaving the individual grains dispersed and cemented on the slide. The slide is then placed under the optical microscope of the Quantimet 720. By setting class limits, the instrument can be programmed to measure the total particle area larger or smaller than any of the given limits. In using this technique, the class limits are based on the diameter of a circle with an equivalent area. In practice, accuracies of better than 1 percent can be obtained when the measured area covers more than 5 percent of the viewing area (Peach and Perrie, 1974). For each of the suspended sediment samples analyzed, over 2000 grains were counted on each slide. Results of the grain-size analysis for the specified size classes, <1.0, 1.0-2.5, 2.5-10.0 and 10.0  $\mu\text{m}$  are shown in Table 2.

TABLE 2. Grain Size Characteristics of Suspended Sediments

SITE	GRAIN SIZE DISTRIBUTION OF AEROSOLS (% FREQUENCY)						MEAN SIZE ( $\mu\text{m}$ )	STANDARD DEVIATION ( $\mu\text{m}$ )	SHEAR VELOCITY (cm/sec)
	< 1.0 $\mu\text{m}$	1.0 - 2.5 $\mu\text{m}$	2.5 - 10.0 $\mu\text{m}$	10.0 $\mu\text{m}$	10.0 $\mu\text{m}$	10.0 $\mu\text{m}$			
Mesa, AZ (agricultural)	1	24.81	40.88	30.30	4.01		3.31	2.74	62.9
	2	33.32	34.61	24.01	8.05		3.23	3.04	43.7
	3	28.96	35.09	28.75	7.20		3.44	3.00	43.4
	4	48.24	27.20	18.68	5.88		2.59	2.88	50.3
	5	44.95	31.41	21.91	1.73		2.45	2.52	53.4
	6	36.78	26.63	28.17	8.42		3.39	3.16	55.5
Glendale, AZ (construction)	1	42.00	31.68	21.61	4.70		2.72	2.79	22.1
	2	32.16	37.13	23.68	7.02		3.15	2.95	36.7
	3	65.53	30.65	1.19	2.63		1.28	1.69	49.4
	4	17.48	21.33	42.38	18.80		5.15	3.33	62.6
Maricopa, AZ (agricultural)	1	14.21	23.31	38.76	23.71		5.43	3.41	58.9
	2	24.76	24.92	31.59	18.73		4.55	3.53	66.1
	3	19.68	27.30	38.54	14.48		4.59	3.281	41.1
	4	21.46	17.64	35.61	25.28		5.30	3.60	80.1
	5	27.12	32.68	29.46	10.73		3.78	3.21	72.3
Yuma, AZ (disturbed desert)	1	10.88	15.75	43.46	29.90		6.19	3.27	27.5
	2	14.28	16.79	36.98	31.95		6.01	3.49	38.3
	3	9.49	21.62	52.69	16.20		5.54	2.97	59.6
	4	9.42	13.11	45.15	32.32		6.48	3.16	36.6
	5	14.36	23.81	44.00	17.83		5.19	3.23	55.9



TABLE 2. (Continued)

SITE		GRAIN SIZE DISTRIBUTION OF AEROSOLS (% FREQUENCY)					MEAN SIZE ( $\mu\text{m}$ )	STANDARD DEVIATION ( $\mu\text{m}$ )	SHEAR VELOCITY (cm/sec)
		< 1.0 $\mu\text{m}$	1.0 - 2.5 $\mu\text{m}$	2.5 - 10.0 $\mu\text{m}$	10.0 $\mu\text{m}$	10.0 $\mu\text{m}$			
Yuma, AZ (agricultural)	1	17.17	21.54	40.99	20.30	5.21	3.37	29.6	
	2	14.03	27.59	44.69	13.69	4.89	3.12	31.9	
	3	14.15	20.41	43.42	22.01	5.50	3.31	34.6	
	4	13.19	20.31	48.16	18.34	5.44	3.16	57.0	
	5	10.91	18.14	45.12	24.83	5.89	3.21	51.7	
Algodones, CA (dune flats)	1	23.22	23.10	29.55	24.13	4.91	3.67	26.7	
	2	16.15	16.72	41.64	25.49	5.67	3.41	34.3	
	3	13.46	24.45	49.33	12.77	5.04	3.04	50.4	
	4	20.04	32.24	37.74	9.98	4.19	3.11	49.7	
	5	27.42	32.88	25.53	14.17	3.87	3.37	48.7	
	6	10.93	11.20	41.31	36.56	6.62	3.27	40.4	
Yuma, AZ (scrub desert)	1	46.77	1.74	29.84	21.65	4.37	3.91	50.5	
	2	31.09	30.12	17.18	21.60	4.04	3.72	40.4	
	3	15.09	17.33	44.46	23.12	5.62	3.32	41.3	
	4	23.00	21.33	40.41	15.26	4.69	3.35	46.7	
	5	30.95	23.11	30.92	15.03	4.13	3.47	21.4	
Tucson, AZ (Santa Cruz river terrace)	1	31.75	29.12	25.36	13.76	3.77	3.39	30.8	
	2	26.99	24.99	33.30	14.72	4.27	3.41	41.7	
	3	6.88	13.31	50.09	29.72	6.53	2.97	34.5	
	4	9.48	20.47	48.61	21.43	5.76	3.10	18.9	
	5	10.78	16.51	47.90	24.82	5.97	3.16	35.1	

TABLE 2. (Continued)

SITE	GRAIN SIZE DISTRIBUTION OF AEROSOLS (% FREQUENCY)						MEAN SIZE ( $\mu\text{m}$ )	STANDARD DEVIATION ( $\mu\text{m}$ )	SHEAR VELOCITY (cm/sec)
	< 1.0 $\mu\text{m}$	1.0 - 2.5 $\mu\text{m}$	2.5 - 10.0 $\mu\text{m}$	10.0 $\mu\text{m}$	10.0 $\mu\text{m}$	10.0 $\mu\text{m}$			
Tucson, AZ (construction)	1	26.70	36.49	30.74	6.07	6.07	3.47	2.92	18.5
	2	12.36	17.87	45.12	24.64	24.64	5.82	3.26	30.9
	3	22.07	23.80	30.33	23.80	23.80	4.94	3.64	30.4
	4	13.43	18.56	47.11	20.90	20.90	5.59	3.21	50.2
	5	36.71	27.44	23.68	12.16	12.16	3.49	3.35	49.1
Ajo, AZ (mine tailings)	1	22.15	23.02	35.76	19.07	19.07	4.80	3.48	26.8
	2	28.68	20.02	30.46	20.84	20.84	4.61	3.65	31.2
	3	16.85	22.75	46.13	14.27	14.27	4.96	3.17	25.9
	4	31.05	27.33	23.22	18.40	18.40	4.06	3.60	51.4
Hayden, AZ (mine tailings)	1	15.85	22.99	47.10	14.06	14.06	5.01	3.14	33.2
	2	27.90	22.37	25.85	23.88	23.88	4.66	3.75	24.6
	3	15.64	14.98	33.28	36.10	36.10	6.15	3.60	27.5
	4	14.66	15.33	36.03	33.98	33.98	6.11	3.52	41.7
	5	30.02	26.79	32.72	10.47	10.47	3.86	3.25	34.6
	6	30.35	30.90	21.31	17.44	17.44	3.89	3.54	41.7
Mesa, AZ (salt river)	1	23.07	10.98	56.75	9.20	9.20	4.94	3.04	17.7
	2	13.36	16.65	47.16	22.84	22.84	5.75	3.23	22.2
	3	30.05	26.67	22.89	20.39	20.39	4.21	3.67	41.7
	4	9.59	18.62	42.47	29.35	29.35	6.11	3.26	34.2
	5	28.17	24.83	25.78	21.22	21.22	4.44	3.68	29.6
Casa Grande, AZ (abandoned agricultural)	1	25.25	43.73	27.42	3.60	3.60	3.14	2.67	36.7
	2	32.82	28.19	29.37	9.63	9.63	3.59	3.21	22.0
	3	12.16	16.64	45.60	25.60	25.60	5.92	3.25	35.5
	4	9.31	20.18	50.63	19.88	19.88	5.73	3.05	34.5

## 4. TEST RESULTS

### 4.1 Threshold Shear Velocity

Threshold shear velocities for the sampled surfaces vary markedly and range from 17.2 to 58.2 cm/s (Table 3). These values are similar to threshold values found by Gillette, *et al.* (1980) for a variety of undisturbed and disturbed desert sites in the Mojave Desert.

Also included in Table 3 are the associated 10m wind velocities required to initiate particle motion and the mean vertical aerosol fluxes (F). The 10m velocities were computed using the Prandtl equation (Eq. 1) and the roughness lengths found during the wind tunnel tests. Although there is considerable overlap between the threshold values of the undisturbed and disturbed sites, the disturbed surfaces in general have considerably lower threshold wind speeds. This finding is also consistent with the data of Gillette, *et al.* (1980).

The 10m threshold velocities indicate that wind erosion could be initiated at all sites under most normally occurring natural wind conditions. However, the relatively high threshold values found at the Algodones dune flat site and the three active agricultural sites would suggest that major wind erosion events would be relatively infrequent considering the range of naturally occurring wind velocities.

Chepil (1951) and Gillette, *et al.* (1980) have shown a general increase in threshold shear velocity with an increase in the modal size of the surface aggregate size distribution. It should be noted, however, that the empirical relationships shown by these authors are relatively weak and demonstrate the inherent variability in natural sediments. Results from the wind tunnel tests showed no clear relationship between mean grain size and threshold shear velocity ( $u_*$ ) for the 13 Arizona sites. This most likely results from the similarity of modal diameters for the sampled sites and the complicating effects of other surface parameters, such as vegetation and surface crusting, which are not evaluated in a simple bivariate relationship. A significant relationship at the 0.1 confidence level, however, was found to exist between threshold shear velocity and the percentage of aggregates <0.84m (Fig.4). This best-fit least squares relationship is:

$$u_{*t} = 20.09 (\% \text{ aggregates } > 0.84 \text{ mm})^{0.202} \quad (2)$$

$$r = 0.58$$

$$n = 13$$

TABLE 3. Aerosol Emission Test Results

SITE	U <sub>t</sub> (m/sec)	U <sub>10m</sub> (m/sec)	z <sub>0</sub> (cm)	mean F (g/cm <sup>2</sup> sec)	mean grain size (μm)	SURFACE SEDIMENTS		
						standard deviation (μm)	% silt clay	% aggregates > .84mm
Mesa, AZ (agricultural land)	0.569	15.63	0.0331	7.27 x 10 <sup>-9</sup>	1077.0	1844.0	18.6	26.8
Maricopa, AZ (agricultural land)	0.578	13.82	0.1255	1.90 x 10 <sup>-8</sup>	749.3	1003.4	11.2	37.3
Yuma, AZ (agricultural land)	0.582	16.59	0.0224	4.88 x 10 <sup>-8</sup>	642.6	1686.6	8.8	18.5
Casa Grande, AZ (abandoned agricultural land)	0.246	7.80	0.0067	2.97 x 10 <sup>-8</sup>	234.4	307.3	26.6	2.4
Glendale, AZ (construction site)	0.530	14.69	0.0301	5.65 x 10 <sup>-8</sup>	1275.1	2499.0	24.7	27.9
Tucson, AZ (construction site)	0.251	7.26	0.0191	1.83 x 10 <sup>-7</sup>	1010.9	2001.5	14.3	21.0
Ajo, AZ (mine tailings)	0.228	6.68	0.0176	6.75 x 10 <sup>-8</sup>	335.3	202.4	8.9	0.5
Hayden, AZ (mine tailings)	0.172	5.11	0.0141	3.25 x 10 <sup>-7</sup>	271.8	528.3	27.3	3.0
Algodones, CA (dune flats)	0.625	18.31	0.0166	1.83 x 10 <sup>-8</sup>	2794.0	2819.4	15.2	60.3
Yuma, AZ (scrub desert)	0.386	11.33	0.0163	1.83 x 10 <sup>-8</sup>	1038.8	1897.4	17.2	22.4
Yuma, AZ (disturbed scrub desert)	0.320	8.11	0.0731	8.89 x 10 <sup>-8</sup>	591.8	1145.5	3.2	7.7
Tucson, AZ (Santa Cruz river terrace)	0.180	7.26	0.0204	7.90 x 10 <sup>-8</sup>	1950.7	3251.2	20.9	37.4
Mesa, AZ (Salt River channel)	0.218	6.68	0.0100	1.65 x 10 <sup>-7</sup>	398.7	693.4	27.7	11.3

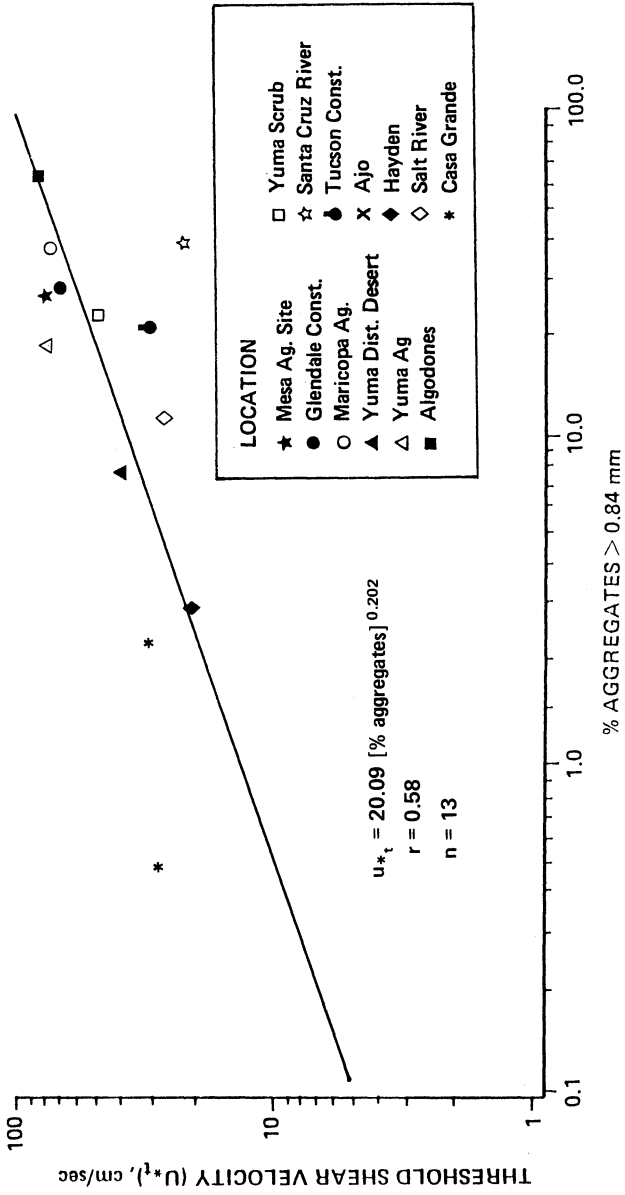


Figure 4: Variation of average threshold shear velocity ( $u_{*t}$ ) with percentage of aggregates > 0.84 mm.

Chepil (1951) and Gillette, *et al.* (1980) have also shown similar relationships between soil erodibility and percentage of aggregates for agricultural and natural desert soils respectively. The relative concentration of large particles or aggregates at the surface affect threshold shear velocity in at least two ways. First, larger grains or aggregates which may be too large to be transported at a given velocity protrude above the surface and absorb a large proportion of the shearing stress exerted by the wind. This effect is noticeable even when the concentration of these non-erodible units is relatively small (Chepil, 1951). Second, larger stationary particles tend to shield smaller, more easily entrained particles from the wind shear. Consequently as the concentration of non-erodible units increases, the threshold shear velocity also increases.

Bagnold (1941), from theoretical considerations and empirical observations, found that threshold shear velocity for dry, well-sorted sands can be defined by:

$$U_{*t} = A \left( \frac{\sigma - \rho}{\rho} \cdot g \cdot D_p \right)^{0.5} \quad (3)$$

where  $\sigma$  and  $\rho$  are the particle and air densities, respectively,  $g$  — the acceleration due to gravity,  $D_p$  — the mean particle diameter, and  $A$  — an empirical coefficient equal to approximately 0.1 for particle friction Reynolds numbers ( $B$ )  $> 3.5$  ( $B = u_* D_p / \nu$ , where  $\nu$  is the kinematic viscosity of air).

Although the Bagnold equation is quite reliable for predicting the threshold velocity of well sorted sands  $>0.1$  mm mean diameter, it is much less satisfactory in the prediction of thresholds for agricultural and natural soils (Gillette, *et al.*, 1980; Nickling, 1984). Naturally occurring sediments, no matter how well sorted, usually contain a wide range of grain sizes; including clays that cause significant variation in threshold shear velocity. Moreover, non-erodible roughness elements (such as vegetation, pebbles and boulders) decrease the momentum transfer to smaller, shielded soil particles thereby increasing the shear velocity required to initiate motion. Similarly, other surface effects such as moisture, soluble salts, organic residues and clay crusts tend to stabilize the surface decreasing entrainment (Gillette, *et al.*, 1980; 1982 and Nickling, 1984).

## 4.2 Vertical Aerosol Fluxes

Direct field observations by several investigators have shown that the concentration of suspended sediment over eroding surfaces decreases as a power function of height, with exponents ranging from approximately -0.25 to -0.35 (e.g. Chepil and Woodruff, 1957; Shinn, *et al.*, 1976; Gillette, 1977 and Nickling, 1978). This relationship can be expressed by:

$$\frac{dn}{dz} = P \frac{n}{z} \quad (4)$$

where  $n$  is the dust concentration at height  $z$  and  $P$  is the average slope of the concentration against height relationship ( $\sim -0.3$ ).

Gillette, *et al.* (1972) and Shinn, *et al.* (1976) suggest that the established power law relationship found in the concentration profiles allows the vertical dust flux ( $F$ ) to be described by:

$$F = K \frac{dn}{dz} \quad (5)$$

where  $K$  is the eddy diffusivity. Under neutral stability conditions,

$$K = u_* k z \quad (6)$$

where  $u_*$  is shear velocity and  $k$  is von Karman's Constant ( $\sim 0.4$ ).

Assuming that the dust concentration follows a power law distribution with height and combining equations 4, 5, and 6, the vertical aerosol flux ( $F$ ) from a point concentration can be estimated by:

$$F = k P u_* n \quad (7)$$

The suspended sediment concentration ( $n$ ,  $\mu\text{g}/\text{m}^3$ ) at the 50 cm sampling height in the wind tunnel during each test run was calculated by:

$$n = \frac{W}{Rt} \quad (8)$$

where  $W$  is the dry weight ( $\mu\text{g}$ ) of sediment collected on the membrane filter,  $R$  is the flow rate ( $\text{m}^3/\text{s}$ ) through the sampler nozzle and  $t$  is the length of the sampling period (seconds). The mean concentration during each test was computed by averaging the concentration values measured on

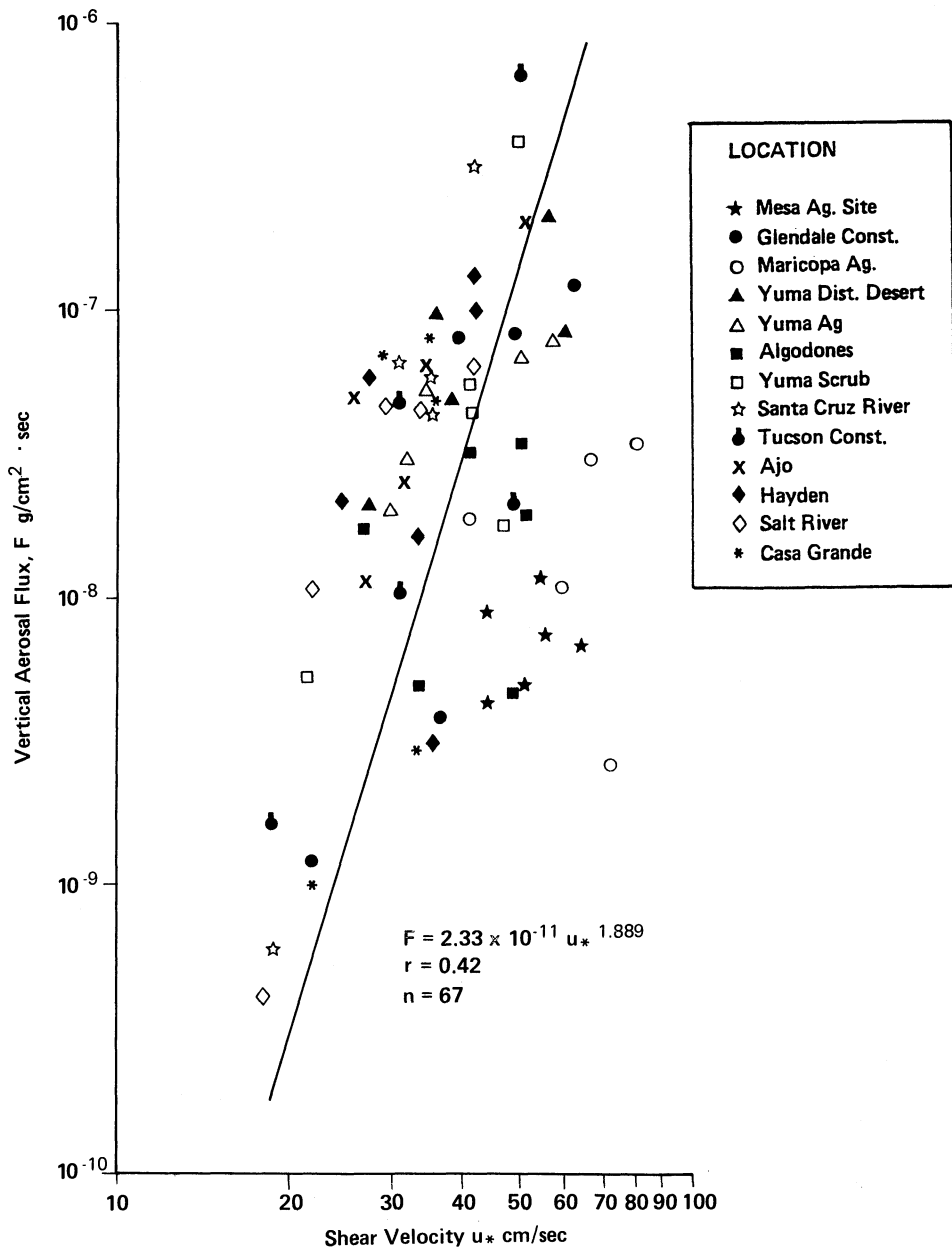


Figure 5: Variation of vertical aerosol flux (F) with increasing shear velocity (u\*).



the two filters installed in the wind tunnel for each test. In almost all cases the differences in the two measured concentrations were less than 10%, indicating the relatively good reproducibility of the sampling technique.

The mean vertical aerosol fluxes ( $F$ ) measured at the thirteen selected sites are given in Table 3. The measured fluxes range from  $1.0 \times 10^{-9}$  to  $6.5 \times 10^{-7}$  g/cm<sup>2</sup> sec and show wide intersite variability. Shear velocities associated with the vertical fluxes range from 17.7 to 80.1 cm/sec.

As shown in Figure 4, there is a general increase in the vertical flux with increasing shear velocity. Although there is a considerable degree of data scatter, the data can be described by the following least squares regression which is significant at the 0.1 confidence level.

$$F = 2.33 \times 10^{-11} u_*^{1.889} \quad (9)$$

$$r = 0.42$$

$$n = 68$$

The degree of scatter in the data is not unexpected considering the intersite variability in surface characteristics such as soil texture, the absence or presence of a surface crust, and the type and percentage of vegetative cover. The erosion system is not a simple bivariate relationship between vertical aerosol flux and shear velocity but multivariate, with surface characteristics interacting and influencing the availability of particles for transport and therefore the flux rates.

It is noteworthy that the data shown in Figure 4 compares very favorably with that presented by Gillette (1977) in terms of both the range of vertical fluxes observed and the degree of data scatter. Gillette's data were collected in West Texas during a four-year period over nine agricultural fields with varying textural characteristics.

To investigate the scatter in the data set, it was partitioned on the basis of the percentage of silt and clay measured in the surface sediments (Figs. 6 and 7) and also on the similarity of surface morphology and land use.

Figure 6 shows the vertical flux against  $u_*$  for soils having a combined silt and clay content >25%. For these silty loams, a relatively high correlation exists between increasing vertical flux and  $u_*$ :

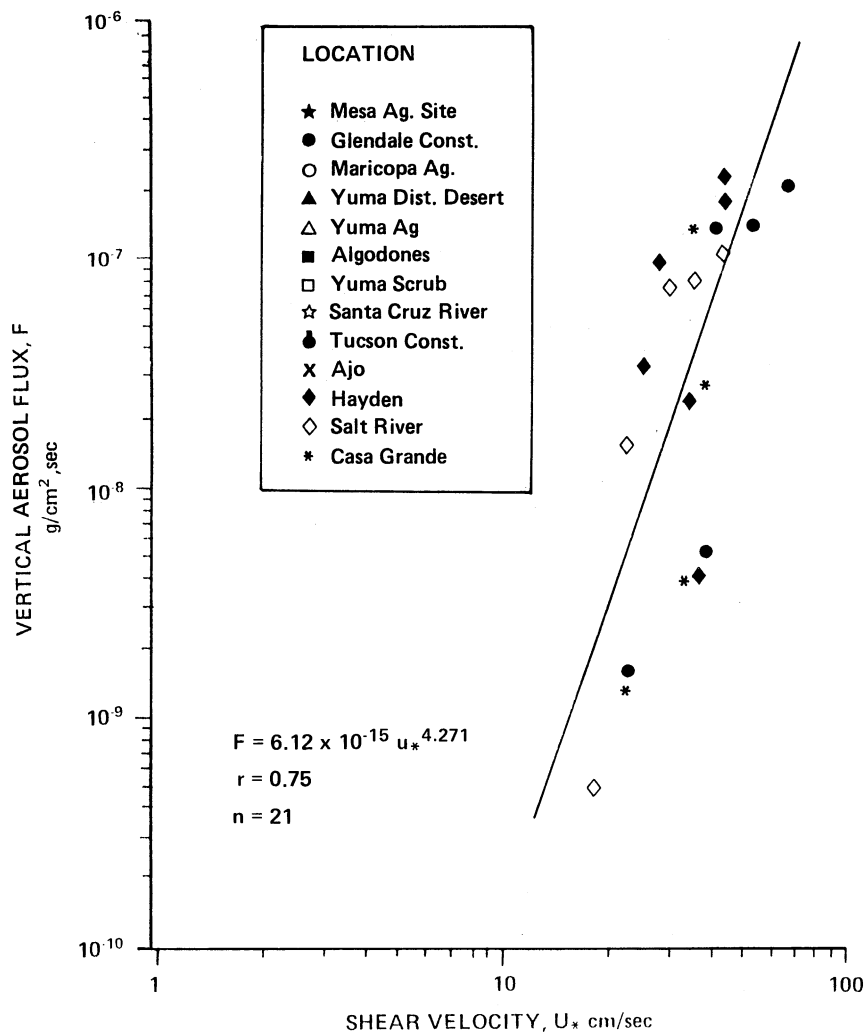


Figure 6: Variation of vertical aerosol flux (F) with increasing shear velocity ( $u_*$ ) for soils with silt and clay content > 25%.

$$F = 6.12 \times 10^{-15} u_*^{4.271} \quad (10)$$

$$r = 0.75$$

$$n = 21$$

The variation of vertical flux with increasing  $u_*$  for the sandy soils (silt and clay >15%) is shown in Figure 7. The relatively poor relationship, which is evident on this plot, primarily results from the inclusion of the Maricopa agricultural site data. This site, although similar in sand content to the other four sites, was considerably different in terms of surface roughness characteristics. The field on which tests were carried out had been very recently ploughed and was characterized by well-defined ridges 15-20 cm in height. In addition, the surface was covered with large clods 8-10 cm in diameter which resulted from ploughing under somewhat moist conditions. These large clods were not broken down by abrasion during the wind tunnel tests, and thus acted as large non-erodible roughness elements which tend to protect the finer soil fractions from deflation (Chepil and Woodruff, 1963). This results in a much less rapid increase in vertical flux with increasing shear velocity than was observed at the other four sites.

If the Maricopa data are omitted from the regression because of the cloddy nature of the soils, the vertical aerosol flux for the sandy soils can be described by:

$$F = 7.79 \times 10^{-13} u_*^{3.027} \quad (11)$$

$$r = 0.77$$

$$n = 19$$

In comparison to the above results, Gillette (1977) found a fairly uniform trend of increasing vertical particle flux with increasing shear velocity for sites with sandy soils. He attributes this relatively good relationship to the uniformity of the dry aggregate structure of the soils investigated in his study. In contrast, the relationship between vertical flux and shear velocity presented by Gillette (1977) for loamy soils showed great variability, which he attributed to the widely different dry aggregate structures of these soils. This argument is similar to that used to account for the lower fluxes found at the Maricopa agricultural site in this study.

Since textural data may not be readily available when estimating emission factors for various surfaces, an attempt was made to partition the data on the basis of surface morphology and land use. Despite the limited data, five classes were established:

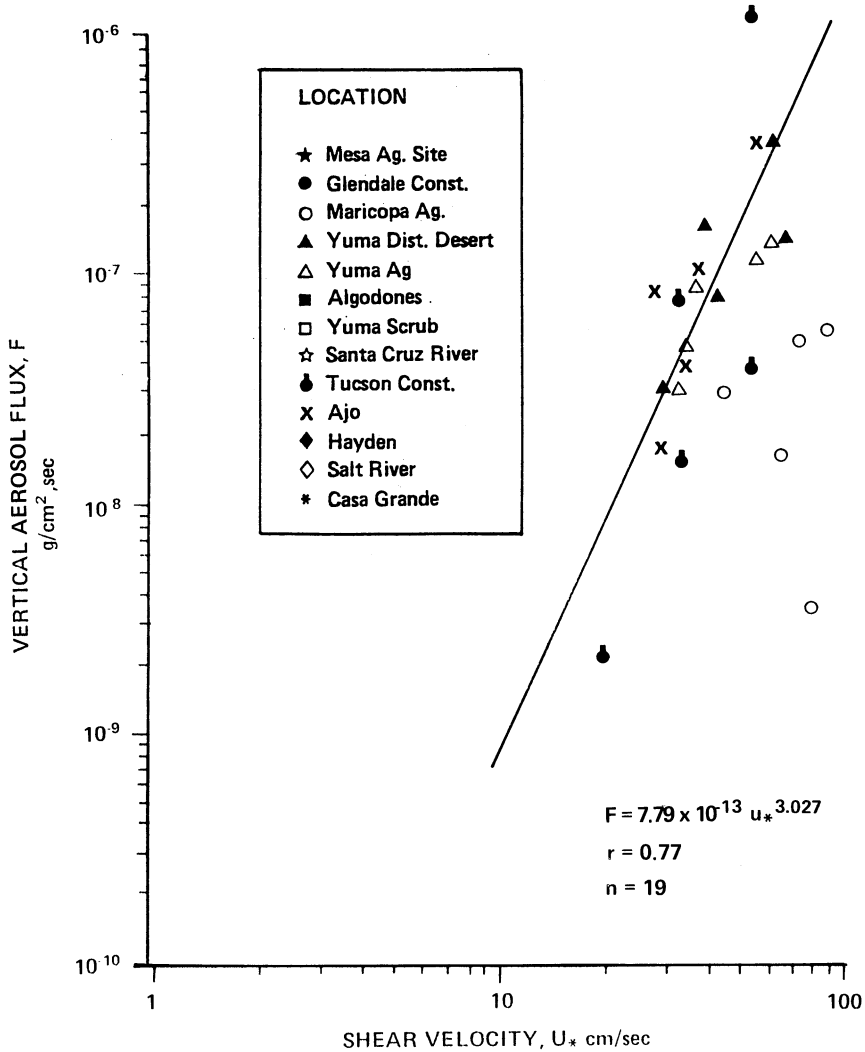


Figure 7: Variation of vertical aerosol flux ( $F$ ) with increasing shear velocity ( $u_*$ ) for soils with silt and clay content < 15%. Maricopa Ag. site data are not included in the regression.

- 1) Natural and Disturbed Desert Sites,
- 2) Sites Developed or Modified by Fluvial Processes,
- 3) Construction Sites,
- 4) Mine Tailings, and
- 5) Agricultural Sites.

Significant regressions were derived for all classes except agricultural sites. In general, the regressions are typified by relatively high correlation coefficients and may prove useful for estimating emission rates from surfaces when textural data are lacking. A great deal of caution must be exercised, however, since the criteria on which the classes were based is somewhat arbitrary.

The regression relationships derived for the morphological land use classes are:

- 1) Natural and Disturbed Desert Sites

$$\begin{aligned}
 F &= 7.99 \times 10^{-13} u_*^{2.99} & (12) \\
 r &= 0.76 \\
 n &= 10
 \end{aligned}$$

- 2) Fluvial Sites

$$\begin{aligned}
 F &= 1.59 \times 10^{-13} u_*^{3.32} & (13) \\
 r &= 0.61 \\
 n &= 16
 \end{aligned}$$

- 3) Construction Sites

$$\begin{aligned}
 F &= 5.82 \times 10^{-15} u_*^{4.24} & (14) \\
 r &= 0.81 \\
 n &= 10
 \end{aligned}$$

## 4) Mine Tailings

$$\begin{aligned}
 F &= 1.59 \times 10^{-12} u_*^{2.93} \\
 r &= 0.76 \\
 n &= 10
 \end{aligned}
 \tag{15}$$

The wide data scatter and the lack of a significant correlation coefficient for the agricultural sites is most likely related to textural and surface parameters which are not accounted for in a simple bivariate relationship. This is borne out by the fact that significant relationships are present for all individual sites except Maricopa.

Several authors have suggested that the vertical emission of aerosols is related to the amount of material transported in saltation and creep. To characterize this relationship, the dimensionless ratio of vertical aerosol flux ( $F$ ) to horizontal soil flux,  $q'$  ( $\text{g}/\text{cm}^2 \text{ sec}$ ) has been plotted in Figure 8. The horizontal soil flux ( $q'$ ) is calculated by dividing the horizontal transport rate  $q$  ( $\text{g}/\text{cm sec}$ ) by the height of the saltation/creep sediment trap (Gillette, 1977).

Despite the data scatter a statistically significant trend is apparent. This relationship can be described by:

$$\begin{aligned}
 (F/q') &= 3.14 \times 10^{-10} u_*^{2.85} \\
 r &= 0.54 \\
 n &= 68
 \end{aligned}
 \tag{16}$$

A somewhat clearer picture is obtained if the data set is partitioned on the basis of soil texture. The more loamy textured soils (silt + clay > 25%) show a significant increase in flux ratio with increasing shear velocity.

$$\begin{aligned}
 (F/q') &= 5.01 \times 10^{-12} u_*^{4.01} \\
 r &= 0.63 \\
 n &= 21
 \end{aligned}
 \tag{17}$$

This result is very similar to that presented by Gillette (1977) who also found that the flux ratio increased with shear velocity with an exponent of approximately 4.0.

A similar, but somewhat weaker, relationship was also found for the sandy textured soils (silt + clay < 15%).

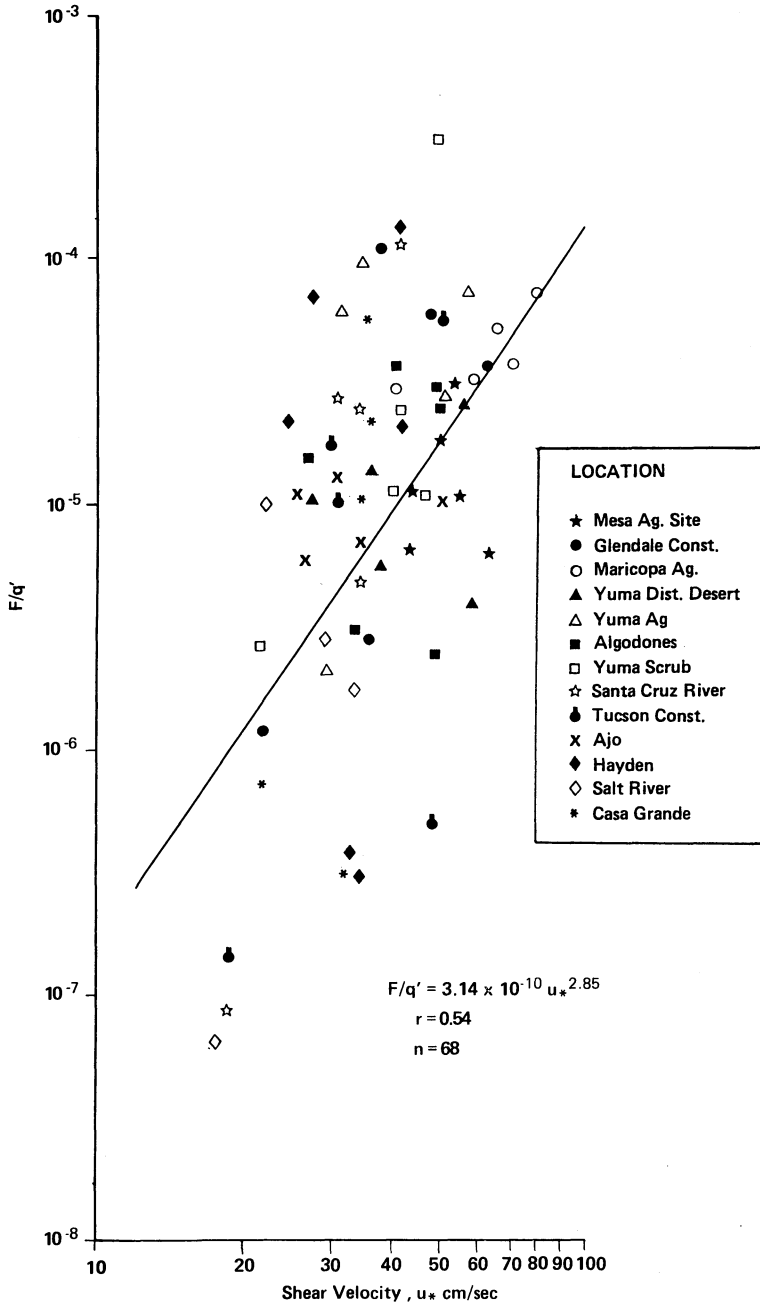


Figure 8: Variation at the ratio of vertical aerosol flux (F) to horizontal soil flux (q') in saltation and creep with increasing shear velocity.<sup>1</sup>

$$(F/q') = 5.37 \times 10^{-9} u_*^{2.10} \quad (18)$$

$$r = 0.51$$

$$n = 19$$

The above relationships demonstrate the importance of soil texture in the emission of fine particulates. In general, soils with finer textures produced more fine dust per unit horizontal soil flux than the coarser textured soils. The increase of the exponent value of  $u_*$  with increasing percentage of silt and clay also indicates that the fine, textured soils produce particulates at a much higher rate as shear velocity increases.

### 4.3 Aerosol Grain-Size Characteristics

Frequency size distributions of the aerosols collected during the wind tunnel tests are shown in Table 2. The mean sizes and standard deviations of both the aerosols and the associated surface sediments are also included.

In general, the aerosols are characterized by unimodal size distributions with weak to moderate positive skewness (i.e. tail of coarser grains). The most striking feature of the size distributions is their similarity. Almost all the distributions have modal diameters in the 2.5-10.0  $\mu\text{m}$  size range. The one major exception to this is the Mesa agricultural site, which has strong modes in the <1.0  $\mu\text{m}$  and 1.0-2.5  $\mu\text{m}$  size classes reflecting the relatively high silt and clay content (18.6%) of the parent soil (Table 3).

The mean size of the aerosols range from 1.28 to 6.62 $\mu\text{m}$ , with a remarkable uniformity of mean sizes. The aerosols are rather poorly sorted, with standard deviations ranging from 1.69 to 3.65  $\mu\text{m}$ , with the majority being from 3.25 to 3.55  $\mu\text{m}$ . The relatively poor sorting of aerosols has also been reported by Gillette, *et al.* (1972), Patterson and Gillette (1977b), and Nickling (1983). It is suggested that the rather poor sorting associated with fine-grained aerosols (1-20  $\mu\text{m}$ ) results from the low sedimentation velocities of these particles.

Gillette (1974) suggests that particles less than 20  $\mu\text{m}$  are sufficiently small and that their sedimentation velocities are usually less than 0.1  $u_*$  for almost all eroding winds and remain in suspension for great distances. Since all particles (<20  $\mu\text{m}$ ) that are ejected into the air stream tend to remain in suspension, the size distributions tend to become more uniform (i.e. poorly sorted) as a result of turbulent mixing regardless of the shear velocity or textural characteristics of the parent soil.



As previously indicated, there is a great similarity in the mean sizes of the suspended sediment despite a considerable difference in the textural characteristics of the surface sediments from which the aerosols were derived. Moreover, no consistent relationship is evident between the mean size and the shear velocity at which the suspended sediments were transported. The lack of consistent relationships between the mean size of aerosols in the 1-10  $\mu\text{m}$  size range with shear velocity and textural characteristics of the parent soils has been noted by several authors.

Patterson and Gillette (1977a), from their study of aerosols over eroding surfaces, suggest that the distributions are characterized by three distinct modes which may not all be present under a given set of conditions. The authors have labelled the characteristic modes A, B and C. Mode A, which contains a majority of particles having diameters between 2 and 20  $\mu\text{m}$ , is characteristic of soil-derived aerosols but does not appear to be related to the size distribution of the parent soil. Mode B is centered between 20 and 200  $\mu\text{m}$ . It is characteristic of the particle size distribution of the parent soil. This mode is present only under conditions of heavy to moderate dust loading. Mode C is centered between 0.04 and 0.1  $\mu\text{m}$ . In general, it is not related to the other modes in composition or origin but is characteristic of a background aerosol concentration related to the transient nuclei mode of Willeke and Whitby (1975).

Gillette and Goodwin (1974) suggest that mode B is characteristic of particles derived from loose soil aggregates, while mode A results from the breakup of aggregates by the saltation process (sandblasting) and the subsequent injection of disaggregated material into the atmosphere. As the wind speed increases over the threshold for erosion, the first particles to be set in motion are those with diameters between 40 and 100  $\mu\text{m}$ . The initial movement is primarily due to saltation in which the particles bounce along close to the surface. These particles collide with other particles on the surface, dislodging and disaggregating smaller particles which are injected into the atmosphere and produce mode A. The larger particles which form mode B (20-200  $\mu\text{m}$ ) quickly settle out because of their high sedimentation velocities. As a result, a relatively narrow range of particle sizes is kept aloft in suspension by the vertical velocity fluctuations.

This selective transport process, related to the turbulent nature of most eroding winds, accounts for the narrow range of mean sizes and poorly sorted distributions associated with samples collected during the wind tunnel tests.

## 5. DISCUSSION

The collected data revealed that in general the natural desert surfaces, including the Algodones dune complex outwash area and the tested agricultural sites, have higher average threshold shear velocities and lower particulate fluxes than the other tested sites. The stability of these areas is associated with several important factors. The crusting of desert soils, resulting from the presence of clay and natural salts, frequently protects these soils from erosion for all but extremely high winds. In addition, the amount of vegetative cover plays a significant role in the reduction of aerosol flux because of momentum partitioning and surface roughness effects. Precipitation is also an extremely important factor in decreasing particulate emissions from desert soils. Although precipitation can decrease emissions by the simple wetting of the surface, this control is relatively short lived because of the high evaporation rates in desert environments. Of greater importance is the indirect effect precipitation has on the vegetation pattern and surface crusting.

During periods of increased rainfall, particularly in the winter months when temperatures and evaporation rates are low, vegetation such as annual grasses may become established thereby stabilizing the surface. Even if these grasses do not survive subsequent summer droughts, the dry stubble can persist for several years acting as an effective control on aerosol emission (Brazel and Nickling, 1986).

The frequency and intensity of precipitation can also affect the development and maintenance of surface crusts. Surface water mobilizes and redistributes clay particles and allows them to seal the surface as they sediment out during infiltration and evaporation. In contrast, heavy rainfall events may break up surface crusts, reducing the bonding effectiveness; thereby increasing the susceptibility of the soil to erosion (Gillette, *et al.*, 1982).

A final consideration for the desert soils is the time interval between disruptions of the surface. Long disturbance-free periods will allow deflation of erodible material and the development of a lag deposit which effectively armours the surface; thereby reducing the emission potential. The stability of these soils can be seriously affected by anthropogenic effects, such as off-road vehicles or overgrazing, which rework the surface making erodible particles available for transport. In contrast, the stability of the agricultural soils is related to their ridged surface and cloddy soil structure which protect the finer soil fractions from deflation and increase the threshold shear velocity.

An important consideration in the determination of aerosol fluxes which is frequently not addressed is the decrease in flux through time as sediment is removed, and a lag of non-erodible grains develops at the surface. The fluxes in this study were measured in the order of minutes and during many of the test runs the deflation of the fine-grained particulates occurred relatively quickly. The surface then became stable as a lag of non-erodible soil units developed ( $>0.84$  mm) which effectively sheltered the erodible soil particles. Consequently, the erosion system involves an emission decay function. The surface will not produce a given aerosol flux for a given shear velocity for an indefinite period of time. This relationship has not been defined, and further research is necessary to examine the decay function for various type surfaces, soil textures and for the degree of disturbance at the surface.

## 6. CONCLUSIONS

This research has shed more light on the question of the relative importance of different surfaces in the production of atmospheric aerosols in southern Arizona. Of the variety of sites tested, it was apparent that those which experience periodic disturbance such as the river channels and mine tailing sites have the greatest potential for increased aerosol production because of the greater sediment supply and lower threshold shear velocities. The natural desert sites, controlled construction sites, and the agricultural sites have reduced emission potential because of their higher threshold shear velocities and lower flux values because sediment supply is limited by factors such as progressive armouring, surface crusting roughness, and vegetation.

This study also clearly indicates the usefulness of *in situ* testing using the portable wind tunnel. Previous to this research, the most detailed data on aerosol fluxes from natural surfaces was that presented by Gillette (1977). His data collection took place over a four-year period, with a limited range of surface conditions. In contrast, data collection for the present study was accomplished in approximately eight weeks for a wide range of velocity and surface conditions with comparable results.

## REFERENCES

- Bagnold, R.A., 1941: *The Physics of Blown Sand and Desert Dunes*, Morrow, New York, 265 p.

- Brazel, A.J., and Nickling, W.G., 1986: The relationship of weather types to dust storm generation in Arizona (1965-1980), *J. Climatol.*, 6: 255-275.
- Chepil, W.S., 1951: Properties of soil which influence wind erosion: IV, State of dry aggregate structure, *Soil Sci.*, 72: 387-401.
- Chepil, W.S., and Woodruff, N.P., 1957: Sedimentary characteristics of dust storms: II, Visibility and dust concentrations, *Am. J. Sci.*, 255: 104-114.
- Chepil, W.S., and Woodruff, N.P., 1963: The physics of wind erosion and its control, *Advances in Agronomy*, 15: 211-302.
- Complin, P.G., and Piersol, P., 1978: Uranium mill tailings area fugitive emissions, Proceedings Third Symposium on Fugitive Emissions Measurement and Control, San Francisco, CA, October.
- Gillette, D.A., 1977: Fine particulate emissions due to wind erosion, *Trans. ASA*, 80: 890-897.
- Gillette, D.A., 1978: A wind tunnel simulation of the erosion of soil: effect of soil texture, sandblasting, wind speed and soil consolidation on dust production, *Atmos. Environ.*, 12: 1735-1743.
- Gillette, D.A., and Goodwin, P.A., 1974: Microscale transport of sand-sized soil aggregates eroded by wind, *J. Geophys. Res.*, 79: 4080-4084.
- Gillette, D.A., Blifford, I.H., Jr., and Fenster, D.R., 1972: Measurements of aerosol on land subject to wind erosion, *J. Appl. Meteorol.*, 11: 977-987.
- Gillette, D.A., Adams, J., Endo, A., Smith, D., and Kihl, R., 1980: Threshold velocities for input of soil particles into air by desert soils, *J. Geophys. Res.*, 85: 5621-5630.
- Gillette, D.A., Adams, J., Muhs, D., and Kihl, R., 1982: Threshold friction velocities and rupture moduli for crusted desert soils for the input of soil particles into air, *J. Geophys. Res.*, 87: 9003-9015.
- Leathers, C.R., 1981: Plant components of desert dust in Arizona and their significance for man, In: Péwé, T. (Ed.), *Desert Dust: Origin characteristics and effects on man*, Geological Society of America Special Paper 186, p. 191.

- Nickling, W.G., 1978: Eolian sediment transport during dust storms: Slims River Valley, Yukon Territory, Canada, *Canad. J. Earth Sci.*, 15: 1069-1084.
- Nickling, W.G., 1983: Grain size characteristics of sediment transported during dust storms, *J. Sed. Pet.*, 53: 1011-1024.
- Nickling, W.G., 1984: The stabilizing role of bonding agents on the entrainment of sediment by wind, *Sedimentology*, 31: 111-117.
- Nickling, W.G., and Brazel, A.J., 1984: Temporal and spatial characteristics of Arizona dust storms, *J. Climatol.*, 4: 645-660.
- Patterson, E.M., and Gillette, D.A., 1977a: Commonalities in measured size distribution from aerosols having a soil-derived component, *J. Geophys. Res.*, 82: 2074-2082.
- Patterson, E.M., and Gillette, D.A., 1977b: Measurements of visibility vs. mass-concentration for airborne soil particles, *Atmos. Environ.*, 11: 193-196.
- Peach, P.A., and Perrie, L.A., 1974: Grain-size distribution within glacial varves, *Geology*, 3: 43-46.
- Perrie, L.A., and Peach, P.A., 1973: Gelatin-coated microscope slides in sedimentary size analysis, *J. Sed. Pet.*, 43: 1174-1175.
- Péwé, T.L., 1981: Desert dust: an overview, In: Péwé, T.L. (Ed.) *Desert Dust: Origin, Characteristics and Effect on Man*, Special Paper 186, The Geological Society of America, Boulder, CO, pp. 1-10.
- Pilat, M.J., and Ensor, D. S., 1971: Comparison between the light extinction aerosol mass concentration relationship of atmospheric and air pollutant emission aerosols, *Atmos. Environ.*, 5: p. 209.
- Prandtl, L., 1932: Meteorologische Anwendung der Stromungslehre, *Beitr., Phys. d. Freien Atmo.*, XIX: 188-202.

- Shinn, J.H., Kennedy, J.C., Koval, J.S., Clegg, B.R., and Porph, W.M., 1976: Observations of dust flux in the surface boundary layer for steady and nonsteady cases, *Proceedings, Atmosphere-Surface Exchange of Particulate and Gaseous Pollutants*, 1974 Symposium, Richmond, Washington, Energy Research and Development Administration Symposium Series CONF-740921, pp. 625-637.
- Willeke, K., and Whitby, K.J., 1975: Atmospheric aerosols: size distribution interpretation, *J. Air Pollution Control Association*, 25: 529-534.
- Wooding, R.A., 1968: A low-speed wind tunnel for model studies in micro-meteorology, 1, *General design considerations, Commonwealth Sci. Ind. Res. Organ., Aust. Div. Plant Ind.*, Canberra City, A.C.T., Tech. Paper 25, pp. 3-24.

RELATIONSHIPS BETWEEN THE CHARACTERISTICS OF SOILS, THE WIND ENERGY AND DUST NEAR THE GROUND, IN THE WESTERN SANDSEA (N.W. SAHARA)

Pierre Rognon and Geneviève Coudé-Gaussen  
UA 722 - CNRS - Laboratoire de Géodynamique des Milieux  
Continentaux.  
Université Pierre & Marie Curie  
4, place Jussieu  
75252 PARIS CEDEX 05 FRANCE

Gilles Bergametti and Laurent Gomes  
UA 717 - CNRS - Laboratoire de Physico-Chimie de l'Atmosphère  
Université Paris VII  
2, place Jussieu  
75251 PARIS CEDEX 05 FRANCE

ABSTRACT: In and around a sandsea of 80,000 km<sup>2</sup>, 120 dust samples have been collected by air filtration during a wind still period, a windy period and several dust storms between March 1985 and March 1986. In relation to these different meteorological conditions, Si concentration in dust increases from 0.5 to 70 µg/m<sup>3</sup>, correlated with the increasing wind energy and has been used as an indicator of the wind erosion intensity. As Si concentration increases, the Ca/Si ratio and the amount of calcite and gypsum decrease. Inversely, the amounts of fine particles (<2µm) and of quartz and clay minerals increase. These results are in good agreement with the "behaviour" of the surface soils towards the deflation. About 60 soil samples have been sampled around the sites and classified according to their ability to be eroded by the wind. For instance the most erodible soils are the carbonated powdery ones, which yield their directly available amount of calcite even when the wind intensity is low.

## 1. INTRODUCTION

In the northern Sahara, very few works have been carried out on the relationships between eolian dust, wind processes and various patterns of soils within an area. In Libya, the dune fields seem relatively unproductive for the generation of dust because the fine particles below 20-30µm have been already strongly depleted (Schütz and Jeanicke, 1974) whereas alluvial deposits and flood plains around mountain ranges are the best sources for Saharan dust (Yaalon and Ganor, 1979). In the last two years, our research group investigated the initial sorting of wind blown particles in a region where some wadis carry silt and clay from the Atlas

mountains as far as the edge of the Western Great Sandsea, about 200km south of the Atlas (fig. 1). This area, of about 80,000 km<sup>2</sup> was selected as study area because of its very arid climate and of the varied types of terrain favourable for dust deflation, and because it shows evidence of intense Late-Holocene wind erosion. Yearly rainfall very rapidly decreases from about 117mm in El Abiodh to 50-60mm north of the sandsea and 20-40mm at its southern edge. Aridity increases as towards the south, because the vegetation, very scattered on the Atlas piedmont, disappears almost completely. The predominant wind direction is from north or north-west in El Abiodh. In summer, a secondary direction is observed from south-west. But the wind data are only available for the period 1935-1950 and are discontinuous (Callot, 1987).

Active dunes, characterized by fine sands overlap the older and larger ones that are built of coarser sand. Many areas around the sandsea are covered with thin sandsheets in connection with this large bulk of quartz sands. Sandsheets, only a few centimeters thick, are ubiquitous. At the northern edge of the sandsea, there are numerous blowout depressions (dayas), some kilometers in diameter and tens meters deep. During the Pleistocene, they were excavated by wind in the substratum of the sandsea (i.e. Tertiary sandstones, clay or calcretes). These dayas have been filled with very various lacustrine deposits (clay, carbonate, gypsum, halite) during the Holocene wet period (from 9000 to 4000 y BP). Since 4000 or 3000 BP, these soft sediments have been intensively eroded by a very active wind erosion (Callot, 1987). Therefore, this area seems a good potential source for the dust transported out of the desert, but we must take the large quartz sand cover into consideration, because it restricts the light wind action in and around the sandsea.

Our research project is supported by the French *Centre National de la Recherche Scientifique* (CNRS) for the purpose of understanding the effects of the wind velocity and turbulence at ground level during the initial sorting of the airborne particles.

## 2. SAMPLING OF DUST NEAR THE GROUND

During three field trips, different types of grounds and dust have been sampled :

- During some dust storms in March 1985 and 1986, dust has been collected on about 50 filters in the little town of El Abiodh Sidi Cheikh. The dust was collected by air filtration on 0-4 $\mu$ m porosity filters. The intake was positioned six meters above the ground. Some sample sequences, which were collected over a period of several days of gale or storming characterize air that is heavily loaded with dust. During the dust storms, the wind direction was always from north to south.



- During a windy period (30th of January to 6th of February 1986), dust was collected on a trip around the sandsea as far as 350 km south of El Abiodh. The purpose of this sampling was to characterize some changes in the dust composition on a regional scale.

- During a quiet period (7-22th of December 1985), a movable apparatus with filters at the top of a 9m high mast and a five stage cascade impactor, one meter high, was successively set up on nine different grounds in the northern part of the sandsea. The duration of the pumping was from 5 to 12 hours at each location. The wind velocities were bet-

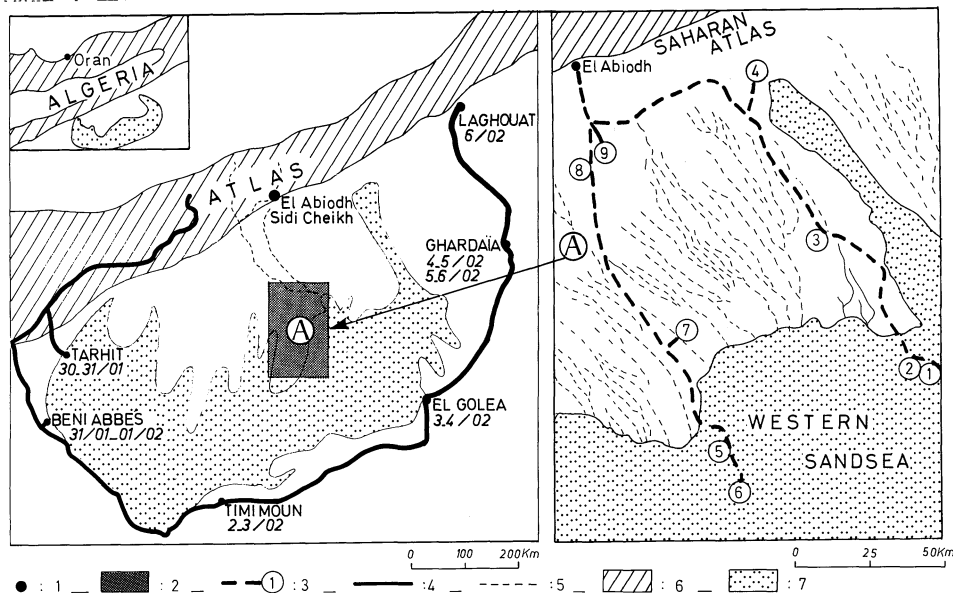


Fig.1- Location map of the studied area : 1- Samples collected during dust storms; 2- field trip area during a quiet period; 3- itinerary followed during this trip, with the nine different stops; 4- trip around the sandsea; 5- wadis, 6- Atlas mountains, 7- Western sandsea.

Most of the samples were collected by bulk filtration (El Abiodh, around the sandsea or at the top of the mast). Cascade impactor samples were used to characterize the grain-size distribution of atmospheric particles from a typical "background" situation with little visible dust entrainment. No rain occurred during the time of sampling.

Thus, about 120 filters and 60 soils samples have been taken above various soil surfaces and in different atmospheric conditions (still air and more or less windy weather) .

The samples collected have been analyzed by X-ray fluorescence, X-ray diffraction (XRD), and scanning electron microscopy (SEM). For samples from very lightly loaded filters, the lack of detection of some minerals by XRD might mean the amount of material is below the detection threshold rather than that the mineral is absent. For instance, a few soils, sampled around the sites contain Na Cl, but there are no detected by XRD Na Cl in the dust samples.

### 3. SAMPLING AND MINERALOGY OF SURFACE SOILS ACCORDING TO THEIR "BEHAVIOR" RELATIVE TO THE WIND ACTION

The surface soils around the sampling sites have been classified according to their erodibility by the wind, their potential availability in fine particles, their size distribution of coarse sand or soil aggregates etc...

- Powdery soils are common in the dayas. They are chemical sediments (carbonates, gypsum, NaCl etc...) due to the evaporation of water supplied through aquifers or wadi underflows during the Holocene wet period. These soils are more or less mixed with clay or silt, without cohesiveness, and can be eroded even by convective swirls. On a regional scale, these soils lie in very small closed depressions, but they seem to have a relation with frequent dust emissions.

- Clayey or silty deposits in general have a better cohesiveness which prevents an easy entrainment by wind, except by ballistic impact. Only relatively strong winds can scour the cracked clay crust in fine wadi deposits and, less easily, the commonly hard clays of the Late Tertiary rocks. On the other hand, loamy lacustrine and swamp deposits are often more erodible by the wind abrasion.

- Sands contain a low percentage of fine particles. But there are some differences between sandy deposits and eolian sands. The former ones are more or less cohesive (Holocene lacustrine deposits, wadi sediments or Late Tertiary sandstone) but they sometimes contain a wide range of grain sizes and some silt and clay constituents. The latter ones are very well sorted by wind. Dune sands which cover the largest areas are coarser ( $Md = 180 \mu m$ ) and fine particles are scarce whereas the sand sheets ( $Md = \text{about } 110 \mu m$ ) lie on various substrats. These are fed with their own deflated material and the ejection of dust particles into the windflow is dependent on the threshold shear velocity required to initiate saltation of all the sand grains.

The mineral components of these different surface soils were identified by using X-ray diffraction. Figure 2 shows that the soils most easily carried by the wind (carbonates or gypsiferous powdery soils) are clustered around the maximum of calcite + gypsum (> 20%). So the importance of these two minerals to form powdery structures is corroborated.

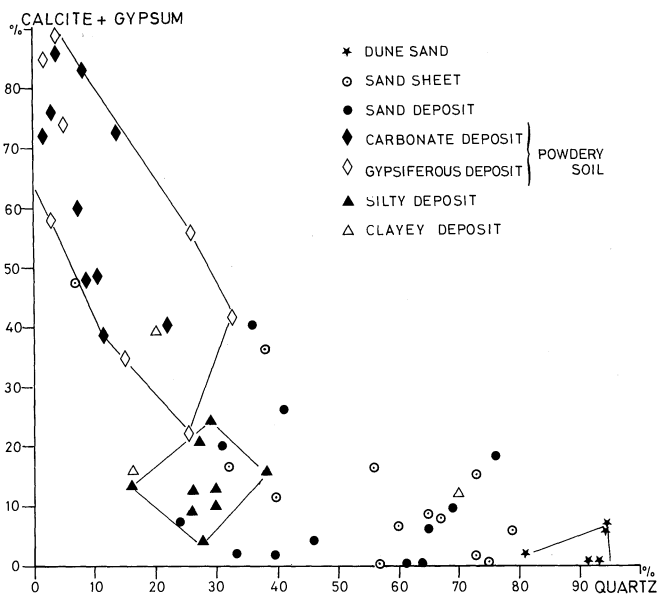


Fig.2- Three mineral components identified by X-ray diffraction for different surface soils.

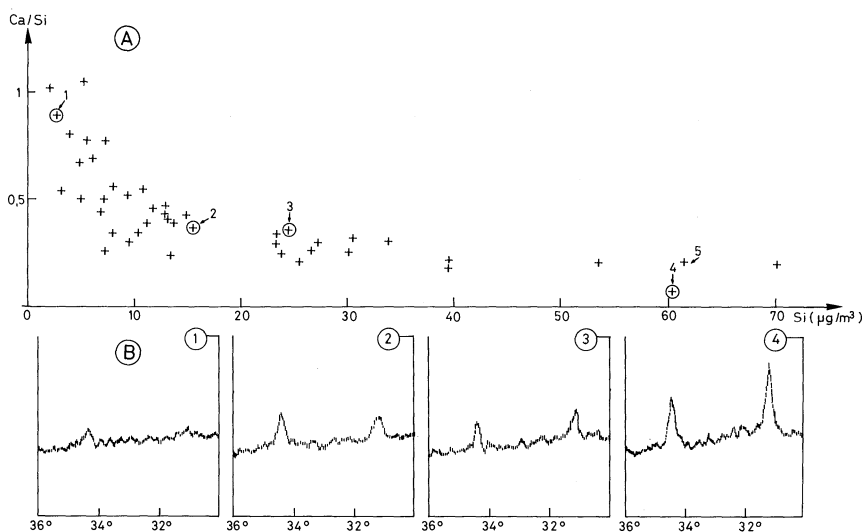


Fig.3- Ca/Si ratio related to the Si concentration : A- Elemental analyses (X-ray fluorescence spectrometry) on dust samples collected in different wind stress conditions; B- Mineralogical analyses (X-ray diffraction) on filters related to increasing wind energy.

In contrast, dune sands (80 - < 90% of quartz) are the richest in quartz. In most cases, the other sands, in which eolian grains are always present, contain also quartz. On the other hand, silty or clayey deposits always contain less than 25% of calcite + gypsum and 15-40% of quartz, but surely some clay minerals.

#### 4. RELATIONSHIPS BETWEEN THE AIRBORNE DUST NEAR THE GROUND AND THE WIND STRESS

Three sets of dust samples were available for very different wind stresses observed in the field. In December 1985, in the northern part of the sandsea, an anemometer was used, but the wind velocities were very low. In fact, it is very difficult to evaluate the wind erosion intensity only from the velocity and not the turbulence or the angle of incidence etc... because the wind processes were very different ranging from convective swirls to sandstorms and to dust storms. Sampling and analytical procedures are the same as those used for our work on the Saharan dust above Fuerteventura in the Canaries islands (Coudé-Gaussen et al., 1987).

##### 4.1. Chemical and mineralogical composition of dust from the bulk filters (fig. 3) :

Elemental analyses have been performed by wave length dispersive X-ray fluorescence spectrometry. The concentration of silicon varies from 2 to 70  $\mu\text{g}/\text{m}^3$  and increases in relation to the wind stress. Since it is very difficult to quantify this stress, we have used the Si concentration as a indicator of the wind erosion intensity.

We have observed that the ratio Ca/Si changes from 0.8 to < 0.2 when the Si concentration increases from 2 to 70  $\mu\text{g}$  (samples collected in El Abiodh during dust storms). This result has been corroborated by the two other field experiments at different weather conditions (Si ranges : 0.5 - 2  $\mu\text{g}/\text{m}^3$  in December 1985 ; 3-25  $\mu\text{g}/\text{m}^3$  in February 1986).

The mineralogy of eolian dust has been studied directly on some filters by X-ray diffraction. During the quiet period, the filters were very lightly loaded and a qualitative examination only shows calcite, gypsum and rarely, trona. By contrast, during dust storms, quantitative analyses chiefly indicate the occurrence of quartz, clay, calcite and mica. For four samples collected in El Abiodh where the Si concentrations were 3, 15, 24 and 60  $\mu\text{g}/\text{m}^3$  respectively (fig. 3,B), calcite is the major mineral in low wind stress conditions (Ca/Si close to 1), but gradually the quartz to calcite ratio increases simultaneously with increasing Si concentration. However, taking into account the only semi-quantitative determination by X-ray diffraction, further investigations will be necessary to confirm the correlation of Ca/Si ratio with increase in quartz content. It is possible that silicon included in clay mineral also contributes significantly to the decrease of Ca/Si ratio.

#### 4.2. Particle size analyses

SEM and EDAX examinations were performed on a bulk filter : Six samples collected during dust storms in El Abiodh (March 1985) have been classified as a function of the increasing Si concentration, from 2.8 to 8-15, then 50-70 $\mu\text{m}$ . For the diameter  $< 25\mu\text{m}$ , all the dusts contain three groups of grain sizes: the first two ones ( $< 1\mu\text{m}$  and about  $2\mu\text{m}$ ) are the same regardless of the Si concentration and the wind stress (tabl. 1). The coarser mode decreases from 12-15 $\mu\text{m}$  to 7-9 $\mu\text{m}$  and finally to 4-5 $\mu\text{m}$  when the Si concentration increases. Gillette and Walker (1977) have shown a similar relationship in loamy soil ; the amount of fine particles ( $< 10\mu\text{m}$ ) increases at higher wind speeds, partly because the breakage of clay aggregates by sandblasting. When the Si concentration increases, EDAX examination shows that the Si and Fe concentrations increase more rapidly than the Ca concentration (fig. 4).

Number of filters	Si concentration ( $\mu\text{g}/\text{m}^3$ )	Grain size modes
3	50-70	4-5 $\mu\text{m}$ 1-2 $\mu\text{m}$ < 1 $\mu\text{m}$
3	8-15	7-9 $\mu\text{m}$ 1-2 $\mu\text{m}$ < 1 $\mu\text{m}$
1	2,8	12-15 $\mu\text{m}$ 3 $\mu\text{m}$ < 1 $\mu\text{m}$

Table 1 : Grain size of dust particles, collected by bulk filtration.

X-ray fluorescence analyses were performed on impactor filters : we have used a five stage cascade impactor EGAI 80 (Bergametti et al., 1983). The largest particles ( $>$  about  $25\mu\text{m}$ ) were collected qualitatively by washing the wall of the inlet funnel with alcohol at every change of filters. For the less than  $< 25$  microns size, the distribution of Ca and Si grain size is related to increasing wind stress (fig. 5). The mass of particles within a diameter interval  $d$  is represented by the area over this interval between 0.1 and  $25\mu\text{m}$ . During a quiet period, the mode of Ca and Si particles is about 3-5  $\mu\text{m}$  and the distribution seems to be log normal. The mass of very small particles ( $< 0-6\mu\text{m}$ ) is insignificant (A on fig.5). In contrast, during dust storms, the percentage of very small particles very rapidly increases from B to C, according to the increasing Si concentration.

For the greater than  $> 25$  microns size, the size of coarser grains, directly sampled on the impactor inlet funnel is mainly between

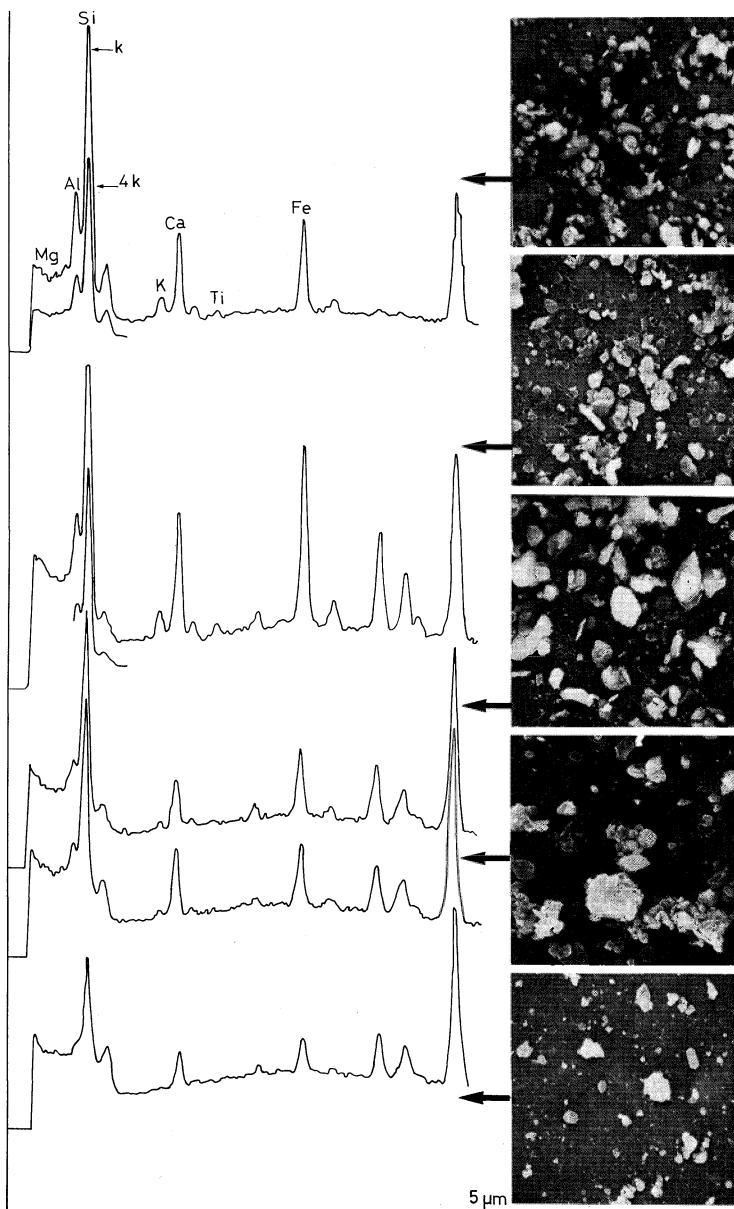


**Fig.4-** SEM and EDXA analyses on bulk filters collected during dust storms in El Abiodh and classified as a function of an increasing Si concentration from 1 ( $2.8 \mu\text{g}/\text{m}^3$ ) to 4 ( $70 \mu\text{g}/\text{m}^3$ ).

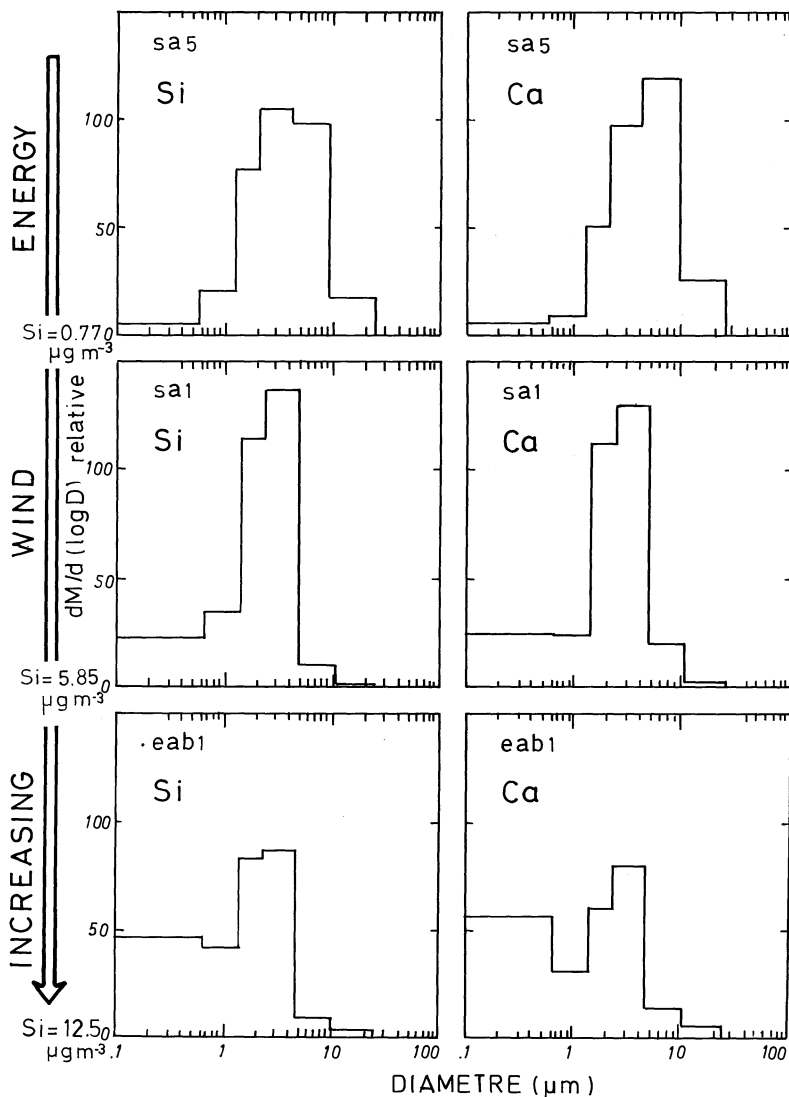


Fig.5- Distribution of Ca and Si grain size related to increasing wind energy. The mass of particles within a diameter interval  $\Delta d$  is represented by the area over this interval between 0.1 and 25  $\mu\text{m}$ .

25 and 150  $\mu\text{m}$ . The dominant minerals are quartz, Ca carbonates grains and clayey aggregates ; however feldspar is rare.

#### 4.3. Relationships between dust and soils

Mineralogical analyses show calcite or/and gypsum are predominant during the quiet periods ( $< 5\text{m/sec}$  wind velocity). This result is in good agreement with the field observation that powdery soils (rich in calcite or/and gypsum) are easily eroded by the winds at present and during the Late Holocene.

When the wind stress is increasing, the concentration of Ca (from calcite or gypsum ?) remains noticeable but the Ca/Si ratio decreases. The Si increase can be related the increase in quartz or clay particles. Moreover, the grain size analysis (by impactor or by SEM) show the very small particles increase in relation to the wind stress. These results also confirm the field observations. The sand sheets yield their finest particles only from a threshold shear velocity, when the wind can shift all sand particles. In the same way, sandy or silty clay deposits are mobilized only by more or less strong winds according to their cohesiveness.

#### 5. SOIL CONTRIBUTION TO DUST IN RELATION TO GRAIN SIZE

The collected soils almost always contain some amount of silt or clay (except in the dune sands), forming more or less coarse aggregates which have an influence on the grain size distribution. Consequently it is necessary to distinguish between :

- the immediately available amount of erodable particles
- the potential amount which is the percentage of small particles that the wind can eject when its energy is strong enough to reduce the interparticle cohesive forces of soils or aggregates. In the majority of the analysed soils, small particles can be mobilized only during the shift of sandsheets or the bombardment of the sandy, silty or clayey deposits by ballistic impact of saltating coarse grains (Gillette et al., 1974).

##### 5.1. The available amount of erodable particles

Two grain size values are used on figure 6 : 40  $\mu\text{m}$  defines the amount of small particles which can remain in suspension over a distance of several hundreds or more than one thousand kilometers ; and 100  $\mu\text{m}$  is the size still currently found in the dust falls on Sal, Canaries or Corsica islands (Jaenicke and Schütz, 1967 ; Glaccum and Prospero, 1980 ; Schütz et al., 1977 ; Coudé-Gaussen et al., 1987). To estimate the percentages of these two amounts in the whole of the soil, samples have been



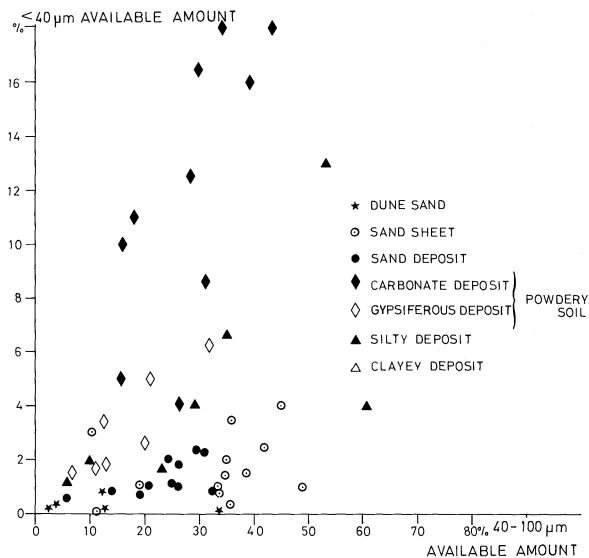


Fig.6- The available amount of soil particles immediatly erodible by wind for two grain size values

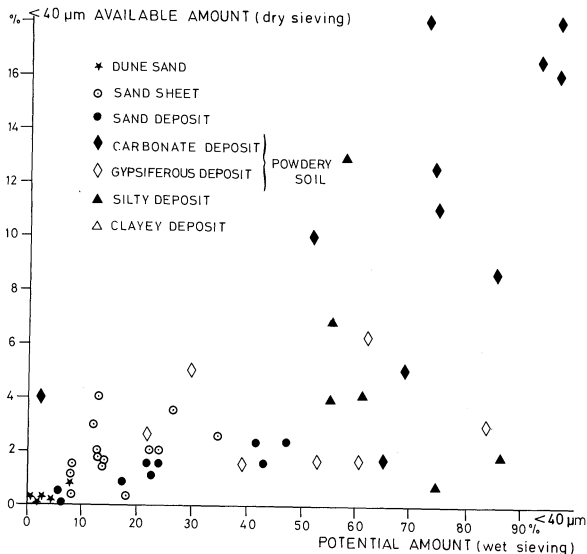


Fig.7- Comparison between available and potential amounts of fine particles in the different types of soils.

sieved, without any preparation except drying for a short time in a dryer to simulate the "arid environment". On figure 6, the carbonated powdery soils appear to be the richest in  $< 40 \mu\text{m}$  available particles (6 to 18%), then followed by the gypsiferous ones (2-6%). This difference is probably explained by the fact that the size of the calcite crystallisation (for instance : micrite or sparite) is smaller than the gypsum one. But in gypsiferous soils, the amount of 40-100  $\mu\text{m}$  sized particles ( $< 40\%$ ) is lower than the percentage in some sand sheets (commonly between 30 and 50%). In contrast, the latter contain very low amounts of less than 40  $\mu\text{m}$  particles (0.3 - 4%). The available amount of small particles in silty deposits is extremely variable both in  $< 40 \mu\text{m}$  and 40-100  $\mu\text{m}$  size ranges. No sample of clay was analyzed because of their hard cohesiveness when dry. Finally, alluvial or lacustrine sands and, especially, the dune sands contain very few available amounts ( $< 35\%$  for 40-100  $\mu\text{m}$  size and, respectively  $< 2.5$  and  $< 0.7\%$  for  $< 40 \mu\text{m}$ ).

### 5.2. The potential amount

This amount results from a wet-sieving in order to destroy all the soft aggregates. This procedure determines the weight of small particles able to be ejected by strong winds. On figure 7, the potential amount of  $< 40 \mu\text{m}$  particles is plotted with the available amount of  $< 40 \mu\text{m}$  particles since these small particles are the most closely concerned with the aggregation processes. The less than 40  $\mu\text{m}$  potential amount is very high (50 to  $> 90\%$ ) both in carbonated powdery soils and in silty deposits. The former principally yield calcite and the later clay minerals. The gypsiferous powdery soils still contain high potential amounts, but these are more variable (20 to 85%), because the gypsiferous aggregates are more cohesive. On the other hand, the sands have a very low potential amount, sometimes yet appreciable in the sandy deposits (5-50%) or in the sand sheets (5-35%), but quasi non-existent in the well sorted dune sands which nevertheless cover the largest area.

### 5.3. Clay mineral composition in $< 40 \mu\text{m}$ fraction

Table 2 shows the clay mineral composition is very similar for the 55 soil analyses. The silty, clayey or sandy deposits are found to be richer in illite than the powdery soils or the sand sheets which contain a little more palygorskite or smectite. But in these four types of soils, illite and polygorskite form about 60% of the sum of the clay minerals. So this assemblage is similar to that found in dust sampled in this region by two meters high filters along a north-south transect from Oran to the southern boundaries of the Algeria (Paquet et al., 1984). Thus, they seem to characterize the "signature" for the clay assemblage of dust on the regional scale.

	ILLITE	SMECTITE	PALYGORSKITE	KAOLINITE	I.C.M. (a)	CHLORITE	<2 $\mu$ m particles in soils (%)
Sandy deposits	40.5	10.4	28.8	6	9.5	4	4.4
Silt and clay	45	14.2	15.2	8	11.3	6.5	28.0
Powdery soils	36.8	17.4	24.3	6	11	6	4.0
Sand sheet	26	20.3	24.6	8	11.2	4	1.8
All the soils	38.3	17	21.7	7.2	10	5	

Table 2 : Association of clays minerals in soils of the sandsea : (a) mixed layer clay minerals.

#### 5.4. The grain size distribution of the fraction 2-200 $\mu$ m

Analyses by a Coulter Counter Multisizer (256 channels) allowed us to distinguish between several particle populations (from 2 to 200  $\mu$ m) and to estimate their relative contribution in volume. From 30 samples, we can point out the following data :

- The carbonate-bearing powdery soils are very homogeneous (only one mode about 35  $\mu$ m, with 70-90% of the whole material < 200  $\mu$ m). This single mode sometimes shifts to very small silts (16  $\mu$ m) or fine sands (70-75  $\mu$ m). On the other hand, two or three modes occur in the gypsiferous powdery soils and their main size is about 60-65  $\mu$ m or even 120-140  $\mu$ m (fig. 8). For this second soil type, when the wind stress increases, the rate of removal by wind decreases relative to an increasing roughness. Therefore, gypsum is less abundant in the dust.

- Among the alluvial or lacustrine deposits, clayey soils contain a very large fraction of small particles with 50-80% of the grains in the 5-10  $\mu$ m range and a second clustering around 30-40  $\mu$ m may also be present (fig. 9). The size distribution is very heterogeneous in the silty deposits, with 2 or 3 grain-size modes, but the main mode is about 25-55  $\mu$ m. In the lacustrine sands, there is a main mode about 110  $\mu$ m (70 to 85%) and in some samples a secondary peak about 50-55  $\mu$ m.

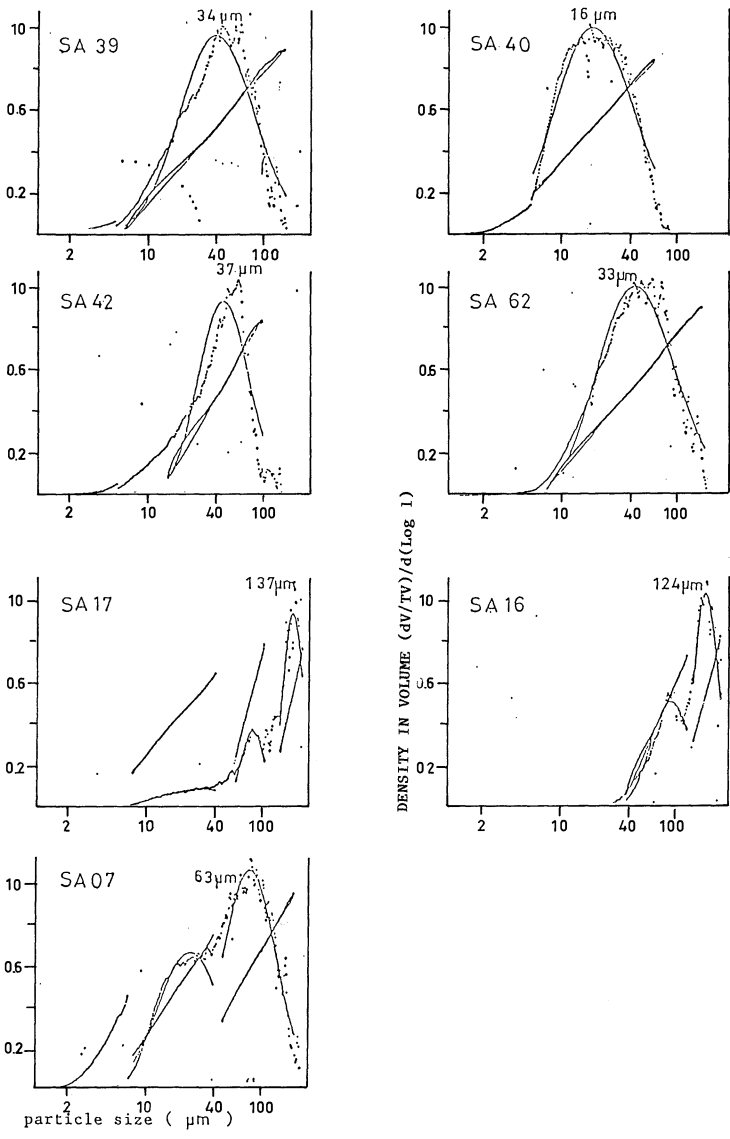


Fig.8- Grain size distribution (2 - 200 μm) of particles in some powdery soils : A- Carbonated soils; B- Gypsiferous soils.

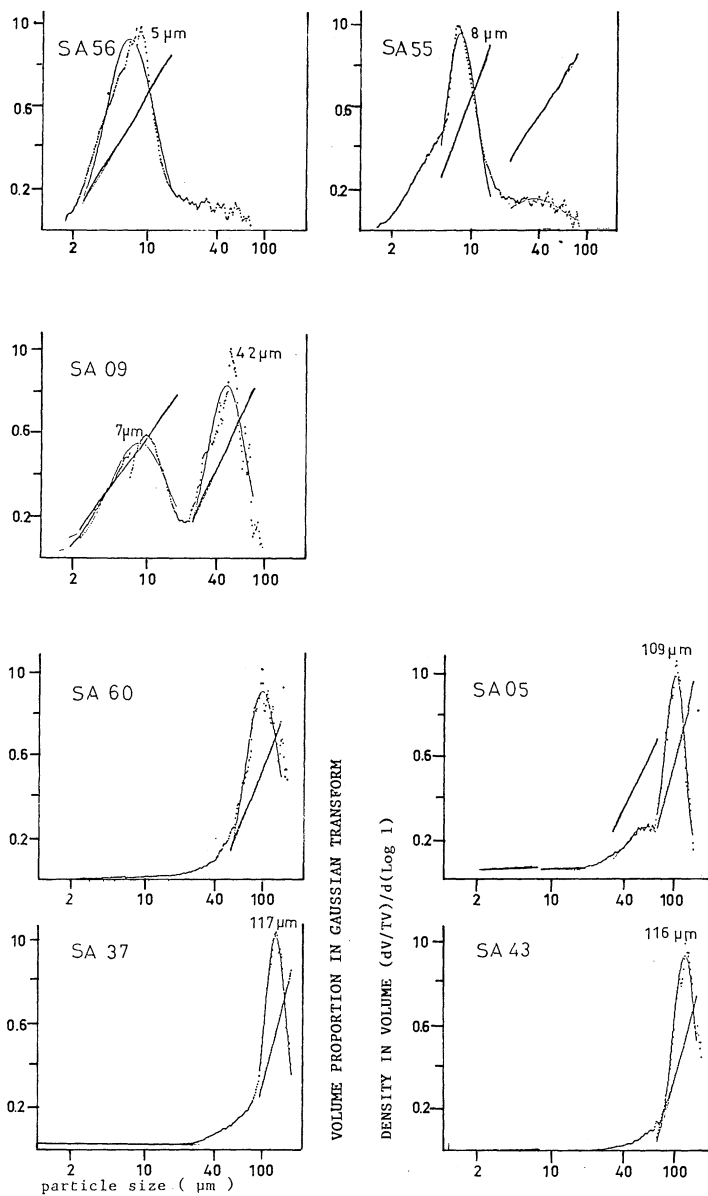


Fig.9- Grain size distribution (2 - 200 μm) of particles in some lacustrine clayey deposits (A) and sand sheets (B).

- Finally, the dune sands contain no fraction less than  $< 60 \mu\text{m}$ ; whereas the sand sheets are very well sorted with only one mode of about  $100 \mu\text{m}$  (70-80%). This diameter requires the minimum threshold velocity to initiate movement (Chepil, 1951) and these sheets include the particles entrained by a direct aerodynamic action.

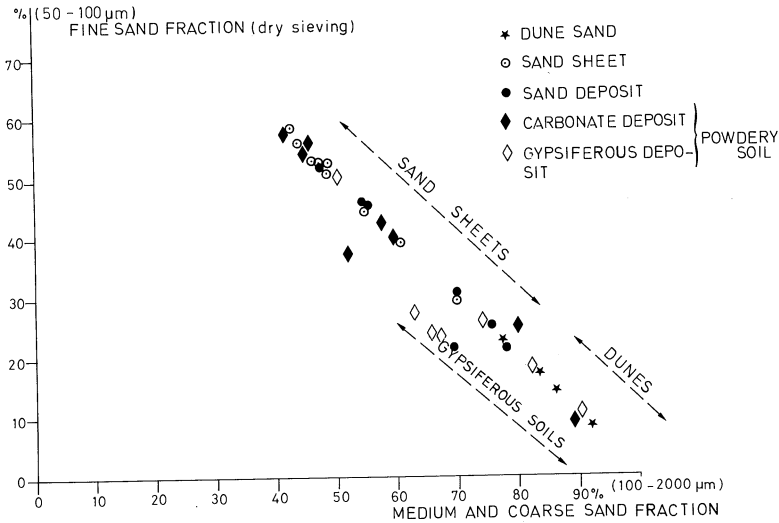


Fig.10- The fraction of coarse sands (100 - 2000 μm) compared to the fine sands (50 - 100 μm) fraction in some surface soils.

### 5.5. The fraction of coarse sands in soils

On fig. 10, only the dry sieved fraction of soils is taken into consideration. The fraction of coarse sand (100-2000 μm) is related to finer sands (50-100 μm). The former, only drifted by saltation or creeping, control the entrainment of the second one, which can be winnowed by the wind. Here, dune sands and gypsiferous powdery soils are the richest in coarse sand fraction and their non erodable fraction is progressively exposed by deflation and induces an increase of the velocity threshold and limit erosion. On the other hand, the sand-sheets and carbonated powdery soils contain very little coarse fraction and the small particles are easily removed.

## 6. CONCLUSION

These first results point out a good relation between the dust composition and the grain size, mineralogy and structure of soils in the Western Sandsea. *During quiet periods*, dust contains more Ca element or calcite mineral because the carbonated powdery soils are the most erodable and yield their directly available amount of calcite ; they also have a large potential amount of about 35  $\mu\text{m}$  sized particles and very small fraction of coarse sand. Gypsum is less abundant in the dust samples because the gypsiferous powdery soils contain only few available fine particles, but much coarser sand. *When the wind stress increases*, the bombardment by ballistic impact of coarse sand more and more ejects particles of quartz and clay aggregates from the alluvial and lacustrine deposits which often contain a large potential amount of fine particles. Moreover, this increasing wind stress allows the entrainment of the fine fraction included in the sand sheets. Consequently, when the winds are strong, smaller particles are more abundant, the Si concentration linked both to quartz and clay minerals increases. Such a study is obviously non-exhaustive, even for the considered region. Taking into account the fact that we are now able to characterize the relationships between main surface soils and dust emissions, it is necessary in this way to promote methods allowing an extrapolation of these data. For instance, dune sands, by far the most widespread soils, yield a very small amount of dust. In the following years, the major topic possibly will be to quantify precisely the areas covered by various types of soils. Unfortunately, maps available are not precise enough to estimate the dust drift potential for the whole region. Consequently, remote sensing methods could allow significant progress by integrating the types and characteristics of soils on a regional scale (Oliva et al., 1983). Such an approach has already been successfully by A. Abd el Hady (1987) in the Southwestern part of the Sinai by using satellite imagery from Landsat and a Thematic Mapper.

## 7. ACKNOWLEDGMENTS

We would like to thank Dr. Y. Callot of the Oran University for his valuable suggestions and discussions during the field experiments , M. N. Le Coustumer of the Center of Geomorphology (CNRS, Caen, France) and P. Blanc of the Department of Micropaleontology (University Pierre and Marie Curie, Paris, France) for their invaluable work on X-ray diffraction analyses. M. Fremont carried out the laboratory procedures in obtaining soil size distributions by Coulter Counter Multisizer. We also wish to thank the Oran University for their general assistance.

## 8. REFERENCES

- Abd el Hady, A., 1987. Etude des sols désertiques en relation avec la télédétection. Sud-Ouest Sinaï (Egypte). Thesis of University P. and M. Curie, Paris, 87-5, 223p.
- Bergametti, G., Vié le Sage, R., Grubis, B., Dulieu, B., and Elichegaray, C., 1983. Relation between particulate concentration in the atmosphere and aerosol collection efficiency, Environ. Technol. Lett., 3, 297-304.
- Callot, Y., 1987. Géomorphologie et paléoenvironnements de l'Atlas saharien au Grand Erg occidental : dynamique éolienne et paléolacs holocènes. Thesis of University P. and M. Curie, Paris, 473p.
- Chepil, W.S., 1951. Properties of soil which influence wind erosion :4, state of dry aggregate structure. Soil Sci. 72, 387-401.
- Coudé-Gaussen, G., Rognon, P., Bergametti, G., Gomes, L., Strauss, B., et Gros, J.-M., 1987. Saharan dust on the Fuerteventura island (Canaries). Chemical and mineralogical characteristics, air-mass trajectories and probable sources. J. of Geophys. Res., 92, 9753-9771.
- Gillette, D. A., Blifford, I.H. and Fryrear, D.W., 1974. The influence of aerosols generated by the wind erosion of soils. Journal Geophys. Res., 79, 4068-4075.
- Gillette, D.A. and Walker, T.R., 1977. Characteristics of airborne particles produced by wind erosion of sandy soil, High Plains of West Texas. Soil Sci., 123, 97-110.
- Glaccum, R.A., and Prospero, J.M., 1980. Saharan aerosols over the tropical North Atlantic. Mineralogy., Mar. Geol., 37, 295-321.
- Jaenicke, R., and Schütz, L., 1967. Studien zur oberen Grenzgröße des natürlichen Aerosoles. Contrib. Atmos. Phys., 40, 129-143.
- Oliva, P., Coudé-Gaussen, G., Delannoy, H., Dorize, L., Rognon, P., and Tabeaud, M., 1983. Etude de la dynamique de quelques lithométéores sahariens par télédétection spatiale. Medit. N° spécial Télédétection, III, 21-52.
- Paquet, H., Coudé-Gaussen, G., and Rognon, P., 1984. Etude minéralogique de poussières sahariennes le long d'un transect entre 19 et 35° de latitude Nord. Rev. Géog. Phys. et Géol. Dyn., 25, 257-266.
- Schütz, L., and Jaenicke, R., 1974. Particle number and mass distribution above  $10^{-4}$  cm radius in sand and aerosols of the Sahara desert., J. App. Meteorol., 13, 863-870.
- Schütz, L., Jaenicke, R., and Pietrek, H., 1977. Saharan dust transport over the North Atlantic Ocean. Proceed. of AAAS Symposium. Desert dust: origin, characteristics and effect on Man. Univ. of Arizona Press.
- Yaalon, D.H., and Ganor, E., 1979. East Mediterranean trajectories of dust carrying storms from the Sahara and Sinaï. in Saharan dust : Mobilisation, transport, deposition, Morales, G., edit., J. Wiley and Sons, 187-193.



## AEOLIAN DUST TRANSPORT IN WEST AFRICA

G. Tetzlaff, M. Peters, W. Janssen, and L. J. Adams  
Institut für Meteorologie und Klimatologie  
der Universität Hannover  
Herrenhäuser Str. 2  
D-3000 Hannover-21  
Federal Republic of Germany

**ABSTRACT.** Deep sea deposits of continental dusts are found in abundance off the coast of West Africa in the Atlantic ocean, transported there in several periods of the geological past. The chemical properties of the deposited materials indicate the area of origin being south of the Sahara desert itself. This long distance dust transport from the continental areas to the oceanic deposition areas is closely connected to specific atmospheric flow systems. In summer the westward dust transport requires several components active in consecutive steps, these are taking the dust from the surface, bringing large enough quantities high enough into the atmosphere and strong enough easterly winds. In an analysis of the synoptic scale flow systems of West Africa the rain bearing disturbances of the Sahel combine all these components and thus contribute to a large extent to the supply of dusts as they are found in the deep sea deposits as well as the supply of water vapour of the region allowing the formation of rain.

### 1. DUST DEPOSITS

The reconstruction of past climates has to rely on information from indirect data. One of the most complete records of climatic history is found on the ocean floors. There the material in large parts of the deep ocean basins remains undisturbed once it has been deposited. Therefore, efforts of many scientists were devoted to contribute to the coupling of such proxy-data with quantitative climatic data. Because of the many scales involved both in time and space this problem can only be solved for individual cases.

In the tropical north Atlantic large quantities of dust were deposited almost through all climatic periods of the recent geological past. The first idea of this dust transport goes back to Arab sea farers, who called this part of the Atlantic situated off the African coast the "dark seas". A detailed record of progress in the research on this topic can be found in Wolter (1981). The main proof for long distance transport from the African continent across the Atlantic towards central

and South America came from the results of Carlson and Prospero (1972, 1977). They sampled dust on Barbados and found an annual cycle as well as variations between dry and wet years in the Sahel. Figure 1 gives the measured data of the dust concentration on Barbados.

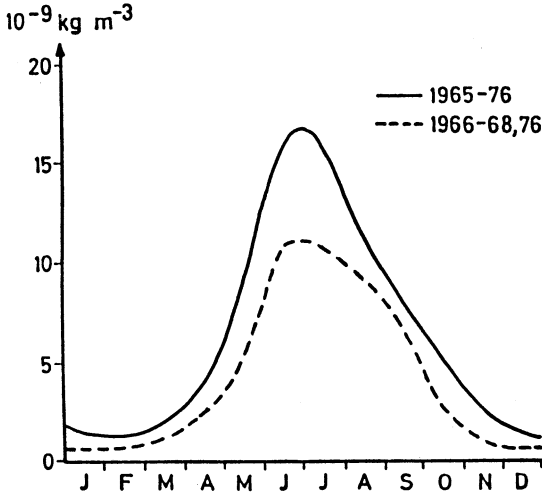


Figure 1. Monthly averages of dust concentration on Barbados for non-drought years (dashed line) and the overall period (solid line) (modified after Carlson and Prospero (1977)).

This material originally came from the African continent. As is necessary this long distance transport has to cross the whole Atlantic ocean. On their path some dust particles fall from the atmosphere on the surface of the ocean waters. It is these particles that form the deep sea sediments. In order to allow any further conclusion as to the atmospheric climate it is necessary that the particles immediately sink to the bottom where they initially hit the water surface. The mechanism of motion of small particles in water is well known, sinking velocities are very small and it would take individual particles years to travel from the surface to the bottom. The presence of an accelerating process is undisputed. Its nature however, seems to be a mixture of several processes. The formation of fecal pellets was held the most important until recently (Szekielta 1978). Modern approaches use additional evidence without altering the general pattern. This then allows to consider the patterns of the deposited materials as related to atmospheric flow systems and to interpret them accordingly.

The materials of the deep sea deposits were investigated systematically by Sarnthein and Koopmann (1980) and by Koopmann (1979). The basic pattern of these studies is represented in Figure 2 and shows information on the relative grain size distribution in the form of isolines of the percentage of the occurrence frequency of a particular quartz grain size. As only continental areas can be the source of this kind of grains the tongue extending from the coastline into the sea

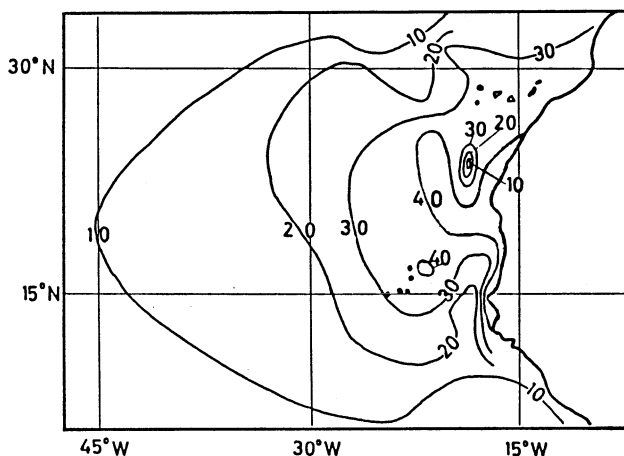


Figure 2. Distribution of percent terrigenous silt  $> 6 \mu\text{m}$  in recent surface sediments in the Atlantic ocean off the African coast (modified after Sarnthein and Koopmann (1980)).

gives the part of the coast where the bulk of the material crosses the coast line. These data were rearranged by Wolter (1981) in a comprising study on the deposited spectral distribution of the granular quartz material. The pattern of these isolines then allows to conclude the transport direction and velocity of the air borne material. These data were applied to deduce an atmospheric flow pattern connected with the deposits (Sarnthein et al. 1981). The samples of deep sea deposits were not only available for present-day conditions but also for other times, in particular for the time slice 18 000 years B.P.. In analogy with present-day results the glacial dust flow patterns were used to derive the corresponding atmospheric flow patterns. The dust found in the Atlantic and on the island of Barbados alone do not allow to define the exact area of origin and the transport path in detail. In addition, the information presented up to now is not homogeneous in itself. The dust samples taken on Barbados cover a period of a few years, while the deep sea quartz deposits cannot be resolved finer than about 500 years due to bioturbation and the small deposition rate. Only if a strong repetitive pattern of the atmospheric flow is active, these two data sets may be interpreted on the same basis.

There is, however, some additional information that allows to specify the source area and to confirm a geometrically fixed flow system. A major portion of the material found at distances of more than 500 km from the coast is stained with a coat of reddish material (Koopmann 1979). The material found at shorter distances from the coast is increasingly unstained. This allowed Sarnthein and Koopmann (1980) to ascribe the stained material to Sahelian source regions in the zone of the lateritic soils and the unstained material to Saharian sources.

## 2. THE ATMOSPHERIC WIND SYSTEMS RELEVANT FOR DUST TRANSPORT

The atmospheric flow system in the area of interest consists of two components: the mean flow and the disturbances. The mean flow is represented by a long term average either for a whole year or for a specific season. The disturbances are short-lived and restricted to only a smaller part of the total area. It can easily be made plausible that the dust transport is connected with disturbances of the average flow field. This requires consideration of the mechanism picking the quartz material from the ground. It is reported from many sources that dust, either air borne in the transport layer of several kilometers aloft or close to the source areas in the Sahel and also in the Sahara, is not present in a constant concentration (Jaenicke 1979, Middleton 1985). The dust injection into the atmosphere occurs by wind action on the surface. The functional dependence is not at all linear. The transport rate of dust is proportional to the force the wind exerts on the surface. This force is proportional to the second power of the wind speed. In order to transform force into power the addition of a length and a time is required, thus producing the third power dependency of the transport rate. The above specified transport rate applies to transport in saltation restricted to the layers close to surface oriented almost parallel to the surface. Suspended load requires an additional velocity component, the vertical velocity, adding to the third power so that the suspended load is proportional to the fourth power of the wind speed. As the vertical and the horizontal wind velocity are closely related and the saltation transport also contains a vertical component, however small, the observed functionality of the suspended load is observed to be between the third and the fourth power (i.e. Westphal et al. 1987).

On the other hand, long distance transport requires a fairly well organized transport process on a horizontal length scale of several thousand kilometers. Such a long extension is connected with a time scale of at least several days. Therefore, several processes are involved to make a considerable amount of dust originating from the zone at the southern fringe of the Sahara cross the Atlantic ocean. It is necessary to have a fluctuating wind speed in the source region, a pumping mechanism to lift the dust in levels high enough to allow long distance transport, and finally a none too variable repetitive flow pattern on the travel path of the dust.

One component of long distance transport is the upper air wind regime where this transport is observed (Carlson and Prospero 1972). In Figure 3 the average zonal flow component of the 70 kPa level is shown for the summer months. The maximum easterly component is found on the continent at 15°N. This was pointed out as the region of the origin of dust. The easterly winds at this level extend right across the Atlantic towards the Caribbean. In addition, these winds show a very small variability, their persistence being higher than 90 % (Newell et al. 1972). This means that dust injected into this air flow travels across the Atlantic under almost any condition. The injection process is to be dealt with later. The deposition pattern of Figure 2 contains a smaller scale bulge where higher transport velocities are directed towards the northwest. This hints an air flow deviating from the mean flow as pre-

sented on Figure 3.

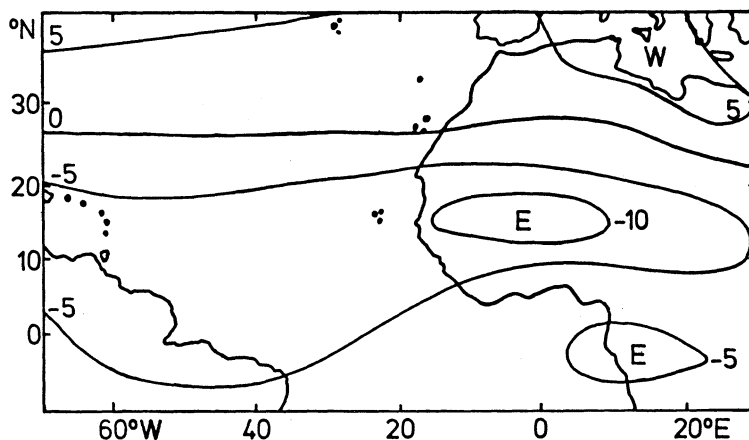


Figure 3. Mean African and Atlantic zonal wind component at 70 kPa, June - August (modified after Newell et al. (1972)).

The setting of the continental land masses and oceans in the region is coupled with a surface temperature pattern. In summer the African land masses are heated and consequently monsoonal air is sucked into the continent from the south in low levels. Because of the temperature gradient between the cool maritime air masses representing the conditions of the Gulf of Guinea and the hot continental air masses over land a substantial easterly air flow is induced at the mid level of the troposphere called African Easterly Jet (AEJ). Thus, surface winds and winds at higher levels are to be expected to blow in different directions with different transport directions of the injected materials such as dust and water vapour. However, the basic forcing of the two wind systems is identical and closely connected with the geographical setting of the land-sea-distribution. This forcing is rather strong because of the different thermal properties of land and sea. Therefore, there is a distinct regional component in the wind system of the West African region.

This is also the reason for the constancy of the smaller-scaled atmospheric flow patterns. Hence it is possible to compare rather short term information on atmospheric flows with more long termed ones. The climatic information is contained in the changes of intensity of the flow system and not in their general geometrical setting.

It was analysed by Tetzlaff and Wolter (1980) and by Carlson and Prospero (1972) that disturbances occur regularly. These disturbances are instabilities of the AEJ and are called Easterly Waves (EW). They were analysed in detail by Reed et al. (1977). The EWs cause the dust trajectories that are shown in Figure 4, where a typical summer situation at the 50 kPa-level is presented. However, the EWs do not change the whole atmospheric flow pattern, only slightly effecting the mean flow as shown in Figure 3.

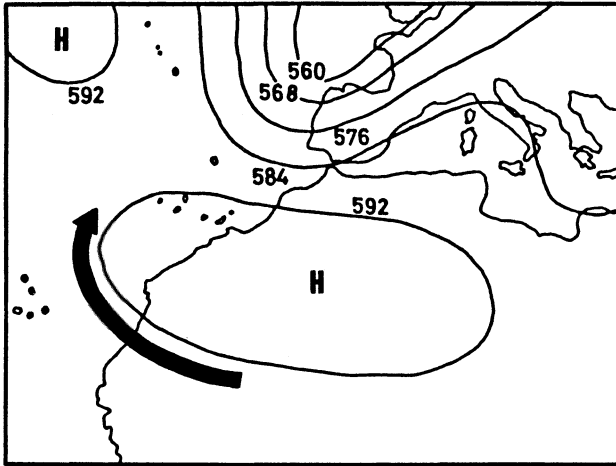


Figure 4. Typical 50 kPa situation in summer in the rear of an Easterly Wave. The arrow indicates the connected dust flow from the continent to the Atlantic ocean (modified after Tetzlaff and Wolter (1980)).

### 3. SYNOPTIC SCALE ATMOSPHERIC FLOW SYSTEMS AND THE DUST LIFTING MECHANISM

Satellite imagery allows to depict the main effect of the disturbances, the vertical motion and the subsequent condensation of water vapour in the form of clouds. The region of interest is located at the latitudinal belt between  $10^{\circ}$  to  $15^{\circ}$ N. There the weather situation is dominated by cloud areas of a size of 400 by 400 kilometers, the Squall Lines (SL). These SLs alter the average flow pattern slightly, because they are rather small compared with the EWs. As can be detected from the presence of clouds in the disturbances, precipitation is related to them as well. It was found by Dhoneur (1970) that SLs generate about 80% of the rains in the Sahel.

Figure 5 shows such an SL as it travels along West Africa in July 1986. The figure shows the Squall Front which is the leading edge of the identifiable cloud cover both in the visible spectral range as in the infrared range. The travel path and the propagation velocity of the cloud exhibit some of the relevant properties of such SLs. The velocity of this SL amounts to about 16 m/s. The travel path is gently bent towards the south generally following the AEJ flow direction. The effect of the EW is distinct in the travel path of the SL as shown in Figure 5. To produce this sort of pattern both a certain ratio of propagation velocities of the SL and the EW and a particular area where the SL is embedded in the EW are necessary. The EWs were analysed to travel at about 8 m/s and their average wave length is about 2500 kilometers. Therefore, the SL moves faster than the EW, even overtaking the air flow of the AEJ which moves at about 12 m/s. It was found by Peters and Tetzlaff (1988) that the origin and the most frequent observations of SLs are restricted to the trough zone of the EW. This hints at the

coupling of EWs and SLs, the EW producing favourable conditions for the SL formation in the region with the highest mean upward motion within the EW. After its initiation the SL moves ahead of the trough zone, decaying after a lifetime of about 35 hours in a somewhat southern position mostly in the ridge zone of the EW.

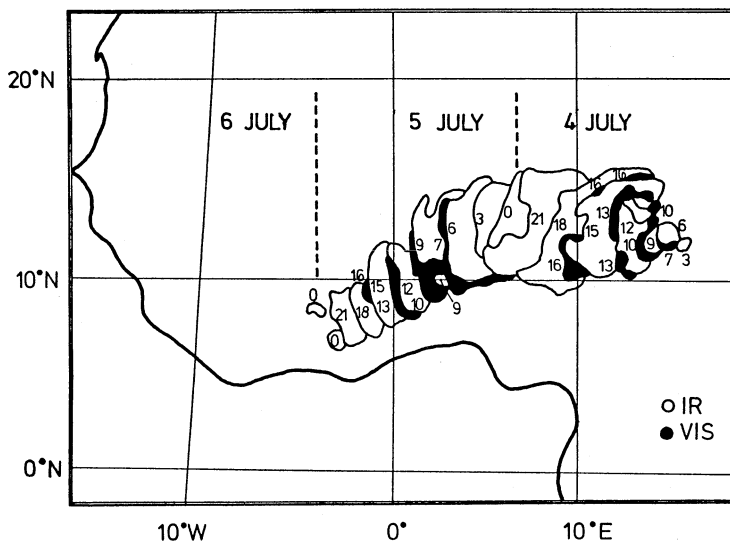


Figure 5. Time sequence of Squall Line cloud contours moving west on the 4 - 6 July 1986. Contours are taken from Meteosat imagery in the infrared ( o ) and the visible ( ● ) (modified after Tetzlaff et al. (1988)).

In a composite analysis of the SL and its environment Tetzlaff and Peters (1988), Peters and Tetzlaff (1988) showed the connection between SL and EW, SL and surface wind velocity, SL and vertical motion, SL and 70 kPa flow, and SL and precipitation.

The surface wind velocity pattern (Figure 6) is spatially organized and exhibits maximum values at the Squall Front with average values of more than 5 m/s at 10 m height above the ground and in an area north of the SL. This area with wind speeds higher than 5 m/s is far more extent than the one at the Squall Front.

There is no direct measurement of the amount of dust taken from the surface, but the routine observations include a diagnosis of dust in the air. It was shown by Tetzlaff and Peters (1986a) that in a northern area about one seventh of all observations indicate dust lifting of all different kinds (Figure 7). This is rather a frequent event, in particular when comparing this to the frequency of such findings in the region south of the SL, where it usually does not occur at all and also to the northern region, which is not SL-influenced and where only less than one twentieth of the observations is occupied by times with dust lifting.

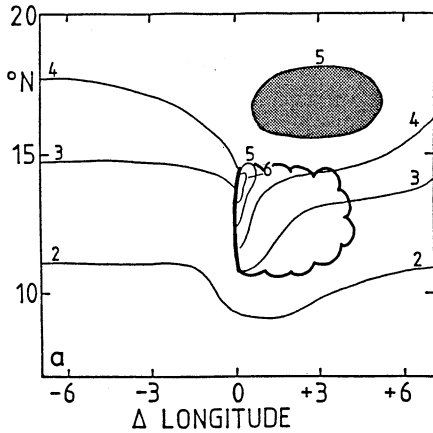


Figure 6. Average surface wind speed in m/s for composited Squall Lines and their environment in summer 1979. Composited fields are shown in a coordinate system moving with the Squall Line. Shaded area A indicates lifting of dust at the surface (modified after Tetzlaff and Peters (1986a)).

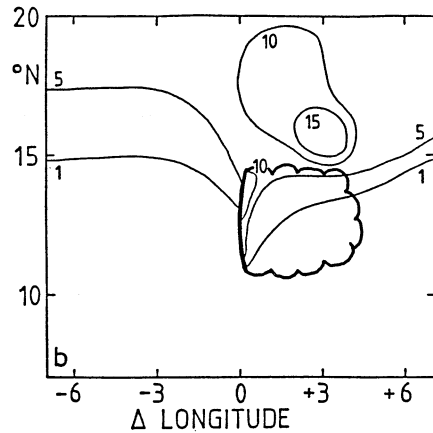


Figure 7. Percentage of surface observations with dust lifting at the surface from the composite of the Squall Lines and their environment in summer 1979 (modified after Tetzlaff and Peters (1986a)).

In the high wind speed region in the north (about 17 to 19°N) surface winds show a distinct convergence. This convergence pertains through to a level of about 1500 m above the surface (Tetzlaff and Peters 1986b). Above this level convergence is converted into divergence, which was clearly analysed in the 70 kPa-level. All this happens under the influence of the monsoonal air at the surface, causing mainly an average stable stratification suppressing vertical motions. Therefore, the average vertical velocity may explain the vertical dust injection into the easterly air flow aloft. On the other hand, convective vertical transport is improbable, because there is only a negligible amount of precipitation observed that far north of the SL itself.

The wind at the main transport level is dominated by the easterly flow of the AEJ which is only slightly modified by the EWs and the SLs. The composite analysis showed average values of about 11 m/s which is close enough to the climate mean value as found by Newell et al. (1972). The horizontal gradient of the wind velocity is rather steep on either side of the jet. At 17°N the velocity has dropped to about 6 m/s, a value found similarly at 7°N. Consequently, the AEJ shows the required wind pattern in order to export large amounts of dust to the Atlantic ocean.



## 4. BUDGETS OF WATER VAPOUR AND LIQUID WATER

The results of the composite studies by Tetzlaff and Peters (1988) and by Peters and Tetzlaff (1988) served also to determine the basic data for the atmospheric moisture field. As was pointed out before dust transport and disturbances of the mean flow field are interrelated.

Peters and Tetzlaff (1988) showed that the moisture flow at different levels is predominantly influenced by the variations in the atmospheric flow system rather than the moisture field itself. Therefore, the few radiosonde stations in the region are sufficient to calculate the horizontal moisture flows, relying on the large number of pilot balloon soundings.

The analysed flow and moisture fields were then used to calibrate a flow model consisting of the mass budget equations of water vapour and of liquid water. These equations were then subsequently solved for a grid containing the SL and its environment.

The basic equations were formulated for the budgets of water vapour, liquid water and surface rainfall (Equations 1, 2, and 3).

$$\frac{\partial q \rho}{\partial t} + \frac{\partial u q \rho}{\partial x} + \frac{\partial v q \rho}{\partial y} + \frac{\partial w q \rho}{\partial z} + \rho C_c - \rho E_{rr} = 0 \quad (1)$$

$$\frac{\partial q_l \rho}{\partial t} + \frac{\partial u q_l \rho}{\partial x} + \frac{\partial v q_l \rho}{\partial y} + \frac{\partial w q_l \rho}{\partial z} - \rho C_c + \rho P_r = 0 \quad (2)$$

$$\frac{1}{g} \int_{p_l}^{p_u} \frac{\partial q_r}{\partial t} dp + \frac{1}{g} \int_{p_l}^{p_u} P_r dp - \frac{1}{g} \int_{p_l}^{p_u} E_{rr} dp = R \quad (3)$$

In these equations the air density  $\rho$ , the gravity acceleration  $g$ , the time  $t$ , the three air flow velocity components  $u$ ,  $v$ , and  $w$ , the mixing ratio for water vapour  $q$ , for liquid cloud water  $q_l$ , and for rain droplets  $q_r$  appear. The condensation rate describing the transformation of water vapour into cloud droplets is  $C_c$ , cloud droplet evaporation is  $E_{rr}$ , the production rate of rain is  $P_r$ , the surface precipitation is  $R$ . Equations 1 and 2 apply to individual levels, Equation 3 is vertically integrated between the lower and the upper boundary of the troposphere,  $p_l$  and  $p_u$ , respectively.

The calculations relied on a horizontal grid of  $0.5^\circ$ , the vertical resolution was 5 kPa, the surface pressure was set at an average value of 97 kPa. The length of the time step was selected to be 1/10 of the time elapsing for the SL to travel from one grid point to the next. This time interval is close to six minutes. The initial flow field was assumed to be free of divergence and cloudfree. The SL then moves into the area with an average propagation velocity of 16 m/s, all SL parameters were assumed to be stationary while wandering across the area of

analysis. This assumption is plausible, because it takes about 8 hours for the SL to travel across the whole area. The technique to solve the equations on the grid used central differences, the details are given in Janssen (1988).

The mass budget of water vapour consists of the horizontal atmospheric fluxes through the vertical walls of the box. The vertical flux through the top of the box is neglected, because both the mixing ratio and the vertical velocity are small quantities there. The flux of evapotranspiration from the surface into the box is assumed to be zero in case of a cloud covered surface. In other cases the evapotranspiration is calculated independently and inserted without feedback.

The initial conditions are assumed to be close to the climatic average conditions for the region, the SL then propagating from the east into the geometrically defined region. The disturbance of the average flow field as caused by the propagating SL then moves into the region and produces a flow convergence.

The convergence of moisture flow causes saturation. Condensation is assumed to begin at a relative humidity of 100%. The excess is transformed into liquid water keeping the relative humidity at 100% in its presence. Condensation nuclei are assumed to be abundant, supersaturation does not occur. Rain formation relies on the droplet growth formulae as given i.e. in Rogers (1979).

$$\frac{d D}{d t} = \frac{\pi}{4} \int_0^{\infty} N(D) \cdot D^2 \cdot v_f(D) \, dD \quad (4)$$

In this equation the diameter of the droplets is  $D$ ,  $N(D)$  is their frequency distribution and an important parameter,  $v_f$  is the terminal fall velocity of the droplets. Both the frequency distribution and the terminal fall velocity are taken from standard empirical findings such as the Marshall-Palmer distribution (Rogers 1979). Inserting the appropriate formulations into Equation 4 allows to calculate the droplet growth. Falling rain drops in some parts of the box enter undersaturated air layers, their evaporation is hence considered. The total amount of condensed vapour results from the convergence calculations in Equation 1 and the rain reaching the surface then results from the whole set of equations.

## 5. THE CALIBRATION OF THE MODEL

The results of the composite analysis which included data from a homogeneous part of the Sahel with a good data coverage by Peters and Tetzlaff (1988) were further developed by splitting the atmospheric flow system in the AEJ-level between 85 and 30 kPa and the monsoon level between the surface and the 85 kPa level (Figure 8a). All flow quantities are given in units of  $10^6$  kg/s. This unit is related to the extension of the areas under consideration which covers the latitudinal

belt between  $10^{\circ}$  and  $15^{\circ}$ N and the longitudes from  $2.5^{\circ}$ E to  $2.5^{\circ}$ W, thus an area of slightly more than  $300\,000\text{ km}^2$ . The composite of the SL is based on all cases when the the Squall Front is located at  $2.5^{\circ}$ W. The balance equation for the water of this atmospheric volume is given by Equation 5.

$$S - \Delta F = E - P \quad (5)$$

$S$  is the rate of change of the water vapour storage in the volume,  $\Delta F$  the budget of the atmospheric water vapour fluxes across the four vertically oriented walls of the box,  $E$  the evapotranspiration from the ground, and  $P$  the losses of water by precipitation.

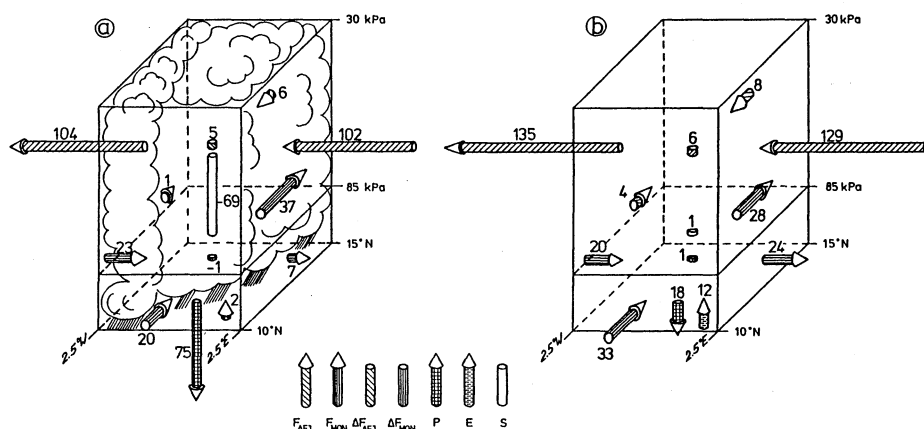


Figure 8a. Budget of water and water vapour in units of  $10^6\text{ kg/s}$  for the atmospheric volume between  $10^{\circ}$  and  $15^{\circ}$ N,  $2.5^{\circ}$ E and  $2.5^{\circ}$ W from the composite data of the Squall Lines of summer 1979. The fluxes are shown separately for the monsoon level (surface to 85 kPa, indexed MON) and the level of the African Easterly Jet (85 kPa to 30 kPa, indexed AEJ).  $S$  is the change of the storage term of water vapour in the atmospheric volume,  $\Delta F$  is the net budget of the atmospheric fluxes through the vertically oriented walls of the box,  $E$  is the evapotranspiration from the ground, and  $P$  is the loss of water of the box by precipitation.

Figure 8b. Budget of water and water vapour as in Figure 8a, but for the climatic average of summer 1979.

The moisture flow data at the SL itself show the two atmospheric flow systems very distinctly. The AEJ supplies the largest moisture flux. This is due to the rather deep layer as well as to the high zonal wind velocities. There is almost no southerly flow in the AEJ-layer. In the monsoon layer the south-westerly monsoonal flow comes out clearly. Especially at the northern margin the southerly fluxes predominate the zonal fluxes. For both layers together the moisture gains by conver-

gence of atmospheric moisture fluxes amounts to only  $4 \cdot 10^6$  kg/s.

The moisture increment of the box by evapotranspiration is a small quantity as well, because the available energy and the saturation deficit are both small underneath the cloud cover of the SL. Contrary, precipitation is a large quantity causing a marked loss of moisture from the box. Thus these losses can only be compensated by the changes in the storage term, i.e. the water vapour content (ppw) of the atmosphere.

The evapotranspiration was estimated using a precipitation-runoff model (Adams and Tetzlaff 1986, Adams 1987). It was calculated using the precipitation values as resulting from the composite. Then the average soil moisture of the summer and the actual rains were added to produce the relevant soil moisture. The results were compared with empirical findings for the region (Flitcroft et al. 1986, Schmidt and Tetzlaff 1987). This was followed by the application of the evapotranspiration model. The necessary soil constants are based on empirical findings (Flitcroft et al. 1986).

The results for the SLs themselves were then extended to an area-averaged budget (Figure 8b). As was shown by Peters and Tetzlaff (1988), the budgets of the SL itself, the zone between SLs and the climatic average have to match each other and can thus be used as a control of the individual results. In the composite results the data for the climatic average were calculated by taking all data -that is 4 times per day- for the whole area, irrespective where a SL might be positioned. The results for the climatic average for the area and the SL itself differ in some significant points. The average AEJ fluxes tend to be larger than the fluxes at the SL. This is plausible, because the AEJ was found to be minimum in the vicinity of the SL (Tetzlaff and Peters 1988). The amount of precipitation is about one quarter of what it is in the SL itself and agrees very well with the climatic data of summer 1979. Evapotranspiration is about double what the convergence term of the atmospheric fluxes reaches. Evapotranspiration is again estimated from the approach of Adams and Tetzlaff (1986). The results depend on the amount of available soil moisture. The assumption is that in the rainy season there are steady state conditions. For the resulting values of soil water, soil properties, and plant coverage a flux of  $12 \cdot 10^6$  kg/s resulted for the evaporative input into the box. This means that two thirds of the water vapour losses due to precipitation originate from reevaporated waters of preceding SLs, only one third is directly supplied by atmospheric fluxes. It is remarkable that a significant inflow occurs from the north into the AEJ-level.

In order to quantify the errors of the fluxes given in Figures 8a and 8b the net storage of water vapour in the atmosphere is taken. In the climatological average this flux should be zero and indeed the composite gives a value of  $1 \cdot 10^6$  kg/s. Similar to the results for the SL itself this emphasizes the plausibility of the results, the formal errors being smaller than  $5 \cdot 10^6$  kg/s. Therefore, all major fluxes are significant.

The flow model needs the moisture flow data as an input. The model equations then allow to calculate the concentration of water vapour and of the rainfall at the surface, the ultimate product of condensation. The model results of the rainfall were intercompared against the

composite results (Figures 9a and 9b). The agreement is very close. The area-integrated values differ less than 5%. The spatial pattern shows some minor deviations such as a symmetric precipitation pattern at the Squall Front instead of a maximum at the southern edge, and a still weaker anvil precipitation. The lack of the anvil rains might result from the different mechanism producing them. They are not caused by a predominant convergence pattern such the rains at the Squall Front (Gamache and Houze 1983). The close agreement of the rainfall patterns prove that the flow model may be used to study the influence of changes in the input flow data on the resulting rainfall both for the SLs itself and for the climatic average.

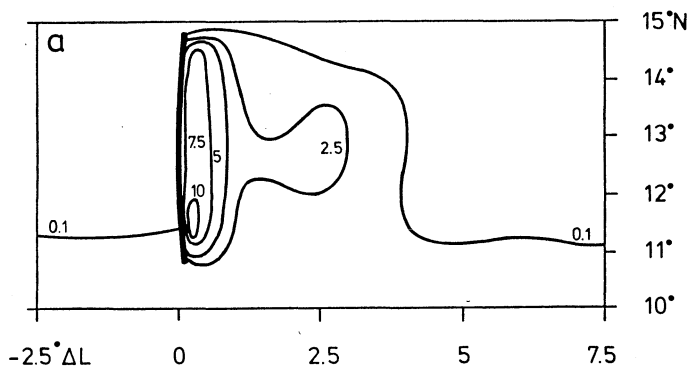


Figure 9a. Rainfall in mm/h as a result from the composite analysis of Squall Lines and their environment of summer 1979.

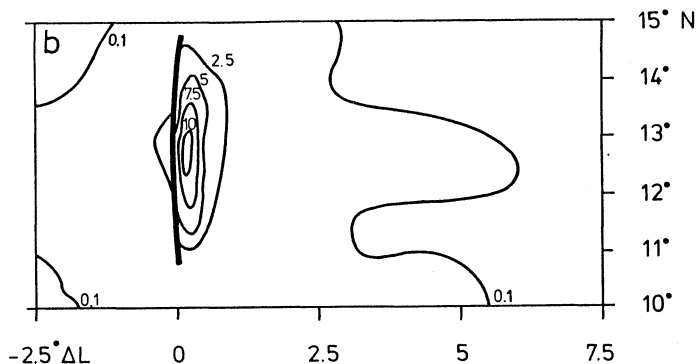


Figure 9b. Rainfall in mm/h from the Squall Line flow model (Equations 1 - 4) using the atmospheric water vapour fluxes, the water vapour content, and the temperature of the Squall Line environment as an input.

## 6. THE PALAEOCLIMATIC CONCLUSIONS FOR 18 000 YEARS B.P.

The main objective is to find palaeoclimatic data appropriate to insert into the flow model. For this purpose it is necessary to find such information. From former other findings (i.e. Gates 1976, Kutzbach and Guetter 1986) it is clear that temperatures in West Africa at 18 000 years B.P. were some 4 K lower than today. This led to a lower moisture content of the atmosphere. The relative humidity was kept constant, an assumption that seems to be plausible. Otherwise, any precipitation process would undergo dramatic changes. The quantitative consequences for the water vapour content are quite effective lowering the fluxes by a factor of almost 2.

As was pointed out before, the flow system is an important contributor to the atmospheric dust fluxes as well. From an analysis of the aeolian dust deposits in the equatorial Atlantic off the African coast a slowing down of the AEJ could be deduced (Sarnthein et al. 1981). On the other side, the amount of dust transported to the Atlantic Ocean was augmented by a factor of 2.5. The shape of the dust plume leaving the African continent was almost unchanged compared with recent conditions. The precipitation in the Sahel belt was lower than today. Estimates cover a range of 25 to 50% of today's values (i.e. Street and Grove 1979, Rognon 1976).

From the shape of the deposited dust plume it can be deduced that the transport mechanism for the dust remained unchanged including the synoptic scale features of the sickle shaped deposits stretching towards the Canary Islands. The combination of lower temperature, less precipitation, lower upper level winds, and higher dust deposits requires higher surface wind speeds. The influence of the different parameters on the amount of dust taken from the surface were investigated in a sensitivity study. In this study the general transport mechanism remained unchanged, because the flow pattern was unchanged as well as the general relative thermal distribution in the region. Furthermore, the SLs provide the mechanism to inject the dust into the mid-level air flow.

The lower wind velocity in the AEJ-level was still sufficient to allow the formation of SLs, because the critical value of the vertical wind shear was exceeded (Dudhia et al. 1987). The horizontal wind shear was large enough to cause the formation of waves within the AEJ-level with favorable zones for the initiation of the SLs.

The parameters quantitatively influencing the amount of dust taken from the surface are surface wind speed, surface roughness, vegetation coverage, extension of the area of high surface winds related to the SLs and SL frequency. To deposit more than the double amount of dust in the Atlantic ocean requires still higher amounts of dust injected into the easterly flow and this finally requires an increased surface wind speed.

In the sensitivity analysis the mentioned parameters were systematically varied starting from today's conditions (Figure 10). At 18 000 years B.P. less vegetation  $V_z$  (about  $-2/3$ ; Agwu and Beug 1984) and therefore a lower roughness length (about  $-1/2$ ; Sud and Smith 1985), a lower SL frequency  $n$  (about  $-1/3$ ), and a smaller area of high surface winds north of the SLs A (about  $-1/5$ , see Figure 7) produce a reduction

of the dust moved at the surface and of the suspended load. A reduced value of  $A$ , according to a lower intensity of the SLs, does not necessarily contradict an increase of potential dust source area, a consequence of reduced vegetation cover at 18 000 years B.P.. In this sense, the area of high surface winds  $A$  in the vicinity of an SL can be regarded as an effective dust source area, which was decreased at 18 000 years B.P.. These effects have to be overcompensated to find the increased amount of deposits in the Atlantic. The figure shows that the relation between surface wind speed and dust transport is nonlinear. It was thus concluded that the surface flow was increased by about 15%.

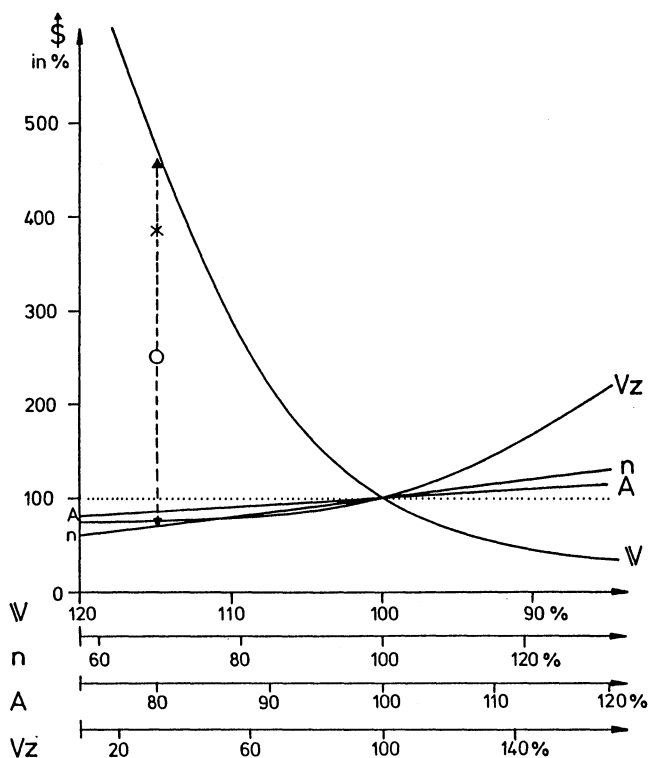


Figure 10. Dust lifting rate ( $\uparrow$ ) as a function of surface wind velocity ( $w$ ), Squall Line frequency ( $n$ ), extension of the dust lifting area ( $A$ ), and vegetation coverage together with surface roughness length ( $Vz$ ). All numbers are given in % of today's values ( $x$ : dust lifting rate at 18 000 years B.P.,  $o$ : dust deposits in the Atlantic ocean at 18 000 years B.P.).

With the higher flow velocities in the monsoon and the lower flow velocities in the AEJ-level, the lower temperature, a constant relative humidity the flow model allowed to calculate the changes of the amount

of SL-related precipitation as a function of the moisture fluxes. Similar to the results of the Figures 8a and 8b the moisture fluxes are presented for the SLs and for the climatic average (Figures 11a and 11b).

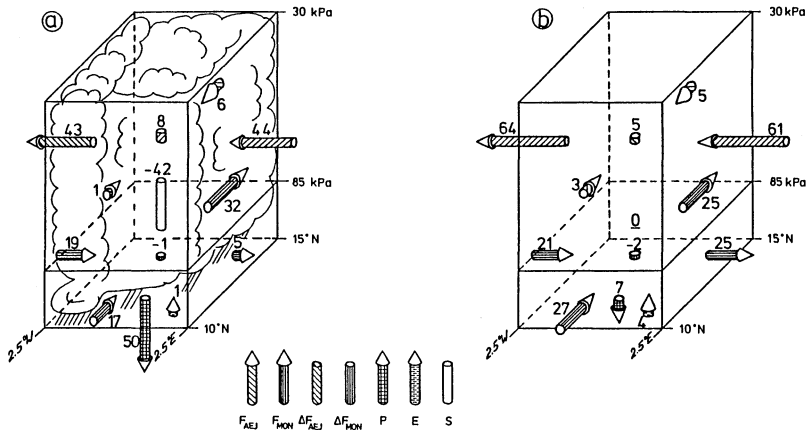


Figure 11a. Budget of water and water vapour as in Figure 8a, but for Squall Lines at 18 000 years B.P.

Figure 11b. Budget of water and water vapour as in Figure 8b, but for the climatic average at 18 000 years B.P.

According to the specified conditions, moisture fluxes in the monsoon layer and in the AEJ-layer are smaller. The decrease in the AEJ-layer is particularly distinct. The precipitation originating from the individual SL results to be about 2/3 of what it is today. The SL mechanism is still active and as such does not allow to drop the amount of precipitation too low. The climatic average values are similarly different as far as the atmospheric moisture fluxes are concerned. The total amount of precipitation is calculated to be close to 35% of today's value. Evapotranspiration supplies a smaller share of the precipitated waters, which is in agreement with the sparser vegetative cover.

These results support the idea that the climate of 18 000 years B.P. was dominated by the same meteorological structures as the weather is today, because a system with many parameters matches all available proxy data findings. The decisive data source are the dust deposits and the consequently derived values of the AEJ-fluxes as well as the the increased monsoon fluxes. The flow model then allowed to estimate the atmospheric fluxes and the resulting precipitation from these values. An error analysis showed that the results are significant. In future more emphasis will be put on the evapotranspiration processes and the soil moisture changes to allow a sensitivity analysis of the influence of the plant coverage on the precipitation formation.



## ACKNOWLEDGEMENT

Financial support was provided by the Bundesministerium für Forschung und Technologie under No. KF 2004/1. Mrs. R. Lorenz carefully prepared the figures, we thank her for her kind assistance.

## 7. REFERENCES

Adams, L.J., 1987: 'Ein Wasser- und Energiebilanz-Modell von abflußlosen Seen und seine Anwendung in der Paläoklimatologie von Nordwest-Afrika.' Ber. Inst. Met. u. Klimat. Uni. Hannover 29, 129 pp.

Adams, L.J. and G. Tetzlaff, 1986: 'Hydrologische Verhaltensmuster von abflußlosen Seen und ihre Rolle in der Paläoklimaforschung'. Ann. Meteorol. (N.F.) 23, 172-173.

Agwu, C.O.C. and H.-J. Beug, 1984: 'Palynologische Untersuchungen an marinen Sedimenten vor der westafrikanischen Küste'. Palaeoecology of Africa 16, 37-52.

Carlson, T.N. and J.M. Propero, 1972: 'The large-scale movement of Saharan Air Outbreaks over the northern equatorial Atlantic'. J. Appl. Met. 11, 283-297.

Carlson, T.N. and J.M. Prospero, 1977: 'Saharan Air Outbreaks: meteorology, aerosols and radiation'. Rep. US GATE Central Program Workshop (NCAR), Boulder, 57-78.

Dhonneur, G., 1970: 'Essai de synthèse sur les théories des lignes de grains en Afrique occidentale et centrale'. Bureau étude et méthode du centre météorologique de Dakar-Yoff 38, 56 pp.

Dudhia J., M.W. Moncrieff and D.W.K. So, 1987: 'The two-dimensional dynamics of West African Squall Lines'. Quart. J. Roy. Met. Soc. 113, 121-146.

Flitcroft, I.D., G. Dugdale and J.R. Milford, 1986: 'Hydrological studies in Niger'. In: ESA-Report SP-248, Proceedings of ISLSCP Conf., Rome 1985, 455-459.

Gamache, J.F. and R.A. Houze jr., 1983: 'Water budget of a mesoscale convective system in the tropics'. J. Atmos. Sci. 40, 1835-1850.

Gates, W.L., 1976: 'The numerical simulation of ice-age climate with a global circulation model'. J. Atmos. Sci. 33, 1844-1873.

Jaenicke, R., 1979: 'Monitoring and critical review of the estimated source strength of mineral dust from the Sahara'. In: C. Morales (ed.): Saharan Dust (SCOPE 14). John Wiley & Sons, Chichester, 233-242.

Janssen, W., 1988: Wasserbilanz westafrikanischer Squall Lines bei Änderungen der klimatischen Bedingungen. M.Sc. thesis, Inst. Met. u. Klimat. Uni. Hannover, 96 pp.

Koopmann, B., 1979: Saharastaub in Sedimenten des subtropisch-tropischen Nordatlantiks während der letzten 20 000 Jahre. Ph.D. thesis, Uni. Kiel, 98 pp.

Kutzbach, J.E. and P.J. Guetter, 1986: 'The influence of changing orbital parameters and surface boundary conditions on climate simulations for the past 18 000 years'. J. Atmos. Sci. 43, 1726-1759.

Middleton, N.J., 1985: 'Effect of drought on dust production in the Sahel'. Nature 316, 431-434.

Newell, R.E., J.W. Kidson, D.G. Vincent and G.J. Boer, 1972: The general circulation of the tropical atmosphere and interactions with extra-tropical latitudes, Vol. I. MIT Press, Cambridge and London, 258 pp.

Peters, M. and G. Tetzlaff, 1988: 'The structure of West African Squall Lines and their environmental moisture budget'. Met. Atmos. Phys. 38 (in press).

Reed, R.J., D.C. Norquist and E.E. Recker, 1977: 'The structure and properties of African wave disturbances as observed during phase III of GATE'. Mon. Wea. Rev. 105, 317-333.

Rogers, R.R., 1979: A short course in cloud physics, 2nd ed. Pergamon Press, Oxford, 235 pp.

Rognon, P., 1976: 'Essai d'interprétation des variations climatiques au Sahara depuis 40 000 ans'. Rév. Géogr. Phys. Géol. Dyn. 18, 251-282.

Sarnthein, M. and B. Koopmann, 1980: 'Late quaternary deep-sea record on NW-African dust supply and wind circulation'. Palaeoecology of Africa 12, 239-253.

Sarnthein, M., G. Tetzlaff, B. Koopmann, K. Wolter and U. Pflaumann, 1981: 'Glacial and interglacial wind regimes over the eastern subtropical Atlantic and north-west Africa'. Nature 292, 193-196.

Schmidt, R. and G. Tetzlaff, 1987: La détermination de l'évaporation dans un territoire semi-aride pendant la phase de dessèchement. Rep. for the Minister Res. and Techn. KF 1014 3, 73 pp.

Street, F.A. and A.T. Grove, 1979: 'Global maps of lake-level fluctuations since 30 000 years B.P.'. Quat. Res. 12, 83-118.

Sud, Y.C. and W.E. Smith, 1985: 'The influence of surface roughness of deserts on the July circulation'. Boundary-Layer Met. 33, 15-49.

Szekielda, K.-H., 1978: 'Eolian dust into the Northwest Atlantic'. Oceanogr. Maritime Biol. Ann. Rev. 16, 11-41.

Tetzlaff, G. and M. Peters, 1986a: 'Deep-sea sediments in the eastern tropical Atlantic off the African coast and meteorological flow patterns over the Sahel'. Geol. Rdschau 75, 71-79.

Tetzlaff, G. and M. Peters, 1986b: 'The atmospheric transport potential for water vapour and dust in the Sahel region'. GeoJ. 12, 387-398.

Tetzlaff, G. and M. Peters, 1988: 'Composite study on early summer Squall Lines and their environment over West Africa'. Met. Atmos. Phys. 38, 153-163.

Tetzlaff, G. and K. Wolter, 1980: 'Meteorological patterns and the transport of mineral dust from the north African continent'. Palaeoecology of Africa 12, 31-42.

Tetzlaff, G., M. Peters, L.J. Adams and W. Janssen, 1988: 'Wasserhaushalt im Sahel'. Die Erde (in press).

Westphal, D.L., O.B. Toon and T.N. Carlson, 1987: 'A two-dimensional numerical investigation of the dynamics and microphysics of Saharan dust storms'. J. Geophys. Res. 92 D3, 3027-3049.

Wolter, K., 1981: Staubtransporte über Nordafrika und dem angrenzenden Atlantik. M.Sc. thesis, Inst. Met. u. Klimat. Uni. Hannover, 176 pp.

## **SECTION 2.**

### **DUST TRANSPORT AND TRANSPORT MODELING**

## MODELING LONG-RANGE TRANSPORT USING TRAJECTORY TECHNIQUES

JOHN T. MERRILL

Center for Atmospheric Chemistry Studies  
Graduate School of Oceanography  
University of Rhode Island  
Narragansett, RI 02882-1197  
U.S.A.

**ABSTRACT.** Trajectory analysis has been used to help identify the source of materials transported through the atmosphere. A review of event-specific meteorological techniques, including isentropic trajectory analysis, is presented. A summary of mineral aerosol observations (both of air concentrations and of depositional flux) in the Pacific Ocean area follows, emphasizing the seasonal and latitudinal variations. Maximum concentrations are found in the North Pacific midlatitudes in the spring months. Examples of aeolian transport of Asian desert dust to the midlatitudes and subtropics of the North Pacific are contrasted with the clean-air flow to tropical South Pacific islands. A technique for synthesizing trajectory and chemical data is discussed, and the results of such an analysis for the SEAREX (Sea/Air Exchange program) mineral aerosol measurements are outlined. The dust from Asia is lifted to high elevations by prefrontal ascent. The dust-laden air moves out over the ocean rapidly in the high-speed, upper tropospheric winds. In the midlatitudes the westerlies provide a direct path, while in the subtropics the air subsides as it moves around anticyclones, descending to the surface trade winds. Similar trajectory analysis techniques have been used to investigate the transport paths to hypothetical sites in the western and central North Pacific (i.e., sites chosen arbitrarily and for which no direct observations are available). These show a similar pattern and indicate a tendency for higher latitude sites to be influenced by higher latitude deserts.

## 1. INTRODUCTION

Meteorological analyses and models can contribute materially to studies of the natural cycling of materials (Merrill, 1986); long range transport of mineral dust is a fine example (Merrill, 1989). Of the meteorological techniques which can be used in studies of global atmospheric transport, I will here discuss two. First, event-specific meteorological data and analyses can be combined with present-day observations of eolian transport and deposition to assess the importance of various source regions, transport paths, and removal mechanisms. Second, some of the same techniques of analysis can be used independent of direct observations of concentrations or deposition, at arbitrary locations, to make partial assessments of the first two of these factors. In this way direct observations of transport can be extended to characterize the meteorological phenomena.

Implicit in the discussion above is the notion that observations over a limited time, e.g., a few years, may yield transport events which are of geochemical and geological significance. This has not been demonstrated in general, but has been shown to be plausible for several substances in several regions. For example, in the central Pacific Ocean area, it has been shown that the mineral aerosol deposition flux is large enough to account for the observed mass accumulation rates of the nonbiogenic sediments (Uematsu, *et al.*, 1985, and the references therein). Initially, the mineralogical similarity of the windborne dust in the Hawaiian Islands to the nearby surface sediments indicated that the pelagic clays there are continental dust from Asia (Rex and Goldberg, 1958; Griffin, *et al.*, 1968). Additional comparisons of present-day mineral aerosol particles have firmly established that they are virtually identical to the surface sediment from various regions of the North Pacific (Buat-Menard, *et al.*, 1983; Blank, *et al.*, 1985). Careful *in situ* sampling of mineral dust concentrations and fluxes in the remote North Pacific has been conducted for less than ten years, but both the identity and the intensity of the dominant source have been confirmed in this brief interval. This connection is important because the recognition of truly significant transport events is the key to the selection of representative cases for meteorological analysis.

## 2. TECHNIQUES

In this work it is appropriate to undertake a direct juxtaposition of Eulerian and Lagrangian characterizations of atmospheric phenomena. In the *Eulerian* approach, one makes observations at a fixed site; such

sampling allows the atmosphere to bring information or material to you. Here, the Eulerian data are mineral aerosol concentrations at a sampling station on the windward coast of islands far from any continent. In the *Lagrangian* approach, one follows hypothetical parcels of air as they move about. The attempt to account for the motion, the accumulation and loss of chemical constituents (e.g., the dust load), and other aspects of the parcel's development is dependent upon meteorological data and analysis techniques.

## 2.1 Mineral Aerosol Observations

Estimates of the concentration of mineral aerosol (dust) have been made at island sites in the Pacific area by Duce, *et al.* (1980), Arimoto, *et al.* (1982), Uematsu, *et al.* (1983), Parrington, *et al.* (1983), Darzi and Winchester (1982), and by others. These estimates are based on trace metal measurements, primarily aluminum and iron, which are indicative of weathered continental crustal material. The analytical determinations are made by instrumental neutron activation or by X-ray excitation on filters pumped in high-volume air sampling apparatus. The samplers are set to pump only when the wind is onshore, to prevent contamination of the filter by dust raised from the soil locally. There have also been direct observations of the deposition of mineral dust to the Pacific. Uematsu, *et al.* (1985) analyzed one year of deposition estimates using two-week long samples of total deposition (i.e., continuously open bucket collections of dry and wet deposition) for dust. Betzer, *et al.* (1988) demonstrated consistent flux values in the air (in deposition collectors and sediment traps at several levels in the water column) at a site near the Hawaiian Islands.

These observations are only the most recent in a continuing series of mineral aerosol observations. A continuously operating Network of stations was established as part of the SEAREX (Sea/Air Exchange) program when it became apparent that there are marked seasonal variations in the amount of continental material transported to the remote Pacific Ocean. A comprehensive synthesis of these observations is to be found in Prospero, *et al.* (1989). Numerous studies in the Atlantic and Mediterranean area have documented the more massive flux from the Sahara (e.g., Prospero and Carlson, 1972). An overview is presented in the recent paper by Chester (1986). It is obvious that the Atlantic and Pacific dust transport problems differ in essentials: the Atlantic transport is in the easterlies, while the Pacific is in the westerlies.

## 2.2 Trajectories and Transport Paths

Event-specific meteorological data have always been used to determine the source area for atmospheric chemistry experiments. Trajectory analysis has been used in many cases. The trajectories have usually been based on manual or machine analyses of radiosonde data (i.e., on upper-air weather charts). These *isobaric* analyses may indicate the motion of the air accurately for short periods, but after as little as a day the motion of the air begins to be substantially anisobaric. This is because the isobaric surfaces are nearly horizontal, and even the large scale motion of the atmosphere includes significant vertical excursion. It has been shown that the motion of the air is *isentropic* to a good degree of accuracy in the free troposphere and that isentropic trajectory analysis more accurately tracks the motion of the air (Danielsen, 1961). The approximation is based on the nearly adiabatic character of the airflow in areas away from the surface boundary layer and from moist convection. The vertical velocity of the air is taken into account implicitly rather than ignored; the parcels move vertically as their motion along the sloping and undulating isentropic surface progresses.

The calculation of such trajectories requires only wind data on the isentropic surfaces for chosen values of the potential temperature. These winds are obtained by a process of vertical interpolation in each column of a grid covering the region of interest, using as the basic data winds and geopotential heights on isobaric surfaces (Bleck, 1984). The required data fields are available globally twice per day in the routine analyses prepared by operational weather services. In my work the 2.5° analysis of the US National Meteorological Center is used. This data set is the product of a sophisticated analysis-forecast-assimilation cycle that takes into account all available meteorological observations (Dey and Marone, 1985).

‣ An example of the input winds and the resultant isentropic data is shown in the pair of height *vs.* latitude cross sections in Fig. 1, which represents the analysis for the indicated longitude at a particular time. The velocities are shown in conventional meteorological notation, by arrows flying with the wind. The average temperature (and thus the average potential temperature) between the isobaric levels is given by the distribution of geopotential heights (not shown). The shape of the intermediate isentropic surfaces is indicated by the thin lines sloping down to the right. It is important to note that no fundamentally new information is present in the isentropic winds here; examination of the plot shows that these winds are merely consistent with the isobaric analysis.



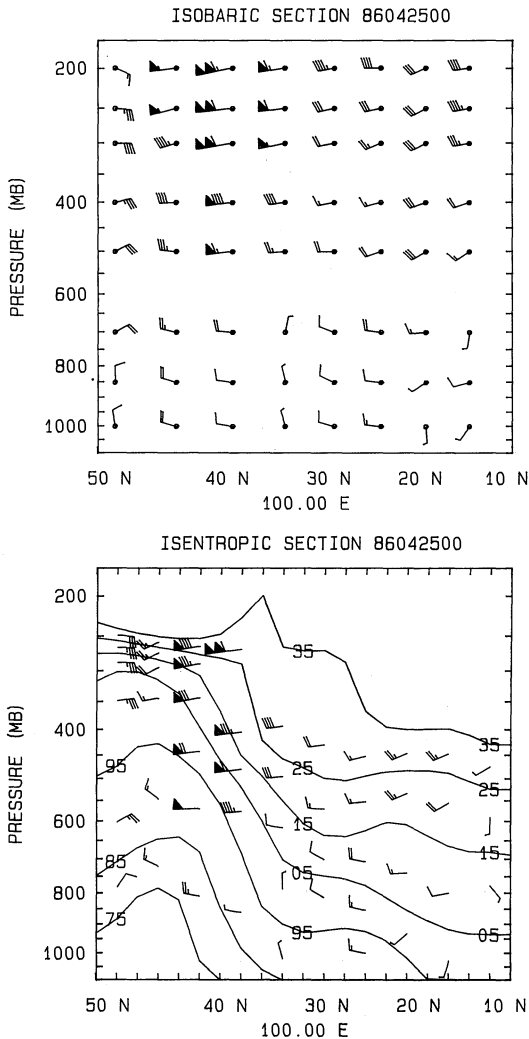


Figure 1: Height *vs.* latitude cross sections for a single longitude and time illustrating the conversion from isobaric to isentropic fields. The winds are shown in conventional meteorological notation, as arrows flying with the wind. Half barbs represent  $2.5 \text{ ms}^{-1}$ , full barbs  $5 \text{ ms}^{-1}$  and feathers (shaded triangles)  $25 \text{ ms}^{-1}$ . The isobaric data marked with a circle at the arrowhead, and are at fixed intervals of  $2.5^\circ$ , but the sections are shown on a Mercator projection. The isentropic winds are shown for 280K, 290K...330K, and the shape of the surfaces for 275K...335K is shown by the sloping lines.

Based on such, wind trajectories can be calculated which will accurately reflect the vertical as well as horizontal motions of the *air* for several days. Because the winds are known imperfectly (especially over the ocean where upper air data are few), errors accumulate rapidly and individual trajectories contain little information after many days. Also, deformation processes inherent in the motion of the atmosphere cause initially compact parcels of air to be stretched into thin filaments; they eventually lose their identity. Finally, diabatic effects and the often very important gravitational settling of aerosol particles increase the differences between the calculated and the actual trajectories. Nevertheless, we can use trajectories extending back from the measurement sites and interpret them with these limitations in mind (Merrill, *et al.*, 1985).

### 3. OBSERVATIONS OF SEASONAL AND LATITUDINAL DISTRIBUTIONS

As noted above, several groups have made observations of mineral dust concentrations in the Pacific region. Here we review some of the data obtained by Uematsu and his co-workers, including recent data. A discussion of the Network and the first year's data for the North Pacific are to be found in Uematsu, *et al.* (1983). Direct measurements of the mass flux are reported and discussed in Uematsu, *et al.* (1985). The review by Prospero, *et al.* (1989) has an informative discussion of the week-to-week variability of the concentrations. Short-term variations in the flux and concentration have also been studied: Darzi and Winchester (1982); Tsunogai and Kondo (1982).

The range of concentrations, the latitudinal variation, and the seasonal variability are all evident in the temporal record of concentrations from the SEAREX Network shown in Table 1. These are monthly geometric mean and standard geometric deviations determined from the number of samples indicated. The estimates are based on weekly samples collected synoptically. The number of samples varies from station to station because some data are missing. Missing data are caused by failure of field equipment or by adverse winds; available samples with less than 10% pumping time are set aside to avoid artifacts caused by local contamination.

In Table 1 the data for 1981-1986 at Shemya, Midway and Oahu are summarized. The concentrations of mineral dust range from less than 0.10 to about 4.5 mg m<sup>-3</sup>. Each station has significant variation through the year, with monthly mean values greater than 1.3 and less than about 0.2 mg m<sup>-3</sup>. The largest values are near the midlatitudes, at Shemya and Midway,

Table 1: Mineral dust concentrations at SEAREX Network sites. Geometric mean,  $\text{mg m}^{-3}$ , and geometric standard deviation, based on data from 1981-1986.

Mon	Shemya			Midway			Oahu		
	Meang	sg	N	Meang	sg	N	Meang	sg	N
JAN	3.03	--	1	0.09	4.09	11	0.56	2.55	10
FEB	0.46	1.45	3	0.88	2.56	15	0.76	2.44	13
MAR	0.88	1.89	7	1.75	2.29	16	1.38	2.10	18
APR	4.49	2.09	6	1.18	2.26	18	0.87	1.78	18
MAY	1.49	3.50	2	1.43	2.12	17	1.38	1.88	16
JUN	0.71	1.32	3	0.33	2.40	11	0.41	1.67	13
JUL	0.25	1.46	4	0.08	2.08	13	0.09	1.95	10
AUG	0.31	2.42	5	0.14	2.65	12	0.12	2.35	12
SEP	0.47	1.92	3	0.13	2.53	10	0.13	2.53	13
OCT	0.20	1.71	3	0.31	2.22	9	0.18	2.60	13
NOV	0.60	1.75	4	0.55	2.47	13	0.18	2.01	9
DEC	1.04	1.20	2	0.22	2.70	12	0.27	2.75	8

while there are generally lower values at Oahu. The data for the lower latitude sites (not shown) show a continuing decrease further from the midlatitudes. The seasonal variation is systematic, with a maximum in the late winter and spring months of February through June and a minimum in the summer months of July - September. There is an indication of a secondary maximum in the months of October and November, particularly at the midlatitude sites.

These relatively high concentration values are to be contrasted with much lower estimates in regions unaffected by eolian transport from continents. At American Samoa the mineral dust concentrations have been found to be nearly independent of season and range around  $0.01 \text{ mg m}^{-3}$  (Arimoto, *et al.*, 1987). As will be illustrated below, the airflow pattern and the finite residence time of mineral dust in the atmosphere make these small values seem reasonable.

#### 4. TRANSPORT PATTERNS IN THE WESTERN AND CENTRAL PACIFIC

It has been known for many years that dust storms in Asia are the source for mineral dust reaching the North Pacific Ocean (e.g., Ing, 1972). A dramatic example is presented by Iwasaka, *et al.* (1983). Combined with the direct observations of mineral dust at the midocean sites, trajectory analysis can confirm the source area and be used to document the transport path.

Examples of trajectories provide an indication of the role of the large scale patterns of airflow in the long range transport process. In Fig. 2 back trajectories from three of the Network sites are shown for March 6, 1981. The trajectories at Midway and Oahu are at 300 K, while that at Enewetak is at 305 K. The dots are at 24 hour intervals (there is one each day at 00 UTC). The map in the lower panel shows the horizontal motion, while the height-longitude cross section in the upper panel shows the vertical component of the motion. All of the trajectories began over Asia at higher elevations. Note that the trajectory reaching Midway was at about 400 hPa when it was over the deserts; this is over 7 km above sea level. The transport path is more or less direct from Asia to Midway in this case. The trajectory reaching Oahu lies at a lower elevation and a lower latitude over China. Further, the air circles slowly around the large anticyclone northeast of the Hawaiian Islands and approaches Oahu from the southeast. This anticyclonic motion is accompanied by subsidence. The trajectory to Enewetak is similar to that at Oahu in that there is a long anticyclonic segment during which the parcel gradually descends towards the surface.

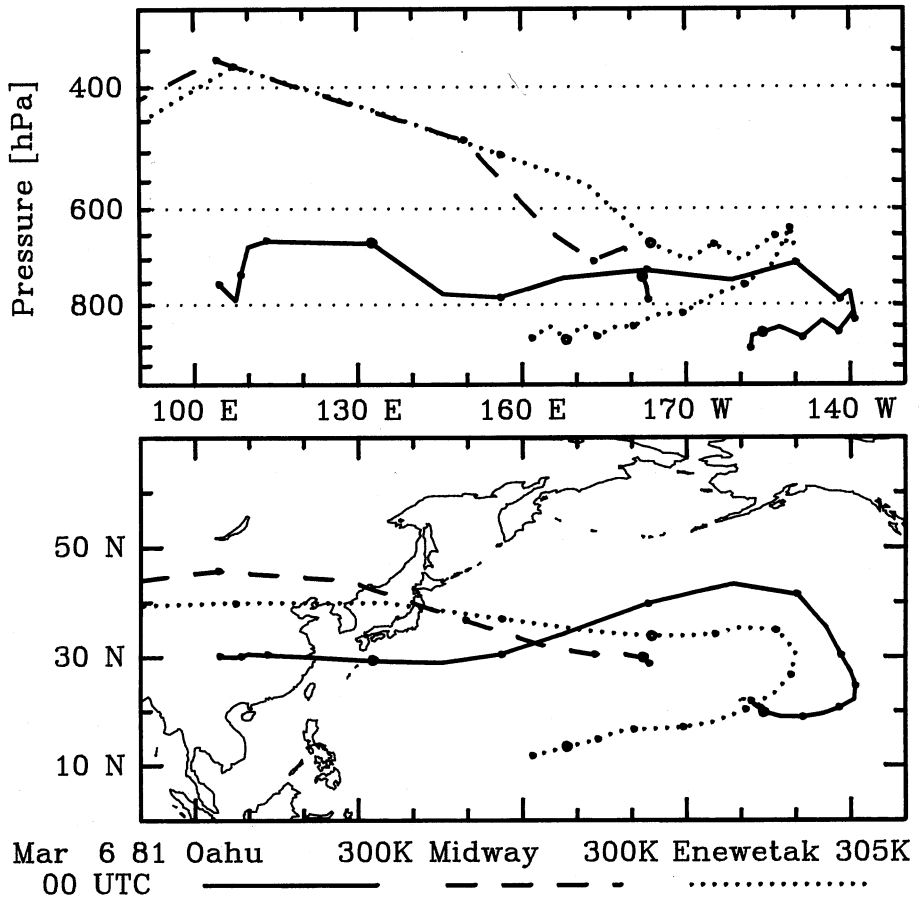


Figure 2: Isentropic trajectories back in time from three Network sites for March 6, 1981. At Midway and Oahu the trajectories are at 300K, while at Enewetak the trajectory is at 305K. The dots are at 00 UTC each day. The lower panel shows the horizontal component of the motion, and the corresponding vertical motion is shown on the panel above. The trajectories started at high elevations over Asia and gradually subsided as they moved out over the ocean.

The potential temperature surfaces were chosen to lie within or just above the atmospheric mixed layer at the latitudes of the sites. The relative speed of motion, indicated by the spacing of the daily dots, is consistently lower on the equatorward flank of the anticyclonic loop, because the trade winds are slower than the upper level westerlies.

There was a major dust outbreak in progress in Asia when these trajectories were over the deserts. This was determined by an examination of routine surface weather observations for that time. The approach is similar to that discussed by Middleton, *et al.* (1986). Also, the mineral aerosol samples for the week including March 6 showed a peak in the dust concentration at each of these island sites. The corroboration of the source of the material by trajectory analysis provides an indication that there is some information in such long trajectories despite the large uncertainty in each individual point. In order for material to be carried such long distances, it must be lifted to great heights to overcome the subsequent inexorable gravitational settling. Several additional examples of trajectories for Enewetak, including cases in the summer season, are to be found in Merrill, *et al.*, (1985). Also to be found there is a brief discussion of the likely cause of the uplifting.

It would seem unlikely to a meteorologist that this pattern of flow could extend deep into the tropics. However, the mineral aerosol observations at Fanning Island (at 4°N in the central Pacific) indicate that such a path exists (Uematsu, *et al.*, 1983). The examples shown in Merrill (1986) indicates that a pattern similar to that at Oahu and Enewetak in Fig. 2 can bring air from Asia deep into the tropics. They also indicate that similar flow patterns can carry material across the equator. Of course most of the material from the deserts has been dispersed or removed by settling or precipitation scavenging by the time the air reaches the equatorial regions.

Further, there are vast regions of the South Pacific Ocean that are relatively isolated from eolian transport from the continents. The trajectories in Fig. 3 go backward in time from April 17, 1984 from the eastern tip of American Samoa. There are four trajectories plotted, starting at intervals of 1 degree in latitude and longitude surrounding the site. This "swarm" calculation is useful for assessing the diffluence of the flow. In this case the diffluence is very small. Here the air approaching Samoa is moving slowly and remains within the marine boundary layer. The air has been isolated from any continent for at least two weeks. The trajectories are representative of the flow to Samoa for most of the year and are consistent with the very low mineral dust concentrations discussed above.

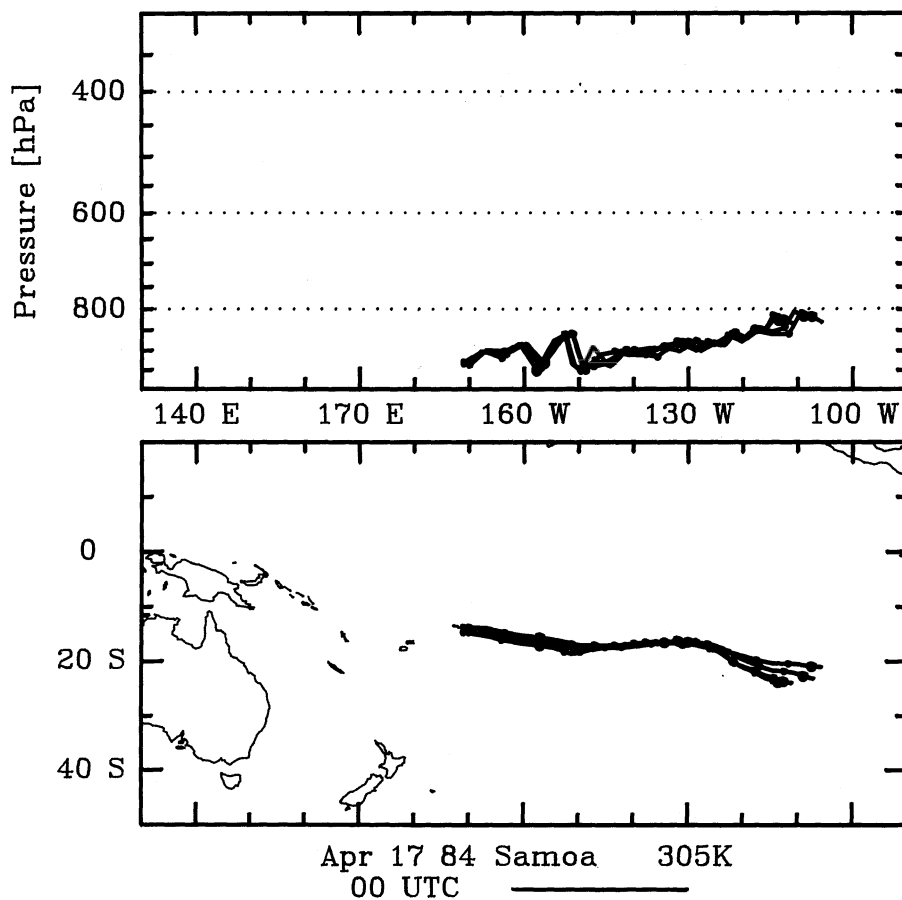


Figure 3: Isentropic trajectories back in time from American Samoa. There are four trajectories, with starting locations displaced by 1 degree of latitude and longitude, surrounding the site. These trajectories show that the air reaching American Samoa neither approached nor crossed any continent for at least two weeks prior to its arrival.

I have prepared trajectories for the entire period of sampling in the SEAREX Network. The collected trajectories contain a wealth of information about transport paths, including an indication of the average or typical path when such exists. Seeking the typical path by a direct superposition of large numbers of trajectories is not informative, because the wide variation in the features of the trajectories makes such a superposition look like pseudo-random scribbling. Also, the covariation of the route of transport and the ambient aerosol concentration in the source region may be important, not only the path itself. This is especially true in the case of mineral aerosol because the uplifting required for long range transport is strongly dependent on the large scale meteorological situation, and the source and transport processes are not independent. However, there are no quantitative measures of the dust source strength that are suitable for use in estimating this covariance. Therefore, I use downstream observations of concentrations at the surface, when the dust is about to enter the ocean.

A technique for synthesizing trajectory results with chemical observations was developed by Poirot and Wishinsky (1986). In this approach the probability that trajectories reaching a chosen site are from any given area is plotted on a map. The chemical observations are used to *select* the trajectories. Thus, periods during which high concentrations of the substance of interest were found may be noted and the corresponding trajectories used in the superposition. If a sufficiently large number of samples (and thus trajectories) is available, the resulting fields of probability are relatively smooth. The smoothness can be enhanced by plotting contours of the cumulative probability rather than the probability itself. There is a strong central tendency in the probability distribution because every trajectory emanates from the chosen site. This is compensated for by a square-law geometric correction applied to the raw probabilities. Use of this technique demonstrates that the source area and transport path ideas discussed above, which were based on trajectory examples chosen rather arbitrarily, are in fact representative of the main transport regime. Further discussion of transport paths for the Pacific region can be found in Merrill, *et al.* (1989).

The approach can be used in a limited way even when no direct chemical observations are available, at least for well-studied environments such as Asia and the Pacific. This is because both the synoptic and seasonal variations in the mineral dust source strength are fairly well known. At the present the maximum in the dust concentration and the dust flux in the western Pacific area is during the months February-June. Using trajectories calculated back in time from arbitrary locations along 155°E and 155°W I



have prepared cumulative probability maps showing the latitudinal and longitudinal variation of the probable source area of air masses during the months of March and April for the years 1984-1987. Because air reaching these locations is so often dusty during those months I have not made use of any restrictive selection. (More fundamentally, there are, in general, no *in situ* data from these locations on which to base the selection.) The resulting areas of peak probability are shown in Fig. 4 and 5 for two latitudinal bands: 25-30°N and 45-50°N.

The peak probability of trajectory passage for the more northern area at 155°E (Fig. 4) lies over the eastern deserts and coastal regions of Asia, while that for the more southern area lies further south. That is, there is a latitudinal shift in probable source areas as a hypothetical "receptor" area moves latitudinally. Thus the transport pattern is an important factor in the distribution of eolian dust. The simplest imaginable pattern is a straight west to east flow; the actual pattern is not this simple (note that the areas of peak probability overlap somewhat). While the details of the areas indicated are not to be believed, because of the limitations of the trajectory analysis and the absence of corroborating data, it is reassuring to note that at intermediate latitudes (not shown) the peak probability extends further west, covering a larger area of the deserts. In Fig. 5 the corresponding peak probability areas for 155°W are shown. A similar latitudinal shift is apparent, indicating that the transport pattern retains its identity at least out to the central part of the ocean. The areas of peak probability are larger, extending further west and especially east of the coast of Asia.

The trajectories themselves are not quantitative, i.e., they offer no indication of the source strength or the dilution and removal along the path. However, since the lower latitude area in these Figures lies south of the deserts of Asia, it is to be expected that the air reaching that latitude band will most often have a lower dust load than that from directly over the desert. The fall-off of the mass accumulation rates with latitude away from the midlatitudes in the sediments is caused, in part, by this transport pattern. In the central Pacific, transport south of about 30°N always involves an anticyclonic loop, as shown in Fig. 2 (Merrill, 1986).

The importance of the transport pattern in the distribution of mineral aerosol is evident in the observed distribution of concentrations and fluxes at present. The observed concentrations decrease markedly from midlatitudes to the tropics and from the dusty season to the clean season; at lower latitudes the seasonal variation of the ambient mineral aerosol is higher because instances of transport in the summer are less frequent there.

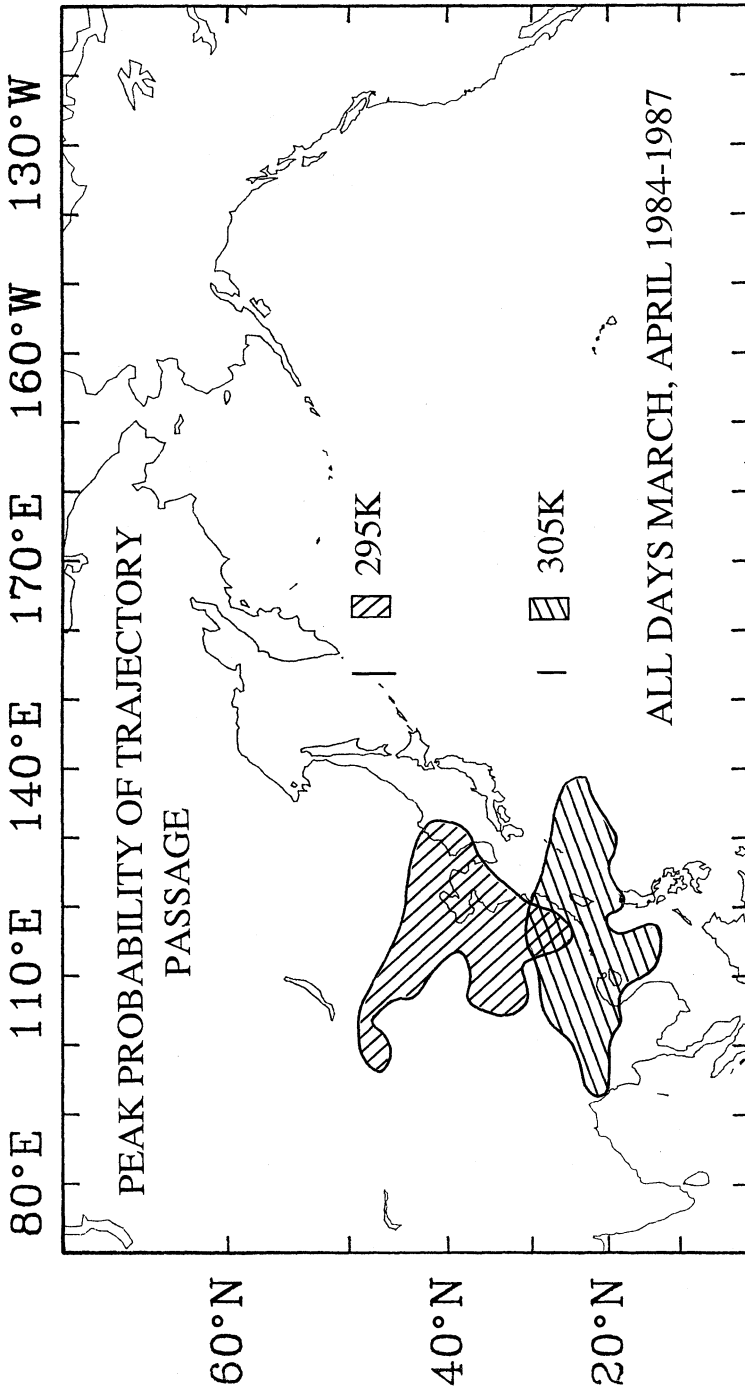


Figure 4: Areas of maximum probability of trajectory passage for two latitude bands at 155°E. The lower latitude area, for trajectories arriving at 25-30°N, is at 305K, while that for 45-50°N is at 295K because of the latitudinal slope of the isentropes. Trajectories, twice per day for March and April for the years 1984-1987, were used in the calculation.

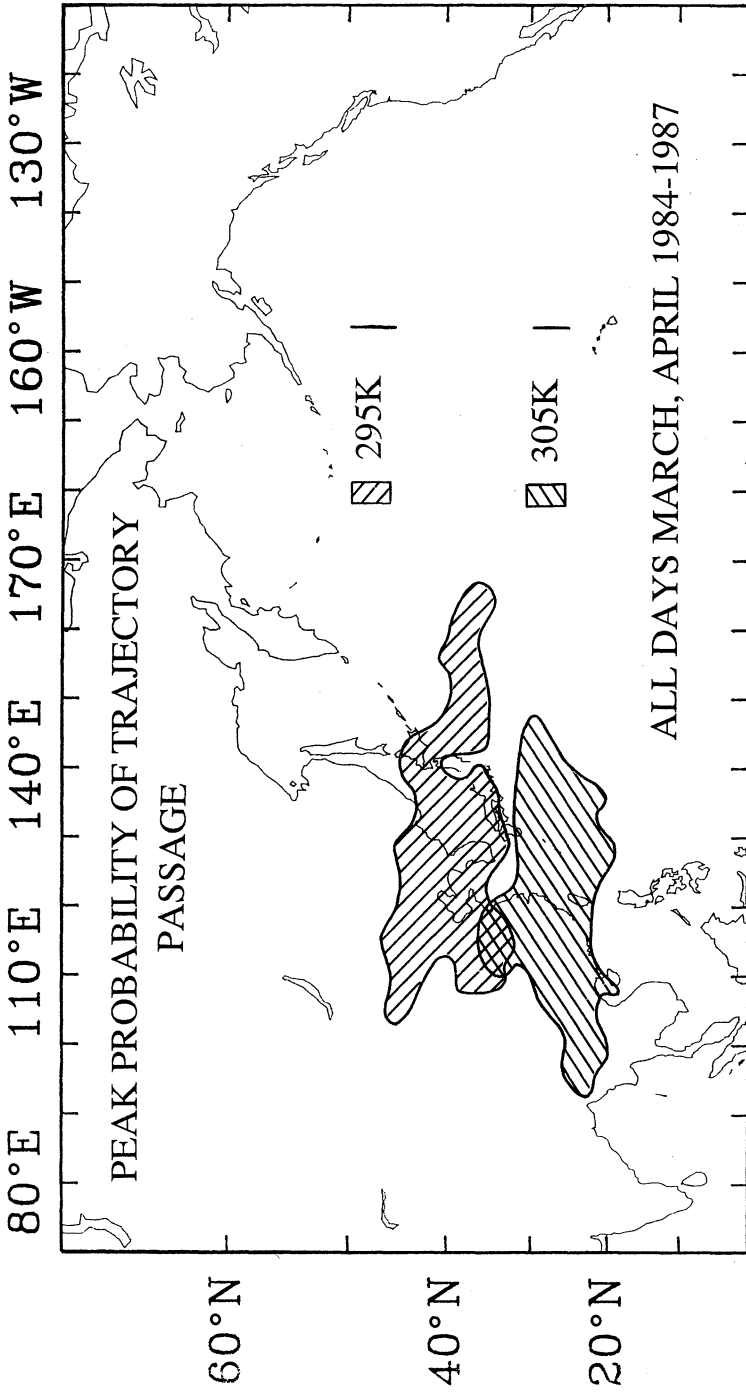


Figure 5: Areas of maximum probability of trajectory passage for two latitude bands at 155°W. The same remarks as in Fig. 4 apply.

However, the latitudinal variation of the downward flux is much less than that of the concentration because greater rainfall at the lower latitudes results in large deposition fluxes.

## 5. CONCLUSIONS

Event specific meteorological data and analyses can be used constructively to assess the transport patterns and dominant source areas of present day eolian transport. The approach discussed here is merely qualitative and is most powerful when applied in conjunction with *in situ* chemical observations (i.e., estimates of the air concentration or the depositional flux). Nevertheless it can be used independently of such observations to discern typical transport patterns. Knowledge of these patterns is needed because they are such an important contributor to the overall distribution of eolian materials.

## ACKNOWLEDGEMENTS

The observations of mineral aerosol in the Pacific Ocean area that were discussed above are those of the Pacific Aerosol Transport and Deposition Network. This Network was developed by J. M. Prospero, Mitsuo Uematsu and R. A. Duce, funded by the US National Science Foundation primarily through grant ATM 83-11694. The meteorological analysis techniques discussed in this paper have been developed in a collaborative effort between the author and his colleague Rainer Bleck of the University of Miami, primarily under NSF funding, most recently grant OCE 84-05608 as part of the Sea/Air exchange program. This paper was completed while the author was supported by NSF grant ATM 87-16432. The computing facilities and meteorological archives of the National Center for Atmospheric Research have been used extensively in my work; NCAR is also funded by NSF. The figures and many of the calculations were prepared with the courteous assistance of Ms. Ruth Platner. It is a pleasure to thank all of these people for their cooperation.

## REFERENCES

- Arimoto, R., R.A. Duce, B.J. Ray, and C.K. Unni, 1982: Atmospheric trace elements at Enewetak Atoll, 2, Transport to the ocean by wet and dry deposition, *J. Geophys. Res.*, 90: 2391-2408.

- Arimoto, R., R.A. Duce, B.J. Ray, A.D. Hewitt, and J. Williams, 1987: Trace elements in the atmosphere of American Samoa: concentrations and deposition to the tropical South Pacific, *J. Geophys. Res.*, 92: 8465-8479.
- Betzer, P.R., K.L. Carder, R.A. Duce, J.T. Merrill, N.W. Tindale, M. Uematsu, D.K. Costello, R.W. Young, R.A. Feely, J.A. Breland, R.E. Bernstein, and A.M. Greco, 1988: A pulse of Asian dust to the Central North Pacific: Long range transport of giant mineral aerosol particles, *Nature*, 336: 568-571.
- Blank, M., M. Leinen, and J.M. Prospero, 1985: Major Asian eolian inputs indicated by the mineralogy of aerosols and sediments in the western North Pacific, *Nature*, 314: 84-86.
- Bleck, R., 1984: Vertical coordinate transformation of vertically discretized atmospheric fields, *Mon. Wea. Rev.*, 112: 2535-2539.
- Buat-Menard, P., U. Ezat, and A. Gaudichet, 1982: Size distribution and mineralogy of aluminosilicate dust particles in tropical Pacific air and rain, In: *Precipitation Scavenging, Dry Deposition and Resuspension, Vol. 2*, (H.R. Pruppacher, R.G. Semonin and W.G.N. Slinn, Eds.), Elsevier, New York, pp. 1259-1270.
- Chester, R., 1986: The marine mineral aerosol, In: *The Role of Air-Sea Exchange in Geochemical Cycling*, P. Buat-Menard, Ed., NATO ASI Series, C185, D. Riedel, Inc., Dordrecht, Holland, pp. 443-476.
- Danielsen, E.F., 1961: Trajectories: isobaric, isentropic and actual, *J. Meteor.*, 18: 479-486.
- Darzi, M., and J.W. Winchester, 1982: Aerosol characteristics at Mauna Loa Observatory, Hawaii, after east Asian dust storm episodes, *J. Geophys. Res.*, 87: 1251-1258.
- Dey, C.H., and L.L. Marone, 1985: Evolution of the National Meteorological Center global data assimilation system: January 1982-December 1983, *Mon. Wea. Rev.*, 113: 303-318.
- Duce, R.A., C.K. Unni, B. Ray, J.M. Prospero and J.T. Merrill, 1980: Long range transport of soil dust from Asia to the tropical North Pacific: Temporal variability, *Science*, 209, 1522-1524.

- Griffin, J.J., H. Windom, and E.D. Goldberg, 1968: The distribution of clay minerals in the world ocean, *Deep Sea Res.*, 15: 433-459.
- Ing, G.K.T, 1972: A dust storm over central China, April, 1969, *Weather*, 27: 136-145.
- Iwasaka, Y., H. Minoura, and K. Nagaya, 1983: The transport and spacial scale of Asian dust-storm clouds: a case study of the dust-storm event of April 1979, *Tellus, Ser. B.*, 35: 189-196.
- Merrill, J.T., Bleck, R., and L. Avila, 1985: Modeling atmospheric transport to the Marshall Islands, *J. Geophys. Res.*, 90: 12,927-12,936.
- Merrill, J.T., 1986: Atmospheric pathways to the ocean, *In: The Role of Air-Sea Exchange in Geochemical Cycling*, P. Buat-Menard, Ed., NATO ASI Series, C185, D. Riedel, Inc., Dordrecht, Holland, pp. 35-63.
- Merrill, J.T., 1989: Atmospheric long range transport to the Pacific Ocean, Chapter in *Chemical Oceanography*, 10, Reiley and Chester, Eds., Academic Press.
- Merrill, J.T., M. Uematsu, and R. Bleck, 1989: Meteorological analysis of long range transport to the Pacific Ocean, *J. Geophys. Res.*, in press.
- Middleton, N.J., A.S. Goudie, and G.L. Wells, 1986: The frequency and source areas of dust storms, *In: Aeolian Geomorphology*, W.G. Nickling, Ed., Allen and Unwin, New York, pp. 237-259.
- Parrington, J.R., W. Zoller, and N.K. Aras, 1983: Asian dust: seasonal transport to the Hawaiian Islands, *Science*, 220, pp. 195-197.
- Poirot, R.L., and P.R. Wishinsky, 1986: Visibility, sulfate and air mass history associated with the summertime aerosol in northern Vermont, *Atmos. Environ.*, 20: 1457-1469.
- Prospero, J.M., and T.N. Carlson, 1972: Vertical and areal distribution of Saharan dust over the western equatorial Atlantic Ocean, *J. Geophys. Res.*, 77: 5255-5265.
- Prospero, J.M., M. Uematsu, and D. Savoie, 1989: Mineral aerosol transport to the Pacific Ocean, Chapter in *Chemical Oceanography*, 10, Reiley and Chester, Eds., Academic Press.

- Rex, R.W., and E.D. Goldberg, 1958: Quartz contents of pelagic sediments of the Pacific Ocean, *Tellus*, 10: 153-159.
- Tsunogai, S., and T. Kondo, 1982: Sporadic transport and deposition of continental aerosols to the Pacific Ocean, *J. Geophys. Res.*, 87: 8870-8874.
- Uematsu, M., R.A. Duce, J.M. Prospero, J.T. Merrill, and R.L. MacDonald, 1983: The transport of mineral aerosol from Asia over the North Pacific Ocean, *J. Geophys. Res.*, 88: 5543-5552.
- Uematsu, M., R.A. Duce, and J.M. Prospero, 1985: Deposition of atmospheric mineral particles in the North Pacific Ocean, *J. Atmos. Chem.*, 3: 123-138.

PRESENT TRANSPORT AND DEPOSITION PATTERNS OF AFRICAN DUSTS TO THE NORTH-WESTERN MEDITERRANEAN.

G. Bergametti, L. Gomes and E. Remoudaki  
Laboratoire de Physico-Chimie de l'Atmosphère  
UA CNRS 717, Université Paris VII  
2, place Jussieu, 75251 Paris Cedex 05  
France

M. Desbois  
Laboratoire de Météorologie Dynamique  
Ecole Polytechnique  
91120 Palaiseau  
France

D. Martin  
Etablissement d'Etudes et de Recherches Météorologiques  
Centre de Recherches en Physique de l'Atmosphère  
78470 Magny les Hameaux  
France

P. Buat-Ménard  
Centre des Faibles Radioactivités, Laboratoire Mixte CNRS-CEA  
91198 Gif/Yvette Cedex  
France

**ABSTRACT.** The elements associated with mineral aerosol particles exhibit, in the Western Mediterranean, sporadic but intense concentration peaks. Twenty dust events were recorded during a one-year sampling period with their frequency being maximum in spring and summer. Three-dimensional air-mass trajectories as well as satellite imagery (Meteosat II) show that all these events are associated with transport of soil dust from Africa. Three principal source-regions have been distinguished by using air-mass trajectories. Each of them seems to be characterized also by the chemical composition of the dust collected in Corsica. Moreover, the emissions and transport of dust particles from these various source-regions were found to occur during different times of the year. This has been explained by the seasonal atmospheric circulation patterns over North Africa and the Western Mediterranean.

Finally, total deposition measurements show that such dust transport events control a large fraction of the yearly atmospheric deposition of mineral aerosol particles to the Western Mediterranean. One single deposition event of short duration was found to account for 30% of the total annual flux for elements such as Si and Al.



## 1. INTRODUCTION

It is now well recognized that a significant fraction of non-biogenic material in deep ocean sediments has an aeolian origin, primarily the mobilization of soil-dust by the effect of wind. Arid and semi-arid areas of the Earth contribute to more than 70% to the total soil-dust content of the atmosphere and consequently, these desertic dusts constitute the major part of the atmospheric component present in ocean sediments (Prospero, 1981).

Many authors (Rex and Goldberg, 1958; Griffin and Goldberg, 1968; Dauphin, 1983; Blank et al., 1985) have observed significant amounts of aeolian minerals (as quartz or illite) in North-Pacific sediments. Similar results have been obtained in the North-Atlantic (between 5°N and 35°N) by Chester et al. (1979) and Sarnthein et al. (1982). These results were of great importance because they suggested that the aeolian components in sediments could provide information on past climatic conditions on the continents and paleoatmospheric circulation patterns (see for example Rea et al., 1985).

However, the atmospheric cycle of particulate matter is rather complicated and any interpretation of the oceanic record requires a thorough understanding of soil dust deflation and long-range transport.

Up to now, the atmospheric studies on mineral particles from arid regions have mainly concerned Saharan dusts transported by the trade winds from the West African coast across the tropical North Atlantic (Prospero and Carlson, 1972; Carlson and Prospero, 1972; Chester et al., 1979). More recently, new investigations have focused on soil-dusts transported from the arid areas of Central Asia to the North Pacific Ocean (Duce et al., 1983; Uetmatsu et al., 1985; Merrill, this issue). The transport of Saharan dusts over the Mediterranean region is poorly documented. Some authors have studied one or two dust events from a meteorological, mineralogical or chemical point of view (Tomadin et al., 1984; Bücher et al., 1983; Prodi et al., 1983; Ganor and Mamade, 1982; Chester et al., 1984; Lefèvre et al., 1986; Löye-Pilot et al., 1986; Dulac, 1987). In fact, since these studies are limited in time, major questions remain about the frequency of Saharan dust events in this region, their source-regions, the transport processes and deposition patterns.

In this paper, we focus on processes which control the temporal variability of the atmospheric inputs of African dusts in the Western Mediterranean region. We try to determine the parameters which are able to explain, at the present time, intra-annual variations in mineral aerosol concentrations and fluxes and we discuss their possible implications for paleometeorological studies.

## 2. SAMPLING AND ANALYSIS

### 2.1. Sampling procedures

Aerosol samples were collected at Capo Cavallo (42°31 N, 8°40 E), Corsica Island (Figure 1), between February 1985 and April 1986. This

site is located 300 m above sea-level and about 700 m distant from the shore line. It is exposed 80% of the time to maritime air-masses from southwest to northeast. Moreover, the closest local pollution sources originating from the city of Calvi are 20 km distant. The aerosol samples were collected at the top of a 10 meters meteorological tower. Bulk filtration samples were obtained on 0.4  $\mu\text{m}$  porosity Nuclepore filters. Sampling duration was 24 hours with a nominal airflow of  $1 \text{ m}^3 \text{ h}^{-1}$ . Blank filters were subjected to all the manipulations made on the filters, except air filtration.

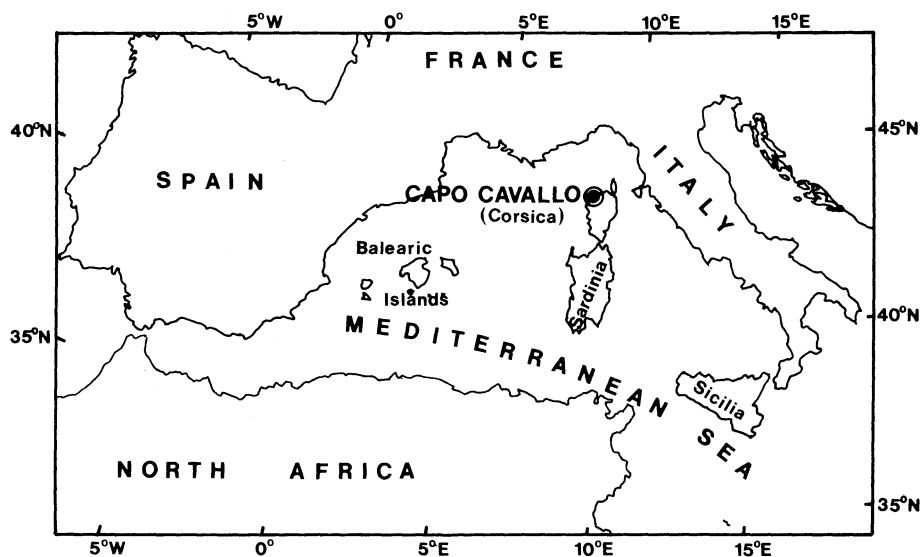


Figure 1. Localization of the sampling station (Capo Cavallo) in the north-western Mediterranean basin.

During the same period, total (wet + dry) atmospheric deposition was sampled in a hemispheric plastic collector ( $0.1 \text{ m}^2$ ). The sampling duration was about 15 days. This collector was connected to a 5-liter plastic bottle for the storage of the sample. Before sampling, the collector was pre-acidified with  $1 \text{ l HNO}_3 \text{ 0.1 N}$  to minimize adsorption effects on the inner sides of the collecting bottle. At the end of sampling, the collector was washed again with  $1 \text{ l HNO}_3 \text{ 0.1 N}$  to recover the deposited particles.

## 2.2 Analytical Methods

For aerosol samples, the concentrations of Al, Si, K, Ca, Ti, Mn, and Fe have been determined by wavelength dispersive X-ray fluorescence spectrometry according to the method described by Elichegaray et al. (1981). Briefly, the sample is placed in an irradiation chamber and the excitation is produced by a X-Ray tube with a Cr (for Al, Si, K, Ca, Ti) or W (for Mn, Fe) target. The intensity of the K-alpha ray of each

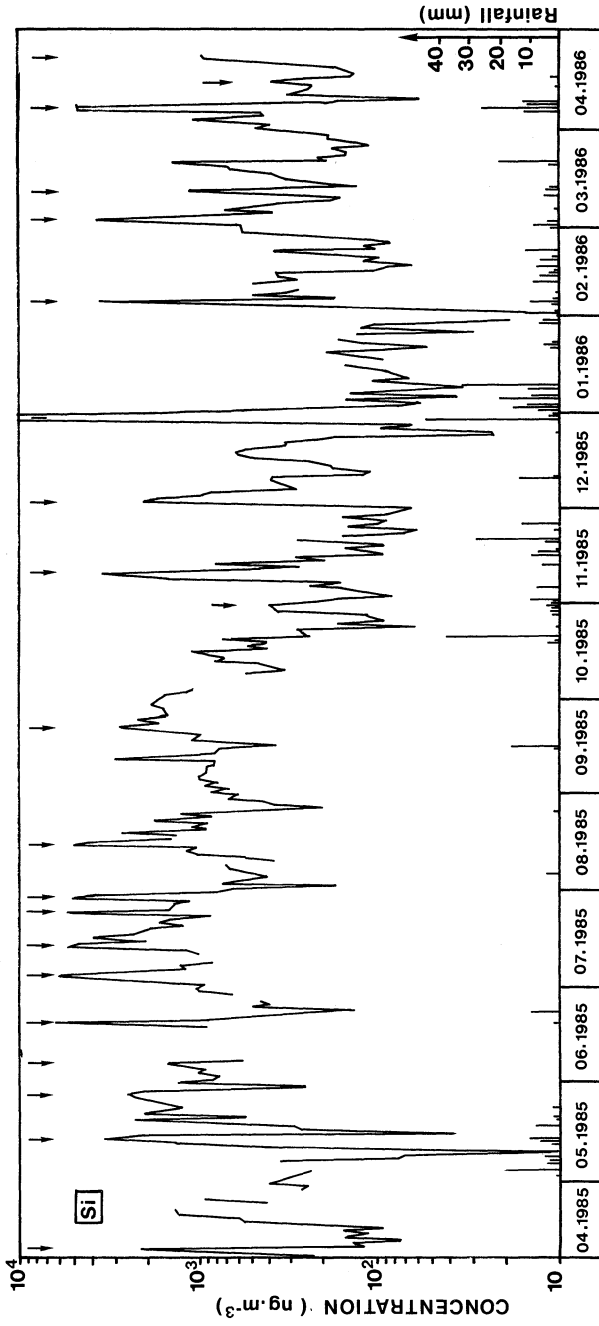


Figure 2. Temporal variations of Silicon concentrations in aerosols samples collected between February 1985 and April 1986 in a coastal site of Corsica Island.

element is counted at least twice for 50 to 70 seconds on a proportional gaseous flux detector. Total counts were corrected for the blank filter contribution. The lack of significant matrix effects was checked by using three standards (Losno et al., 1987). The mean errors on the measurements are generally less than 10 % (Bergametti et al., in press).

Atmospheric deposition samples were filtered on Nuclepore filters (0.4  $\mu\text{m}$  pore size). The particulate fraction was analyzed for Al, Si and Mn by using the same method as for aerosols. The dissolved fraction was analysed by flameless atomic absorption for Al and Mn and by colorimetry for Si. Taking into account the preacidification of samples, the amount of each element in each phase has no geochemical significance and consequently the results will only refer to the total deposition of each element.

### 2.3 Meteorological data and air-mass trajectories

Capo Cavallo is a station of the French meteorological network and all the basic meteorological parameters (wind velocity and direction, amounts of local precipitation) were generally recorded with a three or six hours time step.

Moreover, for each sample, three-dimensional air-mass trajectories backward in time were computed to assess the transport of aerosol particles from their source-regions. The air-mass trajectories were calculated over a period of four days, arriving at the 925, 700 and 500 hPa barometric levels, at the mid-time of each sampling period. The input winds and the vertical velocity are taken from the European Center for Medium Range Weather Forecast of Reading, England (Lorenc et al., 1977) gridded fields every 6 hours for standard pressure levels. The grid space is equal to 1.875 ° on both latitude and longitude. At each 5-mn time step, the new position of the air particle is calculated from linear, spatial and temporal interpolations using a central advance leap frog scheme (see Martin et al., 1987).

## 3. SOIL-DUSTS OVER THE WESTERN MEDITERRANEAN

### 3.1. Frequency of Saharan inputs into the Western Mediterranean

During our sampling period (February 1985 - April 1986) twenty cases of Saharan dust inputs have been observed at Corsica Island (Bergametti, 1987). As shown in Figure 2, these events were easily identified by abrupt increases in concentrations for elements such as Al, Si, Fe or Ti. Moreover, air-mass trajectories have confirmed the African origin of these dusts. The frequency of Saharan inputs over the Western Mediterranean seems to be maximum during spring and summer for the sampling period considered. 80 % of the events are observed between March and October with a greater frequency in July and August. More investigations are needed to confirm our observations and to validate them from a climatological point of view. However, the air-mass flow patterns during the sampling period seem to be quite representative of mean

**Sector 1:****Eastern Algeria, Tunisia, Lybia**

N°	DATE	Si/Al	Fe/Al
1	02/27/85	2.05	0.49
	02/28/85	2.05	0.51
3	04/20/85	2.17	0.61
	04/21/85	2.19	0.52
	04/22/85	2.38	0.54
4	05/12/85	2.35	0.53
	05/13/85	2.51	0.59
	05/14/85	2.23	0.69
5	05/19/85	2.19	0.47
	05/21/85	2.06	0.43
6	05/26/85	2.26	0.58
	05/27/85	2.24	0.50
	05/28/85	2.23	0.49
19	03/01/86	2.04	0.45
	03/02/86	2.13	0.51
20	04/06/86	2.17	0.49
	04/07/86	2.21	0.50

**arith. mean****2.20****0.52****S.D.****0.12****0.06****Sector 2:****Morocco, Western Algeria**

N°	DATE	Si/Al	Fe/Al
2	04/09/85	2.48	0.55
9	07/03/85	2.82	0.73
	07/04/85	2.77	0.68
10	07/16/85	2.49	0.66
	07/17/85	2.56	0.70
11	07/27/85	2.76	0.63
	07/28/85	2.57	0.69
	07/29/85	2.67	0.66
	07/30/85	2.72	0.68
12	08/12/85	2.80	0.77
	08/13/85	2.64	0.64
	08/14/85	2.80	0.74
	08/15/85	2.62	0.62
18	08/16/85	2.70	0.67
	02/04/86	2.65	0.61

**arith. mean****2.67****0.67****S.D.****0.11****0.05****SECTOR 3: South of 30° PARALLEL**

N°	DATE	Si/Al	Fe/Al
8	06/18/85	3.35	1.53
	06/19/85	3.61	1.69
13	09/22/85	2.62	0.69
	09/23/85	2.75	0.76
	09/24/85	2.70	0.66
	09/25/85	2.61	0.80
15	11/09/85	2.85	0.65
	11/10/85	2.91	0.73
16	12/03/85	2.95	0.67
	12/04/85	2.82	0.65
17	12/28/85	2.31	0.45
	12/29/85	2.21	0.51

**Arith. mean****2.92****0.88****S.D.****0.28****0.34**

Table 1. Si/Al and Fe/Al ratios in Saharan dust events collected over the northwestern Mediterranean in relation with the origin of dusts.

annual conditions when compared to air flow climatology statistics over 18 years by Miller et al., (1987).

### 3.2. Source-regions of African dusts for the Western Mediterranean

The classification of these events by using air-mass trajectories as an indicator of geographical origin of dusts allows us to distinguish three different source-regions (Figure 3). These three sectors are defined as :

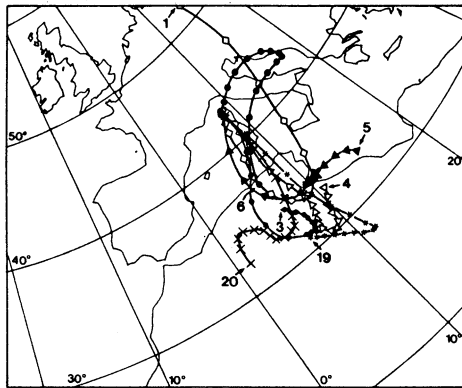
- sector 1: Eastern Algeria, Tunisia, Western Libya;
- sector 2: Morocco, Western Algeria;
- sector 3: South of 30° N.

Eighteen events have been classified in this sectors (Table 1). The events 7 and 14 for which the trajectories are too short to be precisely affected to one sector have been eliminated. Each source-region seems to be characterized by discernably different Si/Al and Fe/Al ratios. Very low Si/Al and Fe/Al ratios (mean value respectively 2.20 and 0.52) are found for events coming from sector 1. By contrast, the events from sector 2 are less rich in aluminium and consequently Si/Al and Fe/Al ratios increase to 2.67 and 0.67 respectively. The differences observed for these two sectors are statistically significant when considering the very low standard deviations found (0.11 and 0.12 for Si/Al ratios in sector 1 and 2 respectively).

These results clearly suggest the existence of various source-regions with different chemical and mineralogical compositions. This observation contrasts with the general finding that, over the oceans, the chemical composition of the mineral aerosol is rather homogeneous (Prospero, 1981). Schütz and Sebert (1987) indicate that this homogenization could be the result of a mixing of various soil-dusts by the effects of continuous uptake and deposition in desertic regions. It seems therefore that the homogenization of the desertic aerosol is strongly dependant on the scale being considered. For example, Paquet et al., (1984) have shown, along a transect between Oran and In Guezzam (Algeria), four different regional sections characterized by various mineralogical associations. The dusts collected in each region had a composition close to that of the associated soils and their composition changed with the pedological environment.

It is therefore likely that the 3 source-regions identified in this study are not homogeneous with respect to the soil types. Taking into account the diversity of soils in each of the identified source-regions, the quite satisfying homogeneity of dusts from sectors 1 and 2 can only result from an important and efficient mixing of dusts from various soils on a regional scale. In contrast, the difference in composition for these two sectors must indicate that the mixing of dusts occurs at a scale smaller than that of the overall African source of Saharan dusts. This can be explained by the prevailing direction of dust storms in each region.

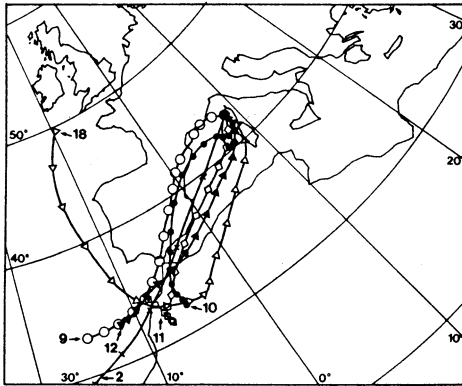
It is very difficult to relate the observed variations of Si/Al and Fe/Al ratios to changes in mineralogy and pedology. Future investigations by electron microscopy and X-Ray diffraction will help to answer this question. However, it is likely that the Si/Al ratios



**SECTOR 1:**

**Si/Al** mean: 2.20  
S.D. : 0.12

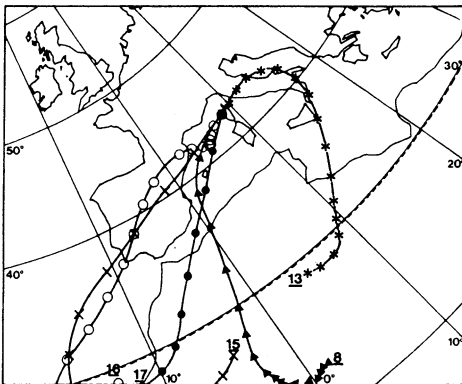
**Fe/Al** mean: 0.52  
S.D. : 0.06



**SECTOR 2:**

**Si/Al** mean: 2.67  
S.D. : 0.11

**Fe/Al** mean: 0.67  
S.D. : 0.05



**SECTOR 3:**

**Si/Al** mean: 2.92  
S.D. : 0.28

**Fe/Al** mean: 0.88  
S.D. : 0.34

Figure 3. Air-mass trajectories associated with dust transport from various African source-regions to the Western Mediterranean Sea. Ending level: 700 hPa; distance between two consecutive points: 6 hours; numbers refer to table 1;

observed for sectors 1 and 2, which are lower than the mean crustal ratio ( $\text{Si}/\text{Al} = 3.4$ ; Mason, 1966) can be interpreted by a high content in clay minerals and/or a low contribution of quartz in the sampled dusts (Rahn, 1976). This could be explained as due to long-range transport allowing sedimentation en route of the coarser quartz particles. Alternatively, this could reflect a North African rather than a pure Saharan origin of these dusts.

Changes in mineralogical composition can also be invoked to explain the differences observed between sectors 1 and 2. The higher  $\text{Si}/\text{Al}$  ratios observed for Moroccan or Western Algerian events (Sector 2) can be related to the presence of a significant amount of smectite (a clay mineral with a low aluminium content) in the soils from these regions (FAO-UNESCO, 1973). This agrees with the observations of Bücher et al., (1983) which found a  $\text{Si}/\text{Al}$  ratio of 2.82, with smectite as the major clay mineral, for a dust event coming from Southern Morocco and Western Algeria. On the other hand, kaolinite (a clay mineral rich in aluminium) is most abundant in the eastern Atlas (FAO-Unesco, 1973) which could explain the lower  $\text{Si}/\text{Al}$  ratio found for dusts from sector 1. We also underline that, although this may be coincidental, there is an agreement between the  $\text{Si}/\text{Al}$  and  $\text{Fe}/\text{Al}$  ratios observed in these dusts and those found for the clay fraction of aeolian loess in Southern Tunisia (2.04 and 0.52 respectively, Goudé-Caussen et al., 1982). It should be pointed out that this interpretation is supported by the results of Prodi and Fea (1979) for a dust event originating from the Jeffara area (near the tuniso-libyan border) and transported to the Italian Peninsula. For this event, kaolinite was found to be the dominant mineral in the clay fraction.

A greater variability of the elemental ratios is observed for the sector 3. This is probably related to the rather crude identification of the source-region as a result of the limited number of recorded dust events. The  $\text{Si}/\text{Al}$  ratios are often high and could indicate a more important contribution of quartz in relation with the large and numerous sandseas in the Saharan and Sahelian regions.

### 3.3. Seasonal pattern of African dust transport

It seems that the three identified transport pathways of the mineral aerosol sampled in Corsica do not occur at the same period of the year. Table 1 indicates that the events originating from sector 1 occur only between the end of February and the end of May. The transports from Moroccan regions or Western Algeria are mainly observed during summer. Finally, southern source-regions seem to be efficient for the Mediterranean Basin during fall and winter. These observations also agree with previous studies: the case studied by Prodi and Fea (1979) (from Tunisia-Libya) occurred in May 1977; the events originating from Morocco studied by Bücher et al., (1983) and Lefèvre et al., (1986) were observed in August.

Therefore, this seasonal trend in transport of African dusts from the various source-regions to the Western Mediterranean is likely related to temporal changes in regional atmospheric circulation.

Although our data set represents only one year of survey and



consequently may not be representative from a climatological point of view, we will try in the following section to define the type of meteorological situation propitious for each type of transport.

### 3.3.1. General climatology of the source-regions

The atmospheric circulation of tropical and equatorial regions is subject to seasonal changes related to the apparent movement of the sun. This circulation is characterized by the presence of the Hadley cells which have their ascending component over the Inter-Tropical Convergence Zone (ITCZ) and their descending component up to the subtropical anticyclonic belt. The whole system moves south to north between the austral summer and the boreal summer, with opposite variations in size and intensity of the southern and northern Hadley cells.

The northward movement of the ITCZ during the boreal summer is important over the Atlantic Ocean but is even more pronounced over Africa. The corresponding subtropical anticyclones (the Azores and Libyan ones) also move to the north but not as much due to a decrease of the size of the Hadley cell. The northern part of these anticyclones comes into contact with colder air masses from polar or temperate regions. This area of contact, which also moves from south to north between summer and winter, is characterized by disturbances resulting in an interpenetration of the two types of air masses. These disturbances generally move from west to east but there are some preferential contact areas between the two air-masses. Thus, the polar air-masses move to the south either over the Eastern Atlantic or over the middle of the European continent. The incursion to the south is obviously more important when the anticyclones are in a southerly position, which is the case in winter.

### 3.3.2. Cyclonic transport from north-western Africa

Radio-soundings and meteorological maps were studied for the eleven events coming from sectors 2 and 3. This kind of transport is characterized by the presence of an anticyclonic wedge over the entire Mediterranean Basin which can extend as far as northern Germany. This wedge of high pressures results from a distortion of the subtropical anticyclone induced by an incursion of a polar air-mass over the Eastern Atlantic. This polar air mass is generally stopped in its incursion to the south by the anticyclonic center. Such a situation generates a south-south-west flow resulting in the transport of dust over the Western Mediterranean.

This type of situation has no seasonal pattern except that the incursion of the polar air mass to the south is controlled by the position of the anticyclone. In summer (Figure 4), the subtropical anticyclone has strongly moved to the North. So, the polar air-mass is stopped early (generally in front of the Iberian Peninsula). Consequently, this situation allows the transport of dusts only from the North-Western part of Africa.

By contrast, in winter, the high pressure moves to the south, associated with the shift of the ITCZ. The polar air mass can penetrate

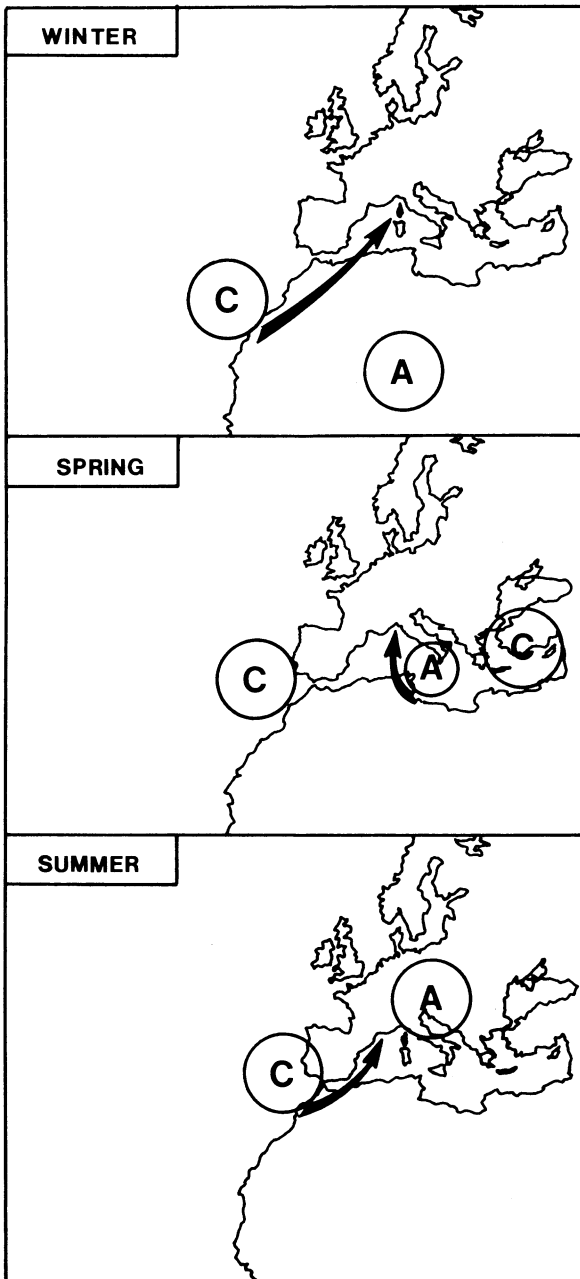


Figure 4. Meteorological situations propitious to dust transport to the Western Mediterranean Sea (A: high pressure; C: low pressure; the arrows indicate the air-flow direction).

more easily to the south, as far as the coast of Mauritania. This situation allows the transport of dusts from more southern source-regions.

### 3.3.3. Transport of dusts from Tunisia and Libya

The meteorological situation associated with these types of transport is not as easy to explain as the previous one. Nevertheless, from the consideration of the meteorological maps, it seems that these transports occur when two polar cold air pools appear, one located over the Eastern Atlantic (as seen in the previous case) and the other one over the European continent, near the Black Sea. Taking into account the intermediate position of the subtropical anticyclone, these cyclones generate an anticyclonic north-south wedge in the Central Mediterranean Sea. This wedge of high pressure gives an anticyclonic flow from the south, resulting in the input of Tunisian and Libyan dusts in the Central Mediterranean Sea (Figure 4).

### 3.4. Transport Processes

The main conclusion of the previous discussion is that these meteorological situations generate: 1° a front (active or not) generally oriented south-west - north-east, and 2° a warm advection from the south.

By using satellite imagery data and three-dimensional air-mass trajectories, we will try to discuss more precisely such transport processes. We have selected two cases corresponding to the Saharan dust inputs observed in Corsica respectively between June 18 and June 20, 1985 and between July 02 and July 04, 1985.

#### 3.4.1 June 18-20, 1985 event

Infra-red satellite imagery (METEOSAT II) shows the formation of a dust storm on June 16, at the north-west of an intense squall-line in Niger. Over Africa, at these latitudes, the squall-lines are usually associated with dust mobilization in their northern part (Dubief, 1979; Kalu, 1979). This squall-line, which comes from east, does not appear on the meteorological maps from the European Center for Medium Range Weather Forecast of Reading. This is due to the limited number of observations over this area. In this case, it is obvious that the conditions for dust mobilization can not be deduced from the large scale meteorological maps and remote-sensing methods are thus more powerful.

This dust cloud is transported in a southerly flow generated by a low pressure center which is off the Moroccan coast on June 17. Due to the presence of the normal high pressure center over North-Africa, this trough moves on the following days to the north-east via Spain and the Gulf of Lions, preserving a predominantly southerly flow over North-Africa and over a large part of the Western Mediterranean Basin. The trajectory of the dust cloud, from June 17 11h30 GMT until June 19 08h30 GMT, has been determined by Infra-Red Meteosat imagery with a

time resolution of 3 hours (Figure 5). After June 19 08h30 GMT, the dust cloud is over the Mediterranean Sea. Unfortunately, its trajectory, using visible wavelength, could not be reconstructed because the dust were completely hidden by clouds.

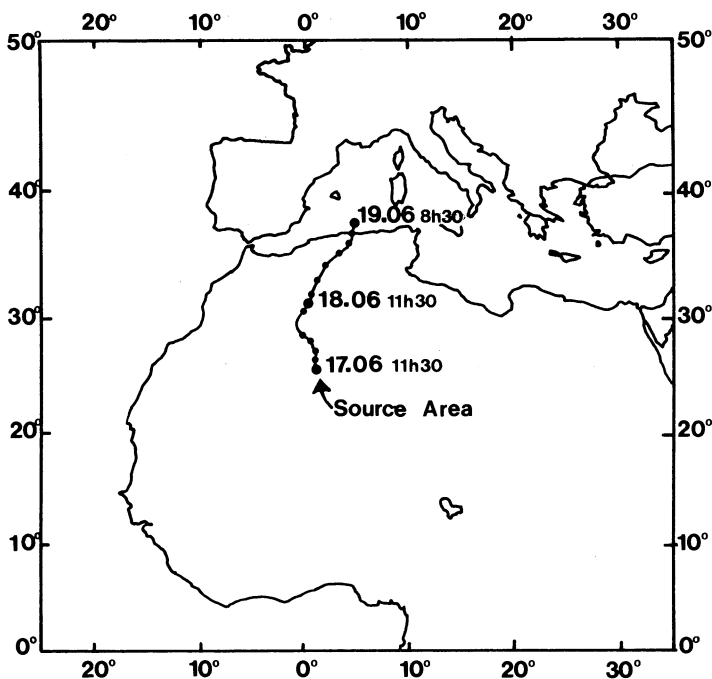


Figure 5. Reconstructed trajectory of the dust cloud using Meteosat II infra-red imagery.

The computed air-mass trajectories arriving at Capo Cavallo (Figure 6) on June 19 12h00 GMT, give very different origins of the air-masses depending on the final barometric level. The lower layers of the local atmosphere are fed with air-masses coming from France. Only the trajectory ending at the 500 hPa barometric level is compatible with the one observed from the satellite imagery. At 00h00 GMT on June 20, some changes occur and the trajectory ending at the 700 hPa level is the only compatible with the trajectory observed by the satellite imagery. The vertical motions of the various trajectories are shown on figures 6 and 7. At the synoptic scale, there is a significant upward movement for the upper trajectories (500 hPa and 700 hPa) and in

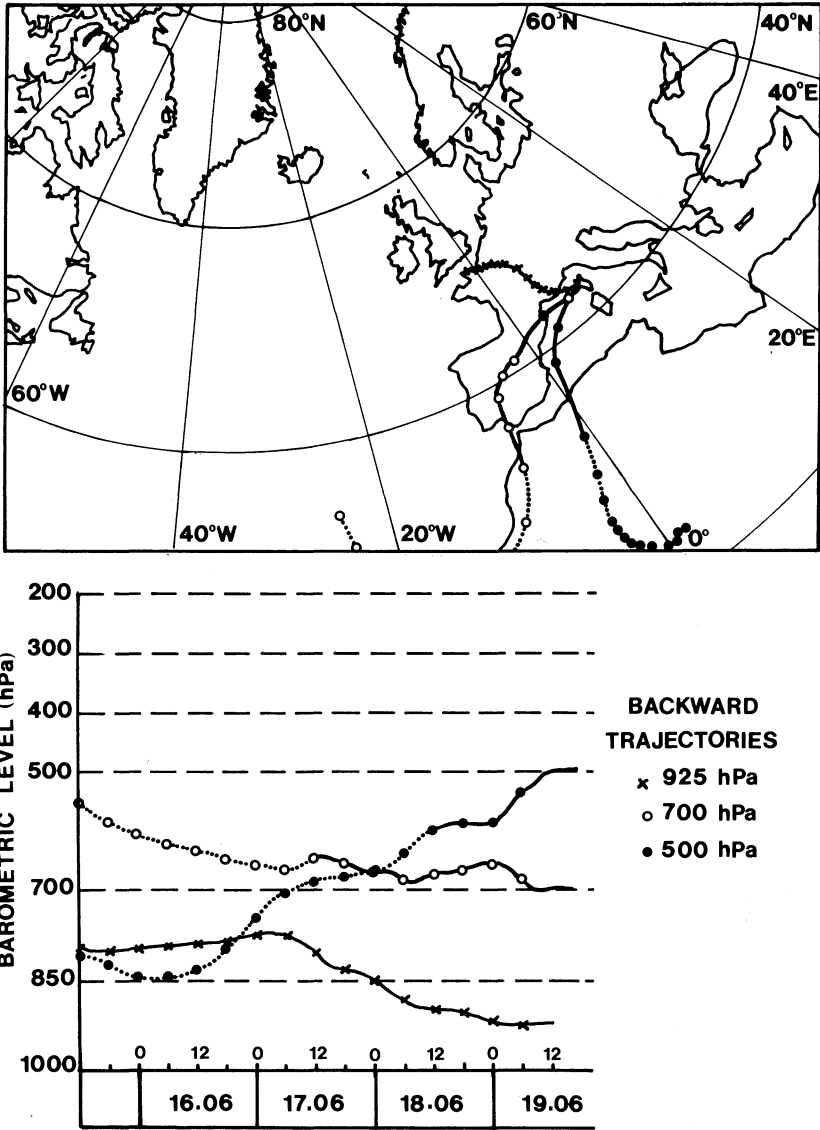


Figure 6. Backward trajectories and vertical movements of the air-masses arriving at Capo Cavallo on June 19, 1985 at 1200 GMT.

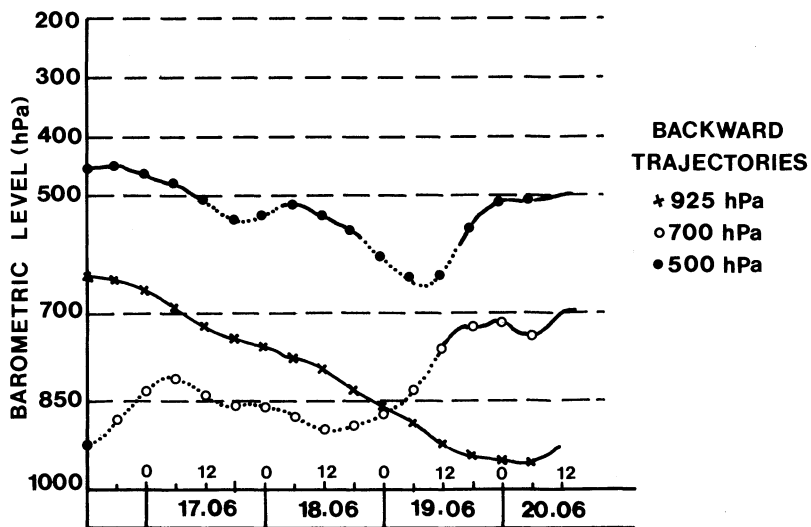
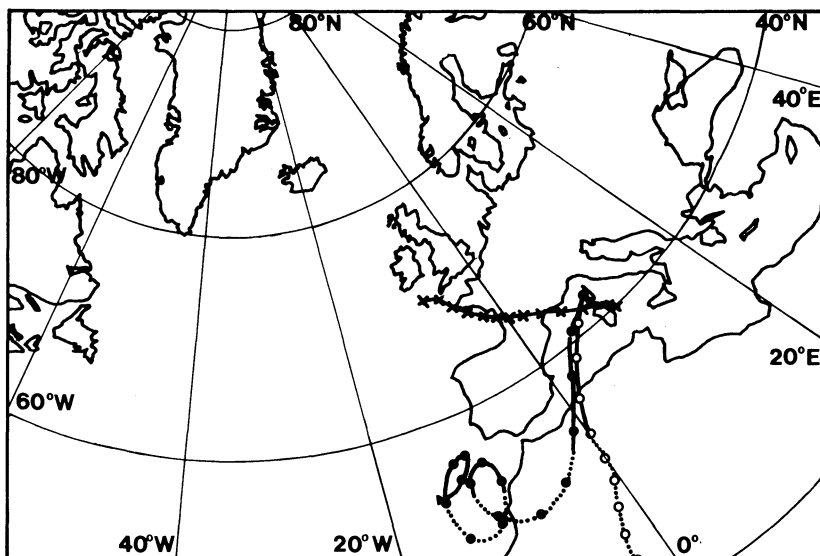


Figure 7. Backward trajectories and vertical movements of the air-masses arriving at Capo Cavallo on June 20, 1985 at 0000 GMT.

contrast, a notable downward movement for the lower trajectories (925 hPa). The upward movement allows the dust to ascend and consequently to be taken in the cyclonic system. The radio-soundings from Ajaccio, Corsica indicate the presence of the dry and warm Saharan layer between 600 and 800 hPa on June 19 at 00h00 GMT. At 12h00, this Saharan air is present in the 800-1000 hPa layers; above this level, the air-mass becomes more humid with the arrival of the trough.

So, these observations strongly suggest that the advection of the Saharan dusts is similar in character to a frontal system. This event is quite similar to that previously described by Prodi and Fea (1979).

#### 3.4.2 July 02-04, 1985 event

As observed in the previous case, the computed air-mass trajectories (Figure 8) arriving at Capo Cavallo on July 3, 4, 5 1985 at 925 and 700 hPa levels differ significantly. Again, the African origin of the air-mass appears more clearly for the highest barometric level. Moreover, the vertical movements of the air indicate the frontal character of the advection of dusts: upward motions occur for the air-masses arriving at the 700 hPa level although downward motions are observed for the final 925 hPa level.

Figure 9 shows the visible satellite imagery data on July 2 and 3. The July 2 data allow us to assess that the dust originated from North-Western Algeria. It can be noted that the transport of dusts occurred ahead of an active cyclonic system which moved from west to east. The dust arrived over Corsica on July 3 in the morning and expanded in a large stretch covering the entire width of the Western Mediterranean Sea.

We computed two forward trajectories starting on July 2 at 06h00 GMT from the eastern and western borders of the source-region as identified by satellite imagery. The initial barometric level was 850 hPa, i.e. close to the altitude of the Atlas mountain in this region. The results (Figure 10) agree satisfactorily with the observations from the satellite. We can also observe an upward movement of the air-mass during transport which indicates a barometric level of about 600 to 700 hPa when these dusts arrived over Corsica, on July 3 between 12h00 and 18h00 GMT.

#### 3.4.3 Conclusion

By studying twenty cases of dust transport from Africa to the Western Mediterranean Sea using both computed trajectories at various final barometric levels, radio-soundings and meteorological maps, we have concluded that the two previous cases are typical of transport processes occurring during such events (Bergametti, 1987). We stress that all these events resulted from frontal transport systems which allowed the dust to ascend. Large updrafts in the vicinity of clouds and frontal systems may also explain why large dust particles (coarser than 10  $\mu\text{m}$ ) are transported far from their source-regions despite their large settling velocities.

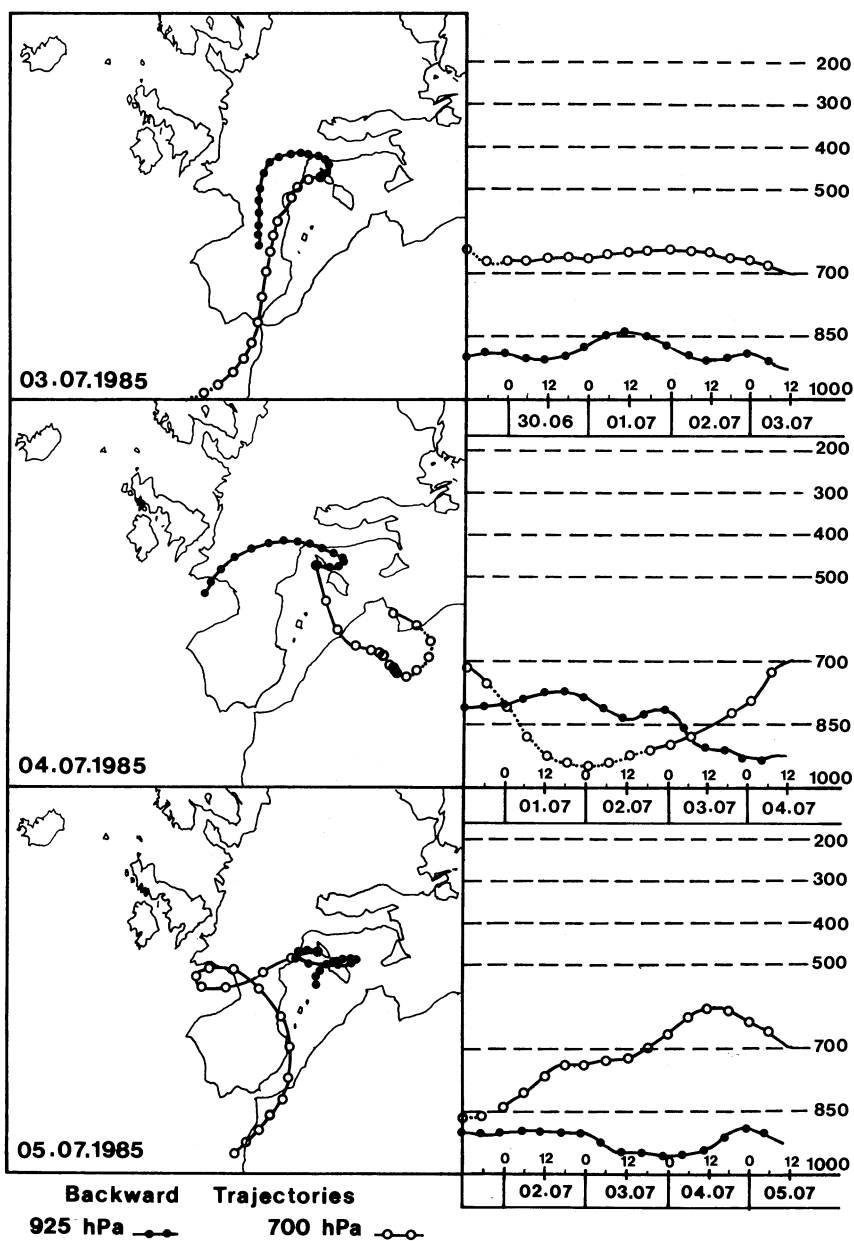


Figure 8. Backward trajectories and vertical movements of the air-masses arriving at Capo Cavallo on July, 2, 3 and 4 1985 at 1200 GMT.



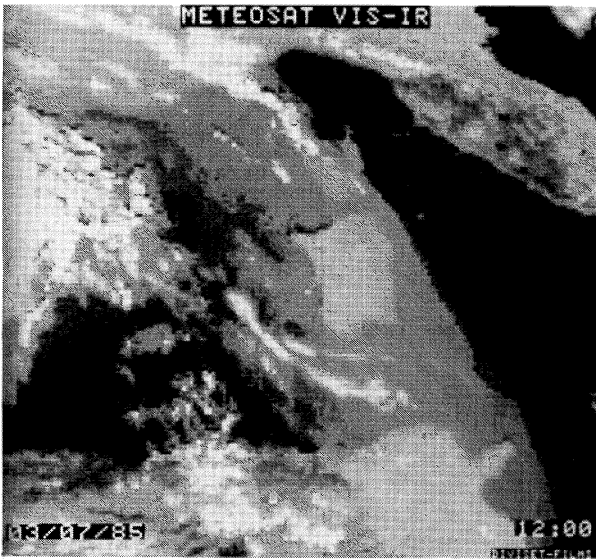
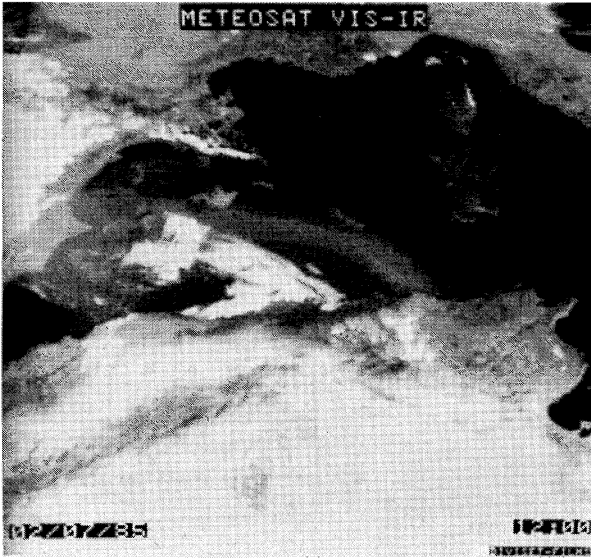


Figure 9. Meteosat II visible images of the African dust event observed over the Western Mediterranean Sea on July 2, 1985(a) and July 3, 1985 (b) at 1200 GMT.

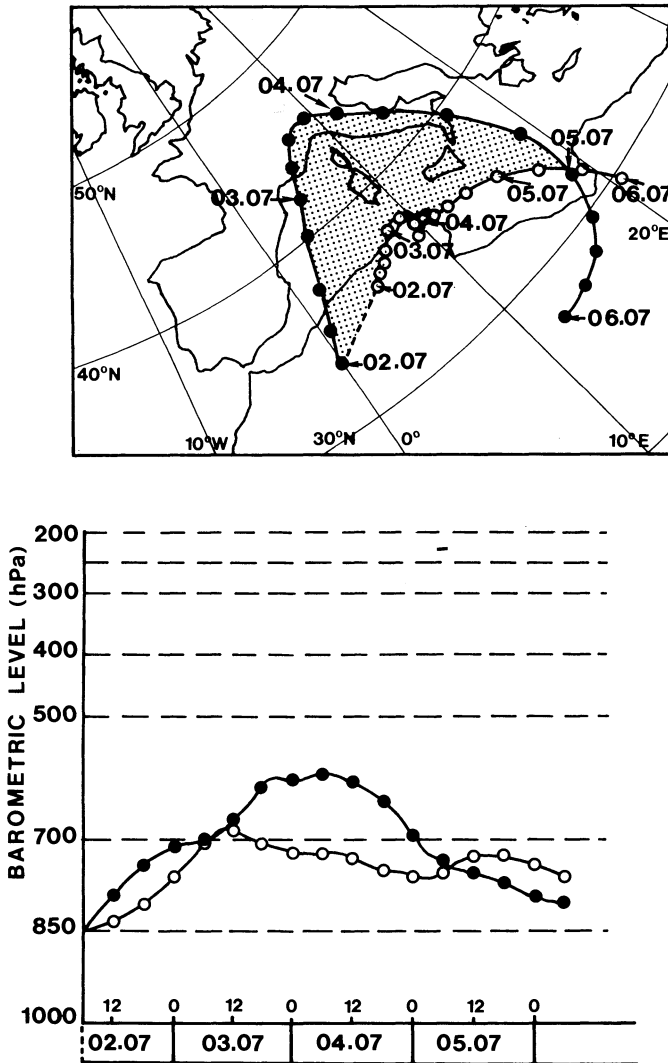


Figure 10. Forward trajectories starting on July 2, 1985 at 0600 GMT from the eastern and western borders of the source-region as observed by satellite imagery. Associated vertical movements are reported below. The initial barometric level is 850 hPa.

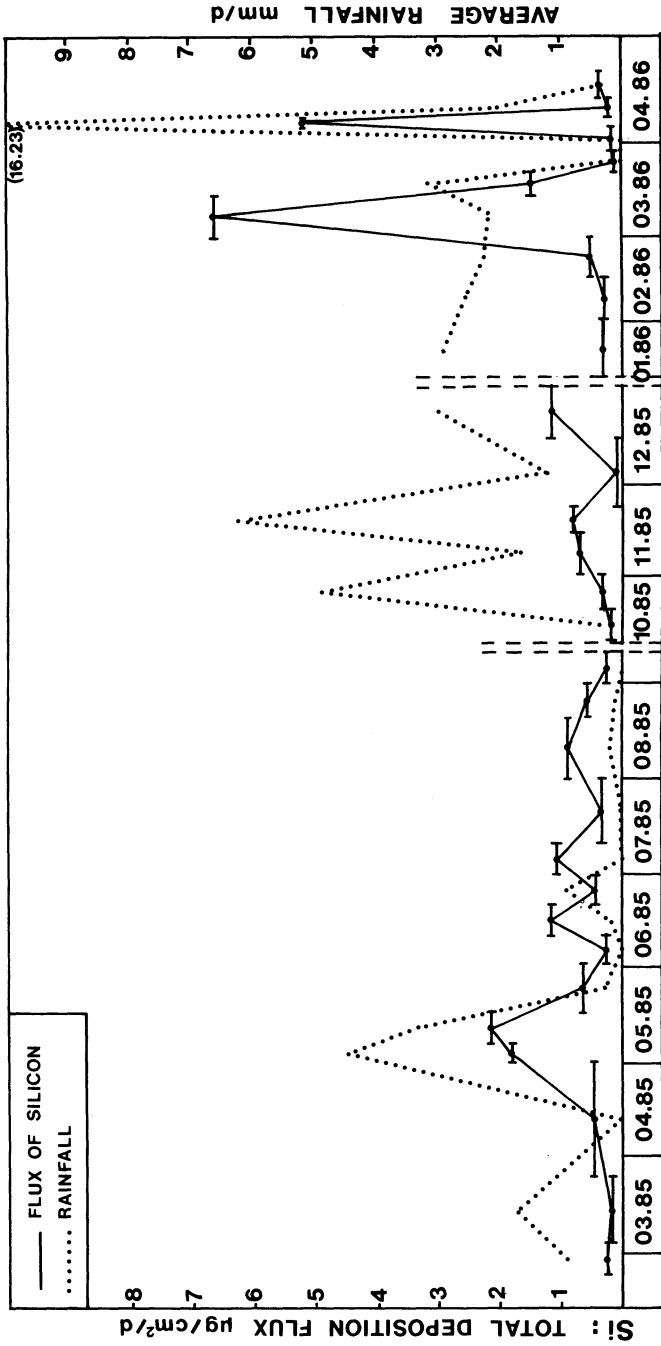


Figure 11. Temporal variations of the atmospheric deposition flux of Silicon and precipitations at Capo Cavallo during the sampling period. The horizontal lines indicate the duration of the sample.

#### 4. DEPOSITION OF AFRICAN DESERTIC DUSTS ONTO THE WESTERN MEDITERRANEAN SEA

##### 4.1 Temporal variability

We have reported in figure 11 the total deposition fluxes of Si as measured from our deposition collector, for the sampling period at Capo Cavallo. The major feature is the great variability of these fluxes from one sample to another. The mean daily fluxes range between 0.09 and  $6.6 \mu\text{g cm}^{-2} \text{d}^{-1}$ . The real variability is even greater since our samples integrated the total deposition over periods of about 10-20 days.

Figure 11 shows also that, during periods with no precipitation, the deposition flux is generally lower. This result agrees with the general observations that wet deposition dominates the total (wet + dry) deposition in various regions and particularly in the mid-latitudes areas (Galloway et al., 1982; Buat-Ménard, 1986).

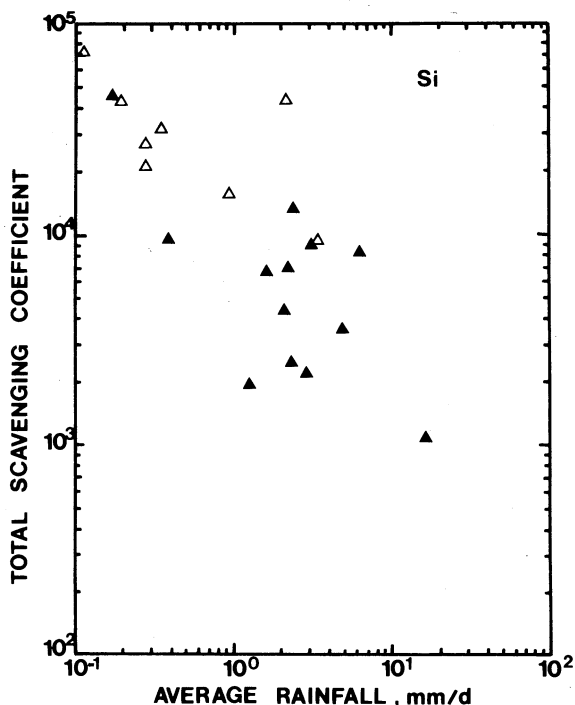


Figure 12. Total Scavenging Coefficients for Silicon versus average rainfall (the black triangles are for the samples collected during fall and winter; the white ones for the samples collected in spring and summer).

Our results indicate also that the temporal variability of atmospheric deposition fluxes measured at Capo Cavallo is related to the occurrence of precipitation. As shown in figure 11, the deposition flux increases with the amount of precipitation. However, the observed variations in the Silicon fluxes are not linearly related with the rainfall amounts. Indeed, total scavenging coefficients (TSC), computed by dividing the measured fluxes by the mean rainfall rate and the mean aerosol concentration for each sampling period, appear highly variable (Figure 12). We observe, especially, a seasonal variability of these TSC's: high TSC values are found in spring and summer and low TSC values are found in fall and winter. Various hypotheses can be offered to explain such a pattern in precipitation scavenging efficiencies. For instance, Jaffrezo, (1987) has shown that the total volume of precipitation can be an important factor in explaining changes in scavenging coefficients since a dilution effect induces lower values of scavenging ratios for precipitations events of strong absolute intensity. However, this effect cannot explain our results since the rainfall amounts are quite similar for the two groups of samples with high and low TSC's. It seems therefore that these differences could rather result from changes in precipitation type. In the Mediterranean region, precipitation occurs mainly as convective storms during the "warm" period, whereas stratiform events are most frequent in winter and fall. Some authors (Scott, 1978; Raynor and Hayes, 1982) have underlined that differences in precipitation patterns certainly affect the precipitation scavenging efficiencies of aerosol particles.

It appears therefore that the amount of dust transferred from the atmosphere to the ocean in a given area is not necessarily directly proportional to the emission rates of dusts in the source-region. Indeed, significant modifications in the source-receptor relationship can be expected mostly due to temporal changes in the deposition rates of aerosol particles. Such changes are mostly controlled by the variability of precipitation scavenging processes.

For the sampling period considered here, it can be underlined that about 30% of the total annual flux of the elements Si and Al resulted from only one single Saharan dust event, which occurred in March 1986. The high input of dust during this period reflects both a dust transport event and a high wet removal efficiency. This indicates that a major fraction of the annual deposition can occur in a small fraction of the days, as observed also by Prospero et al., (JGR, in press) for Saharan dust deposited in Miami (Florida).

#### 4.2 Geochemical significance

Finally, our data set allows to estimate a total atmospheric deposition rate of Al to this part of the Western Mediterranean Sea of  $100 \mu\text{g cm}^{-2} \text{ year}^{-1}$ . About 70% of this rate result from Saharan dust transport (Bergametti, 1987). Assuming that Al represents about 8% of the total mass of the dust (based on Al concentrations in soil), this value represents an African dust annual deposition rate of  $12 \text{ t km}^{-2} \text{ year}^{-1}$ , very close to the estimate of  $14 \text{ t km}^{-2} \text{ year}^{-1}$  by Löye-Pilot et al. (1986). These authors indicate that this value, extrapolated to the

whole Western Mediterranean Basin (277000 km<sup>2</sup>), corresponds to an atmospheric annual flux of 3.9 millions of tons which is of the same order as the average annual downstream flow of solids in the Rhône River (4.3 millions of tons per year). These crude estimates suggest that the atmospheric input of mineral dust is a major source of non-biogenic sediments in this region. This atmospheric mineral flux corresponds to a sedimentation rate of about 10 µm/year.

## 5. CONCLUDING REMARKS

This work was focused on the atmospheric processes which control the transfer of desertic dust from arid and semi-arid regions of Africa to the Western Mediterranean Sea.

Fingerprints of past atmospheric and climatic patterns are certainly recorded in Mediterranean sediments. However, our results indicate that the information contained in these sediments reflect primarily the various factors which affect the atmospheric dust cycle. A major feature is that the temporal variability in time of atmospheric processes such as transport and deposition can generate variable records in sediments for the same amount of dust emitted.

Moreover, considering that one single dust event of a duration of a few days can explain about 30% of the annual mineral dust deposition rate, it is clear that the interpretation of the aeolian signal in Mediterranean sediments does not simply reflect mean atmospheric circulation patterns. Another major problem for interpreting the sediment-record is that the efficiency of the processes involved in dust transfer from the atmosphere to the Mediterranean Sea can be different at a mesoscale level. For example, a small shift in the location of the active trough can induce different dust deposition rates at the same site. This conclusion may not apply however to marine regions where dominant airflows are well established.

Our data suggest that further work on the climatology of intense dust transport events must be performed if we want to improve our understanding of the aeolian signal in deep-sea sediments. A major topic is the need for accurate assessments of the relationship between dust emissions and the occurrence of precipitation events from a climatological point of view. Such studies would allow ultimately the prediction of mineral dust deposition patterns on a spatial and temporal basis.

## 6. ACKNOWLEDGEMENTS

We are grateful to the French National Navy for logistic support and the use of the sampling facilities at Capo Cavallo. We thank B. Chate-net for her technical and editorial support. We also thank G. Senne-quier (E.E.R.M) for his significant contribution for the interpretation of the meteorological maps. The trajectories have been computed by J.M Gros and B. Strauss of the Service des études spéciales of the French Meteorology. We also acknowledge F. Dulac (CFR) for helpful discussions

and comments. This work was supported by the CNRS-PIREN ATP "Aérosols Désertiques" (grant n°982034) and by the French Ministry of the Environment under grant n° 84122.

## 7. REFERENCES

- Bergametti, G., 1987. 'Apports de matière par voie atmosphérique à la Méditerranée Occidentale: aspects géochimiques et météorologiques.' Thèse d'état, Université de Paris VII, 300p.
- Blank, M., M. Leinen, J.M. Prospero, 1985. 'Major asian aeolian inputs indicated by the mineralogy of aerosols and sediments in the Western North Pacific.' Nature, **314**, 84-86.
- Bücher, A., J. Dubief, and C. Lucas, 1983. 'Retombées estivales de poussières sahariennes sur l'Europe.' Rev. Géogr. Phys. Géol. Dynam., **24**, 153-165.
- Carlson, T.N., and J.M. Prospero, 1972. 'The large-scale movement of Saharan air outbreaks over the Northern Equatorial Atlantic.' J. Appl. Meteorol., **11**, 283-297.
- Chester, R., H. Ederfield, J.J. Griffin, L.R. Johnson, and R.C. Pagham, 1972. 'Eolian dust along the eastern margins of the Atlantic Ocean.' Mar. Geol., **13**, 91-105.
- Chester, R., A.G. Griffiths, and J.M. Hirst, 1979. 'The influence of soil sized atmospheric particulates on the elemental chemistry of deep-sea sediments of the northeastern Atlantic.' Mar. Geol., **32**, 141-154.
- Chester, R., E.J. Sharple, G.S. Sanders, and A.C. Saydam, 1984. 'Saharan dust incursion over the Tyrrhenian sea.' Atmos. Environ., **18**, 929-935.
- Coudé-Gaussen, G., C. Mosser, P. Rognon, and J. Tourenq, 1982. 'Une accumulation de loess du Pléistocène supérieur dans le Sud-Tunisien: la coupe de Téchine.' Bull. Soc. Géol. France, **24**, 283-292.
- Dauphin, J.P., 1983. 'Eolian quartz granulometry as a paleowind indicator in the Northeast Equatorial Atlantic, North Pacific and Southeast equatorial Pacific.' Ph. D Thesis, University of Rhode Island, Kingston, Rhode Island (USA).
- Dubief, J., 1979. 'Review of the North African Climate with Particular Emphasis on the Production of Eolian Dust in the Sahel Zone and in the Sahara.' in "Saharan Dust", C. Morales, ed. J. Wiley and Sons, pp 27-48.
- Duce, R.A., R. Arimoto, B.J. Ray, C.K. Unni, and P.J. Harder, 1983. 'Atmospheric trace elements at Enewetak Atoll: 1. Concentrations, sources and temporal variability.' J. Geophys. Res., **88**, 5321-5342.
- Elichegaray, C., A.L. Dutot, B. Grubis, and R. Vié le Sage, 1981. 'Dosage par fluorescence X des aérosols atmosphériques: détermination des facteurs de correction.' Analisis, **9**, 492-497.
- Galloway, J.N., J.D. Thornton, S.A. Norton, H.L. Volchok, and R.A. Mac Lean, 1982. 'Trace metals in atmospheric deposition: a review and assessment.' Atmos. Environ., **16**, 1677-1700.

- Ganor, E., and V. Mamane, 1982. 'Transport of saharan dust across the eastern Mediterranean.' Atmos. Environ., **10**, 1079-1084.
- Griffin, J.J., and E.D. Goldberg, 1968. 'Clay mineral distribution in the world ocean.' Deep-Sea Res., **15**, 333-359.
- Jaffrezo, J.L., 1987. 'Etude du lessivage des aérosols atmosphériques par les précipitations.' Ph D Thesis, Université Paris VII, 183 pp.
- Kalu, A.E., 1979. 'The African dust plume: its characteristics and propagation across West Africa in winter.' in Saharan Dust, C. Morales ed., J. Wiley and Sons, pp 95-118.
- Lefèvre, R., A. Gaudichet, and P. De Félice, 1986. 'Caractérisation chimico-minéralogique des flux microparticulaires dans la basse atmosphère de la Méditerranée moyenne. Permanence et fluctuation des apports atmosphériques à la sédimentation.' C. R. Acad. Sc. Paris, **303**, 1215-1220.
- Lorenc, A., I. Rutherford, and G. Larsen, 1977. 'The E.C.M.W.F analysis and data assimilation scale analysis of mass and wind fields.' ECMWF Technical Report, N°6, Reading, England.
- Losno, R., G. Bergametti, and G. Mouvier, 1987. 'Determination of optima conditions for atmospheric aerosols analyses by X-Ray Fluorescence.' Environ. Tech. Lett., **8**, 77-87.
- Löye-Pilot, M.D., J.M. Martin, and J. Morelli, 1986. 'Influence of saharan dust on the rain acidity and atmospheric input to the Mediterranean.' Nature, **321**, 427-428.
- Martin, D., C. Mithieux, and B. Strauss, 1987. 'On the use of the synoptic vertical wind component in a transport trajectory model.' Atmos. Environ., **21**, 45-52.
- Mason, B., 1966. 'Principles of geochemistry.' 3rd edition, J. Wiley and Sons ed. New-York.
- Miller, J.M., D. Martin, and B. Strauss, 1987. 'A comparison of results from two trajectory models used to produce flow climatologies to the Western Mediterranean.' NOAA Technical Memorandum, ERL ARL-151, NOAA, Air Resources Laboratory, Silver Spring, Maryland (USA).
- Paquet, H., G. Coudé-Gaussen, and P. Rognon, 1984. 'Etude minéralogique de poussières sahariennes le long d'un itinéraire entre 19° et 35° de latitude nord.' Rev. Geol. Dyn. Geogr. Phys., **25**, 257-265.
- Prodi, F., and G. Fea, 1979. 'A case of transport and deposition of saharan dust over the italian peninsula and southern Europe.' J. Geophys. Res., **84**, 6951-6960.
- Prodi, F., G. Santachiara, and F. Oliosì, 1983. 'Characterization of aerosols in marine environments (Mediterranean, Red Sea, and Indian Ocean).' J. Geophys. Res., **88**, 10957-10968.
- Prospero, J.M., and T.N. Carlson, 1972. 'Vertical and areal distribution of Saharan dust over the western equatorial North Atlantic ocean.' J. Geophys. Res., **77**, 5255-5265.
- Prospero, J.M., 1981. 'Eolian transport to the world ocean.' in The oceanic lithosphere, **7**, The Sea, C. Emiliani ed., John Wiley and Sons, New-York.



- Rahn, K.A., 1976. 'Silicon and aluminium in atmospheric aerosols: crust-air fractionation ?' Atmos. Environ., **10**, 597-601, 1976.
- Rea, D.K., M. Leinen, and T. Janecek, 1985. 'A geological approach to the long term history of atmospheric circulation.' Science, **227**, 721-725.
- Raynor, G.S., and J.V. Hayes, 1982. 'Concentrations of some ionic species in Central Long Island (New-York) precipitations in relation to meteorological variables.' Wat. Air Soil Pollut., **17**, 309-335.
- Reiff, J, G.S. Forbes, F.T.M. Spieksma, and J.J. Reynders, 1986. 'African dust reaching northwestern Europe: A case of study to verify trajectory calculations.' J. Climatol. Appl. Meteorol., **25**, 1543-1567.
- Rex, R.W., and E.D. Goldberg, 1958. 'Quartz contents in pelagic sediments of the Pacific Ocean.' Tellus, **10**, 153-159.
- Sarnthein, M., J. Thiede, U. Pflaumann, H. Erkenkeuser, D. Fütterer, B. Koopmann, H. Lange, and E. Seibold, 1982. 'Atmospheric and oceanic patterns off Northwest Africa during the past 25 million years.' in Geology of the Northwest African Continental Margin, edited by U. Von Rad, K. Linz, M. Sarnthein, and E. Seibold, pp. 545-604.
- Schütz, L., and M. Seibert, 1987. 'Mineral aerosol and source identification.' J. Aerosol Sci., **18**, 1-10.
- Scott, B.C., 1978. 'Parametrization of sulfate removal by precipitation.' J. Appl. Meteorol., **17**, 1375-1389.
- Tomadin, L., R. Lenaz, V. Landuzzi, A. Mazucotelli, and R. Vannucci, 1984. 'Wind-blown dusts over the Central Mediterranean.' Oceanologica Acta, **7**, 13-23.
- Uematsu, M., R.A. Duce, and J.M. Prospero, 1985. 'Deposition of atmospheric mineral particles in the north Pacific Ocean.' J. of Atmos. Chem., **3**, 123-128.

## DESERT DUST AND CLIMATE : AN INVESTIGATION USING AN ATMOSPHERIC GENERAL CIRCULATION MODEL

S. Joussaume  
Laboratoire de Météorologie Dynamique  
24 rue Lhomond  
75231 Paris Cedex 5  
FRANCE

**ABSTRACT.** A modeling of the atmospheric cycle of desert dust particles has been introduced within an atmospheric general circulation model to investigate the modifications of this cycle induced by climatic changes. For this purpose, simulations of the present-day and Last Glacial Maximum (LGM) climates have been performed. The results show little changes of the simulated atmospheric dust contents on a global scale but more important changes over some regions. However, the observed large increases over ice-caps for the LGM are not well reproduced.

### 1. Introduction

Records of dust deposits in sea-sediments and ice-sheets exhibit large fluctuations with climate. In East Antarctica (Vostok and Dôme C stations), large increases in the dust amounts are related to cold periods, in particular during the Last Glacial Maximum (18000 years BP) with increases by a factor of 10 to 20 (Petit *et al.*, 1981; De Angelis *et al.*, 1987). Even larger increases have been observed at Camp Century (Greenland) (Thompson, 1977). These changes are larger than the changes of accumulation and therefore reflect changes in the atmospheric aerosol content, at least over high latitudes. These dust deposits, of continental origin, can be related to climate changes through modifications of the source regions and/or changes in the atmospheric circulation.

In order to investigate the link between climate and the transport of desert dust particles, a modeling of the atmospheric desert dust cycle has been introduced in an atmospheric general circulation model and numerical simulations of the present-day and LGM climates have been performed. We present here only the main features of our modeling and of the simulated results. Results from preliminary experiments were described in Joussaume *et al.* (1984, 1985), and a more detailed description of the desert dust modeling and of the present-day simulations will be found in Joussaume (to be submitted).

## 2. Modeling

The atmospheric general circulation model of the Laboratoire de Météorologie Dynamique (Sadourny and Laval, 1984) is a grid point model, whose standard version uses 64 points regularly spaced in longitude, 50 points regularly spaced in sine of latitude (the mesh size is therefore  $400 \times 400 \text{ km}^2$  in mid-latitudes) and 11 levels in the vertical. A modeling of the desert dust cycle has been developed, including parameterizations of the source, diffusion and removal processes, and transport by the simulated winds. The parametrizations of the source and removal processes, which depend on the nature and size of particles, have been defined for dust particles raised by winds over desert areas and corresponding to a size range of  $1 \mu\text{m}$ . In this first approach, particles have been considered as passive scalars without taking into account either their interaction with radiation or with cloud physics (as condensation nuclei). The size range of  $1 \mu\text{m}$  has been chosen as it fairly corresponds to the size range of particles of continental origin experiencing long-range transport and found in dust deposits over Antarctica (Petit *et al.*, 1981).

### 2.1 DUST SOURCE

Particles are raised by winds over source regions. The source flux formulation used is similar to the one commonly used for water vapor in general circulation models, and is proportional to the surface wind speed and the vertical gradient of dust concentrations ; the proportionality coefficient being unknown, all the simulated dust amounts are defined up to an arbitrary constant. Our formulation, however, tends to be oversimplified as neither a threshold velocity for dust mobilisation nor a non-linear dependency with wind speed ( $u^3$  or  $u^4$ ) have been used (Gillette, this volume). The source regions are generated by the model itself and they correspond to the regions that are dry both in winter and summer; this approach has been used, rather than prescribing the source regions, as we deal with paleoclimatic simulations for which source regions are not well known. The corresponding extent of source regions for the present-day climate is displayed in figure 1. The distribution of the major desert areas are fairly well reproduced: the Saharan, Kalahari, Arabian, Asian deserts (Thar, Takla-Makan, Gobi and Turkmenia steppes), the north and south american sources, but the Australian desert is underestimated. Our definition of source regions is, however, simplistic as it does not take into account the nature of soils, and therefore probably leads to an overestimation of the source regions, considering all the desert areas as sources of fine dust.

Dust is raised from the surface layers to the upper layers of the troposphere, through the turbulent diffusion processes within the planetary boundary layer and the diffusion within the simulated convective motions.

### 2.2 DUST REMOVAL

Dust is removed from the atmosphere both by wet and dry removal processes. Wet removal occurs during precipitation events, as particles should act as condensation nuclei. Dry removal occurs by gravitational settling (weak for particles in this size range) and by deposition at the surface through interception by obstacles. Both

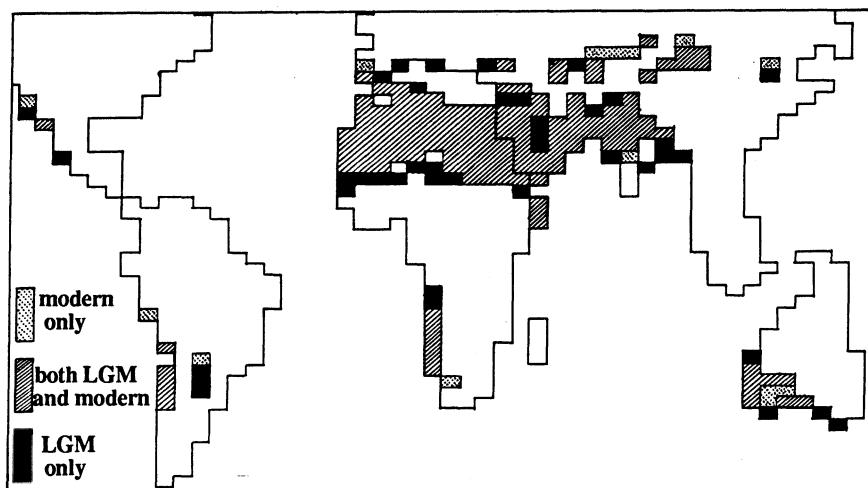


Figure 1. Simulated extent of the desert source regions for present-day and the Last Glacial Maximum (LGM) climates, defined as the dry regions in February and August. Dotted (black) areas for the source regions of the only present-day (LGM) climate, hatched areas for source regions of both climates.

Table 1. Simulated LGM / present-day changes (%) for the global averaged desert dust budgets of source areas, source intensity and atmospheric dust content.

	Source areas	Source intensity	Atmospheric dust content
Estimated annual mean	+ 18%	+ 14%	+ 8%
February	+ 18%	+ 25%	+ 23%
August	+ 18%	+ 7%	+ 1%

processes have been parameterized in a simple way: wet removal is assumed proportional to the precipitation amount and the dust concentration, and dry removal proportional to the surface wind speed and the surface dust concentration. These formulations lead to larger dry removal than wet removal on a global scale (factor 3 to 4), dry removal prevailing near source regions and wet removal prevailing in regions of intense precipitations and at high latitudes. However, our formulation tends to underestimate the wet removal efficiency compared to estimated values based upon observations (e.g., Uematsu *et al.*, 1985). The simulated dry deposition velocities range between .5 to 1. cm/s over oceans and from 1. to 5. cm/s over land. These values are largely overestimated for particles of 1  $\mu\text{m}$  but fairly realistic for a mean size distribution of particles between .5 to 5  $\mu\text{m}$  (Giorgi, 1986); our formulation seems therefore reasonable for desert dust particles near source regions but tends to overestimate the fluxes far from source regions.

### 3. Simulations of the present-day climate

Simulations of 100 days have been performed for February and August present-day climates (Joussaume and Sadourny, 1988). Starting from no dust in the atmosphere, 10 to 20 days are required to reach simulated values of the order of the global mean simulated atmospheric dust content, and, therefore, the simulated results are analysed over the last 60 days of the simulations.

The dust plume patterns, averaged for February and August (estimate of the annual mean), are displayed in figure 2. The overall patterns of the dust plumes are dominated by low-level winds. In the tropics, dust is transported by trade-winds towards the equator, while, in mid-latitudes, transport is controlled by westerlies. A strong transport towards the Pacific Ocean also takes place for Saharan and Arabian dust through the monsoon wind regime in August. A strong seasonal dependency of the dust plumes is simulated by the model, with globally twice more dust in August than in February. This seasonal contrast results from more dust aloft in the mid-troposphere in August, due to a larger vertical mixing over the warm regions of Sahara and Arabia-Asia during that month, the change in the vertical structure leading to a relative decrease of dry removal which depends on the near-surface concentrations (dry removal being more efficient than wet removal).

If the overall patterns of the simulated dust plumes are reasonable, the comparison with observations, although somewhat limited due to the lack of a global climatology of dust plumes, exhibits some discrepancies. Concerning the Saharan dust plume over the Atlantic ocean, the model simulates a too strong seasonal dependency with insufficient dust amounts in February compared to August, in particular the simulated transport towards the Gulf of Guinea is weak (e.g., Prospero, 1981). In August, an important transport of Saharan dust is simulated over the tropical Atlantic Ocean, however, this transport is more continuous than observed and insufficiently confined in the mid-troposphere (e.g., Prospero *et al.*, 1979). In August, the transport towards the east by the monsoon winds is overestimated and extends too far east. Major deficiencies of the simulated dust cycle result either from deficiencies of the simulated atmospheric circulation, like the overestimation of the monsoon wind intensity and of their eastward extent and the underestimation of the mid-tropospheric August easterly winds

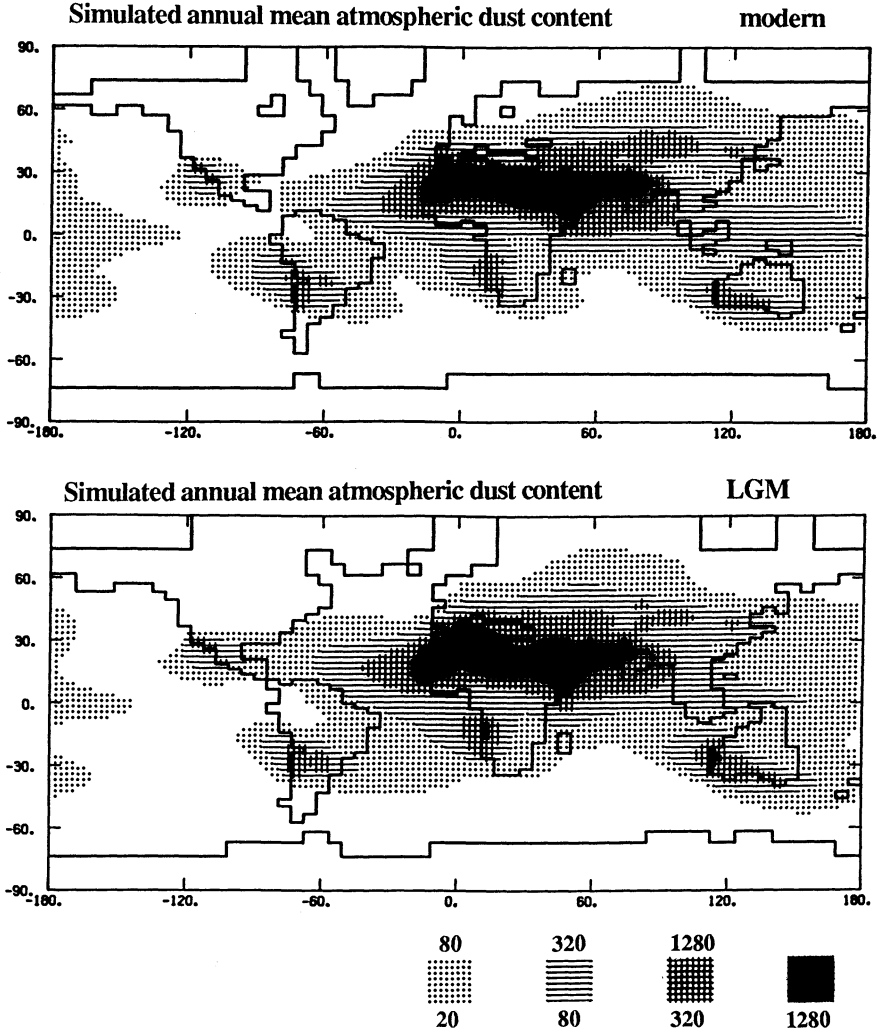


Figure 2 . Simulated annual mean (averaged for February and August) atmospheric dust content (vertically integrated mass of dust ) for: a) the present-day climate and b) the LGM climate. Units in  $\text{kgm}^{-2}$  (defined with an arbitrary constant). Shaded areas in a geometrical progression of ratio 4 : 20-80-320-1280.

over the Atlantic, or from deficiencies in the modeling of the dust cycle, the major critical point being the definition of the source extent and the parameterization of the dust mobilisation flux.

#### **4. Simulations of the Last Glacial Maximum climate**

A simulated atmospheric circulation of the LGM is obtained as the model response to the boundary conditions characteristic of the LGM climate: sea-surface temperature, sea-ice extent, ice-sheets and surface albedo (vegetation and soil types) given by CLIMAP (1981) for February and August and a lower atmospheric CO<sub>2</sub> content (190ppm rather than 330 ppm). Using these boundary conditions, simulations of 200 days have been performed using the LGM solar radiation forcing for February and August, which is very similar to the present-day one. The atmospheric cycle of desert dust particles has been introduced over the last 100 days only and the source regions defined from the first 100 days. As for present-day simulations, the analyses concern the last 60 days of the simulations. This time period is nevertheless relatively short for the simulation of a mean climate which would be unbiased by slow evolving transient circulation patterns.

##### **4.1 GLOBAL AVERAGES**

On a global average, the atmospheric dust amount only increases by 8% for the estimated LGM annual mean (from February and August). This small change is likely to originate in the small increase of the simulated source areas (18%) and source intensity (14%) (table 1). The changes are stronger in February than in August (table 1), which is the season with larger dust concentrations aloft; the seasonal contrast of the dust cycle thus tends to be weakened during the LGM.

##### **4.2 SIMULATED SOURCE REGIONS**

The source area distribution is displayed in figure 1, clearly exhibiting the small changes during the LGM. Compared to paleoclimatic reconstructions of land aridity for the LGM (Sarnthein, 1978), the simulated increase of the Saharan source towards the south-west is realistic, although smaller than observed; the simulated increase of the source extent in South America and in south-east Australia is also reasonable, but the changes in south Africa and north Australia are largely underestimated. The change of the source extent is, however, highly dependent on our definition of the source regions, in particular we consider here all the desert areas as sources of fine dust.

##### **4.3 SIMULATED DUST PLUMES**

The simulated dust plumes averaged for February and August are displayed in figure 2. If on a global scale the changes in the atmospheric dust content are small, regional features can show large changes (figure 3.a). As an example, an important increase takes place over the western north Atlantic ocean resulting, in part, from the LGM source in Central America and, mainly, from a southward shift of the westerlies over

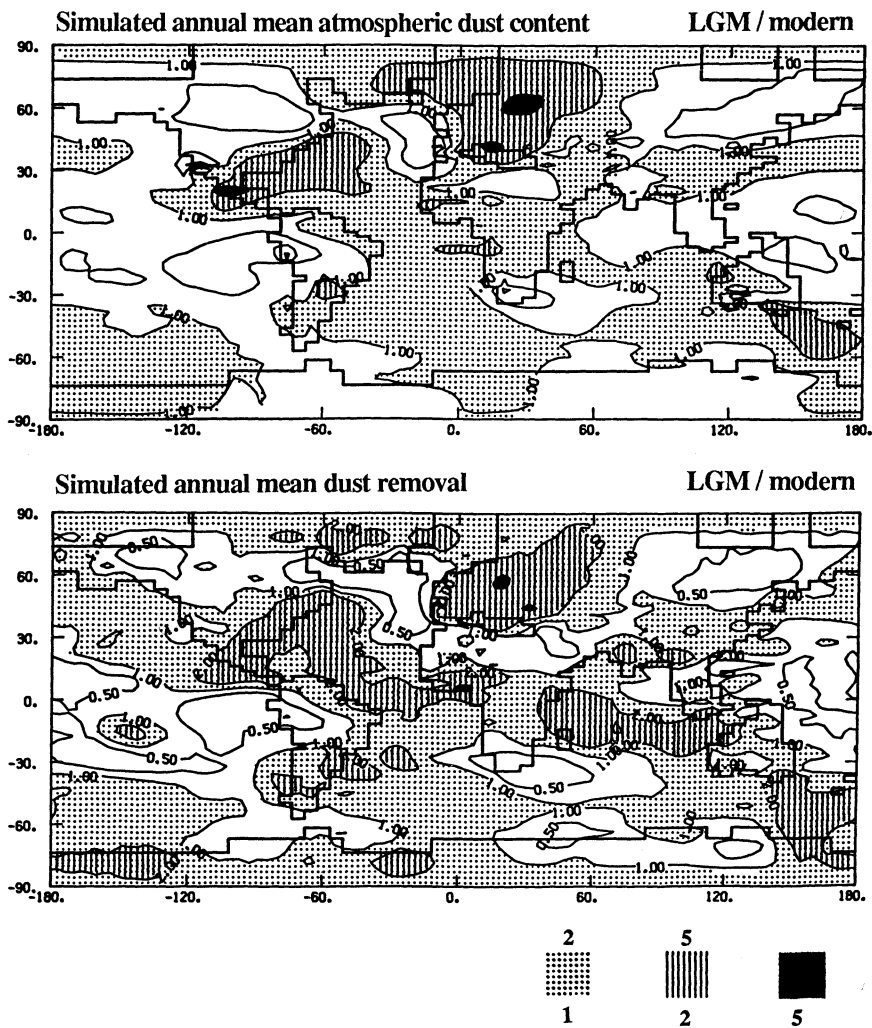


Figure 3 . Simulated LGM / present-day ratios of a) the atmospheric dust content and b) the total dust removal, averaged for February and August. Isolines 1/2, 1, 2 and 5 (shaded areas above 1.)



the Atlantic linked to the southward displacement of the sea-ice margin. Over Europe, the dust amount also greatly increases, both in February and August, due to new sources in southern Europe and changes in the atmospheric circulation. Over south-east Australia, the transport also increases. The weaker LGM Indian monsoon induces lower dust amounts in this region. Other differences are due to the removing of some source regions, as over the eastern Pacific and the south of Africa. The decrease over the northeastern Atlantic ocean give evidence of our short simulations, as it is associated with a northward extent of the subtropical high pressures, a circulation pattern that sometimes occurs in February.

#### 4.4 SIMULATED DUST REMOVAL - COMPARISON WITH OBSERVATIONS

The changes of the dust removal (wet and dry processes) (figure 3.b), on an annual mean, must be used for the comparison between simulated and observed results. The changes of the dust removal are, on the one hand, related to changes in the atmospheric dust content (comparison with figure 3.a) and, on the other hand, related to specific changes of the removal rates: modifications of the precipitation rates (wet removal) and of the surface wind strength (dry removal) between the LGM and present-day climates. Contributions of the removal changes are illustrated, for example, over the Indian ocean and the equatorial eastern Atlantic.

The model simulates an increase of the dust removal by a factor of 2 over eastern Antarctica, between 150°E and 120°W (e.g., Byrd station), and a decrease by at least a factor of 2 between 30°E and 150°E (e.g., Vostok and Dôme C stations). However, these changes are essentially determined by changes in the accumulation rates; indeed, the ratio of the dust removal to the precipitation rate (directly comparable to ice-core data) corresponds to very small changes for the LGM, with values from .8 for Vostok to 1.4 for Byrd. These simulated values are far below the observed changes of 10 to 20 for Vostok and Dôme C, and 4 for Byrd. In Greenland, the ratio of the dust removal to the precipitation rate increases by a factor of 4; however, this increase is smaller than the observed one, with values of the order of 100 at Camp Century. *Therefore, the model does not simulate the observed enhancement of the dust amounts in high latitudes for the LGM.* This shortcoming can be due in part to deficiencies in the atmospheric circulation but, most probably, is related to deficiencies in the simulation of the source regions. This last assumption is corroborated by the fact that, in our simulations, Australia is the major source of dust for East Antarctica, conversely to observations which show very few kaolonite clay type particles, very commonly found in Australian soils (Gaudichet *et al.*, 1986). For Greenland, the simulated dust deposits originate from Sahara and Arabia-Asia, and the LGM increase is due to the development of a cyclonic circulation over Europe with easterlies at high latitudes; other source regions are also certainly required to explain the observed enhancement of dust deposits for the LGM.

In the equatorial eastern Pacific, the quartz content of sea sediments decreases for the LGM (Janecek and Rea, 1984), corroborating the simulated features in this region which result from a higher humidity in the north Atacama desert. In the northwest Pacific, the simulated dust removal and atmospheric dust content increase slightly, due to increased westerlies, whereas observations show similar accumulation rates for both climates (Leinen, this volume); however, longer simulations would be required to

confirm this small discrepancy. Over the Atlantic ocean, the model simulates an increase in the Saharan dust deposits, in agreement with increased accumulation rates in sea sediments (Koopmann, 1981). This simulated increase is due to the enhancement of both the Saharan source intensity and the northeasterly low-level circulation over the Atlantic, both features corroborated by observed results (Sarnthein *et al.*, 1981) ; however, increases in the observed Saharan dust deposits is only controlled by increases in the source strength, as the mid-tropospheric winds, mainly responsible for the Saharan dust transport over the Atlantic (Tetzlaff, this volume), are weakened (Sarnthein *et al.*, 1981), a feature which cannot be seen from the simulated dust plumes as this transport is largely underestimated in the model.

## 5. Conclusion

Although the simulated results for the present-day climate are qualitatively reasonable, some discrepancies with observations appear due to model shortcomings either of the simulated atmospheric circulation, or of the dust cycle. Indeed, our dust modeling must be considered as a first step and still requires improvements, one of the main critical point being the definition of the source regions. Another limiting factor, intrinsically related to the large mesh sizes of AGCMs, remains the non-resolving of meso-scale events, a shortcoming which might be critically important for dust storm formation.

For the LGM climate, the model simulates only small changes of the desert dust cycle on a global scale. However, more important changes are simulated on regional scales, either due to changes in the source extents or to changes in the atmospheric circulation. One of the major change occurs over Europe with an increase of the dust amounts of the order of 2 to 5. Over ice-caps, the model simulates an increase of 4 over Greenland, but little changes over Antarctica (relatively to the same amount of precipitations). These changes at high latitudes are largely underestimated, a shortcoming which seems to be essentially due to deficiencies in the simulated source extents of the LGM but might also come from model deficiencies.

For further investigations, sensitivity experiments are required. For the present-day climate, they should focus on the dust modeling, for example the parameterization of the dust mobilisation and source extent. For the LGM climate, different hypotheses of source changes for the LGM should be tested, in order to better understand the changes of the dust cycle at high latitudes. The introduction of the modeling of the size distribution of desert dust particles should also be a further step and could help to investigate the complex link between the size distribution and the wind velocity as indicated in sea sediments records (e.g., Rea *et al.*, 1985). However, all these model investigations require more observational datasets related to the desert dust cycle both for present-day and past climates, in order to improve the model validation.

**ACKNOWLEDGEMENTS.** I thank R. Sadourny for his important contribution to the development of this work. The computing has been done using the CRAY-1 of the Centre de Calcul Vectoriel pour la Recherche. This work was supported by the Programme

National d'Etude de la Dynamique du Climat. The participation to the meeting was supported by NATO and the Centre National de la Recherche Scientifique.

## References

- CLIMAP (Climate : Long Range Investigation, Mapping and Prediction): 1981. 'Seasonal reconstructions of the earth's surface at the Last Glacial Maximum, *Geological Society of America*, Map Chart Series **MC-36**, Boulder (Colorado).
- De Angelis, M., N.I. Barkov and V.N. Petrov: 1987, 'Aerosols concentrations over the last climatic cycle (160 kyr) from an Antarctic ice core, *Nature*, **325**, pp. 318-321.
- Gaudichet, A., J.R. Petit, R. Lefèvre and C. Lorius: 1986, 'An investigation by analytical transmission electron microscopy of individual insoluble microparticles from Antarctic (Dôme C) ice core samples', *Tellus*, **38B**, pp. 250-261.
- Gillette, D.A., 'Variability of dust production caused by atmospheric and surficial variability', *this volume*.
- Giorgi, F.: 1986, 'A particle dry-deposition parameterization scheme for use in tracer transport models', *J. Geophys. Res.*, **91**, pp. 9794-9806.
- Janecek, T.R. and D.K. Rea: 1984, 'Pleistocene fluctuations in northern hemisphere tradewinds and westerlies', In A. Berger et al. (eds) *Milankovitch and Climate*, part 1, NATO ASI Series C, **126**, pp. 331-348.
- Joussaume, S., S.I. Rasool, R. Sadourny and J.R. Petit: 1984, 'Simulation of the desert dust cycles in an atmospheric general circulation model', *Annals of Glaciology*, **5**, pp. 204-207.
- Joussaume, S.: 1985, 'Simulation of airborne impurity cycles using atmospheric general circulation models', *Annals of Glaciology*, **7**, pp. 131-137.
- Joussaume, S. and R. Sadourny: 1988, 'Simulation of the desert dust cycle using an atmospheric general circulation model', IAMAP Conference on 'Aerosols and Climate', Vancouver 1987, published by A. Deepak.
- Koopmann, B.: 1981, 'Sedimentation von Sahara Staub im subtropischen Nordatlantik während der letzten 25.000 Jahre', *Meteor Forsch.-Ergebnisse*, **C 35**, pp. 23-59.
- Leinen, M., 'The late quaternary record of atmospheric transport to the northwest Pacific from Asia', *this volume*.
- Petit J.-R., M. Briat and A. Royer: 1981, 'Ice age aerosol content from East Antarctic ice core samples and past wind strength', *Nature*, **293**, pp. 391-394.
- Prospero, J.M.: 1981, 'Eolian transport to the world ocean', in C. Emiliani (ed) *The Sea: the oceanic lithosphere*, **7**, pp. 801-873.
- Prospero, J.M., D.L. Savoie, T.N. Carlson and R.T. Nees: 1979, 'Monitoring Saharan aerosol transport by means of atmospheric turbidity measurements', in C. Morales (ed) *Saharan dust: mobilization, transport, deposition*, SCOPE Report **14**, J. Wiley, pp. 171-186.
- Rea, D.K. M. Leinen and T. Janecek: 1985, 'Geologic approach to the long-term history of atmospheric circulation', *Science*, **227**, pp. 721-725.
- Sadourny R. and K. Laval: 1984, 'January and July performance of the LMD general circulation model', In A. Berger and C. Nicolis (eds) *New perspectives in climate*

- modelling*, Developments in Atmospheric Sciences, **16**, Elsevier, pp. 173-198.
- Sarnthein M.: 1978, 'Sand deserts during glacial maximum and climatic optimum', *Nature*, **272**, pp. 43-46.
- Sarnthein, M., G. Tetzlaff, B. Koopmann, K. Wolter and U. Pflaumann: 1981, 'Glacial and interglacial wind regimes over the eastern subtropical Atlantic and North-West Africa', *Nature*, **293**, pp. 193-196.
- Tetzlaff, G., 'Dust transport in West Africa', *this volume*.
- Thompson L.G.: 1977, 'Microparticles, ice-sheets and climate', Institute of Polar Studies, **64**, Ohio State University, pp. 148.
- Uematsu, M., R.A. Duce and J.M. Prospero: 1985, 'Deposition of atmospheric mineral particles in the North Pacific Ocean', *J. Atmos. Chem.*, **3**, pp. 123-138.

**SECTION 3.**

**DUST COMPOSITION AND FACTORS CONTROLLING IT: EVIDENCE  
FROM AEROSOLS AND SEDIMENTS**

EOLIAN DUST OVER THE MEDITERRANEAN AND THEIR CONTRIBUTION TO  
THE PRESENT SEDIMENTATION

L. TOMADIN and R. LENAZ

ABSTRACT

Atmospheric dust has been sampled over the Mediterranean by mesh panels and by filtration during a three years research program. The concentration and the composition of the dust was investigated and have been shown to depend on the origin and mode of transport.

Occasional episodes of direct transport contrast with more continuous nature of "background" indirect transport. Mass concentration values emphasize the indirect eolian supply. Along constant sampling tracks, dust mineralogy shows a clear evolution of typical "mineral assemblages" depending on the source areas of the particulate and on meteorological patterns variable on synoptic scale. The average composition of the dust samples has been compared with that of marine sediments, and it is suggested that wind-blown dust contributes significantly to marine sedimentation in particular areas of the Mediterranean.

1 - INTRODUCTION

Sampling cruises have been carried out in the Mediterranean over a three years period (1980-1983) and atmospheric dust was collected to investigate its composition, provenance, and contribution to the marine sediments (Landuzzi et al., 1982). At the beginning of the research (EOLLO Project), dust was collected on mesh panels. The low collection efficiency of mesh sampling permits analysis but it does not provide accurate mass concentrations (Tomadin et al., 1984; Chester et al., 1984). Subsequently sampling by high-volume air filtration ( $\sim 70 \text{ m}^3/\text{h}$ ) was also carried out to provide mass concentration data. The atmospheric dust was collected close to the seawater air interface along constant and continuous sampling tracks, which enabled the comparison of dust composition and concentration with meteorological conditions on mesoscale. Analytical procedures, previously described by Tomadin et al. (1984), consist of X-ray diffraction analysis, TEM and SEM microscopy, and elemental analysis of the collected particulate.

The first cruises were carried out in the central Mediterranean along latitudinal tracks (Fig. 1, Table 1) and suggested the following (Tomadin et al., 1984; Mazzucotelli et al., 1986): (A) the possibility to distinguish between dust of European and African source, and (B) a quite different meaning for "indirect transport" (normal circulation) of material suspended in the atmosphere, that can be compared with the "direct transport" (dust storm), which mobilizes and blows to the Mediterranean large amounts of Saharan dust. Later the research was extended to the whole Mediterranean Basin with sampling along longitudinal tracks. New evidence has been obtained (Lenaz et al., 1988) that emphasizes the importance of the "background" indirect transport.

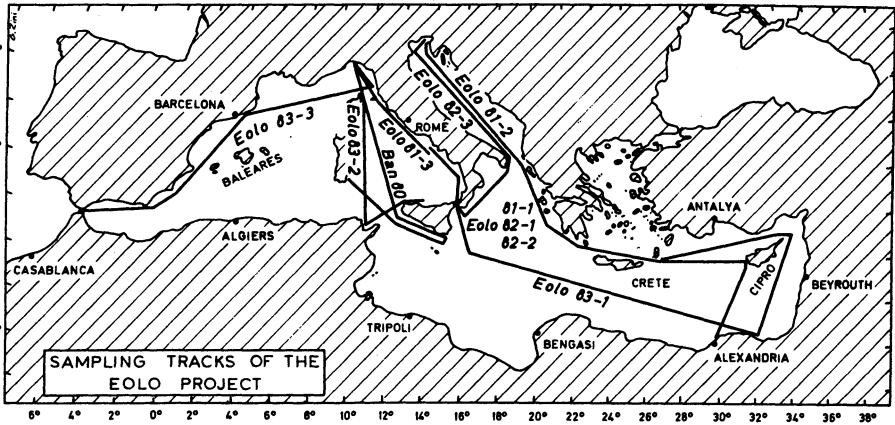


Fig. 1 - Location of continuous sampling tracks for collection of atmospheric dust at seawater-air interface during the EOLO Research Program (1980-1983).

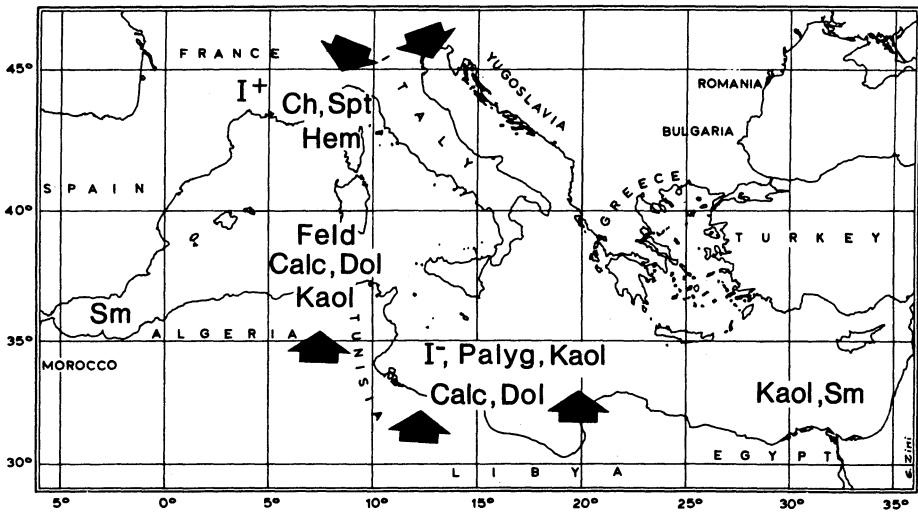


Fig. 2 - Minerals from northern and southern source areas recognized in windborne dust over the Mediterranean. I+: well-organized illite; I-: poorly-organized illite; Ch: chlorite; Kaol: kaolinite; Spt: serpentine; Palyg: palygorskite; Hem: hematite; Sm: smectite; Feld: feldspars; Calc: calcite; Dol: dolomite.

Table 1

Tracks and times of atmospheric dust collection (EOLO Project)

Cruise	Track	Date	
		Start	Finish
BAN 80	Genoa-Malta-Cagliari	19-IX-1980	30-IX-1980
EOLO 81-1	Ancona - Messina	27-III-1981	4-IV-1981
EOLO 81-2	Piraeus - Trieste	31-X-1981	5-XI-1981
EOLO 81-3	Messina - Genoa	18-XII-1981	21-XII-1981
EOLO 82-1	Neaples-Chan.Sicily- Ancona	14-VII-1982	9-VIII-1982
EOLO 82-2	Ancona - Crotone	1-IX-1982	15-IX-1982
EOLO 82-3	Trieste - Neaples	21-XI-1982	25-XI-1982
EOLO 83-1	Reggio Calabria-Port Said	12-II-1983	18-II-1983
EOLO 83-2	Neaples-Sardinia-Genoa	10-VI-1983	19-VI-1983
EOLO 83-3	Genoa-Livorno-Barcelona- Gibraltar	2-X-1983	9-X-1983



The objectives of the present study are: (1) to demonstrate the continuity and the important mass contribution by "indirect transport" with respect to uncommon episodes of "direct transport"; (2) to show where the source area of atmospheric dust suspended at seawater-air interface can be recognized, even during indirect transport; (3) to trace the dispersion mechanisms of fine materials, which permit the identification of a significant windborne input in the present-day marine sediments of the Mediterranean.

## 2 - DUST TRANSPORT AND MASS CONCENTRATION

Eolian dust is generally supplied to the Mediterranean by either direct transport of material deflated from source areas in North Africa or indirect transport of materials already present in the lower atmosphere. Occasional episodes of direct transport contrast with the more continuous nature of "background" indirect transport. A considerable literature deals with the direct transport (Alaimo and Ferla, 1979; Prodi and Fea, 1978, 1979; Venzo and Chiaramonti, 1980; Ganor and Mamane, 1982; Bucher et al., 1983; Bucher and Lucas, 1984; Chester et al., 1984; Loye-Pilot et al., 1986; Nihlén and Solyom, 1986), but there is little information about the indirect transport of dust. Evidence that concerns the frequency of episodes of direct transport is derived from either previous work or the EOLO Research Program. According to Prodi and Fea (1978, 1979) during 10 years of continuous air sampling at the alpine station of Plateau Rosa (3480 m.s.l.), direct transport of Saharan dust occurred only 34 times. During the sampling cruises of the EOLO Project (1980-83), a single dust storm was encountered accidentally (Tomadin et al., 1984). With this exception, most of the eolian dusts have been sampled under meteorological situations favourable for indirect transport (Lenaz et al., 1983, 1988; Tomadin et al., 1984; Mazzucotelli et al., 1986). Mass concentrations that were measured with high-volume sampler have been compared and permit differentiation of the two transport types recognized over the Mediterranean Basin. High concentrations have been observed during severe episodes of direct transport ( $154 \mu\text{g}/\text{m}^3$  according to Tomasi et al., 1979), but significant concentration values are also related to the indirect eolian supply. In fact, recent investigations (Lenaz et al., 1988) gave the following total concentrations (insoluble + soluble fractions) measured at seawater-air interface:  $6-51 \mu\text{g}/\text{m}^3$  (average value:  $22 \mu\text{g}/\text{m}^3$ ) along tracks of the western Mediterranean (EOLO 83-3 Cruise from Genoa to Gibraltar) and  $21-55 \mu\text{g}/\text{m}^3$  (average value:  $38 \mu\text{g}/\text{m}^3$ ) in the south-eastern Mediterranean (EOLO 83-1 Cruise from Reggio Calabria to Port Said) (Fig. 1). These data indicate the important contribution due to the indirect transport of dust. Considerable dust concentrations depend on a concordant air flow both at 500 hPa and at sea level (Lenaz et al., 1988, Fig. 6, 7, 8). Although the values of the northern sampling (EOLO 83-3 data) were obtained in a dry season (more favourable to the transport of atmospheric dust), the highest mass concentrations have been found in the

southernmost belt bordering the basin (EOLO 83-1 data) during a wet season.

### 3 - MINERALOGY OF ATMOSPHERIC DUST COLLECTED DURING BACKGROUND INDIRECT TRANSPORT

Both the mineralogy of the bulk sample and the clay mineralogy (as well as the color and the elemental composition of the particulate - Table 2) give evidence of the provenance of the wind-blown dust, since they reflect these properties in soil of the source areas (Chester, 1972; Prospero, 1981, 1981a). Previous investigations indicated the presence of minerals of northern (European) and of southern (African) provenance in the eolian dust over the Mediterranean (Chester et al., 1977, 1984; Lefevre et al., 1986; Lenaz et al., 1983, 1988; Tomadin et al., 1983, 1984; Mazzucotelli et al., 1986; Nihlén and Solyom, 1986). Dust samples collected along latitudinal and longitudinal tracks permitted close examination of the atmospheric dust of the "background" indirect transport that was recognizable on synoptic scale.

Two different types of dust were analyzed:

#### A - Wind-blown dust from a constant direction

This was observed along the Adriatic Sea and depends on meteorological conditions responsible for the transport of dust by constant winds. In fact, with prevailing winds from South-East (EOLO 81-1 Cruise) or from North-West (EOLO 81-2 Cruise), the composition of atmospheric dust points to typical trends in the areas crossed by the air masses. The particulate that is suspended in the lower atmosphere of the northern Adriatic shows a characteristic mineral assemblage (Fig. 2): well-organized illite ( $I^+$ ), chlorite (Ch), serpentine (Spt), and rare smectite (Sm) as well as hematite and mullite as industrial pollutants. Towards lower latitudes (southern Adriatic, Ionian Sea), the atmospheric particulate shows a gradual change of mineral assemblage: poorly-organized illite ( $I^-$ ), kaolinite (K), palygorskite (Palyg), smectite (Sm), subordinate chlorite (Ch), abundant carbonates, feldspars, quartz and scarce hematite. Subordinate or uncommon minerals like gypsum, talc, imogolite, amphibole, analcime and mullite give additional information about their provenance (cruises BAN 80, EOLO 82, etc. in Fig. 1). For example, imogolite comes from volcanic soils of central and southern Italy (Violante and Tait, 1979); mullite and iron oxides are present in the fly-ash of various industries (Del Monte and Sabbioni, 1984; Mazzucotelli et al., 1986).

The comparison of different meteorological conditions of the same geographical region, permits recognition of minerals from a given proximal source area in the atmospheric dust. For example, in the southern Adriatic a significant input of chlorite (and serpentine) from ophiolitic soils of Albania has been recognized in prevailing winds from southeast (EOLO 81-1 Cruise), but has not been recognized in north-western winds (EOLO 81-2 Cruise) (Tomadin et al., 1984, Fig. 2, 3 and Table 3).

#### B - Wind-blown dust from veering directions

Provenance and composition of atmospheric dust of a given area

Table 2

Differentiation of atmospheric dust by color, mineralogy and elemental composition (Tomadin et al., 1984; Mazzucotelli et al., 1986)

## Differences between dust of

southern provenance

northern provenance

## COLOR

yellow-red (7,5 YR 4/4)

brown-blackish (10 YR 3/2)  
(Munsell soil color charts)

## MINERALOGY

poorly-organized illite,  
kaolinite, smectite,  
palygorskitewell-organized illite,  
chlorite, serpentine

calcite, dolomite, feldspars

(hematite)

## ELEMENTAL COMPOSITION

2-3% organic matter

20-30% organic matter

higher  $\text{SiO}_2 / \text{Al}_2\text{O}_3$  ratiolower  $\text{SiO}_2 / \text{Al}_2\text{O}_3$  ratio

high Ca content

strong Fe, Mg content

scarce trace elements

high Co, Cr, Ni, Cu content

K/Na &gt; 1

K/Na &lt; 1

depend on air mass movements in the days preceding sampling. The atmospheric particulate of a given air mass due to "background" indirect transport shows a characteristic mineral assemblage. The arrival of a new air mass from different source may supply dust of different mineralogy. After changing of the meteorological conditions, the possible dust supply of the initial air mass attenuates and results in more or less active mixing of windborne particulates.

This type of dynamic interaction was most widespread during the sampling cruises of the EOLO Project (Fig. 1, Table 1). For example, during the EOLO 83-3 Cruise in the western Mediterranean, winds from the North were blowing towards the Ligurian Sea a few days before the beginning of sampling. At first, the mineralogy of the atmospheric dust was characterized by the following mineral assemblage:  $I^+$ , Ch, Spt and talc of Ligurian Apennines and western Alps source (Fig. 2) as well as high amounts of hematite from industrial pollution have been detected (Gulf of Genoa and Gulf of Lion). The influence of these air masses on the composition of transported dust continued even when winds veered from the first to the second quadrant. After only several days of Sirocco winds, the mineralogy of dust changed. Serpentine and talc disappeared, chlorite decreased, whereas kaolinite content increased along southwestwards tracks and well-organized illite ( $I^+$ ) was interspersed with poorly-organized illite ( $I^-$ ). In the following days, smectite also appeared, and dolomite, calcite, and quartz contents progressively increased. Dust with an African source (Fig. 2) was attributed to the Sirocco winds, which grew stronger during the preceding days (Lenaz et al., 1988, Table 2 and Fig. 5, 6, 7). In the lower atmosphere of the Alboran Sea, smectite and kaolinite of Iberian source were probably mixed with minerals of southern provenance, because in the last days of sampling the winds veered again from the North.

In the following case, the veering wind direction played a subordinate role on mineralogy of the dust, which was mainly affected by the input from the most important eolian source of the Mediterranean Basin. During the approach to the African mainland, sampling of the EOLO 83-1 Cruise (Fig. 1, Table 1) was dominated by the effects of strong Sirocco winds (Lenaz et al., 1988), which carried clay materials and abundant carbonates. Dolomite and calcite were probably transported from the Cyrenaica reefs (Venkatarathnam and Ryan, 1971). The data in Table 3 summarize the typical clay mineralogy of dust of southern source. The percentage values permit the mineral evolution of sampled dust to be followed as the African coast was approached. The "A" data (Tab. 3) correspond to atmospheric particulate collected in the northern Ionian Sea, whereas the "B" data give the clay mineral contents of dust collected over the Nile cone. In fact, when by cyclonic rotation the winds veer to the South, carbonates disappear and  $I^-$  content decreases, but there is a progressive increase in smectite and kaolinite, which are the most abundant clay minerals of the Nile cone and of surrounding deserts (Venkatarathnam and Ryan, 1971; Chester et al., 1977; Maldonado and Stanley, 1981).

Table 3

Evolution of the "clay mineral assemblage" in the dust with an African source in the prevailing Sirocco wind. Samples were collected in the atmosphere of the eastern Mediterranean.

	I <sup>-</sup>	K	Sm	Ch	Palyg
(A) Ionian atmospheric dust	64*	18	7	11	abundant
(B) Nile cone atmosph. dust	35	39	21	5	abundant

\* Percentages data (Lenaz et al., 1988)

The above examples clearly show that when a wind rotation occurs in a wide area under leveled atmospheric pressure, the eolian dust is not affected by a total change of mineralogy. Part of the atmospheric particulate reflects the dynamics of transport of the days prior to the directional change.

#### 4 - ATMOSPHERIC DUST AND PRESENT-DAY SEDIMENTS

The clay mineralogy of the eolian dust can be compared to that of underlying marine sediments (Table 4). Useful information can be obtained for areas where the eolian supply has not been masked by high terrigenous input from rivers.

In general, illite is more abundant in the dust samples than in the sediments; moreover, little wind-blown smectite was recognized (Table 4). These data agree with general remarks of Windom (1975) and with those of Chester et al. (1977, 1984) in the eastern and in the central Mediterranean. Given the cut-off of the less than 1  $\mu\text{m}$  fraction (Tomadin et al., 1984; Chester et al., 1984), probably the finest smectites were not collected by mesh sampling. Only part of the atmospheric dust suspended close to the seawater-air interface, contributes significantly to the present-day marine sedimentation. The high mobility of the atmospheric particulate (mainly of the clay minerals) leads to their long-range transport. For example, airborne dust of Saharan origin has been carried to Barbados and Miami (Glaccum and Prospero, 1980) and to Scotland (Bain and Tait, 1977).

Data for two different areas of the central Mediterranean are presented in Table 4. In the first one, the recent sedimentation of the Adriatic Sea is highly influenced by the input of the Po River and the minor rivers flowing from Apennines to the Adriatic. The data in Table 4 clearly show that the fluvial supply prevails in respect to the possible eolian supply. It is worth mentioning, however, that kaolinite/chlorite ratio increases to the South both in the sediments (Tomadin, 1981) and in the atmospheric dust of the Adriatic (Tomadin et al., 1983, 1984). It is not easy to determine if this reflects an increase of windborne kaolinite towards the south or an increase of fluvial chlorite towards the north. The smectite of the marine sediments, which was eroded from various geological formations of the Apennines is certainly of fluvial origin (Tomadin et al., 1986, 1988; Curzi and Tomadin, 1987; Tomadin and Borghini, 1987). Sedimentology and dispersion patterns of the clay minerals in the Tyrrhenian Sea are quite different (Tomadin, 1974, 1981). The fluvial input is very negligible, considering only two significant rivers - Tiber and Volturno - and numerous ephemeral creeks are present in the whole circum-tyrrhenian area. One of the most important features of the clay sediment distribution is a tongue-like belt, which extends north of Sicily (Fig. 3 and 4) towards the center of the Tyrrhenian Sea. The main clay components of the "central belt" are kaolinite and illite that is poorly-organized in respect to that of surrounding areas. Moreover kaolinite (Fig. 3b) and low-crystalline illite (Fig. 4 a, b) are more abundant on the top of several seamounts (De Marchi, Vavilov, Marsili, Palinuro, Lametino) (Fig. 3a) than

Table 4 - CLAY MINERALOGY OF ATMOSPHERIC DUST AND PRESENT-DAY SEDIMENTS OF THE CENTRAL MEDITERRANEAN

	Sm	I	K	Ch	Spt	Palyg	References
Indirect transport	0-5	60-75	5-15	15-35	10	--	Tomadin et al., 1983; 1984
from the N							
from the S	5-20	40-65	15-25	10-15	--	present	Mazzucotelli et al., 1986
Direct transport	5-10	55-65	25-35	5-10	--	present	Lenaz et al., 1988
from the S							
Po River	20-25	40-50	10-15	15-20	5	--	Tomadin, 1979
Northern Adriatic	10-20	50-60	10-15	15-20	5	--	Tomadin, 1975
Southern Adriatic	30-35	40-50	10-20	10-15	--	--	Curzi & Tomadin, 1987 Tomadin & Borghini, 1987
Central Tyrrhenian	10-20	45-60	20-25	10-15	--	--	
Southern Tyrrhenian	15-25	40-50	25-35	5-10	--	(*)	Tomadin, 1974, 1981

The percentages correspond to compositional ranges. For symbols, see Fig. 2  
 (\*) sometimes recognized by TEM microscopy in the southernmost marine sediments

ATMOSPHERIC DUST

SEDIMENT

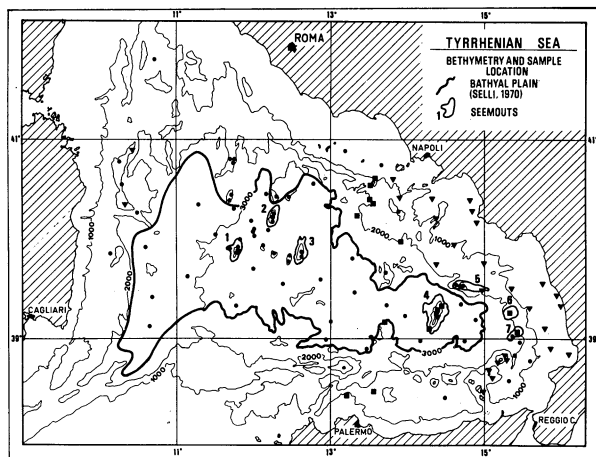


Fig. 3a- Bathymetry, sample location, and main morphological features of the Tyrrhenian Sea. 1-Magnaghi Seamount; 2-De Marchi S.; 3-Vavilov S.; 4-Marsili S.; 5-Palinuro S.; 6-Enotrio S.; 7-Lametino S.

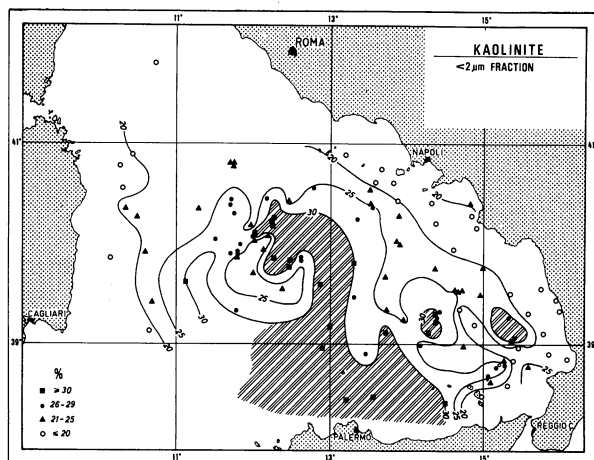


Fig. 3b- Kaolinite distribution in the present-day sediments of the Tyrrhenian Sea. Hachured areas show kaolinite-rich sediments in a belt from north of Sicily towards the center of the basin and on the top of the seamounts.



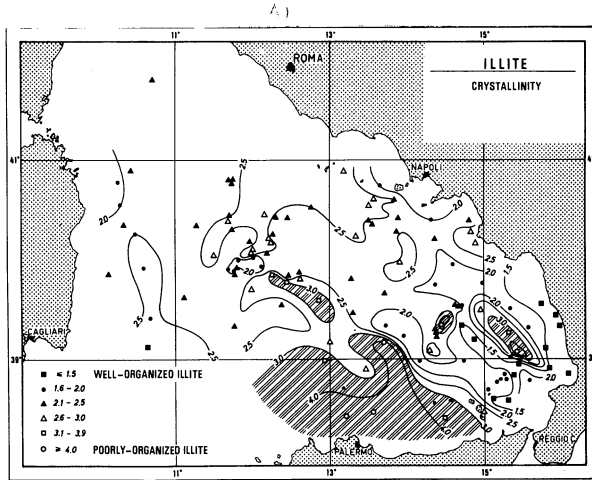
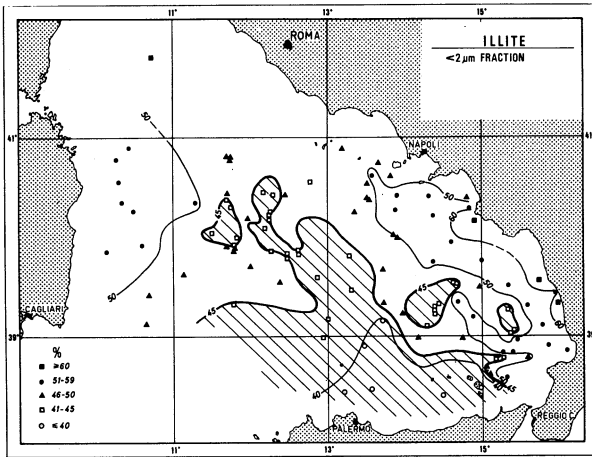


Fig. 4a,b - Illite and illite crystallinity distribution in the Tyrrhenian Sea. Hatched areas show poorly-organized illite of eolian origin in the present-day sediments of the basin.

along their slopes. The comparison between these sediments and those distributed on the Tyrrhenian continental shelf and slope, clearly shows that both minerals have not been supplied by rivers from either Sardinia or the Italian peninsula. A terrigenous kaolinite supply from the geological formations of northern Sicily cannot be excluded (Alaimo and Ferla, 1981; Deconinck et al., 1987); however, the poor hydrography and also the physiography of the Basin do not seem to favor an important input of kaolinite to the Tyrrhenian Sea. In fact, several "perityrrhenian basins" (Ustica, Cefalù and Gioia - see Selli, 1970; Fabbri and Selli, 1972) are able to collect large amounts of the finest sediments. Moreover, with the exception of the Stromboli Canyon, which mainly collects eolian volcanoclastics and crystalline materials, there are no important canyons which could promote clay sediment transport as far as 250 km from Sicily (Fig. 3 and 4).

Two explanations of the anomalous kaolinite distribution in the Tyrrhenian Basin could be invoked: (a) submarine rock alteration by hydrothermal solutions and (b) input of atmospheric dust. The first possibility is rejected on the basis of the petrography of the Tyrrhenian volcanic seamounts, which consist of tholeiitic, calcalkaline, and shoshonitic lavas (Beccaluva et al., 1981). Disregarding the seamounts, one must consider the wide distribution of kaolinite-rich sediments on the Tyrrhenian bathyal plain (Selli, 1970, p. 20); Tomadin, 1974) (Fig. 4). The second hypothesis is supported by the low average kaolinite content of the geological formations, limited fluvial input from southern Italy and Sardinia, and recent mineralogical evidence provided by analysis of airborne dust samples. Recent data (Tomadin et al., 1984); Chester et al., 1984; Lenaz et al., 1988) show that over the Mediterranean, kaolinite and palygorskite, which are minerals characteristic of peridesertic environment (Millot, 1964), increase to the south. Additionally, the data in Table 4 indicate very similar amounts of kaolinite (and illite) measured in the atmospheric dust and in the sediments of the Tyrrhenian Sea.

In conclusion, the effect of eolian transport is evident when downslope gravitational processes, or long-distance transport by water circulation do not prevail. Therefore, the eolian input plays an important and hitherto little known role in the sedimentation of the central Mediterranean.

## 5 - CONCLUSIONS

Windborne dust collected in the lower atmosphere of the Mediterranean over a three years period permit the recognition of the considerable contribution of the "background" indirect transport.

Mass concentrations measured along continuous sampling tracks indicate significant contributions due to the indirect eolian supply when compared with higher values provided by occasional dust storms.

The mineralogy of the atmospheric particulate give evidence of characteristic "mineral assemblages" depending on proximal or

distal source areas and the variable wind direction. Eolian components can only be distinguished in marine sediments when the input of dust is large relative to fluvial or turbiditic sediment supply, as in the Tyrrhenian Sea.

## REFERENCES

- ALAIMO R. and FERLA P., 1979 - Presenza di palygorskite nella polvere trasportata dallo Scirocco in Sicilia. *Ist. Miner. Petrog. e Geoch.*, Univers. di Palermo, Quaderno n. 4, 1-10.
- ALAIMO R. and FERLA P., 1981 - Guidebook for the excursions in Sicily, AIPEA, 7th Internat. Clay Conf., 6-12 September 1981, 1-66.
- BAIN D.C. and TAIT J.M., 1977 - Mineralogy and origin of dust fall on Skye. *Clay minerals*, 12, 353-355.
- BECCALUVA L., GABBIANELLI G., LUCCHINI F., ROSSI P.L., SAVELLI C. and ZEDA O., 1981 - Magmatic character and K/Ar ages of volcanics dredged from the Eolian seamounts (Tyrrhenian Sea). In: *Sedimentary Basins of the Mediterranean margins* (F. C. Wezel Ed.), CNR Italian Project of Oceanography, Tecnoprint, Bologna, 361-368.
- BUCHER A., DUBIEF J. and LUCAS C., 1983 - Retombées estivales de poussières sahariennes sur l'Europe. *Rev. Géol. dyn. Géogr. phys.*, 24, 2, 153-165.
- BUCHER A. and LUCAS C., 1984 - Sédimentation éolienne intercontinentale, poussières sahariennes et géologie. *Bull. Centres Rech. Explor. - Prod. Elf - Aquitaine*, 8, 1, 151-165.
- CHESTER R., 1972 - Geological, geochemical and environmental implications of the marine dust veil. In: *The changing chemistry of the oceans*. Nobel Symposium 20, edited by D. Dyrssen and D. Jagner, Wiley Interscience Div., New York, 291-305.
- CHESTER R., BAXTER G.G., BEHAIRY A.K.A., CONNOR K., CROSS D., ELDERFIELD H. and PADGHAM R.C., 1977 - Soil-sized eolian dusts from the lower troposphere of the Eastern Mediterranean Sea. *Mar. Geol.* 24, 201-217.
- CHESTER C., SHARPLES E.J., SANDERS G.S. and SAYDAM A.C., 1984 - Saharan incursion over the Tyrrhenian Sea. *Atmospheric Environment*, 18, 5, 929-935.
- CURZI P.V. and TOMADIN L., 1987 - Dinamica della sedimentazione pelitica attuale ed olocenica nell'Adriatico centrale. *Giornale di Geologia*, 49, 1, 101-111.
- DECONINCK J.F., BROQUET P., CHAMLEY H., ROBASZYNSKI F. and THIEBAULT F., 1987 - Minéraux argileux de la zone de Sclafani (Madonies, Sicile): Diagenèse et paléoenvironnement du Permien au Miocene. *Géologie Méditerranéenne*, 12-13, 3-11.
- DEL MONTE M. and SABBIONI C., 1984 - Morphology and mineralogy of fly-ash from a coal fueled power plant. *Arch. Met. Geoph. Bioch.*, B 35, 93-104.
- FABBRI A. and SELLI R., 1972 - The Structure and Stratigraphy of the Tyrrhenian Sea. In: *The Mediterranean Sea. A natural Sedimentation Laboratory*, editet by D.J. Stanley, Dowden, Hutchinson & Ross, Stroudsburg, 75-81.

- GANOR E. and MAMANE V., 1982 - Transport of Saharan dust across the eastern Mediterranean. *Atmospheric Environment*, 16, 581-587.
- GLACCUM R.A. and PROSPERO J.M., 1980 - Saharan aerosols over the tropical North Atlantic - *Mineralogy. Mar. Geol.*, 37, 295-321.
- LANDUZZI V., LENA Z R., MAZZUCOTELLI A., TOMADIN L. and VANNUCCI R., 1982 - Updating our knowledge on the eolian input over the Mediterranean Sea. *Giornale di Geologia*, 45, 1, 17-24.
- LEFEVRE R., GAUDICHET A. and DE FELICE P., 1987 - Caracterisation chimico-mineralogique des flux microparticulaires dans la basse atmosphère de la Méditerranée moyenne. Permanence et fluctuation des apports atmosphériques à la sédimentation. *Comptes rendus*, 469, série 2, in print.
- LENA Z R., LANDUZZI V. and TOMADIN L., 1983 - Apporti eolici stagionali sul Mediterraneo centrale. *Atti 5° Congr. AIOL*, Stresa 19-27 Maggio 1982, 559-578.
- LENA Z R., LANDUZZI V. and TOMADIN L., 1988 - Apports et concentrations de masse des poussières eoliennes sur le abssin oriental et occidental de la Méditerranée. *Mem. Soc. Geol. It.*, 36, in print.
- LOYE-PILOT M.D., MARTIN J.M. and MORELLI J., 1986 - Influence of Saharan dust on the rain acidity and atmospheric input to the Mediterranean. *Nature*, 321, 427-428.
- MALDONADO A. and STANLEY D.J., 1981 - Clay mineral distribution patterns as influenced by depositional processes in Southeastern Levantine Sea. *Sedimentology*, 28, 21-32.
- MAZZUCOTELLI A., LANDUZZI V., LENA Z R., OLIVERI F., TOMADIN L. and VANNUCCI R., 1986 - Polveri in sospensione nella bassa atmosfera del mar Tirreno e del Canale di Sicilia (Crociera BAN 80). *Mem. Soc. Geol. It.*, 27, 311-321.
- MILLOT G., 1984 - *Geologie des Argiles*, Masson et Cie, Paris, 499 P.
- NIHLEN T. and SOLYOM Z., 1986 - Dust storm and eolian deposits in the Mediterranean area. *Geol. Foren. Stock. Forhand.*, 108, 235-242.
- PRODI F. and FEA G., 1978 - Transport and deposition of Saharan dust over Alps. *Proc. 15th Int. Tagung Meteorol.*, 1, 179-182.
- PRODI F. and FEA G., 1979 - A case of transport and deposition of Saharan dust over the Italian peninsula and Southern Europe. *J. Geopys. Res.*, 84, 6951-6960.
- PROSPERO J.M., 1981 - Arid regions as sources of mineral aerosols in the marine atmosphere. *Geol. Soc. of America, Special Paper* 186, 71-86.
- PROSPERO J.M., 1981a - 21. Eolian transport to the World Ocean. In: *The oceanic lithosphere* (Ed. C. Emiliani). *The Sea*, vol. 7, Wiley, New York, 801-874.
- SELLI R., 1970 - Ricerche geologiche preliminari nel Mar Tirreno. *Giornale di Geologia*, 37, 1, 1-249.
- TOMADIN L., 1974 - Les minéraux argileux dans les sédiments actuels de la Mer Tyrrhénienne. *Bull. Gr. Fr. Argiles*, 26, 219-228.
- TOMADIN L., 1975 - Clay minerals in the Northern Adriatic Sea: dispersal by drift currents. *Rapports Commission*

- Internationale Mer Méditerranée, 23, 283-285.
- TOMADIN L., 1979 - Clay mineralogy of recent sediments around the Po River Delta. *Giornale di Geologia*, 43, 249-275.
- TOMADIN L., 1981 - Provenance and dispersal of clay minerals in recent sediments of the Central Mediterranean Sea. In: *Sedimentary Basins of Mediterranean Margins* (F. C. Wezel Ed.), CNR Italian Project of Oceanography, Tecnoprint, Bologna, 313-324.
- TOMADIN L., LANDUZZI V. and LENAZ R., 1983 - Influence of the eolian supply on the sedimentation in the Adriatic Sea. *Thalassia Jugoslavica*, 19, 377-382.
- TOMADIN L., LENAZ R., LANDUZZI V., MAZZUCOTELLI A., and VANNUCCI R., 1984 - Wind-blown dusts over the Central Mediterranean. *Oceanologica Acta*, 7, 1, 13-23.
- TOMADIN L., GALLIGNANI P., LANDUZZI V. and OLIVERI F., 1986 - Fluvial pelitic supplies from the Apennines to the Adriatic Sea. I - The rivers of the Abruzzo Region. *Petrogr. Acta*, 29A, 277-286.
- TOMADIN L. FRANCHI R. and LANDUZZI V., 1987 - Apporti pelitici fluviali dall'Appennino al Mare Adriatico. II - I bacini di drenaggio del Marecchia e del Metauro (Marche). *Giornale di Geologia*, 49, 2, 11-21.
- TOMADIN L. and BORGHINI M., 1987 - Source and dispersal of clay minerals from present and Late Quaternary sediments of Southern Adriatic Sea. The 6th Meeting of the European Clay Groups, Sevilla (Spain), 7-10 September 1987, *Summaries-Proceedings*, 537-538.
- TOMASI C., PRODI F. and TAMPIERI F., 1979 - Atmospheric turbidity variations caused by layers of Saharan dust particles. *Beitr. Phys. Atmosph.*, 52, 3, 215-228.
- VENKATARATHNAM K. and RYAN W.B.F., 1971 - Dispersal patterns of clay minerals in the sediments of the eastern Mediterranean Sea. *Mar. Geol.*, 11, 261-282.
- VENZO G.A. and COMIN-CHIARAMONTI P., 1980 - Saharan dust deposited by rain during the night of February 11, 1979 in the zone of Trento, n. Italy. *Studi trentini di Scienze Naturali*, 57, *Acta Geol.*, 3-14.
- VIOLANTE P., and TAIT J.M., 1979 - Identification of imogolite in some volcanic soils from Italy. *Clay Minerals*, 14, 155-157.
- WINDOM H.L., 1975 - Eolian contributions to marine sediments. *J. Sedim. Petrol.*, 45, 520-529.

Luciano Tomadin - Istituto di Mineralogia e Petrografia,  
Università di Urbino,  
via M. Oddi, 14 - 61029 URBINO, ITALY

Renzo Lenaz - Istituto per la Geologia Marina del CNR  
via Zamboni, 65 - 40127 BOLOGNA, ITALY

EOLIAN DUST COLLECTED IN SPRINGTIME (1979 AND 1984 YEARS)

AT THE SEAWATER-AIR INTERFACE OF THE NORTHERN RED SEA

L. TOMADIN, G. CESARI, S. FUZZI, V. LANDUZZI, R. LENAZ, A. LOBIETTI, P. MANDRIOLI, M. MARIOTTI, A. MAZZUCOTELLI, R. VANNUCCI

ABSTRACT

Atmospheric dust samples have been collected over the Red Sea during springtime in 1979 and in 1983 by mesh sampling and by high-volume filters. Mineralogical-, grain-size-, chemical- and biological analyses have been performed to give a first sedimentological picture of the dust present in the lower atmosphere of this area.

The meteorology during both sampling periods was characterized by indirect transport of materials by prevailing northwesterly wind. In this conditions mass concentration values are subordinate to those measured during a moderate episode of direct transport. The grain-size distribution and the clay mineralogy of the dust are controlled by the variable atmospheric dynamics occurred during the two samplings. In particular, a higher wind energy (MR 79 Cruise) is responsible for the transport far away of the finest smectites. Conversely, atmospheric dust collected in dependence on average lower energy level (MR 83 Cruise) is richer in smectite than the former one. Besides factors such as meteorology and energy level, also the land morphology plays an important role for the control of the dust mineralogy (f.i. the "barrier action" due to a chain transverse to the wind flow, and the effect due to the break off of the same chain). The elemental compositions of both insoluble and soluble fractions of the particulate are controlled by the prevailing northwesterly wind. The pollen grains loading decreases with the latitude and testifies a dominant long-range transport of pollen species.

1 - DUST PARTICLE COLLECTION AND ANALYTICAL PROCEDURES

Atmospheric dust samples have been collected in February - March (Cruise MR 79) and in March 1983 (Cruise MR 83) on board of Italian research ships. The sampling was performed along continuous tracks from Suez to Jeddah (Fig. 1 and 3) by mesh panels and by high-volume air filtration. As previously discussed (Prospero, 1981; Tomadin et al., 1984; Chester et al., 1986), the mesh collection, even if affected by poor efficiency for submicron particles, permits sedimentological investigations, providing however only relative information on dust loadings in the atmosphere (Chester, 1986). Mineralogical, chemical and grain-size analyses were performed on materials collected by mesh panels during both sampling periods. On the opposite, the total suspended particulate matter (TSP) and the aerobiological matter were investigated by high-volume

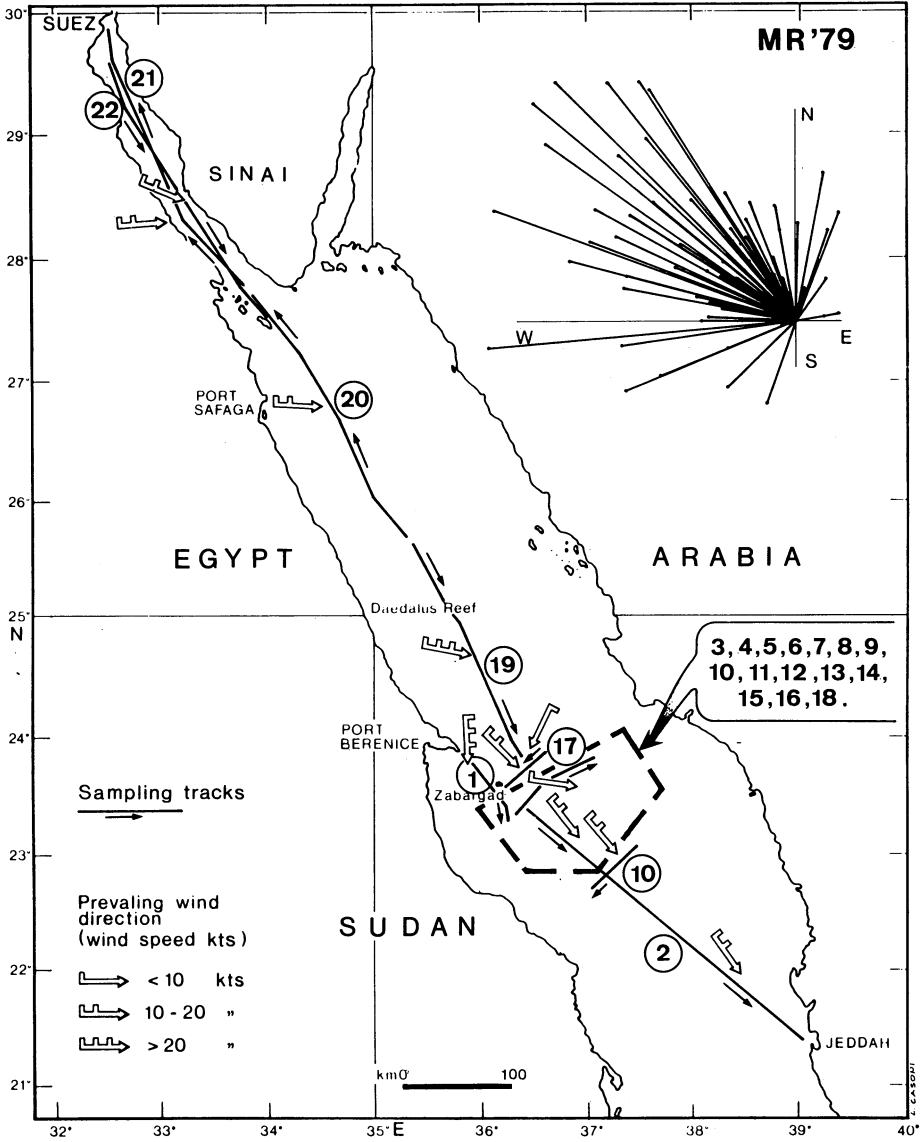


Fig. 1 - Dust sampling tracks, wind directions and diagram of the true wind measured on board during the Cruise MR 79 (Feb-Mar 1979).

filters collected during spring 1983 (compare southbound and northbound tracks of Figures 12, 13, 14 and 16). After the mesh panels have been rinsed in an ultrasonic bath, the dust particles were analyzed by a photo-extinction sedimentometer for grain-size analysis (Simmons, 1959; Gallignani and Magagnoli, 1972). The mineralogy of the dust samples was determined by X-ray diffraction on powders and on oriented smear slides (less than 2  $\mu\text{m}$  fraction). For a convenient identification of palygorskite, TEM microscopy was used as well as SEM for a systematic morphological analysis. Major, minor and trace elements of the eolian dusts were analyzed by AA spectrophotometry and ICP spectroscopy after sample dissolution (Mazzucotelli et al., 1988; Tomadin et al., 1984).

High-volume collection of atmospheric particles was performed by a GMW-2000 sampler on 20x25 cm glass fiber filters, at a flow rate of 72  $\text{m}^3 \text{hour}^{-1}$  (Jutze and Foster, 1967). Spectrograde Gelman filters were used, which ensure low blank values in the chemical analyses. This filter substrate exhibits a collection efficiency of 99,9% for particles larger than 0,3  $\mu\text{m}$ . After the determination of TSP by differential weighting, one-half of the filter was leached in an ultrasonic bath with deionized water to which 5% ethanol had been added. The soluble fraction of TSP was then determined by difference. For aerobiological analysis the second half of the filter was used. The filter was first treated with a surfactant in an ultrasonic bath for 30 minutes to remove all particles. The solution was then filtered through Millipore membrane filters (1,2  $\mu\text{m}$  pores) and observed under the microscope after drying and transparentizing.

## 2 - METEOROLOGICAL CONDITIONS AND MASS CONCENTRATIONS

The mesoscale atmospheric circulation is much more energy-rich in tropical areas than in the higher latitudes (Hastenrath, 1985). In particular, a large variability from local to mesoscale was pointed out in the Red Sea region (Flohn, 1965; Prodi et al., 1983). In the early spring, the meteorology of the Mediterranean controls the circulation over the northern Red Sea, with quick air mass movements towards the East. In this period strong winds blow from NW over the Red Sea (Butzer, 1960; Thompson, 1970). Such meteorological conditions have been noticed also during the MR 79 and MR 83 Cruises. In fact, the representative vectors of the true wind, measured on board and reported in the diagrams of Fig. 1 and 3, show a prevailing direction from Northwest. Moreover the comparison between the two sampling periods allows to recognize higher average wind speed (and therefore transport energy) in spring 1979 than in spring 1983. During the MR 79 Cruise, meteorological patterns at the sea level and at 500 mb (Fig. 2), give evidence of a clear discordance of the wind directions favouring an indirect transport of particles suspended in the lower atmosphere. Concentrations of the mineral fraction have been appreciated as: 2-82  $\mu\text{g}/\text{m}^3$  (Prospero, personal communication). During the MR 83 Cruise, the atmospheric circulation involves again an indirect transport. The corresponding concentration of the mineral fraction was: 4-35



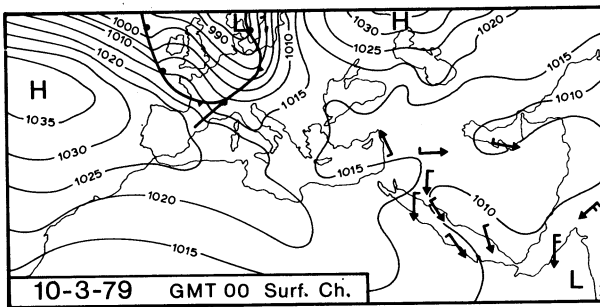
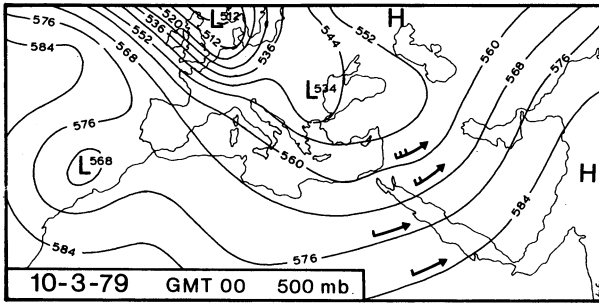


Fig. 2 - Meteorological conditions on 10 March 1979 at the 500 mb (A) and at sea level (B) (from Europ. Wetterb. Deutsch. Wetterdienstes).

$\mu\text{g}/\text{m}^3$ . At the beginning of this latter sampling period, however (compare tracks 8 and 9 of Fig. 3), the meteorological patterns at sea level and at 500 mb (Fig. 4) point out a concordance of wind directions, favouring an episode of direct transport of dust particles. Nevertheless, the low-pressure minimum is located in the eastern Mediterranean and it does not give evidence of mobilization at the surface. The increasing wind speed, measured on board and with a prevailing direction from W-SW, seems however to be able to favor the erosion of weakly aggregated soil. In fact, the higher mineral concentration:  $100\text{--}200 \mu\text{g}/\text{m}^3$  (measured over a 6 hour period) supports a possible direct supply from the African mainland to the Red Sea.

As a matter of fact, the meteorological conditions during the two springtime sampling cruises, give evidence of a prevailing indirect transport of atmospheric suspended materials. The relative mass concentrations are by no means negligible in terms of the possible sedimentation, even if they are clearly subordinate to concentrations due to the direct transport. Similar conditions and concentration values have been also recognized in the lower atmosphere of the Mediterranean (Tomadin and Lenaz, this issue).

### 3 - PARTICLE SIZE AND MINERALOGY

The atmospheric dust collected over the Red Sea exhibits a variable percentage of insoluble particulate (see the following data on the TSP). The total amount collected was sometimes too scarce for a reliable grain-size analysis. The grain-size distribution of the investigated dust samples is reported in Fig. 5 and 6; the dashed line on the top of the less than  $1 \mu\text{m}$  class points out to the above mentioned cut-off for submicron particles. The comparison between representative histograms of the two groups of collected dust samples (5 samples from the MR 79 Cruise and 4 samples from the MR 83 Cruise) shows significant differences. A lower clay content (35-80%) with an important silt fraction and a constant presence of sand characterized the MR 79 dust samples. Conversely, higher clay content (70-90%), scarce silt and rare sand particles were found in the MR 83 samples. More appreciable silt amounts were collected during the episode of direct transport (samples 8 and 9).

The mineralogy of mesh-collected dusts shows that the finest components (less than  $2 \mu\text{m}$  fraction) are in order of decreasing abundance: low-crystalline illite, poorly organized smectite, kaolinite, chlorite and palygorskite. Among the coarsest components were recognized: quartz (the most abundant non-clay mineral), calcite, dolomite, feldspars and occasionally hematite, amphibole, talc and analcyme.

The most remarkable difference between the mineralogy of two series of dust samples is the variable illite/smectite ratio and the kaolinite content. During the MR 79 Cruise illite prevails, whereas in the MR 83 Cruise higher smectite and kaolinite amounts have been recognized (Fig. 7). This significant compositional change was related to the mentioned variations of average energy level. Given the dominant wind direction (from the NW in two

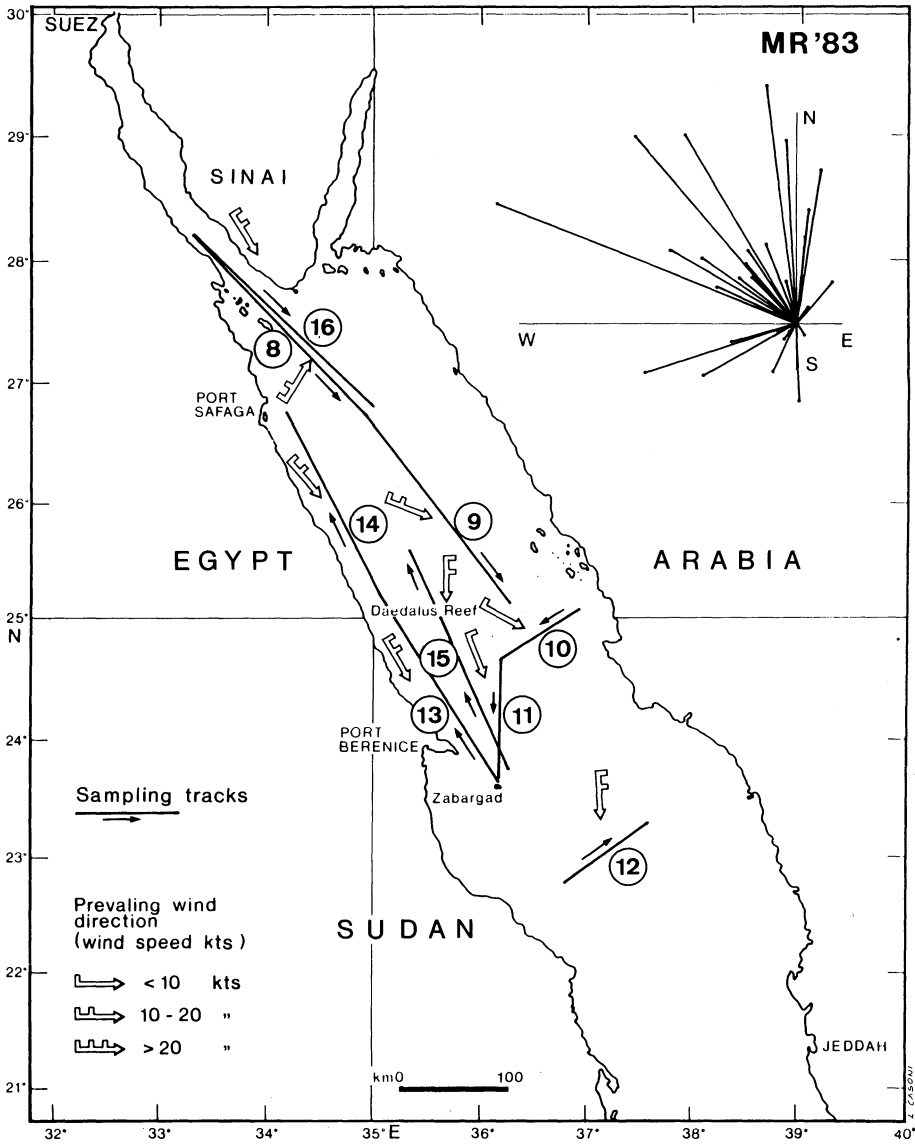


Fig. 3 - Dust sampling tracks, wind directions and diagram of the true wind measured on board during the Cruise MR 83 (Mar 1983).

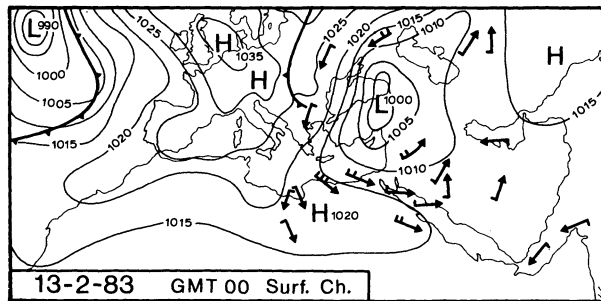
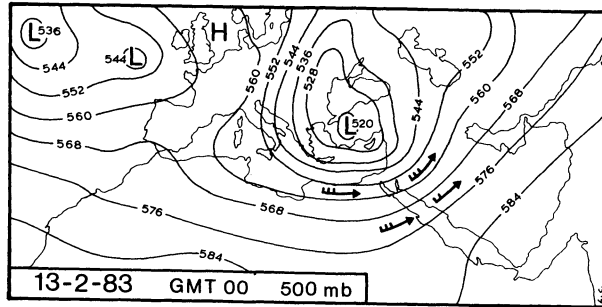


Fig. 4 - Meteorological conditions on 18 February 1983 at the 500 mb (A) and at sea level (B) (from Europ. Wetterb. Deutsch. Wetterdienstes).

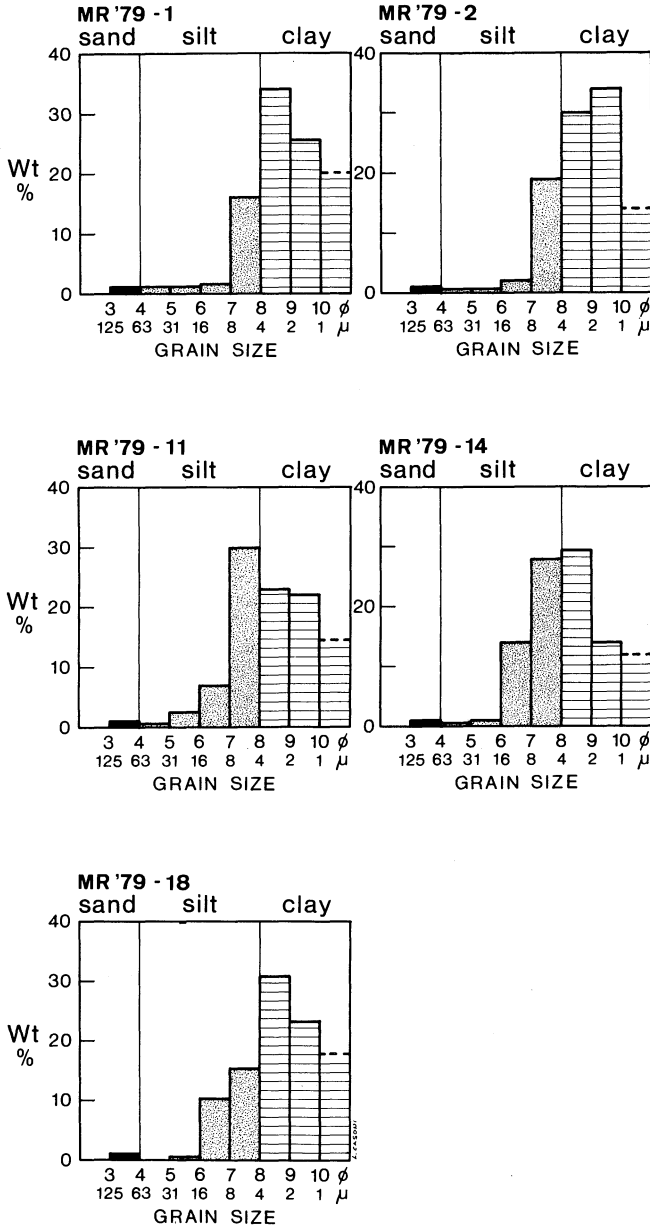


Fig. 5 - Grain-size distribution of dust samples collected at seawater-air interface during the MR 79 Cruise.

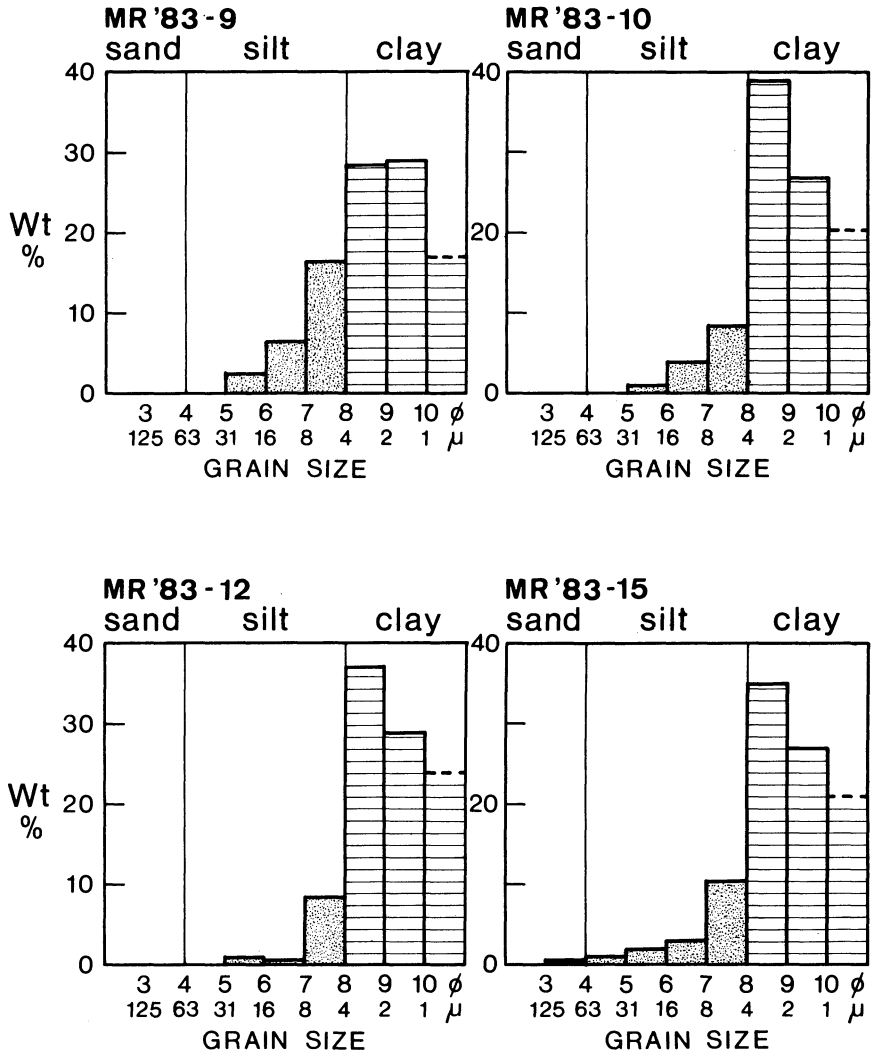


Fig. 6 - Grain-size distribution of dust samples collected at seawater-air interface during the MR 83 Cruise.

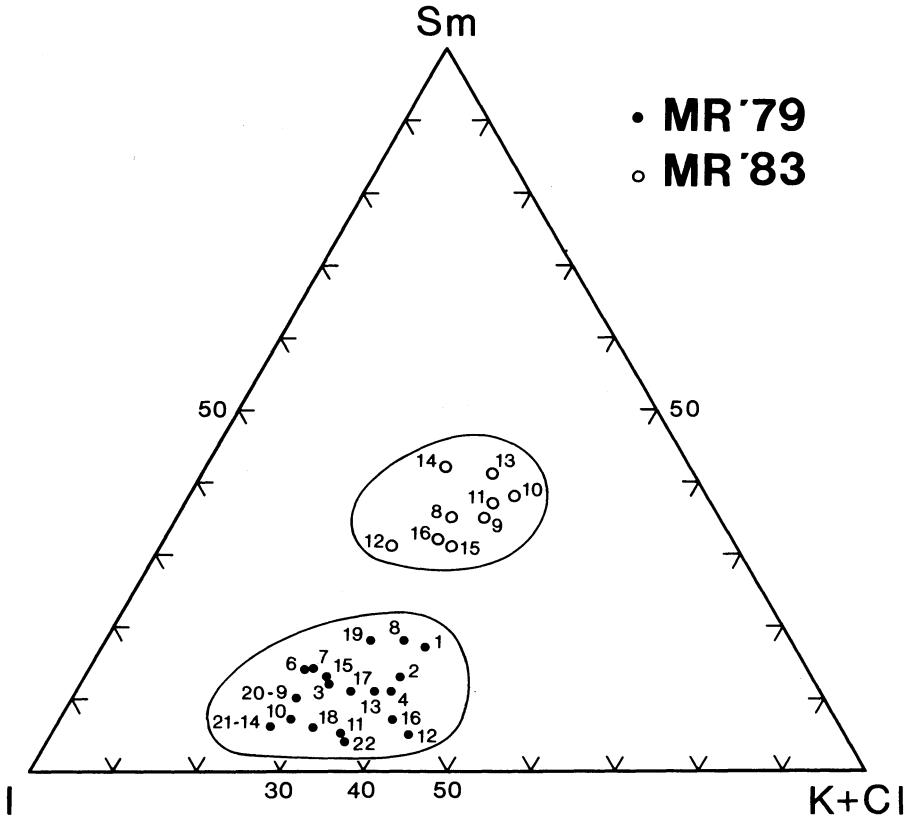


Fig. 7 - Clay mineralogy of the finest components (less than 2  $\mu\text{m}$  fraction) of the eolian dusts over the Red Sea. Sm: smectite; I: illite; K: kaolinite; Ch: chlorite.

different spring seasons) and the prevailing indirect transport of suspended materials (compare the meteorological conditions), an important change in atmospheric dynamics seems in fact much more effective than a possible supply from different source areas. The different situations are depending on the values of the true wind reported in the vectorial diagrams of Fig. 1 and 3. It follows that during the first dust collection (MR 79 Cruise), higher amounts of silts (and relatively more sand) were transported over the Red Sea, as supported by the grain-size distribution (Fig. 5). In addition the finest particles were transported far away from the high-level energy of the wind. The clay mineralogy of the atmospheric dust probably reflects the grain-size distribution of the flying particles. In particular, smectite particles are the finest among the clay minerals (Grim, 1968) and seem to behave as natural tracers in the atmosphere, as they do in the marine environment (Gibbs, 1977; Curzi and Tomadin, 1987). During the second sampling (MR 83 Cruise) indeed the lower average wind speed favoured the settling of the smallest particles. Higher amounts of clay-sized particles (Fig. 6) and a relevant smectite content characterize in fact the wind-borne dust (see Fig. 7) of spring 1983.

The location of sampling tracks greatly affects the mineralogy of the atmospheric dust. Samples collected in the far offshore (compare MR 83 Cruise) show a higher carbonate and kaolinite content (tracks 9, 10 and 16 of Fig. 3); while those collected closer to the shoreline (tracks 13 and 14 of Fig. 3) are richer in smectite and hematite. Feldspars, amphyboles and chlorite recognized in the dust SE of Zabargad Island (leeward tracks) are probably supplied from a local source (igneous and metamorphic formations outcropping in the eastern Egypt and Sudan). In addition, the atmospheric dust at the seawater-air interface of the Red Sea exhibits a gradual trend of mineral concentrations depending on the latitude. A southward increase in smectite, palygorskite and chlorite was observed, together with a parallel decrease in illite, calcite, dolomite and feldspars.

The whole composition of the windborne dust over the Red Sea is very close to that of African source (Lange, 1975; Sarnthein, 1979; Yaalon and Ganor, 1979; Prospero, 1981). The prevailing northwesterly winds and the above mentioned mineralogy give therefore evidence of an eolian supply from the African desert to the Red Sea. Occasional winds blowing from the East in springtime (compare Fig. 1 and 3) let us suppose, however, a moderate contribution of atmospheric dust from Arabian source.

The morphology of the surrounding areas plays an important role in controlling the mineralogy of the eolian dust. The high mountain chain bordering the western rim of the Red Sea is responsible for the mentioned differences between far-to-shore and close-to-shore collected samples, depending on a sort of "barrier action" produced by the chain, transversal to the wind flow (Pye, 1987). In addition, the break off of the chain in correspondence with the Zabargad Fracture Zone (Bonatti et al., 1984) favours the wind blowing from NW and the transport of material from local sources (eastern Egypt and Sudan).

The comparison between the mineralogy of atmospheric dusts and



that of marine sediments of the Red Sea gives more detailed information on the provenance of the materials. During Plio-Pleistocene abundant clastic sediments were introduced into the basin from a metamorphic and igneous Sudan source area (Stoffers and Ross, 1974). Nevertheless the present investigation points out to a considerable contribution of wind transported materials to the surficial sediments of the Red Sea. The occurrence of palygorskite, already recognized in the sediments of this region (Heezen et al., 1965) and whose origin was unknown so far, appears significant in this respect. The hypothesis of a diagenetic origin of palygorskite was already rejected by Stoffers and Ross (1974). The presence of diffuse laths and aggregates of palygorskite (Fig. 8 and 9) in the eolian dust over the Red Sea, testifies now the windborne transport of this mineral from a continental source, f.i. from Southern Arabia (Muller, 1961; Millot, 1964).

#### 4 - ELEMENTAL COMPOSITION

Major element composition of collected dust samples is reported in Tab. 1 and 2. The observed differences are strictly related to the above discussed variations in mineralogy. The sample distribution in the ACF and (Al/3-K) vs. (Al/3-Na) diagrams (respectively in Fig. 10 and 11) clearly shows the evolution of MR 83 dusts towards Al-rich clayey compositions; high Ca and Mg contents are reliable to carbonate presence.

Compared with the data reported by Chester et al. (1985) the present atmospheric Al loadings (max value 31800 ng/m<sup>3</sup>) are higher than the previous recorded values for the Red Sea and the Northern Arabian Sea (respectively 2200 and 20300 ng/m<sup>3</sup>) and close to the highest Al concentrations found for marine regions (Eastern Atlantic, North-east trade winds from Saharan reservoir, 50000 ng/m<sup>3</sup>).

In spite of different major element compositions, MR 79 and MR 83 dust samples are characterized by similar trace element contents. From this it could be deduced that the trace elements are not depending on grain-size and mineralogy. We suggest that part of these elements, characterized by  $EF_C$  higher than 1, are related to anthropogenic pollutants perhaps in oxide form or surface-adsorbed on mineral fraction (Chester et al., 1986). On the basis of crustal enrichment factors ( $EF_C$ , Tab. 3) a crustal source ( $EF_C \leq$

1) is mainly responsible of soil-sized particles, and an anthropogenic one is playing a prevalent role in controlling Pb transition elements such as Cr and Cu.

The transport of pollutants metals from the atmosphere to the sea surface, assuming a 1 cm sec<sup>-1</sup> deposition velocity (Junge, 1963), ranges from 405 to 1080  $\mu\text{g}/\text{cm}^2/10^3$  years for Cr and from 720 to 1730  $\mu\text{g}/\text{cm}^2/10^3$  years for Pb. These Pb values are in broad agreement with the data reported for ETNA 80 dusts (1600  $\mu\text{g}/\text{cm}^2/10^3$  years, Arnold et al., 1983), whilst Cr shows the highest recorded values, the previous data for Cr transport being lower than 100  $\mu\text{g}/\text{cm}^2/$  years (ETNA 80 and PHY 80 Cruises, Arnold et al., 1983).

TABLE 1

## RED SEA '79 DUSTS: ELEMENTAL COMPOSITION

Sample	79-1	79-2	79-3	79-4	79-5	79-6	79-7	79-8	79-9	79-10	79-11	79-12
Al <sub>2</sub> O <sub>3</sub>	10.80	11.26	12.01	11.56	11.80	9.81	12.56	11.02	12.53	10.07	10.81	9.50
Fe <sub>2</sub> O <sub>3</sub>	5.50	4.91	7.55	7.15	5.87	5.92	6.12	6.97	5.59	7.44	6.70	6.57
MgO	5.17	5.90	3.40	3.48	1.64	2.25	0.29	3.15	3.08	3.86	4.41	4.40
CaO	13.04	13.22	1.68	2.33	2.98	3.63	2.94	3.87	7.14	3.50	7.67	5.34
Na <sub>2</sub> O	1.36	1.30	2.00	1.96	6.71	3.35	6.76	3.30	1.56	2.20	2.38	2.67
K <sub>2</sub> O	1.47	1.25	2.02	1.73	1.94	4.01	2.64	2.94	1.49	1.76	1.83	1.80
Co ppm	20	25	22	31	27	30	28	22	35	32	27	28
Cr	150	210	120	105	118	116	150	102	96	105	120	205
Cu	65	80	60	110	65	100	80	72	88	76	110	105
Mn	205	190	210	200	90	108	96	108	120	210	270	260
Ni	89	105	100	120	105	96	90	70	85	76	78	92
Ti	5395	6894	7194	7074	7554	5755	4436	6415	6894	7074	5395	5156
V	120	200	135	150	160	160	192	189	190	220	185	190
Sample	79-13	79-14	79-15	79-16	79-17	79-18	79-19	79-20	79-22	$\bar{x}(21)$	s.d.	
Al <sub>2</sub> O <sub>3</sub>	11.26	12.30	8.90	10.96	10.12	11.56	9.50	12.36	13.10	11.28	1.32	
Fe <sub>2</sub> O <sub>3</sub>	5.86	6.35	5.50	7.09	5.70	5.28	5.69	6.06	5.50	6.16	0.75	
MgO	4.90	4.96	5.26	4.43	4.04	3.72	4.06	3.64	3.79	3.80	1.28	
CaO	3.65	10.95	5.35	3.75	4.33	7.31	7.80	4.30	2.72	5.60	3.37	
Na <sub>2</sub> O	1.86	2.80	1.58	5.56	1.61	1.36	1.70	1.79	1.22	2.62	1.95	
K <sub>2</sub> O	1.47	1.93	1.38	3.06	1.60	1.59	1.59	1.80	1.75	1.95	0.67	
Co ppm	30	30	28	31	30	30	25	40	22	28	5	
Cr	106	200	100	85	105	210	208	160	195	141	45	
Cu	85	93	80	105	92	65	110	60	88	85	17	
Mn	208	210	160	190	205	208	190	195	186	182	50	
Ni	76	85	70	80	110	78	90	110	85	90	14	
Ti	5276	5515	5755	7074	5156	6295	6415	6595	5156	6113	882	
V	205	180	190	210	215	150	210	160	188	181	27	

TABLE 2

## RED SEA '83 DUSTS: ELEMENTAL COMPOSITION

Sample	83-8	83-9	83-10	83-11	83-12	$\bar{x}(5)$	s.d.	83-13	83-14	83-15	$\bar{x}(3)$	s.d.
Al <sub>2</sub> O <sub>3</sub>	20.55	16.01	13.43	16.68	13.90	16.11	2.83	19.35	17.30	14.38	17.01	2.50
Fe <sub>2</sub> O <sub>3</sub>	6.38	5.10	4.40	4.43	4.88	5.04	0.81	6.91	6.91	5.50	6.44	0.81
MgO	2.81	2.90	2.92	3.26	4.31	3.24	0.62	2.49	2.81	3.34	2.88	0.43
CaO	0.08	8.08	2.95	5.65	12.10	7.74	5.19	0.29	0.99	8.09	3.12	4.31
Na <sub>2</sub> O	0.38	0.35	0.24	0.24	0.20	0.28	0.08	0.69	0.27	0.35	0.44	0.22
K <sub>2</sub> O	0.83	0.75	1.08	0.69	1.26	0.92	0.24	0.76	0.72	0.71	0.73	0.03
Cr ppm	123	149	191	219	180	172	37	n.d.	595	262	429*	235
Cu	69	48	46	191	38	78	64	n.d.	174	58	116*	82
Mn	377	347	400	354	408	377	27	339	500	547	462	109
Ni	37	44	48	48	49	45	5	n.d.	129	87	108*	30
Pb	138	86	163	72	n.d.	115**	43	1827	n.d.	n.d.	1827***	-
Ti	4038	4776	4780	4766	4714	4615	324	n.d.	6699	4595		1488

\* = average of 2 samples; \*\* = average of 4 samples; \*\*\* = only one value; n.d. = not determined;  
 83-8/83-12 = RED SEA '83, South-track; 83-13/83-15 = RED SEA '83, North-track.

TABLE 3

CRUSTAL ENRICHMENT FACTORS ( $EF_C$ ) OF RED SEA '83 & '79 DUSTS COMPARED WITH PUBLISHED DATA.

	1	2	3	4	5	6	7	8	9	10	11
Fe	.87	1.00	.80	1.78	1.50	1.30	.90	.90	.60	.73	1.05
Ca	.48	.60	2.55	.49					1.29	.49	1.32
Mg	.68	.74	1.22	1.27					.81	.68	1.36
Na	.97	.25	.44	.77					.08	.13	1.14
K	1.09	1.30	1.57	.58					.35	.27	1.07
Ti	1.00	.78	1.29	1.41				1.07	.79	.91	1.48
Co	.84	.44	1.56	1.34	1.90	.13	1.60	.78			1.54
Cr	3.90	1.70	2.41	2.88	6.10	5.40	2.40	1.67	1.66	3.92	1.94
Cu	1.52	1.17	2.65	1.83	25.00		7.00	1.72	1.37	1.92	2.13
Mn	.96	.76	1.13	1.09				.70	.38	.44	.26
Ni	2.43	1.68	3.24	2.91				1.43	.58	1.32	1.65
Pb					2000	1300	1300	390	8.88	133.66	
V	.78	.26	.18	.33				1.02			1.85

$EF_C = (X/Al)_{DUST} / (X/Al)_{CRUST}$ : Average crust composition from TAYLOR (1964).

1 = BAN 80 dusts (MAZZUCOTELLI et al., 1986); 2 = EOLO 81-1 sea collected dusts (TOMADIN et al., 1984); 3 = EOLO 81-1 land collected dusts (TOMADIN et al., 1984); 4 = EOLO 81-2 dusts (TOMADIN et al., 1984); 5 = ETNA 80 dusts (ARNOLD et al., 1983); 6 = PHY 81 dusts (ARNOLD et al., 1983); 7 = North Atlantic dusts (BUAT-MENARD & CHESSELET, 1979); 8 = Atlantic dusts of Saharan provenance (GLACCUM, 1978); 9 = RED SEA '83 dusts, South-track; 10 = RED SEA '83 dusts, North-track; 11 = RED SEA '79 dusts.

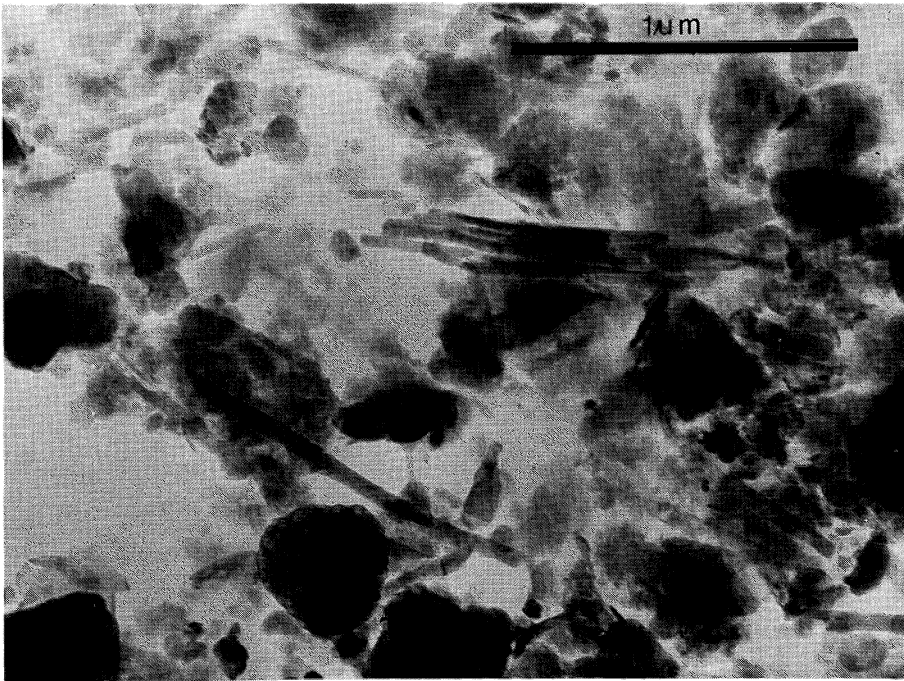


Fig. 8 - Transmission electron micrograph of palygorskite lath of the less than 2  $\mu\text{m}$  fraction in the MR 83-15 dust sample.

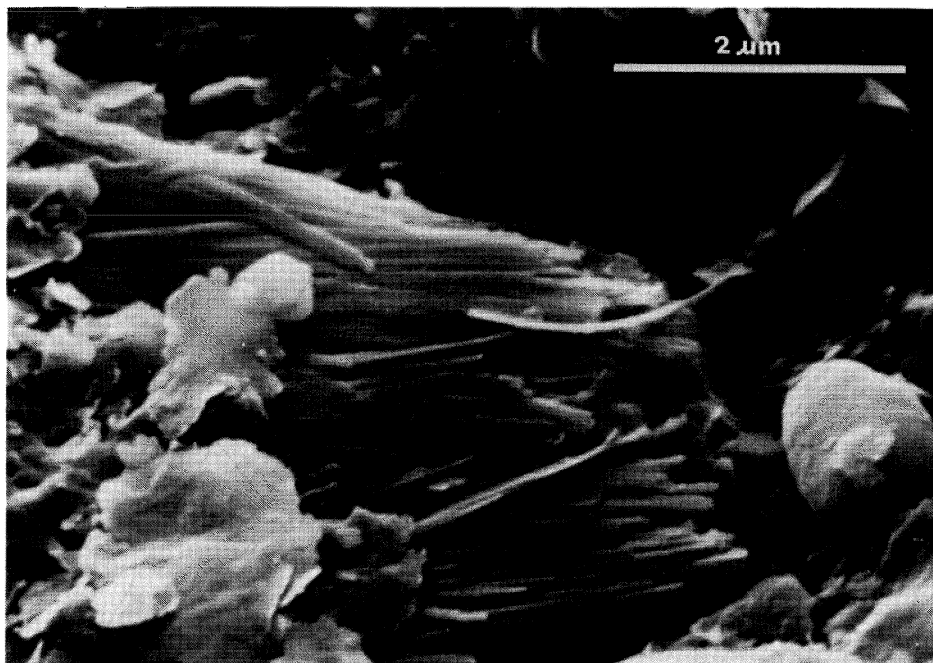


Fig. 9 - Scanning electron micrograph of fibrous palygorskite, exagonal kaolinite and rounded quartz in the MR 83-12 dust sample.

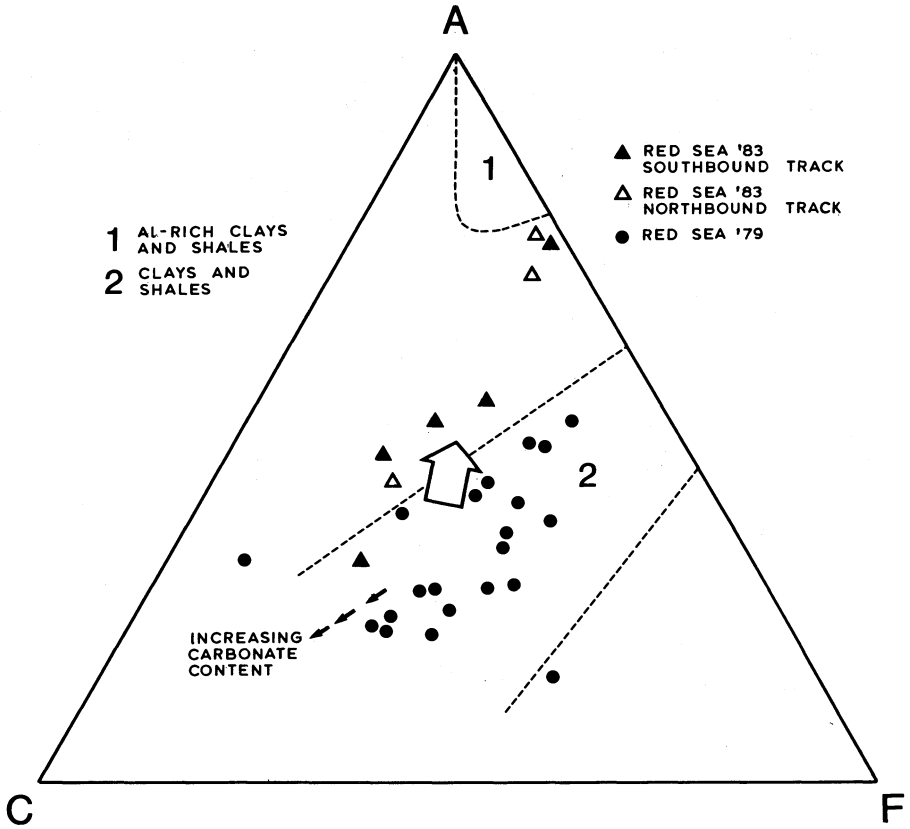


Fig. 10 - Red Sea 79 and 83 eolian dusts on the ACF diagram (Winkler, 1967); the big arrow shows the evolution of the Red Sea 83 dusts towards Al-rich compositions.

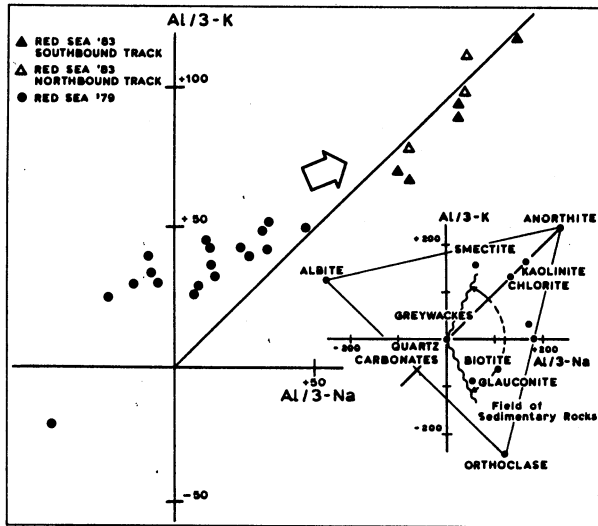


Fig. 11 - Red Sea and 83 dusts on the (Al/3-K) vs. (Al/3-Na) diagram (De La Roche, 1968). The Red Sea 83 samples plot near the clay mineral representing point show a compositional evolution (big arrow).

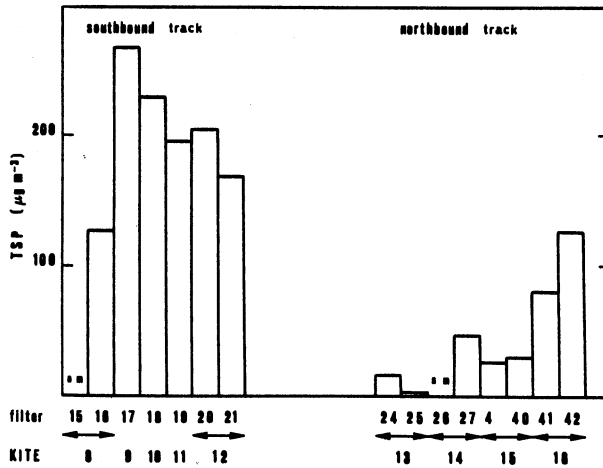


Fig. 12 - Total suspended particulate matter collected during the MR 83 Cruise. KITE numbers correspond to the mesh samples along the tracks of Fig. 3. (nm: not measured).



## 5 - TOTAL SUSPENDED PARTICULATE AND SOLUBLE FRACTION

The amounts of the total suspended particulate (TSP) during the MR 83 Cruise is shown in Fig. 12. The TSP loading is much higher during the southward track with respect to the northward one, and increases approaching the coast (Filters 41 and 42, corresponding to mesh sample 16 of Fig. 3).

Most of the atmospheric particulate consists of soluble materials collected during the northward tracks (Kite 14, 15 and 16 of Fig. 13) in dependence on ship movement against the wind (see Fig. 3); on the contrary, insoluble particulate prevails along the southward track.

$\text{Na}^+$  and  $\text{Cl}^-$  are the major components of TSP soluble fraction (Fig. 14) with minor  $\text{Ca}^{2+}$  and  $\text{SO}_4^{2-}$  presence. Small percentages of  $\text{K}^+$ ,  $\text{Mg}^{2+}$  and  $\text{NO}_3^{2-}$  ions were also detected. Negligible amounts of  $\text{NH}_4^+$  are present in the 22, 27 and 41 samples.

## 6 - AEROBIOLOGICAL ANALYSIS

In spite of the small amounts normally present in the atmospheric particulate, the biological particles can be considered as a good atmospheric tracer, especially when the vegetation is blossoming as during the sampling period. According to Horvat et al. (1974); Zohary (1973); Tutin et al. (1964) and Pignatti (1982), the prevailing vegetation of the Mediterranean and Red Sea regions is reported in Fig. 15. In fact, the potential sources which mainly affect the collected samples are located NW of the sampling areas. The contribution of PALMAE (average 0,5 pollens/ $\text{m}^3$ ) and CHENOPODIACEAE (average 0,2 pollens/ $\text{m}^3$ ) can be assigned to the Saharan-Arabian region (Egypt and southern Mediterranean), whereas BETULACEAE (average 0,05 pollens/ $\text{m}^3$ ) and CORYLACEAE have their origin in the northern Mediterranean and European regions. The size of pollens grains is ranging from 10 to 30  $\mu\text{m}$ , with an average diameter of 20-22  $\mu\text{m}$ . Pollens of higher size (50-200  $\mu\text{m}$ ), usually present in the atmosphere, were not found over the Red Sea, probably due to their sedimentation velocity. The histogram of Fig. 16 shows that the pollen concentrations decrease with the latitude and does not seem to be affected by the distance from the coast (compare the pollen/ $\text{m}^3$  ratio - Fig. 16 - and the number of pollen grains collected on each filter - Fig. 17 - with the location of the sampling tracks of Fig. 15).

With wind blowing from N-NW, a long range transport of pollens prevails, whereas the contribution of blossoming species from the African coast is scarce.

## 7 - CONCLUSIONS

The mineralogical-, grain size-, chemical- and biological data presented in this paper provide a first insight into the nature, the composition and the provenance of atmospheric dust collected in springtime over the Red Sea.

In spite of the poor collection efficiency for submicron particles, the mesh sampling of dust is at present the only method permitting to collect enough material for sedimentological

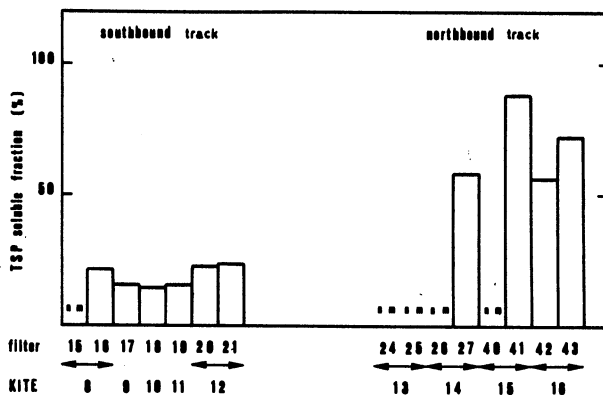


Fig. 13 - Soluble fraction of the suspended particulate matter reported in Fig. 12. (nm: not measured).

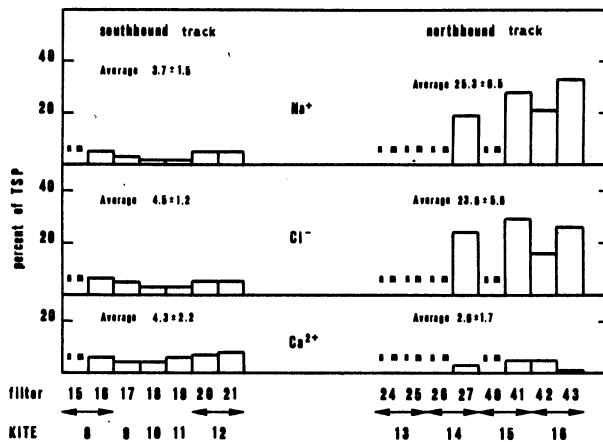


Fig. 14 - Na<sup>+</sup> and Cl<sup>-</sup> content of the suspended particulate matter reported in Fig. 12. (nm: not measured).

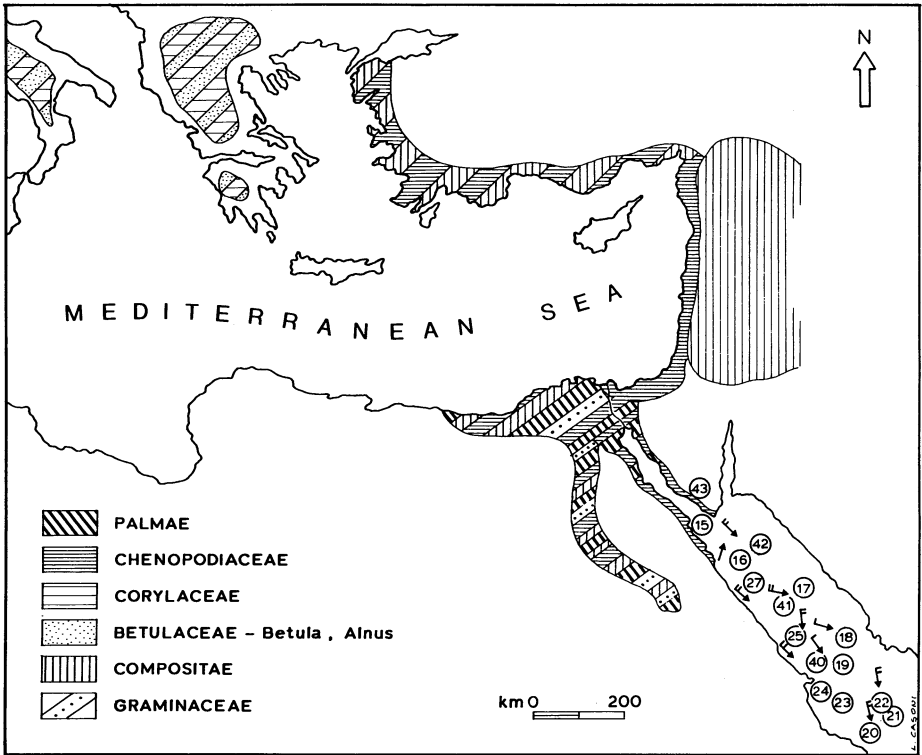


Fig. 15 - Areal distribution of dominant vegetal species whose pollens have been collected over the Red Sea. The filter numbers reported on the right are related to the sampling tracks.

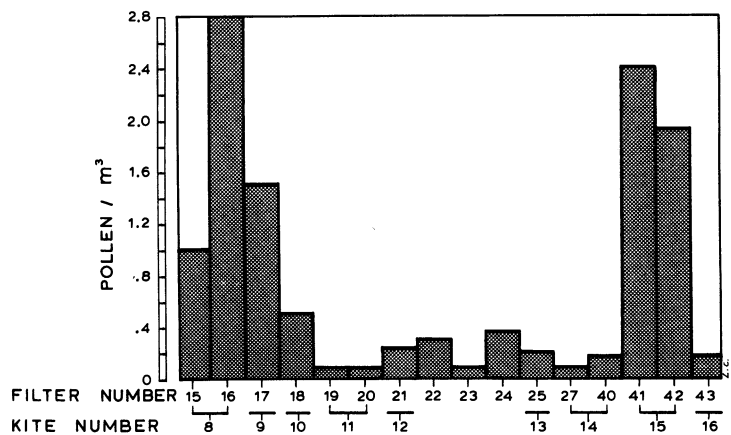


Fig. 16 - Histogram of the different concentrations of pollen species depending on sampling tracks of Fig. 3.

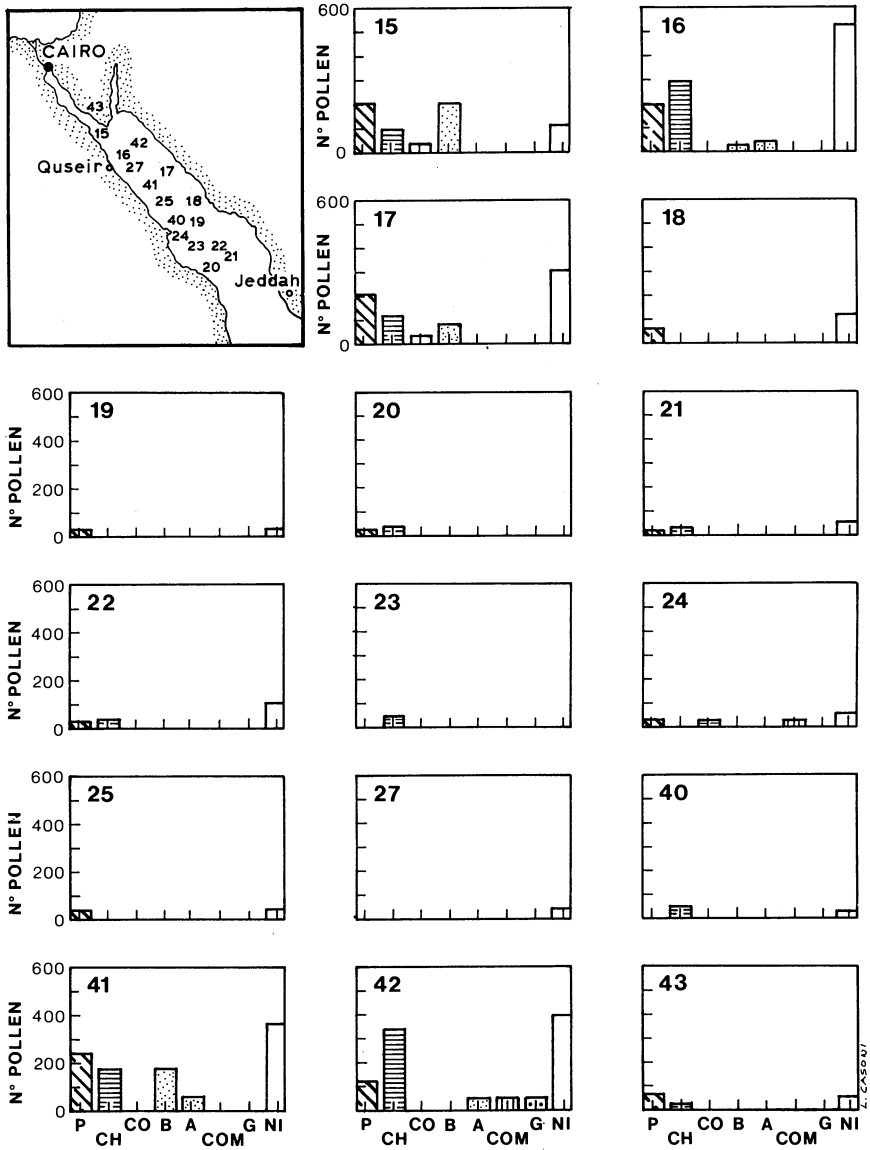


Fig. 17 - Histograms showing the number of airborne pollen grains collected on the filters. The pollen code is reported on the bottom. P: Pinus; CH: Chenopodiaceae; CO: Corilaceae; B: Betula; A: Alnus; COM: Compositae; G: Gramineae; NI: not identified.

analyses. However, in order to obtain reliable information on TSP (and also for aerobiological research), high-volume filters were used.

The meteorological conditions during the sampling periods (Feb - Mar 1979 and Mar 1983) were characterized by indirect transport of atmospheric suspended materials by prevailing northwesterly wind. The relative mass concentrations give evidence of variable but appreciable values, which are still subordinate to concentrations measured during a moderate episode of direct transport (at the beginning of the MR 83 sampling). The grain-size distribution of the dust shows a lower clay content and an important silt fraction during the MR 79 sampling. A dominant clay content is, on the contrary, present in the MR 83 samples. The clay mineralogy and mainly the illite/smectite ratio reflects the grain-size distribution of the suspended particles. These patterns were interpreted in terms of the variable atmospheric dynamics during the two different samplings. With higher wind energy (MR 79 Cruise) the finest clay particles (smectites) were transported far away behaving as natural tracers in the atmosphere.

The mineral distribution shows not only characteristics trends depending on the latitude but also clear differences between dust samples collected farther-to-shore and those collected closer-to-shore (see MR 83 Cruise). In addition to factors such as meteorological conditions and variable energy levels, also the land morphology plays a primary role in controlling the mineralogy of the eolian dust. It consists in a "barrier action" produced by the chain along the western rim of the Red Sea, which is responsible for the different mineral distribution far- and close-to-shore. Moreover, the break off of the coastal chain in correspondence of the Zabargad Fracture Zone, favours the transport by northwesterly wind of dust particles from a local source (eastern Egypt and Sudan).

The comparable meteorological and transport conditions of suspended matter in springtime of the two sampling periods, permit to recognize a prevailing eolian supply of African provenance, even if a moderate contribution of dust of Arabian source cannot be excluded.

The major element chemistry of insoluble particulate reflects the variations observed in the mineralogy and in the grain-size distribution; on the contrary, trace elements are mainly related to anthropogenic pollutants. Between them, Cr and Pb show high transport rates. The soluble fraction, appreciated as 25-70% of the total suspended particulate is controlled by the direction of the prevailing winds.

The pollen concentration of most widespread species points out the long-range transport from the Mediterranean and south European source areas to the Red Sea, superimposed to a closer provenance from the Saharan - Arabian regions.

#### ACKNOWLEDGEMENTS

Authors are indebted to J. Prospero for making his data available and for fruitful discussion.

Thanks also to R. Sartori for stimulating criticism of the text, to L. Casoni for his draughtsmanship and to the captains, officers and crew of the vessels Salernum and Bannock for their collaboration in sampling operations.

## REFERENCES

- ARNOLD M., SEGHAIER A., MARTIN D., BUAT-MENARD P. and CHESSELET R., 1983 - Géochimie de l'aérosol marin au-dessus de la Méditerranée Occidentale. Vies Journées Etud. Pollutions, Cannes, CIESM, 27-38.
- BONATTI E., COLANTONI P., DELLA VEDOVA B. and TAVIANI M., 1984 - Geology of the Red Sea transitional region (22 N - 25 N). *Oceanologica Acta*, 7, 4, 385-398.
- BUAT-MENARD P. and CHESSELET R., 1979 - Variable influence of the atmospheric flux on the trace metal chemistry of oceanic suspended matter. *Earth Planet. Sci. Lett.*, 42, 399-411.
- BUTZER K.W., 1960 - Dynamic climatology of large-scale European circulation patterns in the Mediterranean area. *Meteor. Rsch*, 13, 97-105.
- CHESTER R., 1986 - The marine mineral aerosol. In: *The role of air sea exchange in geochemical cycling*. (Buat-Menard P. Ed.), Reidel, Dordrecht, 443-476.
- CHESTER R., SHARPLES E. J. and SANDERS G.S., 1985 - The concentrations of particulate aluminium and clay minerals in aerosols from the Northern Arabian Sea. *J. Sediment. Petrol.*, 55, 1, 37-41.
- CHESTER R., MURPHY K.J.T., TOWNER J. and THOMAS A., 1986 - The partitioning of elements in crust-dominated marine aerosols. *Chem. Geol.*, 54, 1-15.
- FLOHN H., 1965 - Klimaprobleme am Roten Meer. *Erdkunde*, 19, 179-191.
- GALLIGNANI P. and MAGAGNOLI A., 1972 - Metodologie e tecniche di Sedimentologia fisica. Rapp. Tecnico N. 1, Lab. Geol. Marina, CNR, Bologna, 34 p.
- GIBBS R.J., 1977 - Clay mineral segregation in the marine environments. *J. Sediment. Petrol.*, 47, 1, 237-243.
- GLACCUM R.A., 1978 - The mineralogy and elemental composition of mineral aerosols over the tropical North Atlantic: influence of Saharan dusts. Thesis, Miami University, 161 p.
- GRIM R.E., 1968 - Clay mineralogy. 2<sup>d</sup> Ed., Mc Graw-Hill, New York, 384 p.
- HASTENRATH S., 1985 - Climate and circulation of the tropics. Reidel Pub. Co., Dordrecht, 644 p.
- HEEZEN B.C., NESTEROFF W.D., OBERLIN A. and SABATIER G., 1965 - Découverte d'attapulgit dans les sédiments profonds du Golfe d'Aden et de la Mer Rouge. *C.R. Acad. Sc. Paris*, 260, 9, 5819-5821.
- HORVAT J., GLAVAC V. and ELLENBERG H., 1974 - Vegetation Sudosteuropas, G. Fisher Ed., Stuttgart, 768 p.
- JUNGE C.E., 1963 - Air chemistry and radioactivity. Academic Press, New York, 328 p.

- JUTZE G.A. and FOSTER K.E., 1967 - Recommended standard method for atmospheric sampling of fine particulate matter by filter media high-volume sampler. *JAPCA*, 17-25.
- LANGE H., 1975 - Herkunft und Verteilung von Oberflächensedimenten des westafrikanischen Schelfs und Kontinentalhanges. *Meteor. Forsch. Ergebn.*, C 22, 61-84.
- LA ROCHE H. de, 1968 - Comportement géochimique différentiel de Na, K et Al dans les formations volcaniques et sédimentaires: une guide pour l'étude des formations métamorphiques et plutoniques. *C. R. Acad. Sci. Paris*, 267, série D, 39-42.
- MAZZUCOTELLI A., FRACHE R., DADONE A. and BAFFI F., 1976 - Ion-exchange separation and atomic absorption determination of fifteen major, minor and trace elements in silicates. *Talanta*, 23, 879-882.
- MAZZUCOTELLI A., VALERIO F., BRESIANINI C. and FRACHE R., 1988 - Seasonal variation of Tl, Pb and Cr concentrations in airborne particulate matter collected in an urban area. *Sci. Total Environ.* (in press).
- MILLOT G., 1964 - *Geologie des Argiles*. Masson et Cie., Paris, 499 p.
- MULLER G., 1961 - Palygorskit und Sepiolith in tertiären und quartären Sedimenten von Hadramaut (S-Arabien). *Neues Jahrb. Mineral. Abhandl.*, 97, 275-288.
- PIGNATTI S., 1982 - *Flora d'Italia*, 5 vol., Edagricole, Bologna.
- PRODI F., SANTACHIARA G. and OLIOSI F., 1983 - Characterization of aerosols in marine environments (Mediterranean, Red Sea, and Indian Ocean). *J. Geophys. Res.*, 88, 10597-10968.
- PROSPERO J.M., 1981 - Eolian transport to the world ocean. In: *The oceanic lithosphere* (C. Emiliani Ed.). *The Sea*, 7, Wiley, New York, 801-874.
- PYE K., 1987 - *Aeolian dust and dust deposits*. Academic Press, London, 334 p.
- SARNTHEIN M., 1979 - Indicators of continental climates in marine sediments, a discussion. *Meteor. Forsch. Ergebn.*, C 31, 49-51.
- SIMMONS G.M., 1959 - The photo-extinction method for the measurement of silt-sized particles. *J. Sediment. Petrol.*, 29, 233-245.
- STOFFERS P. and ROSS D.A., 1974 - Sedimentary history of the Red Sea. In: Whitmarsh R. B., Weser O. E., Ross D. A. et al., *Initial Reports of the DSDP*, 23, Washington, 849-865.
- TAYLOR S.R., 1964 - Abundance of chemical elements in the continental crust: A new table. *Geochim. Cosmochim. Acta*, 28, 1273-1285.
- THOMPSON B. W., 1970 - *The climate of Africa*. Oxford Univ. Press., 132 p.
- TOMADIN L., LENAZ R., LANDUZZI V., MAZZUCOTELLI A. and VANNUCCI R., 1984 - Wind-blown dusts over the Central Mediterranean. *Oceanologica Acta*, 7, 1, 13-23.
- TUTIN T. G., HAYWOOD V. H., BURGESS N. A., MOORE D.M., VALENTINE D.H., WALTERS S. M. and WEBB D.A., 1964 - *Flora europea*, 5 vol., University Press, Cambridge.
- WINKLER H.G.F., 1967 - *Petrogenesis of metamorphic rocks*. Springer Verlag, New York, 237 p.
- YAALON D.H. and GANOR E., 1979 - East Mediterranean trajectories



- of dust-carrying storms from the Sahara and Sinai. In:  
Saharan dust. Mobilization, transport, deposition. Scope 14  
(C. Morales Ed.), Wiley, New York, 187-193.
- ZOHARY M., 1973 - Geobotanical foundations of the Middle East, 2  
vol., G. Fischer Ed., Stuttgart.

L. Tomadin - Istituto di Mineralogia e Petrografia  
Università di Urbino  
via M. Oddi, 14 - 61029 URBINO

G. Cesari

S. Fuzzi

A. Lobietti

P. Mandrioli - Istituto FISBAT del CNR  
via dei Castagnoli, 1 - 40126 BOLOGNA

V. Landuzzi

R. Lenaz - Istituto per la Geologia Marina del CNR  
via Zamboni, 65 - 40127 BOLOGNA

M. Mariotti - P.M.P. Sezione Chimica  
via Triachini, 18 - 40138 BOLOGNA

A. Mazzucotelli - Istituto di Chimica Generale  
Università di Genova  
viale Benedetto XV, 3 - 16132 GENOVA

R. Vannucci - Dipartimento di Scienze della Terra  
Sez. Mineralogia, Petrografia e Geochimica  
Università di Pavia  
via Bassi, 4 - 27100 PAVIA

# DESERT AEROSOL: CHARACTERISTICS AND EFFECTS ON CLIMATE

Guillaume A. d'Almeida  
University of Munich  
Theresienstr. 37  
8000 München 2, F.R. Germany

key words: desert dust, mineral aerosol, Saharan dust, source strength, deposition rate, radiative characteristics, aerosol optical properties, Sahara, Africa

## ABSTRACT

Major sources for crustal-derived aerosol are the earth's arid and semiarid regions. Soil size distributions of different locations in the Sahara have, therefore, been analysed and allow us to hypothesize a particle loss mostly for the size range of radius smaller than  $20 \mu\text{m}$  due to erosion. Cumulative mass distributions emphasize an apparent difference in the productivity of the soil types considered. Furthermore, the physical properties and radiative characteristics of desert dust such as size distribution, source strength, deposition rate, extinction, scattering, and absorption coefficients, single scattering albedo, asymmetry factor, and optical depth, that are relevant quantities required to estimate the aerosol impact on present day climate and likely to reconstruct the earth's past climate, have been observed or computed, and discussed. About 600–700 Tg of crustal material are mobilized from the Sahara and 1800–2000 Tg worldwide and injected into the atmosphere each year. A considerable part of that amount contributes to the sediments of the Atlantic, the Mediterranean, and the Pacific. Both computed and observed data indicate desert dust as one of most prominent aerosol types with the highest variability in its microphysical components as well as in its radiative characteristics, and the best absorber in the atmospheric transparency window. It has been pointed out that the presence of desert dust leads to a warming due to the absorption of solar radiation in the dust layer and above the dust layer, a corresponding cooling due to the backscattered solar radiation, and a challenging warming due to the absorption of the thermal infrared radiation below the dust cloud.

## 1. INTRODUCTION

Recent investigations by Sarnthein (1978) and Petit et al. (1981) have yielded the following remark: Geomorphological features and deep-sea core studies indicate that during the last glacial maximum, the southern hemisphere continents were drier and that active sand deserts between 30 degrees North and 30 degrees South were five times larger than today. This statement triggers the following crucial questions: How high are the source strength and the deposition rate of desert dust nowadays? Which role does desert dust play in the present climate? To what extent did the above-mentioned estimate of airborne mineral

dust influence the climate during the glacial maximum?

There exist, indeed, to date too few sensitivity studies on the impact of atmospheric aerosol on climate. Tanre et al. (1984) have used the so-called low-resolution model of the European Center for Medium Range Weather Forecast to show that the effect of aerosol on climate is significant for temperature but is comparable with the noise level for the dynamics. A further sensitivity study performed by Joseph (1977) using the General Circulation Model of the National Center for Atmospheric Research (NCAR - GCM) has indicated that the presence of desert aerosol in the atmosphere yields significant changes of the air temperature over the world's main deserts and over the Atlantic ocean, and a subsequent change in the vertical wind field and a perturbation in the meridional motion. With respect to the atmospheric dynamics, the study by Joseph (1977) leads to the knowledge that the presence of desert aerosol is sensitive over and outside the affected regions. These two investigations, regarded as tentative approaches, are indicative of the importance of atmospheric aerosol particles for climate and, likely, for the atmospheric synopsis.

Coming back to the statement by Sarnthein (1978) and Petit et al. (1981) and considering a recent paper by Shaw (1979a) which indicates that water-insoluble particles encountered in the Antarctic originate from arid and semiarid regions of the southern hemisphere, i.e. Australia, Kalahari Desert, and Atakama Desert, it can be concluded that the transport pattern has not changed at all over thousands of years. As far as the northern hemisphere is concerned, Ehrenberg (1862) and Semmelhack (1934) were the first observers to report on mineral dust fallout over the northern equatorial Atlantic. Carlson and Prospero (1972), Prospero and Carlson (1972), and Schütz (1980) have undertaken the task of estimating the source strength and the deposition rate of Saharan dust towards Barbados. In addition, Prospero (1979) and Prospero et al. (1981) have monitored the average mass concentration of mineral dust over different world oceans. Shaw (1980), Darzi and Winchester (1982), Uematsu et al. (1983), and Braaten and Cahill (1986) have inferred size, composition, mass concentration, and transport patterns from Asian dust events towards the Pacific ocean. All these investigations are, indeed, very useful in quantifying the aerosol mass loading of mineral dust and the amount of material deposited on snow or ice and in the lakes or the oceans as pelagic sediments. They have, however, the commonality of having been performed far away from the real source areas and are therefore likely to be biased, with respect to the aerosol properties in the source regions, as the physico-chemical properties of the dust may increasingly alter within the transport route. Measurements of source-related parameters responsible for wind erosion, mobilisation, and transport of mineral dust have been investigated for the Anglo American deserts only by Gillette (1974) and Gillette et al. (1980).

Any quantitative estimate on productivity and deposition rate of desert dust in the past is contingent upon the reliability to which the origin, the source, and the composition of the 'paleoaerosol' in deep-sea cores, as well as the feature of the modern-age aerosol have been investigated. Furthermore, a quantitative simulation of the aerosol impact on climate in the past requires the knowledge of the physico-chemical behavior of the source-relevant airborne particulate matter. There exist too few scientific reasons to believe that that behavior could have changed over the thousands of years. The present paper reports on measurements of relevant quantities near the source areas of Saharan dust performed between 1979 and 1984, discusses mandatory quantities required to estimate the mineral aerosol impact on present day climate, and outlines the climatic implications due

to the presence of desert dust in the atmosphere. The paper is intended to be both a review of previously published articles (19, 20, 21) and an addendum to them.

## 2. SOIL PRODUCTIVITY AND AEROSOL SIZE DISTRIBUTION

Discussion on the production of aerosol particles should be linked to their source, in order to distinguish between particles stemming from primary sources and those generated by secondary sources. As far as mineral aerosol is concerned, an analysis of soil samples taken in potential source regions is required. With respect to mobilisation and transport, it can be stated, with certainty, that particles with radius above  $100 \mu\text{m}$  are of minor importance. Only soil types and deposits having appreciable fraction of loose and fine grained material can be regarded as productive. A further important, more or less open, question in this connection relates to the types of soil that hold an appreciable fraction of fine material released in the atmosphere as aerosol particles and able to travel over long distances. With the aim of looking for a reliable answer to this question, soil samples have been taken in the whole Sahara and analysed. Figure 1 shows the location of the sampling sites.

- a) Matan is a small village in Senegal on the northeast border with Mauritania situated in the flood plain of the Senegal river. The soil sample of Matan belongs to the so-called alluvial land material.
- b) Goundam is located southwest of Timbuctu in Mali. Its sample is assumed to be representative of a flood plain material of the large Niger river depression.
- c) Dar Albeida is northeast of Timbuctu in Mali and has a dune material, typical of the large sand sea area of the great western central desert.
- d) Tamanrasset is situated in the foothills of the Hoggar mountains. Its sample is supposed to be a highly weathered mountain debris material.
- e) Achegour is located west of Bilma in Niger, in the gravelly soil plain of Tenere.
- f) The sample of the Nubian desert in the northern of Sudan is taken between Dongola and Karima (not shown in Fig. 1 to avoid an overloaded map) on the east side of the Nile.

All these samples are different in color, state of weathering, composition, and granulometry and are thought to represent, to a large extent, the geomorphological features of the soils in the Sahara. The samples have been analysed in terms of number, volume, and mass distributions. Preparation and evaluation procedures have been described in previous papers (22, 19). The differential mass distributions have been converted to cumulative mass distributions as the latter are well suited to indicating which type of soil is particularly affected by wind erosion.

The size of soil particles varies between  $0.02 \mu\text{m}$  and some  $1000 \mu\text{m}$  depending on the soil type. This size range is important as it reflects the smallest size expected for the size spectrum of a pure mineral aerosol. The fact that particles smaller than  $0.1 \mu\text{m}$  are ubiquitous in all soil samples analysed presumes the presence of this size range in the aerosol size distribution as well.

Figure 2 shows the cumulative mass distributions of the soil samples. Thereafter, the samples of Matan and Goundam claim about 70% and 98% of the particles

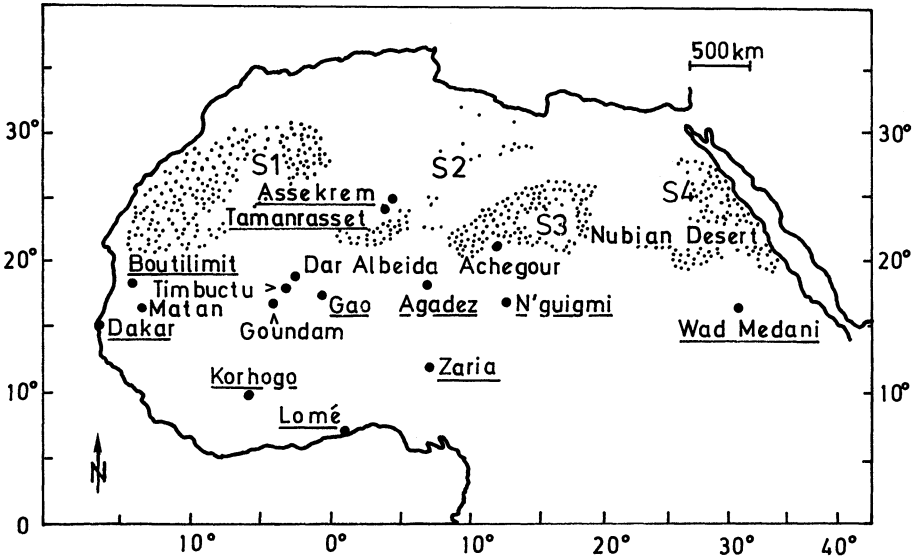


Figure 1:  
 Location of the soil and aerosol sampling sites, and the stations used in the framework of the African turbidity monitoring network (the ATMNI – stations are underlined).

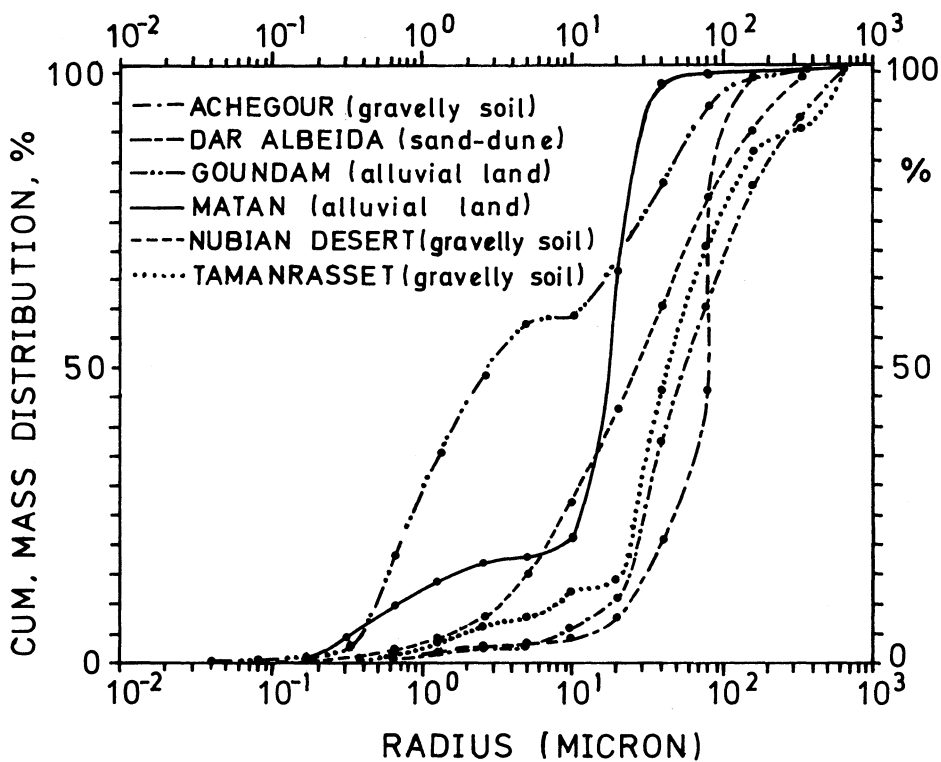


Figure 2:

Cumulative mass distributions of different soil types showing: a) the productivity (i.e. amount of soil wind erosion aerosol having the potential for long-range transport) and b) the particle size range of soil particles.

with radius smaller than 20  $\mu\text{m}$  and 100  $\mu\text{m}$  respectively. Dar Albeida's sample (sand dune) depicts only 7% of the mass of particles smaller than 20  $\mu\text{m}$  and 47% for the particles smaller than 100  $\mu\text{m}$ . Tamanrasset's, Achegour's, and Nubian desert's samples indicate about 11%, 19%, and 43% by mass of the particles smaller than 20  $\mu\text{m}$  radius, and 61%, 70%, and 77% by mass of particles smaller than 100  $\mu\text{m}$  respectively. From these values, it becomes apparent that the alluvian land samples are the most productive of the soil types analysed here. It should be emphasized that the hypothesis of soil erodibility and productivity is very tentative. An additional method would be to analyse the soil samples in their natural environment with respect to their threshold wind velocity, moisture content, and texture, as Gillette et al. (1980) did.

The aim behind the discussion above is to make clear that an arid zone does not necessarily mean a dust production area. Real source regions are rather scattered. Some transport models, designed to estimate the source strength and the deposition rate, need both location and extent of the source areas (section 3.1.5).

The size spectrum of the above-mentioned distributions reflects the smallest size expected from the size spectrum of a purely crustal-derived aerosol size distribution. The fact that submicron-size particles are ubiquitous in the samples analysed points to the presence of that particle size in the aerosol size distribution. Particle sizes smaller than 0.1  $\mu\text{m}$  are normally thought to be the exclusive domain of secondary produced particles within the atmosphere by chemical reactions involving the oxidation of the available atmospheric trace gases. It is not clear to date how such small particles can be generated in soils. Lerman (1979), however, reported on observations that lead to the belief that weathering processes may provide a mechanism for size reduction beyond what can be achieved by breakup alone. For instance, size decrease in soil material may take place by dissolution of the soluble components of minerals. Small amounts of mineral-based material in the submicron-size range may be found in soil and in atmospheric particulate samples. It may be also worth mentioning that, besides biogenically and chemically produced non-sea-salt sulfate particles in clean-maritime environments, Meszaros and Vissy (1974) have identified particles in the size range below 0.1  $\mu\text{m}$  to be pure sea-salt particles. Yet, primary natural sources generate submicron-size particles, though in a very limited amount.

Parallel to the soil samples, 42 mineral aerosol samples have been taken during several field experiments in Matan (Senegal), Timbuctu (Mali), and Agadez (Niger) between February 1979 and February 1982 (Fig. 1). The active sampling time was about 10 weeks, a period in which aerosol was collected almost continuously. Each sample lasted between 10 and 48 hours depending on the prevailing atmospheric situation. During the sampling period, the horizontal visibility varied between some 10 m and more than 30 km and the mass concentration between 30  $\mu\text{g m}^{-3}$  and 9500  $\mu\text{g m}^{-3}$ . Sampling sites, sampling methods, and evaluation procedures are described in some previous papers (21, 19, 20). The above-mentioned mass concentration data reflect the high variability that the physical characteristics of mineral aerosol may undergo. For comparison, an empirical formula by Lovett (1978) indicates sea-salt mass concentrations between 5  $\mu\text{g m}^{-3}$  and 520  $\mu\text{g m}^{-3}$  for wind speeds between 1  $\text{ms}^{-1}$  and 30  $\text{ms}^{-1}$ . Furthermore, the smallest value observed during the 10-weeks field campaign is still more than twice the highest value of 14.2  $\mu\text{g m}^{-3}$  observed by Prospero (1979) over the tropical North Atlantic, and more than fourfold the global background mass concentration estimated by Heintzen-

berg (1980). The complete data set is shown by d'Almeida (1987). Apart from the tentative approach by Joseph (1977) discussed below, too little is known about the impact of the tremendous amount of dust on the atmospheric dynamics.

The aerosol samples have been sorted according to the prevailing horizontal visibility during the sampling period and classified into three categories. The samples corresponding to a visibility range higher than 8 km have yielded a so-called 'background desert dust distribution'. Size distributions observed during dust wind events with a visibility range between 8 km and 2 km have led to the 'wind carrying dust distribution'. The remaining samples were collected during heavy duststorm and sandstorm episodes with a horizontal visibility below 2 km. The resulting average size distribution is referred to as 'sandstorm distribution'. The sampling sites have been chosen to be far away from the major source areas of the dust to allow a well mixed layer during the 1–2 days travel time and close enough to avoid possible interactions with other aerosol components or the change of its physico-chemical characteristics due to scavenging processes. Although horizontal visibility is not a predictable quantity in the synoptic context, we find it opportune to choose it rather than the wind velocity that neither describes the aerosol mass loading nor reflects in a realistic manner the extent of aerosol productivity in deserts or arid regions with their well known geomorphological diversity. Wind velocity may however be a very useful variable to parameterise aerosol physical quantities in a maritime environment.

Figure 3 shows the average number distributions obtained from the classification outlined above. The background distribution is thought to represent the state of aged particles in normal atmospheric conditions, i.e. blue sky, calm weather, wide visibility ranges. The background distribution is characterised by particle number densities between  $250 \text{ cm}^{-3}$  and  $400 \text{ cm}^{-3}$  and an average concentration of about  $320 \text{ cm}^{-3}$ . It denotes the remnant concentration a long time after and shortly before a heavy sandstorm or dustwind. It may be worth mentioning that the so-called background desert aerosol is not to be confused with a background continental aerosol. The latter consists rather of a mixture of dust-like and water-soluble substances. The wind carrying dust and sandstorm distributions are characterised by a larger number of both giant and submicron-size particles, which are to a large extent purely soil-derived, as the soil sample analyses depicted similar features. The size distributions of mineral aerosol cover about six (sandstorm) to nine (background) orders of magnitude in concentrations and four orders of magnitude in particles radius. The curves show a distinct absolute maximum between 0.05 and 0.1  $\mu\text{m}$ . The significant amount of giant particles in wind-carrying dust and sandstorm distributions is responsible for the much higher mass concentration values indicated above. The transition between a sandstorm concentration and a background concentration is characterised by the alteration of the airborne particulate matter due to scavenging processes, mostly consisting of impaction and gravitational settling as dry season prevails. The evaluation procedure of the aerosol size distribution with a scanning electron microscope does not allow secondary produced particles (GPC) to be counted. We are neither aware of any production source of appropriate gases in an unpolluted desert that may yield such particles. They may however be transported from remote continental sources and remain just for a while airborne. Their number density is supposed to be negligible.

### 3. SOURCE STRENGTH, TRANSPORT, AND DEPOSITION RATE

Production areas of desert aerosol are confined to the most insolated parts of



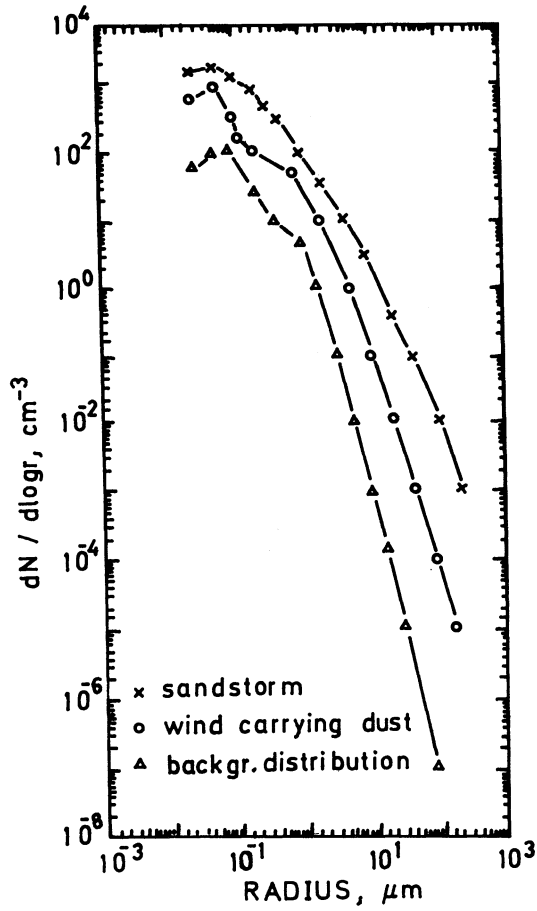


Figure 3:  
 Size distributions of desert aerosol for different atmospheric situations emphasizing the high variability that may occur. The average particle number densities amount respectively to  $322 \text{ cm}^{-3}$ ,  $1721 \text{ cm}^{-3}$ , and  $2533 \text{ cm}^{-3}$  for the background, wind carrying dust, and sandstorm distributions.

the earth's surface. In favorable meteorological conditions, the heated soil induces strong convective processes that facilitate particle mobilisation and ascension. Once embedded in the higher atmospheric layers, desert aerosol can be carried thousands of miles. The occurrence of the dust is a purely random phenomenon. Any attempt to compute the source strength requires a numerical model with observed or assumed input data. Indeed, a main purpose of our extensive study on mineral aerosol was to assess the source strength and the deposition rate of the dust emerging from the Sahara. The monitoring program and the outcome of our endeavor are summarised in the following. A more comprehensive report (20) outlines the choice of the sampling sites, the logistic, the method, the algorithm, the model input, as well as the assumptions made.

### 3.1. Truncated mass balance equation

The mass balance equation is reduced as follow and adapted to the goal of the present study:

$$U(x,z) \frac{dC(x)}{dx} = Q(x) - R(x).$$

The remaining composites to look into are: the aerosol mixing ratio  $\psi(x)$ , the source  $Q(x)$  and the sink  $R(x)$  of the dust, the wind field  $U(x,z)$ , and the aerosol profile. By neglecting possible variations of the air density  $\rho$ , the mean mixing ratio may be expressed in terms of the mean mass concentration  $\psi(x)\rho = C(x)$ . Our effort was then focussed on the way to obtain the aerosol mass concentration over a representative period of time. This can be monitored either directly with a time-consuming and sensitive dust sampler or indirectly with a suitable and maintenance-free device and a subsequent calibration. We opted for the second approach.

#### 3.1.1. African turbidity monitoring network (ATMN)

A 9-channel sunphotometer has been developed (27) and reproduced to set up a network of 11 stations in the Sahara, the Sahel region and the surrounding southern area. The so-called African turbidity monitoring network (ATMN) ran from November 1980 to February 1984. In that period, observations were performed three or four times daily, usually at 0900, 1200, 1500, 1700 or 1800 LT. The frequency of observations could follow the infrequent and rapidly changing turbid state of the atmosphere over the Sahara. Along with the sunphotometric data, meteorological quantities such as temperature, pressure, relative humidity, wind speed, wind direction, visibility, sky cover, and the prevailing weather were reported to allow a better control and an unbiased interpretation of the recorded sunphotometric data. The optical depth time series of the stations close to the source regions, i.e Boutilimit (Mauritania), Gao (Mali), and Agadez (Niger) show distinct peaks that reflect the sandstorm episodes (28, 21). In other words, the frequency of sandstorms can be easily deduced from a turbidity monitoring program.

#### 3.1.2. Atmospheric turbidity and aerosol mass concentration

A 6-weeks field experiment was performed in Agadez (Niger) to calibrate the sunphotometer and find an analytical relationship between aerosol turbidity, i.e dimensionless Angström's turbidity coefficient  $\beta$  and aerosol mass concentration  $C(\beta)$  in  $\mu\text{g m}^{-3}$ . Hereby, a size-fractionation has been made by means of an

impactor between particles with radius  $r$  smaller than  $5 \mu\text{m}$  and the total aerosol because the first size range is more sensitive to extinction processes in the atmosphere and enables a better correlation with the aerosol turbidity parameters. The regression analysis yields a correlation coefficient of 0.95 and the following formula:

$$C(r < 5 \mu\text{m}, \beta) = 404.45 \beta + 19.03.$$

Furthermore, an average ratio between both size ranges is found to be:

$$C(\text{total aerosol}) = 7.8 C(r < 5 \mu\text{m}).$$

The opportunity of a network has been used to obtain a dependence of aerosol turbidity upon a horizontal visibility  $VV$  ranging from some 100 m and 400 km

$$\beta = 2.26 VV^{-0.73}.$$

The combination of both equations permits the horizontal visibility in km to be expressed in terms of aerosol mass concentration in  $\mu\text{g m}^{-3}$  and vice versa

$$C(r < 5 \mu\text{m}, \beta) = 914.06 VV^{-0.73} + 19.03.$$

### 3.1.3. Aerosol profile

To our knowledge, there exists to date no long-term observation on aerosol profile over the Sahara and we were neither equipped during the field campaign to assess such a quantity. The vertical extent of the dust has, therefore, been calculated by assuming a homogeneous dust layer from the ratio between the aerosol optical depth and the aerosol extinction coefficient for a given wavelength of the sunphotometer channels, thus assuming a homogeneous dust layer. The extinction coefficient was calculated with the Mie theory using observed size distributions, inferring the pertaining refractive index from the available literature (Volz, 1973; Grams et al., 1974), and assuming the particle shape to be spherical.

### 3.1.4. Sink: removal processes

The removal processes in the model are confined to dry and wet deposition. The dry deposition accounts for the particle size and density to obtain the sedimentation velocities. The wet deposition considers the washout coefficient, the rainfall intensity over Africa and the seasonal migration of the Intertropical convergence zone (ITCZ). The latter acts as an effective barrier to meridional exchanges. The rainfall data refer to 20–50 years of observations tabulated by Griffiths (1972).

### 3.1.5. Source areas

Number and size of the major source areas are further quantities required. Due to the complexity of the geomorphology in the Sahara, the determination of the source areas turns out to be a difficult task. There are, however, useful methods such as: satellite photographs, monitoring of air mass trajectory, visibility distribution analyses, comparison of element composition and color between aerosol

and soil. Among them, visibility analysis on meteorological charts for unaged aerosol particles, that permits one to follow the generation and the migration of a dust plume, seems to be the easiest and most common technique to date. The identification of the major sources for the present study is based on a) visibility analysis, b) monitoring of air mass trajectory, c) the evaluation of a map for soil erosion in Africa entitled : Provisional methodology for soil degradation assessment jointly published by the World Meteorological Organisation (WMO), the Food and Agriculture Organisation (FAO), and the United Nations Educational, Scientific, and Cultural Organisation (UNESCO), d) last but not least, several trips and substantial discussions with resident observers of the few meteorological stations in the Sahara and the Sahel regions. In Figure 1, the localised sources have been simulated by dotted points. Of course, there exist other sources, that are, from the productivity viewpoint, far less important than those suggested above. A differentiated method to mark potential sources has also been discussed by Schütz (this volume).

### 3.2. Model results

The source strength of Saharan dust has been computed on a monthly basis for the years 1981 and 1982, and for the different transport directions. The transport occurs mainly in three directions: a) the transport towards the Sahel region and the Gulf of Guinea, called south - transport, b) the transport over the tropical equatorial Atlantic known as the west - transport, c) the transport to Europe via the Mediterranean sea and the northern equatorial Atlantic referred to as the north - transport.

The sources are activated throughout the year and particularly strengthened between March and June, a period which coincides with the highest insolation in that region. The direction of transport is determined by the general circulation pattern. The particle fractionation makes it possible to give the source strength for both particles smaller than  $5 \mu\text{m}$  radius and for the total aerosol. The following discussion will be, however, confined to the total aerosol as the removal process already accounts for the rapid depletion of large particles near the source regions. Figure 4 shows the space and time distribution of the dust transport towards different directions. S1, S2, S3, and S4 refer to the production areas marked with dots in Fig. 1. Table 1 below shows monthly average values and the time dependent cumulative distributions of dust emission for 1981 and 1982, even though neither of the two monitoring years shows a distinct seasonal pattern.

**Table 1:** Source strength (differential and cumulative) of Saharan dust towards various directions

month	south - transport		west - transport		north - transport	
	$\text{Tg yr}^{-1}$	%	$\text{Tg yr}^{-1}$	%	$\text{Tg yr}^{-1}$	%
Jan	12.6	3.3	17.8	9.4	0.95	1.0
Feb	45.9	15.4	22.3	21.2	3.5	4.5
Mar	82.3	37.1	24.1	33.9	3.0	7.5
Apr	53.0	51.0	24.1	46.7	4.1	11.7

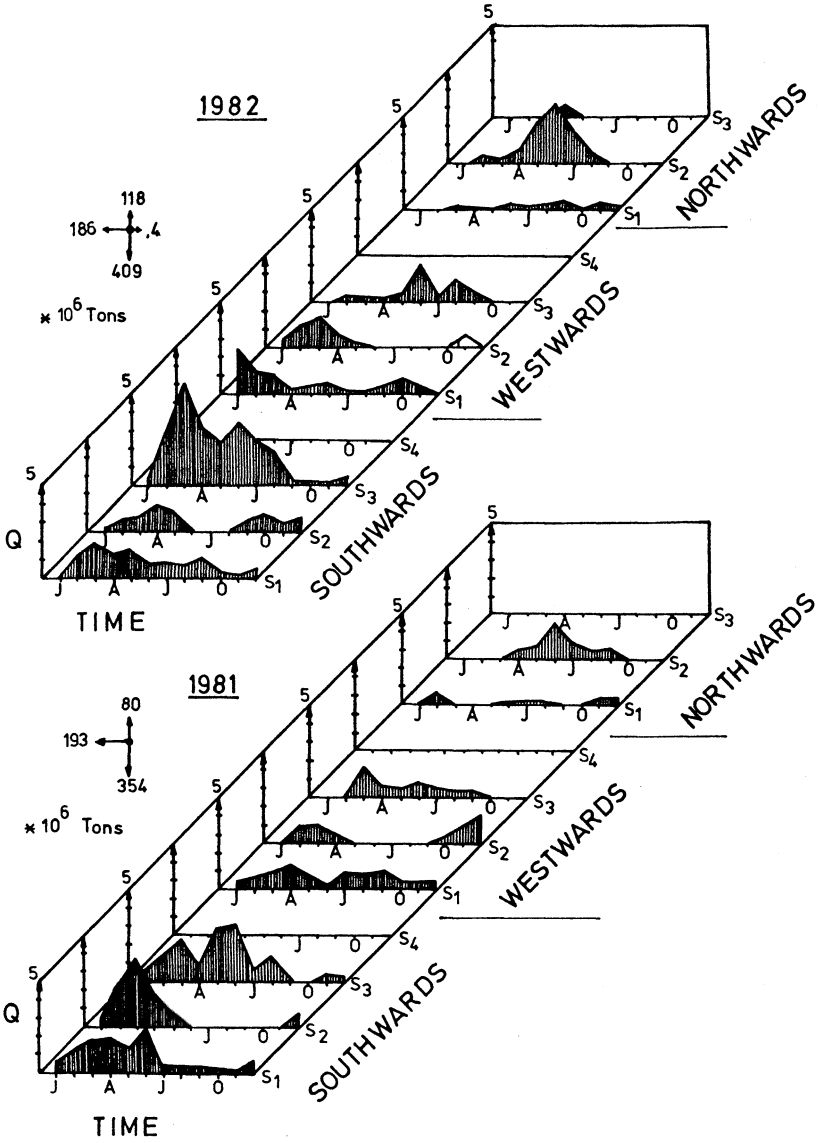


Figure 4:  
 Source strength of Saharan dust as functions of time and transport directions. S1, S2, S3, S4 represent the source regions indicated with dots in Fig. 1. The south-transport indicates the dust transport towards the Gulf of Guinea, the west-transport means the transport over the Atlantic towards the Caribbean Islands, the north-transport specifies the transport to Europe via the Mediterranean and the northern Atlantic.

May	48.1	63.7	12.5	53.3	7.1	18.8
Jun	47.1	76.1	17.5	62.5	24.7	43.7
Jul	22.0	81.8	9.9	67.8	22.3	66.3
Aug	22.7	87.8	9.7	72.9	17.4	83.9
Sep	13.3	91.3	16.6	81.7	8.1	92.1
Oct	9.7	93.9	12.0	88.0	0.45	92.5
Nov	7.3	95.8	11.3	94.0	3.9	96.5
Dec	16.5	100	11.8	100	3.6	100
Total	381	100	189	100	99	100

### 3.2.1. South - transport

The dust plume spreading towards the Sahel region called **Harmattan** and partly deposited in the Gulf of Guinea is of frequent occurrence in wintertime. The total dust export to the south amounts to about  $380 \text{ Tg yr}^{-1}$ . Table 1 and Figure 4 indicate that about 55% of the total mass is shifted between December and April. The airborne dust in the summer months is almost totally scavenged by the monsoon air mass. The region in the southern part of the ITCZ is almost completely shielded from the dust transport. Due to the seasonal position of the front and its considerable precipitable water content, only about  $15 - 20 \text{ Tg yr}^{-1}$  (roughly 2% - 6% of the south - component) are deposited in the equatorial Atlantic. The quasi - totality of the airborne particulate matter transported to the south between May and October (about 30% of the south - production) is washed out in the precipitation zone of the ITCZ and contributes probably to the enrichment of the farming land nutrients.

### 3.2.2. West - transport

As in case of the south - transport, the westward transport occurs all the year round without any seasonal predominance (Tab. 1). The monthly mean mass concentration values observed by Prospero et al. (1981) in Cayenne (French Guiana) between December 1977 and December 1979 depict a prevailing deposition between February and May. This finding corroborates, indeed, the statement made above, as the particles collected in Cayenne or in Barbados (Caribbean Island) are those particles that escape the scavenging process (wet deposition) particularly pronounced in the summer months. The present model indicates that about  $190 \text{ Tg}$  material are emitted every year from the source regions of the Sahara towards the Caribbean Sea. A small portion of about  $44 \text{ Tg}$  is deposited on the continent and the remaining quantity of  $146 \text{ Tg}$  passes over the African western coast. While these estimates agree reasonably well with a previous investigation by Schütz (1980) who has come to compute a source strength of about  $260 \text{ Tg yr}^{-1}$ , they show some discrepancy with the computation by Prospero and Carlson (1972) who have found a semiannual flux of  $37 \text{ Tg}$ . At least, two reasons may explain the obvious difference: a) the dust transport

phenomenon depends upon the highly variable meteorological situation and variations may occur from year to year, b) the different methods used and locations to which the basic observations related are as important as the physico-chemical behavior of aerosol particles alters with lasting residence time and travel distance.

### 3.2.3. North - transport

The north-transport of Saharan dust and its deposition are responsible for the well known **red snow** and **bloody rain** reported in some European regions. This type of transport is infrequent and of a sporadic nature. Table 1 shows a rather pronounced activity between May and September where 73% of the yearly production of about 100 Tg is exported towards Europe via the Mediterranean Sea and/or the northern Atlantic. A long-term monitoring program of the north-transport is being carried out in the French Pyrenees by Bucher (this volume).

### 3.2.4. East - transport

The east-transport from the Sahara does exist, occurs occasionally, and is of a minor importance. The present model indicates a negligible quantity of 0.4 Tg yr<sup>-1</sup> which largely contribute to the pelagic sediment of the Red-sea. The East-transport of Saharan dust is certainly not the only transport pattern towards the Red-sea.

### 3.2.5. Global transport

Besides the Sahara, there exist other deserts about which dust transport has been reported. However, too little is known about the extent of the potential sources, the frequency of dust emission, and other relevant parameters required to quantify the source strength. We are only aware of the following calculations. A case study on the Near-east desert conducted by Joseph et al. (1973), leads to a tentative evaluation of a global mineral dust input into the atmosphere between 64 and 192 Tg yr<sup>-1</sup>. A further estimate by Peterson and Junge (1971), based on average concentrations and residence time, yields global source strength of 500 Tg yr<sup>-1</sup>.

Assuming that our estimate is reliable, and there are no scientific reasons to believe the contrary, the evaluation by Peterson and Junge (1971), and that by Joseph et al. (1973) seem to be very low, even lower than the contribution from the Sahara alone. If we further assume that the extent of the source areas, the productivity of dust, the mechanism, and the frequency of injection into the atmosphere, as well as the physico-chemical behavior of the mineral dust of other deserts of the earth are proportionately similar to those of the Sahara, we come to the conclusion that about 1800 - 2000 Tg of desert material is injected each year into the atmosphere. That figure may appear somewhat high because we consider giant particles up to 100 μm in our model. If we, however, account for the atmospheric conditions under which the dust mobilisation occurs, i.e. high surface insolation along with an unstable layer inducing a strong convective transport, it becomes clear that even giant particles experience both an upward movement and a meridional transport as long as the convective process lasts. A great deal of the giant particles does participate, at least for a while, in the long-range transport before being scavenged out of the atmosphere. Careful soil size analysis of the pelagic sediment may prove this suspicion. From the viewpoints of aerosol transport and residence time, the fact that the background size distribution of desert aerosol observed at stations further than 1000 km from the source areas, holds such particles, supports the hypothesis. Possible local

influences during the sampling were largely shielded.

#### 4. RADIATIVE CHARACTERISTICS

It is nowadays well established that atmospheric aerosol may significantly alter the energy budget of the earth-atmosphere system and, thus, have a regional, and probably a global, climatic impact. As far as the present report is concerned, it is of interest to estimate the extent to which mineral aerosol contributes to the change of the radiative balance. As mineral particles are to a large extent insoluble in water, the following discussion will be confined to dry particles.

The quantities required to compute the impact of aerosol on climate are: scattering and absorption coefficients, asymmetry factor, phase function, and optical depth of aerosol, as well as the reflection properties of the underlying surface, often called surface albedo. The sum of scattering and absorption coefficients is called the extinction coefficient which is the fraction of energy removed per unit path length from an incident wave with energy flux density 1 by a collection of particles in suspension. The energy that then reappears as scattered energy is the scattering coefficient and the energy absorbed is the absorption coefficient. The ratio between scattering and extinction is called single scattering albedo; that means the fraction of energy removed from the incident wave which reappears as scattered radiation. A pure scatterer has a single scattering albedo of 1 while a perfectly absorbing aerosol depicts a single scattering albedo of zero. The asymmetry factor is the average of the cosine of the scattering angle for scattered radiation and gives to a certain extent the portion of the energy scattered in the forward or in the backward direction. The asymmetry factor may have a value between -1 and 1. The phase function gives the angular distribution of the scattered radiation. More details on the basic formulae may be seen in a previous paper by d'Almeida (1987) or elsewhere. It is intended in this section to present the radiative characteristics of the desert dust and compare them with those of other aerosol types.

##### 4.1. Computed radiative characteristics

The optical quantities defined above need size distribution, refractive index, and shape of the aerosol particles to be computed. The Mie computation is performed for very small radius intervals to increase the accuracy of the resulting quantities. For this reason, the observed size distributions described above (Fig. 3) are converted to lognormal distributions as suggested by Davies (1974). A log-normal distribution is defined by a median radius  $r_M$ , a standard deviation  $\sigma$ , and a number density  $N(r)$  of particles with radius smaller than  $r$ . An observed size distribution converted to log-normal distributions consists usually of several partial distributions that very often reflect the sources or the composition (here the different minerals) and the characteristics of the airborne material. The basic equation can be written as follow:

$$\frac{dN(r)}{d(\log r)} = \sum_i \frac{N_i}{(2\pi)^{1/2} \log(\sigma_i)} \exp\left(-\frac{(\log r - \log r_{Mi})^2}{2(\log \sigma_i)^2}\right)$$

with



$$\sum \frac{dN_i(r)}{d(\log r)} = \frac{dN(r)}{d(\log r)} .$$

Although it is possible in principle to take account of irregular particles shape in any detailed treatment, normal practice is to assume all particles to be spherical on the basis that random orientation would ensure that they behave in the mean like spheres of equivalent size.

The refractive index measurements performed by Volz (1973) and Patterson (1977) hold the broadest spectral range of data on the mineral aerosol published so far. We rely on these data for the Mie computation although the values represent only the bulk refractive index which may differ from a particle volume - related mixed refractive index obtained by firstly segregating the particles into small size ranges and subsequently determining their refractive index.

The trimodal size distribution of the wind carrying dust distribution has the following microphysical parameters:  $r_{1,2,3} = (0.052, 0.5, 12)$ ,  $\sigma_{1,2,3} = (2.15, 2.07, 1.7)$ , and  $N_{1,2,3} = (1710, 20.7, 0.005)$ , with  $r_i$ , the modal radii,  $\sigma_i$ , the geometric standard deviations, and  $N_i$ , the partial number densities in  $\text{cm}^{-3}$  of the 3 modes termed mode A, mode B, and mode C. Subscript  $i$  specifies the single components (mineral species). This distribution has been arbitrarily chosen from Fig. 3 as an example to single out the contribution of the different modes. Mode A represents the smallest particles, mode B the transition mode, and mode C the giant particle mode.

In Figure 5, the contribution of the individual modes to the wind carrying dust distribution is presented along with the total contribution of the corresponding radiative characteristics for the spectral range between 0.3 and 40  $\mu\text{m}$ . It becomes apparent that Mode A and Mode C play only a minor role in the scattering and absorption (and thus the extinction) properties. Mode B overlaps the total contribution. The single scattering albedo of the Mode A is predominant in the visible region and becomes nearly zero in the infrared region. This figure points out the sensitivity of the smallest particles to the smaller wavelengths. Mode C, and Mode B to a certain extent, depict nearly neutral extinction and scattering features (wavelength independent pattern) for the whole spectral range. This behavior is due to the large and effective scattering diameter of the particles. The contribution of Mode A to the asymmetry factor is negligible in the infrared region while Mode C is dominant in that spectral range. From the viewpoint of residence time, Mode C is more quickly scavenged while Mode B remains longer airborne and undergoes a long - range transport to mix with other aerosol components in maritime and continental environments and participates in the radiative processes. Mode B claims namely the quasi totality of both the scattered and the absorbed energy in the solar as well as in the thermal infrared regions. Furthermore, Mode A and Mode B have an outstandingly high absorption feature in the atmospheric transparency window between 8 and 12  $\mu\text{m}$  and, thus clog this window. This is a further important peculiarity of mineral aerosol worth stressing.

To demonstrate the absorptivity of desert dust, a world map for computed absorption coefficient values is displayed in Fig. 6 for the wavelength 10  $\mu\text{m}$ , for January, and for an assumed ambient relative humidity of 0%. The computation has been performed by considering possible mixture of aerosol components, i.e. all existing tropospheric aerosol types (Arctic, clean - forest, clean - continental or

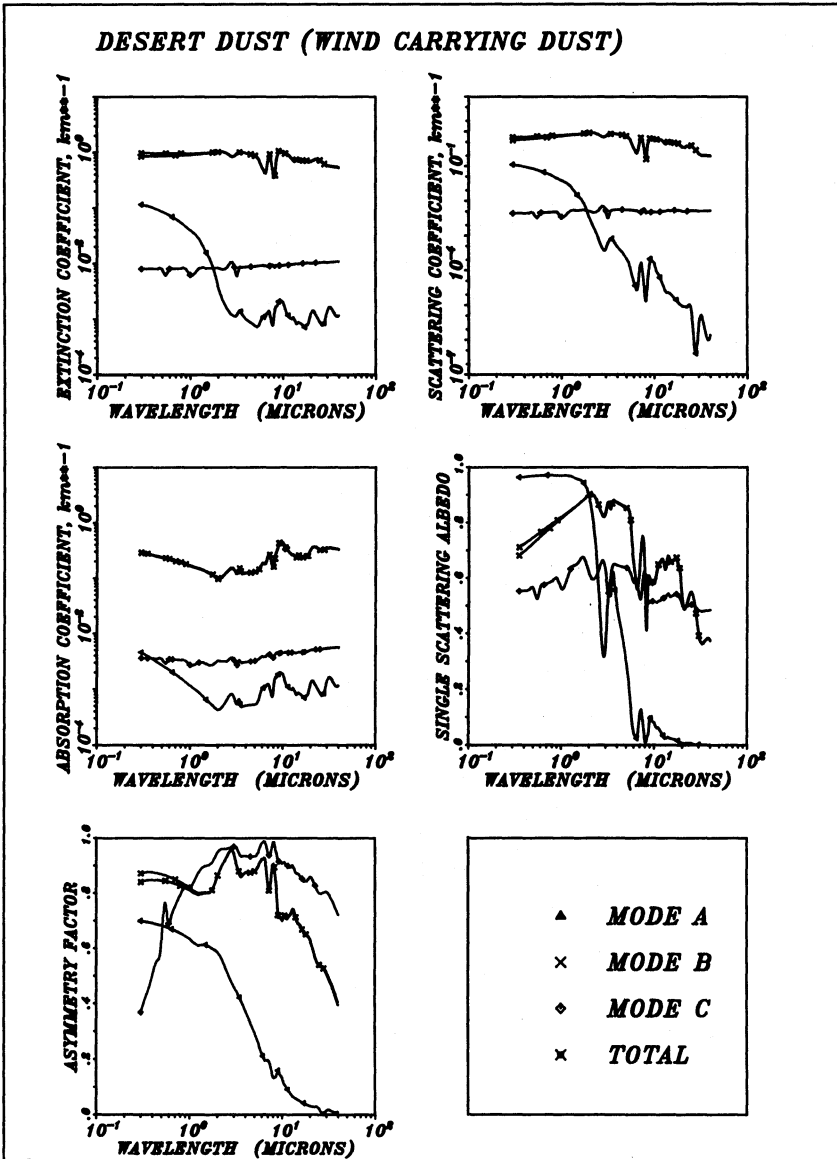


Figure 5:  
Radiative characteristics of desert dust: contribution of the single modes as well as of the sum of the 3 modes. The values refer to the wind carrying dust distribution of Fig. 3.

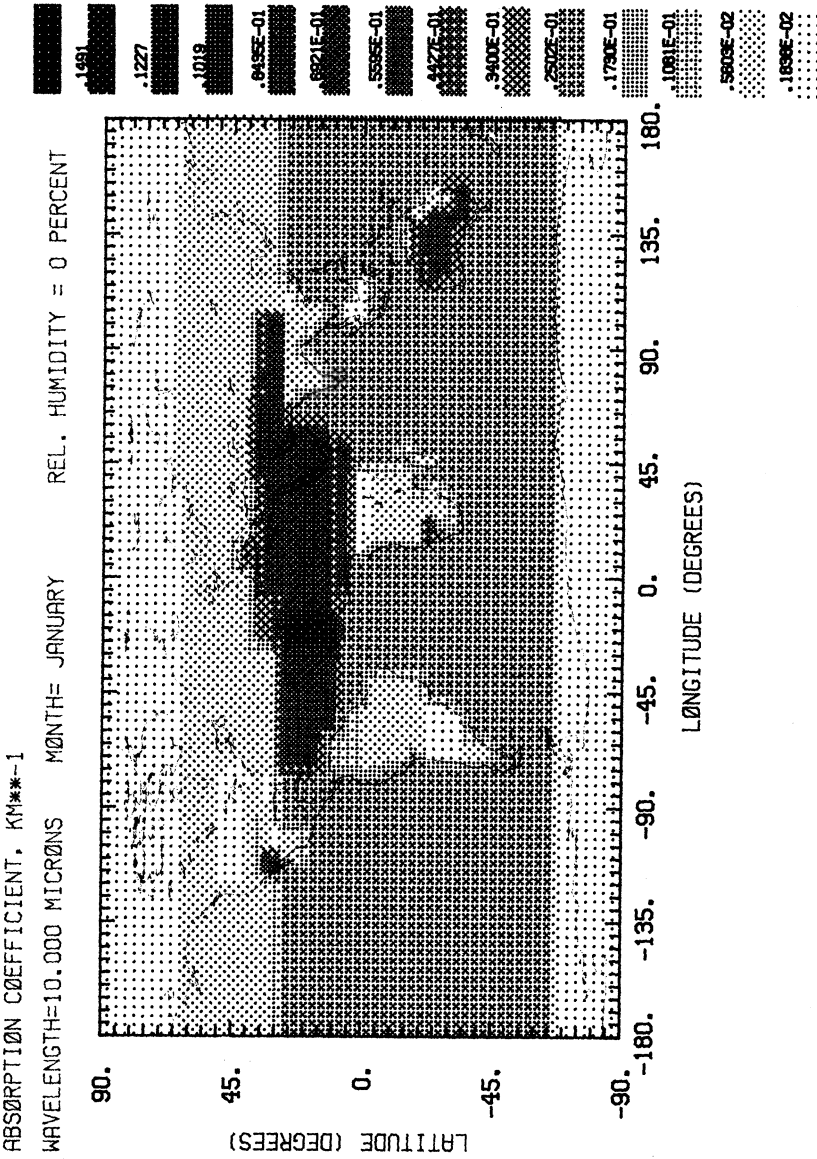


Figure 6:  
Global absorption coefficient for the wavelength 10.0  $\mu\text{m}$ , for January (an example), and for a relative humidity of 0% indicating the desert aerosol as the most prominent aerosol type in the atmospheric transparency window. The map is plotted in half-tone pictures along with the continental outlines. Values lower than  $0.1838 \times 10^{-2}$  are displayed with the lowest intensity.

rural, average – continental, urban, desert, clean – maritime, maritime – mineral, maritime – polluted, and Antarctic) along with their physical – chemical properties and their distribution in a global grid of 5 degrees latitude and 5 degrees longitude. The data have been inferred from the available literature and critically reviewed. More detail about the aerosol model, the computation of the radiative characteristics and the treatment of the relative humidity dependence is given by d’Almeida and Koepke (1988). Figure 6 indicates not only high absorption features in the main arid regions of the world (south – west United States, Sahara, Kalahari, Asian deserts, and central Australia) and the maritime environments influenced by the mineral aerosol component (northern equatorial Atlantic and North – Pacific) but also depicts the most efficient absorber in the atmospheric transparency window. The lowest absorption values occur in the polar regions.

#### 4.2 Desert aerosol optical depth

Aerosol optical depth or aerosol optical thickness is a further versatile quantity required to compute the possible effect of aerosol particles on climate. Aerosol optical depth is the integration of the aerosol extinction coefficient (section 4.1) over a given path length through the atmosphere. As such, it can be computed when the aerosol profile is known, as well as measured. A direct measurement can be performed by means of a sunphotometer equipped with interference filters. This has been done in the framework of the African turbidity monitoring network (see also section 3.1.1). The outcome of that program is presented in the following.

Figure 7 shows the monthly average values of the aerosol optical depth for the wavelength 500 nm and at some selected locations of the ATMN (stations underlined in Fig. 1). The seven stations presented here can be classified into 3 categories.

a) Assekrem (2730 m, Algeria), a mountain station on the northern border of the identified major source areas, is well – suited to assessing the aerosol optical properties of the high troposphere and the stratosphere in wintertime, and the transport pattern to Europe via the Mediterranean Sea in the summertime.

b) Boutilimit (Mauritania), Gao (Mali), and Agadez (Niger) are stations nearer to the source areas and display some peculiarities with respect to the seasonal pattern and the residence time of the aerosol.

c) Dakar (Senegal), Wad Medani (Sudan), and Zaria (Nigeria) are located in the Sahel or in the surrounding southern region and reflect the transport pattern towards the ITCZ and the effectiveness of the latter to interfere with the dust propagation.

Before the eruption of the volcano El Chichon in April 1982, daily optical depth values down to 0.03 (base e) have been observed between December and February for the wavelength 500 nm. A similar value had previously been measured only in Mauna Loa (3397 m, Hawaii) and in the Antarctic by Shaw (1979b, 1982). This low value is to a great deal larger than the Rayleigh scattering at this wavelength and at this station and seems to be characteristic of the clean – stratospheric aerosol. Between April and October, a sensitive increase of the optical depth occurs when dust is transported toward Europe. Daily average values reach sometimes 1.5. Monthly average optical depth in Assekrem amounts to values between 0.08 and 0.8.

Figure 7 indicates that Boutilimit, Gao, and Agadez do have strong seasonal

patterns although less striking than Assekrem. The stations experience an alternation of fair weather (blue sky) and sandstorm or heavy dustwind episodes reducing the horizontal visibility down to 10 m.

The daily turbidity pattern in Boutilimit is characterised by a strong optical depth discontinuity up to 3 (sandstorm) and down to 0.3 (fair weather). This behavior indicates the quick shift and the short local residence time of the aerosol over the areas located in the proximity of the source regions. The monitoring year 1983 in Boutilimit was characterised by very high dust activities which peaked in May with a monthly average value of 1.8 and more than 17 days sandstorm events. For comparison, the previous years indicate sandstorm frequencies less than 9 events. To our knowledge, that value represents the highest monthly average optical thickness value observed so far in a cloud-free atmosphere.

Gao and Agadez are a bit further from their respective sources and the characteristics underlined above are less pronounced. The monthly average values still remain very high with maxima between March and July, a period that coincides with the sunniest season and the lowest rainfall intensities in the region. Joseph et al. (1973) observed also the highest frequency of occurrence of Khamsinic depressions and maximum turbidity values in May.

Dakar is not (or better not yet) a typical arid station with a predominance of mineral aerosol component. The availability of a radiosounding station to retrieve precipitable water and infer aerosol profile supports its choice. At this station, a mixture of soot, sea salt, mineral and sulfate-bearing particles prevails and determines the turbidity pattern with maximum values around 1 in the summer months. Due to the location of Dakar and the prevailing winds, the quasi-totality of the dust passing over the city is subsequently deposited in the Atlantic.

Wad Medani is rather a station better suited to monitoring Saharan dust background concentrations. It was probably erroneously chosen for the purpose of measuring the dust emission from the sudanese desert. During the monitoring years, the dust seemed, however, to have been confined elsewhere.

As far as Zaria is concerned, the optical depth features differ from those of the station discussed above. The turbidity is clearly lower in summer than in winter. The small variation in the seasonal pattern is probably due to the persistence and the relatively longer residence times of the particles (weeks) far away from their sources. The lower summer values are due to intense scavenging processes induced by the monsoon rain that cleanses the atmosphere and reduces the optical thickness to a background value between 0.2 and 0.4.

In order to show the importance of desert aerosol on a global context, a world map for computed optical depth values has been displayed for the wavelength 500 nm (representative of the visible spectral range), for January and for hypothetical dry aerosol particles (Figure 8). The data involved account for all existing aerosol types, their microphysical parameters, and their refractive index as well as the contribution of the stratospheric aerosol. The map is plotted in half-tone along with the continental outlines. Values lower than  $0.1018 \times 10^{-1}$  are displayed with the lowest intensity. More details on the aerosol model and their radiative characteristics are published by d'Almeida and Koepke (1988). The map shows, for instance, that the optical depth of the aerosol in clean-maritime (undisturbed) environment is less than 0.2. For relative humidities near 100%, that value may increase by up to a factor of 15, approaching values encountered in the Saharan atmosphere during sandstorm episodes. It can also be seen from Fig. 8 that the maritime environment influenced by desert dust indicates large values due to the

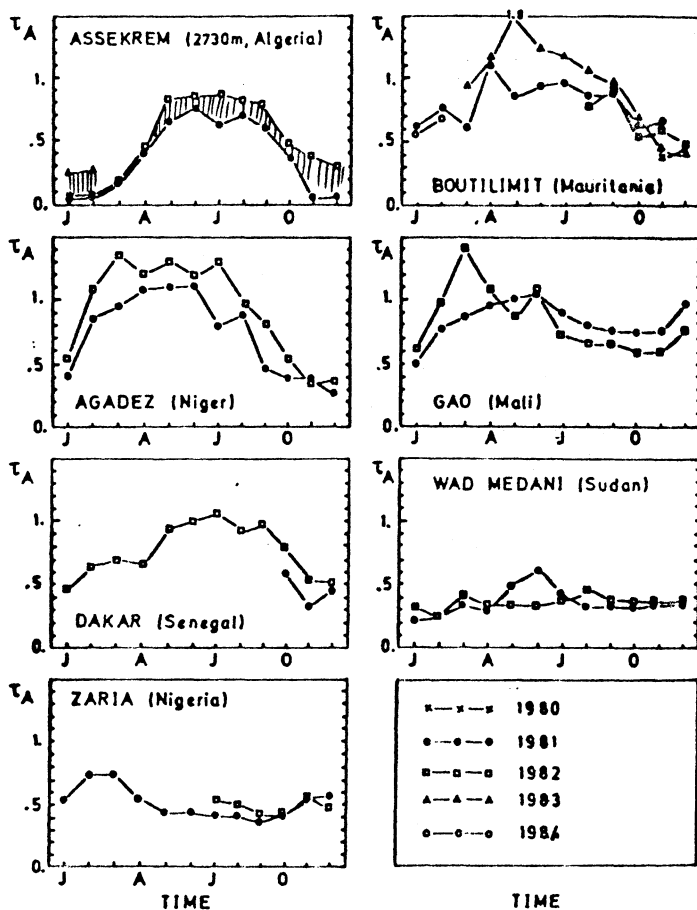


Figure 7:  
Monthly average values of desert aerosol optical depth for some selected stations of the ATMN.

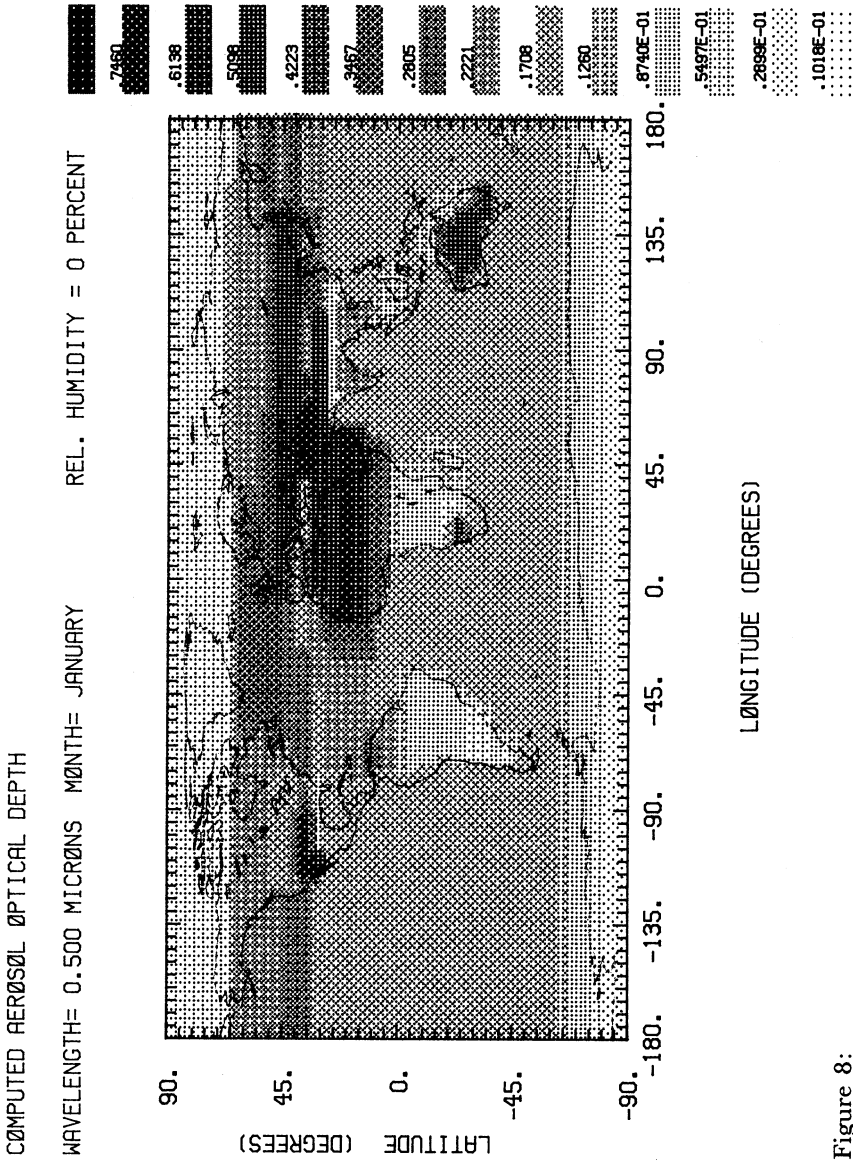


Figure 8:  
 Global optical depth for January (an example), for the wavelength 500  $\mu\text{m}$ , and for a relative humidity of 0% indicating the desert aerosol as the most prominent aerosol type in the visible spectral region. The map is plotted in half-tone pictures along with the continental outlines. Values lower than  $0.1018 \times 10^{-1}$  are displayed with the lowest intensity.

presence of the mineral component.

To describe the aerosol turbidity pattern in the atmosphere, Angström (1964) has suggested the following empirical formula:  $\tau(\lambda) = \beta \lambda^{-\alpha}$ . Here,  $\tau$  is the optical depth for an arbitrary wavelength  $\lambda$ ,  $\beta$  is the so-called Angström's turbidity coefficient, and  $\alpha$ , the wavelength's exponent. The quantities  $\alpha$  and  $\beta$  are wavelength independent.  $\alpha$  is characteristic of the aerosol extinction pattern, while  $\beta$  describes the amount of suspended particulate matter in the atmosphere. Observations by d'Almeida (1985) for the spectral range between 0.4 and 1.025  $\mu\text{m}$ . show, indeed,  $\alpha$ -values between  $-0.5$  and  $+0.5$  during sandstorm and wind carrying dust episodes at stations like Boutilimit, that are in the neighborhood of a source region. The further the monitoring station from the source and the lower the aerosol mass loading, the larger is  $\alpha$ . For instance, normal atmospheric conditions in Boutilimit lead to  $\alpha$ -values between 1 and 2. The same holds for observations made in Wad Medani (Sudan) and in Zaria (Nigeria) indicating a progressive depletion of giant particles of mode C and a modification of the particle population of mode B during the transport process. Our own measurements performed in Mainz and Garmisch-Partenkirchen (both in F.R. Germany) yield  $\alpha$ -values between 1.5 and 3, which are characteristic of urban and continental aerosols.  $\beta$ -values vary between 0.02 and 3.

a) The transition mode (mode B) of the size distribution determines the radiative characteristics, even in the source regions. With increasing distances from the sources, the particle population undergoes some changes expressed by the higher values of the Angström's wavelength exponent.

b) If the giant particle mode (mode C) is disregarded the single scattering albedo value is much larger. In other words, the ratio between particle scattering and extinction becomes higher, the more distant the source areas, i.e. the older the particles. The same holds for the asymmetry factor if mode A is disregarded.

c) The turbidity pattern of all stations, considered together, indicate that wet deposition is the most efficient aerosol removal process in an arid environment. In dry seasons the particles remains airborne for several weeks and participate longer in the radiative exchange processes.

d) Desert aerosol experiences the highest variability of all aerosol types, both by virtue to its physical properties (number density, mass concentration, and residence time) and to its radiative characteristics (scattering and absorption).

e) desert aerosol is the best absorber in the atmospheric transparency window and depicts the highest optical depth value of all aerosol types both in the solar spectral range and in the infrared region.

## 5. CLIMATIC IMPLICATIONS

The effects of aerosol on climate are to affect directly and indirectly the radiation budget of the atmosphere, and to perturb the atmospheric circulation. The direct effect consists of a redistribution in the atmosphere of solar and terrestrial radiation that may cause a cooling or a heating. The indirect influence resides in the ability of the particles to act as condensation nuclei and facilitate the cloud formation process. The attenuation properties of cloud in terms of scattering, absorbing, emitting, and reflecting incident radiation are obvious.

The discussion above is thought to emphasize the peculiarities and the importance of desert aerosol on the scale of all existing aerosol types. Chapter 3 has pointed



out the huge mass of desert dust yearly injected into the atmosphere. Chapter 4 has indicated the radiative characteristics required to estimate the impact of aerosol on climate. The present section attempts to stress the climatic implication of desert aerosol using the previous findings.

Although the estimate of desert dust source strength by Joseph et al. (1973) and Joseph (1977) is much lower than that of the present study, the authors have found by using the NCAR – GCM, possible climatic effects with respect to the atmospheric dynamics. It has been shown that desert dust yields a significantly increased upward motion over the northern hemisphere tropics and the lower part of the desert – containing zone, and a subsequent decrease of the upward motion due to the modification of the Hadley cell by the oceanic aerosol layer. A perturbation of the meridional motion has also been observed.

With respect to the energetic effect, the impacts of desert dust on climate are manifold and more distinct.

Mineral particles are predominantly insoluble in water. As such, they are incapable of acquiring atmospheric water – vapor and undergoing a sudden transition, and becoming saturated or supersaturated. In favorable atmospheric conditions, they may, however, grow by adsorbing water on their surface. The so – called capillary condensation increases the particle size by less than 5 per cent (41). On the other hand, sea – salt particles and non – sea – salt sulfate particles are abundant in the maritime environment and are water – soluble substances. They partly act as condensation nuclei and contribute to cloud formation. The transport of desert dust over the maritime environment and their mixing with maritime air masses and water – soluble components impair the cloud formation processes and, thus, influence the attenuation features of the clouds.

Desert dust has been seen to close the atmospheric transparency window and, thus, to reduce the terrestrial thermal radiation to space. A net warming effect might be created in the layer below the dust, the magnitude of which increases with the thickness of the dust cloud veil.

Furthermore, the deposition of desert dust on ice and snow surface may decrease the planetary albedo and contribute to a local warming.

Yamamoto and Tanaka (1972) have used a slightly modified radiative transfer equation for a turbid atmosphere to compute the effect of atmospheric aerosol on climate. The quantities involved in that model are, among others aerosol size distribution, Angström's turbidity coefficient, aerosol refractive index, and surface albedo. Relying on the model results, the following can be concluded.

- a) For a given imaginary part of the aerosol refractive index, the average heating rate of the earth's atmosphere increases with the turbidity
- b) The higher the surface albedo, the lower the average heating rate of the earth's atmosphere
- c) the higher the absolute value of imaginary refractive index and the lower the surface albedo, the higher is the heating rate of the earth's atmosphere.

Applying these model results on the optical properties stressed in Chap. 4, the influence of desert aerosol becomes apparent. The imaginary part of the aerosol refractive index in the solar spectral range is constant and of about 0.008 (29). For a surface albedo of 0.3 as suggested for Saharan dust and the whole solar spectral range by Cunnington and Rowntree (1986), and a maximum Angström's

turbidity coefficient of 3 as observed by d'Almeida (1985) in sandstorm episodes, an extrapolation of the results by Yamamoto and Tanaka (1972) yields a heating rate of the earth's atmosphere of more than  $2 \text{ K day}^{-1}$  and a decrease of the surface temperature to  $10 - 15 \text{ K day}^{-1}$ . The latter result agrees fairly well with observations made in Agadez (Niger) and reported by d'Almeida (1986). Taking into account the high, at least one-day-lasting, monthly frequency of sandstorm in the Sahara reaching sometimes 17 events, the regional impact of the dust becomes apparent.

Carefully considered studies on interactions between aerosol heating or cooling and atmospheric circulation involving actual data are required to infer the climatological significance of desert dust on a global scale.

## 6. CONCLUSION

The report has attempted to present the physical properties, the radiative characteristics, and the climatic effects of the desert aerosol with special emphasis on the Sahara. We, however, believe that the results discussed above are proportionately representative for all deserts and transferable in the past.

Soil samples have been analysed to indicate a soil type-dependent productivity and to localise the particle populations occurring in the aerosol size distribution. It has been found that submicron-size particles, generally thought to be the domain of particulate matter generated by gas-to-particle conversion, are present both in soils and aerosol. In the future, it would be of interest, to look more closely into the generation processes of this particle population both in the laboratory and during field experiments. Even though the role of the individual particles, with respect to cloud physics, atmospheric radiation phenomena, as well as their contribution to the aerosol mass concentration are negligible, they may, however, impact with larger particles or be deposited on ice or snow and change the planetary albedo. They are also responsible for the increased air electrical conductivity observed during heavy sandstorms.

With respect to the size ranges observed in desert aerosol, a realistic consensus among scientists is required. The number size distribution is the most prominent physical characteristic. The controversial discussion on that parameter encountered in the open literature is very confusing for users.

An extensive sunphotometer network has been set up within the whole Sahara and its southerly border, a regression analysis between aerosol mass concentration and aerosol turbidity coefficients has been performed, and major production sources have been localised, in order to estimate the mass input of the aerosol in the atmosphere, using the mass balance equation. It has been shown that a tremendous amount of Saharan dust participates in the atmospheric circulation and influences the dynamics. From that evaluation, a tentative estimate of the global source strength has been made, the impact of which for the atmospheric dynamics is a further field of research worth being considered in the future.

Based on the outcome of field measurements of aerosol size distribution and on the ATMN-program, the radiative characteristics of the desert dust have been discussed. Both computation and measurement indicate the desert aerosol as one of the most prominent aerosol types with the highest variability. It depicts quasi-neutral extinction and scattering features in the visible and near infrared regions, clogs the atmospheric transparency window in the infrared region and reduces the loss of terrestrial thermal radiation to space, and shows the most significant spatial and temporal variation with respect to the aerosol optical depth.

Due the above - outlined physical properties, radiative characteristics, and climatic effects of the present day desert aerosol, it might be easier to reliably undertake a quantitative reconstruction of the climate in the past. Five times the present amount of desert dust in the atmosphere leads to an outstandingly dramatic warming process due to absorption of solar radiation in the layer and above the layer to which the dust is confined, and a corresponding cooling due to the backscattered solar radiation and a challenging warming due to the absorption of the thermal infrared radiation below the dust cloud. The net and long-term effects require a more comprehensive computation.

## REFERENCES

1. M. Sarnthein: Sand Deserts During Glacial Maximum and Climatic Optimum, Nature, 272, 43 - 46 (1978).
2. J. - R. Petit, M. Briat, A. Royer, 1981: Ice Age Aerosol Content from East Antarctic Ice Core Samples and Past Wind Strength, Nature, 293, 391 - 394 (1981).
3. D. Tanre, J.F. Geleyn, J. Slingo: First Results of the Introduction of an Advanced Aerosol - Radiation Interaction in the ECMWF Low Resolution Global Model, in H.E. Gerber and A. Deepak (eds.), Aerosol and their Climatic Effects, A Deepak Publishing, Hampton, Va., pp. 133 - 177 (1984).
4. J.H. Joseph: The Effect of a Desert Aerosol on a Model of General Circulation, in H. - J. Bolle (ed.), Proceedings of the Symposium on Radiation in the Atmosphere, Science Press, 487 - 492 (1977).
5. G.E. Shaw: Considerations on the Origin and Properties of the Antarctic Aerosol, Rev. Geophys. Space Phys., 8, 1983 - 1998 (1979a).
6. C.G., Ehrenberg: Erläuterung eines neuen wirklichen Passatstaubes aus dem Atlantischen Dunkelmeere von 29. Okt. 1861, Monatsber. Kg. Preuss. Akad. Wiss., Berlin, 202 - 224 (1862).
7. W. Semmelhack: Die Staubfalle in nordwest afrikanischen Gebiet des Atlantischen Ozeans, Annalen der Hydrographie, 62, 273 - 277 (1934).
8. T.N. Carlson, J.M. Prospero: The Large Movement of Saharan Air Outbreak over the Northern Equatorial Atlantic. J. Appl. Meteorol., 11, 283 - 297 (1972).
9. J.M. Prospero, T.N. Carlson: Vertical and Areal Distribution of Saharan Dust over the Western Equatorial North Atlantic Ocean, J. Geophys. Res., 77, 5255 - 5265 (1972).
10. L. Schütz: Long - Range Transport of Desert Dust with Special Emphasis on the Sahara, Ann. N.Y. Acad. Sci., 338, 515 - 532 (1980).
11. J.M. Prospero: Mineral and Sea - Salt Aerosol Concentration in the Various Ocean Regions. J. Geophys. Res., 84, 725 - 731 (1979).
12. J.M. Prospero, R.A. Glaccum, R.T. Nees: Atmospheric Transport of Soil Dust from Africa to South America, Nature, 289, 570 - 572 (1981).
13. G.E. Shaw: Transport of Desert Aerosol to the Hawaiian Islands, J. Appl. Meteorol., 19, 1254 - 1259 (1980).

14. M. Darzi, J.W. Winchester: Aerosol Characteristics at Mauna Loa Observatory, Hawaii, after East Asian Dust Storm Episodes, J. Geophys. Res., 87, 1251 – 1258 (1982).
15. M. Uematsu, R.A. Duce, J.M. Prospero, L. Chen, J.T. Merrill, R.L. McDonald: Transport of Mineral Aerosol from Asia over the North Pacific Ocean, J. Geophys. Res., 88, 5343 – 5352 (1983).
16. D.A. Braaten, T.A. Cahill: Size and Composition of Asian Dust Transported to Hawaii, Atmos. Environ., 20, 1105 – 1109 (1986).
17. D.A. Gillette: On the Production of Soil Wind Erosion Aerosol Having the Potential for Long – Range Transport, J. Rech. Atmos., 8, 735 – 744 (1974).
18. D.A. Gillette, J. Adams, A. Endo, D. Smith, R. Kihl: Threshold Velocities for Input of Soil Particles with the Air by Desert Soils, J. Geophys. Res., 85, 5621 – 5630 (1980).
19. G.A. d'Almeida, L. Schütz: Number, Mass, and Volume Distribution of Mineral Aerosol and Soils of the Sahara, J. Clim. Appl. Meteorol., 22, 233 – 243 (1983).
20. G.A. d'Almeida: A model for Saharan Dust Transport, J. Clim. Appl. Meteorol., 24, 903 – 916 (1986).
21. G.A. d'Almeida: On the Variability of Desert Aerosol Radiative Characteristics, J. Geophys. Res., 93, 3017 – 3026 (1987).
22. L. Schütz, R. Jaenicke: Particle Number and Mass Distribution above  $10^{-4}$  cm Radius in Sand and Aerosol of the Sahara, J. Appl. Meteorol., 13, 863 – 870 (1974).
23. A. Lerman: Geochemical Processes, Water and Sediment Environments, J. Wiley and sons, 481 pp (1979).
24. A. Meszaros, K. Vissy: Concentration, Size Distribution, and Chemical Nature of Atmospheric Aerosol Particles in Remote Oceanic Areas, J. Aerosol Sci., 5, 101 – 109 (1974).
25. R.F. Lovett: Quantitative Measurement of Airborne Sea – Salt in the North – Atlantic, Tellus, 30, 358 – 364 (1978).
26. J. Heintzenberg: Particle Size Distribution and Optical Properties of Arctic Haze, Tellus, 32, 251 – 260 (1980).
27. G.A. d'Almeida, R. Jaenicke, P. Roggendorf, D. Richter: A New Sunphotometer for Network Operation, Appl. Opt., 22, 3796 – 3801 (1983).
28. G.A. d'Almeida: Recommendation on Sunphotometer Measurements in the BAPMoN as Based on the Experience of a Dust Transport Study in Africa, World Meteorological Organisation, WMO/TR – 67, 30 pp, Geneva, (Switzerland) (1985).
29. F.E. Volz: Infrared Optical Constants of Ammonium Sulfate, Saharan Dust, Volcanic Premice, and Flyash, Appl. Opt., 12, 564 – 568 (1973).
30. G.W. Grams, I.H. Blifford, Jr., D.A. Gillette, P.B. Russel: Complex Index of Refraction of Airborne Soil Particles, J. Appl. Meteorol., 13, 459 – 471 (1974).
31. J.F. Griffiths: Climates of Africa, in H.E. Landsberg (ed. in chief),

World Survey of Climatology, Vol. 20, Elsevier Publishing Company, Amsterdam, London, New York, 604 pp (1972).

32. J.H. Joseph, A. Manes, D. Ashbel: Desert Aerosol Transported by Khamsinic Depressions and their Climatic Effects, J. Appl. Meteorol., 12, 792 - 797 (1973).

33. S.T. Peterson, C.E. Junge: Sources of Particulate Matter in the Atmosphere, in W.W. Kellog and G.D. Robinson (eds.), Man's Impact on Climate, MIT Press, 310 - 320 (1971).

34. C.N. Davies: Size Distribution of Atmospheric Aerosol Particles, Aerosol Sci., 5, 293 - 300 (1974).

35. E.M. Patterson: Atmospheric Extinction Between 0.55  $\mu\text{m}$  and 10.6  $\mu\text{m}$  Due to Soil - derived Aerosol, Appl. Opt., 16, 2414 - 2418 (1977).

36. G.A. d'Almeida, P. Koepke: An Approach to a Global Optical Aerosol Climatology, to be published in P. Hobbs and A. Deepak (eds.), Aerosol and Climate (1988).

37. G.E. Shaw: Aerosol at Mauna Loa: Optical Properties, J. Atmos. Sci., 36, 862 - 869 (1979b).

38. G.E. Shaw: Atmospheric Turbidity over the Polar Regions, J. Appl. Meteorol., 21, 1080 - 1086 (1982)

39. A. Angström: The Parameters of Atmospheric Turbidity, Tellus, 16, 64 - 75 (1964).

40. P. Winkler: The Growth of Atmospheric Aerosol Particles as a Function of the Relative Humidity II; An Improved Concept of Mixed Nuclei, Aerosol Sci., 4, 373 - 387 (1973).

41. G. Yamamoto, M. Tanaka: Increase of Global Albedo Due to Air Pollution, J. Atmos. Sci., 29, 1405 - 1412 (1972).

42. W.M. Cunnington, P.R. Rowntree: Simulations of the Saharan Atmosphere Dependence on Moisture and Albedo, Quart. J.R. Met. Soc., 112, 971 - 999 (1986).

LOCAL, PROXIMAL AND DISTAL SAHARAN DUSTS: CHARACTERIZATION  
AND CONTRIBUTION TO THE SEDIMENTATION

Geneviève Coudé-Gaussen  
UA 722-CNRS, Paléoclimats et paléoenvironnements  
en régions arides  
Univ. P. & M. Curie, tour 16-26, 4, Place Jussieu  
75252 Paris Cedex 05  
France.

ABSTRACT. Local, proximal and distal dusts are mainly distinguished by their grain-size distributions in relation to the distance from their desert sources. The coarse particles have an inherited micromorphology derived from the incipient eolian mobilization in the source area. This is shown by SEM examination, image analysis and correspondence factor analyses. Yet, mineralogical identification may be difficult for the finest dust particles. In the presently deposited dusts or trapped dusts in the rock cracks, the grain-size and micromorphological characters, inherited from the previous eolian phase, are well-preserved.

According to the correspondence factor analyses, mineralogical alterations can occur after deposition. Micromorphological and mineralogical markers, such as reddened desert quartz or wind-shaped palygorskite grains, which are well characterized in present atmospheric dusts, are good indicators of Saharan dust contribution in peridesert soils and deposits and in several terrestrial and marine sediments.

## 1. INTRODUCTION

The deserts, and particularly the Sahara, are and have been important suppliers of mineral aerosols. The general aspects of this question concern the production, mobilization, transport and sedimentation of the desert dust, and a recent review of literature addressing these aspects can be found in Pye, 1987. The most important sedimentological problem is to estimate the real contribution of eolian dust to soils, continental and marine sediments beyond the desert area. For this purpose, it is necessary to define criteria to identify sediment of desert origin that has been deposited through eolian transport. The chemical and mineralogical data are reliable criteria for determining the allochtony and, less commonly, the origin of the deposited material, but they are not reliable indicators of exclusively eolian transport. Fluvial run-off and various marine processes such as currents or turbidite dynamics can also

explain fine depositions. Consequently, the real eolian contribution in more general allochthonous sedimentation must be characterized.

The examination of present-day desert dust is a good starting point for the characterization of eolian sediments. The chemical and mineralogical characters must be determined but also the size and the micromorphology of the particles. Indeed, the shapes and surficial micro-features of these particles examined by SEM are interesting indicators of their predepositional history. We have studied about 300 Saharan dust samples taken from filters of a five-stage cascade impactor, EGAI 80 (Bergametti *et al.*, 1983), bulk filtrations on a 10 meter mast or on a top 25 meter building, bulk samples on the soil surface during dust-falls, deposited dusts commonly trapped in rock cracks and eolian material from sea cores etc. All these samples come from various Saharan and peri-Saharan areas (Tanezruft, Hoggar, North-Mali, Great Eastern Erg, Great Western Erg, South-Tunisia, South-Morocco, Gulf of Gabes, Canary Islands, Sinai, Israel, Iberian Peninsula, Mediterranean region, Pyrenees, Normandy and Paris in France).

## 2. LOCAL, PROXIMAL AND DISTAL DUSTS

During the eolian phase of dust cycle, some sedimentological characteristics of the air-loaded material are dependent on the distance covered from the desert source area. As a result, it is possible to distinguish among local dust from the immediate area, proximal dust, which has been transported above the continental or marine peridesert areas, and distal dust which has been transported longer distances over seas.

### 2.1. The grain-size differences between these dusts

Generally, the local, proximal and distal dusts are differentiated by increasing fineness (Fig. 1). The cumulative grain-size curves of local dust show a main coarse fraction with a median located in the silt/fine sand size (50-65 $\mu$ m). The finest fraction of such material may have a distant desert source and may be derived from an continuously reworked Saharan dust material. However, the coarse fraction comes from the nearby substratum or from the comminution of dune sands as is shown on various mineralogical materials by field observations and laboratory experiments (see reviews in Busche *et al.*, 1984; Pye, 1987; and particularly Kuenen, 1960; Coudé-Gausson *et al.*, 1982; Coudé-Gausson *et al.*, 1984; Mazzulo *et al.*, 1986; Whalley *et al.*, 1987). The role of the coarse fraction and limit size of their particles (which can reach 200 $\mu$ m and more) are controlled by the wind strength which is responsible of the dust storm.

On the desert margins, the proximal dusts are fairly well sorted. The coarse fraction is reduced and it has a median grain-size between fine and coarse silts (20-25 $\mu$ m).

The distal dusts are finest. Various samples from southern Europe have a median grain-size around 5-10 $\mu$ m and the Saharan aerosols sampled above western Atlantic Ocean are finer still.

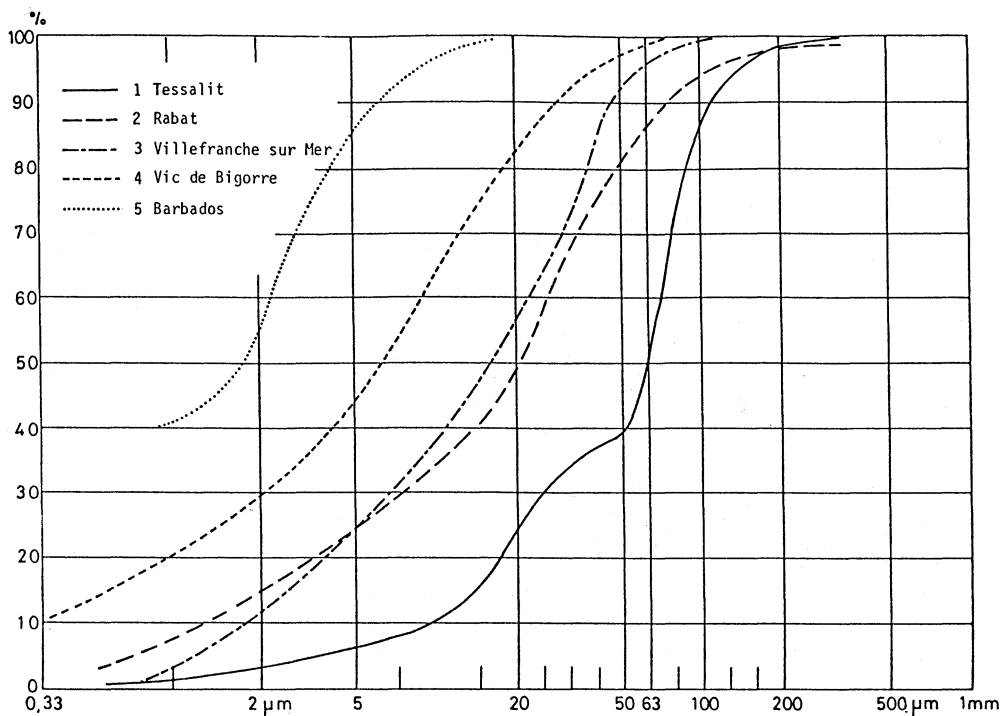


Fig. 1.- Cumulative grain-size curves of varied Saharan dusts: 1/ Local dust, Tessalit, central Sahara; 2/ Proximal dust, Rabat, Morocco; 3/ "Coarse" distal dust, Villefranche-sur-Mer, France; 4/ Distal dust, Vic de Bigorre, France; 5/ Distal dust, Barbados (from Glaccum & Prospero, 1980).

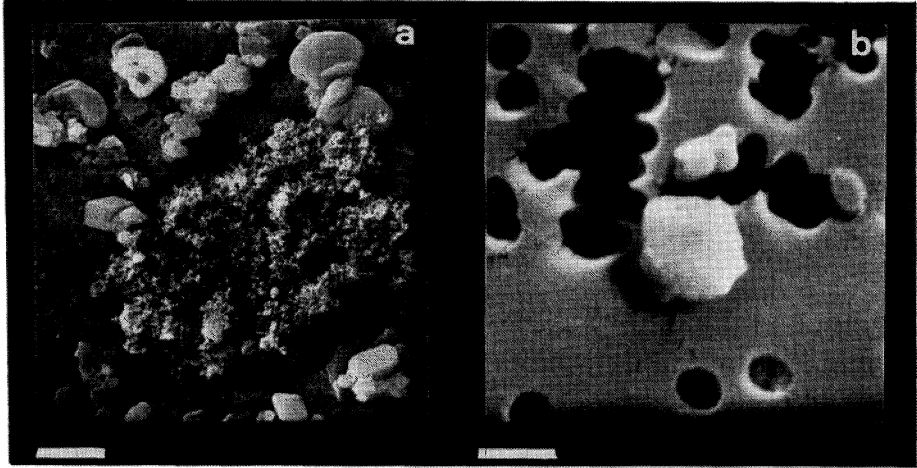
Large overlaps of grain-size occur among these three groups of Saharan dust. For example, the dust sampled in July 1981 in Villefranche-sur-Mer (Mediterranean France) shows grain-size nearer to a proximal dust than those of a distal one. In summer, when the Sirocco blows over Maghreb, a lower Saharan air layer loaded with coarse particles may reach southern Europe.

2.2. The common mineralogical and micromorphological properties of similarly-sized particles of these dust groups

2.2.1. Method. Dust grains have been examined by SEM (magnification X 200 to 30 000) on a JEOL SM2 and chemical data have been obtained on an ORTEC energy dispersive spectrometer (\*). The mineralogical identification of the coarser particles (>20μm) is made easy by the EDS chemical analyses. Furthermore, the shapes and surficial microfeatures seen with the SEM commonly provide confirmation of mineral's identity (for example if crystalline microstructures are obvious).

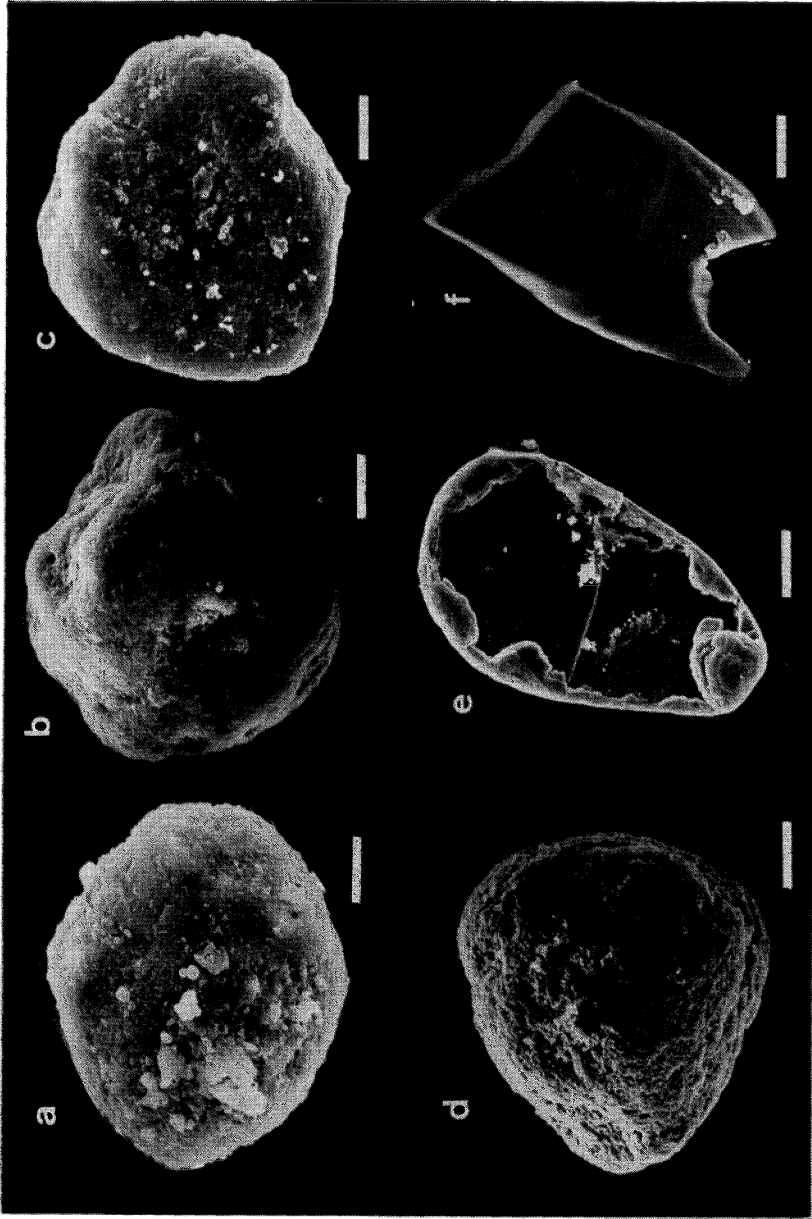


However, the mineralogical characterization of the finest particles (micrometer to sub-micrometer) is more difficult. This problem is encountered with complex clay mixtures that yield enigmatic chain-aggregate shapes or for the siliceous particles which may be quartz, opal or chalcedony (Pl.1).

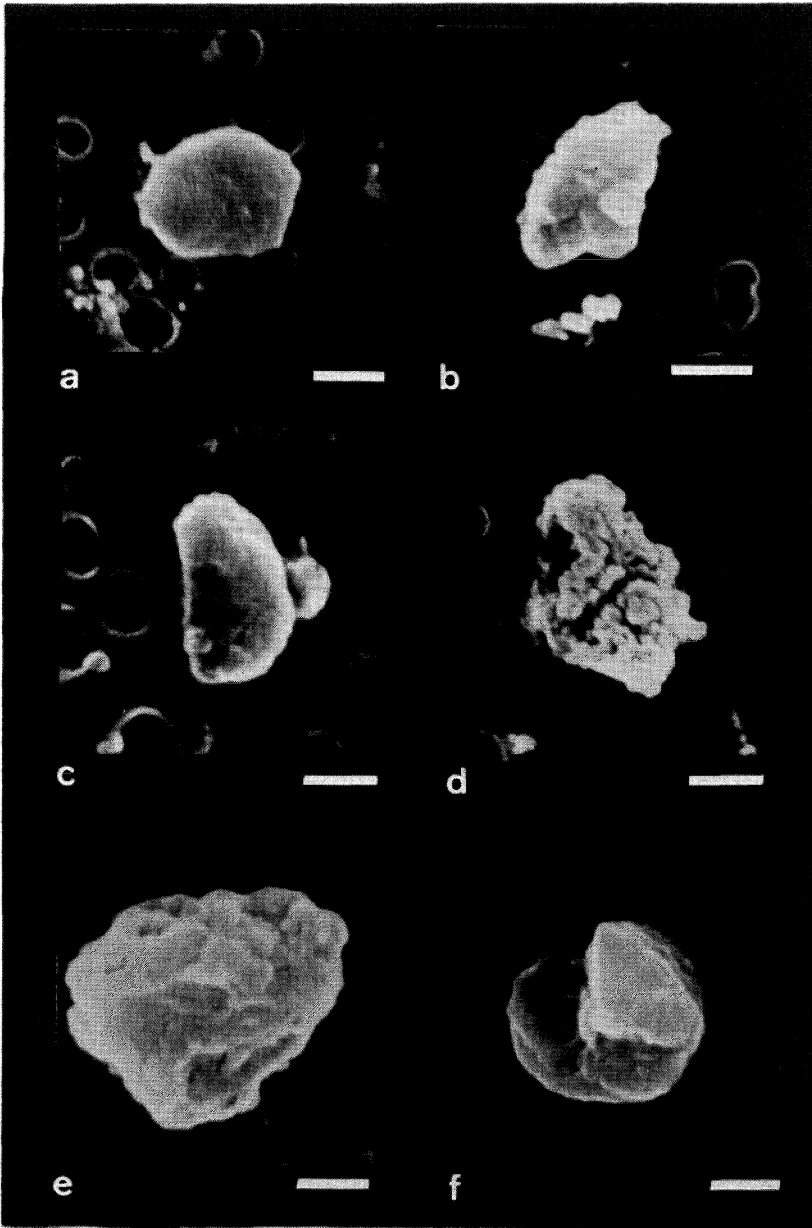


Pl. 1: a/ chain aggregate (Al, Si, K, Ca, Fe), scale= 6 $\mu$ m; b/ Si particle (quartz?), sc= 2 $\mu$ m.

2.2.2. The micromorphological and mineralogical criteria. In the local, proximal and distal dusts, the coarse grains commonly show a micromorphology inherited from their incipient desert phase of mobilization, before their air transport (Pl. 2). For example, the rounded desert quartz, commonly found in local dusts, are derived from dune or sand sheet material where the grains have been shaped by rolling and saltation. Numerous surficial microfeatures, well-known in SEM examination, relate to these high energy eolian processes (Krinsley and Doornkamp, 1973; Le Ribault, 1977). The shapes of other mineral particles developed similarly. Grains of Ca carbonate, heavy minerals or K feldspar or clay particles (palygorskite, kaolinite etc) have also been rounded before their transport as dust. Other coarse particles show angular or sub-angular forms which suggest an immediate dust mobilization from the substratum (rocks, regolites or soils); examples are arenitic quartz, chips of quartz or feldspars etc. In other respects, "flying" shapes like flakes of micas or gypsum are particularly favorable to the input as dust and explain the larger size of such particles. This corroborates previous observations such as the occurrence of large African micas in the Atlantic atmosphere (Glaccum & Prospero, 1980). Finally, all these micromorphological characters are good criteria of eolian mobilization



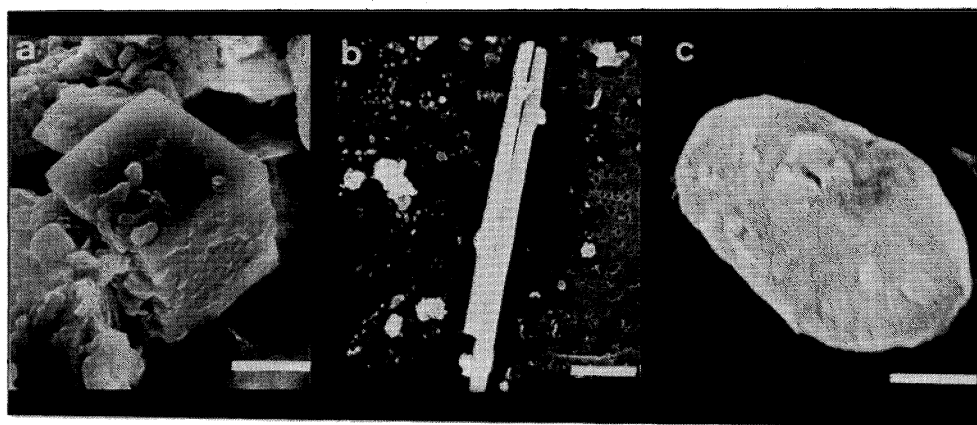
Pl. 2: Coarse particles a/ rounded clayey grain,  $sc = 18\mu m$ ; b/ rounded reddened quartz,  $sc = 20\mu m$ ; c/ rounded K feldspar,  $sc = 20\mu m$ ; d/ rounded Ca carbonate grain,  $sc = 22\mu m$ ; e/ wind-shaped mica,  $sc = 40\mu m$ ; f/ quartz flake,  $sc = 20\mu m$ .



Pl. 3: Fine particles a/ mica,  $sc=1\mu m$ ; b/ Si (quartz?),  $sc=1\mu m$ ; c/ Ca carbonate,  $sc=1\mu m$ ; d/ clayey mixing,  $sc=1\mu m$ ; e/ Al carbonate,  $sc=1\mu m$ ; f/ Fe (hematite?),  $sc=1\mu m$ .

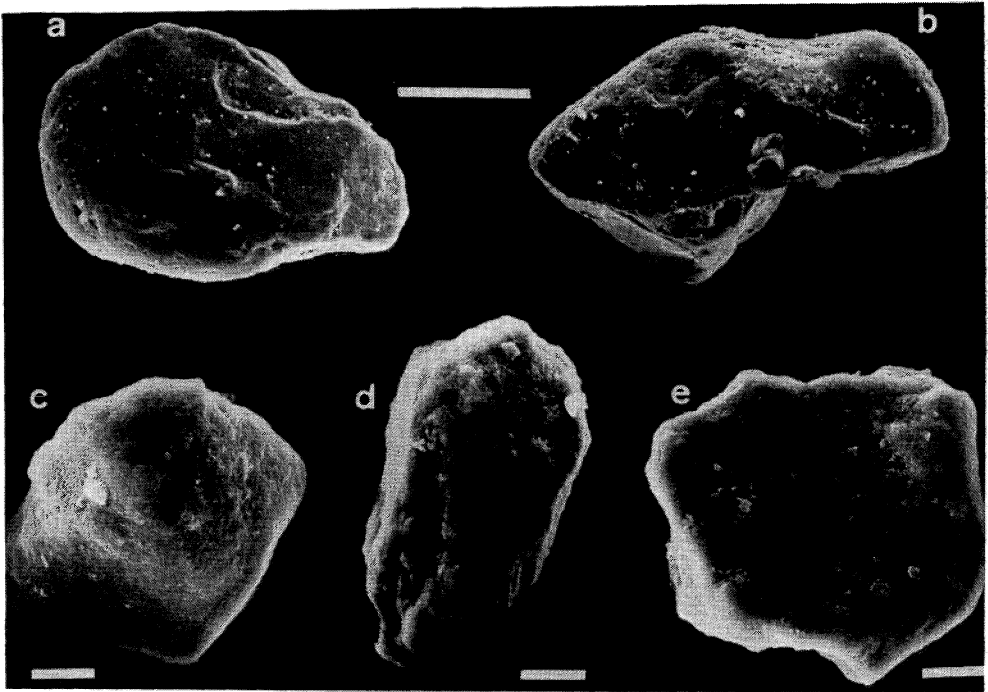
and transport. Since they are inherited from the incipient mobilization phase in the desert, they are not modified during the subsequent transportation as dust.

In spite of the uncertainties of the mineralogical identity noted above, numerous micromorphological similarities are found among the fine fraction of mineral dusts of various origins (Pl. 3 and 4). Crystalline forms (Beta quartz, needles of calcite, calcite rhombohedrons) may be observed. Oblong shapes of the small siliceous particles ( $2\mu\text{m}$ ) suggest a phytolith origin, but some crystal-cleavage planes may confirm the presence of quartz.



Pl. 4: a/ calcite rhombohedron,  $sc = 3\mu\text{m}$ ; b/ needles of calcite,  $sc = 3\mu\text{m}$ ; c/ "oblong" quartz (?),  $sc = 1\mu\text{m}$ .

2.2.3. The problem of the "large" particles in the proximal and distal dusts. Coarsest particles which may be over  $100\mu\text{m}$  across are abundant in dusts, not far from their mobilization area. As a consequence, their occurrence in Saharan dusts sampled in Fuerteventura (Canary Island), in Corsica or in southern France is more surprising. Yet, these particles show indisputable evidence of their Saharan origin, such as the micromorphological and mineralogical characteristics mentioned above. For example, typical rounded reddened quartz have been often observed by SEM (Pl. 5). Similar observations have been made off the African coasts (Game, 1964; Jaenicke & Junge, 1967; Schütz *et al.*, 1977; Glaccum & Prospero, 1980; Carder *et al.*, 1986). Until recently, the possibility of a long distance transport of these large particles by Saharan outbreaks was neglected by theoretical assumptions which were particularly adapted to finest particles (Schütz, 1977; 1979). So it seems now necessary to emphasize the role of such "giant" grains in the deposition budgets, particularly in the soils and sediments of peridesert areas (Coudé-Gausen *et al.*, 1987a).



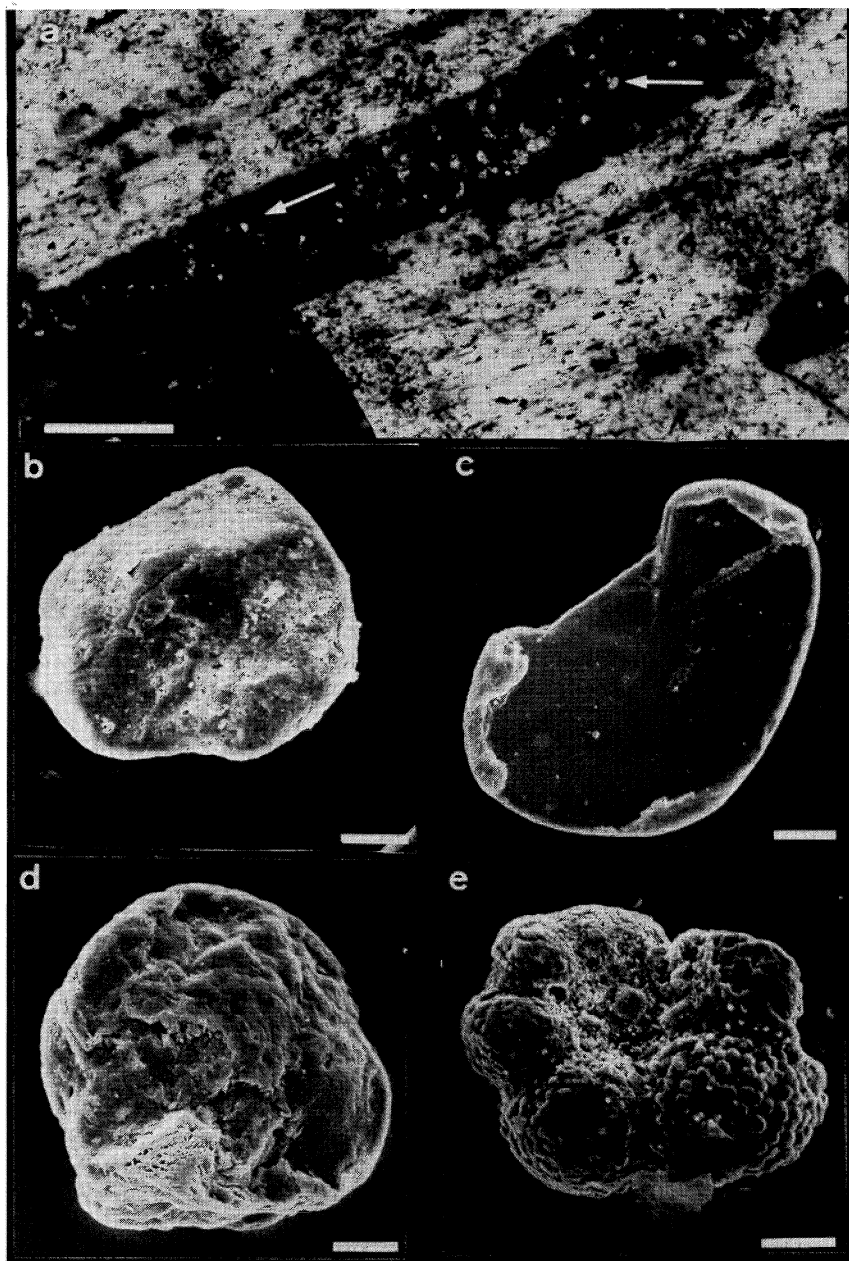
Pl. 5: a & b/ "huge" wind-shaped quartz grains, note the mechanical eolian cups on the edges,  $sc = 75\mu m$ ; c, d & e/ reddened quartz from Saharan dusts upon Canary islands,  $sc = 18\mu m$ .

### 3. ATMOSPHERIC DUSTS AND DEPOSITED DUSTS

Before their incorporation into soils or sediments, dusts are deposited on the soil surface and in cracks of rocks. They are not completely altered by pedogenesis or postdepositional processes and their study can yield information about either inherited desert characteristics or the first postdepositional reworkings.

#### 3.1. The inherited grain-size and micromorphological characteristics of local or proximal dusts

3.1.1. Dusts trapped in rock cracks. Examples of these dusts were sampled in granite cracks of inselbergs in the Sinai and have similar grain-size properties to the atmospheric dusts also sampled in this desert (Coudé-Gaussen *et al.*, 1984). The polarizing microscope examination of thin-plates from various fissured rocks of Sinai, Hoggar, southern-Morocco and eastern Canary Islands has corroborated the existence of trapped dusts and indicated that they have smoothed and even rounded shapes. From the SEM study, their microfeatures are typically eolian and very similar to those previously described for atmospheric dusts (Pl. 6).



Pl. 6: a/ infilling of eolian dusts in rock crack (thin-plate, Sinai granite),  $sc = 200\mu m$ . Wind-shaped grains from granite cracks in Sinai b/ quartz,  $sc = 30\mu m$ ; c/ wind-shaped mica,  $sc = 25\mu m$ ; d/ wind-shaped palygorskite,  $sc = 30\mu m$ ; e/ foraminifera,  $sc = 25\mu m$ .

3.1.2. The morphometrical characterization by Image Analysis and Correspondence Factor Analysis. This study has concerned 375 particles trapped in cracks in andesitic (Ifni, South-Morocco), quartzitic (Jebel Bani, South-Morocco) and schisteous rocks (Anti-Atlas, South-Morocco).

3.1.2.1. Methods. Image analysis has been made by a VICOM System (\*\*) and 8 morphometrical parameters have been selected from the 41 possible ones of the CYTIX Program. The selected parameters were: area (total surface of pixels), perimeter (outline length), mean radius (2S/P), Max. Feret diameter (max. length), Min. Feret diameter (min. dimension perpendicular to Max. Feret), irregularity (convex outline/real outline), circularity ( $4\pi \cdot S/P^2$ ), elongation (Max. Feret/Min. Feret).

After statistical sorting of 6 "variables" by parameters, the data have been processed by "correspondence factor analysis" (CFA) according to the method of Benzécri and coll. (1973). CFA is one of the best mathematical methods adapted for the computer processing of groups of data dealing with numerous "individuals" ("p" samples) defined by an important number of "variables" ("n") in multi-dimensional spaces, using n and p dimensions. In these spaces, a point corresponds either to a "n" value for a given sample or to a "p" value for a given variable. However, because the spaces relative to each point are not directly understandable, the method substitutes "factorial spaces", selected to reduce as far as possible the deformation. The factorial spaces that correspond to the variables and individuals are superimposed and represented simply in a space of fewer dimensions. Hence, the distances between the points can be more easily understood; they translate degrees of similarity between individuals or degrees of correlation between individuals and variables. CFA is graphically presented by a projection of "individual points" and "variable points" on a plane defined by a combination of the first seven "factorial axes" taken two by two.

3.1.2.2. Results. Attributes of grains can be related to various CFA axes. The trapped particles in the andesitic rocks are nearly rounded and regular grains of 80-140 $\mu$ m size. More irregular large grains (150-170 $\mu$ m) also occur. As all these grains are quartz and allochthonous, since quartz is not present in the andesitic rocks, we assume that they are eolian material (typical rounded desert grains) powdered by wind on the andesitic hills. The irregular shapes of other coarse quartz suggests that they were not transported far.

From the CFA, the trapped particles of the quartzites are also regular, circular and not very elongated. Their size varies between 80 and 140 $\mu$ m and they are fine desert sand brought by the wind. However, in this material, there are also some non-circular grains (100-120 $\mu$ m) which may be a non-eolian, local quartzitic contribution.

Finally, in these two previous examples, the rounded shape of grains (well-known in the coarse fraction of local dusts), is a good indicator of an eolian contribution into the crack fillings. In contrast, the trapped material of the schisteous rock induces another factor because the characteristics selected by CFA are not typically eolian and suggest a local origin and a crack filling by slope processes from the nearby rocks. There is no sorting (material between 80 and 170  $\mu$ m), with low roundness, irregularity and high elongation.

### 3.2. The mineralogical differences between the atmospheric and the deposited dusts

The mineralogy of the dust samples has also been processed by two "correspondence factor analyses". The first analysis treats only the clay fraction and the second, the mineralogy of the whole sample.

**3.2.1. Methods.** Clay fractions of 86 samples of atmospheric dusts from two north-Saharan transects (Oran-Hoggar and Tripoli-Hoggar) and deposited and trapped dusts on various substratums (Canary Islands, Sinai, South-Morocco, South-Tunisia) have been studied with CFA. In relation to the rate values, 7 mineralogical parameters (kaolinite, expandable clay interlayers, smectite, illite, chlorite, clay interlayers, palygorskite) have been statistically sorted in 4 variables each. The 7 first axes of CFA give 65% of the information (35% for the 3 first). The complete mineralogy of 61 samples that were processed by the second CFA are from atmospheric dusts of the Oran-Hoggar transect and deposited dusts (Canary Islands, Sinai, South-Morocco, South-Tunisia). 10 mineralogical parameters (quartz; plagioclases, K feldspars, oxides, gypsum, ankerite, calcite sensu stricto, dolomite, aragonite, Mg calcite) and 2 other parameters (percentages of mineralogical clays and Ca CO<sub>3</sub>) have been also sorted in 2 to 4 variables each in relation to their percentages. In this CFA, the 7 first axes give 67% of the information (39% for the 3 first).

**3.2.2. Results and discussion.** The comparison of characteristics on the two CFA axes indicates regional differentiation of dust. For example, the "flying" dust of the two Saharan transects is characterized, on the clay CFA, by abundant smectite (>40%) in Hoggar (Axis II+) but smectite is absent northward in the limestone plateaus and hamadas of northern Sahara (Axis II-). This is well explained by the regional lithology, because the Hoggar soils are composed of weathered volcanic rocks that contain smectite. In contrast, the sandstone plateaus of Tassili and the eastern Murzuk area have dusts that are particularly rich in kaolinite (>15%) and have a notable palygorskite (<20%) content (Fig. 2, Axis I-). All these results agree with previously published data showing that at a large Saharan regional scale there is a geographical relation between the dust mineralogy and the lithology of the substratum (Paquet et al., 1984). In the same way, the trapped dusts of southern Morocco (>25% of illite and absence of palygorskite on the Axis III+) are distinct from all the other deposited dusts of various origin which were rich in palygorskite (>40%) and kaolinite (10-15%) on the Axis I+.

Even without the relation to sampling location or source origin of the dusts, the two CFA results illustrate the general difference between the atmospheric dusts and the deposited ones. Hence, in the clay CFA (Fig. 2), a group of deposited dusts (Axis I+) that are rich in palygorskite (>40%) and kaolinite (10-15%) is contrasted with a group of atmospheric dusts (Axis I-) with higher kaolinite content (>15%) but lower palygorskite content (<20%). Likewise, the trapped dusts of Axis III+ (illite >25%) are distinguished from the "flying" dusts (Axis III-)



which are poorer in illite (15-25%) but have a higher palygorskite content (20-40%). For the CFA of the whole material, the deposited dusts are located on the Axes I+ and II- with either high calcite percentages (>45%) or high quartz values (>65%); in contrast, the atmospheric dusts

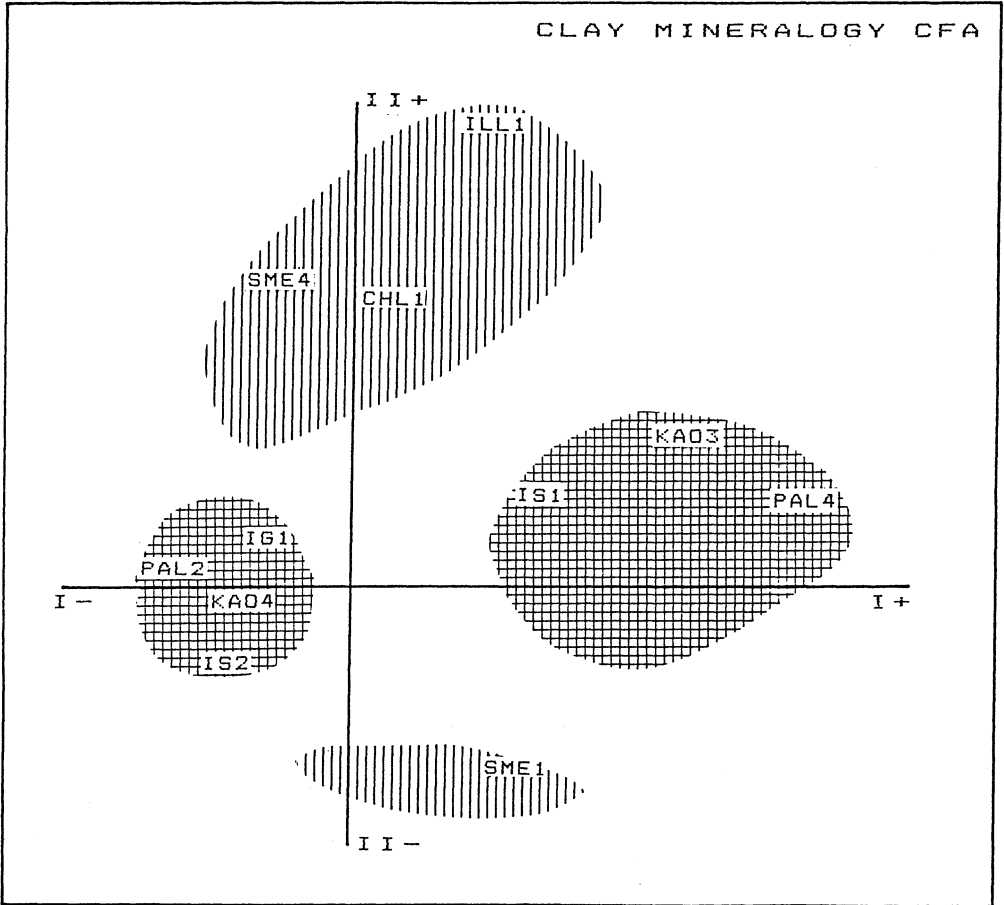


Fig. 2.- Clay mineralogy CFA: Axis I+: trapped dusts in rock cracks (PAL4: palygorskite >40%; KA03: kaolinite 10-15%; IS1: absence of interlayers). Axis I-: atmospheric dusts sampled during the two north-Saharan transects (PAL2: palygorskite <20%; IS2: occurrence of interlayers; KA04: kaolinite >15%; IG1: absence of expandable interlayers). Axis II+: calcite deposits of eolian origin unconformable on varied calcite free substrates (SME4: smectite >40%; ILL1: illite <10%; CHL1: chlorite <5%). Axis II-: atmospheric dusts sampled during the western north-Saharan transect (SME1: absence of smectite).

are characterized by low calcite (10-30%) and clay contents greater than 3%. Such a discrimination suggests that the mineralogical evolution of the dusts begins immediately after their deposition. Neogenic palygorskite seems to be added to the inherited eolian one which may explain explain the high percentages registered in the deposited dusts.

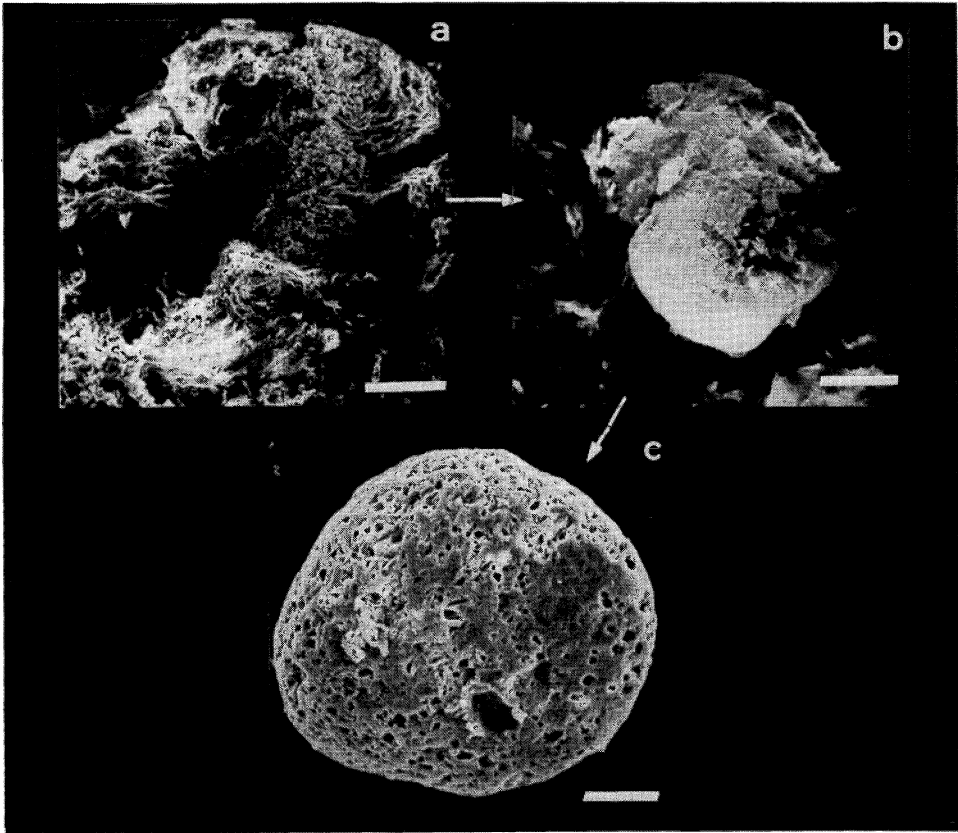
#### 4. CRITERIA OF THE SAHARAN DUST CONTRIBUTION IN THE SEDIMENTATION

The question is to identify mineralogical and micromorphological markers well distinguished by their Saharan origin and eolian dynamics in the continental and marine sediments.

##### 4.1. Occurrence of markers in the present eolian desert dusts

4.1.1. Several markers have been examined by SEM/EDS in proximal dusts sampled by bulk filtrations and cascade impactor. The samples were collected during dust outbreaks in April 1984 and July 1985 on Fuerteventura (Canary Islands), 100km West of the Saharan coasts. The African origin of these atmospheric dusts was proved by remote sensing (Meteosat II, NOAA 7) and computing air-masses trajectories (Coudé-Gausson *et al.*, 1987a). The identification of allochtoneous particles from the African basement has been made easier because the volcanic rocks of the islands do not contain quartz (Coudé-Gausson *et al.*, 1987b). A lot of quartz, mainly the reddened desert variety (2 to >100µm) has been collected. Some of the grains are angular, but some are typically rounded and covered by a surficial film of amorphous silica inherited from mechanical processes of the incipient phase of mobilization in the desert. K feldspars, micas and various rounded and wind-shaped carbonate grains occurred also in the samples. Desert clays such as kaolinite and palygorskite have been identified; this last mineral occurs either as coating of fibres trapped by the surficial hollows of other mineral grains (quartz, micas etc...) or as well-rounded grains entirely composed of clay which makes them very significant markers of Saharan origin and eolian dynamics.

4.1.2. The wind-shaped palygorskite grains: a typical desert marker. This fibrous clay is found in many Saharan areas, such as the large limestone "torba" plateaus or outcrops of clay-rich paleolake deposits. The eolian mobilization and shaping in grains of the clay is well known from the study of a small clay rich sand-sea in northern Mali, the Erg Ine Koussamene (Coudé-Gausson *et al.*, 1983; Coudé-Gausson *et al.*, 1984). Not far from the sedimentary source which was an Holocene lacustrine clay, the dunes have a significant grey colour due to the very high palygorskite content. Farther away, the dunes have a yellow colour due to enrichment in quartz and disappearance of clay. This modification results from deflation processes which selectively remove the small clay particles as dust. From various samples along the sand-sea, it has been observed that the clay particles (Pl. 7) that are irregular near the paleolake area become rounded by rolling and saltation in the sand dunes.



Pl. 7: wind shaping of palygorskite, Erg Ine Koussamene (North-Mali) a/ initial clayey sediment,  $sc=50\mu m$ ; b/ sub-rounded palygorskite particle,  $sc=15\mu m$ ; c/ well-rounded palygorskite grain with its surficial fibers compaction,  $sc=15\mu m$ .

They are slowly comminuted and are entrained in the air when they become small enough ( $<150\mu m$ ).

SEM examination of such wind-shaped palygorskite grains shows a notable surficial alteration of the fibrous microstructure. The incipient mobilization of the grain has modified the fiber assemblages by compaction and abrasion giving the surfaced "felt-like" structure. This cortex explains the relative hardness of the grains and their survival in dusts and sediments. Today, such wind-shaped palygorskite grains have been found in atmospheric desert dusts (Tanezruft, Sinai, Canary Islands), in soils (Canary Islands), recent sediments as peridesert loess (South-Tunisia, Negev), wadi terraces (South-Tunisia, South-Morocco) and sea cores of the Gulf of Gabes, Mediterranean Sea (Coudé-Gaussen & Blanc, 1985; Coudé-Gaussen, 1987a). The importance of palygorskite as a significant marker of Saharan origin has also been supported by Schütz and Sebert (1987), but particular attention should be paid to its occurrence as wind-rounded grains.

4.1.3. Occurrence of such markers in distal dusts. Quartz, dolomite, kaolinite and palygorskite have been previously used as African markers. However, the fineness of these particles may make the identification of an eolian shaping difficult. The best indicator of their origin is their presence in characteristic mineral assemblages of typical Saharan dust outbreaks.

#### 4.2. The dust contribution to the continental and marine sediments

The dust contribution to soils and sediments has been most important near the desert source area. Hence, the eolian deposition might be massive during the Pleistocene on the Saharan margins, as is shown by the peridesert loess in southern Tunisia and all around the Sahara (Coudé-Gaussen, 1987b). On the contrary, the dust contribution has been more scattered in the soils, continental or marine sediments and its identification is more difficult.

4.2.1. The allochthonous and topographical location. The allochtony and unconformity of a deposit on a substratum is the best evidence of past sedimentation of dust and is well known in many examples. For example, the Pleistocene loess of the Matmata plateau (South-Tunisia), which has a major quartz component, lie on Mesozoic limestones (Coudé-Gaussen & Rognon, 1988a). In the same way, numerous calcretes lying on non-carbonate rocks of southern Morocco or Fuerteventura (Canary Islands) are derived from carbonate eolian dusts (Coudé-Gaussen & Rognon, 1988b).

The topographic location is another evidence of dust contribution. The summit location of an unconformable deposit can only be explained by a dust contribution as has been shown by calcretes or infillings in quartzitic or volcanic hills. The air transport is indeed the only explanation for the allochthonous particles sampled in Canary Islands.

4.2.2. The identification in marine sediments. In such deposits, the sparse dust particles are often difficult to distinguish from other terrigenous contributions. Quartz or reddened desert quartz contents have previously been used as indicators of eolian contribution in marine sediments (Window, 1975; Diester-Haass, 1976; Diester-Haass, 1979; Kolla *et al.*, 1979; Sarnthein, 1979; Sarnthein *et al.*, 1981; Sarnthein *et al.*, 1982; Dauphin, 1983).

In the Gulf of Gabes sea cores, dust contributions are evident all along the Pleistocene marine sedimentation. This is shown by the SEM micromorphological criteria. Gypsum and carbonate rounded aggregates, typical wind-shaped quartz and palygorskite grains are good indicators. A clear relationship may be established between the sands of the Saharan Great Eastern Erg and the loess of Matmata; and between this loess and the eolian contribution to the marine sediments of Gulf of Gabes.

TABLE I Dust particle shapes related to their attributes

SIZE	TYPE OF SHAPES	SHAPE ORIGINAL INHERITED	MINERAL/GENETIC ATTRIBUTIONS
<i>GEOMETRICAL</i>			
	globule	+	organic matter
	ball	+	pollution/volcanism
	cube/parallelep.	+	NaCl
	hexagon	+	Ca sulfate
	needle	+	gypsum/epsomite
<i>ANY SHAPE</i>			
0,5-5 $\mu$ m	chain aggregate	?	?
	fluffy	?	clayey mixtures
	micro-aggregate	?	clayey mixtures
	flake	+	{ quartz/micas quartz/K feldspars albite/carbonates heavy minerals gypsum/hematite zeolite/calcite phyllites
	sub-angular	+	
	sub-rounded	?	
<i>GEOMETRICAL</i>			
	rod	+	gypsum/NaCl/Ca carb.
	fibre	+	gypsum
	cube/parallelep.	+	NaCl/trona/chlorides
<i>ANY SHAPE</i>			
10-20 $\mu$ m	chain aggregate	?	?
	elongated	+	vegetal fibres
	chip	+	quartz/volc.minerals quartz/palygorskite
	sub-angular	+	{ clayey mixtures/ K feldspar/kaolinite Ca carb./phyllites
	sub-rounded	+	
	rounded	+	
<i>GEOMETRICAL</i>			
	rhombohedron	+	calcite/dolomite
	disk/pipe	+	diatoms/phytolithes
<i>ANY SHAPE</i>			
>20 $\mu$ m	elongated	+	gypsum/microcodium vegetal fibres
	angular	+	quartz/volc.minerals gypsum
	sub-angular	+	{ quartz/palygorskite Ca carb./K feldspars clayey mixtures/micas heavy minerals Zn/Ca phosphorites
	sub-rounded	+	
	rounded	+	

## 5. CONCLUSIONS

Sedimentological data (mainly grain-size) allows local, proximal and distal dusts, whose characters vary in relation to the desert source distance, to be distinguished. In order to characterize the role of dust in relation to terrigenous contribution in the soil or sediment materials, it seems necessary to supplement the mineralogical and chemical data with more complete micromorphological study of the particles themselves.

Our SEM/EDS observations that concern the shapes, microfeatures and genetic attributes of all the dust samples studied here, are summarized in the Table 1 where the particle size modes are about 0,5-5 $\mu$ m, 10-20 $\mu$  and >20 $\mu$ m. In this table, three kinds of genetic attributes are distinguished: a marine origin for some crystalline particles from Canarian samples, an anthropogenic origin related to industrial activities around the desert, and a mineral and detrital origin. Strictly speaking, this last origin is only significant for a Saharan source. On the other hand, some particle shapes are given as "original"; this means that they do not have any erosional modifications. But many associated particles (mainly mineral) have been reworked, aggregated or comminuted by various weathering and erosional processes until their subsequent air loading. In the coarser fractions, the particles commonly show shapes and surficial microfeatures inherited from the mechanical processes of the incipient eolian phase. Chemical solution/deposition microfeatures are often observed on the finest particles. However for these last particles, the problem is to decide if some microfeatures and shapes may have been obtained during the air-transport. For example, the formation of chain-aggregates could not be attributed to static electricity and the smoothing of smallest quartz to chemical solution by droplets in wet clouds?

Furthermore, significant markers of desert origin can be characterized by their microfeatures and mineralogical compositions. Knowledge of the present Saharan dusts seems to be a good guide for the understanding of dust contribution to past sedimentation around deserts.

**ACKNOWLEDGEMENTS.** The author is grateful for help and stimulating discussion with Dr. P. Blanc \* (Centre de Microscopie, Univ. P. & M. Curie, Paris) and Dr. L. Humbert \*\* (Institut de Géodynamique, Univ. Bordeaux, France).

## REFERENCES

- Benzécri, J.P. et collab.: 1973, 'L'analyse des données. T.1. La Taxinomie. T.2. Analyse des correspondances'. - Dunod, Paris, 615p. + 619p.
- Bergametti, G., Vié Le Sage, R., Grubis, B., Dulieu, B. and Elichegaray, C.: 1983, 'Relation between particulate concentration in the atmosphere and aerosol collection efficiency'. - *Environ. Technol. Lett.*, 3, pp. 297-304.

- Busche, D., Draga, M. and Hagedorn, H.: 1984, 'Les sables éoliens. Modèles et dynamique. La menace éolienne et son contrôle'. GTZ n° 162, Eschborn, FRG., 770 p.
- Carder, K.L., Steward, R.G., Betzer, P.R., Johnson, D.L. and Prospero, J.M.: 1986, 'Dynamics and composition of particles from an aeolian input event to the Sargasso Sea'. - *J. Geophys. Research*, 91, D1, pp. 1055-1066.
- Coudé-Gaussen, G.: 1987a, 'Observations au MEB de fibres de palygorskite transportée en grains par le vent'. In N. Fedoroff, L.M. Bresson and M.A. Courty (eds.), *Micromorphologie des sols*, AFES, Paris, pp. 199-205.
- Coudé-Gaussen, G.: 1987b, 'The perisaharan loess: sedimentological characterization and paleoclimatical significance'. In M. Pecci (ed.), *Studies on the distribution, origin, subdivision of loess and related deposits*, *GeoJournal*, Special Issue INQUA Congress Ottawa 1987, 15, 2, pp. 177-183.
- Coudé-Gaussen, G. and Blanc, P.: 1985, 'Présence de grains éolisés de palygorskite dans les poussières actuelles et les sédiments récents d'origine désertique'. *Bull. Soc. géol. Fr.*, 1, 4, pp. 571-579.
- Coudé-Gaussen, G. and Rognon, P.: 1988a, 'The Upper Pleistocene loess of Southern Tunisia: a statement'. *Earth Surf. Proc. Landf.* 13, pp.137-151.
- Coudé-Gaussen, G. and Rognon, P.: 1988b, 'Encroûtements calcaires d'origine éolienne sur l'île de Fuerteventura (Canaries orientales)'. *Geoderma*, 42 (in press).
- Coudé-Gaussen, G., Riser, J. and Rognon, P.: 1983, 'Tri éolien et évolution du matériel dunaire par vannage et fragmentation: l'Erg Ine Koussamène (Nord-Mali)'. - *C.R. Acad. Sci. Paris*, 296, 2, pp. 291-296.
- Coudé-Gaussen, G., Riser, J. and Rognon, P.: 1984, 'L'Erg Gris d'Ine Koussamène: un exemple d'erg à dunes d'argile'. - In N. Petit-Maire and J. Riser (eds.), *Sahara ou Sahel? Publ. CNRS et Ministère des Relations Extérieures*, pp. 97-119.
- Coudé-Gaussen, G., Rognon, P. and Fedoroff, N.: 1984, 'Piégeage de poussières éoliennes dans des fissures de granitoïdes du Sinaï oriental'. *C.R. Acad. Sci. Paris*, 298, 2, 8, pp. 369-374.
- Coudé-Gaussen, G., Rognon, P. and Hoyos-Gomez, M.: 1987b, 'Indicadores mineralógicos de polvo de origen sahariano recogido en la Isla de Fuerteventura (Canarias)'. *Estudios Geológicos* (in press).
- Coudé-Gaussen, G., Rognon, P. and Weisrock, A.: 1982, 'Evolution du matériel sableux au cours de son déplacement dans un système dunaire - les barkhanes du Cap Sim au Sud d'Essaouira (Maroc)'. *C.R. Acad. Sci. Paris*, 295, 2, pp. 621-624.
- Coudé-Gaussen, G., Rognon, P., Bergametti, G., Gomes, L., Strauss, B., Gros, J.M. and Le Coustumer, M.N.: 1987a, 'Saharan dust on the Fuerteventura Island (Canary Islands): chemical and mineralogical characteristics, air-mass trajectories and probable sources'. *J. Geophys. Research*, 92, D8, pp. 9753-9771.

- Dauphin, J.P.: 1983, 'Eolian quartz granulometry as a paleowind indicator in the Northeast Equatorial Atlantic, North Pacific and Southeast Equatorial Pacific'.- PhD Thesis, Univ. Rhode Island, USA., 335p.
- Diester-Haass, L.: 1976, 'Late Quaternary climatic variations in northwest Africa deduced from East Atlantic sediment cores'.- *Quaternary Res.*, 6, pp. 299-314.
- Diester-Haass, L.: 1979, 'Indicators of continental climates in marine sediments'. A reply.- "*Meteor" Forsch. Ergebnisse*, C, 31, pp. 53-58.
- Game, P.M.: 1964, 'Observations on a dust fall in the eastern Atlantic, February 1962'.- *J. Sediment. Petrol.*, 34, pp. 355-359.
- Glaccum, R.A. and Prospero, J.M.: 1980, 'Saharan aerosols over the tropical North Atlantic, mineralogy'.- *Mar. Geol.*, 37, 3/4, pp. 295-321.
- Jaenicke, R. and Junge, C.: 1967, 'Studien zur oberen Grenzgrösse des natürlichen Aerosols'.- *Beitr. Phys. Atmos.*, 40, pp. 129-143.
- Kolla, V., Biscaye, P.E. and Hanley, A.F.: 1979, 'Distribution of quartz in Late Quaternary Atlantic sediments in relation to climate'. *Quaternary Res.*, 11, pp. 261-277.
- Krinsley, D.H. and Doornkamp, J.C.: 1973, '*Atlas of Quartz Sand Grain Surface Textures*', Cambridge Univ. Press, New York, 91p.
- Kuenen, P.H.: 1960, 'Experimental abrasion. IV. Eolian action' *J. Geol.*, 68, pp. 427-449.
- Le Ribault, L.: 1977, '*L'exoscopie des quartz*'. Masson, Paris, 150p.
- Mazzullo, J., Sims, D. and Cunningham, D.: 1986, 'The effects of eolian sorting and abrasion upon the shapes of fine quartz sand grains'. *J. Sed. Petrol.*, 56, pp. 45-56.
- Paquet, H., Coudé-Gaussen, G. and Rognon, P.: 1984, 'Etude minéralogique de poussières sahariennes le long d'un itinéraire entre 19 et 35° de latitude Nord'. *Rev. Géol. dyn. Géogr. phys.*, 25, 4, pp. 257-265.
- Pye, K.: 1987, '*Aeolian dust and dust deposits*', Academic Press, London, 352p.
- Sarnthein, M.: 1979, 'Indicators of continental climates in marine sediments. A discussion'.- "*Meteor" Forsch. Ergebnisse*, C, 31, pp. 49-51.
- Sarnthein, M., Tetzlaaf, G., Koopmann, B., Wolter, K. and Pflaumann, U.: 1981, 'Glacial and interglacial wind regimes over the eastern sub-tropical Atlantic and northwest Africa'.- *Nature*, 293, pp. 193-196.
- Sarnthein, M., Thiede, J., Pflaumann, U., Erlenkeuser, H., Fütterer, D., Koopmann, B., Lange, H. and Seibold, E.: 1982, 'Atmospheric and oceanic circulations patterns off Northwest Africa during the past 25 Million years'.- In C. Von Rad, K. Hinz, M. Sarnthein and E. Seibold (eds.), *Geology of the Northwest African continental margin*.- Springer-Verlag, Berlin, pp. 545-604.
- Schütz, L.: 1977, 'Die Saharastaube-Komponente über dem subtropischen Nord-Atlantik.' PhD. Thesis, Univ. Mainz, FRG., 153p.



- Schütz, L.: 1979, 'Sahara Dust Transport Over the North Atlantic Ocean - Model Calculations and Measurements'. In C. Morales (ed.), *Saharan Dust: Mobilization, Transport, Deposition*.- Wiley, Chichester, UK., pp. 267-277.
- Schütz, L. and Seibert, M.: 1987, 'Mineral aerosols and source identification'.- *J. Aerosol Sci.*, 18, 1, pp. 1-10.
- Schütz, L., Jaenicke, R. and Pietrek, H.: 1977, 'Saharan dust transport over the North Atlantic Ocean'.- In T.L. Péwé (ed.), *Desert Dust: Origin, Characteristics and Effect on Man*.- Spec. Paper, Geol. Soc. Amer., 186, pp. 87-100.
- Whalley, W.B., Smith, B.J., McAlister, J.J. and Edwards, A.: 1987, 'Aeolian abrasion of quartz particles and the production of silt-size fragments, preliminary results and some possible implications for loess and silcrete formation'. In I. Reid and L. Frostick (eds.), *Desert sediments Ancient and Modern*. Blackwell, Oxford (in press).
- Windom, H.L.: 1975, 'Eolian contribution to marine sediments'.- *J. Sed. Petrol.* 45, pp. 520-529.

## ATMOSPHERIC MINERAL DUST - PROPERTIES AND SOURCE MARKERS

Lothar Schuetz  
Institute for Meteorology  
Johannes Gutenberg-University  
P.O. Box 3980  
6500 Mainz  
Federal Republic of Germany

**ABSTRACT.** Mineral dust particles from arid regions of the earth are a substantial fraction of the atmospheric aerosol. Due to long range transport mineral dust is found in all types of airmasses and thus in remote regions too. Physical and chemical properties allow to distinguish mineral aerosols easily from other types of aerosols. Many characteristic features are similar to those of global average crust. Only major deviations from this mean composition are reflected by the mineral aerosol composition. In order to derive source characteristic features from mineral dust samples advanced statistical methods coupled with various analytical tools from the mineralogy and chemistry must be applied.

### 1. INTRODUCTION

Atmospheric mineral dust is found in all geographical regions of the earth. This omnipresence is due to long range transport over thousands of kilometers in the atmosphere. Sources are the arid and semi-arid regions of the continents. In many respects, there is evidence for the importance of airborne dust influencing many processes in the atmosphere and the hydrosphere. For instance, during the course of formation and deposition of precipitation, dust particles are incorporated in droplets and thus play an important role in the cycle of atmospheric hydrometeors. Scattering and absorption of solar radiation due to the presence of dust particles causes atmospheric turbidity and changes the radiation budget. Once deposited in the hydrosphere, major and minor compounds of the dust are released and incorporated various cycles until the material reaches the sediments. Therefore many ocean sediments have a strong aeolian component. On the continents, airborne mineral dust contributes significantly to the soil formation. The great Loess areas are examples for past aeolian deposits.

Mineral dust is produced by weathering of soil and deflation. This liberation of dust particles can be considered mostly as a natural process. However, in highly populated desert regions and areas with bad land use practices, the rate of deflation can be significantly enhanced. About one third of the continental surfaces can be addressed as potential dust sources. Therefore, soil dust is an important aerosol component in the

atmosphere.

The goal of this contribution is to describe major physico-chemical properties of atmospheric mineral dust. Total number and mass concentrations, the size distribution and its alteration during transport are discussed as well as optical properties. Beside these physical properties, the chemical composition with respect to elements and mineral compounds will be presented. Based on this overview, possibilities are discussed to find source specific markers in order to detect contributions of different source regions.

According to the fact that desert regions are very remote and some of them rather difficult to access, the data basis for mineral aerosols from arid areas is often very poor. Despite many logistical and travel problems, the Sahara (the largest desert of the world) is the best investigated source area for mineral dust. Long range transport from the Sahara to other continents and deposition into the oceans is rather well investigated too. This explains why in this contribution mostly Saharan related data will be used. However, many of the major conclusions from Saharan studies may easily be addressed as basic characteristics which are valid for other sources and mineral aerosols too.

## 2. PHYSICAL PROPERTIES OF MINERAL AEROSOLS

In all kinds of air masses aerosol particles including soil derived material can be found. Aerosol particles cover usually a size range between 0.001  $\mu\text{m}$  and roughly 100  $\mu\text{m}$  radius. Aerosol particles are produced mainly by two basic processes, "gas to particle conversion" (GPC) and "bulk to particle conversion" (BPC). GPC is responsible for the particle production in the small size particle regime. BPC describes the desintegration of bulk material, for instance, by weathering of terrigenous matter. Mineral particles derived from this process cover a size range from about 0.01  $\mu\text{m}$  up to more than 100  $\mu\text{m}$  radius. The erosion process by which particles from soil surfaces are liberated is very complex and depends on a number of micrometeorological and soil parameters as described comprehensively by GILLETTE (1981). Source areas for soil dust are surfaces with unconsolidated material and areas with active weathering like alluvial fans, outwashes, wadis etc. Thus dust productive soil surfaces are usually of small scale and are not easy to determine. Some of these source related characteristics are described by d'ALMEIDA (1987) and PYE (1987). Concentrations and size distributions of particles in the atmosphere, therefore, depend not only on the availability within the sources but also on transport, transformation, deposition and resuspension processes.

In order to distinguish different aerosol types, key parameters like total concentrations and size distributions are used. Both concentrations and size distributions are closely related to each other, because the total concentration is the integral over the distribution. On the basis of number distributions, other parameters like mass- and volume distributions and derived from this, total mass and volume concentrations can be calculated. Total number concentrations can be measured also

directly with Aitken nuclei counters and mass concentrations can be determined by gravimetric air filter evaluation. With respect to many air chemistry applications and characterisation of airmasses, the total number concentration  $N$  is used as a typical measure. This number varies tremendously over a range with number concentrations  $N \ll 100 \text{ cm}^{-3}$  in very clear aged polar airmasses up to values of  $N \gg 100000 \text{ cm}^{-3}$  in polluted air masses. Table (1) shows a compilation of average total number concentrations  $\bar{N}$  from dust carrying airmasses over the Sahara, in vicinity of the Sahara and within the long range transport over the North Atlantic Ocean. Under normal atmospheric conditions values of  $N$  do not exceed  $900 \text{ cm}^{-3}$  over the source area and near the source area over the ocean. During dust storms, concentrations in the range of  $600 \text{ cm}^{-3}$  and  $2000 \text{ cm}^{-3}$  were found. When considering that concentrations in remote continental airmasses (without strong dust sources) are on the order of  $500 \text{ cm}^{-3}$ , it becomes clear, that the mineral soil dust production is not controlling the total number concentration of mineral aerosols in Saharan airmasses. The moderately enhanced concentrations up to about  $2000 \text{ cm}^{-3}$  during sand storm conditions may be explained perhaps by incorporation of polluted airmasses into cyclonic disturbances during the formation of dust storms. Thus, total number concentrations of mineral aerosols are similar to the 'background' and 'remote continental' aerosol values.

This categorisation, however, does not hold true when comparing number size distributions of such aerosols with each other. Fig.1a shows number size distributions in a double logarithmic presentation, where  $dN/d\log r$  in  $\text{cm}^{-3}$  is plotted as a measure of concentration versus particle radius  $r$ . As an example for typical desert aerosols average size distribution during strong dust winds, turbid and clear atmospheric conditions from a measuring campaign at Agadez, Niger, are presented. Highest concentrations are found during strong dust storms and lowest for clear atmospheres over the whole size range. The shape of the mineral distribution shows a continuous concentration decrease for particles with  $r > 0.3 \mu\text{m}$ , which indicates, that no major size selective deflation processes take place. At about  $0.1 \mu\text{m}$  radius the maximum of the size distribution can be expected. Below  $0.1 \mu\text{m}$  radius extreme variable concentrations (not included in Fig.1) were observed. The average tendency with this size range is towards decreasing concentrations with decreasing radius, as indicated by d'ALMEIDA and SCHUETZ (1983). The variability among each type of distribution is very large and ranges roughly from about one order of magnitude in the submicron range up to more than two orders of magnitude in the ultra-giant particle size range with  $r > 20 \mu\text{m}$ . Especially, during sandstorms the variability is extreme because under

these conditions such large particles are lifted up temporarily as the 'desert dust storm' type distribution shows. Particles with radii of hundreds of micrometers can easily be found airborne. Size distributions of other desert airmasses by d'ALMEIDA and SCHUETZ (1983) and average desert type distributions by d'ALMEIDA (1987) show a similar behaviour. Based on these features, approximations of desert type distributions in between 'background', 'remote continental' and even 'urban' type ave-

TABLE 1 : Total particle number concentration  $\bar{n}$  in Saharan airmasses

region	average concentration $\bar{n}$ , $\text{cm}^{-3}$		reference
	normal atm. conditions	strong dust wind	
source:			
Agadez (Niger)	400 - 800	800 - 2000	Author
source near:			
West African Coast	400 - 600	600 - 800	Dreiling et al. 1988
long range transport:			
Cape Verde Islands	870	870	Jaenicke 1978
Eastern -		710, 860*	*Jaenicke et al. 1971
Central -	440		
Western -	370		
Subtropical North Atl.			

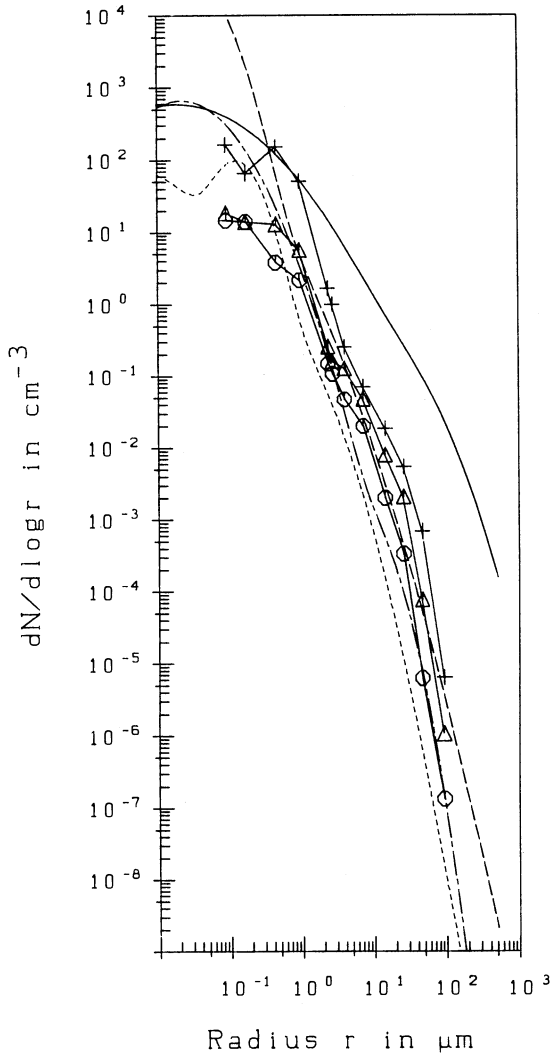


Fig.1a: Mineral aerosol size distributions over the Sahara: Agadez, Niger: + - + dustwind,  $\Delta$  -  $\Delta$  turbid and O - O clear atmospheric conditions versus model distributions (JAENICKE, 1988): ---- desert-dust storm, - - - "urban", - . - . "remote continental"- and - - - "background"-aerosols

rage distributions are not justified. Desert type aerosol number distributions, therefore, must be accepted as its own category. Concentrations in the submicron range are similar to 'background' and 'remote continental' aerosols, but, concentrations of the supermicron range easily exhibit values of 'urban' aerosols. For the use in calculations, parameters of such distributions can be found in a compilation of physical and chemical aerosol properties by JAENICKE (1988). Conversion of the number distributions from Fig.1a into volume distributions (Fig.1b) emphasizes strongly the variability of the size distribution especially in the supermicron range. Simply by multiplying by a uniform particle density such distributions can be converted into mass distributions. Fig.1b also shows that most of the mineral aerosol volume or mass is confined to the size range of about 0.1  $\mu$ m and 100  $\mu$ m radius.

This general statement can be taken as representative for desert regions. However, when dust laden airmasses emerge from the source region and are subject to long range transport, very characteristic alterations of the shape of the distributions take place. For instance, due to sedimentation and scavenging processes large particles are removed from the dust plume. Fig.2 shows in the upper part this sand and dust fractionation process compiled by JUNGE (1979) on the basis of surface air aerosol measurements and model calculations by SCHUETZ (1979). Starting with the original soil material, the mass distribution shows lower concentrations with progression of the fractionation and increasing transport distances. The modes of the mass distributions will be shifted towards smaller particle sizes. As a first product of dust deposition in a distance of a couple of hundreds of kilometers around source areas Loess deposits are formed. During further atmospheric long range transport of more than about 1000-2000km distances the larger particles with radii  $r > 5 - 10 \mu$ m will be strongly depleted. However, actual measurements made several thousands kilometers from the sources over the oceans and in sediments show the presence of giant single particles of the order of 50  $\mu$ m radius (CARDER et al., 1986). In contrast to model calculations (SCHUETZ, 1979 and WESTPHAL, 1987), the existence of such particles can only be explained by assuming strong atmospheric updrafts and convective motions in the vicinity of frontal systems. However, the major mineral aerosol mass, which is able to travel long distances, is restricted to the size range with radii less than about 5  $\mu$ m.

This feature also explains the enormous variations among mineral aerosol mass concentrations which are measured over the deserts and after being transported for long distances. The data base for a survey of mineral dust concentrations (Fig.3) for different air mass regimes is rather good. Air chemistry measurements, total mass concentrations have been determined, and many elemental concentrations determined in various regions of the atmosphere allow us to estimate mineral dust concentrations on the basis of mean crustal proportions. According to Fig.3 (a revised version of a survey proposed by JUNGE (1979)) shows mass concentrations of the desert dust between about 50  $\mu$ g/m<sup>3</sup> under clear atmosphere conditions up to hundreds of thousands micrograms per cubic meter during heavy sandstorms. Lowest mineral concentrations can be found in polar regions with values less than about 0.01  $\mu$ g/m<sup>3</sup>. The whole range

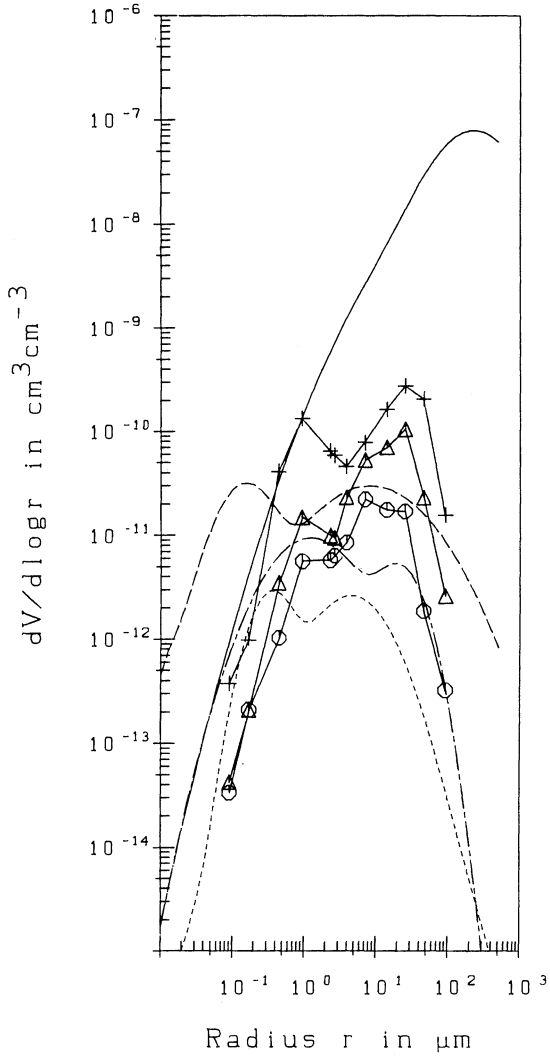


Fig.1b: Volume distributions of Fig.1a



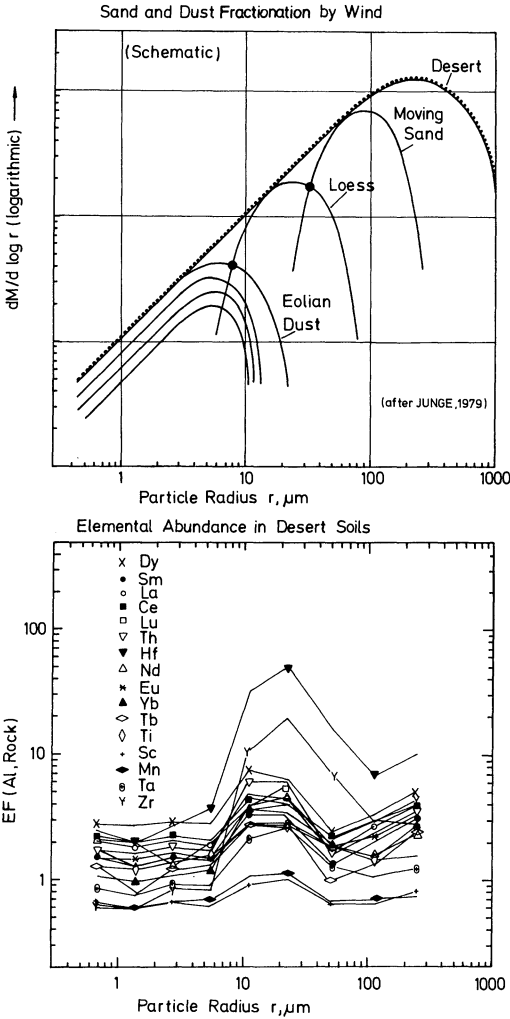


Fig.2: Upper section: Schematic sand and dust fractionation by wind. Characteristic development of mass distributions from desert soils being eroded and injected into the atmosphere and progressive aeolian long range transport (after JUNGE, 1979 and Schuetz, 1979). Lower section: elemental abundances relative to crustal average rock of rare earth and other related elements in desert soils versus particle size expressed as enrichment factors EF(Al,rock) (after SCHUETZ and RAHN, 1982) © Schütz and Sebert (1987) Atmos. Env. 16, pp. 171-176 Pergamon Press.

## Survey of the Concentration Ranges of Mineral Dust in the Troposphere

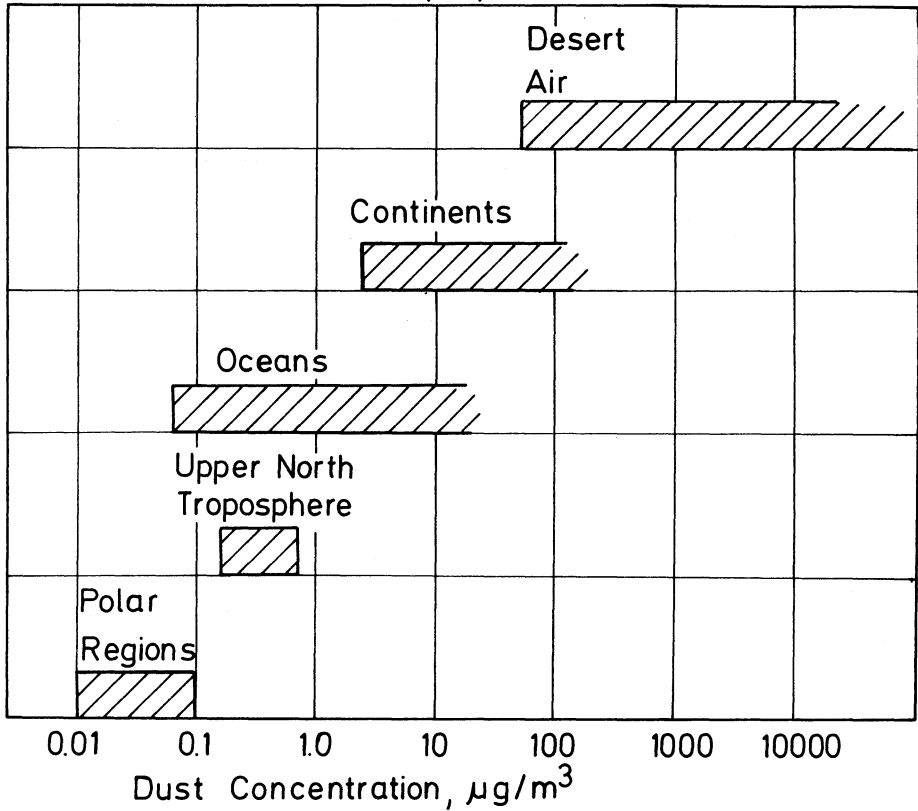


Fig.3: Survey of mineral aerosol mass concentrations in different air-masses after JUNGE (1979)

© Schütz (1987) In: Atmosphärische Spurenstoffe, R. Jaenicke, Ed., pp. 341-357 VCH-Verlagsgesellschaft, 6940 Weinheim, FRG.

of mass concentrations covers about eight orders of magnitude. This survey may justify the very first statement of this contribution, that mineral dust is omnipresent. Obviously, over the source regions, mineral aerosol is always available for any long range transport. Insolation over the desert creates strong turbulence in the boundary layer, forcing wind erosion, by which particles are injected into the atmosphere. Strong convection also lifts particles up into elevations of the middle troposphere. Such processes build up a particle reservoir over the desert which is always present. For example, an investigation of time series of the Linke turbidity factor over the western Sahara by JAENICKE (1979) shows long-term average values of 4. This factor expresses total columnar mass loads of trace substances in terms of pure molecular atmospheres. An average turbidity factor of 4 can be taken as a good evidence for an appreciable 'background' of dust. The permanent availability of dust also is expressed by Fig.4, where mass concentrations versus windspeed are plotted for mineral aerosols and sea salt respectively. This picture is based on a compilation of world wide mineral dust and sea salt measurements by JAENICKE and SCHUETZ (1988a). Except a generally assumed windspeed dependency for mass concentrations, Fig.4 shows clearly that even under low windspeed conditions mineral dust in concentrations of about 50 - 100  $\mu\text{g}/\text{m}^3$  is present. Additionally, Fig.4 also stresses that deserts obviously have a much higher productivity of particulate matter than the oceans, when assuming, that similar production processes in the BPC size range are dominant. Very recent estimates on the global annual production of various aerosol components (JAENICKE, 1988) show values of about 2000 x  $10^{10}$  tons of mineral dust injected into the atmosphere compared to about 1000 x  $10^{10}$  tons of sea salt matter.

In order to determine radiative effects of aerosols, informations on the size distributions and on optical properties are required. Optical properties usually are expressed as a number of different parameters like complex index of refraction, coefficients related to extinction, single scattering albedo, asymmetry factor and optical depth. Among these parameters the complex index of refraction is the fundamental property which is needed to describe scattering and absorption of incident sunlight. Therefore the complex index of refraction will be discussed in this section. The importance of the other parameters in relation to soil dust aerosols is covered by the contribution of d'ALMEIDA (1987). The complex index of refraction  $m$  is expressed by the relation:  $m = n_{\text{S1ReT}} - i n_{\text{S1ImT}}$ . The real component  $n_{\text{S1ReT}}$  is usually known as the refractive index.  $n_{\text{S1ImT}}$ , the imaginary component is an absorption parameter that is related to the usual bulk absorption coefficient. Both  $n_{\text{S1ReT}}$  and  $n_{\text{S1ImT}}$  show a dependence of wavelength in the visible and infrared region of the spectrum. A review of optical properties of crustal derived aerosols by CARLSON and BENJAMIN (1980) and PATTERSON (1981) and a compilation of properties for different aerosol types by JAENICKE (1988) show very distinct patterns of the wavelength dependency. Within the visible part of the spectrum,  $n_{\text{S1ReT}}$  has a value of approximately 1.5 for the major aerosol types including soil dust aerosols. The wavelength dependency of  $n_{\text{S1ReT}}$  is only slight. Values of  $n_{\text{S1ImT}}$  are on the order of  $10^{-2}$  with a well expressed wavelength dependency. PATTERSON (1981) showed that

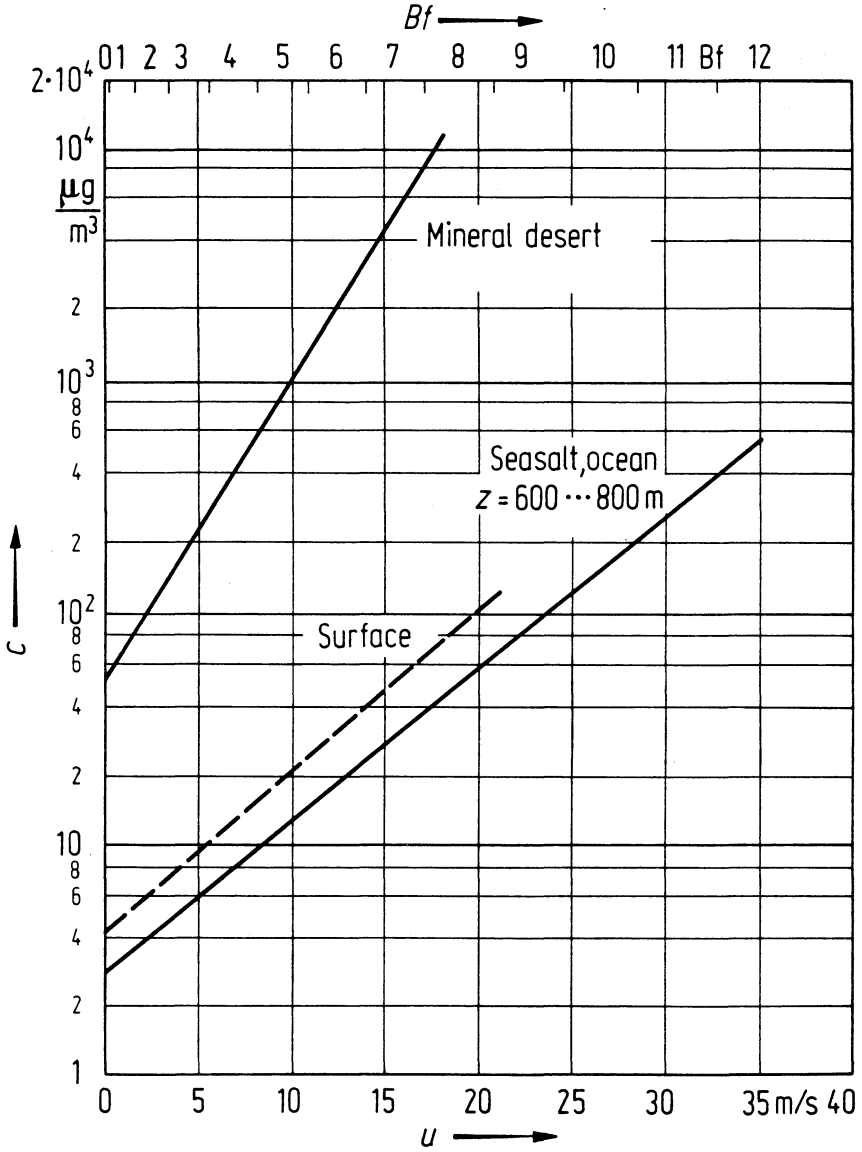


Fig.4: Mineral aerosol and sea salt aerosol mass concentrations versus windspeed after JAENICKE AND SCHUETZ (1988)

© Jaenicke and Schütz (1988 a + b) Landolt-Boernstein New Series, Group V Springer Verlag.

for pure crustal aerosols primarily consisting of clay minerals there was a great uniformity among many measurements on a global basis. In the case of Saharan aerosol over the Atlantic Ocean (PATTERSON et al., 1977) the pattern of both  $n_{SIR}$  and  $n_{SIM}$  showed no significant differences for samples near the West African Coast or near the Caribbean. However, the most notable features can be seen in the infrared part of the spectrum for both  $n_{SIR}$  and  $n_{SIM}$ . Especially  $n_{SIM}$  shows a lot of structure of the absorption spectrum with different peak locations and strength which are characteristic for different aerosol types (PATTERSON (1981) and JAENICKE (1988)). In this part of the spectrum is the range of the "atmospheric window", where except for a smaller  $OS_{13T}$  absorption line, almost no other gas type absorber is found. This range is dominated by strong silicate and clay mineral absorption lines between about 8  $\mu$ m and 12  $\mu$ m. Therefore, measurements of infrared transmission spectra (Fig.5) for different Saharan soils and mineral aerosols were carried out. The soil material consisted only of the fraction of particles with  $r < 5 \mu$ m, which can be addressed as the long range transport fraction of soils produced by a dry laboratory fractionation procedure (SCHUETZ and SEBERT, 1987). The samples were selected from very different areas of the Sahara. The aerosol samples originating from the desert and off the West African Coast were treated like the soil samples using the KBr pellet technique. Despite, some uncertainties and possible errors associated with this type of transmission measurement (PATTERSON, 1981), the spectra in Fig.5 show a number of very important features. The general pattern of both types of samples is rather similar with a typical broad absorption range due to soil derived silicates and clay minerals in the atmospheric window region. This similarity, especially between the different soils (except the sample from Northern Libya from carbonate rich soils) and the mineral aerosols from the desert shows that the material is rather uniform. Thus for radiation calculations values of the real and imaginary refractive index can be used within very narrow limits. Similar measurements from the great North American deserts by HOIDALE and BLANCO (1968) came to the same conclusions as well as a comparison of a number of global crustal derived aerosol data by PATTERSON (1981).

As a conclusion for this section it can be stated that this aerosol component is distinct from others and is quite uniform geographically. However, with regard to defining source markers when dealing with long range transport of atmospheric trace substances, only crude distinctions are possible, and no specific source area can be pointed out. Number concentrations and size distributions do not show any typical behaviour in this respect. Mass concentrations show a tremendous wide range of concentrations, but no range can be addressed as typical for a specific source region. The optical properties show also a great deal of similarity with respect to the complex index of refraction. As part of this, the infrared transmission spectra for both desert soils and aerosols may stress this conclusion. However, one typical soil sample from the Northern Sahara with a broad carbonate absorption line (Fig.4) around 7  $\mu$ m wavelength indicates, that perhaps compositional differences might be used as source specific markers.

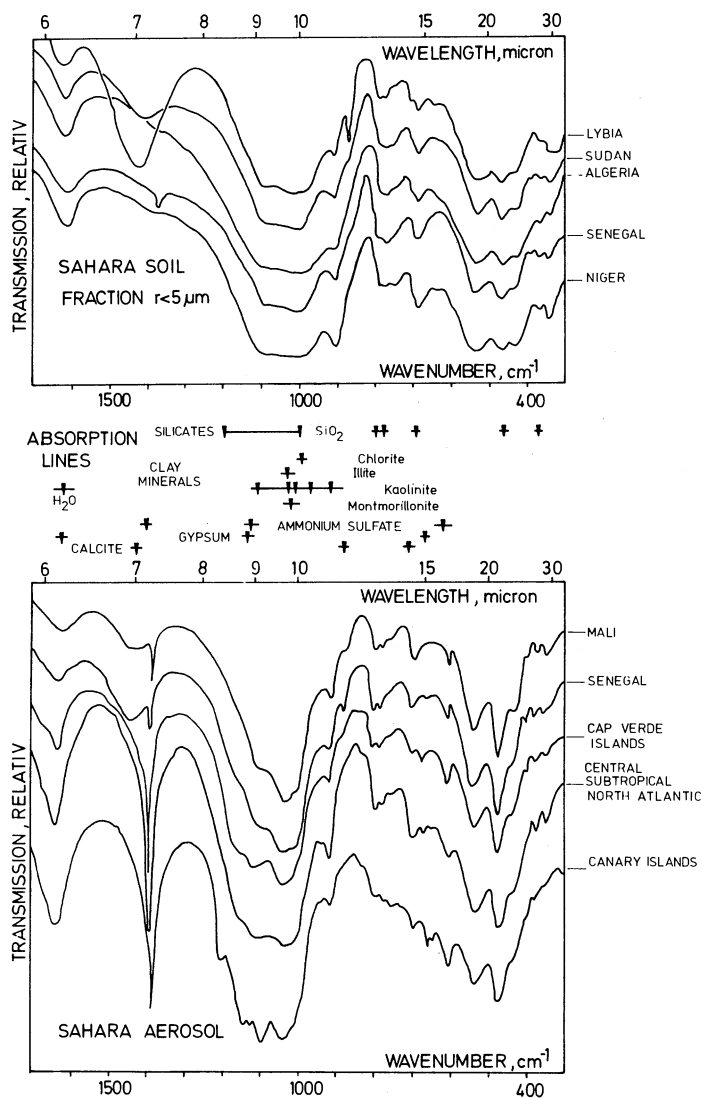


Fig.5: Infrared transmission spectra determined with the KBr method: for Saharan soil material ( $r < 5 \mu\text{m}$ ) (upper section) and mineral aerosols (lower section) together with the location of absorption lines of major compounds in the middle section

### 3. CHEMICAL PROPERTIES OF MINERAL AEROSOLS

Mineral dust in the atmosphere originates almost exclusively from soils and rocks of the arid regions of the earth. Since mineral dust consists of many inert compounds, there should be a close relationship between the compositions of soil and airborne matter for both elements and minerals. However, with respect to Fig.2, where a physical fractionation process caused very characteristic changes for sand and airborne dust particles, chemical fractionation processes and compositional changes during dust production and transport must be expected too. Among other reasons, this stimulated investigations on the elemental and mineral composition of soil and aerosol samples as well. Studies for bulk samples on Saharan aerosol, for example, are reported by RAHN et al. (1979), GLACCUM and PROSPERO (1980) and a review of data from other desert aerosols is given by PROSPERO (1981). On the basis of minor and trace element concentrations and on the mineral composition of clay and silt size particles it was concluded, that the dust composition is rather similar to average crustal material. This is in contrast to other aerosols and especially those having a pollution derived component. For instance, urban aerosols are enriched in many elements from anthropogenic sources. This difference usually is expressed by the term 'enrichment factor' EF. The EF for any element X in an aerosol relative to an assumed reference material, such as global average crustal rock, is defined as  $EF(Al, crust) = (X/Al)_{S1AerosolT} / (X/Al)_{S1crustT}$ . The reference element is one with unappreciable pollution sources, like Al, Sc, Fe etc. EF's with values higher than about 5 therefore suggest any other than crustal sources. Pollution derived elements like Pb, Cd, V, etc. usually are highly enriched even in remote regions, where the aerosol has been transported over long distances. Within Saharan airmasses most terrigenous elements were found in crustal proportions. Tab.2 shows EF's for a selection of elements for various regions in the vicinity of the Sahara and within the strong dust plume over the Subtropical Northern Atlantic. Most of the elements with  $EF < 3$  can be addressed as crustal derived. Those like Cu, Zn, Pb, and Cd over the Mediterranean and the Atlantic indicate with  $EF > 5$  pollution origin most probably from Europe. The reference material for EF is global average crustal rock as is usual in such studies. However, this seems to be rather inappropriate, because crust is unweathered and therefore soil would be much more suitable. Knowledge about the sand and dust fractionation processes suggests the use of the small size fraction of soil which can be transported over great distances, rather than to use any bulk material. In fact, RAHN et al. (1979) found that the composition of particles in desert soil with radii less than 16  $\mu$ m differed markedly from the bulk soil composition. Fig.6 summarizes these results compared to bulk crustal rock, soil and shale (JAENICKE and SCHUETZ, 1988b). Except for Si, which has usually higher concentrations in bulk samples, all other analysed elements were found to be enriched in the small size fraction of the soils. These results on one hand and the findings, of desert aerosols in crustal proportions on the other hand, seem to be very controversial. This stimulated an elemental analysis of soils as a function of particle size

TABLE 2 : Enrichment Factors in Saharan Aerosols

Element	Enrichment Factor EF(Crust)			
Al	1)*		1)*	.9
K		.4		.7
Ca		1		.7
Sc			.6	.7
Ti		1	1	1.4
V			.9	.9
Cr	2.9		2.1	1
Mn	.8	.8	.7	1.1
Fe	.9	1)*	.9	1)*
Co			.8	.8
Ni	2.8		1.8	2.4
Cu	5.6	1.4		<20
Zn	5.6	2.8		2.3
Rb		2.3		1
Sr		1.5		
Zr			1.1	2.2
Pb	46			
Cd	96			<200
Ba			2.6	2.3
La			2.6	1.8
Geographical region	Mediterranean	West African Coast	Cape Verde Islands	Subtropical North Atlant.
Reference	Chester et al. 1984	Author	Glaccum 1978	Rahn et al. 1979

1)\* Reference Element



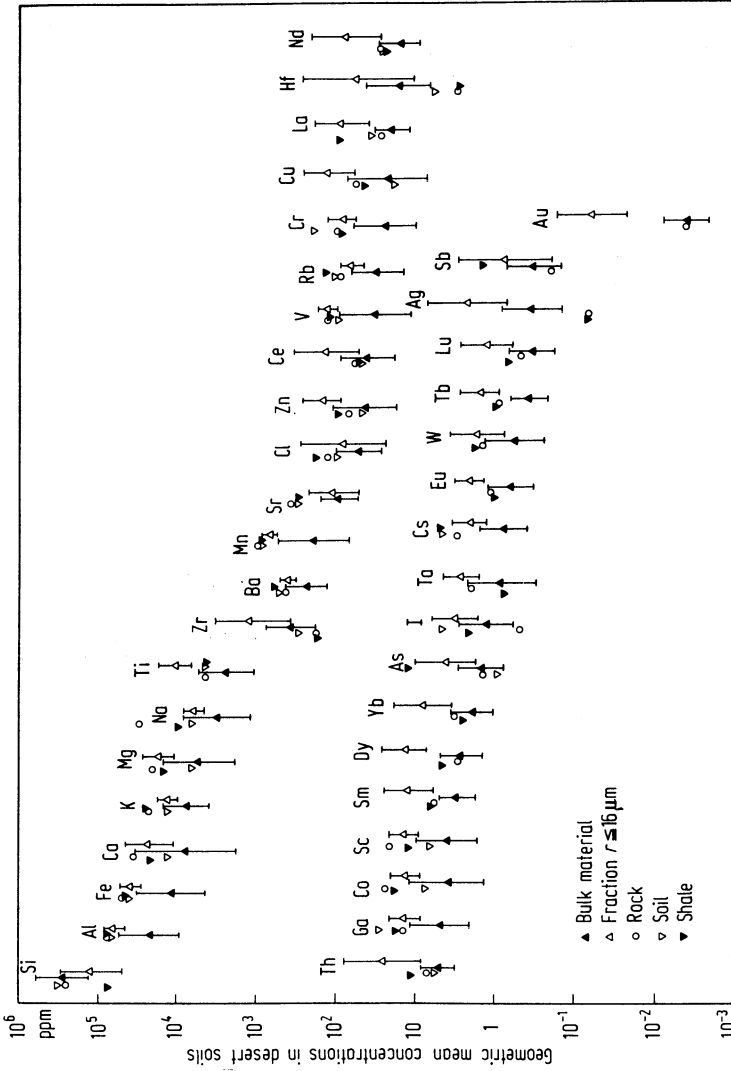


Fig. 6: Elemental concentrations in desert soils for bulk material and the fine particle fraction with  $r < 16 \mu\text{m}$  compared to three major reference materials ('Rock' after MASON, 1966; 'Soil' after VINOGRADOV, 1959 and 'Shale' after TUREKIAN and WEDEPOHL, 1961) © Jaenicke and Schütz (1988 a + b) Landolt-Boernstein New Series, Group V Springer Verlag.

with special attention to the small particle size ranges. Soil samples from the Sahara and North American deserts were fractionated and analysed by neutron activation analysis by SCHUETZ and RAHN (1982). As a general feature one finds the elemental concentrations, except for Silicon, increasing with decreasing particle size down to about 30 - 50  $\mu$ m radius. Below 10 - 20  $\mu$ m a broad plateau of concentrations, with a greater or lesser maximum near 20  $\mu$ m is observed. But in order to find any commonalities among the samples or elements, instead concentrations enrichment factors (EF(Al,crust)) were determined too. This allowed to answer two important questions: 1) How does the elemental composition change during airborne transport as the particle size decreases? 2) How valid is the use of bulk crustal rock as reference material in enrichment factor calculations for remote areas for mineral dust and for other trace elements (as also discussed in this volume)? A number of elements like Fe did not show any size dependency. The EF's for the rare earth elements group on the other side showed a well expressed pattern (Fig.2, lower section) with a maximum around 10 - 20  $\mu$ m radius. This result in combination with the physical fractionation process during transport (Fig.2, upper section) shows, that for certain elements higher enrichments must be expected when transport distances very close to source areas are investigated. During long range transport, however, transport distances are larger than about 1000 - 2000km and most of the aerosol mass consists of particles with less than 5 - 10  $\mu$ m radius. In such a case most of the elements are found in crustal proportions. In the Sahara dust plume over the Atlantic Ocean, for instance, RAHN et al. (1979) found most elements with EF's close to unity and with very small standard deviations indicating a very homogenous crustal derived aerosol. GLACCUM (1978) and GLACCUM and PROSPERO (1980) came to the conclusion with respect to the elemental and mineral composition during the course of a comparative investigation of several dust outbreaks studied at the Cape Verde Islands, Barbados and Miami. This also agrees with the measurements of the optical properties by PATTERSON (1981) as mentioned above. Therefore, it can be concluded, that the mineral dust component which is subject to global long range transport, can be regarded as rather homogeneous in composition close to average crustal material.

These conclusions may be influenced by the fact that all these investigations are made in same geographical region, which is supplied by the same source. But in general, soil dusts are expected to be strikingly different from different source regions. Different mineralogies of the soil material also can be expected to cause different source aerosols. Aerosol studies in the Northern Sahara by PAQUET et al. (1984) and ROGNON et al. (1987) confirm this assumption. They showed that mineral aerosol collected at different sites were in accord with local soil material. However, the fact that a homogenous aerosol is emerging from a large desert area like the Western Sahara may be due to mixing of the different contributions within the source area itself. For this reason, soil and aerosol samples from the different locations in the Sahara were analysed with X-ray diffraction by SCHUETZ and SEBERT (1987). In order to achieve an appropriate comparison between aerosol and soil material, only the

long range transport fraction of the soils with  $r < 5$  m was sampled and analysed after a dry fractionation process. The composition of the soils from the Northern, Western, Central and Southern Sahara showed a great similarity. For most minerals of the silt and clay size range abundances in the range less than 20% relative to quartz were found. This takes also in consideration the standard deviation of the means and the uncertainty of the X-ray diffraction method. Drastic differences, however, were found in Northern Saharan samples with low quartz contents and high values of calcite (see also Fig.5) and palygorskite. This behaviour reflects the general petrography of North Africa, where larger marine carbonate deposits in form of calcite and (some together with dolomite) are present especially in Northern Algeria and parts of Libya. Palygorskite followed closely the concentration pattern of calcite. In contrast, aerosol samples taken at Matam (Senegal), Tombouctou (Mali) and Agadez (Niger) showed no area specific variations. The general concentration pattern was similar to soils from Western, Central and Southern Sahara regions. No specific contributions, for instance, from northern sources could be noticed. The aerosol over the desert is obviously well mixed and rather homogenous. Regional surface characteristics, which can be seen from petrographic maps are not seen in both small size soil fractions and aerosols. Continuous deflation, transport, deposition and resuspension seems to equalize many minor and regional characteristics. Local features may only be apparent in the composition of sandstorms lifting up appreciable amounts of larger particles. Samples taken in the strong Saharan dust plume over the subtropical North Atlantic Ocean also showed a similar concentration pattern as the Saharan aerosols. Individual concentration values are close to the findings of GLACCUM and PROSPERO (1980), which stresses the strong homogeneity of the Sahara dust. Samples with progressing distance from the source show increasing clay mineral-to-quartz ratios as in the investigation of GLACCUM and PROSPERO (1980). The appearance of gypsum, which was also recognized in the infrared spectrum (Fig.5) is most probably an artificial product formed on the filters during sampling as mentioned by GLACCUM and PROSPERO (1980).

The large uniformity of Saharan aerosols extending from the interior of the desert up to the Caribbean as result of mineralogical, elemental and optical measurements seems to confirm the concept of a well mixed body of a mineral background aerosol. This result, however, must not be a discrepancy to authors like SARNTHEIN et al. (1982) who claim a non-uniform aerosol composition in airmasses from the Sahara. They report striking differences between shipboard aerosol samples off North Africa, the North-West African coast and the trade wind regions with the strong Saharan plume. Northern samples are among other features higher in calcite abundances. Significant calcite concentrations and the occurrence of palygorskite in aerosols off the African Coast is also reported by COUDE-GAUSSEN et al. (1987). This agrees well with the findings on the high calcite and palygorskite concentrations of North African soils and sedimentary deposits analysed by COUDE-GAUSSEN (1985). Therefore, it may be concluded, that the homogeneity of an aerosol body must not necessarily correlate with a major geographical source region rather than a major transport region coupled with a specific source composition.

Compositional differences are not easy to detect, except for major features. Any other small scale features like regional characteristics require very specific tracers. Such source markers are strongly needed.

#### 4. SOURCE MARKERS

The preceding sections have shown that single physical or chemical properties can be used to distinguish between major aerosol categories. If single ones do not work, then combinations of parameters usually are successful. Source identifications within one particular particle category like mineral dust, however, seem to be only possible if drastic deviations from mean global averages as the mineral composition of North African soils, are available. As a consequence, source identification is often carried out by tracing movements of airmasses back to their origin. Airmass trajectories, however, in areas with low data density - as over desert regions - are not easy to determine. Thus there is always the need for source specific tracer being pointed out.

From a number of pollution studies elemental tracer and typical elemental ratios are known to serve as markers for different anthropogenic particulate sources. European and North American air pollution studies carried out by RAHN and LOWENTHAL (1984) are successful examples for an application of elemental tracer techniques. Thus, the elemental composition of mineral aerosols and soils by RAHN et al. (1979) and SCHUETZ and RAHN (1982) was investigated, as mentioned in the preceding section. This study, unfortunately, showed that the elemental composition of the long range transport size fraction of the soil was very similar to bulk crustal material and similar to airborne mineral dust. Additionally, no clear source-discerning properties were observed. This, however, must not preclude the possibility that source characteristics can be found in such samples. As an example, HEIDAM (1985) studied enrichment factors of arctic aerosols using statistical multivariate methods. A time series of enrichment factors of Mn with a systematic seasonal variation ranging from 0.5 - 5 would here been described normally to a purely crustal origin. Although this variation constituted only a small part of the total Mn signal, it revealed that the non-crustal Mn-component was of pollution origin. Multivariate statistical methods obviously should be considered for the analysis of time series for suitable sets of elemental data and elemental ratios. The elemental ratio technique has been applied by BERGAMETTI et al. (1987) to Saharan dust episodes over Corsica. By using Si/Al and Fe/Al ratios in the aerosol three different source regions in the Northwestern Sahara could be distinguished. TOMADIN et al. (1987) also used elemental ratios like K/Na and Si/Al in order to distinguish between Saharan and non-Saharan airmasses over the Mediterranean.

Another possibility for characterization of source regions of airborne mineral dust may be isotopic ratios of elements. GROUSSET et al. (1987) studied Nd, Sr and Pb isotopes of Atlantic Ocean sediments in order to derive the origin of the aeolian component. S087TSr/S086TSr ratios were used by BISCAYE et al. (1974) in Southern Atlantic Ocean sediments to

distinguish aeolian dust contributions from the Sahara and a second plume from the Southwest African deserts.

Traditional mineralogical methods must be considered also. As mentioned in the previous section calcite and palygorskite minerals found in North African mineral dust by COUDE-GAUSSSEN and BLANC (1985), SCHUETZ and SEBERT (1987) and TOMADIN et al. (1987) can be used as tracer for airmasses derived from this region. Asian dust and material from North America collected over Enewetak in the Pacific Ocean could be distinguished by their illite and kaolinite components. Eastern Pacific aerosol samples in equatorial regions investigated by PROSPERO and BONATTI (1969) constituted two mineral groups. High pyroxene and plagioclase contents suggested a source in Mexico, whereas high concentrations of illite and quartz could be attributed to sources of the coastal deserts of Peru and Northern Chile.

Micromorphological identification of particles using scanning electron microscope methods must be mentioned within this context too. This method, applied to single mineral particles with radii larger than about 5 - 10  $\mu$ m by KRINSLEY and DOORNKAMP (1973) and COUDE-GAUSSSEN et al. (1987) show a number of features from the surface texture, that can be used identifying different sources. Within the submicron size range, however, the successful application of this method is limited, because the surface morphology is only definable for very broad features like cubic, plate-like and other structures. This also holds true for energy dispersive X-ray spectrometer studies (SCHUETZ (1976) and COUDE-GAUSSSEN et al. (1987)), which can only provide some qualitative information on the major elemental composition.

Molecular signatures of various organic compounds such as lipids from marine and terrestrial plants and animals are discussed also as source markers. These features along with plant debris can be easily mobilized together with soil material and will become subject to long range transport. The use of such tracers is discussed by GAGOSIAN (1986) and POYNTER et al. (1987). Within the context of organic matter that may constitute potential source markers pollens must be mentioned. They seem to be very important tracers, because they are highly differentiated in form and structure. Under appropriate conditions, pollen can be injected into the atmosphere directly from the plants or along with soil material. Pollen are produced in very large numbers and their presence may reveal the connection between sources, transport and deposition. If different vegetation zones are present in areas where the major deflation takes place, different source contributions will be reflected by the pollen component in the airborne dust. In studies of marine sediments off Northwestern Africa, HOOGIEMSTRA et al. (1986) identified seven pollen groups characterizing five different vegetation zones or mineral dust source contributions respectively.

As a conclusion, it can be stated that there are only a few straight forward source markers available like high amounts of single mineral groups, which can be taken to identify major source regions. Regional differences can not easily be detected except using combinations of source relevant parameters. Chemical or compound related parameters seem to be most successful rather than physical parameters like concentra-

tions, size distributions, optical parameters and particle shape or morphology.

## 5. CONCLUSION

Mineral dust is a very important component of the atmospheric aerosol. Mineral particles originating from arid areas of the continents are found in all types of airmasses. With respect to total number concentrations desert dust and aerosols have rather low concentrations on the order of  $500 - 2000 \text{ cm}^{-3}$ . Mass concentrations, however, cover about 8 orders of magnitude, ranging from hundreds of thousands  $\text{g/m}^3$  during sandstorm down to less than a tens of a  $\text{g/m}^3$  in extreme remote regions. This indicates, that size and mass distribution of mineral dust particles change drastically during long range transport. After transport distances of about  $1000 - 2000 \text{ km}$  from the source most of mineral dust mass with particle sizes larger than  $5 - 10 \text{ }\mu\text{m}$  is removed from the atmosphere. The smaller size fraction contributes to the global atmospheric background aerosol and thus influences the radiation balance and formation and chemistry of precipitation in the atmosphere. Deposited material contributes significantly to the sediments especially in remote areas of the earth. Optical properties and chemical signatures show characteristics of average global crustal material. As a consequence of this, mineral can be easily distinguished from all other types of aerosols, but within its own group of particulate matter different source contributions are not easy to detect. Source detection using conventional methods of the mineralogy, elemental chemistry, electron microscopy etc. succeed only if probable source materials are very different from average crustal matter. However, advanced statistical methods coupled with traditional approaches may succeed very well. Additionally, tracers derived from all kinds of biogenic origin carrying source specific signatures must be considered in the future too.

## ACKNOWLEDGEMENTS

This work was supported by the German Science Foundation through its Sonderforschungsbereich 73 ("Atmosphere Trace Substances") and its Sonderforschungsbereich 233 ("Dynamics and Chemistry of Hydrometeors").

- d'ALMEIDA, G.A. and L. SCHUETZ (1983): 'Number, Mass and Volume Distributions of Mineral Aerosol and Soils of the Sahara'. J. Climate and Applied Meteorol. 22, 233-243.
- d'ALMEIDA, G.A. (1987): 'Source strength and deposition rate of Saharan dust'. NATO Advanced Research Workshop: Paleoclimatology and Paleometeorology'. Oracle, Arizona, Nov. 15-19
- BERGAMETTI, G., L. GOMES, D. MARTIN, M. DESBOIS and P. BUAT-MENARD (1987): 'Sources, Transport and Deposition of African Dusts over the Western Mediterranean'. NATO Advanced Research Workshop: Paleoclimatology and Paleometeorology'. Oracle, Arizona, Nov. 15-19
- BISCAYE, P.E., R. CHESSELET and J.M. PROSPERO (1974): 'Rb - Sr, S087TSr/S086TSr isotope system as an index of provenance of continental dusts in the open Atlantic Ocean'. J.Rech.Atmos. 8, 819-829.
- CARDER, K.L., R.G. STEWARD, P.R. BETZER, D.L. JOHNSON, J.M. PROSPERO (1986): 'Dynamics and Composition of Particles from an Aeolian Input Event to the Sargasso Sea', J.Geophys.Res. Vol. 91, 1055-1066
- CARLSON, T.N. and S.J. BENJAMIN (1980): 'Radiative heating rates for Saharan dust', J.Atmos.Sci. 37, 193-213.
- CHESTER, R., E.J. SHARPLES and G.E. SANDERS (1984): 'Saharan Dust Incursion over the Tyrrhenian Sea', Atm.Env. 18, 929-935.
- COUDE-GAUSSSEN, G. and P. BLANC (1985): 'Présence de grains de palygorskite dans les poussières actuelles et les sédiments récents d'origine désertique', Bull.Soc.Géol. France 8, 571-579
- COUDE-GAUSSSEN, G., P. ROGNON, G. BERGAMETTI, L. GOMES, B. STRAUSS, J.M. GROS and M.N. LE COSTUMER (1987): 'Saharan dust on Fuerte Ventura Island (Canaries): Chemical and mineralogical characteristics and probable sources', J.G.R 92, 9753-9771.
- DREILING, V., L. HELMES, R. MASER and L. SCHUETZ (1988): 'Properties of marine background and Saharan aerosol off West Africa'. In preparation.
- GAGOSIAN, R.B. (1986): 'The air-sea exchange of particulate organic matter', In: The role of air-sea exchange in geochemical cycling', Ed. P. Buat-Menard. D. Reidel Publishing Company, Dordrecht, 409-442.
- GILLETTE, D.A. (1981): 'Production of dust that may be carried great distances', In: Desert Dust: Origin, Characteristics and Effects on Man. Ed. T.L. Pewe, Geol. Soc. America, 11-26
- GLACCUM, R.A. (1978): 'The Mineralogy and Elemental Composition of Mineral Aerosols over the Tropical North Atlantic: The Influence of Saharan Dust', Scientific Report, Univ. of Miami, 161 pp.

- GLACCUM, R.A. and J.M. PROSPERO (1980): 'Saharan Aerosols over the Tropical North Atlantic - Mineralogy', Mar. Geol. 37, 295-321.
- GROUSSET, F.E., P.E. BISCAYE and A. ZINDLER (1987): 'Nd, Sr, Pb, Isotopes as Tracers of wind transport in Atlantic Holocene Sediments', NATO Advanced Research Workshop: Paleoclimatology and Paleo-meteorology, Oracle, Arizona, Nov. 15-19.
- HEIDAM, N.Z. (1985): 'Crustal Enrichments in the Arctic Aerosol', Atm. Env. 19, 2083-2097.
- HOOGHIEMSTRA, H., O.C.A. CHIORI and H.-J. BEUG (1986): 'Pollen and spore distribution in recent marine sediments: a record of NW African seasonal wind patterns and vegetation belts'. 'METEOR'-Forsch. Ergebnisse C40, 87-135.
- HOIDALE, G.B. and A.J. BLANCO (1968): 'An Infrared Spectroscopic view of the nature of giant and large particles of Atmospheric Dust', J.Rech. Atm. 3, 293-299.
- JAENICKE, R. (1978): 'Aitken particle size distributions in the atlantic north trade winds', METEOR-Forschungsergebnisse Reihe B, No. 13, 1-9.
- JAENICKE, R. (1979): 'Monitoring and Critical Review of the Estimated Source Strength of Mineral Dust from the Sahara'. In: Saharan Dust, C. Morales (Ed.), J. Wiley & Sons, Chichester, 233-242.
- JAENICKE, R. (1988): Aerosol Physics and Chemistry. In: 'Meteorology: Physical and Chemical Properties of Air', Landolt-Boernstein, New Series, Group V, Volume 4b, Fischer, G. (Ed.), Springer-Verlag, 391-457.
- JAENICKE, R. and L. SCHUETZ (1988a): 'Wind speed and vertical flux of aerosols'. In: Aerosol Physics and Chemistry. In: 'Meteorology: Physical and Chemical Properties of Air', Landolt-Boernstein, New Series, Group V, Volume 4b. Fischer, G. (Ed.), Springer-Verlag, 403-405.
- JAENICKE, R. and L. SCHUETZ (1988b): 'Elemental composition of potential sources for bulk-to-particle conversion (BPC)'. In: Aerosol Physics and Chemistry. In: 'Meteorology: Physical and Chemical Properties of Air', Landolt-Boernstein, New Series, Group V, Volume 4b. Fischer, G. (Ed.), Springer-Verlag, 395-400.
- JAENICKE, R., C. JUNGE and H.J. KANTER (1971): 'Messungen der Aerosol-groessenverteilungen über dem Atlantik ueber dem Atlantik', 'METEOR'-Forsch. Ergebnisse B, 1-54
- JUNGE, C. (1979): 'The importance of Mineral Dust as an Atmospheric Constituent'. In: Saharan Dust, C. Morales (Ed.), J. Wiley & Sons,



Chichester, 49-60.

- KRINSLEY, D.H. and J.C. DOORNKAMP (1973): 'Atlas of quartz sand surface textures'. Cambridge Univ. Press, 72 pp.
- MASON, B. (1966): Principles of Geochemistry, 3rd.Ed. J. Wiley & Sons, New York.
- PAQUET, H., G. COUDE-GAUSSEN and P. ROGNON (1984): 'Etude minéralogique de poussières sahariennes le long d'un itinéraire entre 19° et 35° de latitude nord', Rev.Géol.Dyn.Géogr.Phys., 25, 257-265.
- PATTERSON, E.M., D.A. GILLETTE and B.H. STOCKTON (1977): 'Complex Index of Refraction between 300 and 700 nm for Saharan Aerosols', J.G.R. 82, 3153-3160.
- PATTERSON, E.M. (1981): 'Optical Properties of the Crustal Aerosol: Relation to Chemical and Physical Properties', J.G.R. 86, 3236-3246.
- POYNTER, J.G., P. FARIMOND and G. EGLINTON (1987): 'Lipid signals recording aeolian contributions to marine sediments', NATO Advanced Research Workshop: Paleoclimatology and Paleometeorology, Oracle, Arizona, Nov. 15-19.
- PROSPERO, J.M. and E. BONATTI (1969): 'Continental dust in the atmosphere of the eastern equatorial Pacific', J.G.R. 74, 3362-3371.
- PROSPERO, J.M. (1981): 'Aeolian transport to the World Ocean'. In: The Sea, Vol.7, C. Emiliani (Ed.), Wiley Interscience, 801-874.
- PYE, K. (1987): 'Origin and nature of particulates that are transported great distances'. NATO Advanced Research Workshop: Paleoclimatology and Paleometeorology, Oracle, Arizona, Nov. 15-19.
- RAHN, K.A., R.D. BORYS, G.E. SHAW, L. SCHUETZ and R. JAENICKE (1979): 'Long range impact of Desert Aerosol in Atmospheric Chemistry: Two Examples'. In: Saharan Dust, C. Morales (Ed.), J. Wiley & Sons, Chichester, 243-266.
- RAHN, K.A. and D.H. LOWENTHAL (1984): 'Elemental Tracers of Distant Regional Pollution Aerosols', Science 223, 123-139.
- SARNTHEIN, M., J. THIEDE, U. PFLAUMANN, H. ERLLENKEUSER, D. FUETTERER, B. KOOPMANN, H. LANGE and E. SEIBOLD (1982): 'Atmospheric and Oceanic Circulation Patterns off Northwest Africa during the last 25 million years'. In: Geology of the Northwest African Continental Margin. U. von Rad et al. (Ed's), Springer-Verlag, Berlin, 545-604.
- SCHUETZ, L. (1976): 'Analysis of Atmospheric Aerosol Particles using a

- Scanning Microscope (SEM)', Beitr. elektronenmikroskop. Direktabb.  
Oberfl. 9, 365-384.
- SCHUETZ, L. (1979): 'Saharan Dust Transport over the North Atlantic  
Ocean - Model Calculations and Measurements'. In: Saharan Dust,  
C. Morales (Ed.), J. Wiley & Sons, Chichester, 233-242.
- SCHUETZ, L. and RAHN, K.A. (1982): 'Trace-element concentrations in  
erodible soils', Atmos. Env. 16, 171-176.
- SCHUETZ, L. and M. SEBERT (1987): 'Mineral aerosols and source identi-  
fication', J. Aerosol Sci. 18, 1-10.
- TOMADIN, L., R. LENAZ and R. VANNUCCI (1987): 'The eolian dusts over  
the Mediterranean', NATO Advanced Research Workshop: Paleo-  
climatology and Paleometeorology, Oracle, Arizona, Nov. 15-19.
- TUREKIAN, K.K. and K.H. WEDEPOHL (1961): 'Distribution of the elements  
on some major units of the earth crust', Bull. Geol. Soc. Amer.  
72, 175-192.
- VINOGRADOV, A.P. (1959): The Geochemistry of Rare and Dispersed Chemi-  
cal Elements in Soils, 2nd Ed., Consultants Bureau Inc., New York.
- WESTPHAL, D.L. (1987): 'A Case Study of a Saharan Dust Storm', NATO  
Advanced Research Workshop: Paleoclimatology and Paleometeorology,  
Oracle, Arizona, Nov. 15-19.

Nd AND Sr ISOTOPES AS TRACERS OF WIND TRANSPORT: ATLANTIC AEROSOLS AND SURFACE SEDIMENTS.

F. E. GROUSSET<sup>1,2</sup> and P. E. BISCAYE<sup>1</sup>

1. Lamont-Doherty Geological Observatory  
of Columbia University  
Palisades, N.Y., 10964  
USA.

2. U.A. CNRS 197, IGBA, Université Bordeaux I  
351 Crs. de la Libération  
33405 Talence Cedex,  
France.

ABSTRACT. A study of Nd and Sr isotopes in the detrital fraction of surface sediments and aerosols permit distinction between different continental sources and the deduction of transport mechanisms of particulate matter to and within the Atlantic Ocean. Nd isotope ratios and Rb-Sr "model ages" are the most informative aeolian transport tracers. Isotopic ratios display consistent patterns for both present-day aerosols and Upper Holocene surface sediments. Important sources of aeolian particles are connected with major atmospheric circulation systems: the "Trades" and the "Westerlies". In the tropical present-day aerosols, Rb-Sr model ages allow us to distinguish between "old" particles coming from the north-west part of the Saharan desert, transported during summer periods, and "young" particles coming from the south-east part of tropical Africa and transported during winter periods. The use of these tracers to evaluate wind flux and trajectory evolution would be fruitfully extended to the entire Quaternary period.

1. INTRODUCTION

A number of studies of the oceans have used fine-fraction (clay) mineralogy to deduce origins of the sediments, and, from the observed distribution patterns, something of the mechanisms responsible for transporting the sediments to their deposition site (Biscaye, 1965; Griffin et al., 1968; and Rateev et al., 1969). The latter two suggested that, possibly along with other mechanisms, aeolian transport by the westerlies across the entire North Atlantic was important. In the area of the northern Mid Atlantic Ridge

(MAR), Grousset and Chesselet (1986), using clay mineralogy, trace-element, and R.E.E. analyses, saw evidence in the sediments for aerosols transported from North America by the Westerlies. Chester and Johnson (1971) and Prospero (1979) also described aeolian transport by the Trade winds off the African coast. Unfortunately mineralogical tracers are not sufficiently discriminative to distinguish unequivocally between the various source areas surrounding the Atlantic Ocean.

To increase our ability to resolve continental source areas, additional tracers are necessary. Radioactive and radiogenic isotope tracers have the potential for reflecting the geologic age and petrologic nature of the continental source rocks. Some work has been done using Sr isotopes as tracers of provenance (Dasch, 1969; Biscaye and Dash, 1971; Biscaye, 1972; Biscaye et al., (1974), Grousset and Chesselet, 1986; Biscaye et al., in prep.). However, Dasch (1969) and Biscaye (1972) showed that, although Sr isotopic ratios are good tracers of the geologic origin of detrital sediments, the results are influenced by the size frequency distribution of the samples analyzed:  $^{87}\text{Sr}/^{86}\text{Sr}$  ratios generally increase with decreasing grain-size. To further increase resolution of sediment provenance while minimizing the problems of grain size sorting, the utility of the Sm-Nd isotope system has been explored (Goldstein et al. 1984; Grousset et al., 1988a). Nd isotopic ratios of the detrital fraction of the sediment reflect both the petrologic nature and geologic age of their parent rocks, and they appear not to be influenced by variations in grain-size (Goldstein et al., 1984).

We report here Sr and Nd isotope ratios, and Nd and Sr model ages derived from those ratios, measured on surface deep-sea sediments and on aerosol samples mainly from the Atlantic Ocean. In the context of previous mineralogical and Nd- and Sr-isotopic parameters, these data are used to locate sources of continental detritus and then, to deduce wind-transport mechanisms.

## 2. SAMPLES AND ANALYTICAL PROCEDURES

Surface sediment samples were recovered with box and gravity corers on French cruises (University of Bordeaux). Sample locations are listed in Grousset et al. (1988a). Core-tops were sliced aboard ship and immediately frozen. Only Upper Holocene samples from the first centimeter below the sediment-water interface were analyzed. Stratigraphic control was provided by studies of planktonic foraminifera. For box cores,  $^{14}\text{C}$  analyses were run on the biogenic carbonate fraction. Ultra pure water was used to wash salt from sediment samples, after which they were dried and ground to powder. Biogenic carbonate, which would carry a sea-water

isotope signal, was leached with ultra-clean Na-acetate (pH 4.5-buffered acetic acid). Organic matter was removed by oxidation through dropwise addition of ultrex-H<sub>2</sub>O<sub>2</sub>. The remaining residue is designated the "detrital fraction" of the sediment. This fraction may contain a minor authigenic component, e.g. Fe-Mn-oxides. Sr isotope measurements on such oxides may display a range from typical crustal- ( $\approx 0.730$ ) or mantle-derived signals ( $\approx 0.703$ ), different from that of the acid-leached fraction which displays a typical sea-water signal ( $\approx 0.7092$ ). Because of the low Nd content of carbonate, Nd isotope measurements on the bulk sediments (including carbonates), however, are little affected by the sea-water signal. For example, in one sample from shelf around the Azores, where the sea-water signal in the Northeast Atlantic is always a negative value ( $E_{Nd}(0) \approx -10$  to  $-12$  after Piepgras and Wasserburg, 1983),  $E_{Nd}(0)$  in the bulk sample (including carbonate) was  $\approx +4.5$ , and in the decarbonated residue was  $\approx +4.9$ , or a difference of only  $\approx -0.4$ .

All aerosol samples were collected by means of a pair of one meter square, woven, monofilament mesh panels that were mounted normal to the wind (Chester and Stoner, 1974). Mineral dust particles were collected by impaction onto the 1mm. diameter monofilament fibers. The dust particles were removed in distilled and deionized water. The suspensions were allowed to settle out, the supernatant liquid was decanted and the remaining slurry centrifuged. The subsequent preparation for isotopic measurements was the same as that for surface sediments. All samples were collected aboard ships with the exception of those from Barbados and Miami which were collected from the tops of towers located on the windward coasts. At all sites, the collectors were positioned at least ten meters above the surface to minimize the possibility of contamination from local soils and from surf spray. Those aerosol samples were kindly provided by Drs. Jo. Prospero, R. Chester and R. Lenaz. The collection efficiency of meshes and filters is discussed in Grousset et al. (1988a) and in Blank and Prospero (in prep.).

Isotopic analytical work was carried out at Lamont-Doherty Geological Observatory, using chemical and mass spectrometer techniques previously described (Zindler et al., 1984; Grousset et al., 1988a). For Sr and Nd isotopes, samples weighing  $\approx 5$  to  $\approx 10$ mg., were dissolved for two days in pressurized PTFE bombs, at a temperature of about 215 °C in a 2b[HF+HClO<sub>4</sub>+HNO<sub>3</sub>] mixture.  $^{87}\text{Sr}/^{86}\text{Sr}$  ratios have been corrected for mass fractionation by normalizing to  $^{86}\text{Sr}/^{88}\text{Sr} = 0.11940$ , and adjusted to correspond to a value of 0.70800 for the E & A Standard. "Sr model-ages" (My) were calculated by assuming an arbitrary  $^{87}\text{Sr}/^{86}\text{Sr}$  initial value of 0.7025.  $^{143}\text{Nd}/^{144}\text{Nd}$  ratios have been corrected for mass fractionation by normalizing to  $^{146}\text{Nd}/^{144}\text{Nd} = 0.7219$ , and

adjusted to correspond to a value of 0.512650 for BCR-1 ( $\approx 0.511875$  for the La Jolla Nd standard). Nd and Sm blanks averaged 0.078 and 0.034 ng, respectively, and were negligible in all cases; amounts correspond to 0.01% and 0.05% respectively of the Nd and Sm in total samples. Uncertainties in concentrations are  $<0.3\%$ . Results are expressed as:  $E_{Nd}(0) = \left[ \frac{^{143}Nd}{^{144}Nd} (\text{measured}) / 0.512638 \right] - 1 \times 10^4$ , using the present-day CHUR value of Jacobsen and Wasserburg (1980). Nd model-ages (Ga) were calculated by assuming an arbitrary  $^{143}Nd/^{144}Nd$  present-day value of 0.51316. This is the mean "present-day depleted mantle" value of Goldstein et al. (1984) and is high enough to avoid future ages. The "model-age" concept has been discussed for fluvial sediments (Goldstein et al., 1984); we use it not in any absolute age sense, but merely to add an age-related fingerprint to our set of particle tracers.

### 3. RESULTS AND DISCUSSION

#### 3.1. Sr isotopes

3.1.1. Results. The distribution of Sr isotope ratios has been extensively described in the Atlantic sediments by Dasch (1969), Biscaye and Dasch (1971), Biscaye (1972) and Biscaye et al. (1974). Additional results have been obtained more recently in both sediments and aerosols (Biscaye et al., in prep.). The isotopic data we present here are taken from those papers.

The most interesting information is given by model-ages, derived from Rb- and Sr-isotope ratios, using isotopic geochronology methods. The Rb-Sr isochron age of an igneous or high-grade metamorphic rock normally is defined by the slope of a best fit line through the  $^{87}Rb/^{86}Sr$  vs  $^{87}Sr/^{86}Sr$  values determined on separated mineral phases or on several rock samples. If only one set of values of  $^{87}Rb/^{86}Sr$  and  $^{87}Sr/^{86}Sr$  are available (for example from only one mineral or from one whole-rock analysis), a calculated or assumed age may be obtained by connecting this point to an arbitrary "initial ratio", of  $^{87}Sr/^{86}Sr$  (at  $^{87}Rb/^{86}Sr=0$ ). To calculate an analogous "model-age" for individual sediment samples, one must know or assume an initial  $^{87}Sr/^{86}Sr$  ratio, which must be sufficiently low to preclude any negative model-ages. For this reason, we decided to use an arbitrary value: the MORB ratio, which is close to the ratios of Mid-Atlantic-Ridge-derived sediments. The validity of this parameter as something related to geological age, is given by the consistency of these results with the geological ages of surrounding continents, and with information obtained with a completely independent parameter: windborne lacustrine diatoms occurring in the sediments (after Pokras and Mix, 1985). These tests are extensively described in Biscaye et

al. (in prep.).

### 3.1.2. Distribution and interpretation.

The distribution of model-ages in units of million years for these samples is shown in Fig.1.

-North Atlantic. The oldest model-ages are found in sediments of the Labrador Sea ( $\approx 3200$  my). This part of the Ocean is bordered by the oldest cratonic area around the North Atlantic, --the Canadian shield and Greenland (Hurley and Rand, 1969). In the western North-Atlantic, the decrease in model-ages of the deep-sea sediments to the south, parallels a decrease in Hurley and Rand's (1969) age provinces from  $\geq 1700$  my through  $\approx 800-1700$  my to  $\approx 0-800$  my in the southeastern United States. A feature pertinent to the subject of this workshop is the eastward extension of North American material across the MAR: sediments older than 500 my occur as far east as  $\approx 15^\circ$  W. This kind of pattern has been observed for the concentrations of chlorite and rubidium in sediments (Grousset and Chesselet, 1986) and was explained in term of wind transport.

-Equatorial Atlantic. On the African side of the Atlantic, the north-to-south trend toward lower model-ages is interrupted by values in the range of  $\approx 700$  my in the Cape Verde Basin. The Cape Verde data reflect sediment sources in the West Saharan shield area. This interpretation is consistent with east-west gradient previously observed in this area for quartz (Biscaye, 1965; Chester and Johnson, 1971; Kolla et al., 1979) and explained as transport by the Trade and/or Harmattan winds.

## 3.2. Nd isotopes

3.2.1. Results. Nd and Sm concentrations,  $^{143}\text{Nd}/^{144}\text{Nd}$  and model ages (expressed in Ga) are from Grousset et al. (1988) and are listed there. The range of Nd and Sm concentrations, 5.6-90.2 ppm Nd and 1.1-14.8 ppm Sm, is larger than the range reported by Goldstein et al. (1984) for fluvial sediments (16-52 ppm Nd and 3-9.2 ppm Sm).  $^{143}\text{Nd}/^{144}\text{Nd}$  ratios of 0.511892-0.512890 and  $^{147}\text{Sm}/^{144}\text{Nd}$  ratios of 0.087 -0.218 also exceed the corresponding ranges for fluvial sediments reported by the same workers (Goldstein et al., 1984). If we plot the  $E_{\text{Nd}}(0)$  distribution in the North Atlantic surface sediments and aerosols (Fig. 2), it is possible to identify different main components. Positive  $E_{\text{Nd}}(0)$  (more radiogenic) values are observed around the Azores islands (+3.9, +4.9). An area with values between -2.5 to -10 occurs between the Alboran Sea (western Mediterranean) and the Azores. To the north and south, values are more negative (-12 to -15), i.e. less radiogenic. Although the data are not sufficiently closely spaced to show trends quantitatively, samples in the

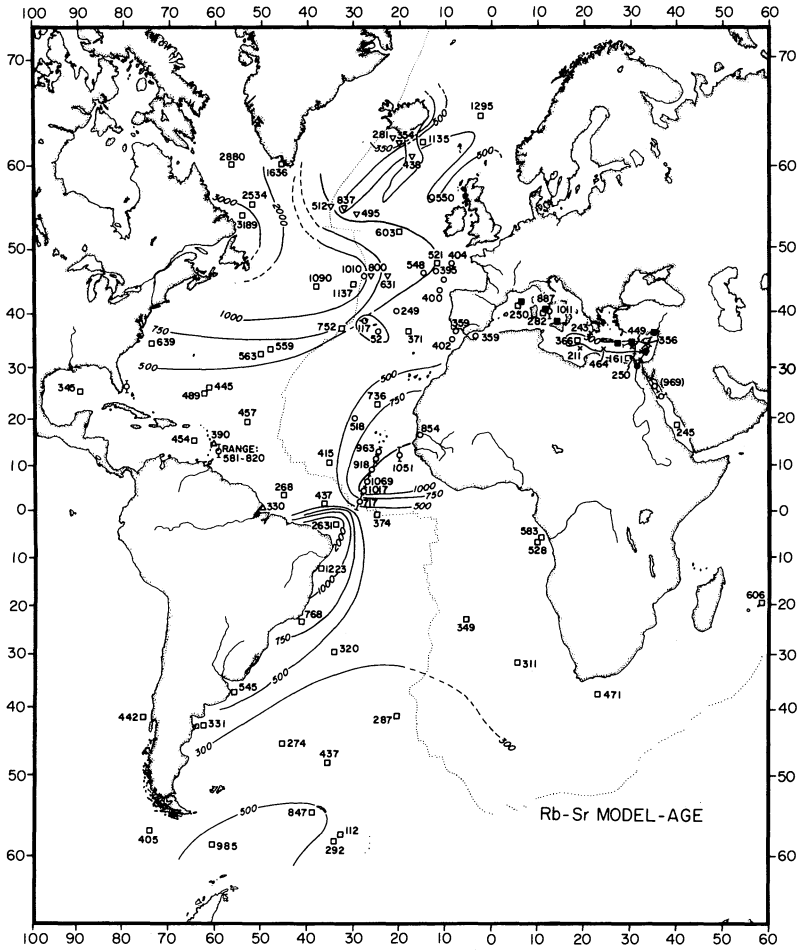


Figure 1: Rb/Sr model-age (My) distribution in Atlantic surface sediments and aerosols. Open circles: this work (aerosol samples are those symbols crossed by a bar). Other symbols are data from the literature ( Dasch, 1969, Kolla et al., 1972, Goldstein and O'Nions, 1981, Goldstein et al., 1984, Frost et al., 1986 and Biscaye et al., in prep.).



regions around 45°N. and 10°N. appear to define gradients of eastward- and westward-decreasing  $E_{Nd}(0)$ , respectively (Fig. 2). Definition of the eastward gradient at ≈40-55°N and of the westward gradient at 5-25°N is based also on gradients of other sedimentary tracers --chlorite and rubidium concentrations and strontium isotope compositions-- in a much larger set of samples than is reported here (Grousset and Chesselet, 1986; Biscaye et al., in prep.). Aerosols from Barbados may define the western distal part of the 5-25°N gradient.

Two of our Mediterranean aerosols are comparable to those in the tropical Atlantic (-12 to -12.4), but the third one (#SH9/79-M8) and the Red Sea aerosol sample have slightly more positive values (-10.1 and -9.1).

All the model ages calculated on our samples are between ≈0.1 and ≈2.2 Ga and correlate very well with the  $E_{Nd}(0)$  values ( $r=0.95$ ) mainly because Sm/Nd ratios are roughly constant. Only a few samples do not fit this correlation because of extremes in the Sm/Nd ratio. Thus, the geographic pattern of model ages is quite similar to that of  $E_{Nd}(0)$  (Grousset et al., 1988a). In the neighbourhood of the Azores, model age are younger than ≈1 Ga. A narrow band of young ages (<1.5 Ga) occurs in Azores area, and eastward as far as the Alboran Sea in the western Mediterranean: they are probably induced in part, by a specific Mediterranean Sea particulate matter contribution as reported by Grousset et al. (1988b). We observe two areas characterized by "old" model ages (>1.75 Ga) which are the same west-to-east gradients in the  $E_{Nd}(0)$  seen at 40-55°N. latitudes and an east-to-west gradient seen in the tropical latitudes.

3.2.2. Interpretation. The average value for Atlantic river sediments reported by Goldstein et al. (1984) was  $E_{Nd}(0) \approx -10.6$ , and the average of all the North Atlantic sediments in Fig.2 is  $E_{Nd}(0) \approx -8.6$ . If it were assumed that the average river sediments value represents the general crustal average input to the North Atlantic, the patterns of Fig.2 appear as areas characterized by sediments greater and less than this value.

Aerosol samples from the Tyrrhenian Sea are probably of African origin, based on the frequency of African dusts in Europe (Chester et al., 1984), and on the similarity of  $E_{Nd}(0)$  values (-12, -12.4) to that of our other equatorial aerosol samples. Only one Tyrrhenian aerosol value (-10.9) is more radiogenic than those two previous values and suggests a sporadic input of some volcanic dusts from surrounding volcanoes. On this basis, it would appear that the aerosol input to the Mediterranean is much less important than the riverine input, which is consistent with a previous evaluation (Frost et al., 1986).

Goldstein et al. (1984) reported a value of  $E_{Nd}(0) \approx -8.5$

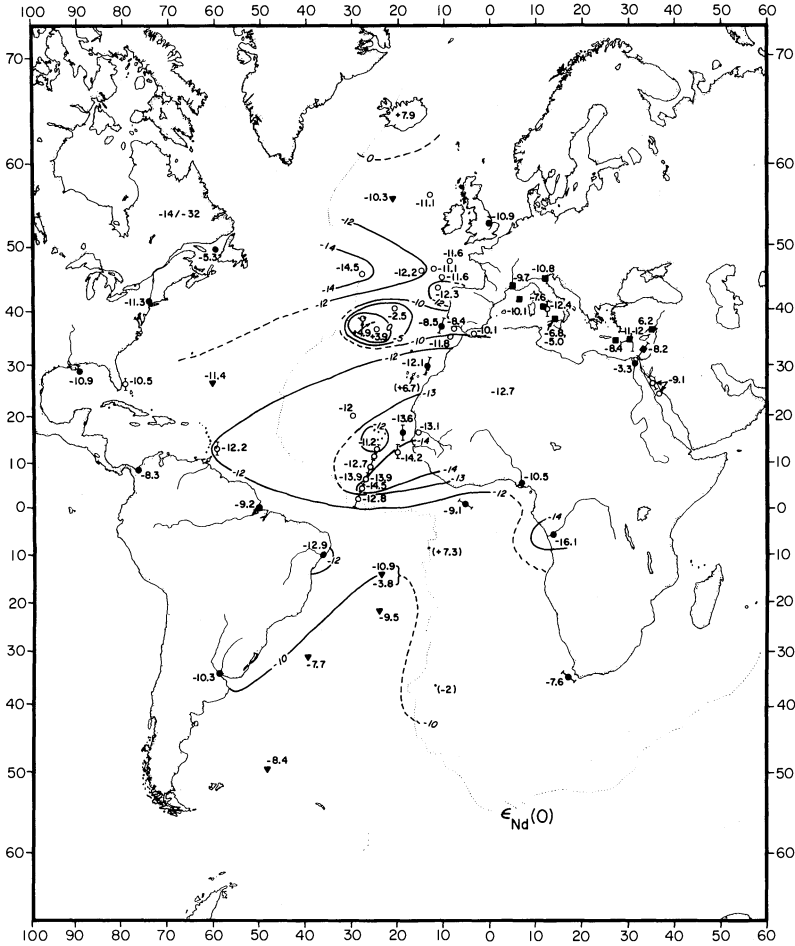


Figure 2:  $\epsilon_{Nd}(0)$  distribution in Atlantic surface sediments and aerosols, with  $\epsilon_{Nd}(0) = [((^{143}\text{Nd}/^{144}\text{Nd})_{\text{meas.}}/0.512638) - 1] \cdot 10^4$ . Open circles: this work (aerosol samples are those symbols crossed by a bar). Other symbols are data from the literature (McCulloch and Wasserburg, 1978, Zindler et al., 1979, Allègre and Ben Othman, 1980, Goldstein and O' Nions, 1981, Goldstein et al., 1984, Miller and O' Nions, 1985, Frost et al., 1986 and Grousset et al., 1988a). Contours in the latitudes of the westerlies for the "northern gradient" are guided by prior knowledge derived from a much larger set of data, which included the distributions of chlorite and rubidium concentrations (Grousset and Chesselet, 1986) and of Rb-Sr isotopes (Fig.1, from Biscaye et al., in prep.).

in one aerosol sample collected about 300 km west of Gibraltar during an easterly (east-to-west) wind. This aerosol most likely originated from the Iberian region, because most of the aerosols of Saharan origin have less radiogenic values down to  $\approx -14.2$  (Tab.1). One Tyrrhenian aerosol sample display a less radiogenic value  $-10.9$ , which agree well with values reported for the Mediterranean Sea deposits (Frost et al., 1986). This more radiogenic value must also be related to the "youngest" and more volcanogenic rocks and terrains occurring in the region of the Mediterranean Sea.

Those low values west of Gibraltar could imply that a particulate flux is transported westward, through the atmosphere, at Mediterranean latitudes, and can seasonally influence a region as far west as the Azores. The mean atmospheric circulation pattern reported for the Upper Holocene (Lamb, 1971), and the present-day pollen distribution in aerosols (Melia, 1984) are consistent with this assumption.

This central axis of volcanogenic influence from the eastern Mediterranean to the Azores is bracketted to the north and south by broad areas of less radiogenic, highly negative values:  $-12 < E_{Nd}(0) < -14.5$ . The Eastern Tropical Atlantic Basin lies within the Trade Wind latitudes and the influence of aeolian transport has been extensively studied by many authors (Radczewski, 1939; Biscaye, 1965; Chester and Johnson, 1971; Biscaye et al., 1974; Chester et al., 1979; Schutz, 1980; Sarnthein et al., 1981; Prospero, 1981)). Using sedimentological, mineralogical and geochemical data, those authors have described an east-to-west gradient, which traverses the MAR axis, and is fed by aeolian transport from the Saharan region. This desert area is a tremendous source of detrital particles, which are removed by the northeast Trade Winds, and carried over the Atlantic Ocean as far as Barbados (Delany et al., 1967; Prospero, 1979-1981; Prospero et al., 1981; Glaccum and Prospero, 1980) and Central America (Folger, 1970). The Nd isotopic values that we have measured in sediments of the eastern equatorial Atlantic ( $E_{Nd}(0) \approx -12$ ) are consistent with our measurements of aerosol samples:  $-12$  to  $-14.2$  and with data on aerosols by Goldstein et al. (1984):  $-12.1$  to  $-13.6$ . The isotopic ratio of the Senegal river sediment is in the same range  $\approx -13.1$ , but this is a negligible influence on the sediment composition of the nearby ocean, since the suspended matter input of this river represents only 2 to 4% of the atmospheric flux (Gac and Kane, 1986) There are few Nd isotopic data on Saharan desert rocks, but some samples from several locations were analyzed by Allegre and Ben Othman (1980). For example, for Inzize (Tanezrouft) granitoids, they reported a  $E_{Nd}(0)$  of about  $\approx -12.7$ , which is consistent with our tropical Atlantic sediment and aerosol data. Moreover, these aerosols and

TABLE 1. Sediment (top core) and aerosol locations and Nd isotope analytical results. Reported errors (2 sigmas on the mean) are expressed in parts per million

Samples:	Latitude	Longitude	$^{143}\text{Nd}/^{144}\text{Nd}$	ENd(0)	Model-Ages (Ga)
<b>Sediments:</b>					
Flux-6	40°07.8 N	21°08.2 W	0.512510±16	-2.5	0.83
Flux-7	46°22.0 N	12°23.7 W	0.512067±20	-11.1	1.58
Flux-8	47°30.8 N	08°31.6 W	0.512043±27	-11.6	1.64
Inter-B2	43°45.0 N	11°50.0 W	0.512007±19	-12.3	2.21
CV-2	19°24.0 N	29°44.0 W	0.512010±15	-12.2	1.78
KS 8231	36°09.0 N	03°13.0 W	0.512117±49	-10.1	1.49
K-12	37°57.2 N	26°07.8 W	0.512890±16	4.9	<0.01
KS 7929	46°18.3 N	15°04.0 W	0.512014±18	-12.2	1.87
KS 7920	45°37.5 N	27°44.8 W	0.511892±19	-14.5	2.13
KS 8228	35°50.0 N	08°43.0 W	0.512033±16	-11.8	1.81
KC 8221	36°53.0 N	07°39.0 W	0.512207±56	-8.4	1.36
KS73134	56°31.3 N	13°15.1 W	0.512069±22	-11.1	1.71
Senegal River (mouth sediments)			0.511838±31	-13.1	1.96
<b>Aerosols:</b>					
Glomar-#36	12°29N.	20°03W.	0.511911±17	-14.2	1.93
M19(10)	Cape Verde Basin		0.511984±23	-12.8	1.84
M20(10)	from 0°1N.	from 30°27W	0.511895±23	-12.7	1.96
M21(10)	-	-	0.511923±13	-13.9	1.91
M22(10)	-	-	0.511987±11	-12.7	1.82
M23(10)	-	-	0.511985±40	-12.7	1.82
M24(10)	to 14°14N.	to 25°17W.	0.512065±17	-11.2	1.77
Miami #157	25°50N.	80°15W.	0.512098±39	-10.5	1.71
Barbados-1	13°15N.	50°30N.	0.512068±14	-11.1	1.31
Barbados-2	13°15N.	50°30N.	0.512036±19	-11.7	1.76
Barbados-3	13°15N.	50°30N.	0.512014±24	-12.2	1.93
Barbados-4	13°15N.	50°30N.	0.511984±41	-12.8	1.83
Med.S.M08	39°40N.	12°40W.	0.512077±23	-10.9	1.63
Med.S.M09	"	"	0.512022±18	-12	1.82
Med.S.M10	"	"	0.512000±19	-12.4	1.45
Red S.MR83	26°N	35°E.	0.512172±16	-9.1	1.55
St. Louis (Missouri)			0.511826±40	-15.8	

sediments display the "oldest" model ages (1.74 to 1.98 Ga), which are also consistent with model ages reported for North West African granitoids (1.93 to 2.01 Ga).

Based on our analyses, it appears that the Nd isotopic distribution in tropical North-East Atlantic detrital sediments is mainly controlled by wind transport from Saharan Africa, consistent with a conclusion based on the Rb-Sr isotope system (Biscaye et al., 1974). Because primary productivity is very high in this region (Berger et al., 1986), aerosols falling on the sea surface are likely to be quickly scavenged and transported to the sediments by biogenic processes. In this region, light-REE surface-water enrichments were previously explained by a Saharan aerosol input (Elderfield and Greaves, 1982).

The transport of these aerosols to Barbados by the northeast Trades, previously reported in terms of dust loadings and mineralogy (Prospero, 1979-1980) and Sr isotopes (Biscaye et al., 1974) are further confirmed by Nd results (Grousset et al., 1988). The four Barbados samples that we analyzed display a narrow  $E_{Nd}(0)$  range:  $\approx -11.1$  to  $-12.8$  (the average:  $\approx -12.2$  is plotted on Fig.2), consistent with Saharan aerosol values observed between Africa and the MAR.

If we average model-ages of three of the four Barbados aerosols, we obtain  $\approx 1.84$  Ga. Of the four aerosols, however, one displays a much younger model-age (1.31 Ga) than the other three (1.76; 1.83; 1.93). This is consistent with the two-source hypothesis that we proposed in Biscaye et al. (in prep.) and referred to above for Rb-Sr model ages in that the sample with the lower model age was collected in winter and was derived from the area of younger African rocks.

In surface sediments to the north of the Mediterranean-Azores volcanogenic axis is another cluster of highly negative values (Fig.2;  $-12.2 \leq E_{Nd}(0) \leq -14.5$ ). Although the Nd data alone are not sufficient in number or extent --they do not extend to the western Atlantic-- they suggest a west-to-east gradient. Indeed such a gradient in concentrations of the mineral chlorite and of rubidium (Grousset and Chesselet, 1986) and with Rb-Sr isotope data (Biscaye et al., in prep.) has been observed from a much more extensive data set. This west-to-east gradient has been attributed to aerosol transport by the westerlies. In that analysis we tended to discount watermass transport for the reasons given in Grousset and Chesselet (1986) and Grousset et al. (1988).

McCulloch and Wasserburg (1978) reported an average value on North American shale ( $E_{Nd}(0) \approx -14.4$ ), an Iowa loess value ( $E_{Nd}(0) \approx -14.1$ ) and some Canadian Shield values which are much more negative than our North Atlantic data, with  $E_{Nd}(0)$  as low as  $-31.5$ . Present-day Saint Louis, Missouri, aerosols, however, display values consistent with ours:

$E_{Nd}(0) \approx -15.8$  (Grousset et al., 1988). These upwind sources are sufficiently nonradiogenic to explain our North Atlantic sediment data in the latitudes of the westerlies by aeolian transport. This North American signal is also characterized by high model ages ( $\approx 1.87$  to  $2.13$  Ga), which is consistent with data reported by many authors for Canadian Shield rocks ( $\approx 2.74$ - $2.96$  Ga and  $\approx 2.75$ - $3.15$  Ga (Miller and O'Nions, 1985)), for Iowa Loess ( $\approx 1.93$  Ga) or for North American Shales ( $\approx 2.08$  Ga) (McCulloch and Wasserburg, 1978). It appears likely that the westerlies blow over North American shales, loess and shield, and the mean Nd signal of the aerosols is an average of the different ages ( $1.93$ - $3.15$  Ga).

Our data, suggesting a westerly-transported source, is also consistent with the results of Folger (1970), who collected aerosols from Newfoundland to Great Britain, and observed a west-east gradient of North American particles: lacustrine diatoms, minerals, fungi, phytoliths. Based on previous work using Sr isotopes (Grousset and Chesselet, 1986), it appears that sediments on the MAR (between  $\approx 40$  and  $\approx 50^\circ$ N.) have two different provenances: transport from Iceland by bottom currents, and aeolian transport from North America. Our  $E_{Nd}(0)$  are consistent with this interpretation and we applied this interpretation and a two-member mixing model to our MAR sample (KS7920) to see if the estimate of aerosol contribution is similar to that derived from Sr isotopes. We obtained a North American aeolian contribution to the MAR (at the site of core KS7920) of about 56%, in very good agreement with the 58% aerosols estimate based on Sr isotope data, which corresponds to an aeolian flux of about  $\approx 0.5 \text{ g} \cdot \text{cm}^{-2} \cdot (10 \text{ Ky})^{-1}$  (Grousset and Chesselet, 1986). Thus we interpret the  $E_{Nd}(0)$  patterns reported here as displaying mainly the influence of an aerosol transport superimposed on a background of fluvial input to the North Atlantic.

#### 4. CONCLUSIONS:

A study of Nd and Sr isotopes in the detrital fraction of surface sediments and aerosols permits distinction between different continental sources and deduction of transport mechanisms of particulate matter to and within the Atlantic Ocean.

Nd isotope ratios and model ages, and Rb-Sr model ages are very informative aeolian transport tracers. Isotopic ratios display consistent patterns for both present-day aerosols and Upper Holocene surface sediments. In the North Atlantic, the two major sources of aeolian particles are the Saharan Shield and North America. Dust transport from those sources to the Atlantic Ocean are respectively connected with the Trade and Westerly major atmospheric circulation systems.

In the present-day tropical aerosols, Rb-Sr model ages allow us to distinguish between old particles coming from the north-west part of the Saharan desert, transported during summer periods, and young particles coming from the south-east part of tropical Africa and transported during winter periods. A much smaller number of Sm-Nd model age are consistent with this conclusion.

Aknowledgements: We are very grateful to Drs. J.M. Prospero, R. Lenaz and R. Chester, who provided aerosol samples. We thank very much Dr. A. Zindler who provided ultra-clean laboratory and mass-spectrometer facilities at Lamont, and thank Dr. Carol D. Frost and two anonymous reviewers for their helpful and pertinent comments. We thank the officers and crews of R/V Le Noroit, Le Suroit, Jean Charcot and Marion-Dufresne, for their help in raising the cores. This work was funded by a French CNRS program: "ATP-FMO" and by a "NSF/ CNRS" exchange grant to FG (#INT-85-13011).

#### REFERENCES:

- Allègre C.J. and Ben Othman, D. (1980) 'Nd-Sr isotopic relationship in granitoid rocks and continental crust development: a chemical approach to orogenesis', *Nature* 286, 335-342.
- Berger, W.H., Fischer, K., Lai, C., Wu, G. (1986) 'Primary production and organic carbon flux in the World Ocean', *Trans. Amer. Geoph. Union*, EOS 66, 1302.
- Biscaye, P.E., (1965) 'Mineralogy and sedimentation of recent deep-sea-clay in the Atlantic Ocean and Adjacent Sea and Oceans', *Geol. Soc.of Amer. Bull.* 76, 803-832.
- Biscaye, P.E., (1972) 'Strontium isotope composition and sediment transport in the Rio de la Plata Estuary', *Geol. Soc. Amer. Mem.* 33, 349-357.
- Biscaye, P.E., and Dasch, E.J. (1971) 'The rubidium, strontium, strontium isotope system in deep-sea sediments: Argentine Basin', *J. Geoph. Res.* 76, 5087-5096.
- Biscaye, P.E., Chesselet, R., Prospero, J. (1974) 'Rb-Sr, <sup>87</sup>Sr/<sup>86</sup>Sr isotope system as an index of the provenance of continental dust in the open Atlantic Ocean', *J. Rech. Atmos.* 8, 819-829.
- Biscaye, P.E., Dasch, J., Grousset, F.E., 'Rb-Sr model-ages in deep-sea sediments in the Atlantic Ocean', (submitted to *Earth & Planet. Sci. Lett.* )
- Chester, R., Griffiths A.G., Hirst, J.M. (1979) 'The influence of soil-sized atmospheric particulates on the elemental chemistry of the deep-sea sediments of the northeastern Atlantic', *Mar. Geol.* 32, 141-154.
- Chester, R., and Johnson, L.R. (1971) 'Atmospheric dusts collected off the West African coast', *Nature* 229, 105-107.
- Chester, R., Sharples, E.J., Sanders, G.S., Saydam, A.C. (1984) 'Saharan dust incursion over the Tyrrhenian Sea', *Atmos.*

- Environ. 18, 929-935.
- Chester R., and Stoner, J.H. (1974) 'The distribution of zinc, nickel, cadmium, copper and iron in some surface waters from the world Ocean', *Mar. Chem.* 2, 17-32.
- Dasch, E.J. (1979) 'Strontium isotopes in weathering profiles, deep-sea sediments and sedimentary rocks', *Geochim. & Cosmo. Acta* 33, 1521-1552.
- Delany, A.C., Delany, A.C., Parkin, D.W., Griffin, J.J., Goldberg, E.D., Reimann, B.E. (1967) 'Airborne dusts collected at Barbados'. *Geochim. & Cosmo. Acta* 31, 885-909.
- Elderfield, H. and Greaves, M.J. (1982) 'The rare earth elements in seawater', *Nature* 296, 214-219.
- Folger, D.W. (1970) 'Wind transport of land-derived mineral biogenic and industrial matter over the North Atlantic', *Deep-Sea Res.* 17, 337-352.
- Frost, C.D., O'Nions, R.K., Goldstein, S.L. (1986) 'Mass balance for Nd in the Mediterranean Sea', *Chem. Geol.* 55, 45-50.
- Gac, J-Y. and Kane, A. (1986) 'Le fleuve Sénégal: I. Bilan hydrologique et flux continentaux de matières particulaires à l'embouchure' *Sci. Géol. Bull. Strasbourg* 39(1), 99-130.
- Glaccum, R.A. and Prospero, J.M. (1980) 'Saharan aerosols over the tropical North-Atlantic: mineralogy', *Mar. Geol.* 37, 295-321.
- Goldstein, S.L. and O'Nions, R.K. (1981) 'Nd and Sr isotopic relationships in pelagic clays and ferromanganese deposits' *Nature* 292, 324-327.
- Goldstein, S.L., O'Nions, R.K., Hamilton, P.J. (1984) 'A Sm-Nd isotopic study of atmospheric dusts and particulates from major river systems', *Earth & Planet. Sci. Lett.* 70, 221-236.
- Griffin, J.J., Windom, H., Goldberg, E.D. (1968) 'The distribution of clay mineral in the world Ocean', *Deep-Sea Res.* 15, 433-459.
- Grousset, F.E., and Chesselet, R. (1986), 'The Holocene sedimentary regime in the northern Mid-Atlantic Ridge region', *Earth & Planet. Sci. Lett.* 78, 271-287.
- Grousset, F.E., Biscaye, P.E., Zindler, A., Prospero, J.M., Chester, R., (1988a) 'Neodymium isotopes as tracers in marine sediments and aerosols: North Atlantic', *Earth & Planet. Sci. Lett.* 87, 367-378.
- Grousset, F.E., Joron, J-L., Biscaye, P.E., Latouche, C., Treuil, M., Maillet, N., Faugères, J-C., Gonthier, E. (1988b) 'Mediterranean outflow through the Strait of Gibraltar since 18,000 yrs.B.P.: mineralogical and geochemical arguments', *Geo-Mar. Lett.* 8, 25-34.
- Hurley, P.M. and Rand, J.R. (1969) 'Predrift continental nuclei', *Science* 164, 1229-1242.
- Jacobsen S.B. and Wasserburg, G.J. (1980) 'Sm-Nd isotopic evolution of chondrites', *Earth & Planet. Sci. Lett.* 50, 139-155.
- Kolla, V., Biscaye, P.E., Ryan, B.F. (1972) 'Origin and disper-



- sal of Holocene sediments in the Eastern Mediterranean Sea', *The Mediterranean Sea*, D.J.Stanley, (ed), pp.455-469.
- Kolla, V., Biscaye, P.E., Hanley, A. (1972) 'Distribution of quartz in Late Quaternary sediments in relation to climate', *Quat. Res.* 11, 261-277.
- Lamb, H.H. (1971) 'Climates and circulation regimes developed over the northern hemisphere during and since the last ice age', *Paleo. Paleo. Paleoc.* 9, 125-162.
- McCulloch, M.T. and Wasserburg, G.J. (1978) 'Sm-Nd and Rb-Sr chronology of continental crust formation', *Science* 200 (4345), 1003-1011.
- Melia, M.B. (1984) 'The distribution and relationship between palynomorphs in aerosols and deep-sea sediments off the coast of North-west Africa', *Mar. Geol.* 5, 345-371.
- Miller R.G. and O'Nions R.K. (1985) 'Source of Precambrian chemical and clastic sediments', *Nature* 314, 325-330.
- O'Nions, R.K., Hamilton, P.J., Hooker, P.J. (1983) 'A Nd investigation of sediments related to crustal development in the British Isles', *Earth & Planet. Sci. Lett.*, 63, 229-240.
- Pokras, E.M. and Mix, A.C. (1985) 'Eolian evidence for spatial variability of Late Quaternary climates in tropical Africa', *Quater. Res.* 24, 137-149.
- Piepgras D.J., and Wasserburg, G.J. (1983) 'Influence of the Mediterranean Outflow on the isotopic composition of neodymium in waters of the North Atlantic', *J. of Geophys. Res.* 88(C10), 5997-6006.
- Prospero, J.M. (1979) 'Mineral and sea-salt aerosol concentrations in various ocean regions', *J. Geoph. Res.* 84, 725-731.
- Prospero, J.M. (1981) 'Eolian transport to the World Ocean', *The Oceanic Lithosphere*, C.Emiliani (ed.), *The Sea* 7(21), 801-874.
- Prospero, J.M., Glaccum, R.A., Nees, R.T. (1981) 'Atmospheric transport of soil dust from Africa to south America', *Nature* 289, 570- 572.
- Radczewski, O.E. (1939) 'Eolian deposits in marine sediments', *Recent Marine Sediments*, Am. Assoc. Petr. Geol. Symp., P. D.Trask (ed.), pp.496-502.
- Rateev, M.A., Gorbunova, Z.N., Lisitzyn, A.P., Nosov, G.L. (1969) 'The distribution of clay minerals in the Ocean', *Sedimentology* 13, 21-43.
- Sarnthein, M., Tetzlaff, G., Koopmann, B., Wolter, K., Pflaumann, U. (1981) 'Glacial and interglacial wind regimes over the eastern subtropical Atlantic and North-West Africa', *Nature* 293, 193-196.
- Schutz, L. (1980) 'Long-range transport of desert dust with special emphasis on the Sahara', *Ann. N-Y. Acad. Sci.* 338, 515-532.
- Zindler, A., Hart, S.R., Frey, F., Jakobsson, S.P. (1979) 'Nd and Sr isotope ratios and REE abundances in Reykjanes

Peninsula Basalts: evidence for mantle heterogeneity beneath Iceland', *Earth & Planet. Sci. Lett.* 45, 249-262.

Zindler, A., Staudigel, H., Batiza, R. (1984) 'Isotope and trace element geochemistry of young Pacific seamounts: implications for the scale of upper mantle heterogeneity', *Earth & Planet. Sci. Lett.* 70, 175-195.

WIND-BORNE DEPOSITS IN THE NORTHWESTERN INDIAN OCEAN: RECORD OF  
HOLOCENE SEDIMENTS VERSUS MODERN SATELLITE DATA

FRANK SIROCKO and MICHAEL SARNTHEIN

ABSTRACT

A study of deep sea cores shows that eolian dust plumes from Arabia dominate the Holocene non-turbiditic lithogenic sedimentation in the northwestern Indian Ocean; fluvial supply controls only the proximal deposition near India, off Kenya, and off Oman, where also the suspension load of the intermediate water from the Persian Gulf is added. A survey of modern dust outbreaks as depicted on satellite images from 1979 was used to calibrate the paleoclimatic and paleometeorological record of lithogenic sediment accumulation in the deep sea.

Dolomite, chlorite and illite-rich sediments mark the dispersal of Shamal wind-borne dust from the Persian Gulf and Gulf of Oman. Palygorskite and kaolinite are linked to the dust outbreaks from and near the Gulf of Aden. The outer margin of the steep gradient of dust accumulation rates, which runs from the Horn of Africa to India near 20°N, parallels the position of the southwesterly low-level Somali Jet.

The average of annual dust accumulation in the Arabian Sea during the last 8000 years amounted to about  $100 \cdot 10^6 \text{t y}^{-1}$ . This number compares well with a transcoastal dust flux of 115 to  $215 \cdot 10^6 \text{t y}^{-1}$  derived for 1979 from satellite images.

1. INTRODUCTION

Southern Asia, from the Red to the Chinese Sea is influenced by intense southwest monsoon summer precipitation, which is of vital importance to the social and economic life of the whole region. Accordingly, there is a major concern about the stability of the climatic system in terms of both year by year forecasting (Bryson & Campbell, 1982) and long-term variations during the Quaternary (Prell & Van Campo, 1986, Prell & Kutzbach, 1987).

Long-term change in the monsoonal regime has been assessed by both climatic modelling (Kutzbach, 1981, Kutzbach & Guetter, 1986) and direct proxydata (Prell, 1984 a, b, Duplessy, 1982). In the deep-sea record three kinds of proxydata can trace past monsoonal winds. Surface salinity patterns, as calculated from the isotopic composition of planktonic Foraminifera were used to outline areas of monsoon-controlled precipitation over the ocean (Duplessy, 1982). The composition of foraminiferal assemblages has provided information on wind-induced upwelling and monsoonal wind strength via zonal anomalies of sea surface temperatures (Prell & Hutson, 1979, Prell & Curry, 1981). Last but not least, wind supplied particles, mineral dust, and pollen carry a significant message. For example, Van Campo (1986) and Van Campo et al. (1982) used pollen to reconstruct the Late Quaternary vegetation of East Africa and India and to estimate the respective precipitation figures over land.

Mineral dust, however, which is a common feature over the Arabian

Sea during present-day summers (McDonald, 1938), has not yet been studied on Pleistocene timescales, except for the record of a sediment core by Kolla & Biscaye (1977) and an early investigation by Olausson & Olsson (1968), who restricted their interest to the Holocene of the Gulf of Aden. Stewart et al. (1965), Goldberg & Griffin (1970), von Stackelberg (1972), Mattiat et al. (1973), Marchig (1974), Kolla et al. (1976, 1981 a,b), and Kolla & Biscaye (1977) mapped the mineral and chemical composition of surface sediments across the Arabian Sea in detail and defined its modern sedimentological provinces. They generally agreed that the lithogenic sediment fraction is composed of a mixture of eolian and river-borne particles, but their estimates of source proportions, source areas, and transport mechanisms differ strongly. Likewise, their early studies of sediment cores led to only vague suggestions regarding climatic change, which moreover were poorly defined in terms of age.

During the last 15 years, stable isotope stratigraphy (Shackleton & Opydyke, 1973, Duplessy, 1978) has provided an effective means to overcome the dating problem. In the Northwestern Indian Ocean, it was employed by Moyes et al., (1978), Prell et al. (1980), Van Campo et al. (1982), Van Campo (1986), and Fontugne & Duplessy (1986) to date Late Pleistocene and Early Holocene climatic change on the encompassing continents.

## 2. THE OBJECT OF THIS STUDY

In our present study we present data from 54 hemipelagic sediment cores and 9 surface samples (Sirocko, 1989) covering the Arabian Sea north of 10°S to characterize and quantify the modern and past eolian sediment input (Fig.1). Accordingly, data from 15 sediment profiles disturbed by any sediment transport near the sea floor such as turbidites, were rejected. Only 39 cores (Table 1) contained undisturbed hemipelagic sections of the Late Quaternary. They were dated by oxygen isotope stratigraphy. Accumulation rates were calculated for the last 27,000 years. In this study we only present data from the last 8000 years; the Pleistocene sediment record is described elsewhere (Sirocko, 1989).

Employment of sediment and particle accumulation rates provides major advantages over the use of concentrations. For example, mutual dilution effects of different sediment components are excluded. Moreover, the accumulation rates enable us to interpret the sediment data in terms of flux. Finally, accumulation rates allow direct comparison of the sedimentary record with flux data derived from satellite images, estimates of river discharge, sediment traps, and aerosol measurements.

In addition to the study of sediment cores, we processed in a pilot study satellite images from 1979 to measure the aerosol turbidity over the ocean.

Both records are used to construct a mass balance of the Holocene aerosol input to the Arabian Sea. We are aware that the accuracy of our two calculation methods is limited. Likewise, the satellite data from one year hardly form an adequate analogue to the sediment record averaging 8000 years, especially since the Late Holocene climate clearly differs to that from the Early Holocene (Kutzbach, 1981).

Table 1. Location of Sediment Cores

	core	latitude [ ° ]	longitude [ ° ]	waterdepth [ m ]
SO 42	15KL	14 52.82 N	64 44.79 E	3920
	26KL	15 30.86 N	68 45.61 E	3776
	36KL	17 04.49 N	69 02.68 E	2055
	43GB	17 54.40 N	69 02.60 E	3410
	51KL	20 57.92 N	65 33.54 E	2644
	57KL	20 54.47 N	63 07.32 E	3422
	64KL	19 04.62 N	64 41.01 E	3281
	70KL	17 30.69 N	61 41.82 E	3810
	71KL	16 14.17 N	60 15.35 E	4029
	74KL	14 19.26 N	57 20.82 E	3212
	79KL	13 38.84 N	58 19.56 E	4351
	82KL	12 41.09 N	58 40.62 E	4416
	87KL	10 30.05 N	57 44.22 E	3773
SO 28	05KL	06 39.75 N	61 08.03 E	3335
	11KL	05 23.36 N	60 15.09 E	3859
	18KL	01 53.99 N	67 20.47 E	3035
ORGON 4	KS 8	23 28.00 N	59 11.50 E	2900
IOE	105KK	11 16.00 N	53 32.50 E	3535
	114KK	08 00.50 N	51 12.80 E	3843
	143KK	01 15.00 N	44 47.00 E	1522
	162KK	04 05.00 S	40 28.80 E	940
	169SK	03 33.50 S	53 38.70 E	3620
	181SK	07 30.10 N	71 03.50 E	4122
	182SK	08 46.20 N	73 42.00 E	2234
	223SK	20 04.00 N	66 53.00 E	2686
	232SK	21 47.00 N	64 36.00 E	3098
	OSIRIS	76123	06 23.50 N	78 39.50 E
76125		08 35.00 N	75 20.00 E	1878
76127		12 05.40 N	73 54.00 E	1610
76128		13 08.00 N	73 19.00 E	1712
76132		16 59.40 N	71 30.80 E	1430
76135		14 26.60 N	50 31.80 E	1895
76136		12 52.30 N	46 48.90 E	1649
77191		07 30.10 N	76 43.00 E	1254
77194		10 28.00 N	75 14.00 E	1222
77200		16 32.50 N	67 53.50 E	2910
	77202	19 13.30 N	60 40.90 E	2427
	77203	20 41.90 N	59 34.10 E	2442
	Meteor 5	422-6	24 23.40 N	59 02.50 E

	surface	latitude	longitude	waterdepth
	samples:	[ ° ]	[ ° ]	[ m ]
SO 42	93GB	09 55.19 N	57 42.46 E	4160
ORGON 4	KR 4	13 47.75 N	51 36.90 E	4727
	KS 5	16 45.90 N	57 30.70 E	4010
IOE	112	07 43.20 N	51 53.30 E	5067
	115	08 07.80 N	50 48.10 E	3200
	126	05 33.50 N	49 25.80 E	2835
	129	05 04.00 N	50 26.00 E	4719
	130	04 56.30 N	50 48.00 E	4729
	132	01 54.00 N	49 02.00 E	4614
	136	02 47.00 N	48 00.00 E	3515
	146	00 31.00 N	45 36.00 E	3625
	148	00 00.00 N	46 02.50 E	4027
	170SK	02 46.00 S	57 59.50 E	4356
	179SK	02 12.00 N	57 51.50 E	4231
	180SK	05 15.00 N	65 56.30 E	4494
	221	18 21.80 N	69 39.50 E	2793
	234	22 32.50 N	65 24.00 E	2254
	236	23 25.00 N	65 53.00 E	1220
Osiris	77201	17 56.70 N	63 09.80 E	3665
	77204	19 18.00 N	58 26.00 E	1430
Meteor 5	419	22 30.10 N	61 56.20 E	3098
	420	23 02.20 N	61 29.40 E	3334
Vema	V 19-181	08 14.00 N	66 57.00 E	2449
Conrad	RC 9-160	12 03.10 N	63 08.80 E	2270

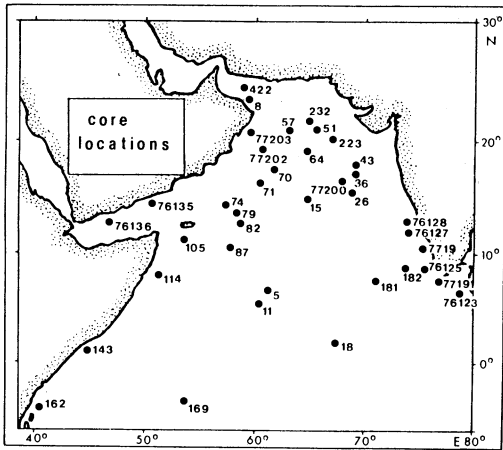


Fig.1. Location of sediment cores used for the calculations of recent accumulation rates. Additional surface sediment samples (compare Table 1).

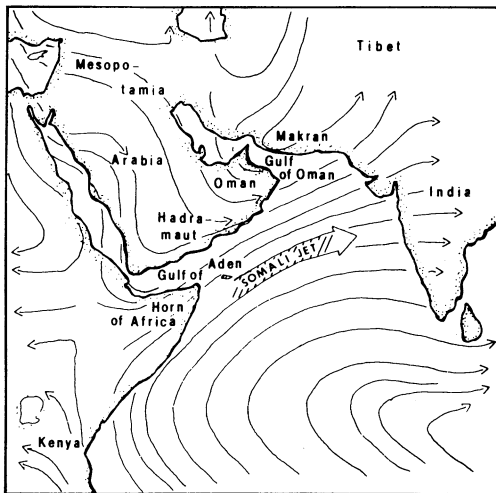


Fig.2. 850 mb mean winds for 1 July to 31 July, taken from Krishnamurti et al.(1980), including position of the Somali Jet (Findlater, 1969).

### 3. METEOROLOGICAL SETTING

The meteorology over the Northern Indian Ocean is marked by the well established seasonal system of monsoonal winds that also controls dust transport. Ramage et al. (1972 a, b) and Krishnamurti et al. (1982) show that during winter northeasterly monsoons blow from India, Pakistan, and Afghanistan toward the Arabian Sea in the surface layer of the atmosphere, below 1500 m height. The high Himalayas separate the strong Siberian anticyclone from the Indian Ocean and cause a weak pressure gradient between North India and the Arabian Sea; this results in gentle wind speeds of 2-3 m/s as a mean value for the winter months in the Arabian Sea (Ramage, 1969).

Forced by strong gradients of solar heating during summer, continental heat lows are maintained near the surface of Iran, Tibet and North India. The resulting landward-directed south-north pressure gradient generates the strong low level southwesterly monsoons over the Arabian Sea with windspeeds of 5-15 m/s (monthly means after Ramage et al., 1972) (Figure 2).

Pant (1978) summarized the vertical structure of the summer troposphere over the Arabian Sea (Figure 3). The low-level monsoon layer (below 600-1000 m) is divided into a near ground mixed layer in the northwest with a potential for eastward dust transport and a cloud layer in the southeast where the dust is rained out. In the northwest, immediately off Arabia, the top of the monsoon layer is marked by an inversion, the base of which is gradually lifting towards southeast (Narayanan & Rao, 1981). The inversion results from a dry and warm midtropospheric air mass that overlies the cooler and moist air mass of the low level monsoon. The dry air mass aloft originates from Arabia, extends up to 6000 m above surface and carries an ongoing dust load to the south during summer (McDonald, 1938, Ackerman & Cox, 1982). This transport is punctuated by occasional major dust outbreaks (Foda et al., 1985, Chen, 1986, Ackerman & Cox, 1988). Southward flux of dust over the northern Arabian Sea is accomplished by northwesterly winds, called Shamal in the Persian Gulf region, which below 500 mb tend to turn toward the east above the monsoonal inversion, that is roughly parallel the low-level monsoon above the Arabian Sea (Ramage et al., 1972, Chen, 1986).

Further to the east and southeast (Figure 3), the monsoon inversion weakens and is penetrated by cumulus and cumulonimbus clouds. They reach to and through the middle troposphere and largely bar any further dust transport to the east, to India.

The summer monsoon and its cloud layer are centered around the ' Somali or East African Low Level Jet ' ( Findlater, 1969, Figure 2, 3). During July it moves from the Horn of Africa towards the southern flank of the North Indian heat low and marks the southernmost reach of the Arabian northwesterlies (Findlater, 1969).

In summary, the distribution pattern of dust in sediments from the Arabian Sea is likely to reflect the following meteorological and climatic structures of the encompassing land masses,

i) the southern margin of dust dispersal marks the latitudinal position of the monsoon inversion at about 500 mb (Findlater, 1969) and of the underlying Somali Jet;

ii) the flux of dust is controlled by the continental aridity in the entrainment regions, i.e. Arabia and Mesopotamia, and by the



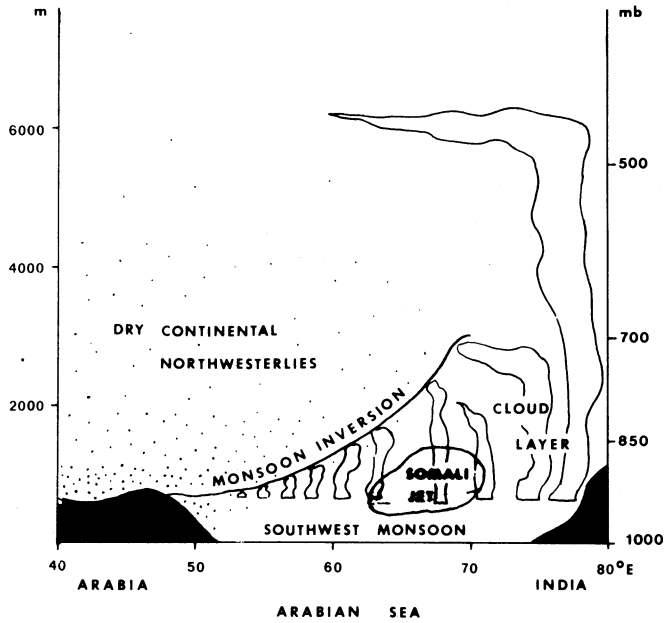


Fig.3. Generalized profile of the low and mid troposphere during June and July at 16°N, modified after Pant (1978). Dust concentrations indicated by stipples (after Ackerman & Cox, 1982).

frequency and speed of the Arabian northwesterlies;

iii) dust grain sizes record both the transport distance and the strength of Shamal and southwest monsoonal winds;

iv) indirectly, the latitudinal position of the Somali Jet and the associated monsoon inversion may outline the northern limit of summer precipitation over northwest India.

#### 4. ANALYTICAL TECHNIQUES: SEDIMENT DATA

Age control was based on well-defined events of oxygen isotope stratigraphy such as the onset and end of glacial Termination I (Broecker & van Donk, 1970). Recent  $^{14}\text{C}$  ages by accelerator mass spectrometry (Bard et al., 1987, Broecker et al., 1988) date the onset of Termination I at about 15,000 y.B.P., the end at about 8,000 y.B.P.. The age of the sediment surface in the cores of this study was determined by upward extrapolation of the age-depth curves (Sirocko, 1989). As a result, absolute ages for the core tops range between 0 and 4000 years B.P..

Dry bulk densities were determined from wet samples of known volume (usually 5 ccm) by drying and subsequent weighing of the dry sample. The bulk accumulation rates were calculated from equation (1), following the technique of van Andel et al. (1975) and Thiede et al. (1982).

$$\text{ARb} = \text{S} * \text{Dbd} * 10 \quad (1)$$

where

$$\begin{aligned} \text{ARb} &= \text{bulk accumulation rate} \quad [ \text{g} / \text{m}^2 \text{ y} ] \\ \text{S} &= \text{sedimentation rate} \quad [ \text{cm} / 1000 \text{ y} ] \\ \text{Dbd} &= \text{dry bulk density} \quad [ \text{g} / \text{cm}^3 ] \end{aligned}$$

Dolomite was determined by X-ray diffractometry of bulk sediment samples using the calcite/dolomite ratio of Tennant & Berger (1957). Bulk carbonate concentrations were measured by IR absorption of  $\text{CO}_2$ . The proportions of marine and lithogenic carbonate form two end members of a mixing line, which are distinguished by their respective oxygen isotope ratios. The  $\delta^{18}\text{O}$  of marine carbonates largely equals the oxygen isotope record of *Globigerinoides ruber*, which also served for stratigraphy. This species forms its tests in the warm surface layer of the ocean (Duplessy et al., 1981), which results in the most negative oxygen isotopic values of all planktonic Foraminifera ranging between -1.5 and -2.5 ‰. In contrast, Precambrian, Paleozoic and Mesozoic limestones, which are abundant near the Persian Gulf region, provide  $\delta^{18}\text{O}$  ratios of -4.0 to -7.0 ‰ (Degens & Epstein, 1962, Renard, 1986). Detrital silt-sized particles of limestone with this isotopic composition are found in the plankton-free sediments from the deepest part of the Oman Gulf (Degens & Hunt, unpubl. report, Sirocko, 1989). Likewise, the bulk carbonate fraction of a dust sample from the Horn of Africa (Sirocko, 1989) has a  $\delta^{18}\text{O}$  composition of -6.8 ‰. Hence, we defined the averaged  $\delta^{18}\text{O}$  value of lithogenic calcium carbonate, the terrigenous end member of the mixing line, at -6.0 ‰.

The resulting estimates of detrital lithogenic carbonate in the bulk  $\text{CaCO}_3$  fraction are regarded as quasi-conservative since the shell and test carbonate of many marine planktonic and benthic species is

Table 2. Sources of Error Contained in the Aerosol Quantification Based on Satellite Images.

(Equation (6):)

: The analytical errors of the McIDAS image processing system range at 0.1 units of  $V$

(Equation (7):)

\*constant 3.75: Assumption of a constant to calculate the dust loading from turbidity units. However the constant depends on the specific aerosol extinction coefficient (here 0.267), which varies with mineralogy, grain size, and transport distance of dust (Westphal, et al., 1985). The error cannot be quantitated.

(Equation (8):)

\*TM : Estimates of monthly averages of TM being based on  $V$  samples of no more than 6 days per month. The relative error of  $V$  range within 30 and 200 %, due to the occasional dust outbreaks.

j : Definitions of coastline sectors considered homogenous in terms of  $V$ , wind speed and direction. (Deviations see TM)

k : Definition of air layers according to the availability of meteorological data restricts the vertical resolution of different horizontal layers of dust transport.

TA : Arbitrary selection of a single year (1979) for estimating the trans-coastal dust discharge. E.g., 1979 was marked by unusual droughts and dust outbreaks (Wolter, pers.comm.)

U\* : Low lateral resolution of wind data (50 grid spacing in Ramage et al., 1972); Use of monthly means of wind direction (wind steadiness ranges during July along the Arabian coast in the layer 0-1 km at 84%, 1-2 km not given, 2-4.5 km 68 %, 4.5-7 km 82 %). Ephemeral outbreak trajectories generally follow the wind tracks at 700 mb (Chen, 1986).

\*\*A : Basic assumptions contained in vertical dust concentration profiles solely based on 5 aircraft transects across Arabia (4) and the Arabian Sea (1) during the pre-onset season of the southwest monsoon 1979 (Ackerman & Cox, 1982). Concentrations for the level 0-1km range between 40.5 and 70.8 %, for 1-2 km between 14.3 and 34.1 %, for 2-4.5 km between 10.6 and 22.8 %, for 2.5-7 km between 0.6-2.5 %.

\* : Error sources regarded as most significant.

likely to be more enriched in  $^{18}\text{O}$  than that of *Globigerinoides ruber*, which has been defined as marine endmember of the  $\text{CaCO}_3$  mixing line.

Biogenic opal was separated quantitatively from the carbonate-free sand and silt fractions by means of a density liquid of  $2.14 \text{ g/cm}^3$  (Potassium-poly-tungstate, Bohrmann, 1988). This technique does not apply to the fraction  $< 2 \mu\text{m}$  diameter. However, only minor opal concentrations are expected in this fraction because of increased efficacy of silica dissolution.

Based on bulk accumulation rates and the concentrations of marine carbonate and biogenous opal, the accumulation rate of the lithogenic fraction ( $\text{AR}_1$ ) was determined by equation (2):

$$\text{AR}_1 = \text{AR}_b - [(\text{AR}_b/100) * C_m] - [(\text{AR}_b/100) * B] \quad (2)$$

[ g / m<sup>2</sup> y ]

where

$\text{AR}_b$  = bulk accumulation rate [ g/m<sup>2</sup>y ] see eq. (1)

$C_m$  = marine carbonate content [ % of bulk sample ]

$B$  = biogenous opal content [ % of bulk sediment  $> 2 \text{ m}$  ]

For this calculation the input of volcanic ash and extraterrestrial material was assumed to be neglectible.

The accumulation rate of the siliciclastic fraction ( $\text{AR}_{\text{sil}}$ ) is calculated by equation (3):

$$\text{AR}_{\text{sil}} = \text{AR}_1 - [(\text{AR}_b/100)*C_1] - [(\text{AR}_b/100)*D] \quad (3)$$

[ g / m<sup>2</sup> y ]

where

$C_1$  = lithogenic carbonate content [% of bulk sample]

$D$  = dolomite content [% of bulk sample]

Finally, the total lithogenic accumulation rate for the Arabian Sea north of the equator (Tab. 3) was derived by multiplying the mean lithogenic accumulation rate of a homogenous area (deduced from the isolines of Fig. 5a) with its areal extent.

The grain sizes of the carbonate- and carbon-free sediment fraction were measured on a Sedigraph 5000 D (Stein, 1985). These measurements were not corrected for biogenous opal, which might result in a small error for samples collected off the Horn of Africa where opal concentrations reach peak values of 10 % of the siliciclastic fraction. For the rest of the Arabian Sea they are lower than 5 % (Sirocko, 1989). Thus, the accumulation rate of clay ( $\text{AR}_{<2}$ ) was calculated by equation (4):

$$\text{AR}_{<2} = ( \text{AR}_{\text{sil}} / 100 ) * \text{GS}_{<2} \quad (4)$$

[ g / m<sup>2</sup> y ]

where

$\text{GS}_{<2}$  = grain size  $< 2 \mu\text{m}$  [ % of siliciclastic fraction ]

The clay fraction  $< 2 \mu\text{m}$  was analyzed by X-ray diffractometry of oriented samples. To quantify quartz, we run a sample several times with varying additions of a laboratory standard of pure quartz, measuring the peak area at  $4.26 \text{ \AA}$ . Palygorskite produces two diffraction peaks, one each at  $6.4 \text{ \AA}$  and  $10.5 \text{ \AA}$ , the latter one overlapping with the illite

Table 3. Annual Average of Non-turbiditic Lithogenic Sediment Deposition in the Arabian Sea below 1000 m Water Depth (Based on Fig. 5a; see Analytical Techniques Section)

Areas (north of the equator)	Mass accumulation rate [ $10^6\text{t y}^{-1}$ ]
West of 70°E	107
East of 70°E	32
	total: 139
Gulf of Oman	20

Table 4. Vertical Variability of Dust Flux over 1979 Based on Equation (8). (Vertical Resolution of Data based on Monex Aircraft Data for May 1979; Ackerman & Cox, 1982)

sector	transcoastal dust flux in 1979 [ $10^6\text{t y}^{-1}$ ]				
	0-1 km	1-2 km	2-4.5 km	4.5-7 km	sum:
	( height over ground)				
1	0.0	0.0	0.0	0.1	0.1
2	21.3*	11.0	7.8	0.0	40.1
3	0.0	6.9	0.0	0.0	6.9
4	0.0	10.2	20.2	0.0	30.4
5	78.4*	30.6	7.1	0.4	116.5
6	0.0	6.3	13.7	1.0	21.0
sum:	99.7	65.0	48.8	1.5	215.0

\* the marked values are subject to large errors, (see Mass Balance Section)

Table 5. Trans-coastal Dust Flux to the Arabian Sea 1979, Based on Equation (8) (locations of sectors see Fig. 10 a)

sec- tor	monthly trans-coastal dust flux in 1979 [ $10^6\text{t y}^{-1}$ ]								annual sum:
	Jan- March	April	May	June	July	Aug.	Sept.	Oct.- Nov.	
1	0.0	0.0	0.0	0.0	0.0	0.1	0.0	0.0	0.0
2	0.0	0.0	0.2	10.3	15.2	14.4	0.0	0.0	40.1
3	0.0	0.0	0.0	2.9	2.6	1.5	0.0	0.0	7.0
4	0.0	0.0	0.0	22.4	6.0	2.1	0.0	0.0	30.5
5	0.0	4.7	3.8	32.1	50.1	25.5	0.4	0.0	116.6
6	0.0	4.2	1.2	4.1	4.4	5.3	1.9	0.0	21.1
								sum:	215.3

peak at 10 Å. Hence, we used the peak area at 6.4 Å to approximate the abundance of palygorskite. This method is based on unpublished experiments of H. Lange, Kiel University, with laboratory standards (Sirocko & Lange, in prep.). Other clay minerals were determined using the established factors of Biscaye (1965) with the illite peak at 10 Å additionally corrected for the overlap of palygorskite.

The accumulation rates of various clay minerals (AR<sub>cm</sub>) were determined by equation (5):

$$AR_{cm} = \{ [AR_{<2} - (AR_{<2}/100) * Q] / 100 \} CM \quad (5)$$

[ g / m<sup>2</sup> y ]

where

Q = quartz percentage of siliciclastic fraction < 2 μm

CM = clay mineral percentage of bulk clay mineral fraction

## 5. THE SEDIMENT RECORD

The highest sedimentation rates and bulk accumulation rates in the Northwestern Indian Ocean (Figure 4a, b) occur in the Gulf of Aden (120 g/m<sup>2</sup>y) and in the Gulf of Oman (150 g/m<sup>2</sup>y). From these two maxima the rates decrease to less than 20 g/m<sup>2</sup>y east of 70° E and south of 17° N. Further east, between the Lakkadive Ridge and the Indian continent, Figure 4b shows a small-scale lobate distribution pattern with values reaching 318 g/m<sup>2</sup>y.

Accumulation rates of non-turbiditic lithogenic sediment (Figure 5a) produce a similar distribution pattern, however, with the maximum values marking the Gulf of Oman (130 g/m<sup>2</sup>y) and still high values in the Gulf of Aden (70g/m<sup>2</sup>y). Near the tip of India, we again observe small-scale extremes of up to 143 g/m<sup>2</sup>y. This patchy distribution pattern suggests the local origin of these sediments. For comparison we present a map of the Indus turbidites (Figure 5b), modified after Kolla & Coumes (1984), which shows a high turbidite abundance in the central to southeastern Arabian Sea while the rest of the Arabian Sea is turbidite free. The 4 cores inside the area of abundant turbidites in Figure 5b are located on sea-mounts or reveal turbidites below the Holocene section.

In Figures 6-8 we document the raw percentages of minerals on the left side of each double-figure and present the accumulation rate on the right side.

The accumulation rates of dolomite (Figure 6b), which mostly consists of silt-sized rounded grains (Stewart et al, 1965), outline a transport direction from the Oman coast down to southern India. Terrigenous carbonate debris (Figure 6d) shows a similar distribution pattern. Both variables indicate a transport from Arabia towards the east, up to an area near 17°N 70°E.

The accumulation rates of siliciclastic grain-size fractions (Figures 7a-f) also reveal distribution patterns similar to those of other variables. The >6 μm fraction (Figure 7d) indicates a transport as far as 800 km, possibly up to 1500 km distance offshore from South Arabia. The high accumulation of coarse silt >20 μm (Fig. 7b) is restricted to a zone of about 400 km width, parallel to the coastline of Arabia with a maximum in the outer Gulf of Aden. The accumulation rate of clay (Fig. 7f) culminates near the Arabian coast with a pronounced maximum in the Gulf of Oman.

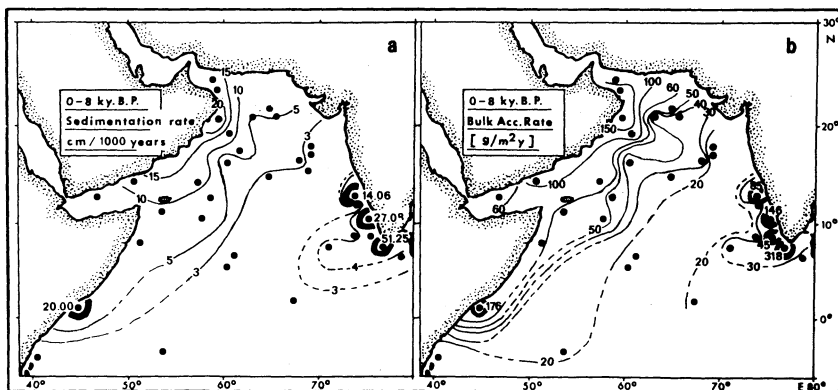


Fig.4. (a) Sedimentation and (b) bulk accumulation rates for the last 8000 years.

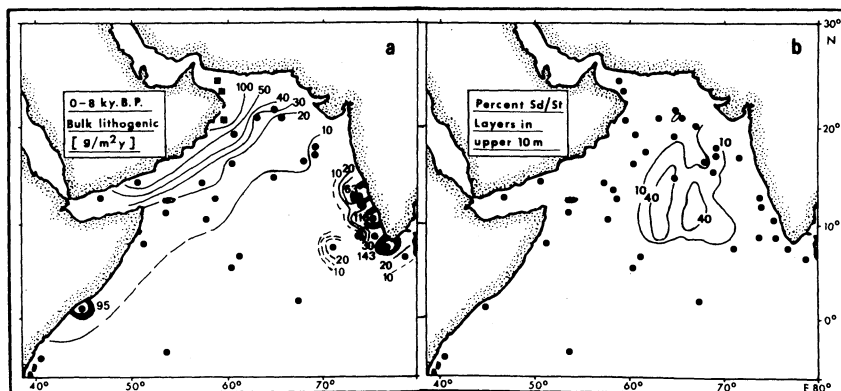


Fig.5. (a) Annual lithogenic accumulation rates for the last 8000 years. Sample positions marked by squares are samples with river-borne deposits. (b) Abundance of sand silt layers, i.e. turbiditic sediments of the river Indus (modified after Kolla & Coumes, 1984).

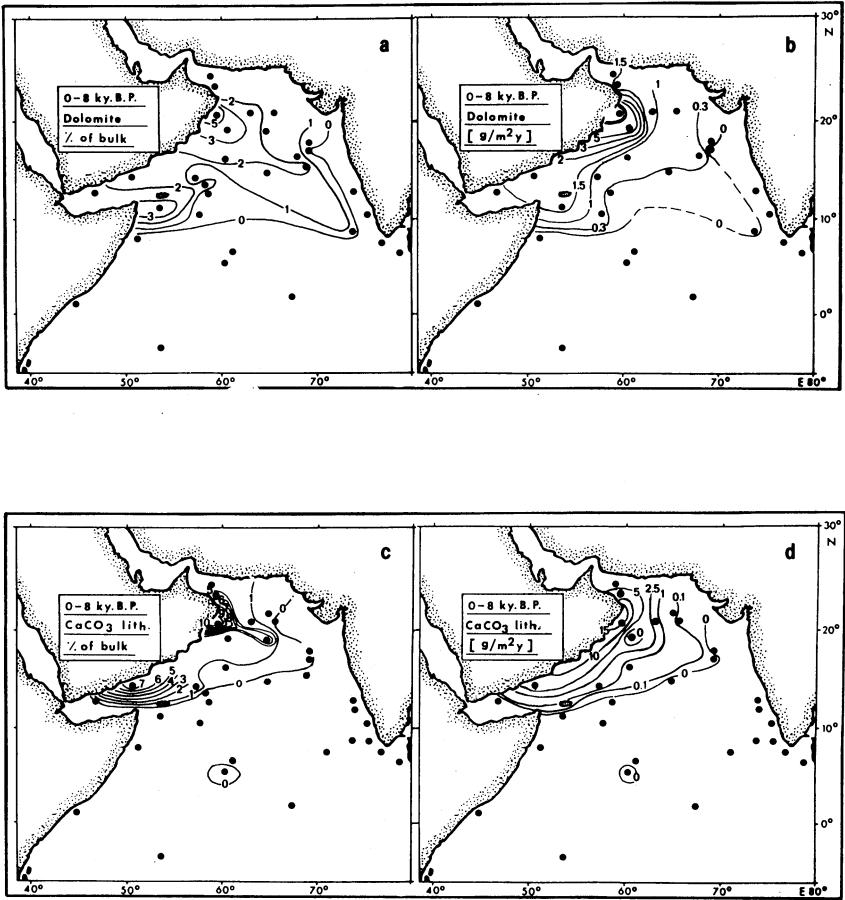
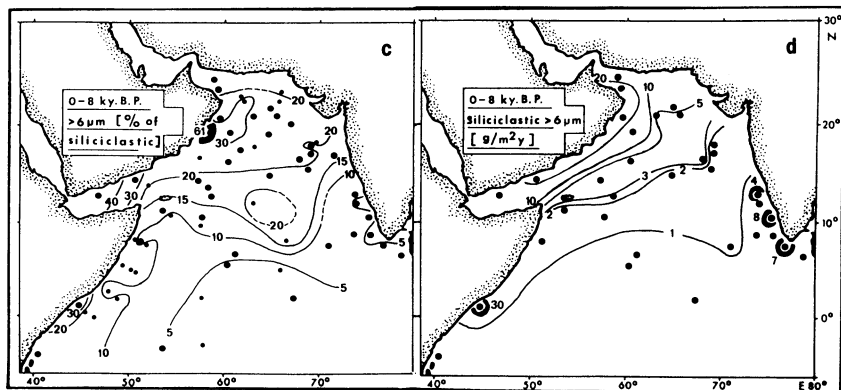
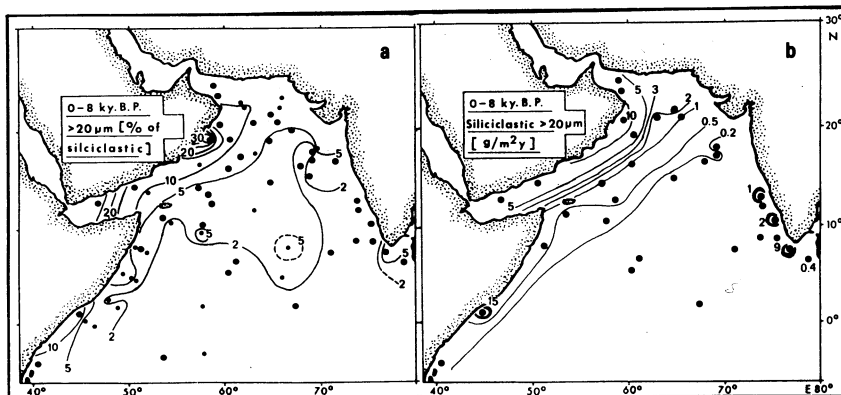


Fig.6. Percentages and accumulation rates of lithogenic carbonates in the bulk fraction. (a, b) Dolomite; (c, d) detritic CaCO<sub>3</sub>.





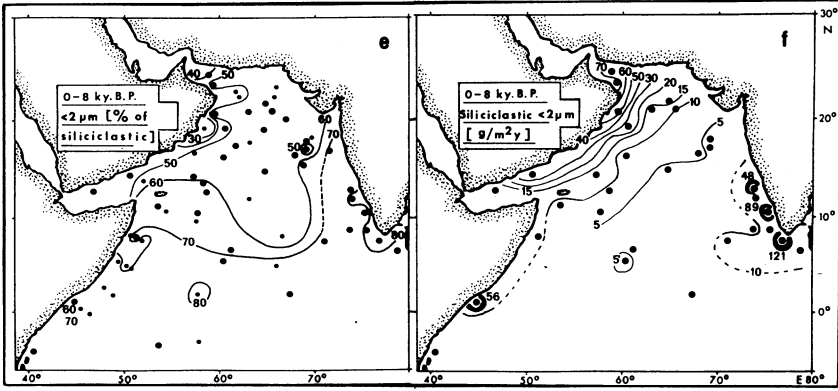


Fig.7. Percentages and accumulation rates of siliciclastic grain size fractions (annual average during the last 8000 years). (a, b) > 20 m, (c, d) > 6 m, (e, f) < 2 m. Large dots are Holocene average values, small dots are true surface samples, tentative isolines are hatched.

The maximum accumulation rates of the various clay sized components (Figures 8a-1) lie either in the Gulf of Oman or in the Gulf of Aden and hence, may indicate different continental source areas. For example, the maximum accumulation rates of chlorite in the Gulf of Oman are ten times, those of quartz and illite three times higher than those in the Gulf of Aden. Contrarywise, accumulation rates of palygorskite in the Gulf of Aden exceed those in the Gulf of Oman by a factor of two, whereas kaolinite and smectite is equally abundant in both regions. Likewise, the maximum accumulation rate of bulk clay < 2  $\mu\text{m}$ , quartz, detritic carbonate and dolomite are characteristic of the sediments in both the Gulf of Oman and Gulf of Aden.

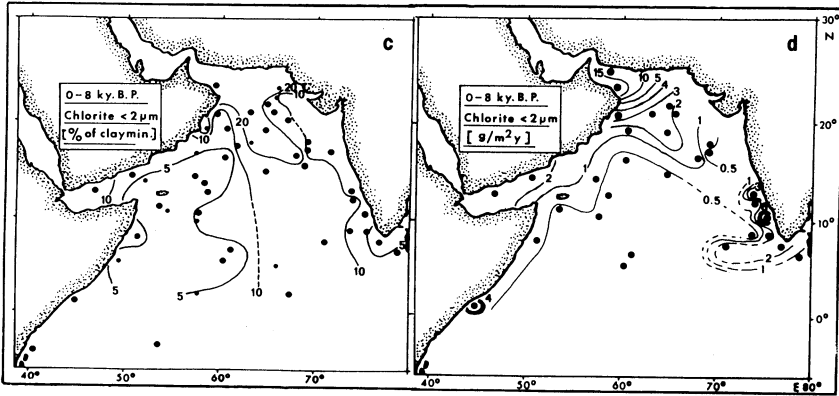
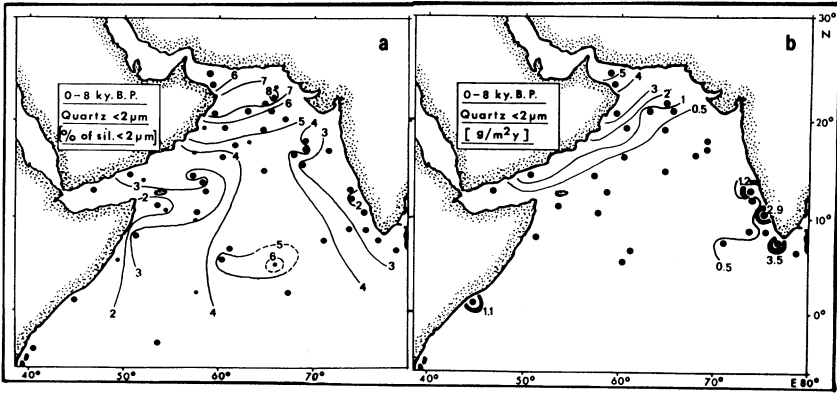
In summary, we can distinguish two major source regions for terrigenous sediment in the Arabian Sea and in addition, a number of local sources. Based on accumulation rates, the Gulf of Oman appears as deposition center of the large sediment lobe extending to the latitude of Bombay. Nevertheless, the high rates of clay deposition in the outer part of the Gulf are linked in part to near-shore local distribution patterns such as the sediment supplied by the Persian Gulf outflow water (Hartmann et al., 1971, Ziegenbein, 1966) or by rivers from Makran (Sarnthein, 1971) and Oman. The Gulf of Aden forms the second center of long-range sediment supply. A mixture of sediments from both source areas covers the central Arabian Sea. Offshore from India and south of Bombay, the distribution of lithogenic sediments is characterized by the small scale, lobate and patchy patterns, which lie on the continental rise and are typical for proximal river- and shelf-borne and redeposited material (von Stackelberg, 1972, Koopmann, 1981).

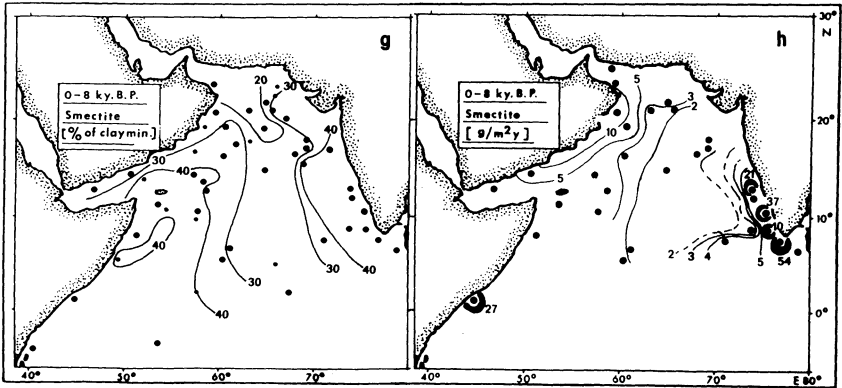
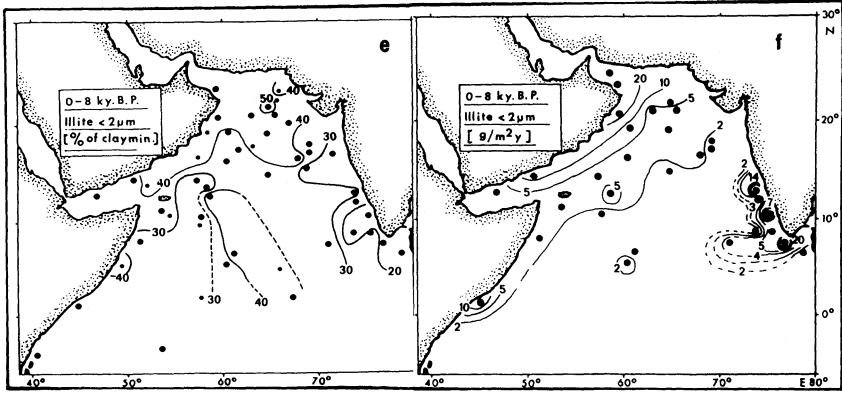
#### 6. THE INTERPRETATION OF THE SEDIMENT DISTRIBUTION PATTERNS

Dust carrying wind is the prime candidate for long-range sediment transport, especially off large deserts such as the Great Arabian Sand Sea and the deserts of Iran, Afghanistan, and Northwest India.

The extreme near-shore maxima of accumulation rates in cores off Makran, east Oman, and Hadramaut ( Figures 4-7), however, are indicative of riverine deposits that are supplied from nearby wadis and washed downslope. In general, non-turbiditic fluvial sediments can be expected to spread up to 200 km offshore in the nepheloid layer ( e.g., Koopmann, 1981). A grain-size test (Figure 9), i.e., a comparison of carbonate-free silt modal grain sizes with the percentage of carbonate-free fraction > 6 $\mu\text{m}$  (sensu Koopmann, 1981, Stein, 1984) has shown that most Holocene samples of the cores immediately offshore from Oman (marked by quadratic signs in Figure 5a ) probably contain river supplied lithogenic sediment fraction, except for the most modern surface sediments (Sirocko, 1989).

Indus sediments do not appear in our sediment distribution patterns for various reasons. Most riverine sediments are deposited on the continental shelf or are transported through turbidite channels to the deep sea (Bouma et al., 1985). Kolla & Coumes (1984) showed that the top 10 m sediment of the Indus sediment fan largely consist of turbidites (Figure 5b). In its center turbiditic sands and silts form up to more than 60 % of the total sediment thickness. These deposits were carefully bypassed by our sample selection. The hemipelagic chlorite depleted sediments outside the immediate turbidite channel system along the Indian continental margin (Figure 8e) do not show a composition that is





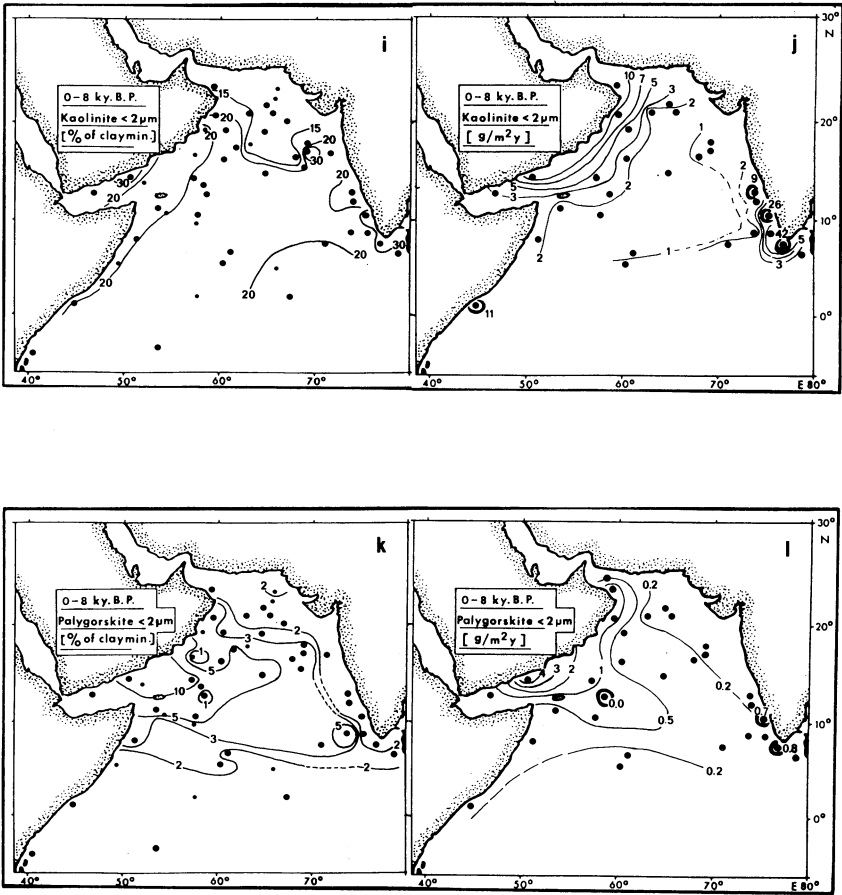


Fig.8. Percentages and accumulation rates of minerals in the fraction < 2 μm (annual average during the last 8000 years). (a, b) quartz, (c, d) chlorite, (e, f) illite, (g, h) smectite, (i, j) kaolinite, (k, l) palygorskite. Further explanations see Figure 4.

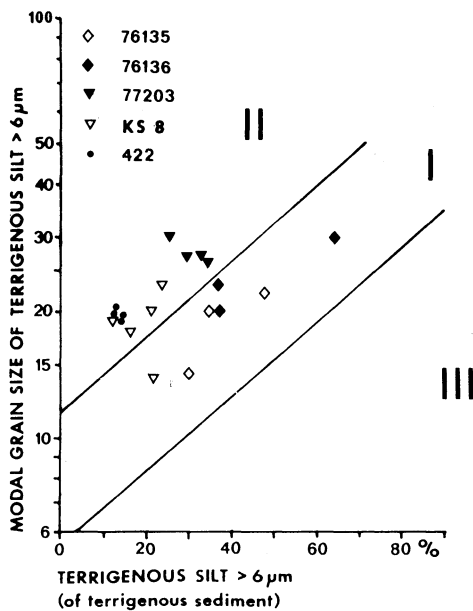


Fig.9. Proportions of the siliciclastic silt fraction > 6 m vs. modal grain size of siliciclastic silt: sample group I. well-sorted grain sizes characteristic of eolian dust; II. sample group with a relative excess of clay (river-borne); sample group III: relative deficit of clay indicating sediment winnowing on sea floor.

characteristic of deposits supplied by the Indus river, which are defined by abundant chlorite (Guptha & Hashimi, 1985). Instead dolomite and lithogenic carbonates, characteristic of Persian Gulf dust, are abundant in front of the Indus delta. Thus we regard the lithogenic fraction as largely wind-borne also in hemipelagic sediments from the northeastern Arabian Sea.

The southeastern margin of the high concentrations and accumulation rates of wind-borne sediments about 500-800 km off south Arabia (most visible in Figure 6b) parallels the average July position of the Somali low level jet (Figures 2, 3) (Findlater, 1969) which forms the core of the southwest monsoon. Hence the outer margin of the sediment gradient, for example the 20 % isoline of the grain-size fraction  $> 6 \mu\text{m}$  (Figure 4c) may serve as record of the long-term average position of this low-level jet.

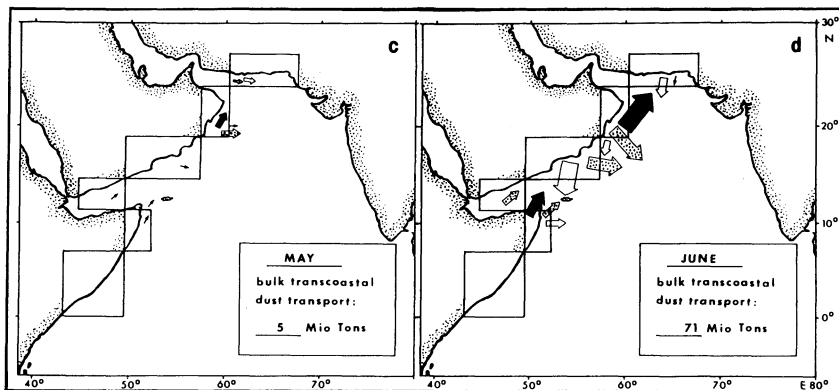
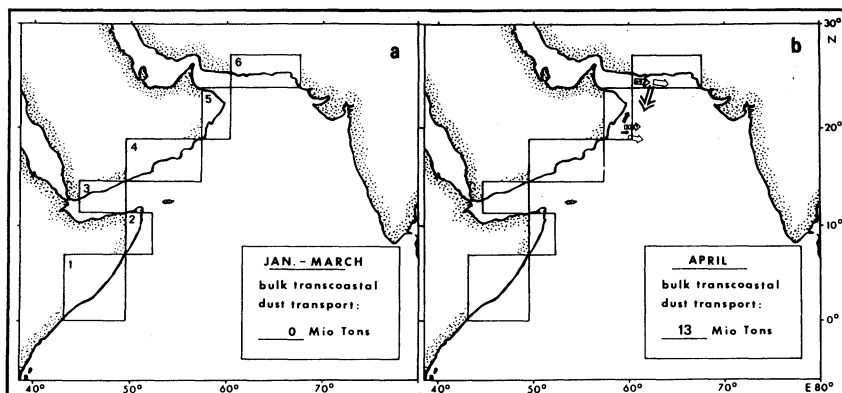
Unexpectedly, the transport directions of the eolian sediment towards the southeast and south do not match the pattern of the prevailing southwest monsoon surface winds during summer. Hence, the vigour of monsoon winds cannot be inferred from the grain-size composition of dust deposits. The bulk of the dust must be related to a different wind system, most likely to the persistent northwesterly winds from Arabia (Goldberg & Griffin, 1969, Kolla et al., 1976, 1981) and the Persian Gulf, the Shamal. In addition mega-scale dust outbreaks from the Arabian desert have been reported from the evaluation of satellite imagery and from aerosol measurements with an aircraft (Foda et al. 1985, Chen, 1986, Ackerman & Cox, 1988). These events may greatly enforce the general dust transport from the northwest.

## 7. METHODS OF AEROSOL QUANTIFICATION

Based on GOES satellite visible images, Chen (1986) mapped the atmospheric turbidity of a severe dust outbreak from Arabia in June 1979. She calibrated the GOES data for Norton's et al. (1980) turbidity model, which was originally designed for the SMS1 satellite and for Saharan dust. Furthermore, she verified the model by means of grain-size distributions of Arabian dust (Tomasi & Prodi, 1982). Dusts from both the Sahara and Arabia were similar in their grain-size distributions and optical properties. Accordingly, methods of image processing developed for Saharan dust can be also applied to Arabian dust.

In extension of the work of Chen (1986) one of us (FS) has determined the variations in aerosol turbidity over the ocean along the Arabian Sea coast from Somalia to India (Figures 10 a-h) during the year 1979. During this year, the GOES satellite was located over the Indian Ocean in support of the summer MONEX. By means of Norton's et al. (1980) turbidity model (implemented at the McIDAS image processing system of the University of Wisconsin-Madison) the aerosol turbidity was studied at 1130 GMT every 5th, 10th, 15th, 20th, 25th and 30th day of each summer month (April - September) and on the 15th of each winter month. The days in between were surveyed on hardcopies of the images. The spatial scale of the measurements were 16 pixel. In all sectors (Figure 10 a) 1 to 3 turbidity values were measured during the outlined key dates. The sample positions were chosen to be representative of the cloud-free marine atmosphere. Arrows in each sector of Figures 10 a-h represent a monthly mean for the different air layers and are based on





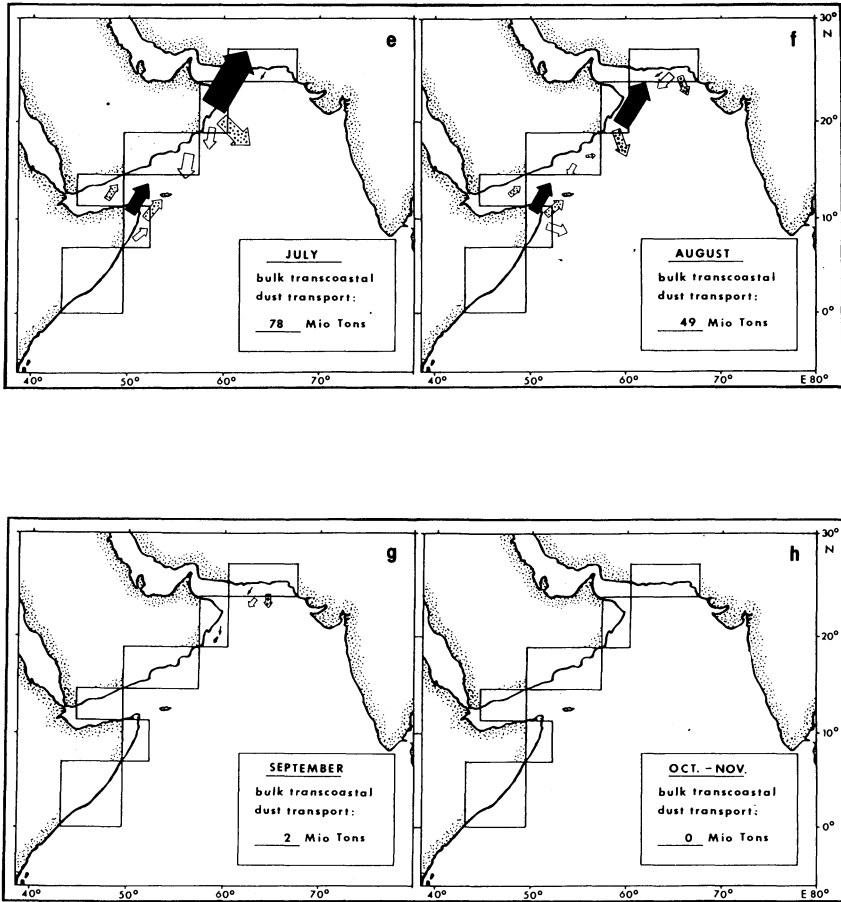
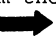
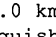
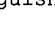



Fig.10. Monthly transcoastal dust discharge during 1979 (a-h) for six coastal image sectors (given in a) and four air layers. Size of arrows represent amount of monthly mean dust mass (Table 5) discharged from the respective sector in the air layers 0.0-1.0 km , 1.0-2.0 km , 2.0-4.5 km , 4.5-7.0 km . For minimum transport air layers are not distinguished.

the following derivations.

The Volz aerosol turbidity ( $\tau_v$ ), i.e. the measuring output of the McIDAS image processing system, was converted to optical aerosol depth (  $\tau$  ) by equation (6) (Chen, 1986):

$$\tau = \tau_v * 2.303 \quad (6)$$

With the conversion formula (equation 7) of Carlson & Caverly (1977):

$$M = 3.75 * \tau \quad (7)$$

we obtained from the optical aerosol depth the mass loading (M) of a dust column of 5000 m height, which is the average thickness of the Arabian dust layer in summer (Ackerman & Cox, 1982).

It was impossible to map these dust loadings across the whole Arabian Sea, because only a narrow band extending 300-500 km offshore from Arabia was cloud free during summer.

To calculate the transcoastal dust discharge in a given sector, air-layer and month ( $T_{mjk}$ ) we used the near-shore mass loading of the dust column (M) (determined by McIDAS), its vertical concentration profile (A) (Ackerman & Cox, 1982) and the mean monthly wind speeds (U) and -directions (L) of the air levels (k) at 1000 mb, 850 mb, 700 mb, 500 mb (Ramage et al. 1972 a, b). The annual trans-coastal dust transport (TA) into the Arabian Sea was then calculated by the sum of the air layers, the sectors and months (equation 8):

$$TA = \sum_{m=1}^{11} \sum_{j=1}^6 \sum_{k=1}^4 T_{mjk} \quad (8a)$$

$$T_{mjk} = (U_{mjk} * 2592000 * L_{mjk}) * ((M_{mj}/100) * A) * 10^9 \quad (8b) \quad [ 10^6 t \ y^{-1} ]$$

where

m = months of 1979, January to November

j = sectors of the coastline

k = air layers

U = monthly mean of windspeed in respective air level [ m/s ]

2592000 = seconds per month

L = length of coastline in a sector which is perpendicular to wind direction [ km ]

M = monthly mean of mass loading of a dust column calculated from eq.(7) [ g/m<sup>2</sup> ]

A = dust concentration in distinct air layers k [ % ]

0.0-1.0 km, 56% ( 1000 mb)

1.0-2.0 km, 23% ( 850 mb)

2.0-4.5 km, 19 % ( 700 mb)

4.5-7.0 km, 2 % ( 500 mb)

Some variables used in equation (8) are little substantiated by observations. We were unable to specify the precise error range of the aerosol data due to their complexity. Instead we list in Table 2 a number of possible errors for each variable contained in equation (6, 7, 8).

Finally, our calculations are based on the assumption that all dust particles crossing the south Arabian, Makran and Somali shorelines are

deposited in the ocean. As shown in Figure 3, most dust particles will be trapped indeed and rained out during summer by the high convective band of clouds over the eastern Arabian Sea and especially along the Indian margin. However, during outbreak conditions minor portions finally penetrate the Indian subcontinent (Martin, pers. comm.). Arabian dust, crossing the Gulf of Aden and again entering East Africa near the Horn of Africa in the mid-troposphere forms the only exception from this rule (to be considered with the data from sector 2).

#### 8. THE SATELLITE RECORD OF DUST DISPERSAL

Figures 10 a-h and Table 4, 5 present the monthly rates of trans-coastal dust discharge during 1979. From January to March (Figure 10a) there is no offshore turbidity along the coast from Somali to India. During April (Figure 10b) dust is visible off Oman and Makran. Generally low turbidity values ( $\tau_v = 0.1-0.2$ ) and alongshore winds off Makran limit the monthly dust discharge to about  $13 \cdot 10^6 \text{ t y}^{-1}$ , including an ephemeral dust outbreak on 30 April from the Makran coast towards the south and southeast. Averaging the mean turbidity ( $\tau_v \geq 3.0$ ) over the outer Gulf of Oman this ephemeral dust outbreak amounts to  $3-4 \cdot 10^6 \text{ t y}^{-1}$ . The outbreak was released by unusual winds from the northeast. It possibly originated from the inner Iranian and Northern Indian squall lines during spring ( Middleton, 1986, Bryson & Baerreis, 1967 ). For the rest of the year the visible dispersal of dust followed the monthly means of winds, which were fairly persistent during summer (Ramage et al, 1972a, b).

During June (Figure 10d) the bulk trans-coastal dust transport to the Arabian Sea increased dramatically to an apparent figure of  $71 \cdot 10^6 \text{ t y}^{-1}$ . Most of this dust was raised in the lowlands of Mesopotamia, from Syria to Iran during a severe dust storm that passed the south Arabian coast in two pulses from 22-27 June (Chen 1986, Ackerman & Cox, 1988). The dust plumes spread across Arabia and separated as they rose over the southwest monsoon into a northeastern branch following the topographic contours to Oman and a southern branch in the midtroposphere that reached the Gulf of Aden.

During July (Figure 10e), the dust transport continued to be high over the northwestern Arabian Sea. From Oman it spread to the northeast in the surface layer and to the southeast higher up. The extremely high near-surface transport from northeast Oman towards northeast was linked to monsoonal trajectories. The dust load, however, was laterally advected by Shamal winds from Iraq passing south of the Oman mountains to the Arabian Sea. From August (Figure 10f) to September (Figure 10g) turbidity values and wind speeds gradually fell resulting in a reduced discharge of dust. During fall 1979 (Figure 10h) turbidity values again were zero and wind velocities of the northeast monsoon season were low.

#### 9. MASS BALANCE OF THE SEDIMENTARY AND SATELLITE RECORD

Based on the areal integration of bulk lithogenic sediment accumulation rates (Figure 5a), Table 3 shows that the total non-turbiditic sediment supply from East Africa, Arabia, and India to the Arabian Sea below 1000 m water depth amounted to an annual average of about  $140 \cdot 10^6 \text{ t y}^{-1}$  during the last 8000 years.

Out of this sum, about  $30 \cdot 10^6 \text{ t y}^{-1}$  are found east of  $70^\circ \text{E}$  within

small-scale patchy sediment lobes off South India that are largely ascribed to Indian river supply. Von Stackelberg (1972) shows that fluvial sediments led to an, at least, similar order deposited on the Indian shelf and upper slope. Thus, the total non-turbiditic riverine sediments off south India may approach 30-60  $\times 10^6\text{t y}^{-1}$ . We are aware of the fact that further north the Indus river supplies an additional sediment load (150-400  $\times 10^6\text{t y}^{-1}$ , Milliman & Meade, 1983) which largely exceeds our outlined cumulative value. However, the bulk of the Indus discharge is deposited on the shelf and in turbidites of the Indus fan (Figure 5b), both settings which we bypassed with our sampling grid.

West of 70°E, the total non-turbiditic lithogenic sediment deposition below 1000 m water depth amounts to an annual average of 107  $\times 10^6\text{t y}^{-1}$  (Table 3). As outlined in the Sediment Record Section, the spatial distribution pattern of lithogenic sediment accumulation (Figs. 6-8) suggest that most of this sum can be related to the supply of the Arabian northwesterly winds. Offshore Oman, however, about 20  $\times 10^6\text{t y}^{-1}$  lithogenic sediments were deposited (Tab. 3), considerable proportions of which originate from local fluvial discharge and Persian Gulf outflow (Figure 9). Thus the bulk annual eolian accumulation rate can be approximated to about 100  $\times 10^6\text{t y}^{-1}$  of dust during the last 8000 years.

Since the climate of Arabia and India was subject to severe deterioration during the last 6000 years ( McClure, 1976, al Sayari & Zötl, 1978, Singh et al., 1972, Sirocko, 1989) we surmise that the actual modern annual average of dust supply may be substantially higher than the annual average of the humid middle Holocene.

Table 4 and 5 present the satellite record of transcoastal dust transport. Accordingly the bulk dust discharge amounts to 215  $\times 10^6\text{t y}^{-1}$ , most of which (100  $\times 10^6\text{t y}^{-1}$ ) is transported in the surface layer, 65  $\times 10^6\text{t y}^{-1}$  in the air layer 1-2 km, 50  $\times 10^6\text{t y}^{-1}$  between 2 and 4.5 km, while the transport at 4.5 -7 km can be neglected in all 6 sectors.

The near surface dust estimates for image Sectors 2 (Horn of Africa) and 5 (offshore Oman), which amount to about 20 and 80  $\times 10^6\text{t y}^{-1}$  respectively (Table 4), are regarded as a crude estimate. From June to August, when most dust is supplied in the Sectors 2 and 5, the southwest monsoon migrates across the shoreline (Figure 2) into these sectors and therefore only little dust is laterally supplied across the monsoonal inversion to the Arabian Sea in the air layer up to 1 km above the surface. Accordingly, the general vertical profiles of dust concentrations underlying equation (8) are no more valid for the surface layer during summer. If we assume a total cut off effect of dust in the sectors 2 and 5 we must reduce the trans-coastal dust transport to about 115  $\times 10^6\text{t y}^{-1}$  during 1979. Thus, the actual amount of discharged dust to the Arabian Sea in 1979 was a value between 115 and 215  $\times 10^6\text{t y}^{-1}$ .

At least by the order of magnitude, this dust flux in 1979 closely compares with the average eolian sediment accumulation during the Holocene. Additionally, the distribution patterns of dust dispersal e.g. the gradient offshore from Arabia match in both the sedimentary and the satellite records.

## 10. CONCLUSIONS

The recent and modern patterns of eolomarine sediment dispersal in the Arabian Sea were obtained from studying both deep sea sediment cores and

satellite images. The eolian flux dominates lithogenic sedimentation in areas of hemipelagic, non-turbiditic deposition in the Arabian Sea. Both the sediment and satellite records indicate that the main source regions lie in Arabia and Mesopotamia and that northwesterly winds dominate the dust trajectories. Ephemeral massive dust outbreaks originating from Mesopotamia follow and reinforce the general dispersal pattern. The amount of aerosol discharge in 1979 ( $115-215 \cdot 10^6 \text{t y}^{-1}$ ) nearly equals the average late Holocene eolian sediment flux observed in deep sea cores (about  $100 \cdot 10^6 \text{t y}^{-1}$ ).

Based on mineralogy, grain sizes, and stable isotopes several sedimentary provinces can be distinguished in the Arabian Sea; these reflect different source regions and pathways of terrigenous sediment input apart from turbidite deposition.

i) Dust that originates in the Arabian northwesterly winds crossing Oman during summer dominates the northern sector of the Arabian Sea up to  $17^\circ\text{N}$ ,  $70^\circ\text{E}$ . Its mineral composition consists of coarse grained siliciclastics with abundant chlorite, dolomite and lithogenic carbonate.

ii) The Holocene sediments in the Gulf of Oman and adjacent to the southern coast of Oman receive clay rich terrigenous matter largely from the Persian Gulf outflow water and rivers from Makran and Oman.

iii) The dust offshore Hadramaut and in the Gulf of Aden is marked by abundant palygorskite and smectite. It is supplied by the southwestern branch of the Arabian northwesterlies and originates in central Arabia and hence cannot serve as marker of monsoon intensity.

iv) The southern margin of the steep gradient in lithogenic sediment distribution patterns off south Arabia, for example the 20 % isoline of the grain-size fraction  $> 6 \mu\text{m}$  (Fig. 4c) appears to document the northernmost position of the Somali Jet, which forms the core of the southwest monsoon.

v) Riverborne suspensions from south Indian rivers form patchy sediment lobes along the Indian continental margin. Indus-borne massive turbiditic sediments were bypassed in this study.

#### ACKNOWLEDGEMENTS

We thank Jean Claude Duplessy / Paris, Venu Ittekkot / Hamburg, Ulrich von Stackelberg / Hannover, Peter Stoffers / Kiel, Jean Moyes / Bordeaux and the curatorial services of Lamont-Doherty Geological observatory / New York for generous support with the acquisition of core samples. During the visit of one of us (F.S.) at the Meteorological Department of Colorado State University / Fort Collins and the University of Wisconsin-Madison, David Martin, Steven Ackerman, Felicia Chen, and David Santek gave encouraging support and practical advice for the satellite-image study.

Richard Arimoto, Jean Claude Duplessy, Francis Grousset, David Martin, John Merrill and Gerd Tetzlaff reviewed the manuscript and helped to improve the final version of the paper with their critical and constructive comments.

We gratefully acknowledge the support of Heinz Lange / Kiel in supervising the clay mineral analyses, Ute Doering and Hartmut Schulz for technical assistance.

This research was generously funded by the German National Program of Climatic Research ( Bundesministerium für Forschung und Technik,

grant no. 07KF2045).

REFERENCES:

- ACKERMAN, S.A. & COX, S.K. (1982): The Saudi Arabian heat low: Aerosol distribution and thermodynamic structure. - *Journal of Geophysical Res.*, Vol.87, No. C 11, pp.8991-9002.
- ACKERMANN, S.A. & COX, S.K. (1988): Dust outbreaks associated with the southwest monsoon region. - In press, *Meteorology and Atmospheric Physics*.
- AL SAYARI, S. S. & ZOETL, J. G. (1978): *Quaternary period in Saudi Arabia*. - Springer Verlag, Wien, New York
- BARD, E., ARNOLD, M., DUPRAT, J., MOYES, J. & DUPLESSY, J.C. (1987): Reconstruction of the last deglaciation: deconvolved records of  $\delta^{18}O$  profiles, micropaleontological variations and accelerator mass spectrometric  $^{14}C$  dating. - *Climate Dynamics*, Vol.1, pp.101-112.
- BISCAYE, P.E. (1965): Mineralogy and sedimentation of recent deep sea clay in the Atlantic Ocean and adjacent seas and oceans. - *Geol. Soc. Amer. Bull.*, Vol.76, pp.803-832.
- BOHRMANN, G. (1988): Zur Sedimentationsgeschichte von biogenem Opal im noerdlichen Nordatlantik und dem Europaeischen Nordmeer (DSDP/ODP-Bohrungen 408, 642, 643, 644, 646 und 637). - *Ber. Sonderforschungsbereich 313, Univ. Kiel, 9*, 150 S.
- BOUMA, A.H., NORMARK, W.R. & BARNES, N.E. (1984): *Submarine fans and related turbidite systems*. - Springer Verlag.
- BROECKER, W.S. & VAN DONK, J. (1970): Insolation changes, ice volumes and the  $\delta^{18}O$  record in deep-sea sediments. - *Rev. Geoph. Space Phys.*, 8, pp.169-191.
- BROECKER, W. S., ANDREE, M., WOLFLI, W., OESCHGER, H., BONANI, G., KENNETT, J. & PETEET, D. (1988): The chronology of the last deglaciation: Implications to the cause of the younger Dryas event. - *Paleoceanography*, Vol. 3, No. 1, pp. 1-19.
- BRYSON, R.A. & CAMPBELL, W.H. (1982): Year-in advance forecasting of the Indian monsoon rainfall. - *Environmental Conservation*, Vol.9, No.1, pp.51-56
- BRYSON, R.A. & BAERREIS, D.A. (1967): Possibilities of major climatic modification and their implications: Northwest India, a case for study. - *Bull. Amer. Met. Soc.*, Vol.48, No.3, pp.136-142.
- CARLSON, T.N. & CAVERLY, R.S. (1977): Radiative characteristics of Saharan dust at solar wavelengths. - *Journal of Geophysical Res.*, Vol.82, No.21, pp.3141-3152
- CHEN, F.H. (1986): Analyses of a major dust outbreak over the Arabian Sea during Monex. - *Thesis at the University of Wisconsin - Madison*.
- DEGENS, E, & HUNT, J.M. (unpubl.): Data on the distribution of stable isotopes and amino acids in Indian Ocean sediments. - *Woods Hole Oceanographic Institution*, Reference No.68-4.
- DEGENS, E.T. & EPSTEIN, S. (1962): Relationship between  $O_{18}/O_{16}$  ratios in coexisting carbonates, cherts and diatomites. - *Amer. Assoc. Petr. Geol. Bull.*, Vol.46, pp.534-542.
- DUPLESSY, J.C. (1978): Isotope studies. - In: Gribbin, J.

- (ed.), *Climatic Change* (Cambridge University Press): pp.46-67.
- DUPLESSY, J.C. (1982): Glacial to interglacial contrasts in the northern Indian Ocean. - *Nature*, Vol.295, pp.494-498.
- DUPLESSY, J.C., BLANC, P.L. & BE, A.W.H. (1981): Oxygene-18 enrichment of planktonic foraminifera due to gametogenic calcification below the euphotic zone. - *Science*, Vol.213, pp.1247-1249.
- FINDLATER, J. (1969): A major low level air current near the Indian Ocean during the northern summer. - *Quart.J.R.Met.Soc.*, 95, pp.362-380.
- FODA, M.A., KHALAF, F.I. & KADI-AL, A.S. (1985): Estimation of dust fallout rates in the northern Arabian Gulf. - *Sedimentology*, 32, pp.595-603
- FONTUGNE, M.R. & DUPLESSY, J.C. (1986): Variations of the monsoon regime during the upper quaternary: Evidence from carbon isotopic record of organic matter in North Indian Ocean sediment cores. - *Palaeogeography, -climatology, -ecology*, 56, pp.69-88.
- GOLDBERG, E.D. & GRIFFIN, J.J. (1969): The sediments of the northern Indian Ocean. - *Deep-Sea Res.*, Vol.17, pp.513-537.
- GUPTHA, M. V. S. & HASHIMI, N. H. (1985): Fluctuations in glacial and interglacial sediment discharge of the river Indus as seen in a core from the Arabian Sea. - *Ind. Journal of Marine Sciences*, Vol.14, pp.66-70
- HARTMANN, M., LANGE, H., SEIBOLD, E. & WALGER, E. (1971): Oberflaechensedimente im Persischen Golf und Golf von Oman. - *Meteor Forsch. Erg.*, Reihe C, No.4, pp.1-76
- KOLLA, V. & COUMES, F. (1984): Indus Fan, Indian Ocean. - In: BOUMA, A.H., NORMARK, W.R. & BARNES, N.E., *Submarine fans and related turbidite systems*. Springer Verlag.
- KOLLA, V. & BISCAYE, P. E. (1977): Distribution and origin of quartz in the sediments of the Indian Ocean. - *Journal. of Sed. Pet.*, Vol.47, No.2, pp.642-649.
- KOLLA, V., KOSTECKI, J.A., ROBINSON, F. & BISCAYE, P.E. & RAY, P.K. (1981): Distribution and origin of clay minerals and quartz in surface sediments of the Arabian Sea. - *Journal of Sed.Pet.*, Vol.51, No.2, pp.0563-0569.
- KOLLA, V., HENDERSON, L. & BISCAYE, P. (1976): Clay mineralogy and sedimentation in the western Indian Ocean. - *Deep-Sea Res.*, Vol.23, pp.949-961.
- KOLLA, V., RAY, P.K. & KOSTECKI, J.A. (1981): Surficial sediments of the Arabian Sea. - *Marine Geology*, Vol.41, pp.183-204.
- KOOPMANN, B. (1981): Sedimentation von Saharastaub im subtropischen Nordatlantik waehrend der letzten 25,000 Jahre. - *'Meteor' Forsch. Ergebn.*, C, Vol. 35, pp.23-59.
- KRISHNAMURTI, T.N., GREIMAN, P., RAMANATHAN, Y., PASCH, R., ARDANY, P. (1980): *Quick look summer monex atlas*, Part 1,2,3, - FSU Report, No.80-4
- KUTZBACH, J.E. (1981): Monsoon climate of the early holocene: Climate experiment with the earth's orbital parameters for 9000 years ago. - *Science*, Vol. 214, pp.59-61.
- KUTZBACH, J.E. & GUETTER, P.J. (1986): The influence of changing



- orbital parameters and surface boundary conditions on climate simulation for the past 18000 years. - *Journal of the atmospheric science*, Vol. 39, No. 6, pp. 1177-1187.
- MARCHIG, V. (1974): Zur Geochemie rezenter Sedimente des Indischen Ozeans II, Arabisches Meer, afrikanischer Kontinentalrand und Vergleich mit dem indisch-pakistanischen Kontinentalrand. - *Meteor Forsch. Erg.*, Reihe C, No.18, pp.1-34.
- MATTIAT, B., PETERS, J. & ECKHARDT, F.J. (1973): Ergebnisse petrographischer Untersuchungen an Sedimenten des indisch-pakistanischen Kontinentalrandes (Arabische See). - *Meteor Forsch. Erg.*, Reihe C, No.14, pp.1-50.
- McCLURE, H. A. (1976): Radiocarbon chronology of late Quaternary lakes in the Arabian Desert. - *Nature*, Vol. 263, pp. 755-756.
- McDONALD, W.F. (1938): *Atlas of climatic charts of the ocean*. - U.S. Dept. Agr. Weather Bur., No. 1, 247, charts 59-62.
- MIDDLETON, N.J. (1986): A geography of dust storms in Southwest Asia. - *Journal of Climatology*, Vol. 6, pp. 183-196.
- MILLIMAN, J.D. & MEADE, R.H. (1983): World-wide delivery of river sediment to the oceans. - *Journal of Geology*, 91, pp.1-21.
- MOYES, J., DUPRAT, J., FAUGERES, J.-C., GONTHIER, E. & PUJOL, C. (1978): Etudes stratigraphique et sedimentologique. - In: *Orgon 4: Golf dden, Mer dman*
- NAINI, B.R. & KOLLA, V. (1982): Acoustic character and thickness of sediments of the Indus fan and the continental margin of western India. - *Marine Geology*, Vol.47, pp.180-195.
- NARAYANAN, M.S. & RAO, B.M. (1981): Detection of monsoon inversion by Tiros-N satellite. - *Nature*, Vol.294, pp.546-548
- NORTON, C.C., MOSHER, F.R., HINTON, B., MARTIN, D.W., SANTEK, D. & KUHLOW, W. (1980): A model for calculating desert aerosol turbidity over the oceans from geostationary satellite data. - *Journal of Applied Meteorology*, Vol.19, No.6, pp.633-644
- OLAUSSON, E. & OLSSON, I.U. (1968): Varve stratigraphy in a core from the Gulf of Aden. - *Palaeogeography, -climatology, -ecology*, Vol.6, pp.87-103.
- PANT, M.C. (1978): Vertical structure of the planetary boundary layer in the West Indian Ocean during the Indian summer monsoon as revealed by ISMEX data. - *Indian J. Met. Hydrol. Geophys.*, 29, 1 & 2, pp.88-98
- PRELL, W. L., CURRY, W. B. (1981): Faunal and isotopic indices of monsoonal upwelling: western Arabian Sea. - *Oceanologica Acta*, Vol.4, No.1, pp.91-98
- PRELL, W., HUTSON, W.H. (1979): Zonal temperature-anomaly maps of Indian Ocean surface waters: Modern and ice-age patterns. - *Science*, Vol.206, pp.454-456.
- PRELL, W., HUTSON, W.H., WILLIAMS, D.F., BE, A.W., GEITZRENAUER, K., and MOLFINO, B. (1980): Surface circulation of the Indian Ocean during the last glacial maximum, approximately 18,000 yr B.P.. - *Quaternary Res.*, Vol.14, pp.309-336.
- PRELL, W.L. & KUTZBACH, J.E. (1987): Monsoon variability over

- the past 150000 years. *J. Geophysical Res.*, 92, pp. 8411-8425
- PRELL, W.L. & VAN CAMPO, E. (1986): Coherent response of Arabian Sea upwelling and pollen transport to late Quaternary monsoonal winds. - *Nature*, 323, pp.526-528.
- PRELL, W.L. (1984): Variation of Monsoonal Upwelling: A response to changing solar radiation. - In: *Climate Processes and Climate Sensivity, Geophysical Monograph 29, Maurice Ewing Volume 5*
- PRELL, W.L. (1984): Monsoonal climate of the Arabian Sea during the late quaternary: A response to changing solar radiation .  
In: *Milankovitch and climate*, edited by: Berger, W. & Imbrie, J., Part 1, pp.349-366.
- RAMAGE, C.S. (1969): Indian Ocean surface meteorology. - *Oceanogr. Mar. Biol. Ann. Rev.*, 7, pp.11-30
- RAMAGE, C.S., MILLER, F.R. & JEFFERIES, C. (1972): *Meteorological atlas of the international Indian Ocean expedition*. - By: U.S. National Science Foundation and India Meteorological Department.
- RAMAGE, C. S. & RAMAN, C. V. R. (1972): *Meteorological atlas of the international Indian Ocean expedition*. - By: U.S. National Science Foundation and India Meteorological Department.
- RENARD, M. (1986): Pelagic Carbonate Chemostratigraphy (Sr, Mg, <sup>18</sup>O, <sup>13</sup>C). *Marine Micropaleontology*, 10, pp. 117-164.
- SARNTHEIN, M. (1971): Oberflaechensedimente im Persischen Golf und Golf von Oman. II. Quantitative Komponentenanalyse der Grobfraktion. - *'Meteor' Forsch. Erg.*, C, No. 5, pp.1-113.
- SHACKLETON, N.J. & OPDYKE, N. (1973): Oxygene isotope and paleomagnetic stratigraphy of equatorial Pacific core V28-238: Oxygene isotope temperatures and ice volume on a 10<sup>5</sup> and 10<sup>6</sup> \* 10<sup>4</sup> year scale. - *Quat. Res.*, 3, pp.39-55.
- SINGH, G., JOSHI, R. D. & SINGH, A. B. (1972): Stratigraphic and radiocarbon evidence for the age and development of three salt lake deposits in Rajasthan, India. - *Quaternary Res.*, Vol.2, pp.496-505.
- SIROCKO, F. (1989): Zur Akkumulation von Staubsedimenten im nördlichen Indischen Ozean: Anzeiger der Klimageschichte Arabiens und Indiens .- *Berichte - Reports, Geol. - Paläont. Inst. Universitaet Kiel*, Nr. 27, 114 S..
- SIROCKO, F. & LANGE, H. (in prep.): Accumulation rates of clay minerals in Arabian Sea sediments
- STEIN, R. (1985): Rapid grain size analyses of clay and silt fraction by Sedigraph 5000 D: comparison with Coulter Counter and Atterberg methods. - *Journal of Sedimentary Petrology*, Vol.55, No.4, pp.590-593.
- STEIN, R. (1984): Zur neogenen Klimaentwicklung in Nordwest-Afrika und Palaeo-Ozeanographie im Nordost-Atlantik: Ergebnisse von DSDP-Sites 141, 366, 397 und 544B. *Berichte-Reports, Geologisch-Palaeontologisches Institut der Universitaet Kiel*, Nr.4, 210 S.
- STEWART, R.A., PILKLEY, O.H. and NELSON, B.W (1965): Sediments of the northern Arabian Sea. - *Marine Geology*, Vol.3, pp.411-427.

- TENNANT, C.B. & BERGER, R.W. (1957): X-ray determination of dolomite - calcite ratio of a carbonate rock. - *Amer. Mineralogist*, 42, pp. 23-29.
- THIEDE, J., SUESS, E. & MUELLER, P. (1982): Late quaternary fluxes of major sediment components to the sea floor at the Northwest African continental slope. - In: von Rad, U., Hinz, K. et al. (eds.), *Geology of the Northwest African continental margin*, Springer Verlag Berlin, pp. 605-631.
- TOMASI, C. & PRODI, F. (1982): Measurements of atmospheric turbidity and vertical mass loading of particulate matter in marine environments. (Red Sea, Indian Ocean and Somalian Coast) - *Journal of Geophysical Res.*, Vol.87, No.C2, pp.1279-1286.
- VAN ANDEL, T.H., HEATH, G.R., & MOORE, T.C. (1975): Cenozoic history and paleoenvironment of the Central Equatorial Pacific Ocean. - *Geol. Soc. Amer.*, Memoir 143.
- VAN CAMPO, E., DUPLESSY, J.C. & ROOSIGNOL-STRICK, M. (1982): Climatic conditions deduced from a 150-kyr oxygen isotope-pollen record from the Arabian Sea. - *Nature*, Vol.296, pp.56-59.
- VAN CAMPO, E. (1986): Monsoon fluctuations in two 20,000-Yr B.P. oxygen-isotope /pollen records off Southwest India. - *Quaternary Res.*, 26, pp.376-388.
- VON STACKELBERG, U. (1972): Faziesverteilung in Sedimenten des indisch-pakistanischen Kontinentalrandes. - *Meteor Forsch. Erg.*, Reihe C, No.9, pp.1-73.
- WESTPHAL, D.L., TOON, O.W. & CARLSON, T.N. (1987): A two-dimensional investigation of the dynamics and microphysics of Saharan dust storms. - *Journal of Geophysical Res.*, Vol.92, NO.D3, pp.3027-3049.
- ZIEGENBEIN, J. (1966): Truebungsmessungen im Persischen Golf und im Golf von Oman - *'Meteor' Forsch. Erg.*, A 1, pp.59-79.

Frank Sirocko, Michael Sarnthein  
 Geologisch Palaeontologisches Institut  
 Universitaet Kiel  
 Olshausenstr. 40-60  
 D 2300 Kiel, Federal Republic of Germany

## AEOLIAN-DERIVED HIGHER PLANT LIPIDS IN THE MARINE SEDIMENTARY RECORD: LINKS WITH PALAEOCLIMATE

J.G.Poynter, P.Farrimond, N.Robinson and G.Eglinton.

Organic Geochemistry Unit, University of Bristol, School of  
Chemistry, Cantock's Close, Bristol BS8 1TS, U.K.

**ABSTRACT.** The abundances and distributions of terrestrial higher plant lipids have been investigated in two cores from the Equatorial North Atlantic. Two distinct populations of *n*-alkanes (C<sub>23</sub>-C<sub>35</sub>) have been recognised, a predominant higher plant distribution and a subordinate distribution of unknown, possibly bacterial, origin. The abundance, flux and distribution of the predominantly higher plant component is shown to be linked to palaeoclimatic change. The utilization of the higher plant *n*-alkane distribution is proposed as a potential palaeoclimatic tool reflecting the temperature and/or the aridity of the continental dust source region. The abundance of presumed higher plant *n*-alkanols has been found to covary with higher plant *n*-alkanes.

### 1. INTRODUCTION

Several series of straight-chain compounds, ranging from C<sub>20</sub> to C<sub>37</sub>, are well known as the major component of epicuticular leaf waxes (e.g. Eglinton and Hamilton, 1967). These include C<sub>20</sub>-C<sub>37</sub> *n*-alkanes with a strong odd/even predominance and C<sub>20</sub>-C<sub>32</sub> fatty acids and *n*-alkanols with a strong even/odd predominance. They have been found in soils (Morrison, 1969), lacustrine sediments (e.g. Cranwell, 1973) and deep and shallow marine sediments (Simoneit, 1976, among many others). The application of these compounds as biological markers is an established method, their distribution being regarded as the signature of the biological system which synthesised them (Eglinton and Calvin, 1967). Their mode of transport through the environment is thought to include fluvial and aeolian mechanisms. They have been found in aeolian dusts, first over the Atlantic near the African margin (Simoneit and Eglinton, 1975), subsequently at Enewetak Atoll in the Pacific (Gagosian *et al.*, 1981) and later at North Island off New Zealand (Gagosian *et al.*, 1987). The observation of aeolian lipids at Enewetak Atoll illustrates the great distances over which these compounds can be transported, *i.e.* 5000km from S.E. Asia and 8000km from the North American continent (Gagosian *et al.*, 1981).

Table I. Results of aeolian dust analyses (taken from various literature sources) showing the latitude dependence of the modal *n*-alkane chain length. The Antarctic sample (marked with an asterisk) is a sediment extract included, in the absence of an aeolian sample, to represent a high latitude sample. Despite the broad latitude dependence, a regional (longitude) dependence is also noted; hence, those from a single longitude (off the west African coast) are underlined.

Latitude (range) of source	Modal <i>n</i> -alkane carbon no.	Sample site (source)	Reference
<u>30-45°N</u>	27	West African Coast (source- N.W. Europe/N.W. Africa)	Simoneit <i>et al.</i> , 1977
≈40°N	29	Enewetak Atoll (source- Chinese dust storms)	Gagosian <i>et al.</i> , 1981,1986
<u>15-25°N</u>	27-29	West African Coast (source- Sahara)	Simoneit <i>et al.</i> , 1977
≈15°N	31	Enewetak Atoll (source- Central America)	Gagosian <i>et al.</i> , 1981,1986
<u>0-20°N</u>	29	West African Coast (source- Sahara/Southern Africa)	Simoneit <i>et al.</i> , 1977
<u>≈15°S</u>	29-31	West African Coast (source- Southern Africa)	Simoneit <i>et al.</i> , 1977
<u>15-30°S</u>	31	West African Coast (source- Southern Africa)	Simoneit <i>et al.</i> , 1977
≈30°S	31	Ninety Mile Beach (source- Southern Australia)	Gagosian <i>et al.</i> , 1977
≈40°S	29	Ninety Mile Beach (source- New Zealand)	Gagosian <i>et al.</i> , 1977
*75-65°S	27	Wilkes Land continental margin and Ross Sea (source unknown)	Kvenvolden <i>et al.</i> , 1987

Different plant species synthesise differing proportions of the various homologues (e.g. Stranksy *et al.*, 1967; Borges del Castillo *et al.*, 1967). Homologues are defined as members of a series of compounds which have the same general structure and the same functional group, differing only in their molecular formula by an incremental repeating unit, such as  $-CH_2-$ . One of the few studies of variations in higher plant lipids in the sedimentary record has shown that the  $C_{20}$ - $C_{33}$  *n*-alkane distribution of sediments from oligotrophic lakes in N.W.England and Scotland is dependent upon the vegetation of the drainage region (Granwell, 1973). Furthermore, changes in the sedimentary higher plant

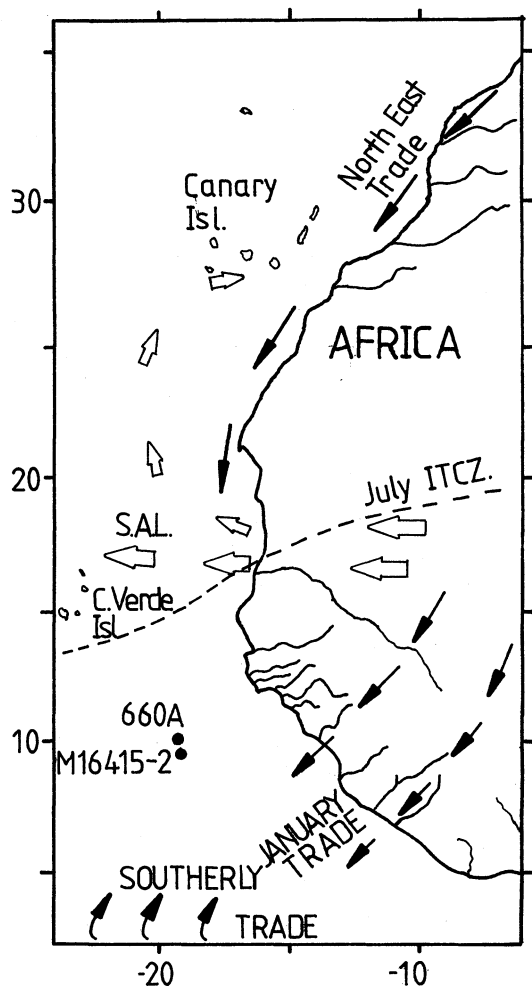


Figure 1. Locations of cores M16415-2 and 660A relative to the major wind systems of the N.E. Equatorial Atlantic. Solid arrows indicate surface winds (*i.e.* N.E. Trades, January Trades and Southerly Trades); open arrows indicate zonal winds at higher altitudes (*i.e.* African Easterly Jet or Saharan Air Layer SAL). Modified from Hooghiemstra and Agwu (in prep). The approximate July position of the Intertropical Convergence Zone (ITCZ) near the surface is shown (modified from Sarnthein *et al*, 1981); its position in winter is near the equator.

lipids of Priest Pot (Lake District, U.K.) were shown to be consistent with documented alterations in the lakeside vegetation (Cranwell *et al.*, 1987). Marine sediments have not received such a source study, although literature data shown in Table I show that the distributions of *n*-alkanes in aeolian dust samples vary grossly with latitude (with longer *n*-alkane chain lengths predominating at lower latitudes). However, it is apparent that the modal *n*-alkane chain length may also vary with longitude at a given latitude, presumably reflecting the input of higher plant waxes from different regional climatic regimes (compare the data of Simoneit with that of Gagosian; Fig. 1). A future literature survey of the modal carbon chain lengths of higher plant *n*-alkanes from Holocene sediments around the world might delineate these regional changes as well as the overall latitudinal dependence. Furthermore, an investigation of the lipid abundances and distributions off the coast of Africa revealed that dusts derived from the Sahara contained the lowest amounts of lipid material whilst those from more tropical regions yielded the highest (Simoneit *et al.*, 1977).

More recently, evidence has been obtained which indicates that the distribution of higher plant lipids in aeolian dusts can be used to infer their geographical source and hence the trajectory of dust transport (Gagosian *et al.*, 1987). Four aeolian dust samples were collected from Ninety Mile beach on the N.W. shore of North Island, New Zealand (position 34.6°S & 172.8°W) over a period of 2 months. During this time the proposed source (inferred from prevailing wind directions) changed from predominantly Australian to New Zealand. Associated with this change a shortening of the average and modal higher plant *n*-alkane chain length was observed, interpreted as being due to the more temperate flora of the latter region (Gagosian *et al.*, 1987). This apparent climatic dependence of plant waxes in aeolian dusts had been noted earlier in samples collected at Enewetak atoll in the tropical North Pacific (Gagosian and Peltzer, 1986). In cooler temperate regions, predominantly shorter chain compounds are biosynthesized, whereas in warmer tropical regions longer chain compounds are produced (Table I).

### 1.1 Aims and scope of the present study

The present paper examines the abundance and distribution of presumed higher plant lipids in two short sediment cores from the Equatorial North Atlantic (Fig.1). Several aims are addressed: (i) to investigate any covariance of *n*-alkanes and *n*-alkanols, thus examining the hypothesis that they have a common source in higher plants; (ii) to relate the flux (i.e. the rate of incorporation into the sediment) of aeolian-derived higher plant *n*-alkanes to changes in the palaeoenvironment such as changes in continental aridity and the intensity of palaeocirculation (presumably linked to glacial/

interglacial fluctuations) and; (iii) to identify any link between the chain-length distribution of *n*-alkanes and transitions between glacial and interglacial conditions during the late Quaternary.

A common doubt associated with the use of organic molecules as biomarkers is related to their ability to survive incorporation into the sediment record. However, it would appear that terrestrial lipids are less susceptible to degradation than marine lipids (Prahl and Pinto, 1987). Calculations of fluxes of a terrestrial sterol and higher plant fatty acids through the water column have shown no apparent decrease with depth, whilst marine sterols and fatty acids decreased to 15% and 5% respectively, of their original values at 52m depth (Gagosian *et al.*, 1983; Wakeham *et al.*, 1983). Consequently, it was inferred that terrestrial lipids are less easily assimilated by the marine biomass in the photic zone. In view of this and the stability of long chain compounds (Brassell *et al.*, 1978) we assume as a temporary working hypothesis that quantitative incorporation of higher plant *n*-alkanes occurs.

A second problem lies in the decoupling of the long-chain *n*-alkanes of higher plant origin from homologues derived from other possible sources. A wide range of organisms are known to biosynthesise aliphatic alkanes including marine algae (*n*-C<sub>14</sub> to *n*-C<sub>21</sub>, odd/even preference maxima at C<sub>15</sub> and C<sub>17</sub>; Clark and Blumer, 1967) and bacteria (non-photosynthetic bacteria have been found to have a bimodal distribution maximizing at C<sub>15</sub> and C<sub>25</sub>, a low odd/even preference and a chain length range of C<sub>15</sub>-C<sub>29</sub>; Han and Calvin, 1970). Clearly, both higher plants and bacteria can produce a similar range of *n*-alkane homologues. Hence, whilst striving to achieve our targets we must remain aware of the possibility of multiple sources of *n*-alkanes.

## 1.2 Geographical and environmental position of core M16415-2 and Site 660A

The positional information concerning site M16415-2 ('Meteor' cruise N<sup>o</sup>. 65) and Site 660A (Ocean Drilling Program, Leg 108) is given in Table 2. Analysis of core M16415-2 has produced a high resolution data set spanning the last two glacial cycles (185 Ka) whilst the analysis of Hole 660A provides a lower resolution data set spanning a slightly longer period (250 Ka).

It has been stated that this area receives the bulk of its aeolian input from the N.E. Trade Winds during the period November to May. During this time the Intertropical Convergence Zone (ITCZ) is located to the south of this region, hence allowing only material from the northern areas to reach these latitudes (Hooghiemstra and Agwu, in press). This is due to the associated rain wash belts of the ITCZ forming a sharp cut off to aeolian dust transport. From June to October



Table 2 The position and water depths from which the cores studied were recovered and an estimate of the time of deposition of the section studied.

Site	M16415-2	108/660A
Latitude	9°34'N	10°01'N
Longitude	19°06'W	19°15'W
Water depth	3841 m	4327 m
Core section studied mbsf	0-2.46 m	0-5.56 m
Approx. time spanned by core	0-170 ka	0-250 ka

the average position of the ITCZ is north of the site, potentially allowing an influx of dust *via* the southerly trades (Fig. 1). In reality however, hardly any aeolian material is transported to the site by this wind system (Hooghiemstra and Agwu, in press).

It has also been suggested that a large aeolian component may be derived from the Southern Saharan and Sahel regions *via* the Saharan Air Layer (SAL; Fig. 1); *i.e.* dust in the SAL reaching the coast at about 14-22°N may be displaced south by means of the underlying near surface trade winds and be washed out by precipitation in the study area (Sarnthien and Koopman, 1980). The amount of dust reaching our sites at 10°N from each source will be dependent on a combination of the following factors:-

1) The intensity of the surface trades increases during the glacial stages (isotopic stages 6, 4 and 2). Hence, an increased flux of dust will be carried to the study region *via* the N.E. Trades during the cold stages.

2) The amount of dust from the southern Sahara/ Sahel region would be expected to rise due to increased continental aridity arising from the depletion of the ITCZ water budget (Tetzlaff and Peters, this vol.).

We conclude that the volume of dust reaching our site should rise during the cold stages. However, the composition of the dust (Tradewind/SAL) will depend on the balance between the increase in SAL dust reaching our site due to glacial aridity, and the increased supply of tradewind material *via* the strengthened N.E. Trades during glacial periods.

The summer and winter positions of the ITCZ are thought to have remained constant throughout the glacial and interglacial stages (Sarnthien *et al.*, 1981). Consequently, the source regions and trajectories of the dusts are expected to have remained constant.

## 2. EXPERIMENTAL

### 2.1 Extraction procedure

The method used to separate organic biomarkers from the largely inorganic sediment matrix involved sonication in an organic solvent. Each sample was extracted wet in a polar solvent (methanol), followed by extractions with progressively less polar solvents, finally extracting with dichloromethane alone. The polarity of the organic phase was controlled by adjusting the proportion of dichloromethane. The extract thus obtained was a two phase system, comprising of a highly polar phase containing extracted salts and water, and a less polar phase containing organic biomarkers; this method is analogous to one proposed by Bligh and Dyer (1959).

Whilst this procedure reproducibly extracts the biomarkers considered in this study it does not extract the entire organic fraction of the sample.

### 2.2 Sample extract preparation

Organic geochemists typically fractionate lipid extracts into compound classes prior to analysis. However, in this study, to maintain the simplicity and speed of the method, each sample was analysed as a total lipid extract after derivatisation with commercial grade bis-trimethylsilyl-trifluoroacetamide (BSTFA).

### 2.3 Analysis and Quantitation

The organic extracts were analysed by capillary gas chromatography using a Carlo Erba Mega series 5300 instrument equipped with an on-column injector and an OV-1 equivalent (methylsilicone; 0.17 $\mu$ m film thickness) fused silica column (50m x 0.32mm i.d.). Hydrogen was used as the carrier gas with a flow rate of 50cm/sec, and a temperature program of 50°C for one minute, 50°C to 150°C at 15°C/min, 150°C to 300°C at 4°C/min and 30 minutes at isothermal, was used.

The components in the lipid extract were quantitated by comparing individual peak areas, acquired using a Minichrom data system, with those of internal standards added to the sediment prior to extraction. The resulting calculations and data processing was carried out using Lotus 123 software on an IBM AT, and SAS version 5.16 on a Vax 11/750 computer.

### 2.4 Climatic Stratigraphy of M16415-2

The stratigraphy used in this study was primarily based upon the  $\delta^{18}O$  record of the planktonic foraminifer *G. sacculifer* (largely recording fluctuations in global ice volume) as reported by Brassell *et al.*,

(1986b) and Hooghiemstra and Agwu (in press), and the downhole  $U^{k}_{37}$  index (recording local palaeoseasurface water temperatures; Brassell *et al.*, 1986a and b). Comparison of data derived in this study was made relative to one or both of these climatic records.

2.5 Determination of higher plant n-alkane flux rates at site M16415-2

Conversion of lipid abundances to fluxes depends upon a knowledge of the sedimentation rate and the bulk dry density of the sediment. An estimate of the sedimentation rate (Fig.2) was made based on the oxygen isotope taxonomy devised by Prell *et al.*, (1986) and the chronology of Imbrie *et al.*, (1984). The bulk dry densities were obtained from

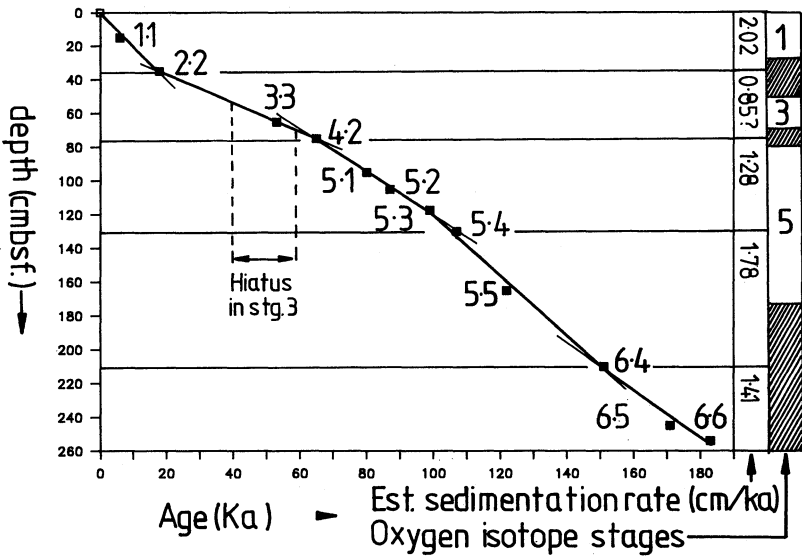


Figure 2. A plot of age versus depth for core M16415-2 estimated by recognition of the isotopic events (marked with squares) proposed by Prell *et al* (1986). The estimated sedimentation rate and oxygen isotope stages are shown on the right of the Figure. Full details of the assignments of oxygen isotopic events and the method used to estimate the sedimentation rate are given in the Experimental section.

Mienert (1986) and linearly interpolated to the depths of the lipid samples. Lipid abundances were then converted to fluxes using the following formula:

$$\text{flux} = \text{Concentration} \times \text{dry bulk density} \times \text{sedimentation rate}$$

$$(\mu\text{g cm}^{-2} \text{Ka}^{-1} = \mu\text{g g}^{-1} \times \text{g cm}^{-3} \times \text{cm Ka}^{-1})$$

The sedimentation rate was determined as follows. The assignment of isotopic events 3.3, 4.2, 5.1, 5.2, 5.3, 5.4, and 5.5 were taken from Hooghiemstra and Agwu (in press), whilst events 1.1, 2.2, 6.5, and 6.6 were assigned by the authors using the  $\delta^{18}\text{O}$  curves of *G. sacculifer* and *G. ruber* reported in Brassell *et al.*, (1986b). Event 6.2 previously assigned as occurring at 210 cmbsf. (Hooghiemstra and Agwu, in press) was reassigned 6.4 in this study, due to strong evidence from the  $\text{U}^{235}/\text{U}^{238}$  curve and higher plant *n*-alkane data (Fig. 11; see later text) that suggests isotopic event 6.2 occurred between 170-200 cmbsf., a region from which foraminiferal  $\delta^{18}\text{O}$  values could not be determined due to carbonate dissolution. The sedimentation rate was estimated by plotting the depths (cmbsf.) of these assigned events against their accepted chronology (Ka.; Imbrie *et al.*, 1984) and fitting least squares regression lines to those points that appeared to lie on a straight line (Fig. 2). A hiatus of unknown duration occurred in sediment deposition during stage 3 (Brassell *et al.*, 1986b); this contributes to the low estimated sedimentation rate during this portion of the core. Hence, this section was not used to determine higher plant lipid flux.

2.6 Determination of parameters used to assess higher plant *n*-alkane composition.

Molecular parameters recording average chain length (ACL) and odd/even carbon number preference were determined using the following formulae:

$$\text{ACL} = (\Sigma[\text{C}_i]xi)/\Sigma[\text{C}_i] \quad \text{for } i=23 \text{ to } 33$$

Where  $[\text{C}_i]$  is the concentration of the *n*-alkane containing *i* carbon atoms.

$$\text{Odd/Even} = (5x[\text{C}23]+[\text{C}25]+[\text{C}27]+[\text{C}29]+[\text{C}31]+[\text{C}33])/ \\ (6x[\text{C}24]+[\text{C}26]+[\text{C}28]+[\text{C}30]+[\text{C}32])$$

2.7 Principal components analysis

Principal components analysis (PCA; Pearson, 1901) was routinely performed on a VAX 11/750 computer using the SAS Princomp procedure to investigate the variance/co-variance structure of each data set. This method makes no assumptions about the data but merely identifies the components of correlated variance within the data set. Principal components analysis can be defined as "an objective way of combining the original variables into linear combinations (eigenvectors) which effectively describe the principal patterns of variation in a few primary components, leaving the less coherent aspects ("noise") for the last few components" (quoted from Bradley, 1983; after Sachs, *et al.*, 1977).

The data sets and the scaling used during each analysis were as follows:-

1) Seven variables from 26 samples from the upper 5.5 meters of Core 660A. The variables used were sums of the concentrations of the selected biomarkers *i.e.*: the C<sub>29</sub>, C<sub>31</sub> and C<sub>33</sub> *n*-alkanes; the C<sub>28</sub> and C<sub>30</sub> *n*-alkanols; dinosterol; the C<sub>32</sub> alkane-1,15-diol; the U<sup>k</sup><sub>37</sub> index which is thought to be related to seasurface water temperature (Brassell *et al.*, 1986a and 1986b);  $\Sigma$ di-unsaturated alkenones ( $\Sigma$ C<sub>37:2</sub>Me and C<sub>38:2</sub>Me); and  $\Sigma$ tri-unsaturated alkenones ( $\Sigma$ C<sub>38:2</sub>Me and C<sub>38:3</sub>Me). The tri-unsaturated ketones are found to be more abundant relative to the di-unsaturated compounds in areas of cooler seasurface waters (Brassell *et al.*, 1986a and 1986b). The data were scaled prior to analysis by standardising each column of variables so that they had a mean of zero and a standard deviation of one.

2) Eleven variables from 43 samples from the upper 2.5 meters of core M16415-2. The variables used were the concentrations of the C<sub>23</sub>-C<sub>33</sub> *n*-alkanes. The data used were scaled prior to analysis by normalising the sum of the variables from a given sample to unity and standardising each column of variables so that it had a standard deviation of one and a mean of zero.

3) Six variables from 36 samples from the upper 2.5 meters of core M16415-2. Data for the samples occurring at 16, 51, 122, 126, 156 and 241 cmbsf were omitted. The variables used were the concentrations of the *n*-alkanes containing an odd number of carbon atoms between 23 and 33. The data used were scaled prior to analysis by normalising the sum of the variables from a given sample to unity and standardising each column of variables so that it had a standard deviation of one and a mean of zero.

### 3. RESULTS AND DISCUSSION

#### 3.1 Correlation of presumed higher plant lipids

A gas chromatographic trace of the free lipid extract of a modern sediment sample from the Equatorial Atlantic showing many of the biomarker compounds we consider is shown in Figure 3. The averaged *n*-alkane and *n*-alkanol distributions (normalised to the highest single component) for the two cores studied here are shown in Figure 4 alongside two previous analyses of aeolian dust samples. The *n*-alkane distributions of all four samples maximize at or around *n*-C<sub>31</sub> and display a predominance of odd carbon-numbered compounds. This distribution is regarded as a typical signature of higher plant input (Brassell *et al.*, 1978). The dominance of the C<sub>31</sub> *n*-alkane homologue in the sediment samples is consistent with the observation that longer chain lengths dominate in the waxes of higher plants from warmer climates (Gagosian and Peltzer, 1986).

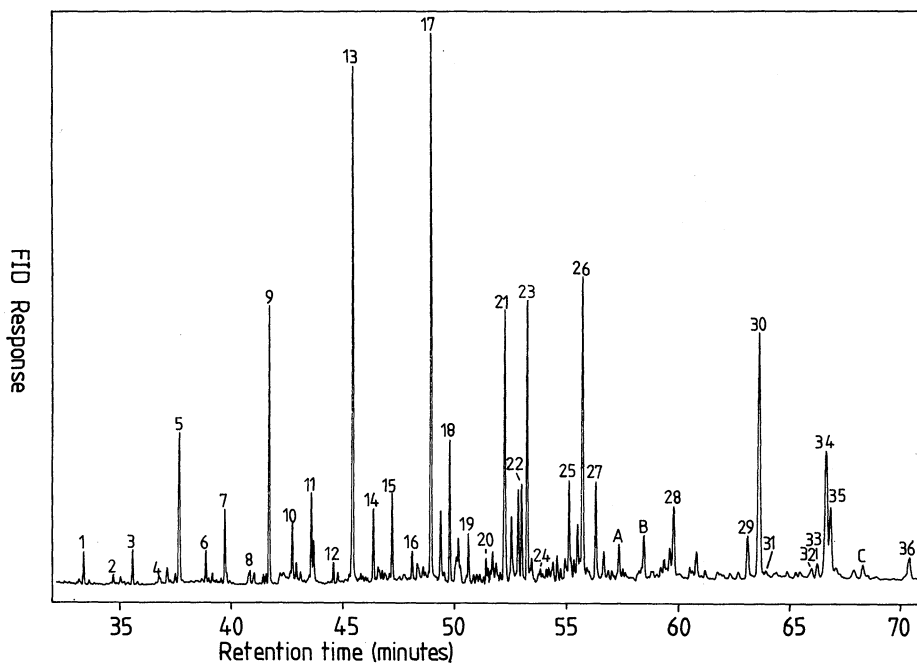


Figure 3. A typical gas chromatographic trace of the BSTFA derivatised free lipid extract of a recent sediment sample from the N.E. Equatorial Atlantic (Site M16415-2). Compound assignments are as follows: 1,3,5,7,9,11,13,15,17,19,21, 24 and 25 are the  $C_{23}$ - $C_{35}$  *n*-alkanes ascribed to higher plants (Eglinton and Hamilton, 1967); 2,4,6,8,10,12,14, 16,18,20 and 22 are the  $C_{20}$ - $C_{30}$  *n*-alkanols and 27 is the  $C_{32}$  *n*-alkanol also ascribed to higher plants (Eglinton and Hamilton, 1967); 29,30,32,33,34,35 and 36 are the  $C_{37}$ :3Me,  $C_{37}$ :2Me,  $C_{38}$ :3Et,  $C_{38}$ :3Me,  $C_{38}$ :2Et,  $C_{38}$ :2Me and  $C_{39}$ :2Et alkenones respectively, and 31 is the  $C_{37}$ :2Me ester, collectively ascribed to Prymnesiophyte algae (Volkman *et al*, 1980; Marlowe *et al*, 1984); 22 is dinosterol ascribed to dinoflagellates (Boon *et al*, 1979); and 26 and 28 are the  $C_{30}$  and  $C_{32}$  alkan-1,15-diols ascribed to cyanobacteria (Morris and Brassell, 1988). The internal standards (A, B and C) are the  $C_{36}$  *n*-alkane, cholesteryl hexanoate and  $C_{40}$  *n*-alkane, respectively.

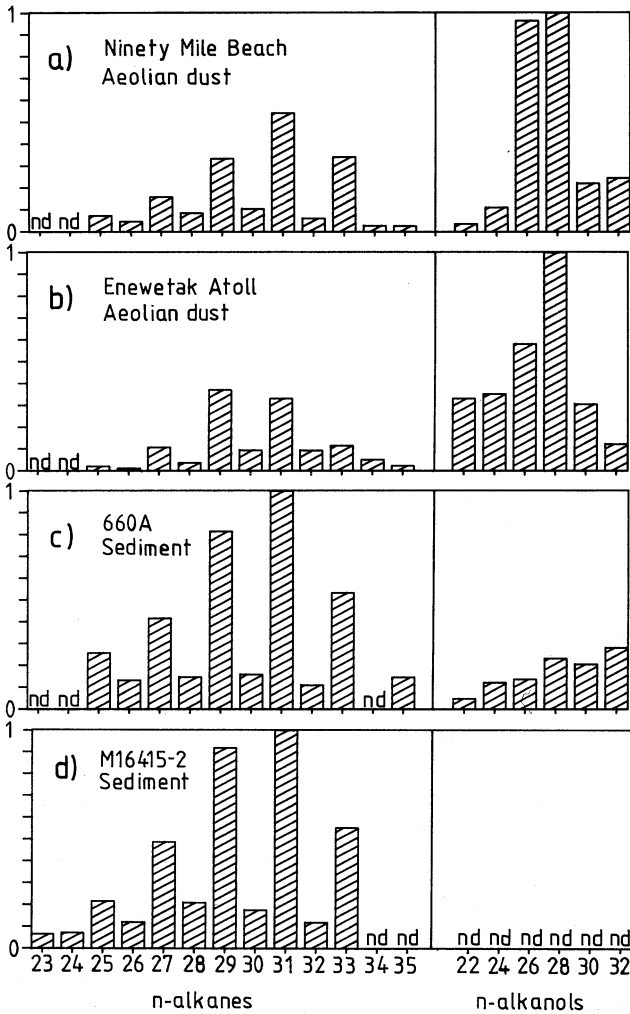


Figure 4. Distributions of the C<sub>23</sub>-C<sub>35</sub> n-alkanes and even C<sub>22</sub>-C<sub>32</sub> n-alkanols are shown for: a) an aeolian dust sample collected from Ninety Mile Beach New Zealand (modified from Gagosian *et al.*, 1987; the source proposed therein was Southern Australia); b) an aeolian dust sample collected from Enewetak Atoll (modified from Gagosian *et al.*, 1981; the source proposed therein was Chinese dust storms); c) the average of the 26 sediment samples taken from the first 5.5m of a core from Site 660A; and d) the average of 43 samples taken from the top 2.5m of core M16415-2. The abundances of those compounds marked with n.d. were not determined.

Higher plant *n*-alkanols show a dominance of even numbered homologues. In this work only these even carbon numbered *n*-alkanols were quantitated since they are more abundant and hence, easier to quantify. The lower abundances of *n*-alkanols relative to *n*-alkanes in our sediment samples, as compared to the aeolian dust samples (Fig. 4), suggests that these compounds may be partially lost prior to incorporation into the sediments (Tissot and Welte, 1984). It has been suggested that selective loss of *n*-alkanols relative to *n*-alkanes may occur in the water column due to selective degradation in oxic conditions (ten Haven *et al.*, 1987).

The correlation between the downhole abundances of *n*-alkanols and *n*-alkanes in the top 5.5m of Site 660A is high ( $r^2=0.98$ ) whilst the correlation between these compounds and marine biomarkers is low (in the range  $r^2=0.38$  for dinosterol to 0.67 for the diunsaturated alkenones; Fig. 5). The differing chemistries of the *n*-alkanes and *n*-alkanols should result in the latter being degraded or becoming bound to the sediment faster than the former. In this case the high correlation between these compounds downhole suggests that once in situ in the sediment, they remain intact in the unbound fraction of the sediment. This is taken as evidence that the apparent loss of *n*-alkanols must occur prior to incorporation into the sediment either in the water column or near the sediment water interface.

Covariance between variables can be demonstrated by principal components analysis. The output from such an analysis, [see Experimental section 2.7(1) for explanation and scaling] shows the correlations of each variable upon the major factors of variation within the data set (Fig. 6), calculated for 24 samples from the top 5.5m of Site 660A. The first three factors (principal components) account for 87% of the total variance in the data set. The alkenones, diols, and presumed higher plant lipids are all highly correlated with the most important factor (PC1<sup>660</sup>; PC1 of site 660A); this simply reflects the abundance of lipid material in the sediment. However, the "aeolian" compounds closely covary, and are discriminated from the alkenones and diols along the second and third PCs. This supports the hypothesis that the alkanols and alkanes are derived from a common source which is different from that of the other biomarkers.



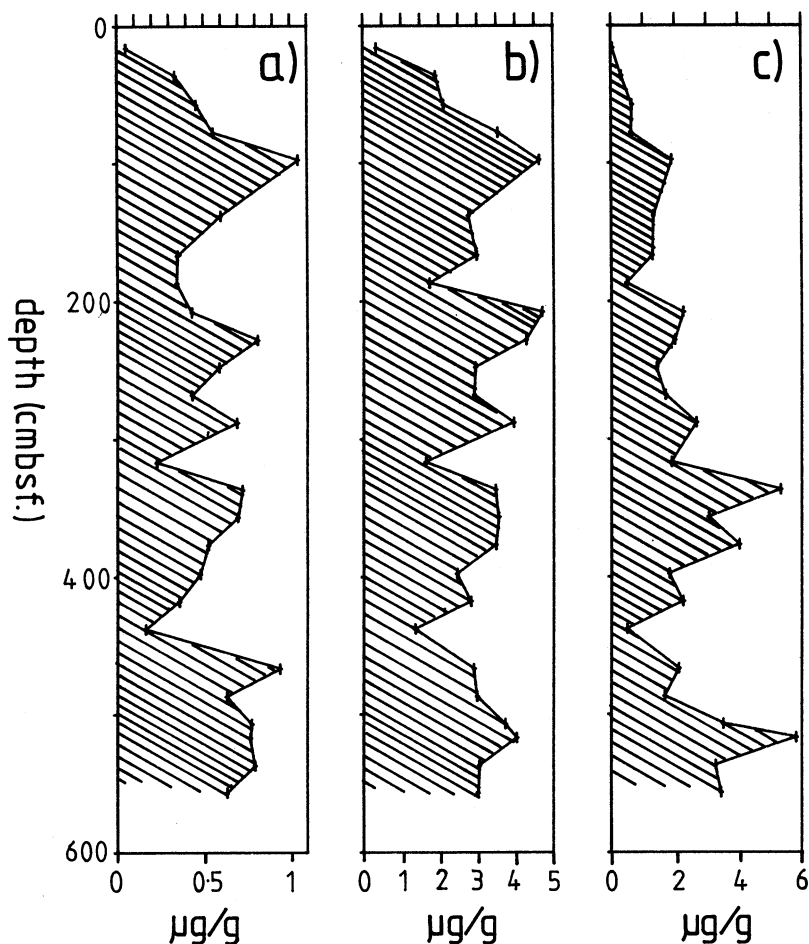


Figure 5. Downhole profiles of selected biomarker abundances in the top 5.5m of Core 660A (ODP Leg 108): a) the sum of the concentrations of the C<sub>28</sub> and C<sub>30</sub> *n*-alkanols; b) the sum of the concentrations of the C<sub>29</sub>, C<sub>31</sub> and C<sub>33</sub> *n*-alkanes; and c) the sum of the concentrations of the C<sub>37</sub>:2Me, C<sub>37</sub>:3Me, C<sub>38</sub>:2Me and C<sub>38</sub>:3Me alkenones.

### 3.2 Down-hole abundance of higher plant *n*-alkane lipids in core M16415-2

A higher resolution study of higher plant lipids was undertaken with core M16415-2, where the abundance of these lipids varies considerably with depth. In Figure 7, the downhole *n*-alkane abundance is compared

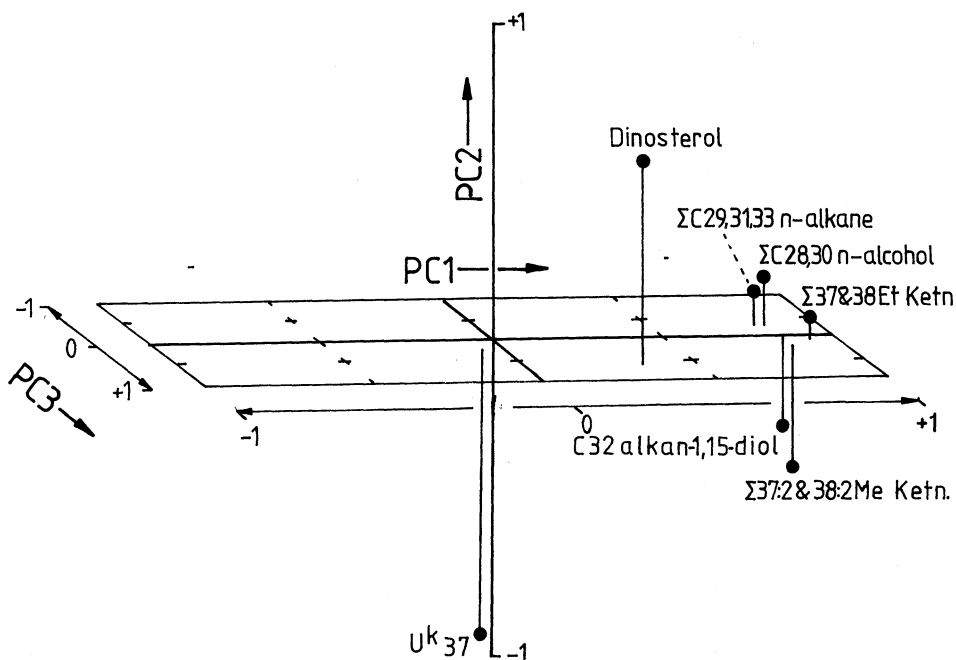


Figure 6. Part of the output from the principal components analysis of a "reduced" data set comprised of 26 samples from the top 5.5 meters of Core 660A and seven measured variables. The position of each variable upon each axis shows the correlation of each variable with the three major components of variance within the data set. Full details of the data and the scaling used are given in the Experimental 2.7(1). Ketn. = Ketone.

with the  $\delta^{18}\text{O}$  record of *G. sacculifer* and the  $U^k_{37}$  index. If quantitative addition of higher plant *n*-alkanes to marine sediments is assumed as a working hypothesis, then the two key factors controlling their abundance in the sediment are: 1) the original flux of higher plant lipids, and 2) the dilution effect of the sedimentation rate. It should be noted however, that the "sealing effect" of a high sedimentation rate is considered an important factor enhancing organic carbon preservation (Suess, 1980; Meyers *et al.*, 1984; Sarnthein *et al.*, in press). In calculations concerning the latter, organic carbon is

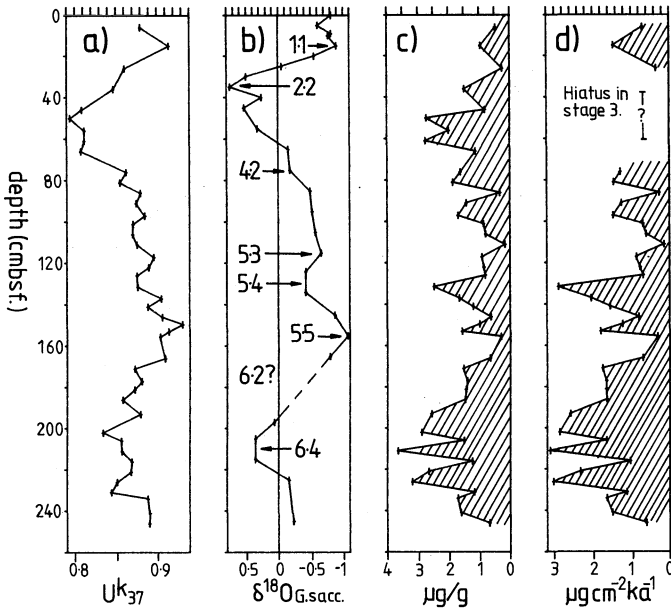


Figure 7. Downhole profiles (core M16415-2) of: a)  $U_k^{37}$  Index (proposed as a measure of palaeosea-surface water temperature; Brassell *et al.*, 1986b); b) the oxygen isotope composition of the planktonic foraminifera, *G. sacculifer* (mainly documenting the global ice volume with a minor sea surface water temperature component Brassell *et al.*, 1986b); c) the downhole abundance of the sum of selected higher plant *n*-alkanes ( $C_{29}$ ,  $C_{31}$  and  $C_{33}$ ); and d) the flux of these higher plant lipids into the sediment. Full details of how the flux rate was estimated is given in the Experimental.

regarded as a homogeneous substance. In contrast, we anticipate that the inert and hydrophobic nature of higher plant *n*-alkanes will render them relatively resistant to degradation, and therefore in regions with slow sedimentation rates we would expect them to be enriched relative to total organic carbon.

The aeolian transport of higher plant lipids can take place either directly from the leaf surface or by the subsequent ablation and redeposition of soils and lake sediments during times of aridity. The dominance of tropical pollen in this area, both at present and during the last glacial maximum (Hooghiemstra *et al.*, 1987), suggests that direct sloughing from leaf surfaces was the important mechanism since diminished aeolian transport of soil material is expected in humid conditions. However, even in humid regions extreme seasonality may give rise to soil deflation and hence, this component cannot be ruled out. Clearly, recognition of the presence or absence of freshwater

diatoms from dessicated lake sediments (Stabell, 1986; Pokras and Mix, 1987) would help resolve this uncertainty.

Lower concentrations of higher plant lipids have been found in dusts from areas which have remained dessicated for prolonged periods (Simoneit *et al*, 1977); hence, although the area may receive a large component from the Southern Sahara *via* the SAL we do not anticipate a high flux of higher plant biomarkers associated with this input.

In the region considered we expect an increased input of higher plant lipids (*via* sloughing) during glacial stages due to the intensification of the offshore/alongshore tradewinds and possibly an increased input from the Sahel region due to a depletion in the moisture budget of the ITCZ (see Introduction).

Assuming that the sedimentation rate remained more or less constant, then the variability of the higher plant *n*-alkane abundance curve (Fig. 7) leads one to infer that aeolian flux at this site varied more rapidly than the major climatic fluctuations. However, close inspection of the alkane abundance curve does reveal similarities with the established palaeoclimatic curves, *i.e.* oxygen isotope and  $U^{k}_{37}$ . During the last three cold stages (isotope stages two, four and six), higher plant lipid concentrations were high on average, whilst the last interglacial optimums (event 5.5 and 1.1) are marked by reduced higher plant lipid concentrations. The climatic deterioration at event 5.4 features a surprisingly high concentration of plant lipid material. Also, although stage 5.2 is not well delineated by the planktonic oxygen isotope record of *G. sacculifer*, there is an associated rise in plant *n*-alkane abundance in the position where this event is seen to occur in the  $\delta^{18}O$  record of *G. ruber* (Brassell *et al.*, (1986). However, full interpretation of the higher plant lipid (*n*-alkane) signal can only be undertaken if fluxes rather than abundances are known.

### 3.3 Down-hole flux of higher plant *n*-alkanes in core M16415-2

The method used to convert higher plant *n*-alkane abundances to fluxes is given in the Experimental section. It should be noted that the resulting higher plant lipid fluxes are subject to the sedimentation rate being accurately known.

During the interglacial extremes (1.1 and 5.5) we have estimated sedimentation rates of 2.02 and 1.78 cm/Ka, whilst during the sections of core deposited during the colder (non extreme interglacial events 5.1, 5.2, 5.3 and 6.4, 6.5, 6.6) the sedimentation rate was calculated to be lower (1.28 and 1.41 cm/Ka; Fig.2 and Fig.7). The extreme low value of 0.85 cm/Ka between events 2.2 and 4.2 is in part due to the hiatus that occurred during the top of isotope stage three (Brassell *et al.*, 1986) and hence, will not be considered further. The observed decrease in the estimated sedimentation rate (Fig. 2) during the remaining (non interglacial extreme) cold portions of the curve is in

accordance with the following geological model: in a pelagic sediment, such as M16415-2, receiving most of its input from the overlying photic zone, the sediment accumulation rate is dominated by the primary productivity and the corrosiveness of the bottom waters with respect to calcium carbonate. These two factors have opposite effects on the sedimentation rate; an increased primary productivity produces more carbonate tests (occurring in this core during the cold stages); whereas the associated increased supply of oxidisable carbon increases the corrosiveness of bottom waters (Müller and Suess, 1979). These locally induced changes in bottom water corrosiveness are of course additive with oceanwide fluctuations. In a core containing an appreciable carbonate content one might expect the latter to hold sway, as illustrated by core M13519 from the nearby Sierra Leone Rise (Sarnthein *et al*, 1984).

The most striking details of the thus determined higher plant *n*-alkane flux curve (Fig.7d) are the maxima occurring during oxygen isotope stage six and event 5.4. This, combined with the minimum in *n*-alkane higher plant flux near oxygen isotope event 5.5 supports the view that aeolian input increased during the cooler stages, possibly due to intensification of the N.E. Trade winds. Other contributing factors may be an increased proportion of SAL ( being deflected south by the N.E. Trades) due to an enhanced continental aridity.

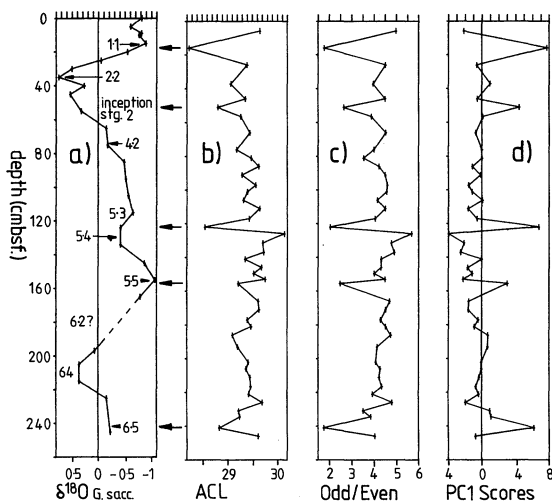


Figure 8. Three methods of representing distributions of *n*-alkanes are shown for the upper 2.5 metres of core M16415-2: b) average chain length (ACL.) of all of the C<sub>23</sub>-C<sub>33</sub> *n*-alkanes; c) odd/even ratio; and d) a down-hole scores plot of the first principal component (PC1) of the data set. Details of the data used and scaling are given in the Experimental section 2.7(2). The oxygen isotope record (*G. sacculifer*) is also shown for comparison (redrawn from Brassell *et al.*, 1986b).

### 3.4 Higher plant lipid (*n*-alkane) composition

The modal carbon number of aeolian transported higher plant lipids has been observed as being dependent upon the geographical location of particulate sources (Table 1), presumably being either directly or indirectly dependent on the prevailing climatic conditions of the growth habitat and the plant communities therein (e.g. Gagosian and Peltzer, 1986). Whilst this phenomenon has been reported in aeolian dusts it has not been studied in the sedimentary record.

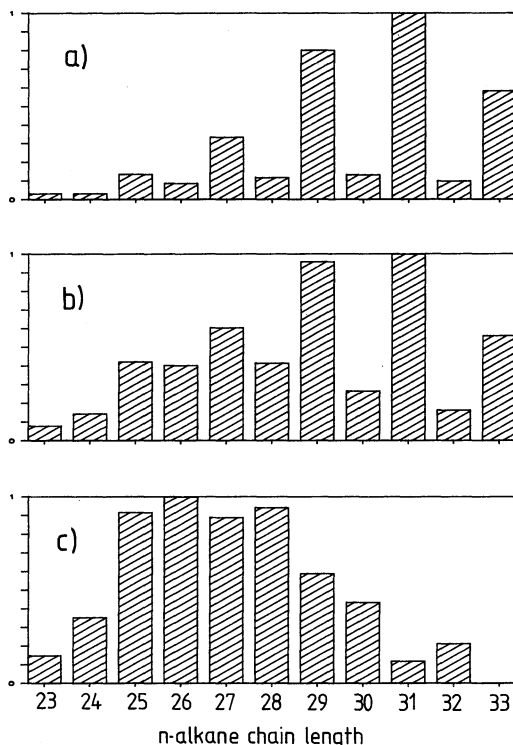


Figure 9. Representative distributions of *n*-alkanes (C<sub>23</sub>-C<sub>33</sub>) in the data set calculated by summing the determined *n*-alkane distribution from the following samples: a) 6, 126 and 226 cmbsf., thought to represent a higher plant *n*-alkane signal; b) 16, 122 and 241 cmbsf., thought to represent a mixture of higher plant *n*-alkanes with another unknown distribution; and c) an estimate of the unknown distribution calculated from distribution (a) and (b), see Experimental section for details.

The downhole record of higher plant *n*-alkane distributions was investigated by determining the average chain length, the odd/even carbon chain length preference and the PC1 scores. See Experimental

section 2.7(2) for explanation and scaling. These parameters all appear to contain approximately the same signal. In each case the curves bear little similarity to the  $\delta^{18}\text{O}$  record (dominant palaeoclimatic cycle; see Fig. 8). However, it is notable that high PC1 scores occur close to the warm peaks in the isotopic curve, *i.e.* events 1.1, 5.3, 5.5, 6.5 and the inception of cold stage 2.

In order to aid the interpretation of the PC1 downhole signal we calculated two "extreme distributions", by separately summing the *n*-alkane distributions of the samples from 16, 122 and 241 cmbsf, and those from 6, 126 and 226 cmbsf. (Fig. 9). These samples were selected on the basis of their PC1 Scores. From these histograms it is apparent that we have two contributing *n*-alkane distributions superimposed on each other. The first distribution (a) is the recognised higher plant distribution. The unknown distribution (c) was calculated by subtracting the first distribution (a) from another (b) so that  $\text{C}_{33}$  becomes zero). To clarify, this can be represented by the following formula:

$$[\text{C}_i]_c = [\text{C}_i]_b - ([\text{C}_{33}]_b / [\text{C}_{33}]_a) \times [\text{C}_i]_a \quad \text{for } i=23 \text{ to } 33$$

$[\text{C}_i]_c$  is the concentration of the *n*-alkane containing *i* carbon atoms in the distribution c. The letters a, b and c refer to the distributions shown in Fig. 9a, 9b and 9c accordingly. The second distribution (shown in Fig. 9c) is of unknown origin (possibly bacterial; Han and Calvin, 1969). It would appear that the dominant factor in the data (PC1; Fig. 8) is dependent on the proportions of these two *n*-alkane distributions. The correlation of the variables with this major factor (PC1; Fig. 10a) corroborates this finding. The dominant higher plant *n*-alkanes  $\text{C}_{29}$ ,  $\text{C}_{31}$  and  $\text{C}_{33}$  are negatively correlated with PC1, whilst the remainder, particularly the even numbered shorter chain *n*-alkanes, are positively correlated.

A more direct link between the *n*-alkane distribution and the prevailing climatic conditions is found if we decouple the higher plant and unknown (possibly bacterial) components. This was performed crudely by excluding samples containing a large proportion of the unknown *n*-alkane distribution. (A greatly improved method for decoupling these mixed inputs in the data set is reported by Yendle *et al.*, submitted). Since we have assumed that PC1 describes this mixture effect we could eliminate all samples with high PC1 scores. However, as we aim to find the variance in the main group of samples we first attempt to eliminate all extreme values. The plot of the samples scores on the first and second principal components (Fig. 10b) shows most of the samples grouped together with a few outliers (samples 16, 51, 122, 156 and 241 cmbsf.). These "outliers" having high PC1 scores typically contain a large contribution from the unknown (possibly bacterial) source. The

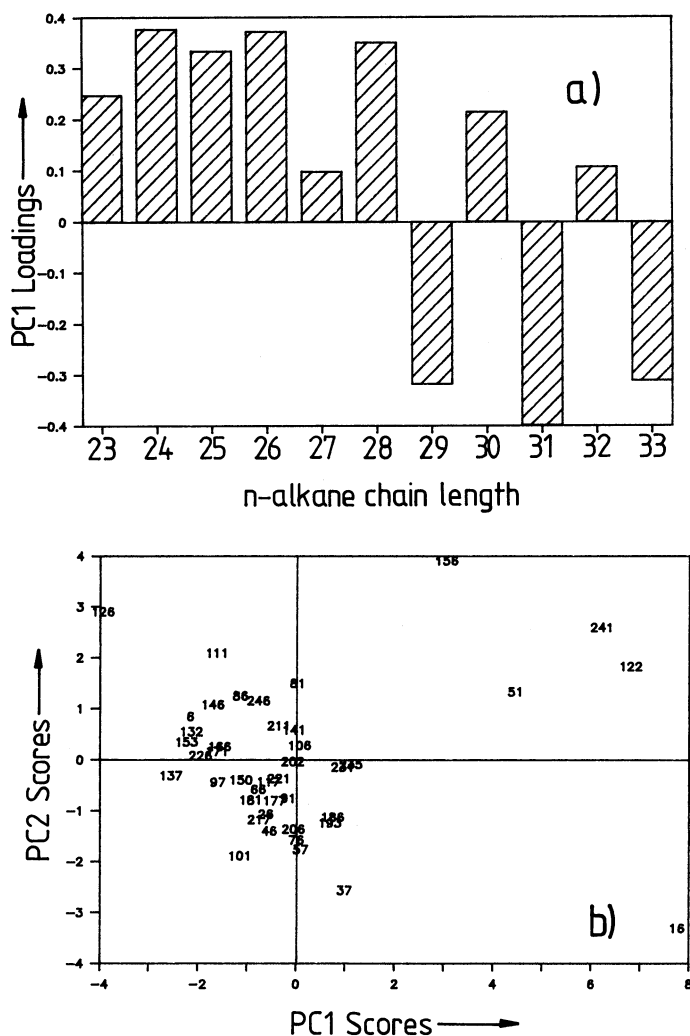


Figure 10. Part of the output from the principal components analysis of the distributions of 11 variables ( $C_{23}$ - $C_{33}$  *n*-alkanes) in 43 samples from the top 2.5m of core M16415-2: a) the correlations of the  $C_{23}$ - $C_{33}$  *n*-alkanes with the major component of variance (PC1); and b) the distribution of each sample (labelled by depth cmbsf.) upon the two major factors in the data (PC1 and PC2). The factor score of each distribution on the largest single component of variance (PC1) was shown previously (Fig.8d). See Experimental section 2.7(2) for details of data and scaling.



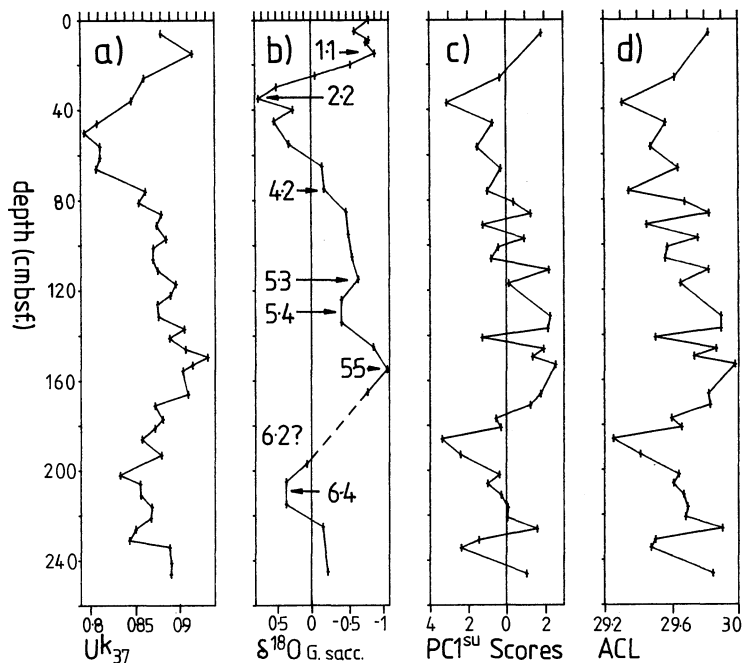


Figure 11. Downhole profiles of selected parameters proposed to contain climatic information for the upper 2.5m of core M16415-2: (a)  $U^k_{37}$  index (proposed seasurface water temperature parameter); (b) planktonic oxygen isotope composition of *G. sacculifer* (global ice volume and sea surface water temperature); (c) the first principal components ( $PC1^{su}$ ) scores calculated for 36 selected samples, see Experimental section 2.7(3) for details of data and scaling; (d) the average chain lengths of the odd homologues from  $C_{23}$ - $C_{33}$  (for the 36 selected samples).

sample from 126 cmbsf. also plotted independently of the main group and hence, was also considered an outlier.

These outliers were rejected. Furthermore, to increase the weight of higher plant *n*-alkanes in the data, only odd carbon chain lengths were considered. Subsequent supervised principal component analysis of the reduced data set afforded a first principal component  $PC1^{su}$  which appears to closely parallel the  $\delta^{18}O$  palaeoclimatic fluctuations (Fig. 11), see Experimental section 2.7(3) for scaling. Although the numerical correlation coefficient is relatively low ( $r^2=0.66$ ; derived by linearly interpolating  $PC1^{su}$  scores to oxygen isotope depths), a similarity between the curves is apparent. During the penultimate cold

stage, (stage 6) the PC1 scores are on average higher (shorter chains dominate); this stage is split into two positive maxima, the last occurring between the oxygen isotope data points, probably recording event 6.2 (inferring a misassignment of Stage 6.2 in the sedimentation rate calculation; see Experimental section). The last interglacial (event 5.5) is characterised by generally lower scores (longer chain lengths), whilst the slow deterioration in climate (events 5.5 to 2.2) has associated with it fluctuating scores superimposed on a steadily increasing mean (chain length decreasing). Finally, the present interglacial (event 1.1) is characterised by low scores, reflecting a higher chain length in the aeolian higher plant *n*-alkanes.

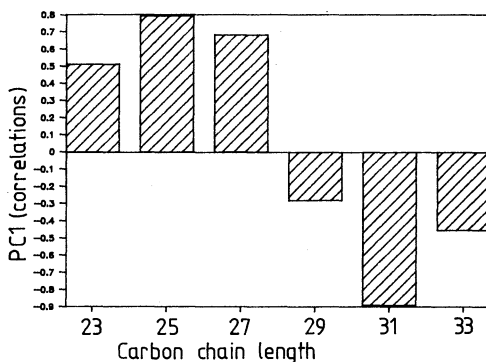


Figure 12. Part of the output from the principal components analysis of the reduced data set (36 samples) of the top 2.5m of core M16415-2, showing the correlations of the 6 variables (odd *n*-alkane homologues C<sub>23</sub>-C<sub>33</sub>) with the major component of variance (PC1<sup>su</sup>). Details of the samples rejected and the scaling used are given in the Experimental section 2.7(3).

The correlations of the variables (*n*-alkanes) with PC1<sup>su</sup> are shown in Figure 12. These correlations are largely dependent on chain length, the C<sub>23</sub>, C<sub>25</sub> and C<sub>27</sub> compounds being positively correlated, while the longer chain lengths are negatively correlated. This chain length dependence was investigated further by calculating the average chain length for each sample in the reduced data set (Fig. 11); this parameter correlates highly with our determined factor ( $r^2=0.91$ ). The interpretation of these results fits well with the suggestion that the plant waxes of vegetation from warmer climates is, in general, characterised by longer alkane chain lengths (Table I), a proposition which warrants further study. In particular a similar study should be undertaken based on other higher plant lipids such as *n*-alkanols and *n*-alkanoic acids.

Iso pollen maps (Hoogiemstra and Agwu, 1988) show an increased input of pollen from more northerly regimes to the region during

glacial stages, due to the intensification of the N.E. Trades. Likewise, we infer an increased input of epicuticular waxes from plants growing in cooler more temperate regions during the cold phases, based upon the observation of a slight shortening of the average higher plant *n*-alkane chain length in sediments deposited during the ice age stages of this core. This observation could also be due to an increased input of N.E. tradewind dust, relative to that transported by the SAL from the warmer Sahel region, during the cold stages (see Section 1.2).

#### 4. CONCLUSIONS

Reinspection of higher plant *n*-alkane data drawn from the literature has revealed a dependance between modal carbon chain length and source latitude and by inference growth temperature. The major conclusions from this study of the two cores from off N.W. Africa are as follows:

1) The carbon number distributions of C<sub>23</sub>-C<sub>33</sub> *n*-alkanes are interpretable in terms of two superimposed signals; a recognised higher plant distribution and an unrecognised (possibly bacterial) distribution having a maximum at C<sub>25</sub> and a low odd/even chain length preference.

2) Over the time period investigated (less than 300 Ka), sedimentary higher plant *n*-alkanols and *n*-alkanes show no apparent preferential degradation or incorporation into the bound organic fraction, presumably having undergone little or no diagenetic or biological transformations once incorporated into the sediment. Furthermore, their covariance is consistent with their having the same biological source.

3) The estimated flux of higher plant *n*-alkanes into core M16415-2 increased during the cold events 5.4 and stage 6 reaching a maximum of approximately 3  $\mu\text{g cm}^{-2} \text{Ka}^{-1}$ , possibly due to increased sloughing off from plant surfaces and/or deflation of the pertinent dust sources. The *n*-alkane flux for the interglacial events (1.1, 5.3 and 5.5) was lower falling between 0.5 to 1.5  $\mu\text{g cm}^{-2} \text{Ka}^{-1}$ .

5) The chain length distribution of the higher plant *n*-alkanes preserved in the sedimentary record of site M16415-2 appears to be linked to palaeoclimate, the average chain length becoming shorter during cold stages, thought to be due to a change in source region. Thus, from such studies the composition of aeolian dust in terms of source regions might be determined and used to assess changes in aeolian processes during climatic change.

## Acknowledgements

We thank NERC for GC-MS facilities (GR3/2951), for S.A.S. (GR3/3758), and for grants supporting Molecular Stratigraphy (GR3/5957) and (GR3/02/247). The Royal Society are acknowledged for funding the Minichrom data system. We also thank P. Yendle for writing the interpolation and three dimensional plot programs and for productive discussions of chemometrics, and S.C. Brassell for discussions during the early stages of this study. Furthermore, we thank Ann Gowar and Lynne Dyas for running and maintaining laboratory equipment including the GC-MS facility. The authors are also grateful to those who aided in the collection of samples, notably Prof. M. Sarnthein, and the crews of the R.V. Meteor and the JOIDES Resolution (ODP Leg 108). Finally we would also like to thank M. Sarnthein for helpful discussions, and the two reviewers for constructive comments on the original manuscript.

## REFERENCES

- Bligh E.G. and Dyer W.J. (1959) 'A rapid method of total lipid extraction and purification' *Can. J. Biochem. Physiol.* **37**, 911-917.
- Boon J.J., Rijpstra W.I.C., de Lange F., de Leeuw J.W., Yashioka M. and Shimizu Y. (1979) 'Black sea sterol-molecular fossil for dinoflagellate blooms' *Nature* **277** 125-127.
- Borges del Castillo J., Brooks C.J.W., Cambie R.C., Eglinton G., Hamilton R.J. and Pellitt (1967) 'The taxonomic distribution of some hydrocarbons in Gymnosperms' *Phytochemistry* **6**, 391
- Bradley R.S. (1985) 'Quaternary paleoclimatology' *Allen and Unwin* 472pp.
- Brassell S.C., Eglinton G., Maxwell J.R. and Philp R.P. (1978) 'Natural background of alkanes in the aquatic environment' In: *Aquatic pollutants*, (eds Hutzinger O., Van Lelyveld I.H. and Zoeteman B.C.J.) pp69-86
- Brassell S.C., Brereton R.G., Eglinton G., Grimalt J., Liebezeit G., Marlowe I.T., Pflaumann U. and Sarnthein M., (1986a) 'Palaeoclimatic signals recognised by chemometric treatment of molecular stratigraphic data. In Leythausen D. and Rullkötter J. (Eds.), *Advances in Organic Chemistry 1985. Org Geochem.*, **10**, 649-660.
- Brassell S.C., Eglinton G., Marlowe I.T., Pflaumann U. and Sarnthein M. (1986b) 'Molecular stratigraphy: a new tool for climatic assessment' *Nature* **320**, 129-133.
- Clark R.C. and Blumer M. (1967) 'Distributions of *n*-paraffins in marine organisms and sediments' *Limnol. oceanogr.* **12**, 79-87.
- Cranwell P.A. (1973) 'Chain-length distribution of *n*-alkanes from lake sediments in relation to post-glacial environmental change' *Freshwat. Biol.* **3**, 259-265.

- Cranwell P.A., Eglinton G. and Robinson N. (1987). Lipids of aquatic organisms as potential contributors to lacustrine sediments - II. *Organic Geochemistry* **11**, 513-527.
- Eglinton G. and Calvin M. (1967) 'Chemical fossils' *Sci. Am.* **216**, 32-43.
- Eglinton G. and Hamilton R.J. (1967) 'Leaf epicuticular waxes' *Science* **156**, 1322-1335.
- Gagosian R.B. and Peltzer E.T (1986) 'The importance of atmospheric input of terrestrial organic material to deep sea sediments' *Org. Geochem.* **10**, 661-669.
- Gagosian R.B., Peltzer E.T. and Zafiriou O.C. (1981) 'Atmospheric transport of continentally derived lipids to the tropical North Pacific' *Nature* **291**, 312-314.
- Gagosian R.B, Nigrelli G.E. and Volkman J.K. (1983) 'Vertical transport and transformation of biogenic organic compounds from a sediment trap experiment off the coast of Peru. In: *Coastal Upwelling: Its sediment record*, (Eds. Suess E. and Theide J.) Plenum press, New York pp241-272.
- Gagosian R.B., E.T. Peltzer and J.T. Merrill (1987) 'Long-range transport of terrestrially derived lipids in aerosols from the South Pacific' *Nature* **325**, 800-803.
- Han J. and Calvin M. (1970) 'Branched alkanes from blue-green algae' *J. Chem. Soc. Chem. Commun.*, **1460**
- Hooghiemstra H. (1988) 'Changes of major wind belts and vegetation zones in NW Africa 20,000-5000 yr B.P. as deduced from a marine pollen record near Cap Blanc. *Review of palaeobotan. and palynology.*
- Hooghiemstra H., Bechler A. and Beug H.J. (1987) 'Isopollen maps for 18,000 years B.P. of the Atlantic offshore of Northwest Africa: Evidence for Paleowind circulation' *Palaeocirculation* **6**, 561-582
- Hooghiemstra H. and Agwu C.O.C. (in press) 'Changes in the vegetation and trade winds in the Equatorial Northwest Africa 140,000-70,000 as deduced from two marine pollen records' *Palaeogeog. palaeoclim. palaeoecol.*
- ten Haven H.L., Baas M., de Leeuw J.W. and Schenck P.A. 'Late Quaternary Mediterranean sapropels, II. Organic geochemistry and palynology of S<sub>1</sub> sapropels and associated sediments' *Chemical Geology.* **64** 149-169
- Imbrie J., Hays J.D., Martinson D.G., McIntyre A., Mix A.C., Morley J.J., Pisias N.G., Prell W.L. and Shackleton N.J. (1984) 'The orbital theory of Pleistocene climate: support from a revised chronology of the marine  $\delta^{18}\text{O}$  record' In: *Milankovitch and climate* **1**, (Eds. Berger A.L. et al) 269-305
- Marlowe I.T., Green J.C., Neal A.C., Brassell S.C., Eglinton G. and Course P.A. (1984) 'Long chain (*n*-C<sub>37</sub>-C<sub>39</sub>) Alkenones in the Prymnesiophyceae. Distributions of Alkenones and lipids and their Taxonomic Significance' *Br. phycol. J.* **19**, 203-216.

- Meyers P.A., Kawka O.E. and Whitehead D.R. (1984). Geolipid, pollen and diatom stratigraphy in post-glacial lacustrine sediments. *Organic Geochemistry* 6, 727-732.
- Mienert J. (1986) 'Akustostratigraphie im äquatorialen Ostatlantik: zur entwicklung der tiefenwasserzirkulation der tiefenwasserzirkulation der letzten 3,5 millionen jahre "Meteor" *Forsch-Ergebnisse* 40, 19-86.
- Morris R. and Brassell S.C. (1988) 'Long-chain alkanediols: Biological markers for cyanobacterial contributions to sediments' *Lipids* 23, 256-258.
- Morrison R.I. (1969) 'Soil lipids' In: *Organic Geochemistry: methods and results* (Eds. Eglinton G. and Murphy M.T.J.) Springer-verlag, Berlin pp558-575.
- Müller P.J. and Suess E. 'Productivity, sedimentation rate and sedimentary organic matter in the Oceans - Organic carbon preservation' *Deep sea research* 26A, 1347-1362.
- Pearson K. (1901) 'On lines and planes of closest fit to systems of points in space' *Philosophical Magazine* 6, 559-572.
- Pokras E.M. and Mix A.C. (1987) 'Earths precession cycle and quaternary climatic change in tropical Africa' *Nature* 326, 486-487.
- Prahl F.G. and Pinto L.A., 'A Geochemical study of long-chain *n*-aldehydes in Washington coastal sediments' *Geochimica et Cosmochimica Acta* 51, 1573-1582.
- Prell W.L., Imbrie J., Martinson D.G., Morley J.J., Pisias N.G., Shackleton N.J. and Streeter H.J. (1986) 'Graphic correlation of oxygen isotope stratigraphy application to the late quaternary' *Paleoceanography* 2, 137-162.
- Sachs M.H., Webb T. and Clark D.R., (1977) 'Paleoecological transfer functions' *Ann. Rev. Earth Planet. Sci.* 5, 159-78.
- Sarnthein M. (1984) 'Stable-isotope stratigraphy for the last 750-000 years: 'Meteor' core 13519 from the eastern equatorial Atlantic' *'Meteor' Forsch-Ergebnisse* 38, 9-38.
- Sarnthein M. and Koopman B. (1980) 'Late Quaternary deep-sea record on Northwest African dust and wind circulation' *Palaeocology of Africa* 12, 239-253.
- Sarnthein M., Tetzlaff G., Koopmann B., Wolter K. and Pflaumann U. (1981) 'Glacial and interglacial wind regimes over the eastern subtropical Atlantic and north west Africa' *Nature* 293, 193-196.
- Sarnthein M., Winn K. and Zahn R. (in press) 'Paleoproductivity of Oceanic upwelling and the effect on Atmospheric CO<sub>2</sub> and climatic change during deglaciation times' In: *Abrupt climatic change* (Eds. Berger W.H. and Labeyrie L.D.).
- Simoneit B.R.T. (1976) 'Sources of the solvent-soluble organic matter in the glacial sequence of DSDP samples from the Norwegian-Greenland Sea, Leg 38' *Initial reports of the Ocean drilling project XXXVIII* U.S. Government printing office Washington, 805-806.

- Simoneit B.R.T. and Eglinton G. (1977) 'Organic matter of eolian dust and its input to marine sediments' In: *Advances in Organic Geochemistry 1975*, (Eds Campos R. and Goni J. 415-430.
- Simoneit B.R.T., Chester R. and Eglinton G. (1977) 'Biogenic lipids in particulates from the lower atmosphere over the eastern Atlantic' *Nature* **267**, 682-685.
- Stabell B. (1986) 'Variations of diatom flux in the Eastern Equatorial Atlantic during the last 400,000 years 'Meteor' cores 13519 and 13521' *Marine Geology* **72**, 305-323.
- Stranský K., Streibl M. and Herout V. (1967) 'Distribution of wax hydrocarbons in plants at different evolutionary levels' *Col. Czech. Chem. Commun.* **32**, 3213-3220.
- Suess E. (1980) 'Particulate organic flux in the Oceans-surface productivity and oxygen utilization' *Nature* **288**, 260-263.
- Tissot B.P. and Welte D.H. (1984) 'Petroleum formation and occurrence' 2nd edition. Springer-Verlag, Berlin. 538pp.
- Volkman J.K., Eglinton G., Corner E.D.S. and Sargent J.R. (1980) 'Novel unsaturated straight-chain C<sub>37</sub>-C<sub>39</sub> methyl and ethyl ketones in marine sediments and a coccolithophore *Emiliana huxleyi*' (Eds. Douglas A.G. and Maxwell J.R.) In: *Advances in organic geochemistry*, Pergamon press, Oxford, pp219-227.
- Wakeham S.G. and Farrington J.W. (1983) 'Fatty acids, wax esters, triglycerols and alkyldiacylglycerols associated with sinking particles collected in the Peru upwelling' *Advances in organic geochemistry 1981*' (Eds. M. Bjorøy et al) pp185-197.
- Yendle P.W., Poynter J.G., Farrimond P. Macfie H.J.H. and Eglinton G. (Submitted) 'Identification and quantitation of multiple *n*-alkane inputs to sediments using iterative target transformation factor analysis'.

### Glossary of Terms

ITCZ = Intertropical convergence zone

SAL = Saharan Air Layer

BSTFA = bis-(trimethylsilyl)trifluoroacetamide

SAS = Statistical Analysis System

CMBSF = cm below sea floor

Ka = Thousand year before present

Σ = The sum of

ACL = Average chain length

[C<sub>i</sub>] = Concentration of the *n*-alkane containing *i* carbon atoms

PCA = Principal components analysis

PCs = Principal components

[C<sub>i</sub>]<sub>n</sub> = Concentration of the *n*-alkane containing *i* carbon atoms in the distribution *n*

Contribution to the NATO Advanced Research Workshop:  
Paleoclimatology and Paleometeorology:  
Modern and Past Patterns of Global Atmospheric Transport  
15–19 November 1987, Oracle, Arizona

Lithogenic sediment on Arctic pack ice:  
Potential aeolian flux and  
contribution to deep sea sediments

Stephanie Pfirman, Ingo Wollenburg, Jörn Thiede  
GEOMAR  
Research Center for Marine Geoscience  
The Christian-Albrechts University  
Wischhofstr. 1–3, Building 4  
2300 Kiel 14, Federal Republic of Germany

and

Manfred A. Lange  
Alfred-Wegener Institute for Polar and Marine Research  
Postfach 120161  
Columbusstraße  
2850 Bremerhaven, Federal Republic of Germany

463



## Abstract

Potential aeolian input of lithogenic sediment to sea ice and possible contribution from sea ice to sedimentation in Eurasian Arctic deep basins are discussed for modern and glacial environments. Low atmospheric fluxes estimated by previous investigations of snow samples from Amerasian Basin sea ice and the Greenland ice cap indicate that atmospheric deposition from long range sources probably provides only low quantities of lithogenic material to the Eurasian ice surface. Other likely sources for the predominantly fine-grained sediment in the Eurasian Arctic ice are entrained river, nearshore and shelf sediments.

Particles deposited both on the sea ice surface and within the upper ice column will affect ice characteristics. Especially in multiyear ice which experiences extensive surface melting during summer, particles within the melted snow and ice will be concentrated at the ice surface. If particle concentrations are high, the ice surface will become darkened or discolored, changing ice albedo and melting patterns. Sediment may aggregate to form more or less cohesive pellets during repeated freeze-thaw cycles. Implications for deposition from particle-laden sea ice to the sea floor are discussed.

High dust content in Greenland ice formed during the last glacial maximum indicates that at that time atmospheric flux of lithogenic material was much higher than today. Correspondingly large fluxes may be expected to the surface of sea ice during the last glacial maximum.

## 1. Introduction

Although the occurrence of particle-laden sea ice is often commented on by Arctic investigators (e.g. Nansen, 1897; Clark and Hanson, 1983), its importance remains unknown because its distribution has not been systematically surveyed. During the 1893–1896 FRAM expedition in the eastern Eurasian Basin, Nansen (1897, p.436–7) noted that the “upper surface of the floes is nearly everywhere of a dirty brown colour, or, at least, this sort of ice preponderates, while pure white floes, without any traces of a dirty brown on their surface, are rare...” (July 18, 1894 at approximately 81° 30'N, 125°E). Observations of the ice surface north of Svalbard indicated that as much as 10% of the ice surface may exhibit discolorations from sediments (Drewry, 1986; p. 229). In the Barents Sea, areal coverage of brownish ice was sometimes observed to be as high as 20–30% of a given ice area (Vinje, 1985). Larssen et al. (1987), in their investigation which preferentially sampled particle-laden ice in Fram Strait, found that an average of 20% of total ice volume contained sediment debris. Concentrations of particulate material ranged up to 3 g/l. Particles were predominately fine-grained: 30–60% of the bulk material in particle-laden ice was less than 2  $\mu\text{m}$ , with only minor grains coarser than 63  $\mu\text{m}$ .

Because much of the sediment in Arctic sea ice is observed to be fine-grained, an obvious source to be considered is aeolian dust (Nansen, 1897). However, fine-grained sediment may be incorporated in sea ice also by other mechanisms. Fine-grained sea floor sediments from shallow continental shelves can be incorporated in sea ice by formation of

anchor ice and frazil ice, sediment underplating and ice gouging (e.g. Kindle, 1924; Barnes et al., 1982; Clark and Hanson, 1983; Osterkamp and Gosink, 1984; Drewry, 1986; Reimnitz et al., 1987; Reimnitz and Kempema, 1988). Anchor ice, which forms when supercooled water encounters the sea bed, can raft bottom sediments and organics to the sea surface or the underside of the ice. Frazil ice formation can freeze-in or scavenge sediment which is suspended in the water column. Sediment could be in suspension due to storms, current activity (including tides), and ice scour. Sediment underplating of ice floes can also occur when the water column contains high particle loads. Sediments were recently observed by Vinje (1987) to accumulate on the underside of the ice and between ice floes during March over Spitsbergenbanken. Water samples showed that the water column contained large quantities of suspended sediment. Ice gouging of the sea floor by pressure ridges can result in accumulation of sediments on the underside of ice. In addition, fine-grained fluvial sediment may be contributed to sea ice. Sediment-laden river ice may discharge to the sea and turbid river water may flood over and under the nearshore ice when river ice breaks up in spring.

At present, the relative importance of these various sources for incorporation of lithogenic particles in sea ice of the Arctic Basin is unknown. Also not well documented are the processes which modify particle distributions during seasonal melting/freezing cycles in multiyear ice and mechanisms involved in release of particles to the underlying water column. In this paper characteristics of sediment-laden, multiyear ice are discussed in view of studies by other investigators and observations of several sea ice samples recently collected from the Eurasian Basin. In addition, the possible flux of aeolian lithogenic sediments in the Arctic region is reviewed. Geologic implications are discussed for modern and glacial periods in view of information on atmospheric characteristics and Greenland ice cores. Emphasis is placed on aeolian deposition of lithogenic material, not because it is thought to be the major source for sediment in sea ice or in the sea floor sediments of the Arctic Basin, but because atmospheric transport was the focus of the Workshop.

## **2. Eurasian Arctic Sea Ice Samples**

In July and August 1987, biological, chemical, geological, geophysical, oceanographic and meteorological investigations were conducted from the German ice-breaking research vessel RV POLARSTERN in the central Eurasian Basin of the Arctic Ocean (POLARSTERN Shipboard Scientific Party, 1988; Thiede, 1988; figures 1 and 2). The northernmost station was at 86°11'N and 22°04'E. During this expedition the first transect of sea ice cores and surface snow/ice samples was obtained from the Arctic Ocean margin into the central Eurasian Basin (figure 2). Geologic objectives of sea ice investigations were concerned with: 1) determining the amount and composition of particles contained in pack ice, 2) understanding the processes by which this material is incorporated, 3) determining how material in sea ice may be modified by melting/freezing cycles during transport, 4) identifying possible depositional environments/locations on the sea floor and 5) estimating the contribution of material transported by sea ice to the sedimentary budget of the Arctic Ocean.

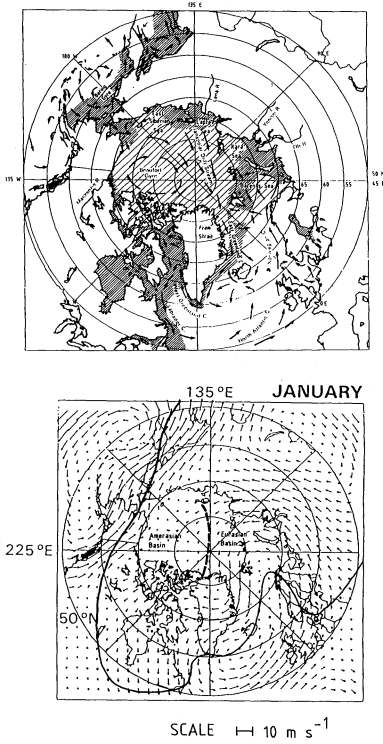


Figure 1 (A) Surface circulation pattern in the Arctic Ocean and surrounding seas (Parkinson et al., 1987). The four rivers providing major inflow to the Arctic Ocean are also indicated. Hatched region shows four-year average (1973–1976) maximum and minimum sea ice extent (i.e. concentrations exceeding 15% as contoured from interpretation of satellite passive-microwave observations, Parkinson et al., 1987).

(B) Mean monthly climatological geostrophic winds for January calculated from mean monthly climatological sea-level pressures (Parkinson et al., 1987). Arrows indicate the directions and magnitudes of the wind vectors. Mean position of the arctic front (which conforms approximately to the mean position of the  $-5^{\circ}\text{C}$  surface level isotherm) in January (solid line) from Barrie and Hoff (1984). Heavy dashed line indicates approximate position of the Lomonosov Ridge which divides the Amerasian and Eurasian Basins.

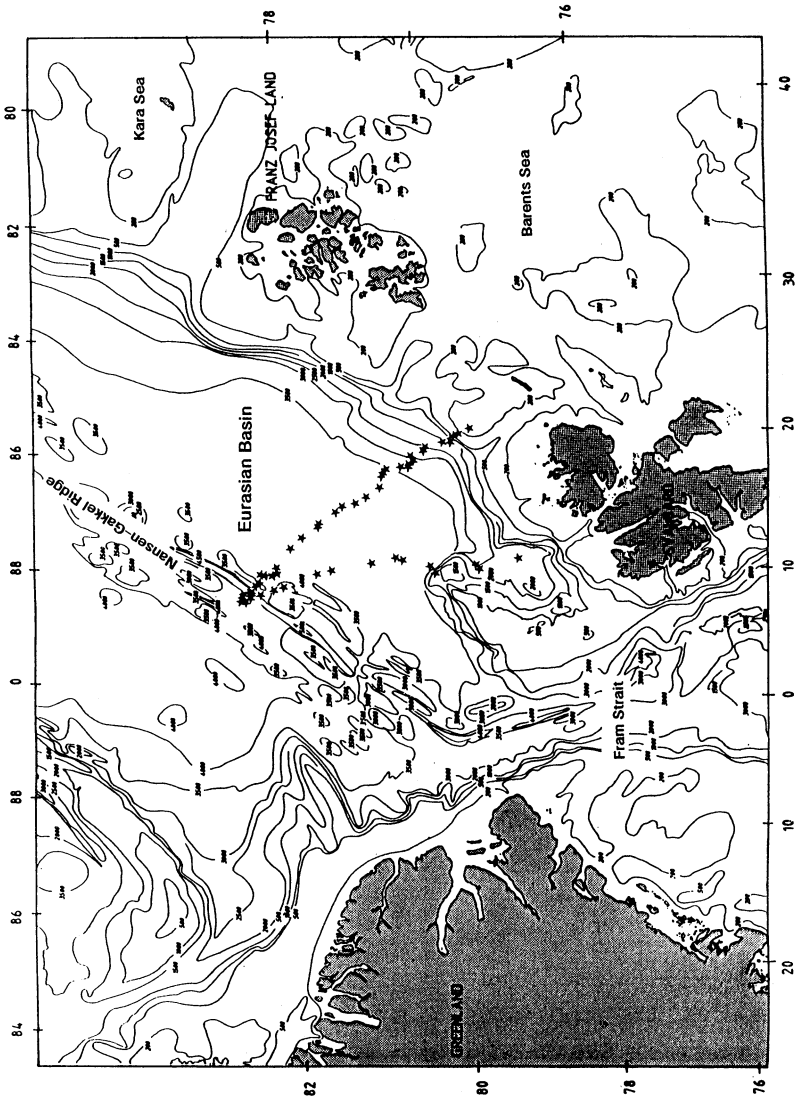


Figure 2 Sea ice/snow sample locations during July and August 1987 with the RV POLARSTERN in the Eurasian Basin.

The transect of ice samples ranged the Svalbard margin to the Nansen–Gakkel Ridge, between 81°N and 86°11'N latitude and 15 to 32°E longitude (figure 2). Ice sampling was carried out from both RV POLARSTERN and the accompanying helicopter. Cores were obtained, usually through the entire ice floe, primarily at or near dirty ice locations with a 10 cm diameter ice coring auger. A total of 72 cores (average length 3 m) were drilled at 31 stations, amounting to about 173 m of ice and averaging two cores per sampling site. The shortest core was 38 cm, the longest one was 455 cm. In the field, cores were photographed, described and the temperature measured every 50 cm downcore. Cores were placed in a –27°C freezer as soon as possible on returning to the ship. In addition to the ice cores, 102 samples of surface snow and/or surface accumulations of particulate material were taken, and observations were made of the surface characteristics of the ice floes, including snow/ice grain size and temperature, for correlation with satellite images in conjunction with other investigators.

Observations of the distribution of dirty patches on the sea ice, percentage of ice cover, ridges and meltwater ponds, were obtained during 36 helicopter flights from aboard the RV POLARSTERN. More detailed mapping of ice characteristics were carried out 6 times by flying over an 8 mile grid (e.g. figure 3).

On shore, the ice cores are being examined for structure and textural parameters in order to understand the growth processes of the sampled floe and the relationship of particulate material to ice classification (Lange, 1988). Following this investigation, cores are analyzed in sections according to ice texture for the following parameters: salinity, pH, O<sup>18</sup> (Institut für Umweltphysik, Heidelberg) and incorporated biogenic and lithogenic material. Examinations of the distribution of particulate material are used to: 1) determine lithogenic and biogenic concentrations in ice cores and surface samples, 2) analyse bulk composition, and particle grain size, mineralogy and surface microtextures, 3) compare the Eurasian Basin ice data with ice samples from the Amerasian Basin and Greenland, and with sediment cores obtained in the Arctic basin, Fram Strait and the Barents Sea in order to determine the contribution of sea ice rafted material.

### **3. Character of Eurasian Arctic Sea Ice and Sediment Inclusions**

The primary result of the “dirty” ice investigation is that the sea ice we encountered in the central Eurasian Basin contains a considerable amount of particulate material. Although sampling along only one transect does not permit areal mapping, it appears that the highest concentrations of particle-laden floes occur north of about 84° N and especially near our northernmost stations, at about 86°N (figure 3). This location is over the crest of the sea-floor Nansen–Gakkel Ridge in the region of the Siberian Branch of the main Transpolar Drift stream (figure 1). Ice coring showed that the ice here was generally 4 m or more thick, and appeared to be several years old. The relatively smooth ice had many surface meltwater ponds, often affecting more than 50% of the ice surface, and weathered ridges. Sea ice with surfaces darkened by particle accumulations occurred in patches, with

## FLIGHT OBSERVATIONS

Ship Position: N 86° 09' 34", E 22° 00' 94"

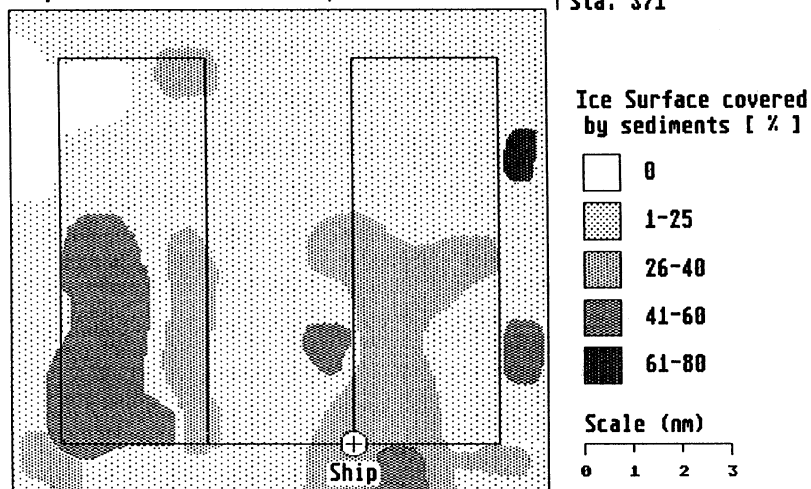


Figure 3 Example of a helicopter survey to estimate the distribution of sediment accumulations on the ice pack. Observations were made at 2 nm intervals with continual notation of special features. The percent of the ice surface affected by accumulations of particulate material is shown. 100% means that the entire ice surface was covered.

concentrations of discolored ice floes ranging up to 80% (figures 3 and 4). The discolorations were mainly brown to black, with some yellow and red patches, most likely depending on concentration and composition of particulate material. Often one floe with extensive surface deposits was embedded in much cleaner floes, and vice versa. In general, when surface particle accumulations are observed particles are enriched in small pockets in the uppermost 15 cm of the ice column. Occasional deeper layers were also observed.

Preliminary data indicate that the surface discolorations and particle accumulations are due to a highly variable combination of biogenic and lithogenic material. Therefore, visual observations from the helicopter or ship cannot be used to estimate lithogenic concentration, unless accompanied by actual samples of the particular ice floe. Analysis of 12 surface samples with the highest concentrations of particulate material show that the lithogenic component consists of > 90 % clay- and silt- sized material. The clay fraction is generally about 50% percent. The bulk of the silt fraction is less than 16  $\mu\text{m}$ . Concentrations of total particulate material in these very "dirty" samples ranged from 3 to 560 g/kg. The coarsest lithogenic material observed to date are 1–2 mm diameter rock fragments which were observed at one station, located at 82° N and 32° E.

In the silt and sand fraction examined to date, quartz is most abundant and is accompanied by heavy minerals, plagioclase and orthoclase feldspars, and silt- and sandstone-fragments. Diatoms dominate the biogenic component with minor amounts of radiolarians, brown algae and copepods. Grass fragments were also observed. Reddish patches formed by ice algae were identified by P. Mudie on board as *Chlamydomonas nivalis*, living on the ice surface.

Particle accumulations and sea ice occurred in five different combinations:

1. a clean, white surface with or without particle accumulations underneath;
2. a "dirty" surface layer, mostly between 3 and 15 cm thick, with or without particle accumulations down core;
3. meltwater ponds, which contain particle accumulations in small holes often 9–20 cm deep, 3–5 cm in diameter with a discolored surface surrounding the pond, and with or without deeper particle accumulation;
4. ridges with deformed sediment layers and lenses; and
5. surface discolorations of snow and ice, often only affecting one side of ridges.

Particulate material on the ice surface generally formed small mm-sized aggregates. In extreme cases, these aggregates accumulated in up to 2 cm thick layers, resembling mud, at the surface and in cylindrical holes in and near meltwater ponds (figure 4). Larger round to elongate pellets were found on the ice surface near our northernmost location, at 86° N. These pellets were 1–3 cm in diameter, very cohesive and consisted of mostly biogenic material with lesser amounts of clay and silt-sized mineral grains.

Preliminary investigations of several ice cores from the northernmost portion of the transect indicate that columnar ice predominates, but that the ice texture is variable (figure 5). For example, we describe the structure of a typical core obtained on a floe 3.66 m

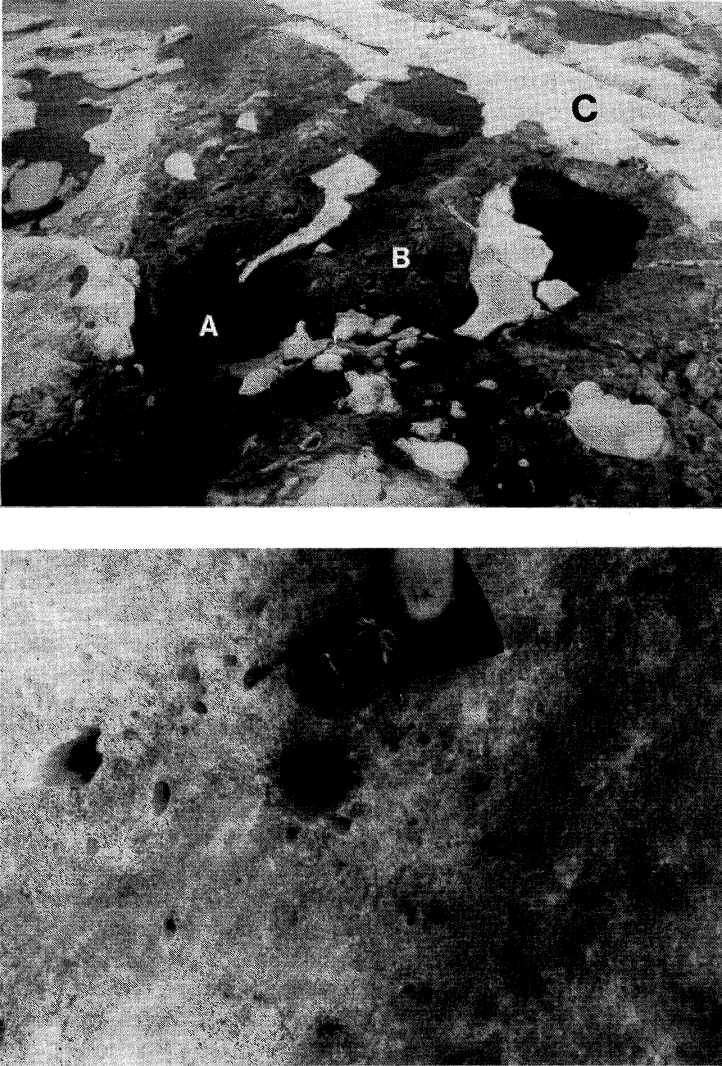


Figure 4 (A) Photograph of ice floe from helicopter showing showing “A” meltwater ponds, and “B” dark ice surface with high particle content and “C” lighter snow/ice surface with lower particle content. Width of photographed area is estimated to be between 30–50 m.

(B) Photograph of biogenic and lithogenic material collected on the ice surface in small pockets and cylindrical pits several centimeters in diameter (cryoconites). Scale is shown by glove which is approximately 35 cm long.



thick at 86°05'N and 21°59'E on 3 August 1987. Approximately the upper 1 m of the core (figure 5) represents the "classical" sequence from snow ice to granular ice and over the transition zone to extensive columnar ice. The uppermost and the second thin section photographs show vertical sections through the granular and transition zone to columnar ice. Visible inclusions of particulate material were only observed in the uppermost 0.09 m of this core.

The upper two fabric diagrams represent the c-axis distributions corresponding to the granular ice and the beginning of the columnar part of the ice core. Both the thin sections and the fabric diagrams support the structural classification as mentioned above (c.f. Weeks and Ackley, 1982; Gow et al., 1987). The c-axis of the frazil ice show the expected random distribution in directions, while the first columnar fabric diagram clearly shows the trend towards horizontal alignment of c-axis. The thin section of the transition zone ice displays the gradual increase in grain size as well as typical signs of congelation growth, i.e. brine pockets and the encroachment of large grains on smaller ones.

At around 1.10 m depth, a thin zone (about 3 cm) of granular ice, followed by a poorly defined transition zone most probably marks the beginning of a different floe that was rafted under the upper portion of the top floe. The band of granular ice represents the rapid filling of a gap that originated in the rafting event.

The middle thin section and fabric diagram show the typical characteristics of columnar ice, i.e. large, elongated crystals with strongly preferred horizontal c-axis orientations. The clearly defined azimuthal distribution of the c-axis orientations can be related to the under ice flow regime during growth of the ice cover (c.f. Weeks and Gow, 1978; Lange et al., in prep.). Both the salinity distribution, as well as profiles of  $O^{18}$  show similar patterns in the upper two columnar sections. This supports the hypothesis that this part of the core represents two rafted floes.

Between about 2.15 and 2.86 m a zone of granular and mixed granular/columnar ice is observed. This might indicate a second rafting event of a floe that again resulted in a large gap, which was subsequently mainly filled by granular ice. An alternative interpretation is that this zone represents quickly frozen meltwater that ran off the floe, either over the sides or through enlarged brine channels, and accumulated underneath the existing floe. This is a plausible hypothesis, since most of the melting probably represents accumulated, salt-poor snow with a freezing point above the ambient water temperature. The lowermost thin sections and fabric diagrams show a granular ice zone and a transition zone towards the bottom section of congelation ice, respectively. While the bottom-most fabric diagram shows the expected trend towards horizontal c-axis distribution, the supposed frazil fabric diagram displays a surprising concentration of c-axis directions towards the horizontal. This might indicate that characterization of this section as pure frazil ice is in error and has to be re-examined. The lower columnar section probably represents second year growth. Thus the floe may be characterized as two-year ice. This

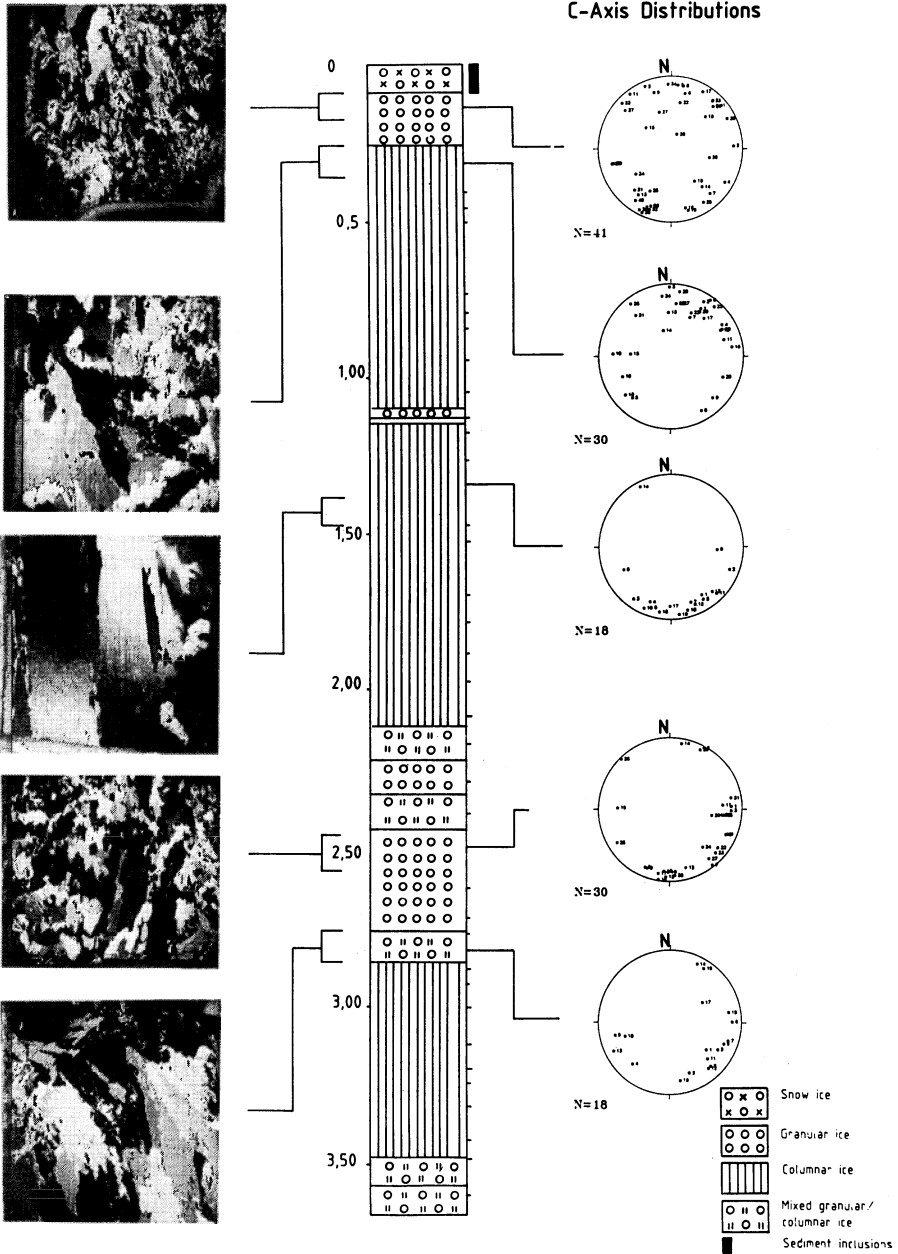


Figure 5 Example of sea ice texture analysed from thick and thin ice sections at 86° 05' N and 21° 59' E. Photographs on left show examples of ice crystal structure. C-axis analyses on right show crystal orientation.

supports the alternative interpretation of the granular section as refrozen summer meltwater run-off.

In summary, the texture of this core exemplifies the complex nature of the formation processes of sea ice in the Arctic Ocean. It is obvious that the approach of multiple measurements on the same core sections represents the most promising method to unravel the growth history of Arctic sea ice.

#### 4. Discussion

The fine grain size of most lithogenic material investigated to date is consistent with an aeolian origin but it does not exclude other sources such as fine-grained shelf and river sediments. Associated heterogeneous biogenic components indicate a variety of influences, terrestrial, fluvial and marine. The patchy distribution of "dirty" ice floes embedded in predominantly cleaner ice, and vice versa, indicates rafting of some floes from a source region with high particulate incorporation. Determining the origin and relative importance of various sources is the goal of present multidisciplinary investigations on the ice samples. Following, we discuss processes associated with sediment inclusions in eastern Arctic Basin sea ice and the potential atmospheric flux of lithogenic material to sea ice. Not considered are atmospheric fluxes of other aerosols, such as soot. Such particles will also have important effects on sea ice albedo (Clarke and Noone, 1985) and melting characteristics but discussion must await future analyses.

##### 4.1. Sea Ice Formation and Transport

An important source for sea ice in the Eurasian Basin is the Siberian shelf (e.g. Nansen, 1897; Koch, 1945; Colony and Thorndike, 1985). This continental shelf is shallow, broad, and influenced by river input, and therefore has the potential of including sediment in ice from marine, littoral, fluvial and aeolian sources (Larssen et al., 1987). Shelf or shorefast sea ice which escapes from the Laptev and East Siberian Seas and is included in the polar ice pack will generally be transported westward with the Transpolar Drift across the Eurasian Basin (figure 1; Nansen, 1897; Koch, 1945; Gordienko and Laktionov, 1969; Hibler, 1979; Colony and Thorndike, 1984). Much of this ice exits through Fram Strait (Colony and Thorndike, 1985) in the East Greenland Current after undergoing several years of melting, refreezing, and deformation. Based on analysis of particle content of sea ice samples, Nansen (1897) believed that particle-laden ice floes observed in the East Greenland Current contained biogenic and lithogenic material from along the Siberian coast.

The transit from north of the Siberian shelf to Fram Strait is thought to average about 2 to 3 years (Koch, 1945; Colony and Thorndike, 1985; Weeks, 1986) with a mean-maximum drift period of 5 years (Koerner, 1973). Ice is exported from both the Kara and Barents Seas to the Arctic Basin during winter and imported during summer (Zacharov, 1976; Vinje, 1985). In the Amerasian Basin, the sea ice rotates in the clockwise Beaufort Gyre (figure 1), and is generally older than Eurasian ice (Colony and Thorndike, 1985). A mean-maximum

drift period of 16 years was proposed by Koerner (1973). The Beaufort Sea is an important source for sea ice in this region (Colony and Thorndike, 1985).

#### 4.2. Surface Melting and Particle Redistribution

Multi-year ice in the Transpolar Drift will be exposed to several seasons of melting and freezing which will influence the characteristics of the sea ice and incorporated particles. Although changes in ice characteristics are relatively well known, processes involved in modification and redistribution of particles have not been extensively investigated.

According to Vowinckel and Orvig (1970), annual precipitation over the central Arctic Ocean is mainly in the form of snow and falls during autumn and late spring. The average annual water equivalent is approximately 13.5 cm, and snow thickness may reach a maximum of 35–40 cm by late spring (Vowinckel and Orvig, 1970). Surface melting of snow begins in late May–early June, and by July the ice is usually snow free (Vowinckel and Orvig, 1970, Barry et al., 1984). Meltpond coverage on multiyear ice may briefly reach values of 50 to 60%, but quickly decreases to about 30% once the snow cover has been removed (Maykut, 1985). Each year 40 to 50 cm of the upper sea ice column may melt in summer while new ice is added to the base of multiyear floes in fall and winter in the central Arctic (Nansen, 1897; Vowinckel and Orvig, 1970; Untersteiner, 1986). Undeformed multiyear ice thicknesses of 3–4 m are eventually attained (Maykut and Untersteiner, 1971; Hibler, 1979). Along the peripheral areas towards the American and Eurasian continents, melting of 1.5 to 2.0 m may occur (Vowinckel and Orvig, 1970).

Observations during our 1987 expedition indicated that extensive surface melting had occurred, affecting more than half of the ice surface in some regions. Surface melting will have several important effects:

1. Ablation of snow and sea ice with incorporated particles will result in surface accumulation of particles contained in the entire melted snow and sea ice column. A “dirty” brownish surface will form if particle concentration is high. This effect will be particularly important in multiyear floes. Sverdrup (1938) observed that material originally attached to the bottom of coastal sea ice, appeared at the ice surface after about 3 years. A consequence of extensive surface melting is that the original relationships between the melted snow/sea ice section and particle accumulations cannot be distinguished.
2. Biogenic material, primarily diatoms and algae may grow on the ice surface in association with accumulations of lithogenic material. This biogenic growth appears to be highly variable from year to year (e.g. Blessing in Gran, 1904).
3. Melting and surface material accumulations are interrelated, due to radiation absorption by particle accumulations. Vinje (1985) noted that the albedo of brownish ice in the Barents Sea was 5–10% less than that of melting ice, and may occur in quantities significant for the heat budget of the ice fields in the Barents Sea. Current models of sea ice albedo do not consider such extensive surface accumulations of biogenic and lithogenic material as observed during the 1987 expedition.

4. Due to higher absorption of solar radiation by surface material accumulations, cylindrical pits form on sea ice with accumulations of particles at the bottom (figure 4; Nansen, 1906; Poser, 1933; Crary, 1958; Barnes and Reimnitz, 1974). In the glaciological literature the cylindrical pits are known as dust wells or cryoconite holes ("Kryokonitlöcher") and the accumulations of particles are called cryoconites ("Kryokonit": Nordenskiöld, 1870; Brandt, 1931a,b and 1932; Steinbock, 1936; Wagner, 1938; Drygalski and Machatschek, 1942; Sharp, 1949; Hoinkes, 1956). Cryoconites generally include a mixture of biogenic and fine-grained lithogenic material. In thin floes, or where extensive melting occurs, the cryoconite holes may enlarge allowing particles to be released to the underlying water column. On the surface of thick multiyear floes, cryoconite accumulations may run off with meltwater if the floe tips or enough meltwater accumulates (Nansen, 1904). However, particles may also be retained in the cryoconite holes during meltwater runoff.
5. Material retained in cryoconite holes may accumulate into pellets containing biogenic and lithogenic material. Spherules of sediment 1 to 3 mm in diameter are often observed in sea ice (Poser, 1933; Barnes and Reimnitz, 1974; Osterkamp and Gosink, 1984). The 1–3 cm pellets we observed at the northernmost stations are larger and more cohesive than is usually described although mud balls with a maximum diameter of 2 cm were observed on Alaskan glaciers (Ray, 1935). Cohesion of these pellets could be enhanced over several freeze–thaw cycles by ice pressure, biologic activity, freeze–thaw consolidation (Barnes, pers. commun., 1988) and perhaps periodic desiccation.
6. Surface melting may also result in repositioning surface material along pre-existing brine channels. As brine channels enlarge during melting particulate material may be lost, provided connected brine channels exist that reach the bottom of the floe.

Shipboard observations of ridging on multiyear floes and preliminary ice texture analysis indicate that ice deformation and rafting may be extensive. As much as 40% of the total mass in the Arctic ice pack may be contained in deformation structures (Wadhams, 1980). Rafting under other ice floes will result in a complex ice stratigraphy and repositioning of surface particle accumulations. Such rafting events may explain the observations of subsurface layers with particle accumulations.

#### 4.3. Ice Floe Disintegration and Particle Release

Release of particulate material from sea ice is not well understood. Because incorporated material, of aeolian and other origins, is concentrated mostly at the ice surface in multiyear floes, it appears likely that deposition on the sea floor will occur primarily along the drift path of the ice floe as it finally disintegrates. As noted above, deposition may also occur during seasonal melting. During ice rafting events some particles may be scraped or washed off of the submerged floe, resulting in release to the water column (Nansen, 1904). In addition, wave and water action along the periphery of the ice floes will result in release of particles and cryoconite deposits (Poser, 1933) along the edges of the floe.

Sea ice concentration in the marginal ice zone of Fram Strait is dependent on the radiation balance, waves, winds and eddies (Gascard et al., 1988). Thus, greatest ice floe disintegration, and therefore potential for sediment deposition, is expected to occur along the ice margin, near polynyas and large leads (figure 1). These regions are located mostly along the Arctic Basin perimeter, in the Fram Strait or in the Norwegian–Greenland and Barents seas. In particular, deposition of ice–rafted sediments is expected to occur along the East Greenland margin where ice is rapidly (about 10–30 cm/sec; Vinje and Finnekåsa, 1986) advected into a region of melting (figure 1). Gow et al. (1987) estimated that during June and July 1984 more than 75% of the ice in this region was multiyear ice (most likely less than 4–5 years old) and much of it was deformed. These authors note that the sampled ice appeared to be remarkably free of particulate material. This observation indicates either that the ice was not originally formed on the Siberian shelf, or that if the ice was formed there then sediment incorporation is patchy or particulate material was already been released to the water column.

Cryoconite formation and aggregation of sediment in multiyear ice is important to understand because it may result in accelerated settling of fine–grained material released from disintegrating ice floes. Cohesive cryoconite pellets may settle intact to the sea floor. If the cohesive pellets form during freeze–thaw cycles, accumulations of such deposits in sea floor sediments may indicate deposition from sediment–laden ice which has experienced extensive surface melting/refreezing. However, pellets are also formed in glacier ice (Ovenshine, 1970). Observation of pelletoids with heterogeneous composition in deep–sea cores has been attributed to iceberg rafting (Clark et al., 1980; Goldstein, 1983; Minicucci and Clark, 1983). Analysis of biogenic components may aid in distinguishing between sea ice and iceberg rafted pellets (P. Mudie, pers. commun., 1987).

#### 4.4. Aeolian Deposition of Lithogenic Particles

Most of the aeolian material deposited in the Arctic Basin will settle on sea ice. Winter ice cover within the central Arctic region is generally thought to be greater than 95% (Koerner, 1973; Hibler, 1979). In summer, it disappears entirely in many marginal seas (figure 1), and decreases within some parts of the central region by about 10–20% (Hibler, 1979; Maykut, 1985).

Aeolian fluxes of particles measured on the Greenland ice sheet and in snow samples from the Amerasian Basin may be considered for estimation of fluxes in the Eurasian Basin. Fluxes on Greenland show large seasonal variation with maximum deposition in spring (Hammer, 1977a; Langway et al., 1977; Thompson, 1977; Steffenson, 1988). Seasonal variations in particle flux are thought to be associated with the autumn movement of the atmospheric Polar Front to the south (figure 1), permitting influx of dust to the polar air mass from continental sources during winter (Heidam, 1984; Barrie, 1986; Steffenson, 1988). The Arctic reservoir therefore has highest dust content in spring just before the Polar Front moves north and is isolated from the major sources (Steffenson, 1988).

Because of high elevation and distance from local sources, deposition of particles on ice sheets such as Greenland provide information mainly on the distant tropospheric aerosol (Junge, 1977; Steffensen, 1985). Dust content of Greenland snow may therefore be used as the minimum value to be expected for snow falling on Arctic sea ice. According to Windom (1969), mineral dust accumulated at 21 mg/(cm<sup>2</sup>1000yrs) in a northwestern Greenland snowfield (79° 59'N and 56° 04'W, elevation 2000m). It consisted of about 37% mica, 23% quartz and 16% feldspar and the largest particles were 40 µm. Wagenbach and Geis (this volume) calculated a mineral dust input of 4.7 µg/(cm<sup>2</sup>yr) from Boutron's (1978) reported average Al content for a transect across the Greenland plateau. Grain sizes of particles tend to be between 0.1 < R < 2 µm (Hammer et al., 1985). Sources for terrigenous dust are thought to be dry regions in North America (Hammer, 1977b, 1978; Gayley and Ram, 1985) and Eurasia (Davidson et al., 1985). These sources are similar to the regions proposed as sources for Arctic haze pollutants and crustal aerosol (Rahn et al., 1977; Rahn and McCaffrey, 1980; Davidson et al., 1985; Barrie, 1986). The composition of Arctic haze greatly resembles that of the Saharan aerosol (K.A. Rahn, L. Schütz and R. Jaenicke, unpublished data cited in Rahn et al., 1977).

Four snow samples (Mullen et al., 1972) from the Arctic ice island T-3 had an average particle fallout rate of 14 µg/(cm<sup>2</sup>yr) (1.04 mg/kg (Darby et al., 1974)), and the particles were mostly less than 2 µm in diameter. In a later study, Darby et al. (1974) investigated snow samples obtained approximately 500 km north of the Alaskan north coast. Total particle fallout rates were calculated at 3.3 µg/(cm<sup>2</sup>yr) (0.36 mg/kg). The grain size of these particles was mostly less than 5 µm and the average grain size > 5 µm was 18 µm. One sample was determined to consist of about 50% biogenic material. Mullen et al. (1972) and Darby et al. (1974) estimated that if airborne dust observed in these snow samples is deposited on the sea floor, it may contribute 0.09 mm to 0.02 mm/1000yr (respectively) of sediment in the Amerasian Basin.

Based on these investigations, the minimum average atmospheric deposition of lithogenic dust on sea ice in the Arctic Basin may be expected to range between 3.3 to 21 µg/(cm<sup>2</sup>yr) (Windom, 1969; Mullen et al., 1972; Darby et al., 1974; Wagenbach and Geis, this volume). Even if the sea ice was relatively old, for example 5 years, only small surface accumulations would be expected from these annual fluxes: 0.02 - 0.13 mm/yr × 5 years = 0.1 - 0.65 mm (assuming a sediment density of 1.6 g/cm<sup>3</sup> and complete snow melting). Because ice in the Beaufort Sea is generally older than ice in the Transpolar Drift region, total surface accumulations of atmospheric dust may be greater on sea ice in the Amerasian Basin. However, atmospheric deposition rates of dust might be expected to be higher in the Eurasian Basin because it is closer to proposed long range European and Asian sources. Also average wind velocities are higher than in the Amerasian Basin (figure 1), perhaps resulting in greater particle transport.

The particle accumulations observed in our surface samples and by Larssen et al. (1987) appear too high to be explained entirely by aeolian deposition, unless intense dust storms transport sediment onto the ice. Jackson et al. (1973) estimate that vertical fluxes of soil-derived aerosols can reach the order of 10 µg/(cm<sup>2</sup>sec) locally during dust storms.

Around the perimeter of the Arctic Basin, it is possible that locally-derived wind-blown dust from snow and ice free terrain onto the near shore regions contribute significantly to the particle content of the sea ice surface (Kindle, 1924). Maykut (1985) notes that areally averaged albedos may be lowered in regions where dust is deposited from nearby land areas. On pack ice, blowing snow and local wind transport may also redistribute particulate material from regions with high surface accumulations.

Because the Siberian shelf is proposed as a source for much of the multiyear ice in the Transpolar Drift, wind conditions on this shelf are of special interest. The following summary is abstracted from Borisov (1965). Along the northern coast of Siberia there is a general monsoonal circulation. Winds blow from the continent to the Arctic Basin in winter and in summer winds are from the sea. In the Kara Sea in winter, winds are mainly southeasterly averaging 8–9 m/sec, while in summer the winds are northeasterly and about 5–6 m/sec. Wind velocities sometimes reach 40–50 m/sec in the southern part of the sea during boras. In the Laptev Sea the winter winds are generally light and from the south and south-east with strong winds during rare periods when depressions penetrate from the Kara Sea. During July and August the winds are strong and are predominantly from westerly and northwesterly directions. In the East Siberian Sea cold southerly and southeasterly winds from land prevail from October to May. Northwesterly winds are more frequent in eastern half of the seas. In summer, cool northwesterly winds from the Arctic Ocean occur in the western half with southeasterly winds prevailing in the eastern half of the seas. Thus, aeolian transport to Siberian shelf sea ice may occur during winter monsoonal winds from the land, but will depend on specific wind, snow, soil and sea ice characteristics.

## **5. Aeolian Deposition during the Last Glacial Maximum in the Arctic Basin**

During the last glacial maximum the Arctic environment was very different than it is today. At maximum glaciation, ice sheets covered much of northern North America and Greenland, northern Europe, western Asia and the Barents and Kara Seas. Extensive loess deposits, sand dunes and deserts formed south of the continental ice sheets in response to strong winds and arid climate (Flint, 1971; Sarnthein, 1978). Sea level was lower, exposing Siberian continental shelves and closing the Bering Strait. The oceanic Polar Front was displaced from the Norwegian–Greenland Sea to well south of the Greenland–Faroe Ridge. Perennial sea ice is thought to have covered the entire Arctic Ocean and a considerable portion of the Norwegian–Greenland Sea (CLIMAP, 1976; Kellogg, 1977, 1980; Gard, 1988).

Observations of continental dust in concentrations 3 to 70 times higher than today in Greenland ice older than 10,750 years indicate increased aeolian transport in the Arctic during the glacial maximum (Petit et al., 1981; Thompson and Mosley–Thompson, 1981; Hammer et al., 1985; Paterson and Hammer, 1987). At the end of the last glacial maximum, average particle concentrations were about 12 times that observed in post-glacial ice in the Greenland Camp Century core (Thompson and Mosley–Thompson,



1981). Rapid fall-off in concentration of particles occurred during the transition into the Holocene (Thompson and Mosley-Thompson, 1981). Reduced precipitation during the glacial maximum would account for a factor of 2 to 3 increase in particle concentration (Paterson and Hammer, 1987). According to Thompson (1977) the fraction of large particles, greater than or equal to 1.65  $\mu\text{m}$ , decreases in the Wisconsin ice, while the total number of particles increases. Although an increase in particles is also observed in Antarctic ice cores during the last, and previous glacial maxima (Petit et al., 1981; Thompson and Mosley-Thompson, 1981; De Angelis et al., 1987), the Arctic dust contains a large alkaline component (Hammer et al., 1985) indicating a different source.

Models proposed for Arctic atmospheric circulation during the glacial maximum do not point to a specific source for the dust, although general flow appears to have been from west to east. Lamb (1977) notes that there was a reversal of atmospheric circulation over the inner Arctic with cyclonic (counterclockwise) rotation. The atmospheric general circulation models of Manabe and Broccoli (1985) and Kutzbach and Guetter (1986) also indicate strong westerly flow along the northern flanks of the Laurentide and Eurasian ice sheets. Hammer et al. (1985) stated that the high dust concentrations observed in the Greenland ice are most likely caused by large source regions for loess. But based on the increased content of calcium-rich carbonates in this predominately silicate dust (Thompson 1977), a new source of alkaline aerosol from exposed high and mid-latitude continental shelves was proposed by Cragin et al. (1977) and Hammer et al. (1985). Fisher (1979) and Hammer et al. (1985) specifically proposed the exposed Siberian and Alaskan shelves as a large source region. Vast areas of the eastern Siberian shelf (northern Yakutia) are apparently covered by loess (Tomirdiaro, 1984) or loess-like (Konishchev, 1987) silts. The silts contain ice, are saline, are saturated with pollens of grasses, and have grain sizes largely in the range of 10–30  $\mu\text{m}$ . Tomirdiaro (1984) proposes that wind transport may have been onshore, based on high salinity of deposits in the Lena River basin. Konishchev (1987) has disputed the proposed aeolian nature of these sediments. No comment was made on the carbonate content. At least the modern surface sediments in the East Siberian Sea, which appear to have a large river influence, do not appear to contain calcium carbonate (based on 147 samples, Naugler et al., 1974). Other possible sources for the Greenland dust are exposed shelf regions in mid-latitudes or continental regions. For example, Eurasian and North American loess deposits are also carbonate-rich (Taylor et al., 1983; Wright, 1987, respectively).

Although the specific source is not known, large quantities of continental dust must have been transported a long distance in order to form the deposits observed in the Greenland ice cores during the glacial maximum. Fisher (1979) noted that dust would have blanketed all the Arctic ice cover during the late Wisconsin period. If annual fluxes of fine-grained material were 1–25 times higher than today (reducing the 3–70 times observed for the Greenland ice by about a factor of 3 to account for decreased precipitation (Paterson and Hammer, 1987)), minimum fluxes on the order of 10–100's  $\text{ug}/(\text{cm}^2\text{yr})$  might be expected on the Arctic ice pack during portions of the last glacial period. In addition, a coarser component might have been deposited. Research on modern wind transport indicates that up to about 1000 to 2000 km from the source (depending on the strength of the aeolian

transport, Sarnthein et al., 1981), the size of aeolian material continually decreases due to deposition of the larger grain size material (Schütz, 1980; Janecek and Rea, 1985). The distance to Greenland, directly over the North Pole from the Siberian Shelf, is more than 2000 km. Therefore, if Europe or Asia was a source for dust deposited on Greenland, by inference large quantities of dust composed of the larger size fraction of resuspended calcium-rich carbonates and silicates probably were also deposited on sea ice of the Arctic Basin. In particular, high deposition rates may have occurred in the vicinity of the exposed Siberian and Alaskan shelves.

High aeolian particle flux in the absence of increased snowfall would reduce ice albedo. For example, particle concentrations of  $0.1 \text{ mg/cm}^3$  in surface snow in central Japan resulted in an albedo of about 60% (Higuchi and Nagoshi, 1977). Particle concentrations of  $3 \text{ mg/cm}^3$  reduced the albedo to about 20%. If ambient temperatures are near the freezing point, increased absorption of solar radiation may lead to surface melting, further reducing surface albedo. Areal averaged albedos as low as 20% have been reported from nearshore sea ice influenced by extensive seasonal melting (Langleben, 1966). Similarly low albedos (20–30%) have been recorded over wet, dirty snow (Warren and Wiscombe, 1980), and a mid-summer, mature meltpond may have a total albedo of 22–29% (for clear and overcast skies, respectively, Grenfall and Maykut, 1977). If surface sediment concentrations are too high, melting is reduced. Experiments conducted by Higuchi and Nagoshi (1977) show that maximum melting of snow was observed when a layer of sand 0.5 cm thick was spread over the snow surface. If the sand layer is more than 2 cm thick, melting of snow is reduced.

Global cooling of 2–3° C due to an increase in atmospheric aerosols at the end of the last glacial maximum has recently been proposed (Harvey, 1988). However, possible surface particle accumulations on sea ice have not been considered in the atmospheric general circulation models constructed to date for glacial environments. Manabe and Broccoli (1985) used a thick sea ice albedo of 70% north of 66.5°N, reducing it to 45% when surface temperature reached the melting point to reflect the presence of meltwater ponds. Kutzbach and Guetter (1986) used an average sea ice albedo of 70%.

Under present conditions, a 15 to 20% decrease in summer albedo would result in complete disappearance of perennial Arctic ice (Maykut and Understeiner, 1971; Maykut, 1985). In view of the generally colder surface temperatures during the last glacial maximum most likely prohibiting seasonal surface melting, it is not clear what effect increased dust content of surface snow from long range sources would have. Bloch (1965) proposed that redistributed loess could cause discolorations of Arctic ice masses and reverse the balance of radiation, pushing back the limits of the glaciers of the north polar sea. However, Cragin et al. (1977) note that increased dust content in the Greenland glacial ice did not cause visible dust layers.

Minicucci and Clark (1983) believe that wind-blown loess contributed significantly to sea ice sedimentation during glacial maxima, forming silty lutites on the sea floor of the Amerasian Basin. In order for sea-floor sedimentation from sea ice and atmospheric

deposition to occur, periodically open water or disintegration of ice floes (perhaps accelerated by sediment accumulations?) may have occurred. Sediment may also have been washed from the ice surface during ice rafting events. The observed sedimentation rates, on the order of 1–3 mm/1000yrs (Clark et al., 1986; Morris, 1988; Thiede et al., 1988), could be achieved by a flux of 160–480 ug/(cm<sup>2</sup>yr) (assuming a sediment density of 1.6 g/cm<sup>3</sup>). This flux is of the same order as the higher end of the range of fluxes estimated above (order of 10–100's ug/(cm<sup>2</sup>yr)) for the long range component of wind-blown dust on the Arctic ice pack. Other possible sources for Arctic deep sea lithogenic sediments during the last glacial maximum are 1) deposition from sea ice of sediment with sources other than long range aeolian deposition, 2) iceberg rafting, 3) distal turbidite deposition and 4) redistribution by ocean currents of sediments resuspended from the sea floor, contributed by eastern Siberian river run-off or discharged in turbid glacial meltwater.

Ice drift paths and melting locations during glacial maxima must have been very different than today. Presently winds determine to a large degree the mean ice movement in the Arctic Basin (Thorndike and Colony, 1982; Colony and Thorndike, 1984; McLaren et al., 1987). By analogy to the modern situation, high velocity (5–10 m/s, Kutzbach and Guetter, 1986) westerly winds during the last glacial maximum along the northern flanks of the ice sheets (Lamb, 1977; Manabe and Broccoli, 1985) may have resulted in reversal of surface ocean and sea ice circulation to form a cyclonic gyre around the North Pole (Lamb, 1977).

Along the East Greenland margin, Manabe and Broccoli (1985) and Kutzbach and Guetter (1986) show strong northerly winds in winter (during summer, Kutzbach and Guetter (1986) show southerly winds in this region). The flow of cold air is considered responsible for formation of thick sea ice in this region. It may also have increased southerly transport of sea ice from the Arctic to the Norwegian–Greenland Sea. However, ice transport through Fram Strait may have been restricted. Lowered sea level could expose banks along the East Greenland margin, narrowing Fram Strait by about one-fourth. Also perennial sea ice cover on the northern Norwegian–Greenland Sea (CLIMAP, 1976; Kellogg, 1977, 1980; Gard, 1988) may have hindered ice movement through Fram Strait.

Therefore it is not known to what degree Arctic sea ice and incorporated sediment would be rafted into the Norwegian–Greenland Sea. Ruddiman and McIntyre (1977) envisage that limited melting of sea ice and icebergs occurred north of the oceanic Polar Front, allowing ice to pass southeastward with minimal loss of load. It is clear from analysis of upper Quaternary sediments in the North Atlantic and the Norwegian–Greenland Sea by Kolla et al. (1979) that the location of quartz depocenters shift between the Holocene surface layer and sediments deposited during the last glaciation. Similarities between patterns of quartz accumulation and ice-rafted sediment in the North Atlantic (> 63 µm, Ruddiman 1977a,b) indicate that quartz distribution is probably related to ice rafting (Kolla et al., 1979). Samples are lacking from the western Norwegian–Greenland Sea which is presently covered by sea ice. In the absence of information on this area, two main regions of modern accumulation of ice-rafted quartz-rich sediments are defined by Kolla et al. (1979): in the Irminger Basin south of Denmark Strait and east of Labrador–Newfoundland

(although this may include reworked deposits) where accumulation rates are greater than 50 mg/(cm<sup>2</sup>1000yrs). In the North Atlantic during the last glacial maximum, a depocenter for quartz-rich sediments existed at 45°N and 28°W, indicating a locus for ice rafting and melting along the northern border of the 18,000 BP oceanic Polar Front (CLIMAP, 1976; Kolla et al., 1979; Ruddiman and McIntyre, 1977). In the central Norwegian Sea, similarly high quartz percentages (>15 % of carbonate-free sediments) are observed (Kolla et al., 1979). Other sources for deep sea lithogenic sediment, besides sea ice and iceberg rafting, may have been glacial meltwater discharge, and redistribution of sea-floor sediments by ocean currents, turbidity currents and debris flows.

During deglaciation of the Arctic Basin margin, flooding of continental shelves and glacier retreat with associated extensive calving of icebergs, sediment entrainment by sea ice, and discharge of sediment-laden rivers and glacial meltwater would provide increased sediment input to the Arctic deep sea region. In the Amerasian Basin foraminifer-poor sandy lutites with associated erratics, pelletal mud clasts, and pink-white and white layers have been described (Clark et al., 1980). These sediments are interpreted by Minicucci and Clark (1983) to represent increased calving of glacial ice along the basin margin following glacial maxima, and deposition from icebergs in the central Arctic region with comparatively little contribution from aeolian sources.

## 6. Summary

The primary finding from geologic investigations of Eurasian sea ice is that in the region of the Transpolar Drift the ice surface contains a large amount of particulate material, lithogenic and biogenic, often affecting more than half of the ice surface. Part of the material is undoubtedly accumulated from long range atmospheric deposition, but the concentrations appear too large for this to be the only process. Following Nansen (1897) and Larssen et al. (1987), we propose that particles are also incorporated in ice when it forms on the Siberian shelf region. Particles may be derived from biogenic, aeolian, fluvial, littoral and marine sources.

During transport with the Transpolar Drift, seasonal melting results in accumulation of particulate material as cryoconites at the ice surface in small pockets and cylindrical pits. In addition, diatoms and other biogenic material grow on the ice surface in summer. From observations of Blessing during Nansen's FRAM expedition it appears that this growth does not occur every year (reported in Gran, 1904).

As yet unresolved are the processes involved in release of particles from sea ice to the water column. Some deposition may occur during ice rafting events and seasonal melting. However, the bulk of incorporated sediments may be released in regions where the entire ice floe melts and disintegrates. If this is true, deposition should occur mainly along the East Greenland margin. Here particle-laden multiyear ice, transported with the Transpolar Drift from the Siberian shelves, is advected into a region of melting. Cryoconite formation may be important in accelerating deposition by aggregating fine-grained material into

more or less cohesive pellets. Horizons of such pellets in marine sediments may indicate disintegration regions of sediment-laden ice which has experienced extensive melting/refreezing.

During the last glacial maximum, westerly winds along the northern flanks of the continental ice sheets (Lamb, 1977; Manabe and Broccoli, 1985; Kutzbach and Guetter, 1986) most likely caused reversal of the modern sea ice circulation to form a counterclockwise gyre in the Arctic Basin (Lamb, 1977).

High concentrations of particles in Greenland ice older than 10,750 years and formation of continental loess and sand dune deposits, indicate that long range aeolian dust transport was significantly greater during the last glacial maximum in the Northern Hemisphere (e.g. Flint, 1971; Sarthein, 1978; Fisher, 1979; Petit et al., 1981; Thompson and Mosley-Thompson, 1981; Hammer et al., 1985; Paterson and Hammer, 1987). The Arctic sea ice surface most likely received correspondingly increased deposition of aeolian dust. Accumulations of silty lutite in the Amerasian Basin during glacial maxima, proposed to be derived from wind-blown loess onto sea ice (Minicucci and Clark, 1983), would indicate periodic deposition from the ice pack.

Many questions posed in this paper will be answered when analyses of investigations conducted during the 1987 expedition are completed. In addition to our ice analyses, studies are presently being carried out on the following subjects (Thiede, 1988): pollen, spores and dinoflagellates in surface snow and sea floor sediment samples by P. Mudie and chrysophytes and archeomonads by S. Lichti-Federovich at Atlantic Geoscience Center/Bedford Institute of Oceanography; diatoms and radiolarians from the ice surface by A. Abelmann at Alfred-Wegener-Institut für Polar- und Meeresforschung; chemistry and origin of surface waters by L. Anderson at University of Göteborg and E.P. Jones at Bedford Institute of Oceanography; particle flux and under-ice currents by S. Honjo at Woods Hole Oceanographic Institution; and ice transport and possible deposition locations of ice rafted debris will be determined in cooperation with J.-C. Gascard at the University of Paris and his deployment of satellite-tracked buoys on the ice.

## 7. Acknowledgements

We thank J.-C. Gascard, Laboratoire d'Océanographie Dynamique et de Climatologie, Paris, for discussion of sea ice melt patterns. Peter Schlosser, Institut für Umweltphysik, Heidelberg, provided preliminary results of the pilot  $^{18}\text{O}$  analyses. A. Elverhøi, Norsk Polarinstitut, Oslo and P.W. Barnes, U.S. Geological Survey, Menlo Park, provided valuable comments on the manuscript. E. Reimnitz, U.S. Geological Survey, Menlo Park, brought to our attention the translation of Tomirdiaro's 1976 work. Some sampling equipment and materials were kindly provided by J.-C. Gascard and S. Honjo, Woods Hole Oceanographic Institution. We would like to thank RV POLARSTERN's operating institution, the Alfred-Wegener Institute for Polar and Marine Research, Bremerhaven; the Captain, Heinz Jonas and crew of RV POLARSTERN; and the pilot, Günther Mahler and technician, Volker Lundström from Helicopter Service, Wasserthal. This research was supported by U.S. Office of Naval Research contract N00014-85-G-0124 and the

Bundesministerium für Forschung und Technologie, F.R. Germany. This is contribution number 112 of the Alfred-Wegener Institute for Polar and Marine Research.

## 8. References

- Barnes, P.W. and E. Reimnitz: 1974, 'Sedimentary processes on Arctic Shelves off the northern coast of Alaska', in: J.C. Reed and J.E. Sater (eds.) *The Coast and Shelf of the Beaufort Sea*, Arctic Institute of North America, Arlington, Virginia, pp. 439–476.
- Barnes, P.W., E. Reimnitz, D. Fox: 1982, 'Ice rafting of fine-grained sediment, a sorting and transport mechanism, Beaufort Sea, Alaska', *J.Sediment.Petrol.* 52(2), 493–502.
- Barrie, L.A.: 1986, 'Arctic air pollution: an overview of current knowledge', *Atmosph.Environ.* 20(4), 643–663.
- Barrie, L.A. and R.M. Hoff: 1984, 'The oxidation rate and residence time of sulphur dioxide in the Arctic atmosphere', *Atmosph.Environ.* 18(12), 2711–2722.
- Barry, R.G., A. Henderson-Sellers, K.P. Shine: 1984, 'Climate sensitivity and the marginal cryosphere', in: J.E. Hansen and T. Takahashi (eds.) *Climate Processes and Climate Sensitivity*, Geophysical Monograph 29, Maurice Ewing Volume 5, American Geophysical Union, Washington, D.C., pp.221–237.
- Bloch, M.R.: 1965, 'A hypothesis for the change of ocean levels depending on the albedo of the polar ice caps', *Palaeogeogr.Palaeoclimatol.Palaeoecol.* 1, 127–142.
- Borisov, A.A.: 1965, '*Climates of the U.S.S.R.*', Adline Pub.Co., Chicago, 255 pp.
- Boutron, C.: 1978, 'Influence des aérosols naturels et anthropogénic sur la géochimie des neiges polaires', Thesis, University of Grenoble, Grenoble, France.
- Brandt, B.: 1931a, 'Über Kryokonit in der Magdalenenbucht in Spitzbergen', *Zeit.f.Gletscherk.* 19, 125–126.
- Brandt, B.: 1931b, 'Kryokonit auf Flusseis in Mitteleuropa', *Zeit.f.Gletscherk.* 19, 317–320.
- Brandt, B.: 1932, 'Beobachtungen und Versuche über die Entwicklung der Kryokonitformen', *Zeit.f.Gletscherk.* 20, 84–93.
- Clark, D.L., M. Andree, W.S. Broecker, and A.C. Mix: 1986, 'Arctic Ocean chronology confirmed by accelerator <sup>14</sup>C dating', *Geophys.Res.Lett.* 13(4) 319–321.
- Clark, D.L. and A. Hanson: 1983, 'Central Arctic Ocean sediment texture: Key to ice transport mechanisms', in B.F. Molnia (ed.): *Glacial-Marine Sedimentation*, Plenum Press, pp. 301–330.
- Clark, D.L., R.R. Whitman, K.A. Morgan, and S.D. Mackay: 1980, 'Stratigraphy and glacial-marine sediments of the Amerasian Basin, central Arctic Ocean', *Geol.Soc.Am.Spec.Paper* 181, 57 pp.
- Clarke, A.D. and K.J. Noone: 1985, 'Soot in the Arctic snowpack: A cause for perturbations in radiative transfer', *Atmos.Env.* 19(12), 2045–2053.

- CLIMAP Project Members: 1976, 'The surface of the ice-age earth', *Science* 191, 1131–1137.
- Colony, R. and A.S. Thorndike: 1984, 'An estimate of the mean field of Arctic sea ice motion', *J.Geophys.Res.* 89(C6), 10623–10629.
- Colony, R. and A.S. Thorndike: 1985, 'Sea ice motion as a drunkard's walk', *J.Geophys.Res.* 90(C1), 965–974.
- Cragin, J.H., M.M. Herron, C.C.Jr. Langway, G. Klouda: 1977, 'Interhemispheric comparison of changes in the composition of atmospheric precipitation during the late Cenozoic era', in M.J. Dunbar (ed.) *Polar Oceans*, Proc. Polar Oceans Conf., McGill Univ. Montreal, May 1974, Calgary, Alberta, Arctic Inst. North Am., pp. 617–631.
- Crary, A.P.: 1958, 'Arctic ice island and ice shelf studies', *Arctic* 11,(1), 3–42.
- Darby, D.A., L.H. Burckle, and D.L. Clark: 1974, 'Airborne dust on the Arctic pack ice, its composition and fallout rate', *Earth Planet.Sci.Lett.* 24, 166–172.
- Davidson, C.I., S. Santhanam, R.C. Fortmann, and M.P. Olson: 1985, 'Atmospheric transport and deposition of trace elements onto the Greenland Ice Sheet', *Atmos.EnvIRON.* 19, 2065–2081.
- De Angelis, M., N.I. Barkov, and V.N. Petrov: 1987, 'Aerosol concentrations over the last climatic cycle (160 kyr) from an Antarctic ice core', *Nature* 325, 318–321.
- Drewry, D.: 1986, *Glacial Geologic Processes*, Edward Arnold Ltd, London, 276 pp.
- Drygalski, E.v. and F. Machatschek: 1942, *Gletscherkunde*, Franz Deuticke, Wien.
- Fisher, D.A.: 1979, 'Comparison of 10<sup>5</sup> years of oxygen isotope and insoluble impurity profiles from the Devon Island and Camp Century Ice Cores', *Quat.Res.* 11, 299–305.
- Flint, R.F.: 1971, *Glacial and Quaternary Geology*, John Wiley and Sons, Inc. New York, 892 pp.
- Gard, G.: 1988, 'Late Quaternary calcareous nannofossil biochronology and paleo-oceanography of Arctic and Subarctic seas', *Meddel.Stockholms Universitets Geologiska Inst.* 275, 8–45.
- Gascard, J.-C., C. Kergomard, P.-F. Jeannin and M. Fily: 1988, 'Diagnostic study of the Fram Strait marginal ice zone during summer from 1983 and 1984 Marginal Ice Zone Experiment Lagrangian observations', *J.Geophys.Res.*, 93(C4), 3613–3641.
- Gayley, R.I. and M. Ram: 1985, 'Atmospheric dust in polar ice and the background aerosol', *J.Geophys.Res.* 90(D7), 12921–12925.



Goldstein, R.H.: 1983, 'Stratigraphy and sedimentology of ice-rafted and turbidite sediment, Canada Basin, Arctic Ocean', in B.F. Molnia (ed.): *Glacial-Marine Sedimentation*, Plenum Press. pp. 367-400.

Gordienko, P.A. and A.F. Laktionov: 1969, 'Circulation and physics of the Arctic basin waters', in *Annals of the International Geophysical Year, Oceanography*, Pergamon, New York 46, 94-112.

Gow, A.J., W.B. Tucker, III and W.F. Weeks: 1987, 'Physical properties of summer sea ice in the Fram Strait, June-July 1984'. *CRREL-Rep.* 87-16.

Gran, H.H.: 1904, 'Diatomaceæ from the ice-floes and plankton of the Arctic Ocean', in F. Nansen (ed.), *The Norwegian North Polar Expedition 1893-1896*, Scientific Results, 4(11), Oslo.

Grenfall, T.C. and G.A. Maykut: 1977, 'The optical properties of ice and snow in the Arctic Basin', *J. Glaciol.* 18, 445-463.

Hammer, C.U.: 1977a, 'Dating of Greenland ice cores by microparticle concentration analyses', in *Isotopes and Impurities in Snow and Ice*, Proc. IUGG Symp., Grenoble, August-September 1975, IAHS-AISH Publ. No. 118, pp. 297-301.

Hammer, C.U.: 1977b, 'Dust studies on Greenland ice cores', in *Isotopes and Impurities in Snow and Ice*, Proc. IUGG Symp., Grenoble, August-September 1975, IAHS-AISH Publ. No. 118, pp. 365-370.

Hammer, C.U., H.B. Clausen, W. Dansgaard, N. Gundestrup, S.J. Johnsen, and N. Reeh: 1978, 'Dating of Greenland ice cores by flow models, isotopes, volcanic debris, and continental dust', *J. Glaciol.* 20(82), 3-26.

Hammer, C.U., H.B. Clausen, W. Dansgaard, A. Neftel, P. Kristinsdottir, and E. Johnson: 1985, 'Continuous impurity analysis along the Dye 3 deep core', in *Greenland Ice Core: Geophysics, Geochemistry, and the Environment*, Geophysical Monograph 33, American Geophysical Union, Washington, D.C. pp. 90-94.

Harvey, L.D.D.: 1988, 'Climatic impact of ice-age aerosols', *Nature* 334, 333-335.

Heidam, N.Z.: 1984, 'The components of the Arctic aerosol', *Atmos. Environ.* 18(2), 329-343.

Hibler, W.D. III: 1979, 'A dynamic thermodynamic sea ice model', *J. Phys. Ocean.* 9, 815-846.

Higuchi, K. and A. Nagoshi: 1977, 'Effect of particulate matter in surface snow layers on the albedo of perennial snow patches', in *Isotopes and Impurities in Snow and Ice*, Proc. IUGG Symp., Grenoble, August-September 1975, IAHS-AISH Publ. No. 118, 95-97.

Hoinkes, H.: 1956, 'Die Bedeutung des aufgefrorenen Eises (superimposed ice) für die Entstehung von Kryokonitlöchern', *Zeit. Gletscherk.* 3, 305-312.

- Jackson, M.L., D.A. Gillette, E.F. Danielsen, I.H. Blifford, R.A. Bryson, and J.K. Syers: 1973, 'Global dustfall during the Quaternary as related to environments', *Soil Sci.* 116(3), 135-145.
- Janecek, T.R. and D.K. Rea: 1985, 'Quaternary fluctuations in the Northern Hemisphere trade winds and westerlies', *Quat. Res.* 24, 150-163.
- Junge, C.E.: 1977, 'Processes responsible for the trace content in precipitation', in *Isotopes and Impurities in Snow and Ice*, Proc. IUGG Symp., Grenoble, August-September 1975 IAHS-AISH Publ. No. 118, pp. 63-77.
- Kellogg, T.B.: 1977, 'Paleoclimatology and paleo-oceanography of the Norwegian and Greenland Seas: the last 450,000 years', *Mar. Micropaleon.* 2, 235-249.
- Kellogg, T.B.: 1980, 'Paleoclimatology and paleo-oceanography of the Norwegian and Greenland Seas: glacial-interglacial contrasts', *Boreas* 9, 115-137.
- Kindle, E.M.: 1924, 'Observations on ice-borne sediments by the Canadian and other Arctic expeditions', *Am. J. Sci.* 7, 251-286.
- Koch, L.: 1945, 'The East Greenland Ice', *Meddelelser om Grønland* 130(3), 373 pp.
- Koerner, R.M.: 1973, 'The mass balance of the sea ice of the Arctic Ocean', *J. Glaciol.* 12(65), 173-185.
- Kolla, V., P.E. Biscaye, and A.F. Hanley: 1979, 'Distribution of quartz in Late Quaternary Atlantic sediments in relation to climate', *Quat. Res.* 11, 261-277.
- Konishchev, V.N.: 1987, 'Origin of loess-like silt in northern Yakutia, USSR', *GeoJournal* 15(2), 135-139.
- Kutzbach, J.E. and P.J. Guetter: 1986, 'The influence of changing orbital parameters and surface boundary conditions on climate simulations for the past 18,000 years', *J. Atmosph. Sci.* 43(16), 1726-1759.
- Lamb, H.H.: 1977, *Climate: Present, Past and Future, Vol 2, Climatic History and the Future*, Methuen and Co., London, 835 pp.
- Lange, M.A.: 1988, 'Basic properties of Antarctic sea ice as revealed by textural analysis of ice cores', *Ann. Glaciol.* 10, 95-101.
- Langleben, M.P.: 1966, 'On the factors affecting the rate of ablation of sea ice', *Can. J. Earth Sci.* 3, 431-439.
- Langway, C.C.Jr., G.A. Klouda, M.M. Herron and J.H. Cragin: 1977, 'Seasonal variations of chemical constituents in annual layers in Greenland deep ice deposits', in *Isotopes and Impurities in Snow and Ice*, Proc. IUGG Symp., Grenoble, August-September 1975, IAHS-AISH Publ. No. 118, pp. 302-306.

- Larsen, B.B., A. Elverhøi, and P. Aagaard: 1987, 'Study of particulate material in sea ice in the Fram Strait – a contribution to paleoclimatic research?', *Polar Res.* 5(3), 313–315.
- Manabe, S. and A.J. Broccoli: 1985, 'The influence of continental ice sheets on the climate of an ice age', *J.Geophys.Res.* 90(C2), 2167–2190.
- Maykut, G.A.: 1985, 'The ice environment', in R.A. Horner (ed.) *Sea Ice Biota*, CRC Press, Boca Raton, Florida, pp. 21–82.
- Maykut, G.A. and N. Untersteiner: 1971, 'Some results from a time-dependent thermodynamic model of sea ice', *J.Geophys.Res.* 76(6), 1550–1575.
- McLaren, A.S., M.C. Serreze, and R.G. Barry: 1987, 'Seasonal variations of sea ice motion in the Canada Basin and their implications', *Geophys.Res.Lett.* 14(11), 1123–1126.
- Minicucci, D.A. and D.L. Clark: 1983. 'A late Cenozoic stratigraphy for glacial-marine sediments of the eastern Alpha Cordillera, central Arctic Ocean', in B.F. Molnia (ed.), *Glacial-Marine Sedimentation*, Plenum Press, New York, pp. 331–365.
- Morris, T.H.: 1988, 'Stable isotope stratigraphy of the Arctic Ocean: Fram Strait to central Arctic', *Palaeogeogr.Palaeoclimatol.Palaeoecol.* 64, 201–219.
- Mullen, R.E., D.A. Darby, and D.L. Clark: 1972, 'Significance of atmospheric dust and ice rafting for Arctic Ocean sediment', *Geol.Soc.Am.Bull.* 83, 205–211.
- Nansen, F.: 1897, *Farthest North*, Archibald Constable and Co. Whitehall Gardens.
- Nansen, F.: 1904, 'The bathymetrical features of the North Polar Seas', in: F. Nansen (ed.), *The Norwegian North Polar Expedition 1893–1896, Scientific Results*, 4(13), Longmans, Green and Company. London, 232 p.
- Nansen, F.: 1906, 'Protozoa on the ice-floes of the North Polar Sea', in F. Nansen (ed.), *The Norwegian North Polar Expedition 1893–1896, Scientific Results*, 5(16), Longmans, Green and Company. London, 22 p.
- Naugler, F.P., N. Silverberg, and J.S. Creager: 1974, 'Recent sediments of the East Siberian Sea', in Y. Herman (ed.), *Marine Geology and Oceanography of the Arctic Seas*, Springer-Verlag, Heidelberg, pp. 191–210.
- Nordenskiöld, A.E.: 1870, 'Redegörelse för en expedition till Grönland år 1870' Öfversigt af K. Svenska Vetenskaps – Akad. Förhandl, 10.
- Osterkamp, T.E. and J.P. Gosink: 1984, 'Observations and analyses of sediment-laden sea ice', in P.W. Barnes, D.M. Schell and E. Reimnitz (eds.) *The Alaskan Beaufort Sea, Ecosystems and Environments*, Academic Press, Inc., pp. 73–93.
- Ovenshine, A.T.: 1970, 'Observations of iceberg rafting in Glacier Bay, Alaska, and the identification of ancient ice-rafted deposits', *Geol.Soc.Am.Bull.* 81, 891–894.

- Parkinson, C.L., J.C. Comiso, H.J. Zwally, D.J. Cavalieri, P. Gloersen, and W.J. Campbell: 1987, *Arctic Sea Ice, 1973–1976: Satellite passive-microwave observations*, NASA SP-489, National Aeronautics and Space Administration, Washington, D.C., 296 pp.
- Paterson, W.S.B. and C.U. Hammer: 1987, 'Ice core and other glaciological data', in W.F. Ruddiman and H.E. Wright, Jr. (eds.) *Geology of North America, Vol K-3, North America and adjacent oceans during the last deglaciation*, Geol.Soc.Am. pp. 91–109.
- Petit, J.-R., M. Briat, and A. Royer: 1981, 'Ice age aerosol content from East Antarctic ice core samples and past wind strength', *Nature* 293, 391–394.
- Polarstern Shipboard Scientific Party: 1988, 'Breakthrough in Arctic deep-sea research: The R/V Polarstern expedition 1987', *Eos Trans.* 69(25), 665, 676–678.
- Poser, H.: 1933, 'Über Abschmelzformen auf dem ostgrönländischen Packeise und Landeise', *Zeit.f.Gletscherk.* 21, 1–20.
- Rahn, K.A., R.D. Borys and G.E. Shaw: 1977, 'The Asian source of Arctic haze bands', *Nature* 268, 713–715.
- Rahn, K.A. and R.J. McCaffrey: 1980, 'On the origin and transport of the winter arctic aerosol', *Ann.New York Acad.Sci.* 338, 486–503.
- Ray, L.L.: 1935, 'Some minor features of valley glaciers and valley glaciation', *J.Geol.* 43, 297–322.
- Reimnitz, E. and E.W. Kempema: 1988, 'Ice rafting: an indication of glaciation?', *J.Glaciol.* 34(117), 254–255.
- Reimnitz, E., E.W. Kempema, P.W. Barnes: 1987, 'Anchor ice, seabed freezing, and sediment dynamics in shallow Arctic seas', *J.Geophys.Res.* 92(C13), 14671–14678.
- Ruddiman, W.F.: 1977a, 'Late Quaternary deposition of ice-rafted sand in the subpolar North Atlantic (lat 40° to 65°)', *Geol.Soc.Am.Bull.* 88, 1813–1827.
- Ruddiman, W.F.: 1977b, 'North Atlantic ice-rafting: A major change at 75,000 years before the present', *Science* 196, 1208–1211.
- Ruddiman, W.F. and A. McIntyre: 1977, 'Late Quaternary surface ocean kinematics and climate change in the high-latitude North Atlantic', *J.Geophys.Res.* 82, 3877–3887.
- Sarnthein, M.: 1978, 'Sand deserts during glacial maximum and climatic optimum', *Nature* 272(5648), 43–46.
- Sarnthein, M., G. Tetzlaff, B. Koopmann, K. Wolter, U. Pflaumann: 1981, 'Glacial and interglacial wind regimes over the eastern subtropical Atlantic and north-west Africa', *Nature* 293, 193–196.

Schütz, L.: 1980, 'Long range transport of desert dust with special emphasis on the Sahara', *Ann. New York Acad. Sci.* 338, 515–532.

Sharp, R.P.: 1949, 'Studies of superglacial debris on valley glaciers', *Am. J. Sci.* 247, 289–315.

Steffensen, J.P.: 1985, 'Microparticles in snow from the South Greenland ice sheet', *Tellus* 37B, 286–295.

Steffenson, J.P.: 1988, 'Analysis of the seasonal variation in dust, Cl<sup>-</sup>, NO<sub>3</sub><sup>-</sup>, and SO<sub>4</sub><sup>2-</sup> in two central Greenland firn cores', *Ann. Glaciol.* 10, 171–177.

Steinbock, O.: 1936, 'Über Kryokonitlöcher und ihre biologische Bedeutung', *Zeit. f. Gletscherk.* 24, 1–21.

Sverdrup, H.U.: 1938, 'Notes on erosion by drifting snow and transport of solid material by sea ice', *Am. J. Sci.*, 35, 370–373.

Taylor, S.R., S.M. McLennan, and M.T. McCulloch: 1983, 'Geochemistry of loess, continental crustal composition and crustal model ages', *Geochim. Cosmochim. Acta* 47, 1897–1905.

Thiede, J.(ed.): 1988, 'Scientific Cruise Report of Arctic Expedition ARK IV/3', *Reports on Polar Research*, 43, 237 pp.

Thiede, J., D. Clark, and Y. Herman: 1988, 'Late Mesozoic and Cenozoic paleoceanography of northern polar oceans', *Geology of North America, Vol. L, Arctic Ocean Region*, Geol. Soc. Am.

Thompson, L.G.: 1977, 'Variations in microparticle concentration, size distribution and elemental composition found in Camp Century, Greenland, and Byrd station, Antarctica, deep ice cores', in *Isotopes and Impurities in Snow and Ice*, Proc. IUGG Symp., Grenoble, August–September 1975, IAHS–AISH Publ. No. 118, pp. 351–364.

Thompson, L.G. and E. Mosley–Thompson: 1981, 'Microparticle concentration variations linked with climatic change: evidence from polar ice cores', *Science* 212, 812–815.

Thorndike, A.S. and R. Colony: 1982, 'Sea ice motion in response to geostrophic winds', *J. Geophys. Res.* 87, 5845–5852.

Tomirdiaro, S.V.: 1984, 'Arctic loess–ice plain as a bridge between America and Asia and its thermokarstal disintegration in the Holocene', in V.L. Kontrimavichus (ed. in chief) *Beringia in the Cenozoic Era*, pp. 87–110. Vladivostok, 1976, U.S. Department of Interior and National Science Foundation translation 1984, Washington, D.C.

Untersteiner, N.: 1986, 'Glaciology – A primer on ice', *Oceanus* 29, 18–23.

Vinje, T.: 1985, 'Drift, composition, morphology and distribution of the sea ice fields in the Barents Sea', *Norsk Polarinst. Skr.* 179C, 26 pp.

Vinje, T.: 1987, 'Morphology and dynamics of the Barents Sea ice fields', in W.M. Sackinger and M.O. Jeffries (eds.) *Proceedings of the Ninth International Conference on Port and Ocean Engineering Under Arctic Conditions*, Fairbanks, August 17–22, 1987 University of Alaska.

Vinje, T. and Ø. Finnekåsa: 1986, 'The ice transport through the Fram Strait', *Norsk Polarinst.Skr.* 186, 39 pp.

Vowinkel, E. and S. Orvig: 1970, 'The climate of the North Polar Basin', in S. Orvig (ed.), *Climates of the Polar Regions, vol 14 of the World Survey of Climatology*, Elsevier, Amsterdam. pp. 129–252.

Wadhams, P.: 1980, 'Ice characteristics in the seasonal ice zone', *Cold Regions Sci.Tech.* 2, 37.

Wagenbach, D. and K. Geis: (this volume), 'The mineral dust record in a high altitude alpine glacier (Colle Gnifetti, Swiss Alps)'.

Wagner, A.: 1938, 'Zur Entstehung von Kryokonitlöchern', *Zeit.f.Gletscherk.* 26, 129–137.

Warren, S.G. and W.J. Wiscombe: 1980, 'A model for the spectral albedo of snow II: snow containing atmospheric aerosols', *J.Atmos.Sci.* 37, 2734–2745.

Weeks, W.F.: 1986, 'The physical properties of the sea ice cover', in B.G. Hurdle (ed.) *The Nordic Seas*, Springer-Verlag, New York, pp. 87–100.

Weeks, W.F. and S.F. Ackley: 1982, 'The growth, structure and properties of sea ice', *CRREL. Mon.* 82–1.

Weeks, W.F. and A.J. Gow: 1978, 'Preferred crystal orientations in the fast ice along the margins of the Arctic Ocean', *J.Geophys.Res.* 83, 5105–5121.

Windom, H.L.: 1969, 'Atmospheric dust records in permanent snowfields: implications to marine sedimentation', *Geol.Soc.Am.Bull.* 80, 761–782.

Wright, H.E., Jr.: 1987, 'Synthesis; The land south of the ice sheets', in W.F. Ruddiman and H.E. Wright, Jr. (eds.), *Geology of North America, Vol K-3, North America and adjacent oceans during the last deglaciation*, Geol.Soc.Am. pp 479–488.

Zacharov, V.F.: 1976, 'Cooling of the Arctic and the ice cover of the Arctic seas', *AAVIII, Trudy*, 337, 94(96) pp. (Russian text translated by, Norsk Polarinstittutt, Oslo).

## **SECTION 4.**

### **MODELING ATMOSPHERIC CIRCULATION IN THE PAST**

## PAST AND PRESENT OCEANIC ENERGY BALANCE PATTERNS

REGINALD E. NEWELL & JANE HSIUNG

Department of Earth, Atmospheric, and Planetary Sciences

54-1522

Massachusetts Institute of Technology

Cambridge, MA 02139

U.S.A.

**ABSTRACT.** Present-day oceanic energy balance patterns are discussed from the point of view of the role wind-stress changes play in controlling the annual cycle, interannual changes, and glacial/interglacial changes in sea-surface temperature. Particular reference is made to Pacific-Atlantic differences and the relationship with salinity changes.

### 1. INTRODUCTION

Atmospheric flow patterns over the ocean play a major role in controlling sea-surface temperature so that when they change, during the annual cycle or from one year to the next or in a transition from glacial to interglacial climate, sea-surface temperature patterns are also expected to change. Factors which contribute to sea-surface temperature fluctuations include meridional oceanic energy flux transport changes, alterations in the solar energy reaching the surface due to cloudiness changes or Milankovitch-type changes, and variability of surface energy loss by the ocean as sensible and latent heat. All of the internal changes, including cloudiness, depend on atmospheric flow patterns. In addition meridional energy transport depends on the thermohaline circulation which is governed by density gradients and therefore partly by salinity which depends on precipitation and evaporation, so that again atmospheric flow patterns are involved. Insofar as maximum air temperatures over the ocean are dependent on sea-surface temperature (the difference averaging less than one kelvin), it is clear that knowledge of these flow patterns for the past and present is of major importance. It is also well known that the



atmosphere and ocean are closely coupled so that the atmospheric flow patterns themselves are strongly related to the underlying surface temperature and that this sort of coupling can only be satisfactorily taken into account in an interactive general circulation model. Until this is generally available, there is still some value in studying the mechanisms involved by themselves. Indeed this sort of exercise can be of considerable use in formulating coupled models.

Here we examine the relationship between atmospheric flow patterns and oceanic energy flux in three contexts: the annual cycle of sea-surface temperature in the middle-latitude Atlantic and Pacific and the possible reasons why the temperatures differ; the changes in ocean temperatures in the past 30 years; and the changes in North Atlantic temperature that may have accompanied the last glacial/interglacial transition, particularly around the Younger Dryas period. The data that will be brought to bear on these points is mostly winds over the ocean and oceanic temperatures and salinities collected since 1949.

## 2. PACIFIC-ATLANTIC DIFFERENCES AND THE ANNUAL CYCLE

Zonal mean sea-surface temperatures for high northern latitudes (55-60°N) are higher for the Atlantic than the Pacific, while between 20°N and 35°S the Pacific is the warmer ocean (see Table 1). Figures 1 and 2 give examples of the annual cycle in the two oceans and show that the inter-ocean difference is a minimum during the warmest period and a maximum in the coldest. The zonal mean surface energy flux for the two regions selected shows that the energy flux difference is largest in the cold periods and, paradoxically, that the warmest ocean has the smallest energy flux. The North Atlantic loses much more energy than the North Pacific in winter, mostly by evaporation. This is manifested also in salinity differences as the North Atlantic is saltier than the North Pacific at the same latitude. Likewise the South Pacific loses more energy than the South Atlantic. At 55-60°N there is an increase in temperature in March and April accompanying a surface energy loss and balance can only be achieved by a meridional energy transport from lower latitudes. The relevant energy fluxes are shown in Figure 3 (see also Hsiung *et al.*, 1987) with the North Atlantic being larger than the North Pacific and being particularly large when the inter-ocean temperature difference is large. Because the warmest ocean has the smallest surface energy flux it, must be the larger meridional energy transport that is responsible for the Atlantic

TABLE 1. Differences Between Atlantic and Pacific Zonal Mean Temperatures

LATITUDE	JAN	FEB	MARCH	APRIL	MAY	JUNE	JULY	AUG	SEPT	OCT	NOV	DEC
60-65°N	4.8	5.3	4.8	4.1	4.4	3.8	1.2	0.8	0.9	2.8	3.5	4.0
55-60°N	3.5	3.7	3.8	4.0	4.0	2.9	1.7	1.1	1.0	2.1	3.1	3.4
50-55°N	4.0	3.8	4.0	4.3	4.5	3.8	3.2	2.3	2.0	2.7	3.5	4.0
45-50°N	4.0	3.8	4.1	4.2	4.3	4.5	4.6	3.7	2.9	3.0	3.8	4.0
40-45°N	3.5	3.4	3.5	3.7	3.9	4.3	3.9	2.6	2.2	2.6	3.3	3.5
35-40°N	3.3	3.4	3.4	3.3	3.3	3.5	2.8	1.8	1.7	2.1	2.7	2.9
30-35°N	2.3	2.5	2.4	2.4	2.3	2.1	1.6	1.2	1.1	1.5	1.6	2.0
25-30°N	1.4	1.6	1.6	1.6	1.3	1.4	1.2	1.3	1.0	1.1	1.0	1.2
20-25°N	0.6	0.6	0.6	0.5	0.4	0.2	0.2	0.3	0.3	0.5	0.5	0.5
15-20°N	-0.3	-0.5	-0.5	-0.6	-0.8	-0.8	-0.7	-0.5	-0.1	0.1	0.0	-0.1
10-15°N	-0.8	-1.2	-1.5	-1.6	-1.6	-1.2	-1.0	-0.7	-0.2	-0.2	-0.1	-0.4
5-10°N	-0.4	-0.8	-1.0	-1.2	-1.1	-0.9	-1.0	-0.8	-0.5	-0.3	-0.2	-0.2
0-5°N	0.4	0.4	0.4	0.4	0.1	-0.5	-0.9	-1.1	-0.8	-0.4	0.0	0.4
0-5°S	0.1	0.2	0.3	0.5	-0.1	-1.3	-2.0	-1.8	-1.4	-1.1	-0.7	-0.3
5-10°S	-1.1	-0.6	-0.3	-0.4	-0.7	-1.1	-1.5	-1.8	-2.1	-2.2	-2.1	-1.8
10-15°S	-2.0	-1.4	-1.1	-1.3	-1.5	-1.7	-2.0	-2.3	-2.7	-2.7	-2.7	-2.5
15-20°S	-2.2	-1.7	-1.2	-1.5	-1.6	-1.9	-2.2	-2.3	-2.6	-2.9	-2.6	-2.5
20-25°S	-1.5	-1.3	-1.1	-1.0	-1.2	-1.4	-1.5	-1.6	-1.8	-1.8	-1.9	-1.5
25-30°S	-0.6	-0.2	-0.2	-0.5	-0.6	-0.6	-0.7	-0.8	-0.7	-1.0	-1.0	-0.7
30-35°S	-0.3	0.0	-0.1	-0.2	-0.1	-0.4	-0.2	-0.4	-0.4	-0.5	-0.4	-0.4
35-40°S	-0.1	0.2	-0.2	-0.1	0.4	0.7	0.6	0.3	0.8	0.7	0.4	0.2

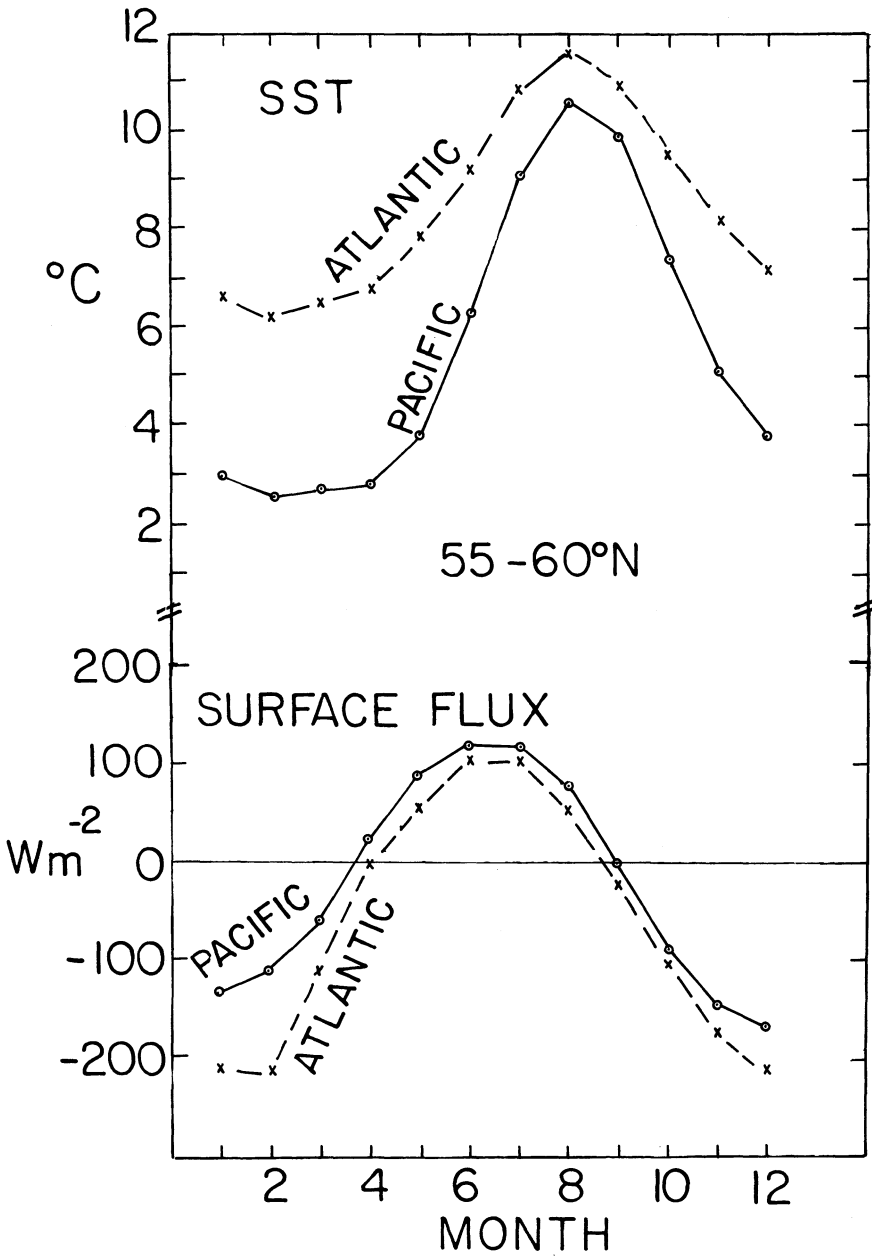


Figure 1: Sea-surface temperature and surface energy flux (Hsiung, 1986) for Atlantic and Pacific, 55-60° N. Units and °C and  $Wm^{-2}$ .

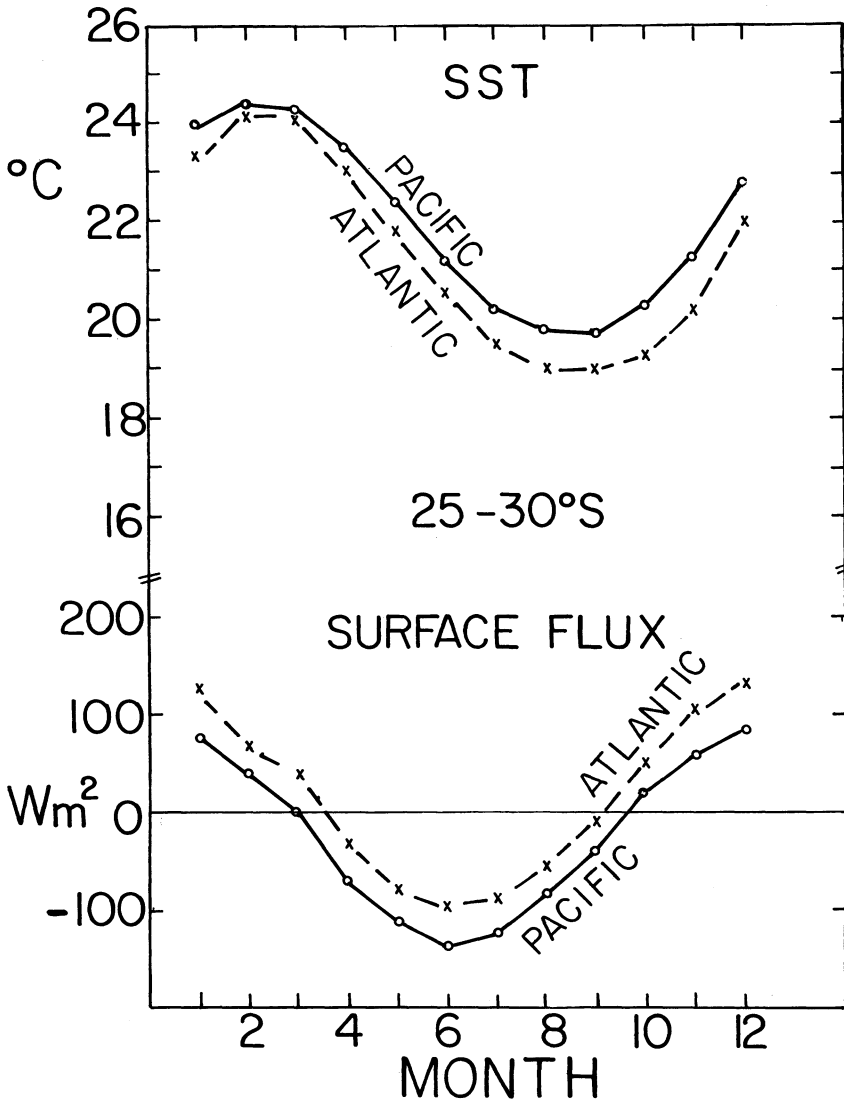


Figure 2: Same as Fig. 1 for 25-30°S.

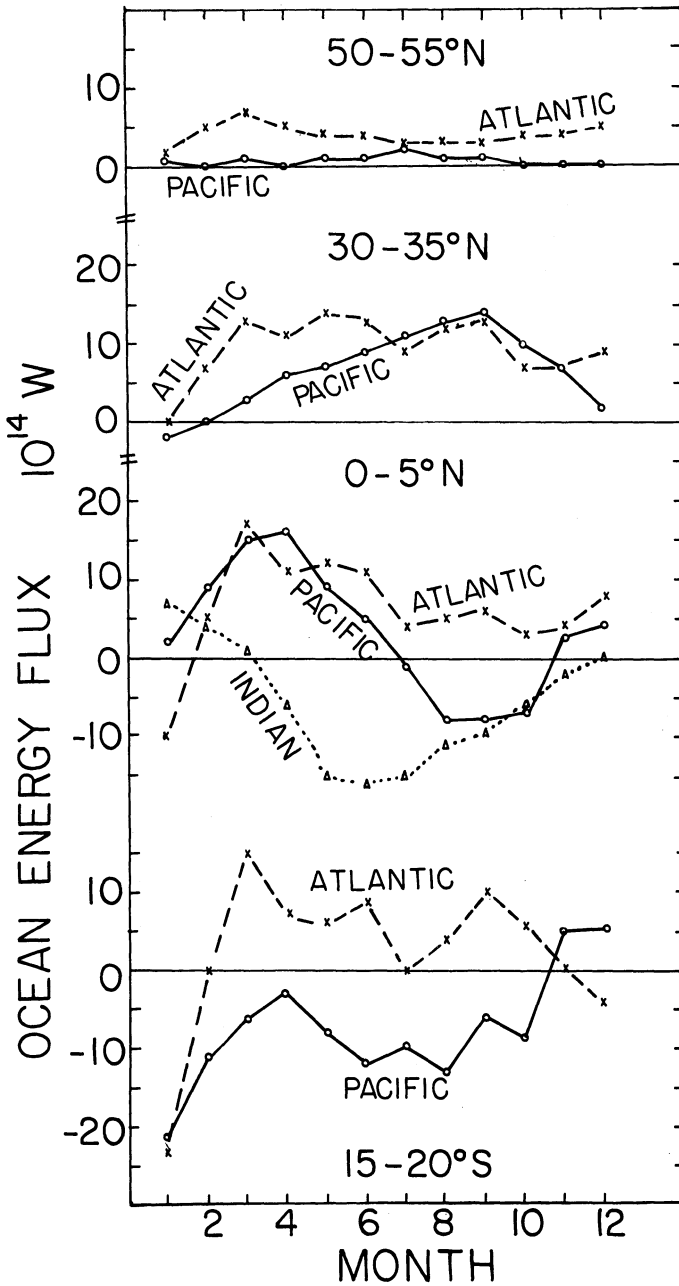


Figure 3: Meridional oceanic energy flux. Units:  $10^{14}$ W. (Data source described in Hsiung *et al.*, 1987.)

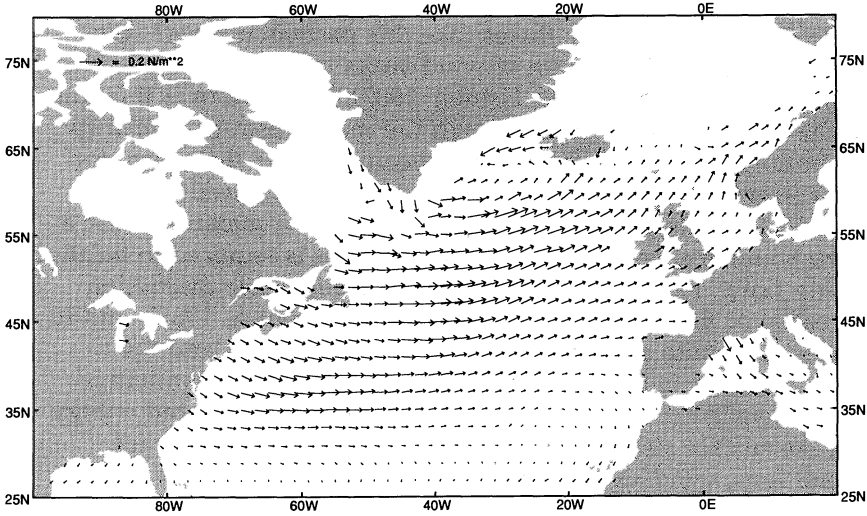
warmth. In the 25-30°S region, the Pacific flux is southwards and the Atlantic is northwards — which would act to produce a warmer Pacific, as observed.

Why do the oceanic energy fluxes take this particular form? We believe this is related to the pattern of wind-stress curl at the ocean surface (see Newell *et al.* 1982; Newell and Hsiung, 1987); this pattern is thought to control the oceanic energy flux through the mechanism of Sverdrup transport. In the case of a westerly wind maximum over the ocean, for example, the Sverdrup transport is towards the north polewards of the maximum, and towards the south equatorwards of the maximum; for a fixed eastern boundary, an eastward flowing current is required to balance this diverging flow. However, there has been considerable discussion about the reality of this transport (Wunsch and Roemmich, 1985), and its deduced pattern is quite sensitive to the wind observations and their uncertainties. Thus, it is difficult at present to construct a quantitative relationship between the observed flow patterns and the deduced energy flux. From the surface stress patterns shown in Figure 4 for average January conditions, wind-stress curl patterns have been deduced and are shown in Figure 5. (Wind data are taken from COADS, 1985). It is the orientation of the zero line of the wind-stress curl that we think is relevant to the oceanic energy flux: this is aligned NE-SW in the Atlantic but more nearly E-W in the Pacific in the example shown in Figure 5; we suggest that the Atlantic configuration is associated with a larger polewards flux. In fact estimation of the orientation of the zero line from 12 monthly sets of maps like Figure 5 shows that the Atlantic is aligned more in the SW-NE sense than the Pacific in the period December-July, except for March, and as may be seen from Figure 3, the oceanic flux at 30-35°N is greater in the Atlantic than the Pacific in those months. But at the present stage this association needs much more investigation both from theory and observations before a definitive linkage can be established and before the relative roles of the wind-stress-forced circulation and the thermohaline circulation (discussed briefly below) can be assessed. A definite link with the Sverdrup transport is as yet unproven.

Another consequence of the larger energy loss, mostly by evaporation, from the surface in the Atlantic is the difference in salinity between the two oceans. As may be seen from Figure 6, the North Atlantic is considerably saltier than the North Pacific; the evaporational forcing of salinity may well be augmented by additional poleward water transport from the salty subtropical regions, which according to Figure 3 is greater for the Atlantic. In the North Atlantic and South Pacific, the salinity forcing field (evaporation minus precipitation) is close to zero and

Mean Surface Wind Stress  
January, 1949-1979

Min. Obs. = 3  
Min. Yrs. = 15/31  
Smoothed



Mean Surface Wind Stress  
January, 1949-1979

Min. Obs. = 3  
Min. Yrs. = 15/31  
Smoothed

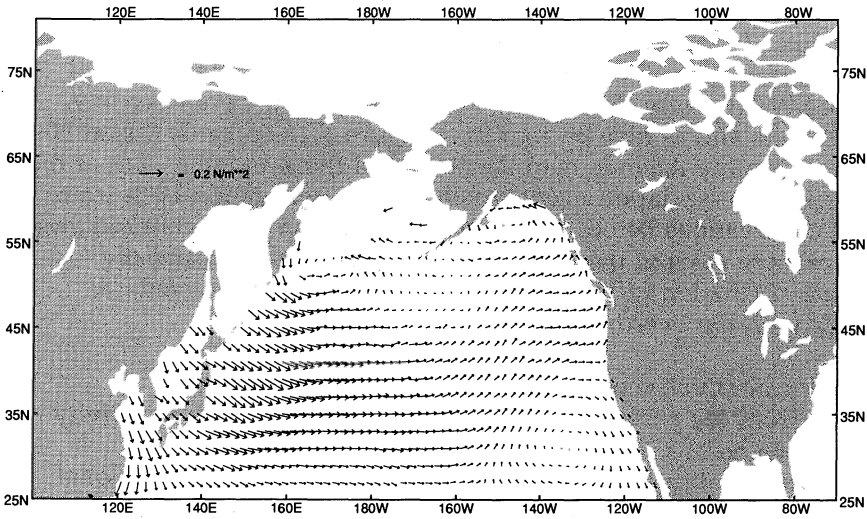
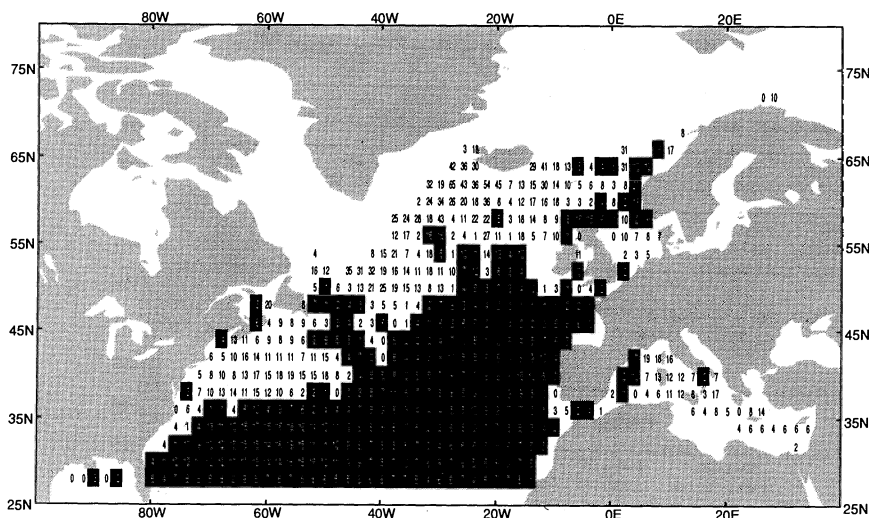


Figure 4: Wind-stress patterns for January 1949-79. North Pacific and Atlantic. Units:  $Nm^{-2}$ .

Curl of the Surface Wind Stress  
January, 1949-1979

Min. Obs. = 3  
Calculation B  
Min. Yrs. = 15/31  
Smoothed



Curl of the Surface Wind Stress  
January, 1949-1979

Min. Obs. = 3  
Calculation B  
Min. Yrs. = 15/31  
Smoothed

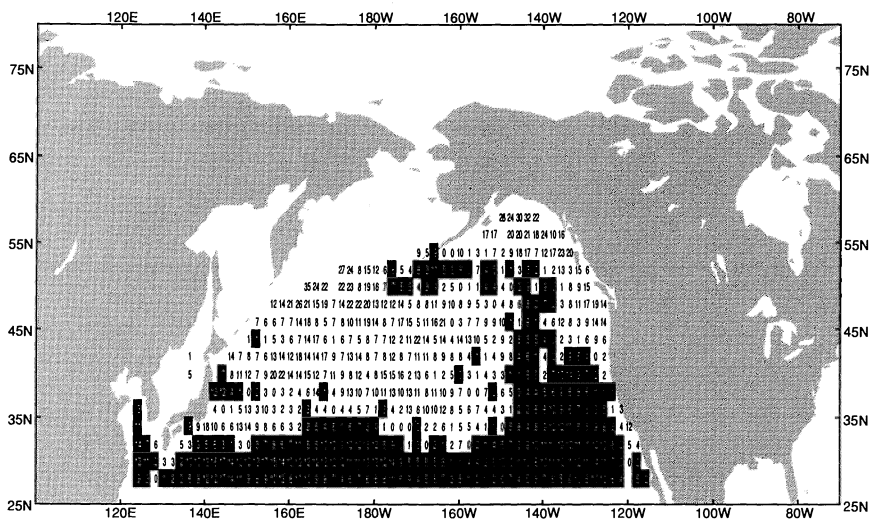


Figure 5: Wind-stress curl for January 1949-79. North Pacific and Atlantic. Shaded regions are negative values. Units:  $10^{-8} \text{kg m}^{-2} \text{s}^{-2}$ .



### Evaporation-Precipitation versus Salinity

Units- E,P,E-P: m/yr  
Salinity: parts/thousand  
Sources: (P)Jaeger,1975  
(E)Hsiung,1986 (S):MOODS

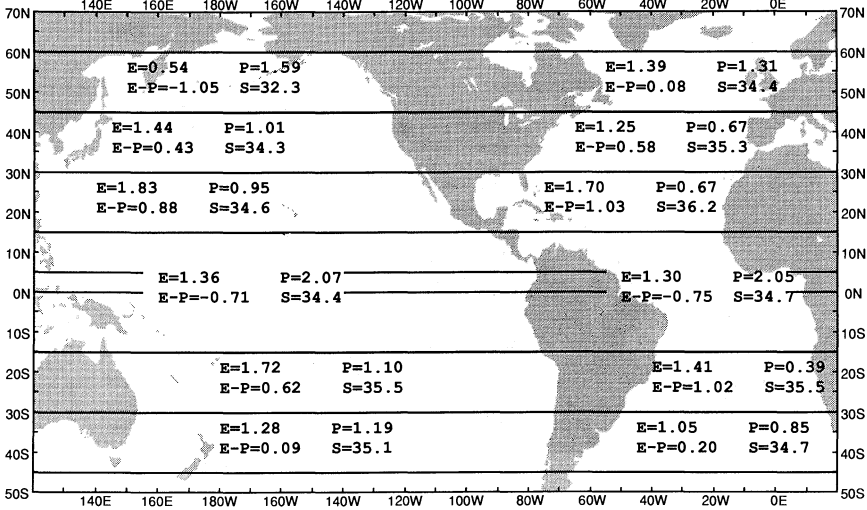


Figure 6: Evaporation (see Hsiung, 1986) minus precipitation (Jaeger, 1976) versus salinity. Units: salinity parts per million, E, P: m yr<sup>-1</sup>.

from meridional cross-sections of salinity, both regions show evidence of downwelling. Thus, surface processes control both the thermohaline circulation and the wind-stress-forced circulation, making the atmospheric flow patterns a major factor in climate.

### 3. RECENT INTERANNUAL SEA-SURFACE TEMPERATURE PATTERNS

Eigenvector analysis of global sea-surface temperature patterns for the 1949-79 period showed that the first eigenvector and its time series corresponded to the El Niño-Southern Oscillation mode (Hsiung and Newell, 1983). We have summarized how this mode is related to air temperature (Newell and Hsiung, 1987) and to changing surface wind patterns (Newell *et al.*, 1982); middle latitude winds are quite important in these changes. The second eigenvector showed a downward trend for the North Atlantic and North Pacific (Hsiung and Newell, 1983) accompanied by warming in the southern regions of these oceans. These large-scale changes have been related to drought in the Sahel (Folland *et al.*, 1986; Newell and Hsiung, 1987), which became more pronounced in the 1970s. During the drought both the North Atlantic and North Pacific were colder, particularly at high latitudes, and the South Atlantic was warmer. Possible relationships between changing oceanic energy transport and surface flux have been discussed elsewhere (Newell and Hsiung, 1987); flux changes within the North Atlantic, into the North Atlantic from the South Atlantic, and through the surface of the Atlantic or Indian Ocean are all possibilities and all depend upon the surface atmospheric flow patterns. The energy loss from the North Atlantic corresponding to the observed cooling was about  $1.2 \times 10^{14} \text{W}$  or  $3 \text{ Wm}^{-2}$ . This may be compared with an annual mean cross-equatorial flux of  $6 \times 10^{14} \text{W}$  so that a relatively small change in this flux could be responsible.

Hsiung (1983) has argued that the northward energy flux in the Atlantic ocean may be controlled by surface energy received in the Indian Ocean. She found that the surface energy flux was smaller by about  $7 \times 10^{14} \text{W}$  during the period 1965-1979 when the northern ocean temperatures were cooler than the period 1949-1964. Sea-surface temperature data and surface wind data were divided into these periods (1949-1964, 1965-1979) in order to deduce any possible relationships between sea-surface temperature changes and the wet and dry periods in the Sahel. In general, we found the northern oceans to be cooler and the

southern oceans warmer during dry years as in the eigenvector analysis. However, the differences in derived quantities, such as wind-stress curl between 1949-64 and 1965-79, are not significant.

#### 4. RELEVANCE TO GLACIAL/INTERGLACIAL CHANGES INCLUDING THE YOUNGER DRYAS

Production of an ice age, such as that at 18,000 B.P., involves the formation of about  $47 \times 10^6 \text{ km}^3$  of ice north of  $30^\circ\text{N}$  from atmospheric water vapor. This involves the release of about  $2.8 \times 10^6 \text{ J kg}^{-1}$  of latent heat to the atmosphere which must be lost to space, giving a loss at high latitudes relative to present conditions of about  $1.3 \times 10^{24} \text{ J}$ , which must be uncompensated by transport of energy from low latitudes. If the ice cap build-up occurs in 30,000 years or  $9.4 \times 10^{11}$  seconds (which may occur in steps rather than continuously), then the anomalous energy flux involved amounts to about  $1.4 \times 10^{14} \text{ W}$ , corresponding to about  $1 \text{ Wm}^{-2}$  for the region north of  $30^\circ\text{N}$ . The meridional energy flux by the ocean at  $30^\circ\text{N}$  is about  $16 \times 10^{14} \text{ W}$ , 9.6 in the Atlantic and 6.7 in the Pacific, so that an ice age could be produced by reducing the meridional energy transport in the Atlantic by 15%, or that in the Pacific by 21%, or by an equivalent combination of reductions in both oceans. There is, of course, an energy balance for the system as a whole in the present configuration with the same amount of energy leaving high latitudes as enters at low latitudes. During the ice formation, there is an energy imbalance with more leaving at high latitudes than is provided by the meridional flux from low latitudes. During melting more energy flows polewards than is lost to space, but because the latent heat required for melting is much less than that required for vaporization, the energy involved is much smaller. This difference was suggested earlier to be the reason for the relatively rapid decay of ice ages when compared with their time of formation (Newell, 1974).

The formation of additional ice of mass about  $47 \times 10^{18} \text{ kg}$  in 30,000 years is equivalent to a flux of water vapor crossing  $30^\circ\text{N}$  of about  $5 \times 10^7 \text{ kg sec}^{-1}$ . This compares with a normal water vapor flux across  $30^\circ\text{N}$  of about  $6 \times 10^8 \text{ kg sec}^{-1}$  (e.g., see Peixoto and Oort, 1983). Hence, there is clearly no difficulty in balancing the water vapor budget with current circulation mechanisms. During the period of ice accumulation at high northern latitudes (that is between about 100 kyr BP and 20 kyr BP), there must be

less ocean-atmosphere energy flux than the present across 30°N, while no change is required in the water vapor flux; during the melting period, say 16 to 8 kyr BP, the combined energy flux must exceed present values.

Milankovitch variations in incoming radiation are expected to influence climate in two ways: they alter the differential solar radiation between pole and equator, which is the main factor involved in controlling the overall energy flux; and they alter the energy which can be involved in oceanic storage and which can be transported by the ocean — this latter role depending on the way they control atmospheric flow patterns. The importance of the meridional flux varies with month, latitude, and ocean as can be seen from Figure 3. For example, if minimum radiation just to the south of 30°N occurs in May and/or September, while minimum flux just south of the equator occurs in March, there may be a smaller than average flux at the equator and 30°N at the same time leading to an energy deficit north of 30°N. To test this idea requires an optimization approach once the factors involved in controlling the temperature of the upper oceanic layers are understood.

During the Last Glacial Maximum, the sea temperature isotherms drawn by CLIMAP (1981) have an almost east-west alignment between North America and Spain. Because the present day isotherms in the middle-latitude Atlantic and Pacific are closely parallel to the zero line of the wind-stress curl, we assume that such was the case also at 18,000 BP implying a more east-west atmospheric flow pattern in the Atlantic. This implication is not in disagreement with the flow patterns deduced by Kutzbach (1987) from experiments with climate models, though it should be borne in mind that these models do not permit ocean-atmosphere coupling as surface boundary conditions are generally fixed although these conditions can of course be varied to correspond to different times in the past.

In the present circulation, the surface flow over the North Atlantic is governed by the large-scale planetary waves which depend on land-sea temperature differences, topographical forcing and zonal wind speeds. All of these were different in the last Ice Age, particularly with the existence of the Laurentide ice sheet. Furthermore, the topographical forcing was highly variable as the sheet melted and the changing interference pattern between the topographical forcing by the Rockies and this sheet could quite conceivably have been responsible for the Younger Dryas atmospheric flow fluctuations and concomitant oceanic flux changes in the Atlantic.

It is suggested that this surface flow interference pattern changed in the Younger Dryas Oscillation so that the zero line of the wind-stress curl in the Atlantic changed from E-W (the current Pacific and 18,000 BP Atlantic mode) to SW-NE (the current Atlantic mode) then back again before its final move to present conditions.

Changes in salinity patterns would have accompanied these flow pattern changes. For example, at the Last Glacial Maximum the poleward advection of salty water in the Atlantic would have decreased as the flow became more E-W although the evaporative component in middle latitudes may have been larger under the influence of the stronger winds which have been inferred (e.g., by Newell, *et al.*, 1981).

Several authors have suggested that the climate system can operate in two preferred modes (Newell, 1974; Broecker, *et al.*, 1985). Newell proposed that the difference between the modes was in the partitioning of the energy flux between the atmosphere and the ocean. Broecker, *et al.*, suggest that the mode difference lies in weak and strong production of deep water in the North Atlantic; they also show production of deep water in the North Pacific in the cold mode. One difference with the information given here is that they indicate a southward flux of energy in the present day North Pacific, whereas a northward flux is indicated in Figure 3. Clearly there is much work to be done on all these ideas.

## 5. CONCLUSIONS

Atmospheric flow patterns, through their control of oceanic currents, play a major role in governing oceanic energy transport and high latitude temperature. This transport also seems to control the temperature difference between the North Atlantic and North Pacific and between the southern oceans as well as contributing to interhemispheric temperature changes. Annual variations of sea-surface temperature and salinity can only be explained satisfactorily when meridional oceanic energy transports are taken into account. The importance of meridional energy transports is not new, and elsewhere we have intercompared mean annual values (Newell *et al.*, 1981; Hsiung, 1985). The annual cycle is now being considered in detail, and we think this cycle is an important part of the mechanism of climatic fluctuations. The same ideas can be applied to study interdecadal temperature changes and glacial/interglacial changes. It is of major importance to try to reconstruct the surface flow patterns of the past so that possible changes in oceanic and salt fluxes may be assessed.

## ACKNOWLEDGEMENTS

We greatly appreciate the help of Francis Tourneur and Steven Walker who processed the COADS data. Support was provided by the National Science Foundation, Climate Dynamics Program under Grant ATM-8517107.

## REFERENCES

- CLIMAP project members, 1981: Seasonal reconstruction of the earth's surface at the last glacial maximum, *Geol. Soc. Amer. Map Chart Series*, MC-36.
- COADS (Comprehensive Ocean-Atmosphere Data Set), Release 1, 1985, CIRES, ERL, NCAR, NCDC, Boulder, CO, 267 pp.
- Broecker, W.S., Peteet, D.M., and Rind, D., 1985: Does the ocean-atmosphere system have more than one stable mode of operation?, *Nature*, 315: 21-26.
- Folland, C.K., Palmer, T.W., and Parker, D.E., 1986: Sahel rainfall and worldwide sea temperatures, 1901-85, *Nature*, 320: 602-607.
- Hsiung, J., 1983: Large-scale, sea-air energy fluxes and global sea-surface temperature fluctuations, Ph.D. Thesis, MIT, 240 pp.
- Hsiung, J., 1985: Estimates of global oceanic meridional heat transport, *J. Phys. Oceanogr.*, 15: 1405-1413.
- Hsiung, J., 1986: Mean surface energy fluxes over the global ocean, *J. Geophys. Res.*, 91: 10,585-10,606.
- Hsiung, J., Newell, R.E., and Houghtby, T., 1987: Annual variation of heat transport in the Pacific and Indian Oceans, *Nature*, 325: 518-520.
- Jaeger, L., 1976: Monatskarten des Niederschlags für die ganze Erde, *Ber. Dt. Wetterd.*, 18, No. 139, 38 pp.
- Kutzbach, J.E., 1987: Model simulations of the climatic patterns during the deglaciation of North America, *In: The Geology of North America, U.K-3 North America and adjacent oceans during the last deglaciation*, Geol. Soc. Amer., pp. 425-446.

- Newell, R.E., 1974: Changes in the poleward energy flux by the atmosphere and ocean as a possible cause for ice ages, *Quat. Res.*, 4: 117-127.
- Newell, R.E., Chiu, L.S., Ebisuzaki, W., Navato, A.R., and Selkirk, H.B., 1981: The oceans and ocean currents: their influence on climate, International Conference, Climate and Offshore Energy Resources, London, England, The Royal Society/American Meteorological Society, Boston, Mass., pp. 59-112.
- Newell, R.E., Gould-Stewart, S. and Chung, J.C., 1981: A possible interpretation of paleoclimatic reconstructions for 18,000 BP for the region 60°N to 60°S, 60°W to 100°E, *Palaeoecology of Africa*, v. 13, J.A. Goltzee and E.M. Van Zinderen Bakker Sr., Eds., A.A. Balkema, pp. 1-20.
- Newell, R.E., and Hsiung, J., 1987: Factors controlling free air and ocean temperature of the last 30 years and extrapolation to the past, *In: Abrupt Climatic Changes*, W.H. Berger and L.D. Labeyrie, Eds., D. Reidel, pp. 67-87.
- Newell, R.E., Selkirk, H.B., and Ebisuzaki, W., 1982: The southern oscillation: sea-surface temperature and wind relationships in a 100-year data set, *J. Climatol.*, 2, pp. 357-373.
- Peixoto, J.P. and Oort, A.H., 1983: The atmospheric branch of the hydrological cycle and climate, *In: Variations in the Global Water Budget*, A. Street-Perrott, M. Beran and R. Ratcliffe, Eds. D. Reidel, pp. 5-65.
- Wunsch, C., and Roemmich, D., 1985: Is the North Atlantic in Sverdrup balance?, *J. Phys. Oceanogr.*, 15: 1876-1880.

# POSSIBLE EFFECTS OF ORBITAL VARIATIONS ON PAST SOURCES AND TRANSPORTS OF EOLIAN MATERIAL: ESTIMATES FROM GENERAL CIRCULATION MODEL EXPERIMENTS

JOHN E. KUTZBACH  
IES-Center for Climatic Research  
University of Wisconsin-Madison  
1225 West Dayton Street  
Madison, WI 53706  
U.S.A.

**ABSTRACT.** Paleoclimate simulation experiments for various orbital configurations of precession, tilt and eccentricity (for 9000 and 125,000 years ago) and for glacial-age boundary conditions (for 18,000 years ago) provide examples of possible variations in sources/sinks and transports of eolian material. These types of experiments are likely to play an increasingly important role in helping to interpret the eolian sediment record.

## 1. INTRODUCTION

Variations of the sources, sinks and transports of eolian material are an important aspect of earth's changing climate. There are many records of eolian material in the soil, in lake and ocean sediments, and in ice sheets. It is outside the scope of this paper to review these records, except to note that the orbital periods of precession (about 22,000 years), or axial tilt (about 41,000 years), or eccentricity (about 100,000 years) are found in eolian deposits in ocean sediment cores (see, for example, Pisias and Leinen, 1984; Janecek and Rea, 1985); in the loess record from China (Liu Tungsheng, *et al.*, 1985) and aerosol records from the Antarctic ice cap (Petit, *et al.*, this volume). In this paper, I will speculate (based upon the results of our paleoclimate simulation experiments with general circulation models) on possible variations of source/sink patterns and transports of eolian material that might occur at the periods of orbital variation over the past million years.



## 2. MODEL SIMULATIONS

Because general circulation models simulate atmospheric flow patterns and the hydrologic cycle, the results can be used to help infer sources/sinks and transports of eolian material. We have made a number of paleoclimate simulation experiments for different geologic times. We simulated the climatic effects of orbital changes by using the latitudinal and seasonal distribution of solar radiation that occurred for different orbital configurations. We also simulated the glacial-age climate using boundary conditions (ice sheets, etc.) appropriate for glacial times. Our main set of experiments for 18 ka (thousands of years ago) to present, at 3000 year intervals, are described in Kutzbach and Guetter (1986) and in COHMAP members (1988); other experiments will be referenced as needed.

### 2.1 *Variations in the Season of Perihelion: the 22,000-year precession cycle*

Our experiments for 9 ka and 125 ka provide examples of climates with increased range of the seasonal cycle of solar radiation in the northern hemisphere and decreased range in the southern hemisphere, compared to present (Kutzbach, 1981; Kutzbach and Otto-Bliesner, 1982; Kutzbach and Guetter, 1986; see also Royer, *et al.*, 1984, for 125 ka and 115 ka experiments with a general circulation model that was different from the one we used). At 9 ka and 125 ka perihelion occurred in July rather than January (the present condition). These particular times were also periods of increased axial tilt that enhanced the increased seasonality of solar radiation in the north.

The increased seasonality of solar radiation in the northern hemisphere at 9 and 125 ka increased the seasonal range of temperature (warmer summers, colder winters) and increased the intensity of summer and winter monsoon circulations. In the northern tropics the strengthening of the summer monsoon produced increased rainfall and increased precipitation-minus-evaporation (compared to present) in parts of North Africa and south and east Asia. In the northern mid-latitude continental interiors, near the limit of the reach of summer precipitation, evaporation under the warmer summertime conditions increased more than precipitation; this caused a decrease of precipitation-minus-evaporation compared to present. Our first series of experiments, referenced above, were made with general circulation models using prescribed (non-interactive) soil moisture. We and others have repeated the experiments for 9 ka using models with interactive soil moisture and

interactive mixed-layer oceans (Gallimore and Kutzbach, 1988; Kutzbach and Gallimore, 1988; Mitchell, *et al.*, 1988). These new experiments generally confirm the previous results.

A conceptually simple climatic pattern emerges from these experiments: there is increased aridity in the northern continental interiors and increased moisture (decreased aridity) in the northern tropics at times of July perihelion (9 ka, 125 ka) and the reverse at times of January perihelion (0 ka, 115 ka). Based on these model results and neglecting lag effects, one might expect to find 22,000-year variations in the source strength of eolian material, with maxima in source strength in northern continental interiors and the southern tropics and minima in source strength in the northern tropics occurring near times of July perihelion.

Records of lake levels from the northern tropics over the past 20,000 years (Kutzbach and Street-Perrott, 1985), from North Africa around 125 ka (Petit-Maire, 1986) and from northern mid-latitudes over the past 12,000 years (Street-Perrott, 1986), appear to be in fair agreement with the changes in surface hydrology as simulated for different orbital configurations. A 30,000-year eolian sediment record from the Northwest Pacific contained the greatest dust flux (a measure of source aridity) around 6 ka and is also consistent with the simulated maximum of northern mid-continental aridity around 6 ka to 9 ka (Rea and Leinen; 1988).

We have used our model results to estimate time series of monsoon precipitation for regions of North Africa and South Asia for the past 125,000 years (Prell and Kutzbach, 1987). We then made comparisons between the simulated aridity record and eolian records of African climate as contained in marine sediment cores from the Atlantic (Pokras and Mix, 1985). Once again, we found relatively good agreement and therefore additional support for a physical link between orbital variations and variations of eolian material.

Variations in the sources of eolian material are of course only one potential cause of variability in geologic records of eolian sediments. Variations in transports and sinks must also be considered. We found in our 9 and 125 ka experiments that increases in the intensity of summer monsoon circulations were accompanied by increases in the strength of the subtropical anticyclones over the North Pacific and North Atlantic and by increased wind speed in the subtropical easterly jet stream over south Asia and North Africa. We can, therefore, expect that air trajectories were different from present at these times (cf Merrill, this volume, for

examples of trajectory calculations). Simulation experiments with general circulation models provide the data sets needed to evaluate these changes in air trajectories.

## **2.2 Variations in Axial Tilt: the 41,000 year obliquity cycle**

We have made a series of experiments to begin to explore the climatic effects of tilt and precession separately and in combination (Prell and Kutzbach, 1987). Changes in axial tilt have their greatest direct effects on the climates of middle and high latitudes. However, our experiments also showed that changes of tilt and season of perihelion may combine to produce a wide range of climatic responses at all latitudes. Our studies of tilt and combined tilt/precession effects are too incomplete at this stage to speculate further on implications for eolian records, other than to note that both 41,000-year and 22,000 year variability is to be expected.

## **3. GLACIAL PERIODS**

For studying the sources/sinks and transports of eolian material during glacial periods, we have at our disposal a relatively large number of general circulation model experiments for the last glacial maximum around 18 ka. Because the marine oxygen isotope record contains evidence of variations in the volume of continental ice sheets with periods around 100,000 years, 41,000 years and 22,000 years (Hays, *et al.*, 1977), we may expect to find variations in the eolian sediment record at all of these orbital periods and especially at the dominant 100,000-year period. (The relation between the dominant 100,000-year glacial/interglacial cycle in the geologic record and the very weak orbital forcing provided by the 100,000-year eccentricity cycle is the subject of a great deal of current research.)

Our experiments for 18 ka show that major changes in surface moisture regimes and in the strength and location of atmospheric jet streams and storm tracks occur in connection with glacial-age boundary conditions (Kutzbach and Guetter, 1986; Kutzbach and Wright, 1985; Kutzbach, 1987; Webb, *et al.*, 1987). Similar (but not identical changes) are found in glacial-age simulations with other models (Manabe and Broccoli, 1985; Broccoli and Manabe, 1987; Rind and Peteet, 1985). Some examples of these glacial-age changes are: drier conditions in the regions of North America and Eurasia south of the ice sheets; wetter conditions in the vicinity of the southward-shifted jet streams and storm tracks over the southwestern United States and over parts of the Mediterranean and North Africa.

The detailed data sets that are available from these experiments for glacial climates provide opportunities to compare source/sink and trajectory analyses with information from the eolian sediment record for glacial times. The availability of simulations for both significantly different orbital conditions (such as 9 and 125 ka) and for glacial-age boundary conditions (such as 18 ka) may help to separate the more direct effects of orbital variations on sources/sinks and transports of eolian material from the more indirect effects associated with the extreme climatic states accompanying maximum glacial conditions.

### ***3.1 Other Processes Involving Eolian Material Not Generally Included in Climate Models***

In the future, it will be possible to construct climate models with interactive source/sink and transport processes for eolian material. These models will include parameterizations for injection, transport and removal mechanisms; as well as essential interactions between the aerosols and radiative, cloud, and chemical processes. Important steps in this direction are being achieved in connection with the so-called "nuclear-winter" aerosol experiments (Covey, *et al.*, 1984; Covey, *et al.*, 1985; Thompson, 1985; Thompson, *et al.*, 1987). Other important first steps are sensitivity experiments on the climatic impact of glacial-age aerosols (Harvey, 1988).

## **4. CONCLUSIONS**

The primary purpose of my talk has been to give examples (obtained from paleoclimate simulation experiments) of possible effects of orbital variations on past sources/sinks and transports of eolian material. Computer simulations of paleoclimates will no doubt play an increasingly important role in helping to interpret the eolian sediment record.

## **ACKNOWLEDGEMENTS**

Research grants to the University of Wisconsin-Madison from the National Science Foundation's Climate Dynamics Program (Grants ATM-86-03295 and ATM-87-13227) supported this work. The computations were made at the National Center for Atmospheric Research (NCAR), which is sponsored by the National Science Foundation, with a computing grant #35381017 from the NCAR computing facility.

## REFERENCES

- Broccoli, A.J., Manabe, S., 1987: The influence of continental ice, atmospheric CO<sub>2</sub>, and land albedo on the climate of the last glacial maximum, *Climate Dynamics*, 1: 87-99.
- COHMAP Members, 1988: Climatic changes of the last 18,000 years: Observations and Model Simulations, *Science*, 241: 1043-1052.
- Covey, C., Schneider, S.H., and Thompson, S.L., 1984: Global atmospheric effects of massive smoke injections from a nuclear war: Results from general circulation model simulations, *Nature*, 308: 21-25.
- Covey, C., Thompson, S.L., and Schneider, S.H., 1985: Nuclear Winter: A diagnosis of atmospheric general circulation model simulations, *J. Geophys. Res.*, 90: 5615-5628.
- Gallimore, R.G., and Kutzbach, J.E., 1988: Effects of soil moisture on the sensitivity of a climate model to earth orbital forcing at 9000 yr BP, *Climatic Change*, accepted pending revision.
- Harvey, L.D.D., 1988: Climatic impact of ice age aerosols, *Nature*, in press.
- Hays, J.D., Imbrie, J., and Shackleton, N.J., 1976: Variations in the Earth's orbit: Pacemaker of the ice ages, *Science*, 194: 1121-1132.
- Janecek, T.R., and Rea, D.K., 1985: Quaternary fluctuations in the northern hemisphere trade winds and westerlies, *Quat. Res.*, 24: 150-163.
- Kutzbach, J.E., 1981: Monsoon climate of the early Holocene: Climate experiment with the Earth's orbital parameters for 9000 years ago, *Science*, 214: 59-61.
- Kutzbach, J.E., 1987: Model simulations of the climatic patterns during the deglaciation of North America, In: Ruddiman, W.F. and H.E. Wright, Jr., Eds., *North America and Adjacent Oceans during the Last Deglaciations, The Geology of North America Vol. K-3, Geological Society of America, Boulder, CO, Chapter 19, pp. 425-446.*
- Kutzbach, J.E., and Gallimore, R.G., 1988: Sensitivity of a coupled atmosphere/mixed-layer ocean model to changes in orbital forcing at 9000 yr BP, *J. Geophys. Res.*, 93: 803-821.

- Kutzbach, J.E., and Guetter, P.J., 1986: The influence of changing orbital parameters and surface boundary conditions on climate simulations for the past 18,000 years, *J. Atmos. Sci.*, 43 (16): 1726-1759.
- Kutzbach, J.E., and Otto-Bliesner, B.L., 1982: The sensitivity of the African-Asian monsoonal climate to orbital parameter changes for 9000 yr B.P. in a low-resolution general circulation model, *J. of Atmos. Sci.*, 39 (6): 1177-1188.
- Kutzbach, J.E., and Street-Perrott, F.A., 1985: Milankovitch forcing of fluctuations in the level of tropical lakes from 18 to 0 kyr BP, *Nature*, 317: 130-134.
- Kutzbach, J.E., and Wright, H.E., Jr., 1985: Simulation of the climate of 18,000 yr BP: Results for the North American/North Atlantic/European sector and comparison with the geologic record, *Quat. Sci. Rev.*, 4: 147-187.
- Liu Tungsheng, An Zhisheng, Yuan Baoyin and Han Jiamao, 1985: The loess-paleosol sequence in China and climatic history, *Episodes*, 8: 21-28.
- Manabe, S., and Broccoli, A.J., 1985: The influence of continental ice sheets on the climate of an ice age, *J. Geophys. Res.*, 90,: 2167-2190.
- Merrill, J.T., 1987: Modeling long-range transport using trajectory techniques, Paper presented at the NATO Advanced Workshop on Paleoclimatology and Paleometeorology: Modern and past patterns of global atmospheric transport, Oracle, Arizona, Nov. 15-19, 1987.
- Mitchell, J.F.B., Grahame, N.S., and Needham, K.H., 1988: Climate simulations for 9000 years before present: seasonal variations and the effect of the Laurentide ice sheet, *J. Geophys. Res.*, 93: 8283-8303.
- Petit, J., 1987: Vostok ice core: The dust-record over the last climatic cycle, Paper presented at the NATO Advanced Workshop on Paleoclimatology and Paleometeorology: Modern and past patterns of global atmospheric transport, Oracle, Arizona, Nov. 15-19, 1987.
- Petit-Maire, N., 1986: Palaeoclimates in the Sahara of Mali. A multi-disciplinary study, *Episodes*, 9: 7-16.

- Pisias, N.G., and Leinen, M., 1984: Milankovitch forcing of the oceanic system: evidence from the northwest Pacific, *In: Berger, A., J. Imbrie, J. Hays, G. Kukla, and B. Saltzman, Eds., Milankovitch and Climate, Understanding the Response to Astronomical Forcing, Part 1*, D. Reidel Publishing Co., Hingham, Mass., pp. 307-330.
- Pokras, E.M., and Mix, A.C., 1985: Eolian evidence for spacial variability of late Quaternary climates in tropical Africa, *Quat. Res.*, 24: 137-149.
- Prell, W.L., and Kutzbach, J.E., 1987: Monsoon variability over the past 150,000 years, *J. Geophys. Res.*, 92: 8411-8425.
- Rea, D.K., and Leinen, M., 1988: Asian aridity and the zonal westerlies: late Pleistocene and Holocene record of eolian deposition in the northern Pacific Ocean, *Paleo., Paleo., Paleo.*, in press.
- Rind, D., and Peteet, D., 1985: Terrestrial conditions at the last glacial maximum and CLIMAP sea-surface temperature estimates: Are they consistent?, *Quat. Res.*, 24: 1-22.
- Royer, J.F., Deque, M., and Pestiaux, P., 1984: A sensitivity experiment to astronomical forcing with a spectral GCM: simulation of the annual cycle at 125,000 BP and 115,000 BP, *In: Berger, A., J. Imbrie, J. Hays, G. Kukla, and B. Saltzman, Eds., Milankovitch and Climate, Part 2*, D. Reidel, Hingham, Mass., pp. 733-764.
- Street-Perrott, F.A., 1986: The response of lake levels to climatic change - implications for the future, *In: Climate Vegetation Interactions, Report OIES-2, Office for Interdisciplinary Earth Studies (OIES), University Corporation for Atmospheric Research (UCAR), Boulder, CO*, pp. 77-80.
- Thompson, S.L., 1985: Global interactive transport simulations of nuclear war smoke, *Nature*, 317: 35-39.
- Thompson, S.L., Ramaswamy, V., and Covey, C., 1987: Atmospheric effects of nuclear war aerosols in GCM simulations: influence of smoke optical properties, *J. Geophys. Res.*, in press.

Webb, T., III, Bartlein, P.J., and Kutzbach, J.E., 1987: Climatic change in eastern North America during the past 18,000 years: Comparisons of pollen data with model results, *In*: Ruddiman, W.F. and H.E. Wright, Jr., Eds., *North America and adjacent oceans during the last deglaciations*, *The Geology of North America Vol. K-3*, Geological Society of America, Boulder, CO, Chapter 20, pp. 447-462.



**SECTION 5.**

**INFERENCES FROM THE SEDIMENTARY RECORD: LOESS, ICE CORES,  
AND OTHER LAND EVIDENCE**

# CLIMATIC CHANGES IN ISRAEL DURING HISTORICAL TIMES AND THEIR IMPACT ON HYDROLOGICAL, PEDOLOGICAL AND SOCIO-ECONOMIC SYSTEMS

A. Issar\*, H. Tsoar\*\* and D. Levin\*

\* The Jacob Blaustein Institute for Desert Research and

\*\*Department of Geography

Ben-Gurion University of the Negev

Sede Boqer Campus, 84993 Israel

**ABSTRACT.** A change from the deposition of loess to that of sand was observed in the southern coastal plain of Israel at the end of the Pleistocene (starting ca. 20 K B.P.). This was explained by a northward movement of the ITCZ (Inter-Tropical Convergence Zone) over East Africa which reduced the number of dust rain storms with a simultaneous northward movement of the East African Monsoonal Belt, which caused a rise in the level of the Nile and with it an increase in the supply of sand to the Mediterranean. Such a change in deposition was also observed at the transition from the Byzantine to the Arab periods (ca. 650 A.D.), and thus a similar climatic change for this historical period, was also suggested. This raised the question whether, prior to this change, a more humid phase did not affect the Levant while a dry spell affected the East African monsoon belt.

The environmental data from this period, such as  $^{18}\text{O}$  and  $^{13}\text{C}$ , as well as pollen of olive and oak trees in a core in the Sea of Galilee, records of the Dead Sea Level and the level of the Nile, indeed show that during the Hellenistic, Roman and Byzantine periods (from about 300 BC. to 600 A.D.) these paleo-environmental conditions existed.

During the more humid period agricultural settlements expanded into the desert and vice versa.

## 1. INTRODUCTION

Until recently, the dominant opinion with regard to the climate of Israel during historical times was that there has been no significant climatic change since the end of the Chalcolithic period. All changes in the flourishing of settlements or desertification, as well as geomorphological changes (such as erosion of stream beds and deposition of sands) were attributed to human activities (Riefenberg 1953, Issar 1968, Evenari et al. 1971).

The need to look for a paleo-climatic model different from the contemporaneous one started with the need to explain the isotope anomaly, as well as the high sulfate content of the paleo-water of

Uppermost Pleistocene age (dated by  $^{14}\text{C}$  to be between 40 to 20 K years old) found in the Nubian sandstone aquifer discovered under the Sinai and Negev deserts (Issar et al. 1972). An explanation was also needed for the observation that during the Uppermost Pleistocene the main layers deposited in the deserts of Sinai and the Negev were loess (Issar and Bruins 1983), while at the end of this period (starting 20 K) sand dunes invaded the region and, simultaneously, the loess of the highlands began to erode (Bowman et al. 1986). The conceptual model which was developed in order to explain all these observations (Issar et al. 1987) suggested that, during the Last Glacial Period, the ITCZ moved southward. This caused a deflection of the trajectories of the rain storms to the south, causing them to enter Sinai and the Negev over northern Africa which resulted in dust and rainstorms laden with airborne salts. These recharged the Nubian Sandstone aquifers with brackish water and deposited loess rich in gypsum and carbonates. The same conceptual model held also for the aridization phase which affected the entire region at the end of the Pleistocene period. This was connected with a northward movement of the ITCZ.

An invasion of sand dunes to the coastal plains which occurred at the end of the Byzantine period (7th century A.D.), was formerly explained by the first author as due to anthropogenic reasons (Issar 1968). The new model for the end of the Pleistocene induced him to shift the blame from man and to put it on nature (Issar and Tsoar 1987). This change of approach triggered an examination of other historical variations in the hydrological and depositional environments in order to find out whether climatic changes may not have been the cause of changes in the socio-economic systems and not vice versa.

In the present article the results of this examination are presented. The observations and the paleo-climatic conceptual model for the transition period from the Uppermost Pleistocene to the beginning of the Holocene, will be described first, followed by the description of the pertinent observations related to historical periods and their explanation in the framework of a similar model.

## 2. OBSERVATIONS RELATED TO THE TRANSITION PERIOD FROM THE UPPERMOST PLEISTOCENE, LOWERMOST HOLOCENE (20 K TO 10 K B.P.)

### 2.1. Lake Levels

The most pronounced event is that of the change in the level of Lake Lisan, the precursor of the Dead Sea (Neev and Emery 1967, Begin et al. 1974). This lake reached its maximum level of about 190 m below MSL at about 20,000 B.P. and dropped to about -400 m sometime between 14,000 and 10,000 B.P.

Shallow lakes existed during the Uppermost Pleistocene also in Wadi Feiran in Central Sinai (Issar and Eckstein 1969). Their  $^{14}\text{C}$  age was

found to be about 20,000. These lakes dried up towards the end of the Pleistocene period.

## 2.2. Paleo-groundwater Different from Contemporary Groundwater

The  $^{14}\text{C}$  dates for the paleo-groundwater found in the sandstones of Lower Cretaceous age under the Sinai and Negev are in the same range as those of the water under the Sahara (Issar et al. 1972, Klitzsch et al. 1976), yet the environmental isotope composition ( $^{18}\text{O}$ ,  $^2\text{H}$ ) and the  $\text{SO}_4$  content of the water differs (Issar et al. 1972).

2.2.1. Environmental Isotopes. It was shown by Gonfiantini et al. (1976) and Sonntag et al. (1979) that the paleo-water found in the "Intercalaire continental" under the Sahara shows a pronounced depletion of the  $^{18}\text{O}$  and  $^2\text{H}$  as one travels from the Atlantic coast eastwards. This was explained by Sonntag et al. (op. cit.) as a function of the continental effect due to the fact that the rainstorms which recharged the sandstones of the Sahara aquifers came from the Atlantic Ocean. On the other hand, the paleo-water in Sinai and the Negev, were found not to follow the continental effect pattern and, though remaining on the global meteoric line, were found to be heavier than those of the Eastern Sahara.

The isotopic composition of the paleo-water of Sinai and the Negev differ also from the isotopic composition of contemporary groundwater. The latter are similar in composition to that of the precipitation of most of the storms at present coming along the northern and northwestern trajectories to the Negev. In this respect they fall on the Mediterranean line of  $d = +22\text{‰}$  (Gat and Dansgaard 1972). It was shown, however, that some of them which arrive along western or southwestern trajectories are similar to the paleo-water (Leguy et al. 1983, Rindsberger et al. 1983, Gat and Rindsberger 1985). In order to explain these anomalies it was suggested that, during the Last Glacial period, rainstorms reached Sinai and the Negev after entering the continent over the coast of Libya and Egypt (Issar et al. 1987).

2.2.2. Sulfate Anomaly. The paleo water under the Sinai and Negev are characterized by high  $\text{CaSO}_4$  content which differs from the paleo-water of the Sahara as well as from the contemporary groundwater of the Negev. This anomaly corresponds with the high sulfate content found in the loess layers of the same age (Uppermost Pleistocene ca. 80 K to 20 K) found in the Negev (Issar et al. 1988).

Gypsum layers of the same age are found along the Mediterranean coast of Egypt. The enrichment in gypsum was explained as a function of the retreat of the sea due to the Last Glacial, exposing a very shallow shelf. This caused the formation of sabkhas. The rainstorms coming over these sabkhas were enriched by halite, sulfate and carbonate. These recharged the Nubian Sandstone aquifers and were deposited together with the loess.

### 2.3. Loess Deposits (Figs. 1,2)

Thick loess deposits are the characteristic sediments of the Uppermost Pleistocene (Bruins and Yaalon 1979). Issar and Bruins (1983) suggested that the special climatic conditions prevailing during the Last Glacial period caused heavy dust storms to precipitate heavy dust loads on the Negev. Towards the end of the glacial period, at ca. 20 K, deposition of the loess was reduced and the encroachment by sand dunes started. In the highlands of the Negev, the loess layers went through an erosion phase (Bowman et al. 1987).

The same as other loess deposits in the world, the Negev loess consists of a high content of coarse silt (31-62  $\mu\text{m}$ ), which decreases in size from its source. As rainfall increases, the rate of leaching and weathering of deposited dust is boosted (Pye and Tsoar, 1987), giving it pedogenetically-altered appearance which displays numerous carbonate horizons (Issar and Bruins 1983, Goodfriend and Magaritz 1988).

The pedogenetically-altered loess of the Negev exhibits up to seven palaeosols each of which with a calcic horizon. This succession of palaeosols indicate wet periods of pedogenesis and intermittent drier periods during which extensive erosion took place.  $^{14}\text{C}$  dating of the upper three calcic horizons retrocedes us to ages of 37,000; 28,000 and 13,000 years B.P., respectively (Goodfriend and Magaritz 1988). No loess deposits occurred after the end of the Upper Pleistocene. The periods between the above mentioned ages are regarded as dry and cold whereas the palaeosols are attributed to warm phases of the last glacial period (Goodfriend and Magaritz 1988).

Modern dust deposition rates in Israel lie in the range of 0.020 - 0.083  $\text{mm yr}^{-1}$  (Ganor 1975, Yaalon and Ganor 1975), well below the critical value of 0.5  $\text{mm yr}^{-1}$  suggested by Pye (1984) for accumulation of recognizable loess in semi-arid areas. Most of the coarse and medium silt deposited by contemporary dust storms in Israel originates probably from local sources and only part of the particles finer than 20  $\mu\text{m}$  comes from North Africa (Tsoar and Pye 1987).

In conclusion, Negev loess deposits stems mainly from the late Pleistocene (Issar and Bruins 1983, Issar et al. 1987) when northern Sinai was covered, not by sand dunes as today, but by poorly sorted fluvial deposits (Sneh 1982) which could have been the source of dust. Several lines of evidence indicate that cyclonic rain-bearing winds were then more frequent and that the climate of the Negev and Sinai was wetter during glacial times (Issar and Bruins 1983, Issar et al. 1987). Resulting more frequent wadi flow (read greater silt supply), increased windness, and a more vigorous growth of silt-trapping vegetation in the northern Negev should all have been tantamount to generous loess accumulation at that time. Progressive dessication during the Holocene caused stripping of loess from interflaves and its redeposition in valleys and closed basins. Much of today's Negev loess was re-deposited by running water (Sneh, 1984).

#### 2.4. Sand Dunes

The source of Israel's southern Mediterranean beach sand is the Nile, as shown by Pomerancblum (1966) who used a heavy-mineral analysis, and by Emery and Neev (1960) showing a decrease in grain-size northwards until Tel Aviv, and a posterior uniformity of grain-size up to Haifa, attributed to the eroded aeolianite cliffs there as an additional sand source.

The Nile sediments are carried eastward by the longshore currents along the shores of Sinai and Israel. The fact that the Israeli coastal dune strip is wider (5 to 6 km) than the Sinai one (2 to 3 km) is attributed to the wind. In Sinai the shoreline runs parallel to direction of the winter wind storms and perpendicular to the summer low and moderate winds. Towards Israel the beach turns more perpendicular to the winter W and SW high winds and also to the summer sea breeze. Recent field measurements for the coast of Israel between Gaza and AKko show that the aeolian net sand transport from the beach to the dunes is  $42,000 \text{ m}^3 \text{ yr}^{-1}$  (Goldsmith and Golik 1980, Goldsmith et al. 1988). Hence, the formation of coastal dunes along the Israeli coasts requires the delivery of adequate supplies of sand by longshore currents, as also onshore storm winds that blow perpendicularly to the shorelines and are capable of moving the sand. The climate is, however, not a limiting causative (Pye 1983).

Two main groups of active sand dunes are known in Israel and northern Sinai. One encompasses the inland sand dunes and the other coastal dunes of northern Sinai between the Suez Canal in the west, and the northwestern Negev, in the east. They became gradually stabilized toward the northeast, where they underwent pedogenic development and were eventually covered by coastal dunes (Fig. 1).

Active coastal sand dunes extend themselves parallel to the shoreline, from the eastern part of the Bardawil lagoon in northern Sinai unto Tel-Aviv, and also in some isolated areas north of Tel-Aviv up to Haifa Bay.

All loess deposits are overlain by inland dune sand thus indicating their older age (Fig. 2). It is clear from field observations that coastal sand dunes are younger than inland ones. Some indications are that ancient and defunct drainage channels in inland dune areas were blocked and covered by coastal sand dunes. The color of the sand in northern Sinai becomes progressively redder as it departs from the coast (Tsoar 1976), which is indicative of greater age and longer distance of transport (Norris 1969, Walker 1979).

Absolute age of sand is ascertainable by archaeological finds. The first known aeolian sand penetrated into Sinai and the Negev toward the late Upper Paleolithic (ca. 20,000 B.P.; Goldberg, 1986, Goren and Gilead 1986). In the Shunera sand dunes of the Negev there is some evidence pointing at Upper Paleolithic and Epi-Paleolithic ages (ca. 20,000 to 10,000 B.P.) for fixed sands (Goring-Morris 1987). These dune deposits probably spring from increased aridity at 20,000 - 19,000 B.P. (Goodfriend and Magaritz 1988). They presumably stabilized during the

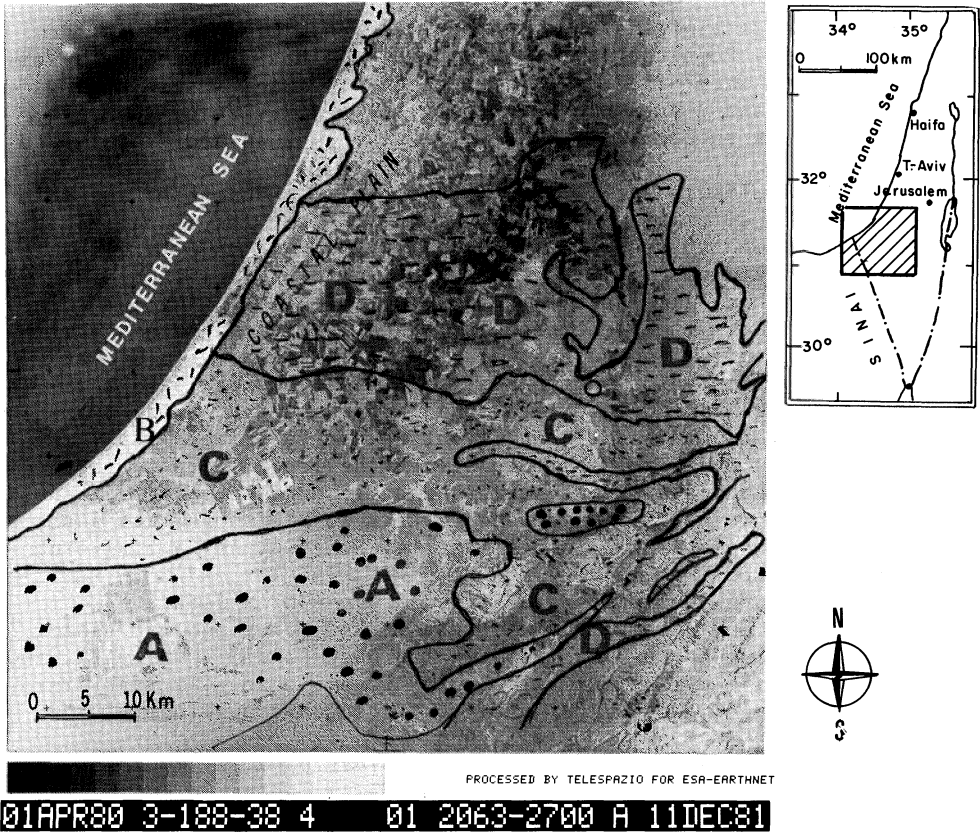


Fig. 1: Satellite image of Western Negev.

- Legend:
- A: Inland sand dunes;
  - B: Coastal sand dunes;
  - C: Stabilized sand
  - D: Loess.



Fig. 2: Sand dunes overlying loess in Western Negev



later Epi-Paleolithic when wetter conditions prevailed. The sand dunes covering most of northern Sinai and western Negev may be younger. The youngest archaeological discoveries within inland dune sand go back to the Chalcolithic (ca. 5,000-6,000 B.P., Goren and Gilead 1986).

From the above findings we can conclude that the encroachment of the inland sand dunes dates back from 20,000 to 5,000 B.P. It is possible that this invasion occurred in several phases during this long period. It is generally accepted that during the period from 5,000 to 1,300 B.P. no invasion of sand took place and that the inland dunes became stabilized.

### 3. OBSERVATIONS RELATED TO PROTO-HISTORICAL AND HISTORICAL PERIODS

#### 3.1. Dead Sea Levels

A prehistorical high level was found to have occurred at the Upper Neolithic period ( $6660 \pm 400$  years B.P.) (Goodfriend and Magaritz 1987). The mapping of historical shore lines of the Dead Sea was carried out by Klein (1981). The most pronounced one is a high sea level from about 50 B.C. to 100 A.D. (Fig. 3), which reached a maximum level of -330 m (namely, 70 meters above the present level). This change in level and volume was run on an hydrological mathematical model which equated levels of the Dead Sea and precipitation, as well as runoff from its drainage basin. This model was prepared by TAHAL (Water Planning for Israel) to predict size by the level of the Dead Sea in case the Mediterranean Dead Sea Project is executed. It showed that an increase in precipitation of about 50% is needed in order to bring up the level of the Dead Sea 70 meters during that period.

#### 3.2. Sediments of the Sea of Galilee

In 1979 several cores were recovered from Lake Kinneret, Israel. The sediments were dated by  $^{14}\text{C}$  and analyzed for their carbonate contents and  $^{18}\text{O}/^{16}\text{O}$   $^{13}\text{C}/^{12}\text{C}$  ratios (Stiller et al. 1984). Their microbotanical (pollen and algae) and microfaunal (diatoms) compositions were also investigated (Baruch 1986). The periodic variations, especially of the pollen, were interpreted as reflecting environmental changes due to human intervention (Stiller et al. 1984, Baruch 1986).

Reanalysis of the data presented in these investigations was prompted by the conclusion of the present authors reached from a more general study that humid climatic conditions prevailed in the Negev desert of Israel from ca. 300 B.C. to ca. 600 A.D. This raised the question whether the data from Lake Kinneret, especially the  $^{18}\text{O}$  (which is a good paleo-climate indicator) might not be used as supporting evidence in the paleo-climatic research of the Negev desert. The reanalysis was done by using the moving average of 12 data points, plotted vs. the time scale, evenly divided. This statistical method was

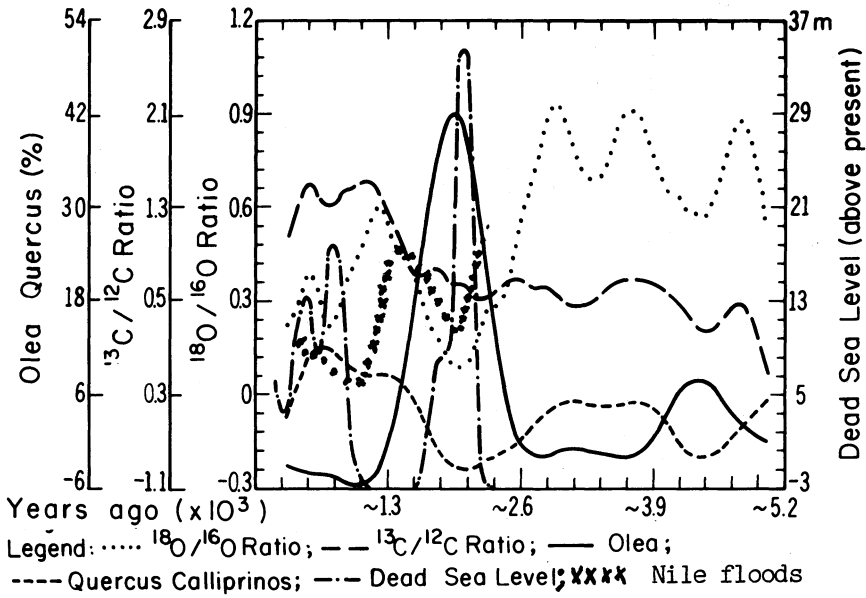


Fig. 3: Moving average of  $^{18}\text{O}/^{16}\text{O}$ ,  $^{13}\text{C}/^{12}\text{C}$   
 Olea/Quercus pollen ratio relative to present (Stiller et al, 1984). Ancient levels of the Dead Sea relative to present (Klein, 1982). Nile floods ancient levels (Nicholson, 1980).

chosen in order to smooth out short-term variations. The average was calculated relative to contemporary levels of variants as recorded in the top layers of this core (Fig. 3). The 12 data points average ensured that most recent anthropogenic changes (drying up of Lake Hula, pumping of water from Lake Kinneret) would not affect the calculations drastically.

The most pronounced co-variation (between 190 and 290 cm depth) was found, according to  $^{14}\text{C}$  dating, to have taken place between ca. 2,300 and ca. 1,400 years B.P. At the peak of this period (260 cm depth; about 2,010 years B.P.) the Olea constituted about 95% of the total arboreal pollen (Baruch 1986). Parallel to the increase in Olea, there is a reduction in Quercus pollen as well as a depletion of  $^{18}\text{O}/\text{oo}$  and  $^{13}\text{C}/\text{oo}$ . These results reflect, in the opinion of the present authors, a cooler and more humid climate. These climatic changes are reflected in the assemblage of the pollen which co-variate. The reason for the change in the olive and the oak content is due to the fact that the basin of Lake Kinneret is semi-arid; thus humid climate led the inhabitants to cut the natural oak vegetation and plant olive trees instead. The drying up caused the plantations to become non-economic and consequently they were deserted.

The other pronounced co-variation in the assemblage of pollen as well as in the environmental isotopes occurs in the layers between 400cm and 430cm, calculated according to the  $^{14}\text{C}$  dating to be between ca. 4,300 and ca. 4,000 B.P. (Fig. 3). Though quantitatively the rate of change is smaller, the co-variation is similar to that mentioned above. This suggests a similar climatic change, which triggered the cutting of the natural vegetation and the planting of olive trees, also at this early date in human history.

The other low  $^{18}\text{O}$ , and thus presumably cold phases observed in the core of Lake Kinneret (Fig. 3), are that at around 5,200 B.P. (Lower Early Bronze), and that around 3,400 B.P. (Late Bronze to Iron Age). This agrees with Goodfriend's (1988) estimates that during the period between 2,790 to 3,350 B.P. a shift southward (of about 20 to 30 km) of the isohyets, which implies a two-fold increase in mean annual rainfall occurred. He based his estimation on the changes in the  $^{13}\text{C}/^{12}\text{C}$  in land snails from this period. Another depletion of  $^{18}\text{O}$  is that of ca. 750 and a low level of  $^{18}\text{O}$  is also observed in the Kinneret core, sometime from the middle to the end of the last century.

### 3.3. Groundwater Levels

In the western part of Israel, Rosen (1986) found that the groundwater table during the Byzantine period was higher than today's level and the Wadi bed was about 2.5 to 3.5 meters above the present channel. She suggests that the climate may have been more moist than the present. Nir and Eldar (1987) found that the groundwater table in a Byzantine well in the coastal plain was higher than the preceding and following periods.

### 3.4. Alluvial Processes

Bruins (1986) observed that at the end of the Byzantine period a severe erosive process started at the head of a stream bed draining to Wadi El-Arish of Sinai. This conforms with the observation of Rosen stated above, namely, that during the Roman-Byzantine period the Wadi beds were higher.

### 3.5. Sand Dunes

Issar (1968) found that the youngest layers covered by the dunes of the coastal plain of Israel (Fig. 1) contain ample Hellenistic to Roman-Byzantine artifacts, from which he concluded that the dunes are post-Byzantine. This conclusion has been confirmed by later archaeological investigations (Dotan 1982, 1985).

### 3.6. Nile River Levels

As these sands are derived from the Nile Delta (Emery and Neev 1960) it is interesting to compare the levels of the Nile (Nicholson 1980) with the levels of the Dead Sea (Fig. 3). This shows that there exists covariation but in opposing directions between these two curves.

## 4. THE SYNTHESIS

In the first place the contemporary climatic model has to be described.

The Negev of Israel lies at the northern boundary of the Sahara belt. During the summer the arid climate is decided by this high-pressure zone. During winter, when this zone moves south, the Negev comes under the influence of the Westerlies which blow from the Atlantic over Europe and are then deflected by the Mediterranean Sea into a more southern trajectory. Here they pick up more moisture which is precipitated as winter rains. Thus the humidity of the countries along the southern and eastern Mediterranean shores is decided by the southern migration of the ITCZ the Sahara and the Westerlies low pressure zones in its wake. The further from the seashore a place is situated, the less rain it gets, with the positive exception of high altitude areas and negative exception of areas located in the rain-shadow, like the Jordan-Dead Sea rift valley.

During spring and autumn the interplay between low-pressure marine air mass and high-pressure continental air mass causes dry winds to blow from the desert causing heavy dust storms. A rain storm which may follow such a dry, usually hot, wind will cause the dust to settle and be carried by floods.

Egypt is fed by the water of the Nile which is fed by the tropical and subtropical rains. These rains fall on the mountains of Eastern Africa and drain to the Nile. The tropical rains feed the White Nile

during most of the year, while the Blue Nile gets its supply from the monsoonal rains which come from the Indian Ocean and fall on the central and northern highlands of Ethiopia during the summer. These monsoonal rains depend also on the northern migration of the ITCZ. When this belt fails to move northward enough to allow the monsoons to reach these highlands the summer floods of the Nile will diminish.

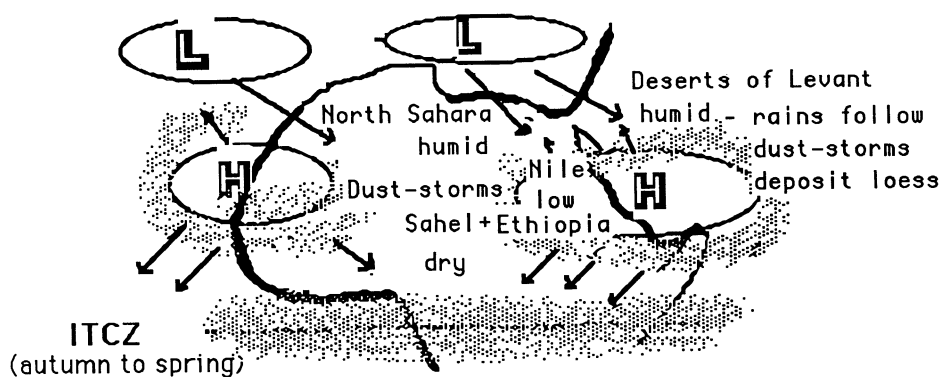
These floods carry tremendous quantities of silt and sand which are carried into the Mediterranean where they are picked by counterclockwise currents and brought to its south eastern coast. Here they are washed ashore by the waves, picked by the winds and driven inland as sand dunes.

It is assumed by the present authors that during the Uppermost Pleistocene (Last Glacial period) the ice covering northern Europe created a strong meridional temperature gradient to the south of its margins, displacing the westerlies southward into North Africa. This was accompanied by a southward displacement of the main tracks of cyclonic storms. Thus many disturbances were presumably moving over the Libyan and Egyptian deserts during the cold season. Several of these storms were associated with strong surface winds that raised dust into the atmosphere ahead of their cold fronts. It is believed that a majority of the winter precipitation of that period in the Sinai and the Negev was accompanied by heavy dust depositions which caused the formation of the loess layers in these regions (Issar and Bruins 1983). All observations show that at the same time the monsoon system was much weaker which resulted in low levels of the African lakes and the Nile (Prell and Kutzbach 1987, Kutzbach 1987). The end of the Pleistocene evidenced a severe reduction in the number of this type of dust-rainstorm and thus a decrease in the rate of deposition of the loess. On the other hand, the monsoon system became stronger as the Nile started bringing large quantities of sand which covered northern Sinai and central Negev (Fig. 4). As at approximately the middle of the first millenium A.D. the same encroachment of sand dunes over loessial soils has been observed in the southern part of the coastal plain of Israel, it is suggested to apply the Pleistocene-Holocene model of climatic change to this period too. This suggestion is substantiated by the observations from the sediments of the Sea of Galilee. These also show that, at approximately the middle of the first millennium B.C., a global cold period started which affected the Levant most probably causing it to be more humid.

## 5. CONCLUSIONS

Climatic fluctuations from more humid to more arid affected Israel at the end of the Pleistocene and at the middle of the first Millenium A.D. An opposite change occurred in the monsoonal zone of East Africa. The simultaneity of the changes speak for a movement of the ITCZ, as both zones are situated, one on the northern, the other on the southern,

## PLEISTOCENE [ GLACIAL ] PALEOCLIMATE



## HOLOCENE [ INTER-GLACIAL ] CLIMATE

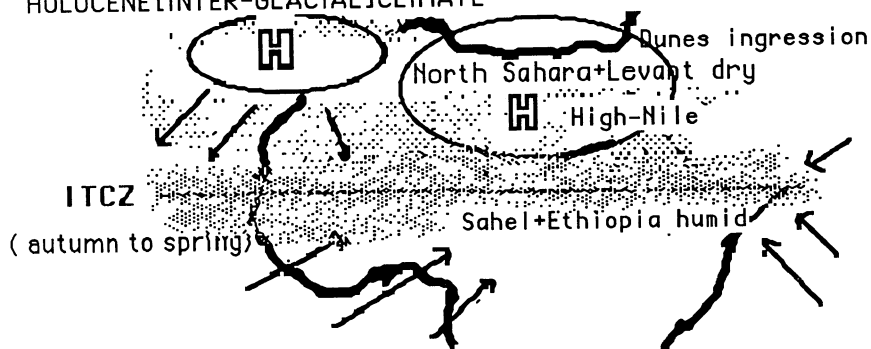


Fig. 4: Paleo-climatic maps. (Based on Nicholson and Flohn, 1980).

margins of the ITCZ. The humid periods were characterized in Israel by dust and rainstorms causing the deposition of loess, and the arid periods, by the encroachment of sand dunes originating in the Nile and transported by sea and wind.

The humid periods were characterized by the settlement of man in the desert and vice versa.

A similar humid stage affected Israel also during the Early Bronze (ca. 2200 B.C.).

Another conclusion from the conceptual model suggested in this work is that the climate in monsoonal East Africa will behave in a opposite manner to that of the Levant, namely that dry periods in the Mediterranean will synchronize with wet period in East Africa. Proof that this was the case has already been shown on the Nile floods curve. Other similar proof for example is that of Lake Turkana in Kenya (Owen et al. 1982) and Lake Abbe in Ethiopia (Nicholson 1980).

#### 6. REFERENCES

- Begin Z.B., Ehrlich A. & Nathan Y. (1974). 'Lake Lisan, the Pleistocene precursor of the Dead Sea.' Bull. No. 63. Geological Survey, Ministry of Commerce & Industry, State of Israel, 30 p.
- Baruch, U. (1986). 'The Late Holocene vegetational history of Lake Kinneret' (Sea of Galilee), Israel. Paleorient Vol. 12/2:137-148.
- Bowman D., Karnieli A., Issar A. & Bruins H.J. (1986). 'Residual colluvio-aeolian aprons in the Negev highlands, Israel, as a paleo-climatic indication.' Paleoqeoq. Paleoclimat. Paleobot., 56:89-101.
- Bruins H.J. (1986). 'Desert environment and agriculture in the central Negev and Kadesh-Barnea during historical times.' Midbar Foundation / Nijkerk, The Netherlands, 219 p.
- Bruins H.J. & Yaalon D.H. (1979). 'Stratigraphy of the Netivot section in the desert loess of the Negev (Israel).' Act. Geol. Acad. Scient. Hungaricae, 22(1-4):161-169.
- Dotan T. (1981). Deir El Balah, Prelim. Report. Israel Exp. J. 31:126-131.
- Dothan, T. (1982). 'Lost outpost of the Egyptian Empire'. National Geographic 62:739-769.
- Emery K.D. & Neev D. (1960). 'Mediterranean beaches of Israel.' Geol. Survey Israel, Bull. 26, 1-24 p.
- Evenari M., Shanan L. & Tadmor N. (1971). The Negev: The Challenge of a Desert. Harvard University Press, Cambridge, Mass., 345 p.
- Ganor, E. (1975). Atmospheric Dust in Israel - Sedimentological and Meteorological analysis of Dust Deposition. Ph.D. Thesis, Hebrew University of Jerusalem. (In Hebrew).
- Gat J.R. & Dansgaard W. (1972). 'Stable isotope survey of fresh water occurrence in Israel and the Jordan Rift Valley.' J. Hydrology 16:177-211.

- Gat J.R. & Rindsberger M. (1985). 'The isotopic signature of precipitation originating in the Mediterranean Sea area.' Israel J. of Earth Sciences 34:80-85.
- Goldberg, P. (1986). 'Late Quaternary Environmental History of the Southern Levant.' Geoarchaeology 1:225-244.
- Goldsmith, V., & A. Golik (1980). 'Sediment Transport Model of the Southeastern Mediterranean Coast.' Marine Geology 37:147-175.
- Goldsmith, V., P. Rosen, & Y. Gertner (1988). 'Eollian Sediment Transport on the Israeli Coast'. Final Report to U.S. - Israel BSF, Jerusalem.
- Gonfiantini R., Conrad G., Fontes F.C., Sauzay G. & Payne B.R. (1974). 'Etude isotopique de la nappe du Continental Intercalaire et de ses relations avec les autres nappes du Sahara septentrional.' Isotope Techniques in Groundwater Hydrology (Proc. Symp. Vienna, 1974) 1:227, IAEA, Vienna.
- Goodfriend, G.A. (1988). 'Mid-Holocene rainfall in the Negev desert from  $^{13}\text{C}$  of land snail shell organic matter.' Nature 333:757-760.
- Goodfriend C.A. & Magaritz M. (1987). 'A high stand of the Dead Sea at the end of the Neolithic Period.' Climatic Change 9:349-356.
- Goodfriend, G.A., & M. Magaritz (1988). 'Palaeosols and Late Pleistocene Rainfall Fluctuation in the Negev Desert.' Nature 332:144-146.
- Goren, Y., & I. Gilead (1986). 'Man and Environment in Nahal Seker, Northern Negev, during the Quaternary.' Mitkofat Aeven 19:58-70 (In Hebrew).
- Goring-Morris, A.G. (1987). At the Edge. Bar, Oxford.
- Issar A. (1968). 'Geology of the central coastal plain of Israel.' Israel J. Earth Science 17(1):16-29.
- Issar A. & Eckstein Y. (1969). 'The Lacustrine beds of Wadi Feiran, Sinai.' Israel J. Earth Science 18(1):29-32.
- Issar A., Bein A. & Michaeli A. (1972). 'On the ancient water of the Upper Nubian sandstone aquifer in central Sinai and southern Israel.' J. of Hydrol. 17:353-374.
- Issar A. & Bruins H. (1983). 'Special climatic conditions in the Sinai and Negev during the Most Upper Pleistocene.' Paleogeog. Paleoclimat. Paleoeco. 42: 63-72.
- Issar A. & Tsoar H. (1987). 'Who is to blame for the desertification of the Negev Israel; the influence of climatic variability on the hydrologic regime and water resources.' Proc. Vancouver Symp. IAHS, Publ. No. 168:577-583.
- Issar A.S., Tsoar H., Gilead Y. & Zangvil A. (1987). 'Paleoclimatologic model to explain depositional environments during Late Pleistocene, in the Negev, Israel.' In: Progress in Desert Research, (eds.) Berkofsky, L. & Wurtele, M.G., Rowman and Allanhead, 302-309
- Issar A., Bahat D & E. Wakshal. (1988). 'Occurrence of secondary gypsum veins in joints in chalks in the Negev, Israel.' Catena 15:241-242.
- Klein C. (1982). 'Morphological evidence of lake level changes, western shore of the Dead Sea.' Israel J. Earth Sciences 31:67-94.



- Klitzsch von E., Sonntag C., Weistroffer K. & El Shazly E.M. (1976). 'Grundwasser der Zentralsahara: Fossile vorrate.' Geol. Rundschau 65(1):264-287.
- Kutzbach J.E. (1987). 'The changing pulse of the monsoons.' In: Monsoons (Eds. Fein J.S. & Stephens P.L.), John Wiley & Sons Inc. 247-267.
- Leguy C., Rindsberger M., Issar A. & Gat J. (1983). 'The relation between  $^{18}\text{O}$  and deuterium content of rainwater in the Negev and air masses trajectories.' J. of Isotope Geosciences 1:205-218.
- Neev D. & Emery K.D. (1967). 'The Dead Sea: Depositional processes and environments of evaporites.' Geol. Surv. Israel Bull. 41:147.
- Nicholson, S.E. (1980). 'Saharan climates in historic times.' In: Sahara and the Nile, (eds.) Williams, M.A.J. & Faure, H.J., Balkema, Rotterdam, 173-200.
- Nicholson S.E. & Flohn H. (1980). 'African environmental and climatic changes and the general circulation in the Late Pleistocene and Holocene.' Climatic Change 2(4):313-348.
- Nir Y. & Eldar I. (1987). 'Ancient wells and their geoarchaeological significance in detecting tectonics of the Israel Mediterranean coastline region.' Geology 15:3-6
- Norris, R.M. (1969). 'Dune Reddening and Time.' Jour. Sed. Petrology 39:7-12.
- Owen, R.B., Barthelme, J.W., Renaut, R.W. & Vincens, A. (1982). 'Palaeolimnology and Archaeology fo Holocene Deposits North-East of lake Turkana, Kenya.' Nature 298(587):523-529.
- Pomerancblum, M (1966). 'The Distribution of Heavy Minerals and their Hydraulic Equivalent in Sediments of the Mediterranean Continental Shelf of Israel.' Jour. Sed. Petrology 36:162-179.
- Porath, Y. (1975). 'Kayseri Gardens.' Gadmoniot 8:90-93. (In Hebrew).
- Prell W.L. & Kutzbach J.E. (1987). 'Monsoon variability over the past 150,000 years.' J. of Geophysical Res. 92 (10.D7):8411-8425.
- Pye, K. (1983). 'Coastal Dunes.' Progress in Physical Geography 7:531-557.
- Pye, K (1984). 'Some perspective on loess accumulation.' Loess Lett. 11:5-10.
- Pye, K. & H. Tsoar (1987). 'The Mechanics and Geological Implications of Dust Transport and Deposition in Deserts with Particular Reference to Loess Formation and Dunes Diagenesis in the Northern Negev, Israel.' In: Desert Sediments: Ancient and Modern, (eds.) Frostick, L. & Reid, I., Geological Society Special Publication 35:139-156.
- Riefenberg, A. (1953). 'Desert Research.' Res. Counc. Isra. Bull. Jerusalem 3:378-391.
- Rindsberger M., Magaritz M., Carmi I. & Gilad D. (1983). 'The relation between air mass trajectories and the water isotope composition of rain in the Mediterranean Sea area.' Geophys. Res. Lett. 10:43-46.
- Rosen A.M. (1986). Cities of the Clays: The Geoarchaeology of Tells. University of Chicago Press, 280 p.

- Sneh, A. (1982). 'Drainage Systems of the Quaternary in Northern Sinai with Emphasis on Wadi El-Arish.' Z. Geomorph. N.F. 26:179-195.
- Sneh, A. (1984). 'Redeposited Loess from the Quaternary Besor Basin, Israel.' Israel J. Earth Science 32:63-69.
- Sonntag C., Neureuther P., Lalinke Ch., Munnich K.O., Klitzsch E. & Weistroffer K. (1976). 'Zur Paläoklimatik der Sahara. Kontinentaleffekt im D- und O-18-Gehalt pluvialer Saharawasser.' Naturwissenschaften 63:479.
- Stiller, M., Ehrlich, A., Pollinger, U., Baruch, U. & Kaufman, A. (1984). 'The Late Holocene sediments of lake Kinneret (Israel) - multidisciplinary study of a 5m core.' In: Geological Survey of Israel, Ministry of Energy and Infrastructure, Jerusalem, Israel.
- Stuvier, M. (1970). 'Oxygen and Carbon Isotope Ratios of Fresh Water Carbonates as Climatic Factors.' J. of Geophys. Res. 75(27): 5247-5257.
- Tsoar, H. (1976). 'Characterization of Sand Dune Environments by their Grain-Size, Mineralogy and Surface Texture.' In: Geography in Israel, (eds.) Amiran, D.H.K. & Ben-Ariueh, Y., IGU, Jerusalem, p. 327-343.
- Tsoar, H. and Pye, K (1987). 'Dust Transport and the Question of Desert Loess Formation'. Sedimentology 34:139-153.
- Walker, T.R. (1979). 'Red Color in Dune Sand'. In: A Study of Global Sand Seas, (ed.) McKee, E.D., U.S. Geol. Surv. Prof. Paper, 1052, 61-81.
- Yaalon, D.H. and E. Ganor (1975). 'Rate of Aeolian Dust Accretion in the Mediterranean Desert Fringe Environments of Israel.' 1th Congr. IAS, Nice, pp. 169-174.

## THE MINERAL DUST RECORD IN A HIGH ALTITUDE ALPINE GLACIER (COLLE GNIFETTI, SWISS ALPS)

Dietmar Wagenbach and Klaus Geis  
Institut für Umweltphysik  
Universität Heidelberg  
Im Neuenheimer Feld 366  
D-6900 HEIDELBERG, FRG

**ABSTRACT.** Ice-core and snow-pit samples from a non-temperated glacier in the summit range of Monte Rosa, Swiss Alps (4450 m.a.s.l.) has been analyzed for total mineral dust and the size distribution of insoluble particulate matter in the size range 0.63-20 microns. Based on a 50 years-record Saharan dust accounts for two third of the mean mineral dust flux of  $60 \mu\text{gcm}^{-2}\text{yr}^{-1}$ . Both, background and Saharan dust influenced samples show a distinct mode in the volume size distribution of insoluble particles over the optical active size range with a typical volume mean diameter of 2.5 and 4.5  $\mu\text{m}$ , respectively. These two size distribution categories are attributed to the insoluble fraction of the long lived background aerosol and to the relatively short lived aerosol dominated by soil derived dust (i.e. ground-level aerosol in aride areas).

### 1. INTRODUCTION

Up to now the most detailed and best preserved long term records on the chemical and physical properties of the tropospheric background aerosol have been retrieved from ice cores of the polar ice-sheets Greenland and Antarctica. Among others, convincing long term records of glacial concentrations of terrigenous particles and major ions (mineral acids, sea-salt) have been reconstructed for the polar zones of both hemispheres back into the last ice age (Langway *et al.*, 1985, Legrand *et al.*, 1988). Since there is no aerosol production on the surface of the ice-sheets, these records are representative on a large scale and predominantly reflect the history of the aerosol source-strength and/or the poleward long-range transport pattern of the aerosol components in question (disregarding the influence of a change in the local precipitation rate) (see Petit, this issue). A quite different situation holds true for records from glacier fields situated in the mid-latitude and tropical zones. These glaciers are always located within the principal source areas of continental aerosol species, the high elevation of these mountain glacier sites guarantees their existence and will generally control the clean air status, and, hence, the spatial representativeness of the glacio-chemical records (Wagenbach, 1988). From this it becomes evident that the impurity content of high altitude mountain glaciers may rather be representative on a meso- or even regional scale, making these glaciers a very sensitive receptacle for all kinds of particulate matter originating from the continental source areas.

## 1.1 The Environment Archive of Alpine Glaciers

Unfortunately, the major part of mountain glaciers does not show the glacio-meteorological and topographical features which are needed to establish well preserved and datable glacio-chemical records. The most important criteria to select glaciers for ice-core studies of this kind are:

- 1) high elevation (corresponding to a mean annual air temperature well below 0°C) to prevent disturbances of the chemical and isotopic stratigraphy by melt water percolation
- 2) sufficient glacier thickness relative to the annual net snow accumulation to ensure long term records
- 3) large extension and relatively flat surface topography to minimize the influence of glacier flow and of non-homogeneous snow accumulation on the vertical stratigraphy.

The criteria mentioned before are easily accomplished with the polar ice-sheets, but can hardly be achieved simultaneously for the always relatively small areas representing the uppermost part of the accumulation zone of mountain glaciers. Therefore, only a few glaciers from non-polar regions have been used for extensive ice core studies such as Mt. Logan, North-West Canada (Holdsworth *et al.*, 1988), Quelccaya Ice Cap, Peru (Thompson *et al.*, 1985), recently Dunde Ice Cap, China (Thompson *et al.*, 1988) and Colle Gnifetti (Monte Rosa, Swiss Alps), which latter is discussed in this paper.

During a Swiss-German field campaign in 1982 two ice cores have been drilled to the bedrock at the Colle Gnifetti site. Presently these cores are the only ones capable of providing well preserved glacial records from the Alpine environment far beyond the change of the last century. The major objectives of the Colle Gnifetti ice-core program are related to the deposition history of anthropogenic and natural aerosol components in central Europe and to the flow dynamics of high altitude Alpine firn areas (Oeschger *et al.* 1978). Glacio-chemical studies carried out so far on ice core and snow-pit samples from the Colle Gnifetti site (Haeberli *et al.*, 1983; Schotterer *et al.*, 1985; Wagenbach, 1981) show evidence that the bulk impurity content of the glacier is dominated by mineral dust input, which in turn is largely made up of Saharan dust. The transport of Saharan dust to the Alpine region which is frequently accompanied by the occurrence of "red snow or rain" is known to be a common phenomenon (Prodi and Fea, 1978, Haeberli, 1978). Some of the most striking events sometimes observed up to 1000 km north to the Alps are well documented in the literature (Valentin, 1902). In this way the Colle Gnifetti ice cores may offer the opportunity to reconstruct a long term record of the mineral dust burden in the mid - to upper tropospheric level of the mid latitude westerlies. To some extent this record may reflect the history of the northward transport of subtropical air masses to central Europe.

In the present contribution the main feature of the mineral dust record found in the upper part of this Alpine glacier will be presented. Despite chemical and mineralogical properties, the particle size distribution will be most fundamental in gaining a qualitative characterization of the dust deposited. Conclusions based on aerosol and cloud radiative properties, precipitation forming processes as well as on the mean aerosol residence time are very sensitive to the particle size distribution of the dust component concerned. A characterization of the size distribution of the insoluble particulate matter contained in Colle Gnifetti snow and ice-samples which are predominantly affected by clean air conditions or instead by the long range transported Saharan dust is therefore presented in addition. The potential of the Colle Gnifetti dust record in providing reliable information on the past atmospheric dust burden of the Alpine region will be discussed. Important in this context are the clean air status of the site, the time scale covered by the cores and the spe-

cific shortcomings of this glacial archive due to the small scale character of the sampling site.

## 2. DESCRIPTION OF THE SAMPLING SITE

The Colle Gnifetti site (hereafter referred to as CG) forms a small firn col in the summit range of the second highest peak (Monte Rosa) of the Alps. Situated close to the Swiss-Italian border at an elevation of 4450 m a.s.l., the drilling site is exposed to a very steep slope at its southern margin. Due to this specific orographical situation the glacier is directly influenced by air masses advected from southerly directions (see maps in fig. 1). The glacio-meteorological and topographical features of the CG site, known so far from previous field studies, are reported elsewhere (Alean *et al.* 1984, Haeberli *et al.* 1988, Haeberli and Alean 1985). In brief, the glacier thickness of about 130 m in connection with a relatively low annual snow accumulation of 0.2-0.4 m water equivalent per year as well as the low firn temperature close to  $-15^{\circ}\text{C}$  qualify the CG site to provide well preserved long term glacio-chemical records. On the other hand, due to the exposed situation of this small glacier the net snow accumulation is predominantly controlled by wind erosion of the snow surface preventing any regular snow deposition. As a consequence dating by annual-layer counting is impossible. Automatic snow-gauge readings and the  $\delta^{18}\text{O}$  stratigraphy in snow pits clearly indicate that a large fraction of the dry winter precipitation is lost by wind erosion (Beck, unpublished), consequently the CG ice-cores may mainly reflect the air and precipitation chemistry as well as the past climatic conditions of the summer seasons.

The present day clean air status of CG can be characterized as follows: located even during most parts of the summer season well above the dust loaded mixing layer the glacier site usually "sample" air attributable to the continental background aerosol. Note that the mean mineral dust air concentration between May and August was there found to be about  $1 \mu\text{g m}^{-3}$  only (Wagenbach *et al.*, 1985). Important interruptions of this background situation occur episodically by events of intense vertical mixing (e.g. during thunderstorms) and by the advection of air-masses loaded with Saharan dust. Evidence for the marked long-term influence of the CG site by its regional environment is demonstrated by a significant downcore decrease of the (pollution related) sulfate and nitrate level during the last 100 years by a factor 4 and 5 respectively (Wagenbach *et al.*, 1988).

## 3. METHODS

The mineral dust concentration of CG ice-cores was recorded routinely along with the DC and liquid conductivity, pH and  $\delta^{18}\text{O}$ ,  $\delta\text{D}$  to establish a basic ice-core stratigraphy. Decontaminated subsamples of about 50g were passed through Nuclepore membrane-filters (pore-size  $0.4 \mu\text{m}$ ) which were afterwards examined for titanium by (isotope induced) x-ray fluorescence analysis. The total mineral dust content of the samples was calculated referring to the crustal Ti-abundance of 4.40 % given by Mason (1966). This procedure is assumed to provide reliable results since owing to the extremely low solubility of Ti-components, the Ti concentration in the filtered melt-water was found to be almost insignificant.

The volume size distribution of insoluble particulate matter was analyzed by the Coulter Counter technique (being a measurement of the individual particle volumes) under class 100 clean room conditions from re-cored subsamples. Depending on the total particle concentration usually a particle diameter range of  $0.63\text{-}16 \mu\text{m}$  or  $0.8\text{-}20 \mu\text{m}$  was

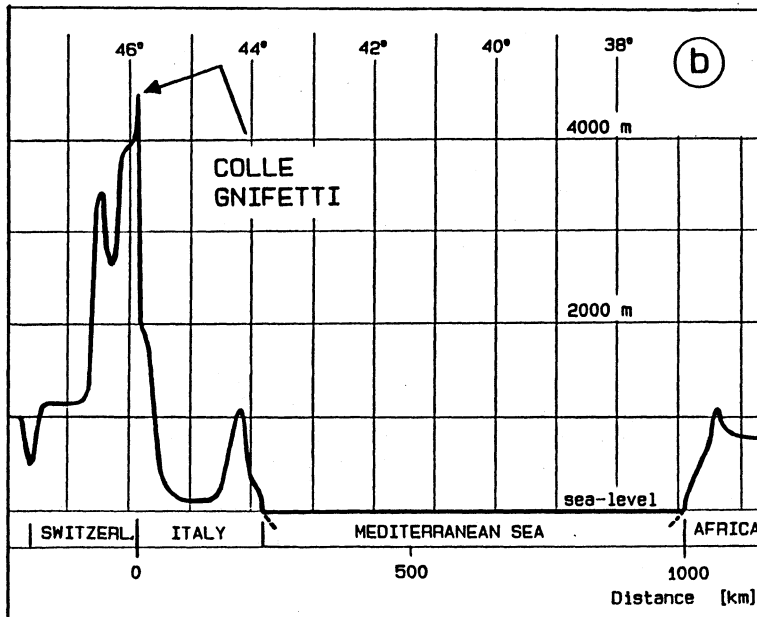
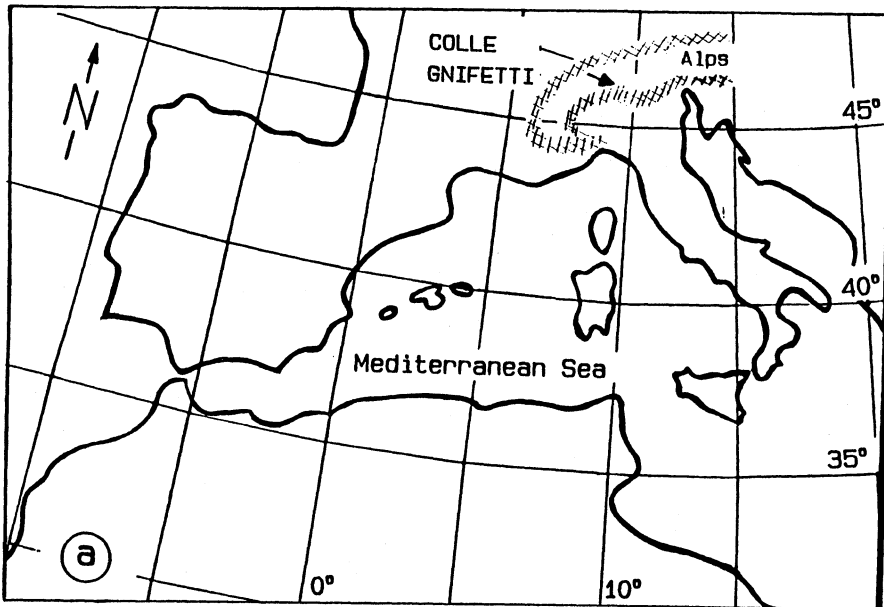


**Figure 1:**  
 a) Location of the Colle Gnifetti drilling site  
 b) General orographical feature of north-south transect crossing the Colle Gnifetti site

used. High resolution size distributions were achieved by connecting the Coulter Counter via an ADC to a 2048-channel analyzer and performing triplicate analytical runs (Geis, 1988). Prior to counting the insoluble particles have to be suspended in a 2%-NaCl working solution. It is presently unclear, whether this inevitable analytical step will seriously change the size distribution of insoluble particulate matter originally embedded in the ice lattice. Experimental evidence for a relative increase of the small particle fraction by shedding of submicron - to micron particles from large mineral particles sampled in water is given by Rosinski and Langer (1974). A concurrent, but more pronounced effect was observed by Geis (1988), if the melt-water was subjected to even a slight ultra-sonic treatment. Homogenization of the suspension was performed therefore always by stirring.

## 4. RESULTS AND DISCUSSION

### 4.1. Glacial Mineral Dust Concentration

The quasi-continuous mineral dust record over about the last 50 years which was extracted from an ice-core drilled in the flat saddle region of Colle Gnifetti is displayed in figure 2 (the uppermost part of the profile was measured on snow-pit samples). As mentioned, annual layer counting (e.g. from the  $\delta^{18}\text{O}$  stratigraphy) to date the CG cores is not feasible. The time scale of this core section has therefore been established by means of reference horizons related to the 1963 maximum of the thermonuclear bomb produced tritium (Schotter, personal communication) and by prominent Saharan dust deposition events clearly documented for the Alpine region (Bücher, 1986 and Bücher, this issue).

In addition to these most prominent dust falls indicated in figure 2 by the year of deposition numerous dust peaks in the concentration range of about 1.5 to 8 mg kg<sup>-1</sup> and exceeding the mean background level by up to two orders of magnitude appear in the record. Inspection of the filter residue for reddish to yellowish colour along with the individual pH and liquid conductivity data indicate that most of these dust peaks may be attributed to the deposition of Saharan dust. Note that enhanced levels of crustal impurities as found in snow layers subject to extended periods without any net snow accumulation can be easily distinguished from those probably related to Saharan dust through the relatively low pH and the dark filter colour caused by soot particles.

The present investigation indicates that most of the ice-core samples exceeding the background mineral dust level by about 1.5 mg kg<sup>-1</sup> are markedly influenced by the deposition of long range transported crustal impurities from remote regions. Presently it is not clear whether all these dust peaks can really be related to the northward transport of Saharan dust. Unequivocal evidence for a Saharan provenance should therefore be stated by studying the chemical, mineralogical, and micromorphological dust properties (Tomadin, this issue and Tomadin *et al.*, 1984) as well as by pollen analysis. However, some evidence for a Saharan origin of the dust producing the numerous peaks above the 1.5 mg kg<sup>-1</sup> level may be drawn so far from the following facts:

- From a snow pit study at CG it is shown that only in those samples marked by a typically reddish colour of the filter residue and an unusually high mineral dust content *Artemisia* and *Ephedra* pollen (originating from the south) were found (Haeberli *et al.*, 1983).

- Prodi and Fea (1978) also reported a relatively high frequency of Saharan dust events in the Alps. By examination of aerosol filters sampled at the Plateau Rosa (3480 m a.s.l.) which is located in the vicinity of the CG site, they were able to identify 35 strong Saharan dust falls during a period of ten years.

The total mineral dust deposition rate on the CG saddle region during approximately the last 50 years is found to be 60  $\mu\text{g cm}^{-2}\text{yr}^{-1}$  corresponding to 0.3 mm per 1000

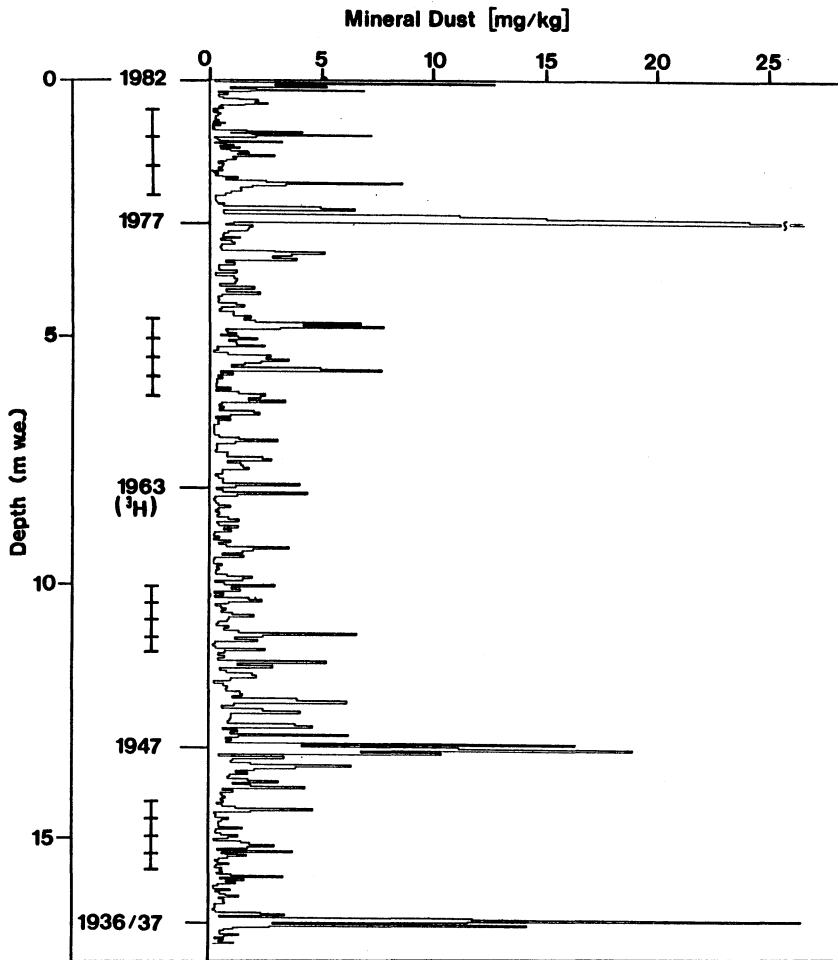


Figure 2:

Mineral dust concentration over about the last 50 years measured from an ice-core drilled in the saddle region of Colle Gnifetti. The depth scale is given in meters of water equivalent, the indicated time scale refers to well known Saharan dust falls and the maximum of bomb produced  $^3\text{H}$ . The mean annual layer thickness of different depth (time) intervals is shown up at the left margin of the plot by individual scales.



years if a density of  $2 \text{ g cm}^{-3}$  is assumed. This number must be regarded as a lower limit since due to snow erosion effects the mean net snow accumulation rate is always smaller than the mean precipitation rate. According to the Al content in Greenland snow reported by Boutron (1978) a present bulk mineral dust input onto the Greenland plateau of about  $4.7 \mu\text{g cm}^{-2} \text{ yr}^{-1}$  can be deduced, which is lower by a factor of 13 compared to the CG site. On the other hand, the data of Loye-Pilot *et al.* (1986) measured at 1200 m a.s.l. in Corsica (Mediterranean Sea) show an annual dust input of about  $1700 \mu\text{g cm}^{-2}$  exceeding the CG mineral dust input by a factor of 28. It is assumed that 84% of the total dust deposited on Corsica may be attributed to the Saharan source.

Summing up all ice core samples obviously not influenced by Saharan dust results in a mean mineral dust flux density of about  $20 \mu\text{g cm}^{-2} \text{ yr}^{-1}$  only, i.e. roughly one third of the value given before can be attributed to true background conditions. Provided that there is no relevant long range transport from other source areas of mineral dust this figure indicates that almost two third of the total mineral dust inventory of this ice core section has been exported from the Saharan region. The figure of  $40 \mu\text{g cm}^{-2} \text{ yr}^{-1}$  representing the long term average of Saharan dust flux on CG is to be compared with the most intense dust fall (1977) in this record which alone accounts for an enormous standing crop of  $540 \mu\text{g cm}^{-2}$ .

Outside of the framework of this paper, one of the most obvious impacts of the Saharan dust spikes is the "disturbance" of other glacio-chemical records like those of the mineral acid components which are related to anthropogenic activities. This disturbance is mainly due to the relatively large and extreme varying amounts of calcite, sulfate and to a lesser extent nitrate carried along with the dust particles (Wagenbach *et al.*, 1988). The latter two species may be partly associated to the external mixing of its gaseous precursors with the alkaline dust particles.

There emerge two conspicuous periods in the 50 year dust record: the late fifties to early sixties marked by a relatively low dust level ( $\approx 0.7 \text{ mg kg}^{-1}$ ) and the late forties showing a much higher mean dust concentration ( $\approx 2.5 \text{ mg kg}^{-1}$ ). The latter period is found to be characterized by a relative maximum in the melt-layer frequency, as well as in the running mean of  $\delta^{18}\text{O}$  and in the mean summer temperatures recorded at high altitude Alpine sites (Schotterer personal communication, Schotterer *et al.*, 1981). Indeed, it would be reasonable to suggest a long term relationship of this type between the glacial dust content (dominated by Saharan dust) and the mean (summer) air temperature (see e.g. Glawion, 1938) for the relationship of Saharan dust and Alpine "Föhn"). But in view of the complex temporal pattern in the snow accumulation on the CG site reliable climate interferences from the dust record would be possible only after examination of a much longer and well dated time period.

#### 4.2. Atmospheric Mineral Dust Concentration

To illustrate the time pattern of a "Saharan dust" episode at CG, figure 3 displays the airborne mineral dust concentration as measured on aerosol filters by neutron-activation analysis of the crustal reference elements Mn and K indicated along with the atmospheric Radon-222 activity. There is a rapid change by about one order of magnitude in the atmospheric mineral dust concentration (connected with a significant increase of air temperature) leading to a mean peak level of  $8.2 \mu\text{g SCM}^{-1}$ . This concentration is comparable with the mean of  $10.5 \mu\text{g SCM}^{-1}$  observed by Savoie and Prospero (1977) in ground-level air at Miami during advection periods of long range transported Saharan dust. In view of the large difference of both sampling sites with respect to altitude and distance to the source area this result has not been expected. On the other hand the C.G. concentration appears to be lower by a factor of 3 if compared with the mean of about  $25 \mu\text{g m}^{-3}$

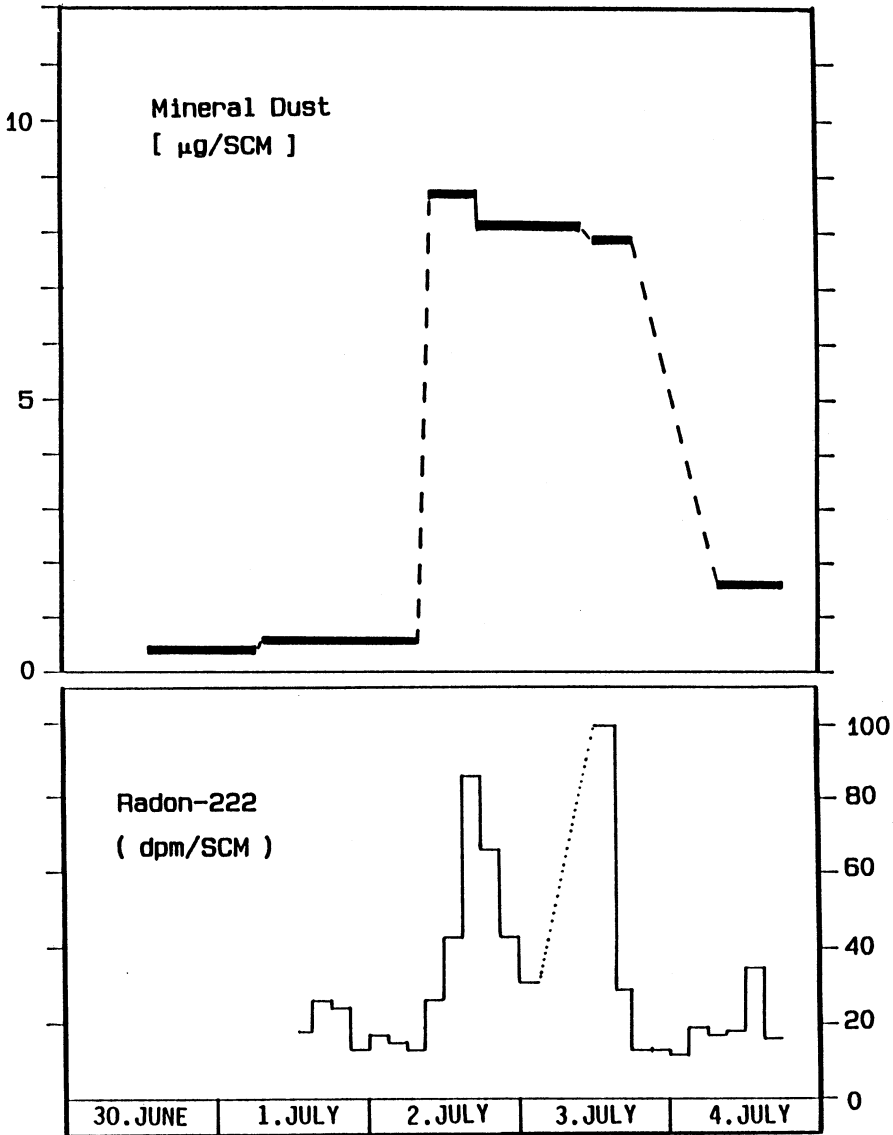


**Figure 3:**  
Time pattern of air-born mineral dust concentration and atmospheric  $^{222}\text{Rn}$ -activity at Colle Gnifetti during a Saharan dust episode in July 1982.

(adopted from the atmospheric Al concentrations) reported by Chester *et al.*, (1984) from ship-board observations made during "Scirocco" episodes, midway Italy and Sicily. In the latter case, the travel distance of the dust plume was found to be in the order of about 1000 km only.

During the dust event recorded at CG only a small amount of precipitation (sleet) occurred but in this specific case the night time formation of surface hoar from overlying clouds was observed to be another relevant dust removal process at this site. Three days after the dusty episode obviously a second event of Saharan dust advection occurred which was easily identified at various ground level sites by large amounts of "red dust" washed out by precipitation. Hence, a highly complex time pattern of air born mineral dust burden might be expected during Saharan dust events at CG. Primarily this might be due to the episodic nature of the mobilization, transport and scavenging processes involved.

Being a good tracer for continental air masses (Dörr *et al.*, 1983) the radioactive noble gas  $^{222}\text{Rn}$  clearly indicates the onset and breakdown of the advection of  $^{222}\text{Rn}$  and mineral dust enriched air masses at CG. The same phenomenon was observed by Weiss *et al.* (1985), at a mountain top in the Black Forest (ca. 300 km north to CG). The  $^{222}\text{Rn}$  exhalating from the desert surface at a fairly constant rate being independent of the nature of dust remobilization is only removed from the atmosphere by radioactive decay (life time 5.5 d). The  $^{222}\text{Rn}$ -concentration observed during the dusty period at CG may therefore be mainly due to dilution of the dust plume by low  $^{222}\text{Rn}$  air (e.g. from maritime or higher tropospheric air masses) and the radioactive decay during the long range transport. In this context the monitoring and interpretation of the long range transport of desert dust to marine and high elevation sites (normally depleted in  $^{222}\text{Rn}$ ) appears to be facilitated by recording the atmospheric  $^{222}\text{Rn}$ -activity in parallel.

### 4.3. Insoluble Particles in Glacial Meltwater

**4.3.1. Total Microparticle Concentration.** To illustrate the role of the CG site as a receptor of the insoluble aerosol component the range of total particle concentrations as measured in typical snow-pit samples and pronounced Saharan dust layers from one of the ice-cores drilled to the bed rock are presented in figure 4. The concentration range observed by other authors in polar, subtropical and tropical glaciers is also indicated to facilitate comparison. On a global scale the mean glacial microparticle concentration is shown to vary by about 2 orders of magnitude, roughly depending on the geographical situation and the snow accumulation rate of the glaciers. Disregarding the Saharan dust events the CG concentration level seems to be just intermediate between that one found in the remote polar ice sheets and the (sub) tropical glaciers, respectively (which are more directly influenced by their dusty environment). On the other hand, the concentration range associated with Saharan dust events at CG clearly cover the upper range of the concentration scale demonstrating the exceptional impact of this phenomenon on the CG-site.

**4.3.2. Size Distribution.** The general form of the size distribution derived from the grand average of surface snow samples not influenced by Saharan dust and displayed in figure 5a is found to be inherent to a large part of the insoluble particulate matter deposited on CG. In the diameter range examined (0.63 - 16  $\mu\text{m}$ ) there always appears a distinct mode in the volume size distribution which can frequently be fitted by a log-normal distribution, and, as a result, the particle number in this size range will also be log-normal distributed. In this case the geometric standard deviation  $\sigma_g$  is common to all moments of the distribution. Hence, the modal diameter of the volume distribution (equivalent to the volume mean diameter  $D_v$ ) can be easily transformed to the corresponding number mean diameter  $D_N$  and surface mean diameter  $D_s$  of the particle population in question (see e.g. Aitchinson

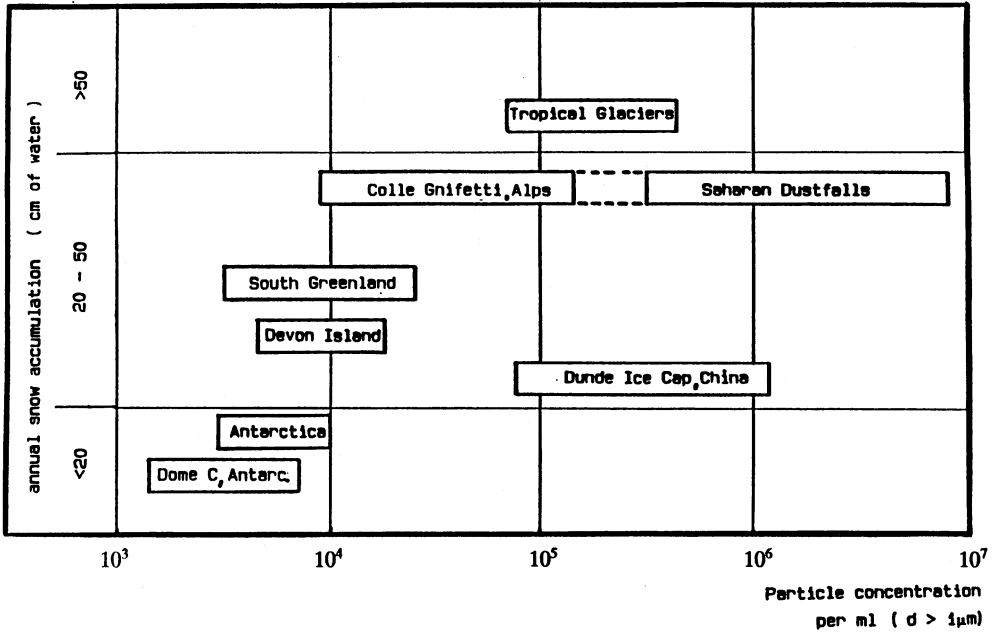


Figure 4:  
 Typical concentration range of insoluble particles observed in glaciers of different latitudes. To facilitate comparison the lower particle size limit always is chosen to  $d > 1 \mu m$  and the range of mean snow accumulation is indicated in addition.

- Antarctica (Thompson & Mosley-Thompson, 1982)
- Dome C., Ant. (Petit *et al.*, 1981)
- South Greenland (Steffenson, 1985)
- Devon Island, High Arctic (Koerner, 1977)
- Colle Gnifetti (this work)
- Duende Ice Cap (Thompson *et al.*, 1988)
- Tropical glaciers (Thompson *et al.*, 1984)

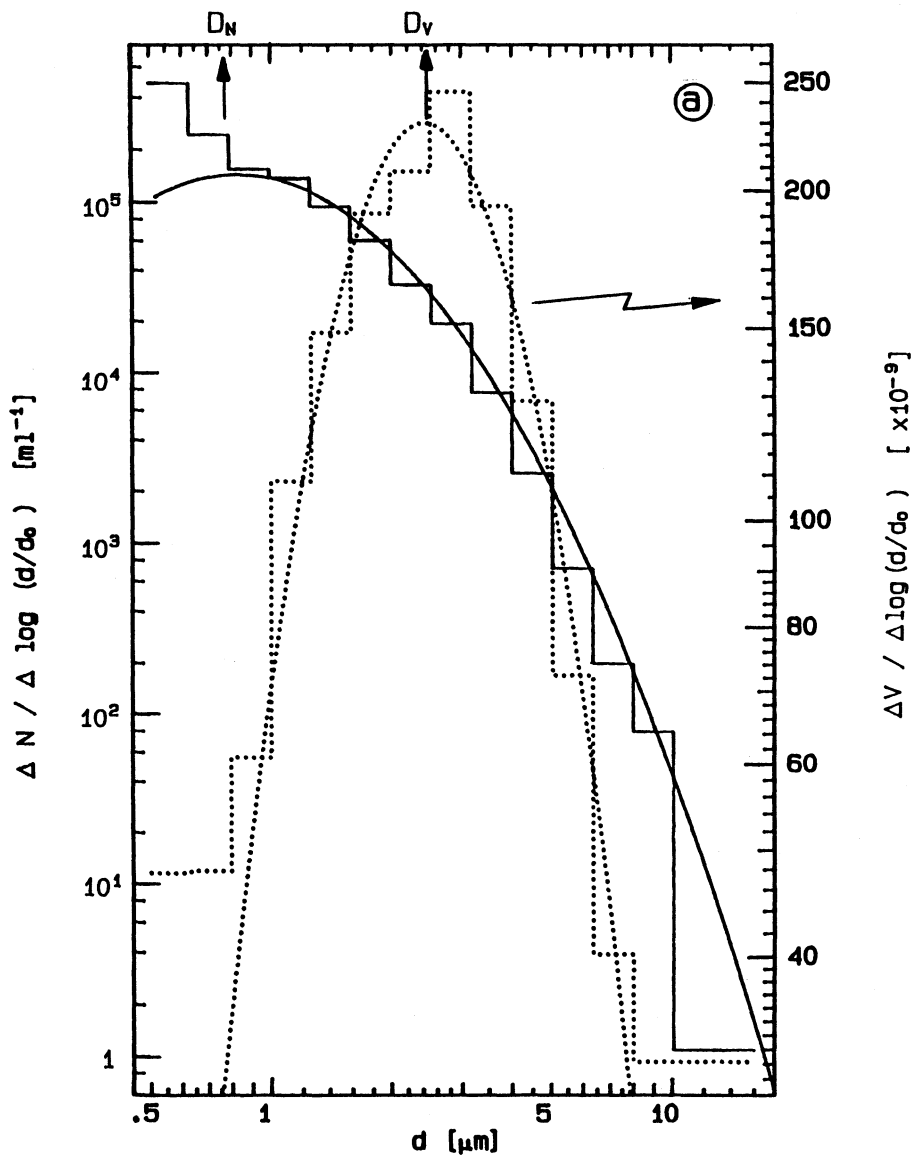


Figure 5:

a) Number and volume size distribution of insoluble particles in the diameter range 0.5 - 16  $\mu\text{m}$  measured in Colle Gnifetti snow pit samples. The distribution is presented by the grand average of 57 snow samples not influenced by Saharan dust falls. The volume size distribution obtained from the Coulter Counter readings by assuming spherical particles is fitted to a log-normal distribution (dotted lines) which in turn is transformed to the log-normal fit of the experimental number size distribution (solid lines).

and Brown, 1957). As shown in figure 5a, a typical volume mean and number mean diameter of about 2.5 and 0.7  $\mu\text{m}$ , respectively can be inferred from the distributions. From figure 5b where a much higher size resolution can be applied to the analysis of a summer snow horizon it becomes immediately evident that the number size distribution in the size range indicated will not be represented in a reasonable way by the Junge power law (as frequently used in aerosol research) with  $dN/d\log(d/d_0) \propto (d/d_0)^{-\beta}$ . In the example shown in figure 5b the slope  $\beta$  increases systematically from about 1.5 close to 1  $\mu\text{m}$  to about 5 at the upper end of the size range.

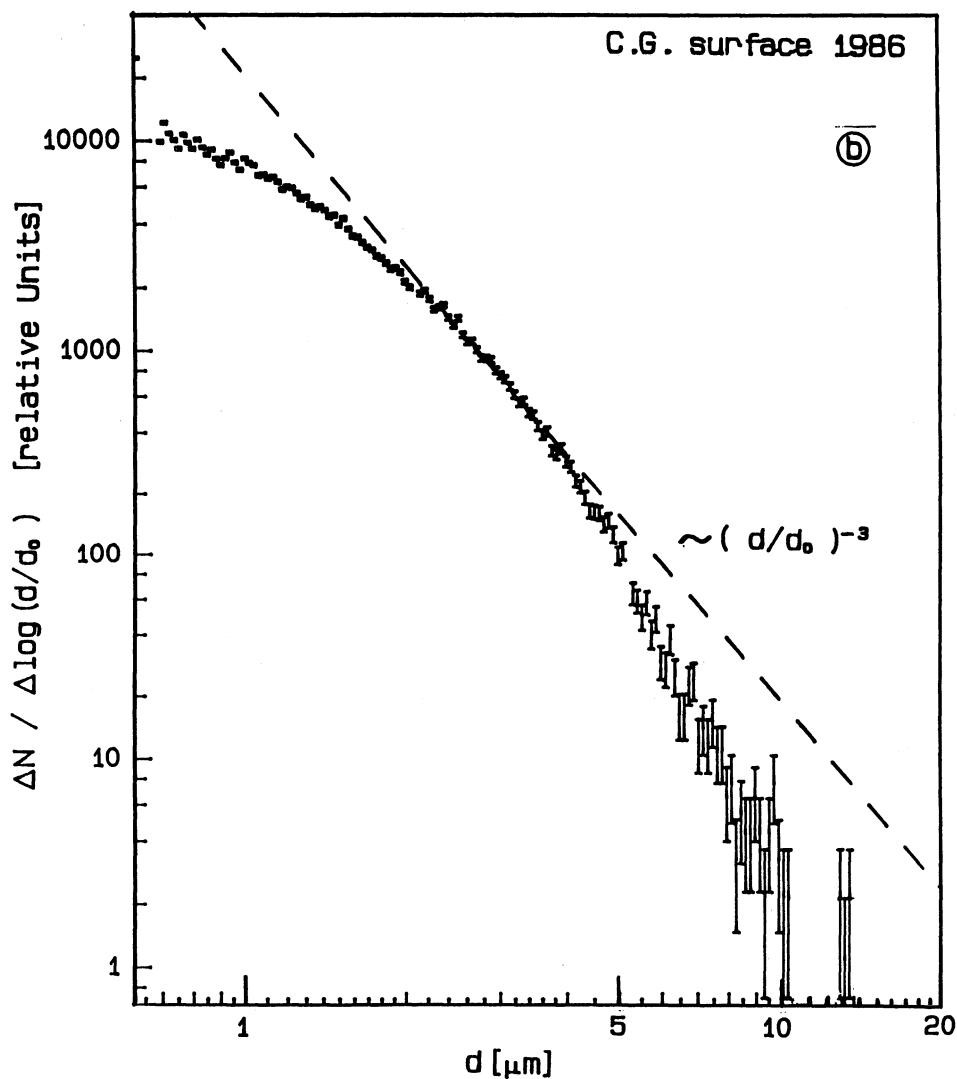
Being derived from a series of consecutively excavated snow-pits, the record of insoluble microparticles in well-dated surface snow layers is presented in figure 6 by plotting the total particle concentration and the apparent volume mean diameter  $D_v$  together with the  $\delta^{18}\text{O}$  stratigraphy. In connection with the definite time horizons the  $\delta^{18}\text{O}$  profile confirms the predominance of precipitation deposited during the summer half year. Note the coincidence of Saharan dust layers with relative  $\delta^{18}\text{O}$  maxima (generally  $\delta^{18}\text{O}$  will be positively correlated with the temperature of the precipitating air mass).

As always shown by the record of mineral dust large variations of microparticle concentrations are introduced by the advection of Saharan dust. Furthermore a conspicuous shift of  $D_v$  towards larger values appears for those samples falling significantly above the background level. This is especially true for the 1983 summer layer (most probably influenced by dry deposited particles during the extreme dry summer season) and for those samples, assumed as directly affected by Saharan dust. Referring to the 1983 summer horizon an enhanced input of insoluble particulate matter (e.g., during dry weather periods) seems to be indicated by a change in the volume mean diameter in a more unequivocal way as than it is for the particle concentration itself.

The question arises whether the size distribution parameters of the Saharan dust deposited differ significantly from those of dust deposits related to more regional source areas or even to the background aerosol. As indicated in figure 7 the volume size distribution of the two Saharan dust events is indeed significantly shifted towards larger particles.  $D_v$  is in this case larger by 60 % than for the non-influenced samples. Following Jaenicke and Schütz (1988), the mass size distribution of the Saharan dust plume at the source region is centered around a diameter of 100  $\mu\text{m}$ . The much smaller  $D_v$  observed at CG is obviously due to gravitational settling and predepositional wet-removal during transportation of the dust particles. Consequently, it seems reasonable to attribute individual differences in the size distribution of the Saharan dust deposited on CG to different transport times which in turn means different transport velocities and/or different lengths of the trajectories.

To find out what range might be covered by the mode parameters  $D_v$  and  $\sigma_g$  of the most prominent Saharan dust layers, individual visible dust layers found in one of the two entire ice-cores were analysed in the size range 0.8-20  $\mu\text{m}$ . Figure 8 shows the two extreme volume size distributions occurring, displaying the largest and smallest  $D_v$  from a total of 16 samples analysed. For the other samples, showing on the average a  $D_v$  of 4.5  $\mu\text{m}$ , the size distributions cannot always approximated by a single log-normal distribution. In contrast to the usually estimated  $\sigma_g$  of 1.9-2.0, in this case,  $\sigma_g$  is found to be 2.2, approximately. Following Jaenicke and Davies (1976), this might be an indication for the apparent multimodal character of these particle populations.

It is presently still an open question what the major process may be, responsible for the large variation of size distribution parameters observed at the endpoint of the atmospheric life time of the Saharan dust. One promising candidate might be the fairly large difference in the length of the two principal transport ways of Saharan air masses reaching the Alps. Following Prodi and Fea (1978) the straight way crossing the Mediterranean Sea and the diverted anticyclonic pathway over part of the western North Atlantic are



b) Example of a highly resolved number size distribution measured in summer surface snow at Colle Gnifetti. The size range  $0.65\text{-}16\ \mu\text{m}$  is represented by 145 channels, error bars refer to the statistical counting errors only. The straight line corresponds to Junge's power law with an exponent  $\beta = 3$ .

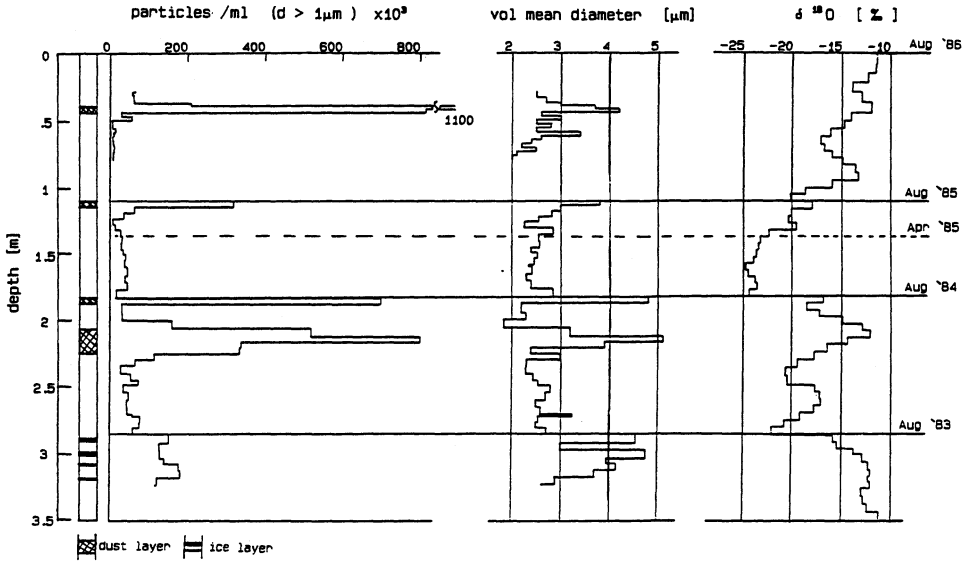


**Figure 6:** Total concentration of insoluble particles  $d > 1 \mu\text{m}$ , volume mean diameter  $D_v$ , and  $\delta^{18}\text{O}$  stratigraphy in surface snow layers at Colle Gnifetti. The depth profiles refer to a sequence of five snow-pits each dug at the date indicated (overlapping sections not shown). Note that the  $\delta^{18}\text{O}$  of CG precipitation is expected to be positively correlated to the mean annual cycle of local air temperature.



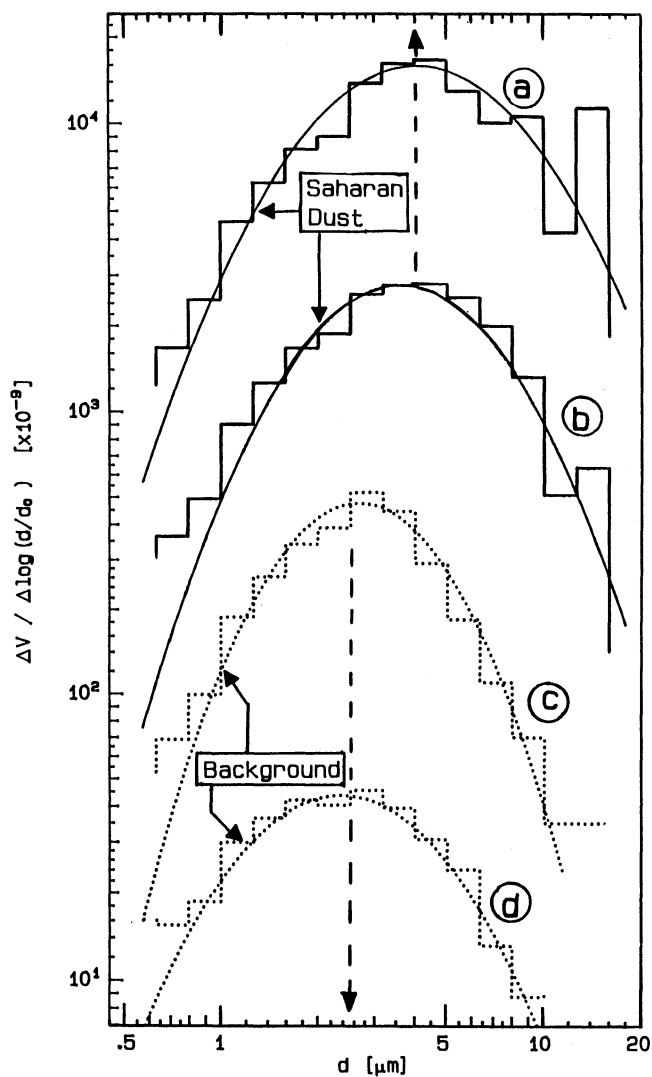


Figure 7:  
Volume size distribution of insoluble particles as measured in different sample categories in the snow-pit shown in figure 6.

Saharan dust (full lines): snow layer at 0.4 m depth (a), at 1.1 m depth (b).

Background (dashed lines): average over the depth interval adjacent to the upper boundary of the Saharan dust peak at 0.4 depth (c), lower boundary (d).

The dashed lines indicate the typical volume mean diameter of the sample categories (a,b) and (c,d).

(fits to the data by log-normal distribution)

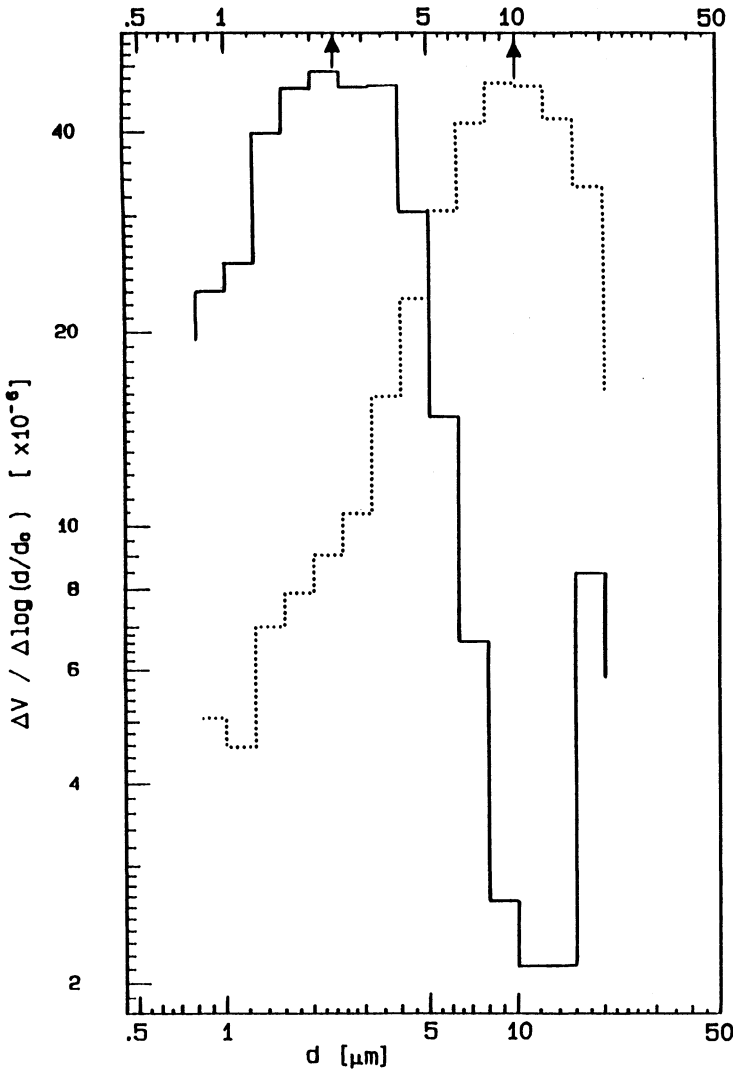


**Figure 8:** Volume size distributions of insoluble particles in Colle Gnifetti ice-core samples marked by visual Saharan dust layers.

Out of 16 identified dust layers the two one characterized by the lowest volume mean diameter with  $D_v = 2.5 \mu m$  (solid line) and the largest one with  $D_v = 10 \mu m$  (dotted line) are presented.

Total volume concentrations are  $35 \cdot 10^{-6}$  and  $32.5 \cdot 10^{-6}$ , respectively. Deposition date of the small particle dust is attributed to the serie of intense dust falls at turn of the century (1901-1903), the true age of the large particle sample is unknown (probably more than 500 years )

found to be the most probable dust trajectories, and these are quite obviously different in their mean transport length.

For the spectral window between 0.63 and 20  $\mu\text{m}$  the size distribution parameters yet measured at CG are summarized and grouped into two different sample populations: one assumed to be mainly represented by the contribution from the continental background and the regional aerosol body and a second one obviously dominated by relatively large amounts of Saharan dust. The number and surface mean diameters ( $D_N$ ,  $D_S$ ) as calculated from  $D_v$  and  $\sigma_g$  in the case of unimodal distributions are given in addition. The mode parameters of the first population show a surprising similarity to those measured by Royer *et al.* (1983) in Antarctic precipitation samples by the same method used here, the mean particle concentration (Petit *et al.*, 1981), however, is, as expected, always lower by more than one order of magnitude (see table I). It is assumed, therefore, that the typical mode parameters  $D_v \approx 2\text{--}2.5 \mu\text{m}$  and  $\sigma \approx 2$  observed at these two clean air sites universally characterize the aged and widespread fraction of the insoluble aerosol component inherent to the global background aerosol.

TABLE I: Total number and total particle volume concentration as well as mode parameters of the particle size distribution of different snow and ice sample populations from Colle Gnifetti compared to Antarctic ice and aerosol from arid regions

	$C_N$ ( $d \geq 1 \mu\text{m}$ ) [per ml]	$C_{\text{vol}}$ [ $10^{-9}$ ]	$D_v$ [ $\mu\text{m}$ ]	$\sigma_g$	$D_N$ [ $\mu\text{m}$ ]	$D_S$ [ $\mu\text{m}$ ]
COLLE GNIFETTI (Background and local influence)	$3.7 \cdot 10^4$	140 $\pm 100$	2.5 $\pm .38$	1.9 $\pm .14$	0.67	1.65
COLLE GNIFETTI (Saharan dust)	$1.25 \cdot 10^6$	9300 $\pm 1400$	4.5 $\pm 1.5$	2.2 $\pm .2$	1	2.75
ANTARCTICA (after Royer et.al., 1983)	$3200^{(1)}$ $\pm 1330$	$40^{(2)}$ $\pm 25$	2 $\pm .6$	2.2 $\pm .2$	0.5 $\pm .16$	$1^{(3)}$
SOIL DERIVED AEROSOL (after Patterson and Gilette, 1977)			5.6	2.2	0.8	3

(1) after Petit *et al.* (1981)

(2) calculated from mass concentration, assuming a density of  $2.5 \text{ g cm}^{-3}$

(3) calculated from  $D_v$  via  $\sigma_g$ .

On the other hand, the Saharan dust population shows an interesting resemblance to the mode parameters compiled by Patterson and Gillette (1977) from various ground-based aerosol measurements representative for atmospheric conditions which are dominated by soil-derived aerosol particles. There remain always some uncertainties about the compatibility of this data set with that one derived from the Saharan dust influenced samples from the CG site. This is mainly due to the different analytical methods used (see caption 3) and to the assumption that prior to the analysis all of the CG dust samples were most probably subjected to the size selective wet-removal processes. Nevertheless, the analogy in the mode parameters is evident and may be traced back to the fact that both data sets are representative for the soil-derived aerosol fraction which is characterized by a relatively low atmospheric residence time.

## 5. OUTLOOK

The most essential factor in assessing the paleoclimatic potential of the dust record buried in the CG glacier is to know the time scale on which records with a sufficient time resolution can be achieved. Primarily this problem is equivalent to the appropriate dating of the ice-core. Since at present in case of C.G. suitable dating methods beyond last 100 years are not available a rough depth-age relationship was established based on glacier-flow modelling (Haeberli *et al.*, 1988). As shown in figure 9 the CG ice-cores will cover a good deal of the present millenium, and in particular contain the important climatic stage of the Little Ice Age. However dating accuracy decrease rapidly with depth as does the annual layer thickness and, consequently, in the lower part of the cores time resolution will for practical reasons be no better than a few years approximately. Apart from serious effects on the interpretation of the lower core section, due to the topographical constraints of the small glacier site, lack of a suitable time scale so far prevents the extraction of reliable paleoclimatic information from a dust record, covering the entire length of the ice-core.

The phenomenon of intense Saharan dust falls (as well as the deposition of volcanic sulphuric acid) on CG, however, may help to attack the dating problem by extending the glacial chronology of well known events as far back as possible which, at the same time, would provide a unique history of the Saharan impact on the upper tropospheric dust burden.

## ACKNOWLEDGEMENTS

Financial support was given to this work by the Federal Ministry for Research and Technology (grand No FZ 01Q07291).

Special thanks are to Prof. K.O. Münnich for his encouragement and invaluable criticism and to Dipl.Phys. N. Beck for realizing the actual glacio-meteorological field works.

The friendly collaboration in the field work with our Swiss colleagues from the Physical Institute, University of Bern (in particular U. Schotterer) and from the Glaciological Department of VAW, ETH-Zürich (in particular P.D.Dr. W. Haeberli) as well as important support that was given by the Swiss Army, Air Zermatt and the CAI staff at Cap. Margherita is greatly acknowledged.

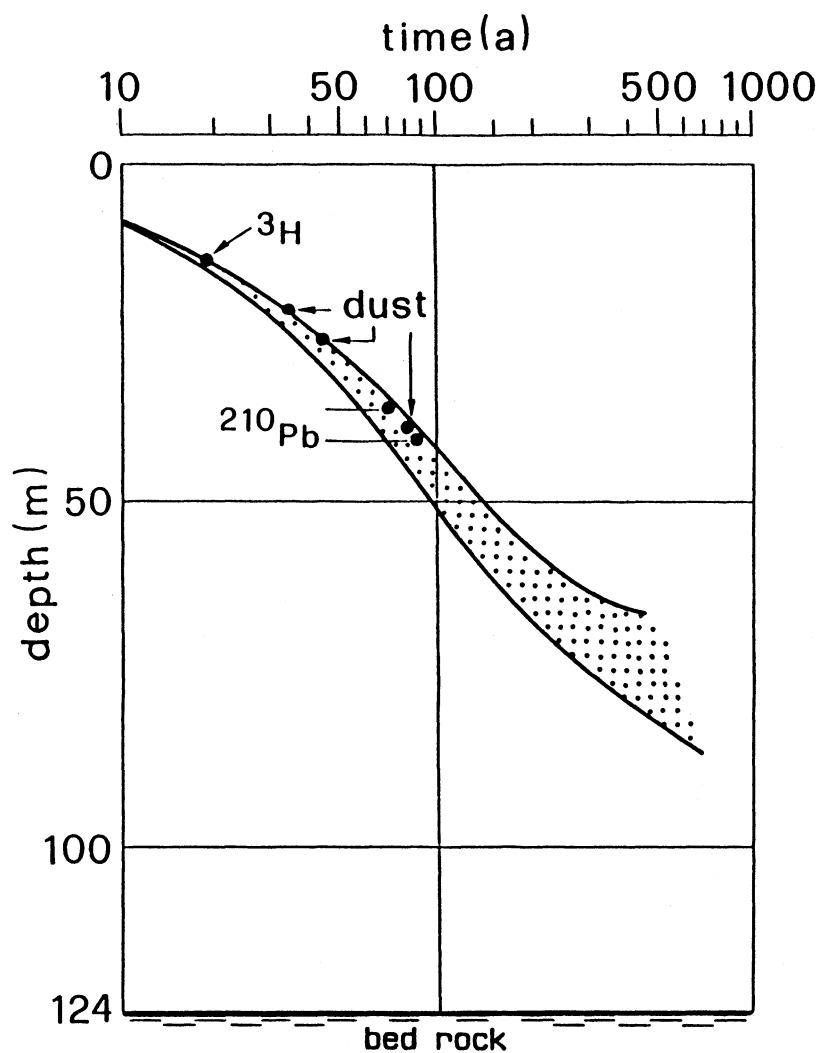


Figure 9: Depth-age relationship at the saddle region of Colle Gnifetti (calculated by means of an ice-flow model based on measured properties of glacier geometry and surface flow (Haeberli *et al.*, 1988)). Shown are the envelopes of greatly different model versions together with the age information provided by known Saharan dust falls, bomb produced  $^3\text{H}$ -maximum and  $^{210}\text{Pb}$ -dating.  $^{210}\text{Pb}$  adopted from Gaggeler *et al.* (1983). The lowest dust-reference horizon is attributed to the famous dust fall period of 1901-1903.

## REFERENCES

- Aitchinson, J. and Brown, J.A. (1957): *The log normal distribution with special reference to uses in economics* Cambridge University Press, Monograph: 5.
- Alean, J., Haeberli, W. and Schaedler, B. (1984): 'Snow accumulation, firn temperature and solar radiation in the area of the Colle Gnifetti core drilling site (Monte Rosa, Swiss Alps): distribution patterns and interrelationships', *Zeitschrift für Gletscherkunde und Glazialgeologie* 19, 2, p. 131-147.
- Boutron, C. (1978): 'Influence des aérosols naturels et anthropogénic sur la géochimie des neiges polaires', *Thesis*, University of Grenoble, Grenoble France.
- Bücher, A. (1986): 'Recherches sur les poussières minérales d'origine saharienne', *Thesis*, University of Reims-Champagne-Ardenne France.
- Chester, R., Shapples, E.J., Sanders, G.S. and Sydam, A.C. (1984): 'Saharan dust intrusion over the Tyrrhenian Sea', *Atmos. Environ.* 18, No. 5, p. 929-935.
- Dörr, H., Kromer, B., Levin, I., Münnich, K.O. and Volpp, H.J. (1983): 'CO<sub>2</sub> and Radon 222 as tracers for atmospheric transport', *J. Geophys. Res.* 88, No. C2, p. 1309-1313.
- Gäggeler, H., von Gunten, H.R., Rössler, E., Oeschger, H. and Schotterer, U. (1983): '<sup>210</sup>Pb-dating of cold alpine firn/ice cores from Colle Gnifetti, Switzerland', *J. of Glaciology* 29, 101, p. 165-177.
- Geis, K. (1988): Master Thesis, Institut für Umweltphysik, University of Heidelberg, FRG.
- Glawion, H., (1938): 'Eine ungewöhnliche Periode von Staubfällen im Mai 1937', *Zeitschrift für angewandte Meteorologie* 54, Heft 9, p.284-289.
- Haeberli, W. (1978): 'Sahara dust on the Alps - a short review', *Zeitschrift für Gletscherkunde und Glazialgeologie*, 13,1-2, p. 206-208. [Appendix to Oeschger and others (1978)].
- Haeberli, W., Schotterer, U., Wagenbach, D., Haeberli-Schwiter, H. and Bortenschlager, S. (1983): 'Accumulation characteristics on a cold, high-Alpine firn saddle from a snow-pit study on Colle Gnifetti, Monte Rosa, Swiss Alps', *J. of Glaciology* 29, 102, p. 260-271.
- Haeberli, W., and Alean, J. (1985): 'Temperature and accumulation of high altitude firn in the Alps', *Annals of Glaciology* 6, p. 161-163.
- Haeberli, W., Schmid, W. and Wagenbach, D. (1988): 'On the geometry, flow and age of firn and ice at the Colle Gnifetti core drilling site (Monte Rosa, Swiss Alps)', *Zeitschrift für Gletscherkunde und Glazialgeologie*, in press
- Holdsworth, G., Krouse H. R. and Peake E. (1988): 'Trace-acid ion content at shallow snow and ice-cores from mountain sites in Western Canada', *Annals of Glaciology* 10, p. 57-62.
- Jaenicke, R. and Davis, C.N. (1976): 'The mathematical expression of the size distribution of atmospheric aerosols', *Journal Aerosol Science* 7, p. 255-259.

- Jaenicke, R. and Schütz L. (1988): 'Wind speed and vertical flux of aerosols', in Fischer, G. (Ed.): *Meteorology: Physical and Chemical Properties of Air*, Landolt-Boernstein, New Series, Group V, Volume 4b., Springer-Verlag, p. 403-404.
- Koerner, R.M. (1977): 'Distribution of microparticles in a 299-m core through the Devon Island ice cap, Northwest Territories, Canada' In: *Isotopes and Impurities in Snow and Ice*, JAHs Publ. No. 118, p. 371-376.
- Langway, C.C., Oeschger, H. and Dansgaard, W. (Editors) (1985): *Greenland Ice Core: Geophysics, Geochemistry and the Environment*, Washington D.C.; AGU Monograph 33.
- Legrand, M.R., Lorius, C., Barkov, N.I. and Petrov V.N. (1988): 'Vostok (Antarctica) Ice-Core: atmospheric chemistry changes over the last climate cycle (160000 years)', *Atmos. Environ.* 22, 2, p. 317-331.
- Loye-Pilot, M.D., Martin, J.M. and Morelli, J. (1986): 'Influence of Saharan dust on the rain acidity and atmospheric input to the Mediterranean', *Nature* 321, p. 427-428.
- Mason, B. (1966): *Principles of Geochemistry*, third edition, Wiley and Sons, Inc., New York.
- Oeschger, H., Schotterer, U., Stauffer, B., Haeberli, W. and Röthlisberger, H. (1978): 'First results from Alpine core drilling projects', *Zeitschrift für Gletscherkunde und Glazialgeologie* 13, 1/2, p. 193-208.
- Patterson, E.M. and Gillette, D.A. (1977): 'Commonalities in measured size distributions for aerosols having a soil-derived component', *J. of Geophys. Res.* 82, p. 2074-2082.
- Petit, J.R., Briat, M. and Royer, A. (1981): 'Ice age aerosol content from East Antarctic ice core samples and past wind strength', *Nature* 293, p. 391-394.
- Prodi, F., Fea, G. (1978): 'Transport and deposition of Saharan dust over Alps', 15. *Internationale Tagung für alpine Meteorologie*, Grindelwald, 19.-23. Sept., Tagungsbericht.
- Rosinski J. and Langer G. (1974): 'Extraneous Particles shed from large Soil Particles'. *Aerosol Science* 5, p. 373-378.
- Royer, A., De Angelis, M. and Petit, J.R. (1983): 'A 30000 year record of physical and optical properties of microparticles from an east Antarctic ice core and implications for paleoclimate reconstruction models', *Climatic Change* 5, p. 381-412.
- Savoie, D.L. and Prospero, J.M. (1977): 'Aerosol concentration statistics for the Northern Tropical Atlantic', *J. Geophys. Res.* 82, 37, p. 5954-5964.
- Schotterer, U., Haeberli, W., Good, W., Oeschger, H. and Röthlisberger, H. (1981): 'Datierung von kaltem Firn und Eis in einem Bohrkern vom Colle Gnifetti, Monte Rosa', *Jahrbuch der Schweizerischen Naturforschenden Gesellschaft*, wissenschaftlicher Teil, p. 48-57.
- Schotterer, U., Oeschger, H., Wagenbach, D. and Münnich, K.O. (1985): 'Information on

paleo-precipitation on a high-altitude glacier, Monte Rosa, Switzerland', *Zeitschrift für Gletscherkunde und Glazialgeologie* 21, p. 379-388.

Schütz, L. (1979): 'Saharan Dust transport over the North Atlantic Ocean - model calculations and measurements', in C. Morales, ed.: *Saharan Dust, mobilisation, transport, deposition*. SCOPE 14, J. Wiley and Sons, New York, p.267-277.

Steffenson, J.P. (1985): 'Microparticles in snow from the South Greenland ice sheet', *Tellus* 37B, p. 286-295.

Thompson, L.G. and Mosley-Thompson, E. (1982): 'Spatial distribution of microparticles within Antarctic snow-fall', *Annals of Glaciology* 3, p. 300-305.

Thompson, L.G., Mosley-Thompson, E., Grootes, P.M., Pourchet, M. and Hastenrath, S. (1984): 'Tropical glaciers: Potential for ice core paleoclimatic reconstructions', *J. Geophys. Res.* 89, p. 4638-4646.

Thompson, L.G., Mosley-Thompson, E., Bolzon, J.F. and Koci, B.R. (1985): 'A 1500-year record of tropical precipitation in ice cores from the Quelccaya Ice Cap, Peru', *Science* 229, p. 971-973.

Thompson, L.G., Xiaoling, W., Mosley-Thompson, E. and Zichu, X. (1988): 'Climatic records from the Dunde Ice Cap, China', *Annals of Glaciology* 10, p. 80-84.

Tomadin, L., Lenaz, R., Landuzzi, V., Mazzucotelli, A. and Vannucci, R. (1984): 'Wind-blown dust over the Central Mediterranean', *Oceanologica Acta* 7, 1, p. 13-22.

Valentin, J. (1902): 'Der Staubfall vom 9. bis 12. März 1901', *Sitzungsbericht der Kaiserlichen Akademie der Wissenschaften in Wien, Mathematische-naturwissenschaftliche Classe* CX 1, Abt. IIa, Mai 1902, p. 50.

Wagenbach, D. (1981): 'Pilotstudie zur Aerosoldeposition auf einer hochalpinen kalten Firndecke', *Ph. D. Thesis*, University of Heidelberg, Heidelberg FRG.

Wagenbach, D., Görlach, U., Haffa, K., Junghans, H.G., Münnich, K.O. and Schotterer, U. (1985): 'A long term aerosol deposition record on a high altitude Alpine glacier', WMO Technical Conference on *Observations and Measurements of Atmospheric Contaminants* (TECOMAT), Vienna 1983, WMO Report No. 647.

Wagenbach, D., Münnich, K.O., Schotterer, U. and Oeschger, H. (1988): 'The anthropogenic impact on snow chemistry at Colle Gnifetti, Swiss Alps', *Annals of Glaciology* 10, Symposium on Ice Core Analysis, Bern 1987, p. 183-187.

Wagenbach, D. (1988): 'Records in alpine glaciers', in Oeschger, H. and Langway, C.C., eds.: *The environmental record in Glaciers and Ice Sheets*. Dahlem Konferenzen. Chichester: J. Wiley and Sons, in press.

Weiss, W., Stockburger, K., Sartorius, H., Münnich, K.O., Keller, M., Bühler, Th. and Platt, U. (1985): 'Atmospheric aerosol and radioactivity parameters at the Schauinsland Mountain Top observatory', WMO Technical Conference on *Observations and Measurement of Atmospheric Contaminants* (TECOMAC), Vienna, WMO Report No. 647.



**FALLOUT OF SAHARAN DUST IN  
THE NORTHWESTERN MEDITERRANEAN REGION**

**A. BÜCHER**

**PIC DU MIDI OBSERVATORY**

**65200 BAGNERES DE BIGORRE, FRANCE**

565

## ABSTRACT

The phenomenon of dust fallout from the Sahara occurs in France several times per year. The air masses that transport the dust are responsible for notable temperature increases. This article is also going to show what directions these air masses take, what the National Meteorology Office says about them, in what way weather reports may help, as well as images taken by satellites. Where dust fallout and mud rain in France are concerned, chemical analyses have been undertaken. The north west Saharan is an important source zone and during the period 1951 - 1960, the annual frequency of occurrence of wind sand is shown. After extensive research in literature, 201 cases of Saharan dust fallout have been found and the monthly distribution has been calculated. In addition, 514 other cases are considered. In the appendix, there is a description of the network which is concerned with collecting information of the Saharan dust fallout.

### 1°) INTRODUCTION

The fallout of Saharan dust particles is of great importance, because it represents over 50 % of mineral dust in suspension in the atmosphere. While a great deal of time and study have been devoted to the transport of dust to the west, very little is known about its transport to the north or about the source zones it comes from. The source regions are south west Algeria, Morocco, Mauritania, Niger, (Bilma, Faya Largeau) and the Chad area.

This phenomenon is as old as the Saharan dust and a major question concerns the continual renewal of the dust. In geological terms, the aeolian contribution to detrital sedimentation is far from negligible. The mineralogical composition of the Saharan dust is approximately 50 % quartz, 25 % phyllosilicates, 15 % carbonates and less than 5 % feldspar (A.Bücher 1986). They contribute to the composition of soils and paleosoils which could not come from a local environment. Saharan dust has an extremely wide distribution.

The accumulation of sediments and the size of the particles decrease with the distance from Africa. The average size of those particles which fall in the High Pyrenees, France is somewhere between 3 and 12 microns, and this depends on the varying force of the transporting wind.

### 2°) TEMPERATURE EFFECTS

Fallout of dust or of mud rain in France or Europe from the Sahara is usually transported by a mass of hot air. Such events are accompanied by a notable increase in ambient temperature. During the event of the 2<sup>nd</sup> of August 1980, temperature fluctuation recorded at the Observatory at Pic-du-Midi-de-Bigorre, High Pyrenees France was among the highest 5 % of recorded cases, (A. Bücher, 1973). At Aurillac, in the Massif Central, France, for the dust fallout on the 26<sup>th</sup> - 28<sup>th</sup> July 1983, the previous lowest recorded minimum temperature was exceeded by 3.6° C.

### 3°) TRAJECTORIES

We will show, that arrivals of air masses from the Sahara can occur on the Atlantic side of France. Such an occurrence took place on the 8<sup>th</sup> of January 1982 when the dust was deflected around a high pressure zone over the Atlantic ocean. In a large majority of cases, however, this Saharan dust plume traverses the Mediterranean Sea and Spain and is carried by a strong southerly wind (Fig. 1.1), (Saharan dust fallout on the 25<sup>th</sup> and 26<sup>th</sup> of October 1987, Algeria, France).

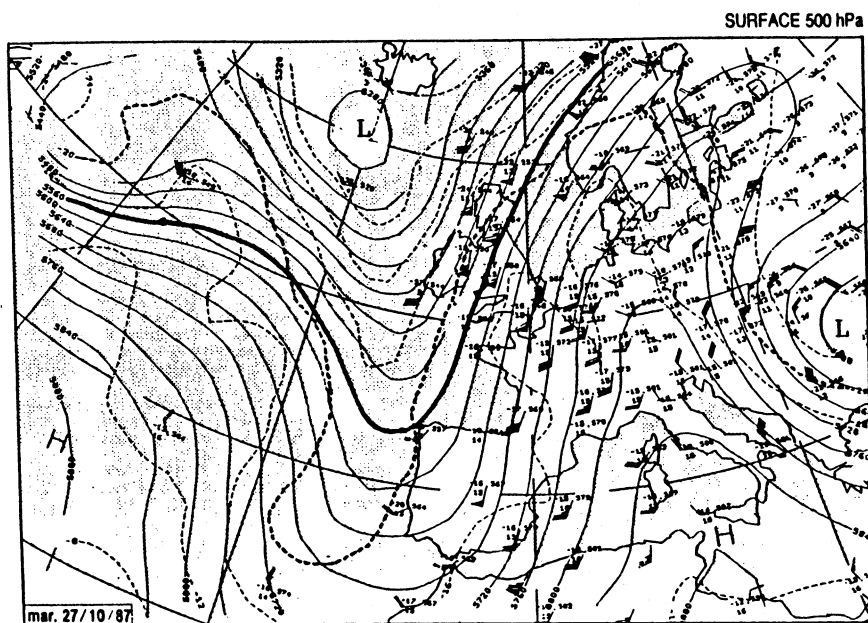


**Figure 1.1**  
 Surface meteorology on 27th October 1987  
 Saharan dust on 25 and 26th October 1987

F. Prodi and G. Féa (1978) have studied the meteorological conditions capable of bringing dust and mud rain to Italy ; they found the three following examples (Fig 1.2, 1.3, 1.4):

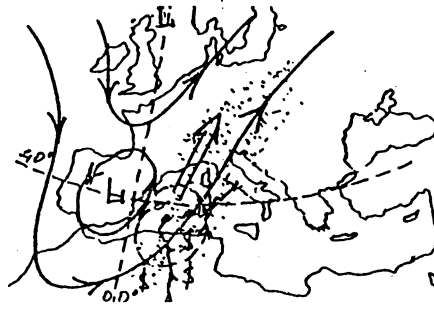


**Figure 1.2**  
Direct transport F. Prodi, G. Féa (1978)

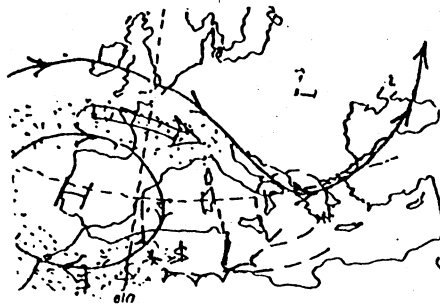


**Figure 1.3**  
Transport deflected by an anticyclone F. Prodi, G. Féa, (1978)

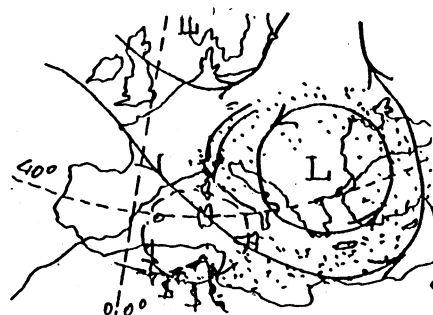


**Figure 1.4**  
Transport deflected by a depression F. Prodi, G. Féa (1978)

Commonly, the second case is responsible for the arrivals of dust and mud rain in the west of France and fallout was most likely to be caused by direct transport over the Mediterranean Sea and northern Italy.

#### **STUDY OF THE ARRIVALS OF SAHARAN DUST AND MUD RAIN.**

When fallout of dust and mud rain occurs, the procedure to be followed consists first of all in consulting the French and European Meteorological Bulletin to verify that the dust is really from the desert.

This is confirmed from photographs taken by the Meteosat and NOAA satellites and provided by the National Meteorology Office (Lannion, France).

For example, the photographs of the dust cloud from the 12<sup>th</sup> - 13<sup>th</sup> and 15<sup>th</sup> August 1987 show this. (The 14<sup>th</sup> of August photo is missing due to dense cloud cover, Fig. 1.5, 1.6, 1.7).

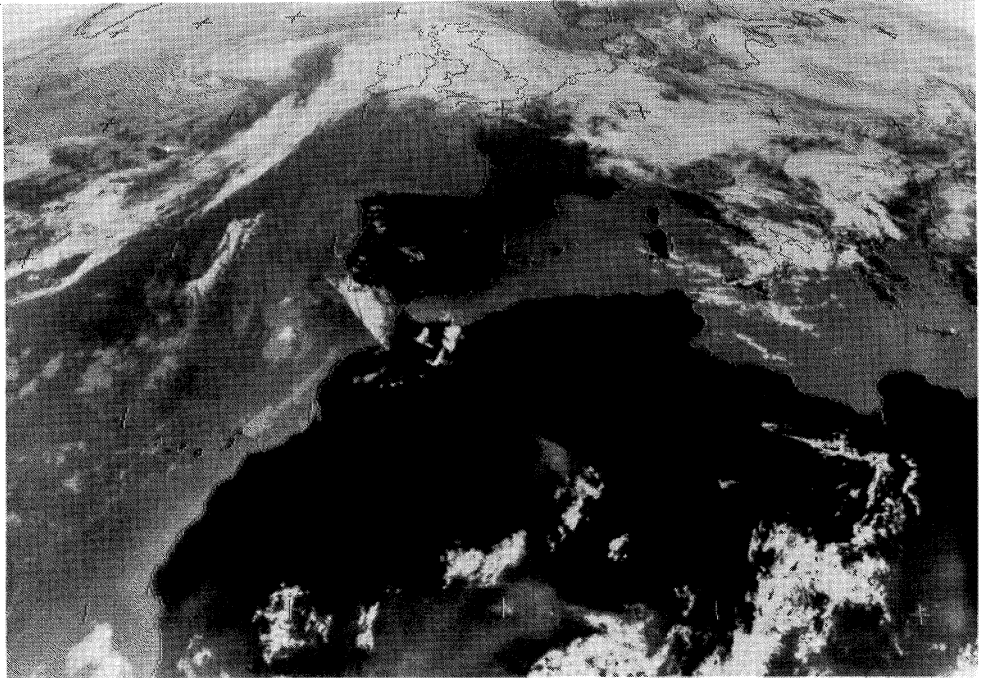


**Figure 1.5**  
Meteosat photograph, 12<sup>th</sup> August 1987; Visible Channel.  
The dust plume in the Sahara milieu is visible.

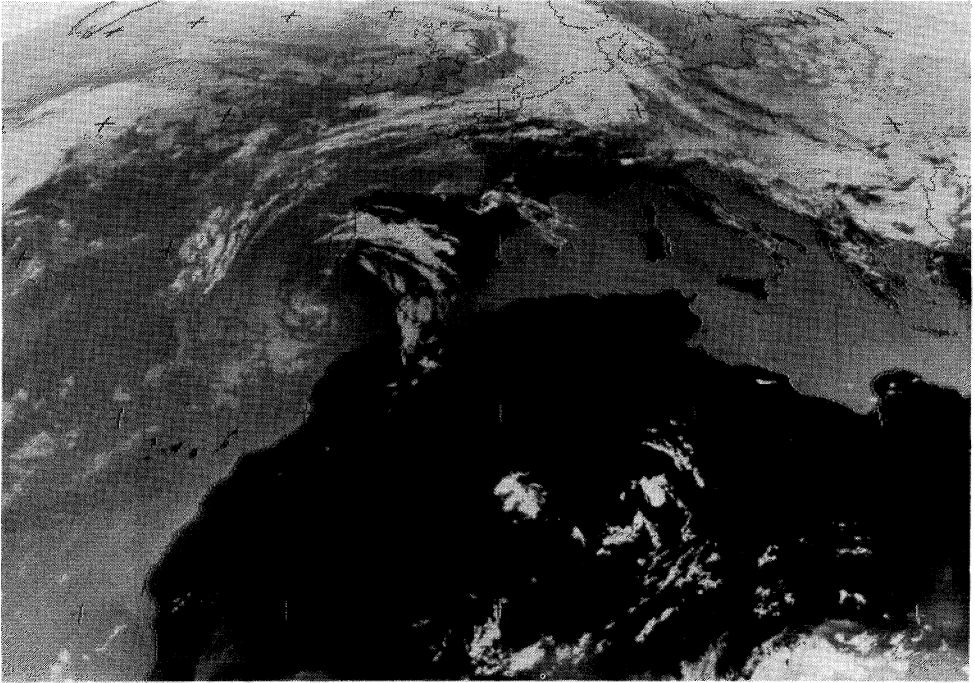


**Figure 1.6**

Meteosat photograph, 13<sup>th</sup> August 1987; Visible Channel.  
The dust plume in the Sahara milieu is visible.



**Figure 1.7**  
N.O.A.A. photograph, 15<sup>th</sup> August 1987; Visible Channel.  
The Saharan dust on the atlantic side of France  
and in its south west quarter.



The National Meteorology Office can also provide "trajectographs" of an air mass, which give a representation of its path on a map, the evolution of pressure from its origin to its fallout place, and the hourly values of longitude, latitude and altitude of the air mass in question. By uniting all this information, one can obtain an idea of the dust source. By studying different pollen of African origin that accompany the dust, some of which are local markers (M. Van Campo 1975), the localization of the source region may be reconstructed.

Unfortunately, "additions" in dust and pollen occur during the transport if the ground winds are turbulent while the dust cloud passes overhead. One can never be certain that the dust that falls on France has exactly the same composition that it had at the outset, the same chemical composition or the same size particles.

Results of the chemical analyses of four important fallouts of Saharan dust and mud rain from the north west Sahara, which arrived in the High Pyrenees, France, since 1972, are shown in table 1.1 (fallout of February 1972, September 1975, August 1980 and July 1983) (A. Bücher, C. Lucas 1972, 1984 ; A. Bücher and al 1983).

**Table 1.1**

Results of the analyses in percentage of four important fallouts of Saharan dust and mud rain in the high Pyrenees, France collected over fresh snow (1972), in a plastic bucket after.

February 1972 Saharan dust

September 1975 coloured snow (Sahara)

August 1980 Saharan dust

July 1983 mud rain (Sahara)

	SiO <sub>2</sub>	Al <sub>2</sub> O <sub>3</sub>	Fe <sub>2</sub> O <sub>3</sub>	CaO	MgO	K <sub>2</sub> O	Na <sub>2</sub> O	TiO <sub>2</sub>	MnO	P <sub>2</sub> O <sub>5</sub>
PM 72	52	16.4	4.2	8.2	2	0.5	0.6	2		
75	56	15	6.4	11	3.2	2.8	1.2	0.95		
80	54.6	17.7	7.07	12.1	3.6	2.4	0.4	1.03	0.1	
83"	56.7	16.2	6.7	9.3	2.8	3	1.7	0.9	0.1	0.13

It is fairly clear that the values recorded in these analyses are similar. In this source zone, ergs (Iguidi, Chech) and hamadas can be found, like those in Draa and many zones of spreading wadi from the Atlas mountains.

## 1°) THE WIND SAND OF THE NORTH WEST SAHARA

In a majority of the cases studied, the source area of the dust seems to be the north west Sahara. Their chemical composition and observations from meteorological stations confirm this.

Andalousi (1966) has studied the number of days of wind sand from 1951 to 1960 in seven stations in the regions of Adrar, Béni-Abbès, Colomb-Béchar, El Bayadh (formerly Geryville), Aïn Sefra, Timimoun, and Tindouf. Two of them are in the northern Sahara, El Bayadh in the Djebel Amour and Aïn Sefra in the Ksour Mountains.

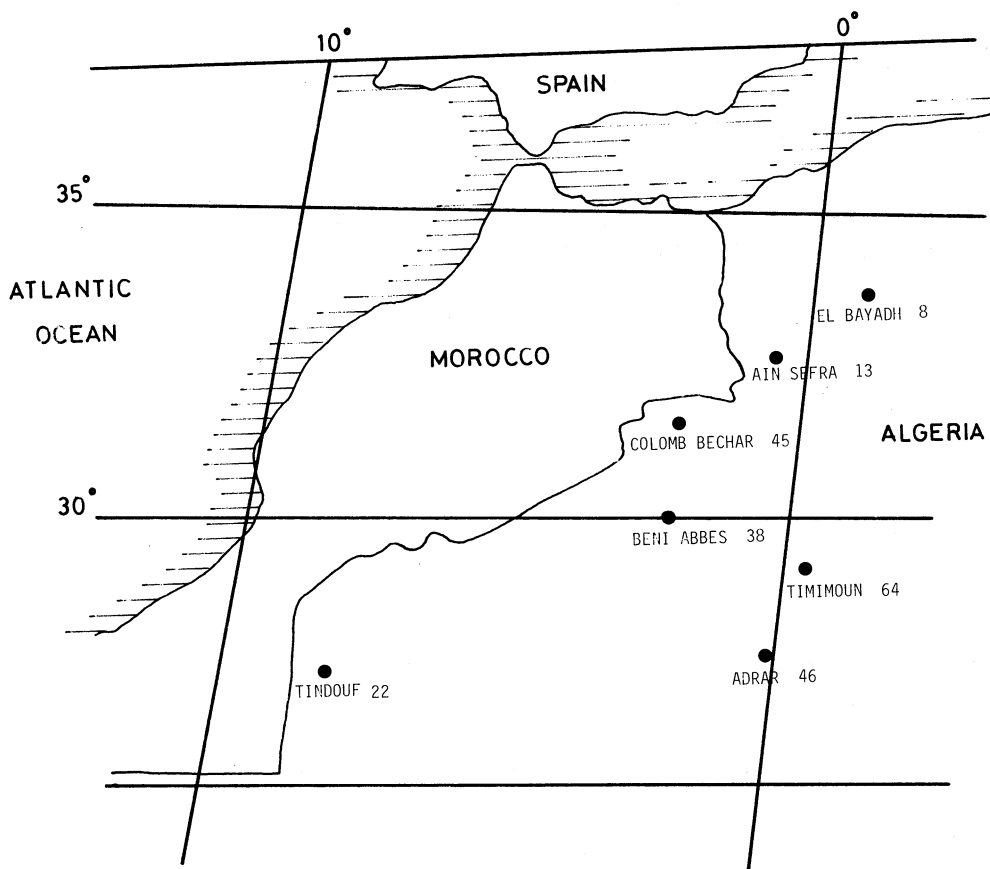
The great Western Erg, a vast stretch of sand, is bordered by Colomb-Béchar to the north, Béni-Abbès 160 km to the south, Timimoun 250 km ESE of the latter, Adrar 150 km south of Timimoun, and Tindouf, which is situated south of the Algerian-Moroccan border. This study was not published, so we have continued and completed it (A. Bücher 1986).

For each of the cited stations, the geographic location and the annual frequency of wind sand is given in map 1.1.

Timimoun is affected by the largest number of these events (64), followed by Adrar (46), Colomb-Béchar (45), Béni-Abbès (38), Tindouf (22), Aïn Sefra (13), and finally El Bayadh (8). The fact that El Bayadh and Aïn Sefra are situated in a mountainous area and are not in the desert region explains the lower number of wind sands.

While Tindouf is to the south of the zone where the Saharan perturbations pass, Timimoun, Adrar, Beni-Abbès and Colomb-Béchar are to the east of this zone. The wind sand is always attended by lighter dust.

The dust storm may occur with a low wind velocity as well as high wind velocity. Certain meteorological conditions, such as heat and turbulence are necessary to provoke the movement of dust particles. Variations in air pressure are also important.



**Map 1.1**

Geographic location of seven stations in the north-west Sahara and their annual frequency of dust storms (1951-1960)

## 2°) STATISTICAL RESEARCH

In order to collect the dates of Saharan dust fallout and mud rain, many articles, books and reviews have been compiled, such as by several authors, "the Nature", "Sky and Earth", the reports of the Academy of Sciences etc.

First of all, only those articles giving precise dates were taken into account. The regions considered are Europe, northern Africa, the Middle-East and the Atlantic Ocean. 201 cases have been listed, with the following average monthly percentages :

	J	F	M	A	M	J	J	A	S	O	N	D
%	9	11	19	12	10	4	8	6	4	6	7	4

During June, September and December, the fallout is rarest, followed by August and October, then November, July, January, May, February, April, March.

Many dates have been found in the works of C.G. Ehrenberg (1849 and 1871). The 201 previously mentioned cases have also been included in a list.

Very often, C.G. Ehrenberg only states the year the event took place, so the results have to be used very carefully.

Whenever 2 similar dates have been found in 2 different author's works, only one date has been retained. 715 cases have been mentioned, between 1577 BC and 1983 AD (Fig. 1.8).

## Numbers of cases

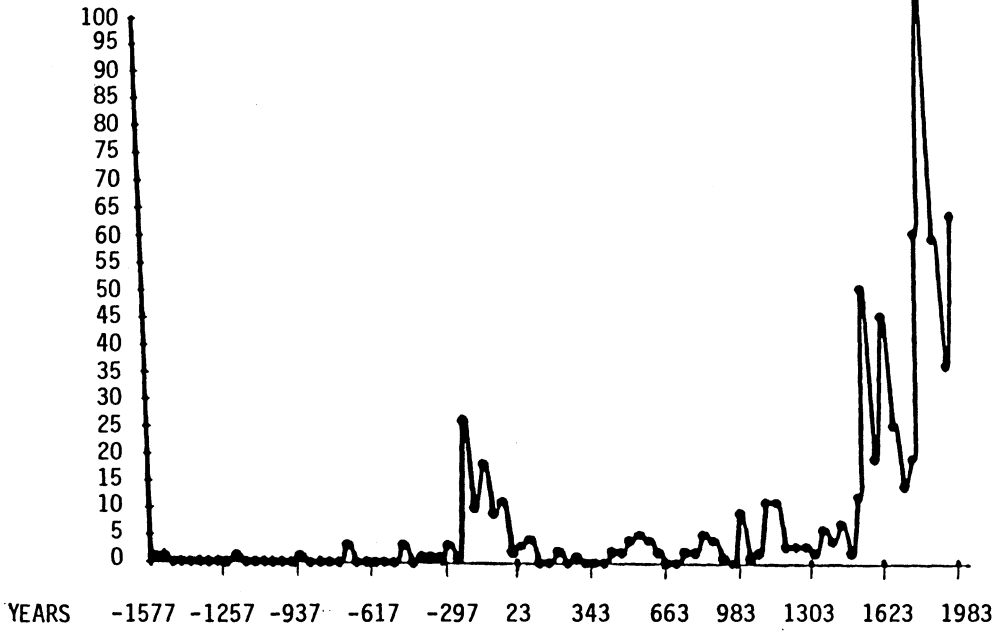


Figure 1.8

Number of cases 40-yr 1577 BC to 1983 AD

One must be struck studying the graphic by the sharp increase in the number of events between the year from about 240 BC to 10 AD. We can be sure, that the events must have been quite wide-spread, since accounts have been kept about them, even though they occurred such a long time ago.

The period from 1500 to 1983 has been studied in greater detail and 417 cases are recorded (Fig. 1.9).

**Numbers of cases**

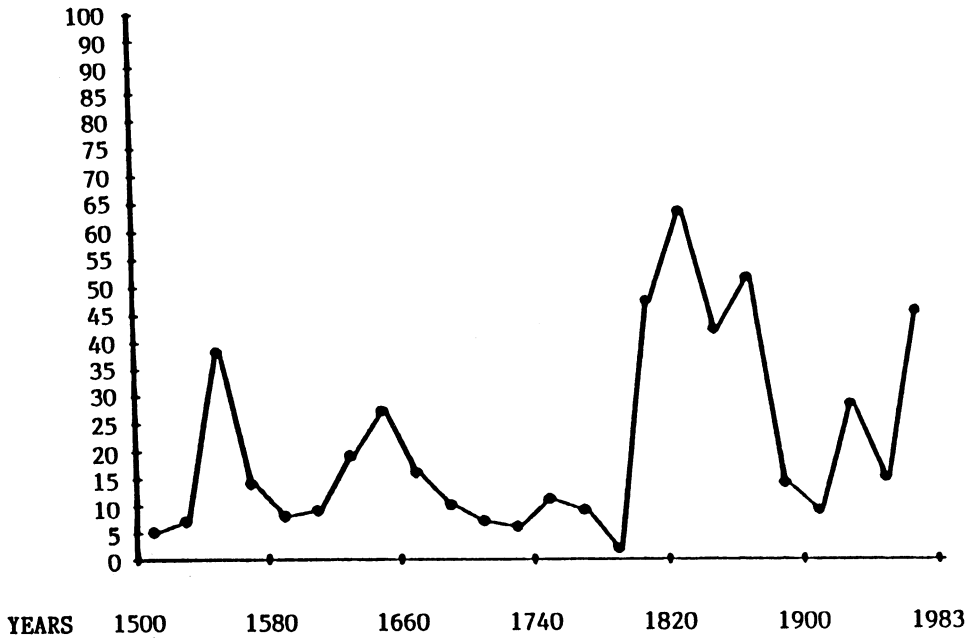


**Figure 1.9**  
Number of cases 20 - yr 1500 to 1983

After a fairly regular decrease from 1640 to 1800, a rapid increase in the cases can be seen from 1800 to 1840. There is currently no explanation for this (A. Bücher 1986).

## APPENDIX

### THE "POUSSAH" NETWORK

In French, "pouss" is the first part of the word for dust "poussière" and "sah" is the first part of Sahara. In hindou "poussah" is a lazy fat man. Our "Poussah" network has two correspondents in Belgium, one in Germany, one in Switzerland, one in Italy, one in Greece, one in Algeria and three in Spain.

In France, a number of institutions and people take part in this research. Special collectors are installed in seven French national parks and also in Spain. They are plastic buckets of 0,250 m<sup>2</sup> with a constant water-level at the bottom, so that the dust cannot be lost once it has been collected and in order to permit also the collection of mud rain and dirty snow.

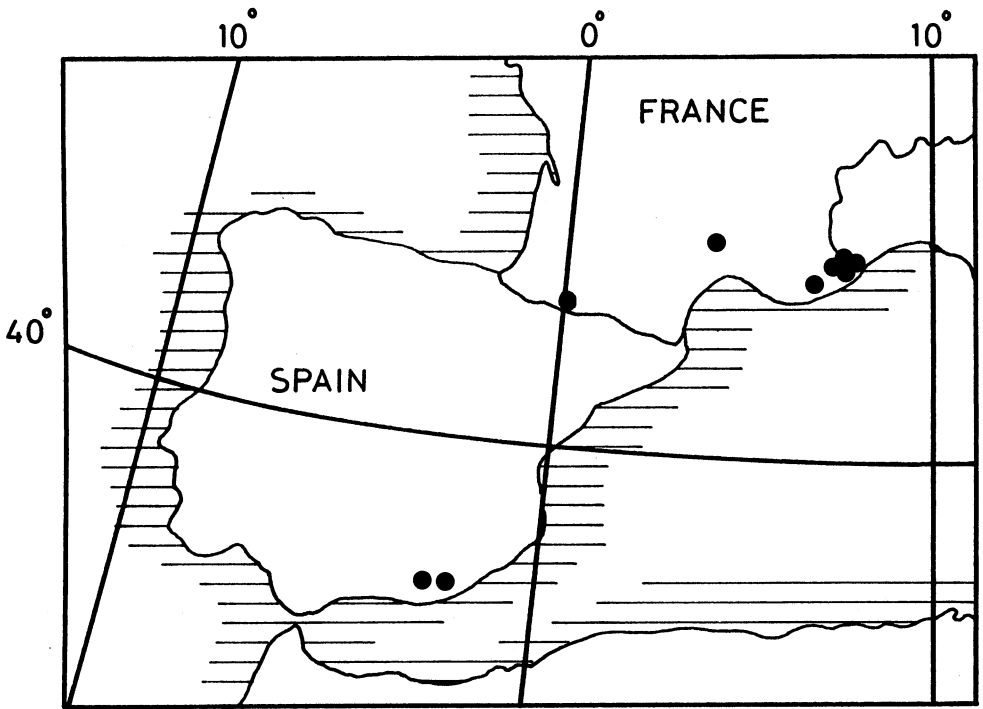
Whenever reddish patches of mud rain and dirty snow occur on cars, the observers complete and dispatch a questionnaire from the collectors. The muddy water from the collectors is poured into plastic bottles with the date on and site of the fallout. Once a year at least, all these bottles are returned to the laboratory and their contents are analyzed.

The advantage of this simple and cheap method is, that it works well in places with no source of pollution (national parks for example). Whenever fallout occurs, samples are collected in areas less likely to be affected by the local geological environment. A. Bücher and C. Lucas (1984) investigated results which do not vary too much in respect to the colour values, particle size and proportions of calcite/quartz. These were obtained at the observatory of Pic-du-Midi- de-Bigorre, a station of reference, High Pyrenees France.

In the context of more precise studies, for which it is necessary to have access to the samples as quickly as possible, these collectors should be replaced by instruments of higher performance that are capable of trapping and sorting fallout, such as "cascade impactors" for example.

The collectors are presently situated in the following places :

- two in southern Spain at 3000 m,
- one at the summit of Pic-du-Midi de Bigorre, High Pyrenees, France, 2870 m,
- one in the Cevennes national park, Lozère France, 1800 m,
- one on the Calern plateau, north of Grasse, Maritimes Alps, 1270 m,
- five distributed over the area of the Mercantour national park, of the Franco-Italian border, 1300 m (map 1.2).



**Map 1.2**  
Geographic location of ten buckets in Spain and in France



The Mercantour national park will be transformed into a model station with the three research objectives :

- a) To determine the mass of dust that falls on the region by extrapolation , through a judicious distribution of the collectors;
- b) to study how the distribution of Saharan dust mass between the various collectors reflects their geographical situation ;
- c) to examine the evolution of items according to the underlying meteorological condition.

The intensity of precipitation and the varying geographical features affect the readings. These factors must always therefore be taken into account.

Since measurements are taken at stations in both Spain and France the particle dimensions as a function of travel distance can be compared. It would be better to measure the particle size around the source zone in the Sahara, but this is difficult and extremely expensive. The particles that are deposited in Spain are obviously larger than those that arrive in France (Fig. 1.10, 1.11).

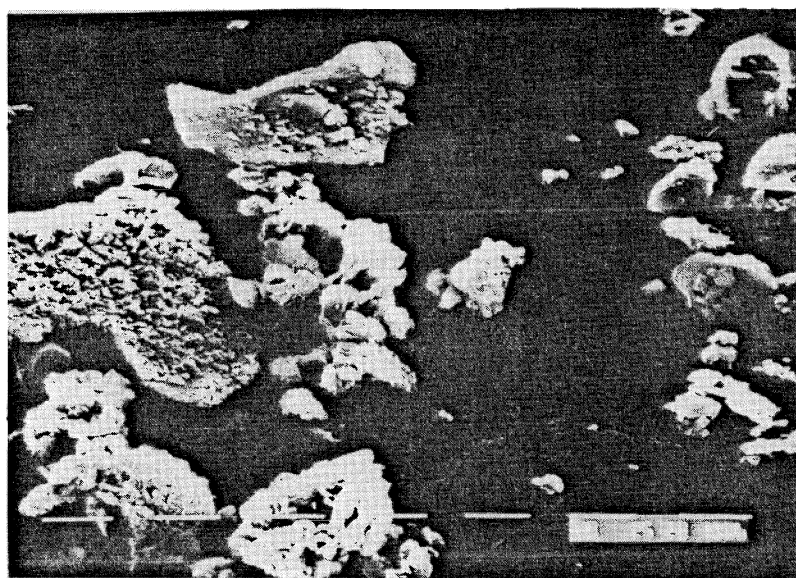


**Figure 1.10**

Saharan dust collected in the Sierra Nevada (Spain), August 1962.

Micas are the largest particles.

Scanning electron microscopy, graphical scale (white bars) = 10 micrometers



**Figure 1.11**

Saharan dust collected by M. Leleubre near St Giron, Ariège, (France). Calcite, micas, quartz, and kaolinite are identified.

Scanning electron microscopy, graphical scale (white bars) = 10 micrometers

The sites at which the collectors are installed were the subject of a preliminary study, because a polluting source can invalidate the analyses as has previously been explained. One may note that fresh snow constitutes an ideal surface for collecting dust, as it can be seen easily. Surface snow visibly containing Saharan dust particles is collected over 1 m<sup>2</sup> and is put into plastic bags, transferred into bottles and subsequently analysed.

It seems more and more evident that European and Mediterranean centres for the collection and the studies of samples of Saharan dust should be established. The experience of the "Poussah" network shows this.

At the present time, researchers concerned with Saharan dust fallout all work independently in their own countries and there is no collaboration between them. The "Poussah" network has however permitted us to understand the importance of the phenomenon of dust fallout, particularly in France.

### AKNOWLEDGEMENTS

I am grateful to C.N.R.S for its help, and to the "Club Alpin Français" who has permitted us to contact nine guardians of mountaineering refuges situated from the upper Rhine to the Alps of High Provence, who have agreed to serve as correspondents.

### BIBLIOGRAPHY

Andalousi, M. (1966) : "Les vents de sable dans le sud-oranais", unpublished report, Météo. Nat. Paris.

Bücher, A. and Lucas, C. (1972) : "Le nuage de poussière rouge du 7 février 1972", Bull. Soc. Hist. Natur. Toulouse 108, 437-445.

Bücher, A. (1973) : "La température au sommet du Pic-du-Midi-de-Bigorre", La Météorologie 28, 19-50.

Bücher, A. Dubief, J. and Lucas, C. (1983) : "Retombées estivales de poussières sahariennes sur l'Europe", Rev. géol. dyn. et géol. phys. 24, fasc. 2, 153-165.

Bücher, A. and Lucas, C. (1984) : "Sédimentation éolienne intercontinentale, poussières sahariennes et géologie", Bull. cent. Rech. Explor. Prod. Elf-Aquitaine 8, 1, 151-165.

Bücher, A. (1986) : "Recherches sur les poussières minérales d'origine saharienne", thèse de Doctorat d'Etat, Université de Reims.

Ehrenberg C.G. (1849) : " Passatstaub und Blutregen, ein grosses organisches Unsichtbares. Wirken und Leben in der Atmosphäre." Abh. K. Preuss. Akad. Wiss. Berlin.

Ehrenberg C.G. (1871) : " Übersicht der seit 1847 fortgesetzten Untersuchungen über das von der Atmosphäre unsichtbar getragene reiche organische Leben" . Abh. K. Preuss. Akad. Wiss. Berlin.

Prodi, F. and Féa, G. (1978) : "Transport and deposition of Saharan dust over Alps", in : 15<sup>e</sup> Internationale Tagung für Alpine Meteorologie, Publ. Inst. Suisse de Météorologie, Grindelwald, 179-182.

Van Campo, M. (1975) : "Pollen analyses in the Sahara", in : Problems in Prehistory : North Africa and the Levant (F. Wendorf and A. E. Marks, eds.), So. Methodist Univ. Press, Dallas, 45-64.

LATE QUATERNARY CLIMATIC CHANGES IN THE AFRICAN RAIN FOREST : FOREST REFUGIA AND THE MAJOR ROLE OF SEA SURFACE TEMPERATURE VARIATIONS.

Jean MALEY

ORSTOM, UR A3 et CNRS, UA 327

Laboratoire de Palynologie

Université des Sciences et Techniques du Languedoc

34060 MONTPELLIER cedex, FRANCE.

ABSTRACT. The question of forest refugia in Africa is briefly presented from a historical and evolutionary point of view. Main pollen evidence, which goes back to about 25-28,000 yr BP, is presented for two lakes situated in African lowland rain forest.

- The pollen data from Lake Bosumtwi (Ghana) show the disappearance of rain forest from ca. 28,000 to ca. 9000 yr BP. During this time interval the vegetation was a grassland of the montane type with sparse clumps of trees. There is synchronism between montane vegetation disappearance and rain forest reappearance. This phenomenon occurred abruptly between about 9000 and 8500 yr BP.

- In Lake Barombi Mbo (West Cameroon) the pollen data show clearly that from ca. 24,000 yr BP until recent time, rain forest persisted with limited variations, and thus, this area represents a refuge area. One also notes an extension of montane vegetation to low elevation which disappears near the beginning of Holocene time.

After a short synthesis of the palaeobiogeography of Afromontane vegetation, one discusses the palaeoclimatology. In the light of the present-day annual climate anomalies which relate mainly to sea surface temperature variations and upwelling of cold water in the Guinea Gulf, one points out the drying and cooling role of stratiform cloud cover, particularly during the time of fragmentation of the forest area. For the Ghanaian rain forest one also discusses on the weather types responsible for the forest extension after 9000 yr BP and during the major transgression of Bosumtwi lake during mid-Holocene time. One relates these two phenomena to the disappearance of the present-day summer "little dry season". The reappearance of this "little dry season" in late Holocene time, linked to the deterioration of the water budget, is probably responsible for the abrupt lacustrine regressions and also for the opening of the "Dahomey Gap".

1. INTRODUCTION. THE QUESTION OF FOREST REFUGIA

In the equatorial zone, the rain forest biome has long been considered

to be a quasi-fixed entity, sheltered from climatic fluctuations. In Africa, botanists such as AUBREVILLE (1949,1962) or SCHNELL (1950) and zoologists as BOOTH (1958), MOREAU (1963,1966) or CARCASSON (1964) who described the large floristic and faunistic heterogeneity of this region, were among the first who came to the following conclusion : the forest biome had also undergone profound modifications. In the end, the continuation of research led to the hypothesis that during climatically unfavorable periods, the biological richness of the forest was conserved in refugia, privileged sectors where the climate would have remained favorable. The first schematic maps of forest refugia in equatorial Africa were published by AUBREVILLE (1949, p.66; 1962, p.62).

Nevertheless, until recently, research on the question of forest refugia have increased, especially in South America, in the Amazon Forest (PRANCE, 1982; WHITMORE et PRANCE,1987), firstly in order to locate the position of refugia, secondly to study the speciation processes associated with the geographical isolation of refugia. Indeed, for many authors, the biologic richness of forest biome could at least partly be explained using the model of allopatric speciation (vicariance) (HAFFER,1982). However, according to the results of studies of animal and plant groups, the existence of refugia has been questioned because the proposed areas were not always superposed or had surfaces of different size (cf.examples given in WHITMORE et PRANCE,1987). Yet these authors consider that those differences could be linked mainly to the dynamics of each animal or plant group, without denying the refugia. Moreover, some authors, as ENDLER (1982), considering the African forest model, estimate that its biological richness could result uniquely from parapatric speciations. Indeed, the necessary isolation for the emergence of new species could be achieved only by the presence in this biome of numerous ecological niches (FEDOROV, 1966; RICHARDS, 1969; etc). In refuting some of ENDLER's arguments (1982), MAYR and O'HARA (1986) re-affirmed evidence supporting allopatric speciation due to fragmentation of the African rain forest area.

All these authors finally estimate that the better arguments supporting the former existence of refugia and fragmentation of the rain forest area could be provided by pollen analyses on deposits from arid phases.

The first aim of this paper is to present the main pollen results answering this question. The second aim is to discuss the climatic conditions which led to fragmentation of the African rain forest into isolated refugia and later on to forest recolonization.

## 2. POLLEN ANALYSES IN AFRICAN RAIN FOREST

During the last few years, pollen analyses were carried out on upper Quaternary deposits from two lakes situated at low elevation in the lowland African rain forest : the Bosumtwi lake in Ghana and the Barombi Mbo lake in West Cameroon (Fig.1).

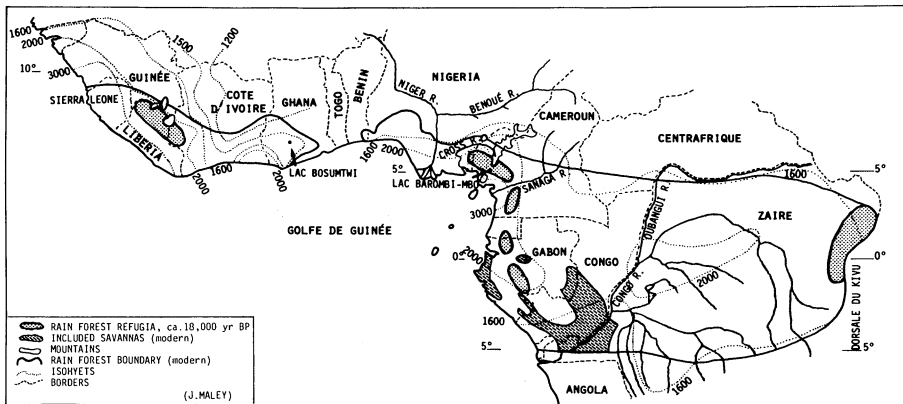


**Figure 1** - Diagram of lowland rain forest refugia in equatorial Africa during maximum of the last great dry and cold period (about 18,000 yr BP). The refugia of Upper Guinea and Eastern Zaire are adapted from ENDLER (1982) and MAYR et O'HARA (1986), from data of MOREAU (1966,1969) and HALL et MOREAU (1970). The modern conditions (forest boundary, included savannas and main isohyets) are adapted from WHITE (1983, fig.5 and map) (figure extracted from MALEY,1987).

### 2.1. Lake Bosumtwi in Ghana

This lake with a water level near 100m ASL (Above Sea Level) is situated in semi-deciduous rain forest that is characterized by the families of Ulmaceae, particularly with *Celtis*, and Sterculiaceae with *Triplochiton* and other genera (HALL et SWAINE, 1981). Climatically, this type of forest is adapted to a slightly less humid conditions than the evergreen type which will be presented below (§ 2.2). The semi-deciduous forest appears when the yearly number of "dry" months (rainfall below about 100mm) reach three. The two months of the "little dry season" in August and September (§ 4.2; Fig.9) are quasi rainless, but because the atmospheric humidity remains high, these two months must not be added (see the Gabon forest example, § 4.2) to the three months dry season of northern winter (December to February).

The core studied from lake Bosumtwi, has a length of about 17m and reaches back to about 28,000 yr BP (Fig.2). The geological study of this core and outcrops of lacustrine deposits, permitted the reconstruction of the lacustrine fluctuations which were very distinct, with a maximum lake level in middle Holocene time and a very low lake level from about 20,000 to 15,000 yr BP (TALBOT et al., 1984; TALBOT et KELTS, 1986; MALEY, 1987).

The principal pollen results (MALEY et LIVINGSTONE, 1983; TALBOT et al., 1984; MALEY, 1987) (Fig.2 and 3) clearly show that before about 9000 yr BP, forest was not present in this region. Indeed, between the present and about 8500 yr BP arboreal pollen percentages oscillated from 75 to 85%, while before 9000 yr BP arboreal pollen percentages were generally below or close to 25%, except near the base of the core, where they were close to 50%. During the period between about 19,000 and 15,000 yr BP, arboreal pollen percentages reached minimum values of about 4 and 5%. At the same time trees had almost completely disappeared from the landscape and had been replaced by the herbaceous plants, essentially Gramineae and Cyperaceae which reached frequencies of 91 to 94%. Today such percentages of pollen grains from herbaceous and arboreal plants are common in the Sahelian zone (MALEY, 1981).

Other important evidence resulting from pollen analyses is the presence of a montane element in the period from the core base to its quasi disappearance around 8500 yr BP, near the time when the rain forest reappeared (Fig.3). This montane element includes the mountain olive, *Olea hochstetteri*, which today are only present 700 km westward, near 1200m ASL on the Momy Mountain in the Dan Massif of western Ivory Coast (SCHNELL, 1977). Eastward, the nearest modern location of this tree is in Nigeria on the Jos Plateau, and further eastward mainly in the mountains of the Cameroonian Ridge (LETOUZEY, 1968). Until about 8500 yr BP, the presence of a montane element at low elevation around the Bosumtwi lake, where the highest surrounding hills reach maximally elevations from 400 to 550m ASL, imply a lowering of the montane vegetation belt with minimally 600m. This corresponds to a temperature decrease of 3° to 4°C (MALEY et LIVINGSTONE, 1983) when applying a mean temperature gradient of 0.6°C for every 100m displacement of the vegetation belt (WALTER et BRECKLE, 1985) (§ 4.1). This temperature decrease has also been reached by



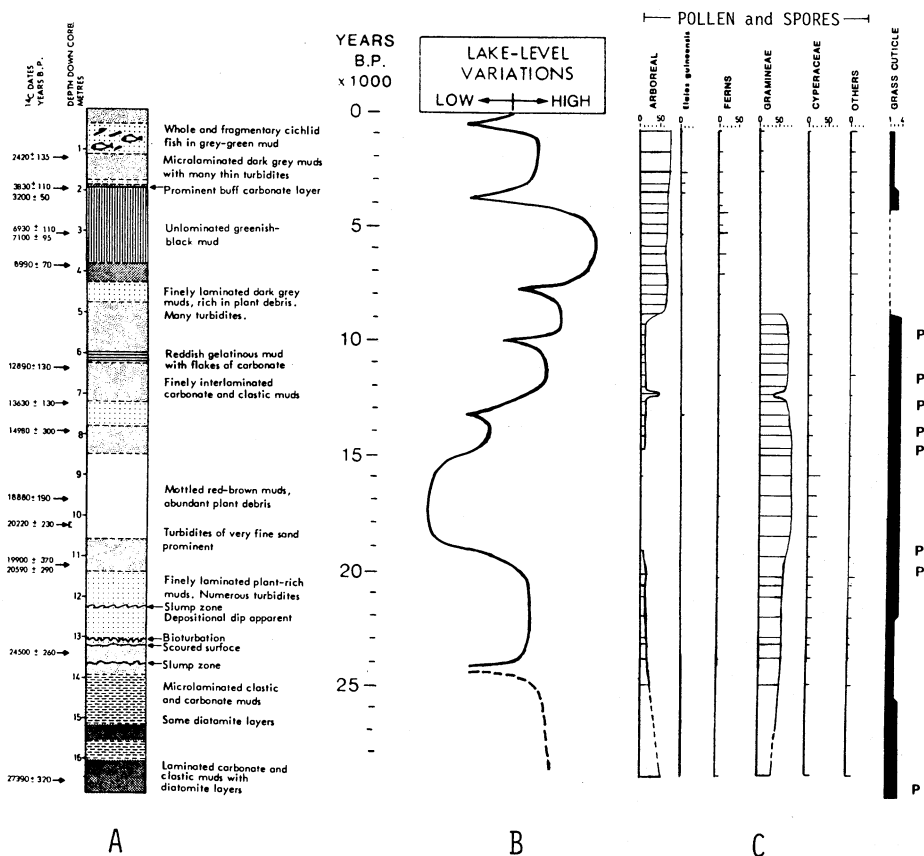


Figure 2 - Lake Bosumtwi in Ghana.

A - Stratigraphy of core B-7, from TALBOT *et al.* (1984).

B - Lake level variations adapted from TALBOT *et al.* (1987); before about 15,000 yr BP the curve is modified by reference to pollen data (cf. Fig. 3).

C - Pollen data from TALBOT *et al.* (1984) and MALEY (1987). P - Cuticles of Pooidae (Afro-montane Gramineae) by PALMER, in TALBOT *et al.* (1984).

LAKE BOSUMTWI POLLEN ANALYSES (J.MALEY)

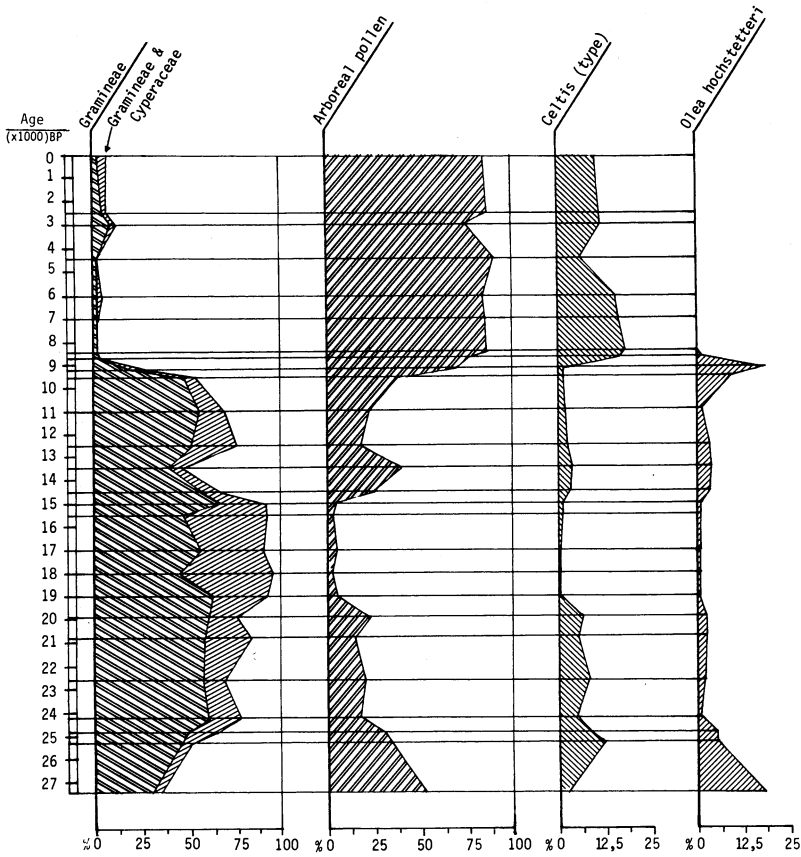


**Figure 3** - Lake Bosumtwi pollen analyses (J.MALEY). The chronology of the core is based on 15 radiocarbon dates (after TALBOT et al., 1984).

PALMER (1982; in TALBOT et al.,1984) by determining in the same section of the core the grass cuticle fragments belonging to the tribe of Pooideae. Today this tribe occurs in the tropical zone only on the high mountains (CLAYTON, 1976; LIVINGSTONE et CLAYTON, 1980), such as on Mount Cameroon where representatives have been recorded only above ca. 2000m altitude (LETOUZEY, 1968,1985). The presence of Pooideae flora below 550m altitude could involve an important decrease of temperature (TALBOT et al.,1984) which should be approximately 6°C, a value comparable to estimates from East Africa (§ 3).

Thus, before 9000 yr BP the forest was absent and it gave way to a mountain type grassland with sparse clumps of trees. Near the base of the core, dated about 27 - 28,000 yr BP, arboreal pollen percentages of about 50% are indicative of the presence of some kind of mountain forest. A remarkable feature is that the scattered trees in the open vegetation belonged in great majority to the semi-deciduous forest flora and not to the Sudano-Guinean savanna flora. Under modern conditions, only the Guinean montane grasslands of middle elevation (submontane belt) include isolated clumps of trees which, in addition to typical mountain species, contain a large set of species which are found from low elevations to the submontane belt (SCHNELL,1977; LETOUZEY,1968, 1985).

## 2.2. Lake Barombi Mbo in West Cameroon

Lake Barombi Mbo has a water level near 300m ASL and is situated in the lowland rain forest of West Cameroon (Fig.1). Around the lake two principal forest formations can be recognized in an area with about 10 km radius (RICHARDS, 1963; LETOUZEY, 1968, 1985; D.THOMAS, pers.commun.):

- The evergreen forest of Biafrean type is a richer variety of the Guineo - Congolan type. It spreads around the Bay of Biafra from east Nigeria to as far south as the boundary of Cameroon and Equatorial Guinea (LETOUZEY, 1985; WHITE, 1983). This forest type is characterized by its richness in Leguminosae, especially Caesalpiaceae and is present when the dry season does not exceed two months.
- The semi-deciduous forest (§ 2.1) forms islets in the evergreen forest which remains largely dominant (LETOUZEY,1985).

So far only the lower half of the longest core (BM-6: 23.50m, from the base to about 11,000 yr BP) has been studied in detail (28 samples spaced every 30 or 60 cm have been analyzed : BRENAC,1988; MALEY et al.,1988(b), to be published). Samples at 2 or 3m intervals have also been studied from the upper part of the core (MALEY et BRENAC, 1987). Below 21m depth in the core, perturbed section interrupts the continuity of pollen spectra . However the dates obtained near the base and the pollen content (Fig.4) show that the lowermost part of the core is probably reversed (MALEY et al.,1988(b) to be published).

The following principal results are to be noted (Fig.4):

### Zone I

From the base of the core (greater than 24,000 yr BP) to a level with an age of about 20,000 yr BP, pollen grains of Gramineae, Cyperaceae

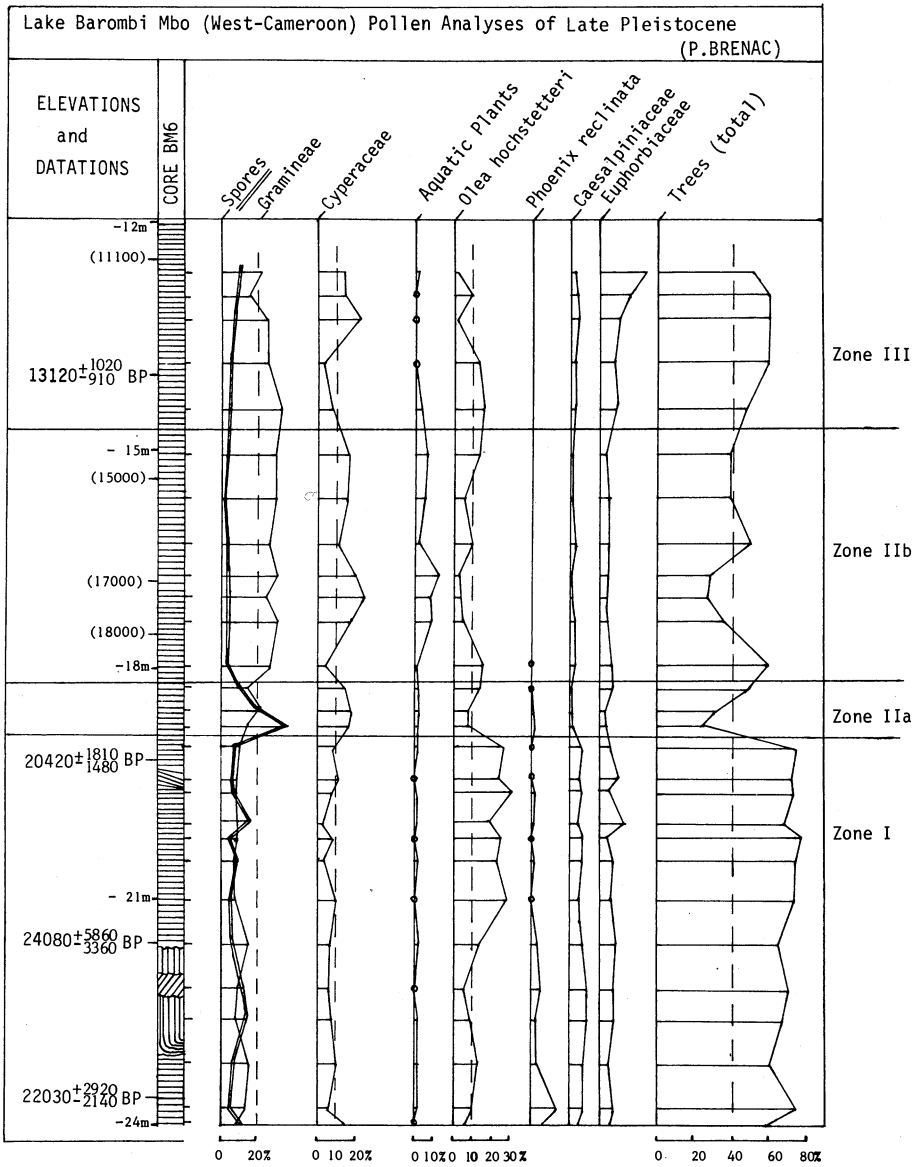


**Figure 4** - Lake Barombi Mbo pollen analyses (P.BRENAC). (from BRENAC, 1988; MALEY et al., 1988, b, to be published).

and shoreline plants are scarce. Gramineae pollen is represented from 6 to 15%. Among the arboreal pollen, the mountain olive, *Olea hochstetteri*, is abundant with percentages between 10 and 30%. *Phoenix reclinata* (Palmae), which is found today in the Cameroon mountains frequently associated with *Olea hochstetteri* (LETOUZEY, 1978), is also relatively frequent in this section. Besides these two montane taxa, pollen of forest taxa is abundant with percentages from 60 to 75%. Among these, Caesalpiniaceae and Euphorbiaceae are particularly well represented (BRENAC, 1988).

Under modern conditions, the association of mountain taxa in combination with typical lowland evergreen forest flora is found in Cameroon, for example, on the hills' summits around Yaoundé (between 900 and 1200m ASL) (ACHOUNDONG, 1985). On the plain around these hills the forest is semi-deciduous, but on the hills' summits climate is more humid and cool because of the high frequency of clouds which favor this particular cloud forest association (BRENAC, 1988).

#### Zone II

Around 20,000 yr BP, a very sharp change occurs in the pollen spectra. Percentages of mountain olive pollen grains decrease to values of 5 to 15%. Forest taxa decrease as well, particularly Caesalpiniaceae and Euphorbiaceae. Percentages of arboreal pollen grains oscillate around 40% until ca. 14,000 yr BP. During the same period, grass pollen grains increase to about 25%. It is the same for Cyperaceae and other aquatic plants.

These data are indications of a relatively dry and cool climate. The increase of Cyperaceae and shoreline plants is probably related to a lower water level, which is in accordance with a decrease in rainfall. By analogy with pollen analyses of modern samples of soils and lacustrine sediments (BRENAC, 1988), the increase in herbaceous plants is indicative of the development of more open forest vegetation or the development of a mosaic pattern of forest and open formations.

#### Zone III

Between ca. 14,000 and 10,000 yr BP the forest taxa increase again, with percentages close to 60%. Among the tree taxa, some representatives of the semi-deciduous forest, such as *Celtis*, replace those of the evergreen forest present before 20,000 yr BP. One notes also pioneer forest taxa typical of secondary natural formations. Around the beginning of Holocene time, Gramineae percentages decrease to about 20%. In Zone III, percentages of mountain olive pollen increase again around 13,000 yr BP to disappear again near the beginning of Holocene (BRENAC, priv. commun.). One can conclude that this period was humid again, but not as cool as before 20,000 yr BP.

From about 10,000 yr BP to the present, the few data so far available show a relatively stable vegetation, dominated by semi-deciduous forest elements accompanied by many taxa of secondary natural formations (MALEY et BRENAC, 1987).

### 2.3. Conclusions

The pollen data presented here are particularly important because they

show that during the last great arid phase, from about 20,000 to 14,000 yr BP, the rain forest disappeared in Ghana, particularly in the Bosomtwi sector, but persisted in West Cameroon. These conclusions have been associated with various biogeographic data obtained from studies on plants, birds, mammals, amphibians, butterflies, etc., from Cameroon and other parts of the forested zone, as well as palaeoclimatic data, in order to establish a new schematic map of lowland forest refugia in equatorial Africa during the last great arid phase, about 18,000 yr BP (Fig.1) (see MALEY, 1987, for a more detailed discussion). Another important result is the spread to low elevation of a montane element that are characterized by *Olea hochstetteri*. This indicates a temperature cooling which seems similar for the two sites studied.

### 3. PALAEOBIOGEOGRAPHY OF AFROMONTANE VEGETATION

To understand the problem of extension of montane vegetation to lowland, the modern composition of the African montane flora and fauna of middle altitudes from about 1000m to 3000m ASL must be recalled. Indeed, between the different mountain massifs of equatorial Africa, a great similarity has often been noted. For example, according to HALL (1973), the plant species common to Mount Cameroon and Eastern Africa are 53% for the montane forest and 49% for the montane grassland. In order to explain these similarities, many authors have assumed that during climatic changes and especially during cooler periods of the Quaternary, the montane floras and faunas must have extended to the lowlands which facilitated migration between mountain massifs (MOREAU, 1966; WHITE, 1981; MALEY, 1987).

The extension of montane vegetation to lower elevation in Eastern Africa has been known for several decades, and for this reason temperatures are believed to have been 5° to 9°C lower (COETZEE, 1964; VAN ZINDEREN BAKKER et COETZEE, 1972; HAMILTON, 1973, 1982; FLENLEY, 1979). Moreover, in southern Congo Republic (CARATINI et GIRESSÉ, 1979; ELENGA et al., 1987) and in northern Angola (VAN ZINDEREN BAKKER et CLARK, 1962), several pollen analyses also clearly show extensions of montane vegetations to low elevation (MALEY, 1987). The most important data has been obtained on the Plateaux Batéké, about 40 km north of Brazzaville, in a small depression near 600m ASL (ELENGA et al., 1987). The pollen analyses carried out on a short core show that from the base until around the beginning of Holocene time, the pollen spectra were dominated by Afromontane taxa; the pollen grains of *Podocarpus milanjanus* (syn. *P. latifolius*), *Ilex mitis* and *Olea welwitschii* (syn. *O. hochstetteri*, cf. TROUPIN, 1985) constituted about 60% of the pollen spectra, dominated by *Podocarpus* with about 50% (ELENGA et al., 1987).

Between the mountain massifs of Eastern Africa and Cameroon, several typical Afromontane taxa had been observed in various isolated stations (WHITE, 1981), on the southern rim of the Zaire river catchment, and along the Guinea Gulf on the ridge of hills connecting Angola to Cameroon. For *Podocarpus latifolius*, there is a station near

700m ASL on the Congolese slope of Chaillu Mountain (MALEY et al.1988 (a), to be published) and another about 900m ASL near the top of an isolated inselberg in south Cameroon, near the Gabon border (LETOUZEY,1968). The cumulative evidence from these stations and the pollen data presented above show the pattern of a preferential junction way which could have operated intermittently during the Quaternary between East Africa and Angola, and subsequently expanded to the hill ridge of Mayombe, Chaillu, Monts de Cristal until eventually the Cameroon mountains (MALEY,1987; MALEY et al.1988 (a), to be published) (Fig.5).

#### 4.PALAEOCLIMATOLOGY

##### 4.1. Introduction. The hypothesis of lapse rate variation

During the Last Glacial Maximum (LGM) (about 18,000 yr BP) the extension of glaciers and vegetation belts to altitudes much lower than those of today are now widely accepted data (see for example the synthesis of FLENLEY, 1979). Many authors have tried to explain the temperature lowering which can be deduced from these data (generally between 5° and 9°C) with palaeoclimatic models (WEBSTER et STRETEN,1978; WHITMORE et al.,1982; FLENLEY, 1984; RIND et PETEET, 1985; MORLEY et FLENLEY,1987; etc). The paper of WEBSTER and STRETEN (1978) is a good example of one of these essays. The authors (*op cit.*) discuss about tropical Australasian palaeoclimates during the LGM, and like for tropical Africa, much of the data show a 6° to 8°C lowering of temperatures in New Guinea mountains. For the surrounding tropical oceans, the data from the CLIMAP Group (1976,1981) suggest only a 2°C cooling or less. The value is similar for the seas around tropical Africa, except in a small sector of the Guinea Gulf where a 3°C cooling is indicated. WEBSTER and STRETEN (*op cit.*) try to explain these opposite results from Australasia with several detailed palaeoclimatic reconstructions.

The principal hypothesis that is discussed in detail is the variation of the vertical lapse rate (WEBSTER et STRETEN,*op cit.*). About this physical phenomenon, WALTER and BRECKLE (1985, their Fig.120) used many temperature records from various mountain slopes in Venezuela to obtain a linear temperature elevation relationship, and from this relation calculated a vertical lapse rate of 0.57°C per 100m from sea level to 5000m. Using the temperature recorded during vertical ascent in free atmosphere for several stations in Australia and New Guinea, WEBSTER and STRETEN (*op cit.*) have shown that this value (about 0.6°C/100m) corresponds to the moist adiabatic lapse rate, but that in dry atmosphere the lapse rate is steeper and close to 0.8°C/100m. The principal point is that this dry atmosphere lapse rate fits quite well the palaeoclimatic data for the LGM. Because the climate was dry at about 18,000 yr BP, WHITMORE et al.(1982), FLENLEY (1984) and MORLEY and FLENLEY (1987), relying on this hypothesis, have estimated that the atmosphere was dry also at this time and, for this reason, had a steeper lapse rate. However WEBSTER and STRETEN (*op cit.*)

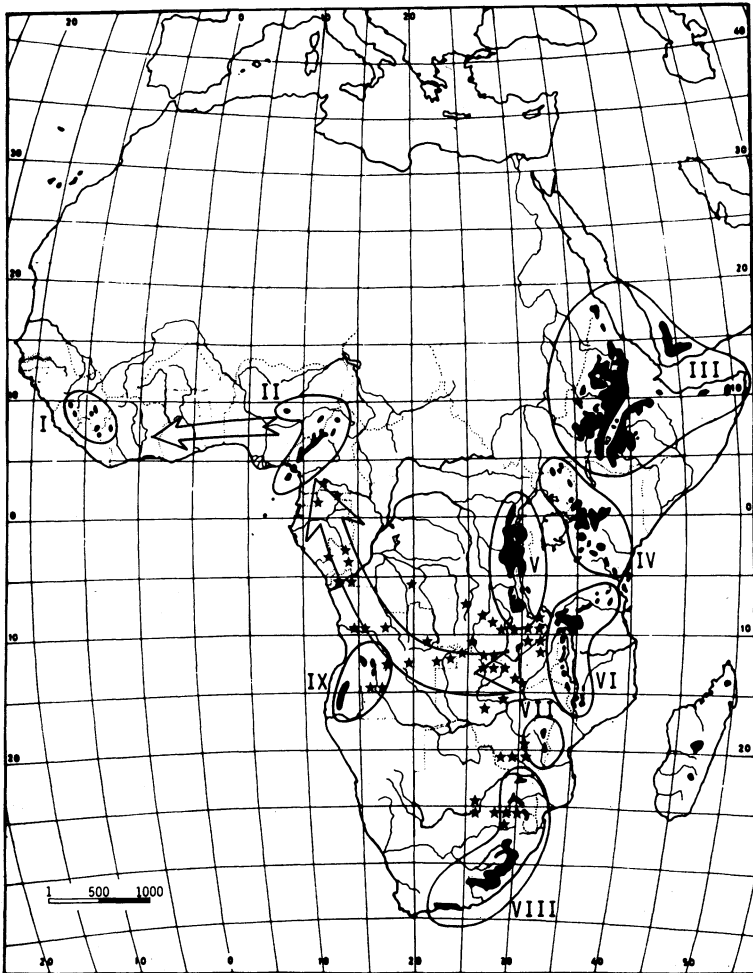


**Figure 5** - Distribution of the nine African regional mountain systems. I, West-African; II, Cameroon-Jos; III, Ethiopian; IV, Imatongs-Kenya-USambara; V, Ruwenzori-Kivu; VI, Uluguru-Mlanje; VII, Chimanimani; VIII, Drakensberg; IX, Angolan. The stars show many distant populations of Afromontane plant species outside the large mountain systems represented by black areas (adapted and completed from WHITE, 1978, 1981). The two arrows schematically represent a possible migration path of Afromontane taxa from East Africa to Angola and subsequently via Cameroon to West Africa.



criticize this hypothesis because (*op cit.*, p.305) the thermodynamics determining the atmospheric structure in the vertical are governed by strict physical laws. The vertical temperature profile are expected to be close to moist adiabatic even if the atmosphere were drier, as indicated by the winter temperature-height diagrams of Darwin, Cloncurry and Charleville. WEBSTER and STRETEN (*op cit.*) also expect similarity between the temperatures above the adjacent ocean regions and at corresponding levels on elevated terrain.

Additionally, in an important paper, RIND and PETEET (1985) conclude (*ibid.*, p.18) that at low latitudes the current lapse rate is consistently close to the moist adiabatic value and that, for this reason, the lapse rate would not have changed if sea-surface temperatures remained warm during the LGM.

Consequently an alternative hypothesis is necessary to explain the LGM data. The starting point of the alternative hypothesis presented here is that one observes today on some mountains a natural extension of mountain vegetation to lower elevations. The new hypothesis, which has been already formulated (MALEY et LIVINGSTONE, 1983; MALEY, 1984, 1987), is based partly on the fact that ecologists studying present-day mountain conditions have demonstrated the primordial role played by the cloud covers and fogs (GRUBB et WHITMORE, 1966; BAYNTON, 1968; GRUBB, 1971, 1974, 1977).

#### 4.2. Some present-day models of localized montane extensions to lower elevations

The montane biotopes appear generally above 1000m ASL; this limit forms a fundamental biological barrier which is characterized by changes in flora and fauna and also commonly by physiological modifications (MOREAU, 1966; HOWARD, 1970; GRUBB, 1971, 1974; WHITMORE, 1975; LEIGH, 1975; BERNARDI, 1979; etc.). However, one can locally observe the extension of normally montane faunas or floras to low elevation.

Outside of Africa, there are many examples of this phenomenon in the Antilles islands and around the Caribbean Sea (BAYNTON, 1968; HOWARD, 1970; etc.). In the northern tip of Colombia, SUGDEN (1982) describes a cloud forest on the Serrania de Macuira which attains a maximum elevation of 865m about 25 km inland from the coast. The slopes from about 500m to the summit are covered by a mountain forest formation. In the lowland the mean monthly temperature is 28°C and varies little throughout the year (SUGDEN, *op cit.*). At 500m ASL SUGDEN (*op cit.*) recorded a mean temperature of about 22.5°C and so, one obtains a temperature lowering of 5.5°C for 500m. Usually, with a lapse rate of 0.6°C / 100m (see above § 4.1) one can calculate a temperature lowering of 3°C for an elevation of 500m. The extra 2.5°C of cooling must be related to the extensive cloud formation and fog which enshroud the summit.

Other examples exist on the Atlantic coast of Africa, but apparently, without temperature measurements. The hills of Freetown in Sierra Leone present one example. These hills rise from the sea to an elevation of about 900m ASL and, from 500m ASL upwards, they support a

set of montane plants (MORTON,1968), such as *Olea hochstetteri* (HEPPER,1963). Further to the east on the seaward south flank of Mount Cameroon, typical montane trees (THOMAS,1986) and birds (SERLE,1964) are found above 500m ASL. Further to the south on the Angola Escarpment, which rises above the sea to the level of the Plateau above 1000m, a cloud forest is found from 200 or 300m ASL with the implication that montane conditions already appear at this low elevation (EXELL et MENDONCA,1937; AIRY-SHAW,1947; WHITE et BERGER,1978). Other examples exist in East Africa near the Indian Ocean on the Usambaras Mountains (MOREAU,1935, 1938, 1966). All these occurrences show that this is a non-fortuitous ecological phenomenon which allows the extension of the climatic conditions normally found above 1000 to 1500m to lower elevations. The data presented above for the Serrania de Macuira in Colombia are an example of magnitude of temperature reduction in such environment.

Most authors who have considered this phenomenon have attributed it to persistency of cloud cover and fog which are particularly frequent on slopes facing the sea (AIRY-SHAW,1947; MOREAU,1966; SERLE,1964; HOWARD,1970; GRUBB, 1971; etc). The Angolan Escarpment is a particularly important model because it shows how the abundance of cloud cover depends directly on the low clouds coming from the sea where the cold Benguela current flows. HOFELICH (1972) has shown how this current produces a thick mantle of stratiform clouds which influence greatly the climate of the neighboring continent by reducing the rainfall and lowering the temperature there.

#### 4.3. The present day climatic role of upwelling and stratiform clouds

Recent research in the tropical Atlantic sector have shown that the interannual variability of the climate is related to enhancement or reduction of the annual cycle (HASTENRATH,1984; NICHOLSON and ENTEKHABI,1987). For example, HIRST and HASTENRATH (1983a, b), studying the variation of rainfall over the Zaïre river catchment, have found positive correlations between the evolution of the two principal rainy seasons and sea surface temperature (SST) off Angola. The periods with warmer (colder) SST are correlated with above (below) normal rainfalls. SST modulate rainfall by controlling moisture and stability in the lower atmosphere which are also related to cloudiness. But another positive correlation exist between upper air conditions and rainfall over the Zaïre catchment (HIRST et HASTENRATH, 1983a). Probably large scale atmospheric conditions influence both parameters (NICHOLSON et ENTEKHABI,1987). In this way, SST variations and upwelling of cold waters (Fig.6) are indeed directly and remotely governed by the intensity of the winds which are related to the activity of the South Atlantic High (MERLE,1980; HASTENRATH,1984; SERVAIN et al.,1985; NICHOLSON et ENTEKHABI,1987). This relation could account for the coherence of the interannual SST variations and particularly that of the upwelling throughout the Guinea Gulf, with particular years or periods having warmer (colder) sea surface waters (MERLE,1980) (Fig.7). Such synchronicity on interannual scale amplifies

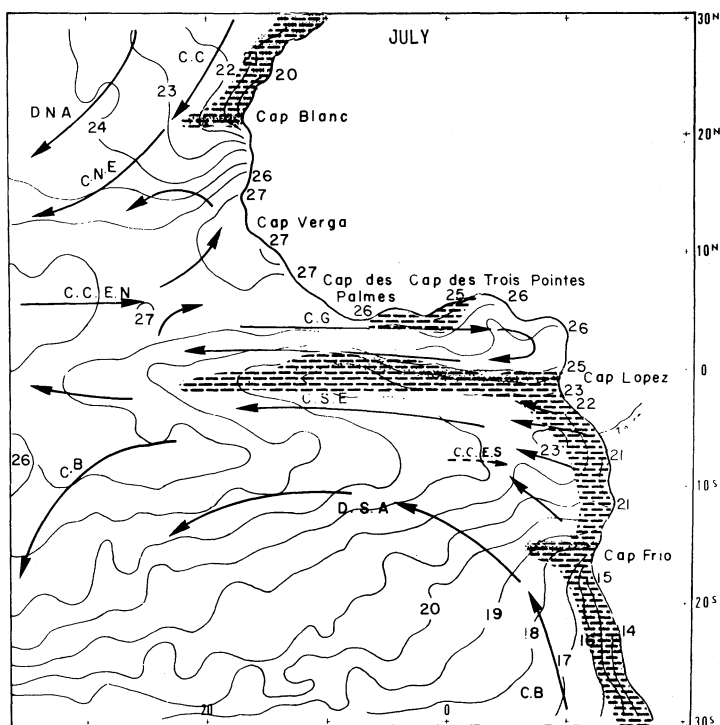


**Figure 6** - Temperature distribution of surface water, surface water circulation and upwelling in the tropical Atlantic Ocean for July. The currents (from north to south): CC, Canary current; DNA, North Atlantic drift; CNE, North equatorial current; CCEN, North equatorial counter current; CG, Current of Guinea; CSE, South equatorial current (equatorial upwelling); CCES, South equatorial counter current; DSA, South Atlantic drift; CB, Benguela current (from WAUTHY, 1983, fig. 20A). The upwelling areas are shaded.

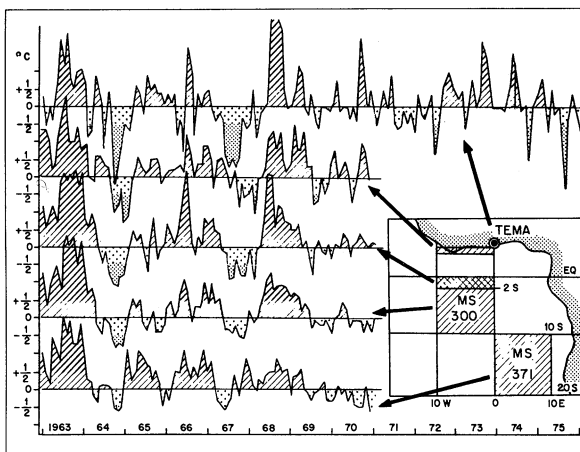


**Figure 7** - Interannual sea surface temperatures (SST) anomalies for some successive years of the recent past in the Guinea Gulf (Figure adapted from MERLE, 1980).

Temperature anomalies

- Oblique shading : Positive anomalies ("warm waters")
- Large dots : Negative anomalies from 0 to 0.5°C (upwelling, "cold waters").
- Small dots : Large negative anomalies of more than 0.5°C (strong upwelling, "cold waters").

The recorded anomalies concern, from north to south :

- Tema, a coastal locality, south of Ghana, and four marine areas (homogenized NANSEN data, NOAA, Asheville, USA),
- latitudinal strip of 10° longitude (0-10°W) between 4° and 5°N along the northern shore of the Guinea Gulf,
- north of Marsden square 300 (MS 300), an equatorial band 2° wide (equator - 2°S) between 0° and 10°W. This band corresponds to the equatorial upwelling area,
- the entire Marsden square 300 (MS 300) (0-10°W; 0-10°S),
- the entire Marsden square 371 (MS 371) (0-10°E; 10°S-20°S).

MERLE(1980) note that the choice of these areas has been mainly determined by the density and the quality of the data. The coherence of anomalies throughout the Guinea Gulf is the principal feature of this figure.

the impact of SST variations on the climate of the adjacent continent.

An example of this relation between SST and climate can be found during southern winter in the appearance of the "little dry season" (generally 2 months) in the rain forest north of the Guinea Gulf (DROCHON, 1976; BAKUN, 1978; HISARD, 1980) (Fig. 8, 9). This dry season, which is also the coldest period of the year (Fig. 9), depends directly on the presence in the lower troposphere of non-precipitating stratiform clouds, generated by the upwelling of cold waters at this time of the year (DROCHON, 1976). On the adjacent continent, the subsidence maintained aloft by the anticyclonic conditions spreading northward during southern winter explains the persistence of the stratiform clouds above the rain forest region (Fig. 8). East of the Guinea Gulf, closer to the equator, the impact of the upwelling is larger because the same chain of oceanic and atmospheric anomalies prevails during four months. This four month dry season in the regions of Gabon and Congo is characterized by a quasi-permanent and non-precipitating stratiform cloud cover which extends at least 800 to 1000 km inland and reduces temperature and evaporation and, as a consequence, maintains a moist atmosphere (SAINT-VIL, 1977). Without this atmospheric humidity a four month dry season would have resulted in a replacement of the forest by savanna.

The relation between this dry season of southern origin and the lowering of SST is very clear and is the most obvious phenomenon in the chain of atmospheric and oceanic anomalies. This conclusion is also supported by the observation that in some particular recent years (for example 1968 or 1984) warm waters persisted (Fig. 7) because the upwelling were weak or absent. This phenomenon is similar to the "El Nino" of the eastern Pacific Ocean (HISARD, 1980; MERLE, 1980). During the "warm" years this season was not dry whatever, but instead it was very wet with heavy rainfalls (HISARD, 1980; GUILLOT, 1985).

#### 4.4. Major role of upwelling in the climatic changes of the rain forest region

The various present-day examples mentioned above (§ 4.1 and 4.2) of the climatic action, either drying or (and) cooling of stratiform cloud covers, show that the generation of upwelling have a basic role in the climate system (cf. FLOHN, 1982, 1983). Some authors have already shown that the upwelling of cold waters have influenced the palaeoclimates of Africa (VAN ZINDEREN BAKKER, 1982) or other regions (FLOHN, 1986).

##### 4.4.1. The last phase of maximum aridity, about 18,000 yr BP

In the tropical Atlantic Ocean and particularly in the Guinea Gulf, the reconstruction of SST by the assemblages of planktonic foraminifera and radiolaria shows that at about 18,000 yr BP the equatorial cold waters upwelling maintained a nearly constant position, and were 4° - 8°C lower than those of the present southern winter (Fig. 10) (PRELL et al., 1976; MORLEY et HAYS, 1979; MIX et al., 1986). Further, PRELL et al. (1976) have shown that during the southern summer (February), which

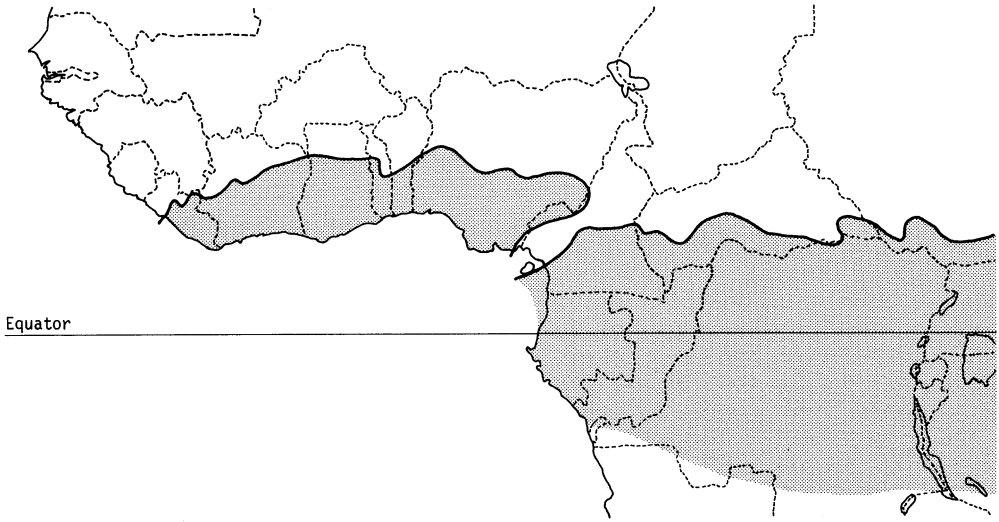


**Figure 8** - Geographical distribution of southern winter dry season in equatorial Africa (adapted from LEROUX,1983). The length of this dry season increases from about 2 months in the north (= "the little dry season") to more than 4 months a year southwards. Note in West Cameroon the absence of this dry season, replaced by a pluvial paroxysm.

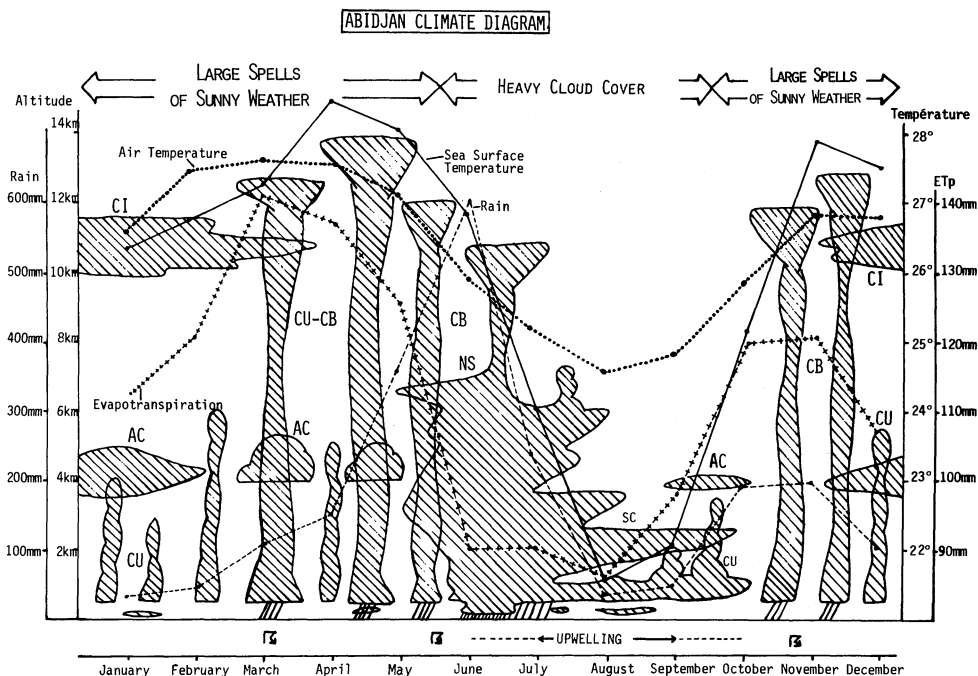


**Figure 9** - Diagram of seasonal climatic change in Abidjan (Ivory Coast), showing the succession of the main types of clouds (adapted from DROCHON 1976) and the principal elements of climate : rain, air temperature, evapotranspiration and sea surface temperature (data from ORSTOM and ASECNA). The Abidjan station is representative of the western sector of the rain forest area.

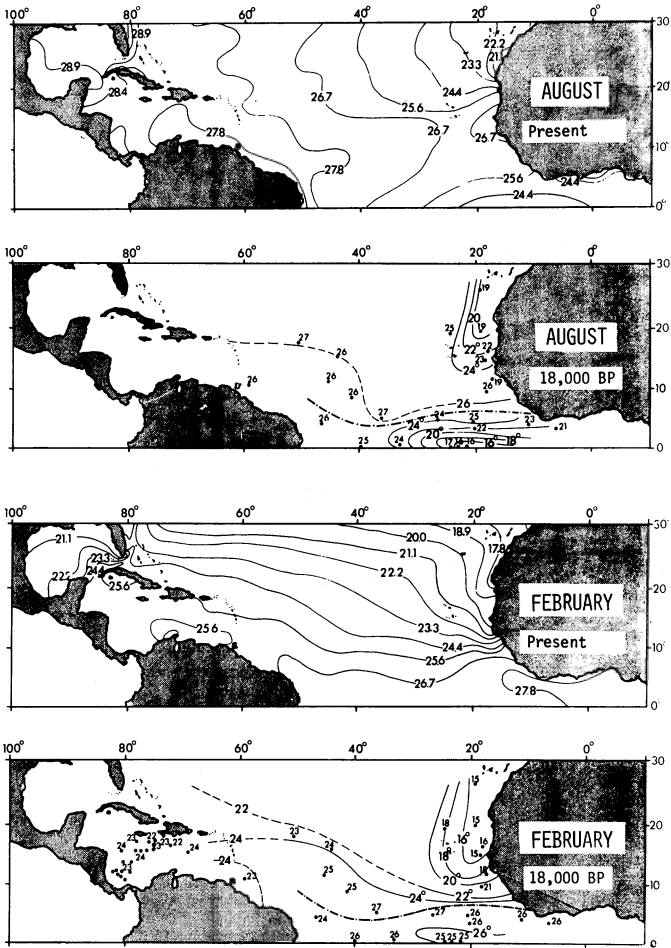


Figure 10 - Sea surface temperatures estimates (August and February) according to transfer functions of foraminiferal assemblages in the north tropical Atlantic Ocean during the last glacial maximum, ca. 18,000 yr BP. Present-day values are provided for comparison (from PRELL et al., 1976, fig.11 and 12, in Geol. Soc. America Memoir, 145).



is the season of warmest water, the surface temperatures were 3 degrees lower than today. This suggests that the upwelling of cold waters would have been a nearly year-round feature. From what we know from the present-day atmospheric phenomena related to upwelling, these data mean also a very powerful anticyclonic high pressure above the Southern Atlantic associated with very strong trade winds. Indeed, research in this field has shown an important strengthening of trade winds around 18,000 yr BP (NEWELL et al., 1981). In conclusion the present-day interannual synchronism throughout the upwelling areas in the Guinea Gulf (equatorial and coastal) (Fig.7) means that in the past the SST variations have had a large climatic impact on the equatorial regions of Africa, mainly those covered today with rain forest. These phenomena and the action of stratiform cloud cover inland could explain (1) the aridification of the climate and the disappearance of large areas of rain forest and (2) the cooling effect of these quasi-permanent cloud covers and the accompanying extension of montane biotopes to lower elevations.

#### 4.4.2. The abrupt change near 9000 years BP and the reappearance of the lowland rain forest

In West Africa, pollen evidence and other data from the Bosumtwi lake (§ 2.1) show that the near absence of forest and the extended spreading of montane vegetation to low elevations lasted until about 9000 yr BP. This coincided with important warming at higher latitudes in both hemispheres which began about 15,000 yr BP (LORIUS et al., 1979; BARD et al., 1987; SARNTHEIM et al., 1981). Pollen data (ROCHE, 1979; CARATINI et GIRESE, 1979; M'BENZA-MUAKA et ROCHE, 1980) and geological data (DE PLOEY, 1969; GIRESE et LANFRANCHI, 1984; PEYROT et LANFRANCHI, 1984; KADOMURA et al., 1986) from the Zaire river catchment, the western Congo and southern Cameroon, show a comparable history of lowland rain forest reappearance. The foraminiferal data of PRELL et al. (1976) suggest that in the belt of equatorial upwelling, SST values at 9000 or 10,000 yr BP became close to those of the present. This change coincided with the rain forest reappearance and climate warming (disappearance of the montane element).

The increase in temperature from ca. 15,000 to 9000 yr BP affected mainly middle and high latitudes but in tropical regions and particularly in the African rain forest, the change was small. As explained above (§ 4.3), this phenomenon is probably related to the persistence of cold waters upwelling throughout the Guinea Gulf. The SST outside the upwelling areas increased (MIX et al., 1986), which provided more water vapor for the monsoon and resulted in more cloud covers inland and probably an increase in rainfall. At the time of the rain forest reappearance, the level of Bosumtwi lake was already very high above the present-day level (Fig.2,B). Since lower temperatures prevailed at that time (presence of montane vegetation until ca. 9000 yr BP), we could infer that the high lake level was partly caused by low evaporation rates, but also by increase in precipitation. These deductions indicate that the reappearance of the rain forest near 9000 yr BP was not solely dependent on rainfall and

humidity, which were very sufficient several millenia before this date, but also on temperature and chiefly amount of sunshine. For this reason, we believe that the reappearance of the rain forest was mainly governed by the variations of cloud covers and cloud types.

One could estimate that between 15,000 and 9000 yr BP the present-day July-type weather with major rain produced by massive nimbostratus clouds (Fig.9), had progressively dominated each year during several months before July. Because we know that the lowland rain forests require large sunlight intensity during many months (LEIGH,1975; WALTER et BRECKLE,1985; etc), the reappearance of the rain forest could be due to a subtle balance between this July-type weather and the March to May-type weather which is characterized by longer periods of sunshine (Fig.9).

#### 4.4.3. The Holocene period between about 9000 and 4000 years BP

The SST data for the Holocene of PRELL et al.(1976) are not sufficiently precise to detect and date temperature variations, but some other indirect data show that SST anomalies have had an important impact on the climate and the rain forest.

Near the coast of western Congo widespread savannas are presently found; however DECHAMPS et al.(1988) and SCHWARTZ et al.(to be published) have studied several extensive palaeosols with in situ remains of numerous tree stumps which belong to a rain forest flora. Several tree stumps and also some samples of organic matter from the palaeosols were radiocarbon dated. A first series of 10 samples were dated from about 6500 to 3100 yr BP and a second series of 3 samples were dated about 500 to 600 yr BP. Because the present-day savannas of this region are mainly related to a long dry season (MAKANY,1964) which are caused by the cold water upwelling (SAINT-VIL,1977) (§ 4.3), their replacement by rain forest was probably caused by a suppression or reduction of upwelling in this area.

Other data related to the upwelling suppression or reduction in the Gulf of Guinea during parts of Holocene time can be obtained by the study of the Bosumtwi lake sediments. Today, this lake is stratified with anoxic waters below about 10m, with a maximum water depth of about 80m (BEADLE,1974), but almost each year an overturn of deep anoxic waters occurs. Because LIVINGSTONE (private commun.) counted about one lamination for one radiocarbon year in the core collected in the lake (Fig.2), the laminations of the sediment correspond to this yearly phenomenon. The overturn is mainly related to a lowering of air temperature in August and September which is induced by the non-precipitating stratiform cloud covers generated by the upwelling (§ 4.3) (Fig.9). This cooling also affects the water column which at this time becomes more or less homothermal (BEADLE,1974). Because, at the same time, the wind stress from the southwesterlies is at its maximum, the instable waters are overturned (BEADLE,1974; WHYTE,1975). But for the core (Fig.2,A), a large part of the Holocene sediment is un laminated and of sapropel type between about 9000 yr BP, when the rain forest reappeared, and about 3700 yr BP, when the laminations reappear suddenly (TALBOT et al.,1984). So,

this unlaminated interval of the core and the high lake level of this period (at maximum 105m above present-day lake level) can be related to an absence or reduction of the "little dry season". Either an annual prolongation through August and September of the June-type weather (Fig.9) which is characterized by heavy precipitation from nimbostratus clouds, or the annual early start of the October-November-type weather (Fig.9) which numerous towering cumuliform clouds are typical, probably occurred. For sedimentological reasons (in West Africa fluvial sediments show a transition from clay type deposits to more sandy type near 7000 yr BP, cf. MALEY, 1981, p.519 ; MALEY, 1982, 1983) we estimate that the June-type weather dominated until about 7000 yr BP and after, the October-November-type weather (Fig.9) dominated until about 3700 yr BP. The yearly rainfall was certainly higher than today (ca. 1520 mm) (§ 4.4.4), but, because the pollen data for this period exhibit no particular change, the composition of the forest must have remained of a semi-deciduous type (MALEY et LIVINGSTONE, 1983, and unpublished data: spectra have only very few pollen grains of Caesalpiniaceae - characteristic of the evergreen forest type, see § 2.2 and BRENAC, 1988). Consequently one concludes that during this period the northern winter dry season had the same length as today, i.e. three months (December to February) (Fig.9). Present conditions in West Cameroon may be representative of those for the period 9000 yr BP to about 3700 yr BP in the Bosumtwi region and probably also for other parts of the African rain forest. In West Cameroon indeed, the three months from July to September represent the rainiest season of the year (Fig.8), and are described as a "pluvial paroxysm" by SUCHEL (1972).

#### 4.4.4. The regression of the lake Bosumtwi during late Holocene time

After 9000 yr BP, the present-day interruption of the rain forest area which is called the "Dahomey Gap" was probably absent, because of higher humidity (§ 4.4.3), and for biogeographical reasons (see the discussion in MALEY, 1987). The Dahomey Gap probably appeared between 4000 and 3000 years ago, when lake Bosumtwi abruptly regressed.

The abrupt regression of the lake, more than 120m, is dated at about 3700 yr BP which is the date of the sudden reappearance of the laminations (TALBOT et al., 1984), and is to be associated with the reappearance of the "little dry season" inland and to the upwelling of cold water in the Guinea Gulf. However the pollen data from this period show the persistence of the rain forest (Fig.2 and 3). In order to explain this, the present-day water budget of the lake which is slightly positive (average rainfall on the crater catchment is 1520mm /year with evaporation at only 1450mm/year - TALBOT et DELIBRIAS, 1977) should be considered. There is an average excess of 70mm which explains the present-day transgressive phase of the lake which has apparently been underway for several centuries (TALBOT et al., 1984, fig.6), because a lacustrine minimum probably occurred in 15th century AD (MALEY, in shed.). This regression phase, like the one dated between 4000 and 3000 yr BP, was caused by a deterioration of

the lacustrine water budget that linked a rainfall decrease to a probable evaporation increase. If this rainfall decrease was distributed over the same number of months, then, provided the total precipitation does not reach values below 1200mm/ year, rain forest could have remained, based on observations that today some northern parts of rain forest in Ghana and Ivory Coast receive yearly rainfall in this range (Fig.1). Thus, provided minima are not below 1200mm/year, the essential factor to maintain the rain forest in late Holocene time is good distribution of rainfall throughout the year, rather than the annual total.

## 5. CONCLUSIONS

After having briefly introduced the problem of rain forest refugia during the last glacial maximum and shown the pollen data which clearly demonstrate that the African rain forest area has been fragmented indeed and survived the glacial period in some refugia, one had attempted to reconstruct the weather types which may account for the recorded vegetational and lacustrine variations. Particular attention has been paid to the climatic reconstruction (1) during the phase of fragmentation of the rain forest belt and the extension of montane biotopes to lower elevation, (2) during the forest recolonization and its extension in early and middle Holocene time, and (3) the return to its present-day limits during the last four millenia and particularly the opening of the "Dahomey Gap". The latter phenomenon is probably related to a deterioration of the water budget, which is also responsible for the regressions of Lake Bosumtwi.

The question of why forest refugia have been formed and how were climatic conditions there, remains without precise answer. One of the major proposed refugia is located in West Cameroon (Fig.1) (MALEY,1987), where today climatic conditions are atypical because this area experiences no "little dry season" during southern winter (Fig.8). For this reason the yearly rainfall is very high. This particularity could account for the survival of the tropical rain forest during dry periods. However, we see that there have been other refugia in regions which experience today a dry season during southern winter such as in Gabon and southern Cameroon. This suggests that other factors are necessary to explain the geographical position of refugia.

The study of climatic conditions of West Cameroon could provide the necessary informations to allow the development of a hypothese. The exact reasons of the present-day July to September pluvial paroxysm of West Cameroon are not well understood (SUCHEL,1972) and could be the result of several causes. It could be related first to the geographic position at the far end of the Guinea Gulf where today the SST seem to be unaffected by the upwelling phenomenon or to the presence of high mountains with possible orographic effects and strong dynamic lifting associated with upper air circulation.

As we have seen above (§ 2 and 3), during colder periods, lowland rain forest and montane vegetation were probably close

together such as in West Cameroon. Presently, as hypothesis, one suggests the transformation of non-precipitating stratiform clouds to precipitating nimbo-stratus or cumuliform clouds through orographic or dynamic lifting of air masses (MALEY,1982; see examples of physical processes in LUDLAM,1966; etc). In this way, locally, prevailing higher temperatures and rainfall necessary for lowland rain forest to survive could have been achieved.

More detailed climatological studies in West Cameroon and in restricted areas where today montane biotopes extend to low elevations, may bring new data leading to a better understanding of the African rain forest palaeoclimatology.

=====

#### ACKNOWLEDGEMENTS

This paper is a contribution to a research program on the Palaeoenvironments of the African rain forest and particularly of West Cameroon. The program results from collaboration between several Cameroonian scientific Institutions (MESRES, ISH, CGN, CRH, IRGM, Yaoundé University), ORSTOM, France (J.MALEY, Research Unit A3 and GEOCIT Program) and the Zoology Department of Duke University, USA (D.A.LIVINGSTONE). For helpful discussions, thanks are due to J.L. AMIET (Zoology Dept., Yaoundé Univ.), R.LETOUZEY (Museum Hist. Nat.,Paris), D.A. LIVINGSTONE (Duke Univ.,Durham, USA), S.MORIN (Geography Dept.,Yaoundé Univ.) and D.W.THOMAS (Missouri Botanical Garden and IRA, Kumba SWP). The author is also grateful to W.L.PRELL (Lamont Geological Observ.,New-York) for permission to reproduce material published in Geological Society of America Memoir (1976, vol.145, fig.11 and 12). Thanks are done also to two anonymous reviewers for constructive remarks and to J. SCHUHMACHER (Mineralogisches Inst.,Kiel Univ.) who greatly improve the English. The cores from Lake Bosumtwi, Ghana and Lake Barombi Mbo, Cameroon, were collected by crews led by D.A.LIVINGSTONE. The funding of coring operations in Cameroon was provided by ORSTOM, CNRS, NSF and Duke University, and in Ghana by NSF.

#### KEYWORDS

Africa - Lake Bosumtwi, Ghana - Lake Barombi Mbo, West Cameroon. - Lowland Rain Forest - Montane vegetation - Pollen Analyses - Forest Refugia - Biogeography - Speciation - Dahomey Gap - Upper Quaternary - Climatic Change - Palaeoclimatology - Tropical Atlantic - Sea Surface Temperatures - Upwelling - Cloud - Stratiform clouds -

**REFERENCES**

- ACHOUDONG, G. 1985, Etude écologique et floristique de la végétation des collines de Yaoundé au-dessus de 1000m. Thèse Univ.Yaoundé, Ecologie Végét., 301 pp.
- AIRY-SHAW, H.K. 1947, The vegetation of Angola. J.of Ecology, 35,23-48.
- AUBREVILLE, A. 1949, Contribution à la paléohistoire des forêts de l'Afrique tropicale. Soc.Edit.Géogr.Marit. et Colon., 99 pp.
- AUBREVILLE, A. 1962, Savanisation tropicale et glaciations quaternaires. Adansonia, 2,16-84.
- BAKUN, A. 1978, Guinea current upwelling. Nature, 271,147-150.
- BARD, E., ARNOLD, M., DUPRAT, J., MOYES, J. et DUPLESSY, J.C. 1987, Reconstruction of the last deglaciation : deconvolved records of  $\delta$  180 profiles, micropaleontological variations and accelerator mass spectrometric 14C dating. Climate Dynamics, 1, 101-112.
- BAYNTON, H.W. 1968, The ecology of an elfin forest in Puerto Rico. 2. The microclimate of Pico del Oeste. J.of Arnold Arbor., 49, 419-430.
- BEADLE, L.C. 1974, The inland waters of Africa. An introduction to tropical limnology. Longman, London, 365 pp.
- BERNARDI, G. 1979, Contribution à la biogéographie des montagnes africaines. I. Généralités. C.R.Soc.Biogéogr. 479,6-10.
- BOOTH, A.H. 1958, The Niger, the Volta and the Dahomey Gap as geographic barriers. Evolution, 12,48-62.
- BRENAC, P. 1988, Evolution de la végétation et du climat dans l'Ouest Cameroun entre 25.000 et 11.000 ans BP. Actes Xème Symposium Ass.Palynologues Langue Française, Trav.Sect.Sci. & Tech.Inst. Français Pondichéry, 25,91-103
- CARATINI, C., et GIRESSE, P. 1979, Contribution palynologique à la connaissance des environnements continentaux et marins du Congo à la fin du Quaternaire. C.R.Acad.Sc., série D, 288,379-382.
- CARCASSON, R.H. 1964, A preliminary survey of the zoogeography of African butterflies. East Afr.Wild Life J., 2,122-157.
- CLAYTON, W.D. 1976, The chorology of African mountain grasses. Kew Bull., 31, 273-288.
- COETZEE, J.A. 1964, Evidence for a considerable depression of the vegetation belts during the Upper Pleistocene on the East African mountains. Nature, 204,564-566.
- DECHAMPS, R., GUILLET, B. et SCHWARTZ, D. 1988, Découverte d'une flore forestière mi-Holocène (5800-3100 BP) conservée in situ sur le littoral ponténégrin (R.P. du Congo). C.R.Acad.Sc., série II, 306, 615-618.
- DE PLOEY, J. 1969, Report on the Quaternary of western Congo. Palaeoecology of Africa, 4,65-68.
- DROCHON, A. 1976, Données climatologiques au sol et en altitude pour la station d'Abidjan. Note ASECNA (Agence Sécurité Naviga. Aérienne), 55, 14 pp.
- ELENGA, H. 1987, Les Plateaux Batéké (Congo). Paléoenvironnements Quaternaires d'après l'étude du sondage du bois de Bilanko.

- Diplôme d'Etudes Approfondies, Université d'Aix-Marseille II, 41 pp.
- ENDLER, J.A. 1982, Pleistocene forest refuges: fact or fancy. in G.T.Prance (ed) Biological diversification in the tropics, Columbia Univ.Press, New-York, pp.641-657.
- EXELL, A.W et MENDONCA, F.A. 1937, Conspectus Florae Angolensis. I, Ranunculaceae - Malvaceae. Inst. Bota. Coimbra. 176 pp.
- FEDOROV, A.A. 1966, The structure of the tropical rain forest and speciation in the humid tropics. J.Ecology, 54, 1-11.
- FLENLEY, J.R. 1979, The equatorial rain forest : a geological history. Butterworths, London, 162 pp.
- FLENLEY, J.R. 1984, Late Quaternary changes of vegetation and climate in the Malesian Mountains. Erdwissensch. Forsch., Wiesbaden, 18, 261-267.
- FLOHN, H. 1982, Oceanic upwelling as a key for abrupt climatic change. J.Meteo. of Japan, 60, 268-273.
- FLOHN, H. 1986, Singular events and catastrophes now and in climatic history. Naturwissenschaften, 73, 136-149.
- GIRESE, P. et LANFRANCHI, R. 1984, Les climats et les océans de la Région Congolaise pendant l'Holocène. Bilans selon les échelles et les méthodes de l'observation. Palaeoecology of Africa, 16, 77-88.
- GRUBB, P.J. 1971, Interpretation of the "Massenerhebung" effect on tropical mountains. Nature, 229, 44-45.
- GRUBB, P.J. 1974, Factors controlling the distribution of forest-types on tropical mountains: new facts and a new perspective. in J.R.Flenley (ed), Altitudinal zonation in Malesia, Trans.3rd Aberdeen-Hull Symp. on Malesian Ecology, pp.13-45.
- GRUBB, P.J. 1977, Control of forest growth and distribution on wet tropical mountains, with special reference to mineral nutrition. Ann.Rev.Ecol.Syst., 8, 83-107.
- GRUBB, P.J. et WHITMORE, T.C. 1966, A comparison of montane and lowland rain forest in Ecuador. II. The climate and its effects on the distribution and physiognomy of the forests. J.Ecology, 54, 303-333.
- GUILLOT, B. 1985, Température de surface de la mer et pluviosité autour du Golfe de Guinée. Veille Climatique Satellitaire, Lannion, 6, 13-14.
- HAFFER, J. 1982, General aspects of the refuge theory. in G.T.Prance (ed), Biological diversification in the tropics, Columbia Univ.Press, New-York, pp.6-24.
- HAMILTON, A.C. 1973, The history of the vegetation. in E.M. Lind et M.E.S. Morrison (eds), The vegetation of East Africa, Longman, London, pp.188-209.
- HAMILTON, A.C. 1982, Environmental history of East Africa. A study of the Quaternary. Academic Press, London, 311 pp.
- HALL, J.B. 1973, Vegetational zones on the southern slopes of Mount Cameroon. Vegetatio, 27, 49-69.
- HALL, J.B. et SWAINE, M.D. 1981, Distribution and Ecology of vascular plants in a tropical rain forest : Forest vegetation in Ghana.

- W.Junk, The Hague, 383 pp.
- HASTENRATH, S. 1984, Interannual variability and annual cycle : mechanisms of circulation and climate in the tropical Atlantic sector. Monthly Weather Review, 112, 1097-1107.
- HEPPER, N. 1963, Flora of West tropical Africa. in J.Hutchinson et J.M. Dalziel (ed), Crown Agents for Oversea Govern.Publ., London, vol.2.
- HIRST, A.C. et HASTENRATH, S. 1983(a), Diagnostics of hydrometeorological anomalies in the Zaïre (Congo) basin. Quat.J.R.Met. Soc., 109, 881-892.
- HIRST, A.C. et HASTENRATH, S. 1983(b), Atmosphere-Ocean mechanisms of climate anomalies in the Angola-Tropical Atlantic sector. J.Phys.Oceanogr., 13, 1146-1157.
- HISARD, P. 1980, Observationn de réponse de type 'El Nino' dans l'Atlantique tropical oriental, Golfe de Guinée. Oceanologica Acta, 3, 69-78.
- HOFLICH, O. 1972, Die meteorologischen Wirkungen kalter Auftriebswassergebiete. Geoforum, 11, 35-46.
- HOWARD, R.A. 1970, The "Alpine" plants of the Antilles. Biotropica, 2, 24-28.
- KADOMURA, H., HORI, N., KUETE, M., TAMURA, T., OMI, G., HARUKI, M. et CHUJO, H. 1986, Late Quaternary environmental changes in southern Cameroon: a synthesis. in H.Kadomura (ed), Geomorphology and Environmental changes in tropical Africa. Case studies in Cameroon and Kenya. Hokkaido Univ., pp.145-158.
- LEIGH, E.G. 1975, Structure and climate in tropical rain forest. Annual Rev.Ecology & Systematics, 6, 67-86.
- LEROUX, M. 1983, Le climat de l'Afrique tropicale. Champion, Paris, 633 pp. & Atlas, 250 maps.
- LETOUZEY, R. 1968, Etude phytogéographique du Cameroun. Encyclopédie Biologique, Paris, 49, 508 pp.
- LETOUZEY, R. 1978, Notes phytogéographiques sur les Palmiers du Cameroun. Adansonia, 18, 293-325.
- LETOUZEY, R. 1985, Notice de la carte phytogéographique du Cameroun au 1/500.000 Inst.Carte Intern.Végétation, Toulouse & Inst.Rech. Agron., Yaoundé.
- LIVINGSTONE, D.A. et CLAYTON, W.D. 1980, An altitudinal cline in tropical African grass floras and its paleoecological significance. Quat.Res. 13, 392-402.
- LORIUS, C., MERLIVAT, L., JOUZEL, J. et POURCHET, M. 1979, A 30,000 yr isotope climatic record from Antarctic ice. Nature, 280, 644-648.
- LUDLAM, F.H. 1966, Cumulus and cumulonimbus convection. Tellus, 18, 687-698.
- MAKANY, L. 1964, La côte Atlantique du Congo : cadres géographiques et géologiques, leur influence sur la répartition de la végétation et sur les possibilités agricoles du territoire. Actes Symposium Pékin, pp.891-907.
- MALEY, J. 1981, Etudes palynologiques dans le bassin du Tchad et paléoclimatologie de l'Afrique nord-tropicale de 30.000 ans à l'époque actuelle. Trav. & Documents ORSTOM, Paris, 129, 586 pp.



- MALEY, J. 1982, Dust, clouds, rain types and climatic variations in tropical North Africa. Quat. Res., 18, 1-16.
- MALEY, J. 1983, Histoire de la végétation et du climat de l'Afrique nord-tropicale au Quaternaire récent. Bothalia, 14(3-4), 377-389.
- MALEY, J. 1984, Influence des nuages sur les paléoenvironnements : quelques exemples pris dans le Quaternaire africain. 10ème Réunion Ann.Sc.Terre, Bordeaux, p.373 (Abstract).
- MALEY, J. 1987, Fragmentation de la forêt dense humide africaine et extension des biotopes montagnards au Quaternaire récent : nouvelles données polliniques et chronologiques. Implications paléoclimatiques et biogéographiques. Palaeoecology of Africa, 18, 307-334.
- MALEY, J. 1988, L'importance de la tradition orale et des données historiques pour la reconstitution paléoclimatique du dernier millénaire sur l'Afrique nord-tropicale. (manuscrit), 6 pp.
- MALEY, J. et BRENAC, P. 1987, Analyses polliniques préliminaires du Quaternaire récent de l'Ouest Cameroun : mise en évidence de refuges forestiers et discussion des problèmes paléoclimatiques Mém.Trav.Ecole Pratiq.Htes.Inst.Montpellier, 17, pp.129-142.
- MALEY, J., CABALLE, G. et SITA, P. 1988(a), Etude d'un peuplement résiduel à basse altitude de *Podocarpus latifolius* sur le flanc Congolais du Massif du Chaillu. Implications paléoclimatiques et biogéographiques. Etude de la pluie pollinique actuelle. In D.Schwartz et R.Lanfranchi (ed), Paysages Quaternaires de l'Afrique centrale, Trav.& Documents ORSTOM, 14 pp. (to be published).
- MALEY, J., GIRESSE, P., THOUVENY, N., BRENAC, P., KELTS, K., LIVINGSTONE, D.A., KLING, G., STAGER, C., HAAG, M., FOURNIER, M., BANDET, Y., WILLIAMSON, D. et ZOGNING, A. 1988 (b), Lithostratigraphy, Volcanism, Paleomagnetism and Palynology of Quaternary lacustrine deposits from Barombi Mbo (West Cameroon) : preliminary results. J.Volcano. and Geoth.Res., 18 pp. (to be published).
- MALEY, J. et LIVINGSTONE, D.A. 1983, Extension d'un élément montagnard dans le sud du Ghana (Afrique de l'Ouest) au Pléistocène supérieur et à l'Holocène inférieur : premières données polliniques. C.R.Acad.Sc., série 2, 296, 1287-1292.
- MAYR, E. et O'HARA, R.J. 1986, The biogeographic evidence supporting the Pleistocene forest refuge hypothesis. Evolution, 40, 55-67.
- M'BENZA-MUAKA et ROCHE, E. 1980, Exemple d'évolution paléoclimatique au Pléistocène terminal et à l'Holocène au Shaba (Zaire). Symposium "Palynologie et Climats", Mém.Museum Nat.Hist.Nat., série Botanique, 27, 137-148.
- MERLE, J. 1980, Variabilité thermique annuelle et interannuelle de l'Océan Atlantique équatorial est. L'hypothèse d'un "El Nino" Atlantique. Oceanologica Acta, 3, 209-220.
- MIX, A.C., RUDDIMAN, W.F. et MCINTYRE, A. 1986, Late Quaternary paleoceanography of the tropical Atlantic. 2: The seasonal cycle of sea surface temperatures, 0-20,000 years B.P. Paleoceanography, 1, 339-353.
- MOREAU, R.E. 1935, A synecological study of Usambara, Tanganyika

- Territory, with particular reference to birds. J.Ecology, 23, 1-43.
- MOREAU, R.E. 1938, Climatic classification from the standpoint of East African biology. J.Ecology, 26, 467-496.
- MOREAU, R.E. 1963, The distribution of tropical African birds as an indicator of past climatic changes. in F.C.Howell et F.Bourlière (ed), African ecology and Human evolution, Aldine Press, Chicago, pp.28-42.
- MOREAU, R.E. 1966, The bird faunas of Africa and its islands. Academic Press, New-York, 424 pp.
- MORLEY, J.J. et HAYS, J.D. 1979, Comparison of glacial and interglacial oceanographic conditions in the south Atlantic from variations in calcium carbonate and Radiolarian distributions. Quat.Res., 12, 396-408.
- MORLEY, R.J. et FLENLEY, J.R. 1987, Late Cainozoic vegetational and environmental changes in the Malay archipelago. in T.C.Whitmore (ed), Biogeographical Evolution of the Malay Archipelago. Clarendon Press, Oxford, pp.50-59.
- MORTON, J.K. 1968, Sierra Leone. in I.& O.Hedberg (ed), Conservation of vegetation in Africa south of the Sahara. Acta Phytogeographica Suec. 54, 72-74.
- NEWELL, R.E., GOULD-STEWART, S. et CHUNG, J.C. 1981, A possible interpretation of paleoclimatic reconstructions for 18,000 BP for the region 60°N to 60°S, 60°W to 100°E. Palaeoecology of Africa, 13, 1-19.
- NICHOLSON, S.E. et ENTEKHABI, D. 1987, Rainfall variability in equatorial and southern Africa: relationships with sea surface temperatures along the southwestern coast of Africa. J.Climate & Appl.Meteo., 26, 561-578.
- PALMER, P.G. 1982, A stratigraphic analysis of fossil grass cuticles from lake Bosumtwi, Ghana, West Africa and its paleoecological significance. XInd Intern.Quat.Congress, Moscow, Abstracts, I, p.244.
- PEYROT, B. et LANFRANCHI, R. 1984, Les oscillations morphoclimatiques récentes dans la vallée du Niari. Palaeoecology of Africa, 16, 265-281.
- PRANCE, G.T. (ed), 1982, Biological diversification in the Tropics. Columbia Univ. Press, New-York, 714 pp.
- PRELL, W.L., GARDNER, J.V., BE, A.W.H. et HAYS, J.D. 1976, Equatorial Atlantic and Caribbean foraminiferal assemblages, temperatures and circulation : interglacial and glacial comparisons. Geological Soc.America Memoir, 145, 247-266.
- RICHARDS, P.W. 1963, Ecological notes on West African vegetation. II.Lowland forest of the southern Bakundu Forest Reserve. J.Ecology, 51, 123-149.
- RICHARDS, P.W. 1969, Speciation in the tropical rain forest and the concept of the niche. Biol.J.Linn.Soc., 1, 149-153.
- ROCHE, E. 1979, Végétation ancienne et actuelle de l'Afrique centrale. African Economic History, 7, 30-37.
- SAINT-VIL, J. 1977, Les climats du Gabon. Ann.Univ.Nat.Gabon, 1, 101-125.

- SARNTHEIN, M., ERLLENKEUSER, H., et ZAHN, R. 1982, Termination I: the response of continental climate in the Subtropics as recorded in deep-sea sediments. Bull. Inst. Géol. Bassin Aquitaine, 31, 393-407.
- SCHNELL, R. 1950, La forêt dense. Introduction à l'étude botanique de la région forestière d'Afrique occidentale. P. Lechevalier (ed), Paris, 330 pp.
- SCHNELL, R. 1977, Introduction à la phytogéographie des pays tropicaux. 4 : La flore et la végétation de l'Afrique tropicale. Gauthier-Villars (ed), Paris, 378 pp.
- SCHWARTZ, D., GUILLET, B. et DECHAMPS, R. 1988, Etude de deux flores forestières mi-Holocène (6000-3000 BP) et subactuelle (500 BP) conservées in situ sur le littoral Pontenegrin (Congo). in D. Schwartz et R. Lanfranchi (ed), Paysages Quaternaires de l'Afrique Centrale, Trav. et Documents ORSTOM, 16 pp. (to be published).
- SERLE, W. 1964, The lower altitudinal limit of the montane forest birds of the Cameroon mountains, West Africa. Bull. British Ornith. Club, 84, 87-91.
- SERVAIN, J., PICAUT, J. et BUSALACCHI, A.J. 1985, Interannual and seasonal variability of the tropical Atlantic Ocean depicted by sixteen years of sea-surface temperature and wind stress. in J.C.J. Nihoul (ed), Coupled Ocean-Atmosphere models. Elsevier, Amsterdam, pp. 211-237.
- SUCHEL, J.B. 1972, La répartition des pluies et les régimes pluviométriques au Cameroun. Trav. & Documents Géogr. Trop., CEGET, Bordeaux, 5, 287 pp.
- SUGDEN, A.M. 1982, The vegetation of the Serrania de Macuira, Guajira, Colombia: a contrast of arid lowlands and an isolated cloud forest. J. Arnold Arb., 63, 1-30.
- TALBOT, M.R. et DELIBRIAS, G. 1977, Holocene variations in the level of Lake Bosumtwi, Ghana. Nature, 268, 722-724.
- TALBOT, M.R. et KELTS, K. 1986, Primary and diagenetic carbonates in the anoxic sediments of Lake Bosumtwi, Ghana. Geology, 14, 912-916.
- TALBOT, M.R., LIVINGSTONE, D.A., PALMER, P.G., MALEY, J., MELACK, J.M., DELIBRIAS, G. et GULLIKSEN, S. 1984, Preliminary results from sediment cores from Lake Bosumtwi, Ghana. Palaeoecology of Africa, 16, 173-192.
- THOMAS, D.W. 1986, Vegetation in the montane forests of Cameroon. in S.N. Stuart (ed), Conservation of Cameroon Montane Forests, Report of Int. Council Bird Preserv., Cambridge, UK, pp. 20-27.
- VAN ZINDEREN BAKKER, E.M. 1982, African palaeoenvironments 18,000 years B.P. Palaeoecology of Africa, 15, 77-99.
- VAN ZINDEREN BAKKER, E.M. et CLARK, J.D. 1962, Pleistocene climates and cultures in north-eastern Angola. Nature, 196, 639-642.
- VAN ZINDEREN BAKKER, E.M. et COETZEE, J.A. 1972, A re-appraisal of late Quaternary climatic evidence from tropical Africa. Palaeoecology of Africa, 7, 151-181.
- WALTER, H. et BRECKLE, S.W. 1985, Ecological systems of the Geobiosphere. 1, Ecological principles in global perspective. Springer-Verlag, Berlin.

- WAUTHY, B. 1983, Introduction à la climatologie du Golfe de Guinée. Océanographie tropicale, ORSTOM, 19, 103-138.
- WEBSTER, P.J. et STRETEN, N.A. 1978, Late Quaternary Ice Age climates of tropical Australasia: interpretations and reconstructions. Quat. Res. 10, 279-309.
- WHITE, F. 1978, The Afromontane region. in M.J.A. Werger (ed) Biogeography and Ecology of southern Africa, W. Junk, The Hague, 2, 463-513.
- WHITE, F. 1981, The history of the Afromontane archipelago and the scientific need for its conservation. Afr. J. Ecology, 19, 33-54.
- WHITE, F. 1983, The vegetation of Africa. UNESCO/AETFAT/UNSO, Maps & Memoir, 356 pp.
- WHITE, F. et WERGER, M.J. 1978, The Guineo-Congolian transition to southern Africa in M.J.A. Werger (ed), Biogeography and Ecology of southern Africa. W. Junk The Hague, 2, 601-620.
- WHITMORE, T.C. 1975, Tropical rain forests of the Far East. Clarendon Press, Oxford.
- WHITMORE, T.C., FLENLEY, J.R. et HARRIS, D.R. 1982, The tropics as the norm in biogeography? Geogr. J. 148, 8-21.
- WHITMORE, T.C. et PRANCE, G.T. 1987, Biogeography and Quaternary History in tropical America. Clarendon Press, Oxford, 214 pp.
- WHYTE, S.A. 1975, Distribution, trophic relationships and breeding habits of the fish populations in a tropical lake basin (Lake Bosumtwi, Ghana). J. Zool., London, 177, 25-56.

# THE REGIONALIZATION OF CLIMATIC CHANGE IN WESTERN NORTH AMERICA

OWEN K. DAVIS

Department of Geosciences  
University of Arizona  
Tucson, AZ 85721  
U.S.A.

**ABSTRACT.** Although displacement of atmospheric circulation patterns is a common and attractive explanation for climatic change, some recent paleoclimatic records from western North America indicate that although relative strengths have changed, the positions of some major circulation features have remained the same during the late Quaternary.

## 1. HOW DOES CLIMATE CHANGE?

### 1.1 *Proxy Records*

Evidence began to accumulate in the middle of the last century that climate of the recent geologic past had been very different from that of today. Geological evidence for Pleistocene glacial advance, collected by Louis Agassiz and his colleagues, was later supplemented by biological evidence for climatic change during the postglacial (Iversen, 1941). In northern Europe, palynological records of vegetation change were accurately dated through varved sediment exposed by isostatic rebound of the Baltic Basin (De Geer, 1912; Iversen, 1941).

A climatic chronology for Western North America was first proposed by Ernst V. Antevs, a student of De Geer's who came to study the varve sequences of Eastern North America in 1920 (Smiley, 1976; for a review of Antevs' varve work see Schove, 1987). After studying the playas and arroyos of western North America, Antevs (1938) proposed a climatic chronology clearly based on the Baltic varve sequence, with dates of 7500 - 4000 ya (years ago) for the period of maximum warmth — well before

Libby's (1955) development of radiocarbon dating. Although Antevs' "Altithermal" was roughly contemporaneous with the Atlantic period of Europe, the Atlantic was a moist interval, whereas the Altithermal was defined as a hot-dry period accompanied by low lake levels.

Antevs' climatological explanation of the Altithermal is important for this discussion because, like the geologists who followed him, Antevs explained the "great drought" in terms of semi-permanent features of atmospheric circulation. He used a seasonal analog to explain late-Quaternary changes in precipitation:

"The precipitation on the Pacific slope and in the Great Basin is now, and was in the past (to a considerable degree) controlled by the Pacific anticyclone. . . . In summer, when this is strong and to the north (Lat. 40°N.), it blocks storms. . . . In winter, when it is weaker and located to the south (Lat. 30°N.), cyclonic storms reach the continent and bring rains. . . . During the glacials, the ice sheets in Canada and in the northern states forced the pressure and precipitation belts south of their modern positions. The Pacific anticyclone did not develop to block summer cyclones. . . . The cold and rainy season was longer." (Antevs, 1955).

## 1.2 *General Atmospheric Circulation*

Probably all of the earth's major circulation features (e.g., the Aleutian and Greenland lows, the east-Pacific and Bermuda highs, and the Inter-Tropical Convergence Zone) have been used in explanations of climatic change. Winstanley (1973) coupled the position of the ITCZ with the general strength of zonal circulation to explain contrasting histories between the Sahel and the Northern Sahara during this century. Westerly (zonal) circulation peaked in the 1920s when monsoonal precipitation was greatest in the Sahel. At the same time, winter precipitation reached a minimum along the south and west coasts of the Mediterranean. Winstanley postulated that during periods of strong zonal circulation the circumpolar vortex contracts, the ITCZ moves poleward, and the northern hemisphere experiences a general warming. Winstanley's (1973) teleconnections have not been substantiated by subsequent research (e.g., Byrne *et al.*, 1982).

Although ambitious and sophisticated, Winstanley's approach resembles earlier studies in that it uses a seasonal analog and calls for displacement of major circulation features by amounts comparable to those of annual changes. This annual-analog approach is inappropriate for

explaining global climatic change for several reasons. The first is the difference in scale of insolation change between annual and glacial/interglacial climatic change. The annual variation in temperate latitudes is many times greater than the difference between full glacial minima and interglacial maxima. At 45°N the difference between December and July insolation is presently 645 Langleys per day. The difference (at 45°N) between glacial minimum 22,200 ya and the Holocene maximum 11,600 ya is only 186 Langleys per day, annually (calculations based on the equations of Berger, 1978). A second difference between annual and glacial/interglacial climatic change is in geographical transformations. Prior to 9000 ya, the huge continental ice sheets probably dominated global climate. Sea-surface temperatures and sea level were lower. These geographical differences far exceed those of the annual cycle, but the insolation differences of the glacial/interglacial cycle are much smaller. Both contrasts make the annual analog inappropriate for explaining long-term climatic change on a global scale.

### 1.3 *Climate Models*

The seasonal analog is satisfying in its simplicity, but it does not embody the appropriate magnitude of variations of climatic forcing functions involved with glacial/interglacial climatic change. During the last decade, geologists have come to rely on computer simulations to simultaneously consider the many atmospheric, oceanic, and terrestrial processes involved in climatic change. In turn, computer modelers have relied on geological evidence of sea-surface temperature, ice volume, and atmospheric aerosols and gases as boundary conditions for their programs. The models produce specific, testable scenarios that go beyond the input data. An exciting example is work the COHMAP group (Kutzbach and Wright, 1985; Kutzbach, 1987), whose community climatic model predicts a splitting of the North American jet stream into northern and southern limbs during the last glaciation (Fig. 1). The bifurcation is an unanticipated result of the model, but the displacement of the southern limb from 45° to 30°N is reminiscent of traditional scenarios in one way. Like the paleoclimatic explanations of Antevs (1955) and Winstanley (1973), it calls for a displacement of the mean position of the jet relative to today.

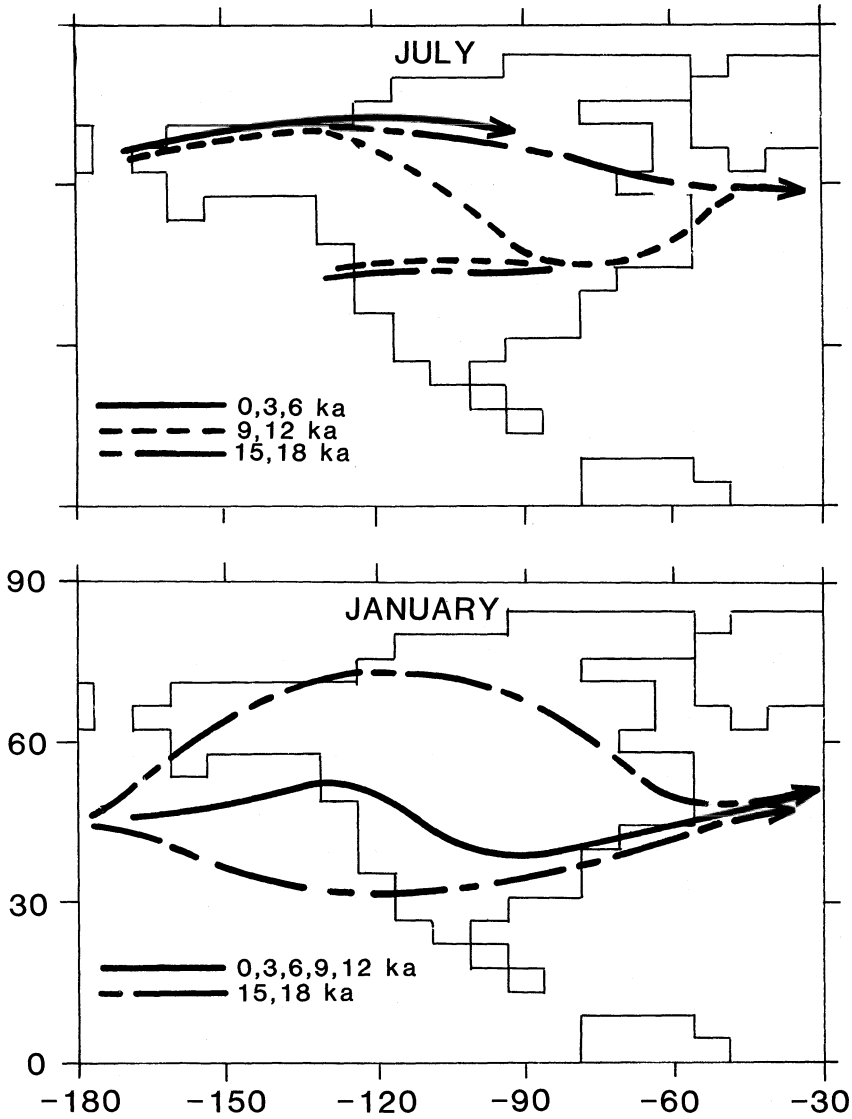


Figure 1: Schematic map of North America showing average position of the jet stream for January and July for 0, 3, 6, 9, 12, 15, and 18 ka (thousands of years before present). The COHMAP climatic model indicates a splitting of the jet around the continental ice sheet and a southward displacement of the southern limb of the jet, relative to its modern position (after Kutzbach, 1987).



## 2. REGIONALIZATION OF CLIMATE

In contrast to the general tendency to explain climatic change in terms of displacement, some evidence indicates circulation patterns may not have changed during the late Quaternary. In certain areas, significant climatic change may have occurred without the displacement of semi-permanent features of atmospheric circulation. On a shorter timescale, Miles and Follard (1974) and Tanaka *et al.* (1975) reviewed Winstanley's data and found no evidence for a southward shift in climatic zones since the 1920s.

### 2.1 *Glacial-Age Climate*

During the full glacial, Saharan Africa was hyperarid. But during the early Holocene, monsoonal precipitation increased so that lakes filled and savanna animals and humans occupied the arid core. It is very tempting to explain this sequence via shifts in the ITCZ, trade winds, and East African jet. Remarkably, investigation of ocean cores by Sarnthein (1987) and Hooghiemstra (1987) indicate that the position of the trade winds and East African jet were the same 18,000 and 9000 years ago as today! Although the strengths of these circulation features varied through time, their positions did not.

Similar conclusions have been reached for western North America. Throughout this region snowlines were roughly 1000m lower at the height of the last glaciation (Zielinski & McCoy, 1987). The actual elevation of the cirques of individual mountain ranges depends on the amount of moisture available in the mountain range today. The equilibrium line elevations (ELAs) are higher in dry ranges than in wet ranges. This relationship can be quantified through a regression of Pleistocene ELAs versus spring snow-water equivalent at the ELA (Zielinski & McCoy, 1987).

The pattern formed by the residuals to this regression (Fig. 2) demonstrates that full-glacial circulation patterns were similar to those of today. Mountain ranges of the northern Great Basin have negative residuals (greater lowering relative to today), whereas southern mountain ranges have positive residuals (less lowering). Most importantly, the line separating the areas of negative and positive residuals coincides with the modern climatic boundary (Mitchell, 1976) in this area, which I will call the "plateau" climatic boundary. The climatic change that produced 1000m lowering of glacier cirques was not accompanied by a shift of the plateau climatic boundary!

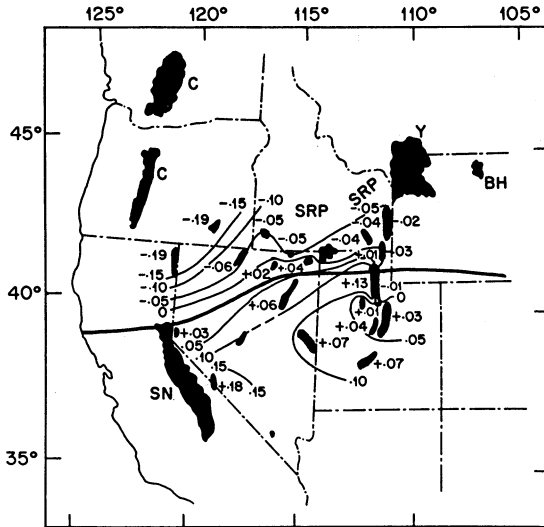


Figure 2: Relative residuals of the regression of Pleistocene equilibrium line elevations vs. snow - water equivalent of April first snowpack in meters. Relative residuals are the absolute residuals expressed as a proportion of the predicted value. Heavy line shows position of the "plateau" climatic boundary (from Zielinski & McCoy, 1987).

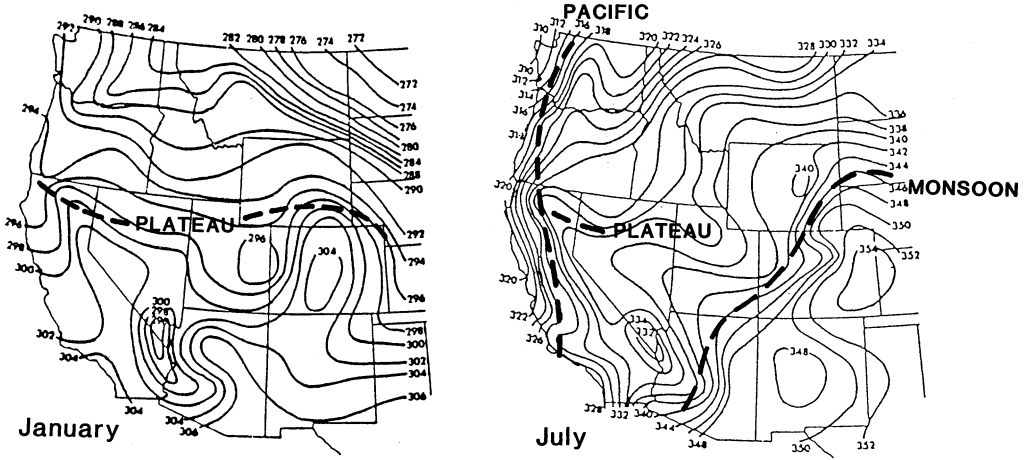
Oviatt (1988) has interpreted lake-level data to indicate long-term stability of the same climatic boundary. Low lake levels in the Great Salt Lake Basin from 12,000 to 10,000 are consistent with climatic history of the Pacific Northwest (Hebda and Mathewes, 1984; Barnosky, 1984; Davis *et al.*, 1986; Petersen *et al.*, 1983). Since the Great Salt Lake Basin obtains most of its water from the Bear and Ogden rivers, which originate north of the plateau boundary, the chronology is consistent with a stable climatic boundary (see discussion in section 3.2). However, Oviatt (1988, p. 18) postulates instability of the "monsoon" climatic boundary, because he suggests it shifted northward of its present position.

## 2.2 Modern Climatic Regions

The climatic regions of western North America primarily follow topographic features. Mitchell (1976) delimited air-mass boundaries based on equivalent potential temperature. The boundaries are marked by the clustering of isolines (Fig. 3). Winter (January) boundaries are sharpest along the east slope of the Rocky Mountains and along the Colorado River valley. Summer (July) boundaries are sharpest along the Pacific coast and the Colorado River valley. In both seasons a weaker, "plateau" boundary begins in the gap between the Cascade and Sierra Nevada mountains, crosses the northern Great Basin along the Humboldt River valley and Great Salt Lake Basin, and ends near the Rawlins Gap of Wyoming.

The "plateau" boundary approximates the northern limit reached by summer precipitation originating in the Gulf of Mexico and the western Pacific (Pyke, 1972). Recent climatological analyses by Tang and Reiter (1984) demonstrate that the intermountain plateau of western North America functions in the same way as the Tibetan highland in producing both summer and winter monsoonal circulation. Although the North American plateau is substantially lower than the Tibetan plateau, a strong anticyclonic shear line, comparable to that over Sinkiang on the Tibetan Plateau, forms in summer months along the climatic boundary that ends in the Rawlins Gap. The shear line is the northern boundary of the strong convection that occurs over the North American plateau in summer (Tang and Reiter, 1984). The same line forms a sharp boundary between wind streamlines in winter (Mitchell, 1976, Fig. 3). The position of this line coincides with the paleoclimatic boundary shown in Figure 2.

### EQUIVALENT POTENTIAL TEMPERATURE (K°)



Mitchell, 1975

Figure 3: Maps of equivalent potential temperature (oK) for January and July based on data from 67 weather stations in western North America (from Mitchell, 1976, copyright American Meteorological Society). Heavy dashed lines show positions of climatic boundaries.

### 3. CLIMATIC CHANGE IN WESTERN NORTH AMERICA

#### 3.1 *Temperature vs. Precipitation*

The number of radiocarbon-dated, climatic chronologies for western North America has increased dramatically over the last decade. These records generally show a major shift of vegetation and climate at the termination of the last glaciation, between oxygen isotope stages 1 and 2, but superimposed on this trend are many regional differences. These differences are most apparent in low-elevation sites; i.e., those where moisture is limiting. In contrast high-elevation sites, where moisture is abundant, tend to reflect the Pleistocene - Holocene temperature change. Paired high- and low-elevation sites on the Snake River Plain demonstrate this temperature - precipitation dichotomy (Davis, 1984). At high elevation, vegetation migrated upward rapidly ca. 11,000 yr B.P. (radiocarbon years Before Present) and reached its highest elevation during the mid-Holocene. At low elevation, the timing of vegetation migration is different. The Pleistocene - Holocene transition is not abrupt, and vegetation zones are highest during the early Holocene 10 - 8000 yr B.P. (Fig. 4).

#### 3.2 *Northwest - Southwest Paleoclimatic Contrast*

The Pacific Northwest was dry at the glacial termination, while the Southwest was wet. Pluvial Lakes north of ca. 40 °N lakes were dry by 11,500 yr B.P. (Smith and Street-Perrott, 1983; Benson and Thompson, 1987), and xeric vegetation was most extensive before 8000 yr B.P. (Hebda and Mathewes, 1984; Barnosky, 1984; Davis *et al.*, 1986; Petersen *et al.*, 1983). In sharp contrast, mesic herbs in Packrat middens from southern Nevada indicate greater summer precipitation 12,000 to 8000 years ago (Spaulding and Graumlich, 1986). From 11,000 to 8500 years ago, thermophilic species (such as New Mexico locust and netleaf hackberry) occupied slopes of the eastern Grand Canyon that are presently too dry for them (Cole, 1981). Pollen indices show that summer precipitation was greatest in southern Utah from approximately 12,000 - 9000 yr B.P. (Davis and Anderson, in prep).

While lakes in the Northwest were drying, many lakes in the Southwest rose. Glacial Lake Mojave overflowed from ca. 15,500 - 10,500 yr B.P. (Wells *et al.*, 1987), and Searles Lake overflowed ca. 11,000 yr B.P. (Smith and Street-Perrott, 1983). In the Las Vegas Valley, many "black mat" deposits indicate renewed spring activity from 11,700 and 10,200 yr B.P. (Quade, 1986). The most elegant demonstration of this lake-level contrast between the Northwest and Southwest is in the Lake Bonneville Basin. At an elevation

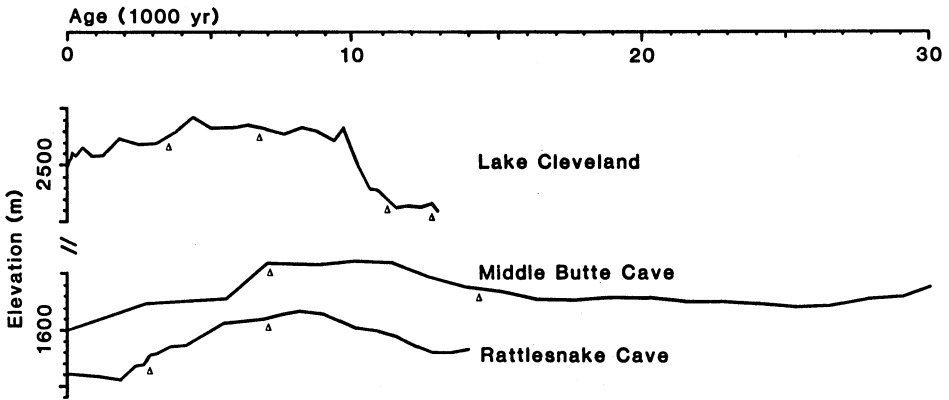


Figure 4: Elevation of vegetation zone boundaries based on pollen indices of three sites in southern Idaho. Scale interval is 10m for the boundaries. Checks indicate positions of radiocarbon dates (from Davis, 1984; copyright American Association for the Advancement of Science).

of ca 1390m, the Bonneville Basin is divided into a northern and a southern (Gunnison) basin. From 12,490 +/- 130 to 10,070 +/- 130, the southern basin overflowed into the nearly dry northern basin through the "Old River Bed" (Oviatt, 1988). Water is supplied to the northern Basin primarily from rivers (chiefly Bear River) that originate north of the "plateau" climatic boundary.

## 4. HOW CLIMATE CHANGES

### 4.1 *Implications of Paleoclimatic Studies*

The boundary between the areas of contrasting climatic history follows that of modern airmass boundaries. Late-glacial and early-Holocene aridity occurs north of the boundary, but sites south of the boundary show a moisture maximum from ca. 12,000 to 10,000 yr B.P. During the full glacial, the lowering of snowlines was greater north of the boundary and less south of it (Zielinski & McCoy, 1987). Thus, as in West Africa (Sarnthein, 1987; Hooghiemstra, 1987), the geographical position of circulation features has remained the same. However, the chronology of climatic change differs across the boundary. Mitchell (1976) delimited climatic boundaries that coincide roughly with topographic features. These same features separate areas of relatively homogeneous climatic change.

It would be premature to claim that modern climatic regions in general have different climatic histories. However, I think the evidence is sufficient to suggest that the regionalization of climatic change should be considered as an alternative to displacement of circulation patterns to explain patterns of climatic change. In topographically diverse regions where meteorological patterns are sharp, boundaries between regions of paleoclimatic change may be equally sharp.

### 4.2 *A Test of the Deflection Hypothesis*

The Northwest - Southwest climatic contrast could be explained by displacement of circulation patterns. The climatic contrast outlined in section 3.2 could result if the jet were deflected south of 39°N from 12,000 to 10,000 ya. Such a deflection would have reduced precipitation and lake levels north of 39°N, but would have had the opposite effect between 33° and 39°N. The COHMAP climate model (Kutzbach and Wright, 1985; Kutzbach, 1987) shows no change in the summer position of the southern limb of the North American jet from 18,000 to 9000 ya (Fig. 1), but its position in winter moves from 30° to 45°N between 15,000 and 12,000 ya.

Benson and Thompson (1987, p.83) suggest that the 14,000 to 12,500 yr B.P. high stand of Lake Lahontan occurred when the jet was most intense at ca. 39°- 42°N.

Fossil records from west of the Great Basin can show that southward deflection of the jet cannot explain the NW-SW climatic contrast. If the jet were displaced southward, precipitation should have increased all along its path, particularly where it crosses major mountain barriers. However, fossil pollen records from 37°N in the western Sierra Nevada indicate greater aridity prior to 9000 yr B.P. rather than greater moisture (Davis *et al.*, 1985; Davis and Moratto, 1988).

Figure 5 includes summary moisture curves for the Northwest and Southwest. The Northwest curve was prepared by combining and smoothing pollen indices of moisture for 4 low-elevation sites on the Snake River Plain (Swan Lake: Bright, 1966; Murphey's Rockshelter: Henry, 1984; Rattlesnake and Middle Butte Caves: Davis *et al.*, 1986). The Southwest moisture curve combines pollen indices from three sites (Cowboy Cave, Lindsay, 1980; Spaulding and Petersen, 1980; Bechan Cave, Davis *et al.*, 1984; and Fishmouth Cave: Betancourt, 1984) with macrofossil records of mesic shrubs from three other sites (Grand Canyon: Cole, 1981; Southern Nevada: Spaulding, 1985; Picacho Peak: Cole, 1986). The moisture indices are the ratio of *Artemisia* to *Chenopodiaceae-Amaranthus* for pollen and the abundances of mesic shrubs for the macrofossils. The technique is discussed in detail by Davis and Anderson (in prep.).

The Southwest - Northwest moisture contrast was greatest at the termination of the last glaciation. Peak moisture for the Northwest curve occurs before 13,000 yr B.P., maximum aridity ca. 7600 yr B.P. The Southwest curve indicates a strong moisture maximum ca. 11,200 yr B.P. at the termination of the last glaciation. Although the two curves are not exactly out of phase, the contrast could be explained either by displacement of the jet, or by regionalization of climatic change.

However, displacement of the jet cannot have produced the 12,000 - 10,000 yr B.P. wet period in the Southwest. Summary curves for the two western Sierra Nevada sites (Davis *et al.*, 1985; Davis and Moratto, 1988) show reduced precipitation in the early Holocene when precipitation east of the Sierra Nevada is greatest. The jet could not have moved storms into the Southwest without also having increased precipitation in the western Sierra Nevada.



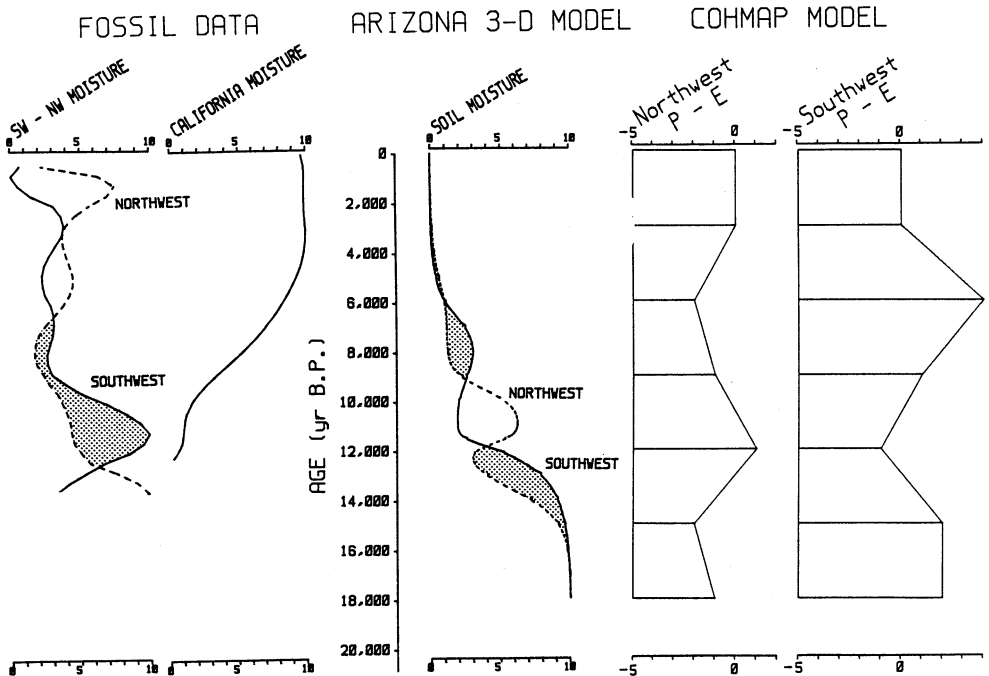


Figure 5: Moisture curves for western North America. The fossil data are based on pollen ratios and macrofossils of mesic shrubs. The curves are for smoothed combinations of data from 4 Northwestern, 6 Southwestern, and 2 Californian sites (from Davis and Anderson, in prep.). The Arizona 3-D climate model curve is for soil moisture (ws) in summer (June, July, and August) for two model grid points -- (southwest) 35°N, 115°W and (northwest) 45°N, 115°W (from Davis and Sellers, in prep.). The precipitation minus evaporation (P - E) curves from the COHMAP model are averages of several grid points (after Kutzbach, 1987). The moisture curves are on arbitrary scale from dry (0) to wet (10) for the fossil and Arizona 3-D curves and from -5 to +5 for the COHMAP model.

### **4.3 Regionalization of Climatic Change**

For western North America, the persistence of climatic boundaries throughout the late Quaternary probably resulted both from the stability of major topographic features during this interval, as well as the relatively constant position of major circulation patterns. Precipitation is brought to the Pacific Northwest and western California by cyclonic storms and fronts driven eastward by the Aleutian Low. The Southwest also receives winter storms, but the relative importance of summer precipitation increases southeastward. The summer precipitation pattern, named the "Arizona Monsoon" by Bryson and Lowrey (1955), is driven by two circulation processes. First, anticyclonic circulation around the Bermuda high brings moist air northward and eastward from the Gulf of Mexico and Gulf of California. Second, the plateau-monsoon circulation brings moist air northward into the eastern Great Basin and Colorado Plateau (Tang and Reiter, 1984).

Variations in the relative strength of these two circulation patterns could have produced the regional climatic histories outlined in this paper. In particular, the precipitation maximum from 12,000 to 10,000 yr B.P. in the Southwest could have resulted from increased summer precipitation at the same time winter precipitation in the Northwest was reduced. However, since the southwestern precipitation maximum coincides with the annual insolation maximum (12,000 - 11,400 ya at 35°N) rather than the July insolation maximum (10,000 - 9200 ya at 35°N), a simple insolation - circulation relationship is unlikely. Simple relationships of the insolation maximum to precipitation in the Northwest are even more difficult to explain. Other factors, such as sea-surface temperature and feedbacks from the continental ice sheet, must be involved.

### **4.4 Model Results**

Both the COHMAP model and the Arizona 3-D climate model indicate a Northwest - Southwest contrast in climatic histories (Kutzbach, 1987; Davis and Sellers, in prep.). The Arizona model (Sellers, 1983, 1984) is equivalent to a coarse grid (10 X 10°) GCM with simplified dynamics. It includes an interactive ocean and variable cloud cover, and three tropospheric and two stratospheric layers. The governing equations of the model are modified versions of the basic equations that control the dynamics and thermodynamics of the earth's surface and atmosphere. The major simplifications are the use of a geostrophic wind approximation

above the boundary layer and the assumption that the mean tropospheric flow is nondivergent. Air-sea interaction is accomplished through variable ice and snow cover, parameterized ocean currents, and the hydrologic cycle.

For the Arizona model, the Southwest moisture maximum (soil moisture) from 8000 to 10,000 ya is preceded by a Northwest maximum from 11,000 to 12,000 ya (Fig. 5). A single grid-point is used for each region, one centered in central Idaho (45°N, 115°W) and the other centered near the southern tip of Nevada (35°N, 115°W). The maxima are roughly 2000 years later than those derived from fossil data. The true age of radiocarbon dates of this range is poorly constrained, but may be 1000 yrs too young (Stuiver *et al.*, 1986), thereby increasing the discrepancy to 3000 yrs.

The moisture curves (precipitation minus evaporation) from the COHMAP model are averages of several grid points (Fig. 5). The Southwestern moisture (P-E) maximum is later than that of the Arizona model — 6000 ya *vs.* 8000 ya. During the late glacial (12,000 ya), the Southwest is drier than at present while the Northwest is wetter — just the opposite of the pattern described in section 3.2. The COHMAP model indicates times in the past that were both drier and wetter than today, whereas the Arizona 3-D model indicates progressive drying since the full glacial. Neither model produces curves that match those derived from the fossil data, but they do indicate the Southwest-Northwest contrast, which is consistent with the regionalization outlined in section 4.1.

Both climate models are strongly affected by the extent of continental glaciers (also see Manabe and Broccoli, 1985). The model runs that produced Figure 5 used a linear decrease in ice extent (after Figure 1 of Kutzbach and Guetter, 1986). The difference between the model results and fossil reconstructions may result from discrepancies between the dates used by the models and the actual deglaciation chronology, and from differences between radiocarbon dates and the "real" ages used by the models for insolation calculations.

## 5. CONCLUSIONS

In western North America, the chronologies of climatic change in the Northwest and Southwest have been different. The boundaries between these regions of climatic change coincide with modern climatic boundaries. Sarnthein (1987) and Hooghiemstra (1987) demonstrate that circulation

patterns in western Africa were similar 18,000 yr B.P., 9000 yr B.P., and today. In both areas the strength of circulation features has changed through time although the position has not.

### 5.1 *Continued Research*

Future investigations in western North America should focus on climatic chronologies of paired sites across climatic boundaries. The discrepancy between model results and fossil data should be investigated with more realistic deglaciation chronologies, and computer model runs later in the Holocene should be performed to determine similarities with the fossil curves for Northwest and Southwest moisture.

### ACKNOWLEDGEMENTS

This research was supported by NSF Grant ATM 8619467. This manuscript benefited from editing by Andy Cohen, Judy Parish, and an anonymous reviewer.

### REFERENCES

- Antevs, E., 1938: Postpluvial climatic variations in the southwest, *Bull. Amer. Met. Soc.*, 19: 30-33.
- Antevs, E., 1955: Geologic-climatic dating in the west, *Amer. Antiquity*, 20: 317-355.
- Barnosky, C.W., 1984: Late Pleistocene and early Holocene environmental history of southwestern Washington State, U.S.A., *Can. J. Earth Science*, 21: 619-629.
- Benson, L.V., and Thompson, R.S., 1987: Lake-level variation in the Lahontan Basin for the past 50,000 years, *Quat. Res.*, 28: 69-86.
- Berger, A.L., 1978: Long-term variations of daily insolation and Quaternary climatic changes, *J. Atmo. Sci.*, 35:2362-2367.
- Betancourt, J.L., 1984: Late Quaternary plant zonation and climate in southeastern Utah, *Great Basin Naturalist*, 44: 1-35.

- Bright, R.C., 1966: Pollen and seed stratigraphy of Swan Lake, southeastern Idaho: Its relation to regional vegetational history and to Lake Bonneville history, *Tebiwa*, 9: 1-47.
- Bryson, R. A., and Lowry, W.P., 1955: Synoptic climatology of the Arizona summer precipitation singularity, *J. Amer. Met. Soc.*, 36: 329-339.
- Byrne, R., Granger, O., and Monteverdi, J., 1982: Recent rainfall trends on the margins of the subtropical deserts: a comparison of selected northern hemisphere regions, *Quat. Res.*, 17:14-25.
- Cole, K.L., 1981: Late Quaternary environments in the eastern Grand Canyon: Vegetational gradients over the last 25,000 years, Ph.D. dissertation, University of Arizona, Tucson.
- Cole, K.L., 1986: The lower Colorado River Valley: A Pleistocene desert, *Quat. Res.*, 25: 392-400.
- Davis, O.K., 1984: Multiple Thermal Maxima During the Holocene, *Science*, 255: 617-619.
- Davis, O.K., and Anderson, R.S. (in prep.): Climatic change and the extinction of the Rancholabrean megafauna: evidence from mammoth diet from the Colorado Plateau, U.S.A, MS submitted and being revised for *Quaternary Research*.
- Davis, O.K., Agenbroad, L.D., Martin, P.S., and Mead, J.I., 1984: The Pleistocene dung blanket of Bechan Cave, Utah, *In: Genoways, H.H. and M.R Dawson (Eds.), Contributions in Quaternary Vertebrate Paleontology: A volume in memorial of John E. Guilday, Carnegie Museum of Natural History Spec. Publ.*, 8: 267-282.
- Davis, O.K., Anderson, R.S., Fall, P.L., O'Rourke, M.K. and Thompson, R.S., 1985: Palynological evidence for early Holocene aridity in the southern Sierra Nevada of California, *Quat. Res.*, 24: 322-332.
- Davis, O.K., and Moratto, M.J., 1988: Evidence for a warm-dry early Holocene in the western Sierra: pollen and plant macrofossil analysis of Dinkey and Exchequer Meadows, *Madrono*, 35: 128-145.

- Davis, O.K., and Sellers, W.D. (in prep.): The effects of seasonal insolation on the history of the Arizona Monsoon, *In: Gunn, J. (Ed.), Mechanisms of Climate and Culture Change*, Plenum Publishers (submitted).
- Davis, O.K., Sheppard, J.C., and Robertson, S., 1986: Contrasting climatic histories for the Snake River Plain resulting from multiple thermal maxima, *Quat. Res.*, 26: 321-339.
- De Geer, G., 1912: A geochronology of the last 12,000 years, Eleventh International Geological Congress, Stockholm 1910, *Compte Rendu*, 1: 241-258.
- Hebda, R.J., and Mathewes, R.W., 1984: Holocene history of cedar and native Indian cultures of the North American Pacific coast, *Science*, 225: 711-712.
- Henry, C., 1984: Holocene paleoecology of the western Snake River Plain, Idaho, M.S. thesis, University of Michigan, Ann Arbor.
- Hooghiemstra, H., 1987: Trade wind history as evidenced by marine sediments off NW Africa: Changes in pollen transport efficiency during the last 140,000 yr, this volume.
- Iversen, J., 1941: Land occupation in Denmark's stone age, *Danmarks Geol. Under.*, Ser. 2, No. 66, 68 pp.
- Kutzbach, J.E., and Guetter, P.J., 1986: The influence of changing orbital parameters and surface boundary conditions on climate simulations for the past 18,000 years., *J. Atmo. Sci.*, 43: 1726-1759.
- Kutzbach, J.E., and Wright, H.E., Jr., 1985: Simulation of the climate of 18,000 years B.P.: results for the North American/North Atlantic/European sector and comparison with the geologic record of North America, *Quat. Sci. Rev.*, 4: 147-187.
- Libby, W.F., 1955: *Radiocarbon dating*, Univ. Chicago Press.
- Lindsay, L.W., 1980: Pollen analysis of Cowboy Cave cultural deposits, *In: Jennings, J.D. (Ed.), Cowboy Cave*, University of Utah Anthropological Papers, 104: 163-177.

- Manabe, S., and Broccoli, A.J., 1985: The influence of continental ice sheets on the climate of an ice age, *J. Geol. Res.*, 9: 2167-2190.
- Miles, M.K., and Follard, C. K., 1974: Changes in the latitude of the climatic zones of the Northern hemisphere, *Nature* (London) 242: p. 616.
- Mitchell, V.L., 1976: The regionalization of climate in the western United States., *App. Met.*, 15: 920-927.
- Oviatt, C.G., 1988: Late Pleistocene and Holocene lake fluctuations in the Sevier Lake Basin, Utah, USA, *J. Palaeolimnology*, 1: 9-21.
- Quade, J., 1986: Late Quaternary environmental changes in the upper Las Vegas Valley, Nevada, *Quat. Res.*, 26: 240-357.
- Petersen, K.L., Mehringer, P.J., Jr., and Gustafson, C.E., 1983: Late-glacial vegetation and climate at the Manis Mastodonsite, Olympic Peninsula, Washington, *Quat. Res.*, 20: 215-231.
- Pyke, C.B., 1972: Some meteorological aspects of the seasonal distribution of precipitation in the western United States and Baja California, University of California Water Resources Center Contribution, 139, 205 pp.
- Sarnthein, M., Teidemann, R., and Pflaumann, U., 1987: Dust record of late Neogene and Quaternary paleoclimate and paleometeorology in the south Sahara, this volume.
- Schove, D.J., 1987: Sunspot cycles and weather history, *In*: Rampino, M. R., J.E. Sanders, W.S. Newman and L.K. Koningsson (Eds.), *Climate, History, Periodicity, and Predictability*, Van Nostrand Reinhold Co., New York, pp. 355-377.
- Sellers, W.D., 1983: A quasi-three-dimensional climate model, *J. Climate App. Met.*, 22: 1557-1574.
- Sellers, W.D., 1984: The response of a climate model to orbital variations, *In*: Berger, A., et al. (Eds.) *Milankovitch and Climate: Understanding the Response to Astronomical Forcing*, D. Reidel Publ. Co., Dordrecht, Holland, pp. 765-788.
- Smiley, T.L., 1976: Memorial to Ernst Valdemar Antevs 1888 -1974, *Geol. Soc. Amer.*, 7 pp.

- Smith, G.I., and Street-Perrott, E., 1983: Pluvial lakes of the western United States, *In: Porter, S.C. and H.E. Wright (Eds.), Late Quaternary Environments of the United States*, University of Minnesota Press, Minneapolis, pp. 190-212.
- Spaulding, W.G., 1885: Vegetation and climates of the last 45,000 years at the Nevada Test Site and vicinity, *U.S. Geol. Sur. Prof. Paper*, 1329.
- Spaulding, W.G., and Graumlich, L.J., 1986: The last pluvial climatic episodes in the deserts of southwestern North America, *Nature (London)* 320: 441-444.
- Spaulding, W.G., and Petersen, K.L., 1980: Late Pleistocene and early Holocene paleoecology of Cowboy Cave, *In: Jennings, J.D. (Ed.), Cowboy Cave*, University of Utah Anthropological Papers, 104: 163-177.
- Stuiver, M., Kromer, B., Becker, B., and Ferguson, C.W., 1986: Radiocarbon age calibration back to 13,300 years BP and the  $^{14}\text{C}$  age matching of the German oak and U.S. bristlecone pine chronologies, *Radiocarbon*, 28 (2B): 969-979.
- Tanaka, M., Weare, B.C., Navato, R., and Newell, R.E., 1975: Recent African rainfall patterns, *Nature (London)*, 255: 201-203.
- Tang, M., and Reiter, E.R., 1984: Plateau monsoons of the northern hemisphere: a comparison between North America and Tibet, *Monthly Weather Review*, 112: 617-637.
- Wells, S.G., McFadden, L.D., and Dohrenwend, J.C., 1987: Influence of late Quaternary climatic changes on geomorphic and pedogenic processes on a desert piedmont, eastern Mojave Desert, California, *Quat. Res.*, 27: 130-146.
- Winstanley, D., 1973: Recent rainfall trends in Africa, the Middle East and India, *Nature (London)*, 245: 190-194.
- Zielinski, G.A., and McCoy, W.D., 1987: Paleoclimatic implications of the relationship between modern snowpack and late Pleistocene equilibrium-line altitudes in the mountains of the Great Basin, Western U.S.A., *Arctic and Alpine Research*, 29: 127-134.



# INTERGLACIAL ENVIRONMENTS IN PRESENTLY HYPERARID SAHARA : PALAEOCLIMATIC IMPLICATIONS

N. PETIT-MAIRE

Laboratoire de Géologie du Quaternaire - CNRS -  
Case 907 - Luminy - 13288 MARSEILLE Cedex -FRANCE-  
IGCP 252 (Past and future Evolution of Deserts)

**ABSTRACT.** A lacustrine transgression took place in the whole Sahara, during the warm 5e stage, and lasted at least 50 000 years. During the early Holocene, a sahelian biotope existed up to 23°N and a sahelo-sudanian one up to 20°N; the limnological and biological optimum was between 8 500 and 6 500 B.P., the onset of the wet phase at c 9 500 B.P. A weakening of current and upwelling along the saharan atlantic shore is evidenced between 6 000 and 4 000 B.P. Palaeoprecipitations are estimated.

Palaeometeorological models which take into account the influence of changing Earth orbital parameters (Berger and Tricot, 1986) show major changes in global monsoons during the last climatic cycle (Kutzbach, 1981; Kutzbach and Otto-Bliesner, 1982; Kutzbach and Guetter, 1986; Kutzbach, 1987; Prell and Kutzbach, 1987). The response of continental West Africa to interglacial conditions is recorded in oceanic sedimentation (Sarnthein, 1976, 1982; Rossignol-Strick, 1983) and for the last climatic optimum, by the lacustrine evolution in the tropical belt (Kutzbach and Street-Perrott, 1985).

In this paper, we shall discuss the climatic situation of three now hyperarid areas of the Sahara (Leroux 1983) during the last two interglacials. They provided a good Th/U and <sup>14</sup>C time resolution for palaeohydrological, palaeobotanical, palaeontological and palaeoanthropological data, observed on the surface and, in the case of northern Mali, along continuous sections and cores.

## 1. The last Pleistocene interglaciation

Important extensions of surface water existed in the Sahara during the interglacial phase which marked the end of the Mid-Pleistocene.

The first evidence was observed in Libya, at 27°30'N (Petit-Maire *et al.*, 1980). Along both the northern and southern sides of the large (125 km x 10-20 km) endoreic Shati depression (fig.1), strikingly thick (1 to 7 m) coquina line the past shores of a lake, 40 to 50 m above the present floor of a sebkha. Foraminifera (*Ammonia beccarii*, *Protelphidium paraliun*, *Criboelphidium sp.*, *Rosalina globularis*), Ostracods (*Cyprideis sp.*) and Mollusca (*Cerastoderma glaucum*, *Melania tuberculata*, *Hydrobia sp.*) are associated in the deposits. All of them are euryhaline: *C. glaucum*, the dominant species, can tolerate a very wide range of 3 to 60‰ (Rosso and Gaillard, 1982) and even 90‰ (Klitzsch, 1972), while *M. tuberculata*, normally only 3 to 10‰, was observed

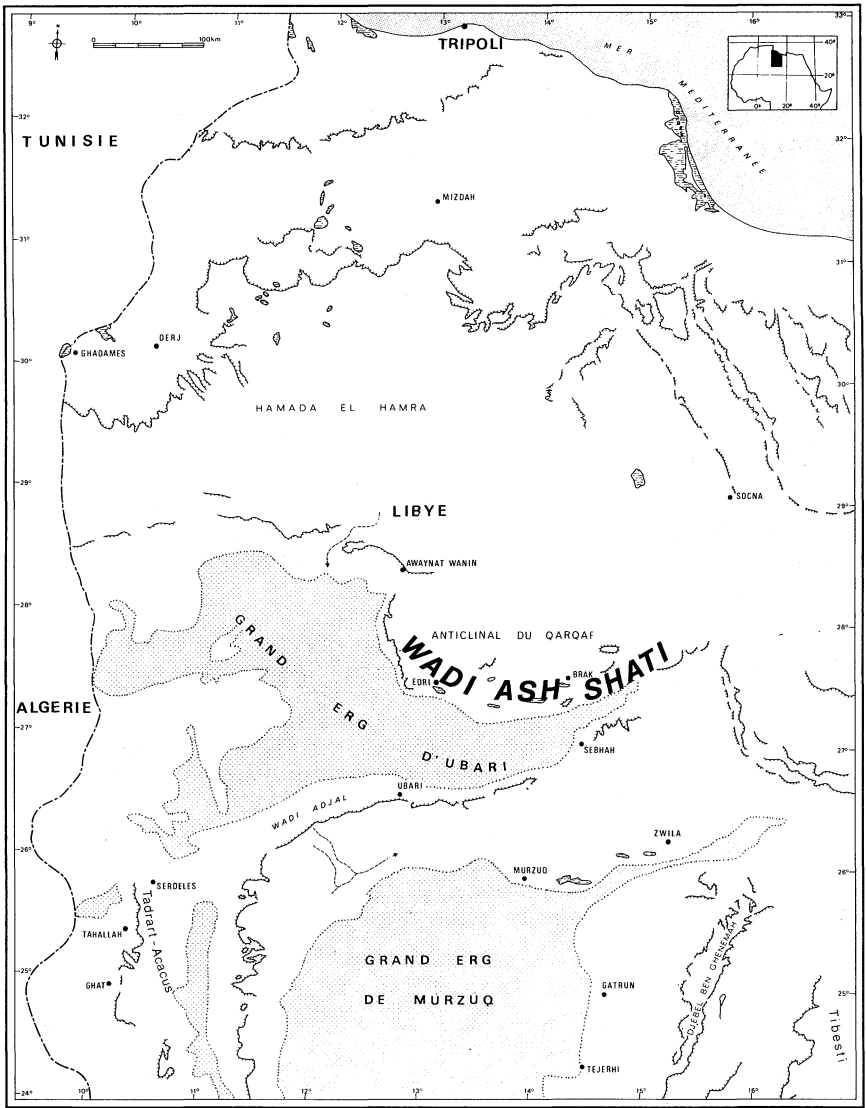


Fig. 1. Situation du Wadi Shati en Libye occidentale.

alive in the Senegal delta at nearly 30‰ (Monteillet et Rosso, 1977; Rosso et Gaillard, 1982). The morphological variations of the Ostracods and the isotopic ratios in the Mollusca shells however indicate a low ionic activity corresponding to oligohaline conditions in a permanent lake where salinities frequently varied from only 3 to 10‰ in well oxygenated waters (Petit-Maire *et al.*, 1980; Gaven *et al.*, 1981; Carbonel, 1982; Blanc-Vernet, 1982; Hillaire-Marcel, 1982). The lacustrine conditions were due to rise of the aquifer -now 5 m below sebkha floor- fed by possibly more remote inputs, but certainly also by local surface run off. This latter is shown by important drainage features at the foot of the Qarquaf massif, with terraces containing the same evolved Acheulean artefacts as around the shores, and pebble-gravel inputs into the cardium beds of the northern shore. To the East, a wide fluvio-lacustrine area with layers of fresh water shells (*Corbicula africana*, *Caelatura lacoini*, *Lymnaea natalensis*) intercalated in alluvial deposits, indicate heavy run off from the Jebel Harruj area.

The Shati palaeolake was Th/U dated on *C. glaucum* shells. Seven ages from its eastern margin cover two episodes: 173-125 Ka B.P. in the lower layers and 90 Ka B.P. in the upper layers. Fourteen ages from coquina mounds along both sides of the lake range from 165 to 122 Ka B.P. with two isolate ages at 92 and 40 Ka B.P. Correction of these dates result into 130 Ka for the hydrological optimum (Causse and Hillaire-Marcel, 1986).

The summer and winter local rainfall implied by the existence of a c 50 billion m<sup>3</sup> permanent lake is totally inconsistent with the present mean (30 mm) and atmospheric patterns in the Fezzan. Precipitations from the south and from the Mediterranean certainly reached the 27<sup>th</sup> parallel during the Eemian marine transgression (max. at -125.000 years), but it is difficult to estimate their importance, due to the lack of information upon other than hydrological data.

Recent observations now confirm the existence of this lake phase throughout the Sahara.

In northern Mali, at Telig, Sbeita and Taoudeni (fig. 2) the emergence of the karstic nappe of Hammada el Haricha is marked by successive layers of thin calcareous crusts and of travertines with vegetal debris and *M. tuberculata*, suggesting alternative swamp and lake phases ; at Sbeita, Mousterio-Levalloisian sites are associated with these formations (Raimbault, in prep.), some 25 m above the level of the holocene lakes (Fabre, 1983; Fabre and Petit-Maire, 1983; Petit-Maire, 1986). A first approximate Th/U age also corresponds to isotopic stage 5 (Causse, pers. comm., 1988).

At Bir Tarfawi, a depression in the Egyptian western desert, mid-palaeolithic sites are also associated with lake episodes dated 90 000 and 125 000 B.P. ; electro-spin resonance analyses of tooth-enamel from the base of one lake suggest even older ages (Wendorf *et al.*, 1987).

In northern Sahara, similar lacustrine episodes are also recorded in Algeria and Tunisia by Fontes *et al.* (1987) and Ballais and Ben-Ouezdou (1987).

These data fit models, as well as the pollen evidence in marine sediments, for a maximal extension of the tropical forest around 124 000 B.P. (Hooghiemstra, in press) which may corroborate frequent arrival of tropical depressions up to 27°N.

## 2. The Holocene interglacial

The range of continental responses to the successive steps of last deglaciation (Duplessy *et al.*, 1981; Duplessy and Ruddiman, 1984; Berger *et al.*, 1985; Lorius *et al.*, 1985; Mix and Ruddiman, 1985), has been well explored in the last ten years and general trends can now be defined, in spite of differences due to opposed local geographical situations. In this scope, two saharan areas with extreme aridity have been compared. One, the Taoudeni basin in Mali, is as free as possible from oceanic influence while the other, the Tarfaya basin and Fuerteventura saharan island, are, to the contrary, exposed to a full oceanic regime.

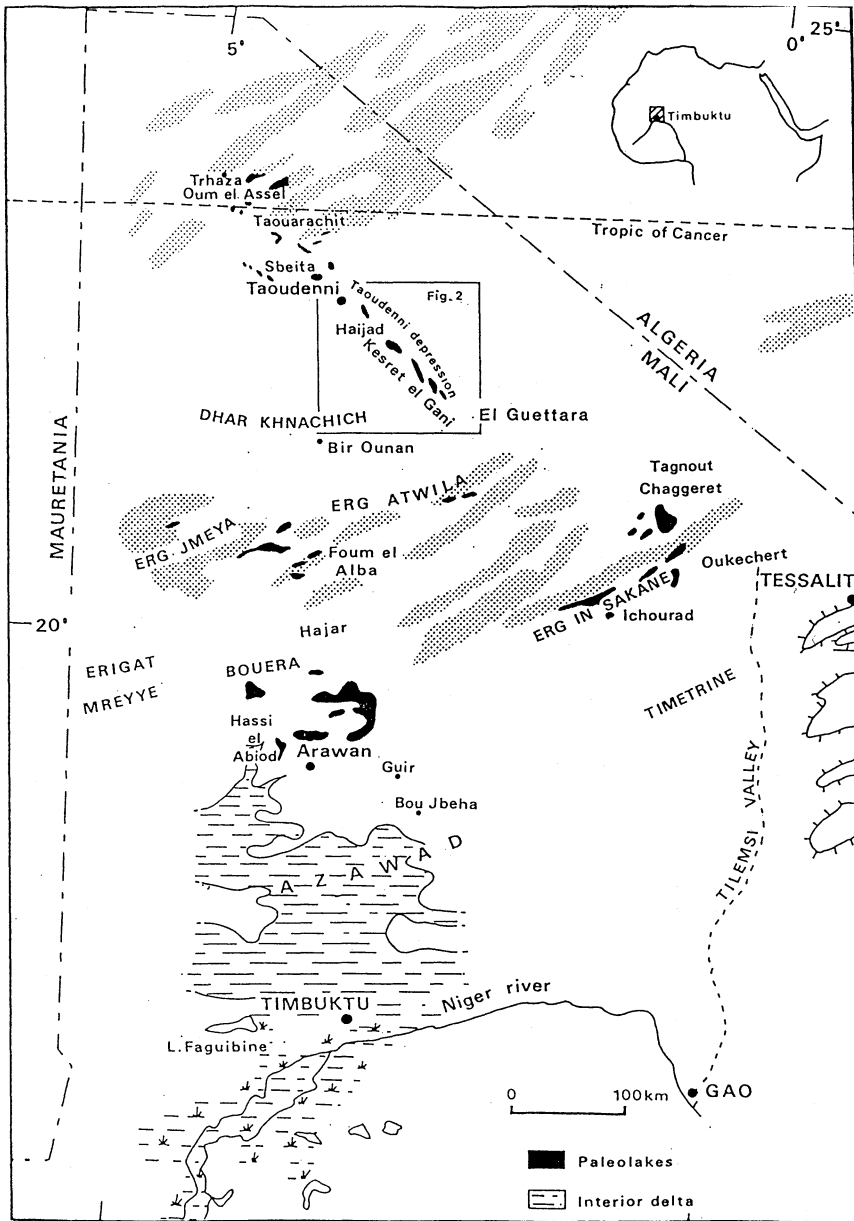


Fig. 2. Holocene lakes observed in malian Sahara. Presently, the area receives 170 mm mean annual rainfall at Timbuktu, 5 mm at Taoudenni and no surface water exists out of the Niger interior delta.

## 2.1. Malian Sahara

The malian part of the Sahara covers some 450 000 km<sup>2</sup> North of the Niger bend and receives mean annual precipitations grading from c 60 mm at Arawan (19°N) to c 5 mm at Taoudeni-Trhaza (23-24°N), near the Tropic of Cancer. The environmental evolution in three hydrological basins has there been observed (fig. 2) and widely radiocarbon dated (table 1).

a. To the N.E., the Erg Ine Sakane-Tagnout Chaggeret area is related to drainage from the Timetrine, the Adrar of Iforas and the Hoggar. During the Upper Pleistocene, the dunes were active; their slightly consolidated sandstones under and along the present erg testify to the unvarying direction of enforced trade-winds, which corroborates Sarnthein *et al.* (1981) and Hooghiemstra (1987) research on marine sedimentation and pollen transport. At 9 500 B.P., a lacustrine phase initiates and small pools (in the former interdune depressions) or large lakes (in the major depressions) are fed by the outcrops of the dunes phreatic nappes and by run off from the Timetrine, as evidenced by alluvial fans interbedding the lake deposits (Riser *et al.*, 1983). A fresh water fauna is plentiful (Blanc-Vernet, 1983; Carbonel, 1983; Gayet, 1983): Foraminifera, Ostracods (*Cyprideis sp.*), Molluscs (*Lymnaea natalensis*, *Bulinus truncatus*, *Biomphalaria pfeifferi*, *Spathopsis sp.*, *Melania tuberculata*) and fish (*Lates niloticus*, *Alestes sp.*) showing at least sporadic surface connections with the Tilemsi system. *Crocodylus niloticus* (Buffetaut, 1983) reached the area (through an implied string of rivers, swamps or lakes) as well as large savanna mammals: hippopotamus, rhinoceros and six species of large antelopes among which *Hippotragus equinus*, *Alcelaphus buselaphus* and *Limnotragus spekei* (Guérin et Faure, 1983). Neolithic man lived in all this region on a hunter-gatherer economy (Dutour et Petit-Maire, 1983; Raimbault, 1983; Camps-Fabrer, 1983).

These environments are dated 9 500-4 000 B.P. (table 1) on lake shells, brown palaeosols, animal and human bones (Petit-Maire and Riser, 1981, 1983). A high level episode was dated at 9 000 B.P. (Riser *et al.*, 1983; Hillaire-Marcel *et al.*, 1983).

Local palaeoprecipitations are not easy to define for that area, since no estimation can be made of the relative parts of allochthonous drainage and local rainfall. However, the grassland implied by the herbivorous fauna suggests values not lower than 300 mm.

b. The flat Azawad only slopes 8 m between the Niger bend and the Bouera, some 400 km to the north. It was shown that, during the Holocene, it was flooded by the rise of the Niger nappe but also fed by surface channels up to 18°30'N (Petit-Maire and Gayet, 1984; Riser and Petit-Maire, 1986; Petit-Maire and Riser, 1987). The inundated lacustrine areas varied with the seasonal river regime and a network of surface connections reached the Mreyyé (19°20'N) as late as c 5 500 B.P. while, to the South, the lacustrine phase lasted until 3 500 B.P. (fig. 3).

The lake deposits and large middens around the shores contained a rich aquatic and semi-aquatic fauna of Foraminifera (Blanc-Vernet, 1983), Ostracods (Carbonel, 1983), Molluscs (Rosso, 1983), large fish among which *L. niloticus* requires a quantity of running fresh water (Gayet, 1983; Petit-Maire et Gayet, 1984), big turtles (de Broin, 1983), crocodiles (Buffetaut, 1983), big python snakes (det. Rage) and hippopotamus (Guérin et Faure, 1983). The environment was a wooded savanna, as proved by the association of the giraffe with rhinoceros, elephants, phacochoerus and many species of large antelopes (det. Guérin, Petit-Maire, 1986). Man lived a sedentary life in this area at 7 000 B.P., as proven by Dutour (1986) palaeoethnological studies. These populations were surprisingly recognized as Cromagnoids,

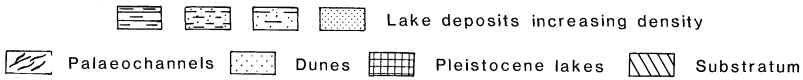
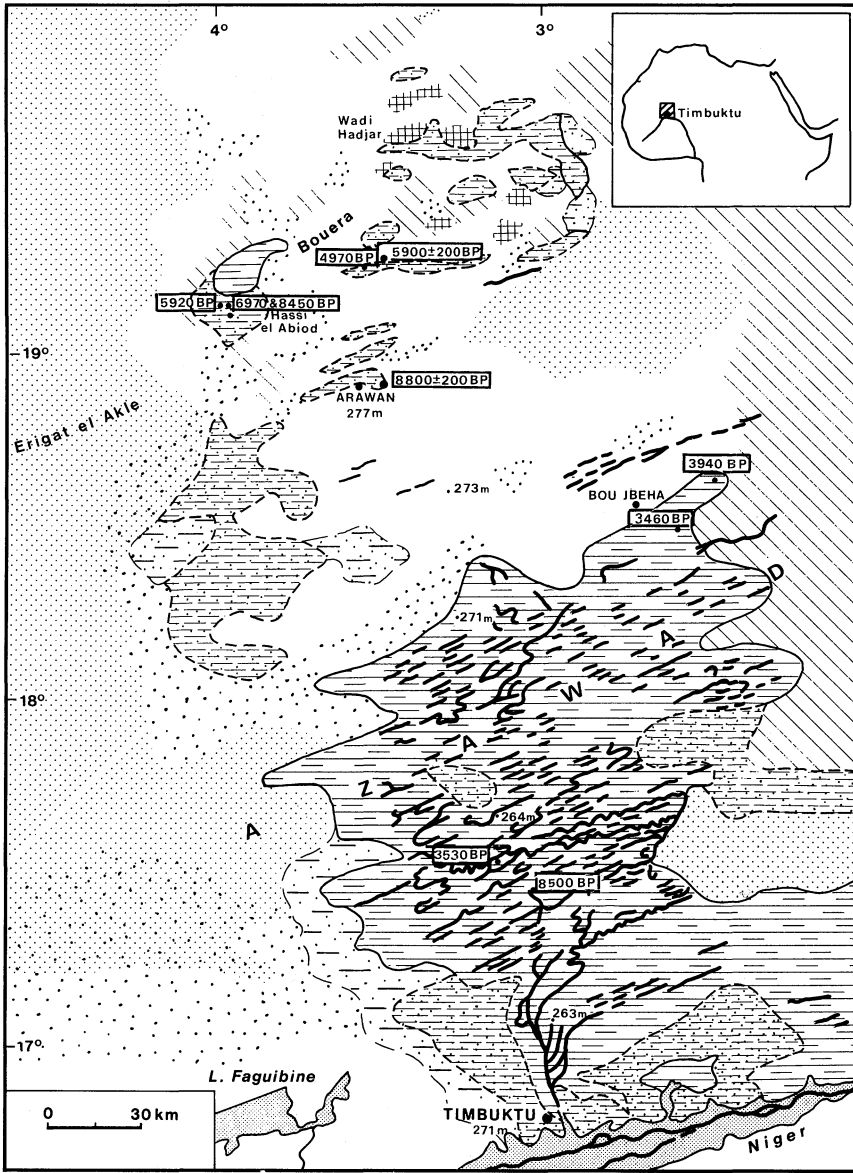


Fig. 3. Holocene lakes in the Azawad and Bouera.

Ages B.P.	Sample	Long.	Lat.	Material	Lab. n°
2000 ± 210	AZ25	1°00'W	19°20'N	Human bones	GIF 5230
2160 ± 250	AZ 15	0°15'E	20°50'N	Human bones	GIF 5306
2850 ± 100	AZ 20	0°40'W	20°50'N	Human bones	GIF 5440
3460 ± 90	MN 25	2°34'W	18°28'N	<i>Limicolaria sp.</i>	GIF 6459
3530 ± 90	MN 2	3°06'W	17°31'N	<i>Melania tuberculata</i>	GIF 6460
3600 ± 180	AZ 21	0°40'W	20°50'N	Human bones	GIF 5441
3680 ± 100	AZ 41	0°45'W	20°35'N	Bone (large herbivora)	GIF 5445
3750 ± 100	AZ 21	0°40'W	20°50'N	Charcoal	GIF 5227
3840 ± 250	MT 7/16	4°00'W	22°40'N	Wood in lake clay	GIF 6122
3940 ± 90	MN 20	2°35'W	18°40'N	<i>Limicolaria sp.</i>	GIF 6463
3990 ± 130	AZ 21	0°40'W	20°50'N	Burnt bone (large herbivora)	GIF 5442
4040 ± 110	MK 22	4°35'W	20°40'N	Charcoal	GIF 5815
4110 ± 90	AZ 26	0°40'W	20°40'N	<i>Melania tuberculata</i>	U.Q. 251
4400 ± 105	AZ 35	0°50'W	20°50'N	<i>Melania tuberculata</i>	U.Q.
4440 ± 270	MT 6/1	3°40'W	22°34'N	<i>Melania tuberculata</i>	GIF 6197
4470 ± 110	AZ 19	0°50'W	21°00'N	Ashy soil	GIF 5439
4480 ± 110	MT 30	3°46'W	22°38'N	<i>Zoothecus insularis</i>	GIF 6125
4480 ± 110	MK 42	0°40'W	21°20'N	<i>Melania tuberculata</i>	GIF 5813
4520 ± 110	AZ 56	0°50'W	21°00'N	Human bones	GIF 5469
4710 ± 120	MK 42	0°40'W	21°15'N	Charcoal	GIF 5818
4710 ± 110	AZ 48	0°45'W	20°50'N	<i>Limicolaria sp.</i>	U.Q.
4720 ± 90	MT 7bis/ 15	4°00'W	22°40'N	Wood in lake clay	GIF 6903
4800 ± 100	17867	3°35'W	19°00'N	<i>Aspatharia sp.</i>	U.Q. 1043
4880 ± 110	AZ 36	0°50'W	20°50'N	<i>Aspatharia sp.</i>	U.Q.
4970 ± 60	AR 6	3°35'W	19°15'N	<i>Caelatura lacoini</i>	U.Q. 370
5010 ± 110	AZ 4	0°50'W	21°00'N	Palaeosoil	GIF 5229
5020 ± 105	AZ 30	0°50'W	20°50'N	<i>Melania tuberculata</i>	U.Q. 173
5270 ± 130	MK 21	5°00'W	21°00'N	Palaeosoil	GIF 5814
5370 ± 100	AZ 50	0°50'W	20°50'N	<i>Limicolaria sp.</i>	U.Q.
5500 ± 130	MC3	4°00'W	22°40'N	<i>Zoothecus insularis</i>	GIF 7874
5590 ± 90	AZ 37	0°45'W	20°50'N	<i>Melania tuberculata</i>	U.Q. 333
5640 ± 150	MT 7/10	4°00'W	22°40'N	Wood in lake clay	GIF 3443
5700 ± 100	MT 27	4°30'W	23°00'N	Charcoal	GIF 6630
5800 ± 800	MT 19	4°35'W	23°35'N	<i>Melania tuberculata</i>	U.Q. 1151
5820 ± 150	AZ 57	0°35'W	20°45'N	<i>Limicolaria sp.</i>	U.Q.
5900 ± 200	AR 5	3°35'W	19°15'N	<i>Biomphalaria pfeifferi</i>	U.Q. 1078
5900 ± 800	MT 7/-3 à -4	4°00'W	22°40'N	Wood in lake clay	GIF 6900
5920 ± 100	MN 32	3°58'W	19°10'N	<i>Melania tuberculata</i>	GIF 6462
6000 ± 110	AZ 20	0°40'W	20°50'N	<i>Limicolaria sp.</i>	U.Q.
6010 ± 120	AZ 54	0°50'W	20°50'N	<i>Melania tuberculata</i>	U.Q.
6050 ± 90	MT 18	4°50'W	23°33'N	<i>Melania tuberculata</i>	GIF 6195
6130 ± 130	AZ 25	1°00'W	19°20'N	<i>Melania tuberculata</i>	GIF 5225
6165 ± 130	AZ 4	0°15'W	20°30'N	<i>Limicolaria sp.</i>	U.Q.
6220 ± 310	AZ 32	0°40'W	20°40'N	Fish bones	GIF 5443
6340 ± 130	AZ 22	0°40'W	20°50'N	Charcoal	GIF 5228
6480 ± 208	AZ 22	0°40'W	20°50'N	<i>Limicolaria</i>	LGQ 46
6500 ± 100	MT 7-0	4°00'W	22°40'N	Wood in lake clay	GIF 6469
6540 ± 130	AZ 22	0°40'W	20°50'N	<i>Limicolaria sp.</i>	GIF 5232
6590 ± 320	AZ 54	0°50'W	20°50'N	Fish bones	GIF 5444
6605 ± 140	AZ 22	0°40'W	20°50'N	<i>Melania tuberculata</i>	U.Q. 317
6640 ± 100	MT 7/6	4°00'W	22°40'N	Wood in lake clay	GIF 6123
6650 ± 130	MK 42	0°44'W	21°15'N	<i>Melania tuberculata</i>	GIF 5812

6680 ± 110	MT 27s	4°30'W	23°00'N	<i>Zoothecus insularis</i>	GIF 6124
6720 ± 90	AZ 29	0°40'W	20°40'N	<i>Melania tuberculata</i>	U.Q. 252
6760 ± 110	MT 7/ 3	4°00'W	22°40'N	Wood in lake clay	GIF 6862
6760 ± 130	AZ 41	0°40'W	20°40'N	<i>Limicolaria sp.</i>	U.Q.
6790 ± 70	MT 6/i	3°40'W	22°34'N	Organic matter	GIF 6863
6970 ± 130	AR 7	3°55'W	19°10'N	Fish bones	GIF 5495
6980 ± 320	MT 25	4°50'W	23°33'N	Charcoal	GIF 6198
6990 ± 130	MK 30	4°45'W	20°40'N	<i>Melania tuberculata</i>	GIF 5810
7050 ± 80	MK 22	4°35'W	20°40'N	<i>Melania tuberculata</i>	U.Q. 367
7054 ± 357	MC 10	4°00'W	22°40'N	<i>Melania tuberculata</i>	LGQ 150
7235 ± 135	AZ 46	0°50'W	20°30'N	<i>Caelaturae lacoini</i>	U.Q.
7295 ± 95	AZ 22	0°40'W	20°50'N	<i>Melania tuberculata</i>	U.Q. 318
7450 ± 130	MK 36	4°46'W	20°40'N	<i>Melania tuberculata</i>	GIF 5811
7470 ± 130	AZ 33	0°40'W	20°50'N	<i>Melania tuberculata</i>	U.Q. 271
7535 ± 135	AZ 55/57	1°00'W	20°50'N	<i>Melania tuberculata</i>	U.Q.
7550 ± 100	AZ 22	0°40'W	20°50'N	Calcified <i>Phragmites</i>	U.Q. 308
7600 ± 100	MT 23	4°50'W	23°40'N	<i>Melania tuberculata</i>	U.Q. 1144
7628 ± 217	MC 6	4°00'W	22°40'N	<i>Melania tuberculata</i>	LGQ 149
7680 ± 130	AZ 32	0°38'W	20°50'N	<i>Melania tuberculata</i>	U.Q. 256
7790 ± 70	AZ 19	0°40'W	21°00'N	<i>Biomphalaria pfeifferi</i>	GIF 5226
7790 + 80	MT 7/1	4°00'W	22°40'N	Organic matter in lake clay	GIF 7895
7830 ± 185	AZ 34	0°40'W	20°50'N	<i>Melania tuberculata</i>	U.Q. 270
7930 ± 145	AZ 55/58	0°55'W	20°50'N	<i>Melania tuberculata</i>	U.Q.
7980 ± 100	AZ 22	0°40'W	20°50'N	<i>Melania tuberculata</i>	U.Q.
8100 ± 140	AZ 53	0°55'W	20°50'N	<i>Melania tuberculata</i>	U.Q.
8300 ± 100	MT 6b	3°40'W	22°34'N	<i>Melania tuberculata</i>	GIF 6196
8440 ± 320	AZ 45	0°40'W	20°30'N	<i>Biomphalaria pfeifferi</i>	U.Q. 275
8450 ± 60	AR 8	3°55'W	19°10'N	<i>Melania tuberculata</i>	U.Q. 368
8500 ± 120	MN 1	3°02'W	17°25'N	<i>Melania tuberculata</i>	GIF 6461
8540 ± 120	MF 18	2°35'W	22°00'N	<i>Melania tuberculata</i>	GIF 6864
8560 ± 90	AZ 43	0°45'W	20°40'N	<i>Melania tuberculata</i>	U.Q. 332
8560 ± 90	AZ 23	0°40'W	20°50'N	<i>Melania tuberculata</i>	U.Q. 332
8600 ± 100	MT 27a	0°40'W	23°00'N	<i>Melania tuberculata</i>	U.Q. 1142
8700 ± 100	MT 28	4°35'W	23°00'N	<i>Melania tuberculata</i>	GIF 6194
8700 ± 200	AR 5	3°35'W	19°15'N	<i>Melania tuberculata</i>	U.Q. 1019
8800 ± 100	MT 30d	3°46'W	22°40'N	<i>Melania tuberculata</i>	U.Q. 1148
8800 ± 200	AR 1	3°00'W	18°50'N	<i>Melania tuberculata</i>	U.Q. 1021
8990 ± 200	AZ 36	0°40'W	20°50'N	<i>Melania tuberculata</i>	U.Q.
9120 ± 100	MC 10	4°00'W	22°40'N	Travertine	Gd 5436
9236 ± 268	MT 9/1	4°30'W	23°10'N	Calcified <i>Phragmites</i>	LGQ 62
9250 ± 100	AR 2	3°00'W	18°00'N	<i>Melania tuberculata</i>	U.Q. 1051
9320 ± 260	AZ 22	0°40'W	20°50'N	<i>Melania tuberculata</i>	U.Q. 272
21000 ± 300	MT 32	3°10'W	22°20'N	<i>Melania tuberculata</i>	U.Q. 1149

**Tabl. 1 - Radiocarbon ages for malian Sahara from material associated with a humid climate: lake fauna, calcified stems of aquatic plants and travertine, paleosols, human settlements.**

**Dating:** S. Biéda, R. Lafont (LGQ) ; G. Delibrias, M. Fontugne (GIF) ; C. Hillaire-Marcel, S. Ochiatti, P. Pagé (UQ) ; M. Pazdur (Gd).



previously only known in the Upper Pleistocene of the Maghreb and Nubia and the Lower Holocene of southern Morocco. This shows the possibility of migration throughout the Sahara between the end of the arid phase in northern Sahara, at c 9 300 B.P. (Gasse *et al.*, 1987), and 7000 B.P. (Dutour, 1986; Petit-Maire and Dutour, 1987).

Fish remains were never collected in the part of the 90 000 m<sup>2</sup> interior delta where an organized hydrographical system was observed, while they are plentiful in the dry lakelets to the N. of Arawan: the surface connections feeding the inundation flat retracted southwards progressively between 9 000 and 3 500 B.P., allowing species migration back to the Niger, while seasonal small channels between the Mreyyé-Bouera pools and the delta dried up rapidly enough to trap the aquatic fauna in the henceforth closed shallow depressions.

A strong increase of rainfall upon the Fouta-Djalou at around 9 000 B.P. is implied by such a wide expanding of the Niger volume, upstream the Taoussa defilé, possibly partly obstructed by Upper Pleistocene eolian barriers.

A tentative estimation of local palaeoprecipitations over the Azawad can only be made through environmental data, since the respective parts of the Niger (nappe and surface effluents) and of rainfall in the lacustrine rise cannot be appreciated. The evidence for sahelo-sudanian trophic chains in a wooded grassland points to annual means of c. 400 mm, considering the present repartition of biotopes in West Africa (Maley, 1981).

c. The northern part of malian Sahara, located between Dhar Khnachich and Trhaza (22°-24°N, fig. 2) provided with the most significant palaeoclimatic data, since it closely fits the requirements for unbiased palaeometeorological interpretations (remoteness from oceanic and high areas, no allocthonous hydrological inputs, no anthropic action upon the environments) and supplied with continuous sections and cores throughout the Holocene. Large structural depressions and doleritic dykes forming natural barriers promoted lake formation during wet phases, while the deep geological structure impeding communication with other basins (Villemur, 1967 and private documents) allows interpretation in terms of rainfall.

Between 1982 and 1985, holocene lakes were observed all over this area, their radiocarbon ages covering a span of time from 9 000 to 4 500 B.P.; aquatic (Ostracods, Molluscs), terrestrial faunas (Pulmonae snails, crocodiles, rhinoceros, elephants, hippopotamus, large antelopes) and man lived during that phase in this presently wholly desertic area, given 5 mm mean annual rainfall (Petit-Maire, 1986). Fish was never found in the deposits, to the difference of the basins described *infra*, thus confirming the absence of surface connections with the Niger, Tilemsi or other systems (the larva of Ostracods and Mollusca being transported from lake to lake by migrating birds, to the difference of more fragile fish eggs).

In the last 4 years, continuous fossiliferous sedimentary sequences (natural sections and cores) were studied from two palaeolakes -Haijad and Agorgott- in the proper Taoudeni area, at 22°-23°N/3°-4°W. They provided a sharp time resolution for the Holocene climatic evolution, together with a rich pollen record (Petit-Maire, 1986, 1987, 1988; Petit-Maire *et al.*, 1987; Schulz, 1987; Aucour, 1988; Fabre and Petit-Maire, 1988; Petit-Maire, 1988; Schulz, 1988).

Haijad clayey-carbonated dissected deposits rest in disconformity upon Carboniferous red impervious clays, in their contact area with the large calcareous glaciais of Hammada el Haricha. They are dated 8 300 at the base and 4 400 at the top (table. 1) and contain Ostracods and Molluscs, but very few pollen.

At Taoudeni, the lowest depression in the basin, the evolution was saline (the famous salt layers are worked since the XVI<sup>th</sup> century). The study of the mining section was completed by coring, in 1985 and 1988. To this day, the span of time covered by radiocarbon dating of wood debris and

organic matter in green clays ranges from 3 800 B.P. at the top (last clay layer under the surface clayey sandstones) to 7 760 B.P. (clay below the main halite deposition, still not the lake bottom). Pollen abound in the whole sequence. Five meters above the present sebkha level, a layer of calcareous concretions around *Phragmites* stems border a was bed and were dated at 9 236 B.P.

Both Haijad and Taoudeni sequences are finely stratified. Their hydrological and biological evolutions could be defined and correlated as follows, according to 10 radiocarbon dates (table 1, fig. 4).

- c 9 000 B.P.: Climatic change and initiation of the humid phase. Swampy soils form upon the palaeozoic red clays. At 8 800 B.P., shallow lakes exist. Mud cracks and fine calcareous crusts infer seasonal rainfall.

- c 8 500/8 300 B.P. to c 6 700 B.P. high lake levels are reached. The sedimentation rates increase. Lakes become permanent, although levels vary. At Haijad, Molluscs (*Bulinus truncatus*, *Biomphalaria pfeifferi*, *Lymnaea natalensis*, *Corbicula africana*, *Caelatura lacoini*) indicate low salinities confirmed by the Ostracods, exceptionally plentiful in all layers (*Cyprideis sp.*, *Cyprinotus sp.*, *Darwinula sp.*): the Sr/Ca and Mg/Ca ratio in *Cyprideis* shells indicate values of 2 to 6‰. According to Ostracod morphology, seasonal contrast is slight. At Agorgott, only *Cyprideis sp.* can live, in small quantity and in a less favourable biotope, but however showing still tolerable salinities in Taoudeni lake as confirmed by sediment study (Aucour 1988). The pollen content of the glauberitic muds, rich in organic matter, at the base of the 1985 core (> 6 760 B.P. correlated with a > 6 790 B.P. layer at Haijad) is of sahelian species (Combretaceae, Sapindaceae, *Securinega*, *Diospyros*, *Celtis*, *Lannaea*, *Maerua*, *Salvadora*, *Capparis*, *Cadaba*, *Fagonia*, *Cassia*, *Grewia*, *Acacia seyal*) demonstrating the existence, up to 23°N at least, of an environment nowadays found at 17°N. This terrestrial vegetation subsisted until 6 000 B.P., at least 500 years after the beginning of the hydrological change.

- 6 700 - 4 500 B.P.: Climatic deterioration. All the sedimentary and biological data in both lakes point of a deep P/E change at c 6 700 B.P. At Haijad, sedimentation rates are 5 times lesser than before; the presence of the Ostracods *Candona neglecta* and *Limnocythere africana*, together with a greater polymorphism of *Cyprideis sp.*, indicate a higher alkalinity at Haijad. At Agorgott, thick halite layers are deposited (about 7 million tons in a 16 km<sup>2</sup> lake). However, both lakes remain permanent, although their levels become more variable. No sand layer is observed in any section, which excludes at Taoudeni the aeolian episode described elsewhere in northern Mali (Riser *et al.*, 1983). The environment, after 6 000 B.P., endures a progressive degradation. Sahelian species are progressively replaced by a saharo-sahelian vegetation. Man seems to have lived in the area at around 7 000 B.P. which fits the necessary time of migration for semi-nomadic groups; the short duration of the occupation is probably due to the rapid decrease in food resources.

- 4 500 B.P.: End of the humid phase. Lake deposits upstream the Taoudeni depression turn into swamp travertines and heavy sheet-floods show a type of run off already characteristic of arid lands. At 4 500 B.P., the Haijad lake dries up; at 4 000 B.P., mud cracks appear on the margins of Agorgott lake while fine sand layers now show in the sequences. The top layers suddenly change into gross clayey sandstone, presently ploughed by the sebkha saline efflorescences. The lack of salt in the upper layers also indicate a quick lowering of the aquifer, due to a drastic change in the Precipitation/Evaporation ratio. Terrestrial Pulmonae (*Zoothecus*

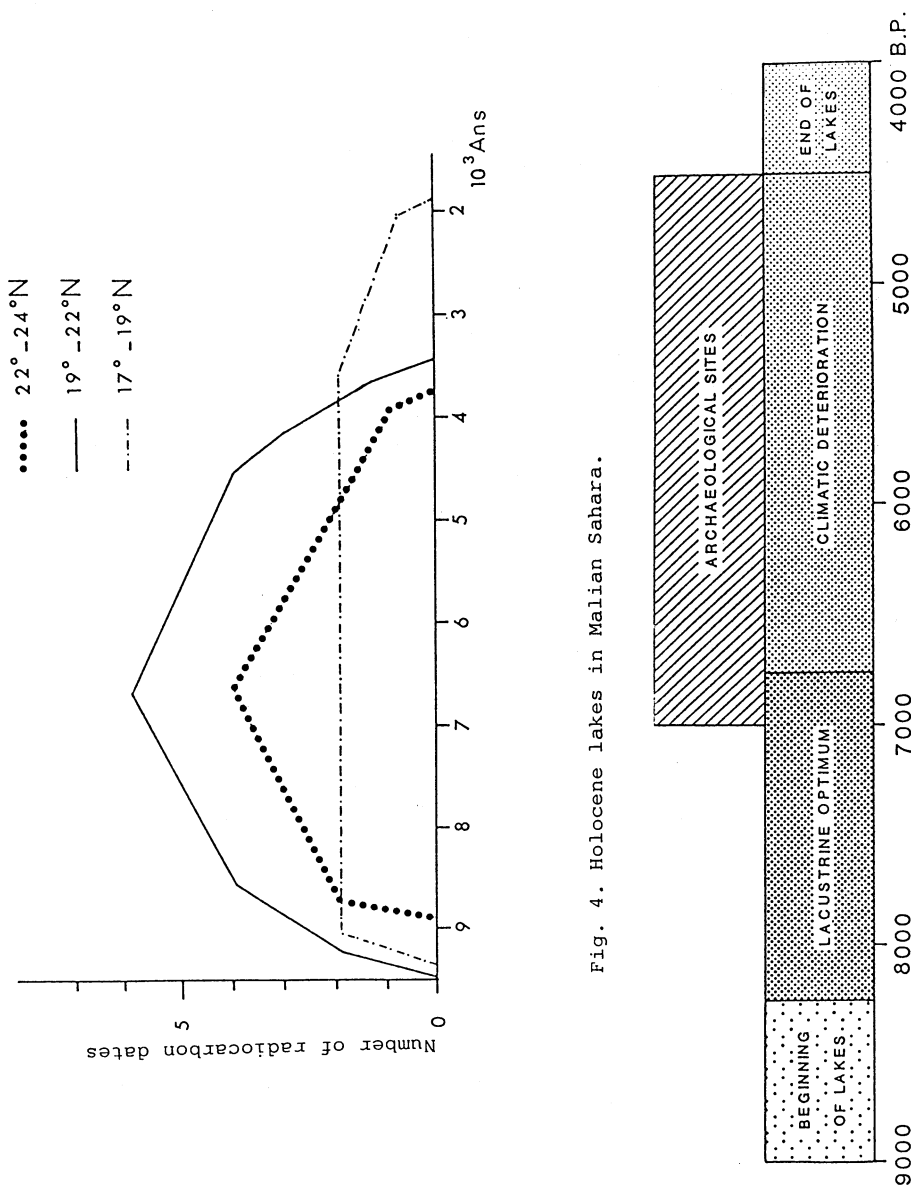


Fig. 4. Holocene lakes in Malian Sahara.

Fig. 4. Holocene lakes in Malian Sahara.

*insularis*) live in the wet clayey infilling of Holocene and Pleistocene travertines until 4 500 B.P. but, except for short incursions of nomadic groups, man has long left the area. At 4 500 B.P., the vegetal cover is of a fundamental saharan type but some sahelian trees (*Acacia seyal*, *Balanites*, *Maerua*) still live near the depression.

At 4 000 B.P. all lakes are dry, except for some residual water at Agorgott, and the present saharan environment has settled. The sahelian fauna and man have long emigrated into more hospitable areas. To-day, the salt mines around two magnesian wells are the only active point in this vast region.

The humid conditions thus had, in this isolate area, a minimal duration of 2 000 years for the optimum itself (8 500-6 500 B.P.) and 5 000 years on the whole.

A tentative estimation of the palaeoprecipitations can be made out of two elements: vegetation and water volume. The presence of a sahelian vegetation between 7 000 and 6 000 B.P. implicates mean annual rainfall ranging from 100 mm to 500 mm, the former corresponding to the present northern limit of the Sahel (Maley, 1981). Besides, for a total drainage basin of only  $c$  34 000 km<sup>2</sup>, the volume of surface fresh water in the 50 km long depression between El Guettara and Taoudeni (fig. 4) varied, according to changes in level, between a maximum of 3 billion m<sup>3</sup> and a minimum of 73 million m<sup>3</sup>: even considering that nebulosity reduced albedo and evaporation, it suggests that the pluvial amount accounting for such numbers could have reached some 300 mm, although no element allows, in his moment, any precise calculation.

The origin of these precipitations is shown by pollen transport and reduced seasonality. The pollen content at Taoudeni indicates, between 7 000 and 6 000 B.P., a monsoonal regime with frequent intrusions of northern depressions (Schulz, 1987) and, after 6 000 B.P., a high predominance of southern markers. The reduced seasonality shown by lake permanence and Ostracods morphology (Carbonel in prep. and also examined after isotopic ratios under way by Sarnthein and Tetzlaff), also implies occurrence of winter rains due to either meridional (as those observed at Taoudeni in february 1988) or boreal depressions. The observation of holocene lakes in northern Sahara (Callot, 1984; Fontes *et al.*, 1985; Gasse *et al.*, 1987), of brown paleosols and fresh water Molluscs in the Tanezrouft, confirm the anthropological inferences (cf. *supra* and Dutour, 1986; Petit-Maire and Dutour, 1987) of a total disappearance of the hyperarid belt in the early Holocene, northern and southern rains covering the whole of present Sahara (Petit-Maire, 1986, 1987).

## 2.2. The atlantic margin of the Sahara

The climate of coastal Sahara between 28° and 19°N (including the lowlands in Fuerteventura island) is presently strongly influenced by the cold Canary current (always less than 20°C in temperature) and the strong northeastern trade winds. This dynamic and thermic barrier results, especially North of Cape Blanc where the stream is parallel to the shore, into a foggy and windy desert with mean annual rainfalls ranging from 52 mm at Laayoune and on the eastern coast of Fuerteventura, to 28 mm at Nouadhibou (Dubief, 1963).

Palaeoenvironmental research in 1970-1979 (Petit-Maire ed., 1979; Petit-Maire, 1979; Rosso and Petit-Maire, 1979; Petit-Maire, 1980) and in 1985-1987 (Petit-Maire *et al.*, 1986, 1987, 1988), supported by 112 radiocarbon dates, resulted into the following main conclusions.

In the Tarfaya basin and Fuerteventura island (some 100 km across) saharan dust deposited during the Late Pleistocene, due to a strong increase of the trade-winds (Sarnthein *et al.*, 1981) and of continental Sahara deflation. However, well stratified layers of terrestrial Molluscs (Helicidae, *Rumina decollata*) and surprisingly plentiful nests of Hymenoptera interrupted aeolian deposition at 15 000 B.P., 13 500-12 500 B.P. and 10 500-9 800 B.P. (Petit-Maire *et al.*, 1986, 1987), testifying to brief soil development. Near Tarfaya, epipaleolithic groups can live on already fixed dunes at 10 400 B.P., at some kilometers from the shore, considering the c 40 km extension of the continental plateau and the sea-level then still about 35 m below present m.s.l. No other biogeographical data (the only mammal found was *Lycaon pictus*, the african wolf, rather insignificant considering the nearby high areas) infer great environmental change quickly associated with the end of aeoliation, which may be related to the fact that, at Cape Juby, cold waters are still implied by presence of *Amygdala decussata* at 8 000 B.P.

The holocene marine transgression deeply modified the low shoreline of occidental Sahara. Deep palaeobays, now turned into paralic sebkhas, as well as the neolithic middens lining them, provided information on the evolution of the Mollusc fauna in the last 10 000 years. Between 6 000 and 2 500 B.P., striking changes took place in the distribution of 30 species (fig. 5). The frequency of occurrence and the density of shells indicate a progressive shift in ecological conditions, with an optimum towards 4 500 B.P. Among them, the most significant tropical species (*Cymbium tritonis*, *C. marmoratum*, *Anadara senilis*, *Venericardia ajar*, *Donax rugosus*) which nowadays live down to the Angola coast, reached Cape Juby (28°N) or Rio de Oro Bay (24°N) and proliferated in undoubtedly warm waters, even in those parts of the shore where morphology did not allow shallow warmer gulfs. Since larva were unable to ascend strong streams or stand cold waters, one must assume a weakening or a cessation of the Current and of the upwelling, during that period. These data corroborate the research by Sarnthein and Koopmann (1980), Diester-Hass (1980) and Rossignol-Strick and Duzer (1979), concluding to a breakdown of the anticyclonic cell over the East-Atlantic margin and a generally sluggish harmattan. On land, human life had become possible but sites are scarce and probably nomadic or semi-nomadic. This could mean that the populations did not live along the coast before that time, but only roamed from inland to collect sea-food. High lake levels and big game remains (fig. 6), found 50 to 100 km inland (Delibrias *et al.*, 1976), well explain that the coastline may have seemed less attractive to a primitive economy than a biotope richer in Gramineae.

After the end of the major transgressive episode at 4 200 B.P., despite the occurrence of two positive oscillations at 3 500 and 2 500 B.P. (Einsele *et al.*, 1974) the shallow holocene gulfs turn into lagoons which, at 2 000 B.P., have completely evaporated (Ortlieb, 1975; Delibrias *et al.*, 1976). The proliferation of tropical Molluscs lasted until 3 000 B.P. to the south of 23°N, but the shells get smaller and thinner, due to abnormal salinity. Mangrove still spreads up to Cape Tafarit (Hébrard, 1973). Inland, lakes only dry up totally at 3 000 B.P. (Delibrias *et al.*, 1976), possibly in relation with the marine level impact upon the phreatic nappes. In opposition with the 6 000- 4 000 period, the large number of neolithic sites all along the coast (Petit-Maire *et al.*, 1973 to 1979; fig. 7) proves continuous (south of Cape Blanc) or seasonal occupation, still made possible by the relictual environments due to oceanic humidity. Pollens show a rate of Gramineae of 22%, which is very high, considering the normal dominance of Chenopodiaceae in littoral areas (Bonnefille et Vincens, 1977), and may correspond to a 80% rate inland (pers. comm. Rossignol-Strick, 1979).

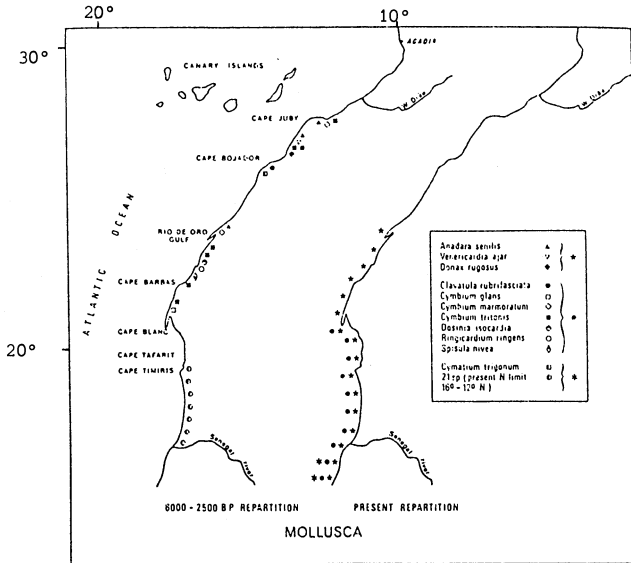


Fig. 5. Comparative distribution of marine Mollusca in the last 6 000 years.

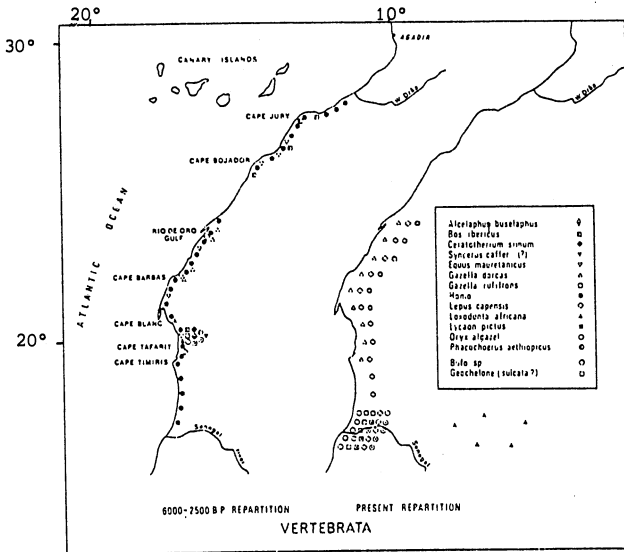


Fig. 6. Comparative repartition of large mammalian fauna and human occupation, in the last 6 000 years.

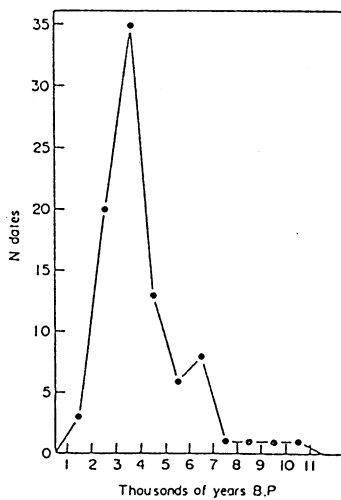


Fig. 7. Radiocarbon dates for human sites  
28° - 19°N.

This is confirmed by the presence, up to 20°30'N, at 4 500 and up to 3 000 B.P., of sahelian mammals (elephant, phacochoerus, hippopotamus, white rhinoceros and large ungulates such as *Alcelaphus buselaphus*). They live nowadays at a maximal latitude of c. 16°N (fig. 6), but hunting losses should be considered for valuable argumentation on mammalian presence or absence.

At 2 500-2 000 B.P., the shores of atlantic Sahara are deserted, although a nomadic natural life is still possible along the coastline north of the Seguiet-el-Hamra, due to wadi inflows from the high areas.

These data imply persistence of semi-arid conditions in the coastal Sahara at least until 3 000 B.P. Although the coast N. of Cape Blanc was always drier than the more southern area, the attenuated wind and current processes still resulted there into environmental improved conditions.

### 3. Conclusions

1. The first deglaciation steps in the Late Pleistocene (Duplessy *et al.*, 1981; Mix and Ruddiman, 1985) resulted into immediate wetter conditions in the most oceanic areas of the Sahara. They seem to have had no effect upon the presently hyperarid basins at continental longitudes along the Tropic of Cancer.

2. The Late-Pleistocene interglacial global stage had, in the Sahara, major effects than the Holocene one as reflected by lakes extension and depth. In the Taoudeni basin, Eemian lake levels are 20-25 m higher than the Holocene ones in the same depressions. In the Fezzan and Shati valley, the > 2 000 km<sup>2</sup> stage 5e lake has nothing in common with the shallow strings of holocene lakelets also recorded in the area (Petit-Maire and Delibrias, 1979; Petit-Maire, 1982). The holocene wet phase had, at Taoudenni, a duration of 4 500-5 000 years with a short optimum of only 2 000 years. Glacial conditions are already prevailing in wind regime in the Sahara (Sarnthein *et al.*, 1981), even in its oceanic belt.

3. Sahelian environmental conditions at 8 000-6 000 B.P., up to 23°N at least, are proved for western Sahara. Ritchie and Haynes (1987) and Pachur and Kröpelin (1987) corroborate the fact in eastern Sahara (Sudan). Biogeographical factors implicate total disappearance of the hyperarid belt at least for one or two milleniums before 7 000 B.P. This can be related with Callot (1984), Fontes *et al.* (1985) and Gasse *et al.* (1987) research between 28° and 30°N in Algeria, showing optimal hydrological conditions during the same span of time.

Monsoon rains, tropical depressions, atlantic and mediterranean rains have to be implicated to account for the observed processes, which fits the models by Berger (1978) and Kutzbach (1979 to 1988).

The Sahel northern limit shifted about 1 000 km to the north between 18 000 and 8 000 B.P. and about 600 km to the south between 6000 B.P. and the present (fig. 8). The assession by Cloudsley-Thompson (1977) that a shift in climatic zone of 1° in 100 years corresponds to a rainfall difference of 40-50%, would imply values widely over those tentatively estimated in this paper.



## RECENT CHANGES IN SAHARA-SAHEL LIMIT

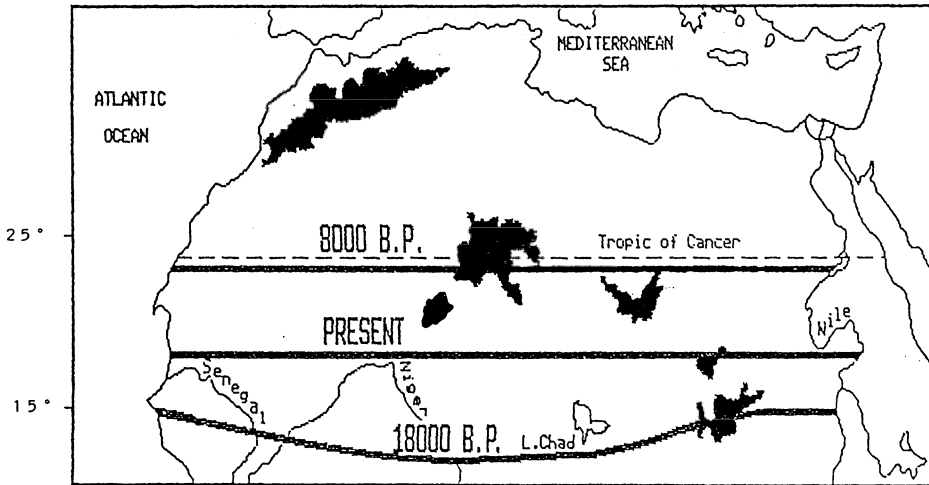


Fig. 8 . Recent changes in Sahara-Sahel limit.

4. In both interglacial phases, the end of the optimum appears to have occurred sharply, provoking large thanatocoenosis. The Shati and Taoudeni palaeolakes, on account of their size and fossiliferous vegetal and animal material, in an extant hyperarid context, could provide further key information upon differential change at the onset and degradation of stages 5 and 1 climatic phases. Surface palaeobiological observations should there again precise and complete the hydrological data, in order to define with greater confidence the real part of local rainfall in the variations of surface water volumes.

#### 4. References

- Aucour, A.M. (1988), 'Le paléolac de Taoudenni (Sahara malien). Etude sédimentologique et implications paléoclimatiques'. In: H. Hagedorn and R. Baumhauer (Eds.) *Geowissenschaftliche Untersuchungen in Afrika*: 87-102. (Würzburger geographische Arbeiten, 69).
- Aucour, A.M. (1988), 'Sédimentologie des dépôts lacustres holocènes de la région de Taoudenni (Mali). Implications paléoclimatiques'. Université Aix-Marseille, 2: Thèse Doctorat, 1988. 165 p.
- Ballais, J.L. and Ben Ouezdou, H. (1987), 'Formes et dépôts du Quaternaire continental de la bordure présaharienne du Maghreb oriental. Essai de synthèse provisoire'. *Conférence P.I.C.G.* 210: 18-19.
- Berger, A.J., Tricot, C. (1986), 'Global climatic change and astronomical theory of palaeoclimates'. In: A. Cazenave (Ed.) *Earth Rotation: solved and unsolved problems*: 111-129. Dordrecht (NL): Reidel.
- Berger, A.L. (1978), 'Long-term variations in daily insolation and Quaternary climatic changes'. *Journal of atmospheric Sciences*, 35: 2362-2367.
- Berger, W.H., Killingley, J.S., Metzler, C.V., and Vincent, E. (1985), 'Two-step deglaciation: 14C-dated high-resolution 18O records from the tropical Atlantic Ocean'. *Quaternary Research*, 23: 258-271.
- Blanc-Vernet, L. (1982), 'Les faunes d'Invertébrés: Foraminifères'. In: N. Petit-Maire (Ed.) *Le Shati, lac pléistocène du Fezzan*: 72-77. Paris: CNRS.
- Blanc-Vernet, L. (1983), 'Foraminifères'. In: N. Petit-Maire and J. Riser (Eds.) - *Sahara ou Sahel? Quaternaire récent du Bassin de Taoudenni*: 181. Marseille (FR): Imprimerie Lamy.
- Bonnefille, R., and Vincens, A. (1977), 'Représentation pollinique d'environnements arides à l'Est du lac Turkana (Kenya)'. In: *Recherches françaises sur le Quaternaire, INQUA 1977*: 235-247. (Suppl. Bull. Ass. Fr. Et. Quatern., 50).
- Broin, F. de (1983), 'Chéloniens'. In: N. Petit-Maire and J. Riser (Eds.) - *Sahara ou Sahel? Quaternaire récent du Bassin de Taoudenni*: 211-233. Marseille (FR): Imprimerie Lamy.
- Buffetaut, E. (1983), 'Crocodyliens'. In: N. Petit-Maire and J. Riser (Eds.) - *Sahara ou Sahel? Quaternaire récent du Bassin de Taoudenni*: 235-238. Marseille (FR): Imprimerie Lamy.
- Callot, Y. (1985), 'Dépôts lacustres et palustres quaternaires de la bordure nord du Grand Erg Occidental (Algérie)'. *Comptes Rendus de l'Académie des Sciences, Paris (D)*, 299: 1347-1350.

- Camps-Fabrer, H. (1983), 'Parures et engins de pêche'. In: N. Petit-Maire and J. Riser (Eds.) *Sahara ou Sahel? Quaternaire récent du Bassin de Taoudenni*: 367-401. Marseille (FR): Imprimerie Lamy.
- Carbonel, P. (1982), 'Ostracodes'. In: N. Petit-Maire (Ed.) *Le Shati, lac pléistocène du Fezzan*: 69-70. - Paris: CNRS.
- Carbonel, P. (1983), 'Ostracodes et paléohydrologie'. In: N. Petit-Maire and J. Riser (Eds.) *Sahara ou Sahel? Quaternaire récent du Bassin de Taoudenni*: 173-179.
- Causse, C. and Hillaire-Marcel, C. (1986), 'Radiochronologies fondées sur le déséquilibre du  $^{230}\text{Th}$  appliquées à l'étude des lacs africains'. In: *Changements globaux en Afrique durant le Quaternaire*. H. Faure, L. Faure and E. Diop (Eds.) *orstom*: 61-63.
- Cloudsley-Thompson, J.L. (1977), 'Man and the biology of arid zones'. Londres (GB): Arnold. 182 p.
- Delibrias, G., Ortlieb, L. and Petit-Maire, N. (1976), 'New  $^{14}\text{C}$  dates for the Atlantic Sahara. Tentative interpretations'. *Journal of human Evolution*, 5: 535-546.
- Diester-Hass, L. (1976), 'Late Quaternary climatic variations in Northwest Africa deduced from East Atlantic sediment cores'. *Quaternary Research*, 6: 299-314.
- Diester-Hass, L. (1980), 'Upwelling and climate off Northwest Africa during the late Quaternary'. In: M. Sarnthein, E. Seibold and P. Rognon (Eds.) *Sahara and the surrounding seas*: 229-238. Rotterdam: Balkema. (Palaeoecology of Africa, 12).
- Dubief, J. (1963), 'Le climat du Sahara, 2'. Alger: Inst. Rech. sahariennes. - (Mémoire h.s.).
- Duplessy, J.C. (1981), 'Oxygen isotope studies and Quaternary marine climates'. In A. Berger (Ed.) *Climatic variations and variability*: 181-192. Dordrecht: Reidel.
- Duplessy, J.C. (1982), 'Glacial to interglacial contrasts in the northern Indian Ocean'. *Nature*, 295: 494-498.
- Duplessy, J.C. and Ruddiman, W.F. (1984), 'La fonte des calottes glaciaires'. *La Recherche*, 156: 806-818.
- Dutour, O. (1986), 'Anthropologie écologique des populations néolithiques du bassin de Taoudenni (Mali)'. Univ. Aix-Marseille 2: Thèse Doct., 1 vol.: 305 p. + Ann.
- Dutour, O. and Petit-Maire, N. (1983), 'Sépultures et restes osseux. In: N. Petit-Maire and J. Riser (Eds.) (1983), *Sahara ou Sahel? Quaternaire récent du Bassin de Taoudenni*'. Marseille (FR): Imprimerie Lamy. 473 p.
- Einsele, D., Herm, D. and Schwarz, H. (1974), 'Sea-level fluctuation during the past 8000 yr at the coast of Mauritania'. *Quaternary Research*, 4: 282-289.

- Fabre, J. (1983), 'Esquisse stratigraphique préliminaire des dépôts lacustres quaternaires'. In: N. Petit-Maire and J. Riser (Eds.) *Sahara ou Sahel? Quaternaire récent du Bassin de Taoudenni*: 421-441. Marseille (FR): Imprimerie Lamy.
- Fabre, J. and Petit-Maire, N. (1983), 'Lacs pléistocènes de la région de Taoudenni (Sahara malien)'. In: *Bassins sédimentaires en Afrique. Séance spécialisée Société géologique de France, Marseille, mars 1983. Résumés des communications*: 99-100. (Trav. Lab. Sci. Terre, Marseille-St-Jérôme, A15).
- Fabre, J. and Petit-Maire, N. (1988), 'Holocene climatic evolution at 22° - 23° N from two paleolakes in the Taoudenni area (northern Mali)'. *Palaeogeography, Palaeoclimatology, Palaeoecology*, 65:133-148.
- Fontes, J.C., Gasse, F., Callot, Y., Plaziat, J.C., Carbonel, P., Dupeuble, P. and Kaczmarska, I. (1985), 'Freshwater to marine-like environments from Holocene lakes in northern Sahara'. *Nature*, 317: 608-610.
- Gasse, F., Fontes, J.C., Plaziat, J.C., Carbonel, P., Kaczmarska, I. De Deckker, P., Soulié-Marsche, I., Callot, Y. and Dupeuble, P.A. (1987), 'Biological remains, geochemistry and stable isotopes for the reconstruction of environmental and hydrological changes in the Holocene lakes from North Sahara'. *Palaeogeography, Palaeoclimatology, Palaeoecology*, 60: 1-46.
- Gaven, C., Hillaire-Marcel, C. and Petit-Maire, N. (1981), 'A Pleistocene lacustrine episode in southeastern Libya'. *Nature*, 290: 131-133.
- Gayet, M. (1983), 'Poissons'. In: N. Petit-Maire and J. Riser (Eds.) *Sahara ou Sahel? Quaternaire récent du Bassin de Taoudenni*: 183-209. Marseille (FR): Imprimerie Lamy.
- Guerin, C. and Faure, H. (1983), 'Mammifères'. In: N. Petit-Maire and J. Riser (Eds.) *Sahara ou Sahel? Quaternaire récent du Bassin de Taoudenni (Mali)*: 239-260. Marseille (FR): Imprimerie Lamy.
- Hillaire-Marcel, C. (1982), 'Paléohydrologie isotopique'. In: N. Petit-Maire (Ed.) *Le Shati, lac pléistocène du Fezzan*: 34-43. Paris: CNRS.
- Hillaire-Marcel, C. (1983), 'Paléohydrologie isotopique des lacs de l'erg Ine-Sakane'. In: N. Petit-Maire and J. Riser (Eds.), *Sahara ou Sahel? Quaternaire récent du Bassin de Taoudenni*: 87-95. Marseille (FR): Imprimerie Lamy.
- Hooghiemstra, H. (1987), 'Pollen in diepzeesedimenten als informatie dragers van Klimaatsveranderingen'. *Vakbl. Biol.*, 67: 345-350.
- Hooghiemstra, H. (in press), 'Late Quaternary changes in vegetation and climate in NW Africa: pollen evidence from marine sediments'.
- Klitzsch, E. (1972), 'Salinität und Herdunft der Grunwassers im mittleren Nordafrika'. *Geologisches Jahrbuch (C)*, 2: 251-260.

- Kutzbach, J.E. (1981), 'Monsoon climate of the early Holocene: climate experiment with the Earth's orbital parameters for 9000 years ago'. *Science*, 214: 59-61.
- Kutzbach, J.E. (1987a), 'The changing pulse of the monsoon'. *Monsoons*: 247-268.
- Kutzbach, J.E. (1987b), 'Model simulations of the climatic patterns during the deglaciation of North America'. *Geology of North America*, 3: 425-445.
- Kutzbach, J.E. and Guetter, P.J. (1986), 'The influence of changing orbital parameters and surface boundary conditions on climate simulation for the past 18,000 years'. *The atmospheric Sciences*, 43/16: 1726-1759.
- Kutzbach, J.E. and Otto-Bliesner, B.L. (1982), 'The sensitivity of the African-Asian monsoonal climate to orbital parameters changes for 9000 years B.P. in a low resolution general circulation model. *Journal of atmospheric Sciences*, 39: 1177-1188.
- Kutzbach, J.E. and Street-Perrott, F.A. (1985), 'Milankovitch forcing of fluctuations in the level of tropical lakes from 18 to 0 Kyr B.P.'. *Nature*, 317: 130-134.
- Leroux, M. (1983), 'Le climat de l'Afrique tropicale'. Paris: Champion, 1983. 2 tomes: 636 p.; 250 cartes.
- Lorius, C., Jouzel J., Ritz, C., Merlivat, L., Barkov, N., Korotkevich, Y. and Kolyatkov V. (1985), 'A 150 000 years climatic record from Antarctic ice'. *Nature*, 316: 591-596.
- Maley, J. (1981), 'Etudes palynologiques dans le bassin du Tchad et paléoclimatologie de l'Afrique nord-tropicale de 30 000 ans à l'époque actuelle. Paris (FR): Orstom. (Trav. Docum.).
- Mix, A.C. and Ruddiman, W.T. (1985), 'Structure and timing of the last deglaciation: oxygen isotope evidence' *Quaternary Science Reviews*, 4: 59-108.
- Monteillet J. and Rosso, J.C. (1977), 'Répartition de la faune testacée actuelle (mollusques et crustacés cirripèdes) dans la basse vallée et le delta du Sénégal'. *Bulletin de l'Institut fondamental d'Afrique noire (A)*, 39/4: 789-819.
- Pachur, H.J. and Kröpelin, S. (1987), 'Wadi Howar: paleoclimatic evidence from an extinct river system in the south eastern Sahara'. *Science*, 237: 298-300.
- Petit-Maire, N. (1979), 'Cadre écologique et peuplement humain: le littoral ouest-saharien depuis 10.000 ans'. *L'Anthropologie*, 83/1: 69-82.
- Petit-Maire, N. (Ed.) (1979), 'Le Sahara atlantique à l'Holocène. Peuplement et écologie'. Alger: C.R.A.P.E. 340 p. (Mém., 28).

- Petit-Maire, N. (1980), 'Holocene biogeographical variations along the northwestern African coast (28° - 19° N). Paleoclimatic interpretations'. In: M. Sarnthein, Seibold and P. Rognon (Eds.) *Sahara and the surrounding seas*: 365-377. - Rotterdam: Balkema. (Palaeoecology of Africa, 12).
- Petit-Maire, N. (Ed.) (1982), 'Le Shati, lac pléistocène du Fezzan'. - Paris/Marseille (FR): CNRS. - 118 p.
- Petit-Maire, N. (1986), 'Paleoclimates in the Sahara of Mali: a multidisciplinary study'. *Episodes*, 9/1: 7-16.
- Petit-Maire, N. (1987), 'Local responses to recent global climatic change: hyperarid central Sahara and coastal Sahara'. In: G. Matheis, H. Schandelmeier (Eds.) *Current Research in African Earth Science*: 431-434. Rotterdam (NL): Balkema.
- Petit-Maire, N. (1988), 'Taoudenni Basin (Mali), Holocene palaeolimnology and environments'. In: H. Hagedorn and R. Baumhauer (Eds.) *Geowissenschaftliche Untersuchungen in Afrika*: 45-52. (Würzburger geographische Arbeiten, 69).
- Petit-Maire, N., Casta, L., Delibrias, G. and C. Gaven with an appendix by A.M. Testud (1980) 'Preliminary data on quaternary paleolacustrine deposits in the Wadi ash Shati, Libya'. In: M.J. Salem and M.T. Busrewil (Eds.) *The geology of Libya*, 3: 797-807. London (GB): Academic Press.
- Petit-Maire, N. and Delibrias, G. (1979), 'Late Holocene palaeoenvironment in the Ghadames area'. *Maghreb Review*, 4: 138-139.
- Petit-Maire, N., Delibrias, G., Méco, J., Pomel, S. and Rosso, J. (1986), 'Paléoclimatologie des Canaries orientales (Fuerteventura)'. *Comptes Rendus de l'Académie des Sciences, Paris*, 303: 1241-1246.
- Petit-Maire, N. and Dutour, O. (1987), 'Holocene populations of the Western and Southern Sahara; Mechtoids and paleoclimates'. In: Close A. (Ed.) *Prehistory of arid North Africa*: 259-286. Dallas (US): Southern Methodist University Press.
- Petit-Maire, N., Fabre, J., Carbonel, P., Schulz, E. and Aucour A.M. (1987), 'La dépression de Taoudenni (Sahara malien) à l'Holocène'. *Géodynamique*, 2/2: 61-67.
- Petit-Maire, N., Gayet, M. (1984) - 'Hydrographie du Niger (Mali) à l'Holocène ancien'. *Comptes Rendus de l'Académie des Sciences, Paris* (2), 298: 21-23.
- Petit-Maire, N. and Riser, J. (1981), 'Holocene lake deposits and palaeoenvironment in central Sahara, northeastern Mali'. *Palaeogeography, Palaeoclimatology, Palaeoecology*, 35: 45-61.
- Petit-Maire, N. and Riser, J. (Eds.) (1983), 'Sahara ou Sahel? Quaternaire récent du bassin de Taoudenni (Mali)'. Marseille : Imprimerie Lamy. 473 p.

- Petit-Maire, N. and Riser, J. (1987), 'Holocene palaeohydrology of the Niger'. In: J.A. Coetzee (Ed.) *Palaeoecology of Africa*, 18: 135-141. Rotterdam (NL): Balkema.
- Prell, W.L. and Kutzbach, J.E. (1987), 'Monsoon variability over the past 150,000 years'. *Journal of geophysical Research*, 92: 8411-8425.
- Raimbault, M. (1983), 'Industrie lithique'. In: N. Petit-Maire and J. Riser (Eds.) - *Sahara ou Sahel? Quaternaire récent du Bassin de Taoudenni (Mali)*: 317-341. Marseille (FR): Imprimerie Lamy.
- Riser, J., Hillaire-Marcel, C. and Rognon, P. (1983), 'Les phases lacustres holocènes'. In: N. Petit-Maire and J. Riser (Eds.) *Sahara ou Sahel? Quaternaire récent du Bassin de Taoudenni*: 65-86. Marseille (FR): Imprimerie Lamy.
- Riser, J. and Petit-Maire, N. (1987), 'Les formations lacustres du bassin d'Araouane et leur rapports avec le paléo-Niger holocène'. In: E. Bonifay (Ed.) - *Travaux français en Paléolimnologie*: 255-260. Le Puy-en-Velay (FR): Imprimerie Jeanne-d'Arc. (Documents du CERLAT, Mémoire, 1).
- Ritchie, J.C. and Haynes, C.V. (1987), 'Holocene vegetation zonation in the eastern Sahara'. *Nature*, 330: 645-647.
- Rosignol-Strick, M. (1983), 'African monsoons, an immediate climate response to orbital insolation'. *Nature*, 304: 46-49.
- Rosignol-Strick, M. and Duzer, D. (1980), 'Late Quaternary West African climate inferred from palynology of Atlantic deep sea cores' In: M. Sarnthein, Seibold and P. Rognon (Eds.) *Sahara and the surrounding seas*: 227-228. Rotterdam: Balkema. (*Palaeoecology of Africa*, 12).
- Rosso, J.C. (1983), 'Mollusques'. In: N. Petit-Maire and J. Riser (Eds.) - *Sahara ou Sahel? Quaternaire récent du Bassin de Taoudenni*: 157-171. Marseille (FR): Imprimerie Lamy.
- Rosso, J.C. and Gaillard, J. (1982), 'Mollusques testacés (macrofaune)'. In: N. Petit-Maire (Ed.), *Le Shati, lac pléistocène du Fezzan*: 55-68. Paris: CNRS.
- Rosso, J.C., Petit-Maire, N. (1978), 'Amas coquilliers du littoral atlantique saharien'. *Bulletin du Musée d'Anthropologie préhistorique de Monaco*, 22: 79-118.
- Sarnthein, M. (1978), 'Sand deserts during glacial maximum and climatic optimum'. *Nature*, 272: 43-46.
- Sarnthein, M. (1979), 'Indicators of continental climates in marine sediments'. *Meteor Forschung-Ergebnisse (C)*, 31: 49-51.
- Sarnthein, M., Erlenkeuser H. and R. Zahn (1982), 'Termination 1: the response of continental climate in the subtropics as recorded in deep-sea sediments'. *Actes du Colloque international CNRS, Bordeaux (FR), septembre 1981*: 393-407. (Bulletin de l'Institut de Géologie du Bassin d'Aquitaine, 31).



- Sarnthein, M. and Koopmann, B. (1980), 'Late Quaternary deep-sea record in Northwest African dust supply and wind circulation'. In: M. Sarnthein, Seibold and P. Rognon (Eds.) *Sahara and the surrounding seas*: 239-253. Rotterdam: Balkema. (Palaeoecology of Africa, 12).
- Sarnthein, M. Tetzlaff, G., Koopmann, B., Wolter, K. and Pflaumann, U. (1981), 'Glacial and interglacial wind regimes over the eastern subtropical Atlantic and North-West Africa'. *Nature*, 293: 193-198.
- Schulz, E. (1987), 'Die holozäne Vegetation der zentralen Sahara'. In: J.A. Coetzee and E.M. Van Zinderen Bakker (Eds.) - *Palaeoecology of Africa*, 18: 143-161. Rotterdam (NL): Balkema.
- Schulz, E. (1988), 'Der Sudrand der Sahara'. In: H. Hagedorn and R. Baumhauer (Eds.), *Geowissenschaftliche Untersuchungen in Afrika*: 45-52. (Würzburger geographische Arbeiten, 69).
- Stein, R., Sarnthein, M. (1984), Late Neogene events of off shore NW Africa : high resolution record from deep-sea sediments. In : J.A. Coetzee, E.M. Van Zinderen Bakker (Eds.). *Palaeoecology of Africa*, 16 : 9-36. Rotterdam: Balkema.
- Villemur, J.R. (1967) - 'Reconnaissance géologique et structurale du Nord du Bassin de Taoudenni', Paris: Bureau de Recherches géologiques et minières. 151 p., Mémoire, 51).
- Wendorf, F., Close, A., Schild, R. (1987), 'Recent work on the Middle Paleolithic of the eastern Sahara'. *African archaeological Review*, 5: 49-63.

**SECTION 6.**

**REPORT OF THE GROUP STUDYING: INFERENCES FROM THE MARINE  
SEDIMENTARY RECORD**

# NORTHEAST ASIAN CLIMATIC CHANGE OVER THE LAST 140,000 YEARS INFERRED FROM POLLEN IN MARINE CORES TAKEN OFF THE PACIFIC COAST OF JAPAN

LINDA E. HEUSSER

Lamont-Doherty Geological Observatory of Columbia  
University, Palisades, NY 10964  
U.S.A.

**ABSTRACT.** Pollen analyses from deep-sea sediment cores V28-304, RC14-99, and RC12-401 provide continuous chronostratigraphic records of the regional vegetation of the Pacific coast of the Japanese archipelago over the last 140,000 years. These detailed pollen time series (with samples at ~2000-year intervals) monitor the changing composition of temperate and boreal montane forests prior to and through the last full glacial cycle. Except for brief intervals, as in the Holocene, conifers were more abundant than deciduous taxa; nonarboreal elements were even less significant in the vegetation of Japan. *Pinus* and *Picea* characterize glacial intervals, and *Cryptomeria*, along with *Sciadopitys*, dominates warm temperate forests of the central and southern coast between ~120,000 and ~70,000yr B.P. Precipitation and temperature indices derived from these pollen/vegetation assemblages show fluctuations related to changes in the northeast Asian summer and winter monsoon.

## 1. INTRODUCTION

The Japanese archipelago is climatically dynamic and diverse. Annual changes in the temperate climates of Japan are characterized by sharp seasonal contrasts — from the winter monsoon winds associated with the northern Siberian, Okhotsk, and Aleutian pressure centers to the summer southern-dominated monsoons (Fig. 1a). Present distribution of the major vegetation zones of Japan reflects these climatic processes (Fig. 1b), particularly atmospheric circulation over the Eurasian continent and Pacific Ocean. For instance, the division between warm and cool temperate forests

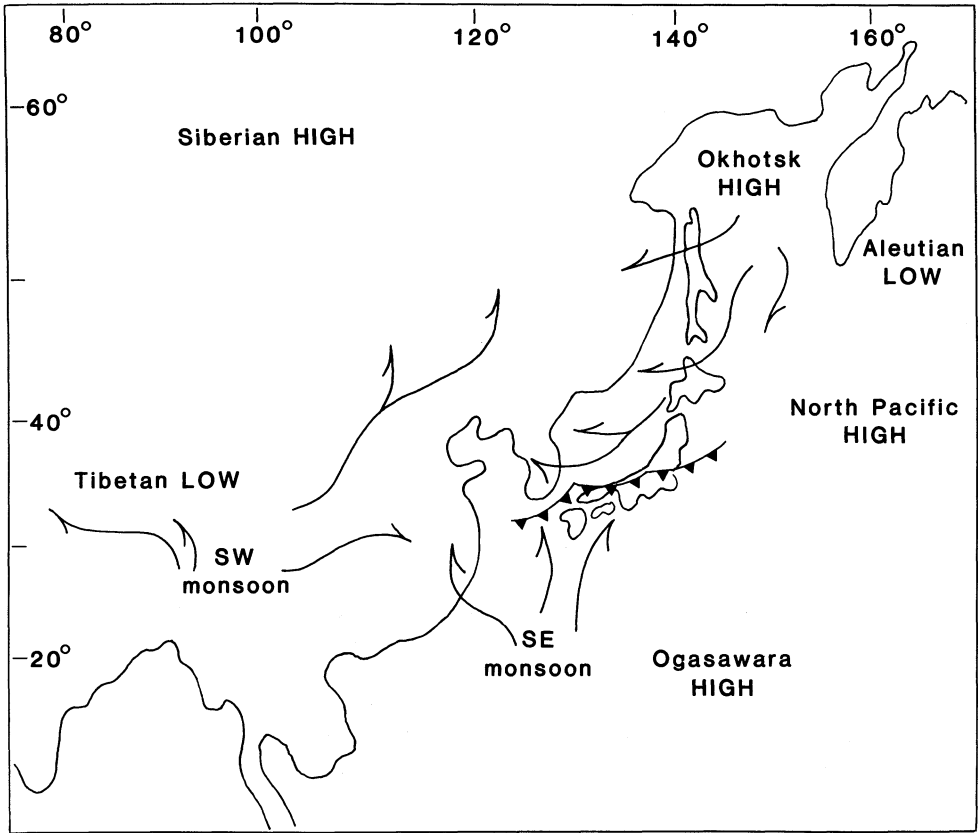


Figure 1a: Dominant atmospheric pressure cells and surface airflow of eastern Asia during the summer. Note the correlation between the position of the atmospheric frontal zone (represented by the dark-toothed line crossing the main island of Honshu, Japan ~39°N) and the marine polar front offshore (the confluence of the subtropical and subarctic gyre, see Figure 1b).

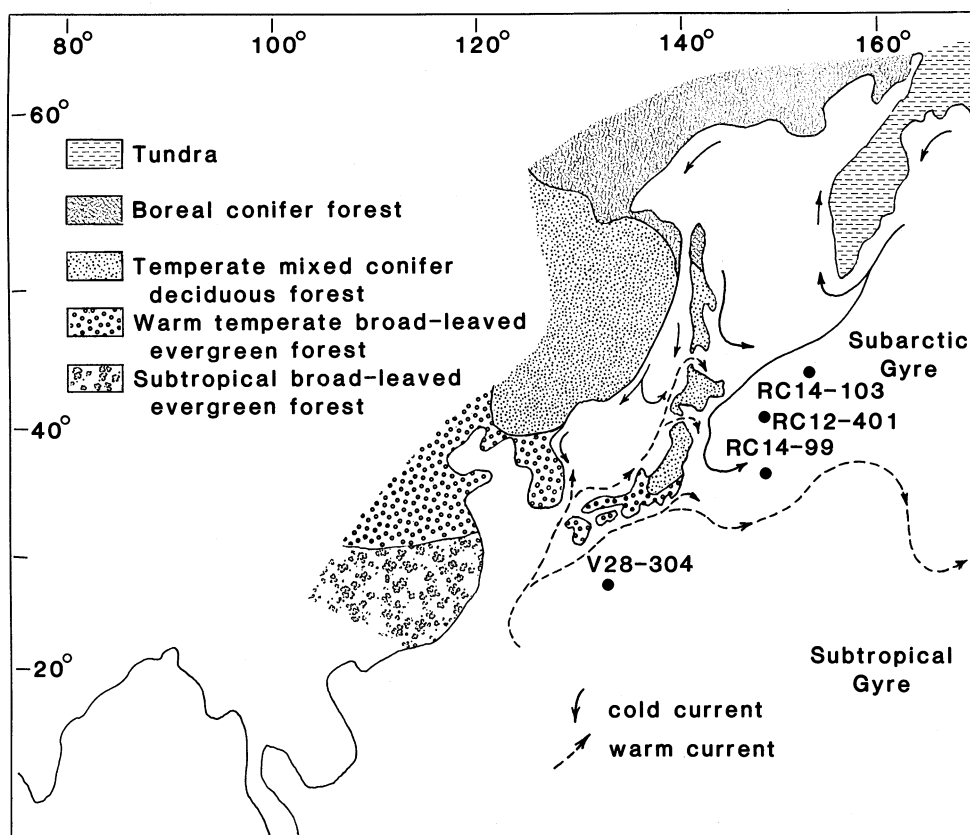


Figure 1b: Schematic distribution of northeast Asian vegetation, locations of marine cores (V28-304, RC14-99, RC12-401, and RC14-103), major surface currents and water masses in the Pacific Ocean. The warm, northflowing Kuroshio current merges with the cold southflowing Oyashio current  $\sim 39^{\circ}\text{N}$ . Zonal distribution of vegetation, closely related to latitudinal temperature and precipitation variations, is highly influenced by large-scale circulation changes associated with seasonal variations in the Asian monsoon. In Japan, average summer temperature and mean annual precipitation range from  $26^{\circ}\text{C}$  and 3000mm in the south to  $18^{\circ}\text{C}$  and 1000mm in the north (Fukui, 1977; Numata, 1974).

(~39°N) corresponds with the position of the atmospheric polar front and adjoins the marine front, the confluence of the two major North Pacific water masses (the subtropical and subarctic gyres).

The flora of the Japanese islands has been stable, with no evidence of plant extinction or migration from the Asian continent since the Middle Pleistocene and possibly since the Pliocene (Jimbo, 1932; Numata, 1974; Tai, 1973). During this time, vegetation of Japan was not totally disrupted nor physically displaced by the physical presence of large ice sheets nor by volcanism.

Although the flora of Japan has been stable for ~2 million years, the composition of Pliocene-Pleistocene vegetation in the Japanese island arc has changed repeatedly (Tai, 1973). In the present and in the past, climate appears to be a principal determinant of changes in vegetation distribution in Japan. Because plant species now growing in Japan have been present in the Japanese archipelago throughout the late Pleistocene, recent vegetation/climate relationships can serve as fairly reliable models to interpret paleoclimates.

The "natural" vegetation of Japan can be divided into three major forest groups: (1) warm-temperate evergreen broadleaf, (2) temperate conifer and deciduous broad-leaf, and (3) subalpine (subboreal) conifer forests (Miyawaki and Sasaki, 1985). It should be noted that these "natural" vegetation zones are all montane; lowland vegetation, which covers less than 17% of the Japanese archipelago, has been severely disturbed for more than 2,000 years. The nature of undisturbed lowland vegetation is essentially unknown. The warm-temperate forests of southern Japan, which reach as far north as 39°30'N on the Pacific coast, include *Castanopsis* (*Chinquapin*) and *Quercus* (oak) with *Sciadopitys verticillata* (umbrella pine), *Tsuga sieboldii* (hemlock), and/or *Abies firma* (fir) in highlands (Toyohara, 1979). Characteristic genera of the mid- and cool-temperate forests which form the primary part of the Japanese flora include: *Fagus* (beech), *Quercus*, *Tsuga*, and *Abies*. Above ~1600-1800m, temperate forests with *Abies mariesii*, *Betula ermanii* (birch), *Picea jezoensis* (spruce), *Tsuga diversifolia*, and *Pinus pumila* (pine) develop (Franklin, et al., 1979; Saito, 1979; 1981; Saito, et al., 1980). Moors and alpine dwarf scrub, with *B. ermanii* and *P. pumila*, occur above ~2400m. On the northernmost island of Hokkaido, broad-leaved deciduous forests merge with forests dominated by *Picea jezoensis* and *P. glehnii*, *Abies sachalinensis*, *B. ermanii*, *P. pumila*, and *Quercus mongolica*. Coastal vegetation is characterized by extensive *Sphagnum* bogs, *Alnus* (alder) swamps, and mixed stands of conifers and hardwoods (Numata, 1974; Watanabe, 1979).

Distribution of Japanese vegetation is primarily related to temperature because precipitation is relatively abundant (1000 to >4000mm *per annum*) throughout the archipelago. Like other mid-latitude oceanic climates, Japan has a small range of annual mean temperature (~6°C to 18°C). Isotherms, which curve northwards on both sides of the islands, reflect the influence of the warm, north-flowing Kuroshio current (Fig. 1a). Southward extension of the cold Oyashio current is responsible for the extremely low summer temperatures on the Pacific coast of Hokkaido (Fukui, 1977).

Climates of Japan are intimately related to dynamics of North Pacific and northeast Asian marine and atmospheric climate processes. Differential heating of the Himalaya-Tibetan massif is a fundamental determinant of the monsoon climates of Japan. Spring (Bai-u) and summer precipitation are primarily related to the southern monsoons, northward movement of the subtropical jet stream, and the intensity of the Ogasawara and North Pacific High. The nature of winter monsoons depends on the development of the Aleutian Low and the Siberian and Okhotsk High pressure systems (Fukui, 1977; Fig. 1a).

Reconstruction of Quaternary climates from pollen recovered from sediments deposited in lakes and bogs in Japan began in the 1930s (i.e., Jimbo, 1932). Some pollen records cover the last 600,000 years (Fuji, 1984); however, the constraints of dating terrestrial sediments > ~30,000 years, place limitations on interpreting such older records of Japanese vegetation and climate. The abundance and diversity of pollen in recent and past marine sediments deposited off the coast of Japan provide detailed, continuous records of Quaternary Japanese vegetation and climate with sample resolution as high as 200 years in rapidly-deposited sediment (Kalil, *et al.*, unpub.). Because each marine-pollen sample is directly correlated with marine paleoclimatic indices from a subset of the same sample, marine pollen data can be precisely correlated with both regional and global chronologies (Imbrie, *et al.*, 1984; Morley, *et al.*, 1982). Thus, pollen records from the northwest Pacific directly relate past changes in vegetation of the Japanese archipelago and in northeast Asian atmospheric circulation to environmental changes in the northwest Pacific Ocean and to global changes in atmospheric and marine circulation.

This paper will focus on pollen records from the last 140,000 years and pollen records from three northwest Pacific Ocean cores with continuous terrestrial and marine paleoclimatic signals (Fig. 1b, Table 1). Cores V28-304, RC14-99, and RC12-401, taken ~1000km east of Japan (along with core RC14-103, Heusser and Morley, 1985b), form a transect across northeast

Table I. Core Data

Core	Latitude	Longitude	Water Depth (m)	Core Length (m)
RC14-103	44 02'N	152 56'E	5365	1528
RC12-401	40 49'N	148 08'E	5415	818
RC14-99	36 58'N	147 56'E	5652	1639
V28-304	28 32'N	134 08'E	2942	824

Table II. Pollen Assemblage Zones for Cores RC12-401, RC14-99, and V28-304

Depth in Core (cm)	Pollen Zone
	<b>RC12-401</b>
0-75	1) Quercus-Pinus
75-200	2) Quercus
200-300	3) Betula-Alnus
300-460	4) Pinus-Compositae-Alnus
460-620	5) Quercus-Pinus-Alnus-Betula
620-700	6) Picea-Alnus-Betula
700-790	7) Pinus-Picea-Tsuga
	<b>RC14-99</b>
0-20	1) Pinus-Cryptomeria
20-60	2) Tsuga-Picea-Abies
60-130	3) Tsuga-Picea-Abies-Cryptomeria
130-190	4) Betula-Sphagnum
190-270	5) Tsuga-Picea
270-340	6) Pinus-Cyperaceae-Sphagnum
340-390	7) Cryptomeria-Sciadopitys
390-450	8) Alnus-Betula-Quercus
450-510	9) Cryptomeria-Sciadopitys
510-560	10) Pinus-Betula
560-600	11) Cryptomeria
600-640	12) Quercus-Betula
640-700	13) Tsuga-Picea-Alnus-Pinus
	<b>V28-304</b>
0-30	1) Pinus
30-80	2) Quercus-Betula-Alnus-Compositae
80-180	3) Tsuga-Quercus-Cyperaceae
180-230	4) Pinus-Tsuga
230-280	5) Alnus-Betula-Cyperaceae
280-310	6) Pinus-Picea
310-340	7) Cryptomeria-Pinus
340-370	8) Pinus-Tsuga
370-420	9) Cryptomeria-Sciadopitys
430-460	10) Pinus-Tsuga
460-480	11) Quercus-Alnus-Compositae



Asian marine and atmospheric fronts ~30-44°N. Climatic data from these cores will be used to reconstruct climates on the Pacific coast of Japan over the past 140,000 years.

## 2. MATERIALS AND METHODS

Samples from cores V28-304 and RC14-99 (taken at 10cm intervals) and RC12-401 (taken at 20cm intervals) were subdivided for pollen, radiolarian, and isotopic analyses. Our sampling strategy was to avoid described or visible tephra layers and core breaks. Pollen preparation (Heusser and Stock, 1984) included addition of exotic pollen to determine pollen concentration and to serve as a reference to estimate effects of staining with Safranin O and other preparation techniques (Berglund, 1986). Variations in pollen preservation meant that criteria used by some Japanese palynologists to distinguish subgenera of *Quercus* (*Cyclobalanopsis* and *Lepidobalanus*) were often not clearly apparent; therefore, pollen identification, using reference collections of modern pollen and spore taxa along with morphological descriptions and keys (including Maeda, 1970; Miyoshi, 1983a,b; Miyoshi and Yano, 1986; Nakamura, 1957; Ueno, 1959) was generally restricted to generic level. Botanical nomenclature follows Ohwi (1984).

Pollen percentages are based on the total pollen number of arboreal and nonarboreal pollen (~300 pollen grains per sample), including *Alnus* and *Cyperaceae* (sedge), pollen types sometimes excluded from basic pollen sums in Japanese pollen diagrams to reduce local over-representation (Tsukada, 1958). Percentages of spores (spores/spores + pollen) are calculated outside the basic pollen sum, as are other microfossils; such as dinoflagellates and charcoal particles (40-150 microns). Pollen data from cores V28-304, RC14-99, RC12-401, and RC14-103 are also synthesized using Q-mode factor analysis. Pollen influx will not be determined until a detailed chronology is established.

Pollen records for each core are divided into site-specific (local) pollen zones and biostratigraphic zones (Birks, 1986), which are restricted to the individual core in which they are described (Table 2, Figs. 2 to 4). At this time, use of local or regional Japanese pollen zone nomenclature (Nakamura, 1952; Tsukada, 1986b) does not seem appropriate for marine pollen zones, even though pollen zones from northwest Pacific cores are correlative with late Pleistocene and Holocene pollen zones from Japan. Note that pollen zones are independent of, and not necessarily coincident with, other stratigraphic zones.

**Table III. Varimax Factor Score Matrix**

	Picea	Quercus	Pinus	Cryptomeria
Pinus	-0.233	0.075	0.932	0.138
Tsuga	0.091	-0.057	0.127	0.144
Larix	0.028	-0.004	-0.001	-0.009
Abies	0.119	-0.035	0.058	-0.042
Cryptomeria	-0.154	-0.027	-0.057	0.812
Picea	0.478	-0.133	0.009	-0.118
Taxaceae	-0.004	0.011	-0.035	0.284
Sciadopitys	-0.059	-0.025	-0.006	0.265
Quercus	-0.331	0.732	0.123	-0.094
Castanea	-0.006	0.01	0.002	0.007
Alnus	0.439	0.316	-0.245	0.339
Celtis	-0.003	0.009	0.001	-0.003
Fagus	-0.052	0.125	0.003	0.047
Betula	0.183	0.512	-0.104	-0.08
Myrica	0.012	0.067	-0.01	-0.008
Corylus	-0.017	0.083	0	-0.002
Ulmus	-0.007	0.118	-0.004	-0.004
Carpinus	-0.003	0.003	0.005	0
Juglans	-0.0101	0.025	0	0.012
Pterocarya	-0.002	0.01	0.002	-0.003
Rosaceae	-0.001	0.011	-0.001	0.007
Salix	0.013	0.015	-0.007	0
Acer	0	0	0	0.001
Tilia	-0.001	0.002	0.001	-0.001
Ericaceae	0.009	0.002	-0.002	-0.001
Ilex	-0.001	0.003	0.001	0
Gramineae	0.088	0.046	-0.006	-0.002
Cyperaceae	0.49	0.035	-0.113	-0.025
Compositae	0.283	0.164	-0.089	0.028
Chenopodiaceae	0.014	0.025	-0.01	0.02

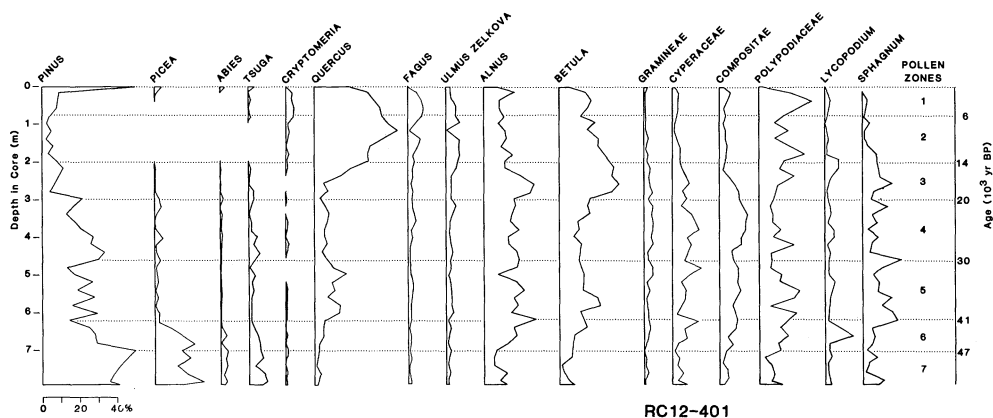


**Figure 2:** Depth plots of percentages of selected pollen and spores from core RC12-401, located at the northern edge of the subarctic front east of cool-temperate, mixed conifer deciduous forest of northern Japan. Pollen assemblage zones (Table 2) are shown on the right. Ages of pollen zone boundaries appear on the far right, and depth in core (meters) is on the left.

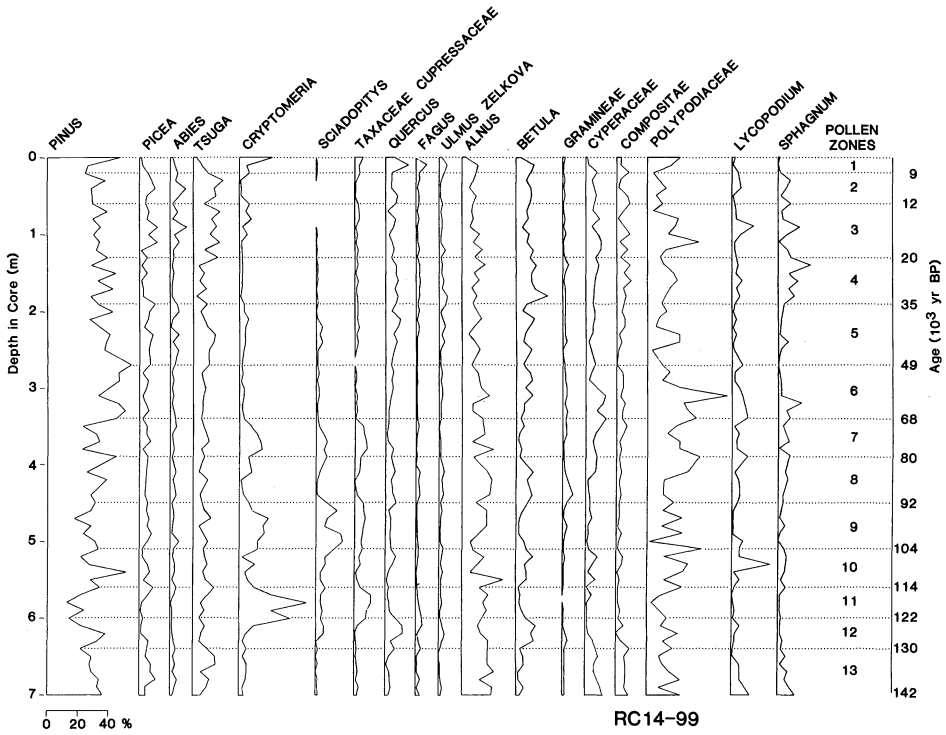


Figure 3: Depth plots of percentages of selected pollen and spores from core RC14-99, located in the marine transition zone between subtropical and subarctic gyres and adjacent to the transition between warm and cool temperate Japanese vegetation. Pollen assemblage zones (Table 2) are shown on the right. Ages of pollen zone boundaries appear on the far right, and depth in core (meters) is on the left.

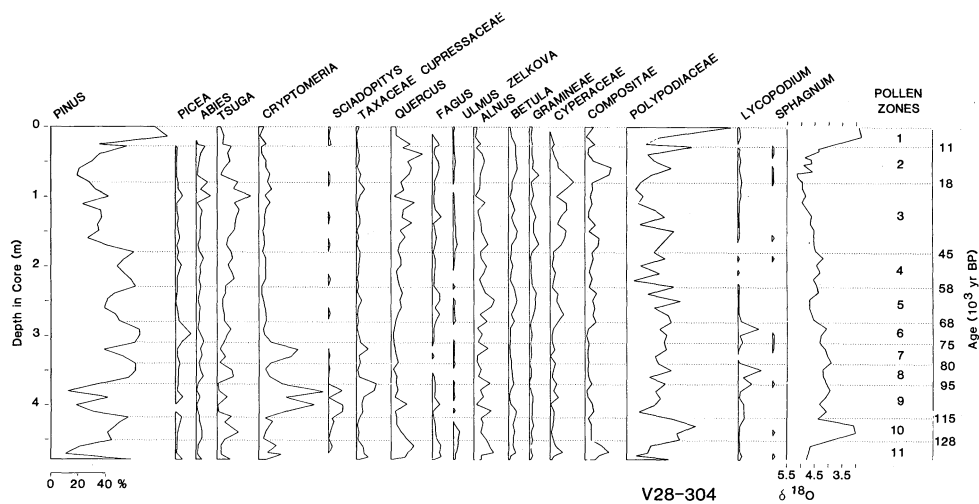


Figure 4: Pollen diagram showing percentages of principal pollen and spores from core V28-304 located east of the warm temperate vegetation of the southernmost islands of the Japanese archipelago in the subtropical gyre. Local pollen assemblage zones (Table 2) are shown on the right. Time series of oxygen isotope values are on the right. Ages of pollen zone boundaries appear on the far right, and depth in core (meters) is on the left.

### 3. TIME CONTROL

For cores RC12-401 and RC14-99, the abundance pattern of the radiolarian *Cycladophora davisiana* provided a detailed, continuous stratigraphic framework. This pattern is similar to, and correlative with, the *C. davisiana* records from other high-latitude sites which have been directly or indirectly tied to the global oxygen isotope stratigraphy (Morley and Hays, 1979; Morley, *et al.*, 1982). The last abundant appearance datum (LAAD) of *Lychnocanium grande*, identified in both cores, provided additional control points verifying the continuous *C. davisiana* stratigraphy.

Specifically, two levels were used in RC12-401 to construct a chronology: (1) the most recent maxima in *C. davisiana* abundance (260cm) with an estimated age of 17,000yr B.P., and (2) the LAAD of *L. grande* (740cm) with an estimated age of 49,000yr B.P. (Morley, *et al.*, 1982). For RC14-99, four control points were used to develop a chronology: (1) the most recent maxima in the *C. davisiana* abundance pattern, occurring at 110cm with an estimated age of 17,000yr B.P., (2) the LAAD of *L. grande* at 260cm with an estimated age of 49,000yr B.P., and (3-4) correlation of *C. davisiana* minima 'e<sub>1</sub> (390cm) and 'e<sub>3</sub> (600cm) with oxygen isotope substages 5a and 5e with estimated ages of 80,000 and 122,000yr B.P., respectively (Imbrie, *et al.*, 1984).

The chronology for core V28-304 was obtained from benthic oxygen isotope measurements (Fig. 4) provided by N.J. Shackleton (written comm.). This isotope curve was correlated with the SPECMAP stacked isotopic record selecting ages corresponding to specific isotope events based upon the SPECMAP timescale (Imbrie, *et al.*, 1984). In all three marine cores, diagnostic pollen events (which were correlated with similar events in radiocarbon-dated cores from Japan) were used for minor revision of the late-Holocene sequences.

The time-series data presented in Figures 5 and 6 were generated using age models defined by the control points described above for each of the records interpolating between datum levels. Selection of time intervals for each of these time series was made by calculating the average time between consecutive samples. With these various chronologies, time series for RC 12-401, RC14-99, and V28-304 were generated using time intervals of 1250, 2000 and 2000 years, respectively.

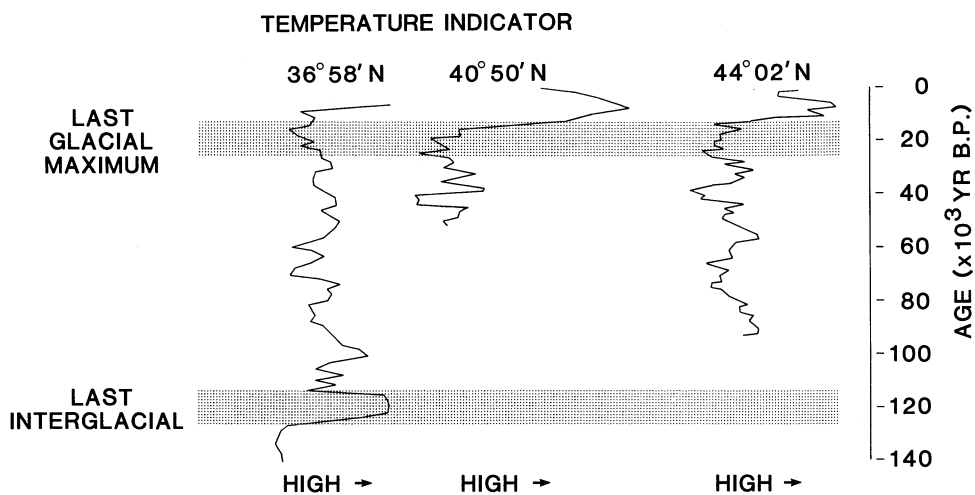


Figure 5: Time series showing relative changes in temperature along a south-north transect on the Pacific coast of Japan inferred from pollen data in cores RC14-99, RC12-401, and RC14-103. Ages are shown on the right. Two major climatic events: the last interglacial and the last glacial maximum, are each delineated by a stippled bar. (Curves are derived from the *Picea* pollen assemblage) .

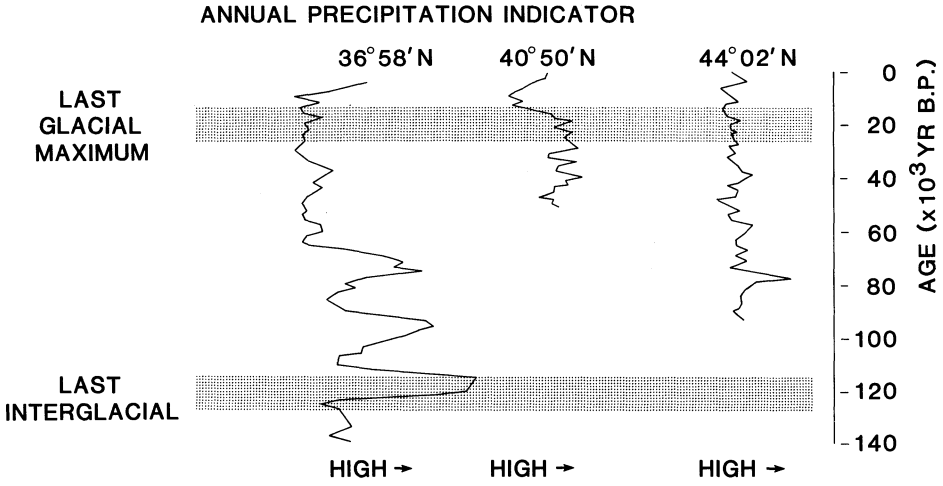


Figure 6: Time series showing relative changes in precipitation along a south-north transect on the Pacific coast of Japan inferred from pollen data in cores RC14-99, RC12-401, and RC14-103. (Curves are derived from the *Cryptomeria* assemblage). Ages are shown on the right. Two major climatic events: the last interglacial and the last glacial maximum, are each delineated by a stippled bar.



## 4. RESULTS

Diagnostic pollen types of Japanese vegetation zones are present in all samples analyzed. Indicator taxa (such as *Selaginella selaginoides*, *Cyathea*, *Castanopsis*, and *Podocarpus*) occur periodically downcore. Conifers (including *Pinus*, *Tsuga*, *Picea*, *Cryptomeria* (Japanese cedar), and *Sciadopitys* (umbrella pine) are generally more abundant than broad-leaved arboreal taxa or herbs. Most abundant are *Pinus*, *Cryptomeria*, *Quercus*, and *Alnus* types produced and/or dispersed with high frequency (Igarashi, 1979, 1987). Taxa which are under-represented in terrestrial deposits (i.e., *Fagus* and *Abies*) are also not well represented in samples from cores V28-304, RC14-99 and RC12-401 (Hibino, 1976; Miura, 1985).

Pollen concentration (# pollen grains/gram dry weight sediment) is low, ranging from ~100/gm in V28-304 to 2,500/gm in RC14-99. In cores RC14-99 and RC12-401, as in other cores from the region (Heusser, 1987), concentration is greater during nonglacial than in glacial intervals.

### 4.1 Pollen Stratigraphy

In core RC12-401, conifer and nonarboreal pollen and spores basically characterize glacial pollen zones 7-4 (Fig. 2, Table 2). Successional types, (*Betula* and *Alnus*) are prominent in the late glacial, and *Quercus* dominates the Holocene — excluding the topmost sediments in which *Pinus*, *Tsuga*, *Picea*, and *Cryptomeria* expand. Conifer pollen, except for *Cryptomeria*, is conspicuously absent from the *Quercus* zone.

*Cryptomeria* and *Pinaceous* pollen types are present continuously in samples from core RC14-99 (Fig. 3, Table 2). Between ~3 to 6m depth, high-amplitude fluctuations in *Cryptomeria*, three peaks of decreasing amplitude alternate with pollen assemblages characterized by increased *Quercus*, *Pinus* and *Betula* (pollen zones 12-7). *Pinus* reaches optimal representation in zone 6 and remains fairly prominent throughout the last 50,000 years. Increased *Tsuga* and *Picea* occur between ~50,000 to ~35,000 and between ~20,000 to 9,000yr B.P. (pollen zones 5, 3, and 2). The *Betula-Sphagnum* zone (pollen zone 4), which immediately precedes the last glacial maximum (pollen zone 3), has a minimal amount of *Taxodiaceous* pollen. In pollen zone 3, and in earlier glacial intervals (pollen zones 13, 10, and 6), *S. selaginoides* is present consistently. The uppermost sediment in the core (pollen zone 1) contains increased amounts of *Pinus*, *Cryptomeria*, and *Quercus*.

In core V28-304 conifers dominate, and *Pinus* is better represented than in cores RC14-99 and V28-304 (Fig. 4, Table 2). As in RC14-99, *Cryptomeria* peaks between ~107,000-95,000yr B.P. and ~80,000-70,000yr B.P. (pollen zones 9 and 7 characterize the early part of the last glacial cycle). During the last interglacial, ~123,000yr B.P., *Pinus* forms about half of the pollen, *Tsuga* (? *T. sieboldii*) reaches 30%, and *Cryptomeria* (though present) is not a major component of pollen zone 10. In the basal zone of the pollen diagram deposited at the end of the penultimate glaciation (140,000-128,000yr B.P.), *Compositae* and *Quercus* are prominent as they are in pollen zone 2, which encompasses the last glacial maximum ~17,000yr B.P.

## 5. DISCUSSION

### 5.1 Marine Pollen Sedimentation

Sedimentation of pollen in the northwest Pacific Ocean deserves some discussion. Our core sites lie more than 500km from land, and two (RC14-99 and RC12-401) are located ~1000km at sea. Theoretical and empirical evidence shows that eolian pollen concentration decreases exponentially within a few meters of the source and that long-distance, atmospheric pollen transport is comparatively small compared with pollen production and local deposition, much of which is washed into streams (Akers, *et al.*, 1979; Raynor, *et al.*, 1972; Tauber, 1967; Traverse, 1988). Although unequivocal identification of eolian or fluvial pollen transport is rarely possible, one example of eolian pollen transport to the northwest Pacific can be definitely identified. *Ephedra*, which is not and has not been part of the Japanese flora, is carried >3000km from China and/or the Himalayas to our core sites (Hou, 1984; Ohwi, 1984).

Winds can carry pollen locally from coastal vegetation to sea, although the limited range of initial pollen dispersal means that most wind-borne pollen will be deposited in shallow water and only a small amount will be blown to deeper waters offshore. Pollen concentration in marine aerosols varies from 0-3 grains•cm<sup>-2</sup>•day<sup>-1</sup> to 4-40 pollen and spores•m<sup>-3</sup> (Melia, 1984; Mudie, 1982); however, using these numbers to estimate the atmospheric component of marine pollen flux is hazardous because these data are essentially singular sampling events, and atmospheric transport (like pollen production) is highly variable on daily and seasonal time scales (Melia, 1984).

Fluvial pollen transport, including pollen resuspended by runoff, is a significant component of marine pollen sedimentation (Traverse, 1988) — at least in non-arid regions. Although data are not available from Japan, rivers in temperate regions elsewhere carry from  $\sim 10^3$  to  $10^{12}$  pollen grains/100 liters water (Heusser, 1985; Traverse, 1988), and the high river runoff in Japan probably carries substantial amounts of pollen. In Japan, arboreal pollen is mainly produced in late spring ( $300$  pollen grains/ $\text{cm}^2\text{day}^{-1}$ ), and maximum shrub and herb pollen dispersal occurs in late summer — a season of high rainfall and river discharge on the Pacific coast (Fukui, 1977).

Once deposited in the ocean, pollen sedimentation (like that of fine-grained terrigenous particles) involves both vertical flux and lateral transport. Some effect of lateral transport, that of the Kuroshio Current (Fig. 1b), is seen in the northeastward trends of pollen distribution in surface sediments; however, the overall correspondence between the major patterns of vegetation distribution onshore and of pollen distribution offshore is excellent (Heusser, 1988; Heusser and Morley, 1985b; Uchiyama, 1978).

## 5.2 Pollen Records

**RC12-401.** Between  $\sim 50,000$  and  $\sim 20,000$ yr B.P., vegetation in northeast Japan (Fig. 2) changed from *Pinus*- and *Picea*-dominated conifer forests to mixed forests with *Alnus*, *Betula*, and *Quercus*, which were replaced by open woodlands and moorlands with *Pinus*, *Alnus*, *Betula*, herbs, (*Compositae* and *Cyperaceae*) *Lycopodium*, and *Sphagnum*. Open birch woodland became even more prominent between  $\sim 20,000$  and  $14,000$ yr B.P. (the interval in which the last appearance of the arctic/alpine indicator, *S. selginoides*, occurs). Development of mixed *Quercus* forests culminated in mid-Holocene followed by conifer expansion in the last few thousand years.

These changes are corroborated by the pollen record from core RC14-103, which lies to the north (Fig. 1; Heusser and Morley, 1985b) and are similar to northeastern Japanese pollen records from the same time interval; however, the regional nature of marine pollen records integrates some local details of terrestrial pollen records. For example, the basal and postglacial pollen assemblages of RC12-401 correlate with coeval pollen deposits in Hokkaido and in fluvial and coastal sediments  $\sim 6$  km offshore (Igarashi and Kumano, 1981; Uchiyama, 1978). On the other hand, brief or

local developments, such as the rise of *Ulmus* between 34,000 and 31,000yr B.P. and again between 26,000 and 25,000yr B.P. in Hokkaido (Igarashi and Kumano, 1981), are not apparent in RC12-401.

**RC14-99.** Vegetation of the Pacific coast of central Japan at the end of the last two glaciations was similar, consisting of conifer forests in which spruce (*Picea*) and well-developed heath and moorlands was prominent (Fig. 3, Table 2). The subsequent deglacial intervals were characterized by the rise of pioneer birch/alder (*Betula/Alnus*) assemblages followed by the establishment of temperate interglacial forests.

Vegetation of the last interglacial (oxygen isotope substage 5e, Heusser and Shackleton, 1979) and present interglacial differ substantially: the former consisted of *Cryptomeria*-dominated conifer forests and the latter by *Quercus/Fagus*-dominated broad-leaf and mixed forests. Conifers (*Cryptomeria*, *Sciadopitys*, and *Taxaceae-Cupressaceae*) also distinguish interstadial forests between 104,000-92,000 and 80,000-68,000yr B.P. (Heusser and Morley, 1985a, b). Intervening stadials (zones 10 and 8) are characterized by more open vegetation; i.e., woodlands with *Pinus*, *Alnus*, *Betula* and *Sphagnum*-moors. After ~68,000yr B.P., except for a minor rise ~40,000yr B.P., the *Taxodiaceae* (which developed so markedly during the last interglacial) played a minor role in plant assemblages of eastern Japan until the Holocene. As to the north, forests of *Pinus*, *Tsuga*, *Picea*, and *Abies*, with varying amounts of broad-leafed trees (*Quercus*, *Fagus*, *Ulmus-Zelkova*, *Alnus* and *Betula*) were widespread on the central Pacific coast of Honshu during the last glacial. According to our age model, temperate conifer forests dominated central Japan from 20,000 until ~9,000yr B.P., followed by development of temperate-mixed and deciduous broad-leaf forests.

*Cryptomeria*-dominated forests have also been reconstructed from pollen data in central Japan. The youngest *Cryptomeria*-rich assemblage from Pliocene-Pleistocene deposits in Osaka basin, described as interglacial (Tai, 1973; Tsukada, 1986a; unpub.), may correlate with the *Cryptomeria* assemblage from the last interglacial in RC14-99. *Cryptomeria* forests were well-developed in the Kanto region south of Tokyo between 90,000 and 60,000yr B.P. (Tsuji, *et al.*, 1984a), and the expansion of *Cryptomeria* sediments deposited in Lake Biwa in the first half of the last glaciation (Fuji, 1976, 1984) correlates with the expansion of *Cryptomeria* seen in RC14-99 during the same time.

It is clear from the pollen record of RC14-99 that the endemic Japanese conifer *Sciadopitys verticillata* was an important component of central Japanese forests prior to 70,000yr B.P., producing >40% of the pollen sum in marine sediments deposited >1000km offshore between ~92,000 and 104,000 yr B.P. Now restricted to temperate regions of southern Japan between 300 and 1500m altitude and represented by pollen percentages of less than 10% (Tsukada, 1963), *S. verticillata* clearly expanded on the Pacific coast of Japan during warm periods at the beginning of the last glaciation. Presumably, earlier Pliocene-Pleistocene range extensions occurred during warm intervals as well, although *Sciadopitys* pollen is reported to have been last abundant in a cold interval, possibly correlated with the Mindel glaciation (Tsukada, 1963).

The importance of conifers such as *Pinus*, *Picea*, and *Tsuga* in central Japanese forests during the last glacial is documented in numerous sites on Japan, as well as in marine sediments of core RC14-99 (Miura and Yamanaka, 1975, 1980; Morita, 1985; Sohma, 1984; Tsuji, *et al.*, 1984a,b). Regional lowering of tree line (>1000m has been suggested by Tsuji, *et al.*, 1984a) related to temperature depression is the usual interpretation, although changes in winter winds may also be a factor (Okitsu and Ito, 1984).

**V28-304.** In southernmost Japan, forest development following Termination II is strikingly different from that of central and northern Japan. During the oxygen-isotope minimum 5e (the last interglacial), *Pinus* and *Tsuga* (? *T. sieboldii*), not *Cryptomeria*, are the leading conifers in a mixed temperate forest with *Abies* (*A. firma*) and hardwoods (Fig. 4, Core V28-304, pollen zone 10). Subsequent expansion of *Cryptomeria* accompanied by *Sciadopitys* and *Taxaceae/Cupressaceae* during the two subsequent warm intervals in oxygen-isotope stage 5 between 115,000 and 95,000 and 80,000-75,000yr B.P. (pollen zones 9 and 7), is essentially the same as in records from RC14-99 (Fig. 3). The *Cryptomeria* zones in V28-304 may be correlative with one or more of the *Cryptomeria* zones described from southern Kyushu (Hase and Hatanaka, 1984), which have been assigned to the Middle-Late Pleistocene or Late Pleistocene.

The *Sciadopitys verticillata* peak in V28-304, between ~95,000 and ~115,000yr B.P. (approximately the same as in core RC14-99), confirms the abundance of this species on the Pacific coast of Japan during this warm interval in the early part of the last glaciation. It is clear from the palynological records of cores V28-304 and RC14-99 that the Tertiary relic *Sciadopitys* was still widely distributed in southern Japan prior to the onset

of the last full glacial (~70,000yr B.P.), unlike northwest Europe where *Sciadopitys* disappeared after "an early (? Pliocene-Pleistocene) glaciation" (Tshudy and Scott, 1969).

The prominence of *Pinus* in southernmost Japan over the past 140,000 years (pollen zones 4, 6, 8, and 10) is corroborated by the abundance of pine inferred from the Pleistocene *Pinus* zones of southern Kyushu sediments (Hase and Hatanaka, 1984). The mixed composition of these Pleistocene forests — conifers (primarily *Pinus* and *Tsuga*) and hardwoods now found in cool-temperate as well as warm-temperate forests — may have no modern analogue.

In the southern part of the Japanese archipelago, after the last glacial maximum (pollen zone 2), the importance of *Quercus* in forests is similar to the role of oak at the end of the penultimate glaciation (pollen zone 11). In the following interglacial forests (those represented by pollen zones 1 and 10), *Pinus* is more prominent in the Holocene than during the last interglacial. The Late-glacial and Holocene pollen record from V28-304 correlates with a 13,000yr record from the Osaka region (Yasuda, 1978) in which subalpine forests (including *Pinus*, *Picea Abies* and *Tsuga*) covered lowlands between 13,000-10,000yr B.P. and were abruptly succeeded ~10,000yr B.P. by temperate *Quercus* forests. Pollen composition of the uppermost sediments in V28-304 also compares with pollen in recent sediments deposited off southern Japan — an assemblage composed of *Pinus*, *Cryptomeria*, *Abies*, *Quercus*, *Podocarpus*, and *Castanopsis*, with *Gramineae* — the dominant nonarboreal pollen (Uchiyama, 1978).

### 5.3 Summary

Pollen records from the northwest Pacific are dominated by arboreal pollen, which suggests that forests were present on the Pacific coasts of the Japanese archipelago throughout the past 140,000yr B.P. When and where present, nonarboreal subalpine or subarctic vegetation (such as that now found north of the Kurile Islands, for example) was never as extensive as forest vegetation. The prominence of conifer pollen in samples analyzed from cores RC12-401, RC14-99, V28-304, and RC14-103 (and in correlative samples from terrestrial sediments onshore) clearly indicates that conifers were the major component of Japanese Pleistocene forest associations.

The complex fluctuations in the marine-pollen time series and the multiplicity of pollen assemblage zones suggest that components of Japanese vegetation units changed frequently over the last 140,000 years,

perhaps on the order of 2,000 to ~10,000 years like the present forest associations of Japan (Morita, 1984; Tsukada, 1986b).

## 6. CLIMATIC SYNTHESIS

Variations in the vegetation of Japan inferred from pollen records in cores from the northwest Pacific Ocean appear to be systematically related to climatic changes over the last 140,000yr B.P. Assuming that the continued presence of components of the present Japanese flora in the Japanese island arc during the last two glaciations indicates that climatic fluctuations during that time did not exceed modern extremes for any extended interval, existing relationships between vegetation, pollen assemblages, and climatic parameters can be used (with discretion) as a basis for paleoclimatic reconstruction in the Japanese archipelago.

Diagnostic pollen types used in reconstructions of northeast Asian climate are present in the marine cores described in this paper. In Japan, *Cryptomeria* is probably the most widely used climatic indicator because of the present close association between high precipitation (not less than 1200mm and usually in excess of 1600mm annually) and the distribution of *Cryptomeria* (Kawamura, 1979; Tsukada, 1982; 1986a). Relative abundance of *Picea* is frequently used as a temperature indicator, and *Betula* pollen is associated with relatively low (<8°C) mean annual temperatures (Jimbo 1964; Nakamura, 1952; Tsukada, 1983, 1988).

To extract climatic signals from northwest Pacific pollen records, pollen data were synthesized using Q-mode factor analysis (Morley and Heusser, 1989). Although this procedure obscures some taxonomic details, it reduces problems inherent in interpreting percentage data and of comparing data from different vegetational regions. Of the four arboreal assemblages identified (Table 3), two (*Picea* and *Cryptomeria*) are dominated by climate-indicator types. The relative importance (factor loading) of these two factors is used to construct time series (see Time Control) of precipitation and temperature trends for the temperate Pacific coast of Japan over the past 140,000 years (Figs. 5 and 6).

Between 120,000yr B.P. and 70,000yr B.P., there are three intervals with significantly high precipitation in central Japan. Temperatures peaked between ~125,000 and 116,000yr B.P. and briefly between ~102,000 and 100,000yr B.P. and at ~80,000yr B.P. The 70,000-60,000yr B.P. glacial event is.

marked by decreased temperatures and precipitation. Throughout the last glacial, temperatures and precipitation are generally low. The late glacial/Holocene transition is marked by an abrupt rise in temperature.

These proxy climatic curves appear to reflect differences between present and past interglacial climates in Japan; particularly higher temperatures and precipitation in central Japan during the last interglacial. If the temperature and precipitation curves are interpreted as summer temperature and precipitation (the season of plant growth on the Pacific coast of Japan), then differences in the position and intensity of the frontal zone and summer monsoons are inferred. A strong and slightly north-northeastward shift of the southeastern monsoon, a northward shift of the frontal rainband, and a weaker Okhotsk High would result in higher rainfall and warmer temperatures on the Pacific coast of Japan during the last interglacial (Fukui, 1977).

In the two younger climatic events (centered at ~100,000yr B.P. and ~80,000yr B.P.), early spring and summer monsoon patterns were more like those of the present (i.e., the front was farther south than during the last interglacial) producing warm, wet climates in southern and central Japan. By 70,000yr B.P. summer and winter monsoons had shifted into a glacial mode. Low temperatures suggest weakened southern summer and intensified winter monsoons — possibly reflecting effects of northern hemisphere glaciation on regional atmospheric circulation. Holocene temperature and precipitation fluctuations on land are related to strengthened summer monsoons between ~12,000yr B.P. and 6000yr B.P.

## ACKNOWLEDGMENTS

Research for this paper was supported by a grant from the Climate Dynamics Division of the National Science Foundation to L. Heusser and J. Morley. I would like to acknowledge the contributions to various aspects of this paper of: J.J. Morley, C.J. Heusser, N.J. Shackleton, E. Stock, and particularly to the organizers of the Paleoclimatology and Paleometerology Conference — M. Leinen and M. Sarnthein.



## REFERENCES

- Akers, T., Edmonds, R., Kramer, C., Lighthart, B., McManus, C., Schlichting, H., Solomon, A., and Spendlove, J., 1979: Sources and characteristics of airborne materials, *In*: Edmonds, Ed., *Aerobiology*, Stroudsburg, PA, Dowden, Hutchinson & Ross.
- Berglund, B. (Ed.), 1986: *Handbook of Holocene Palaeoecology and Palaeohydrology*, New York, Wiley.
- Birks, H. J. B., 1986: Numerical zonation, comparison, and correlation of Quaternary pollen-stratigraphical data, *In*: Berglund, Ed., *Handbook of Holocene Palaeoecology and Palaeohydrology*, New York, Wiley, pp. 743-774.
- Franklin, J., Maeda, T., Ohsumi, Y., Matsui, M., and Yagi, H., 1979: Subalpine coniferous forests of central Honshu, Japan, *Ecol. Mono*, 49: 311-334.
- Fuji, N., 1976: Palaeoclimatic and paleovegetational changes around Lake Biwa, central Japan during the past 100,000 years, *In*: Horie, S., Ed., *Palaeolimnology of Lake Biwa and the Japanese Pleistocene*, 4: 316-356.
- Fuji, N., 1984: Pollen Analysis, *In*: Horie, S., Ed., *Lake Biwa, Dordrecht, The Netherlands*, pp. 497-529.
- Fukui, E. (Ed.), 1977: *The Climate of Japan*, New York, Elsevier.
- Hase, V., and Hatanaka, K., 1984: Pollen stratigraphical study of the Late Cenozoic sediments in Southern Kyushu, Japan, *Quat. Res. (Japan)*, 23: 1-20.
- Heusser, L., 1985: Quaternary palynology of marine sediments in the northeast Pacific, northwest Atlantic, and Gulf of Mexico, *In*: Bryant and Holloway, Eds., *Pollen Records of Late-Quaternary North American Sediments*, Dallas, AASP Foundation, pp. 385-403.
- Heusser, L., 1987: Patterns of atmospheric circulation in northeast Asia over the last 150,000 years., *Paleoclimatology and Paleometeorology: Modern and Past Patterns of Global Atmospheric Transport*, NATO Advanced Research Workshop, November 15-19, 1987, Oracle, AZ, U.S.A.

- Heusser, L., 1988: Pollen distribution in marine sediments on the continental margin off northern California, *Mar. Geol.*, 80: 131-147.
- Heusser, L., and Morley, J., 1985a: Correlative 90 kyr northeast Asia-northwest Pacific climate records, *Nature*, 313: 470-472.
- Heusser, L., and Morley, J., 1985b: Pollen and radiolarian records from deep-sea core RC14-103: climatic reconstructions of northeast Japan and northwest Pacific for the last 90,000 years, *Quat. Res.*, 24: 60-72.
- Heusser, L., and Shackleton, N., 1979: Direct marine-continental correlation: 150,000-year oxygen isotope-pollen record from the North Pacific, *Science*, 204: 837-839.
- Heusser, L., and Stock, C., 1984: Preparation techniques for concentrating pollen from marine sediments and other sediments with low pollen density, *Palynology*, 8: 225-227.
- Hibino, K., 1976L: Air-borne pollen and presumption of vegetation, *Ecol. Rev.*, 18: 211-223.
- Hou, H., 1984: Vegetation of China with reference to its geographical distribution, *Annals of the Missouri Botanical Garden*, 70: 509-549.
- Igarashi, Y., 1979: Pollen incidence and wind transport in central Hokkaido, *Journal of the Faculty of Science, Hokkaido University*, 19 (Series IV): 257-264.
- Igarashi, Y., 1987: Pollen incidence and wind transport in central Hokkaido (II), *Research Bulletins of the College of Experiment Forests, Faculty of Agriculture, Hokkaido University*, 44: 477-506.
- Igarashi, Y., and Kumano, S., 1981: Vegetational changes during the Last Glacial Age in Hokkaido, *Quat. Res. (Japan)*, 20: 129-141.
- Imbrie, J., Hays, J.D., Martinson, D., McIntyre, A., Mix, A.C., Morley, J.J., Pisias, N.G., Prell, W.L., and Shackleton, N.J., 1984: The orbital theory of Pleistocene climate: support from a revised chronology of the marine  $\delta^{18}O$  record, In: Berger, A., et al., Eds., *Milankovitch and Climate*, Part I, Boston, Reidel Publishing Co., pp. 269-305.

- Jimbo, T., 1932: Pollen analytical studies of peat formed on volcanic ash, *Science Reports Tohoku Imperial University*, 7 (4th Series, Biology): 129-132.
- Jimbo, T., 1964: The pollen flora of Japan since Pliocene time and its macrobotanical background, *Science Reports of Tohoku University*, 30, (4th Series, Biology): 27-41.
- Kawamura, T., 1979: Palynological studies of bog deposits in Tohoku district - special reference to the distribution of *Cryptomeria japonica*, *Quat. Res. (Japan)*, 18: 79-88.
- Maeda, Y., 1970: Palynological study of the Latest Pleistocene marine clay in the Itami area, Kinki, Japan, *J. Geo. Sciences, Osaka City University*, 13: 99-112.
- Melia, M.B., 1984: The distribution and relationship between palynomorphs in aerosols and deep-sea sediments off the coast of northwest Africa, *Mar. Geol.*, 58: 345-371.
- Miura, O., 1985: A preliminary investigation into the pollen preservation in peat and soil, *Ecol. Rev.*, 20: 309-319.
- Miura, O., and Yamanaka, M., 1975: Palynological study of Late Pleistocene deposits on the Hakkoda Mountains, *Ecol. Rev.*, 18: 127-132.
- Miura, O., and Yamanaka, M., 1980: Palynological study of the latest Pleistocene deposits on Hakkoda Mountains, *Ecol. Rev.*, 19: 167-174.
- Miyawaki, A., and Sasaki, Y., 1985: Floristic changes in the *Castanopsis cuspidata* var. *sieboldii*-forest communities along the Pacific Ocean coast of the Japanese Islands, *Vegetatio*, 59: 225-234.
- Miyoshi, N., 1983a: Pollen morphology by means of scanning electron microscope, *Bulletin of the Hiruzen Research Institute, Okayama University of Science*, 8: 41-53.
- Miyoshi, N., 1983b: Pollen morphology of the genus *Castanopsis* (*Fagaceae*) in Japan, *Grana*, 22: 19-21.

- Miyoshi, N., and Yano, N., 1986: Late Pleistocene and Holocene vegetational history of the Ohnuma Moore in the Chugoku Mountains, western Japan, *Review of Palaeobotany and Palynology*, 46: 355-376.
- Morita, Y., 1984: The vegetational history of the subalpine zone in northeast Japan, *Japanese Journal of Ecology*, 34: 347-356.
- Morita, Y., 1985: Pollen diagrams of some peat moors in the subalpine zone in the Shinshu District, Japan, *Ecol. Rev.*, 20: 301-307.
- Morley, J., and Hays, J.D., 1979: *Cycladophora davisiana*: A stratigraphic tool for Pleistocene North Atlantic and interhemispheric correlation, *Earth Planet. Sci. Ltrs.*, 44: 1485-1499.
- Morley, J., Hays, J., and Robertson, J., 1982: Stratigraphic framework for the late Pleistocene in the northwest Pacific Ocean, *Deep-Sea Res.*, 29: 1485-1499.
- Morley, J., and Heusser, L., 1989: Late Quaternary Atmospheric and Oceanographic Variations in the Western Pacific inferred from Pollen and Radiolarian Analyses, in prep.
- Mudie, P., 1982: Pollen distribution in recent marine sediments, eastern Canada, *Can. J. of Earth Sci.*, 19: 720-747.
- Nakamura, J., 1952: A comparative study of Japanese pollen records, *Kochi Daigakugakujutsukenkyuhokoku*, 4: 1-20.
- Nakamura, J., 1957: Pollen analyses from two swamps of the Amami Islands, *Reports of the Usa Marine Biological Institute, Kochi University*, 4: 1-14.
- Numata, M. (Ed.), 1974: *The Flora and Vegetation of Japan*, New York, Elsevier.
- Ohwi, J., 1984: *Flora of Japan*, Smithsonian Institution, Washington DC.
- Okitsu, S., and Ito, K., 1984: The relation of forest limit to the W115 in mountains of Kokkaido, *Japanese Journal of Ecology*, 34: 341-346.

- Raynor, G.S., Odgen, E.C., and Hayes, J.V., 1972: Dispersion and deposition of timothy pollen from experimental sources, *Agri. Meteor.*, 9: 347-366.
- Saito, K., 1979: A note on subalpine coniferous forests in north Honshu, *Bull. Yokohama Phytosoc. Soc. Japan*, 16: 177-188.
- Saito, K., 1981: Species diversity of subalpine coniferous forests on Mt. Hakoda, north Honshu, Japan, *Hikobia Supplement, ISBN*, 1: 73-82.
- Saito, K., Sugawara, K., and Fukuda, H., 1980: Natural and semi-natural vegetation on Mt. Goyo in the Kitakami massif, north Honshu, Japan, *Saito Ho-on Museum Research Bulletin*, 48: 25-42.
- Sohma, K., 1984: Two Late-Quaternary pollen diagrams from northeast Japan, *Sci. Rep. Tohoku University 4th Ser. (Biology)*, 38: 351-369.
- Tai, A., 1973: A study on the pollen stratigraphy of the Osaka Group, Plio-Pleistocene deposits in the Osaka Basin, *Memoirs of the Faculty of Science, Kyoto University*, 39 (Series of Geology and Mineralogy): 123-165.
- Tauber, H., 1967: Investigations on the mode of pollen transfer in forested areas, *Review Palaeobotany and Palynology*, 3: 277-286.
- Toyohara, G., 1979: Forest vegetation on rocky sites in Hiroshima Prefecture southwestern Honshu, *Bull. Yokohama Phytosoc. Soc. Japan*, 16: 167-175.
- Traverse, A., 1988: *Paleopalynology*, Winchester, Unwin Hyman, Inc.
- Tschudy, R.H., and Scott, R.A., 1969: *Aspects of Palynology*, New York, Wiley Interscience.
- Tsuji, S., Minaki, M., and Osawa, S., 1984a: Paleobotany and paleoenvironment of the Late Pleistocene in the Sagami Region, central Japan, *Quat. Res. (Japan)*, 22: 279-296.
- Tsuji, S., Minaki, M., and Suzuki, M., 1984b: Plant fossil assemblage of the Latest Pleistocene at Ninomiya-cho, southern Tochigi Prefecture, Central Japan, *Quat. Res. (Japan)*, 23: 21-29.

- Tsukada, M., 1958: Untersuchungen über das Verhältnis zwischen dem Pollengehalt der Oberflächenproben und der vegetation des Hochlandes Shiga, *Journal of the Institute of Polytechnics, Osaka City University*, 9 (Series D): 217-234.
- Tsukada, M., 1963: Umbrella pine, *Sciadopitys verticillata*: past and present distribution in Japan, *Science*, 142: 1680-1681.
- Tsukada, M., 1982: *Cryptomeria japonica*: glacial refugia and late-glacial and postglacial migration, *Ecology*, 63: 1091-1105.
- Tsukada, M., 1983: Vegetation and climate during the Last Glacial Maximum in Japan, *Quat. Res.*, 19: 212-235.
- Tsukada, M., 1986a: Altitudinal and latitudinal migration of *Cryptomeria japonica* for the past 20,000 years in Japan, *Quat. Res.*, 26: 135-152.
- Tsukada, M., 1986b: Vegetation in prehistoric Japan: the last 20,000 years. *Windows on the Japanese past: studies in archeology and prehistory*, Ann Arbor, University of Michigan.
- Tsukada, M., 1988: Japan, In: Huntley, B. and T. Webb, II, Eds., *Vegetation History*, Boston, Kluwer Academic Publishers.
- Uchiyama, T., 1978: Palynological studies of marine sediments in Urado Bay, Kochi Prefecture, and Sendai Bay, Miyagi Prefecture, *Ecol. Rev.*, 19: 37-44.
- Ueno, J., 1959: Some palynological observations of *Taxaceae*, *Cupressaceae* and *Araucariaceae*, *Journal of the Institute of Polytechnics, Osaka City University*, 10 (Series D): 75-87.
- Watanabe, S., 1979: The subarctic summer green forest zone in northeastern Asia, *Bull. Yokohama Phytosoc. Soc. Japan*, 16: 101-111.
- Yasuda, Y., 1978: Vegetational history and paleogeography of the Kawachi Plain for the last 13,000 years, *Quat. Res. (Japan)*, 16: 211-229.

## THE LATE QUATERNARY RECORD OF ATMOSPHERIC TRANSPORT TO THE NORTHWEST PACIFIC FROM ASIA

MARGARET LEINEN

Graduate School of Oceanography  
University of Rhode Island  
Narragansett, RI 02882-1197  
U.S.A.

**ABSTRACT.** Late Quaternary Asian dust composition and transport to the Pacific was studied in sediments from a north-south transect of piston cores which extends from 25° to 46°N between 140° and 157°E. Principal component factor analysis was used to identify end-member clay mineral assemblages. Three clay mineral assemblages explain 84% of the variance in clay-size fraction sedimentation along the transect. The first end-member is most abundant in sediments from the northern end of the transect and from east Japan. It probably represents clays which have a contribution from andesitic soil dust. The second end-member is most abundant in illite, smectite and quartz and probably represents loess. The final end-member is dominated by illite and is most abundant in sediments from the northern and southern ends of the transect, but it accumulates most rapidly at the latitude of present-day maximum dust accumulation.

Time slices along the transect demonstrate that the spatial distribution and flux of individual mineral groups and of the end-member assemblages has changed with time, however the flux is always greatest between 35 and 42°N, the latitude which now has the greatest probability of receiving dust transported from the desert regions of central Asia. The greatest fluxes occurred between 4 and 7 KY BP and between 23 and 27 KY BP. Factors 1 and 3 were especially important in the sediments deposited between 4 and 7 KY BP. Factor 2 is most abundant in sediments deposited 10-25 Ka. Mineral fluxes during the last glacial maximum were similar to those of today. Longer records of eolian quartz deposition in the region suggest that the composition of dust is dominated by variance at the precession frequency, 23 KY. These data, together with the data presented

here, suggest that dust flux and composition may be more strongly influenced by the seasonality of climate in Asia than by the more dramatic effects of glacial stages.

## 1. INTRODUCTION

The non-biogenic fraction of deep-sea sediment from the northwest Pacific is dominated by terrigenous material transported to the region from Asia. Surface sediments from the northwest Pacific are virtually identical in mineral composition to modern mineral aerosol being transported to the North Pacific from Asia, which is collected at the same sites (Blank, *et al.*, 1985). Thus, the mineral fraction of the sediment is a useful indicator of the amount and composition of Asian dust transported to the Pacific in the past.

Previous studies of the concentration of one atmospherically transported component of the sediment quartz have suggested that it varies periodically in sediments from the northwest Pacific and that these variations are statistically related to changes in Earth's orbital parameters (Pisias and Leinen, 1984; Morley, *et al.*, 1987). The mechanisms by which variations in orbital parameters are translated through the climate system into processes which control the concentration of eolian quartz have never been determined, however. Nonetheless, these preliminary studies suggest that further studies of eolian sediments might increase our understanding of the nature and causes of climate change. The northwest Pacific is a particularly sensitive region for such studies because it lies beneath the transport path of mineral dust deflated from the arid regions of Asia, which are a major source of tropospheric dust (Duce, *et al.*, 1980). Furthermore, these arid regions and the atmospheric circulation systems which transport the dust are strongly influenced by the Indian-Asian monsoonal circulation. Thus, their study is an important complement to studies which have been made of changes in monsoonal circulation through the Quaternary (e.g. Prell and Kutzbach, 1987).

The quartz which has been studied previously is but a single component of mineral aerosol. An understanding of the variations in the entire atmospherically transported mineral assemblage would substantially improve our understanding of the climatic control on mineral aerosol composition and deposition in the past. Recent studies of the transport paths of modern mineral aerosols (Merrill, this volume; Merrill, *et al.*, in prep.) and their control on the mineralogy of mineral aerosols (Leinen, *et al.*, in prep.) suggest that the mineralogy of eolian deep-sea sediments can reveal changes in the sources as well as the flux of Asian dust to the Pacific



during the last glacial cycle. The purpose of the study described here was to determine the nature of mineralogical variation in late Pleistocene and Holocene atmospherically transported sediment and to determine whether the variations could be related to changes in source area.

## 2. SAMPLES AND STRATIGRAPHY

### 2.1 *Sample Locations*

The mineralogy of the late Quaternary eolian sediments from the northwest Pacific was studied in a transect of six cores (Table 1; Fig. 1), which extends from 28.26°N to 49.53°N. The transect is oriented northeast-southwest so that sites are at roughly equal distances from the Asian continent. Two additional cores are located east of the transect. All of the cores are located well east of the trench system that forms the western boundary of the abyssal North Pacific so that material that has been transported down slope from the margin should be minimal. The cores are also east of known areas of active bottom-current circulation and bottom-current winnowing (Damuth, *et al.*, 1983; Jacobi, *et al.*, 1985). It serves as a useful index of the changes in composition that might be caused by ice-rafting. Thus, the locations of the transect cores have been chosen to minimize the influence of non-eolian terrigenous contributions to the sediments. V21-171 is located far east of the transect in a region that was influenced by ice-rafting during the last glacial maximum.

The mineralogy of surface sediments from cores near the transect has been analyzed by Blank, *et al.* (1985) with methods identical to those used in this study and compared to the mineralogy of present-day mineral aerosol collected in mesh samplers. This comparison demonstrated that the mineralogies of the <2  $\mu\text{m}$  fraction of the two types of material were identical (with the exception of the smectite content) and that the accumulation rate of the terrigenous fraction of the sediment was similar to the mineral aerosol deposition flux. Thus, the nature of the area chosen for study and previous comparisons of the clay-sized fraction of the sediment to that of present-day mineral aerosol suggests that the clay-sized fraction of older sediments from the cores should reflect eolian contributions to the sediment.

Samples were taken from depths in the cores which represented six time intervals: 0-3 KY, 4-7 KY, 10-11 KY, 17-19 KY, 24-25 KY, and 29-30 KY (Table 1). The data from the time intervals form "snapshot" images of eolian deposition along the transect at six times through the latest

Table 1. Core locations, sample depth intervals and ages. (Cores that are part of the transect are marked with an asterisk.)

CORE	LATITUDE N	LONGITUDE E	SAMPLE DEPTH (cm)	SAMPLE AGE (ky)	CORE	LATITUDE N	LONGITUDE E	SAMPLE DEPTH (cm)	SAMPLE AGE (ky)
V24-109	0.26	158.48	0.0	0.0	RC14-105*			147.0	24.2
			50.0	18.0				153.0	25.2
V28-238	1.01	160.29	1.0	0.5				158.5	26.1
			34.5	17.3				168.5	27.8
V28-239	3.15	159.11	3.5	2.3	V21-148	42.05	160.36	3.0	2.7
			29.5	19.7				20.0	18.0
V28-243	11.04	138.32	0.0	0.0	V20-126*	42.09	155.52	18.5	3.0
			20.0	18.0				41.5	6.7
V28-249	14.35	147.52	0.0	0.0				68.8	11.1
			20.0	18.0				115.0	25.8
V28-255	20.06	142.27	0.0	0.0				149.0	33.5
			16.0	19.2				184.0	41.1
V28-294*	28.26	139.58	1.0	1.2	V21-173	44.22	163.33	0.0	0.0
			16.0	19.2				21.0	21.6
RC10-167*	33.24	150.23	5.5	2.3	V20-122*	46.34	161.44	10.0	2.3
			10.5	4.3				27.0	6.1
			42.2	17.3				49.0	11.0
V20-129*	37.41	156.35	11.0	1.4				80.0	18.0
			45.0	5.8				107.0	24.1
			139.5	18.1				133.5	30.0
			185.0	24.0	V21-172	47.4	164.21	0.0	0.0
			231.0	29.9				35.0	18.0
RC14-105*	39.41	157.33	1.0	0.0	V21-151	52.16	163.38	0.0	0.0
			20.0	3.3				10.0	18.0
			34.5	5.7	V21-171*	49.53	164.57	3.0	3.4
			45.0	7.4				10.5	7.3
			59.0	9.7				16.5	18.6
			65.5	10.7				21.8	24.5
			85.0	13.9	V32-126	35.3	177.9	27.0	30.4
			97.5	16.0				0.0	0.0
			111.0	18.2				14.5	6.4
			135.5	22.3				39.5	17.6
			143.0	23.5				54.5	24.2

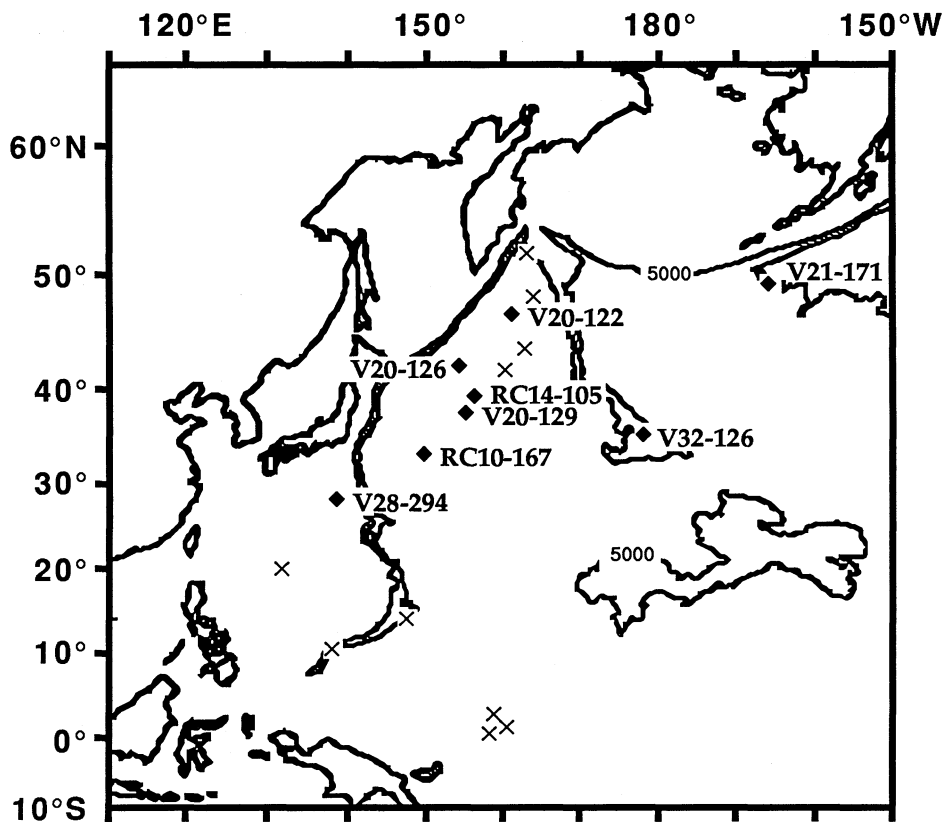


Figure 1. Core locations. Cores for which mineralogical data were collected at 6 KY intervals as part of the transect are marked with a diamond. Cores for which 0 and 18 KY BP total quartz content data were available from CLIMAP (1976) are marked with an "x".

Quaternary. The specific time intervals were chosen at roughly 6 KY intervals to provide a coarse time series of time slices. Several of the specific time intervals include climatic events which were hypothesized to be associated with atmospheric circulation, or source area climate. These include:

- 0-3 KY (present-day conditions),
- 4-7 KY (the climatic "optimum" or period of maximum warmth sometimes called the Altithermal; Antevs, 1938),
- 10-11 KY (the interval of rapid floral and hydrological adjustment to retreat of glacial ice sheets; Webb, *et al.*, 1987),
- 17-19 KY (the maximum extent of continental ice sheets, Shackleton and Opdyke, 1973),
- 23-25 KY
- 27-30 KY (an interval of strong seasonality related to precession; Kutzbach and Guetter, 1981)

Quartz concentration data for total sediment for the time intervals 0-3 KY and 17-19 KY were available for several additional cores in the northwest Pacific (Leinen, *et al.*, 1986). One core (RC14-105; 39°41'N, 159°33'E, Fig. 1), which is located near the present-day maximum of mineral aerosol deposition identified by Rea and Leinen (1988), was selected for more detailed time series analysis (Table 1). Fourteen samples which represent roughly 2 KY intervals in the core were analyzed. Quaternary biogenic and eolian sediments from this core have been studied in great detail by Robertson (1975) and by Pisias and Leinen (1983).

## 2.2 Stratigraphy

Each of the cores chosen for study were part of the CLIMAP data set (CLIMAP, 1976; Moore, *et al.*, 1980). The 18 KY level was identified in cores which contained calcium carbonate (essentially all those south of 20° and V32-126) based on the oxygen isotopic composition of foraminifera and the chronology of Imbrie, *et al.* (1984). For cores north of 20°N which do not contain calcium carbonate, the stratigraphies are based on the abundance maximum of the radiolarian species, *Cycladophora davisiana*, which is

associated with the maximum ice extent 18 KY BP (Morley, *et al.*, 1982). Additional correlations based on other maxima in the abundance of *C. davisiana* were also used to choose depths of samples. The accuracy of the ages assigned to each depth varies between cores, but averages about  $\pm 0.5$ -1 KY for the 18 KY datum and  $\pm 1$ -2 KY for the other age datums.

### 2.3 Lithology

With the exception of V28-294 and V32-126, all of the transect core locations are below the depth of the calcite compensation depth (CCD) in the northwest Pacific and contain no calcium carbonate. The samples comprise pelagic silty clays with varying amounts of biogenic silica. The siliceous biogenic component is dominated by radiolarians, but diatoms are common. A few of the samples also contained small amounts of dispersed volcanic ash. V32-126 lies on the Hess Rise, and the biogenic component of its sediment is dominated by calcareous microfossils.

### 2.4 Other Available Information

The mass flux of the total sediment, the percentage and flux of the eolian component of the sediment, and the grain size of the eolian sediment for the transect cores were determined by Rea and Leinen (1988).

## 3. ANALYTICAL METHODS

### 3.1 Clay Mineralogy

The mineralogy of the samples was determined by two methods, one for quantitative mineralogical analyses of the  $<2 \mu\text{m}$  fraction and one for quantitative determination of the total quartz content. The mineralogy of the  $<2 \mu\text{m}$  sediment fraction was determined using a modification of the techniques of Heath and Piasias (1979). Freeze-dried samples were leached with acetic acid buffered to pH 5.6 with sodium acetate to remove calcium carbonate. This procedure and subsequent washing of the sample in deionized water also removed sea salt from interstitial pore water in the sample. Amorphous iron and manganese oxide and oxyhydroxide phases were removed using sodium dithionite buffered with sodium citrate and bicarbonate (Mehra and Jackson, 1960). Amorphous biogenic silica (opal) was removed by treating the sample with sodium carbonate (Ellis and Moore, 1973). The  $<2 \mu\text{m}$  size fraction was isolated by repeated settling (according to Stokes law) and was saturated with magnesium to allow the quantitative comparison of chlorites and smectites to standards. A quantity

of  $<2 \mu\text{m}$  talc (prepared by Stokes settling) equal to 1/9 of the sample weight was added as an internal standard while the sample was wet and was homogenized with the sample. Samples were mounted as oriented aggregates on silver filters, and swelling clays were expanded with ethylene glycol.

Each sample was x-rayed over the interval  $3^\circ\text{-}30^\circ 2\theta$  using Ni-filtered, monochromatized,  $\text{CuK}\alpha$  radiation at 45kV and 35 ma. The peak areas of smectites, chlorites, kaolinite, illite, plagioclase, amphibole and quartz were determined using an interactive peak area determination program. Duplicate samples were x-rayed without glycolation and after heating to  $490^\circ\text{C}$  for 2 hrs. to aid in the identification of mixed layer clays. The overlapping {001} illite and {001} talc peaks and the overlapping {002} kaolinite and {004} chlorite peaks were resolved using an interactive curve resolving program. The weight percents of each of the clay mineral groups, plagioclase, amphibole and quartz were estimated by converting the peak areas to weight percent in the sample using the weighting factors developed by Heath and Piasis (1979) for surface sediments of the North Pacific.

### 3.2 Total Quartz Analysis

In preparation for determining the concentration of quartz in the total sample, the samples were treated with buffered acetic acid to remove calcium carbonate. They were then ground wet in automatic corundum grinders to achieve a more uniform grain size. After drying, a quantity of  $\alpha$ -alumina equal to half the sample weight was added as an internal standard, the samples were fired at  $1000^\circ\text{C}$  for 24 hours to remove clay mineral interferences (Till and Spears, 1969), and were powdered and x-rayed in duplicate over the {012} (3.48 Å)  $\alpha$ -alumina peak and the {101} (3.34 Å) quartz peak. The ratio of quartz/alumina peak areas was converted to weight percent quartz in each sample by reference to a calibration curve determined by standard additions of quartz to samples from core RC14-105. A more detailed description of the total quartz determination technique is given by Leinen (1985).

### 3.3 Accumulation Rates

In order to compare the amount of each mineral group accumulating in cores along the transect, it is necessary to calculate mass accumulation (flux) rates for each of the cores at each sample depth. This is because the concentration of the various mineral groups varies in response to the input of each other sedimentary component. The mass flux measured in

$\text{g}(\text{cm}^2 \cdot 10^3 \text{ yr})^{-1}$  of the individual components is the product of the linear sedimentation rate in  $\text{cm}(10^3 \text{ yr})^{-1}$ , the dry bulk density of the sediment in  $\text{g}(\text{cm}^3)^{-1}$ , and the concentration of the individual components in wt%. The sedimentation rates were calculated from the stratigraphies indicated above and range from 0.9 - 7.8  $\text{cm}(10^3 \text{ yr})^{-1}$ . The dry bulk densities were calculated by Rea and Leinen (1988) and ranged from 0.2 - 0.3  $\text{g}(\text{cm}^3)^{-1}$ .

## 4. RESULTS

### 4.1 *Mineralogy of Transect Cores*

Each mineral in the  $<2 \mu\text{m}$  fraction has a variable spatial and temporal abundance distribution along the transect (e.g. Fig. 2, Table 2). Because an internal standard was used, the minerals in the clay-sized fraction are not forced to sum to 100%. There were trace amounts of other minerals and mineral groups present in the sample, including mixed-layer clays, amphiboles, and iron oxides, but these phases never accounted for more than 1 or 2% of the total diffracting material. Thus, differences in sum of the minerals and mineral groups reflect differences in the overall amount of crystalline material in the sample. The remaining, non-diffracting, material will include amorphous oxides and oxyhydroxides, refractory organic material, biogenic silica incompletely removed by the sodium carbonate dissolution, and volcanic ash. The percentages of diffracting material along the transect range from about 40 to 100% (Table 2). This range is in agreement with that found by Heath and Pisias (1979) in northwest Pacific surface sediments.

Core V21-171 was not included in Heath and Pisias' (1979) study of surface sediment clay mineralogy. It is in a location at the western extreme of distal turbidite influence and was within the area influenced by ice-rafting during the glacial maximum (Conolly and Ewing, 1970). Its sediment grain size is generally a factor of two larger than that of sediments from cores along the transect (Rea and Leinen, 1988). Nonetheless, the accumulation rates of total sediment, of the  $<2 \mu\text{m}$  sediment fraction, and of the mineral groups in the core are generally lower than those of the transect. One time interval (24-25 KY) had an unrealistically high total for diffracting material (149%), and one time interval (10-12 KY) had an unrealistically low total (10%; Table 2). The mineral ratios in the sediment are unaffected by these differences in inferred crystallinity, but the mineral percents and accumulation rates are influenced.

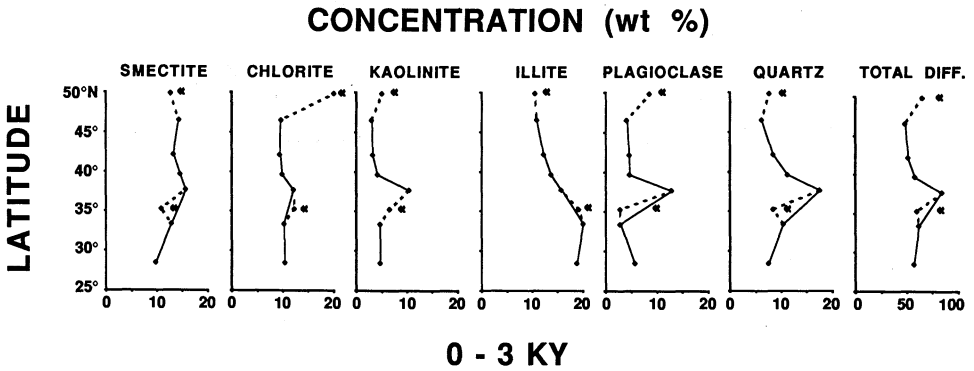


Figure 2. The concentration (in wt %) of mineral groups and individual minerals in the  $<2\mu\text{m}$  fraction of samples along the transect during the 0-3 KY time interval. Data for the concentrations of minerals in the two cores east of the transect are also included and are indicated with an arrowhead.



Table 2. Mineral abundances (wt %) in the <2 $\mu$ m fraction of northwest Pacific cores.

Depth	Age	Smectite	Chlorite	Kaolinite	Illite	Plagioclase	Quartz	Total
<b>V28-294</b>								
1.0	1.2	9.78	10.32	4.64	18.76	5.59	7.49	56.57
16.0	18.6	9.59	11.49	2.88	14.40	3.13	7.47	48.95
<b>RC10-167</b>								
5.5	2.3	12.90	10.18	4.60	20.93	2.82	10.41	61.83
10.5	4.3	14.41	10.36	4.45	17.64	2.87	9.85	59.58
<b>V20-129</b>								
11.0	1.4	15.68	12.13	10.40	15.67	12.90	17.50	84.27
45.0	5.8	35.12	14.65	10.25	14.59	9.51	14.41	98.52
85.0	10.9	17.45	8.75	5.85	13.86	2.51	7.08	55.49
185.0	24.0	18.31	12.79	7.55	15.65	5.83	15.42	75.56
231.0	29.9	12.65	7.80	4.29	18.44	6.20	6.85	56.23
<b>RC14-105</b>								
1.0	0.2	14.56	9.83	4.22	13.69	4.72	11.18	58.20
20.0	3.3	12.82	14.20	3.78	11.86	5.88	13.12	61.65
34.5	5.7	5.69	11.83	8.93	21.56	2.63	5.51	56.15
45.0	7.4	13.71	12.80	6.90	18.95	7.76	10.61	70.74
59.0	9.7	18.13	9.58	4.11	20.94	3.29	10.24	66.30
65.5	10.7	16.47	6.98	3.92	16.34	3.40	10.25	57.36
85.0	13.9	19.00	11.15	5.79	20.02	4.01	12.80	72.77
97.5	16.0	23.63	10.12	5.26	20.28	3.30	10.93	73.52
111.0	18.2	15.48	9.19	5.92	20.79	3.95	11.93	67.25
135.5	22.3	14.74	10.08	4.77	22.10	2.29	8.21	62.20
143.0	23.5	21.89	12.64	5.43	19.49	4.23	10.73	74.41
147.0	24.2	9.44	7.87	5.26	18.62	1.41	7.19	49.80
153.0	25.2	19.77	9.35	6.03	19.43	3.85	10.54	68.98
158.5	26.1	24.52	11.71	8.50	17.32	5.21	12.66	79.91
168.5	27.8	41.32	16.73	8.17	16.41	7.13	10.24	100.00
<b>V20-126</b>								
18.5	3.0	13.28	9.42	3.12	12.27	4.52	8.44	51.03
41.5	6.7	8.78	8.19	3.69	10.31	4.03	6.17	41.18
68.8	11.1	10.05	10.11	5.01	10.44	4.02	7.18	46.80
115.0	18.6	19.23	13.70	8.01	15.06	7.85	10.60	74.44
149.0	24.1	10.06	9.40	4.44	10.77	3.66	7.97	46.30
184.0	29.7	15.52	19.31	5.14	10.48	7.35	5.15	62.95
<b>V20-122</b>								
10.0	2.3	14.36	9.64	2.91	10.86	4.04	6.16	47.97
27.0	6.1	17.34	8.65	3.72	34.64	6.19	10.35	80.89
49.0	11.0	11.62	10.50	5.16	11.99	4.78	8.60	52.65
80.0	17.9	11.84	16.09	7.95	20.64	4.80	10.11	71.44
107.0	23.9	20.54	17.35	8.93	14.85	10.48	13.71	85.86
133.5	29.9	14.82	11.45	3.64	12.53	2.88	9.62	54.94
<b>V32-126</b>								
0.0	0.0	10.86	12.20	6.58	19.19	2.82	8.39	60.05
14.5	6.4	9.79	14.43	4.79	17.07	3.37	11.83	61.27
39.5	17.6	24.10	18.79	4.45	19.99	5.21	15.50	88.03
54.5	24.2	5.68	9.60	3.39	14.33	2.08	7.42	42.49
<b>V21-171</b>								
3.0	3.4	12.73	20.22	5.06	10.46	8.52	7.60	64.59
10.5	11.4	1.75	2.27	3.69	0.76	0.24	0.88	9.58
16.5	18.0	29.53	19.07	3.95	10.12	11.30	10.93	84.89
21.8	23.9	51.72	30.24	14.97	34.40	14.94	2.80	149.08
27.0	29.3	20.33	13.38	5.26	14.53	3.64	12.76	69.91

Illite and smectite are the most abundant minerals along the transect (illite average = 16.7%, smectite average = 16.2%) and have the maximum concentrations (illite maximum = 34.6%, smectite maximum = 41.2%). Kaolinite and plagioclase are the least abundant minerals along the transect (kaolinite average = 5.7%, plagioclase average = 5.1%) and have the minimum concentrations (kaolinite minimum = 2.9%, plagioclase minimum = 1.4%). The average concentration of chlorite along the transect is 11.3% and the average concentration of quartz in the <2  $\mu\text{m}$  fraction is 9.9%.

All minerals are presently most abundant between 34 and 37°N, the latitude at which the probability of eolian transport from the arid regions of Asia is presently greatest (Merrill, this volume). For all minerals except illite the concentrations are lower north and south of this latitude. Illite has its highest concentrations in the southern half of the transect. Core V21-171 has high concentrations of chlorite, plagioclase, and quartz (minerals commonly associated with physical weathering of sedimentary rocks).

The abundance of quartz has been calculated as a percentage of the non-biogenic sediment (Fig. 3, Table 3) using values for calcium carbonate determined by acid dissolution and values for biogenic silica determined during the quartz analysis. Quartz abundance is also greatest between 33 and 39°N, but is greater above this mid-latitude peak than below it both at present and during the glacial maximum (Fig. 3).

#### **4.2 Mineral Fluxes in Transect Cores**

The fluxes of each mineral in the <2  $\mu\text{m}$  fraction were also calculated (Fig. 4, Table 4). The flux or accumulation rate is independent of the variation in input of any other component of the sediment and is therefore the parameter most representative of true variation along the transect. The differences between the distribution of mineral percents (Fig. 2) and fluxes (Fig. 4) for the 0-3 KY interval clearly show the influence of dilution on percentage data. For example, the illite concentration south of 35°N is large, but the flux of illite is much lower at these latitudes than between 35 and 40°N. The flux of the total sediment and the eolian fraction calculated by Rea and Leinen (1988) and of the <2  $\mu\text{m}$  fraction (calculated for this study) are also shown for comparison. Mineral fluxes at the two sites east of the transect are included on the diagrams.

For each time interval the flux of the total sediment, the eolian fraction, the <2  $\mu\text{m}$  fraction, and of most mineral groups is greatest between 37° and 42°N. The overall pattern of flux along the transect is strongly

## QUARTZ CONCENTRATION (WT % IN NON-BIOGENIC SEDIMENT)

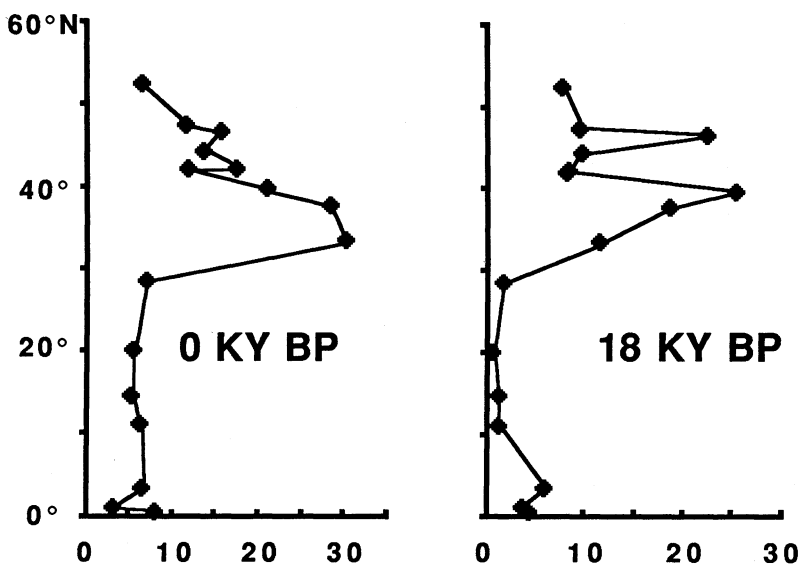


Figure 3. The concentration (in wt %) of quartz in the non-biogenic fraction of northwest Pacific surface sediments and in sediments deposited during the glacial maximum, 18 KY BP.

Table 3. Concentration and accumulation rate of quartz (total sediment) of northwest Pacific sediments.

Depth (cm)	Age (ky)	Accum Rate (g/cm <sup>2</sup> /ky)	%Qz (g/cm <sup>2</sup> /ky)	Quartz Rate (g/cm <sup>2</sup> /ky)	Depth (cm)	Age (ky)	Accum Rate (g/cm <sup>2</sup> /ky)	%Qz (g/cm <sup>2</sup> /ky)	Quartz Rate (g/cm <sup>2</sup> /ky)	Depth (cm)	Age (ky)	Accum Rate (g/cm <sup>2</sup> /ky)	%Qz (g/cm <sup>2</sup> /ky)	Quartz Rate (g/cm <sup>2</sup> /ky)
<b>V24-109 (0°26'N 158°48'E)</b>														
0.0	0.0	2778	8.4	234	<b>RC10-167 (83°24'N 150°23'E)</b>									
50.0	18.0	2778	9.8	272	5.5	2.3	483	30.7	148	<b>V21-173 (44°22'N 163°33'E)</b>				
<b>V28-203 (0°57'N 179°25'W)</b>					10.5	4.3	519	29.7	154	21.0	21.6	190	14.1	27
1.0	0.5	682	3.6	25	42.2	17.3	0	17.0	0	<b>V20-122 (46°34'N 161°44'E)</b>				
6.5	2.9	687	4.2	29	<b>V20-129 (97°41'N 156°35'E)</b>									
9.5	4.3	700	3.6	25	11.0	1.4	1540	28.9	446	10.0	2.3	813	16.1	131
14.5	6.5	844	3.6	30	45.0	5.8	2404	5.2	125	27.0	6.1	1046	8.7	91
21.0	9.5	953	25.8	246	85.0	10.9	2085	32.4	674	49.0	11.0	1149	28.0	322
25.0	11.3	1120	5.3	59	139.5	18.1	1618	24.0	388	80.0	17.9	858	28.0	240
27.0	12.2	1120	7.1	80	185.0	24.0	2287	30.4	694	107.0	23.9	1207	29.6	357
<b>RC14-105 (89°41'N 157°33'E)</b>														
31.5	14.0	1191	6.5	78	231.0	29.9	2101	25.6	539	<b>V20-120 (47°24'N 167°45'E)</b>				
39.0	17.6	1282	5.5	70	1.0	0.0	1141	21.5	245	0.0	0.0	576	9.4	94
43.0	18.5	1191	6.9	82	11.0	1.8	1586	22.1	350	10.0	2.7	85	8.5	85
47.0	21.2	1104	8.7	96	20.0	3.3	1208	17.3	209	16.0	4.4	11.7	11.7	11.7
51.0	23.0	960	7.5	72	34.5	5.7	2220	12.5	277	33.5	9.2	209	6.5	13.0
58.0	26.1	953	9.5	90	45.0	7.4	1556	26.0	404	43.5	11.9	314	14.5	15.2
61.5	27.7	1011	6.0	60	59.0	9.7	1366	23.0	314	55.5	15.8	504	12.8	14.4
65.5	29.5	1138	6.4	73	65.5	5.7	1745	28.9	504	66.5	18.0	314	14.5	14.5
71.0	32.0	1162	5.0	58	85.0	13.9	1220	30.7	375	76.5	20.0	375	12.8	12.8
<b>V28-238 (1°01'N 160°29'E)</b>														
1.0	0.5	2000	3.8	77	97.5	16.0	1330	28.9	384	83.5	21.4	384	13.0	13.0
34.5	17.3	2000	9.1	181	111.0	18.2	1128	30.7	347	94.5	23.6	347	13.7	13.7
3.5	2.3	1500	7.1	107	135.5	22.3	1122	26.7	300	102.0	25.1	300	13.0	13.0
29.5	17.3	1500	11.4	171	142.5	23.3	1200	29.0	347	106.5	26.0	347	11.8	11.8
0.0	0.0	510	6.7	34	147.0	24.2	1326	30.7	407	116.5	28.7	407	14.2	14.2
20.0	18.0	510	6.6	34	153.0	25.2	1092	30.0	328	126.5	31.5	328	13.1	13.1
0.0	0.0	510	6.6	34	158.5	26.1	1152	31.1	338	<b>V21-172 (47°34'N 164°21'E)</b>				
20.0	18.0	510	6.6	34	168.5	27.6	1344	29.5	396	0.0	0.0	381	13.3	51
0.0	0.0	510	5.8	30	18.5	3.0	997	18.0	179	35.0	18.0	381	11.8	45
20.0	18.0	510	6.6	34	41.5	6.7	1448	18.6	269	<b>V21-171 (49°53'N 164°57'W)</b>				
0.0	0.0	510	6.6	34	68.8	11.1	823	16.6	136	3.0	3.4	278	8.0	22
20.0	18.0	510	6.0	22	114.5	18.6	1708	13.6	233	6.5	6.0	316	5.3	17
0.0	0.0	361	6.0	22	149.0	24.1	1269	13.6	173	10.5	11.4	586	2.7	16
16.0	19.2	361	6.0	22	184.0	29.7	997	27.1	270	16.5	18.6	311	4.8	15
1.0	1.2	361	7.4	27	<b>V21-148 (42°05'N 160°36'E)</b>									
16.0	19.2	361	7.1	26	2.0	2.7	219	12.3	27	27.0	30.4	502	6.5	33
<b>V28-294 (28°26'N 139°58'E)</b>														
1.0	1.2	361	7.4	27	3.0	2.7	219	12.3	27	<b>V21-151 (52°16'N 163°38'E)</b>				
16.0	19.2	361	7.1	26	20.0	18.0	219	13.8	30	0.0	0.0	109	6.9	8
<b>V21-151 (52°16'N 163°38'E)</b>														
1.0	1.2	361	7.1	26	20.0	18.0	219	13.8	30	10.0	18.0	109	6.9	8
16.0	19.2	361	7.1	26	20.0	18.0	219	13.8	30	10.0	18.0	109	6.9	8
<b>V21-151 (52°16'N 163°38'E)</b>														
1.0	1.2	361	7.1	26	20.0	18.0	219	13.8	30	10.0	18.0	109	6.9	8
16.0	19.2	361	7.1	26	20.0	18.0	219	13.8	30	10.0	18.0	109	6.9	8

Table 4. Accumulation rates (g/cm<sup>2</sup>/ky) of <2μm mineral components of northwest Pacific sediments.

Depth (cm)	Age (ky)	%Clay	Accumulation Rates (g/cm <sup>2</sup> /ky)									
			Total	Eolian	Clay	Smectite	Chlorite	Kaolinite	Illite	Plagioclase	Quartz	
<b>V28-294</b>												
1.0	1.2	27	206	55	15	1	2	1	3	1	1	
16.0	18.6	34	474	211	72	7	8	2	10	2	5	
<b>RC10-167</b>												
5.5	2.3	22	483	411	90	12	9	4	19	3	9	
10.5	4.3	26	519	452	118	17	12	5	21	3	12	
<b>V20-129</b>												
11.0	1.4	34	1540	999	340	53	41	35	53	44	59	
45.0	5.8	29	2404	1596	463	163	68	47	68	44	67	
85.0	10.9	28	2085	1301	364	64	32	21	50	9	26	
185.0	24.0	27	2287	1591	430	79	55	32	67	25	66	
231.0	29.9	34	2101	1431	487	62	38	21	90	30	33	
<b>RC14-105</b>												
1.0	0.2	28	1141	658	184	27	18	8	25	9	21	
20.0	3.3	30	1208	643	193	25	27	7	23	11	25	
34.5	5.7	22	2220	1678	369	21	44	33	80	10	20	
45.0	7.4	33	1556	1001	330	45	42	23	63	26	35	
59.0	9.7	28	1366	880	246	45	24	10	52	8	25	
65.5	10.7	35	1745	1108	388	64	27	15	63	13	40	
85.0	13.9	22	1220	845	186	35	21	11	37	7	24	
97.5	16.0	32	1330	879	281	66	28	15	57	9	31	
111.0	18.2	27	1128	725	196	30	18	12	41	8	23	
135.5	22.3	25	1122	746	187	27	19	9	41	4	15	
142.5	23.5	35	1200	739	259	57	33	14	50	11	28	
147.0	24.2	30	1326	846	254	24	20	13	47	4	18	
153.0	25.2	26	1092	692	180	36	17	11	35	7	19	
158.5	26.1	23	1152	722	166	41	19	14	29	9	21	
168.5	27.8	27	1344	896	242	100	40	20	40	17	25	
<b>V20-126</b>												
18.5	3.0	34	997	557	189	25	18	6	23	9	16	
41.5	6.7	23	1448	1028	236	21	19	9	24	10	15	
68.8	11.1	29	823	627	182	18	18	9	19	7	13	
114.5	18.6	22	1708	1346	296	57	41	24	45	23	31	
149.0	24.1	26	1269	947	246	25	23	11	27	9	20	
184.0	29.7	30	997	720	216	34	42	11	23	16	11	
<b>V20-122</b>												
10.0	2.3	28	813	486	136	20	13	4	15	6	8	
27.0	6.1	31	1046	769	238	41	21	9	83	15	25	
49.0	11.0	34	1149	671	228	27	24	12	27	11	20	
80.0	17.9	34	858	651	221	26	36	18	46	11	22	
107.0	23.9	34	1207	911	310	64	54	28	46	32	42	
133.5	29.9	27	1605	1209	326	48	37	12	41	9	31	
<b>V32-126</b>												
0.0	0.0	29	540	ND								
14.5	6.4	29	540	ND								
39.5	17.6	29	585	201	58	14	11	3	12	3	9	
54.5	24.2	29	720	130	38	2	4	1	5	1	3	
<b>V21-171</b>												
3.0	3.4	29	278	211	61	8	12	3	6	5	5	
10.5	11.4	29	586	492	143	2	3	5	1	0	1	
16.5	18.0	29	311	244	71	21	13	3	7	8	8	
21.8	23.9	29	571	489	142	73	43	21	49	21	4	
27.0	29.3	29	502	397	115	23	15	6	17	4	15	

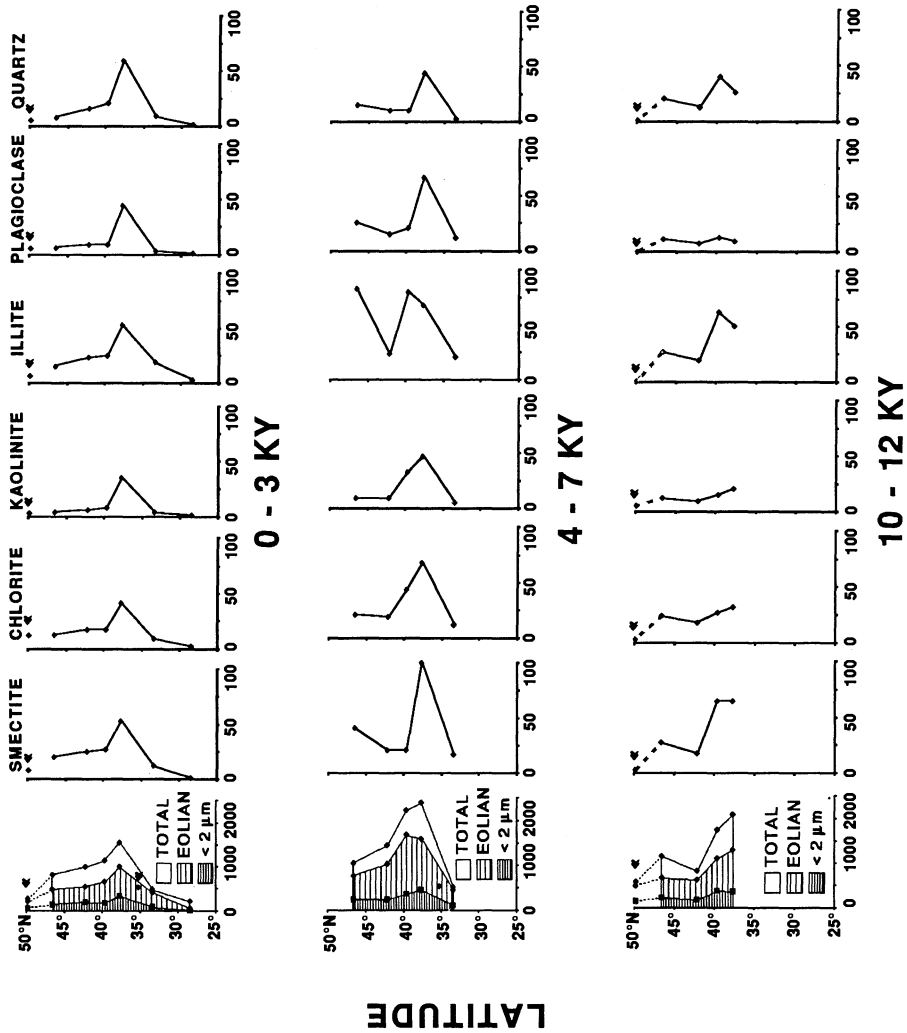
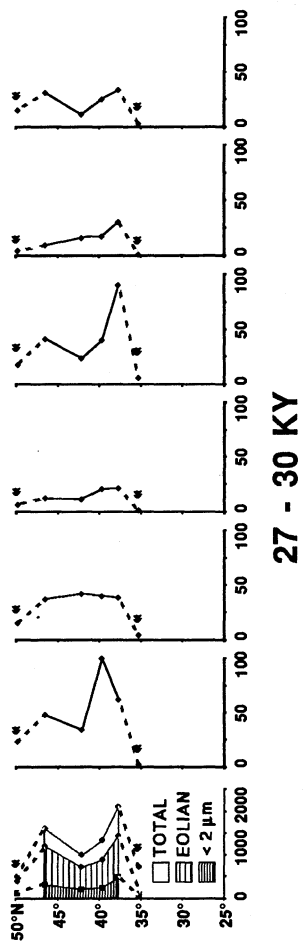
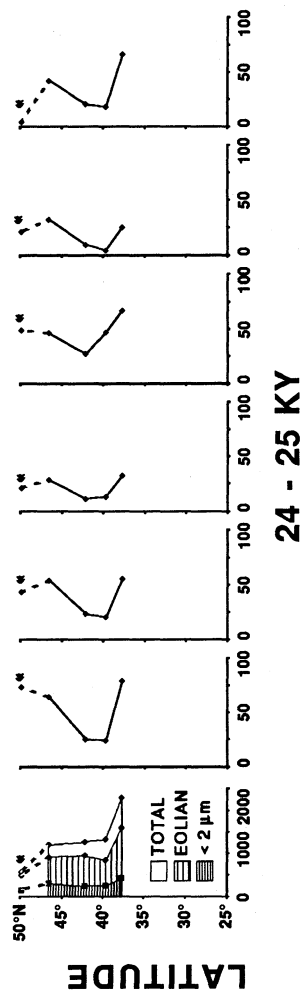
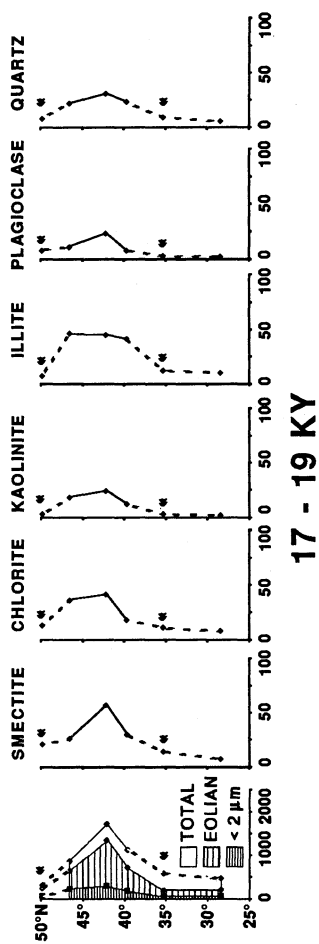


Figure 4. The accumulation rate (in  $\text{g}/\text{cm}^2/\text{ky}$ ) of the total sediment, the eolian fraction of the sediment (Rea and Leinen, 1988), the  $<2\mu\text{m}$  fraction of the sediment, and of individual minerals and mineral groups along the transect during the six time intervals. Data for the accumulation rates in the two cores east of the transect are also included and are indicated with an arrowhead.



LATITUDE

influenced by the high rates of accumulation during all time intervals at V20-129 (37°41'N). The accumulation rates increase toward the latitude of V20-129 during all but the 24-25 KY interval, however, and there is no evidence from the lithology or appearance of the core or the core location to suggest that the accumulation rates at this site are anomalous.

There is a decrease in eolian flux,  $<2 \mu\text{m}$  flux, and the flux of most mineral groups to the south of 37°N for all time intervals which have core data south of this latitude. The decrease in these fluxes to the north of 42°N is not consistent, however. The 0-3 KY and 17-19 KY intervals show a consistent drop in flux to the north, while other time intervals have a minimum at 42°N. The rates of accumulation of mineral groups and of the total  $<2 \mu\text{m}$  fraction during all time intervals at V20-126 (42.2°N) are relatively low for its latitude. During all time intervals except 24-25 KY, the total sediment flux and the eolian flux calculated by Rea and Leinen (1988) for this site was relatively large, however. Thus, a greater proportion of the eolian flux is in larger size fractions at this core site. This highlights the need for mineral data for the  $>2 \mu\text{m}$  fraction in the future to understand both the composition and flux of eolian sediment in the oceans.

The data from the two cores sites east of the transect were included in the profiles and are marked on the figures with arrows. For intervals with data along the entire transect, it is clear that the eastern sites always have lower accumulation rates than do the sites along the transect. This pattern is in agreement with both present-day mineral aerosol deposition rates in the North Pacific (e.g. Blank, *et al.*, 1985) and the accumulation rate of eolian sediment in other North Pacific sites (Janecek, 1985), both of which show an exponential decrease in total eolian deposition with increasing distance from the Asian continent. It is particularly interesting that core V21-171 has low accumulation rates at all time intervals. It is south of the limit of ice-rafted debris in glacial-age sediments from the North Pacific (Conolly and Ewing, 1970). It is also in a location which could receive fine-grained nepheloid layer transport from North America. Contributions from these sources were not as large as the accumulation rate of fine-grained material from eolian transport further west.

The complexity of the distribution of individual mineral fluxes along the transect contrasts with the latitudinal patterns of mineral distribution in the Atlantic (Biscaye, 1965). There is no consistent increase in the rate of plagioclase or chlorite accumulation, minerals characteristic of physically weathered sedimentary rocks, to the north along the transect. Likewise there is no consistent increase in the rate of kaolinite accumulation or in the ratio of kaolinite to chlorite toward the south along the transect.



The most important mineral along the transect varies from interval to interval. For example, quartz has the peak concentration and accumulation rate along the 0 - 3 KY transect, but illite is more abundant along the entire transect. Chlorite has the peak concentration along the 4-7 KY transect. Plagioclase is generally the least important mineral in the assemblage.

There is great variation in the overall patterns of mineral distribution from one time interval to another. The time intervals which have the most similar rates are the 0-3 KY and 17-19 KY intervals. This was quite surprising as the 17-19 KY interval represents the last glacial maximum and a time interval during which abundant atmospherically transported loess was being deposited in Asia (Liu Tung-sheng, *et al.*, 1982). These data suggest that while the amount of  $<2 \mu\text{m}$  material was similar to 17-19 Ka, it was concentrated about  $5^\circ$  further north during the glacial maximum. Time intervals other than 0-3 KY and 17-19 KY have far greater overall accumulation of clay minerals. Rea and Leinen (1988) also found greater accumulation of the total eolian component of the sediment at 4-7 and 10-12 KY.

### 4.3 Time Series of Mineralogy of RC14-105

RC14-105 ( $39^\circ 41' \text{N}$ ) is located within the zone of maximum eolian sedimentation. It was sampled at approximately 2 KY intervals to form a time series of mineral accumulation for the past 30 KY that would be representative of the temporal changes in eolian sediment composition and accumulation at the latitudes of maximum eolian influence. The rate of accumulation of the total eolian fraction and the  $<2 \mu\text{m}$  fraction (Fig. 5) is greatest about 5 Ka. Studies of the accumulation of the eolian fraction along the entire transect (Rea and Leinen, 1988) show that this is the case at all of the core locations.

The clay-sized fraction of the sediment in RC14-105 is dominated by smectites and illite as is the clay fraction along most of the transect (Table 2). Kaolinite and plagioclase are the least important minerals. Although the rate of  $<2 \mu\text{m}$  quartz accumulation is low, quartz is an important component of the total sediment (Table 3) comprising 20-30 wt%. It accounts for only about 10% of the  $<2 \mu\text{m}$  fraction. This composition is also typical of all cores along the transect. Thus, the core should be a good representative of the changes in eolian influence through time.

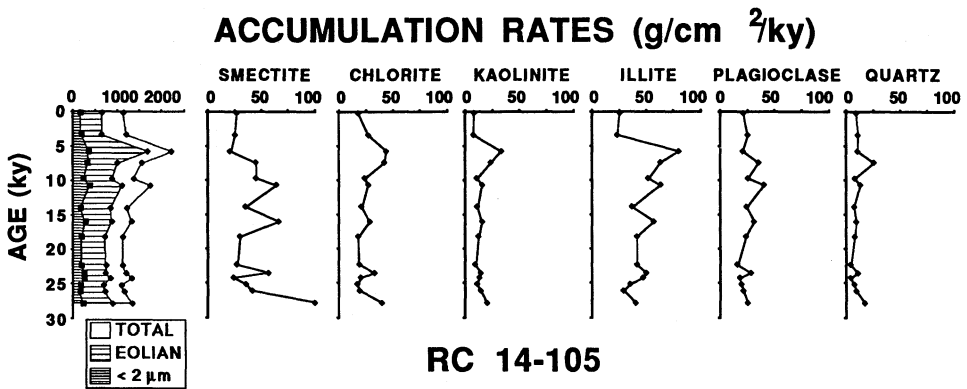


Figure 5. The accumulation rate (in  $\text{g/cm}^2/\text{ky}$ ) of the total sediment, the eolian fraction of the sediment (Rea and Leinen, 1988), the  $<2\mu\text{m}$  fraction of the sediment, and of individual minerals and mineral groups at RC14-105 for the past 30 KY.

The temporal patterns of mineral accumulation show quite clearly that although the sediment is dominated by smectites and illite, the two mineral groups are not correlated. Each has a distinctive pattern of variation through time: the maximum accumulation rate of illite occurred about 5-10 Ka while that of smectite occurred 10-18 Ka and before 27 Ka. Most minerals have their maximum flux between 5 and 10 Ka, some earlier in the interval and some later. Only kaolinite and plagioclase have temporal accumulations patterns that are somewhat similar.

One of the most surprising conclusions from the RC14-105 data is that the eolian sediment does not increase in accumulation toward the period of maximum glacial extent 17-19 Ka with a decrease after that interval. Most minerals do have minor accumulation rate maxima during that time, however. Thus, the interval which is characterized by extensive eolian deposition of loess on the continent is not associated with enhanced eolian deposition in the North Pacific.

## 5. MODELING RESULTS

### 5.1 Factor Analysis

An interpretation of the areal or temporal distribution and flux of individual minerals in sediments, even those thought to be dominantly eolian, ignores the important facts that the source rocks and soils for the sediment are not monomineralic and that many minerals are common to more than one source area. Recent studies of modern mineral aerosol transported to the North Pacific indicate that it is best described by assemblages of minerals (Leinen, *et al.*, in prep.). In order to determine whether the variation in mineral composition of the northwest Pacific clays could be explained by the variation of mineral groups instead of individual minerals, the  $<2 \mu\text{m}$  mineral data for both the transect cores and for the more closely spaced samples of RC14-105 (for a total of 40 samples with 6 variables) were analyzed using Q-mode factor analysis with VARIMAX factor rotations (Klovan and Imbrie, 1971).

The model results suggest that 84% of the sums of squares of the data set can be explained by 3 mineral assemblages or "factors". This 3-factor model explains more than 80% of the variance in each mineral except kaolinite (76%) and smectite (64%). The factor "score" for each mineral indicates the importance of the variance of the mineral in describing the end-member or factor. Factor 1 explains 45% of the sums of squares and is dominated by the variance of quartz and plagioclase (Table 5, Fig. 6). Factor

2 explains 21% of the sums of squares and is dominated by the variance of illite and quartz. Factor 3 explains 17% of the sums of squares and is dominated by the variance of illite, but has a strong inverse relationship with quartz (Table 5).

Because data were also available for the total quartz content of the sediment, a second model was run including total quartz as a variable. The results of this model indicated that total quartz is poorly correlated with the <2  $\mu\text{m}$  fraction quartz: total quartz was segregated as a separate factor in the model. The remaining 3 factors were virtually identical to those of the model run in which total quartz was not included. This was not surprising because the grain-size data of Rea and Leinen (1988) suggest that only 20-30% of the sediment is in the <2  $\mu\text{m}$  size fraction. This experiment emphasizes that the clay-size mineralogy generally studied for deep-sea sediments cannot be extrapolated to represent the total sediment.

The factor scores discussed above indicate which minerals dominate the variance of the data, but the factors cannot be used to describe the composition of the mineral assemblages. Miesch (1976) has shown that composition information can be extracted from the analysis if the data have been summed to a constant. Because the x-ray diffraction data indicate that there are no minerals present in greater than trace amounts in the <2  $\mu\text{m}$  fraction of the sediments that are not included in the analysis, summing the six mineral groups to a constant percentage (in this case 100%) is warranted. The compositions indicated by such a transformation using Miesch's (1976) EQMAIN program (Fig. 6, Table 5) suggest that while the variations in illite, quartz, and plagioclase indicated by the factor analysis are very important, the mineral assemblages also contain substantial amounts of other minerals. Factor 1, which was dominated by the variance of plagioclase and quartz, actually contains more smectite and chlorite than quartz and plagioclase. Factor 2, dominated by the variance of illite and quartz, is also rich in smectite. Factor 3, dominated by the variance of illite, is also rich in chlorite.

The distribution of factors in samples along the transect (Fig. 7) shows that Factor 1 is most abundant in samples at the northern end of the transect, as well as in samples at the latitude of the eolian maximum. The distributions of Factor 2 and Factor 3 are highly variable along the transect.

**Table 5. VARIMAX Scores and composition vectors**

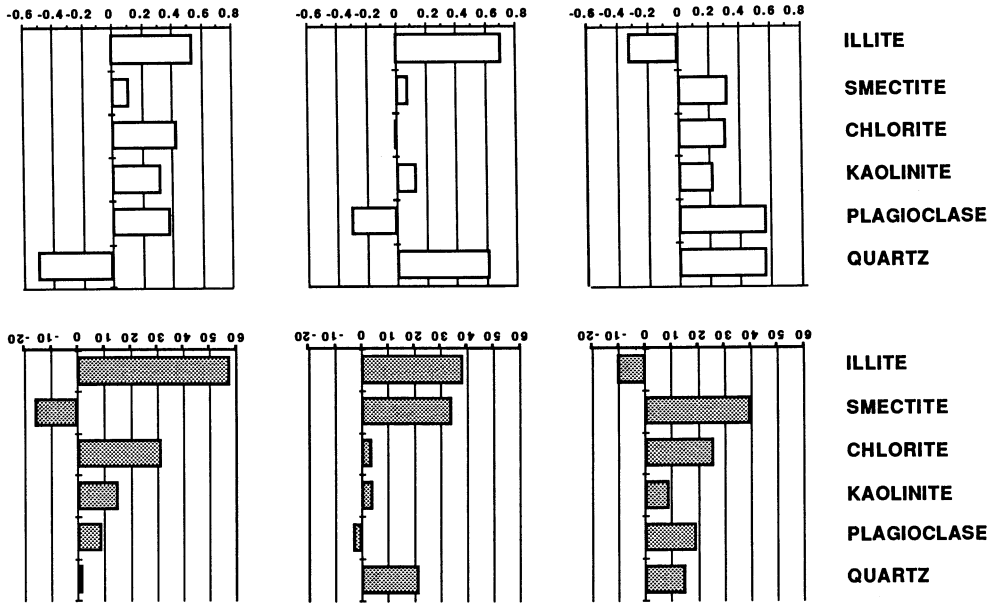
## VARIMAX Scores

	Factor		
	I	II	III
Illite	-0.32	0.71	0.54
Smectite	0.32	0.08	0.11
Chlorite	0.31	-0.01	0.43
Kaolinite	0.22	0.13	0.32
Plagioclase	0.57	-0.31	0.38
<2 $\mu$ m Quartz	0.57	0.62	-0.51

## Composition vectors from EQMAIN

	Factor		
	I	II	III
Illite	-10.09	38.26	57.39
Smectite	40.07	34.57	-15.96
Chlorite	25.95	4.1	31.79
Kaolinite	9.26	4.14	15.58
Plagioclase	19.45	-2.83	9.28
<2 $\mu$ m Quartz	15.33	21.74	1.9

## FACTOR SCORE



## CONCENTRATION (wt%)

Figure 6. The VARIMAX factor scores and factor compositions from a Q-mode factor analysis of the mineral data.

## 6. DISCUSSION

### 6.1 *Factor Compositions and Eolian Sources*

Although the model fits well in terms of explaining the variance in the data set and in all the minerals except smectite and kaolinite, there is some lack of fit as is clear from the small negative concentrations indicated for illite in Factor 1 and smectite in Factor 3. The EQMAIN model does not force the composition values to be positive as do other such transformations (e.g. Leinen and Pisias, 1984; Full, *et al.*, 1982).

Q-mode factor analysis modeling of the mineral composition of present-day mineral aerosol transported to the North Pacific (Leinen, *et al.*, in prep.) indicates that present-day mineral assemblages are also dominated by the variation in quartz, plagioclase, and illite. Furthermore, the present-day aerosol assemblages are very similar to those from this sedimentary data set.

Without the information about present-day aerosol assemblages, the factor scores and compositions for the sediments would be much more difficult to interpret. The factor scores of Factor 1 suggest that the variance in the end-member is dominated by plagioclase and quartz, but that it is rich in smectite and chlorite. Thus, it has characteristics of both high-latitude physical weathering products (chlorite, plagioclase) and temperate-latitude chemical weathering products (smectite, quartz). The abundance of the end-member in samples from sub-polar site V21-171 (Table 6) suggest that it represents physical weathering products of high latitude environments. However, the transformed compositions of the factor indicate that the end-member is actually richest in smectite and chlorite and that it contains nearly as much quartz as plagioclase. Modern aerosols collected from the northwest Pacific also contain a plagioclase-rich factor analysis end-member (Leinen, *et al.*, in prep.). These aerosols have air mass trajectories which are heavily influenced by low-altitude transport over Japan, where soils derived from weathering of andesitic volcanics add plagioclase to dust in the air (Merrill, *et al.*, in prep.). The high accumulation rate of Factor 1 in surface sediments from V20-129 and RC14-105, which lie due east of Japan, suggests that the sediments are also influenced by soil material from Japan. Such soils are also rich in smectite. Heusser (this volume) has shown that Late Quaternary and Holocene sediments from nearby core RC14-99 contain pollen typical of Japanese flora. The modern aerosols which are influenced by Japanese dust are not without Asian components, however. This component is rich in quartz. Thus, Factor 1 has been interpreted as an end-member with a significant contribution from andesitic sources.

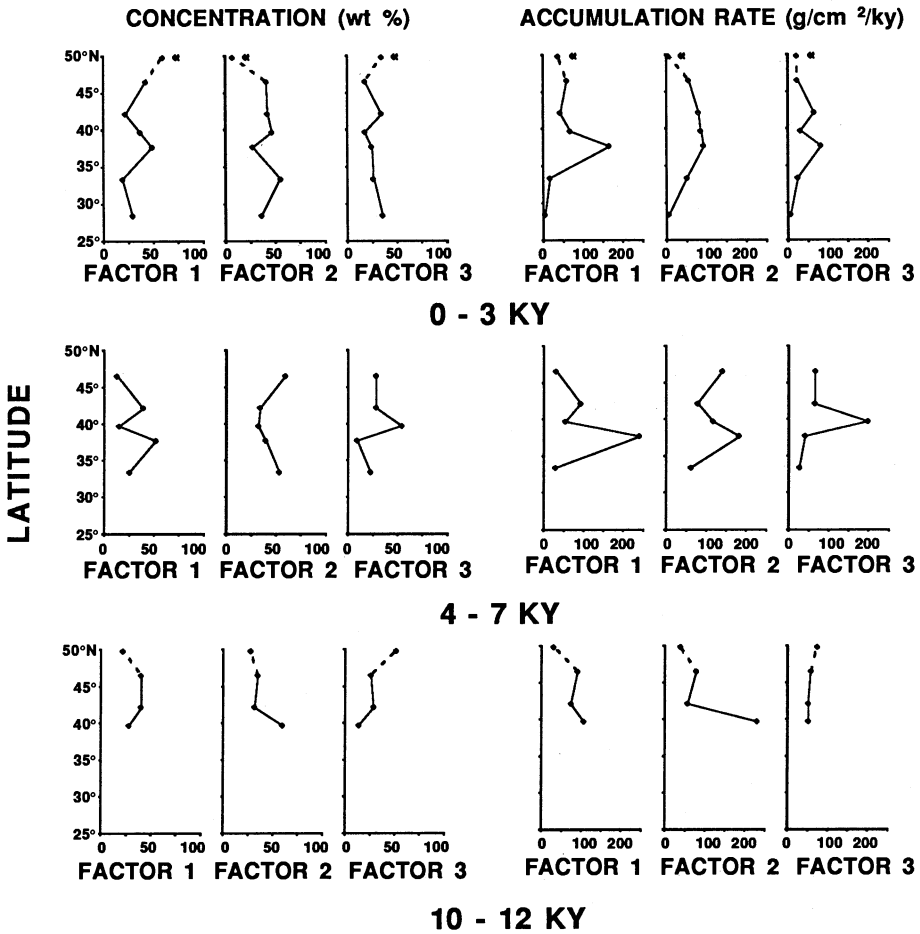
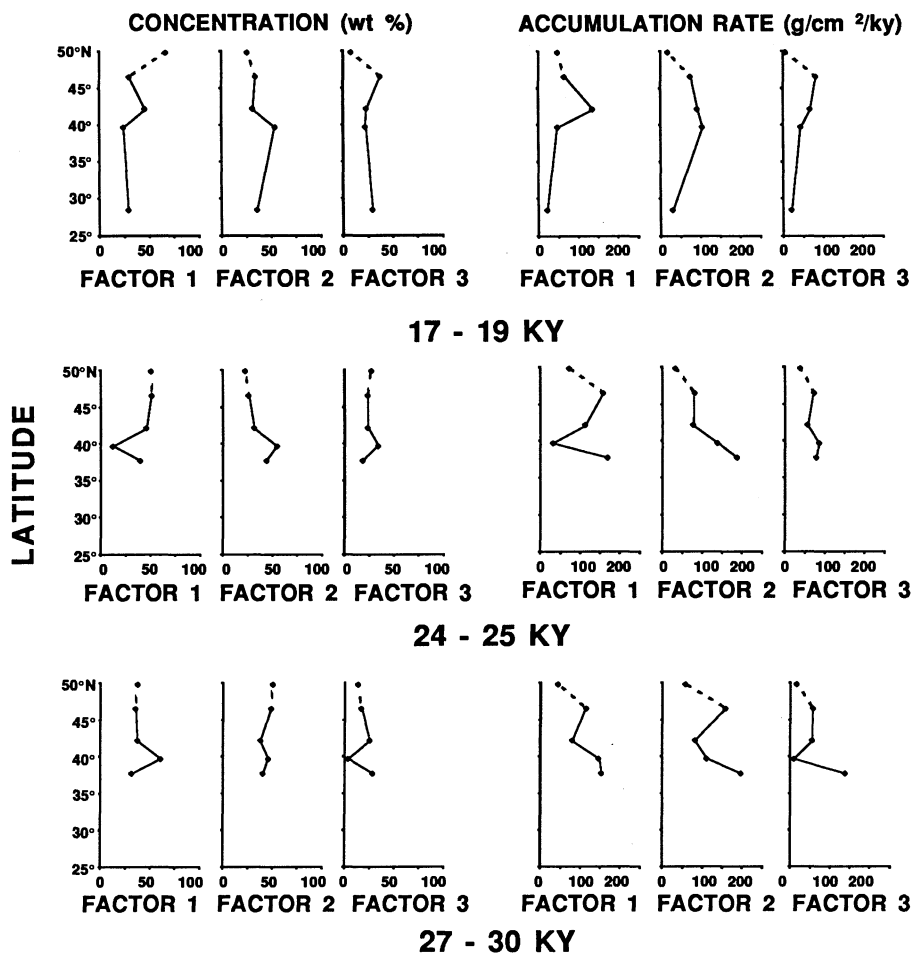


Figure 7. The concentration (in wt %) and accumulation rate (in g/cm<sup>2</sup>/ky) of the three composition factors along the transect during the six time intervals. Data for the concentration and accumulation rates in V21-171 are included and are indicated with an arrowhead.





**Table 6. Concentrations and rates of accumulation (g/cm<sup>2</sup>/ky) of end-member factors in the <math><2\mu\text{m}</math> fraction of northwest Pacific sediments.**

Core	Depth (cm)	Age (ky)	Concentration			Accumulation Rates		
			Factor 1	Factor 2 (wt %)	Factor 3	Factor 1	Factor 2	Factor 3
V28-294	1.0	1.2	29.1	36.0	34.8	4	5	5
	16.0	18.6	29.1	41.5	29.4	21	30	21
RC10-167	5.5	2.3	19.1	54.9	26.0	17	50	24
	10.5	4.3	25.1	52.9	22.0	29	62	26
V20-129	11.0	1.4	48.8	27.0	24.2	166	92	82
	45.0	5.8	51.7	39.6	8.7	239	183	40
	185.0	24.0	39.2	43.6	18.2	168	187	78
	231.0	29.9	31.5	40.2	28.3	153	196	138
RC14-105	1.0	0.2	36.7	46.3	16.9	68	85	31
	20.0	3.3	43.8	36.4	19.8	84	70	38
	34.5	5.7	14.6	31.7	53.6	54	117	198
	45.0	7.4	37.7	32.2	30.1	125	106	99
	59.0	9.7	23.0	59.1	17.9	57	146	44
	65.5	10.7	27.5	59.3	13.2	107	230	51
	85.0	13.9	28.3	53.7	18.1	53	100	34
	97.5	16.0	27.6	60.2	12.2	78	169	34
	111.0	18.2	24.1	53.6	22.3	47	105	44
	135.5	22.3	16.2	56.6	27.2	30	106	51
	142.5	23.5	31.8	51.4	16.8	82	133	43
	147.0	24.2	12.0	54.3	33.6	30	138	85
	153.0	25.2	28.0	54.5	17.5	50	98	31
	158.5	26.1	37.2	47.7	15.1	62	79	25
168.5	27.8	60.6	45.7	3.6	147	111	9	
V20-126	18.5	3.0	22.3	42.2	34.0	42	80	64
	41.5	6.7	38.8	33.6	27.7	92	79	65
	68.8	11.1	40.0	31.6	28.3	73	57	51
	115.0	18.6	45.8	31.1	23.1	136	92	68
	149.0	24.1	45.8	31.1	23.1	113	77	57
	184.0	29.7	37.2	37.6	25.2	80	81	54
V20-122	10.0	2.3	42.6	40.5	16.9	58	55	23
	27.0	6.1	12.8	59.3	27.8	31	141	66
	49.0	11.0	39.8	34.7	25.6	91	79	58
	80.0	17.9	29.4	33.6	37.0	65	74	82
	107.0	23.9	51.0	25.8	23.2	158	80	72
	133.5	29.9	34.9	48.4	16.7	114	158	55
V21-171	3.0	3.4	59.3	6.7	34.0	36	4	21
	10.5	11.4	21.7	26.8	51.4	31	38	73
	16.5	18.6	66.5	25.8	7.7	47	18	5
	21.8	24.5	50.6	22.6	26.8	72	32	38
	27.0	30.4	36.7	49.9	13.3	42	57	15

Factor 2 is dominated almost exclusively by the variance of illite and quartz. Its composition is much less varied than that of Factors 1 and 3 and is almost totally made up of illite, smectite and quartz. It is most abundant in the sediments deposited between 10 and 25 Ka at RC14-105. It accumulates most rapidly in sediments deposited between 10 and 25 Ka at RC14-105 and V20-129. Modern aerosols collected from the northwest Pacific have no end-members with compositions similar to Factor 2 (Leinen, *et al.*, in prep.). The illite-smectite-quartz assemblage is very much like loess (Zheng Hong-han, 1984), which is presently abundant in China and Soviet Central Asia (Pecsi, 1984), and which had its most rapid period of accumulation during the glacial period. The importance of this factor in sites directly downstream of the loess plateaus and its abundance during the glacial interval suggest that this factor represents a fine-grained equivalent of loess which was transported to the North Pacific during the time that loess was being deposited south of the ice margin in Asia.

Factor 3 is dominated by the variance of illite, but unlike Factor 2, it is inversely related to quartz variance. The composition vector suggests that it comprises illite and chlorite with lesser amounts of plagioclase. It contains little quartz. Although the model fit for this vector is poorer than that of the other end-members (the model predicts a relatively large negative concentration of smectite), it is clear that the end-member is a diverse mineral assemblage rich in illite and chlorite and poor in quartz and smectite. The factor is most abundant in sediments deposited 5-8 Ka at RC14-105. Modern northwest Pacific aerosols also have mineral assemblage end-members that are rich in illite, but they are generally richer in quartz and poorer in chlorite than Factor 3 (Leinen, *et al.*, in prep.). The modern aerosol end-member that is closest in composition to Factor 3 is associated with air mass trajectories that originate in northern Asia and travel over Japan at high altitude before sinking over the North Pacific (Merrill, *et al.*, in prep.). Thus, Factor 3 is most likely to represent Asian weathering products which are not mixed with Japanese sources.

## 6.2 *Temporal Changes in Factor Accumulation Rates and Eolian Sources*

The accumulation rate of the end-member factors changes along the transect with time (Fig. 7). Factors 1 and 2 accumulate at the greatest rates along the transect — for most time intervals Factor 3 accumulates at roughly half the rate of Factor 1 or 2. This would imply that most atmospheric transport to the transect over the last 30 KY has been dominated by Asian transport trajectories, which include low-latitude transport over Japan, and by trajectories which transport the fine-grained equivalent of loess to the western North Pacific.

The lack of sample material for the southern half of the transect for most of the early time intervals makes it impossible to determine whether the latitude of the accumulation rate maximum shifted with time. There are, however, clear differences in the importance of eolian accumulation at the northern end of the transect. Factor 1, with Japanese influence, has its peak accumulation during the 4-7 KY interval, but its accumulation rate 24-25 Ka and 27-30 Ka at the northern end of the transect is nearly double its present rate.

Factor 2, which is dominated by the variance of minerals associated with loess — quartz and illite — and is composed of minerals closely associated with loess — quartz, smectite and illite, dominated accumulation along the transect during the glacial maximum 17-19 Ka. These are the first data which provide specific evidence of a loess contribution to northwest Pacific sediments. However, the loess factor was accumulating at the glacial maximum at rates very similar to those of today. This factor did not accumulate most rapidly at the glacial maximum. Its peak accumulation for the entire time period sampled occurred at RC14-105 about 11 Ka, and it accumulated at very high rates along the entire transect 4-7 Ka and 24-30 Ka.

### *6.3 Time Series of Factors at RC14-105*

Factor 2, the loess factor, dominated clay-sized sediment deposition at RC14-105 during most of the past 30 KY (Table 6, Fig. 8). Factor 3, which has been interpreted to represent Asian transport (which has no Japanese influence) is the least important component in RC14-105 fine-grained sediment at all times except the 4-7 KY time interval. It is clear from the time series of factor concentrations and accumulation rates at RC14-105 that the contribution of each of the end-members has changed substantially with time and that factors have independent histories: Factor 1 had its maximum accumulation 28 Ka and between 7 and 11 Ka. The loess factor accumulation rate was greatest at the end of the last glacial stage, 10-16 Ka, when it was accumulating rapidly on the loess plateaus of Asia (Pye and Zhou, 1988). Factor 3 accumulated most rapidly between 4 and 7 Ka, the time of maximum eolian accumulation in the northwest Pacific (Rea and Leinen, 1988).

### *6.4 Implications for the Effects of Climate Change on Eolian Deposition*

Previous studies of eolian deposition in the tropics and subtropics during the Quaternary (e.g. Parkin, 1974; Sarnthein and Koopman, 1980) have found that the greatest difference in the size of eolian sediment grains, and thus in the inferred vigor of atmospheric circulation, was that between

# RC 14-105

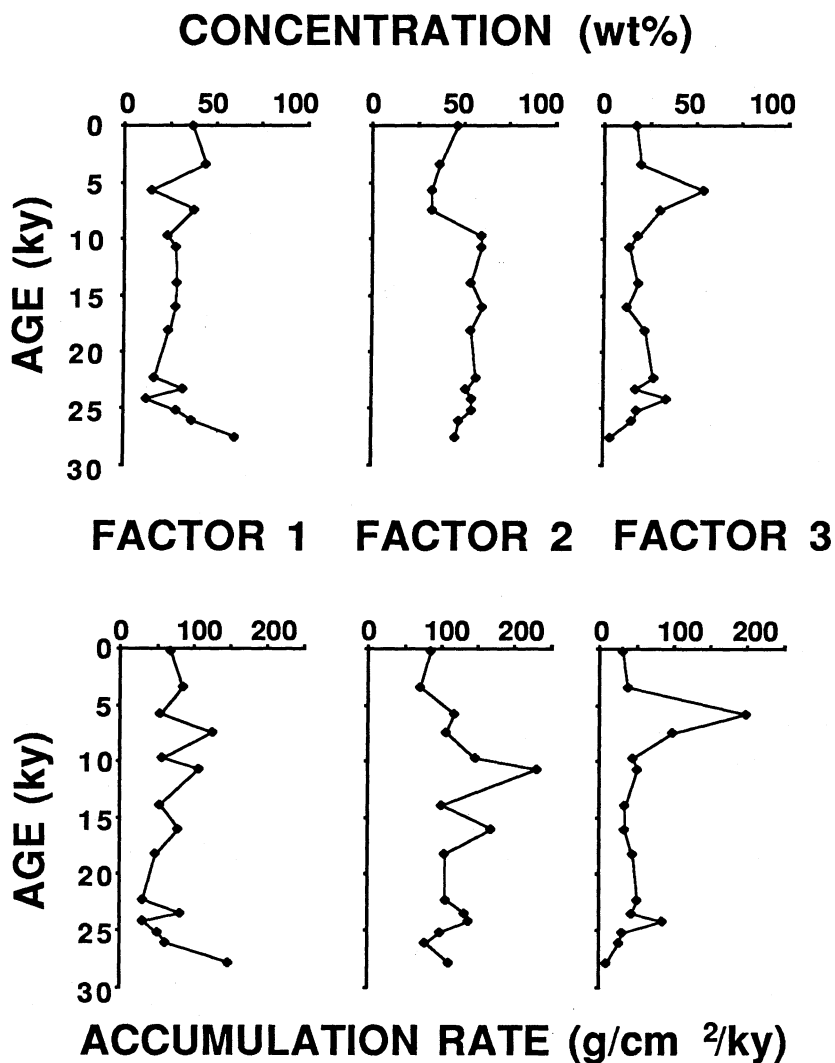


Figure 8. The concentration (in wt %) and accumulation rate (in g/cm<sup>2</sup>/ky) of the three composition factors in RC14-105 for the past 30 KY.

full glacial times and full interglacial times. These studies have concluded that the steepening of the sea-surface temperature gradient during glacials resulted in an equatorward shift of the major wind systems and more vigorous atmospheric circulation (e.g. Parkin, 1974). Most such studies have focussed on the tropics, however. The grain-size data of Rea and Leinen (1988) demonstrate that there has been no similar increase in the size of eolian grains between glacials and interglacials in the northwest Pacific, although the size of eolian sediment was significantly larger during the 4-7 KY interval than before and after that time.

The mineralogical composition of northwest Pacific sediments, their mineral accumulation rates, and the total eolian sedimentation rate show no evidence of a southward shift in the zone of maximum eolian sedimentation at the last glacial maximum. On the contrary, there is evidence from the mineralogical data that the zone of maximum eolian sedimentation shifted to the north. Rea and Leinen (1988) were unable to determine the eolian grain size of the 18.6 KY sample at 42°N (V20-126) because the sample contained dispersed volcanic ash, which was not removed by the sample cleaning procedure. Both the eolian flux and the size of the sample would have been biased by this material. They concluded that the latitudinal position of the flux maximum has remained unchanged at 38° to 40°N for the past 30 KY.

However, the mineralogical determinations are unaffected by the presence of the volcanic ash, and the accumulation rates for the mineral groups are likewise unaffected by other diluents. The accumulation rates for the individual minerals, as well as for the mineral assemblages, indicate that the zone of maximum eolian accumulation moved to the north by about 5° of latitude at the glacial maximum. The lack of adequate sample material for analyses of several time intervals within the cores in the southern half of the transect makes it difficult to determine the maximum rate of accumulation along the transect for all time periods.

Rea and Leinen (1988) concluded on the basis of the eolian deposition rates along the core transect that the aridity of Asian continental environments controlled the flux of eolian material to the northwest Pacific and that aridity was greatest at the time of maximum seasonal contrast about 4-7 Ka (e.g. Kutzbach and Guetter, 1986; Street-Perrott, 1986). The mineralogical data presented here suggest that not all environments and/or transport trajectories contributed to the large flux of eolian sediment 4-7 Ka. The time series of mineral assemblages at RC14-105 (Fig. 8) suggest that it is primarily the accumulation of Factor 3 that is associated with the enhanced flux. This assemblage is similar to that which is presently deposited after

transport from northern Asia. Further south at V20-126, it is the accumulation of Factor 1 (associated today with Asian transport), followed by low-altitude transport over Japan, which is responsible for the increase in flux 4-7 Ka. Thus, the mineral data provide increased resolution of the eolian record and suggest that it is not overall aridity, but the transport of mineral dust from specific source regions or by specific transport paths which controls the total flux of dust to the northwest Pacific.

Information from longer eolian records provides additional insight into the controls on dust transport and composition. The total quartz content of the non-biogenic fraction of RC14-105 sediments was determined by Pias and Leinen (1984). They found that the record was periodic and that the spectrum of quartz variation was dominated by variance at 23 and 19 KY. Furthermore, the quartz variation was coherent and in phase with the variation in the precession index of Earth's orbit. Kutzbach and Guetter (1986) have modeled the circulation of the atmosphere at 3 KY intervals between the present and the maximum extent of glacial ice 18 Ka using a general circulation model. They have highlighted the effect of orbital precession on the seasonality of Earth's climate, especially its effect on seasonal temperature and precipitation contrast. Scientists studying the controls on formation of erodible aggregates (e.g. Brueninger, *et al.*, this volume) and antecedent conditions for dust transport (e.g. Brazel, *et al.*, this volume) have emphasized the importance of enhanced seasonal contrast in rainfall in generating dust and injecting it into the air.

Pye and Zhou (1988) have suggested a model for the difference in temporal importance of eolian loess in continental environments and eolian deposits in the northwest Pacific. They called attention to the inferred importance of low-altitude, ice-margin atmospheric circulation in the deposition of loess on the Asian continent based on its grain size, its local redistribution in valleys and its restricted regional deposition. They also highlighted the demonstrated importance of high-altitude transport mechanisms associated with frontal activity in carrying mineral dust to the Pacific (e.g. Duce, *et al.*, 1981; Merrill, this volume). They reasoned that the low-altitude, ice-margin circulation conditions conducive to loess accumulation on the continents were most common at the time of the maximum extent of continental ice (15-20 Ka) and that frontal activity conducive to high-altitude dust injection and transport was favored during times of maximum seasonal contrast like the period between 4 and 7 Ka. The mineralogy of northwest Pacific eolian sediment is in agreement with the difference in transport mechanisms suggested by Pye and Zhou (1988).

These many associations suggest that it is the seasonality of climate during the Late Quaternary, rather than overall aridity, that controls dust flux from Asia to the northwest Pacific and that may control the source area being eroded. The mineral data by themselves, however, do not indicate which of the many effects of seasonality have dominated the generation, injection, transport and deposition of eolian material to the northwest Pacific. Thus, seasonal variation in soil moisture, vegetative cover, replenishment of erodible surfaces, or storms and frontal activity could all play important roles in the translation of the seasonal signal to the accumulation of Asian mineral dust thousands of kilometers downstream in the northwest Pacific. The correlation of mineral, flux and grain-size data with that from other continental indicators such as pollen, and with climate models will be important efforts in resolving the specific mechanisms by which Asian continental climate and atmospheric circulation respond to climate change.

## 7. CONCLUSIONS

The mineralogy of the clay-sized fraction of terrigenous sediments from the northwest Pacific which are dominated by eolian deposition varies in time and space. While the sediments are generally dominated by illite and smectite, with quartz and chlorite in intermediate concentrations and plagioclase and kaolinite in low concentrations, the clay mineral groups plagioclase and quartz do not vary synchronously and thus indicate that the region receives eolian input from several sources or transport trajectories.

Principal component factor analysis suggests that the sediments bear the imprint of at least three eolian sediment sources and/or transport trajectories. These eolian sources (or end-members) are similar in composition to mineral aerosols accumulating at present in the northwest Pacific. The similarity of sediment and aerosol composition suggests that transport trajectories which combine mineral dust from Asia with dust contributed from Japan during low-altitude transport over the islands have been the most common source of mineral dust to the northwest Pacific over the past 30 KY. Dust rich in illite, quartz, and smectite, and therefore similar in composition to loess, has accumulated at all sites over the past 30 KY, but was most abundant in sediments from 35-45°N and accumulated most rapidly between 10 and 25 Ka. The accumulation rate of this fine loess fraction was not greatest at the time of the maximum extent of glacial ice 17-19 KY BP. A third end-member source, which appears to correspond to



northern Asian sources (which do not experience low-altitude transport over Japan) is also present in the sediments and reaches its peak accumulation about 4-7 Ka.

The maximum in total eolian accumulation along the transect, which occurred 4-7 Ka (Rea and Leinen, 1988), is most closely associated with increases in the accumulation rate of the northern Asian end-member at the northern end of the transect and with the accumulation rate of the Japan-influenced end-member in sites further south. The fact that the accumulation rate peak at 4-7 Ka is associated with specific end-members and not with all end-members suggests that this peak in eolian accumulation was not due to general Asian aridity, but to specific source area and/or transport trajectory changes.

Thus, the mineral composition of northwest Pacific eolian dust and the flux of the mineral assemblages complement data for the total eolian flux to the northwest Pacific, which suggest that dust flux was greatest 4- 7 Ka. The mineral assemblages which comprise the eolian material suggest that there have been changes in the source of eolian material to the northwest Pacific over the past 30 KY, however, and that the distribution pattern of the assemblages has changed over the same time interval. Furthermore, these changes, as well as longer term changes, appear to coincide with times of maximum seasonality in temperature and precipitation on the Asia continent.

## ACKNOWLEDGMENTS

This study has been supported by grants from the Climate Dynamics Program of the National Science Foundation (#ATM81-16301, ATM87-13216, and ATM87-16432). The mineralogical analyses were completed with great care by Tammy Walsh and the manuscript was typed by Rhonda Kenny with her usual expertise and good humor. I would like to thank my colleague in studies of Quaternary North Pacific eolian sediments, David Rea, for many stimulating conversations and thoughtful suggestions about this work. I especially appreciate his forbearance over the years that we have worked on these sites as I fretted and agonized over the interpretation of mineral data which "just didn't fit" my preconceived notions. I would also like to acknowledge my colleagues at URI, John Merrill and Bob Duce, whose discussions of long-range transport trajectories gave me a new perspective on the clay mineralogy of the North Pacific, as well as Eve Arnold and Clark Weaver, who together with John, shared my excitement and delight when the pieces started to fall into place.

**REFERENCES**

- Antevs, E., 1938: Postpluvial climatic variations in the southwest, *Bull. Amer. Met. Soc.*, 19: 30-33.
- Biscaye, P.E., 1965: Mineralogy and sedimentation of Recent deep-sea clay in the Atlantic Ocean and adjacent seas and oceans, *Geol. Soc. Amer. Bull.*, 76: 803-832.
- Blank, M., Leinen, M., and Prospero, J.M., 1985: Major Asian aeolian inputs indicated by the mineralogy of aerosols and sediments in the western North Pacific, *Nature*, 314: 84-86.
- CLIMAP Project Members, 1976: The surface of the ice-age earth, *Science*, 175: 1069-1076.
- Conolly, J.R. and Ewing, J.R., 1970: Ice-rafted detritus in northwest Pacific deep-sea sediments, In: Hays, J.D. (ed.), *Geological Investigations of the North Pacific*, Geol. Soc. Amer. Mem., 126: 263-290.
- Damuth, J.E., Jacobi, R.D., and Hayes, D.E., 1983: Sedimentation processes in the Northwest Pacific Basin revealed by echo character mapping studies, *Geol. Soc. Amer. Bull.*, 94: 381-395.
- Duce, R.A., Unni, C.K., Ray, B.J., Prospero, J.M., and Merrill, J.T., 1980: Long-range atmospheric transport of soil dust from Asia to the tropical North Pacific: temporal variability, *Science*, 209: 1522-1524.
- Ellis, D.B., and Moore, T.C., Jr., 1973: Calcium carbonate, opal and quartz in Holocene pelagic sediments and the calcite compensation level in the south Atlantic Ocean, *J. Mar. Res.*, 31: 210-227.
- Full, W.E., Ehrlich, R., and Bezdek, J.C., 1982: FUZZY QMODEL — A new approach for linear unmixing, *J. Math. Geol.*, 14: 259-270.
- Heath, G.R., and Pisias, N.G., 1979: A method for the quantitative estimation of clay minerals in North Pacific deep-sea sediments, *Clays Clay Mineral.*, 27: 175-184.

- Imbrie, J., Hays, J.D., Martinson, D.G., McIntyre, A., Mix, A.C., Morley, J.J., Pisias, N.G., Prell, W.L., and Shackleton, N.J., 1984: The orbital theory of Pleistocene climate: support from a revised chronology of the marine  $\delta O^{18}$  record, *In: Berger, A., J. Imbrie, J. Hays, G. Kukla, and B. Saltzman, Milankovitch and Climate: Understanding the Response to Astronomical Forcing*, NATO ASI Series, Series C., v. 126, D. Reidel, Dordrecht, Holland, 269-306.
- Jacobi, R.D., Hayes, D.E., and Damuth, J.E., 1985: High resolution seismic studies and site survey results near Deep Sea Drilling Project Sites 576 and 578, Northwest Pacific, *In: Heath, G.R. and L.D. Burckle, et al., (eds.), Init. Repts of the DSDP, v. 86 (U.S. Govt. Printing Office), Washington, DC, 23-50.*
- Janecek, T.R., 1985: Eolian sedimentation in the northwest Pacific Ocean: a preliminary examination of the data from Deep Sea Drilling Project Sites 576 and 578, *In: Heath, G.R. and L.D. Burckle, et al., (eds.), Init. Repts. DSDP, v. 86 (U.S. Govt. Printing Office), Washington, DC, 589-604.*
- Klovan, J.E., and Imbrie, J., 1971: An algorithm and FORTRAN IV program for large-scale, Q-mode factor analysis, *J. Intern. Assoc. Mathem. Geol.*, 3, No. 1.
- Kutzbach, J.E., and Guetter, P.J., 1986: The influence of changing orbital parameters and surface boundary conditions on climate simulations for the past 18,000 years, *J. Atmos. Sci.*, 43: 1726-1759.
- Leinen, M., and Pisias, N.G., 1984. An objective technique for determining end-member compositions and partitioning sediments according to their sources, *Geochim. Cosmochim. Acta*, 48: 47-63.
- Leinen, M., 1985: Quartz content of northwest Pacific Hole 576A and implications for Cenozoic eolian transport, *In: Init. Rept. DSDP, v. 92, Heath, G.R., and L.H. Burckle, et al., (eds). Washington, D.C. (U.S. Government Printing Office), 581-588.*
- Leinen, M., Cwienk, D., Heath, G.R., Biscaye, P.E., Kolla, V., Thiede, J., and Dauphin, J.P., 1986: Distribution of biogenic silica and quartz in recent deep-sea sediments, *Geology*, 14: 199-203.

- Leinen, M., Blank, M., Prospero, J., and Arnold, E.: Mineralogy of aerosols collected during the Deep Sea Drilling Project in the North Pacific, in prep.
- Liu Thung-sheng, an Zhi-sheng and Yuan Baoyin, 1982: Aeolian processes and dust mantles (loess) in China, *In: Wasson, R.J. (ed.), Quaternary Dust Mantles of China, New Zealand and Australia*, Canberra, Australia, Australian National University Press, pp. 1-17.
- Mehra, O.P., and Jackson, M.L., 1960: Iron removal from soils and clays by a dithionite-citrate system buffered with sodium bicarbonate, *Clays Clay Mineral.*, 7: 317-327.
- Merrill, J., Weaver, C., Leinen, M., and Arnold, E.: Airmass trajectories for aerosol samples collected during the Deep Sea Drilling Project in the North Pacific and their implications for mineral composition of the aerosol, in prep.
- Miesch, A.T., 1976: Q-mode factor analysis of geochemical and petrological data matrices with constant row sums, U.S. Geol. Surv. Prof. Paper, 574G.
- Moore, T.C., Jr., Burckle, L.J., Geitzenauser, K., Luz, B., Molina-Cruz, A., Robertson, J.H., Sachs, H., Sancetta, C., Thiede, J., Thompson, P., and Wenkam, C., 1980: The reconstruction of sea surface temperatures in the Pacific Ocean of 18,000 B.P., *Marine Micropaleo.*, 5: 215-247.
- Morley, J.J., Hays, J.D., and Robertson, J.H., 1982: Stratigraphic framework for the Late Pleistocene in the northwest Pacific Ocean, *Deep-Sea Res.*, 29: 1485-1499.
- Parlin, D.W., 1974: Trade winds during the glacial cycles, *Proc. Roy. Soc. London, A*, 337: 73-100.
- Pecsi, M., 1984 (ed.): *Lithology and Stratigraphy of Loess and Paleosols*, Geographic Research Institute, Hungarian Academy of Sciences, Budapest, 325 pp.
- Pisias, N.G., and Leinen, M., 1984: Milankovitch forcing of the oceanic system: Evidence from the northwest Pacific, *In: Berger, A., J. Imbrie, J. Hays, G. Kukla, and B. Saltzman, Eds., Milankovitch and Climate: Understanding the Response to Astronomical Forcing*, NATO ASI Series, Series C., v. 126, D. Reidel, Dordrecht, Holland, 307-330.

- Prell, W.L., and Kutzbach, J.E., 1987: Monsoon variability over the past 150,000 years, *J. Geophys. Res.*, 92: 8411-8425.
- Rea, D.K., and Leinen, M., 1988: Asian aridity and the zonal westerlies: Late Pleistocene and Holocene record of eolian deposition in the northwest Pacific Ocean, *Paleoeco. Paleoclim. Paleoecol.*, 66: 1-8.
- Robertson, J.H., 1975: Glacial to interglacial oceanographic changes in the northwest Pacific, including a continuous record of the last 400,000 years, Ph.D. Thesis, Columbia University, New York, 355 pp.
- Sarnthein, M., and Koopman, B., 1980: Late Quaternary deep-sea record on Northwest African dust supply and wind circulation, *Paleoecology of Africa*, 12: 239-253.
- Shackleton, N.J. and Opdyke, N.D., 1973: Oxygen isotope and paleomagnetic stratigraphy of equatorial Pacific core V28-238: Oxygen isotope temperatures and ice volumes on a  $10^5$  and  $10^6$  scale, *Quat. Res.*, 3: 39-55.
- Till, R., and Spears, D.A., 1969: The determination of quartz in sedimentary rocks using an X-ray diffraction method, *Clays Clay Mineral.*, 17: 323-327.
- Webb, T., Bartlein, P.J., Kutzbach, J.E., 1987: Climatic change in eastern North America during the past 18,000 years; comparisons of pollen data with moderl results and adjacent oceans during the last deglaciation, *Geol. Soc. Amer.*, pp. 447-462.
- Zheng Hong-han, 1984: Paleoclimatic events recorded in clay minerals in loess of China, In: Pecs, M. (ed.), *Lithology and Stratigraphy of Loess and Paleosols*, Geographic Research Institute, Hungarian Academy of Sciences, Budapest, pp. 171-181.

VARIATIONS OF THE NW AFRICAN TRADE WIND REGIME DURING THE LAST 140 000 YEARS: CHANGES IN POLLEN FLUX EVIDENCED BY MARINE SEDIMENT RECORDS.

Henry Hooghiemstra

Institute of Palynology and Quaternary Sciences, University of Göttingen, Wilhelm-Weber-Str. 2, D-3400 Göttingen, F.R.G.

present address: Hugo de Vries-Laboratory, Dept. of Palynology and Paleo/Actuo-Ecology, University of Amsterdam, Kruislaan 318, 1098 SM Amsterdam, The Netherlands.

Pollen was analyzed in 7 eastern Atlantic cores located between 37° and 9°N. The cores lie along a transect in the main trajectory of the northeast trade winds. The northern sector of the transect is close to source areas of pollen; whereas, the southern sector is distant (<2000 km) from the pollen source areas. Winds dominate in the transport of pollen from the northernmost part of the trade wind belt to the coring sites. Therefore, the pollen in the cores is a potential monitor of eolian transport. <sup>18</sup>O and <sup>14</sup>C based time control of the sediment sections made it possible to display the pollen data as influx records. After having estimated latitudinal shifts of the different pollen source areas, spatial and temporal variations in the pollen flux have been used to evaluate changes in the trade wind vigor.

Large influx fluctuations of the mainly trade-wind-transported elements Pinus, Artemisia, other Compositae, and Ephedra in the northern sector parallel synchronous fluctuations of lower magnitude in the southern sector, producing a similar pollen stratigraphy across much of the transect. The pollen recorded 10 phases of wind intensity for the trades. These correlate well with the deep-sea oxygen isotope chronology being largely coeval with the stages 6, 5e through 5a, 4,3,2, and 1. In general, glacial periods (stages 6 and 2) are characterized by a high eolian pollen flux indicating vigorous trade winds, and interglacial periods (stages 5 and 1) are characterized by a low eolian pollen flux indicating weak trade winds. During the two relatively cool intervals of stage 5 (substages 5d and 5b) increased pollen fluxes are indicative of more vigorous trade winds. After phases of pronounced vigor the trade winds weakened in two steps both at about 130 ka BP (Termination II) and 14-12 ka BP (Termination I).

## 1. INTRODUCTION

In the marine sediments off northwest Africa distribution patterns of pollen of northwest African and southwest European provenance have been established for the present-day, 9000 years BP, and 18,000 years BP. Pollen analysis of 109 surface sediment samples from the ocean floor provided the present-day distribution patterns for the region between 35° and 4°N (Hooghiemstra & Agwu, 1986; Hooghiemstra et al., 1986). Pollen analysis of selected intervals of marine cores located between 37° and 9°N yielded the distribution patterns for earlier dates. The Geological Institute of Kiel University provided all samples and time control was provided by oxygen isotope stratigraphy (R. Zahn and M. Sarnthein, Kiel University) and radiocarbon ages (H. Erlenkeuser, Kiel University). Eleven cores located between 37° and 15°N contained data for 9 ka BP (Hooghiemstra, 1988b), and 14 cores located between 37° and 9°N contained data from 18 ka BP (Hooghiemstra, 1988b; Hooghiemstra et al., 1987). The above mentioned studies and that of Melia (1984) showed that although the Canary Current is potentially important for pollen transport along the northwest African continent, eolian pollen transport is dominant. Evidence for river transport of pollen appeared in the modern distribution pattern of Rhizophora in the southern sector (Senegal River). The distribution of pollen in marine sediments is closely related to the geographical position of the pollen source areas (that is the vegetation zones; see Figure 1). The patterns of pollen distribution in the modern marine surface sediments commonly correspond in detail to the average flow patterns of atmospheric circulation. These include such major windsystems as the northeast trade winds, the January trades, and the Saharan Air Layer (African Easterly Jet) (Figure 2). In this region the smearing of pollen input patterns by water currents is apparently minor (see the pollen distribution patterns in Hooghiemstra et al., 1986), and the replication of aerosol distribution patterns in the underlying bottom sediments (Melia, 1984)), and indicates that the residence time of pollen in the water column is short. This observation serves to emphasize the rapid removal of small particles from the surface ocean by large amorphous aggregates and fecal pellet transport (Schrader, 1971; Bishop et al., 1977, 1978; Honjo, 1976, 1980, 1983). The pellets sink at hundreds of meters per day (Janecek & Rea, 1985). Isopoll maps for past times, therefore, potentially provide evidence on possible changes in atmospheric circulation. Isopoll maps for 9 ka BP represent the phase of maximum northward expansion of the vegetation zones south of the Sahara (Petit-Maire & Riser, 1981; Hooghiemstra, 1988a), and maps for 18 ka BP record the last glacial maximum. Maps from these dates were compared with the modern isopoll maps.

Past distribution patterns of many taxa showed the transport of pollen from the Mediterranean area along the northwest African coast to as far south as 5°N, indicating a geographically stationary belt with trade wind transport (Figure 3). The efficiency of pollen transport, however, varied distinctly. This atmospheric circulation model was already hypothesized by, among others, Sarnthein et al., 1981a, 1981b,



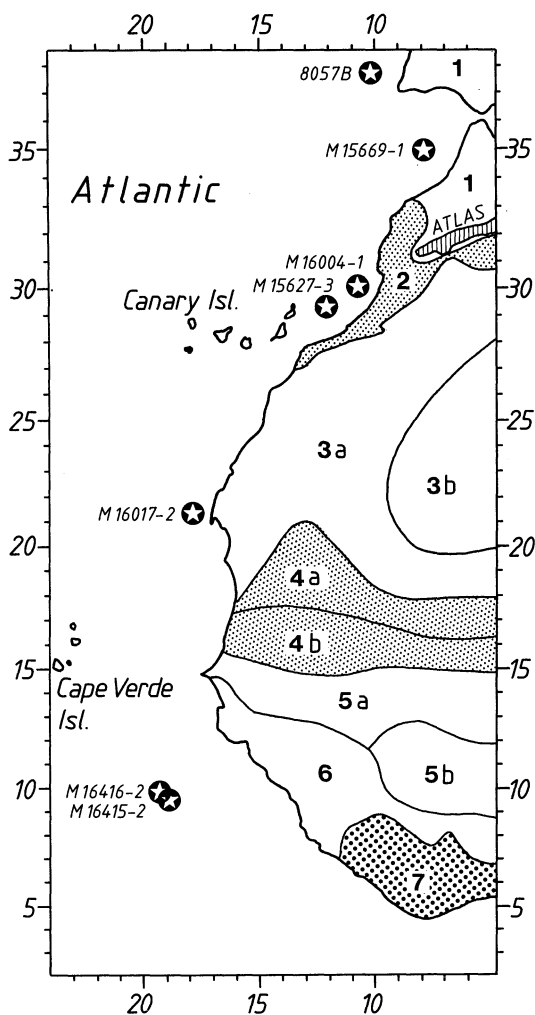


Fig. 1. Vegetation zones of northwest Africa (after White, 1983) and core locations. From north to south: 1, Mediterranean vegetation zone; 2, steppes (semi-desert grassland and shrubland) of the western Atlas region; 3a, deserts and semi-deserts of the Sahara; 3b, desert dunes without perennial vegetation and absolute deserts; 4a, northern Sahel zone: semi-desert grassland and shrubland (dry thorn savannas); 4b, southern Sahel zone: *Acacia* wooded grassland and deciduous bushland; 5a, Sudanian undifferentiated woodland (dry savannas); 5b, Sudanian woodland with abundant *Isoberlinia*; 6, Guinean savanna zone: mosaic of lowland rain forest and secondary grassland; 7, rain forest. (After Hooghiemstra et al., "Meteor" Forschungsergebnisse, C 40, p.89, 1986. With kind permission from Gebr. Borntraeger, Berlin, Stuttgart.)

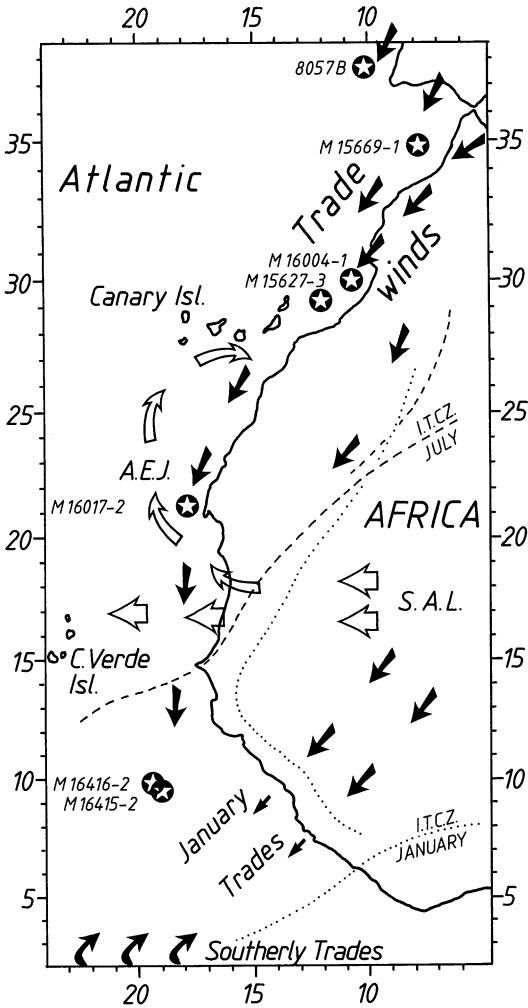


Fig. 2. Major wind belts of northwest Africa (compiled after Leroux, 1983; Tezlaff & Wolter, 1980; and Griffiths & Soliman, 1972) and core locations. Solid arrows indicate surface winds: northeast trade winds, January trades, and southerly trades. The average course of the intertropical convergence zone (ITCZ) and the average geographical position of the discontinuity between coastal-marine air masses (trade winds) and continental air masses ("Harmattan") is indicated for the northernmost July and southernmost January position (dashed lines and dotted lines, respectively). Open arrows indicate zonal winds at higher altitudes: the Saharan Air Layer (S.A.L.) and African Easterly Jet (A.E.J.).

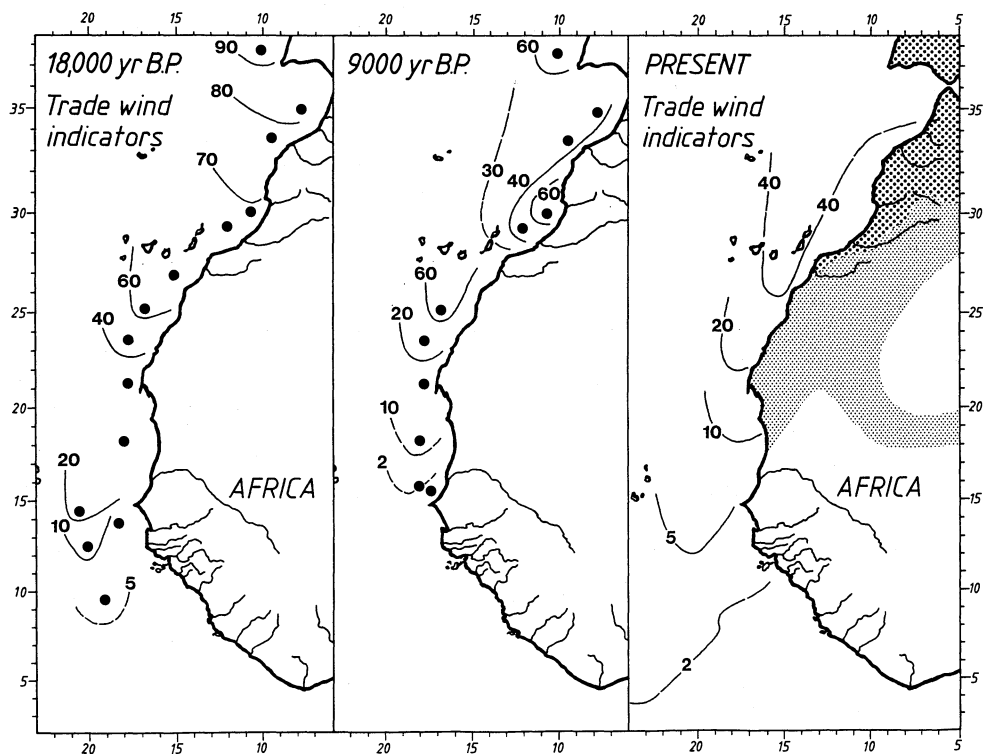


Fig. 3. Isopoll map of the "trade wind indicators" (viz. Pinus, Artemisia, other Compositae, and Ephedra; see text) for the present-day, 9 ka BP and 18 ka BP of the Atlantic off NW Africa. The present-day isopoll map has been based on 109 surface sediment samples located between 35° and 4°N. The 9 ka BP and 18 ka BP isopoll maps have been based on 11 and 14 deep-sea core intervals, respectively (location indicated as solid circles). Area with bold dots indicate main pollen source area; area with thin dots indicate pollen sources of secondary importance. (From Hooghiemstra, Phil. Trans. R. Soc. Lond., B 318, p., 442, 1988. With kind permission from the Royal Society London.)

1982 and contradicts the model of, among others, Rognon (1976, 1987), Nicholson & Flohn (1980) and Pokras & Mix (1985), assuming a displacement of the westerlies and trade wind belt towards the equator. Pollen of taxa whose plants continuously grew mainly north of the Sahara form a useful group for evaluating changes in transport efficiency by the trade winds. This efficiency is mainly related to wind speed. Parkin & Shackleton (1973) report uncertainty about whether it is speed or some function of the speed that is being recorded in their grain size measurements, and they prefer the term wind "vigor". This opinion is adopted here.

The main taxa that are transported by the trade winds are: (1) Pinus whose main source area is in southern Europe (Iberian Peninsula), Morocco, Canary Islands, and the Atlas Mountains; (2) Artemisia whose main source area is in the zone with steppe-like vegetation at the northern fringe of the Sahara; (3) other Compositae whose main source area is restricted to the Mediterranean type of vegetation, and the steppe and desert vegetation along the northern fringe of the Sahara; and (4) Ephedra whose main source area is restricted to southern Europe, Morocco, Canary Islands and parts of the Sahara (in the littoral zone as well as inland). A study of 4 marine pollen records located offshore between Portugal and the Canary Islands (Hooghiemstra et al., submitted) showed that the above mentioned "trade wind indicators" experienced only a limited latitudinal shift during the last glacial-interglacial cycle (Figure 4). Thus changes of the trade wind vigor are indicated by fluctuations of the relative amount (pollen percentages) or the absolute amount (pollen influx: pollen  $\text{cm}^{-2}\text{yr}^{-1}$ ) of trade wind-transported pollen in marine sediments located downwind of the source areas. The percentage of trade-wind-transported pollen versus distance (latitude) is indicated in Figure 5 and uses the data mapped in Figure 3. In offshore Atlantic marine sediments, the percentage values of trade-wind-transported pollen decline from the Iberian Peninsula to as far south as 9°N. As discussed in Hooghiemstra et al. (1987) the graph of the present-day situation (Figure 5, curve A) displays pollen supply from the important source area located north of about 35°N (Iberian Peninsula). Representation of pollen decreases rapidly southward, but between 32° and 27°N representation increases again. This increase reflects pollen supply from the Moroccan source area which is transported by the trade winds across the land-sea boundary at about 30°N. South of 27°N pollen percentages decrease rapidly again, reflecting a low efficiency of pollen transport. The slight increase in representation around 5°N apparently reflects the removal of pollen from the atmosphere at the rain belt that accompanies the intertropical convergence zone (this process was discussed by Tauber, 1965; Schmidt, 1967). The graph for 9 ka BP (Figure 5, curve B) displays the source area on the Iberian Peninsula which supplies mainly Pinus pollen, the Moroccan source area which supplies much of the Compositae pollen, and the source area on the Canary Islands which supplies mainly Pinus pollen, and the rapid decrease in representation south of 25°N is indicative of a low transport efficiency. The graph for 18 ka BP (Figure 5, curve C) approximates a more linear relationship. The area north of about 26°N

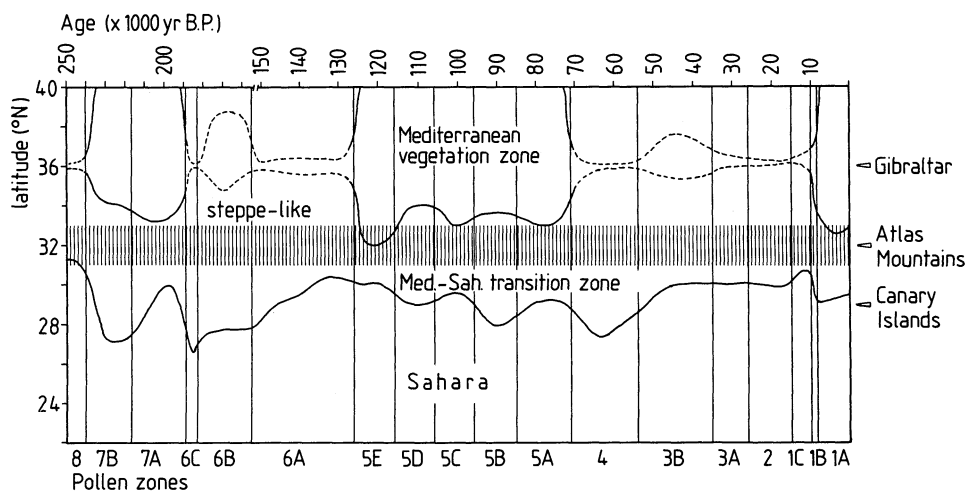


Fig. 4. Schematic representation of the temporal and spatial distribution of source areas of trade-wind-transported pollen in the westernmost Mediterranean area from 250 ka to 5 ka BP. Based on pollen records of the 4 offshore Atlantic cores located between Portugal and the Canary Islands (Fig. 1). The geographical position of the Atlas Mountains is schematically indicated by a hatched zone between  $33^{\circ}$  and  $31^{\circ}$ N. Dotted intervals of the Mediterranean vegetation zone represent periods characterized by a very reduced distribution (relict areas) which are not restricted to the latitudinal zone where they have been schematically drawn. Pinus pollen mainly originate from the Mediterranean vegetation zone and during glacial periods also from the northern part of the Pinus wooded steppe-like vegetation of the Mediterranean-Saharan transition zone. Artemisia pollen mainly originate from the steppe-like vegetation north of the Sahara. Pollen of the group of other Compositae mainly originate from the Mediterranean vegetation zone and the zone with steppe-like vegetation (pollen production in the sparse Saharan vegetation is estimated as of minor importance). Ephedra pollen originate mainly from the Sahara (E. distachya type) and the Mediterranean vegetation (E. fragilis type). (From Hooghiemstra, Stalling & Agwu, manuscript submitted.)

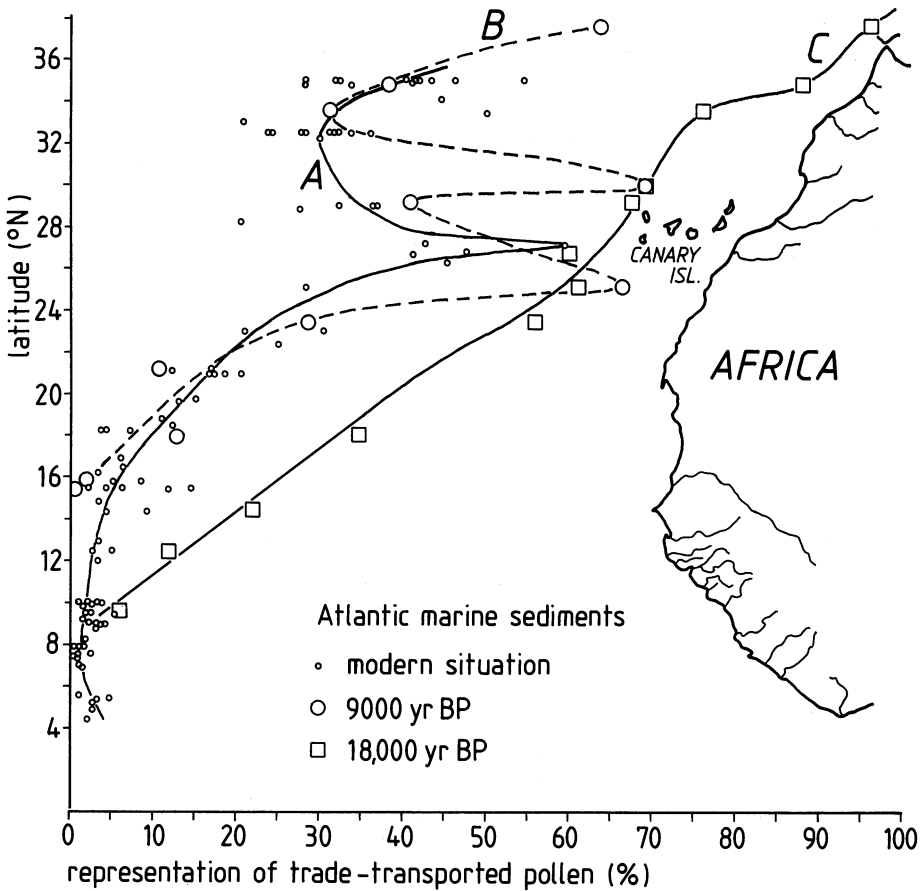


Fig. 5. Percentage of trade-wind-transported pollen versus distance (latitude) for the present-day (curve A), 9 ka BP (curve B), and 18 ka BP (curve C). Based on the data set of surface sediment samples and deep-sea core intervals mapped in Fig. 3. Latitudinal changes in pollen supply to the Atlantic and changes in the efficiency of pollen transport (pollen flux) by the trade winds are reflected. The group of trade-wind-transported pollen include *Pinus*, *Artemisia*, other Compositae, and *Ephedra*. (From Hooghiemstra et al., *Paleoceanography*, 2, p. 580, 1987. Reproduced with kind permission from the American Geophysical Union.)

approximates the situation of an undivided source area in which pollen is transported very effectively. The inclination of this graph seems a measure for the efficiency of pollen transport by the trade winds. This suggests that especially from about 36° to 24°N the vigor of the trade winds had increased during the last glacial maximum.

The Saharan Air Layer (Figure 2) is a zonal wind that moves west above the trade wind inversion between 8° and 23°N (Prospero & Carlson, 1972; Tetzlaff & Wolter, 1980; Tetzlaff & Peters, 1986a, 1986b; Sarnthein *et al.*, 1982). Maximum concentration of transported dust (including pollen) is found around 3000m altitude between 17° and 21°N during July and August when the Saharan Air Layer functions as a jet-like wind (African Easterly Jet). A part of the African Easterly Jet crosses the Atlantic and reaches the Caribbean area, while another component passes around the high pressure system over the western Sahara and forms a sickle-shaped trajectory over the eastern Atlantic into the direction of the Canary Islands. The main source area of dust and pollen of the African Easterly Jet is the southern Sahara and Sahel zone where the modern vegetation is dominated by herbs and shrubs of the families of the Chenopodiaceae and Amaranthaceae (subsequently referred to as "chenopods"). The period of main pollen release of the vegetation is from July to September which is coeval with the period of maximum African Easterly Jet transport. As the chenopods are wind pollinated plants that produce large quantities of pollen, this group is very favorable for tracing wind trajectories. Figure 6 shows the distribution patterns of chenopod pollen in the marine sediments for 18 ka BP, 9 ka BP, and today. The zone between about 19° and 22°N has apparently been continuously characterized by abundant pollen supply from the east, reflecting African Easterly Jet transport. We concluded, therefore, that the belt with distinct African Easterly Jet transport did not shift latitudinally during the last glacial-interglacial transition, which supports our glacial atmospheric circulation model. This model was already hypothesized by Sarnthein *et al.* (1981a, 1981b, 1982) and Koopmann (1981) on the basis of sedimentological studies. This atmospheric circulation model implies that the dominant pollen type in the marine sediments between about 16° and 22°N depends on the type of vegetation present between these latitudes. This implication was substantiated indeed by the palynological study at 21°N of marine core M 16017-2 representing the interval 20 ka to 5 ka BP (Hooghiemstra, 1988a: Figure 13). The period of northernmost expansion of the savanna zone from about 9.2 ka to 7.8 ka BP was reflected in the pollen diagram by a grass pollen maximum, whereas the period older than 9.2 ka BP and the period younger than 7.8 ka BP are characterized by a chenopod pollen maximum.

The marine pollen records of deep-sea cores M 16415-2 and M 16416-2 at 9°N (Hooghiemstra & Agwu, 1988), which cover the interval of 140 ka to 70 ka BP, showed that the pollen concentration and influx rates apparently are related to the trade wind intensity. Pollen of a wide range of provenance (from the Mediterranean area to as far south as the tropical rain forest) fluctuated simultaneously during this interval

indicating a common transport mechanism. The period of maximum expansion of the tropical forest area (viz. during oxygen isotope stage 5e) was represented in the pollen percentage diagram by a maximum of tropical forest pollen, but suffering from accountable low pollen counts. During this period, however, the pollen influx diagram shows a distinct minimum in tropical forest pollen due to low efficiency in pollen-transport by wind.

On the basis of mapped percentages, changes in the trade wind intensity were already noted in previous papers. Transects of pollen influx records yield new insight into pollen transport because the graphed data are independent from each other. The objective of this paper is to evaluate changes in the pollen flux during the interval 140 ka to 5 ka BP between 35° and 9°N off northwest Africa which are indicative of changes of the trade wind vigor.

## 2. MATERIAL AND METHODS

Core data (Table I) were described in Hooghiemstra et al. (submitted: cores 8057B, M 15669-1, M 16004-1, and M 15627-3), Hooghiemstra (1988a: core M 16017-2), and Hooghiemstra & Agwu (1988: cores M 16415-2 and M 16416-2). A linear sediment accumulation rate was assumed for intervals between the age horizons, provided by oxygen isotope stratigraphy and the ages of the SPECMAP time scale (see Imbrie et al., 1984), and a depth versus age graph was produced for each core. In this way, the age of all samples (see Tables II through VIII) and the number of years of pollen production represented in each sample (see Table I) were calculated. The resulting influx values (pollen  $\text{cm}^{-2}\text{yr}^{-1}$ ) for pollen that is mainly transported by the trade winds (Pinus, Artemisia, other Compositae, and Ephedra) are presented in the Tables II through VIII and graphically displayed in the Figures 7 through 10. Figure 11 shows the total pollen influx in all cores.

## 3. RESULTS

### 3.1 General remarks

In order to be able to display the influx values graphically, the scales in the northern sector (core 8057B) have been reduced and those in the southern sector (cores M 16017-2, M 16415-2, and M 16416-2) have been exaggerated in respect of the middle sector (cores M 16004-1 and M 15627-3). This necessary distortion of scales reflects the general decrease in representation of trade-wind-transported pollen in the marine sediments along the transect which is consistent with Figure 5. Core M 15669-1 differs for undetermined reason from this general trend and shows distinctly lower pollen influx values for all groups of pollen.

The zonation of the pollen influx records is based on distinct changes in the pollen influx values. The ages of all samples are approximations which may be the cause of a diminished correlation



Table I. Core data.

Core	Location N W	Water Depth	Time Control	Interval Studied (cm)	Time Interval (yr BP)	Control Points	Reciprocal Sedimentation Rate (yr.cm <sup>-1</sup> )
8057B	37°41' 10°05'	2811	R <sub>p</sub> /R <sub>b</sub>	11-290	19,100-2,900	280 cm- 18,800 yr BP 0 cm- 2,000 yr BP	60.0
M 15669-1	34°53' 07°49'	2030	<sup>18</sup> O/ <sup>16</sup> O	0.5-479.5	121,700-6,300	480 cm-122,000 yr BP 254 cm- 39,000 yr BP 0 cm- 6,000 yr BP	367.3 129.9
M 16004-1	29°59' 10°39'	1512	<sup>18</sup> O/ <sup>16</sup> O	2.0-440.0	142,000-5,700	420 cm-135,000 yr BP 100 cm- 19,000 yr BP 4 cm- 6,000 yr BP	362.5 135.4
M 15627-3	29°10' 12°05'	1024	<sup>18</sup> O/ <sup>16</sup> O	0-360.0	142,200-3,500	522 cm-185,000 yr BP 212 cm-100,000 yr BP 70 cm- 25,000 yr BP 20 cm- 19,000 yr BP 5 cm- 6,000 yr BP	274.2 528.2 120.0 866.7
M 16017-2	21°15' 17°48'	800	<sup>18</sup> O/ <sup>16</sup> O	20.0-322.0	20,650-4,900	300 cm- 19,000 yr BP 230 cm- 13,500 yr BP 37 cm- 7,200 yr BP 13 cm- 3,600 yr BP	78.6 32.7 146.9
M 16415-2	09°34' 19°06'	3841	<sup>18</sup> O/ <sup>16</sup> O	2.0-235.0	143,200-4,500	210 cm-135,000 yr BP 137 cm-110,000 yr BP 75 cm- 65,000 yr BP 43 cm- 15,000 yr BP 3 cm- 4,500 yr BP	342.5 725.8 1562.5 262.5
M 16416-2	09°52' 19°24'	4336	carb.	201.5-409.5	142,800-54,000	384 cm-135,000 yr BP 302 cm-110,000 yr BP 238 cm- 74,000 yr BP	304.9 562.5

Table II. Pollen influx data of deep-sea core 8057 B (lat. 37°41'N, long. 10°05'W; water depth 2811 m). See for time control data Table I.

sample no.	depth (cm)	calculated age (yr BP)	Pollen influx (pollen cm <sup>-2</sup> yr <sup>-1</sup> )				Total
			Pinus	Artemisia	Compositae	Ephedra	
1	11- 20	2,900	2,181	186	1,862	-	9,788
2	21- 30	3,500	2,330	90	1,606	-	9,276
3	31- 40	4,100	3,081	112	1,417	-	9,400
4	41- 50	4,700	4,286	122	1,665	24	12,368
5	51- 60	5,300	3,885	74	1,082	74	13,155
6	61- 70	5,900	2,825	13	591	26	8,475
7	71- 80	6,500	3,913	19	906	-	13,435
8	81- 90	7,100	3,245	13	789	-	10,225
9	91-100	7,700	4,783	30	872	60	13,642
10	101-110	8,300	10,069	37	353	37	16,775
11	111-120	8,900	34,605	156	781	78	56,165
12	121-130	9,500	44,939	285	1,710	95	71,921
13	131-140	10,100	90,400	1,060	3,566	96	115,844
14	141-150	10,700	89,346	1,278	2,850	197	110,773
15	151-160	11,300	60,227	1,953	1,172	391	77,881
16	161-170	11,900	67,806	1,500	1,500	300	81,007
17	171-180	12,500	97,368	2,943	3,583	640	126,796
18	181-190	13,100	81,314	1,724	3,639	383	102,864
19	191-200	13,700	108,251	2,236	4,604	395	138,241
20	201-210	14,300	106,476	2,120	2,690	326	125,554
21	211-220	14,900	169,919	3,087	2,483	470	184,347
22	221-230	15,500	240,246	5,659	3,951	1,602	263,096
23	231-240	16,100	225,086	5,190	2,367	1,912	244,390
24	241-250	16,700	204,347	7,050	2,452	1,533	225,190
25	251-260	17,300	192,395	4,108	1,953	808	206,335
26	261-270	17,900	168,805	3,584	1,624	896	181,183
27	271-280	18,500	168,468	5,728	2,604	1,042	186,782
28	281-290	19,100	147,556	3,929	3,762	920	164,694

Table III. Pollen influx data of deep-sea core M 15669-1 (lat. 34°53'N, long. 07°49'W; water depth 2030 m). See for time control data Table I.

sample no.	depth (cm)	calculated age (yr BP)	Pollen influx (pollen cm <sup>-2</sup> yr <sup>-1</sup> )				Total
			Pinus	Artemisia	Compositae	Ephedra	
1	0.5- 2.0	6,300	0.245	0.004	0.040	-	0.505
2	6.0- 7.5	7,000	0.050	0.006	0.025	0.006	0.283
3	16.0- 17.5	8,200	0.026	-	0.011	0.005	0.100
4	26.0- 27.5	9,500	0.030	-	0.004	0.004	0.080
5	36.0- 37.5	10,700	0.059	-	0.012	-	0.271
6	46.0- 47.5	12,000	0.036	-	-	-	0.041
7	56.0- 57.5	13,300	4.914	0.280	0.409	0.108	7.785
8	66.0- 67.5	14,500	2.228	0.103	0.092	0.044	3.033
9	76.0- 77.5	16,000	1.695	0.563	0.244	0.040	2.937
10	86.0- 87.5	17,200	4.423	0.294	0.186	0.039	5.514
11	96.0- 97.5	18,600	3.289	0.474	0.359	0.065	4.825
12	103.5-105.0	19,500	2.044	0.111	0.138	0.046	2.614
13	113.5-115.0	20,700	1.580	0.129	0.103	0.035	2.091
14	123.5-125.0	22,000	2.063	0.371	0.158	0.042	3.082
15	133.5-135.0	23,300	3.475	0.370	0.197	0.006	4.411
16	143.5-145.0	24,700	0.958	0.105	0.043	0.012	1.264
17	154.0-155.5	26,000	1.067	0.112	0.161	0.036	1.656
18	173.5-175.0	28,500	1.082	0.051	0.026	0.019	1.334
19	183.5-185.0	30,000	4.662	0.242	0.196	0.035	5.905
20	193.5-195.0	31,300	6.558	0.614	0.234	0.117	8.369
21	202.0-203.5	32,500	5.017	0.261	0.120	0.070	6.250
22	212.0-213.5	33,700	3.235	0.155	0.078	0.015	3.793
23	232.0-233.5	36,300	1.495	0.081	0.055	0.010	1.923
24	252.0-253.5	38,800	1.021	0.098	0.067	0.011	1.429
25	272.0-273.5	45,900	0.324	0.007	0.016	-	0.442
26	282.0-283.5	49,700	0.191	0.002	0.006	0.002	0.220
27	292.0-293.5	53,200	0.171	-	0.010	-	0.212
28	301.5-303.0	56,500	0.657	0.003	0.023	0.003	0.736
29	311.5-313.0	60,400	1.833	0.091	0.025	0.017	2.012
30	321.5-323.0	64,000	0.361	0.004	0.002	0.004	0.379
31	331.5-333.0	67,500	0.166	0.002	0.002	-	0.194
32	341.0-342.5	71,300	0.424	0.054	0.057	0.008	0.666
33	371.0-372.5	82,500	0.130	0.001	0.015	0.001	0.183
34	381.5-383.0	86,000	0.452	0.002	0.012	0.002	0.515
35	391.0-392.5	89,600	0.655	0.019	0.058	0.013	0.930
36	402.0-403.5	93,700	0.028	-	0.001	0.001	0.042
37	412.0-413.5	97,500	0.104	0.010	0.021	0.009	0.292
38	421.0-422.5	100,600	0.082	0.006	0.028	0.006	0.251
39	431.5-433.0	104,500	0.124	0.007	0.007	0.003	0.180
40	442.0-443.5	108,500	0.307	0.001	0.006	-	0.333
41	451.0-453.5	111,700	0.224	0.002	0.021	0.006	0.324
42	461.5-463.0	115,500	0.088	0.012	0.023	0.002	0.205
43	471.5-473.0	119,300	0.056	0.003	0.003	0.003	0.068
44	478.0-479.5	121,700	0.084	0.003	0.036	0.002	0.183

Table IV. Pollen influx data of deep-sea core M 16004-1 (lat. 29°59'N, long. 10°39'W; water depth 1512 m). See for time control data Table I.

sample no.	depth (cm)	calculated age (yr BP)	Pollen influx (pollen cm <sup>-2</sup> yr <sup>-1</sup> )				Total
			Pinus	Artemisia	Compositae	Ephedra	
0A	2.0- 3.0	5,700	0.009	0.002	0.057	0.002	0.148
1A	9.0- 10.0	6,900	0.015	0.004	0.041	0.004	0.085
2	12.0- 13.5	7,100	0.011	0.001	0.002	0.003	0.026
3	22.0- 23.5	8,500	0.006	0.001	0.016	0.001	0.044
3A	24.0- 25.0	8,600	0.007	-	0.004	0.002	0.020
4	32.0- 33.5	9,700	0.018	0.001	0.018	0.001	0.059
5	42.0- 43.5	11,200	0.005	-	0.008	-	0.021
6	48.5- 50.0	12,100	176.3	46.3	51.7	39.2	541.6
7	58.5- 60.0	13,500	316.8	82.5	43.4	17.4	655.3
8	68.5- 70.0	15,000	289.3	156.2	33.8	23.2	635.5
9	78.5- 80.0	16,200	301.2	100.4	31.5	33.5	596.5
10	84.0- 85.5	16,800	281.3	191.5	44.9	26.0	711.5
11	88.5- 90.0	17,500	367.4	144.7	69.6	50.1	840.6
12	94.0- 95.5	18,100	313.1	270.4	71.2	49.8	1085.1
13	98.5-100.0	19,000	396.7	554.4	122.1	45.8	1531.0
14	104.5-106.0	20,600	329.5	336.9	51.8	66.6	1110.6
15	108.5-110.0	22,000	184.2	131.4	16.0	20.8	483.8
16	118.5-120.0	25,500	206.0	131.6	47.7	21.0	600.8
17	128.5-130.0	29,000	179.1	81.3	30.3	12.4	414.7
18	138.5-140.0	33,000	186.3	118.5	22.0	18.6	508.0
19	148.5-150.0	36,600	128.0	159.6	19.3	17.5	531.3
20	158.5-160.0	40,500	61.3	88.1	26.9	12.9	324.6
21	168.5-170.0	44,000	101.8	44.9	23.0	18.6	330.6
22	178.5-180.0	47,500	77.9	48.3	35.5	7.9	298.7
23	188.5-190.0	51,000	51.1	16.1	12.9	6.0	139.0
24	198.5-200.0	54,600	67.7	31.7	17.3	9.4	216.9
25	208.5-210.0	58,500	95.5	33.0	3.6	7.8	180.3
26	218.5-220.0	62,000	134.2	44.5	4.6	8.4	230.8
27	228.5-230.0	65,500	157.8	121.6	16.9	10.8	362.5
28	238.5-240.0	69,200	76.0	82.9	28.5	16.4	262.4
29	248.0-249.5	73,000	51.8	65.9	23.5	7.8	240.8
30	258.0-259.5	76,500	30.5	28.7	20.1	5.0	140.4
31	268.5-270.0	80,000	55.1	11.6	33.6	7.7	169.8
32	278.5-280.0	83,700	68.0	29.7	27.6	13.5	216.7
33	288.5-290.0	87,200	62.6	6.9	27.5	8.0	177.9
34	298.5-300.0	91,000	128.5	17.4	31.3	9.6	265.7
35	308.5-310.0	94,500	160.5	21.3	19.5	8.0	271.3
36	318.0-319.5	98,100	25.9	18.0	12.1	1.3	105.9
37	328.5-330.0	102,000	24.2	7.6	10.9	2.0	69.6
38	338.0-339.5	105,500	17.3	6.3	22.6	3.4	77.8
39	348.0-349.5	109,200	61.5	19.1	26.3	14.3	183.4

Table IV (continued)

40	358.0-359.5	113,000	54.0	16.1	23.9	11.9	159.9
41	368.5-370.0	116,500	32.6	60.3	29.5	6.2	197.0
42	378.5-380.0	120,100	30.3	8.8	26.1	6.3	134.0
43	388.5-390.0	123,700	13.9	3.6	9.4	1.9	60.5
44	398.5-400.0	127,500	13.6	1.4	11.0	2.3	64.9
45	407.5-409.0	130,500	125.8	57.5	24.0	7.2	374.9
46	418.5-420.0	134,500	72.5	99.1	20.6	23.0	365.2
47	430.0-431.5	139,000	94.9	61.6	11.7	17.2	234.0
48	438.5-440.0	142,000	96.3	48.2	8.1	12.9	203.5

Table V. Pollen influx data of deep-sea core M 15627-3 (lat. 29°10'N, long. 12°05'W; water depth 1024 m). See for time control data Table I.

sample no.	depth (cm)	calculated age (yr BP)	Pollen influx (pollen cm <sup>-2</sup> yr <sup>-1</sup> )				Total
			Pinus	Artemisia	Compositae	Ephedra	
1	0- 4	3,500	8.6	4.3	5.0	-	48.3
2	10- 14	12,000	52.4	55.1	57.9	46.9	482.4
3	18- 22	19,000	30.3	81.7	12.1	36.3	320.8
4	32- 36	20,500	136.7	89.6	28.3	33.0	424.2
5	40- 44	21,500	533.1	347.9	99.4	126.5	1640.0
6	46- 50	22,200	555.6	253.4	263.2	126.7	1993.2
8	60- 64	24,000	665.7	498.1	330.5	210.7	2816.1
9	68- 72	25,000	266.9	469.9	203.0	46.4	1635.9
11	80- 84	31,500	86.4	49.4	41.4	21.2	306.9
12	90- 94	36,500	46.4	62.5	41.1	35.7	428.7
13	100-104	42,000	30.6	22.3	19.5	6.5	152.1
14	108-112	46,000	27.1	26.3	40.3	5.4	173.5
16	120-124	52,500	52.8	39.3	34.2	2.1	218.5
18	131-135	58,500	31.1	26.8	26.8	5.4	162.8
19	138-142	62,000	301.6	81.2	11.6	27.1	514.3
20	145-149	66,000	45.8	366.4	58.0	21.4	775.6
21	160-164	73,500	12.0	7.4	11.7	1.9	53.2
22	170-174	79,000	71.3	93.5	46.7	54.1	634.8
23	180-184	84,500	28.9	16.8	50.5	31.3	214.2
24	185-189	87,200	19.0	10.5	22.7	14.2	122.3
25	190-194	89,500	18.2	31.0	18.2	5.5	123.8
26	200-204	95,000	18.8	1.1	5.5	2.2	46.6
27	205-209	97,500	65.6	89.9	77.8	63.2	609.9
28	215-219	101,500	47.2	79.4	77.5	30.2	487.5
29	220-224	103,000	-	26.7	26.7	-	133.6
30	225-229	104,500	65.1	9.6	50.7	19.3	205.0
31	230-234	105,800	52.7	35.1	42.1	17.6	238.8
32	240-244	108,600	131.7	426.2	178.2	65.9	1402.7
33	250-254	111,500	13.2	24.8	48.0	5.0	147.2
34	260-264	114,500	23.5	109.8	211.8	31.4	792.1
35	272-276	118,000	143.8	165.1	165.1	26.6	1118.5
36	280-284	120,500	68.4	74.6	105.7	12.4	615.6
37	292-296	123,800	10.4	5.2	20.8	10.4	122.1
38	300-304	126,000	52.1	175.8	58.6	26.0	781.5
39	310-314	129,000	148.0	308.2	123.3	61.6	1220.6
40	320-324	131,800	24.8	34.7	34.7	5.0	158.6
41	326-330	133,500	28.0	36.8	36.8	21.0	210.4
44	342-346	138,200	55.5	71.4	21.8	7.9	241.8
45	350-354	140,500	15.2	34.3	22.9	7.6	163.8
46	356-360	142,200	116.2	107.3	35.8	107.3	652.5

Table VI. Pollen influx data of deep-sea core M 16017-2 (lat. 21°15'N, long. 17°48'W; water depth 800 m). See for time control data Table I.

sample no.	depth (cm)	calculated age (yr BP)	Pollen influx (pollen cm <sup>-2</sup> yr <sup>-1</sup> )				Total
			Pinus	Artemisia	Compositae	Ephedra	
1	20- 22	4,900	0.144	0.324	1.386	0.090	11.70
2	30- 32	6,300	0.135	0.474	2.267	0.102	21.32
3	40- 42	7,300	0.504	1.008	2.520	0.420	52.07
4	50- 52	7,650	0.200	0.560	1.519	0.280	24.82
5	60- 62	7,950	0.169	0.760	1.689	0.591	33.01
6	70- 72	8,300	0.202	0.848	1.615	0.606	26.29
7	80- 82	8,650	0.266	0.592	1.124	0.326	17.81
8	90- 92	8,900	0.271	0.296	0.764	0.222	11.58
9	100-102	9,250	0.238	0.980	0.927	0.291	17.71
10	110-112	9,600	0.161	1.031	0.709	0.387	18.40
12	130-132	10,250	0.555	1.457	1.318	0.520	24.84
14	150-152	10,900	0.273	0.819	0.764	1.528	30.08
15	160-162	11,250	0.236	1.729	0.707	0.707	20.51
16	170-172	11,550	0.267	1.639	1.563	0.419	29.66
18	190-192	12,200	0.224	1.031	0.560	0.381	13.92
20	210-212	12,850	0.522	1.565	1.304	0.609	25.65
21	220-222	13,200	0.407	1.518	1.036	0.629	19.14
22	230-232	13,550	0.452	1.144	0.843	0.662	13.43
23	240-242	14,400	0.092	0.437	0.275	0.148	3.69
24	250-252	15,100	0.038	0.420	0.248	0.108	4.29
26	270-272	16,700	0.067	0.183	0.119	0.172	2.05
28	290-292	18,300	0.037	0.252	0.197	0.105	2.70
29	300-302	19,100	0.073	0.669	0.292	0.304	6.83
30	310-312	19,850	-	0.433	0.345	0.098	4.94
31	320-322	20,650	0.103	0.684	0.361	0.103	7.80

Table VII. Pollen influx data of deep-sea core M 16415-2 (lat. 09°34'N, long. 19°06'W; water depth 3841 m). See for time control data Table I.

sample no.	depth (cm)	calculated age (yr BP)	Pollen influx (pollen cm <sup>-2</sup> yr <sup>-1</sup> )				Total
			Pinus	Artemisia	Compositae	Ephedra	
1	2.0- 3.0	4,500	-	-	-	0.077	14.755
2	7.0- 8.0	6,000	0.086	0.086	0.172	0.086	19.123
3	18.5- 19.5	9,500	-	-	0.079	-	2.145
4	28.0- 29.0	11,500	0.001	-	0.001	-	0.028
5	39.0- 40.0	14,000	-	0.0003	0.002	-	0.068
6	48.0- 49.0	24,000	0.001	0.001	0.003	0.011	0.189
7	58.0- 59.0	39,000	0.0004	0.002	0.003	0.011	0.160
8	62.5- 64.0	46,000	0.001	0.018	0.008	0.021	0.334
9	69.0- 70.5	57,000	0.005	0.001	0.002	0.004	0.121
10	72.5- 74.0	63,600	0.001	-	0.001	-	0.057
11	76.0- 77.5	66,400	0.007	0.007	-	0.003	0.314
12	83.0- 84.5	71,300	0.001	0.008	0.012	0.008	0.471
13	88.0- 89.5	75,200	0.004	-	0.002	-	0.139
14	96.0- 98.0	80,600	0.001	0.002	-	0.001	0.055
15	98.0-100.0	82,400	0.001	0.002	0.002	-	0.060
16	100.0-101.5	83,700	0.001	-	-	0.004	0.037
17	103.0-104.5	86,000	0.004	0.014	0.007	0.008	0.304
18	107.0-108.5	88,700	0.003	0.008	0.004	0.009	0.364
19	108.5-110.0	90,000	0.005	0.007	0.003	0.015	0.515
20	115.5-117.5	95,200	0.001	0.002	0.007	0.008	0.484
21	117.5-119.5	96,700	-	0.001	-	0.003	0.072
23	126.5-128.0	102,500	-	0.004	0.004	-	0.153
24	128.0-129.5	104,200	0.002	-	0.001	0.001	0.040
25	135.0-137.0	109,000	0.001	0.001	0.001	-	0.033
26	137.0-138.5	110,200	-	-	-	-	0.068
27	138.5-140.0	110,800	0.003	0.002	-	-	0.034
28	142.5-144.0	112,000	0.002	-	-	0.002	0.070
29	147.0-149.0	113,600	0.004	0.002	-	-	0.106
30	150.5-152.0	114,700	-	-	0.003	-	0.079
31	155.0-156.5	116,400	0.001	0.001	0.001	-	0.199
32	156.5-158.0	116,900	0.004	0.002	-	0.002	0.081
33	158.0-159.5	117,300	-	-	0.002	-	0.048
34	161.5-163.0	118,400	-	-	-	-	0.028
35	170.0-172.0	121,500	-	0.004	-	-	0.082
36	172.0-174.0	122,200	0.003	0.002	-	-	0.156
37	180.0-181.5	124,900	-	0.001	-	0.001	0.066
38	181.5-183.0	125,600	0.005	0.001	0.001	-	0.120
39	183.0-184.5	126,100	0.004	0.005	0.001	0.007	0.269



Table VII (continued)

40	191.5-193.0	128,800	0.008	0.025	-	0.018	0.699
41	193.0-194.5	129,400	0.002	0.004	-	0.021	0.302
42	197.0-198.5	130,800	0.016	-	0.002	0.001	0.116
43	198.5-200.0	131,300	0.005	-	0.001	0.017	0.220
44	200.0-201.5	131,700	0.001	0.001	-	0.007	0.061
45	206.0-207.5	133,700	-	0.010	0.010	0.030	0.466
46	207.5-209.0	134,200	0.003	-	-	0.029	0.173
47	212.5-214.0	136,000	0.012	0.008	0.008	0.062	0.599
48	218.5-220.0	138,000	0.026	0.052	0.016	0.131	1.481
49	227.0-228.5	141,000	0.004	0.030	0.004	0.056	1.565
50	233.5-235.0	143,200	-	0.012	0.014	0.014	0.797

Table VIII. Pollen influx data of deep-sea core M 16416-2 (lat. 09°52'N, long. 19°24'W; water depth 4336 m). See for time control data Table I.

sample no.	depth (cm)	calculated age (yr BP)	Pollen influx (pollen cm <sup>-2</sup> yr <sup>-1</sup> )				Total
			Pinus	Artemisia	Compositae	Ephedra	
1	201.5-203.0	54,000	0.007	0.023	0.007	0.015	0.709
2	209.0-210.5	58,300	0.003	0.002	0.007	0.004	0.122
3	218.0-219.5	63,500	0.001	0.004	0.004	0.001	0.169
4	225.0-226.5	67,200	-	0.001	0.001	-	0.038
5	230.5-232.0	70,000	-	0.004	0.004	-	0.119
6	237.5-239.0	74,000	0.0004	0.002	0.001	-	0.039
7	245.5-247.0	78,500	-	0.001	-	-	0.021
8	251.5-253.0	82,000	0.001	-	-	0.001	0.012
9	259.5-261.0	86,300	0.001	0.006	0.002	0.001	0.071
10	266.5-268.0	90,300	0.003	0.002	0.004	0.014	0.291
11	271.5-273.0	93,200	0.001	0.004	0.007	0.001	0.148
12	277.5-279.0	96,500	0.001	-	0.0003	0.001	0.063
13	284.0-285.5	100,500	-	-	-	-	0.004
14	292.5-294.0	105,000	-	-	-	0.001	0.010
15	301.5-303.0	110,000	0.002	-	0.001	0.001	0.041
16	308.5-310.0	112,000	0.007	0.004	0.006	0.001	0.218
17	317.0-318.5	114,700	0.002	0.003	0.001	-	0.155
18	325.0-326.5	117,200	-	0.002	0.001	0.001	0.093
19	331.5-333.0	119,000	-	-	-	-	0.013
20	338.5-340.0	121,200	-	-	-	-	0.011
21	347.0-348.5	124,000	-	0.001	-	-	0.019
22	354.5-356.0	126,000	0.002	-	-	0.002	0.034
23	362.0-363.5	128,500	-	0.010	0.011	0.010	0.550
24	367.5-369.0	130,100	0.012	0.011	0.016	0.010	0.328
25	375.5-377.0	132,700	0.015	0.029	0.016	0.012	0.832
26	383.5-385.0	135,000	0.013	0.038	0.019	0.027	0.970
27	393.0-394.5	138,100	0.003	0.003	0.001	0.005	0.156
28	400.0-401.5	140,200	0.005	0.006	0.009	0.030	0.325
29	408.0-409.5	142,800	0.005	0.002	0.003	0.008	0.134

between fluctuations of influx records. Records which are located close to the pollen source area are biased by the pollen production of the regional vegetation. For this reason the influx values for Pinus pollen, for example, off Portugal around 18 ka BP are very high. The Iberian Peninsula was covered at that time by a Pinus wooded steppe-like vegetation (Frenzel, 1968; Florschütz et al., 1971; Janssen & Woldrigh, 1981; Pons & Reille, 1984, 1986; Agwu & Beug, 1982; Hooghiemstra et al., submitted) which was replaced by Mediterranean vegetation around 12 ka BP. Also the high influx values of Artemisia pollen off Portugal and northern Morocco around 18 ka BP is apparently biased by the high Artemisia pollen production in the extensive zone with steppe-like vegetation at these latitudes. The major decline of Artemisia pollen influx occurs 18-16 ka BP at 30°N, 15-13 ka BP at 35°N, and 15-11 ka BP at 37°N (Figure 8).

The latitudinal time lag in the decline of the different trade-wind-transported elements illustrates the presence of a "vegetational signal" in the influx records. This "vegetational signal" is a regional-latitudinal difference in vegetational change within the source area that accounts for latitudinal fluctuations of the influx records that are partly independent of changes in the trade wind vigor. This effect has to be accounted for when evaluating the trade wind signal. Studies on vegetational changes from the northwestern-most part of the Sahara to as north as the Iberian Peninsula during the period studied were published by Frenzel (1968), Florschütz et al. (1971), Reille (1976, 1977), Janssen & Woldrigh (1981), Agwu & Beug (1982), Pons & Reille (1984, 1986), Ben Tiba & Reille (1986), Bernard & Reille (1987), Lamb et al. (in press), and Hooghiemstra et al. (submitted).

### 3.2. Pinus

Pollen influx records for Pinus along a transect in the eastern Atlantic are shown in Figure 7. The main source areas of Pinus pollen today are located on the Iberian Peninsula, in Morocco, in the Atlas Mountains, and on the Canary Islands but natural conditions have been obliterated by long human influence in these areas. Based on earlier mentioned land and marine pollen records it is estimated (Hooghiemstra et al., submitted) that the southernmost limit of the distribution of Pinus forsts probably shifted maximally 1 to 2 degrees of latitude southward during the last glacial (Figure 4). Widely distributed Pinus wooded steppe-like vegetation in the westernmost Mediterranean area during the last glacial may account for an increased production of Pinus pollen. We estimated that the centre of Pinus pollen production may not have shifted more than several degrees of latitude southward during the last glacial period (Figure 4) and fluctuations of the influx of Pinus pollen in the southern sector are, therefore, principally a wind signal.

Highest influx values (100 000-240 000 pollen  $\text{cm}^{-2}\text{yr}^{-1}$  at about 37°N to 600-200 pollen  $\text{cm}^{-2}\text{yr}^{-1}$  at about 30°N) occurred between 40 ka and 12 ka BP. At 13-11 ka BP a sharp decline in the pollen influx between 37° and 30°N to about 2.0-0.01 pollen  $\text{cm}^{-2}\text{yr}^{-1}$  is registered.

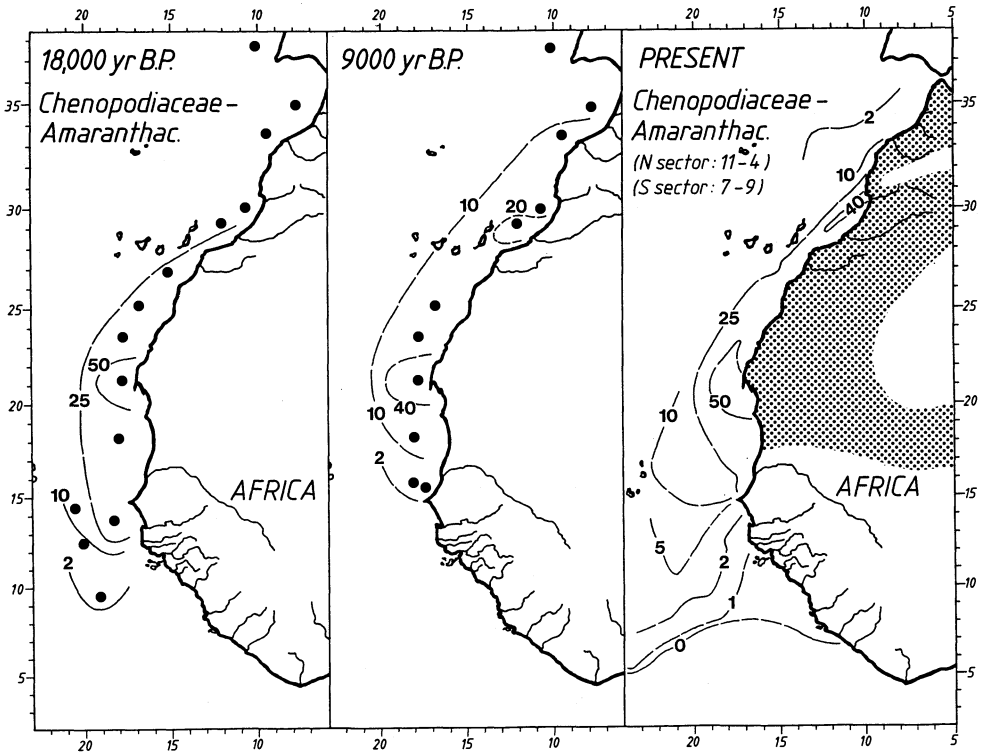


Fig. 6. Isopoll map of the Chenopodiaceae-Amaranthaceae for the present-day, 9 ka BP, and 18 ka BP of the Atlantic off northwest Africa. The present-day isopoll map has been based on 109 surface sediment samples located between 35° and 4°N. The 9 ka BP and 18 BP isopoll maps have been based on 11 and 14 deep-sea core intervals, respectively (location indicated as solid circles). Bold dots indicate main pollen source area, thin dots indicate pollen source areas of secondary importance. Figures in brackets indicate months of main pollen transport. (From Hooghiemstra, *Phil. Trans. R. Soc. Lond.*, B 318, p. 440, 1988. With kind permission from the Royal Society London.)

Core M 15669-1 shows markedly low influx values for Pinus pollen (note the exaggerated scale in Figure 7) for undetermined reasons, but the sequence of fluctuations is consistent with other cores. Core M 16017-2 also shows a decreasing influx between 13 ka and 7 ka BP when two samples (no.3 and 12) are disregarded. The low Pinus influx values between 20 ka and 15 ka BP are not well understood. Increased influx values around 60 ka BP, 90 ka BP, 110 ka BP, and 132 ka BP, and relatively low influx values around 50 ka BP, 80 ka BP, 100 ka BP, and 124 ka BP are expressed by all available pollen records and concordance with the fluctuations of the marine oxygen isotope stratigraphy is evident (Figure 12). The pollen zones dated as 127-120 ka BP, 120-106 ka BP, 106-96 ka BP, 96-84 ka BP, and 84-76 ka BP correspond well with the oxygen isotope stages 5e through 5a.

### 3.3. Artemisia

Pollen influx records for Artemisia along a transect in the eastern Atlantic are shown in Figure 8. The main source area of Artemisia pollen today is the zone with steppe-like vegetation of the Mediterranean-Saharan transition zone (Figure 1). Based on earlier mentioned land and marine pollen records we estimated that this vegetation zone expanded about 4 degrees of latitude northward and 2 degrees of latitude southward (Figure 4) during the interval studied. In glacial times Artemisia-rich vegetation probably expanded markedly in the coastal and littoral areas due to low sea level conditions.

Highest influx values (2000-5000 pollen  $\text{cm}^{-2}\text{yr}^{-1}$  at about 37°N to 100-500 pollen  $\text{cm}^{-2}\text{yr}^{-1}$  at about 30°N) occurred between 40 ka and 12 ka BP. The major decrease of Artemisia pollen influx at the Last Glacial-Holocene boundary occurred 18-16 ka BP at 30°N, 15-13 ka BP at 35°N, and 15-11 ka BP at 37°N. The latitudinal time lag in the decrease of Artemisia pollen influx reflects the vegetational development at the northern fringe of and north of the Sahara (see section 3.1). At 21°N the distinct decrease in Artemisia pollen influx took place about 10 ka BP, and this record is expected to display the most accurate wind signal, since it has been continuously situated south of the source area, which showed slight latitudinal shifts. The low Artemisia influx values in core M 16017-2 between 20 ka and 15 ka BP are not well understood. Increased influx values, especially in the cores M 15627-3, M 16415-2, and M 16416-2, around 66-70 ka BP, 88 ka BP, 110-116 ka BP, and 128-138 ka BP, and relatively low influx values around 55 ka BP, 76 ka BP, 105 ka BP, and 124 ka BP are expressed clearly by most of the records. The pollen zones, which were based on the pollen influx signal of the four groups of trade-wind-transported pollen, are most distinctive in the cores of the southern sector. A concordant sequence of fluctuations can be noted in the cores from the northern sector although these are more influenced by the regional development of the vegetation.

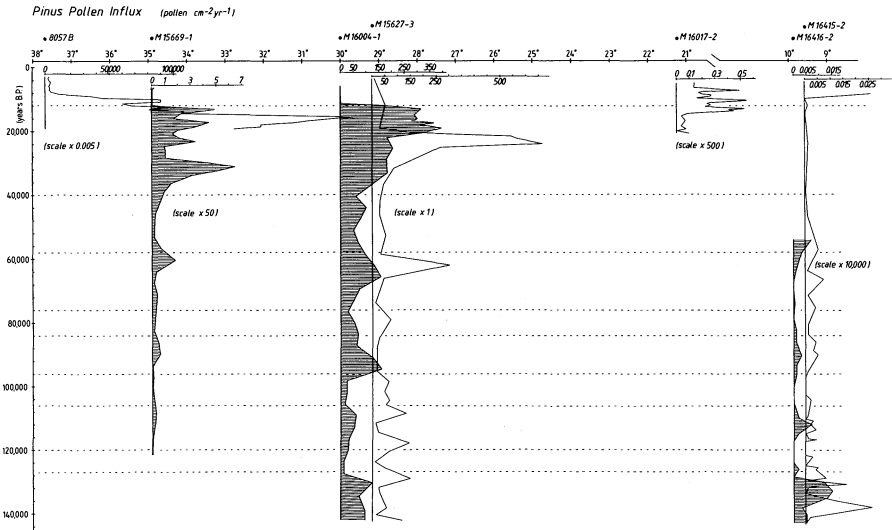


Fig. 7. Relation of pollen influx records for Pinus in 7 eastern Atlantic cores along a transect between 38° and 9°N in the main trajectory of the northeast trade winds. The records represent the interval 140 ka to 4 ka BP and were transformed to a linear time scale. Note the different scales used in the northern and southern sector.

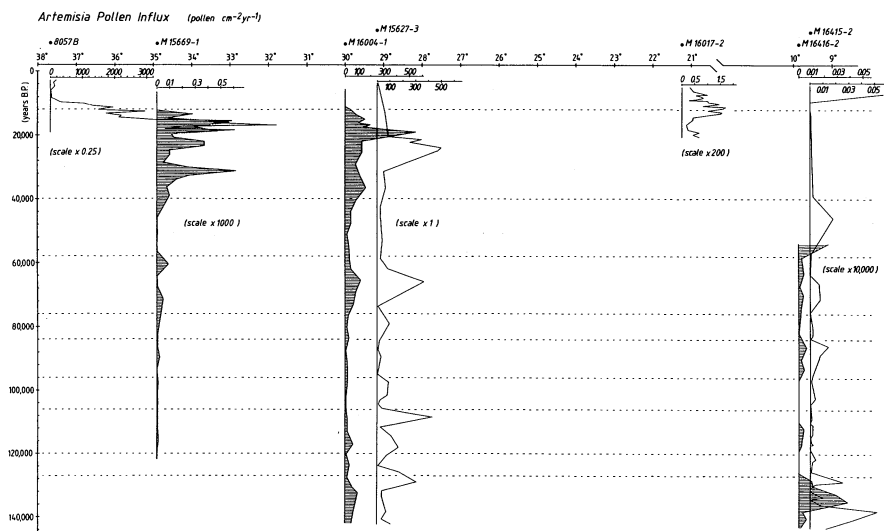


Fig. 8. Relation of pollen influx records for Artemisia in 7 eastern Atlantic cores along a transect between 38° and 9°N in the main trajectory of the northeast trade winds. The records represent the interval 140 ka to 4 ka BP and were transformed to a linear time scale. Note the different scales used in the northern and southern sector.

### 3.4. Compositae (subfamilies Tubuliflorae and Liguliflorae, *Artemisia* excluded)

Pollen influx records for Compositae along a transect in the eastern Atlantic are shown in Figure 9. Compositae are well represented in the vegetation of western Europe, the Mediterranean, the Canary Islands, and the transition zone to the Sahara. Compositae are less common in the Sahara and south of it, and the main modern source area, therefore, may be considered as restricted to the area north of the Sahara. The main source area of Compositae pollen today was reduced during glacial periods when western European and Mediterranean vegetation had been largely replaced by a *Pinus* wooded *Artemisia*-rich steppe-like vegetation. We estimated that the latitudinal position of the total source area has not changed substantially during glacial and interglacial times, but a substantial change in the production of Compositae pollen seems appropriate. The important interglacial source area north of the Sahara was reduced in glacial times and, therefore, the modern, relatively unimportant source area in the Sahara probably increased in relative importance during glacial times.

Highest influx values (2000-4000 pollen  $\text{cm}^{-2}\text{yr}^{-1}$  at about 37°N to 30-200 pollen  $\text{cm}^{-2}\text{yr}^{-1}$  at about 30°N) occurred between 40 ka and 12 ka BP. Core M 15669-1 shows low influx values for Compositae pollen for undetermined reasons (note the exaggerated scale in Figure 9), but the sequence of fluctuations approximates the fluctuations displayed by the other influx records. Core M 16017-2 shows a distinct increase of the influx values of Compositae pollen at 13 ka BP and 9 ka BP. This may be interpreted as reflecting the development of important source areas closer to the core station (Mediterranean vegetation). This interpretation is contradicted by the records for Compositae pollen of more northern latitudes which show at 12 ka BP a sharp decrease in the pollen influx. It is believed that the very abrupt decrease of pollen influx values for all groups of pollen in the cores M 15627-3, M 16004-1, and M 15669-1 reflect neither a "vegetation signal" nor a "wind signal", but has some sedimentological origin. The southernmost records are expected to display the best wind signal: the sequence of fluctuations from 140 ka to 60 ka BP matches well the fluctuations of the oxygen isotope record during the stage 6, 5e through 5a, and 4. A corresponding sequence of fluctuations, although influenced by changes in the vegetation, can be noted in the cores M 16004-1 and M 15669-1.

### 3.5 *Ephedra*

Pollen influx records for *Ephedra* along a transect in the eastern Atlantic are shown in Figure 10. Under modern conditions *Ephedra* is distributed both in the littoral zone and inland from the Iberian Peninsula as far south as the Sahara. During the last glacial maximum the Sahara had expanded southward as far south as about 15°N (Sarnthein, 1978; Petit-Maire & Riser, 1981; Hooghiemstra, 1988a) and the source area reached about 4 degrees of latitude further south than at present. About 9 ka to 8 ka BP the savanna and Sahel zone reached as far north as



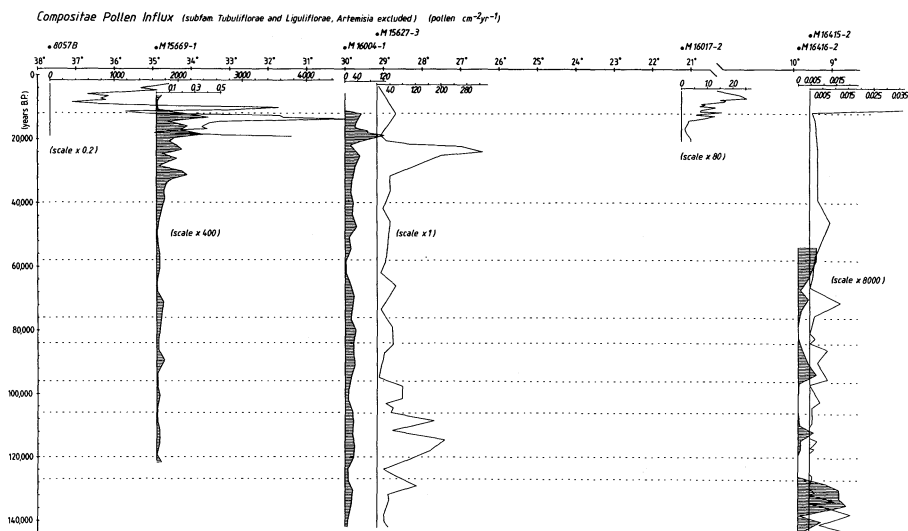


Fig. 9. Relation of pollen influx records for Compositae s.s. (subfamilies Tubuliflorae and Liguliflorae, *Artemisia* excluded) in 7 eastern Atlantic cores along a transect between 38° and 9°N in the main trajectory of the northeast trade winds. The records represent the interval 140 ka to 4 ka BP and were transformed to a linear time scale. Note the different scales used in the northern and southern sector.

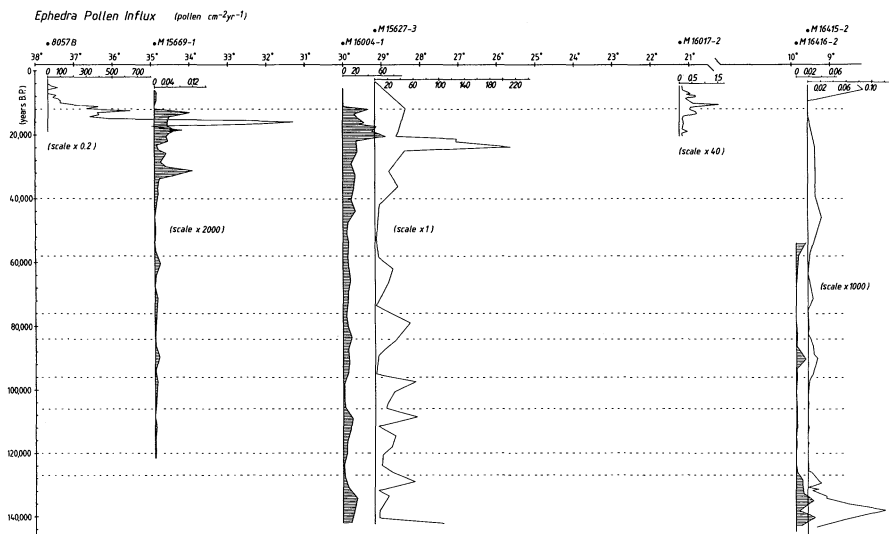


Fig. 10. Relation of pollen influx records for *Ephedra* in 7 eastern Atlantic cores along a transect between 38° and 9°N in the main trajectory of the northeast trade winds. The records represent the interval 140 ka to 4 ka BP and were transformed to a linear time scale. Note the different scales used in the northern and southern sector.

about 24°N (op.cit.). The total shift of the southern boundary of the Sahara amounts about 10 degrees of latitude, and it is estimated to correspond to the southern limit of the main source area of Ephedra pollen. Also, the total production of Ephedra pollen was subject to a considerable change, since, during hyperarid periods, a scarce vegetation cover produced little pollen. Therefore, a considerable effect of the "vegetational signal" in the pollen influx records of Ephedra may be expected.

Highest influx values (400-1900 pollen  $\text{cm}^{-2}\text{yr}^{-1}$  at about 37°N to 40-120(210) pollen  $\text{cm}^{-2}\text{yr}^{-1}$  at about 30°N) occurred between about 40 ka and 12 ka BP. A distinct decrease in pollen influx at 23 ka BP (core M 15627-3), 20 ka BP (core M 16004-1), and 18 ka BP (core M 15669-1) is apparently related to a very low production of Ephedra pollen during hyperarid conditions in the Sahara. Core M 15669-1 shows for undetermined reasons low influx values (note the exaggerated scale in Figure 10), but the sequence of fluctuations is consistent with the other records. Core M 16017-2 shows a distinct increase of influx values for Ephedra pollen at 14 ka BP. This may reflect the development of a more dense vegetation cover in the southern Sahara under more humid conditions (Hooghiemstra, 1988a). In the northern Sahara climate remained arid at 14 ka BP (Figure 4) and a steeper gradient of humidity across the Sahara seems to be recorded. The southernmost records are expected to display the best wind signal; most of the records show increased influx values of Ephedra pollen around 90 ka BP, 110 ka BP, and 135 ka BP, and relatively low influx values of Ephedra pollen around 78 ka BP, 102 ka BP, and 122 ka BP (especially in the cores M 16004-1, M 16415-2, and M 16416-2). This sequence of fluctuations is in agreement with the fluctuations of the oxygen isotope record during the stages 6, 5e through 5a and 4.

### 3.6. Total pollen influx

Changes in the total pollen influx are shown in Figure 11. The fluctuations of the records of the cores 8057B, M 15669-1, M 16004-1, M 16415-2, and M 16416-2 correspond well and show decreasing influx values from north to south. The sequence of fluctuations of core M 15627-3 corresponds with the other cores from 70 ka BP upwards, but the lower part of it is not particularly comparable to the others. For undetermined reasons core M 15669-1 shows low influx values (note the exaggerated scale in Figure 11). The decrease of the total pollen influx at 12 ka BP is very abrupt in the cores M 15669-1, M 16004-1 (and M 15627-3) and nearly as abrupt in core 8057B. Core M 16017-2 shows at 12 ka BP a distinct increase of the total pollen influx with a 7.3 ka BP maximum value which apparently is related to a distinct increase of the total pollen production in the source area of the African Easterly Jet (Hooghiemstra, 1988a). During the period from about 20 ka to 14 ka BP the Sahara was characterized by hyperarid conditions. Sedimentological studies (Koopmann, 1981) suggest the presence of a belt with substantial African Easterly Jet transport at that time. The poor vegetation,

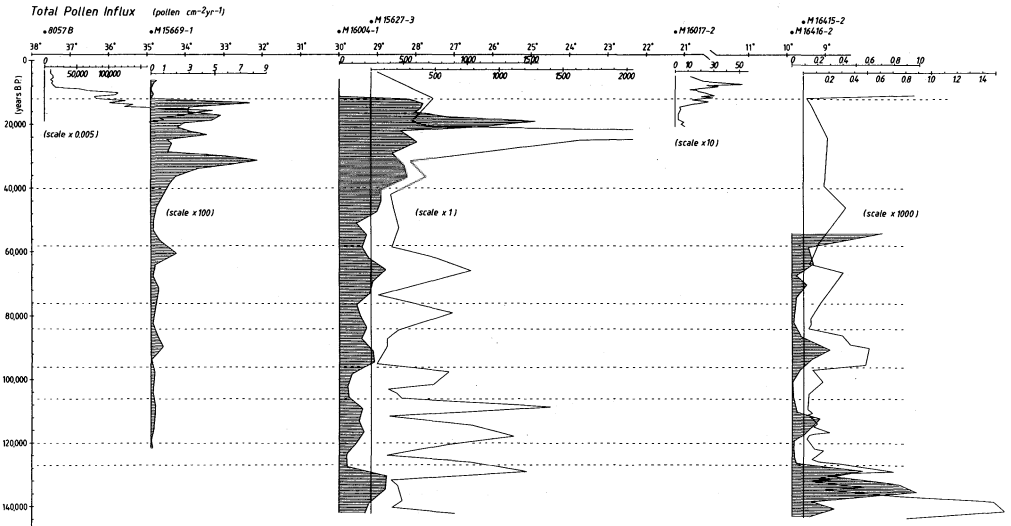


Fig. 11. Relation of records of the total pollen influx in 7 eastern Atlantic cores along a transect between 38° and 9°N in the main trajectory of the northeast trade winds. The records represent the interval 140 ka to 4 ka BP and were transformed to a linear time scale. Note the different scales used in the northern and southern sector.

however, apparently produced so little pollen that there was no functional relation between pollen transport and wind intensity.

North of the Sahara relatively high influx values (100 000-260 000 pollen  $\text{cm}^{-2}\text{yr}^{-1}$  at 37°N to 500-1500 pollen  $\text{cm}^{-2}\text{yr}^{-1}$  at 30°N) occurred between 40 ka and 12 ka BP. Relatively high influx values are expressed by most of the records at 56-65 ka BP, 88-96 ka BP, 108-116 ka BP, and 128-140 ka BP, and relatively low influx values at 48-56 ka BP, 76-82 ka BP, 98-105 ka BP, and 120-126 ka BP. This corresponds with the fluctuations of the oxygen isotope record, representing the stages 4, 5a through 5e, and 6.

#### 4. DISCUSSION

Although core 8057B, M 16017-2, M 16416-2 (and M 16415-2) cover only a part of the period studied, the general sequence of fluctuations of the pollen influx records is clear and provides a base for a reconstruction of changes in the trade wind vigor during the last 140 000 years. The excessive pollen production of Pinus, a well-known phenomenon in literature, is clearly demonstrated by core 8057B. It is shown that also the influx of Pinus pollen decreases distinctly with increasing distance from the source area; consequently, the well-known aerodynamic capacity of Pinus pollen should not be overestimated.

It is remarkable that core M 15669-1 at 35°N shows lower influx values than the cores at 30°N. The assumption that pollen was not transported over this core station (compare the distribution patterns of e.g. Pinus in Melia, 1984; Hooghiemstra *et al.*, 1986) seems unrealistic. Sedimentological reasons are more appropriate to explain the discontinuity in decreasing influx values from north to south.

The influx record of core M 16017-2 requires further discussion. In Hooghiemstra (1988a) the low pollen concentration and pollen influx values between 20 ka and 14 ka BP were explained by the hyperarid conditions in the Sahara which prevented a substantial pollen production in this area. It was assumed that the African Easterly Jet was not able to transport an amount of pollen that had a functional relation to wind vigor. This explanation, however, does not seem appropriate to pollen that is mainly transported by the trade winds which actually blow basically parallel to the shore line. Consequently, it seems remarkable that the pollen influx of Pinus and other trade-wind-transported elements at 21°N were low during a period with vigorous trade winds and increased around 12 ka BP when the trade winds weakened. Although preliminary data of core 16415-2 at 9°N also show an increase of influx values at 10 ka BP, these results are not used to corroborate this observation because of the poor quality of the pollen spectra (see Table VII). In core M 16017-2 there is a rapid increase in the pollen influx of Ephedra, Artemisia, and Pinus at 14 ka BP, followed by a decrease after 10 ka BP. The pollen influx record of the Compositae shows a gradual increase after 14 ka BP and reaches maximum values at 7 ka BP. This difference is clearly related to the vegetational development at

the northern fringe of the Sahara. After 14 ka BP, Ephedra, Artemisia, and Pinus still had a relatively high pollen production in widespread source areas (Figure 4), enabling a rapid response to changing conditions. The main Compositae pollen producing vegetation (Mediterranean vegetation) was around 14 ka BP still in development and became abundant after 10 ka BP.

Another example of the influence of vegetational change on the pollen signal can be found in the Artemisia records. After the last glacial maximum the reduction of Artemisia-rich, steppe-like vegetation at the northern fringe of the Sahara was experienced at first in the southernmost part of the source area (core M 15627-3 and M 16004-1) and later at more northern latitudes (cores M 15669-1 and 8057B). The northward shift of the southern limit of Artemisia-rich vegetation between about 18 ka and 11 ka BP is corroborated by the 18 ka and 9 ka BP isopoll maps.

Additional land based pollen data are needed to evaluate more precisely the displacement of vegetation zones. Conclusions concerning the changing vigor of the trade winds are embodied in Figure 12 and rest on the not yet quantified relation between intensive (vigorous) trade winds, low settling velocity of airborne pollen and, as a consequence, great latitudinal eolian dispersal.

The period of 140 ka to 130 ka BP is characterized by relatively high influx values indicating vigorous trade winds. A two-step weakening of the trade wind intensity around 130 ka BP is suggested by the influx records of both cores at 9°N and is coeval with Termination II. The period of 126 ka to 76 ka BP is generally characterized by low pollen influx values. The intervals 120 ka to 106 ka BP, and 96 ka to 84 ka BP, however, show slightly increased pollen fluxes (see especially the cores M 16415-2 and M 16416-2). In summary, weak trade winds during the intervals 126 ka to 120 ka BP, 106 ka to 96 ka BP, and 84 ka to 76 ka BP, and slightly intensified trade winds during the intervals 120 ka to 106 ka BP and 96 ka to 84 ka BP are indicated. These five intervals match remarkably well with the stages 5e through 5a of the deep-sea oxygen isotope record (see Figure 12). The period of 76 ka to 58 ka BP is characterized by relatively high influx values, especially in the second part of this interval, indicating intensified trade winds which, however, never reached the intensity of stages 6 or 2. This pollen zone corresponds with oxygen isotope stage 4. The period of 58 ka to 40 ka BP shows relatively low influx values, indicating another period of weakened trade winds. After 40 ka BP the pollen flux increased rapidly and very high influx values were registered in the northern sector, indicating vigorous trade winds from 40 ka to 12 ka BP. This period corresponds to the end of oxygen isotope stage 3 and stage 2. Vigorous glacial trade winds were also evidenced by other investigators, e.g. Parkin (1974), Parkin & Shackelton (1973), Parkin & Padgham (1975), and Sarnthein et al. (1981a). Finally, influx records in the middle and northern sectors suggest that between 14 ka and 12 ka BP (Termination I) a two-step weakening of the trade winds occurred. In summary variations

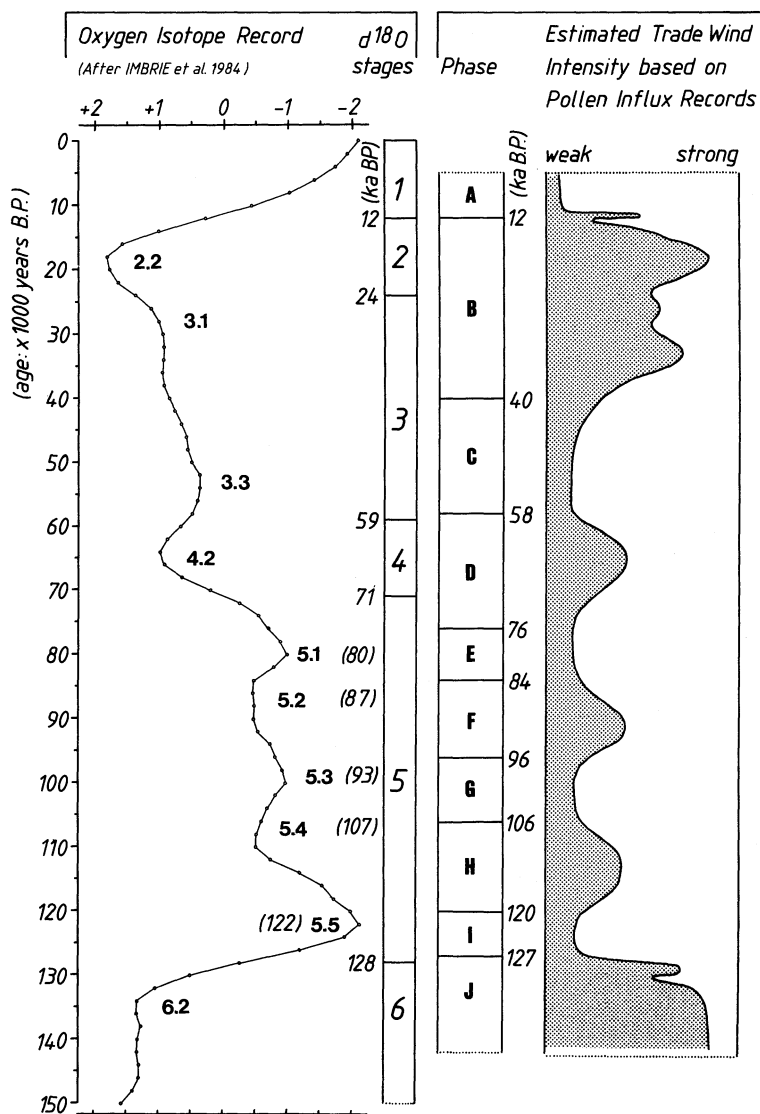


Fig. 12. Summary of suggested changes in the trade wind intensity off northwest Africa for the interval 140 ka to 4 ka BP, and correlation with generalized oxygen isotope record (Imbrie et al., 1984). Rough estimates of the trade wind intensity are based on changes in the pollen flux of mainly trade-wind-transported pollen (viz, *Pinus*, *Artemisia*, other Compositae and *Ephedra*). Phases of trade wind intensity (A through J) are dated by oxygen isotope stratigraphy of the sediment cores (ages used after Imbrie et al., 1984).

in pollen flux suggest that changes in the trade wind vigor are related to changes in global climate as expressed by the oxygen isotope record.

## 5. CONCLUSIONS

1. Accepting that winds dominate in the transport of pollen along the northwest African coast, influx records of pollen from source areas in the northernmost part of the trade wind belt are a potential monitor of changes in eolian transport.

2. Near the pollen source area influx records register changes in the pollen flux as well as vegetational change; at greater distance from the source area influx records are minimally biased by vegetational change but may suffer from low pollen counts during periods with weak wind intensity.

3. Phases of trade wind intensity are more or less coeval with the oxygen isotope stages 6, 5e trough 5a, 4, 3, 2, and 1. In general, glacial periods (stage 6 and 2) are characterized by vigorous trade winds, and interglacial periods (stage 5 and 1) by weak trade winds. The two relatively cool intervals of oxygen isotope stage 5 (substages 5d and 5b) are characterized by slightly intensified trade winds. A correlation between eolian pollen flux time series and the oxygen isotope record is suggested.

4. Two influx records at 9°N suggest a two-step weakening of the trade wind intensity during Termination II (at about 130 ka BP), and five influx records between 37° and 21°N suggest a two-step weakening of the trade wind intensity during Termination I (between about 14 ka and maximally 12 ka BP).

5. In offshore Atlantic marine sediments maximum pollen influx values registered vary from about 250 000 pollen.cm<sup>-2</sup>yr<sup>-1</sup> at 37°N, to 1500 pollen.cm<sup>-2</sup>yr<sup>-1</sup> at 30°N, to 50 pollen.cm<sup>-2</sup>yr<sup>-1</sup> at 21°N, to 1.5 pollen.cm<sup>-2</sup>yr<sup>-1</sup> at 9°N. In offshore Atlantic marine sediments minimum pollen influx values registered vary from about 10 000 pollen.cm<sup>-2</sup>yr<sup>-1</sup> at 37°N, to 60 pollen.cm<sup>-2</sup>yr<sup>-1</sup> at 30°N, to 2 pollen.cm<sup>-2</sup>yr<sup>-1</sup> at 21°N, to 0.01 pollen.cm<sup>-2</sup>yr<sup>-1</sup> at 9°N (core M 15669-1 not considered).

## 6. ACKNOWLEDGEMENTS

This research was carried out in the scope of the German Federal Program of Climate Research (Bundesministerium für Forschung und Technologie, Bonn; grant KF 200041, given to the Institute of Palynology and Quaternary Sciences, Göttingen). All samples were kindly provided by M. Sarnthein (Geological Institute, Kiel University) and his trust in our relatively great claim on core sediments is greatly acknowledged. Pollen analysis was carried out by C.O.C. Agwu (cores M 15627-3 and M 16415-2), H. Stalling (cores 8057B and M 16004-1), and H. Hooghiemstra (cores M 15669-1, M 16017-2, and M 16416-2) at the Institute of



Palynology and Quaternary Sciences, University of Göttingen during 1983 to 1986 while the author was participating in the above mentioned program. H. Erlenkeuser (14C Laboratory, Kiel University) and R. Zahn (Geological Institute, Kiel University; oxygen isotope stratigraphy) kindly provided age control data. I thank M. Sarnthein and U. Pflaumann (Geological Institute, Kiel University), G. Tetzlaff and M. Peters (Institute of Meteorology, Hannover University), H.-J. Beug and L. Dupont (Institute of Palynology and Quaternary Sciences, Göttingen University), and T. Webb III (Brown University, Providence) for discussions, helpful advice, and comments.

This paper was prepared for the NATO Advanced Research Workshop, Oracle, Arizona, November 1987. I thank M. Leinen and M. Sarnthein for enabling me to participate in this workshop. I thank the Hugo de Vries Laboratory, Department of Palynology and Paleo/Actuo-Ecology, University of Amsterdam, for the opportunity to prepare this paper and I thank the Netherlands Organization for Scientific Research (NWO; grant H 75-284) for financial support.

## 7. REFERENCES

- Agwu, C.O.C. & Beug, H.-J., 1982. Palynological studies of marine sediments off the West African coast. "Meteor" Forsch.-Ergeb., C 36: 1-30.
- Ben Tiba, B. & Reille, M., 1982. Recherches pollenanalytiques dans les montagnes de Kroumirie (Tunisie septentrionale): premiers résultats. Ecologia Mediterranea, 8(4): 75-86.
- Bernard, J. & Reille, M., 1987. Nouvelles analyses polliniques dans l'Atlas de Marrakech, Maroc. Pollen et Spores, 29(2-3): 225-240.
- Bishop, J.K.B., Edmond, J.M., Ketten, D.R., Bacon, M.P. & Silken, W.B., 1977. The chemistry, biology and vertical flux of particulate matter from the upper 400 meters of the equatorial Atlantic Ocean. Deep-Sea Research, 24: 511-548.
- Bishop, J.K.B., Ketten, D.R. & Edmond, J.M., 1978. The chemistry, biology and vertical flux of particulate matter from the upper 400 meters of the Cape basin in the southeast Atlantic Ocean. Deep-Sea Research, 25: 1121-1161.
- Florschütz, F., Menéndez Amor, J. & Wijnstra, T.A., 1971. Palynology of a thick Quaternary succession in southern Spain. Palaeogeogr., Palaeoclimatol., Palaeoecol., 10: 233-264.
- Frenzel, B., 1968. Grundzüge der Pleistozänen Vegetationsgeschichte Nord-Eurasiens. Erdwissenschaftliche Forschung, Band I: 326 pp. Steiner Verlag, Wiesbaden.
- Griffiths, J.F. & Soliman, K.H., 1972. The northern desert (Sahara). In: Griffiths, J.F. (ed.), Climates of Africa. World survey of climatology, Vol. 10: pp. 75-131. Elsevier, Amsterdam.
- Honjo, S., 1976. Coccoliths: production, transportation and sedimentation. Mar. Micropaleont., 1: 65-79.
- Honjo, S., 1980. Material fluxes and modes of sedimentation in the mesopelagic and bathypelagic zones. Journal of Marine Research, 38:

53-97.

- Honjo, S., 1983. Transport mechanism of pelagic particles in time and space. Transactions of the American Geophysical Union, 65: 225.
- Hooghiemstra, H., 1988a. Changes of major wind belts and vegetation zones in NW Africa 20,000-5000 yr B.P. as deduced from a marine pollen record near Cap Blanc. Rev. Palaeobot. Palynol., 55: 101-140.
- Hooghiemstra, H., 1988b. Palynological records from northwest Atlantic marine sediments: a general outline of the interpretation of the pollen signal. Phil. Trans. R. Soc. Lond., B 318: 431-449.
- Hooghiemstra, H. & Agwu, C.O.C., 1986. Distribution of palynomorphs in marine sediments: a record for seasonal wind patterns over NW Africa and adjacent Atlantic. Geol. Rdsch., 75(1): 81-95.
- Hooghiemstra, H., Agwu, C.O.C. & Beug, H.-J., 1986. Pollen and spore distribution in recent marine sediments: a record of NW-African seasonal wind patterns and vegetation belts. "Meteor" Forsch.-Ergeb., C 40: 87-135.
- Hooghiemstra, H., Bechler, A. & Beug, H.-J., 1987. Isopollen maps for 18,000 years B.P. of the Atlantic offshore of northwest Africa: evidence for paleowind circulation. Paleoceanography, 2(6): 561-582.
- Hooghiemstra, H. & Agwu, C.O.C., 1988. Changes in the vegetation and trade winds in equatorial northwest Africa 140,000-70,000 yr B.P. as deduced from two marine pollen records. Palaeogeogr., Palaeoclimatol., Palaeoecol., 66: 173-213.
- Hooghiemstra, H. Stalling, H. & Agwu, C.O.C. (submitted). Vegetational and climatic changes at the northern fringe of the Sahara 140,000-5000 years B.P.: evidence from 4 marine pollen records located between Portugal and the Canary Islands. Rev. Palaeobot. Palynol.
- Imbrie, J., Hays, J.D., Martinson, D.G., McIntyre, A., Mix, A.C., Morley, J.J., Pisias, N.G., Prell, W.L. & Shackelton, N.J., 1984. The orbital theory of Pleistocene climate: support from a revised chronology of the marine  $\delta^{18}O$  record. In: Berger, A.L. et al. (eds.), Milankovitch and Climate, Part I, pp. 269-305. Reidel, Dordrecht.
- Janecek, T.R. & Rea, D.K., 1985. Quaternary fluctuations in the northern hemisphere trade winds and westerlies. Quat. Res., 24: 150-163.
- Janssen, C.R. & Woldringh, R.E., 1981. A preliminary radiocarbon dated pollen sequence from the Serra da Estrela, Portugal. Finisterra, 16(32): 299-309.
- Koopmann, B., 1981. Sedimentation von Saharastaub im subtropischen Nordatlantik während der letzten 25.000 Jahre. "Meteor" Forsch.-Ergeb., C 35: 23-59.
- Lamb, H.F., Eicher, U. & Switsur, V.R., in press. An 18,000-year record of vegetational, lake-level and climatic change from the Middle Atlas, Morocco. Journal of Biogeography.
- Leroux, M., 1983. The climate of tropical Africa, Ed. Champion, Paris.
- Melia, M.B., 1984. The distribution and relationship between palynomorphs in aerosols and deep-sea sediments off the coast of northwest Africa. Mar. Geol., 58: 345-371.

- Nicholson, S.E. & Flohn, H., 1980. African environmental and climatic changes and the general atmospheric circulation in Late Pleistocene and Holocene. Climatic Change, 2: 313-348.
- Parkin, D.W., 1974. Trade-winds during glacial cycles. Proc. R.Soc. Lond., A 337: 73-100.
- Parkin, D.W. & Shackleton, N.J., 1973. Trade wind and temperature correlations down a deep-sea core off the Saharan coast. Nature, 245: 455-456.
- Parkin, D.W. & Padgham, R.C., 1975. Further studies on trade winds during the glacial cycles. Proc. R. Soc. Lond., A 346: 245-260.
- Petit-Maire, N. & Riser, J., 1981. Holocene lake deposits and palaeoenvironments in Central Sahara, northeastern Mali. Palaeogeogr., Palaeoclimatol., Palaeoecol., 35: 45-61.
- Pokras, E.M. & Mix, A.C., 1985. Eolian evidence for spatial variability of Late Quaternary climates in tropical Africa. Quat. Res., 24: 137-149.
- Pons, A. & Reille, M., 1984. Originalité de l'histoire climatique des pourtours de la Méditerranée occidentale durant le Pléistocène supérieur par rapport à celle de l'Europe occidentale. Bull. Soc. bot. Fr., 131, Actual. bot., 1984 (2-4): 69-76.
- Pons, A. & Reille, M., 1986. Nouvelles recherches pollenanalytiques a Padul (Granada): la fin du dernier glaciaire et l'Holocene. In: López-Vera, F. (ed.), Quaternary climate in western Mediterranean, pp. 405-420. Universidad Autónoma de Madrid.
- Prospero, J.M. & Carlson, T.N., 1972. Vertical and areal distribution of Saharan dust over the western equatorial North Atlantic Ocean. Journal of Geophysic. Research, 77(27): 5255-5265.
- Reille, M., 1976. Analyse pollinique de sédiments postglaciaires dans le Moyen Atlas et le Haut Atlas marocains: premiers résultats. Ecologia Mediterranea, 2: 153-170.
- Reille, M., 1977. Contribution pollenanalytique a l'histoire Holocène de la végétation des montagnes du Rif (Maroc septentrional). Recherches francaises sur le Quaternaire INQUA, Suppl. Bull. AFEQ, 1977-1(50): 53-76.
- Rognon, R., 1976. Essai d'interprétation des variations climatiques au Sahara depuis 40.000 ans. Rev. Géogr. phys. Géol. dyn., 2, 18(2-3): 251-282.
- Rognon, P., 1987. Late Quaternary climatic reconstruction for the Maghreb (North Africa). Palaeogeogr., Palaeoclimatol., Palaeoecol., 58: 11-34.
- Sarnthein, M., 1978. Sand deserts during glacial maximum and climatic optimum. Nature, 272: 43-46.
- Sarnthein, M., Tetzlaff, G., Koopmann, B., Wolter, K. & Pflaumann, U., 1981a. Glacial and interglacial wind regimes over the eastern subtropical Atlantic and North-West Africa. Nature, 293: 193-196.
- Sarnthein, M., Erlenkeuser, H. & Zahn, R., 1981b. Termination I: the response of continental climate in the subtropics as recorded in deep-sea sediments. Actes Colloque Intern. CNRS, Bordeaux. Bull. Inst. Géol. Bassin d'Aquitaine, Bordeaux, 1982(31): 393-407.
- Sarnthein, M., Thiede, J., Pflaumann, U., Erlenkeuser, H., Fütterer, D., Koopmann, B., Lange, H. & Seibold, E., 1982. Atmospheric and

- oceanic circulation patterns off northwest Africa during the past 25 million years. In: Von Rad, U. et al. (eds.), Geology of the northwest African continental margin. pp. 545-604. Springer Verlag, Berlin.
- Schmidt, F.H., 1967. Palynology and meteorology. Rev. Palaeobot. Palynol., 3: 27-45.
- Schrader, H.J., 1971. Fecal pellets: role in sedimentation of pelagic diatoms. Science, 174: 55-57.
- Tauber, H., 1965. Differential pollen dispersion and the interpretation of pollen diagrams. Danmarks Geologiske Undersøgelse, II, 89: 69 pp. Reitzels Forlag, København.
- Tezlaff, G. & Wolter, K., 1980. Meteorological patterns and the transport of mineral dust from the north African continent. Palaeoecology of Africa, 12: 31-42.
- Tetzlaff, G. & Peters, M., 1986a. Deep-sea sediments in the eastern equatorial Atlantic off the African coast and meteorological flow patterns over the Sahel. Geol. Rdsch., 75: 71-79.
- Tetzlaff, G. & Peters, M., 1986b. The atmospheric transport potential for water vapour and dust in the Sahel region. GeoJournal, 12: 387-398.
- White, F., 1983. The vegetation of Africa. A descriptive memoir to accompany the UNESCO/AEFTAT/UNSO vegetation map of Africa: 356 pp., 3 maps. UNESCO, Paris.

DEFLATION AND HUMIDITY DURING THE LAST 700 KA IN NW AFRICA FROM THE  
MARINE RECORD

Bjørg Stabell  
Geological-Paleontological Institute  
University of Kiel  
Olshausenstrasse 40  
D-2300 Kiel  
F.R. Germany

Mailing adress:  
Bjørg Stabell  
Department of Geology  
University of Oslo  
P.O. Box 1047, Blindern  
N-0316 Oslo 3  
Norway

ABSTRACT

Freshwater diatoms from a core off Cape Blanc have been used to reconstruct atmospheric circulation and climate on the African continent. Maxima in freshwater diatoms occurred mainly in the late phase of interglacial stages. From the freshwater diatom record it can be inferred that intertropical aridity and increased wind strength was initiated just prior to global icegrowth.

1. INTRODUCTION

Freshwater diatoms found in the sediments of the eastern equatorial Atlantic are believed to reflect climatic changes on the adjacent African continent (Parmenter and Folger, 1974; Pokras and Mix, 1985; Stabell, 1986). These investigations assume that the freshwater diatoms are all windblown from Africa, reflecting phases of enhanced deflation and wind transport during dry episodes (Parmenter and Folger, 1974). The easterly trade winds intensified during Late Pleistocene glacial times (Sarnthein et al., 1982). Windblown freshwater diatoms in the Atlantic sediments may thus be used as an index of increased wind strength and the initiation of intertropical aridity.

However, several authors also suggest that freshwater diatoms in the Atlantic sediments may have been derived (at least at some localities) from fluvial transport (see discussion in Gasse et al., in press). In that case, freshwater diatom peaks in Atlantic cores may be indicative of increased river influx, correlated with humid episodes on the continent.

2. MATERIAL AND METHODS

The freshwater diatom record of ODP Site 658 (Stabell, in press) has been investigated (Fig. 1). This Site is located at 20°44.95'N and 18°34.85'W at a waterdepth of 2263 m on the continental slope 160 km

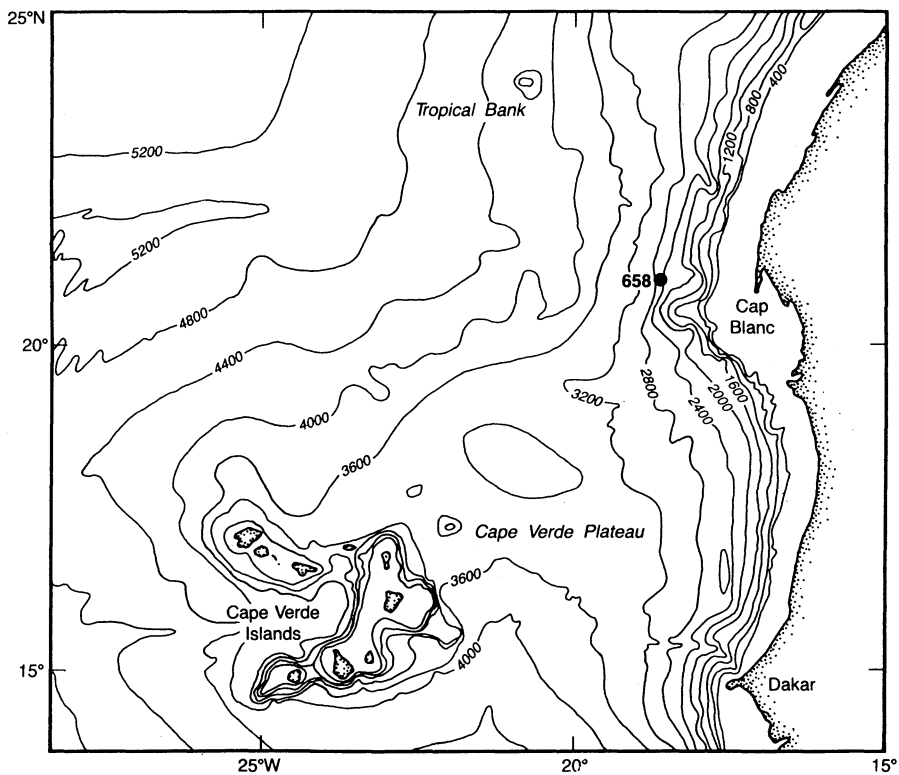


Fig. 1. Location map for ODP Site 658 (from Ruddiman, Sarnthein, Baldauf et al., 1988).

west of Cape Blanc. Sediments deposited at these sites contain eolian dust records dominated by the input from the zonal flow of the Saharan Air Layer (African Easterly Jet). In addition, Site 658 is strongly influenced by dust supply from the meridional trade winds (Ruddiman, Sarnthein, Baldauf et al., 1988). Dust concentrated along the continental margin from 10°N to 25°N originate from the middle of Sahara (Tamanrasset area; Kalu 1979) and is transported westward during northern hemisphere summer. Three holes were cored; 658A, 658B and 658C. Diatom samples were taken from all cores in hole 658A and from cores 2 and 3 in hole 658B. Correlation of holes 658A and 658B was established by means of magnetic susceptibility and oxygen and carbon isotope records. The composite depth values of both sections were taken from Ruddiman, Sarnthein, Baldauf et al. (1988) and Sarnthein and Tiedemann (in press). Pollen analytical information was taken from Dupont et al. (in press).

The diatom samples were prepared based on the procedure described in Kaland and Stabell (1981), adding Dynospheres as a marker for absolute control in quantitative estimates. About 0.02 g dry sediment was oxidized in H<sub>2</sub>O<sub>2</sub> and repeatedly washed. Calcareous matter was removed with HCl. Dynospheres, monosized polymer particles, were added as the last step. For 0.02 g dry sediment about 150.000 Dynospheres were added. With this method only the weight of the sediment sample and the number of Dynospheres added need to be known, the number of diatom valves per g dry sediment can then be calculated. The abundances are based on total sediment, fluctuations in carbonate content will therefore affect the distribution pattern. However, as shown in Stabell (1986), even with large fluctuations in calcium carbonate percentages with time, the general pattern in diatom abundance based on total sediment does not differ significantly from that on a carbonate-free basis.

The time scale is deduced from the  $\delta^{18}\text{O}$  curve, assuming a constant sedimentation rate between midpoint stages as defined by the SPECMAP group (Imbrie et al., 1984; Martinson et al., 1987). The very detailed oxygen-isotope stratigraphy of this core (Sarnthein and Tiedemann, in press) makes it possible to date the fluctuations in freshwater diatom abundance with great accuracy. It was attempted to analyze at least one sample from every core section ( $\geq 1.5$  m between samples). However, sampling gaps occur at 14.88-22.15 mbsf (only one sample at 17.87 mbsf), 30.06-32.15 mbsf, 56.59-60.65 mbsf, 76.98-79.15 mbsf and 86.70-89.35 mbsf. There is a hiatus of 24.26 ky between 8.83 and 9.10 mbsf. The sampling intervals are on the average less than 5 ky between sampling gaps, except at the interval 9.70-14.88 mbsf. Sedimentation rates range from 9.2 cm/ka (152-183 ka) to 26.0 cm/ka (215-225 ka).

The freshwater diatom data of ODP Site 658 are presented as influx values. The influx values are calculated from the concentration values and the sedimentation rates and are plotted against depth.

### 3. RESULTS

Freshwater diatoms (*Aulacoseira granulata* and diverse other taxa) were found in both glacial and interglacial stages (Fig. 2). The detailed influx pattern record fifteen maxima ( $>50 \times 10^2$  valves/g/cm/ka). The majority of these maxima were found in interglacial stages, and are concentrated near the onset of late interglacial cooling (events 15.5,

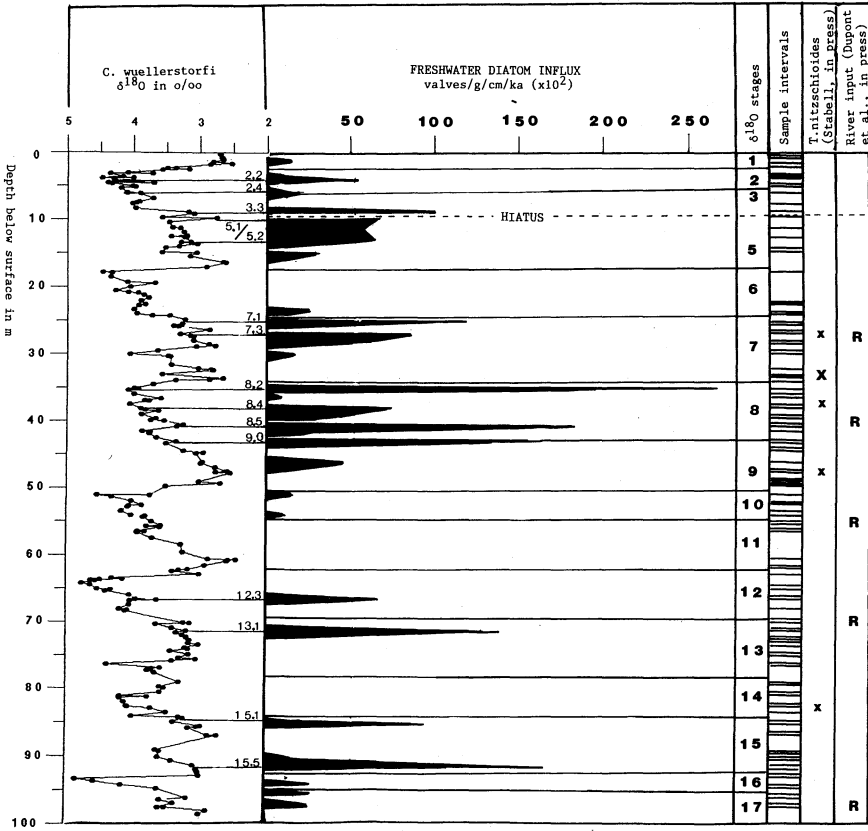


Fig. 2. Freshwater diatom influx versus depth at ODP Site 658. Oxygen isotope curve from Sarnthein and Tiedemann (in press). Only oxygen isotope stages with high freshwater diatom influx have been numbered.



15.1, 13.1, 9.0, 7.32?, 7.1, 5.1 and 3.3), mainly near the onset of global icegrowth (interglacial/glacial stage boundaries). Stage 11 has a large sampling gap. Freshwater diatoms are fairly common in glacial stages 2 and 8, mainly occurring near climatic ameliorations (events 8.4, 8.2, 2.4 and 2.2), with the exception of one peak at interstadial stage 8.5. Glacial stage 4 is missing and glacial stage 6 has a large sampling gap. It is therefore not possible to determine whether freshwater diatoms are common in all glacial stages above stage 9. Below stage 9, however, freshwater diatoms are common in only one sample from a glacial stage; interstadial stage 12.3.

#### 4. DISCUSSION

Parmenter and Folger (1974) proposed that freshwater diatom maxima in marine sediments could be used as an index of equatorial ice-age aridity and suggested that fluctuations in available moisture in the source area are essential for the variability in concentration of freshwater diatoms. However, fluctuations in freshwater diatom abundance, i.e. of dust supply, also reflect changes in wind intensity.

From the information on dust supply in general, one may expect more arid conditions during the late phase of an interglacial. Accordingly lakes would contract, lake beds with abundant diatoms would be exposed, trade winds would strengthen (Sarnthein et al. 1982) and one could expect maxima of freshwater diatoms at the coring localities. It should be noted, however, that freshwater diatom maxima do not necessarily reflect maximum aridity, but rather the interaction of aridification and strengthened trade winds. Pokras and Mix (1987) suggest that depletion of the supply of diatomaceous sediments results in a relatively brief input of *Melosira* (= *Aulacoseira*; freshwater diatoms) to ocean sediments during or immediately following desiccation of lakes, and prior to maximum aridity.

Maxima of freshwater diatoms in cores M13519 and M13521 from the eastern equatorial Atlantic (Stabell 1986) follow exactly this model, as proven by comparison to the global ice record of the  $\delta^{18}\text{O}$  curves.

This pattern was also recorded by Pokras and Mix (1985) from the equatorial region. However, they found increased freshwater diatom abundance in glacial time in their northern area (core V30-49), concluding that the climate of tropical northwest Africa has been most arid during glaciations and glacial stades. It is difficult to compare results from ODP Site 658 directly with those from V30-49 as stage 4 is missing and there is a sampling gap in stage 6 at Site 658. The freshwater diatom abundance at Site 658 is considerably lower (one order of magnitude) than in V30-49. The *Melosira* maximum in the upper Holocene at V30-49 was not found at Site 658. The only maxima that seem to coincide are the ones in glacial stage 2. The long term trends at ODP Site 658, however, rather follow the more general model with high diatom influx ahead of polar ice cap formation. High abundances are, however, common at Site 658 in glacial stages 2 and 8.

The  $\delta^{18}\text{O}$  values of the interglacial events where freshwater diatom maxima occur lie between 3.0 and 3.5 o/oo, with the exception of event 5.1. Interstadials with lower  $\delta^{18}\text{O}$  values (e.g. 1.1, 5.5, 7.53, 9.31, 11.3 and 15.3) do not coincide with freshwater diatom maxima. Also, freshwater diatom maxima are not associated with every interstadial,

indicating that the mechanism behind these maxima are more complex than merely the interaction between aridity and wind strength. Two of the maxima occurring in glacial (12.3 and 8.5) can be explained by the general model, while the maxima at 8.4, 8.2, 2.4 and 2.2 must be explained otherwise. It is possible that the climate in NW Africa (SW Sahara) in the last 300 ka was arid both in ameliorations during glacial intervals and at the onset of global icegrowth.

At events 7.3 and 8.4 the maxima in freshwater diatoms coincide with a maximum of the marine diatom species *Thalassionema nitzschioides* (Stabell, in press), which is regarded as an indicator of river run off by Pokras and Molfino (1986). The maximum at 7.3 also coincides with pollen indicators of river input (Dupont et al., in press). It is therefore possible that the maximum at event 7.3 is due to river run off rather than eolian transport. Further studies in the area searching for fluviatile indicators among the freshwater diatoms (Gasse et al., in press) might clarify whether river input has been an important source of any freshwater diatom maxima. The remaining interglacial maxima must, however, be attributed to deflation at the initiation of intertropical aridity.

It seems that the majority of the freshwater diatom maxima at ODP Site 658 are related to climatic events of intertropical aridity and increased wind strength and that these events occurred just prior to global icegrowth. The general freshwater diatom abundance pattern seems to be similar to that recorded from the equatorial region.

#### ACKNOWLEDGEMENTS

I thank M. Sarnthein for many interesting discussions. This study was supported by the Deutsche Forschungsgemeinschaft.

#### 5. REFERENCES

- DUPONT, L.M., BEUG, H.-J., STALLING, H., and TIEDEMANN, R., in press. Initial palynological results of ODP 661, 659 and 658: Pollen as climate indicators. *Init. Repts. ODP Leg 108. Vol. B.*
- GASSE, F., STABELL, B., IPEREN, J. VAN, and FORTANIER, E., in press. Freshwater diatom influx in intertropical Atlantic; relationships with continental records from Africa. *Quat. Res.*
- IMBRIE, J., HAYS, J.D., MARTINSON, D.G., MCINTYRE, A., MIX, A.C., MORLEY, J.J., PISIAS, N.G., PRELL, W.L., and SHACKLETON, N. J., 1984. The orbital theory of Pleistocene climate: support from a revised chronology of the marine  $\delta^{18}O$  record. in Berger, A.L. et al. (Eds.), *Milankovitch and Climate*. Part 1, D. Reidel Publ. Company, 269-305.
- KALAND, P.E. & STABELL, B. 1981: Methods for absolute diatom frequency analysis and combined diatom and pollen analysis in sediments. *Nord. J. Bot.* 1, 697-700.
- KALU, A. E., 1979. The African dust plume: Its characteristics and propagation across West Africa in winter. in C. Morales (Ed.), *Saharan Dust, Mobilization, Transport, Deposition*. Wiley, Chichester, pp. 95 - 118.
- MARTINSON, D.G., PISIAS, N.G., HAYS, J.D., IMBRIE, J., MOORE, T.C.JR. and SHACKLETON, N.J., 1987. Age Dating and the Orbital Theory of the Ice Ages: Development of a High-Resolution 0 to 300,000-Year Chrono-

- stratigraphy. *Quaternary Research* **27**, 1 -29.
- PARMENTER, C. and FOLGER, D.W., 1974. Eolian Biogenic Detritus in Deep Sea Sediments: a possible index of Equatorial Ice Age aridity. *Science (Washington, D.C.)* **185**, 695-698.
- POKRAS, E.M. and MIX, A.C., 1985. Eolian Evidence for Spatial Variability of Late Quaternary Climates in Tropical Africa. *Quaternary Research* **24**, 137- 149.
- POKRAS, E. M. and MIX, A. C., 1987. Earth's precession cycle and Quaternary climatic change in tropical Africa. *Nature* **326**, 486 - 487.
- POKRAS, E.M., and MOLFINO, B., 1986. Oceanographic control of diatom abundances and species distributions in surface sediments of the tropical and southeast Atlantic. *Marine Micropaleontology* **10**, 165-188
- RUDDIMAN, W., SARNTHEIN, M., BALDAUF, J., et al., 1988. *Proc., Init. Repts. (pt. A), ODP, 108.*
- SARNTHEIN, M., ERLLENKEUSER, H., and ZAHN, R., 1982. Termination I: The response of continental climate in the subtropics as recorded in deep-sea sediments. *Bulletin Institut Géologique du Bassin d'Aquitaine* **31**, 393-407.
- SARNTHEIN, M. and TIEDEMANN, R., in press. Towards a high-resolution stable isotope stratigraphy of the last 3.3 Million years, ODP Sites 658 and 659 off Northwest Africa. *Init. Repts. ODP Leg 108. Vol. B.*
- STABELL, B., 1986. Variations of diatom flux in the eastern equatorial Atlantic during the last 400.000 years ("Meteor" cores 13519 and 13521). *Marine Geology* **72**, 305-323.
- STABELL, B., in press. Initial diatom record of ODP Sites 657 and 658; On the history of upwelling and continental aridity. *Init. Repts. ODP Leg 108. Vol. B.*

PALYNOLOGY OF THE LAST 680,000 YEARS OF ODP SITE 658 (OFF NW-AFRICA):  
fluctuations in paleowind systems.

Lydie M. Dupont

Institute for Palynology and Quaternary Sciences, University  
of Göttingen Wilhelm-Weber-Str. 2, D-3400 Göttingen, F.R.G.

Sediments from ODP Site 658 at 21°N west of Cap Blanc show relatively high pollen concentrations and were deposited at high sedimentation rates. Detailed pollen analysis of the upper 100 m provide a unique record of vegetation and climate of NW Africa for the last 680 ka. With the help of pollen tracers, an estimate is made for the contribution of different transport systems to the total influx of the pollen taxa. High influx values for Poaceae and Cyperaceae that were transported by the African Easterly Jet (AEJ), indicate a northern position of the Sahel-Sahara boundary during periods with warm and humid conditions. During periods with cold and arid conditions the influx values for the NE trade wind transported pollen rise. On the average, pollen transport by the NE trade-winds increases during the last 680 ka; periods with warmest and most humid conditions occur only during the earlier part of the Brunhes Chron.

## 1. INTRODUCTION

The pollen preserved in the marine sediments offshore NW Africa form a rich source of information for studies of the paleovegetation and climatic history of the adjacent continent. The offshore marine sequences often cover a long span of continuous accumulation, and the measurements of oxygen isotopes provide a good stratigraphic and time control (Heusser, 1986/7).

In the sediments offshore NW Africa, pollen from the continent is chiefly transported by wind (Figure 1) and to a much lesser extent by water (Diester-Haass and Müller, 1979; Rossignol-Strick and Duzer, 1979a; Melia, 1984; Hooghiemstra *et al.*, 1986; 1987). West of Cap Blanc three transport mechanisms for pollen grains are of importance:

- (1) transport by the trade winds of pollen grains from Europe, the Mediterranean, and the Northern Sahara;
- (2) transport by the summer maximum (August) of the Saharan Air Layer, the African Easterly Jet (AEJ), of pollen from the Central and Southern Sahara and the Sahel;
- (3) transport by water (e.g. Senegal river) of pollen from plants growing in swamps and from the Guinean and Sudanian vegetation zones (Rossignol-Strick and Duzer, 1979a, 1979b; Caratini *et al.*, 1986; Hooghiemstra *et al.*, 1986; 1987; Hooghiemstra, 1988a; 1988b; this volume).

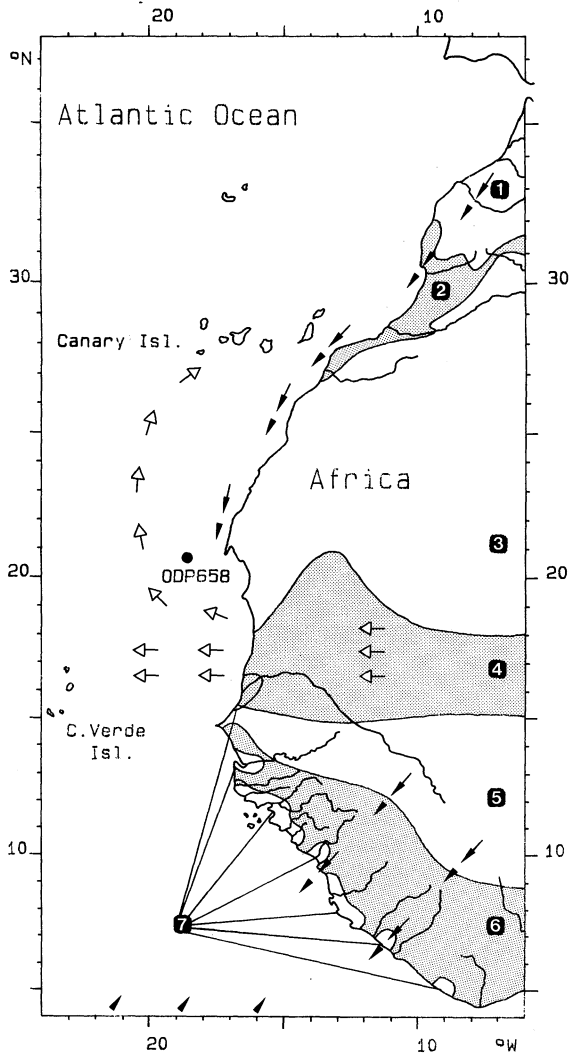


Fig. 1. Summary of the vegetation zones and the major wind belts of NW Africa of the present situation. The solid arrows indicate surface trade-winds and the open arrows the trajectory of zonal winds at higher latitudes (Saharan Air Layer). The numbers indicate the major vegetation zones, from north to south: (1) Mediterranean vegetation zone, (2) steppes of the Western Atlas region, (3) deserts and semi-deserts of the Sahara, (4) Sahel zone, (5) Sudanian woodland and savannas, (6) Guinean savanna zone and rainforest, (7) Mangrove (*Rhizophora*) swamps. The ODP Site 658 is indicated by a dot. After Hooghiemstra et al., 1987 (adapted).

Fluctuations in the wind systems (trades and Saharan Air Layer) are monitored in these sediments by their pollen content (Hooghiemstra, 1988a). The pollen signal displays variations in efficiency of the wind transport which is related to (1) changes in wind speed, (2) changes in the pollen production of the vegetation in the source area (rich or sparse vegetation), and (3) changes in the distance of the source area to the core station (shifting of vegetation zones).

In this paper, it is attempted to estimate the fluctuations of the mentioned transport systems, at 21°N and west of Cap Blanc (ODP Site 658).

## 2. MATERIAL AND METHODS

ODP Site 658 is situated at 20°44.95'N and 18°34.85'W at a water depth of 2263 m on the continental slope 160 km west of Cap Blanc. Three holes were cored: 685A, 685B and 658C. The oldest sediments have an estimated age of 3.5 to 3.8 Ma BP and were reached in hole 658A at a subbottom depth of 300 m (Ruddiman *et al.*, 1987). Pollen samples were taken from all the cores of hole 658A and from the upper 9 cores of hole 658B. Each core was 10 m long. Correlation of 658A and 658B was established using magnetic susceptibility, and the composition depths of both sections were computed (Ruddiman *et al.*, 1987; Sarthein and Tiedemann, *subm.*).

A detailed oxygen isotope stratigraphy of this core was performed by workers at the Geological Paleontological Institute of the University of Kiel. The upper 100 meters of the core represent 680 ka and reaches into oxygen isotope Stage 17 (Stage 4 is lacking in the sediments).

The volume of the samples was determined by water displacement and the wet samples were then fractionated with a 250 µm sieve. The fraction smaller than 250 µm was decalcified with HCl and treated with warm KOH. Lycopodium marker tablets were added together with the HCl. Sand and clay were removed with HF, the sample was acetolysed, and finally, particles smaller than 10 µm were removed by ultrasonic sieving. Pollen grains were mounted in glycerine jelly and counted (by Dr. H. Stalling and myself) until a pollen total of 300 was reached.

The pollen data of Site 658 are presented as influx values and as percentages of the total pollen counted. The influx values were computed from the concentration values and the sedimentation rates. Time control is provided by a very detailed oxygen isotope record with a time resolution of 2700 years (Sarthein and Tiedemann, *subm.*).

## 3. RESULTS

Figure 2 shows the influx values for a selection of curves of the more abundant pollen types. At the lefthand side the relative contributions of 6 groups of pollen taxa (A through E and F) are



indicated. The taxa that make these groups and pollen concentration values per spectrum of the respective taxa are given in Dupont *et al.* (subm.). The oxygen isotope stages (Sarnthein and Tiedemann, subm.) are also given in Figure 2 (extreme left side).

Group A (percentages at the left in Figure 2) includes pollen of Cyperaceae, taxa from swamps and wet localities (e.g. Typha/Sparganium), including pollen of Rhizophora (mangrove), and pollen from the Sudanian and Guinean Savanna (group 5 and 6 of Agwu and Beug, 1982). The influx curves of the Group A taxa are given at the righthand side of Figure 2, all these elements are favoured by humid conditions. Group B consists of Poaceae (grasses). This family has representatives in almost all biotopes, but they are especially abundant in the Savanna. Group C contains desert elements from Sahara and Sahel. It includes Chenopodiaceae-Amaranthaceae mainly from the Sahara and the Sahel (Lezine, 1987), Calligonum mainly from the Sahara (Cour and Duzer, 1976; Rossignol-Strick and Duzer, 1979a; White, 1983), and Capparidaceae and Balanites mainly from the Sahel (Rossignol-Strick and Duzer, 1979; Maley, 1983; Lezine, 1987). Group D contains pollen types coming from Europe (mainly Pinus pollen; group 1 of Agwu and Beug, 1982) and the Mediterranean (mainly Gypsophila; group 2 of Agwu and Beug, 1982). Group E contains elements from dry communities of southern Mediterranean and northern Sahara. It includes Artemisia and other Asteraceae (Compositae), both mainly found in the Mediterranean (vegetation zones VII and XVIII of White, 1983), and Ephedra, mainly of the northern Sahara (vegetation zones VII, XVII, and XVIII of White, 1983). Group F contains all those elements that do not fit one of the groups A through E. In addition, I use the term 'trade-wind indicators' as proposed by Hooghiemstra (1988b) and Hooghiemstra *et al.* (1987). That term covers pollen of Pinus, Ephedra, and Asteraceae (incl. Artemisia). The great majority of pollen grains in group D and E is formed by these trade-wind indicators.

The palynological sequence has been described within reference of the oxygen isotope stratigraphy (Dupont *et al.*, subm.). All isotope stage transitions could be recognised in the pollen diagram with the exception of those of Stage 9. Zone 9 of the pollen diagram spans 331 to 315 k.y., while isotope Stage 9 lasts from 339 to 303 k.y. This means a strongly delayed response of the vegetation to climatic amelioration at the beginning of Stage 9 and an early vegetational response to climatic deterioration at the end of this Stage. The pollen diagram (Figure 2) is divided into 34 zones. The zones are numbered according to the isotope stages. If there are several zones in one isotope stage the zones have been labeled with characters. Zones with high percentages of group D and E (trade wind indicators plus other European and Mediterranean elements) are grouped in drier glacial (G) zones, and those with high percentages of group A (elements from the Guinean and Sudanian savanna, swamps and wet localities, and Cyperaceae) in the more humid interglacial (I) zones. The glacial zones are divided into 4 subtypes (G1-G4) and the interglacial zones types into 3 subtypes (I1-I3). These types will be discussed in section 5.2.



## 4. DISCUSSION

The palynological and sedimentological work on modern and fossil marine sediments in the studied area suggest:

- (1) The NE trade wind and AEJ have permanently contributed to the pollen influx at 21°N (Hooghiemstra, 1988a; this volume);
- (2) The position of the NE trade wind belt remained stable but the transport efficiency (speed) was stronger in colder/arid periods and weaker in warm/more humid ones (Sarnthein *et al.*, 1981; 1982; Hooghiemstra, 1988a; 1988b). The influx of pollen grains from north of the Sahara monitor its vigor (Hooghiemstra, this volume);
- (3) The AEJ belt is also believed to have kept its position (Sarnthein and Koopmann, 1980, Sarnthein *et al.*, 1981; Koopmann, 1981), but until now little has been known about changes in its transport capacity (Sarnthein, this volume). The AEJ component of the pollen supply at 21°N reflects changes in the vegetation of the source area of the AEJ (Hooghiemstra *et al.*, 1987).
- (4) Water transport by the Senegal river into the ocean is apparent during warm/more humid periods, but is low or absent during drier periods (Rossignol-Strick and Duzer, 1979b; Rognon, 1985; 1987).

#### 4.1 Estimation of the individual contributions of the transport systems to the influx of pollen grains.

To estimate the individual contributions of the different transport systems, it is reasoned that the pollen influx brought in by one of the mechanisms (e.g. NE trade wind) may be estimated with the influx of a so-called tracer (e.g. NE trade-wind indicators). For one taxon that is transported by several mechanisms it is presumed that the number of grains transported by one mechanism ( $F_{i,j}$ ) depends only on the total transport capacity of the mechanism and the total available pollen of the taxon. The transport capacity is estimated by the ratio of the total number of transported grains ( $T_i$ ) and the pollen sum ( $S$ ). Dividing by the pollen sum excludes, as much as possible, the effect of varying pollen production in the source area. The number of grains transported by mechanism  $i$  is expressed via the following relation:

$$F_{i,j} = \frac{T_i}{S} P_j, \quad (1)$$

where,  $F_{i,j}$  = the fraction of taxon  $j$  that is transported by mechanism  $i$ ,  $T_i/S$  = estimate of the transport capacity of mechanism  $i$ ,  $S$  = pollen sum, and  $P_j$  = total of pollen grains of taxon  $j$  that are trapped in the sediment.

A tracer for each transport mechanism is needed, that is a taxon or a group of taxa ( $P_{\text{tracer}}$ ) that is (almost) exclusively transported by one mechanism, thus:

$$I_i = P_{\text{tracer}},$$

where,  $I_i$  = total of pollen grains of the tracer that are transported by the mechanism  $i$ . The total number of grains that is transported by mechanism  $i$  ( $T_i$ ) is then given by

$$T_i = I_i + \sum_j F_{i,j}. \quad (2)$$

Substitution of  $T_j$  from equation (2) into equation (1) gives

$$F_{i,j} = \frac{P_j}{S} (I_i + \sum_j F_{i,j}) \quad (3)$$

In addition it is stated that the sum of the fractions  $F_{i,j}$  for one taxon equals the total number of grains of the taxon

$$P_j = \sum_i F_{i,j}$$

namely, the total of pollen grains of a taxon  $j$  is given by the sum of the fractions of all the mechanisms  $i$  that contribute to its pollen influx. The pollen sum ( $S$ ) equals the sum of the grains that are transported by the different mechanisms

$$S = (\text{definition}) \sum_j P_j = \sum_i T_i.$$

For a simplified system with a few taxa equation (3) can be rewritten as:

$$F_{i,1} = I_i \frac{P_1}{S - P_1 - P_2 - P_3},$$

where,  $F_{i,1}$  is the estimate for the part of the pollen of  $P_1$  that are blown into the sediment by mechanism  $i$ ,  $I_i$  = tracer for mechanism  $i$  (taxa that are exclusively transported by this mechanism),  $P_1$  = total pollen of taxon 1 that is partly transported by mechanism  $i$ ,  $S$  = pollen sum, and  $P_2, P_3$  = total pollen of the other taxa (2 and 3) that are partly transported by mechanism  $i$ .

In applying this simplified model to Cap Blanc one has to make additional assumptions that are listed below.

- (1) Not only the trade-wind indicators, but also other pollen from Europe, the Mediterranean area, and the North Sahara are transported by the NE trade-winds (Rossignol-Strick and Duzer, 1979a; Hooghiemstra, 1988a; 1988b).
- (2) Pollen of Rhizophora (Mangrove), pollen from swamp vegetation, and the northbound transport of pollen from the Guinean and Sudanian

savanna is transported chiefly by water (Rossignol-Strick and Duzer, 1979b; Hooghiemstra *et al.*, 1986).

- (3) Pollen grains from the Sahel (e.g. of *Balanites*, the majority of the Capparidaceae) are transported by the AEJ (cf. Cour and Duzer, 1976, Hooghiemstra *et al.*, 1986; cf. Lezine, 1987).
- (4) Pollen grains from the middle and southern latitudes of the Sahara (e.g. of Chenopodiaceae-Amaranthaceae) are transported by the NE trade-wind and by the AEJ (Hooghiemstra *et al.*, 1986; 1987).
- (5) Pollen of the Poaceae (grasses) are transported by the NE trade, the AEJ, and by water (Hooghiemstra *et al.*, 1986; Hooghiemstra, 1988a; 1988b).
- (6) Pollen of the Cyperaceae are transported by the AEJ and by water (Rossignol-Strick and Duzer, 1979a; Hooghiemstra *et al.*, 1986).
- (7) Pollen of taxa that are not characteristic of a particular vegetation zone are thought to be transported by the NE trade, the AEJ and by water.
- (8) The pollen of taxa that are transported exclusively by the AEJ are unfortunately too scarce to be used as a reliable tracer for the AEJ. Therefore, the number of grains assumed to be transported by this wind system is calculated by subtracting the trade transported and the water transported pollen grains from the total.

The curves that were computed according to the described model are given in Figure 3. To clarify the computing method, three examples are given. In these examples, *t* denotes counts of pollen that are chiefly transported by the NE trade-winds, *p* counts of Poaceae, *s* the pollen sum, *c* Chenopodiaceae-Amaranthaceae counts, and *r* counted pollen of the rest group F. The number of trade transported Poaceae in one sample was computed as:  $t.p/(s-p-c-r)$ ; the number of trade transported Chenopodiaceae-Amaranthaceae as:  $t.c/(s-p-c-r)$ ; and the number of the AEJ transported Chenopodiaceae-Amaranthaceae as:  $c-(t.c/(s-p-c-r))$ . All these 'numbers' were multiplied with the concentration factor and the sedimentation rate to obtain influx values.

#### 4.2 Fluctuations in aridity and vigor of the NE trade-winds and the AEJ during the last 680 ka in NW Africa

Driving force of the wind systems (trades and Saharan Air Layer) are the temperature differences between the ocean and the continental landmass (Adams, 1987). As the intensity of the monsoon depends, via these wind systems, on solar radiation (Rossignol-Strick, 1983; Kutzbach and Street-Perrot, 1985; Prell and Kutzbach, 1987), temperature and aridity are highly correlated in NW-Africa. The influence of aridity on the vegetation, however, is greater than that of temperature. This means that the pollen signal chiefly reflects changes in wind intensity and aridity in NW-Africa.

The zones of one type (I1, I2, I3, G4, G3, G2, G1) have enough features in common for combined discussion. The types G1 to G3 represent phases that are colder and more arid and the types I1 to I3 represent warmer and more humid conditions; G4 represents a set of conditions

intermediate between the two groups. Percentages and influx values are given in Figure 2 and estimated contributions of NE trade-winds, AEJ, and water to the pollen influx are given in Figure 3.

The zones 8b, 11a, 13a, 13c, and 17 (type I1) are characterized by low influx values for trade-wind transported pollen and high values for AEJ transported pollen. The influx of AEJ transported Cyperaceae is high, even higher than the influx of AEJ transported Poaceae. The influx values for water transported pollen in these phases are higher than in the rest of the diagram, but still form a minority. The proportion of river transport of pollen into the ocean may be underestimated, since those pollen grains that are thought to indicate the water transport are partly from the tropical forest from plants with a much lower pollen production than e.g. European trees. The highest Poaceae pollen production takes place in the Savannas (Cour and Duzer, 1976; Schulz, 1987). Higher values for the AEJ transported Poaceae are interpreted as a northward position or an extension of the Savannas. Cyperaceae pollen grains will probably be transported in various ways, but, since many representatives of this family are bound to wet conditions, its pollen curve will rise in the more humid stages. Cyperaceae-rich vegetation types also occur at the Sahel-Sahara boundary (Schulz, 1987). These will contribute to the Cyperaceae influx through AEJ transport. Increased water transport and increased AEJ transport are shown for Cyperaceae pollen grains in the zones of type I1. Additionally, *Rhizophora* pollen have been found in the zones of type I1 with the exception of 8b. The pollen grains from the mangrove are almost exclusively carried by the water (Hooghiemstra et al., 1986). The zones 8b, 11a, 13a, 13c, and 17 are thought to present humid periods with a high pollen production and a very effective AEJ transport of pollen grains. The high influx of Cyperaceae and Poaceae indicate a northern position of the Sahel-Sahara boundary at or north of 23°N (Hooghiemstra, 1988a; 1988b).

The zones 1, 5e, 9, 11c, 14a, and 15b (type I2) are characterized by lower values for the influx of AEJ transported pollen when compared with the zones of type I1 and by low influx values for trade transported pollen grains. Overall pollen production and the transport effectivity of the AEJ is probably less. Although the influx values for the water transported pollen grains is lower than in the zones of type I1, the decrease in the influx of the AEJ transported grains when comparing zones of type I2 with I1 is stronger. This explains the high relative values for the water transported grains in the zones of type I2 in Figure 3 (left). AEJ influx of Cyperaceae and Poaceae are of the same magnitude in type I2 zones. The influx of Cyperaceae and Poaceae is higher than the influx of AEJ transported Chenopodiaceae-Amaranthaceae, indicating that the Sahel-Sahara boundary shifted little southwards. The proportion of the Cyperaceae is lower than in zones of type I1. Nevertheless, the zones of type I2 represent probably warm and humid periods comparable to climatic conditions at 9 ka BP (Hooghiemstra, 1988a; 1988b).

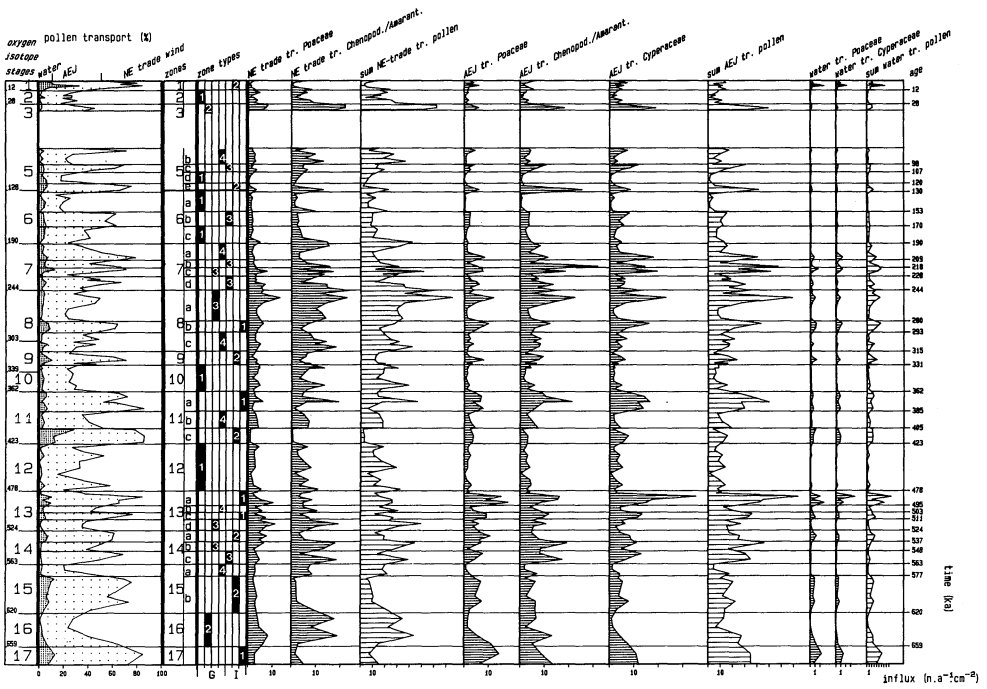


Fig. 3. ODP Site 658: oxygen isotope Stages 1 to 17, proportion of estimated water-, AEJ- and NE trade-winds transport of pollen (percentages), zones 1 to 17, zone types (G1, G2, G3, G4, I3, I2, I1), and influx values (numbers.a<sup>-1</sup>.cm<sup>-2</sup>). The influx values are given for the estimates of the different components of the influx of Poaceae, Chenopodiaceae-Amaranthaceae, and Cyperaceae, grouped per transport mechanism (NE trade, AEJ, or water). Age of the oxygen isotope stage boundaries (extreme left) and age of the zone boundaries (extreme right) are given. The data of the oxygen isotope stages and the vertical time scale (in ka BP) are from Sarnthein and Tiedemann (subm.).

In the zones 5c, 6b, 7b, 7d, and 14c (type I3) the influx values for AEJ transported Chenopodiaceae-Amaranthaceae are at an intermediate level and about the same or higher than the influx of the AEJ transported Cyperaceae or Poaceae. This indicates a more southern position of the Sahel-Sahara boundary than in the zone types I1 and I2, probably at the same latitude as today (see the small rise of the AEJ transported Chenopodiaceae-Amaranthaceae in the upper spectrum of zone I1). The zones of type I3 are thought to represent drier conditions. The Chenopodiaceae-Amaranthaceae are important in the desert vegetation of the Sahara (Cour and Duzer, 1976; Schulz, 1987). Pollen from the northern part will be transported by the NE trade-wind and from the rest of the Sahara by the AEJ (Hooghiemstra *et al.*, 1986; 1987). The AEJ transported pollen grains of these plants will reflect fluctuations in the transport capacity of the AEJ and the pollen production in the Sahara. Periods with large extension of Chenopodiaceae-Amaranthaceae are thought to represent drier phases when the overall pollen production is decreased. In the colder and drier stages (with exception of extreme arid ones), pollen of the Chenopodiaceae-Amaranthaceae may be transported in large quantities by the NE trade-wind. In addition, Chenopodiaceae growing on the dry continental shelf during glaciations may have contributed to a high pollen influx of Chenopodiaceae-Amaranthaceae via the NE trade-wind. In these periods the AEJ probably has a lower capacity (Adams, 1987), but still considerable amounts of pollen are brought in from its source area on the continent. The higher transport capacity of the AEJ in warm and humid periods explains the higher influx of the AEJ transported Chenopodiaceae-Amaranthaceae in zones of type I1.

The zones 5b, 7a, 8c, 11b, 13b, and 15a (type G4) are considered to represent intermediate conditions between the zones of type I and the type G zones described below. For the Chenopodiaceae-Amaranthaceae the NE trade influx is rather high and the AEJ influx rather low. Influx values for Poaceae and Cyperaceae decrease to low levels. The influx of other NE trade transported taxa (e.g. Ephedra, Asteraceae, Pinus) remain low. In comparison to zones of type I1 to I3, these zones probably represent rather dry conditions with decreased AEJ and increased NE trade transport capacity. The Sahel-Sahara boundary is estimated to be a little south of its present position.

The zones 7c, 8a, 13d, and 14b (type G3) are characterized by high influx values for all taxa and the transport capacity of the NE trade-wind becomes larger than that of the AEJ. This indicates an effective trade-wind transport and a high pollen production. Only the estimates for water transport are proportionally low.

The zones 3 and 16 (type G2) show increased influx of Ephedra and Artemisia and high influx values for NE trade-wind transported Chenopodiaceae-Amaranthaceae pollen grains, indicating arid conditions. The rather low influx of AEJ transported Poaceae indicate a more southernly position of the Sahel-Sahara boundary. The relative part of the NE trade transported pollen is high in arid periods, indicating a

high NE trade-wind capacity (Hooghiemstra et al., 1987). Additionally, most of these pollen grains come from plants of steppe and desert communities that favor arid conditions. The influx for species like Ephedra and Artemisia will rise due to both increased transport capacity and increased pollen production. However, under extreme arid conditions (type G1) areas with no or very little vegetation will prevail, decreasing the production of even arid adapted species. So, relatively high pollen influx values for Artemisia and Ephedra are mainly found in the zones of type G2.

The zones 2, 5d, 6a, 6c, 10, and 12 (type G1) indicate extreme arid conditions and lack of vegetation, showing low influx values for all species. Only the influx for Ephedra pollen rises in zone 10 and 12. In the zones of G1 the NE trade-wind is probably strong, but the pollen production in and north of the Sahara is low. They indicate very arid conditions and a southernmost position of the Sahel-Saharan boundary (about 14°N: the same latitude as at 18 ka BP, Hooghiemstra, 1988a; 1988b).

In Figure 4, conclusions derived for the climate of each zone type are plotted against time. For the various zones crude estimates are given for fluctuations in NE trade-wind transport, humidity, and the latitude of the Sahel-Saharan boundary.

Apart from the fluctuations described, there are differences on a still larger scale between the earlier and the later part of the Brunhes Chron:

- (1) Zones of type I1, with most humid and warmest conditions occur only before 280 ka BP;
- (2) oxygen isotope Stage 8 and 14 are surprisingly mild for even Stages, showing no severe arid influence like zone Type G1 or G2; stages 10 and 12 are the oldest showing such arid conditions;
- (3) on the average, the proportion of the NE trade transported pollen grains increased during the Brunhes. The curve in Figure 3 (left) shows more frequent and higher maxima for the trade transport at the expense of the AEJ transport.

Several authors report a change in the paleoclimatic record at 0.4 or 0.3 Ma (Schramm, 1985; Pisias and Rea, 1988). Climatic deterioration in the late Quaternary is reported for the north hemisphere and amelioration for the southern hemisphere and the equatorial regions (Jansen et al., 1986; Chuey et al., 1987). The pollen data of ODP Site 658 indicate a trend toward stronger glacial stages and weaker interglacial stages during the Brunhes Chron. The intensity of the warm and humid stages has been greater during the early Brunhes Chron. The Sahel-Saharan boundary in some of these stages may have been north of its position during the climatic optimum in the Holocene at about 9 ka BP, which implies that the area with extremely arid vegetation types must have been very restricted or even non-existent during such times.

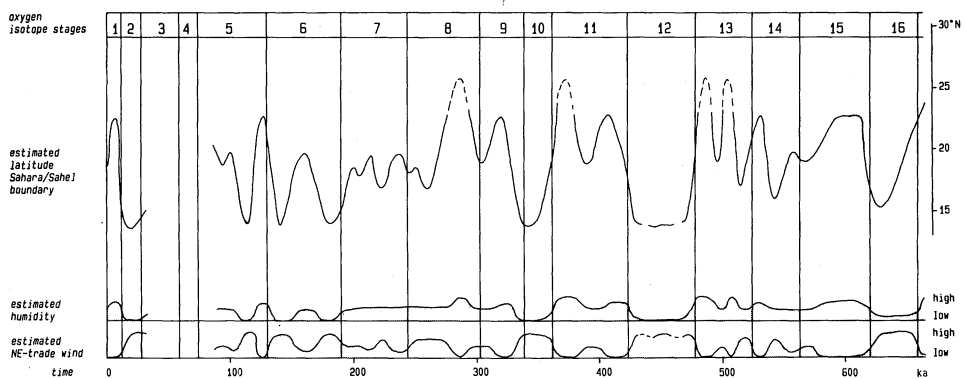


Fig. 4. Estimates for vigor of NE trade-winds, humidity, and latitude of the Sahel-Saharan boundary. Time is plotted on the horizontal axis; in the upper part the oxygen isotope stages are indicated.



## 5. ACKNOWLEDGEMENTS

The author wishes to express her thanks to Prof. Dr. H.-J. Beug and to Dr. H. Hooghiemstra for many helpful discussions and suggestions, to Prof. Dr. Sarnthein and Mr. Tiedemann for providing the time scale and the sedimentation rates in addition to their many useful comments, to Dr. H. Stalling and Mrs. Jaschinski for counting and preparing pollen samples, and to Dr. Agwu for identifying pollen grains. Financial support for the project was given by the Bundesministerium für Forschung und Technologie (Grant KF 2004/1) to the Institute of Palynology and Quaternary Sciences (Göttingen). The author is indebted to the members of the Ocean Drilling Project and the Shipboard party for the supply of the samples.

## 6. REFERENCES

- Adams, L.J., 1987. Ein Wasser- und Energiebilanz-Model von abflußlosen Seen und seine Anwendung in der Paläoklimatologie von Nordwest-Afrika. Berichte des Instituts für Meteorologie und Klimatologie der Universität Hannover, 29: 127pp.
- Agwu, C.O.C. and Beug, H.-J., 1982. Palynological studies of marine sediments off the West African coast. "Meteor"Forsch.-Ergebnisse C, 36: 1-30.
- Caratini, C., Bellet, J. and Tissot, C., 1979. Etude microscopique de la matière organique: palynologie et palynofaciès. Orgon, III: 215-265.
- Chuey, J.M., Rea, D.K. and Pisiás, N.G., 1987. Late Pleistocene paleoclimatology of the central equatorial Pacific: a quantitative record of eolian and carbonate deposition. Quaternary Research, 28(3): 323-339.
- Cour, P. and Duzer, D., 1976. Persistence d'un climat hyperaride au Sahara Central et Méridional au cours de l'Holocène. Revue de Géographie Physique et de Géologie Dynamique 2, 18(2-3): 175-198.
- Diester-Haass, L. and Müller, P.J., 1979. Processes influencing sand fraction composition and organic matter content in surface sediments off W Africa (12-19°). "Meteor"-Forsch. Ergebn., C, 31: 21-47.
- Dupont, L.M., Beug, H.-J., Stalling, H. and Tiedemann, R., submitted. First palynological results from ODP Site 658 at 21°N west off Africa: pollen as climate indicators. In: W.F. Ruddiman, M. Sarnthein, J. Baldauf et al. (eds.). Proceedings of the Ocean Drilling Program. Leg 108, Vol. B. U.S. Govt. Print. Off., Washington.
- Heusser, L.E., 1986/7. Pollen in marine cores: evidence of past climates. Oceanus, 29(4): 64-70.
- Hooghiemstra, H., 1988a. Palynological Records from Northwest Atlantic marine sediments. A general outline of the interpretation of the pollen signal. Phil. Trans. R. Soc. Lond., B 318: 431-449.
- Hooghiemstra, H., 1988b. Changes of major wind belts and vegetation zones in NW Africa 20,000-5,000 yr B.P. as deduced from a marine pollen record near Cape Blanc. Rev. Palaeobot. Palynol., 55(1-3): 101-140.

- Hooghiemstra, H., Agwu, C.O.C. and Beug H.-J., 1986. Pollen and spore distribution in recent marine sediments: a record of NW-African seasonal wind patterns and vegetation belts. "Meteor" Forsch. Ergebn., C, 40: 87-135.
- Hooghiemstra, H., Bechler, A. and Beug, H.-J., 1987. Isopollen maps for 18,000 yr BP of the Atlantic offshore of Northwest Africa: evidence for palaeo-wind circulation. Paleoceanography, 2(6): 561-582.
- Jansen, J.H.F., Kuijpers, A. and Troelstra, S.R., 1986. A Mid-Brunhes climatic event: long-term changes in global atmosphere and ocean circulation. Science, 232: 619-622.
- Kutzbach, J.E. and Street-Perrot, F.A., 1985. Milankovitch forcing of fluctuations in the level of tropical lakes from 18 to 0 kyr BP. Nature, 317: 139-134.
- Maley, J., 1983. Histoire de la végétation et du climat de l'Afrique nord-tropicale au Quaternaire récent. Bothalia 14, (3-4): 377-389.
- Lezine, A.M., 1987. Paléoenvironnements végétaux d'Afrique nord tropicale depuis 12 000 BP. Thèse, Université Aix-Marseille II, Marseille: 180p.
- Melia, M.B., 1984. The distribution and relationship between palynomorphs in aerosols and Deep-sea sediments off the coast on Northwest Africa. Marine Geology, 58: 345-371.
- Pisias, N.G. and Rea, D.K., 1988. Late Pleistocene paleoclimatology of the central equatorial pacific: sea surface response to the southeast trade winds. Paleoceanography, 3(1): 21-37.
- Prell, W.L. and Kutzbach, J.E., 1987. Monsoon variability over the past 150,000 years. J. Geophysical Research, 92(D7): 8411-8425.
- Rognon, P., 1985. The desert. Total information, 10: 4-10.
- Rognon, P., 1987. Les phases d'aridité du Pléistocène supérieur et de l'Holocène au Sahara, arguments sédimentologiques. Palaeoecology of Africa, 18: 111-133.
- Rosignol-Strick, M., 1983. African monsoons, an immediate climate response to orbital insolation. Nature, 304: 46-49.
- Rosignol-Strick, M. and Duzer, D., 1979a. Late Quaternary pollen and dinoflagellate cysts in marine cores off West Africa. "Meteor" Forsch. Ergebn., C, 30: 1-14.
- Rosignol-Strick, M. and Duzer, D., 1979b. West African vegetation and climate since 22,500 BP from deep-sea cores palynology. Pollen et Spores, 21(1-2): 105-134.
- Ruddiman, W.F., Sarnthein, M., Baldauf, J. et al., 1987. Initial Reports of the DSDP/ODP vol. 108 A. U.S. Govt. Print. Off., Washington.
- Sarnthein, M. and Koopmann, B., 1980. Late Quaternary deep-sea record on Northwest African dust supply and wind circulation. Palaeoecology of Africa, 12: 239-253.
- Sarnthein, M., Tetzlaff, G., Koopmann, B., Wolter, K. and Pflaumann, U., 1981. Glacial and interglacial wind regimes over the eastern subtropical Atlantic and North-West Africa. Nature, 293: 193-196.
- Sarnthein, M., Thiede, J., Pflaumann, U., Erlenkeuser, H., Fütterer, D., Koopmann, B., Lange, H. and Seibold, E., 1982. Atmospheric and oceanic circulation patterns off Northwest Africa during the past 25 million years. In: U. von Rad et al. (eds.): Geology of the

- Northwest African Continental Margin. Springer, Heidelberg: 545-604.
- Sarnthein, M. and Tiedemann, R., submitted. Towards a high-resolution stable isotope stratigraphy of the last 3.3 Million years, ODP Sites 658 and 659 off Northwest Africa. In: W.F. Ruddiman, M. Sarnthein, J. Baldauf et al. (eds.). Proceedings of the Ocean Drilling Program. Leg 108, Vol. B. U.S. Govt. Print. Off., Washington.
- Schramm, C.T., 1985. Implications of radiolarian assemblages for the Late Quaternary paleoceanography of the eastern equatorial Pacific. Quaternary Research, 24(2): 204-218.
- Schulz, E., 1987. Die holozäne Vegetation der zentralen Sahara (N-Mali, N-Niger, SW-Lybien). Palaeoecology of Africa 18: 143-162.
- White, F., 1983. The vegetation of Africa. Natural resources research, XX. Unesco: 356p.

**PLIOCENE HISTORY OF SOUTH SAHARAN/SAHELIAN ARIDITY:  
RECORD OF FRESHWATER DIATOMS (GENUS *MELOSIRA*) AND OPAL  
PHYTOLITHS, ODP SITES 662 AND 664**

**EDWARD M. POKRAS**  
Lamont-Doherty Geological Observatory of  
Columbia University  
Palisades, NY 10964  
U.S.A.

**ABSTRACT.** The record of windblown, siliceous microfossils transported from North Africa to the tropical Atlantic provides evidence for times of increased aridity and intensified eolian transport during the Pliocene. Data from ODP Sites 662 and 664, which record climatic changes in the southern Sahara and Sahel, are presented here. These results indicate that cyclical aridification of North Africa began at least 3.8 Ma ago. The data are also consistent with an increase in the severity of arid events approximately 2.3-2.5 Ma ago, although such a change cannot be proved solely on the basis of data presented here.

## **1. INTRODUCTION**

Land-based records of North Africa climate (e.g., pollen profiles, lake deposits) are incomplete and often difficult to date precisely. Much of our understanding of the long-term climatic history of this region has thus relied on studies using records of fluvial and eolian influx to the deep sea. For instance, Sarnthein *et al.* (1982) and Stein (1985) identified several episodes of increased aridity within the last 25 Ma, with the latest phase beginning ~3.2 Ma ago and intensifying ~2.4 Ma ago and again near the Brunhes-Matuyama boundary, ~0.73 Ma ago.

Windblown, freshwater diatoms of the genus *Melosira* (= *Aulacosira*) and opal phytoliths have recently proved to be successful monitors of large-scale fluctuations in the aridity of Saharan and sub-Saharan Africa during the late Pleistocene (Pokras and Mix, 1985, 1987; Stabell, 1986). Pokras and

Mix (1987) demonstrated a strong 23,000-yr periodicity in accumulation rates of *Melosira* valves and interpreted this as indicative of fluctuations in the intensity of the African monsoon. Influx of *Melosira* valves and phytoliths to the deep sea requires substantial fluctuations in aridity/humidity on land, permitting first the abundant production of microfossils and then their deflation (Pokras and Mix, 1985, 1987; Stabell, 1986). This type of climatic fluctuation can result from alternate strengthening and weakening of the African monsoon, either seasonally, over longer periods of time, or both.

This study is an initial analysis of Pliocene eolian input to Sites 662 and 664 of the Ocean Drilling Program, recovered during Leg 108 (Fig. 1). It examines the records of land-derived microfossils at these two equatorial sites. Windblown material found along the equator is apparently derived from the southern Saharan and Sahelian regions, with transport occurring primarily in northern-hemisphere winter (see discussion in Pokras and Mix, 1985). The primary goals of this paper are: (1) to date the inception of eolian influx of siliceous microfossils to the equatorial Atlantic, which should coincide with the onset of cyclic variations in the aridity of north tropical Africa, and (2) to identify major events in the development of North African aridity. Due to the coarse sampling intervals employed here, our data are not suitable for reconstructing the history of shorter-term phenomena, such as orbital-scale cycles. Rather, this paper aims to identify major events in the long-term history of North African aridity cycles.

## 2. METHODS

I examined samples representing the Pliocene sections of Holes 662A and 664D. Hole 664D was examined quantitatively through the interval from 4.25 to 1.75 Ma, at an average sampling interval of 58,000 yr. Due to time constraints, Hole 662A was examined semi-quantitatively. The samples examined from this core ranged from 3.6 to 1.7 Ma old, and the average sampling interval was 58,000 yr.

Sample preparation and analysis followed the methods described by Baldauf and Pokras (in press) for Hole 662A and Pokras and Ruddiman (in press) for Hole 664D. Stratigraphic control was based on biostratigraphic and magnetostratigraphic datums presented in the Site Reports for Sites 662 and 664 (Ruddiman, Sarnthein, Baldauf *et al.*, 1988). Because of the lack of detailed data on sedimentation rate, I cannot convert these per-gram data to absolute accumulation rates. Preliminary stratigraphy suggests that long-term sedimentation rates do not vary substantially (Ruddiman, Sarnthein,

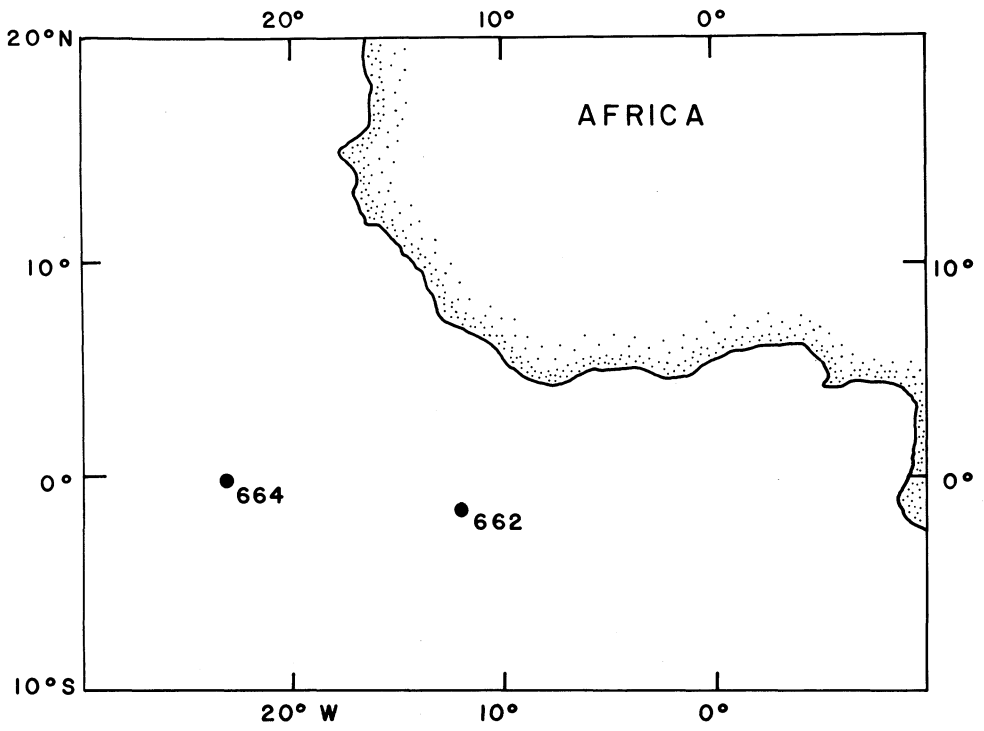


Figure 1: Location of ODP Sites 662, 663 and 664.

Baldauf *et al.*, 1988). Pokras and Mix (1987) showed a close covariance between per-gram abundances and accumulation rates of *Melosira* valves in a piston core near the location of Site 664. Per-gram numbers will thus be used as a first-order substitute for accumulation rate data. To facilitate intercomparison of results from Holes 662A and 664D, all data are presented on the same time scale (4.5-1.5 Ma; Figs. 2 and 3).

The variability in *Melosira* and phytolith time-series from the equatorial Atlantic are dominated by high-frequency (<50,000 yr) cycles (Pokras and Mix, 1985, 1987; Stabell, 1986). Because the sampling intervals used in this study are much too coarse to detect such rapid fluctuations, my records are strongly aliased. The data could also fail to detect short-lived increases in input (Pisias and Mix, in press). The records presented here are thus appropriate only for developing a general overview of changes in North African aridity.

### 3. RESULTS

Both *Melosira* valves and phytoliths first appear in Hole 664D at ~3.8 Ma (Fig. 2). All eleven core-catcher samples older than 3.8 Ma (not shown, maximum age between 8 and 9 Ma) are barren of windblown, siliceous microfossils (Pokras and Ruddiman, in press).

An increase in the amplitudes of both *Melosira* and phytolith maxima occurs at approximately 2.5 Ma, with increased variability in both records after that time. Only 1 of 24 counts older than 2.5 Ma exceeds 10,000 *Melosira* valves per gram, whereas 5 of 16 counts younger than 2.5 Ma exceed that value. In spite of the aliasing problems, the difference in the frequency of high *Melosira* counts before versus after 2.5 Ma (~4% vs 31%) is unlikely to be entirely a sampling artifact. Because the time-series is aliased, the exact timing of the change can only be determined approximately. Specifically, there appears to be a return to low numbers of *Melosira* valves between ~2.5 and 2.3 Ma. This could indicate that the event at 2.5 Ma was transient, and that the event at ~2.3 Ma is a better representation of the actual increase in aridity of the South Saharan and Sahelian areas.

In Hole 662A, *Melosira* valves and phytoliths are present sporadically and in low numbers from 3.6 Ma (the bottom of the hole) to ~2.52 Ma (Fig. 3). A noteworthy change occurs in the *Melosira* curve at that time. Only 1 of 16 samples older than that contain at least few *Melosira* valves, and 6 of the 16 are barren of these fossils. From 2.52 Ma to 1.7 Ma, 10 of the 19 samples contain at least few *Melosira* valves, and only 3 are barren of

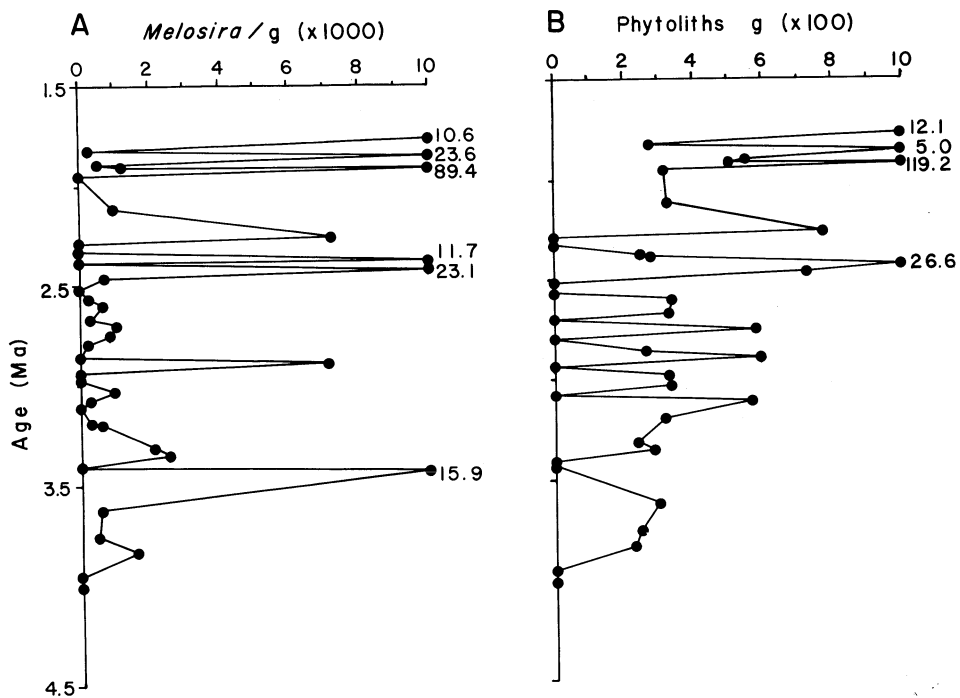


Figure 2: Per-gram abundances of windblown, siliceous microfossils in Hole 664D, 1.75-4.25 Ma. (a) *Melosira* valves. (b) phytoliths.



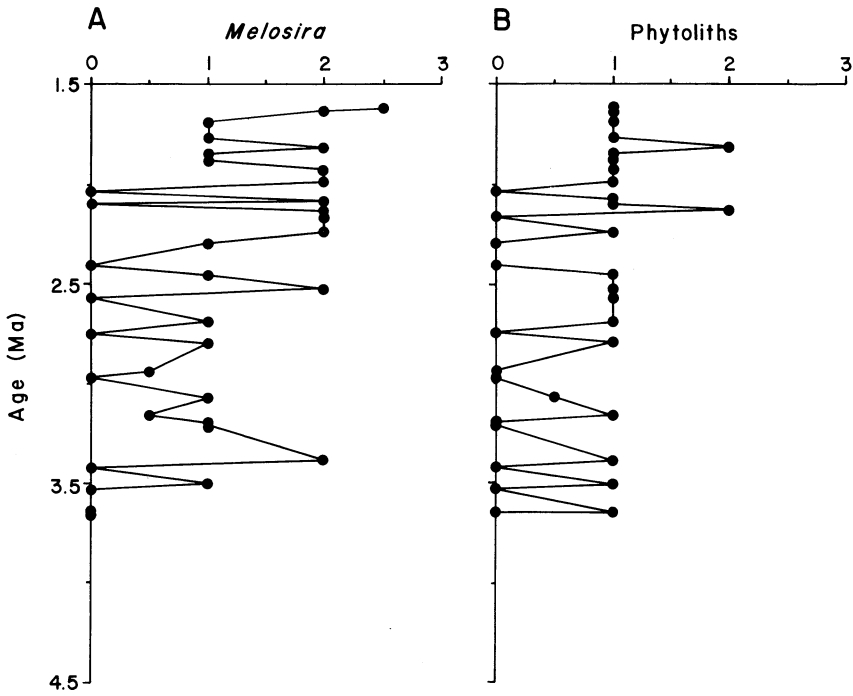


Figure 3: Semi-quantitative estimates of abundances of (a) *Melosira* valves and (b) phytoliths in Hole 662A, from 4.0-1.7 Ma. 0 = barren, 0.5 = very rare, 1 = rare, 2 = few, 3 = common.

*Melosira* valves. Again, it is unlikely that such a marked difference is entirely an aliasing artifact. The aliasing does, however, make it impossible to determine the exact timing of this change, so the assigned date of 2.52 Ma is a very tentative figure. For instance, the maximum at ~2.52 Ma is isolated, so that one could argue that the real change in the nature of the curve occurred closer to 2.3 Ma.

#### 4. DISCUSSION

The presence of both *Melosira* valves and phytoliths 3.8 Ma ago in Hole 664D reveals that eolian supply to the equatorial Atlantic, and hence intermittent aridity in north tropical Africa, began at least 0.6 Ma earlier than suggested by Sarnthein *et al.* (1982) and Stein (1985). This in turn demonstrates at least periodic weakening of monsoonal flow from the equatorial Atlantic into the interior of North Africa since 3.8 Ma. All eleven core-catcher samples in Hole 664D older than 3.8 Ma are barren of marine diatoms as well as *Melosira* valves and phytoliths, so that the absence of land-derived siliceous microfossils could reflect dissolution rather than lack of supply (Pokras and Ruddiman, in press). For that reason, data presented here could underestimate the antiquity of arid episodes in the South Saharan-Sahelian region. In fact, Tiedemann and Sarnthein (1987) have recently presented eolian evidence that aridification had begun at least 4.3 Ma ago farther north in the Sahara.

Continental records indicate that long-term aridification of North Africa was underway during the Pliocene (summarized in Maley, 1980). Evidence includes lower Pliocene eolian deposits in southern Egypt, desert-like faunas and floras in the northern Chad area between 4 and 5 Ma ago, and indications of strong climatic fluctuations in the Chad basin. The fragmentary nature of Pliocene deposits from North Africa and lack of precise chronostratigraphic control make it difficult to establish precise correlations between marine and continental records. Available data are not yet adequate to permit a direct correlation of continental events with the aridification seen at Site 664 near 3.8 Ma. Marine and continental records do, however, concur that aridity was increasing in the early Pliocene. The fact that both *Melosira* and phytolith maxima are generally lower prior to 2.3-2.5 Ma than after that time suggests that the eolian supply was still limited, and suggests that aridity maxima were relatively modest until the late Pliocene. Because the records presented here are aliased, I cannot determine whether the exact timing of the increase in aridity of the South Saharan/Sahelian region was closer to 2.5 or to 2.3 Ma.

Ruddiman and Janecek (in press) report a substantial increase in eolian input of lithogenic sediment to Site 662/663 approximately 2.4 Ma ago. In spite of aliasing, their results are broadly synchronous with the increased influx of *Melosira* valves and phytoliths to Sites 662 and 664 (2.3-2.5 Ma). This coincides with the onset of significant glaciation in the northern hemisphere, as dated by Shackleton, *et al.* (1984) and Ruddiman, *et al.* (1986), and with increasing aridity in tropical Africa (Bonnefille, 1983; Vrba, 1985). There is, however, no corresponding increase in eolian input occurs at Site 659 (18°05'N, 21°02'W; Tiedemann and Sarnthein, 1987). The reason for this discrepancy is not clear.

Changes in the intensity of North African aridity cycles reflect changes in moisture flux from the equatorial Atlantic, due to variations in monsoonal transport (Pokras and Mix, 1985; Prell and Kutzbach, 1987). Increased glaciation at high northern (e.g., Shackleton, *et al.*, 1984) and/or southern (e.g., Ciesielski and Grinstead, 1986 and references therein) latitudes could have had substantial effects on atmospheric and oceanic circulation, and both appear to have occurred at approximately 2.4-2.5 Ma. Another possible forcing function is uplift of large land areas in Tibet and the Himalayas, leading to changes in atmospheric circulation in the tropics (Ruddiman and Janecek, in press).

## 5. CONCLUSIONS

The eolian influx of siliceous microfossils from North Africa to the equatorial Atlantic provides an insight into the broad features of monsoonal circulation in north tropical Africa over the last 4 Ma. The onset of arid climatic events occurred not less than 3.8 Ma ago. Records presented here contain evidence for an increase in the intensity of arid episodes approximately 2.3-2.5 Ma ago, coinciding with an increase in the variability of terrigenous, lithogenic input. These increases appear to result from an increase in the amplitude of monsoonal maxima and minima, leading to a more variable climate in South Saharan and Sahelian Africa. Evidence from other regions suggests that the climatic changes near 2.4 Ma were part of a widespread change in the major features of the earth's climatic system.

## REFERENCES

- Baldauf, J.G., and Pokras, E.M., in press: Diatom biostratigraphic interpretations for the eastern tropical Atlantic Ocean, *Proc. of the Ocean Drilling Program*, 108B.
- Bonnefille, R., 1983: Evidence for a cooler and drier climate in the Ethiopian Highlands towards 2.5 Ma ago, *Nature*, 303: 487-491.
- Ciesielski, P.F., and Grinstead, G.P., 1986: Pliocene variations in the position of the Antarctic Convergence in the southwest Atlantic, *Paleoceanography*, 1: 197-232.
- Maley, J., 1980: Les changements climatiques de la fin due Tertiaire en Afrique: leur conséquence sur l'apparition du Sahara et de sa végétation, In: Williams, M.A.J., and H. Faures, Eds., *The Sahara and the Nile*: Rotterdam (A.A. Balkema), pp. 63-86.
- Pisias, N.G., and Mix, A.C., in press: Aliasing of the geologic record and the search for long period Milankovitch cycles, *Nature (London)*.
- Pokras, E.M., and Mix, A.C., 1985: Eolian evidence for spatial variability of Late Quaternary climates in tropical Africa, *Quat. Res.*, 24: 137-149.
- Pokras, E.M., and Mix, A.C., 1987: Earth's precession cycle and Quaternary climatic change in tropical Africa, *Nature (London)*, 326: 486-487.
- Pokras, E.M., and Ruddiman, W.F., in press: Evolution of North African aridity based on freshwater diatoms and opal phytoliths: ODP Sites 662 and 664, *Proc. of the Ocean Drilling Program*, 108B.
- Prell, W.L., and Kutzbach, J.E., 1987: Monsoon variability over the past 150,000 years, *J. Geophysical Res.*, 92: 8411-8425.
- Ruddiman, W.F., and Janecek, T.R., in press: Plio-Pleistocene biogenic and terrigenous fluxes at equatorial Sites 662/663 and 664, *Proc. of the Ocean Drilling Program*, Vol. 108B.
- Ruddiman, W.F., McIntyre, A., and Raymo, M., 1986: Paleoenvironmental results from North Atlantic Sites 607 and 609, In: Ruddiman, W.F., Kidd, R.B., Thomas, E., et al., Eds., *Init. Repts. DSDP*: Washington (U.S. Govt. Printing Office), 94: 855-878.

- Ruddiman, W.F., Sarnthein, M., Baldauf, J.G., *et al.*, in press: *Proceedings of the Ocean Drilling Program*, 108A.
- Sarnthein, M., Thiede, J., Pflaumann, U., Erlenkeuser, H., Futterer, D., Koopmann, B., Lange, H., and Seibold, E., 1982: Atmospheric and oceanic circulation patterns off northwest Africa during the past 25 million years, *In: von Rad, U., K. Hinz, M. Sarnthein, and E. Seibold, Eds., Geology of the Northwest African Continental Margin: Berlin (Springer-Verlag)*, pp. 545-604.
- Shackleton, N.J., Backman, J., Baldauf, J.G., Desprairies, A., Homrighausen, R., Huddlestun, P., Keene, J.B., Kaltenback, A.J., Krumisek, K.A.O., Morton, A.C., Murray, J.W., and Westberg-Smith, J., 1984: Oxygen isotope calibration of the onset of ice rafting in DSDP Site 552A: history of glaciation in the North Atlantic region, *Nature (London)*, 307: 620-623.
- Stabell, B., 1986: Variations of diatom flux in the eastern equatorial Atlantic during the last 400,000 years ("Meteor" cores 13519 and 13521), *Mar. Geol.*, 72: 305-323.
- Stein, R., 1985: Late Neogene changes of paleoclimate and paleoproductivity off northwest Africa (D.S.D.P. Site 397), *Palaeogeog., Palaeoclimatol., Palaeoecol.*, 49: 47-59.
- Tiedemann, R., and Sarnthein, M., 1989: Late Neogene paleoclimates of the western Sahara: eolian dust record of the last 8 MY (ODP Sites 658 and 659), this volume.
- Vrba, E., 1985: African Bovidae: evolutionary events since the Miocene, *S. Afr. J. Sci.*, 81: 263-266.

# CENOZOIC CLIMATIC VARIATION RECORDED BY QUARTZ AND CLAY MINERALS IN NORTH PACIFIC SEDIMENTS

CYNTHIA T. SCHRAMM  
Graduate School of Oceanography  
University of Rhode Island  
Narragansett, RI 02882-1197  
U.S.A.

**ABSTRACT.** Clay mineral and quartz contents of sediments from two western North Pacific DSDP sites record a history of paleoclimatic and paleoceanographic conditions of the last 65 million years. DSDP Site 436 has recorded an eolian signal of terrigenous material that was transported from Asia. The relatively small range of variation in quartz content indicates that the source of sediment was consistent during the Cenozoic. At DSDP Site 578, the temporal variation of quartz and clay mineral contents in sediments prior to 15MYBP are grossly similar to those recorded in Site 436. However, anomalously low quartz content and accumulation in the bulk sediment since the middle Miocene suggests that the eolian signal at Site 578 was complicated by bottom-current sediment transport.

The evolution of the earth during the last 60MY altered climatic factors that govern the erosion and atmospheric transport of terrigenous material out over the North Pacific. A change in the style of weathering is apparent in the mineralogy of the deep-sea sediments. Low concentrations of kaolinite, indicative of chemical weathering in western North Pacific sediments younger than roughly 20MYBP from DSDP Site 436, reflect increased aridity since that time. Clays associated with cool mechanical weathering gradually increased in relative abundance from climates and the early Miocene, approximately 20MYBP, through the Pliocene at Site 436. However, clay composition at Site 578 does not record an increase in the relative abundance of clays indicative of cool climates and mechanical weathering until the late Miocene. A major change in the quantity of eolian material accumulating in the western North Pacific is not synchronous with the change in weathering deduced from the mineralogy. A large increase in accumulation rates of quartz and clay minerals in the

middle Miocene (approximately 14MYBP) reflects a permanent change in the climatic factors that determine the efficiency of atmospheric transport. Climate models to date do not explain the nature of the climatic response inferred from changes in eolian transport to known tectonic and oceanographic events.

## 1. INTRODUCTION

Deep-sea sediment cores from the North Pacific record a history of eolian sedimentation from which paleoclimatic conditions can be inferred. Such inferences about changes in climatic conditions throughout time provide atmospheric scientists and modelers with information that helps explain long-term processes of atmospheric circulation and the interactions of the atmosphere-biosphere-hydrosphere-cryosphere systems.

The North Pacific is an excellent location for studying long-term climate variation for several reasons. First, very slow sedimentation rates enable recovery of cores containing long temporal records of sedimentation. DSDP Sites 436 (39°55.96'N, 145°33.47'E) and 578 (33°55.56'N, 151°37.74'E; Fig. 1) penetrate sediment that represents most of the Cenozoic. Secondly, the sediments in the central North Pacific are predominantly eolian, transported from continental source regions by the winds (Rex and Goldberg, 1958; Griffin, *et al.*, 1968; Windom, 1969, 1975). Most fluvial input of terrigenous material is trapped by marginal seas and deep trenches that outline the North Pacific, limiting contamination of the eolian signal to distal hemipelagic muds that move offshore in suspension. Previous studies of eolian sedimentation at North Pacific sites DSDP Hole 576A and LL44-GPC3 provide a foundation for unraveling Cenozoic climatic history (Leinen and Heath, 1981; Janecek and Rea, 1983; Janecek, 1985; Leinen, 1985; Lenotre, *et al.*, 1985; Rea, *et al.*, 1985). Long-term trends in eolian sediment composition and grain size at these two sites are quite similar (Rea, *et al.*, 1985), suggesting uniformity of eolian sedimentation over vast distances in the central North Pacific (Leinen, 1985). The sedimentary record at these sites has been affected not only by climatic variation, but also by the northward migration of the underlying Pacific plate. The migration with time of these sites from beneath the tropics to midlatitude climate zones and concomitant increased proximity to the Asian dust source complicate paleoclimatic interpretations from the sedimentary record. Both sites record a general Neogene increase in eolian sediment mass accumulation, but the increases are not synchronous. The eolian sediment records are also characterized by an extremely large increase in mass accumulation rate at approximately 2.5-3MYBP (Leinen and Heath, 1981; Janecek and Rea, 1983;

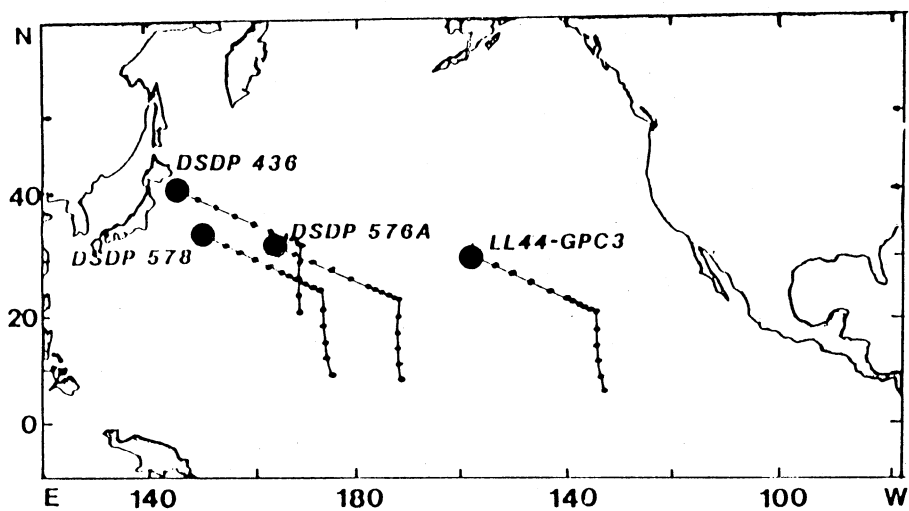


Figure 1: Site Locations and paleopositions of North Pacific sites (from models of van Andel, *et al.*, 1975 and Arthur, *et al.*, 1980 modified from Lancelot and Larson, 1975). Marked intervals represent 5MY.



Leinen, 1985; Janecek, 1985; Rea, *et al.*, 1985). DSDP Site 578 is located in the western North Pacific, approximately 13° west and 1° north of DSDP Site 576A. Because of the uniformity of central North Pacific eolian sedimentation, it was anticipated that the down-core record of sedimentation at this site would be similar to those at DSDP Site 576 and LL44-GPC3. As at site 576A and LL44-GPC3, this site should record changes in sedimentation influenced by both plate migration and climatic change (paleopositions based on a model of van Andel, *et al.*, 1975; Fig. 1). Site 436 is located further northwest of Site 578 (about 800 km) on the edge of the central North Pacific region of pelagic clays and closer to the terrigenous source areas of Asia, and at about 6° higher latitude. Because the paleoposition reconstructions (Arthur, *et al.*, 1980, modified from Lancelot and Larson, 1975) indicate that the site would always have been in the zone in which Asian sources presently dominate eolian sedimentation (Duce, *et al.*, 1980; Merrill, 1987), the primary factor influencing sedimentation at Site 436 was expected to be climate. Because of these differences in settings, quantitative mineralogy at DSDP Sites 436 and 578 should allow a comparison of the sedimentary record at sites that were influenced to different degrees by climatic and tectonic (plate migration) factors. Quartz in deep-sea sediments is solely of terrigenous origin — not formed authigenically. The similarity between the distribution of quartz in North Pacific surface sediments (Leinen, *et al.*, 1986), the wind patterns over the North Pacific (Gray, *et al.*, 1979; Fig. 2), and the many studies which indicate that the quartz is derived from Asia (e.g., Rex and Goldberg, 1958) support the use of quartz as an eolian indicator for this region. Downcore variation in quartz content and accumulation indicate changes in position of the zonal winds, mineralogy of the eolian source region, and the amount and type of material available for transport. Quantitative clay mineralogy augments paleoclimatic interpretations by providing more detailed information pertaining to weathering conditions and source regions. The similarity of the mineralogy of the less-than-two micron fraction of mineral aerosol and surface sediment samples in the North Pacific has been established by Ferguson, *et al.*, (1970) and Blank, *et al.*, (1985).

## 2. STRATIGRAPHY

Sediment samples for this study represent approximately one-million year intervals from two DSDP cores, Site 436 and Site 578. There is not a continuous record of a single type of stratigraphic indicator at either site. The intervals for which various stratigraphic indicators were used are detailed in Table 1. Both sites have relatively unfossiliferous Paleogene sections with very slow sedimentation rates. Very poorly preserved

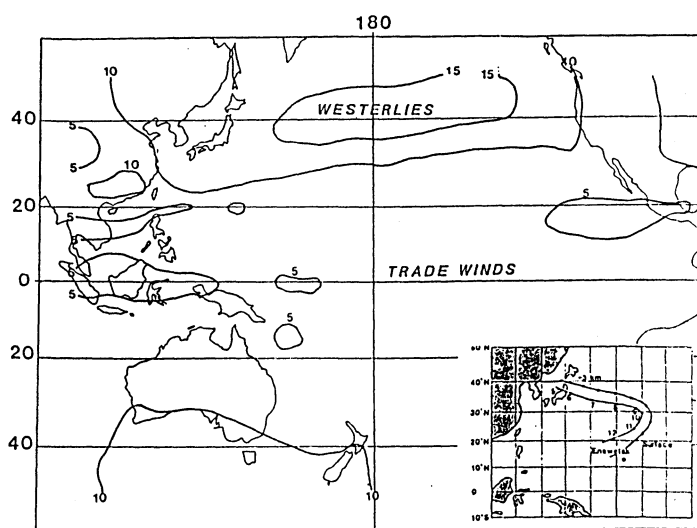
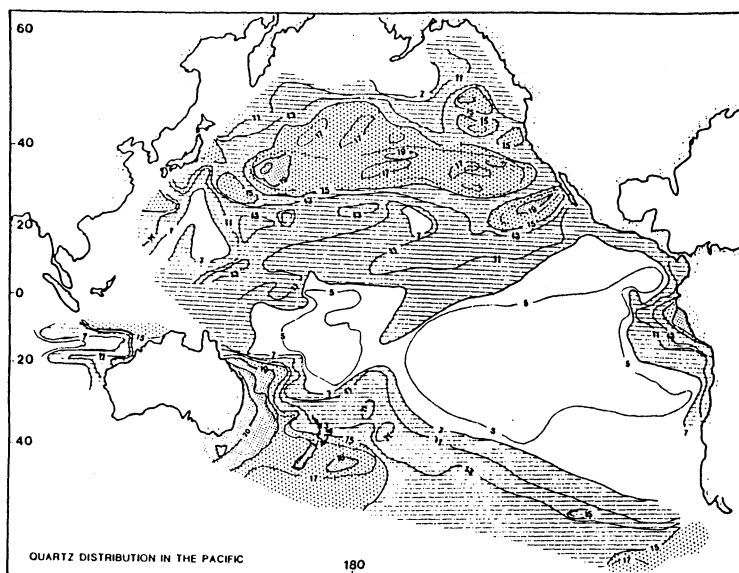


Figure 2: (A) Distribution of quartz content in surface sediments of the North Pacific (Leinen, *et al.*, 1986) closely resembles (B) the 700mb wind patterns in the Spring (Gray, *et al.*, 1979), when most dust transport occurs.

**Table 1. Stratigraphic Model for DSDP Sites 436 and 578**

<b>Interval</b>	<b>Depth (M)</b>	<b>Approximate Age (MY)</b>	<b>Stratigraphic Indicator</b>	<b>Reference</b>
<b><u>DSDP Site 436</u></b>				
Mid Miocene - Present	0-350 0-360	0-13 0-14	Diatoms Radiolaria	Harper, 1980 Sakai, 1980
Paleogene - Mid Miocene	360-378.5	14-63	Ichthyoliths	Doyle & Reidel, 1980
<b><u>DSDP Site 578</u></b>				
Mid Miocene - Present	27.8-144.9	0-15	Paleomagnetic reversal	Heath, <i>et al.</i> , 1985
Paleogene - Mid Miocene	144-168	15-63	Ichthyolith	Doyle & Riedel, 1985

radiolaria present in the lowest core of Site 436 suggest an age of late Albian or Cenomanian (Sakai, 1980). Ichthyolith stratigraphy was used to determine approximate ages of the Paleogene pelagic clays. At Site 436 the Paleocene is probably missing, as Cretaceous ichthyoliths are overlain by those characteristic of the Eocene (Doyle and Riedel, 1980). The onset of biogenic sedimentation at this site during the middle Miocene at about 14MYBP results in greatly improved stratigraphic resolution for younger sediments; sediments older than mid-Miocene are pelagic clays containing only ichthyoliths. The diatom biostratigraphy (Harper, 1980) was correlated with paleomagnetic stratigraphy and radiometric dates to form the stratigraphy of sediments from the last 15MY (Koizumi, *et al.*, 1980). The paucity of fossils in the Paleogene sediments from Site 578 makes hiatuses difficult to identify. It appears that either part of the Oligocene is missing, or the sedimentation rates were extremely low during this interval (Doyle and Riedel, 1985). Magnetic reversal data correlated with the time scale of Berggren, *et al.*, (1985) provide magnetostratigraphy for sediments 15MY old and younger (Heath, *et al.*, 1985). The appearance of siliceous microfossils in late Miocene sediment, 5-6MYBP, provides further biostratigraphic resolution (Morley, 1985).

### 3. METHODS

Both quartz and clay mineral contents were determined by x-ray diffractometry. Two different procedures were used to determine the quartz content of the bulk sample and the clay mineralogy of the less-than-two micron size fraction. For quartz analysis, samples were treated initially with buffered acetic acid to remove calcium carbonate and then ground on automatic grinders for two hours to a uniform grain size. A quantity of alumina equal to 1/2 the sample weight was added to the ground powder as an internal standard. Samples were heated at 1000°C for 24 hours, which removes clay mineral interference from the quartz peak (method modified from Till and Spears, 1969). Duplicate samples were scanned over the alumina and quartz peaks (25.4° 2 $\theta$ , and 26.55° 2 $\theta$ , respectively) on an x-ray diffractometer using CuK-alpha radiation at 35 ma and 45 KV. Peak areas from the diffractogram were converted to weight percents by comparing the ratio of the quartz peak area/alumina standard peak area to standard curves developed for Pacific sediments (Leinen, 1985). To determine clay mineral abundances, samples were treated with acetic acid to remove calcium carbonate. Amorphous iron and manganese oxide and hydroxyoxide phases were removed using sodium dithionite buffered with sodium citrate (as described in Jackson, *et al.*, 1973). Biogenic opal was removed by treatment with sodium carbonate (described in Rea and Janecek, 1981). The less-than-

two micron size fraction was isolated by Stokes settling and saturated with magnesium. A quantity of talc equal to 1/9 of the sample weight was added as an internal standard. Samples were mounted as oriented aggregates on silver filters that have no peaks over the  $2\theta$  diffraction interval in which most clay peaks occur. Each sample was scanned with CuK-alpha radiation at 35KV and 31 ma between 3-30 degrees  $2\theta$ . Peak areas of illite, chlorite, kaolinite, smectite, plagioclase, and quartz were measured and normalized to the talc standard (smectite data of Site 578 in prep.). Weight percents were calculated using the multiplying factors of Heath and Pisias (1979) determined for surface sediments of the North Pacific. Mass accumulation rates ( $\text{g}/\text{cm}^2/\text{my}$ ) measure the change in the quantity of sediment over time. The mass accumulation rate of the bulk sediment was calculated by the formula:

$$\text{mass accumulation rate} = \text{linear sedimentation rate (m/MY)} \times \text{dry bulk density (g/cm}^3\text{)}$$

The dry bulk density (dbd) was calculated from porosity (por) and wet bulk density (wbd) measurements using the relationship:

$$\text{dbd} = \text{wbd} - ((\text{por}/100) \times 1.01)$$

where, 1.01 is the average density of pore waters. The mass accumulation of the less-than-two micron size fraction used for clay analyses is the weight percentage of the less-than-two micron size fraction of the total sample times the bulk mass accumulation rate. Mass accumulation rates for each component are determined by multiplying the weight percent of that component times the mass accumulation rate of the portion of sediment used (either bulk or less-than-two micron). Mineral composition and mass accumulation data are presented in Tables 2 through 5.

#### 4. RESULTS

The temporal variations of quartz content in the bulk sediment from Sites 436 and 578 are distinctly different than those observed in the records from LL44-GPC3 and DSDP Hole 576A (Leinen, 1985; Leinen and Heath, 1981; Fig. 3). The bulk quartz content records at LL44-GPC3 and Hole 576A are both characterized by a trend to increased quartz content in the early-to-middle Miocene. The bulk quartz content of sediments from Site 436 contain no such trend, varying downcore within a narrow range, 6-13%. An anomalously low value at 11 MYBP is due to dilution by volcanic ash. Since the middle Miocene, the concentration of quartz in the

Table 2. DSDP Site 436 Sediment Composition

Depth	Age	Smectite	Chlorite	Kaolinite	Illite	Plagioclase	<2 $\mu$ m Quartz	Bulk Quartz
(m)	my	(wt. %)	(wt. %)	(wt. %)	(wt. %)	(wt. %)	(wt. %)	(wt. %)
210.00	4	3.20	7.45	4.57	13.99	5.08	15.67	12.14
245.50	5	3.57	3.23	7.75	14.39	4.97	18.62	10.59
265.00	6	5.74	6.29	5.38	15.95	6.08	17.65	7.93
278.00	7	4.87	4.23	2.26	13.14	5.66	11.84	7.58
289.50	8	4.59	12.22	1.56	17.50	7.00	17.38	9.03
305.00	9	5.16	2.52	2.49	8.95	1.45	19.27	12.00
310.00	10	3.37	11.91	1.22	20.54	14.33	24.52	11.75
319.80	11	6.60	5.98	3.60	12.27	3.56	8.83	9.89
340.00	12	2.54	2.85	3.64	8.53	4.90	12.78	7.28
350.00	13	3.77	3.47	1.80	14.57	4.96	21.49	8.26
360.00	14	2.92	12.19	0.36	16.71	3.22	21.96	1.09
360.57	15	6.58	4.73	0.60	9.73	1.18	14.43	6.24
361.14	16	1.77	3.57	4.78	5.37	5.71	15.96	7.73
361.71	17	2.12	0.96	2.14	7.51	0.62	13.41	7.26
362.28	18	9.19	7.26	0.38	23.89	1.42	23.22	6.53
362.85	19	3.78	5.06	0.43	14.15	1.94	23.07	9.21
363.42	20	2.94	2.07	3.09	19.20	2.00	20.17	7.08
363.99	21	1.04	2.22	0.20	10.20	3.83	39.55	11.89
364.56	22	1.41	1.24	6.09	14.40	0.56	47.10	8.47
365.13	23	*	*	*	*	*	*	9.04
365.70	24	2.52	1.60	5.85	20.22	0.95	48.39	11.51
366.28	25	5.07	1.34	9.61	24.48	2.60	31.48	7.58
366.86	26	1.84	*	*	*	*	*	7.97
367.44	27	*	0.58	8.39	15.36	1.92	39.50	6.94
369.18	30	*	3.06	10.76	20.12	0.00	40.76	7.70
369.76	31	0.90	2.19	8.35	10.54	0.62	29.92	8.32
370.34	32	4.47	1.68	6.03	12.19	1.34	26.42	8.52
370.92	33	3.77	1.57	9.65	16.49	*	23.16	7.60
371.50	34	2.96	3.25	7.01	18.20	0.16	27.23	7.74
372.08	35	1.84	2.49	7.77	18.83	0.09	30.42	8.16
372.66	36	5.02	1.91	5.40	16.76	*	37.87	9.30
372.79	37	3.19	2.19	3.65	21.11	0.54	21.06	6.02
372.92	38	1.06	0.76	14.49	20.01	1.55	44.20	10.49
373.05	39	1.24	1.30	7.52	22.44	0.24	30.75	8.90
373.18	40	1.60	3.25	9.74	18.96	3.86	30.96	9.56
373.31	41	2.37	1.89	4.69	27.02	5.37	39.92	7.16
373.44	42	0.82	3.63	8.10	13.29	2.66	39.22	5.62
373.57	43	2.99	1.24	3.86	12.84	0.11	13.96	7.74
373.70	44	1.93	1.72	6.59	13.81	1.20	31.19	8.13
373.83	45	0.51	2.28	7.47	12.52	3.14	31.12	7.37
374.09	47	1.72	7.88	5.53	13.39	2.41	18.14	7.05
374.22	48	0.57	0.62	7.00	11.17	0.05	27.67	6.92
374.35	49	1.81	4.31	8.91	12.62	0.85	71.49	7.26
374.61	51	4.44	2.07	9.87	14.68	1.48	23.32	4.75
374.74	52	1.98	3.21	5.57	22.31	2.58	34.83	6.36
374.87	53	2.09	2.52	8.85	15.07	2.76	29.69	6.97
375.00	54	1.52	2.45	6.28	22.74	0.82	49.48	8.29
375.26	56	2.02	3.18	2.28	22.20	0.42	33.01	4.94
375.39	57	1.35	2.35	8.07	20.03	2.07	24.96	5.55
375.52	58	*	*	*	*	*	*	7.03

\* Data not available for this interval.

Table 3. DSDP Site 635 Mass Accumulation Rates

M	Age MY	Sed Rate M/MY	Dry Bulk Density G/CM3	wt.%	Bulk MAR		Smectite		Chlorite		Kaolinite		Illite		Plagioclase		Quartz		Bulk	
					MAR	G/CM2/MY	G/CM2/MY	G/CM2/MY	G/CM2/MY	G/CM2/MY	G/CM2/MY	G/CM2/MY	G/CM2/MY	G/CM2/MY	G/CM2/MY	G/CM2/MY	G/CM2/MY	G/CM2/MY	G/CM2/MY	G/CM2/MY
210.00	4	35.50	0.87	22.00	3088.50	679.47	21.74	50.62	31.05	95.06	34.52	106.47	374.94							
263.50	5	19.50	0.89	23.00	1735.50	393.17	14.25	12.89	30.94	57.44	19.84	74.32	183.79							
265.00	6	13.00	0.86	18.11	1118.00	202.41	11.62	12.73	10.69	32.79	12.31	35.73	88.46							
278.00	7	11.50	0.92	15.00	1068.00	156.70	7.73	6.71	3.59	20.65	5.98	14.79	80.20							
289.50	8	13.50	0.91	27.51	1410.50	387.97	17.81	47.41	6.05	67.89	27.16	67.43	171.37							
305.00	9	5.00	0.99	33.18	495.00	164.24	8.47	4.14	4.09	14.70	2.36	31.65	59.40							
310.00	10	9.00	1.05	30.41	1029.00	312.93	10.55	37.27	3.82	64.28	44.84	76.73	120.91							
319.00	11	20.20	0.92	16.52	1858.00	306.96	20.26	18.96	11.05	37.66	10.93	27.10	163.80							
340.00	12	10.00	0.95	18.69	869.00	177.54	4.51	5.06	6.46	15.14	8.70	22.69	69.16							
350.00	13	10.00	1.10	22.82	1100.00	251.00	9.46	8.71	4.52	36.57	12.45	53.94	90.86							
360.00	14	0.57	1.14	21.77	64.98	14.14	0.41	1.72	0.05	2.36	0.46	3.11	0.71							
360.57	15	0.57	1.14	31.64	64.98	20.56	1.35	0.97	0.12	2.00	0.24	2.97	4.05							
361.14	16	0.57	1.14	26.98	64.98	17.53	0.31	0.63	0.84	0.94	1.00	2.80	5.02							
361.71	17	0.57	1.14	23.34	80.37	18.75	0.40	0.18	0.40	1.41	0.12	2.52	5.83							
362.28	18	0.57	1.14	30.80	64.98	20.02	1.84	1.45	0.08	4.78	0.28	4.65	5.98							
362.85	19	0.57	1.14	29.28	64.98	19.03	0.72	0.96	0.08	2.69	0.37	4.39	5.98							
363.42	20	0.57	1.14	25.80	64.98	16.77	0.49	0.35	0.52	3.22	0.34	3.38	4.60							
363.99	21	0.57	1.28	30.96	72.96	22.59	0.23	0.50	0.05	2.30	0.87	8.93	8.67							
364.56	22	0.57	1.28	28.43	72.96	20.74	0.29	0.26	1.26	2.99	0.12	9.77	6.18							
365.13	23	0.57	1.28	30.65	72.96	22.36	0.54	0.54	0.35	1.26	0.21	10.46	8.55							
365.70	24	0.58	1.28	24.07	74.24	17.87	0.91	0.24	1.72	4.38	0.46	5.63	5.92							
366.28	25	0.58	1.28	28.53	74.24	23.75	0.39	0.39	0.14	1.99	3.65	9.38	5.15							
367.44	27	0.58	1.31	33.72	75.98	25.62	0.24	0.24	0.78	2.76	5.16	10.44	5.85							
369.18	30	0.58	1.31	35.68	75.98	27.11	0.24	0.59	2.26	2.86	0.17	8.11	6.32							
369.76	31	0.58	1.31	35.91	75.98	27.29	1.22	0.46	1.65	3.33	0.37	7.21	6.47							
370.34	32	0.58	1.31	35.06	75.98	26.64	1.00	0.42	2.57	4.39	0.00	6.17	5.77							
370.92	33	0.58	1.31	34.45	75.98	26.17	0.77	0.85	1.83	4.76	0.04	7.13	5.88							
371.50	34	0.58	1.34	36.41	77.72	28.30	0.52	0.70	2.20	5.33	0.03	8.61	6.34							
372.66	36	0.13	1.34	33.85	17.42	5.90	0.30	0.11	0.32	0.99	0.00	2.23	1.62							
372.79	37	0.13	1.34	34.54	17.42	6.02	0.30	0.13	0.22	1.27	0.03	1.27	1.05							
372.92	38	0.13	1.34	32.90	17.42	6.40	0.17	0.05	0.96	1.32	0.10	2.92	1.83							
373.05	39	0.13	1.34	35.29	17.42	6.15	0.08	0.08	0.46	1.36	0.01	1.89	1.55							
373.18	40	0.13	1.34	28.02	17.42	4.88	0.12	0.09	0.54	1.06	0.22	1.73	1.67							
373.31	41	0.13	1.34	28.02	17.42	4.88	0.05	0.23	0.23	1.32	0.36	1.95	1.25							
373.44	42	0.13	1.34	36.23	17.42	6.51	0.05	0.23	0.51	0.84	0.17	2.48	0.98							
373.57	43	0.13	1.34	36.15	17.42	6.43	0.19	0.08	0.25	0.83	0.01	0.90	1.35							
373.70	44	0.13	1.34	33.96	17.42	6.30	0.12	0.11	0.13	0.45	0.18	1.81	1.26							
373.83	45	0.13	1.34	33.96	17.42	5.81	0.05	0.13	0.45	0.75	0.18	1.61	1.26							
374.09	47	0.13	1.34	30.04	17.42	5.37	0.09	0.42	0.30	0.42	0.30	0.72	1.23							
374.22	48	0.13	1.34	36.43	17.42	6.91	0.04	0.04	0.48	0.77	0.00	1.91	1.21							
374.35	49	0.13	1.34	36.43	17.42	6.70	0.12	0.29	0.60	0.86	0.06	4.79	1.28							
374.61	51	0.13	1.34	36.56	17.42	6.72	0.30	0.14	0.66	0.99	0.10	1.57	0.83							
374.74	52	0.13	1.34	36.77	17.42	6.75	0.13	0.22	0.38	1.51	0.17	2.35	1.11							
374.87	53	0.13	1.34	33.22	17.42	5.79	0.12	0.15	0.51	0.87	0.16	1.72	1.21							
375.00	54	0.13	1.33	40.27	6.96	6.96	0.11	0.17	0.44	1.58	0.06	3.45	1.43							
375.26	56	0.13	1.33	38.61	17.29	6.68	0.13	0.21	0.15	1.48	0.03	2.20	0.85							
375.39	57	0.13	1.33	36.83	17.29	6.37	0.09	0.15	0.51	1.28	0.13	1.59	0.96							
375.52	58	0.13	1.33	39.02	17.29	6.75	0.09	0.15	0.51	1.28	0.13	1.59	0.96							

\* Data not available for this interval

Table 4. DSDP Site 578 Sediment Composition

Depth	Age	Chlorite	Kaolinite	Illite	Plagio- clase	<2 Micron Quartz	Bulk Quartz
M	MY	wt. %	wt. %	wt. %	wt. %	wt. %	wt. %
36.36	1.06	4.40	10.01	18.89	6.36	27.49	0.00
60.56	1.92	2.78	7.36	24.50	5.29	21.10	0.63
82.36	3.00	4.66	3.06	20.35	10.68	27.37	0.30
95.46	4.04	5.96	5.09	13.52	6.53	23.91	0.47
102.04	4.63	3.24	5.86	21.95	3.79	18.35	3.73
105.34	4.94	5.49	9.29	16.68	5.74	27.13	4.81
107.81	5.17	3.15	9.81	17.21	5.95	28.27	6.36
111.66	5.52	3.87	9.16	24.49	6.08	46.27	6.88
114.86	5.82	2.38	8.17	21.36	1.86	22.52	3.61
118.06	6.24	3.85	9.49	23.67	7.19	31.45	1.32
120.91	6.79	3.44	8.37	17.73	3.73	14.35	0.63
123.51	7.34	1.57	2.45	14.26	3.89	20.05	0.34
131.46	10.56	1.75	3.09	21.86	1.38	23.08	0.72
133.96	11.45	2.23	3.30	13.25	3.22	13.64	0.54
136.56	12.31	1.99	6.58	14.58	1.79	16.99	2.68
139.31	13.16	1.39	7.90	19.22	0.62	26.29	1.96
142.01	14.30	1.40	8.88	17.58	0.53	17.02	3.92
144.41	15.00	1.16	4.81	17.61	0.74	10.93	0.28
147.34	16.70	2.09	9.73	17.69	2.16	14.22	0.42
149.38	17.87	2.45	8.76	11.64	0.92	24.24	0.87
151.98	21.60	1.95	12.49	12.40	5.05	26.53	0.78
154.28	26.37	1.41	6.10	24.53	1.33	17.55	1.66
156.86	35.00	1.29	8.81	24.09	0.00	37.09	0.58
157.46	36.63	0.48	14.03	13.98	2.63	37.15	0.68
158.06	38.28	2.16	7.22	20.18	0.53	36.50	0.00
158.76	40.29	0.77	13.47	19.08	0.07	33.47	0.00
159.36	42.13	0.00	14.15	23.40	12.17	57.42	2.55
159.86	43.77	2.74	12.35	42.62	0.40	73.66	5.41
160.46	46.05	0.62	17.67	15.03	0.47	47.76	0.67
161.16	49.19	3.82	19.68	29.24	0.45	49.52	0.00
161.76	51.40	0.56	17.10	24.24	0.93	55.61	0.00
162.36	53.19	1.97	9.75	26.77	0.14	24.70	3.91
166.34	60.14	1.56	7.34	20.33	0.00	19.64	0.00
166.93	61.33	2.41	6.75	13.31	0.86	39.54	4.46
167.33	62.09	5.74	3.42	35.73	0.42	32.15	0.00
168.03	63.30	*	*	*	*	*	0.00
168.48	64.03	0.52	10.15	3.32	0.00	41.95	5.18
168.75	64.47	*	*	*	*	*	0.70
169.33	65.36	2.97	16.20	25.64	1.90	58.51	0.00
169.23	66.21	0.26	5.32	12.36	0.28	16.84	0.61
176.26	66.70	6.65	3.13	9.94	1.71	73.32	0.25

\* Data not available for this interval



Table 5. DSDP Site 578 Mass Accumulation Rates

Depth	Age		Sed Rate M/MY	Dry Bulk Density G/CM3	wt. % G/CM2/MY	Bulk MAR	<2Micron MAR	Chlorite G/CM2/MY	Kaolinite G/CM2/MY	Illite G/CM2/MY	Plagio- cline G/CM2/MY	<2Micron Quartz G/CM2/MY	Bulk Quartz G/CM2/MY
	M	MY											
36.36	1.06	28.14	0.54	15.00	1519.56	227.93	10.03	22.82	43.06	14.50	62.66	0.00	
60.56	1.92	20.19	0.46	13.00	928.74	120.74	3.36	8.89	29.59	6.39	25.48	5.85	
82.36	3.00	12.60	0.56	12.00	705.60	84.67	3.95	2.59	17.23	9.04	23.17	2.12	
95.46	4.04	11.15	0.52	17.00	579.80	98.57	5.88	5.02	13.33	6.44	23.58	2.73	
102.04	4.63	10.65	0.53	13.00	564.45	73.38	2.36	4.27	15.98	2.76	13.36	20.89	
105.34	4.94	10.74	0.54	20.00	579.96	115.99	6.37	10.78	19.36	6.66	31.47	27.90	
107.81	5.17	11.00	0.54	25.00	594.00	148.50	4.65	14.47	25.38	8.78	41.70	37.52	
111.66	5.52	10.67	0.49	19.00	522.83	89.34	3.82	9.05	24.20	6.01	45.71	35.78	
114.86	5.82	7.62	0.51	23.00	388.62	89.38	2.13	7.33	19.16	1.67	20.20	14.08	
118.06	6.24	5.18	0.61	15.00	315.98	47.40	1.85	4.56	11.36	3.45	15.10	4.22	
120.91	6.79	4.73	0.51	9.00	241.23	21.71	0.74	1.81	3.83	0.81	3.10	1.51	
123.51	7.34	4.56	0.61	32.00	278.16	89.01	1.41	2.20	12.78	3.49	17.96	0.95	
131.46	10.56	2.47	0.69	28.00	170.43	47.72	0.83	1.47	10.41	0.66	10.99	1.22	
133.96	11.45	3.02	0.75	23.00	226.50	52.10	1.18	1.75	7.01	1.70	7.22	1.24	
136.56	12.31	3.24	0.75	31.00	243.00	75.33	1.48	4.90	10.85	1.33	12.64	6.43	
139.31	13.16	2.37	0.83	33.00	196.71	64.91	0.92	5.21	12.69	0.41	17.35	3.92	
142.01	14.30	3.43	0.70	37.00	240.10	88.84	1.24	7.89	15.61	0.47	15.11	9.41	
154.28	26.37	0.30	0.67	40.00	20.10	8.04	0.11	1.44	1.43	0.58	3.06	0.28	
156.86	35.00	0.37	0.67	33.00	24.79	8.18	0.11	0.73	1.99	0.00	3.06	0.15	
157.46	36.63	0.36	0.97	34.00	34.92	11.87	0.06	1.67	1.66	0.31	4.42	0.24	
158.06	38.28	0.35	0.97	40.00	33.95	13.58	0.29	0.98	2.74	0.07	4.96	0.00	
158.76	40.29	0.33	0.97	32.00	32.01	10.24	0.08	1.38	1.95	0.01	3.43	0.00	
159.36	42.13	0.30	0.97	33.00	29.10	9.60	0.00	1.35	2.24	1.16	5.50	0.74	
159.86	43.77	0.26	0.97	30.00	25.22	7.57	0.21	0.93	3.20	0.03	5.52	1.35	
160.46	46.05	0.22	0.97	32.00	21.34	6.83	0.04	1.19	1.01	0.03	3.21	0.14	
161.16	49.19	0.27	0.97	34.00	26.19	8.90	0.34	1.74	2.58	0.04	4.38	0.00	
161.76	51.40	0.34	0.95	31.00	32.30	10.01	0.06	1.70	2.40	0.09	5.52	0.00	
162.36	53.19	0.57	0.90	34.00	51.30	17.44	0.34	1.69	4.64	0.02	4.28	1.99	
166.34	60.14	0.50	0.90	23.00	45.00	10.35	0.16	0.76	2.10	0.00	2.03	0.00	
166.93	61.33	0.53	0.90	23.00	47.70	10.97	0.26	0.73	1.44	0.09	4.27	2.10	
167.33	62.09	0.58	0.90	23.00	52.20	12.01	0.69	0.41	4.27	0.05	3.85	0.00	
168.03	63.30	0.62	0.90	21.00	55.80	11.72	*	*	0.40	0.00	5.08	2.85	
168.48	64.03	0.61	0.90	22.00	54.90	12.08	*	*	0.40	0.00	5.08	2.85	
168.75	64.47	0.65	0.94	21.00	61.10	12.83	*	*	0.40	0.00	5.08	2.85	
169.33	65.36	0.71	0.94	22.00	66.74	14.68	0.44	0.76	3.78	0.28	8.62	0.00	
169.23	66.21	12.92	0.94	24.00	291.48	291.48	0.74	15.51	36.04	0.82	49.11	7.41	
176.26	66.70	2.64	0.89	22.00	234.96	51.69	3.44	1.62	5.14	0.88	37.91	0.59	

\* Data not available for this interval.

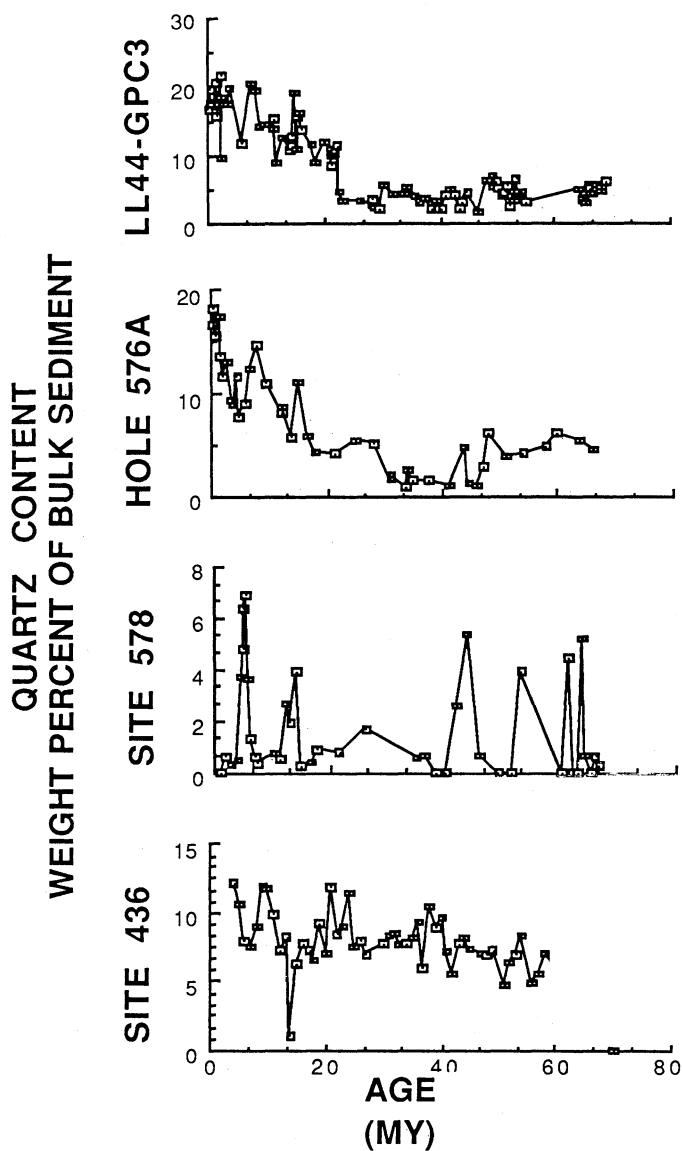


Figure 3: Temporal variation, in quartz content (wt.%), at DSDP Sites 436, 578, 576A and piston core LL44-GPC3.

bulk sediments from Site 578 have been much lower than concentrations in any of the other three North Pacific sites. An increase in quartz content to slightly higher values in Site 578 at 15MYBP occurs at approximately the same time as a larger increase in quartz content at DSDP Hole 576A. The increase at Site 578 (unlike at Hole 576A) is of short duration, as bulk quartz content declined to below 2% by approximately 11MYBP. Only during 4.5-6MYBP did quartz content increase at this site, at which time it reached peak values of almost 8%.

Some similarities in sedimentation between the North Pacific sites are apparent in the records of quartz accumulation in the bulk sediment (Fig. 4). At all four North Pacific sites, quartz accumulation was very low during the Paleogene followed by much higher rates in the Neogene. However, these increases in accumulation are not synchronous. At both Sites 436 and 578, the rate of quartz accumulating increased significantly in the middle Miocene, approximately 14 MYBP. But, from the late Miocene through the Pliocene, bulk quartz accumulation remained high at Site 436, while it decreased sharply at Site 578. Bulk quartz accumulation at Site 578 peaked at 5-6MYBP and then decreased to much lower rates. Bulk quartz accumulation rates increased somewhat earlier in the Miocene at DSDP Hole 576A and LL44-GPC3, at approximately 18MYBP and 23MYBP, respectively. The pattern of the quartz flux at these central North Pacific sites is similar to the flux pattern of the total eolian component (Rea, *et al.*, 1985). At all the North Pacific sites except Site 578, quartz accumulation remained many times higher during the Pliocene. Samples of Site 436 for this study represent sediment older than 4MYBP because of the high Quaternary sedimentation rate. Given the high Pleistocene sedimentation rate and the relatively constant bulk quartz content throughout the Cenozoic, it is estimated that the Quaternary record of bulk quartz accumulation at Site 436 would show a large increase as at LL44-GPC3 and Hole 576A.

Temporal variation in the mineralogy of the material deposited in Sites 436 and 578 indicates a change in sediment composition in the less-than-two micron size fraction from the Paleogene to the Neogene (Figs. 5, 6). The concentrations of kaolinite and quartz (in the less-than-two micron size fraction) drop from Paleogene highs to lower Neogene values in sediments from both western North Pacific sites. At Site 436, where the change is relatively abrupt, it occurs at approximately 20 MYBP and coincides with the onset of a gradual increase in chlorite, plagioclase and smectite contents. The change in sediment composition is more gradual in the record from Site 578. The data may be aliased by the slow Oligocene sedimentation and broader temporal sampling intervals. Nonetheless, kaolinite and less-than-two micron quartz contents were clearly higher

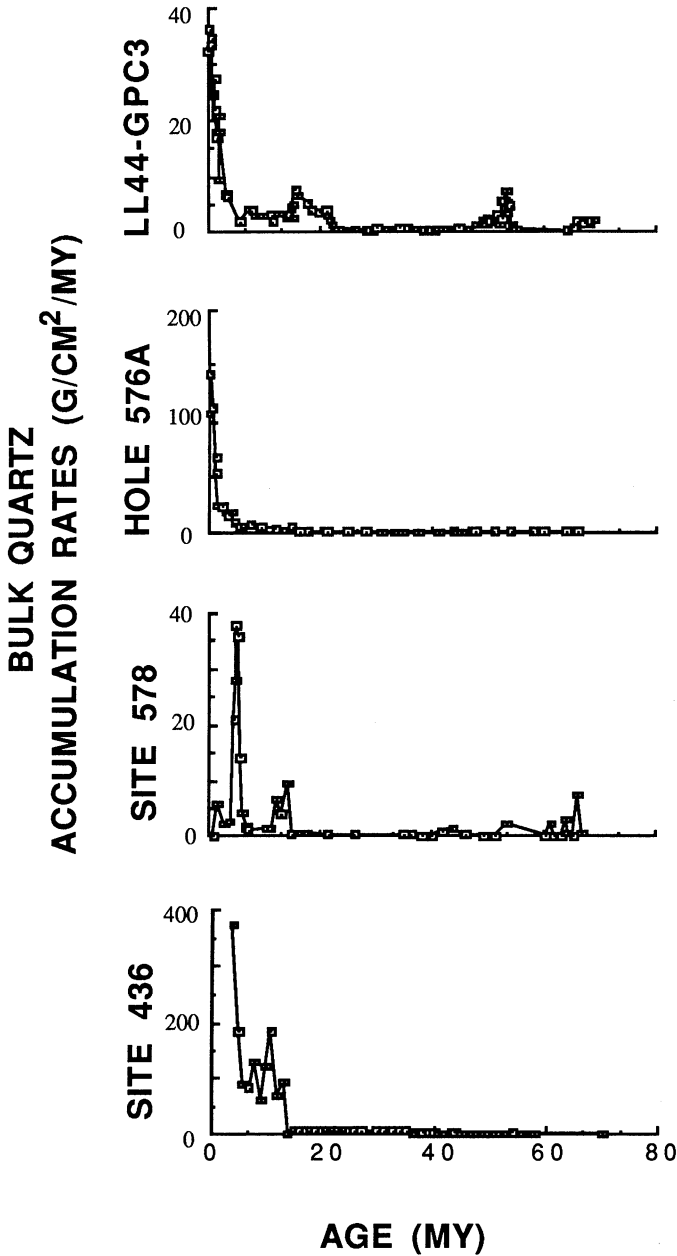


Figure 4: Quartz accumulation rates (g/cm<sup>2</sup>/my) bulk sediment from North Pacific sites.

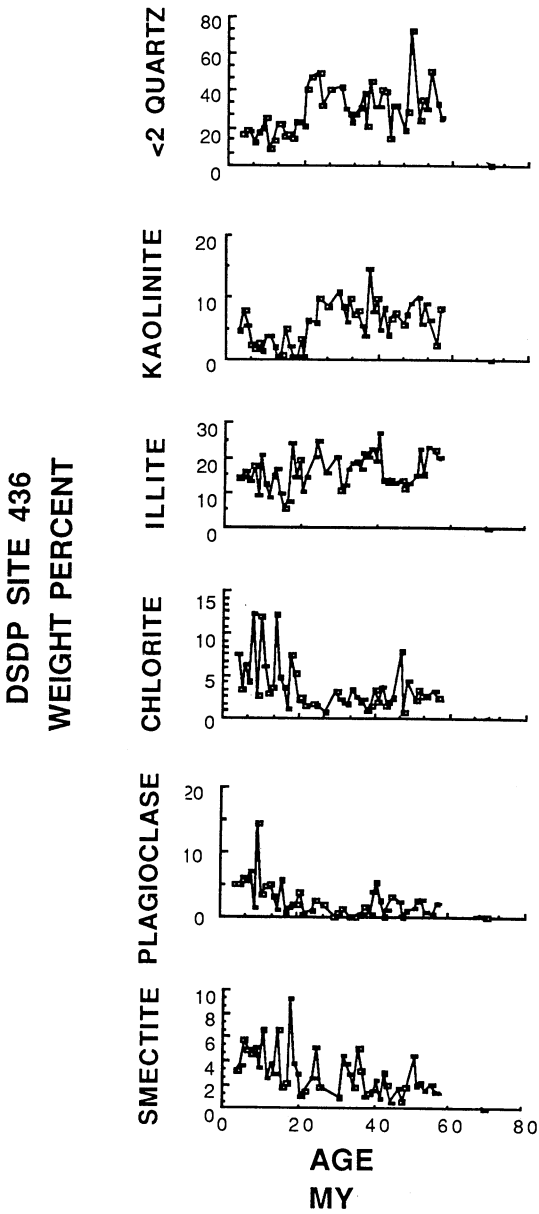


Figure 5: Mineral composition in the less-than-two micron size fraction of sediment from Site 436.

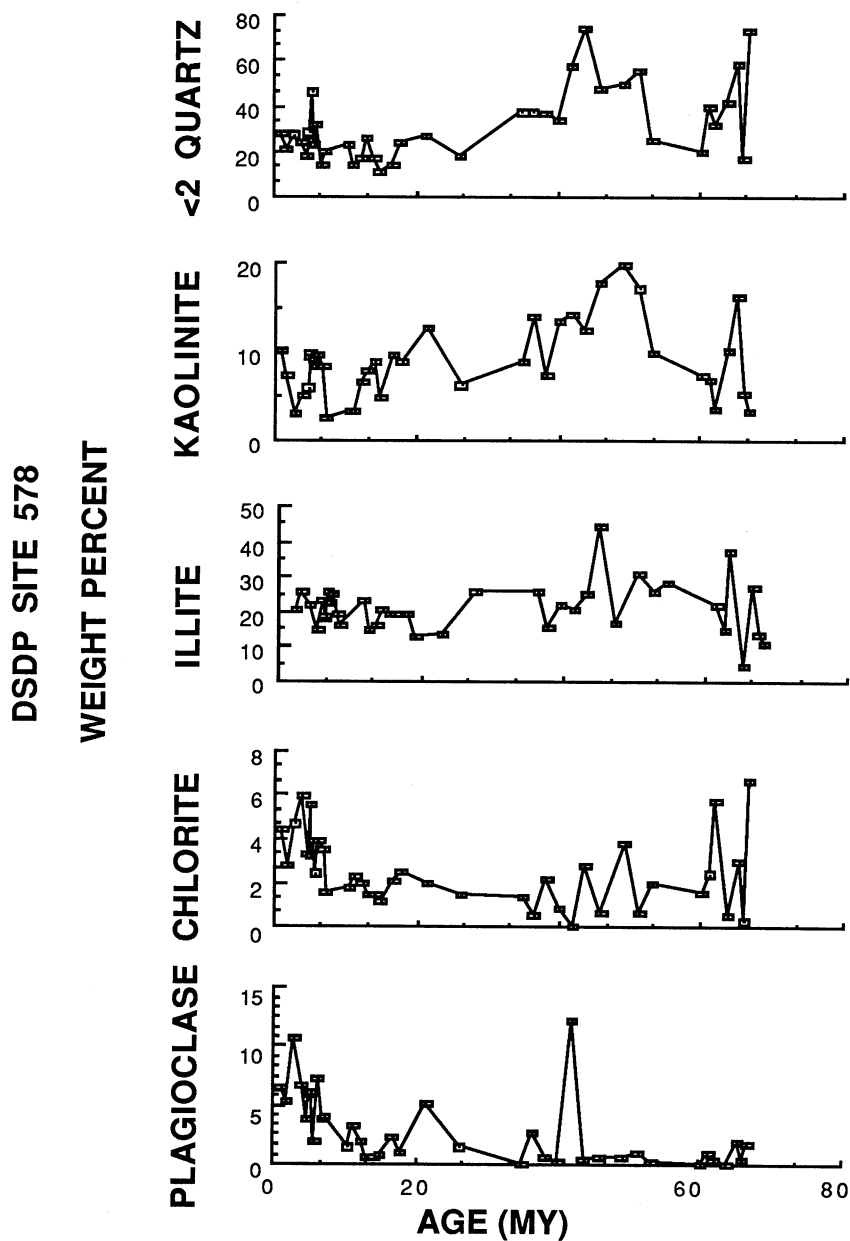


Figure 6: Mineral composition in the less-than-two micron size fraction of sediment from Site 578.

during most of the Paleogene than they were in the Neogene at this site. The concentration of kaolinite in the sediment at both sites is low — between approximately 7-11MYBP at Site 436 and between 3-5MYBP at Site 578. Chlorite and plagioclase concentrations did not increase at Site 578 until the late Miocene.

The mineralogy of Site 578 sediments presented here (calculated using an internal standard) differs from Site 578 mineralogy in Lenotre, *et al.*, (1985). It is difficult to compare clay mineralogy results determined by different analytical procedures. The data of Lenotre, *et al.*, (1985) do not record a change in kaolinite relative abundance from high Paleogene to lower Neogene values. However, they did find a late Miocene/early Pliocene increase in chlorite content occurs at approximately 121m. Although the relative abundances of clay minerals in sediment from Site 436 were determined using sample preparation different from that used in this study, the data of Mann and Muller (1980) exhibit trends similar to the data presented here. Specifically, the chlorite content and chlorite/kaolinite ratio determined by Mann and Muller (1980) were higher in the Neogene, high sedimentation rate portion of the sediment. Kaolinite content was highest in the lowermost sections (below 363m). Mann and Muller's sample spacing was not close enough to identify that the change in sediment composition occurred prior to the change in sedimentation rate.

Mineral group mass accumulation rates were extremely low at both sites for most of the Paleogene (Figs. 7, 8). The accumulation rates of kaolinite, illite, smectite, and less-than-two micron quartz increased slightly at 35 MY at Site 436. A similar change is not apparent in the record of Site 578, perhaps due to the decreased resolution from slow sedimentation rates. An abrupt increase in accumulation of the clay minerals occurred in the middle Miocene at both sites. At Site 436, fluxes of all the mineral groups increased by an order of magnitude at approximately 13-14MYBP. This increase is the result of an increase in total sedimentation rate. The rapidity of the increase is, in part, a function of stratigraphy as it coincides with a switch from broad-range ichthyolith stratigraphy to higher resolution radiolarian and diatom stratigraphy (Table 1). The sedimentation and accumulation rates remained at higher levels for the rest of the Cenozoic. A significant increase in accumulation of kaolinite, illite and less-than-2 micron quartz at Site 578 began at approximately 15 MYBP. Chlorite and plagioclase accumulation also increased at this time at Site 578, but relatively smaller quantities of these two mineral groups have accumulated throughout time. At both sites 436 and 578 a larger increase in the accumulation of all minerals occurred at approximately 5-6MYBP. At Site

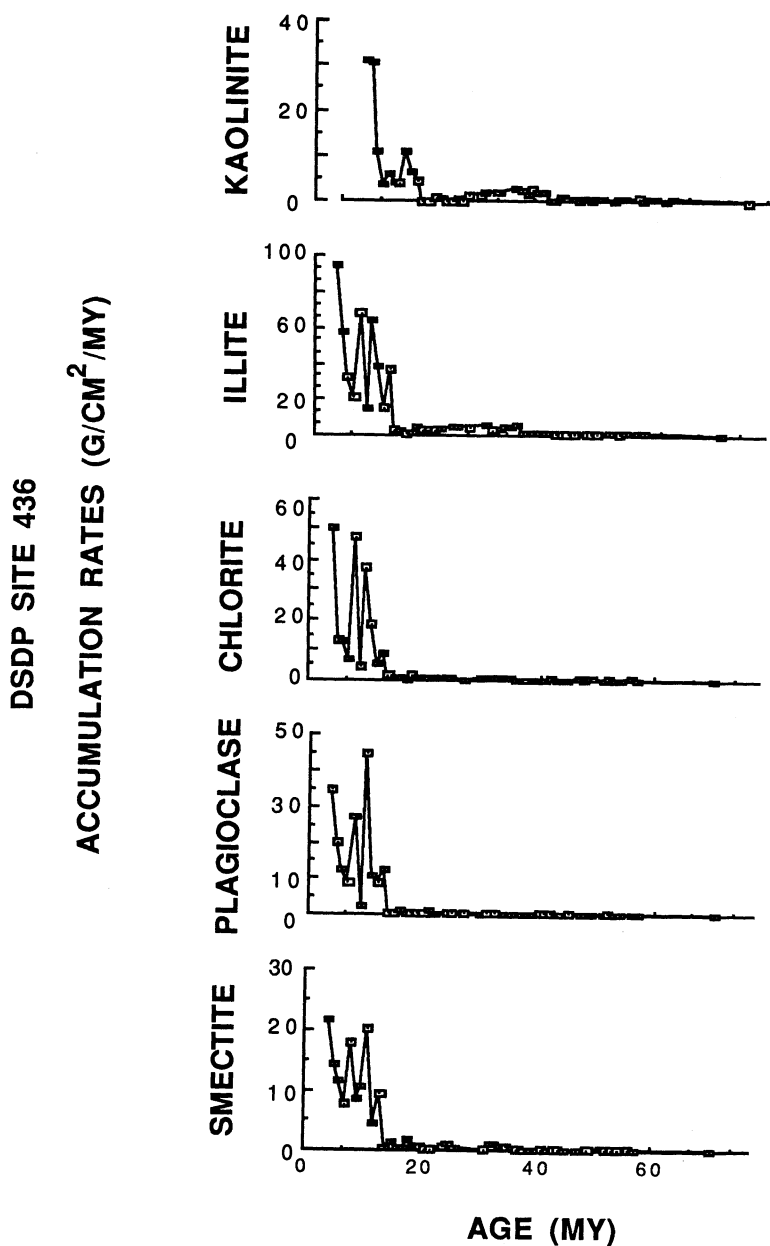


Figure 7: Accumulation rates (g/cm<sup>2</sup>/my) of less-than-two micron size fraction minerals from Site 436.



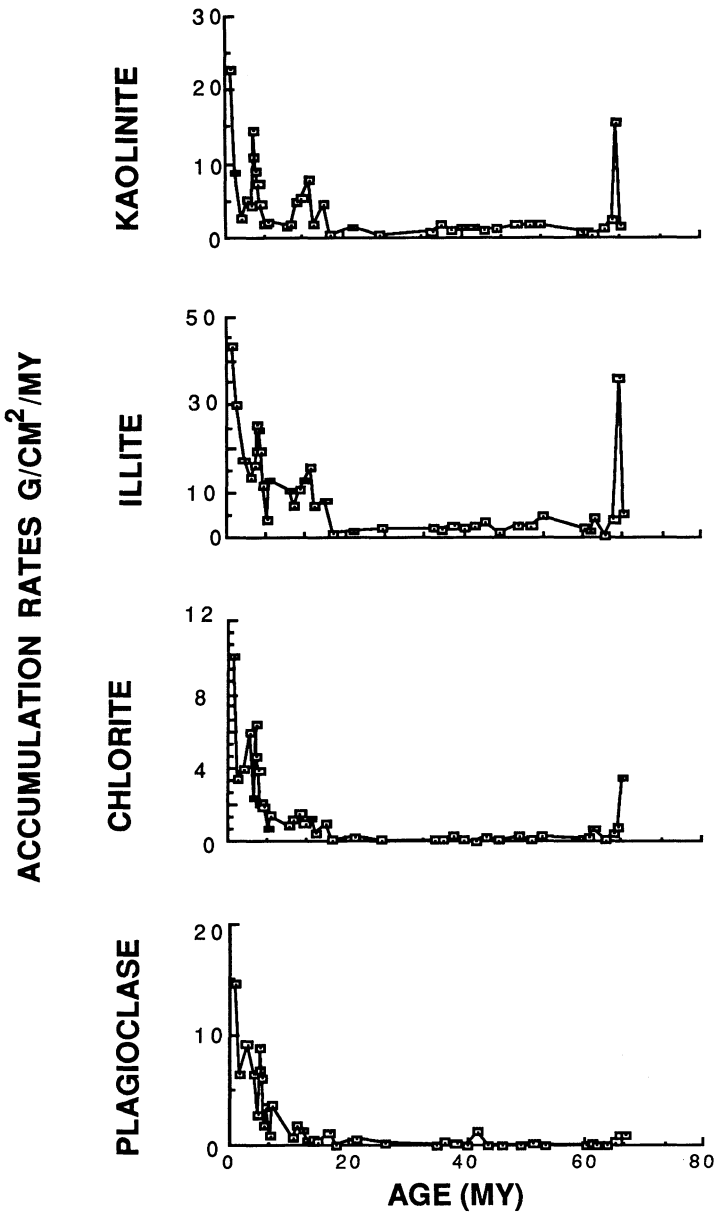


Figure 8: Accumulation rates (g/cm<sup>2</sup>/my) of less-than-two micron size fraction minerals from Site 578.

578 this increase is associated with an increase in the concentration of plagioclase and chlorite. Pliocene mineral accumulation rates were at their highest levels for the Cenozoic at Site 436. Clay mineral accumulation rates are also highest during the Pliocene and Pleistocene at Site 578, but have a large range of variability.

## 5. DISCUSSION

### 5.1 *North Pacific Sedimentation*

The research of Leinen (1985) and Rea, *et al.*, (1985) revealed a striking similarity in the temporal variation in sediment composition and size at Sites LL44-GPC3 and DSDP Hole 576A, which are several thousand kilometers apart in the central North Pacific. The clear difference in the composition and accumulation of sediments between the western North Pacific sites and the central North Pacific sites indicate that the uniformity of eolian sedimentation does not extend across the entire North Pacific. DSDP site 436 is northwest of the central North Pacific sites and closer to the Asian source of terrigenous material. The proximity to source region would result in greater quantities of eolian material accumulating at this site throughout time, as most of mineral aerosol falls out close to its source. Indeed, the accumulation of quartz in the bulk sediment at this site is several times higher than the accumulation rates at the sites more distant from Asia in proportion to the change in the total eolian flux from proximal to distal sites (Janecek, 1985; Fig. 4). The hypothesis of a constant general Asian source for terrigenous material accumulating in Site 436 that was inferred from the paleoposition model (Arthur, *et al.*, 1980, modified from Lancelot and Larson, 1975) and analyses of modern atmospheric transport trajectories (Duce, 1980; Merrill, 1987) is supported by the relative consistency of the bulk quartz content at this site throughout the Cenozoic. Whereas, the central North Pacific sites show an increase in bulk quartz content presumed to be coincident with site migration beneath the westerly wind belt (Leinen and Heath, 1981; Leinen, 1985), bulk quartz content in Site 436 varies within a narrow range.

Although Site 578 is closer to the Asian source of terrigenous material than are Hole 576A and LL44-GPC3, the bulk sediment quartz percent has been much lower than at Hole 576A and LL44-GPC3 since the early Miocene. This low quartz content is inconsistent with eolian transport from Asia and indicates that there may be a disruption of the eolian signal at Site 578 during this time. The Neogene accumulation of quartz at this site is also anomalously low. Total quartz mass accumulation rates in sediment from

sites both northwest (Site 436) and east (Hole 576A) of Site 578 have been greater than Site 578 total quartz mass accumulation rates since the middle Miocene (Fig. 4). As the quantity of total quartz accumulating in the bulk sediment at this site is relatively low, the sediment composition anomaly cannot be due to dilution by other sediment components, but must represent either removal of quartz-rich sediments from the area or a quartz-poor sediment source. Site 578 lies within a region of the Northwest Pacific that has experienced rapid sedimentation during the past 5MY (Damuth, *et al.*, 1983; Jacobi, *et al.*, 1985). The zone of anomalously rapid sedimentation extends from south of Site 578 northward to the Kuril Trench and is believed to be the result of bottom-current activity in this region (Jacobi, *et al.*, 1985). Although sedimentation rates are anomalously high only for the last 5MY, the atypical quartz record suggests that non-eolian processes may have determined sedimentary patterns in this region for the last 15MY. Jacobi, *et al.*, (1985) inferred eastward bottom-water flow patterns in the vicinity of Site 578 from the relative thickness of sediment cover on sides of bathymetric highs and from the east-west strike of the zone of rapid sedimentation.

When the bulk quartz content and accumulation at Site 578 are anomalously low, from the middle Miocene on, there is no change in the composition of clay mineral groups that would indicate a change in source region. Input of material from either the north or the west cannot be resolved. Unlike the concentration of quartz in the bulk sediment, the quartz content in the less-than-two micron size fraction has not been anomalously low since the mid-Miocene, but decreased earlier (approximately 20MYBP) along with kaolinite content. The record of mass accumulation of the less-than-two micron quartz is similar to the other clay components in this site and quite different from the low bulk quartz accumulation record (Fig. 9). The striking difference in the content and accumulation rate records of the two size fractions of quartz are not observed in the Site 436 record. The complication of the eolian signal at Site 578 appears to primarily affect the larger-than-two micron size fraction of sediments. The mean grain size of material in Pliocene-Pleistocene sediments from Site 578 is much larger than the corresponding mean grain sizes in Site 576 and LL44-GPC3 (Janecek, 1985; Janecek and Rea, 1983). Janecek (1985) interpreted this as a reflection of the influence of gravitational settling through the air of larger grains nearer to their source, before the small grains come into equilibrium with the winds. However, the anomalously low quartz content in the bulk sediment suggests that

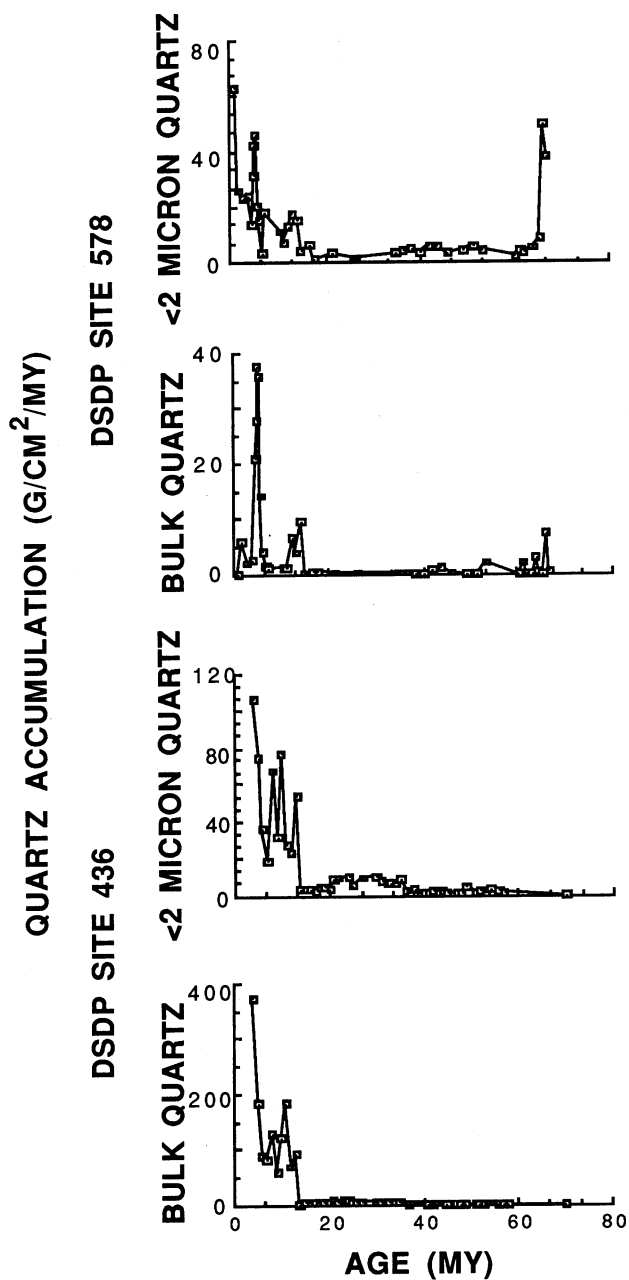


Figure 9: Comparison of quartz accumulation in the bulk and less-than-two micron portions of sediment from Sites 436 and 578.

bottom-water input of coarser-grained, quartz-poor material may have masked the record of eolian sedimentation since the middle Miocene, altering paleoclimatic information contained in the sediment.

## 5.2 *Paleoclimatic Implications*

The variations in mineralogy of sediments from Site 436 reflect changes in the climatic conditions that govern erosion and eolian transport of terrigenous material. Understanding the present-day controls on eolian transport over the North Pacific allows for more detailed paleoclimatic interpretations. In recent years, the mineral aerosol transported over the North Pacific has been monitored at several sampling stations (Uematsu, *et al.*, 1983; Uematsu, *et al.*, 1985). The dominant transport mechanism for Asian dust appears to be severe dust storms that originate in arid regions of China (Uematsu, *et al.*, 1983). Of the approximately 20-million tons of mineral aerosol transported over the central North Pacific per year (Uematsu, *et al.*, 1985), a significant portion (greater than one million tons) may be entrained in a single dust storm (Iwasaka, 1983). The dust storms occur as the passage of successive cold fronts destabilize the air column, allowing for upward injection of terrigenous material to high tropospheric elevations (Avila, 1983). It is this upper level tropospheric injection that allows long-distance transport of the displaced particles. Low-level winds tend to be localized, while most distant transport occurs between 3.5-7 Km (Avila, 1983; Shaw, 1980). The conditions that maximize erosion (Gillette, 1981) and the occurrence of dust storms (Uematsu, *et al.*, 1983) are seasonally dependent. The most frequent of dust storms and the largest quantity of mineral aerosol transported over the North Pacific occurs in the Spring (Uematsu, *et al.*, 1983). Variations in sedimentation rates and composition in the long North Pacific sediment cores provide a basis for examining the record of eolian transport and deposition for changes in these processes through time. Given the dramatic evolution of the earth that took place during the Cenozoic, it is unlikely that the atmospheric conditions which control large-scale dust transport were always similar. During the Cenozoic, tectonic activity altered the pathways for both oceanic and atmospheric circulation. For example, the northward migration of Australia during the Eocene allowed the development of the circum- Antarctic current that increased the thermal isolation of Antarctica, enhancing the development of extensive continental glaciers there (Kennett, 1977). Both the oceanographic changes and the glaciers had a profound effect on climate, altering heat and moisture transport and albedo. Direct tectonic perturbation of the atmosphere occurred as the early Miocene uplift of the Tibetan plateau created a large region elevated so high it interfered with wind paths and heat and moisture transport.

Superimposed on the gradual long-term climatic and tectonic evolution are episodes of more rapid change. The early-to-middle Miocene is a particularly active time in the evolution of the earth. A Himalayan uplift model (based on crustal shortening and paleomagnetism) indicates that significant uplift did not occur until the Miocene (Zeitler, *et al.*, 1985). Copeland, *et al.* (1987), using  $^{40}\text{Ar}/^{39}\text{Ar}$  isotopic analyses and fission track mineral ages of samples from several plutons in southern Tibet, identified spatial and temporal variability in the rates of uplift with the most rapid uplift of this area occurring between 20-17MYBP. Their data suggest that a pulse of uplift as rapid as 4.4mm/yr (the range of error is 17.1mm/yr to 2.6mm/yr) occurred between 17.8-17.0MYBP. This would raise a portion of southern Tibet several kilometers in less than a million years, rapidly altering atmospheric patterns. A middle-Miocene excursion of the oxygen isotopic composition of benthic foraminifera to heavier values reflects expansion of Antarctic ice sheets (Shackleton and Kennett, 1975; Kennett, 1977). Woodruff (1981) sampled this interval in DSDP Site 289 at close spacing and determined that the expansion occurred rapidly between 12-14MYBP. Between the middle and late Miocene, a steepening of the latitudinal temperature gradient, a factor in determining the intensity and position of major wind systems, is recorded in planktonic foraminifera oxygen isotopic values (Savin, *et al.*, 1985; Shackleton and Kennett, 1975; Kennett, 1977).

The eolian sediment record in the western North Pacific shows two periods of dramatic increase in the quantity of material being transported: the middle Miocene and the late Pliocene-early Pleistocene (Figs. 4, 7, 8). The paucity of carbonate material in the sediments of the North Pacific prohibits oxygen isotope analysis, which would improve stratigraphic resolution and allow for a direct comparison of the eolian response to the buildup of glacial ice and sea-surface temperature variations that are recorded in the oxygen isotope signal. Caution must be taken when comparing the timing of uplift of the Tibetan Plateau, based on either the crustal shortening model or the argon isotopic and fission track data, to the timing of changes observed in the sediments that are primarily based on faunal data. Direct correlation of sedimentary changes to climatic causes is not possible in this study, but there are similarities in the timing of climatic events and changes in sedimentation. It was during the middle Miocene (at approximately 14MYBP at Site 436) that the accumulation rates of quartz and clay minerals increased abruptly to consistently higher Neogene values. This indicates the transport of a larger quantity of material over the North Pacific since this time. Greater accumulation rates could result from greater aridity (increased availability of material for erosion), greater injection (dust storm activity), or increased transport efficiency (more vigorous winds).

Clay mineral compositions began to change from those with a large percentage of chemically weathered clays to those with increased contents of mechanically weathered material at approximately 20MYBP, six million years earlier than the increase in accumulation rates. The mineral composition change occurs at approximately 363.42m in brown-black pelagic mud that is characteristic of low sedimentation rates. Analysis of 6 samples taken over the interval 360.57 to 363.42m indicate that this composition change occurred prior to the rapid increase in sedimentation rates and the onset of siliceous sedimentation. The transition from brown-black pelagic mud to the yellowish-brown diatomaceous claystone associated with the high sedimentation rate deposition is gradual between 359.5-360m — about 4-5 million years after the change in mineral composition at 363.4m. The change in weathering conditions recorded by the clay minerals was not sufficient to increase the quantity of atmospherically transported material. The early Miocene change in sediment composition indicative of greater mechanical weathering is roughly contemporaneous with the uplift of southern Tibet (Copeland, *et al.*, 1987). Mid-Miocene increases in eolian mass accumulation at Site 436 are more closely coincident with the expansion of Antarctic glaciation (Woodruff, 1981).

The second major Cenozoic increase in accumulation rates of terrigenous material occurred in the Pliocene, approximately 5 MYBP. This increase occurred during a period of global cooling and Antarctic ice growth (Kennett, 1977; Shackleton and Kennett, 1975). The magnitude of the early Pliocene increase of accumulation rates is even greater than the increase in eolian material accumulating during the middle Miocene. The Tibetan Plateau and Himalayas were well established by this time, with elevations capable of perturbing the climate (Copeland, *et al.*, 1987). Pacific Ocean circulation had changed significantly since the early Miocene (Kennett, *et al.*, 1985; Romine and Lombardi, 1985). Together, the evolution of topography and oceanographic circulation apparently enhanced the sensitivity of the climate to glaciation. It is interesting to note that there is a relatively small increase in sediment accumulation at the time of Antarctic ice growth in the Oligocene, proposed by Miller, *et al.* (1987). This may indicate that the presence of the mountains and the late Miocene oceanographic circulation patterns are key to the erosion and atmospheric transport of large quantities of material or that the Antarctic ice was not extensive enough at that time to have a large climatic effect. The response of eolian transport to Northern Hemisphere glaciation is the extremely large increase in mass accumulation between 2-3MYBP in all North Pacific sediment records.

Sensitivity tests of the NCAR Community Climate Model, a global atmospheric circulation model, to the presence of permanent snow cover and to the effect of topography attempt to identify the relative impact of these factors on climate (Barron and Washington, 1984). Sensitivity tests do not provide a recreation of past climate but identify areas of sensitivity to change of a specific variable and the relative importance of different variables. Using present-day boundary conditions, Barron and Washington (1984) ran the NCAR CCM both with and without Antarctic and Greenland permanent snow cover. The results of this sensitivity test, presented in terms of temperature change, show a globally averaged temperature increase of  $0.8^{\circ}\text{K}$  with extreme regional warming in a snow-free Antarctica. There are regional effects over Asia, with a warming of  $3^{\circ}\text{K}$  over the Himalayas and northwest (north of approximately  $60^{\circ}\text{N}$ ) of the mountains and there are isolated areas with a decrease in temperature of  $3^{\circ}\text{K}$ . Thus, the permanent snow cover had little effect on the global temperature. A comparison of the zonally averaged surface temperatures of the climate model with and without snow shows that the main deviation occurs poleward of  $60^{\circ}\text{S}$ . The steepening of the south pole-to-equator temperature gradient that occurred during the Cenozoic (Savin, *et al.*, 1985; Shackleton and Kennett, 1975; Kennett, 1977, Wolfe, 1978) cannot be accounted for by solely the presence of glacial ice, but involves other climatic parameters. The effect of mountains on climate was examined by removing the topography from the CCM, already without permanent snow cover. The global temperature response to the absence of topography was an increase of  $1.1^{\circ}\text{K}$  over the CCM simulation with no snow cover. The zonally averaged temperature shows that deviation from the no snow simulation is also concentrated in the area south of  $60^{\circ}\text{S}$ . There is more regional variation in the simulation without topography than in the simulation without snow. Regional temperature increases are balanced globally by corresponding decreases in other areas. The temperature in China and the Himalayan region increases between  $6^{\circ}$  and  $12^{\circ}\text{K}$  in this experiment while temperatures to the north and northwest of the mountains decline by  $3^{\circ}$  to  $6^{\circ}\text{K}$ . These temperature differences suggest that without the elevation of the Tibetan Plateau, the midlatitudes of China may have been warmer, making the regional gradient from the midlatitudes to the equator less steep while increasing the steepness of the temperature gradient between middle and high latitudes.

It is clear from the model that although the globally averaged responses to changes in topography and glaciation may be relatively small, there may be significant regional response in the area of Tibet and China. The mesoscale processes of dust storms that dominate the present-day transport of terrigenous material from Asia out over the North Pacific are too small



to be resolved in the climate model. However, larger scale factors that contribute to storm formation and frequency may be identified. In the model experiment without topography, the regional high-latitude, steep-temperature gradient may displace northward the position of the intense winds associated with the jet stream that carry terrigenous material over the North Pacific. Grain-size analyses of sediments from Site 576A and LL44-GPC3 (Janecek, 1985; Rea, *et al.*, 1985) suggest that the intensity of westerly winds transporting Asian dust to the central North Pacific has increased since the early Miocene, roughly 20MYBP, since the uplift of the Tibetan Plateau. The eolian records from these sites also include changes from northward migration beneath the westerlies at an earlier time, about 24MYBP at LL44-GPC3 (Leinen and Heath, 1981; Janecek and Rea, 1983; Leinen, 1985). Moisture content of air masses and warm temperatures would extend farther inland in the absence of a topographic barrier. The uplift of the Tibetan plateau would inhibit the moisture transport to the north, increasing aridity. The change in composition in the western North Pacific sediments at approximately 20MYBP is consistent with such a model. Specific climatic effects of glaciation that would enhance transport efficiency are difficult to determine. The formation and frequency of dust storms may have been affected by regional temperature variation associated with glaciation. The CCM tests of Barron and Washington (1984) did not differentiate between northern and southern hemisphere permanent snow cover. The effect of glaciation on seasonal contrast, which is an important factor in present-day eolian transport, also was not studied in the climate simulations. Climate models should be used to test the sensitivity of these variables to help unravel the change in climatic conditions that resulted in a long-term, several-fold increase in the transport of Asian dust.

## 6. CONCLUSIONS

The eolian sedimentation in the western North Pacific has varied during the Cenozoic in response to changes in climatic and tectonic factors that control erosion and atmospheric transport. Although eolian transport dominates terrigenous sedimentation across the North Pacific, there are regional differences that are a function of proximity to source area, latitude, and bottom-current activity. Hemipelagic or bottom transport of sediment and a possible variation of sediment source complicate the sediment record at DSDP Site 578 since the middle Miocene, as indicated by anomalously low bulk quartz contents and fluxes.

Paleoclimatic interpretations are based on variations in the sediment record, present-day knowledge of controls on atmospheric transport, and temporal changes of those controls. A change in clay mineral composition at approximately 20MYBP to lower kaolinite concentration and relatively increased content of mechanically weathered material, plagioclase and chlorite, suggests a possible increase in aridity of the Asian source region since this time. This change occurred prior to the expansion of Antarctic glaciation, but approximately contemporaneously with the uplift of the Tibetan Plateau. Accumulation rates of terrigenous components were generally low during the Paleogene. Increased accumulation rates at approximately 14MYBP were associated with the onset of siliceous productivity and the expansion of Antarctic glaciation. Accumulation rates increased even further during the early Pliocene at approximately 5MYBP, as global cooling and further Antarctic ice expansion occurred. The largest increase in accumulation rates occurred between 2-3MY, coincident with Northern Hemisphere glaciation. The exact nature of the climatic response to the evolving earth needs to be further explored with both collection of data from key locations and with climate modeling.

## REFERENCES

- Arthur, M.A., von Huene, R., and Adelseck, C.G.: Sedimentary evolution of the Japan fore-arc region off Northern Honshu, Legs 56 and 57, DSDP, In: Langseth, M., Okada, H., *et al.*, (Eds.), *Init. Repts. DSDP*, 56, 57, Washington (U.S. Government Printing Office), pp. 521-568.
- Avila, L., 1983: *Dust storm events over Asia and the mechanism which pumps dust into the Troposphere*, M.S. Thesis, U. of Miami, Coral Gables, FL, 74 pp.
- Barron, E.J., and Washington, W.M., 1984: The role of geographic variables in explaining paleoclimates: Results from Cretaceous climate model sensitivity studies, *J. Geophys. Res.*, 89: 1267-1279.
- Berggren, W.A., Kent, D.V., Flynn, J., and van Couvering, J., 1985: Cenozoic geochronology, *Geol. Soc. Am. Bull.*, 96: 1407-1418.
- Blank, M., Leinen, M., and Prospero, J.M., 1985: Major Asian eolian inputs indicated by the mineralogy of aerosols and sediments in the western North Pacific, *Nature*, 314: 84-86.

- Copeland, P., Harrison, T.M., Kidd, W.S.F., Xu Ronghua and Zhang Yuquan, 1987: Rapid early Miocene acceleration of uplift in the Gangdese Belt, Xizang(southern Tibet) and its bearing on accomodation mechanisms of the India-Asia collision, *Earth and Planetary Sci.Let.*, 86: 240-252.
- Damuth, J.E., Jacobi, R.D., and Hayes, D.E., 1983: Sedimentation processes in the Northwest Pacific Basin revealed by echo character mapping studies, *Geol. Soc. Am. Bull.*, 94: 381-395.
- Doyle, P., and Riedel, W.R., 1980: Ichthyoliths from Site 436, Northwest Pacific, Leg 56, DSDP, In: Langseth, M., Okada, H., et al. (Eds.), *Init. Repts. DSDP*, 56, 57, Washington (U.S. Government Printing Office), pp. 887-894.
- Doyle, P., and Riedel, W.R., 1985: Ichthyolith biostratigraphy of western North Pacific pelagic clays, In: Heath, G.R., Burkle, L.D., et al.(Eds.), *Init. Repts.DSDP*, 86: Washington (U.S. Government Printing Office), pp. 349-366.
- Duce, R.A., Unni, C.K., Ray, B.J., Prospero, J.M., Merrill, J.T., 1980: Long-range atmospheric transport of soil dust from Asia to the tropical North Pacific: Temporal variability, *Science*, 209: 1522-1524.
- Ferguson, W.S., Griffin, J.J. and Goldberg, E.D., 1970: Atmospheric dusts from the North Pacific - a short note on long-range eolian transport, *J. Geophys. Res.*, 75: 1137-1139.
- Gillette, D.A., 1981: Production of dust that can be carried great distances, In: Pewe, T.L. (Ed.), *Desert Dust: Origin, Characteristics, and Effects on Man*, Geol. Soc. Am. Special Paper 186, pp. 11-26.
- Gray, T.I., Irwin, J.R., Krueger, A.F., Varnadore, M.S., 1976: *Average Circulation in the Troposphere over the Tropics, January 1968-August 1972*, NOAA Publication, Washington, D.C.
- Griffin, J.J., Windom, H., and Goldberg, E.D., 1968: The distribution of clay minerals in the world ocean, *Deep Sea Res.*, 15: 433-459.
- Harper, H.E., Jr., 1980: Diatom biostratigraphy of Sites 434, 435, and 436, Northwestern Pacific, Leg 56, DSDP, In: Langseth, M., Okada, H., et al. (Eds.), *Init. Repts. DSDP*, 56, 57, Washington (U.S. Government Printing Office), pp. 633-640.

- Heath, G.R., Rea, D.H., and Levi, S., 1985: Paleomagnetism and accumulation rates of sediments at Sites 576 and 578, Deep Sea Drilling Project Leg 86, western North Pacific', *In: Heath, G.R., Burkle, L.D., et al.*, (Eds.), *Init. Repts. DSDP*, 86, Washington (U.S. Government Printing Office), pp. 459-502.
- Heath, G.R., and Pisias, N.G., 1979: A method for quantitative estimation of clay minerals in North Pacific deep sea sediments, *Clays and Clay Mineral.*, 27: 175-184.
- Iwasaka, Y., Minoura, H., and Nagaya, K., 1983: The transportation and spacial scale of Asian dust storm clouds: a case study of the dust storm of April, 1979, *Tellus*, 35B: 189-196.
- Jackson, M.L., Gillette, D.A., Danielson, E.F., Blifford, I.H., Bryson, R.A., and Syers, J.K., 1973: Global dustfall during the Quaternary as related to environments, *Soil Sci.*, 116: 135-145.
- Jacobi, R.D., Hayes, D.E., and Damuth, J.E., 1985: High resolution seismic studies and site survey results near Deep Sea Drilling Project Sites 576 and 578, Northwest Pacific, *In: Heath, G.R., Burkle, L.D., et al.*, (Eds.), *Init. Repts. DSDP*, 86, Washington (U.S. Government Printing Office), pp. 23-50.
- Janecek, T.R., 1985: Eolian sedimentation in the northwest Pacific Ocean: A preliminary examination of the data from Deep Sea Drilling Sites 576 and 578, *In: Heath, G.R., Burkle, L.D., et al.*, (Eds.), *Init. Repts. DSDP*, 86, Washington (U.S. Government Printing Office), pp. 589-604.
- Janecek, T.R., and Rea, D.K., 1983: Eolian deposition in the North Pacific Ocean: Cenozoic history of atmospheric circulation, *Geol. Soc. Am. Bull.*, 94: 730-738.
- Kennett, J.P., Keller, G. and Srinivasan, M.S., 1985: Miocene planktonic foraminiferal biogeography and paleoceanographic development of the Indo-Pacific region, *In: Kennett, J.P., Ed., The Miocene Ocean: Paleoceanography and Biogeography*, GSA Memoir 163, pp. 197-236.
- Kennett, J.P., 1977: Cenozoic evolution of Antarctic glaciation, the Circum-Antarctic Ocean and their impact on global Paleoceanography, *J. Geophys. Res.*, 82: 3843-3860.

- Koizumi, I., Barron, J., and Harper, H.E., 1980: Diatom correlation of Legs 56 and 57 with onshore sequences in Japan, *In: Langseth, M., Okada, H. et al. (Eds.), Init. Repts. DSDP, 56, 57: Washington (U.S. Government Printing Office), pp. 687-694.*
- Lancelot, Y., and Larson, R.L., 1975: Sedimentary and tectonic evolution of the northwestern Pacific, *In: Larson, R.L., Moberly, R., et al. (Eds.) Init. Repts. DSDP, 32, Washington (U.S. Government Printing Office), pp. 925-940.*
- Leinen, M., Schramm, C., 1986: A comparison of North Pacific mineral aerosol and surface sediment: Implications for paleoclimatic interpretations, *Abstracts with Program, 2nd International Paleoceanographic Congress, Woods Hole, MA.*
- Leinen, M., Cwienk, D., Biscaye, P.E., Heath, G.R., Kolla, V., Thiede, J., and Dauphin, J.P., 1986: Distribution of biogenic silica and quartz in recent deep-sea sediments, *Geology, 14: 199-203.*
- Leinen, M.S., 1985a: Quartz content of northwest Pacific Site 576A and implications for Cenozoic eolian transport, *In: Heath, G.R., Burkle, L.D., et al., (Eds.), Init. Repts. DSDP, 86, Washington (U.S. Government Printing Office), pp. 581-588.*
- Leinen, M.S., 1985b: Techniques for determining opal in deep-sea sediments: A comparison of radiolarian counts and x-ray diffraction data, *Marine Micropaleo., 9: 375-383.*
- Leinen, M.S., and Heath, G.R., 1981: Sedimentary Indicators of atmospheric activity in the Northern Hemisphere during the Cenozoic, *Paleogeography, Paleoclimatology, Paleoecology, 36, 1-21.*
- Lenotre, N., Chamley, H., and Hoffert, M., 1985: Clay stratigraphy at Deep Sea Drilling Project Sites 576 and 578, Leg 86 (western north Pacific), *In: Heath, G.R., Burkle, L.D., et al., (Eds.), Init. Repts. DSDP, 86, Washington (U.S. Government Printing Office), pp. 571-580.*
- Mann, U. and Muller, G., 1980: Composition of sediments of the Japan Trench transect, Legs 56 and 57, *In: Langseth, M., Okada, H., et al. (Eds.), Init. Repts. DSDP, 56, 57: Washington (U.S. Government Printing Office), pp. 939-978.*

- Merrill, J.T., 1987: Atmospheric pathways to the oceans: *In*, Buat-Menard, P., Ed., *The role of air-sea exchange in Geochemical Cycling* NATO ASI Volume C185, pp. 35-63.
- Miller, K.G., Fairbanks, R.G., and Mountain, G.S., 1987: Tertiary oxygen isotope synthesis, sea level history, and continental margin erosion, *Paleoceanography*, 2: 1-19.
- Morley, J.J., 1985: Radiolarians from the Northwest Pacific, Deep Sea Drilling Project Leg 86', *In*: Heath, G.R., Burkle, L.D., et al. (Eds.), *Init. Repts. DSDP*, 86, Washington (U.S. Government Printing Office), pp. 399-422.
- Rea, D.H., Leinen, M., and Janecek, T.R., 1985: Geologic approach to the long-term history of atmospheric circulation, *Science*, 227: 721-725.
- Rea, D.H. and Janecek, T.R., 1981: Mass accumulation rates of the non-authigenic, inorganic, crystalline (eolian) component of deep-sea sediments from the western Mid-Pacific Mountains, DSDP Site 463, *In*: Thiede et al., (Eds.), *Init. Repts. DSDP*, 62, pp. 653-659.
- Rex, R.W., and Goldberg, E.D., 1958: Quartz contents of pelagic sediments of the Pacific Ocean, *Tellus*, 10:153-159.
- Romine, K., and Lombardi, G., 1985: Evolution of Pacific circulation in the Miocene: Radiolarian evidence from DSDP Site 289, *In*: Kennett, J.P., Ed., *The Miocene Ocean: Paleoceanography and Biogeography*, GSA Memoir 163, pp. 273-290.
- Sakai, T., 1980: Radiolarians from site 434, 435, and 436, Northwest Pacific, Leg 56, Deep Sea Drilling Project, *In*: Langseth, M., Okada, H., et al. (Eds.), *Init. Repts. DSDP*, 56, 57: Washington (U.S. Government Printing Office), pp. 695-734.
- Savin, S.M., Abel, L., Barrera, E., Hodell, D.A., Keller, G., Kennett, J.P., Killingley, J., Murphy, M., and Vincent, E., 1985: The evolution of Miocene surface and near-surface marine temperatures: Oxygen isotopic evidence, *In*: Kennett, J.P., Ed., *The Miocene Ocean: Paleoceanography and Biogeography*, GSA Memoir, 163, pp. 49-82.
- Scientific Party, 1980: Site 436, Japan Trench outer rise, *In*: Langseth, M., Okada, H., et al. (Eds.), *Init. Repts. DSDP*, 56, 57, Washington (U.S. Government Printing Office), pp. 399-446.

- Shackleton, N.J., and Kennett, J.P., 1975: Paleotemperature history of the Cenozoic and the initiation of Antarctic glaciation: Oxygen and carbon analyses in DSDP Sites 277, 279, and 281, *In*: Kennett, J.P., Houtz, R.E., *et al.*, Eds., *Init. Repts. DSDP*, 29, Washington (U.S. Government Printing Office), pp. 743-755.
- Shaw, G.E., 1980: Transport of Asian desert aerosol to the Hawaiian Islands, *J. Appl. Meteorology*, 19: 1254-1259.
- Taft, B.A., Ramp, S.R., Dworski, J.G., and Holloway, G., 1981: Measurements of deep currents in the central North Pacific, *J. Geophys. Res.*, 86: 1955-1968.
- Till, R., and Spears, D.A., 1969: The determination of quartz in sedimentary rocks using an x-ray diffraction method, *Clays and clay Minerals*, 17: 323-327.
- Uematsu, M., Duce, R.A., and Prospero, J.M., 1985: Deposition of atmospheric particles in the North Pacific Ocean, *J. Atmos. Chem.*, 3: 123-138.
- Uematsu, M., Duce, R.A., Prospero, J.M., Chen, L.Q., and Merrill, J.T., 1983: Transport of mineral aerosol from Asia to the North Pacific Ocean, *J. Geophys. Res.*, 88: 5343-5352.
- van Andel, Tj., Heath, G.R., Moore, T.C., 1975: Cenozoic history and paleoceanography of the central equatorial Pacific Ocean, *Geol. Soc. Am. Memoir* 143, 134 pp.
- Windom, H.L., 1969: Atmospheric dust records in permanent snow fields: Implications to marine sedimentation, *Geol. Soc. Am. Bull.*, 80: 761-782.
- Windom, H.L., 1975: Eolian contributions to marine sediments, *J. Sed. Pet.*, 45: 520-529.
- Wolfe, J.A., 1978: A paleobotanical interpretation of Tertiary climates in the Northern hemisphere, *Am. Sci.*, 66: 694-703.
- Woodruff, F., Savin, S.M., and Douglas, R.G., 1981: A Miocene stable isotopic record: A detailed deep Pacific Ocean study and its paleoclimatic implications, *Science*, 212: 665-668.

Zeitler, P.K., 1985: Cooling history of the NW Himalayas, Pakistan, *Tectonics*, 4: 127-151.



# GEOLOGIC RECORD OF ATMOSPHERIC CIRCULATION ON TECTONIC TIME SCALES

DAVID K. REA

Department of Geological Sciences  
The University of Michigan  
Ann Arbor, MI 48109-1063  
U.S.A.

**ABSTRACT.** There exists a reasonable geologic record of atmospheric circulation, based on information extracted from eolian dust preserved in deep-sea sediments, that extends back to the late Cretaceous in the northern hemisphere and to the late Oligocene in the southern hemisphere. On tectonic timescales of 500,000 years or longer, important changes in atmospheric circulation do not always occur in conjunction with known paleoenvironmental changes, such as times of ice buildup on continents. There appears to be essentially no change in wind intensity across the Cretaceous-Tertiary boundary. The single greatest change in wind intensity in the Cenozoic occurs at the Paleocene-Eocene boundary, a reduction of higher intensity Mesozoic and Paleocene circulation to the sluggish atmosphere of the middle Tertiary. Circulation intensity remained low throughout the Eocene and increased beginning in the Oligocene to a Plio-Pleistocene maxima. Southern hemisphere records show that the mid-Miocene increase in ice volume at 13 to 14 Ma does not correspond to an increase in wind intensity, suggesting that the inferred direct correspondence of glacial buildup to polar cooling may not always hold. There appears to be little response to the onset of northern hemisphere glaciation in the records of southern hemisphere atmospheric circulation — one indication of the independent behavior of the two hemispheres.

## 1. INTRODUCTION

In the past few years, students of paleoclimatology have come to understand that the earth's environment can be subdivided into several climatic subsystems, each with its own history of variability. Climatic

systems are those naturally occurring systems that are capable of storing, transporting, and releasing both heat and moisture. These systems (the atmosphere, surface ocean, deep ocean, cryosphere, land surface and biosphere) all have different response times to climatic stimuli, and all interact either directly or indirectly. Further, we observe distinct timescales of climatic variability and subsystem interaction ranging from the rather short oceanic timescale of several hundred to a few thousand years, through the orbital timescale of tens of thousands to several hundred thousand years, to the tectonic timescale of half a million or more years.

This paper examines one aspect of paleoclimatology, the history on tectonic timescales of atmospheric circulation as preserved in the deep-sea sedimentary record of eolian dust. The terrigenous mineral component of ocean sediments contains a record of the nature of the continental source area and of the pertinent transport process. In pelagic sediments these terrigenous materials are wind transported and provide both the best proxy indicator of the variability of atmospheric circulation and a useful proxy of continental climate (Rea, *et al.*, 1985).

## 2. EOLIAN TRANSPORT AND DEPOSITION PROCESSES

Most of the dust that we now find incorporated into pelagic sediments originates as soil in an arid or semi-arid climate. That soil material is entrained and elevated by the strong winds of large spring storms and then transported long distances in the middle and upper troposphere by the zonal wind systems. In fact, well over 90% of the total flux of dust to the ocean (about 1015g/yr) is accomplished by a few events each year. We are confident that the mineral component of pelagic sediments away from the influence of hemipelagic, turbidite, and ice-rafting depositional processes is eolian because: (a) dust mineralogy matches that of the surface sediments (Ferguson, *et al.*, 1970; Blank, *et al.*, 1985) and (b) quartz (an unequivocally eolian mineral) shows distribution patterns in surface sediments which match the zonal wind patterns (Leinen and Heath, 1981; Leinen, *et al.*, 1986).

The longest quantitative record of modern dust transport has been compiled by Prospero and his colleagues for material crossing the North Atlantic Ocean from North Africa. These data relate the dust flux to climatic conditions in the Saharan-Saharan source region. Monthly values show increased dust transport during the late spring and early summer with an order of magnitude variation in any given year (Prospero, 1981a; Prospero, *et al.*, 1981). The annual transport cycles correlate with the climatology of arid North Africa, but not with the general intensity of the

Northern Hemisphere trade winds, which are stronger in the winter months. On a longer term basis, the flux of dust across the North Atlantic shows a three-to five-fold increase during the height of the Sahelian droughts demonstrated times of significantly reduced rainfall (Nicholson, 1985) in 1973-1974 and in 1983-1984 in comparison to the more normal years (Prospero and Nees, 1977, 1986). Historical records from China also show that increased dust transport activity occurs during drier times (Zhang, 1984). These data and a similar data set collected in Hawaii (Parrington, *et al.*, 1983), along with ongoing work in the North Pacific (Merrill, 1987), provide the evidence upon which we base our working assumption that on tectonic timescales the flux of dust to the ocean depends upon the availability of material, which in turn depends on the degree of aridity of the eolian source region. Alternatively, the long-term flux of dust to the ocean may depend on the number, intensity, and transport efficiency of dust storms. These processes vary on longer tectonic timescales as zonal or meridional circulation becomes more important, and thus may effect the total amount of material carried to the sea.

Dust raised from the land surface is a complex mixture of sizes and shapes. With increasing injection height and distance from source, however, the size of the eolian load becomes smaller and the distribution more regular (Nickling, 1983; Hobbs, *et al.*, 1985). Both air and land-based sampling (Gillette, *et al.*, 1974; Johnson, 1976; Glaccum and Prospero, 1980) and theoretical calculations (Windom, 1969; Jaenicke, 1979; Schutz, *et al.*, 1981) suggest that beyond 1000 to 2000 km from the source area, the size distribution of the grains changes very little. Along a 3600 km west-to-east transect in the North Pacific, the size of the dust grains in surface sediments changes from  $8.5\Phi$  ( $2.8\mu\text{m}$ ) to  $8.7\Phi$  ( $2.4\mu\text{m}$ ) (Janecek, 1985). Our second working hypothesis then is that these small grains, thousands of kilometers from the source area, are essentially in equilibrium with the transporting zonal winds. Therefore, their size is a measure of the intensity of those winds.

Parkin and his colleagues (Parkin, 1974; Parkin and Shackleton, 1973; Parkin and Padgham, 1975) first used the size of wind-blown grains to make estimates of past wind intensity. Janecek and Rea (1985) have made preliminary attempts to quantify the grain size to wind intensity relationship based on the work of Gillette (Gillette, *et al.*, 1974; Gillette, 1981), but such quantification is not yet well resolved. [See also Tsoar and Pye (1987).]

The eolian grain-size record has been shown to contain important paleoclimatic information in studies conducted of variability on orbital timescales. Periodicities corresponding to the Milankovitch cycles of precession, tilt, and eccentricity are preserved in the grain-size record of the northern hemisphere westerlies (Janecek and Rea, 1985) and the southern hemisphere trade winds (Pisias and Rea, 1988). The grain-size record of wind intensity is coherent and in phase with the radiolarian record of equatorial divergence in the central Pacific (Pisias and Rea, 1988) — quantitatively linking oceanic and atmospheric circulation in the sedimentary record. The success of these studies leads us to believe that this size parameter of the eolian signal also preserves significant paleoclimatic information on tectonic timescales.

In summary, nearly a decade of working with the eolian component of pelagic sediments has revealed that dust flux to the sea floor records the supply function and that supply is related to the climatology of the source region. Dust grain size is determined by the transport process and records both its intensity and variability. The flux and size parameters appear to vary independently (Chuey, *et al.*, 1987) and can be considered to represent the atmospheric analogy of the capacity and competence of rivers. Useful reviews of eolian processes have been given in this volume and by Windom (1975), Prospero (1981b), Rea, *et al.* (1985), and especially in a recent book by Pye (1987).

### 3. EOLIAN PROCESSES ON TECTONIC TIMESCALES: THE CENOZOIC RECORD

#### 3.1 *North Pacific Record*

The best information on the long-term, tectonic timescale history of atmospheric circulation comes from locations in the North Pacific. Early work on eolian deposition at this timescale was done by Leinen and Heath (1981) and Rea and Janecek (1981) for one record of the late Cretaceous and Rea and Janecek (1982) for five Miocene to Recent records. Whole Cenozoic records were compiled by Janecek and Rea (1983) from piston core LL44-GPC3 and by Janecek (1985) from DSDP sites 576 and 578 (Figure 1). Cenozoic records of the mineralogy of the eolian component of North Pacific cores have been presented by Leinen (1985) and by Schramm (this volume).

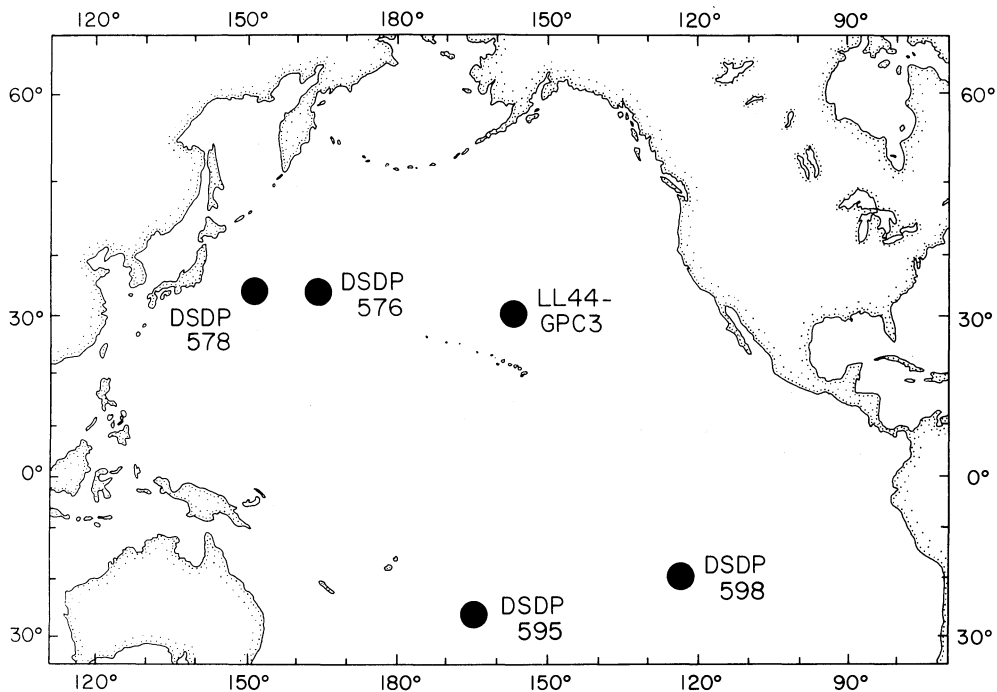


Figure 1: Index map of the Pacific Ocean showing location of some cores having long Cenozoic records of eolian deposition.

Cenozoic flux records (Figure 2) show moderate dust flux, 20 to 40  $\text{mg}(\text{cm}^2 \cdot 10^3 \text{y})^{-1}$ , during the latest Cretaceous and Paleocene, a decline to low values in the middle Tertiary of about 10  $\text{mg}(\text{cm}^2 \cdot 10^3 \text{y})^{-1}$ , a gentle Neogene increase, and finally an order of magnitude increase in dust flux that coincides with the onset of Northern hemisphere glaciation and reaches late Pleistocene values of several hundred  $\text{mg}(\text{cm}^2 \cdot 10^3 \text{y})^{-1}$ . These data agree with our understanding of the middle Tertiary being a time of relatively moist continental climates and increasing Neogene aridity accompanying polar cooling.

The grain-size record (Figure 2) shows relatively coarse grains characterizing the latest Cretaceous and Paleocene, a sudden reduction in grain size in the early Eocene, low grain sizes through the middle Tertiary, and an increase in eolian grain size beginning in the Oligocene and continuing to the Pleistocene. There is only a small increase in the size of eolian grains associated with the onset of Northern Hemisphere glaciation (Rea and Janecek, 1982; Janecek and Rea, 1983; Rea, *et al.* 1985). These data indicate surprisingly vigorous atmospheric circulation during the earlier portion of the record, reduced intensity of circulation during the middle Tertiary, and increasing wind intensity during much of the Neogene.

### 3.2 North Atlantic Record

A few longer term records of eolian deposition suitable for interpretation of climatic change on tectonic timescales have been derived from the North Atlantic (Sarnthein, *et al.*, 1982). Sarnthein and his colleagues have been working on the cores from ODP Leg 108 raised from the Atlantic west of the bulge of Africa. Preliminary results from their longest record (Sarnthien, *et al.*, 1987), which extends back into the late Miocene, show a large increase in the flux of dust to the subtropical Atlantic at 4.5 Ma with flux events or spikes at 3.6 to 3.4 Ma and about 2.2 Ma. They suggest that the average long-term latitudinal position of the Intertropical Convergence Zone may have remained unchanged over the time span of this record.

Stein (1985) presented the Oligocene to Recent record of mineral accumulation on the Sierra Leone Rise at DSDP site 366. There eolian mass accumulation rates show relative maxima in the latest Miocene 5 to 6 Ma, and in the late Pliocene about 2 Ma. The percentage of terrigenous grains coarser than  $6\mu\text{m}$  ( $7.4\Phi$ ) increases from a low of less than 2% to a Pleistocene average of about 7% beginning about 2.5 Ma.

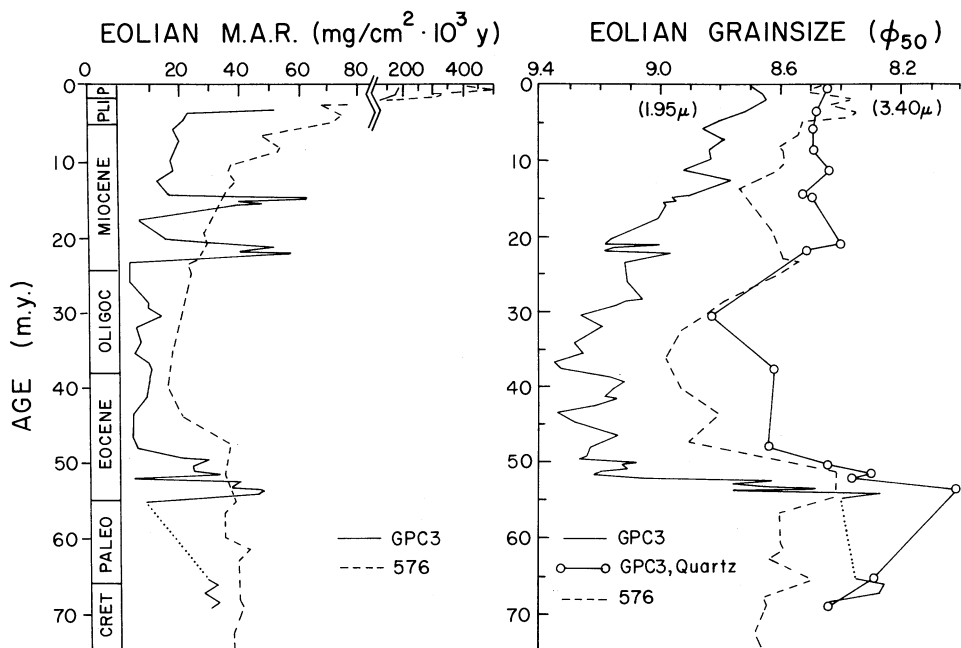


Figure 2: Late Cretaceous to Recent records of eolian deposition from DSDP Site 576 and core LL44-GPC3. Left, flux of dust; right, size of eolian grains. After Rea, *et al.*, 1985.

McCave and Lever described eolian deposition in the North Atlantic for eight time intervals (each a few million years long) from the early Cretaceous to the late Miocene (Lever and McCave, 1983; McCave and Lever, 1986). They do not give a dust flux history, but do determine the grain size of the eolian material. The North Atlantic eolian sediments do show a marked reduction in the size of eolian grains that occurred in the early Eocene in a manner consistent with the North Pacific record shown in Figure 2 (McCave and Lever, 1986).

### 3.3 Southern Hemisphere Record

There have been three studies of eolian deposition in the southern hemisphere that provide information on variability of continental aridity and atmospheric circulation on tectonic timescales. Rea and Bloomstine (1986) examined the Oligocene to recent record of eolian deposition in Leg 92 drill sites located along the west flank of the East Pacific Rise at 19° to 20°S. That study revealed a remarkably low and generally constant flux of dust to the Southeast Pacific, about 1 to 4  $\text{mg}(\text{cm}^2 \cdot 10^3\text{y})^{-1}$ , since 28.5 my ago. These values are more than two orders of magnitude less than the Plio-Pleistocene fluxes to the North Pacific and one order of magnitude less than the pre-Glacial Neogene fluxes. Further, the southern hemisphere record shows no changes in flux or grain size at 2.4 Ma (Figure 3). Together, the several southeastern Pacific sites show only one important change in the eolian grain size — a coarsening from 8.2 $\Phi$  (3.4 $\mu\text{m}$ ) median diameter in older sediments to 7.2 $\Phi$  (6.8 $\mu\text{m}$ ) in younger materials. This change, which we interpret as recording an intensification of the southeast trade winds, is best seen in the data from Site 598 (Figure 3) and occurs at about 10 Ma. It is, therefore, nearly three million years (and three fossil zones) younger than the shift in oxygen isotopic values, which is taken to record the mid-Miocene buildup of ice in Antarctica (Woodruff, *et al.*, 1981) and an equal amount younger than the change in deep water chemistry that allowed the formation of a thick lysocline zone (Rea and Leinen, 1985) — two important mid-Miocene paleoceanographic events. On the other hand, the deposition of biogenic opal in the Pacific equatorial region reaches a maximum of 8 to 10 Ma (Leinen, 1979) — an event which may be linked to the recently intensified trade winds.

These data from the southeast Pacific suggest that the pole-to-equator temperature gradient, which is ultimately responsible for the intensity of the geostrophic winds, may not be directly linked to the volume of ice stored at the poles; a direct ice volume-temperature correlation is a common assumption, but one poorly tested by independent data.



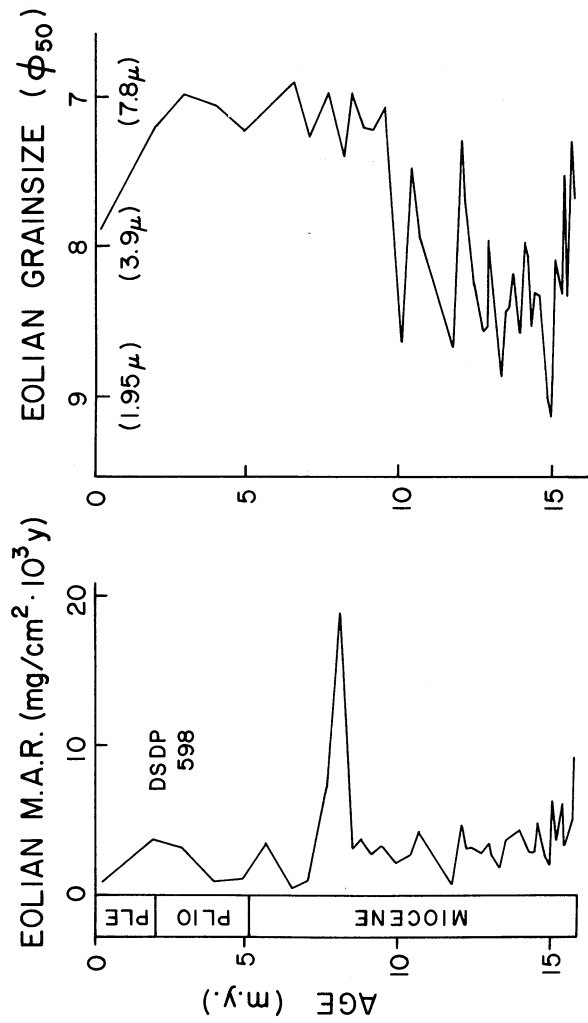


Figure 3: Record of eolian deposition from DSDP Site 598. Left, flux of dust; right, size of eolian grains. After Rea and Bloomstine, 1986.

Schramm and Leinen (1987) examined the eolian quartz in a middle Cretaceous to Pleistocene pelagic clay sequence at DSDP site 595A, about 4500 km east of Australia at 25°S latitude. Their data are sparse but indicate very low dust fluxes throughout the last 100 my and an overall flux pattern consistent with that observed in the North Pacific cores — moderate values in the late Cretaceous, lowest values in the middle Tertiary, and slightly increasing values during the later Neogene. Site 595A also shows no response to the onset of Northern Hemisphere glaciation in the eolian record, although such an event would not be well resolved at the sampling interval used for that study.

Stein and Robert (1985) studied the mineral component of some of the Leg 90 drill sites located between New Zealand and Australia. They provide a Neogene record of the mineralogy of the terrigenous grains in those sediments, fluxes of the non-carbonate fraction, and some types of grain-size information. In those sites the illite to smectite ratio changes dramatically in a sequence from north-to-south that suggests to the authors that there is increasing aridity beginning about 13 Ma in northern Australia and shifting south through the late Miocene. Fluxes of the carbonate-free, mainly terrigenous, fraction of the Leg 90 sediments first increase about 14 Ma, and there is a distinct flux maxima in the early Pliocene. Stein and Robert (1985) associate the flux increases with increasing Australian continental aridity and suggest that aridity increases follow important cooling events. There is little change in the size of the wind-transported mineral grains during the Miocene. Their data also shows very little change at 2.4 Ma, perhaps even a decline in eolian flux beginning then (Stein and Robert, 1985).

#### 4. DISCUSSION

The existing record of atmospheric circulation on tectonic timescales provides a tantalizing glimpse of that climatic subsystem. The full-Cenozoic, northern hemisphere records suggest that latest Cretaceous and Paleocene atmospheric circulation was as vigorous as that of today, a surprising result. The large change in eolian grain size at the Paleocene-Eocene boundary denotes an unexpected indication of a reduction in atmospheric circulation intensity at a time when ocean circulation becomes more vigorous and presents an interesting quandary now being considered by paleoclimatologists (Barron, 1987; Miller, *et al.*, 1987a).

The mid-Eocene to Recent history is, in its general nature, more or less as one would expect from the oxygen isotopic record of cooling and ice volume. It is important to note here that the oxygen isotopic record is

essentially a southern hemisphere record (bottom and deep waters *vs.* subtropical surface water), and the dust records of Figure 2 are a northern hemispheric phenomena.

There are intriguing indications that the changes in atmospheric circulation do not always correspond in time to changes in the isotopic record of increasing ice volume, implying that ice volume build up in Antarctica may not always require much additional cooling. For instance, Kennett (1985) reports that a warming episode may have accompanied some of the mid-Miocene ice buildup at 13-14 Ma. There are more indications of an increase in the intensity of oceanic circulation in the 8-10 Ma time frame, corresponding to the late Miocene increase in atmospheric circulation indicated by the Site 598 record (Figure 3), than at 13-14 Ma. Increased fluxes of biogenic sediments occur in both the equatorial Pacific (Leinen, 1979) and Indian Oceans (Leg 115 Scientific Drilling Party, 1987; A. Zimmerman, written communication, 1988), and canyon cutting occurred on the Atlantic continental margins at about 10 Ma, but perhaps not at 14 Ma (Miller et al, 1987b). The Leg 114 Scientific Drilling Party (1987) reports a "pronounced cooling event" at about 9 Ma, but not at 13-14 Ma. This information suggesting more pronounced changes in oceanic and atmospheric circulation at roughly 9 Ma than at 13-14 Ma, and thus associated with a lesser rather than greater increase in ice volume (Miller, *et al.*, 1987b), bring into question the direct conceptual link between ice volume and global temperature gradient.

Finally, the observation that the southern hemisphere atmosphere does not respond to the onset of northern hemisphere glaciation suggests the circulation of the southern and northern hemispheres may be somewhat independent — each responding to their own, often different, climatic gradients (Flohn, 1981; Rea and Bloomstine, 1986).

## ACKNOWLEDGMENTS

Throughout my work on the eolian paleoclimate record, I have benefitted from discussions with Margaret Leinen, Tom Janecek, and Nick Pisias — discussions all the more useful because we are not always in agreement. I thank the reviewers of this paper for pointing out errors and suggesting revisions. Studies of the eolian component of deep-sea sediments at the University of Michigan has been supported by both the Marine Geology and Geophysics Program of the Oceanic Sciences Division and the Climate Dynamics Program of the Atmospheric Sciences Division of the National Science Foundation.

## REFERENCES

- Barron, E.J., 1987: Eocene equator-to-pole surface ocean temperatures: A significant climate problem?, *Paleoceanography*, v. 2, pp. 729-739.
- Blank, M., Leinen, M., and Prospero, J.M., 1985: Major Asian aeolian inputs indicated by the mineralogy of aerosols and sediments in the western North Pacific, *Nature*, 314, pp. 84-86.
- Chuey, J.M., Rea, D.K., and Pisias, N.G., 1987: Late Pleistocene paleoclimatology of the central Equatorial Pacific: A quantitative record of eolian and carbonate deposition, *Quat. Res.*, 28, pp. 323-339.
- Ferguson, W.S., Griffin, J.J., and Goldberg E.D., 1970: Atmospheric dusts from the North Pacific - A short note on long range eolian transport, *Jour. Geophys. Res.*, 75, pp. 1137-1139.
- Flohn, H., 1981: A hemispheric circulation asymmetry during the late Tertiary, *Geol. Rundschau*, 70, pp. 725-736.
- Gillette, D.A., 1981: Production of dust that may be carried great distances, In: Pewe, T.L., Ed., *Desert Dust: Origin, Characteristics, and Effect on Man*, Geol. Soc. Am. Special Paper 186, Boulder, CO, pp. 11-26.
- Gillette, D.A., Blifford, I.H., Jr., and Fryrear, D.W., 1974: The influence of wind velocity on the size distributions of aerosols generated by wind erosion of soils, *Geophys. Res.*, 79, pp. 4068-4075.
- Glaccum, R.A., and Prospero, J.M., 1980: Saharan aerosols over the tropical North Atlantic - mineralogy, *Mar. Geol.*, 37, pp. 295-321.
- Hobbs, P.V., Bowdle, D.A., and Radke, L.F., 1985: Particles in the lower troposphere over the High Plains of the United States. Part I: Size distributions, elemental compositions, and morphologies, *Clim. Applied Meterol.*, 24, pp. 1344-1356.
- Jaenicke, R., 1979: Monitoring and critical review of the estimated source strength of mineral dust from the Sahara, In: Morales, C., Ed., *Saharan Dust: Mobilization, Transport and Deposition*, John Wiley and Sons, New York, pp. 233-242.

- Janecek, T.R., 1985: Eolian sedimentation in the northwest Pacific Ocean: A preliminary examination of the data from DSDP Sites 576 and 578, *In: Heath, G.R., L.H. Burckle et al., Init. Repts. DSDP, 86: Washington (U.S. Government Printing Office), pp. 589-603.*
- Janecek, T.R., and Rea, D.K., 1983: Eolian deposition in the northeast Pacific Ocean: Cenozoic history of atmospheric circulation, *Geol. Soc. Am. Bull.*, 94, pp. 730-738.
- Janecek, T.R., and Rea, D.K., 1985: Quaternary fluctuations in the northern hemisphere trade winds and westerlies, *Quat. Res.*, 24, pp. 150-163.
- Johnson, L.R., 1976: Mineralogical dispersal patterns of North Atlantic deep-sea sediments with particular reference to eolian dusts, *Mar. Geol.*, 29, pp. 334-345.
- Kennett, J.P., 1985: Miocene to early Pliocene oxygen and carbon isotope stratigraphy in the southwest Pacific, DSDP Leg 90, *In: Kennett, J.P., C.C. von der Borch et al., Init. Repts. DSDP, 90: Washington (U.S. Government Printing Office), pp. 1383-1411.*
- Leg 114 Scientific Drilling Party, 1987: Leg 114 finds complete sedimentary record, *Geotimes*, 32 (10), pp. 23-25.
- Leg 115 Scientific Drilling Party, 1987: Leg 115 tracks oozes and hot spots, *Geotimes*, 32 (11), pp. 13-15.
- Leinen, M., 1979: Biogenic silica accumulation in the equatorial Pacific and its implications for Cenozoic paleoceanography, *Geol. Soc. Am. Bull. Part II*, 90, pp. 1310-1376.
- Leinen, M., 1985: Quartz content of northwest Pacific Hole 576A and implications for Cenozoic eolian transport, *In: Heath, G.R., L.H. Burckle et al., Init. Repts. DSDP, 86: Washington (U.S. Government Printing Office), pp. 581-588.*
- Leinen, M., and Heath, G.R., 1981: Sedimentary indicators of atmospheric circulation in the northern hemisphere during the Cenozoic, *Palaeogeog., Palaeoclim., Palaeoecol.*, 36, pp. 1-21.
- Leinen, M., Cwienk, D., Heath, G.R., Biscaye, P.E., V. Kolla, Thiede, J., and Dauphin, J.P., 1986: Distribution of biogenic silica and quartz in recent deep-sea sediments, *Geology*, 14, pp. 199-203.

- Lever, A., and McCave, I.N., 1983: Eolian components in Cretaceous and Tertiary North Atlantic sediments, *Sed. Petrol.*, 53, pp. 811-832.
- McCave, I.N., and Lever, A., 1986: Wind vigour over the southern North Atlantic Ocean during the last 135 my, Second International Conference on Paleoceanography, Abstracts with Program, Woods Hole Oceanographic Institution, Woods Hole, MA, p. 54.
- Merrill, J.T., 1987: Meteorological analysis of dust transport to the Pacific, Paleoclimatology and Paleometeorology: Modern and Past Patterns of Global Atmospheric Transport, Program and Abstracts, NATO Advanced Research Workshop, Oracle, AZ, p. 36.
- Miller, K.G., Janecek, T.R., Katz, M., and Keil, D.J., 1987a: Abyssal circulation and benthic foraminiferal changes near the Paleocene/Eocene boundary, *Paleoceanography*, 2, pp. 741-761.
- Miller, K.G., Fairbanks, R.G., and Mountain, G.S., 1987b: Tertiary oxygen isotope synthesis, sea-level history, and continental margin erosion, *Paleoceanography*, 2, pp. 1-19.
- Nicholson, S.E., 1985: Sub-Saharan rainfall 1981-1984, *Clim. Applied Meterol.*, 24, pp. 1388-1391.
- Nickling, W.G., 1983: Grain-size characteristics of sediment transported during dust storms, *Sed. Petrol.*, 53, pp. 1011-1024.
- Parkin, D.W., 1974: Trade winds during the glacial cycles, *Proc. Royal Soc. London, A*, 337, pp. 73-100.
- Parkin, D.W., and Padgham, R.C., 1975: Further studies on trade winds during the glacial cycles, *Proc. Royal Soc. London, A*, 346, pp. 245-260.
- Parkin, D.W., and Shackleton, N.J., 1973: Trade wind and temperature correlations down a deep-sea core off the Saharan coast, *Nature*, 245, pp. 455-457.
- Parrington, J.R., Zoller, W.H., and Aras, N.K., 1983: Asian dust: Seasonal transport to the Hawaiian Islands, *Science*, 220, pp. 195-197.
- Pisias, N.G., and Rea, D.K., 1988: Late Pleistocene paleoclimatology of the central Equatorial Pacific: Sea-surface response to the southeast trade winds, *Paleoceanography*, 3, pp. 21-37.

- Prospero, J.M., 1981a: Arid regions as sources of mineral aerosols in the marine atmosphere, *In: Pewe, T.L., Ed., Desert Dust: Origin, Characteristics and Effect on Man*, Geol. Soc. Am. Special Paper 186, Boulder, CO, pp. 71-86.
- Prospero, J.M., 1981b: Eolian transport to the world ocean, *In: Emiliani, C., Ed., The Sea*, Vol. 7 (The Oceanic Lithosphere), John Wiley & Sons, New York, pp. 801-874.
- Prospero, J.M., and Nees, R.T., 1977: Dust concentration in the atmosphere of the equatorial North Atlantic; possible relationship to Sahelian drought, *Science*, 196, pp. 1196-1198.
- Prospero, J.M., and Nees, R.T., 1986: Impact of North African drought and El Niño on mineral dust in the Barbados trade winds, *Nature*, 320, pp. 735-738.
- Prospero, J.M., Glaccum, R.A., and Nees, R.T., 1981: Atmospheric transport of soil dust from Africa to South America, *Nature*, 289, pp. 570-572.
- Pye, K., 1987: *Aeolian Dust and Dust Deposits*, Academic Press, London, 334 pp.
- Rea, D.K., and Bloomstine, M.K., 1986: Neogene history of the South Pacific trade winds: Evidence for hemispherical asymmetry of atmospheric circulation, *Palaeogeog., Palaeoclim., Palaeoecol.*, 55, pp. 55-64.
- Rea, D.K., and Janecek, T.R., 1981: Late Cretaceous history of eolian deposition in the mid-Pacific Mountains, central North Pacific Ocean, *Palaeogeog., Palaeoclim., Palaeoecol.*, 36, pp. 55-67.
- Rea, D.K., and Janecek, T.R., 1982: Late Cenozoic changes in atmospheric circulation deduced from North Pacific eolian sediments, *Mar. Geol.*, 49, pp. 149-167.
- Rea, D.K., and Leinen, M., 1985: Neogene history of the calcite compensation depth and lysocline in the South Pacific Ocean, *Nature*, 316, pp. 805-807.
- Rea, D.K., Leinen, M., and Janecek, T.R., 1985: Geologic approach to the long-term history of atmospheric circulation, *Science*, 227, pp. 721-725.

- Sarnthein, M., Thiede, J., Pflaumann, U., Erlenkeuser, H., Fütterer, D., Koopmann, B., Lange, H., and Seibold, E., 1982: Atmospheric and oceanic circulation patterns off northwest Africa during the past 25 million years, *In: von Rad, U., K. Heinz, M. Sarnthein, and E. Seibold, Eds., Geology of the Northwest African Continental Margin*, Springer-Verlag, Berlin, pp. 545-604.
- Sarnthein, M., Tiedemann, R., and Pflaumann, U., 1987: Dust record of the late Neogene and Quaternary paleoclimate and Paleometeorology in the south Sahara, *Paleoclimatology and Paleometeorology, Present and Past Patterns of Global Atmospheric Transport*, Kluwer Pub. Co., Dordrecht, this volume.
- Schramm, C.T., 1989: Cenozoic climate variation recorded by quartz and clay minerals in North Pacific sediments, *In: Leinen, M., M. Sarnthein, and H. Chamley, Eds., Paleoclimatology and Paleometeorology, Present and Past Patterns of Global Atmospheric Transport*, Kluwer Pub. Co., Dordrecht, this volume.
- Schramm, C.T., and Leinen, M., 1987: Eolian transport to Hole 595A from the Late Cretaceous through the Cenozoic, *In: Menard, H.W., J.H. Natland, T.H. Jordan, J.A. Orcutt et al., Init. Repts. DSDP, 91: Washington (U.S. Government Printing Office)*, pp. 469-473.
- Schutz, L., Jaenicke, R., and Pietrek, H., 1981: Saharan dust transport over the North Atlantic Ocean, *In: Pewe, T.L., Ed., Desert Dust: Origin, Characteristics, and Effect on Man*, Geol. Soc. Am. Spec. Paper 186, Boulder, CO, pp. 87-100.
- Stein, R., 1985: The post-Eocene sediment record of DSDP Site 366: Implications for African climate and plate tectonic drift, *In: Kennett, J.P., Ed., The Miocene Ocean: Paleoceanography and Biogeography*, Geol. Soc. Am. Memoir 163, Boulder, CO, pp. 305-315.
- Stein, R., and Robert, C., 1985: Siliciclastic sediments at Sites 588, 590 and 591: Neogene and Paleogene evolution in the southwest Pacific and Australian climate, *In: Kennett, J.P., C.C. von der Borch et al., Init. Repts. DSDP, 90: Washington (U.S. Government Printing Office)*, pp. 1437-1454.
- Tsoar, H. and Pye, K., 1987: Dust transport and the question of desert loess formation, *Sedimentology*, 34, pp. 139-153.



- Windom, H.L., 1969: Atmospheric dust records in permanent snowfields: Implications to marine sedimentation, *Geol. Soc. Am. Bull.*, 80, pp. 761-782.
- Windom, H.L., 1975: Eolian contributions to marine sediments, *Sed. Petrol.*, 45, pp. 520-529.
- Woodruff, F., Savin, S.M., and Douglas, R.G., 1981: Miocene stable isotope record: A detailed deep Pacific Ocean study and its paleoclimatic implications, *Science*, 212, pp. 665-668.
- Zhang, D. 1984: Synoptic-climatic studies of dust fall in China since historic times, *Scientia Sinica*, 27, pp. 825-836.

**SECTION 7.**

**REPORTS AND RECOMMENDATIONS OF WORKING GROUPS**

## DUST FORMATION, INJECTION, AND CONTINENTAL ARIDITY

**W. Nickling, Chair**

A. Brazel, D. Gillette, N.J. Middleton, K. Pye, P. Rognon, and G. Tetzlaff

### 1. SCALES OF STUDY REQUIRED

Those scientists studying the mechanisms of dust production and injection and their relationship to aridity found a need for two scales of studies of these processes — fine-scale point source studies and broad-scale studies applicable to receptor-type models. Fine-scale point source studies, which are presently being made by geomorphologists, are necessary to understand the type of material which is being generated and injected into the air and the details of the climatic conditions which control that generation and injection. The second scale of studies necessary in the future are broad-scale, receptor-type models which can be translated into formulations for use in global circulation models. Although the group felt that the overall direction of present studies of dust formation and injection is appropriate, they felt that expansion of their studies and a few changes of emphasis would be useful to link their work to that of other scientists studying dust transport and deposition. They also emphasized that some of this work should be co-operative with other groups.

### 2. FINE-SCALE STUDIES

Among the specific types of local sources studies that need to be considered for the future are those which would determine threshold velocity of transport and the distribution and controls on rates of particle size formation. Tracers of specific sources, including mineralogy (e.g., clay assemblages) and chemistry (e.g., rare earth and isotopic studies) will be important. The decay function for size and flux should be determined from the size distribution of particles and aggregates at the source and the particle concentration along the transport path. The temporal and spatial variability in these parameters will also be important — especially to modelers and

paleoclimatologists. Such studies should include a wide range of textural, surficial, and morphological conditions. Erosivity factors within a landscape — exposure to wind energy, etc. — should be studied as well as erodeability. Another broad category of studies which are very important to our understanding of dust injection and generation at this scale are studies of the effects of vegetation on dust production. This information is necessary before we can understand the processes responsible for generation of dust at local and regional levels and how the injection processes act on those sources.

### **3. BROAD-SCALE STUDIES**

In addition to understanding the localized factors which influence dust generation and transport, it will also be necessary to develop models for the dust generation and injection at the synoptic scale that can be used in mesoscale and global circulation models.

### **4. INTERACTION WITH OTHER GROUPS STUDYING TRANSPORT AND DEPOSITION**

In order to provide the information necessary to incorporate realistic dust transport into atmospheric models, it will be necessary to make more detailed studies of the methods by which fine-grained aerosols are injected into the atmosphere. These particles travel great distances at high altitude. Their fallout behavior is generally modeled on the basis of Stokes' Law settling, yet we know that this conceptualization is not appropriate. Thus, additional studies of the setting or fallout behavior of small particles is necessary.

The transport of large particles is poorly understood. Terrestrial investigations suggest that they are aggregates. The generation and injection of aggregates is poorly known and will require further study as well.

The group believes that there is an urgent need for a closer link between geologists studying the deep-sea record of eolian deposition with those studying the continental record of dust deposition. The loess record on land is a great resource, but its correlation with the deep-sea record is poor at present and should be improved. There is also a need for geologists to develop multiple source hypotheses for eolian deep-sea sediments.

The conference demonstrated that there has been too little information exchange between groups studying present-day processes and those studying the geologic record. Better communications between the groups and cooperative projects will be necessary, starting at the objective development stage.

## DUST TRANSPORT AND TRANSPORT MODELING

J. Merrill, Chair

R. Arimoto, G. Bergametti, S. Joussaume, S. Thompson, and D. Westphal

### 1. INTRODUCTION

The techniques used for studying and modeling dust transport range from combining observations with event-specific meteorology to climatological general circulation modeling. It has become possible to use regional or even global-scale, numerical models to simulate eolian transport. A careful reading of the papers presented in the session will reveal that much remains to be done; however, as many of the techniques employed are *ad hoc* and are based on experience or compromise, not on first principles.

In our discussion we focused on coupling findings to recommendations. We chose not to set priorities on our recommendations, but have ordered them to follow the findings. The work of the discussion group benefitted from the comments of several participants who had presented work in other sessions at the workshop.

### 2. THE ROLE OF AEROSOL PARTICLES IN CLIMATE

Eolian dust is a potent indicator of climate change, and reconciling the geological record of dust deposition with theories and models of climate is a challenging, but rewarding effort. Climate can be influenced by dust and by both radiative processes; such as, redistribution of heating in the atmospheric column and by microphysical processes as nucleation. Modeling these factors is at present difficult, but the small amount that has been done has yielded tantalizing results. Because the resultant climate depends upon so many factors, this work impinges upon climate prediction problems of obvious importance to society.

**Recommendation:** Fundamental studies on the role of aerosol particles in the climate system must continue. Sensitivity studies of the various factors which control climate should continue, but the ultimate goal of having as many parameterizations as possible based directly on first principles should not be forgotten. Radiation budget studies should be expanded to explicitly cover the processes and role of mineral aerosols.

### 3. THE PROCESS CONTROLLING AEROSOL GRAIN SIZE

The links between the sediment record and the climate are complex, especially the factors related to particle size. The limited correlation between the average grain size in the sediment and the transporting wind speed is indicative of how far we are from a complete understanding of the problem. Observations of ultra-giant particles thousands of kilometers away from sources remains a perplexing problem.

**Recommendation:** It will be necessary to use several kinds of tools to develop a quantitative model of the processes controlling size distribution of aerosol particles. Many observations of size distributions have been made in the air, fewer in deposition samples, and fewer still in the water column. An assessment must be made of the limitations of these observations (biases in size sampled, representativeness of samples, for example). More fundamentally, as many as possible of these data should be synthesized into estimates of the mass flux as a function of particle size. It will then be a natural step to employ both General Circulation Models and mesoscale meteorological models to study the relationship between the climate and the particles (i.e., to refine the treatments of the source, transport, and deposition to best simulate the observations). It appears that a limited effort addressing the morphology (i.e., aerodynamic characteristics) of ultra-giant particles may be justified.

### 4. THE PROCESSES CONTROLLING DUST MOBILIZATION AND UPLIFT

The present-day climate is a suitable system for study of parts of the paleometeorology and paleoclimatology problems. In particular, the present seasonality in dust mobilization and transport is significant, although variable from region to region. Among the largest source areas, Africa shows seasonal variation in the transport path, while Asia shows

seasonal variation in the source strength. There have been large variations in the mass accumulation rate of eolian sediments in the past varying, for instance, with the glacial-interglacial cycle.

Recommendation: Study of the mobilization and uplifting of mineral dust using modeling techniques should continue, perhaps focused by the preparation of comprehensive test cases chosen from well-observed, large-scale events. High resolution models with event-specific meteorology are an essential component of such studies. For global and climate scale work, continued development of parameterizations for lower resolution models is needed. It is important to continue to refine our knowledge of the distribution of eolian sediments, making quantitative estimates of the rates and grain-size distributions wherever possible.

## 5. DUST TRANSPORT EVENTS

The transport events are sporadic and, in general, cover a wide vertical range, especially in the cases of very long-range transport. Individual dust outbreaks generally include widespread sources, so the particles deposited come from different places and times.

Recommendation: Further study of the types of transport patterns encountered in various regions is needed. Especially important for climate studies are programs which cover large areas and long periods of time, e.g., an entire ocean basin over a decade or so. It is important to be able to estimate the frequency of events and their average paths (including both the mean and the variance). Technique development work for satellite remote sensing of mineral aerosol concentrations should continue.

## 6. DEPOSITIONAL PROCESSES

The deposition processes play a critical role in building the sediment record. Because the individual transport events are dominated by removal, which is highly localized, it is difficult to relate current observations to the sediment record. Too little is known about the processes of removal, including factors such as the region in the vertical over which removal takes place, the evolution of the ambient size range of the particles during precipitation events, and the spatial scales over which such events are active.



Recommendation: We encourage comparative studies of the differences between total deposition and wet-only deposition. Also, using such remote sensing techniques as LIDAR, we encourage studies of the vertical distribution of particles far from the source region. Where possible, it would be desirable to have size distributions of the particles both in the air and in the deposition.

## DUST COMPOSITION AND FACTORS CONTROLLING IT: EVIDENCE FROM AEROSOLS AND SEDIMENTS

**G. Tetzlaff, Chair**

R. Arimoto, G. Bergametti, G. Coude-Gaussen, G. A. d'Almeida, G. Eglinton, F. Grousset, L. Schütz, F. Sirocko, and L. Tomadin

### 0. GOALS

The goals of the interaction between this group of scientists and those working in paleoclimatology and paleometeorology were: 1) to contribute to the understanding and development of methods of determining the shape and nature of particles that are transported by winds, 2) to develop methods which will allow paleoclimatologists to trace sedimentary material back to its source area and to describe the modifications it underwent on its transport path, and 3) to quantify mass fluxes of individual components being transported today — either chemical, mineralogical, or biogenic.

### 1. AEROSOL SAMPLING

One of the most important types of data which could be collected to enhance paleoclimatic interpretation is the effective diameter of particles. The sampling techniques that were described in the various presentations of the workshop have resulted in the collection of valuable data. However, the dust composition working group believes that only extreme care can produce the high quality data necessary for analysis of climate variation. A more systematic and extended effort is necessary to provide an understanding of effective diameter data necessary to evaluate transport mechanisms. The group felt that more emphasis should be placed on specific types of information about effective diameter which are felt to be lacking. One of these is vertical profiling of particle concentration and effective diameter. Such studies should include collection of air samples by aircraft as well as ground- and aircraft-based LIDAR techniques. We need to collect such data from the surface up to an altitude of several kilometers.

Quantitative satellite measurements combined with inversion techniques for the analysis of data should also be used. Continuous sampling should be carried out wherever possible.

## 2. SEDIMENT SAMPLING

In sampling sediments for comparison with atmospheric aerosol, there are several important problems which need to be considered. The difficulty of dating the sediments accurately is inherent to sediment studies and needs careful consideration in all interpretations; indications of the error in age estimates should be included in all reports of sediment studies.

Sediment samples average the aerosol in time and space, and extreme care must be used in comparing these data to those from the present-day mineral aerosol. Nonetheless, there are several potential sources of information about mineral aerosol which were discussed by the speakers at the workshop:

- size distribution and optical properties of mineral dust and source soil material;
- mineral composition and micromorphological aspects of size-fractionated material;
- chemical composition of mineral aerosol including: major elements, trace elements (and rare earths), isotopic composition, radionuclides, molecular components;
- biogenic components of aerosols; such as charcoal, pollen, phytoliths, and freshwater diatoms;
- other biogenic components; such as biochemical markers; and
- radon.

To extract meaningful climatic and paleoclimatic information from the available dust samples and eolian sediments generally requires the application of more than one of the methods described above. One of the shortcomings of many studies is that they rely on data of a single type. The members of the working group strongly emphasize that a combination of methods will bring considerable progress.

There are a great many existing samples of mineral aerosols and of sediments. Although efforts to access these existing sample archives should be supported, many studies will require the collection of new samples from particular locations or new types of samples. The value of these samples can be substantially enhanced if they are collected with some consideration for the potential types of additional analyses that could be done (see above). Whenever possible, scientists in other subdisciplines of atmospheric and paleoclimatologic science should be consulted about the sampling strategies in order to allow the optimum mix of analytical techniques and provide key climatic information.

### **3. IMPORTANT REGIONS FOR STUDY**

There are two regions that the group believed to be particularly worthy of further study of dust composition and controls on the composition. The first is the Sahara, which is the main source of airborne dusts in the world. The study of long distance transport from this region, particularly that affecting Europe and North America, will teach us a great deal about many atmospheric processes. The second region is the southern hemisphere, which has not been studied sufficiently. The composition of material transported to and within the southern hemisphere is poorly known, but is essential in order to understand the record of mineral aerosol preserved in Antarctic ice cores.

## MODELING ATMOSPHERIC CIRCULATION IN THE PAST

**J. Kutzbach, Chair**

S. Joussaumè, R. Newell, and D. Westphal

### 1. INTRODUCTION

We are at the beginning of an exciting period of advances in modeling that, in combination with observational studies, will lead to major improvements in our understanding of climate processes (with emphasis here on aerosol aspects) and significant tests of the accuracy of climate models. The presentations at this workshop emphasize the aspects of this association between observations and models that involve atmospherically transported material.

### 2. CURRENT PALEOCLIMATE MODELING STUDIES WITH GENERAL CIRCULATION MODELS (GCMs)

Paleoclimate modeling studies of the last glacial maximum (around 18,000 yr. BP) have been completed by several general circulation modeling groups (in Great Britain, France, Germany, and the United States). Model studies with changed orbital forcing are also available for periods such as 126,000 yr. BP and 9000 yr. BP (experiments in Great Britain, France, and the United States). These simulations provide "first estimates" of changes in climatic conditions that may have influenced the source, transport, and removal of aerosol. For example, we heard evidence at the meeting of changing midlatitude midcontinent aridity and changing tropical monsoon circulations associated with orbital forcing (J. Kutzbach) and of the patterns of glacial maximum "dust climatology" from the GCM studies of S. Joussaume. Her model included explicit processes for dust sources, transports, and removals. The output from these experiments can now be used to compare with field evidence of sources, sinks, and transports in the past — such as that presented at the workshop by N. Petit-Maire, J. Petit, and M. Leinen.

### 3. IMPROVED PARAMETERS IN GCMs

The work of S. Thompson and S. Schneider showed major progress in adapting the NCAR GCM to include processes of interactive aerosol transport, radiative transfer, scavenging, and removal. Similar work is associated with S. Joussaume's model. Many field studies are needed to improve parameterization of source mechanisms (e.g., relation of dust flux to wind speed, etc.), transport (relation of size distribution to wind speed, etc.), and radiative properties. Several such studies were presented at the meeting. S. Joussaume's model also includes provision for  $O^{18/16}$  isotope "tracking".

Another encouraging development that was apparent from presentations at the workshop is that atmospheric GCMs are being coupled to ocean models and to improved models of soil moisture and biosphere processes. These more complete models of the earth system are essential for dealing with the full range of climate processes — including aerosol processes. For example, A. Juillet-LeClerc illustrated the response of diatoms to upwelling off the coast of California, which is a measure of trade wind intensity. With an ocean-atmosphere coupled model, it may be possible to make quantitative estimates of the wind changes necessary to cause various rates of upwelling. This type of work is useful for recent periods like the past one to three thousand years as well as for the more distant past. Past wind estimates are a valuable adjunct to temperature in understanding past climatic patterns.

### 4. MODEL VERIFICATION

Observational studies of changes in aridity and moisture can be compared with paleoclimatic simulations and thereby help to verify the accuracy of land surface/vegetation parameterizations. This type of work should be encouraged. Given that 20% of the earth's surface is covered by water, the marine sediment record of aerosols (and much else) is extremely important for analyzing the state of the climate at any particular time. Do the positions and strength of the jet streams, storm tracks, the subtropical highs, the ITCZ, and the Tropical Easterly Jet change through time? Eolian records provide many examples to answer these questions, and as pointed out by R. Newell, they can serve the additional critical role of helping to diagnose possible changes in ocean circulation and ocean heat transport.

Professor Newell also emphasized the importance of having a good estimate of volcanic activity through time because of the sensitivity of climate to the presence of volcanic aerosol. Once a comprehensive dust transport model has been completed (like those discussed by Joussaume and Thompson), it should be possible to apply it to volcanic dust as well as to desert dust and loess. This should be helpful in interpreting the marine-core and the ice-core measurements. Such models can be calibrated by measurements of isotope ratios in aerosols (such as the Nd, Sr, and Pb ratios discussed by Grousset, which allow discrete areal sources to be identified ranging from 1000 MY rock formations to 20th century lead in gasoline).

## 5. NESTED MODELS

Papers by Westphal and Tetzlaff illustrated the power of more detailed treatment of the atmospheric dynamical, aerosol, and hydrologic processes on fine spatial grids and for limited areas. With finer grid resolution, it is possible to simulate the detailed processes of injection, transport, and removal of aerosol more accurately. Their models were applied to W. Africa. The availability of nested models to study regional problems in many other areas could significantly improve the "match" between detailed observational evidence and model output. This type of work should also be encouraged (including the difficult problems of matching the global GCM variables to the nested variables along the lateral boundaries of the fine-mesh model).

## 6. MODEL/MODEL COMPARISON

Different GCMs produce somewhat different results for the last glacial maximum and for 9000 yr. BP, for example. It is important to make plans to compare the models with each other and with observations. This would most likely help in finding the best parameterizations.

## 7. COMPUTER TIME AND PEOPLE TIME

The challenge of making long model runs with coupled models requires very significant super computer resources. This problem is heightened by the fact that we must entertain various hypotheses for the climatic forcing (orbital effects, uplift and plate effects, feedback effects of aerosol, CO<sub>2</sub>, etc.). We must also make long runs to test parameterizations.

The task of making the runs and making detailed comparisons with observations and other models will require significant resources of computer time and people time as well as talent.

## 8. MODEL VALIDATION

The encouraging degree of agreement between some observations and some model results (for example, evidence for changes in monsoons 6-9 KY BP and 126 KY BP; the overall Milankovitch/ice age coupling) points to the fact that present generation GCMs are "doing something right". On the other hand, we can still point to significant areas of disagreement. In addition to the intellectual excitement of understanding the past, additional work on model/data comparisons should lead to further improvement in model accuracy. This could in turn have practical applications, such as increasing our confidence in the reliability of doubled CO<sub>2</sub> scenarios.



## **INFERENCES FROM THE SEDIMENTARY RECORD: LOESS, ICE CORES, AND OTHER LAND EVIDENCE**

**J. Maley, Chair**

A. Bücher, A. Issar, J. Petit, N. Petit-Maire, and A. Wagenbach

### **1. INTRODUCTION**

There are many diverse records of eolian activity on land which can be used to study climate change including loess, lake sediments, the dust in glacial ice, and continental sedimentary deposits. While deposits representing the whole of geologic history are available for study, the workshop focussed on Pleistocene eolian material because it can be related to the factors controlling dust composition and injection and transport most reliably. The picture emerging from such studies of the atmospheric circulation is one of great complexity.

### **2. EVIDENCE OF CLIMATE CHANGE OVER THE LAST THREE MILLENNIA**

There were several examples presented at the workshop of research techniques appropriate for study of millenium-scale climate variation. A. Issar presented stratigraphical and archaeological data for the transition of the Roman-Byzantine to Arab periods near the middle first millenium AD. All the data show a process of desertification, which was triggered only by climatic changes. These changes were explained by a northward movement of the ITCZ and of the East African Monsoonal Belt, but it is also possible to consider only an increase in the activity of tropical depressions which are associated with the dynamics of the Subtropical Jet Stream.

A. Wagenbach reported results from the "Monte-Rosa" Massif in the Alps, at Colle Gnifetti, 4500m A.S.L., where the total impurity content of snow from an ice core drilled in one of the glaciers is dominated by mineral

dust — mainly Saharan dust. The record probably extends back to the beginning of the last millenium and may reflect the long-term variation of the south-north transport of subtropical air masses to the Alps.

A. Bücher presented a statistical analysis of 715 outfall events of mineral dust and mud showers of Saharan origin in the Pyrenees covering the last three millenia. The observations, extracted from various historical literature, show that 61% of the events occurred during the five-month interval from January to May.

### 3. EVIDENCE OF CLIMATE CHANGE OVER GLACIAL TO INTERGLACIAL CYCLES

The geologic record from land also holds great promise for understanding climate change between glacials and interglacials. One of the most exciting studies discussed at the workshop was the dust record over the last climatic cycle in Antarctica (Vostok ice core). J. Petit and his colleagues have found that the maximum amplitude of temperature change, ca. 11°C based on the deuterium record, occurred through the large 100 KY glacial-interglacial oscillation. The Vostok record displays an increase in the concentration of dust (up to x20) during the coldest climatic periods. This large increase is attributed to a larger extension in global tropical aridity during the cold periods, coupled with a higher efficiency of the atmospheric circulation.

At the opposite climate regime, N. Petit-Maire presented sediment records for the last 150,000 years from the Sahara which document periods for which there were large lakes in this presently arid region. A paleolake with highest lake levels at 130,000 BP was documented in an area of Libya around 27°30'N, which is presently hyperarid. It covered 2000 km<sup>2</sup>. At Tarfaya in Morocco and at Fuerteventura Island (28°N), which are hyperarid Saharan areas, well-defined layers interrupt eolian deposition at 15,000 BP, 12,500 - 13,500 BP, and from 10,500 - 10,000 BP on. The endoreic, hydrologically-isolated depression of Taoudenni (Mali, 22-23°N, 3-4°W), one of the most desartic areas in the Sahara, shows the following sequence in permanent lakes: 9000 - 8300 BP; 8300 - 6700 BP, climatic optimum with weak seasonality (Sahel limit near 23°N - presently at 17°N); 6700 - 4500 BP, end of lakes, aridification and eolization.

J. Maley presented palynological and biogeographical results documenting the history of the African Rain Forest during late Quaternary. During the last great arid and cold phase (ca. 18,000 BP), the forest

fragmented and remained in three isolated refugia: the Upper Guinea, the Cameroon-Gabon series, and the eastern Zaïre. At the time of fragmentation, montaine biotopes spread to low altitude. These phenomenon are related to aridification of the climate and to lowering of the temperatures. These changes can be explained in terms of an interaction between tropical Atlantic upwellings and cloud formation. In particular, stratiform cloud cover generated by the cold Atlantic waters (maximum annual lowering of 8° to 9°C) caused a cooling and drying of the adjacent land areas.

#### 4. DISCUSSION

While there do appear to be global shifts in aridity with glacial periods having expanded arid regions, especially in the tropics, the presentations at the workshop emphasized the variability of local response and the necessity for putting local studies into regional and global frameworks. This will require new efforts to make temporal correlations between different types of geological information from disparate areas. The potential information from integrated studies using many indicators of atmospheric circulation is very great, however. For example, many of the geological indicators of climate in the circum-Sahara region are sensitive to the position of the Intertropical Convergence Zone: the sediment records of paleolakes in the Sahara, the pollen record of the African Rain Forest south of the Sahara, the geologic record of desertification in the middle East, and the records (both historical and geological) of Saharan dust transported north toward Europe and west toward the Atlantic Ocean.

Interdisciplinary syntheses can reinforce inferences about specific climate and transport phenomena like ITCZ movement, which would be tenuous if based on a single line of evidence. In addition, syntheses of many such types of data from a region are necessary to document the overall relationship between atmospheric circulation and climate change.

#### 5. RECOMMENDATIONS

The working group on inferences from the terrestrial sedimentary record recognized that much of our work is done in areas which are threatened with major environmental changes due to global climate change in the future. We believe our aim should be to understand the relative parts played by natural climatic changes and anthropogenic action in the observed process of aridification and desertification. We call this effort

"Paleoclimatology for Survival". Many of the answers must be found in the near past. While there are key areas (in space) and key periods (in time) that must be studied, we also believe that in order to forecast global evolution in the near future, short cycles may also be important and some effort to determine whether such cycles operating at ~2000-year intervals are present should be made.

### **5.1 Key Isochrons**

In order to understand the regional aspects of climate change, we should study as many types of indicators as are possible at several important times in the past. These include: 18 KY, 9 KY, 6 KY, 3-5 KY, 2 KY. The last Millennium should also be studied, especially the two major events: the Medieval warm optimum (culminating 10-12 century AD), and the Little Ice Age, (culminating ca. 17 century AD).

### **5.2 Key Areas**

Several areas are very important for syntheses based on existing documents and new field research. The key areas for study which would result in a coherent picture of tropical transport phenomena are the Eastern Monsoon regions from South China and India to tropical Africa and the Amazon region of South America. The quasi-periodic El Niño - Southern Oscillation phenomena also has an extremely important effect on tropical meteorology and hydrology, which is probably reflected in atmospheric circulation and transport. In order to understand the impact of this phenomenon with the persistent equatorial atmospheric transport effects, we would need to study the arid and semi-arid regions of South America (Bolivia, Peru, Argentina, Chile) as well.

### **5.3 Methods**

Changes in the climatic belts at the given isochrons must be studied in new syntheses from multidisciplinary sources (geology, hydrology, palynology, paleoenvironments, etc.). Their effect on human and cultural evolution must be considered.

The interaction between groups has been a major strength of this NATO Conference. However, we feel that special focus should be directed toward sampling of rain (chemistry, isotopes), dust, and pollen along special storm trajectories; palaeolacustrine and palaeoenvironmental research in

the key areas/key isochrons defined above, and variations of sea-surface temperature in relation with continental climatic change — the interaction of the clouds.

## REPORT OF THE GROUP STUDYING: INFERENCES FROM THE MARINE SEDIMENTARY RECORD

**M. Sarnthein and M. Leinen, Co-Chairs**

L. Dupont, L. Heusser, H. Hoogheijmstra, A.J. LeClerc, E. Pokras, D. Rea, C. Schramm, B. Stabell, and R. Tiedemann

### 1. INTRODUCTION

The group concerned with paleoclimatic and paleometeorological inference from the marine sedimentary record emphasized the diversity of sedimentary indicators of atmospheric processes in their presentations. These include the mineral and chemical composition of dusts, their size and rate of accumulation, the composition of biological material from the continents (such as pollen and freshwater diatoms), as well as proxy indicators of atmospheric circulation (e.g. isotopic and microfossil evidence for sea surface temperature changes related to upwelling). The group believes that the range of inference from such components will be substantially broadened, and the quality of the inferences improved by new research into the nature of modern climate processes, the provenance of eolian continental material, the stratigraphic links between continental and marine eolian deposits, and by climate modeling.

### 2. MODERN PROCESSES

The greatest concern of the scientists who study the marine record of eolian sediments was that our inadequate understanding of modern processes greatly hinders the interpretations that can be made from the records. The single most important concern was that our understanding of the processes of dust and pollen transport be improved. We need to know the long-term average of dust transport tracks and the seasonality of events. Particle aerodynamics of transported materials, from small clay flakes to "giant" quartz and feldspar grains to pollen, vary greatly. These particles, which are deposited in the deep sea, each provide a different type of information about atmospheric transport, but we are presently unable to

interpret the information. There is particular concern to obtain a quantitative relationship between size of particles and wind velocity. Such research may require tropospheric sampling schemes.

The present climatic regime is becoming reasonably well understood, but more information on the nature of teleconnections, especially those relating atmospheric, sea-surface (i.e. upwelling), and terrestrial (aridity, humidity) variability will be necessary for a complete interpretation of our records. For example, the climatic control on vegetation and pollen production is poorly understood. We also do not know whether eolian input is an important source of oceanic micro-nutrients.

### **3. PROVENANCE**

Sedimentologists are often uncertain about the source of the material recovered in marine and in ice cores. In the case of deep-sea sediments, the eolian record may also be overprinted by the marine sediment subgroup urges provenance studies based upon the nature of recovered materials — their mineralogy, geochemistry, or pollen content. These compositional clues need to be linked in a quantitative manner to continental regions of dust generation. We note that the actual tracers are probably size dependent as the finer grains have a different composition than the coarse ones.

### **4. SAMPLING STRATEGIES FOR MARINE SEDIMENTS**

The nature and causes of environmental variability must be resolved on three timescales of change — tectonic timescales of 0.5my and longer, orbital time scales of 10 to 500ky, and oceanic timescales of a few thousand years and less. There are significant concerns about the seasonality of climate and atmospheric transport at these timescales and whether seasonality changes with time. Several sampling strategies will be required to discover the nature of eolian and climatic variability through time. First, we need long, high-resolution records from climatologically and oceanographically sensitive areas to continue studies in the frequency domain. Second, the strategy of obtaining multi-site transects across important climatic zones will allow us to study lateral variability through time. Finally, areal mapping of carefully chosen time horizons, such as the Emian interglacial (125ky), will pay important conceptual dividends and provide input useful to computer modelers. These strategies can be applied to the particular concerns of the marine sedimentary group. These include

improving the record of eolian deposition in the southern hemisphere, which is especially important to understand the mineral aerosol record in Antarctic ice cores.

The group was also concerned about mid- and long-distance correlations of paleowind phenomena from ocean to ocean and between the hemispheres. Work presented at this meeting suggested that various atmospheric phenomena and responses to climate change have important regional variations.

## 5. LAND RECORDS AND LAND-SEA LINKS

Complementary records from the continents are essential to a complete understanding of climate and climate change. These records may come from lakes and ice caps, loess deposits, etc. Furthermore, these continental records must be linked to the deep-sea record — a problem often complicated by stratigraphic differences. It has been particularly difficult to piece together long-term records from the continents.

Time slice mapping on land will continue to be an important aspect of environmental reconstructions for many times in the past. It will be difficult to achieve this on land, but the effort will be rewarding.

The effects of oceanic phenomena on adjacent or removed continental environments requires a particularly intimate linking of land and sea records. Other, little-used tracers may be important in this particular effort; for example, charcoal.

## 6. NEW ANALYTICAL TECHNIQUES

Many new techniques may provide additional information from the sedimentary record. Molecular stratigraphy is an example. The method involves solvent extraction of sediments and direct quantification of selected lipids (solvent-soluble carbon compounds) by chromatography-mass spectrometry. Organisms produce a wide variety of lipids, some of which (known as biomarkers) are specific to order, class genera, or even species. These biomarkers may survive, intact or modified, death or dissolution of the organism and hence provide a signal in the sedimentary record. Eolian dusts are known to carry biomarkers recognizable as the plant wax components of vascular plants. Hence, profiling these compounds downcore can provide an independent record of terrestrial and



eolian input. Other molecules provide indications of fluvial input (lignin), marine productivity (e.g. dinoflagellate blooms) and of sea-surface temperatures.

The approach has been tested in parallel with  $\delta^{18}\text{O}$  data in cores off NW Africa and stands ready for detailed testing in various ways; for example, as a means of typing dust sources and changes in composition during transport, deposition and incorporation into sediments. It will be particularly important to link it with other studies of mineral particles and organic particles. Sampling should include deflation sites, aerosols over transit routes, water column particulates, and bottom sediments and cores.

Of special interest (in terms of cores) would be deposition at sites of highly anoxic bottom sediment conditions having little or no bioturbation. Such cores will afford the highest quality record of seasonal and annual time resolution; hence, will provide the ability to understand the spectral record. Lake cores may provide the best record for this purpose. Another excellent short-term record is contained within ice cores.

## 7. DATA-MODEL COMPARISON

The marine sedimentological working group recognizes that our understanding of paleoclimatic regimes can be significantly enhanced by application of computer model techniques and strongly encourages that effort.

Many aspects of encouraging cooperation among empirical scientists and computer modelers are matters of communication. Mesoscale and global circulation models require data input as initial boundary conditions and eventually to test model results. Those who construct such models need to communicate their data requirements in terms of spatial or temporal resolution. They must also indicate the most critical sites for data so that those who collect data can invest their effort in the most valuable sites. Those scientists who study the sedimentary record must understand that there are a few critical sites which may be extremely important to determine model reliability.

## 8. LOGISTICS AND CONSTRAINTS

We recognize that there are a number of constraints that tend to impede interactions among investigators and encourage steps that may

reduce the significance of those constraints. Such activities would include intercalibration of instruments that measure similar phenomena, standardization of data formats for storage, retrieval or transmission, etc. These sorts of concerns underlie all interactive scientific endeavors but should not go unmentioned.



<i>African rain forest</i>	
climatic changes in	585-616
<i>African Turbidity Monitoring Network (ATMN)</i>	319
<i>Aggregates</i>	
wind-erodible (formation of)	31-63
sediment, in multiyear ice	475-476
<i>Albedo</i>	
relative to sea ice	475, 479, 481
<i>Alluvial processes in the Sinai</i>	535
<i>Alluvium</i>	11-12, 167, 179
<i>Alpine glacier(s)</i>	
mineral dust record in	543-564
<i>Altithermal</i>	618
<i>American Southwest</i>	
Dust and climate in the	65-96
<i>Andhi</i>	97-132
<i>Antarctica</i>	830, 850
<i>Anthropogenic</i>	133, 161
<i>Arabian Sea</i>	401-433
<i>Arctic Ocean</i>	463-493
<i>Aridity</i>	
continental	3, 16, 861-864
effect of orbital variation	515
environments	3-31, 38, 50, 65-132, 167-184, 311-338, 339-359, 385, 529-532, 543
last phase of, in Africa	601-605
in zone soils	7
paleoclimatic, based upon plant n-alkane distribution	435

<i>Arizona</i>	65-96, 133-166
<i>Asia</i>	721-722, 805-806, 825, 828-832
<i>Atlantic Ocean</i>	
clay mineral flux comparison with Pacific	710
energy flux	498
higher plant lipids in cores from	435-462
particulate flux	842-843, 845-848
salinity	503
transport of aerosols over	385-400
<i>Atmospheric Circulation</i>	665, 734, 741, 841, 844, 848
General Circulation Model (GCMs)	253, 519-521, 618-619, 873-876
Aleutian Low	669
control on energy flux	498
during last glacial maximum	509
Siberian and Okhotsk High	669
<i>Australia</i>	850
<i>Bedding</i>	49
<i>Biogeographical factors</i>	637-661
<i>Biological particles as tracers</i>	302
<i>Bottom Current Deposition</i>	
Pacific Ocean	826
<i>Budgets</i>	
of water vapor and liquid water	193-194
<i>Bulk accumulation rates</i>	408-412
<i>Calcium Carbonate</i>	7, 31-32, 38-39, 57, 167-179, 408-412
leaching	18
<i>Cements</i>	31, 35, 49, 52
<i>Cenozoic</i>	805-839, 844

<b><i>Chemical</i></b>		
solution		7
weathering		7, 15, 18-20, 31, 34
<b><i>China</i></b>		721, 828, 831, 843
<b><i>Circum-Antarctic Current</i></b>		828
<b><i>Clay and clay minerals</i></b>	33, 49-52, 172-179, 273, 283, 349-353, 693-732,	
		805-839
flux and accumulation rate		700-701, 704-711
pelagic		848
sampling and analysis		695-701, 811-812
spatial and temporal variations	701-713, 717, 721-722, 812-825	
stratigraphy		698-699, 711
wind erosion of clayey-siltstone		47
<b><i>CLIMAP</i></b>		698
<b><i>Climate</i></b>		
changes	3, 14-20, 65-96, 236-238, 435-462, 525-542, 585-636,	
		841-842, 877-881
desert dust and, an investigation using AGCM		253-264
control on dust storms		97-132
effects on by desert aerosols		311-338
glacial-age, in North America		620-621
inferred from pollen		665, 684-685
modeling		713-726
effects of mountain building upon		831
stratigraphy		441-442
<b><i>Clouds</i></b>		
climatic role of, in African rain forest		597-606
<b><i>Colle Gnifetti site, Swiss Alps</i></b>		543-564
<b><i>Colloidal matting/material</i></b>		31, 35, 56, 58
<b><i>Colorado Plateau</i></b>		65-96

	893
<b><i>Compression</i></b>	
fracturing	31
molding	31
<b><i>Convection</i></b>	
in relation to dust storms	102-104
<b><i>Correspondence factor analysis (CFA)</i></b>	348
<b><i>Cracking</i></b>	31
shrink/swell	31, 41, 47-48
<b><i>Cretaceous</i></b>	841, 846, 848, 850
<b><i>Cretaceous/Tertiary (K/T) Boundary</i></b>	841
<b><i>Crushing</i></b>	8
<b><i>Cryoconite holes</i></b>	476
<b><i>Cyclonic transport</i></b>	236-237
<b><i>Dead Sea</i></b>	526, 532
<b><i>Deep sea deposits</i></b>	185-203, 228, 267-280, 353, 435-462, 463-493
<b><i>Deep Sea Drilling Program</i></b> (see also: ODP)	
Leg 92	848
Site 366	846
Site 566	844
Site 578	844
Site 595A	850
Site 598	848
<b><i>Deflation</i></b>	771-778
<b><i>Deflection hypothesis</i></b> (of the jet stream)	627-628
<b><i>Deglaciation</i></b>	481-482

<i>Desert(s)</i>		
aerosol: characteristics and effects on climate		311-338
dust and climate		253-263
sand	3-64, 65-97, 97-132, 133-166, 253-263, 339-384,	525, 564-584
<i>Dessication cracking</i>		33
<i>Diatoms</i>		811, 822
freshwater		771-778, 795-804
methods and analysis		773, 796-798
<i>Dinoflagellates</i>		671
<i>Drying</i>		41-50
<i>Dunes</i>	13, 31-64, 161, 167-168, 182, 340, 526, 529-532, 535	
<i>Dust</i> (see also: Aerosol, Particle)		
absorptivity of		329-332
atmospheric	359-384, 401-434, 549-551, 828	
broad-scale studies of formation, injection		861-863
concentration	209, 211-212, 267-284, 360-361	
characterization and contribution to sedimentation		339-358, 385-434
chemical properties of		372-377, 385-400
deposition rates		227-252, 528, 862, 867
desert, and climate		253-263
dispersal, satellite record of		422
fallout (Saharan)		565-584
injection		861-863
markers in	351-358, 359-384, 385-400, 435-462	
mineralogy		842, 844, 846
mobilization and uplift, processes controlling		865-868
near the ground		167-184
physical properties of		360-371
radiative characteristics of	311, 320-333, 368-369	
regional variability		73-74
storms		97-133, 828, 843
trapped in rock cracks		346-351
with relation to soils		176, 543
with relation to wind energy & soil characteristics		167-184



<i>Dust and climate in the American SW</i>	65-96
<i>Dust composition</i>	167-184, 234-235, 267-310, 339-384, 869-872
elemental isotopes as tracers	385-400
mineralogy	167, 170-184, 234-235, 269-271, 281, 283-302, 341-384, 543-564, 566
size	8-13, 16, 32, 38, 142-149, 159-162, 170-184, 186-187, 281, 287-294, 311-358, 386, 464-465, 528, 551-560
source sediment	11
<i>Dust event tracking</i>	106-120
<i>Dust flux</i>	3, 14-20, 134-136, 150-159, 198, 227-252, 256-257, 515, 543-564, 842-844, 849
effect of seasonality in the past	515
<i>Dust frequencies</i>	73-74
<i>Dust Generation</i>	3-63, 65-184
aeolian deflation (weathering)	4-5, 8-9, 15-17, 49, 167, 360
emission rate	14, 133-166
event sequences	4
fluvial processes	4-5, 8, 10-11, 13, 15-16, 19
glacial erosion	4, 9, 14-16, 19
rate of formation	3, 10, 14, 18-19, 861-863
role of moisture in	82-89
role of weather types in	74-82, 89
soil formation	4
sinks and sources	3-4, 9-10, 12-18, 102, 168, 185-203, 227-252, 254, 267-282, 313-325, 339-384, 401-493, 528, 566
storms	10, 53, 73-82, 97-132, 134, 167, 172, 361, 525, 536
terrain types	10
weathering	4-7, 12, 15-16
<i>Dust lifting mechanism</i>	190-192, 866-867
<i>Dust preservation</i>	4
<i>Dust transport</i>	4, 15-18, 97-132, 146-159, 168, 185-203, 207-283, 311-312, 339-434, 544, 566-584, 861-863, 865-868
and deposition patterns of African dusts	227-252
fluvial processes	4, 5, 8, 10-11, 13, 15-16, 19, 401
modeling long-range, using trajectory techniques	207-226

<i>East African Monsoonal Belt</i> (see also: Monsoons)	525
<i>Easterly Waves</i>	189-192
<i>Electrical double layer</i>	8
<i>El Niño - Southern Oscillation</i>	507
<i>Energy Balance</i> role of wind stress	497-512
<i>Eolian</i> (see: Aeolian)	
<i>Eurasian Arctic sea ice</i>	465-474
<i>Flocculation</i>	31, 35, 55-56, 58
<i>Fluvial Transport</i>	734, 771, 776, 781, 784, 787
<i>Foam</i> lofting and floatation	31, 35, 56, 58
<i>Foraminifera</i>	698
<i>Forest refugia</i> as a result of climatic changes in the rain forest	585-616
<i>Forests and Vegetation</i> Africa Japan	738, 755, 758, 763, 779-781, 783 665-692
<i>Fracturing</i> compression by hydration expansion by salt efflorescence tension	31 33-34 34 31
<i>France</i> Saharan dust fallout in	566-584
<i>Freeze/thaw cycle</i>	50-52, 55, 57, 58
<i>Geochemical significance of African dust deposition</i>	248-249

<b><i>Glaciation</i></b>	3
aeolian deposition in the Arctic Basin, during	477-481
northern hemispheric	846, 850
southern hemispheric	848
<b><i>Glacial</i></b>	
-age climate in North America	621
criteria for selection in ice-core studies	544
cycles, evidence of climate change	878-879
energy flux	508
meltwater, insoluble particles in	551-560
<b><i>Glacier</i></b>	
mineral dust record in an alpine	543-564
<b><i>Gobi Desert</i></b>	97, 126
<b><i>Granular disintegration</i></b>	7
<b><i>Great Basin Desert</i></b>	38
<b><i>Greenland</i></b>	463-493, 831
<b><i>Groundwater</i></b>	
paleo-levels in Israel	533
<b><i>Hawaii</i></b>	843
<b><i>Himalays</i></b>	669, 829
rates of uplift	829
<b><i>Holocene</i></b>	3, 15-18, 168, 351, 385-386, 396, 401-434, 526-532, 536, 585, 588, 606-608, 621, 637, 639-652, 665-692, 844, 850
<b><i>Homogeneity of mineral aerosols</i></b>	233
<b><i>Hydration</i></b>	7, 53, 55, 58
<b><i>Hydrological</i></b>	
systems, climatic changes and their impact on	525-542
<b><i>Hydrolysis</i></b>	7

<i>Ice</i> (see: Sea Ice)	
<i>Ice cores</i>	543-564, 877-881
<i>Icthyolith Stratigraphy</i>	811, 822
<i>India/Pakistan</i>	97-132
<i>Indian Ocean</i> wind-borne deposits in	401-434
<i>Inselbergs</i>	8
<i>Inter-Tropical Convergence Zone</i> (ITCZ)	525-526, 535, 538, 618, 621, 846
<i>Isentropic</i>	210
<i>Insolation</i> effect of differing solar insolation on energy flux	509
<i>Isobaric</i>	210
<i>Isotopes</i> carbon radiocarbon dating distribution of environmental, in Israel's paleo-groundwater Nd and Sr, as tracers of wind transport Oxygen age control paleoceanographic indicator precipitation control	773 734 388-396 527 385-400 408, 554, 671, 676, 733-734, 742, 773, 775, 779, 781, 783, 829 829 532-533
<i>Israel</i> climatic changes in	525-542
<i>Japan</i> flora	665, 717, 721 665-692, 717
<i>Jet Stream</i>	669, 832
<i>Lake Barombi, West Cameroon</i>	585-616

	899
<i>Lake Bosumtwi, Ghana</i>	585-616
<i>Lake levels</i>	515, 526-527, 588-591, 605-607, 623
effect of orbital variations	515
<i>Lake Lisan</i>	526
<i>Laminations</i>	49-50
<i>Lapse rate variation hypothesis</i>	595-596
<i>Last Glacial Maximum (LGM)</i>	253, 258, 479-483, 508-510
atmospheric circulation	508-510, 516
<i>Libya</i>	238
<i>'Little dry season' in the rain forest</i>	601, 607
<i>Lithogenic Sediment Transport</i>	802
<i>Loam</i>	11, 31, 32, 49, 57, 157
<i>Loess</i>	3, 9, 11-12, 14, 17-18, 479, 481, 523, 525-538, 721-722, 877-881
<i>'Loo'</i> (see also: Wind)	97-132, 104-105, 118, 122
<i>Lysocline</i>	848
<i>Magnetic Susceptibility</i>	773
<i>Marine sedimentary record, inferences from</i>	883-888
<i>Mass balance equation</i>	319
<i>Mauritania</i>	97, 124-126
<i>Mechanical disturbances</i>	
by animals	32, 35

**Mediterranean**

deposition patterns of African dust to the	227-252
aeolian dust over the	267-282
fallout of Saharan dust in	565-584
supply of sand to	525

**Mineral(s)**

calcite	176-183
clays (see: Clay)	
dust record in an alpine glacier	543-564
gypsum	176-183, 527-528
mica	176, 351
palygorskite	351-353
quartz (see: Quartz)	
silicates	7

<b>Miocene</b>	805, 822, 826, 828-830, 832, 841, 844, 846, 850
----------------	---

**Models**

for African rain forest	586
for Arctic atmospheric circulation	478
for atmospheric circulation, dust and climate	253-264
for atmospheric circulation in the past	873-876
for atmospheric flow from West Africa	185-203
for climate	619, 630-631
for dust transport	207-264, 865-868
for Israel's paleo-climate	525-542
for localized montane extensions to lower ground	596-597
for source strength of Saharan dust	325

<b>Mojave Desert</b>	35, 65-96
----------------------	-----------

**Moisture** (see also: Precipitation, Water vapor)

flow	193-203
fluctuations	8, 15, 82-89
of soil	10

<b>Mongolia</b>	97, 126-129
-----------------	-------------

<b>Monsoons</b>	78, 85, 124, 194-195, 199-200, 401-408, 514, 536, 621, 637, 652, 665, 669, 686, 694, 786, 796, 801
increase in intensity	514

	901
<i>Mud rain</i>	569
<i>n-alkanes</i>	
as paleoclimatic markers	435-462
<i>NCAR</i>	831
community climate model (CCM)	831
<i>Negev Desert</i>	527-528, 535
<i>Neogene</i>	818, 822, 825, 829, 845-846, 848
<i>New Zealand</i>	850
<i>Nile River</i>	525, 529, 535
<i>North America</i>	
climatic change in	617-636
<i>Orbital parameters</i>	513
precession cycle	514-516
obliquity cycle	516
<i>Ocean Drilling Program</i> (see also: Deep Sea Drilling Program (DSDP))	
Leg 108	846
Leg 114	850
Leg 115	850
Site 662	795-804
Site 664	795-804
Site 658	771-777
<i>Oligocene</i>	818, 830, 841, 848, 850
<i>Opal</i>	
biogenic	848
phytoliths	795-804
<i>Organic material</i>	38-41
<i>Pacific Ocean</i>	693-732, 805-839, 843-844, 847
energy flux	498
mineral aerosol observations in	207-226
plate migration (Cenozoic)	806, 825

<i>Pacific Ocean</i> Continued . . .	
pollen	665-692
salinity	503-507
sedimentation	825-828
<i>Paleobiogeography of afromontane vegetation</i>	594-595
<i>Paleoclimate</i>	
calibrated by satellite images	401
for 18000 years BP	198-200
in the Quaternary African rain forest	585-616
implications from	627, 637-661
from pollen record	779, 786
links with aeolian-derived higher plant	
lipids in sediments	435-462
models with circulation modelling	873-876
model for Israel during historic times	525-542
<i>Paleocene</i>	841, 846, 850
<i>Paleocene/Eocene Boundary</i>	841, 846, 850
<i>Paleogene</i>	818, 822, 833
<i>Paleo-groundwater characteristics in Israel</i>	527-542
sulfate content	527
<i>Paleomagnetic Dating</i>	811, 829
<i>Paleosol</i>	15
from pedogenetically-altered loess in Israel	528
<i>Particle(s)</i>	
angularity	8
biological	302
distribution	474-478
entrainment	11
fluvial transport	734
grain size	832, 843-844, 848, 850
insoluble, in glacial meltwater	551-560



<i>Particle(s)</i> Continued . . .	
morphology	341-345, 354
roundness	8
rates of formation	14
size	8, 10, 12, 16, 32, 36, 142-146, 159-160, 170-183, 186-187, 311-347, 543-564
surface roughness	8
<i>Pedogenesis</i>	18
<i>Pedological</i>	
systems, climatic changes and their impact on	525-542
<i>Pellet formation</i>	33, 474-476
<i>Permeability</i>	6
<i>Plant lipids</i>	
as markers of the marine record and paleoclimate	435-462
<i>'Plateau' boundary</i>	623
<i>Playa</i>	
deposits	11, 19
sediments	12
<i>Pleistocene</i>	9, 17-18, 294, 353, 402, 525-530, 536, 617, 637-639, 652, 665-692, 829, 841, 846, 848
<i>Pliocene</i>	785-804, 808, 828, 841, 847, 848
<i>Pollen</i>	533, 573, 665-692, 733-770, 779-794
as evidence for climatic changes in the rain forests	585-616
fluxes	753-763
sampling and methods of analysis	671, 742, 781
Quaternary fluctuations in the North Pacific	665-692
stratigraphy	
Pacific Ocean	679-680
Atlantic Ocean	742, 779-794

<i>Pollen</i> Continued . . .	
taxa	783
transport mechanisms	784-786
<i>Precipitation</i>	6, 10, 15-20, 46, 78-89, 97, 122-129, 161, 168, 191, 193-197, 247-248, 474, 528, 530-535, 585-616, 623-627, 639, 685-686
<i>Present</i> (see: Holocene)	
<i>Pressure gradient</i>	
in relation to dust storms	104-122
<i>Quaternary</i>	3, 9, 14, 19-20, 385, 585-616, 617, 665-692, 779-794, 818, 830
<i>Quartz</i>	7, 176, 348, 351, 693-732, 805-839
methods and analysis	699-701, 811-812
<i>Q-mode Factor Analysis</i>	713-721
<i>Radiocarbon Dating</i> (see: Isotopes)	
<i>Radiolaria</i>	671, 676, 698, 822, 844
<i>Radiometric Dating</i>	637-661, 811
<i>Red Sea</i>	283-310
<i>Regionalization</i>	
of climatic change in North America	617-636
<i>Regolith</i>	12
<i>Reynolds number</i>	11
<i>River Transport</i> (see: Fluvial Transport)	
<i>Roundness</i>	8

- Sahara/Sahel* 167-203, 227-252, 311-338, 339-358, 359-400, 440, 527, 543-584,  
621, 637-661, 733-770, 779,  
795-804, 842  
drought and relation to atmospheric  
circulation 507
- Saharan Air Layer* (see also: African Easterly Jet) 734, 741, 773, 779,  
781, 783, 786-791
- Salt efflorescence* 19, 31-32, 34, 52, 57-59
- Salt weathering* 5-6, 160
- Sand* 8-13, 31-55, 133-184, 525-532, 535, 574
- Sea/Air Exchange (SEAREX)* 207, 209
- Sea ice*  
aeolian flux, contributions to marine sediments 463-493  
formation and transport 473-474
- Sea of Galilee* 532-533
- Sea level* 532
- Seasonality*  
increase due to orbital variation 509-510
- Sea surface temperature (SST)* 597-606  
interannual patterns 507-508  
during last glacial maximum 509
- Sediment(s)*  
dust over the Mediterranean and its  
contribution to 267-310  
contribution from Saharan dust 351-358  
inferences from, regarding loess, ice cores 877-881  
isotopic tracers of wind transport in 385-400  
marine, inferences from 883-888  
of the Sea of Galilee 532-533  
of wind-borne deposits in the Indian Ocean 401-434

<i>Sediment(s)</i> Continued . . .	
on Arctic pack ice, contributions to marine sediment	463-493
rate, determination of	443
sampling	870-871
<i>Senegal River</i>	784
<i>Shale</i>	
wind erosion of	53
<i>Sheeting</i>	8
<i>Sinai Desert</i>	
paleo-climatic changes in	525-542
<i>Slopewash</i>	18
<i>Socio-economic</i>	
systems; climatic changes and their impact on	525-542
<i>Soil(s)</i>	
contribution to dust	176
derived dust	231, 543
desert	133-184, 339-358
mineralogy	170-176
productivity and aerosol size distribution	313-317
salty	31-65
size (see: Particle, Dust composition)	
texture	12, 37-38, 157-160
<i>Soluble fraction</i>	302
<i>Sonoran Desert</i>	65-96
<i>SPECMAP</i>	676, 742, 773
<i>Spores</i> (see: Pollen)	
<i>Squall lines</i>	190-192, 194-197
<i>Strain energy</i>	8

<i>Subtropical Easterly Jet Stream</i> (see also: Jet Stream)	
variation with orbital change	513-516
<i>Surface films</i>	31, 35, 56, 59
<i>Suspended particulate fraction</i>	302
<i>Swiss Alps</i>	543-564
<i>Synoptic forcing</i>	78
<i>Tectonic Time Scales</i>	841-857
<i>Temperature</i>	
effects of fluctuations in	7-8, 831
increases in air masses over France	566
predicted by plant lipids in paleomarine	
sediments	435-462
relative to precipitation	625-627
sea surface (SST)	585-616
<i>Tension</i>	
fracturing	31
<i>Terrigenous Minerals</i>	842, 850
<i>Tertiary</i>	841, 846
<i>Thermal</i>	
expansion	7
gradients	7
shock cracking	8
<i>Threshold shear velocity</i>	10, 139, 142, 146-149, 182
<i>Thunderstorms</i>	102-104, 122
<i>Tibet</i>	669, 828-832
<i>Total scavenging coefficients (TSC)</i>	248
<i>Trades Winds as a Transport Mechanism</i>	733-770, 786-790, 848

<i>Trajectory analysis of transport</i>	207-226
<i>Transgression</i>	637, 649
<i>Troposphere</i>	828, 842
<i>Tunisia</i>	238
<i>Turbidity</i>	
atmospheric	319
pattern of aerosol	333
<i>Unloading</i>	8
<i>Upwelling</i>	597-606
<i>Varve sequence(s)</i>	617
<i>Vegetation</i> (see: Forests)	
<i>Ventifacts</i>	9
<i>Volcanic Ash</i>	722-724
<i>Wadi</i>	
floods	18
sedimentation	18
<i>Water vapor</i>	190, 193-197
<i>Weathering processes</i>	4, 15-17
chemical	7, 15-16, 31, 34, 53
of fined-grained rocks	53
fluvial	15-16
frost	5, 15-16
by hydration	53
glacial	9, 15-16
physical	45-46, 52-53
salt	6, 15-16
thermal effects	7-8
wind	10, 15-16, 167
<i>West Africa</i>	185-203

<i>Wetting and drying</i>	5, 41-50
<i>Wind</i>	
Andhi	97-132
characteristics of dust storms	89-90, 361
contributions to sea ice sediments	479
direction, as a force shaping Israel's beaches	529
disturbances by	10
energy	3, 15, 167-184
erosion	31-63
frequency	17, 89
geostrophic	848
intensity, as a cause for water upwelling	597-601
'Loo'	104-105, 118-122
sand of the Sahara	574
stress	503
with relationship to airborne dust	172
with relation to ocean energy flux	503
transport	188-192, 385-434, 529
Tunnel	135-142, 162
velocity	8, 10-11, 89, 102-118, 138-139, 146-149, 160, 167-184, 285-287, 317, 368
<i>Westerlies</i>	832
<i>Yardangs</i>	9
<i>Younger Dryas</i>	509-510
atmospheric circulation	509-510